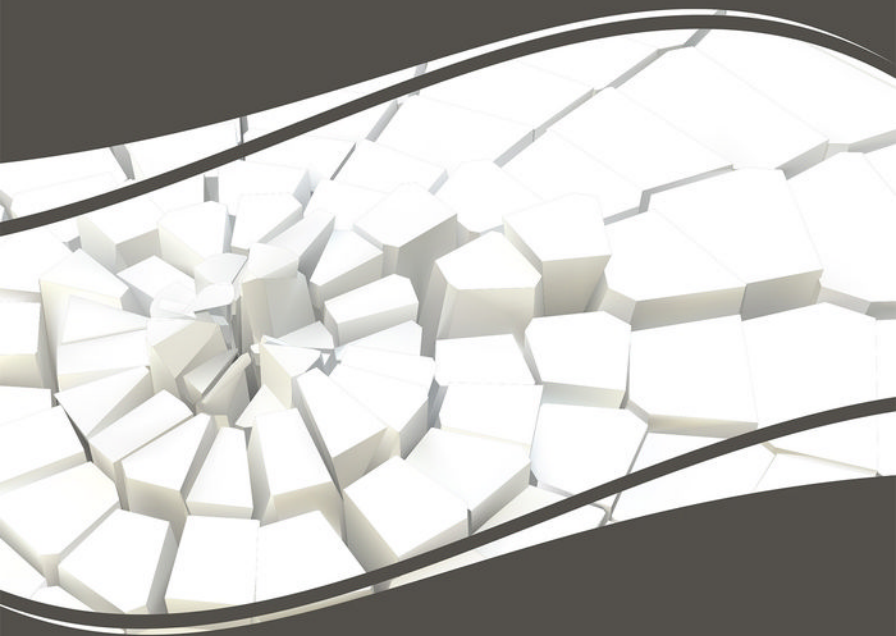


Premier Reference Source

# Fracture and Damage Mechanics for Structural Engineering of Frames

State-of-the-Art Industrial Applications



Julio Flórez-Lopez, María Eugenia Marante, and Ricardo Picón



# Fracture and Damage Mechanics for Structural Engineering of Frames: State-of-the-Art Industrial Applications

Julio Flórez-López  
*University of Los Andes, Venezuela*

María Eugenia Marante  
*Lisandro Alvarado University, Venezuela*

Ricardo Picón  
*Lisandro Alvarado University, Venezuela*

A volume in the Advances in Civil and Industrial  
Engineering (ACIE) Book Series



An Imprint of IGI Global

Managing Director: Lindsay Johnston  
Managing Editor: Austin DeMarco  
Director of Intellectual Property & Contracts: Jan Travers  
Acquisitions Editor: Kayla Wolfe  
Production Editor: Christina Henning  
Development Editor: Brandon Carbaugh  
Typesetter: Cody Page  
Cover Design: Jason Mull

Published in the United States of America by  
Engineering Science Reference (an imprint of IGI Global)  
701 E. Chocolate Avenue  
Hershey PA, USA 17033  
Tel: 717-533-8845  
Fax: 717-533-8661  
E-mail: [cust@igi-global.com](mailto:cust@igi-global.com)  
Web site: <http://www.igi-global.com>

Copyright © 2015 by IGI Global. All rights reserved. No part of this publication may be reproduced, stored or distributed in any form or by any means, electronic or mechanical, including photocopying, without written permission from the publisher. Product or company names used in this set are for identification purposes only. Inclusion of the names of the products or companies does not indicate a claim of ownership by IGI Global of the trademark or registered trademark.

Library of Congress Cataloging-in-Publication Data

Fracture and damage mechanics for structural engineering of frames : state-of-the-art industrial applications / Julio Florez-Lopez, Maria Eugenia Marante, and Ricardo Picon, editors.

pages cm

Includes bibliographical references and index.

ISBN 978-1-4666-6379-4 (hardcover) -- ISBN 978-1-4666-6380-0 (ebook) -- ISBN 978-1-4666-6382-4 (print & perpetual access) 1. Structural analysis (Engineering) 2. Structural engineering. I. Florez-Lopez, Julio, 1958- II. Marante, Maria Eugenia, 1965- III. Picon, Ricardo, 1967-

TG260.F68 2015

624.1'773--dc23

2014022012

This book is published in the IGI Global book series Advances in Civil and Industrial Engineering (ACIE) (ISSN: 2326-6139; eISSN: 2326-6155)

British Cataloguing in Publication Data

A Cataloguing in Publication record for this book is available from the British Library.

All work contributed to this book is new, previously-unpublished material. The views expressed in this book are those of the authors, but not necessarily of the publisher.

For electronic access to this publication, please contact: [eresources@igi-global.com](mailto:eresources@igi-global.com).



# Advances in Civil and Industrial Engineering (ACIE) Book Series

ISSN: 2326-6139  
EISSN: 2326-6155

## MISSION

Private and public sector infrastructures begin to age, or require change in the face of developing technologies, the fields of civil and industrial engineering have become increasingly important as a method to mitigate and manage these changes. As governments and the public at large begin to grapple with climate change and growing populations, civil engineering has become more interdisciplinary and the need for publications that discuss the rapid changes and advancements in the field have become more in-demand. Additionally, private corporations and companies are facing similar changes and challenges, with the pressure for new and innovative methods being placed on those involved in industrial engineering.

The **Advances in Civil and Industrial Engineering (ACIE) Book Series** aims to present research and methodology that will provide solutions and discussions to meet such needs. The latest methodologies, applications, tools, and analysis will be published through the books included in **ACIE** in order to keep the available research in civil and industrial engineering as current and timely as possible.

## COVERAGE

- Hydraulic Engineering
- Transportation Engineering
- Production Planning and Control
- Urban Engineering
- Engineering Economics
- Materials Management
- Coastal Engineering
- Structural Engineering
- Ergonomics
- Optimization techniques

IGI Global is currently accepting manuscripts for publication within this series. To submit a proposal for a volume in this series, please contact our Acquisition Editors at [Acquisitions@igi-global.com](mailto:Acquisitions@igi-global.com) or visit: <http://www.igi-global.com/publish/>.

The Advances in Civil and Industrial Engineering (ACIE) Book Series (ISSN 2326-6139) is published by IGI Global, 701 E. Chocolate Avenue, Hershey, PA 17033-1240, USA, [www.igi-global.com](http://www.igi-global.com). This series is composed of titles available for purchase individually; each title is edited to be contextually exclusive from any other title within the series. For pricing and ordering information please visit <http://www.igi-global.com/book-series/advances-civil-industrial-engineering/73673>. Postmaster: Send all address changes to above address. Copyright © 2015 IGI Global. All rights, including translation in other languages reserved by the publisher. No part of this series may be reproduced or used in any form or by any means – graphics, electronic, or mechanical, including photocopying, recording, taping, or information and retrieval systems – without written permission from the publisher, except for non commercial, educational use, including classroom teaching purposes. The views expressed in this series are those of the authors, but not necessarily of IGI Global.

## Titles in this Series

For a list of additional titles in this series, please visit: [www.igi-global.com](http://www.igi-global.com)

### *Computer-Mediated Briefing for Architects*

Alexander Koutamanis (Delft University of Technology, The Netherlands)

Engineering Science Reference • copyright 2014 • 321pp • H/C (ISBN: 9781466646476) • US \$180.00 (our price)

### *Technologies for Urban and Spatial Planning Virtual Cities and Territories*

Nuno Norte Pinto (The University of Manchester, UK) José António Tenedório (Universidade NOVA de Lisboa, Portugal) António Pais Antunes (University of Coimbra, Portugal) and Josep Roca Cladera (Technical University of Catalonia, BarcelonaTech, Spain)

Information Science Reference • copyright 2014 • 349pp • H/C (ISBN: 9781466643499) • US \$200.00 (our price)

### *Formal Methods in Manufacturing Systems Recent Advances*

Zhiwu Li (Xidian University, People's Republic of China) and Abdulrahman M. Al-Ahmari (King Saud University, Saudi Arabia)

Engineering Science Reference • copyright 2013 • 531pp • H/C (ISBN: 9781466640344) • US \$195.00 (our price)

### *Production and Manufacturing System Management Coordination Approaches and Multi-Site Planning*

Paolo Renna (University of Basilicata, Italy)

Engineering Science Reference • copyright 2013 • 377pp • H/C (ISBN: 9781466620988) • US \$195.00 (our price)

### *Handbook of Research on Industrial Informatics and Manufacturing Intelligence Innovations and Solutions*

Mohammad Ayoub Khan (Centre for Development of Advanced Computing, India) and Abdul Quaiyum Ansari (Jamia Millia Islamia, India)

Information Science Reference • copyright 2012 • 662pp • H/C (ISBN: 9781466602946) • US \$270.00 (our price)

### *Intelligent Industrial Systems Modeling, Automation and Adaptive Behavior*

Gerasimos Rigatos (Industrial Systems Institute & National Technical University of Athens, Greece)

Information Science Reference • copyright 2010 • 601pp • H/C (ISBN: 9781615208494) • US \$180.00 (our price)

### *Manufacturing Intelligence for Industrial Engineering Methods for System Self-Organization, Learning, and Adaptation*

Zude Zhou (Wuhan University of Technology, China) Huaiqing Wang (City University of Hong Kong, Hong Kong) and Ping Lou (Wuhan University of Technology, China)

Engineering Science Reference • copyright 2010 • 407pp • H/C (ISBN: 9781605668642) • US \$180.00 (our price)



[www.igi-global.com](http://www.igi-global.com)

701 E. Chocolate Ave., Hershey, PA 17033

Order online at [www.igi-global.com](http://www.igi-global.com) or call 717-533-8845 x100

To place a standing order for titles released in this series, contact: [cust@igi-global.com](mailto:cust@igi-global.com)

Mon-Fri 8:00 am - 5:00 pm (est) or fax 24 hours a day 717-533-8661

# Table of Contents

<b>Preface</b> .....	x
<b>Acknowledgment</b> .....	xiv
<b>Chapter 1</b>	
Introduction to Structural Mechanics.....	1
1.1 STRUCTURAL MECHANICS, ITS GOALS, AND WAYS .....	1
1.2 APPROACHES FOR THE GEOMETRICAL REPRESENTATION OF A STRUCTURE .....	3
1.3 APPROACHES FOR MATERIAL MODELING .....	7
1.4 SMALL AND LARGE DEFORMATIONS, QUASI-STATIC AND DYNAMIC LOADINGS .....	8
<b>Chapter 2</b>	
Fundamental Concepts of Strength of Materials .....	10
2.1 KINEMATICS OF TIMOSHENKO BEAMS .....	10
2.2 STATICS OF TIMOSHENKO BEAMS.....	14
2.3 CONSTITUTIVE EQUATIONS OF TIMOSHENKO BEAMS .....	18
2.4 EULER-BERNOULLI BEAM THEORY .....	19
2.5 TORSION .....	21
2.6. SUMMARY AND EQUATIONS QUICK REFERENCE .....	23
2.7 EXAMPLES .....	26
2.8. PROBLEMS.....	30
<b>Chapter 3</b>	
Elastic Frames.....	31
3.1 KINEMATICS OF PLANAR FRAMES .....	31
3.2 DYNAMICS OF PLANAR FRAMES .....	40
3.3 CONSTITUTIVE EQUATIONS FOR A SLENDER FRAME MEMBER .....	45
3.4 CONSTITUTIVE EQUATIONS FOR FRAME MEMBERS OF ANY ASPECT RATIO .....	48
3.5 TRIDIMENSIONAL ELASTIC FRAMES .....	54
3.6. SUMMARY AND EQUATIONS QUICK REFERENCE .....	60
3.7. EXAMPLES .....	73
3.8. PROBLEMS.....	81

## Chapter 4

Analysis of Elastic Frames.....	84
4.1 THE DIRECT STIFFNESS METHOD .....	84
4.2 STATIC ANALYSIS OF NONLINEAR ELASTIC FRAMES .....	92
4.3 DYNAMIC ANALYSIS OF ELASTIC FRAMES .....	99
4.4 SUMMARY AND EQUATIONS QUICK REFERENCE .....	101
4.5 EXAMPLES .....	105
4.6 PROBLEMS.....	139
4.7 PROJECTS.....	139

## Chapter 5

Fundamental Concepts of Plasticity.....	141
5.1 EXPERIMENTAL BEHAVIOR OF DUCTILE MATERIALS .....	141
5.2 ELASTO-PERFECT PLASTIC CONSTITUTIVE MODEL.....	143
5.3 ELASTO-PLASTIC MODEL WITH LINEAR ISOTROPIC HARDENING .....	149
5.4 ELASTO-PLASTIC MODEL WITH NONLINEAR ISOTROPIC HARDENING.....	151
5.5 ELASTO-PLASTIC MODEL WITH LINEAR KINEMATIC HARDENING.....	153
5.6 ELASTO-PLASTIC MODEL WITH NONLINEAR KINEMATIC HARDENING .....	157
5.7 ELASTO-PLASTIC SHEAR STRESS-STRAIN RELATIONSHIP .....	158
5.8 SUMMARY AND EQUATIONS QUICK REFERENCE .....	160
5.9 EXAMPLES .....	164
5.10 PROBLEMS.....	171

## Chapter 6

The Plastic Hinge .....	172
6.1 ELASTO-PLASTIC MOMENT VS. CURVATURE RELATIONSHIP .....	172
6.2 THE PERFECT PLASTIC HINGE .....	174
6.3 PLASTIC HINGE WITH HARDENING.....	178
6.4 PERFECTLY PLASTIC HINGE SUBJECTED TO BENDING AND AXIAL FORCES .....	181
6.5 PLASTIC HINGES IN REINFORCED CONCRETE ELEMENTS.....	186
6.6 PLASTIC HINGE WITH PINCHING EFFECT DUE TO SLIP .....	198
6.7 SUMMARY AND EQUATIONS QUICK REFERENCE .....	205
6.8 EXAMPLES .....	217
6.9 PROBLEMS.....	229

## Chapter 7

Elasto-Plastic Frames.....	231
7.1 ELASTO-PLASTIC CONSTITUTIVE MODEL FOR A SLENDER ELEMENT OF A PLANAR FRAME.....	231
7.2 ELASTO-PLASTIC CONSTITUTIVE MODEL FOR SQUAT RC ELEMENTS .....	238
7.3 SHEAR PROPERTIES OF RC ELEMENTS .....	240
7.4 AN ELASTO-PLASTIC CONSTITUTIVE MODEL FOR ELEMENTS OF ANY ASPECT RATIO.....	243
7.5 TRIDIMENSIONAL ELASTO-PLASTIC FRAMES.....	244
7.6 SUMMARY AND EQUATIONS QUICK REFERENCE .....	247
7.7 EXAMPLES .....	256
7.8. PROBLEMS.....	271

## **Chapter 8**

Analysis of Elasto-Plastic Frames.....	276
8.1 THE HINGE-BY-HINGE METHOD FOR PERFECTLY PLASTIC FRAMES .....	276
8.2 ELASTIC PREDICTOR - PLASTIC CORRECTOR ALGORITHM.....	284
8.3 GENERAL ANALYSIS OF ELASTO-PLASTIC FRAMES.....	290
8.4 SUMMARY AND EQUATIONS QUICK REFERENCE .....	292
8.5 EXAMPLES .....	301
8.6 PROBLEMS.....	330
8.7 PROJECTS.....	331

## **Chapter 9**

Fundamental Concepts of Fracture and Continuum Damage Mechanics.....	332
9.1 GRIFFITH CRITERION AND FRACTURE MECHANICS .....	332
9.2 UNIAXIAL DAMAGE MECHANICS MODELS.....	337
9.3 STRAIN AND DAMAGE LOCALIZATION .....	345
9.4 SUMMARY AND EQUATIONS QUICK REFERENCE .....	349
9.5 EXAMPLES .....	355
9.6 PROBLEMS.....	359

## **Chapter 10**

Lumped Damage Mechanics: Reinforced Concrete Frames.....	362
10.1 THE LUMPED DAMAGE MODEL.....	362
10.2 GENERALIZED GRIFFITH CRITERION FOR AN INELASTIC HINGE.....	364
10.3 CRACK RESISTANCE FUNCTION OF AN INELASTIC HINGE.....	365
10.4 YIELD FUNCTION OF A DAMAGED PLASTIC HINGE.....	373
10.5 SOME NUMERICAL SIMULATIONS WITH THE DAMAGE MODEL .....	374
10.6 A MODEL OF DAMAGE FOR RC ELEMENTS CONSIDERING ULTRA-LOW CYCLE FATIGUE EFFECTS.....	379
10.7 ANALYSIS OF DAMAGED FRAMES .....	380
10.8 LIMITATIONS OF THE DAMAGE MECHANICS MODEL .....	388
10.9 SUMMARY AND EQUATIONS QUICK REFERENCE .....	389
10.10 EXAMPLES .....	396
10.11 PROBLEMS.....	408
10.12 PROJECTS.....	409

## **Chapter 11**

Damage Mechanics of Dual Systems.....	412
11.1 EXPERIMENTAL ANALYSIS OF RC ELEMENTS OF VARIOUS ASPECT RATIOS.....	412
11.2 ELASTICITY LAW FOR FRAME MEMBERS OF ANY ASPECT RATIO .....	418
11.3 DAMAGE EVOLUTION LAWS .....	424
11.4 PLASTIC DEFORMATIONS EVOLUTION LAWS.....	429
11.5 ANALYSIS OF DUAL SYSTEMS.....	430
11.6 SUMMARY AND EQUATIONS QUICK REFERENCE .....	438
11.7 PROJECTS.....	444



## **Chapter 12**

Unilateral Damage in Reinforced Concrete Frames .....	445
12.1 ELASTICITY LAW UNDER CYCLIC LOADING .....	445
12.2 INTERNAL VARIABLES EVOLUTION LAWS UNDER CYCLIC LOADING .....	449
12.3 NUMERICAL SIMULATIONS OF THE BEHAVIOR OF RC ELEMENTS OF DIFFERENT ASPECT RATIOS .....	451
12.4 DAMAGE IN A RC WIDE BEAM-COLUMN JOINT .....	460
12.5 TORSION DAMAGE .....	466
12.6 DAMAGE MODEL FOR TRIDIMENSIONAL FRAMES .....	473
12.7 SUMMARY AND EQUATIONS QUICK REFERENCE .....	481
12.8 EXAMPLES .....	488
12.9 PROJECTS .....	501

## **Chapter 13**

Industrial Applications .....	503
13.1 ANALYSIS AND DIAGNOSIS OF VULNERABLE STRUCTURES .....	503
13.2 PORTAL OF DAMAGE .....	506
13.3 INDUSTRIAL APPLICATIONS .....	509
13.4 SUMMARY .....	533

## **Chapter 14**

Lumped Damage Mechanics: Tubular Steel Structures .....	538
14.1 LOCAL BUCKLING DAMAGE MODEL FOR PLANAR MONO-SIGN LOADINGS .....	538
14.2 THE COUNTER-BUCKLING EFFECT AND A MODEL FOR GENERAL PLANAR LOADINGS .....	545
14.3 DAMAGE MODEL FOR TRIDIMENSIONAL STEEL FRAMES .....	554
14.4 ANALYSIS OF STEEL FRAMES WITH LOCAL BUCKLING .....	570
14.5 SUMMARY AND EQUATIONS QUICK REFERENCE .....	580

<b>Compilation of References .....</b>	<b>592</b>
--	------------

<b>About the Authors .....</b>	<b>597</b>
--------------------------------	------------

<b>Index .....</b>	<b>598</b>
--------------------	------------

*To ours sons and daughters: Andrés, Diego, Elena, Julia, and Roberto*

## Preface

Jean Lemaitre, French Mechanician and Engineer, is one of the founders of modern damage mechanics. Sometimes, he starts his books congratulating the reader for opening them. As this book is indebted in many ways to his work and ideas, we would like to start likewise. So, please, read the next paragraph with a Jacques Cousteau accent.

Bravo, dear reader, you have had the courage to open this manuscript! And you were right because you have earned some explanations:

(We suggest that from now on you change your reading accent to that of Sofia Vergara or Ruben Blades)

This is a book on the structural analysis of frames.

Many civil engineering structures such as buildings, bridges, or cranes are modeled as frames. Thus, frame analysis has always been one of the most important themes in structural and earthquake engineering. There is a large number of textbooks on the subject, most of them consider only elastic frames. A more reduced, but still significant, number of books deal with elasto-plastic frames.

Fracture mechanics is also an important branch of engineering mechanics. Many textbooks for many different materials, metals, concrete, rocks, have been written on the subject too. All of them, probably, consider the point of view of continuum mechanics. Damage mechanics is a more recent branch of the engineering mechanics; fewer books on the subject can be found, but, again, they are written in the framework of continuum mechanics.

Frame analysis in the framework of fracture and damage mechanics is a logical development of both subjects. It is also the most recent major extension from both points of view. Paradoxically, even if this is the latest development of damage mechanics, the state of the art on the subject is the more mature for industrial applications.

The primary goal of this book is to describe the structural analysis of frames from the point of view of damage and fracture mechanics; it is intended to be a link between basic knowledge and practical applications, a synthesis between experimental and theoretical results.

However, damage mechanics grew out of fracture mechanics, elasticity, and plasticity and includes them as particular cases. Thus, this book also presents a coherent and comprehensive view of the elastic and plastic analysis of framed structures.

As in any other contemporary engineering field, the computational implementation of the damage models is a priority. Some academic software for the analysis of damaged frames is already available; however, at the time when this book was written, reliable and user-friendly industrial software is still lacking.

This book is also intended as a reference manual for those readers who want to develop computer programs on the subject.

## Preface

We have assumed that the readers of this book have at least a good knowledge of strength of materials, calculus, matrix analysis, and computer programming, as they are taught in standard courses for undergraduate engineering students. Additional courses on structural analysis, reinforced concrete, theory of elasticity (or advanced strength of materials), and design of steel structures would also be very useful.

This book grew out of courses in the Master's and Doctoral programs on Applied Mechanics or Structural Engineering at the University of Los Andes and the Lisandro Alvarado University in Venezuela. Many of the results that are included in the book were developed in the framework of theses at these universities.

## HISTORICAL SKETCH

The need to analyze and predict the failure of structures has been a common preoccupation of humanity since immemorial times. However, the first works of structural engineering in the modern sense of the word are probably due to the Italian scientist Galileo Galilei (1564-1642). He investigated the strength of rods in tension as well as in cantilever beams.

The English scientist Robert Hooke (1635-1703) established the foundations of linear elasticity when he discovered that for many materials displacement under a load is proportional to force. Hooke did not use mathematical language to formulate his law but enunciated it in Latin: "*Ut tensio sic vis.*" Edne Mariotte (1620-1684) in France published similar discoveries in 1680 and applied this concept to the analysis of beams subjected to bending; he remarked that some fibers in the beam elongate while others shorten. He concluded that the limit between both effects corresponds to the middle of the cross-section. The contributions of Sir Issac Newton (1642-1727) changed the history of the science by stating the laws of motion and establishing the basis of infinitesimal calculus in his book *Principia*.

The theory of beams discussed in the textbooks of strength of materials is due to the works of James Bernoulli (1654-1795), Daniel Bernoulli (1700-1782), members of a distinguished family of Swiss mechanicians and mathematicians, and Leonhard Euler (1707-1783). Other important contributions, the equations for normal stresses in a beam subjected to bending, are due to the French scientists Charles Augustine Coulomb (1736-1806) and Louis Marie Henri Navier. Barre de Saint Venant (1797-1886) analyzed the shear stress distribution in beams subjected to bending and also formulated a general theory of torsion that included elements of non-circular cross-sections. The theory of beams was perfected by the Ukrainian engineer Stephen Timoshenko (1878-1972); this improved theory permitted the analysis of short beams, which were not correctly described by the classic one.

The theory of indeterminate structures started with the work of the Scottish physicist James Clerk Maxwell (1830-1879) and the German engineer Otto Mohr (1835-1918); in their procedure, that both of them proposed independently, the problem consisted in the solution of a system of equations; these equations describe the geometrical compatibility of displacements in terms of reactions and internal stresses. The Italian engineer Alberto Castigliano (1847-1884) and the German professor Heinrich Müller-Breslau (1851-1925) improved and generalized the results presented by Maxwell and Mohr. The US structural engineer Hardy Cross (1885-1959) developed the moment distribution method that allowed for the first time the analysis of large structures. In 1969, the US professor H. G. Powell proposed a general formulation for nonlinear elastic frames that is also amendable to the general inelastic case. With the

advent of cheap and powerful digital computers, the analysis of framed structures became the analysis by the finite element method. Its development started in the 1950s with the works of M. J. Turner, R. W. Clough, H. C. Martin, and L. J. Topp in the United States, and by J. H. Argyris and S. Kelsey in Britain.

The general theory of tridimensional elasticity is based on the work of the French mathematician Augustin Louis Cauchy (1789-1857). Within this framework, G. Kirsh obtained in 1898 the stress distribution in a large plate with a circular hole subjected to tractions far from the hole. He showed that the maximum normal stress in this case is equal to three times the nominal value, exposing for the first time the so-called stress concentration phenomenon. Later, the Russian mathematician G. Kolosov (in 1907) and the British engineer Charles Inglis (in 1914) extended these results to the case of elliptical holes. They showed that the maximum normal stress augments when the relationship between the minor and mayor axis decreases. Areas with large stress concentration factors are prone to the development of cracks. The solution of a plate with an elliptical hole was used by the British aeronautical engineer Alan Arnold Griffith (1893-1963) to develop a theory of crack growth that constitutes the basis of fracture mechanics. Other scientists with significant contributions to this theory are the US engineer George R. Irwin (1907-1998) and the US mechanician James Robert Rice.

The theory of plasticity has a history as old as that of elasticity. As early as 1773, Coulomb enunciated the conditions for yielding of soils under normal and shear stresses. The first practical applications of the theory of plasticity are attributed to the French engineer Jean Victor Poncelet (1788-1867) and the Scottish engineer William John Macquorn Rankine (1820-1872). The French engineer Henry Edouard Tresca (1814-1885) studied the conditions for plastic yielding in metals. An improved criterion for plasticity in metals was proposed by the Austrian mathematician Richard von Mises (1883-1953). The mathematical theory of plasticity is due to the contributions of Ludwig Prandtl (1875-1953), Heinrich Hencky (1885-1951), Daniel C. Drucker (1918-2001), William Prager (1903-1980), and Rodney Hill.

Rupture, from the point of view of the fracture mechanics and the theory of plasticity, is considered as a two-state process, failure or no failure, related to critical values of load, stress, strain, or number of cycles. A. Palmgree in 1924 proposed for the first time the use of a variable related to the progressive deterioration of the material preceding to failure. Two decades later, A. M. Miner popularized this approach as a practical tool for design. But it was in 1958 that the Russian scientist L. M. Kachanov published a very famous paper that is considered the cornerstone of damage mechanics. A second significant contribution on damage mechanics, the effective stress concept, appeared a decade later due to the Russian scientist Y. N. Rabotnov. During the 1970s, damage mechanics received a vigorous impulse thanks to the works of the French engineer Jean Lemaitre who introduced the idea of equivalence in strain and several experimental procedures for measuring damage.

## **ORGANIZATION OF THE BOOK**

The chapters are organized as follows: first, the relevant concepts on the subject of the chapter are presented; then, a summary of the equations are listed so that they can be located easily when reading the following chapters and for solving exercises; some examples are solved next to illustrate with simple academic cases the concepts introduced in the chapter. Even if all the examples are presented together in this special section, we suggest the reader look at them when they are referred to in the body of the

## **Preface**

chapter; some unsolved problems are proposed next; those readers who would like to test their comprehension of the chapter should solve them; finally, some projects are proposed; the purpose is to guide the reader interested in the numerical implementation in writing his/her own computer programs; the projects are related to themselves, so they may become a sophisticated software if all of them are carried out.

Chapter 1 is an introduction to structural mechanics.

Chapter 2 contains a compendium of the relevant concepts of the strength of materials for the subjects treated in the book.

Chapters 3 and 4 present the theory of elastic frames. They include not only the classic theory of the structures but also a presentation of the analysis of dual system. These chapters introduce a new notation for the analysis of structures. It differs from the one used in the classic books of structural analysis, but it significantly simplifies the description of the inelastic models.

Chapter 5 introduces the fundamental concepts of the theory of plasticity. Chapters 6 to 8 describe the theory of elasto-plastic frames and dual systems.

Chapter 9 resumes the fundamental concepts of fracture and damage mechanics, while Chapters 10 to 12 present the theory of lumped damage mechanics for reinforced concrete structures.

Chapter 13 shows how these mathematical models can be used in some industrial applications.

Finally, Chapter 14 describes lumped damage mechanics for tubular steel structures.

*Julio Flórez-López*

*University of Los Andes, Venezuela*

*María Eugenia Marante*

*Lisandro Alvarado University, Venezuela*

*Ricardo Picón*

*Lisandro Alvarado University, Venezuela*

# Acknowledgment

We would like to acknowledge our students in the postgraduate programs in Structural Engineering at University of Los Andes, Lisandro Alvarado University, The University of Zulia, Polytechnic University of Madrid, and Sao Paulo University. This book would have not been possible without them.

We would like to thank particularly our colleagues Erick Abarca, Denis Avon, Nelson Briceño, Sebastián Delgado, Rafael Fébres, Néstor Guerrero, Pether Inglessis, María Elena Perdomo, Rosángel Rojas, Edward Thomson, Maylett Uzcategui, and Betsy Vera.

We would like to acknowledge also to Lisandro Alvarado University, which supported us during the redaction of the book.

*Julio Flórez-López*  
*University of Los Andes, Venezuela*

*María Eugenia Marante*  
*Lisandro Alvarado University, Venezuela*

*Ricardo Picón*  
*Lisandro Alvarado University, Venezuela*

# Chapter 1

## Introduction to Structural Mechanics

### ABSTRACT

*Foreign visitors discovering a new country usually start by looking at a map of the place; they identify its regions and their characteristics; they try to acquire a mental chart of the new country. Naturally, they have to choose a city or cities in which they are going to spend long stays. Only in those specific places, the visitors will try to learn about the specifics: street names, places of interests, public transportation network, convenience stores, and so on. In this chapter, a general map of the structural mechanics (the “country” in which the reader of this book is going to “reside”) is first presented. Next, the theory of frames (the “city” that the reader of the book is going to know very well) is placed in this general context. After reading the chapter, the reader will slowly improve his/her knowledge of the specific topic until becoming an expert in the theme. It is fair to say that the theory of frames is equivalent to a Rio de Janeiro in Brazil or a Paris in France or a Saint Petersburg in Russia.*

### 1.1 STRUCTURAL MECHANICS, ITS GOALS, AND WAYS

The goal of structural engineering is to certify the structural integrity of machines, buildings and other solids during its normal operation and, also, during possible accidents or overloads. Structural engineering can be divided into two different but connected sub fields: structural design and structural mechanics. The former consists in the development and application of guidelines and rules that allow for the design of safe structures for a specific use. The latter has as a goal determining how the external forces and actions are distributed among the structural components of an object when its dimensions and properties are known. It is evident that it is not possible to design a structural component if the loads that it has to withstand are unknown. On the other hand, usually, the dimensions and properties of the structural components are not known if the structure has not been designed previously. Thus, in many cases, the process of structural certification is an iterative one where the techniques of the structural design and the structural mechanics are applied successively.

The present is a book on structural mechanics exclusively.

DOI: 10.4018/978-1-4666-6379-4.ch001



Structural mechanics can also be used as a tool for the “diagnosis” of existing structures, in the same way as medical imagenology techniques, such as computerized tomography, are used to diagnose a human patient (see Figure 1). This diagnose is sometimes called structural vulnerability assessment.

In the engineering practice, structural mechanics concepts are usually applied through structural analysis programs. This field has two aspects. The first one is about the mathematical models or equations that describe the behavior of structures under mechanical loading; the second one is about the numerical procedures used to solve these equations. This book deals mainly with the former aspect although the basic notions of the latter are also considered. Table 1 presents a summary of the models used in the structural analysis.

A structural analysis is normally composed choosing one item of every column; for instance, a plastic plate can be analyzed assuming small strains and under dynamic loadings; or a fracture mechanics analysis can be carried out in a solid under a quasi-static loading; any combination is possible. The meaning of each element of the table is explained in the following sections.

Figure 1. “Diagnose” of (a, b) A human patient, (c, d) A structure

1a. MRI-Philips.JPG. (n.d.). Retrieved April 13, 2014 from <http://en.wikipedia.org/wiki/File:MRI-Philips.JPG>

1b PET-image.jpg. (n.d.). Retrieved April 13, 2014 from <http://commons.wikimedia.org/wiki/File:PET-image.jpg>

1c Skyscrapercity.com. (n.d.). Retrieved July 25, 2010 from <http://www.skyscrapercity.com/showthread.php?t=321267&page=17>

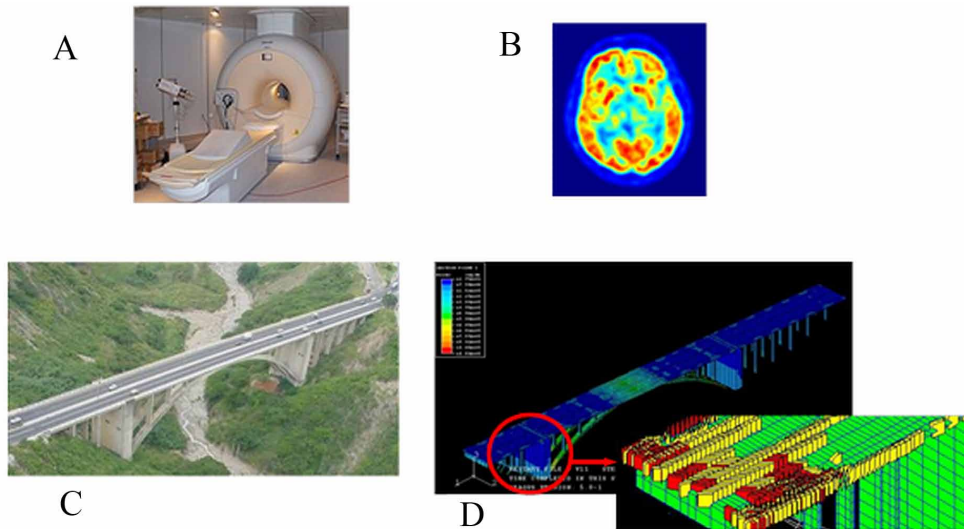


Table 1. Summary of structural mechanics models

Representation of the Structure	Representation of the Material	Representation of the Deformation	Representation of the Loading
Solid theory	Theory of elasticity	Small strains and deformations	Quasi-static loadings
Beam and arc theory	Theory of plasticity	Large strain and deformations	Dynamic loadings
Plate and shell theory	Fracture Mechanics		
Frame theory	Damage Mechanics		

## 1.2 APPROACHES FOR THE GEOMETRICAL REPRESENTATION OF A STRUCTURE

### 1.2.1 Theory of Solids

A structure is always assumed to be the assemblage of a set of basic structural components. The type of the basic unit distinguishes the theories of the first column in Table 1. In the theory of solids, the basic structural component is the solid differential element that is identical to the differential volume element that is introduced in calculus (see Figure 2).

Each solid element is identified using its coordinates  $X, Y, Z$  in a known initial configuration, often this is the blueprint of the structure. Then, some variables for each element are introduced. These are classified into two categories: kinematic variables and dynamic variables. The former define the movement of the solid element (the displacement vector) and its deformation (the strain tensor). The dynamics variables are used to characterize external forces (body or surface vector forces) and the “share” of the external loading that each solid differential element has to withstand (the stress tensor). All these variables depend on the three spatial coordinates that identify each element and, possibly, time.

The analysis of a solid is formulated by introducing three sets of equations; the first one is the kinematic equations that relate the strain field with the displacements, the second one is the equilibrium equation between the external forces and the stress field. The last one is the constitutive equation that relates stresses and strains (see Figure 3). In the general case, those are partial differential equations of the three spatial variables and time.

Figure 2. Basic structural component in theory of solids: the solid differential element

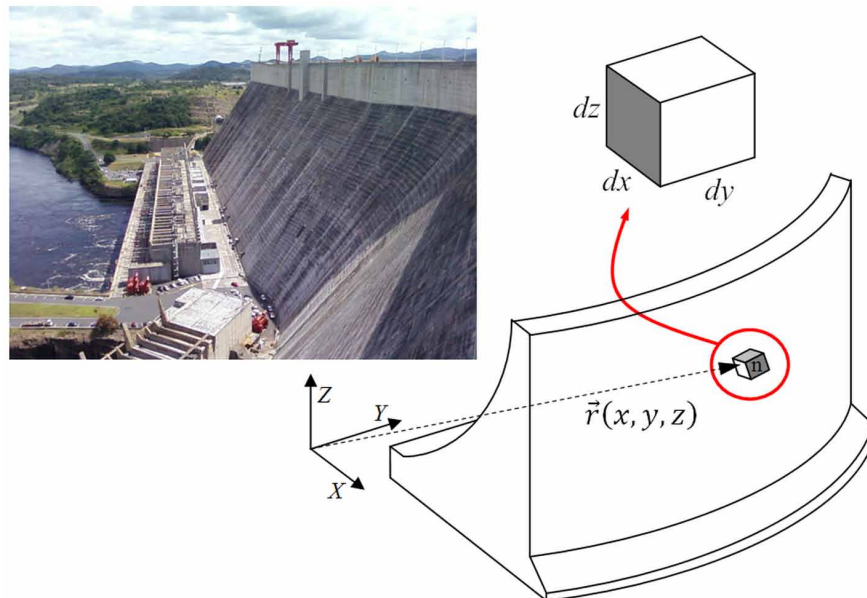
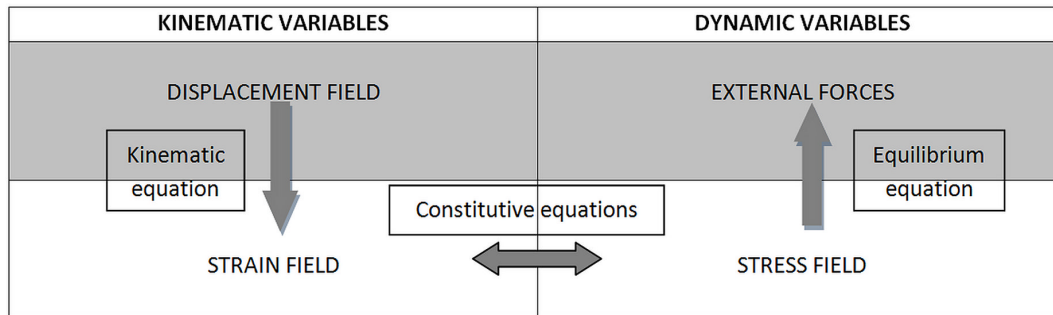


Figure 3. Summary of variables and equations for solids



### 1.2.2 Theory of Beams

The basic structural component in this case is the beam differential element (see Figure 4). Any structure that can be considered as the assemblage of beam elements linked together by an axis, denoted neutral axis, could be analyzed as a beam. Only one independent variable is needed to identify each beam element; this is the distance between the element and the origin of the axis in the initial configuration. In theories of beam, the structural behavior in the cross-section is assumed to be known, thus only variables of the neutral axis are unknowns of the problem. Beam theories are the core of the strength of materials courses and textbooks.

There are several beam theories; the type of behavior of the cross-section differentiates them. In the context of this book, two of them are especially important: the one based on the Euler-Bernoulli hypothesis and another based on the Timoshenko hypothesis. The latter states that a cross-section moves as a rigid body (see Figure 5a); the former indicates that the cross-section not only behaves as a rigid body but that it remains perpendicular to the neutral axis too (see Figure 5b).

The variables in the beam theory can also be grouped as kinematic (deflections or curvatures for instance) and dynamic (moments, axial forces, shear forces, and so on). All these variables depend on the only spatial variable  $x$  and, in some cases, time. The same three set of equations: kinematic, equilibrium and constitutive laws are introduced in order to formulate the beam problem too; but in this case they are ordinary differential equations in simple cases. The scheme shown in Figure 3 is still valid with little modifications.

### 1.2.3 Plate and Shell Theories

The basic structural component of the plate theory, the plate differential element, is shown in Figure 6. Any structure that can be considered as the assemblage of these filaments linked together by a plane, denoted neutral plane, can be analyzed as a plate. Two independent variables are needed to identify each plate element. In this case, the behavior of each filament element is known and only variables of the neutral plane are introduced.

This book is not concerned with plate theory.

Figure 4. Basic structural component in the theory of beams: the beam differential element

4 Michael\_Schumacher\_Ferrari\_2004.jpg. (n.d) Retrieved April 13, 2014 from [http://commons.wikimedia.org/wiki/File:Michael\\_Schumacher\\_Ferrari\\_2004.jpg](http://commons.wikimedia.org/wiki/File:Michael_Schumacher_Ferrari_2004.jpg)

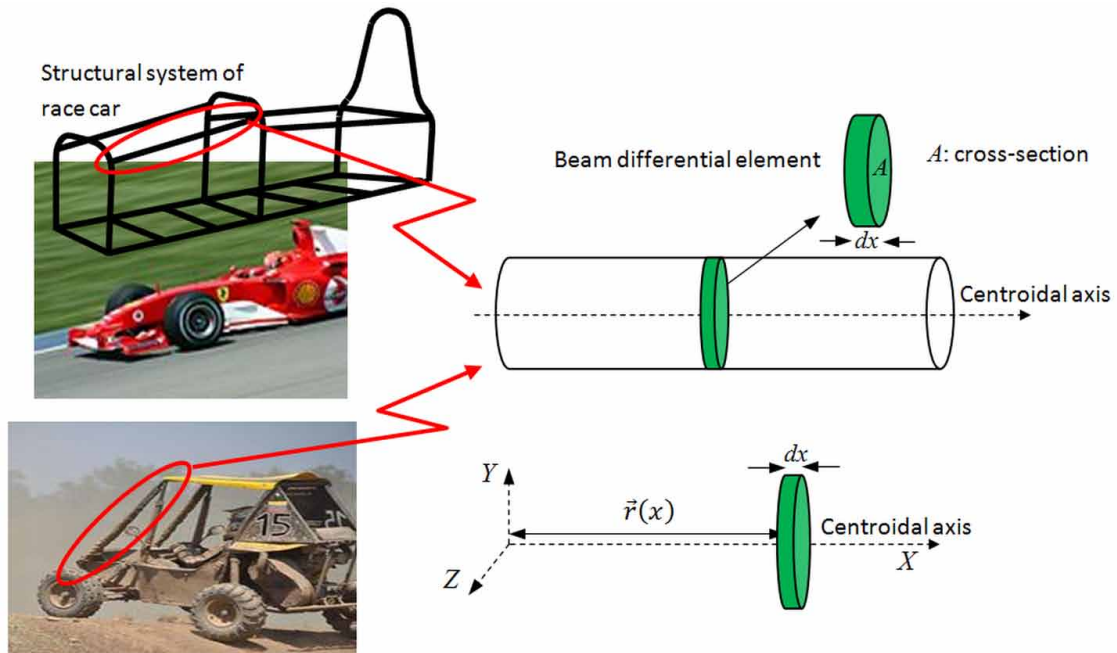


Figure 5. Behavior of the cross-section in two beam theories a) Timoshenko theory b) Euler-Bernoulli theory

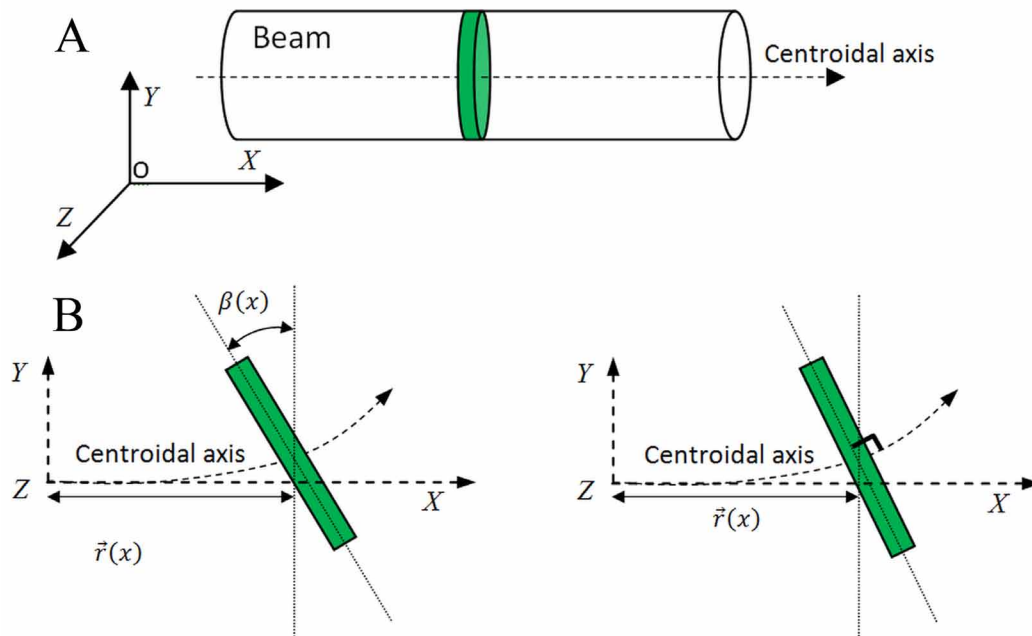
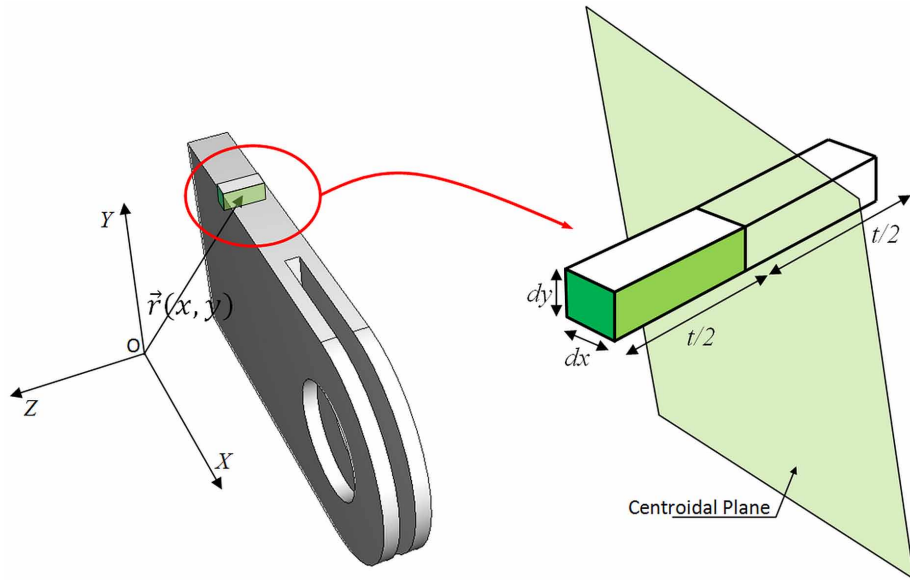


Figure 6. Basic structural component in the theory of plates: the plate differential element

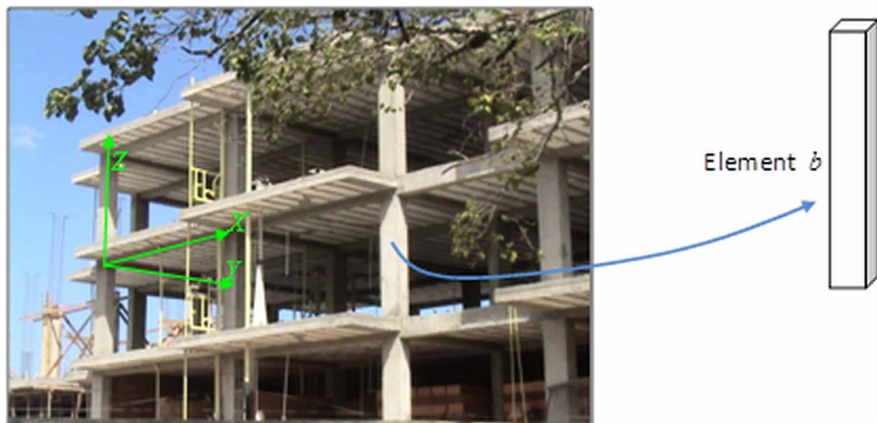


### 1.2.4 Frame Theories

The basic structural component of a frame is the frame element with finite dimensions shown in Figure 7. Only natural numbers are needed to identify each element. Beam and frame theories can be unified in the elastic case, but they are completely different in the inelastic ones: frame theories are based on the concept of plastic hinge, beam theories on the so called multilayer approach.

The goal of this book is to present a general theory of frames.

Figure 7. Basic structural component in the theory of frames



### 1.3 APPROACHES FOR MATERIAL MODELING

Material behavior (second column in Table 1) is characterized through the constitutive equations that relate stresses and strains. The simplest model is the elastic one that assumes a one to one relationship between stress and strain. A classic example is the Hooke's law that postulates a linear relationship between these variables (see Figure 8a). Elastic models assume that the material response is invariable no matter how high are the forces applied on the structure; they do not consider that the material may degrade or the structure bends permanently. Thus, they are used only to analyze structures under service conditions or for design purposes.

Consider now a paper clip; if it is used to hold together a limited number of paper sheets, the clip will recover its original form as soon as the pages are removed: it is then said that its behavior is basically elastic. The paper clip can be used in this way for a big number of cycles. However, if it is used with a large number of pages, the clip will not recover its initial form once the sheets are removed: the two parts of the clip will remain partially open. It is then said that this structure has experienced plastic or permanent deformations. The theory of plasticity, the second item in the second column of Table 1, has as a goal the determination of the structure state when plastic deformations have taken place. As in the example of the paper clip, plasticity theory is often used to evaluate the effect of overloads in the structures. The simplest approach in this case is the model of perfect plasticity that is shown in Figure 8b.

Fracture and damage mechanics deal with the propagation of cracks and structural defects under mechanical loadings. The former theory studies the conditions for the propagation of a single or a small number of cracks as in the case of the structure shown in Figure 9a, the latter considers massive or generalized arrays of meso or micro cracks and defects (Figure 9b).

The most noticeable consequences of these processes are the degradation of strength and stiffness observed in the stress-strain relationships as shown in Figure 8c. The term "stiffness degradation" means reduction of the elastic modulus; "strength degradation" is the term used to indicate that the maximum of the curve strain vs. stress has been over passed.

This book describes the behavior of framed structures from the point of view of all these theories and it is organized following the order indicated in the second column of Table 1: the theory of elastic frames is the object of chapters 2-4, plastic frames are considered in chapters 5-8, models based on fracture and damage mechanics for framed structures are described in chapters 9-14.

Figure 8. Stress –strain relationships for different material models a) Elastic behavior b) Perfect elastic plastic behavior c) Typical damage mechanics behavior

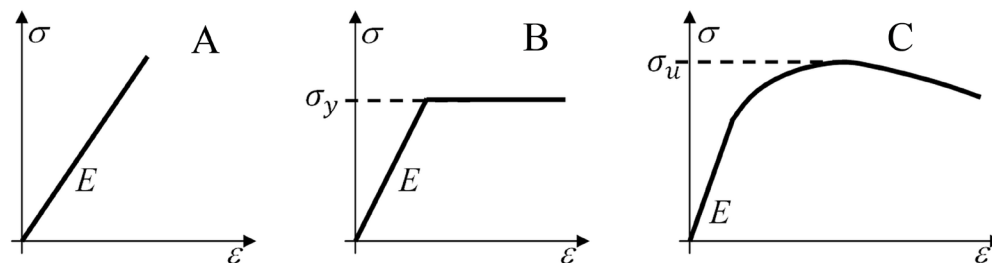
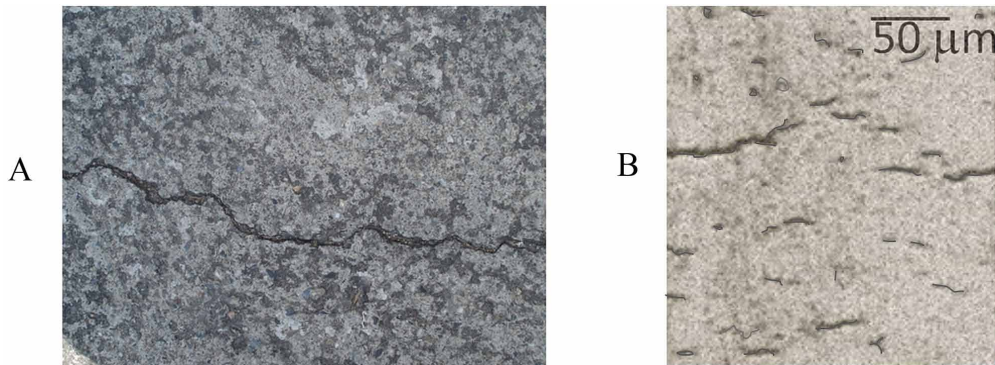


Figure 9. a) Single crack propagation in a floor slab b) Schematic representation of generalized crack-  
ing based on Larrylawson (2005)

9b Larrylawson (2005) Retrieved January 17, 2013 from <http://www.larrylawson.net/pix5/fig5.jpg>



#### 1.4 SMALL AND LARGE DEFORMATIONS, QUASI-STATIC AND DYNAMIC LOADINGS

Consider a simply supported beam as the one shown in Figure 10a. The forces applied on the beam produce the deformation indicated in Figure 10b. The equilibrium of moments gives the maximum flexural moment:

$$M_{\max} = \frac{P.L}{2} + N.\delta_{\max} \quad (1.1)$$

This mathematical operation is not immediate since the value of the deflection  $\delta_{\max}$  must be computed first and the deflection of the beam depends on the flexural moment distribution on it.

A much simpler analysis can be carried out if the deflections of the beam are so small that the term  $N.\delta_{\max}$  can be neglected when compared with

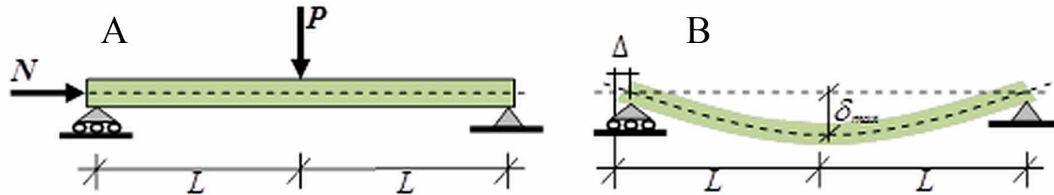
$$\frac{P.L}{2}$$

in Equation (1). In that case, the computation of the maximum moment of the beam becomes immediate:

$$M_{\max} \cong \frac{P.L}{2}.$$

It can be noticed that this result is obtained if the equilibrium of moments is considered in the initial configuration of the beam (Figure 10a).

Figure 10. Simply supported beam under vertical and horizontal loads a) Initial configuration b) Deformed configuration



The latter approach, application of the equilibrium equations in the initial configuration, is called geometrically-linear and corresponds to the first item in the third column of Table 1. The more exact but more complex procedure of considering the deformed configuration corresponds to the second item of column three; in the latter case, the equilibrium equation may become nonlinear. The kinematic equation can also be linear or nonlinear if, respectively, small or large deformations are chosen. This book describes the both cases of equilibrium and kinematic equations for framed structures.

Finally, the last column of Table 1 is also related to the equilibrium equation. In the quasi static case, the inertia forces are neglected. These are the forces that are felt in a bus when it accelerates brusquely. In some cases, earthquake loadings for instance, they are the most significant input and cannot be ignored; this is the dynamic loading case indicated in the second row of column four. This book also considers both forms of the equilibrium equation for framed structures.

## REFERENCES

- Lemaitre, J. (1992). *A course on damage mechanics*. Berlin, Germany: Springer-Verlag. doi:10.1007/978-3-662-02761-5
- Lemaitre, J., & Chaboche, J. L. (1985). *Mécanique des matériaux solides*. Paris, France: Dunod Bordas.
- Rice, J. R. (2010). *Solid mechanics*. Retrieved from [http://esag.harvard.edu/rice/e0\\_Solid\\_Mechanics\\_94\\_10.pdf](http://esag.harvard.edu/rice/e0_Solid_Mechanics_94_10.pdf)
- Sterling, J. (1958). *Indeterminate structural analysis*. Reading, MA: Addison-Wesley Pub. Co.
- Wikipedia. (2010). Retrieved from <http://en.wikipedia.org/wiki/Wikipedia>



## Chapter 2

# Fundamental Concepts of Strength of Materials

### ABSTRACT

*This chapter presents the concepts of strength of materials that are relevant to the analysis of frames. These are the modified Timoshenko theory of elastic beams (Sections 2.1-2.3) and the Euler-Bernoulli one (Section 2.4). These concepts are not presented as in the conventional textbooks of strength of materials. Instead, the formulations are described using the scheme that is customary in the theory of elasticity and that was described in Chapter 1 (Section 1.1.1) (i.e. in terms of kinematics, statics, and constitutive equations). Kinematics is the branch of mechanics that studies the movement of solids and structures without considering its causes. Statics studies the equilibrium of forces; the basic tool for this analysis is the principle of virtual work. The constitutive model that describes a one-to-one relationship between stresses and deformations completes the formulation of the elastic beam problem. Finally, in Section 2.5, some concepts of the elementary theory of torsion needed for the formulation of tridimensional frames are recalled.*

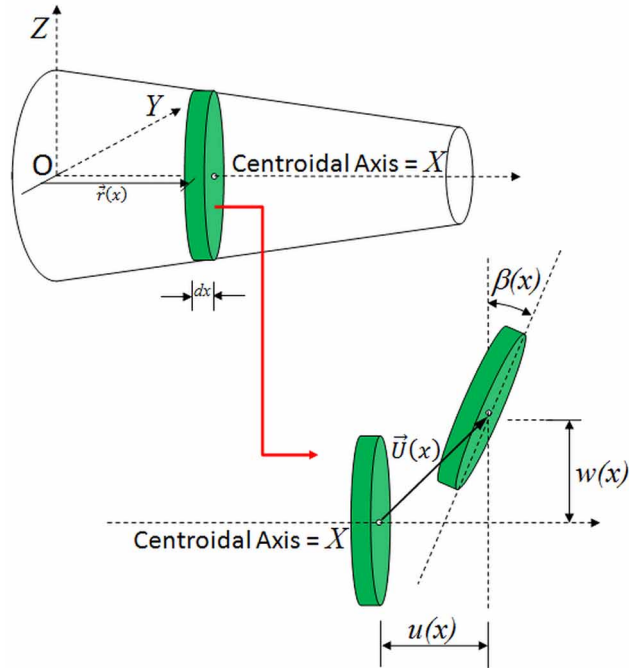
### 2.1 KINEMATICS OF TIMOSHENKO BEAMS

#### 2.1.1 Generalized Displacements of Planar Beams

Consider a beam that displaces only in the plane  $X$ - $Z$  as shown in Figure 1. The axis  $X$  is chosen so that it passes through the centroid of the beam's cross-section; i.e.  $X$  coincides with the centroidal axis of the beam. The fundamental hypothesis of the theory of beams states that a cross-section of the beam moves only as a rigid body.

The movement of a cross-section at a distance  $x$  of the origin is defined by the matrix of generalized displacements  $\{U(x)\}$ :

Figure 1. Graphical representation of the fundamental hypothesis of the theory of beams



$$\{\mathbf{U}(x)\} = \begin{bmatrix} u(x) \\ w(x) \\ \beta(x) \end{bmatrix} \quad (2.1.1)$$

where  $u(x)$  is the displacement in the direction of the axis  $X$  of the particle in the centroid of the cross-section;  $w(x)$  is the displacement of the same point in the direction of the axis  $Z$  and  $\beta(x)$  is the rotation of the cross-section.

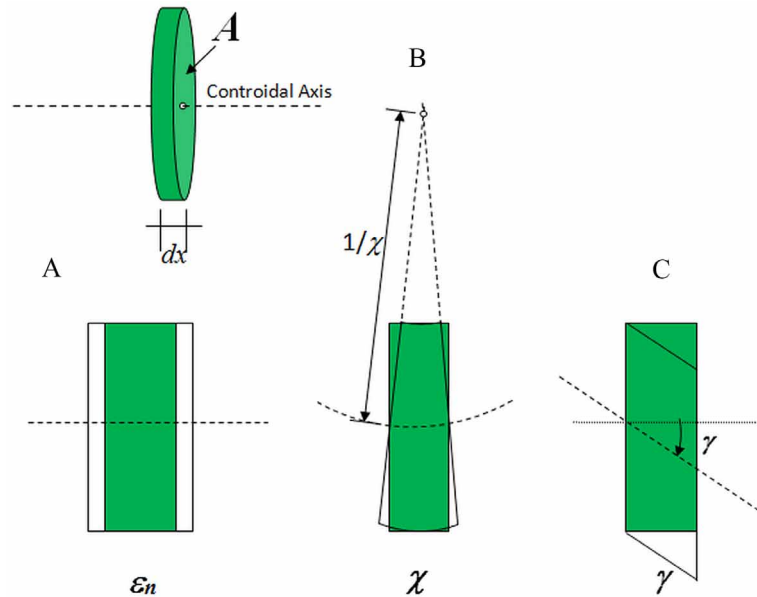
### 2.1.2 Generalized Deformations of Planar Beams

Consider now a beam differential element as the one shown in Figure 1; the modification of its shape is characterized by the following matrix of generalized deformations  $\{\boldsymbol{\varepsilon}(x)\}$  :

$$\{\boldsymbol{\varepsilon}(x)\} = \begin{bmatrix} \varepsilon_n(x) \\ \chi(x) \\ \gamma(x) \end{bmatrix} \quad (2.1.2)$$

where  $\varepsilon_n$  is the normal strain of the fiber in the centroidal axis;  $\chi$  is the curvature and  $\gamma$  the distortion or angular strain (see Figure 2). Notice that the curvature  $\chi$  measures the amount by which the centroidal

Figure 2. Generalized deformations in a beam a) Normal strain b) Curvature c) Angular



axis deviates from being straight; the normal strain  $\epsilon_n$  is related to the elongation of that axis; and the distortion  $\gamma$  measures the modifications in the angle between the centroidal axis and the transversal fibers of the beam differential element.

### 2.1.3 Kinematic Equations

Generalized deformations and displacements are related by a set of expressions called kinematic equations.

Consider an infinitesimal increment of the displacement  $du$  as shown in Figure 3a; notice that as a result, there is an elongation of the centroidal axis; however, it continues being a straight line, i.e. there is no modification in the curvature; and the vertical and horizontal fibers of the cross-section remain perpendicular, i.e. there is no increment of the distortion:

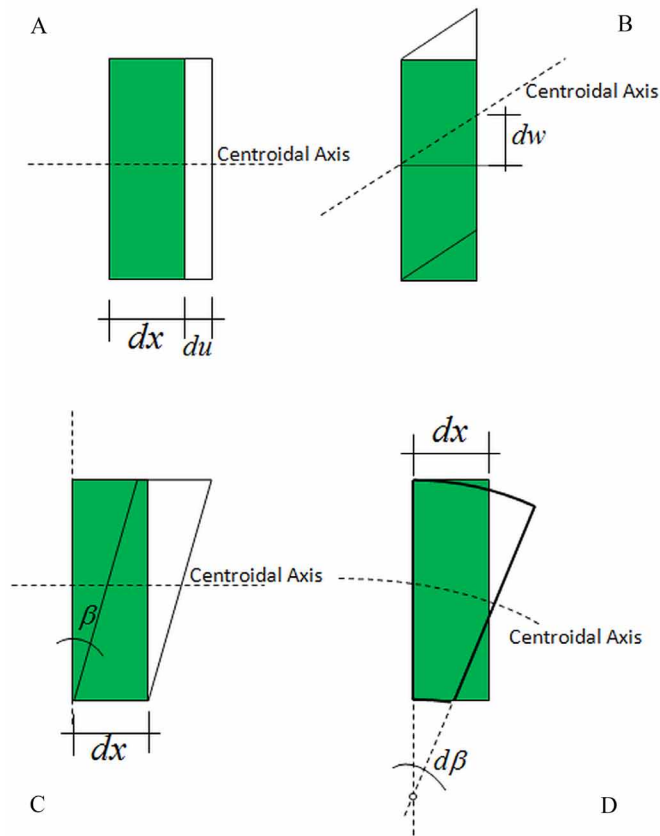
$$\epsilon_n = \frac{(dx + du) - dx}{dx} = \frac{du}{dx}; \chi = 0; \gamma = 0 \quad (2.1.3)$$

Consider now an increment of the displacement  $dw$  as indicated in Figure 3b; notice that the length of the centroidal axis does not change; the cross-sections of both sides of the beam differential element are still parallel (no curvature); but, the vertical and horizontal fibers of the differential element are no longer perpendicular:

$$\epsilon_n = 0; \chi = 0; \gamma = -\frac{dw}{dx} \quad (2.1.4)$$

## Fundamental Concepts of Strength of Materials

Figure 3. Graphical representation of the kinematic equations a) Deformations due to a displacement  $du$  b) Deformations due to a displacement  $dw$  c) Deformations due to a rotation  $\beta$  d) Deformations due to an increment of rotation  $d\beta$



Notice that a rotation  $\beta$ , even if it is the same in both sides of the differential element (Figure 3c), produces an angular deformation; however, the cross-sections are again parallel:

$$\varepsilon_n = 0; \chi = 0; \gamma = -\beta \quad (2.1.5)$$

Finally, if there is an increment of rotation  $d\beta$ , then the cross-sections of the beam differential element are no longer parallel, i.e.  $d\beta$  modifies the curvature:

$$\varepsilon_n = 0; \chi = -\frac{d\beta}{dx}; \gamma = 0 \quad (2.1.6)$$

In the general case, that is considering all displacements simultaneously, the kinematic equation is obtained by adding all the aforementioned contributions:

$$\varepsilon_n(x) = \frac{du}{dx}; \chi(x) = -\frac{d\beta}{dx}; \gamma(x) = -\frac{dw}{dx} - \beta \quad (2.1.7)$$

Additionally, it is also useful to measure the normal strain  $\varepsilon$  of any fiber of the beam differential element (and not only that of the centroidal axis) as a function of the generalized deformations. According to Figures 3a and 3d, the normal strain is:

$$\varepsilon = \frac{(dx + du) - dx}{dx} + \frac{(dx + d\beta.z) - dx}{dx} = \varepsilon_n - \chi.z \quad (2.1.8)$$

where  $z$  is the coordinate of the fiber under consideration.

Notice that the angular strain or distortion of any solid differential element of the beam element is constant and equal to  $\gamma$ .

## 2.2 STATICS OF TIMOSHENKO BEAMS

### 2.2.1 Principle of Virtual Work

Consider a particle subjected to a set of concurrent forces as the one shown in Figure 4. Newton's second law states that the particle is in dynamic equilibrium if:

$$\sum \{\vec{\mathbf{F}}\}_b = \{\vec{\mathbf{F}}\}_1 + \{\vec{\mathbf{F}}\}_2 + \dots = Mass\{\vec{\mathbf{A}}\} \quad (2.2.1)$$

where Mass is, evidently, the mass of the particle and  $\{\vec{\mathbf{A}}\}$  is its acceleration. A scalar multiplication of this vector equation for any arbitrary infinitesimal displacement  $\{\vec{\mathbf{U}}^*\}$ , called virtual displacement, results in:

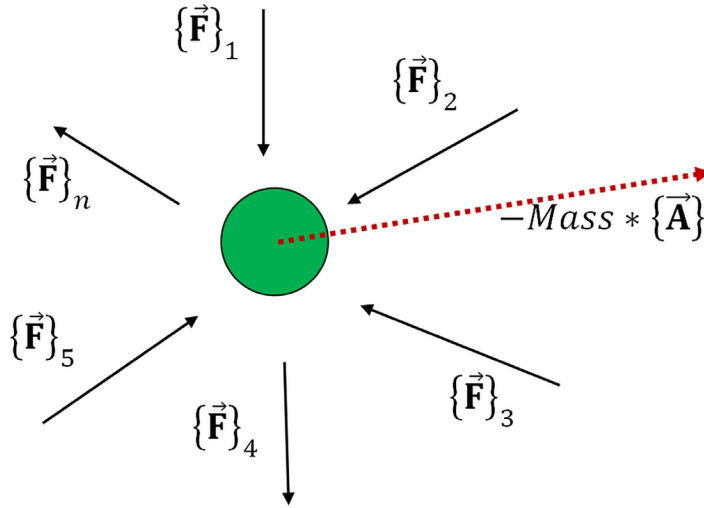
$$\sum \{\vec{\mathbf{U}}^*\}^t \{\vec{\mathbf{F}}\}_b = Mass\{\vec{\mathbf{U}}^*\}^t \{\vec{\mathbf{A}}\} \forall \{\vec{\mathbf{U}}^*\}; \quad (2.2.2)$$

The left hand term of (2.2.2) is denoted virtual work of the external forces or external work and the right hand term is the virtual work of the inertial forces or inertial work. Therefore, Newton's second law leads to the following theorem; the virtual external work is always equal to the virtual inertial work in a particle in dynamic equilibrium:

$$W_{ext}^* = W_{ine}^* \forall \{\vec{\mathbf{U}}^*\} \quad (2.2.3)$$

Alternatively, a state of dynamic equilibrium can be defined by postulating the expression (2.2.3) as a principle (i.e. without need of demonstration) and developing expression (2.2.1) as a theorem. This is the procedure that is followed in this book to define the dynamic equilibrium of a beam or a frame.

Figure 4. Particle subjected to a set of forces in dynamic equilibrium



A difference between a particle and a structure is that the elements in the latter can experience deformations; thus an additional term, that is denoted deformation work, appears in the work equation. The principle of virtual work for a deformable structure is stated as follows:

$$W_{def}^* + W_{ine}^* = W_{ext}^* \forall \{\mathbf{U}^*\} \quad (2.2.4)$$

where  $W_{def}^*$  is the virtual deformation work of the structure,  $W_{ine}^*$  is the inertial work  $W_{ext}^*$  is the external work and  $\{\mathbf{U}^*\}$  is the matrix of generalized virtual infinitesimal displacements. A structure is said to be in a state of quasi-static equilibrium if the inertial work is negligible with respect to any of the two other terms in the work equation.

### 2.2.2 Generalized Stresses of Planar Beams

The deformation work of a planar beam is defined as:

$$W_{def} = \int_0^L \{\varepsilon\}^t \{\sigma\} dx; \text{ where; } \{\sigma(x)\} = \begin{bmatrix} N(x) \\ M(x) \\ V(x) \end{bmatrix} \quad (2.2.5)$$

The matrix  $\{\sigma\}$  is called matrix of generalized stresses. The term  $N$  represents the axial force,  $M$  is the bending moment and  $V$  is the shear force (see Figure 5).

Generalized stresses can also be defined in terms of the stress components of the fibers or solid differential elements of a beam element (see Figure 6):

Figure 5. Generalized stresses in a beam a) Axial force b) Bending moment c) Shear force

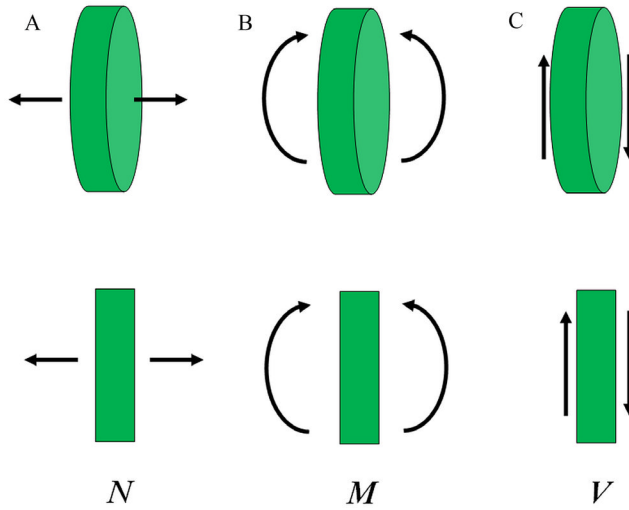
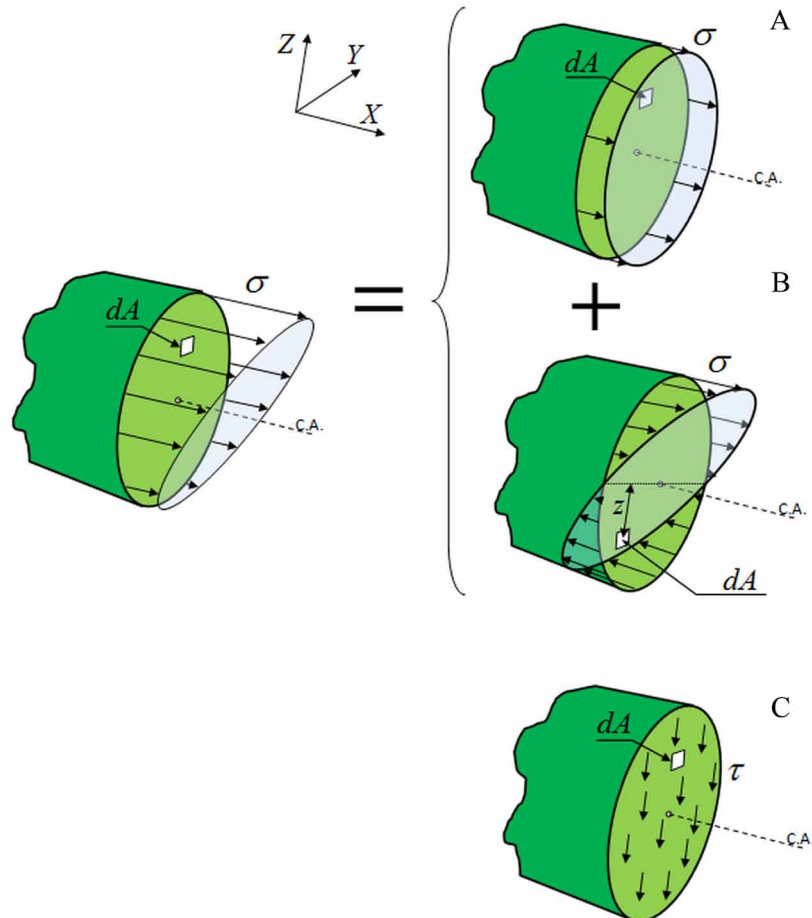


Figure 6. Generalized stresses as functions of stress components a) Axial force b) Bending moment c) Shear force



## Fundamental Concepts of Strength of Materials

$$N = \iint_A \sigma.dA; M = - \iint_A \sigma.z.dA; V = \iint_A \tau.dA \quad (2.2.6)$$

where  $A$  is the area of the cross-section of the beam. Therefore, the axial force  $N$  is the sum of the contributions of each longitudinal fiber ( $\sigma.dA$ ) in the direction of centroidal axis. The bending moment  $M$  is computed integrating the moment produced by these infinitesimal forces with respect to the centroidal axis ( $\sigma.z.dA$ ). Finally the shear force  $V$  is the sum of all the transversal forces ( $\tau.dA$ ) in the cross-section.

### 2.2.3 Quasi-Static Equilibrium Equations of a Planar Beam

Consider the external forces on a beam represented in Figure 7; they are the concentrated external forces  $\{P_0\}^t = (p_{u0}, p_{w0}, m_0)^t$  and  $\{P_L\}^t = (p_{uL}, p_{wL}, m_L)^t$  applied at both ends of the beam and a distributed force  $Q(x)$  in the direction of axis  $Z$ . The external work corresponding to these forces is:

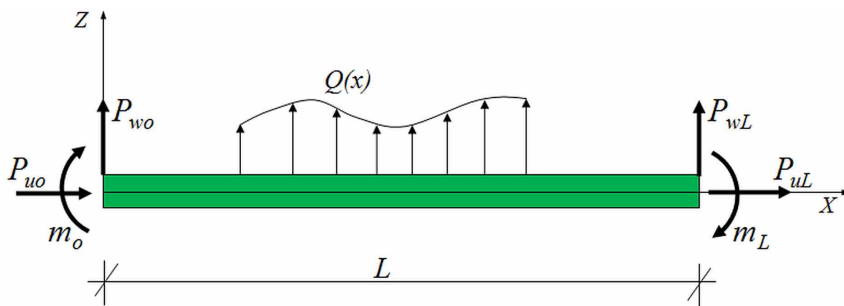
$$W_{ext} = \{U(0)\}^t \{P_0\} + \{U(L)\}^t \{P_L\} + \int_0^L w.Q.dx \quad (2.2.7)$$

If the inertial term is neglected, the principle of virtual work leads to:

$$W_{def}^* = \int_0^L \varepsilon_n^*.Ndx + \int_0^L \chi^*.Mdx + \int_0^L \gamma^*.Vdx = u^*(0).p_{u0} + w^*(0).p_{w0} + \beta^*(0).m_0 + u^*(L).p_{uL} + w^*(L).p_{wL} + \beta^*(L).m_L + \int_0^L w^*.Q.dx = W_{ext}^* \quad (2.2.8)$$

Substitution of the kinematic equations (2.1.7) into (2.2.8) and application of the integration by parts rule on the left part term gives:

Figure 7. External forces on a beam





$$\begin{aligned} & \int_0^L -u^* \cdot \left(\frac{dN}{dx}\right) dx + \int_0^L \beta^* \left(\frac{dM}{dx} - V\right) dx + \int_0^L w^* \cdot \left(\frac{dV}{dx} - Q\right) dx + \\ & -u^*(0) \cdot (p_{u0} + N(0)) - w^*(0) \cdot (p_{w0} + V(0)) - \beta^*(0) \cdot (m_0 - M(0)) + \\ & -u^*(L) \cdot (p_{uL} - N(L)) - w^*(L) \cdot (p_{wL} - V(L)) - \beta^*(L) \cdot (m_L + M(L)) = 0; \forall u^*, w^*, \beta^* \end{aligned} \quad (2.2.9)$$

This expression must be verified for any set of virtual displacements; the only way that this can be accomplished is if every parenthesis in (2.2.9) is nil; in mathematical textbooks, this is called the fundamental lemma of calculus of variations. Therefore, the following quasi-static equilibrium equations derive from the principle of virtual work:

$$\frac{dN}{dx} = 0; \frac{dM}{dx} - V = 0; \frac{dV}{dx} - Q = 0 \quad (2.2.10)$$

With the boundary conditions:

$$N(0) = -p_{u0}; V(0) = -p_{w0}; M(0) = m_0; N(L) = p_{uL}; V(L) = p_{wL}; M(L) = -m_L \quad (2.2.11)$$

Notice that Equations (2.2.10) are the conventional relationship between load, shear force and bending moment defined in the textbooks of statics. In the general case, for any kind of solid or structure, the equilibrium equations represent a relationship between external forces and internal stresses.

### 2.3 CONSTITUTIVE EQUATIONS OF TIMOSHENKO BEAMS

It is assumed in this section that the beam is elastic and that the normal stress obeys the Hooke's law  $\sigma = E \cdot \varepsilon$ ; therefore, the combination of (2.2.6) and (2.1.8) leads to:

$$N = \iint_A \sigma \cdot dA = \iint_A E \cdot \varepsilon \cdot dA = \iint_A E \cdot (\varepsilon_n - \chi \cdot z) \cdot dA = \varepsilon_n \iint_A E \cdot dA - \chi \cdot \iint_A E \cdot z \cdot dA \quad (2.3.1)$$

The axis  $X$  was chosen so that it intersects the beam's cross-section at its centroid, therefore the second integral at the right hand term of Equation (2.3.1) is equal to zero if the beam is homogeneous. The constitutive equation for the axial force is:

$$N = EA \cdot \varepsilon_n = EA \frac{du}{dx} \quad (2.3.2)$$

The constitutive equation of the bending moment is obtained in the same way:

$$M = -\iint_A \sigma \cdot z \cdot dA = -\iint_A E \cdot \varepsilon \cdot z \cdot dA = -\iint_A E \cdot (\varepsilon_n - \chi \cdot z) \cdot z \cdot dA = E \cdot \chi \iint_A z^2 \cdot dA \quad (2.3.3)$$

## Fundamental Concepts of Strength of Materials

Thus

$$M = EI.\chi = -EI \frac{d\beta}{dx} \quad (2.3.4)$$

where  $I$  is the moment of inertia of the cross-section:  $I = \iint_A z^2 dA$ .

Finally, the constitutive equation of the shear force is obtained by assuming that shear stress and strain are related by the elastic relationship  $\tau = G.\gamma$ , where  $G$  is the transverse elastic modulus, thus:

$$V = \iint_A \tau.dA = \iint_A G.\gamma.dA = \gamma \iint_A G.dA \quad (2.3.5)$$

Notice that shear stresses in the cross-section are constant. Again, if the beam is homogeneous the constitutive equation for the shear force is:

$$V = GA.\gamma = -GA \left( \frac{dw}{dx} + \beta \right) \quad (2.3.6)$$

The analysis of a beam using the modified Timoshenko model is described in section 2.7.1.

## 2.4 EULER-BERNOULLI BEAM THEORY

### 2.4.1 Planar Beams

The Euler-Bernoulli beam theory is based on the hypothesis that cross-sections move as rigid bodies and remain perpendicular to the centroidal axis (see Figure 8).

Rotation  $\beta$  is no longer an independent variable but depends on the deflection  $w$  exclusively:

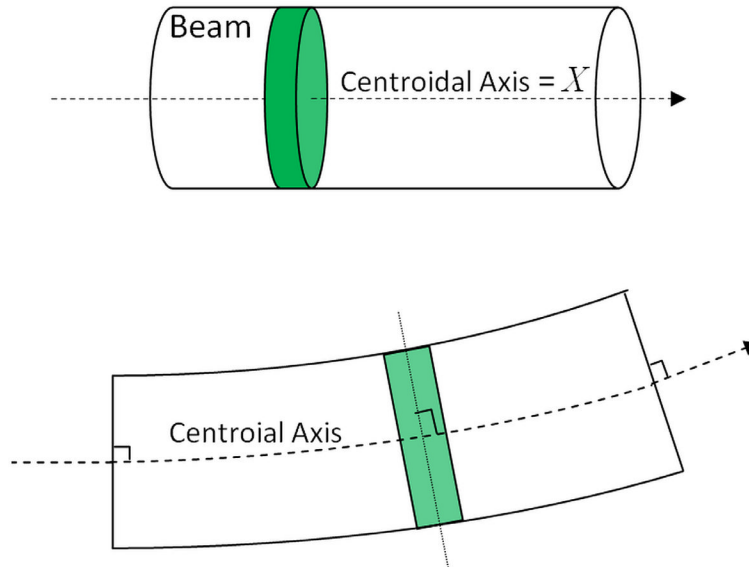
$$\beta = -\frac{dw}{dx} \quad (2.4.1)$$

According to the kinematic Equations (2.1.6) the angular strain  $\gamma$  is always equal to zero. It is then said that the Euler-Bernoulli beam theory neglects shear deformations. This hypothesis is accurate for slender beams with high length/height ratio (see the examples in section 2.7); this relationship is also called “aspect ratio”. The kinematic equations are in this case:

$$\varepsilon_n(x) = \frac{du}{dx}; \chi(x) = \frac{d^2w}{dx^2}; \gamma(x) = 0 \quad (2.4.2)$$

The shear force can be eliminated from the equilibrium Equations (2.2.10) that can now be rewritten as:

Figure 8. Graphical representation of the Euler-Bernoulli's hypothesis



$$\frac{dN}{dx} = 0; \frac{d^2M}{dx^2} = Q \quad (2.4.3)$$

The constitutive equations become:

$$N = EA.\varepsilon_n = EA \frac{du}{dx}; M = EI.\chi = EI \frac{d^2w}{dx^2} \quad (2.4.4)$$

The analysis of a beam using Euler-Bernoulli model is described in section 2.7.2.

## 2.4.2 Tridimensional Beams

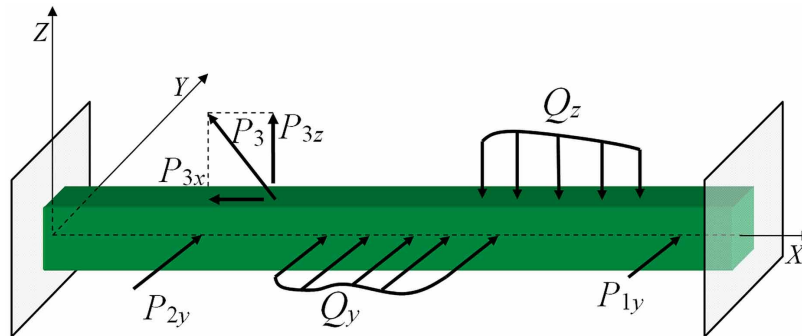
Consider now a beam whose external forces and displacements are not restricted to the  $XZ$  plane. The coordinate axes of the beam are chosen so that  $X$  still matches the centroidal axis.  $Y$  and  $Z$  coincide with the principal axes of the cross-section; in most practical cases, they are the symmetry axes of the section (see Figure 9).

The problem can now be decomposed into several simpler cases. The first one corresponds to the beam subjected to forces and displacements along the axial axe; this case is characterized by the equations:

$$\frac{dN}{dx} = 0; N = EA \frac{du}{dx} \quad (2.4.5)$$

The second problem is that of bending around the axis  $Y$ ; this case was already treated in the precedent section:

Figure 9. Tridimensional beam



$$\frac{d^2 M_y}{dx^2} = Q_z; M_y = EI_y \frac{d^2 w}{dx^2} \quad (2.4.6)$$

where  $M_y$  and  $I_y$  are the bending moment and the moment of inertia of the cross-section around the axis Y:  $I_y = \iint_A z^2 dA$ .

The third problem corresponds to bending around the axis Z:

$$\frac{d^2 M_z}{dx^2} + Q_y = 0; M_z = -EI_z \frac{d^2 v}{dx^2} \quad (2.4.7)$$

where  $M_z$  and  $I_z$  are the bending moment and the moment of inertia of the cross-section around the axis Z:  $I_z = \iint_A y^2 dA$ .

The fourth and last problem corresponds to a beam subjected to torsion that is discussed in the next section.

## 2.5 TORSION

Consider a frame element of circular cross-section subjected to torsion. Let  $\phi_x$  be the relative rotation between the ends of the element, or angle of twist. The term  $m_x$  represents the torque. The fundamental hypothesis of the theory of beams, i.e. the cross-section of the beam moves as a rigid body, is still accepted (see Figure 10).

The element can be considered conformed of concentric rings of infinitesimal width. The angular strain of the solid differential elements that constitute a ring is given by (see Figure 11).

$$\gamma = \frac{\phi_x r}{L} \quad (2.5.1)$$

The torque  $m_x$  can be related to the resulting shear stresses and subsequently with the angle of twist as:

Figure 10. Angle of twist and torque in a frame element of circular cross-section

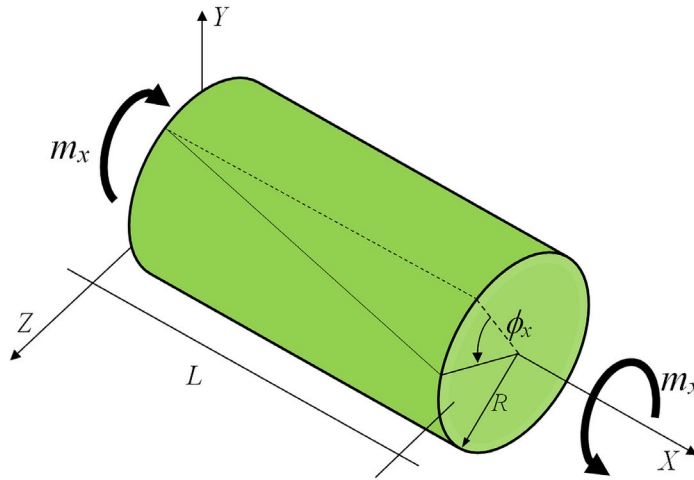
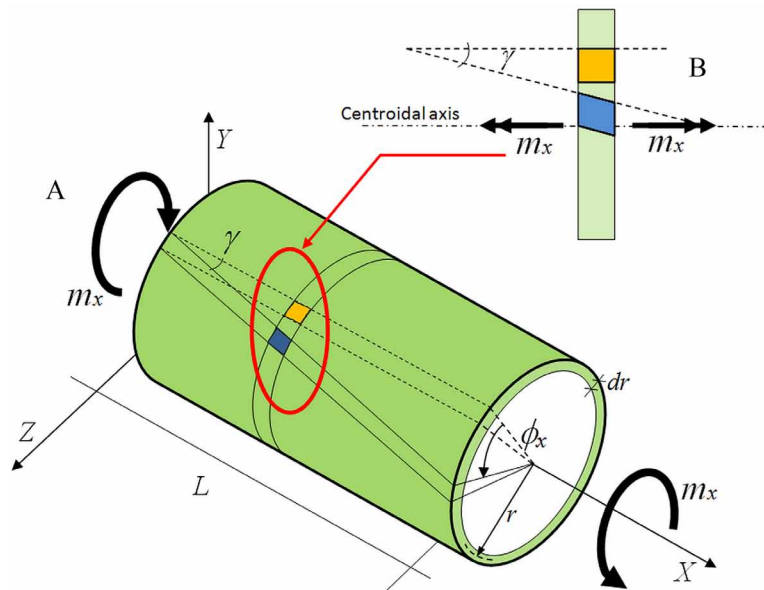


Figure 11. a) Concentric ring of infinitesimal width b) Distortion of a solid element of the ring



$$m_x = \iint_A \tau \cdot r \cdot dA = \iint_A G \cdot \gamma \cdot r \cdot dA = \frac{G \phi_x}{L} \iint_A r^2 dA, \text{ i.e. } m_x = \frac{GJ}{L} \phi_x \quad (2.5.2)$$

where  $J$  is the polar moment of inertia:  $J = \iint_A r^2 dA$ .

If the cross-section is not circular, the beam hypothesis is no longer valid; however Equation (2.5.2b) can still be used. In that case, the term  $GJ$  is called torsional rigidity but  $J$  is not anymore the polar moment of inertia. For instance, in the case of a rectangular cross-section,  $J$  is equal to:

$$J = db^3 \left\{ \frac{1}{3} - 0.21 \frac{b}{d} \left( 1 - \frac{b^4}{12d^4} \right) \right\} d \geq b \quad (2.5.3)$$

where  $d$  and  $b$  are the dimensions of the cross-section.

## 2.6. SUMMARY AND EQUATIONS QUICK REFERENCE

The theory of beams is the main subject of the strength of materials. In the beams theory, variables can be classified into two sets: kinematic and static. The former, is composed by variables that define the movement (longitudinal displacements, deflections and rotations) and deformations (normal strain, curvature, distortion, angle of twist); the set of static variables includes the external forces (concentrate forces, distributed forces) and generalized stresses (axial force, bending moment, shear force, torque). Displacements and deformations are related by kinematic equations, generalized stresses and external forces by equilibrium equations; the constitutive equations link the generalized deformations with stresses.

Two beam theories were discussed in this chapter. The first one, denoted Euler-Bernoulli theory of beams, was introduced in the planar case and the tridimensional one. The second one, the Timoshenko theory was discussed only the planar case. The difference between both theories is that the former neglects shear deformations. Mathematically, only the constitutive equations are different in both theories (See Table 1).

Table 1.

<b>KINEMATICS OF TIMOSHENKO BEAMS</b>
<i>Generalized Displacements of Planar Beams</i>
<p>Matrix of generalized displacements</p> $\{\mathbf{U}(x)\} = \begin{bmatrix} u(x) \\ w(x) \\ \beta(x) \end{bmatrix} \quad (2.1.1)$ <p><math>u(x)</math> = displacement in the direction X of the particle in the centroid of the cross-section  <math>w(x)</math> = displacement of the same point in the direction of the axis Z  <math>\beta(x)</math> = rotation of the cross-section</p>
<i>Generalized Deformations of Planar Beams</i>
<p>Matrix of generalized deformations</p> $\{\boldsymbol{\varepsilon}(x)\} = \begin{bmatrix} \varepsilon_n(x) \\ \chi(x) \\ \gamma(x) \end{bmatrix} \quad (2.1.2)$ <p><math>\varepsilon_n(x)</math> = normal strain of the neutral fiber in the cross-section.  <math>\chi(x)</math> = curvature  <math>\gamma(x)</math> = distortion or angular strain</p>

*continued on following page*

Table 1. Continued

<i>Kinematic Equations</i>
<p>Kinematic equations</p> $\varepsilon_n(x) = \frac{du}{dx}; \chi(x) = -\frac{d\beta}{dx}; \gamma(x) = -\frac{dw}{dx} - \beta \quad (2.1.7)$ $\varepsilon = \varepsilon_n - \chi \cdot z \quad (2.1.8)$ <p><math>\varepsilon</math> = normal strain  <math>z</math> = coordinate of the fiber under consideration</p>
<b>STATICS OF TIMOSHENKO BEAMS</b>
<i>Generalized Stresses of Planar Beams</i>
<p>Matrix of generalized stresses</p> $\{\sigma(x)\} = \begin{bmatrix} N(x) \\ M(x) \\ V(x) \end{bmatrix} \quad (2.2.5)$ <p>N = axial force  M = bending moment  V = shear force</p>
<i>Quasi Static Equilibrium Equations of a Planar Beam</i>
<p>Quasi static equilibrium equations</p> $\frac{dN}{dx} = 0; \frac{dM}{dx} - V = 0; \frac{dV}{dx} - Q = 0 \quad (2.2.10)$
<b>CONSTITUTIVE EQUATIONS OF TIMOSHENKO BEAMS</b>
<p>Constitutive Equation for the Axial Force</p> $N = EA \cdot \varepsilon_n = EA \frac{du}{dx} \quad (2.3.2)$
<p>Constitutive equation of the bending moment</p> $M = EI \cdot \chi = -EI \frac{d\beta}{dx} \quad (2.3.4)$ $I = \iint_A z^2 dA$ <p>I: cross-section's moment of inertia:</p>
<p>Constitutive equation for the shear force</p> $V = GA \cdot \gamma = -GA \left( \frac{dw}{dx} + \beta \right) \quad (2.3.6)$ <p>A: area of the cross-section of the beam  G: transverse elastic modulus</p>
<b>EULER-BERNOULLI BEAM THEORY</b>
<i>Planar Beams</i>
<p>Rotation <math>\beta</math></p> $\beta = -\frac{dw}{dx} \quad (2.4.1)$

continued on following page

## Fundamental Concepts of Strength of Materials

Table 1. Continued

Kinematic equations $\varepsilon_n(x) = \frac{du}{dx}; \chi(x) = \frac{d^2w}{dx^2}; \gamma(x) = 0 \quad (2.4.2)$
Equilibrium equations $\frac{dN}{dx} = 0; \frac{d^2M}{dx^2} = Q \quad (2.4.3)$
Constitutive equations $N = EA.\varepsilon_n = EA \frac{du}{dx}; M = EI.\chi = EI \frac{d^2w}{dx^2} \quad (2.4.4)$
<b>Tridimensional Beams</b>
Beam subjected to axial forces and displacements $\frac{dN}{dx} = 0; N = EA \frac{du}{dx} \quad (2.4.5)$
Beam subjected to bending around the axis Y $\frac{d^2M_y}{dx^2} = Q_y; M_y = EI_y \frac{d^2w}{dx^2} \quad (2.4.6)$ <p> <math>M_y</math>: bending moment around the axis Y  <math>I_y</math>: cross-section's moment of inertia around the axis Y:  <math display="block">I_y = \iint_A z^2 dA</math> </p>
Beam subjected to bending around the axis Z $\frac{d^2M_z}{dx^2} + Q_y = 0; M_z = -EI_z \frac{d^2v}{dx^2} \quad (2.4.7)$ <p> <math>M_z</math>: bending moment around the axis Z  <math>I_z</math>: cross-section's moment of inertia around the axis Z  <math display="block">I_z = \iint_A y^2 dA</math> </p>
<b>TORSION</b>
Angular strain $\gamma$ $\gamma = \frac{\phi_x r}{L} \quad (2.5.1)$
Torque $m_x$ $m_x = \frac{GJ}{L} \phi_x \quad (2.5.2)$
$J = \iint_A r^2 dA$ <p> <math>J</math>: moment of inertia:  <math>GJ</math>: torsional rigidity         </p>

continued on following page



Table 1. Continued

For rectangular cross-section	
$J = db^3 \left\{ \frac{1}{3} - 0.21 \frac{b}{d} \left( 1 - \frac{b^4}{12d^4} \right) \right\}$	$d \geq b$
$d$ and $b$ are the dimensions of the cross-section	

## 2.7 EXAMPLES

### 2.7.1 Determination of the Maximum Deflection in a Simply Supported Timoshenko Beam

Consider the beam shown in Figure 12a. The beam supports a distributed force  $Q = -f$  that produces the deformation that is indicated in Figure 12b.

Under the load condition, the maximum deflection occurs in the middle of the span as can be appreciated in the Figure 12b. The boundary conditions are:  $m_0 = m_L = 0$  and  $w_0 = w_L = 0$ .

The expressions for the shear force and bending moment are obtained by the integration of the equilibrium Equations (2.2.10). The resultant expressions are the following:

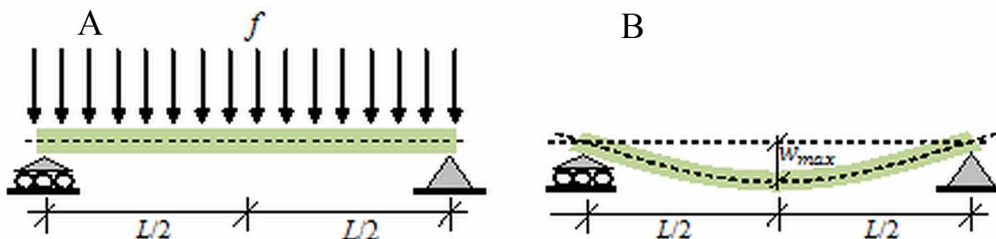
$$V(x) = -fx + C1 \tag{2.7.1}$$

$$M(x) = -\frac{f}{2}x^2 + C1x + C2 \tag{2.7.2}$$

$C1$  y  $C2$  are obtained using the boundary conditions  $m_0 = m_L = 0$ :

$$C1 = \frac{fL}{2}; C2 = 0 \tag{2.7.3}$$

Figure 12. Simply-supported beam subjected to vertical loading a) Initial configuration b) Deformed configuration



## Fundamental Concepts of Strength of Materials

Using the Timoshenko theory, the expression of the rotation  $\beta$  is obtained by the integration of the Equation (2.3.4):

$$\beta(x) = -\frac{1}{EI} \left( -\frac{f}{6} x^3 + \frac{fL}{4} x^2 + C3 \right) \quad (2.7.4)$$

Finally, the expression of the deflection along the beam's length is obtained by the substitution of the rotation  $\beta$  into the constitutive equation of the shear force Equation (2.3.6) and integrating,

$$w(x) = \frac{1}{GA} \left( \frac{f}{2} x^2 - \frac{fL}{2} x \right) + \frac{1}{EI} \left( -\frac{f}{24} x^4 + \frac{fL}{12} x^3 + C3x \right) + C4 \quad (2.7.5)$$

$C3$  y  $C4$  are obtained using the boundary conditions  $w_o = w_L = 0$ :

$$C3 = -\frac{fL^3}{24}; C4 = 0 \quad (2.7.6)$$

The deflection at the middle of the span is obtained when the Equation (2.7.5) is evaluated at  $x = L/2$ .

$$w(x = \frac{L}{2}) = -\frac{1}{GA} \frac{fL^2}{8} - \frac{1}{EI} \frac{5fL^4}{384} \quad (2.7.7)$$

### 2.7.2 Determination of the Maximum Deflection in a Simply Supported Euler-Bernoulli Beam

The same beam shown in Figure 12 is solved now using the Euler-Bernoulli theory. Taking into account that the equilibrium equations are the same in both theories, Timoshenko and Euler-Bernoulli, the expressions for the shear force and bending moment are also identical (Equations 2.7.1 and 2.7.2).

The expression for the deflection along the beam length is obtained by the introduction of the Equation (2.7.2) into the constitutive equation of the bending moment Equation (2.4.4b),

$$\frac{d^2w}{dx^2} = \frac{1}{EI} \left( -\frac{f}{2} x^2 + \frac{fL}{2} x \right) \quad (2.7.8)$$

Integrating twice it is obtained the expression for the deflection along the beam length,

$$w(x) = \frac{1}{EI} \left( -\frac{f}{24} x^4 + \frac{fL}{12} x^3 + C1x + C2 \right) \quad (2.7.9)$$

$C_1$  y  $C_2$  are obtained using the boundary conditions  $w_0 = w_L = 0$ :

$$C_1 = -\frac{fL^3}{24EI}; C_2 = 0 \quad (2.7.10)$$

when the Equation (2.7.9) is evaluated at  $x = L/2$  it is obtained the deflection at the middle of the span, resulting

$$w(x = L / 2) = -\frac{5fL^4}{384EI} \quad (2.7.11)$$

Notice that this expression is identical to the second term of the Equation (2.7.7). The only difference between both results (Equations 2.7.7 and 2.7.11) is the first term of (2.7.7).

### **2.7.3 Analysis of the Maximum Deflection as a Function of the Beam Aspect Ratio**

Consider now the particular case of a beam with rectangular cross-section. Let be  $b$  the base of the cross-section and  $h$  the height:

$$A = bh; I = \frac{bh^3}{12} \quad (2.7.12)$$

The aspect ratio of this element is defined as  $L/h$ . If the material is isotropic,

$$G = \frac{E}{2(1 + \nu)} \quad (2.7.13)$$

where  $\nu$  is the Poisson's ratio that is a material property. The maximum deflection according to the Timoshenko theory can be written as

$$w(x = L / 2) = -\frac{5fL^4}{384EI} \left( 1 + \frac{8}{5} \frac{(1 + \nu)}{(L / h)^2} \right) \quad (2.7.14)$$

Notice that this expression is the maximum deflection of the Euler-Bernoulli theory multiplied by an amplifying factor

$$\left( 1 + \frac{8}{5} \frac{(1 + \nu)}{(L / h)^2} \right).$$

## Fundamental Concepts of Strength of Materials

Figure 13 shows a graph of the amplifying factor in function of the aspect ratio ( $L/h$ ) for a Poisson's constant of 0.20.

For reinforced concrete elements, a beam with aspect ratio larger than 6.5 is called slender; the magnifying factor in this case varies between 1 and 1.05. If the beam has an aspect ratio between 2.5 and 6.5 is called intermediate and the magnifying factor varies between 1.05 and 1.31. Finally, for aspect ratios less than 2.5 the element is called squat and the magnifying factor increases exponentially; for instance, if the aspect ratio is equal to 1, then the magnifying factor is 2.92.

Notice that in the case of slender beams, the Euler-Bernoulli theory gives almost the same result than the Timoshenko theory; for squat elements, the Euler-Bernoulli theory should not be used since it underestimates significantly the deflection value. For intermediate beams the error is not that large but the Euler-Bernoulli theory is still inappropriate for the analysis.

Figure 13. Graph of Amplifying factor vs. Aspect ratio

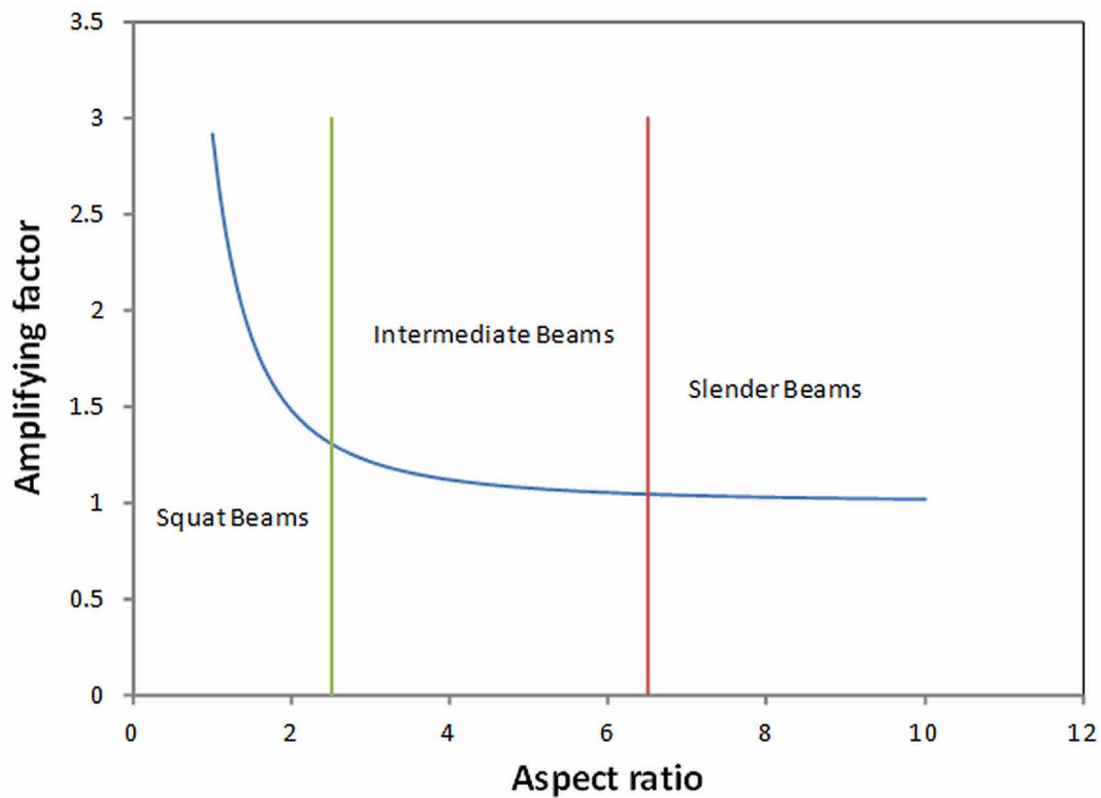
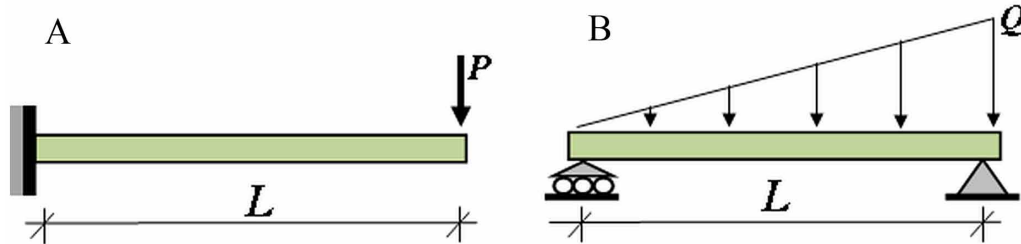


Figure 14. a) Cantilever beam subjected to a concentrated force b) Simply supported beam subjected a linearly distributed force



## 2.8. PROBLEMS

### 2.8.1 Cantilever Beam Subjected to a Concentrated Force

Consider the beam shown in Figure 14a. With the help of an algebraic manipulation program do the following: a) Determine the maximum deflection using the Timoshenko theory and Euler-Bernoulli theory, b) Compute the amplifying factor c) Plot the amplifying factor for aspect ratios between 1 to 10.

### 2.8.2 Simply Supported Beam Subjected to a Linearly Distributed Force

Solve the problem 2.8.1 considering the beam shown in Figure 14b.

## REFERENCES

- Batoz, J. L., & Dhatt, G. (1992). *Modélisation des structures par éléments finis: Poutres et plaques* (Vol. 2). Paris, France: Hermès.
- Jenkins, W. M. (1982). *Structural mechanics and analysis*. Berkshire, UK: Van Nostrand Reinhold Co. LTD.
- Leckie, F. A., & Bello, D.J. (2009). *Strength and stiffness of engineering systems*. New York, NY: Springer.
- Timoshenko, S. (1955). *Strength of materials, part I, elementary theory and problems*. New York, NY: D. Van Nostrand Company.
- Timoshenko, S. (1956). *Strength of materials, part II, advanced theory and problems*. New York, NY: D. Van Nostrand Company.

# Chapter 3

## Elastic Frames

### ABSTRACT

*This chapter describes the mathematical models for the analysis of elastic frames. Again, these theories are not presented as in the conventional textbooks of structural analysis but using the scheme of continuum mechanics and the theory of elasticity that was described in Chapter 1 (Section 1.1.1). The reason is that the conventional presentation is not suitable for generalization of the case of inelastic structures, specifically for fracture and damage mechanics of frames. Several classes of elastic frames are described in this chapter: planar (Sections 3.1-3.4), tridimensional (Section 3.5), linear, nonlinear, based on the Euler-Bernoulli beam theory (Section 3.3), based on the formulation of Timoshenko (Section 3.4), and under quasi-static or dynamic forces.*

### 3.1 KINEMATICS OF PLANAR FRAMES

#### 3.1.1 Tridimensional and Planar Frames

A frame is defined as a set of  $m$  beam-column elements connected by  $n$  nodes. For instance, a chair like the one shown in Figure 1a can be represented by the tridimensional frame with 26 elements and 20 nodes as indicated in Figure 1b. In the general case, the nodes of the frame can have displacement components in any direction.

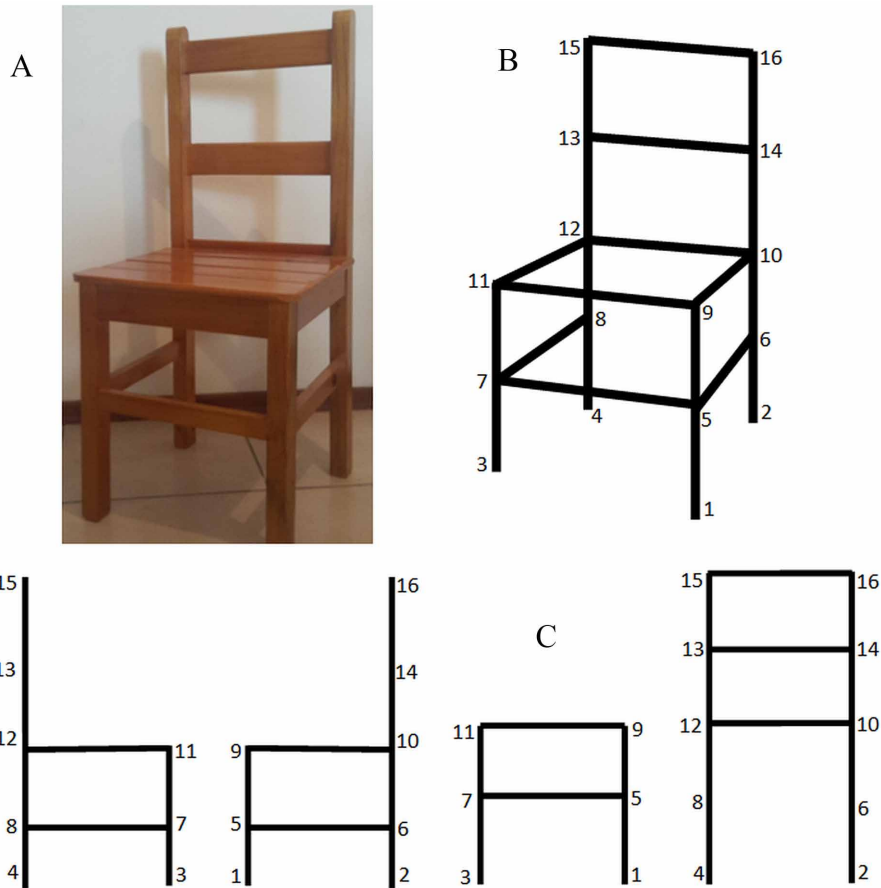
However, another possibility is the decomposition of structures like this into several two-dimensional frames as shown in Figure 1c; those two-dimensional structures are also called planar frames. It is assumed that this kind of structures can move only in their own plane. Thus, some aspects of the behavior are neglected, for instance torsion effects; but the analysis is considerably simpler. Both kinds of formulations are considered in this book, first the planar frame case, then the general one.

#### 3.1.2 Generalized Displacements of a Planar Frame

Consider a planar frame as the one shown in Figure 2. A set of coordinate axis  $XZ$  is introduced. Its initial configuration, i.e. the coordinates of the nodes and the table that indicates how they are con-

DOI: 10.4018/978-1-4666-6379-4.ch003

Figure 1. a) A chair as a structure b) Tridimensional frame representation c) Planar frames representation

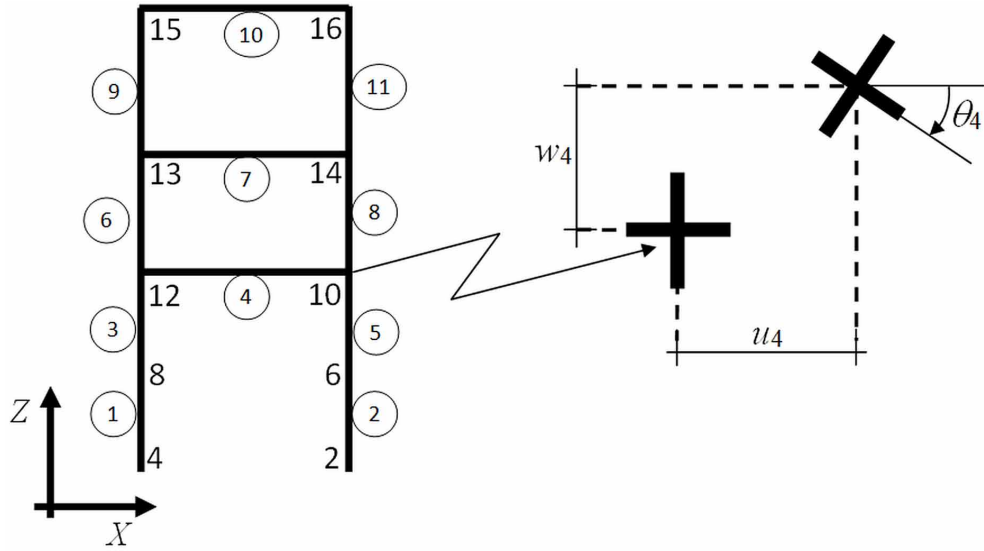


ected by beam column elements, is known. Each node and each element of the frame is labeled using natural numbers as shown in Figure 2. Consider now a node  $i$  of the frame. The movement of this node is characterized by the displacements  $u_i$  in the direction  $X$ , the displacement  $w_i$  in the direction  $Z$  and the rotation  $\theta_i$  as shown in Figure 2. Clockwise rotations of a node are positive, positive displacements follow the conventional rule. The generalized displacement matrix of the frame  $\{\mathbf{U}\}$  includes the displacement of all the nodes of the frame:

$$\{\mathbf{U}\} = \begin{bmatrix} u_1 \\ w_1 \\ \theta_1 \\ u_2 \\ \vdots \\ \vdots \\ w_n \\ \theta_n \end{bmatrix} \quad (3.1.1)$$

**Elastic Frames**

Figure 2. Planar frame and generalized displacements of node



The elements of the frame are also labeled using natural numbers as shown in Figure 2. The generalized displacement matrix of a frame element  $b$  between nodes  $i$  and  $j$  is defined as follows:

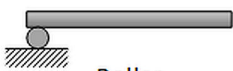






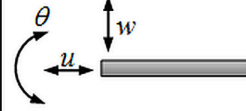
$$\{\mathbf{q}\}_b = \begin{bmatrix} u_i \\ w_i \\ \theta_i \\ u_j \\ w_j \\ \theta_j \end{bmatrix} \quad (3.1.2)$$

One of the goals of a structural analysis is the determination of the generalized displacements as a function of time and the external loading; its computation allows the graphical representation of the frame movement.

Some of the components of this matrix are not computed but must be defined by the analyst in order to formulate a problem with a unique solution. The components of the matrix  $\{\mathbf{U}\}$  with known values are called restricted displacements; the remaining ones are denoted free displacements. The nodes that have one or more restricted displacements are called supports of the frame. The restricted displacements must be chosen so that arbitrary rigid body movements of the frame are impossible. It is customary to represent graphically the supports and their displacements as shown in the Table 1. Often, the restricted displacements are equal to zero; it is then assumed that the foundations of the structure are rigid. However, this is not always the case; non-nil values are sometimes chosen in order to represent settlement of supports or seismic effects on the structure.



Table 1. Graphic representation of frame supports

Type of support	Restricted displacement	Type of support	Restricted displacement
 Roller		 Pinned	
 Fixed guided support		 Fixed support	

### 3.1.3 Generalized Deformation Matrix

The generalized displacement matrix does not characterize shape modifications of the frame. A second set of variables, denoted generalized deformation matrices, is then needed. Consider a frame element  $b$  between nodes  $i$  and  $j$  as shown in Figure 3a. The generalized deformation matrix of the frame element  $b$  is defined as:

$$\{\Phi\}_b = \begin{bmatrix} \phi_i^b \\ \phi_j^b \\ \delta_b \end{bmatrix} \quad (3.1.3)$$

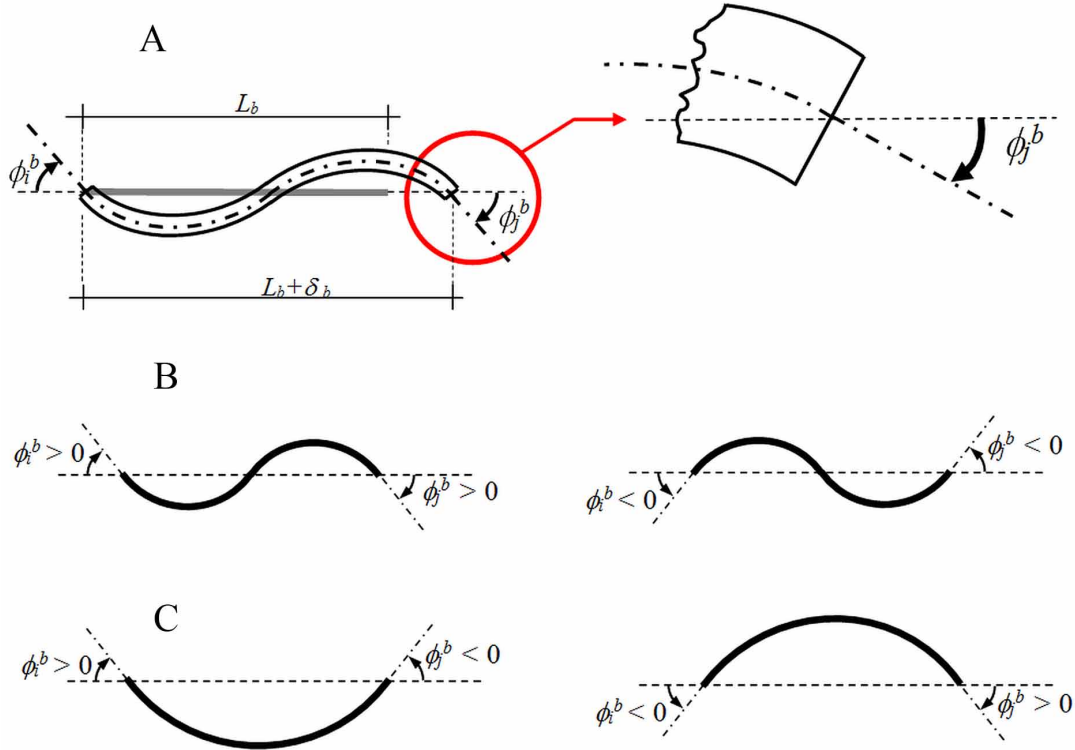
Notice that the deformation  $\phi_i^b$  is the angle between the cord  $i$ - $j$  and the normal to the cross-section at the end  $i$ ; i.e.  $\phi_i^b$  is the relative rotation of this cross-section with respect to the cord. Positive relative rotations go clockwise. The deformation  $\phi_j^b$  corresponds to a relative rotation at the end  $j$  with the same sign convention. The deformations  $\phi_i^b$  and  $\phi_j^b$  are closely related with the concept of story drift ratio. This concept is introduced in structural design textbooks and is discussed in section 3.1.5. Finally, the deformation  $\delta_b$  is the elongation of the cord.

The matrix  $\{\Phi\}_b$  is nil for a rigid body movement of the frame element and vice versa: zero deformations indicate that the element displaces as a rigid body. If the terms  $\phi_i^b$  and  $\phi_j^b$  have the same sign, then the frame element shows a “snake-like” deformed shape (see Figures 3.3b and 3.3c); if those deformations have different sign, the element presents a “hammock-like” final form (see Figure 3d).

The theory of structural design considers that large drift ratios and structural damage are related effects; therefore, a second goal of a structural analysis is the computation of the  $m$  deformation matrices, one for each element of the frame. The kinematics of the structure is completely determined when the free displacements and the deformation matrices have been computed.

## Elastic Frames

Figure 3. a) Generalized deformations of a frame element b) Element shape for positive relative rotations c) Element shape for negative relative rotations d) Element shape for relative rotations of different signs



### 3.1.4 Kinematic Equations

A relationship between deformations and displacements can be established by simple geometrical considerations. This expression is called kinematic equation. Consider a frame element  $b$  between nodes  $i$  and  $j$ . In its initial configuration, the element forms an angle  $\alpha_b^0$  with respect the axis  $X$  and the length of the cord is  $L_b^0$ . Cord angle and length vary with the displacements when the frame moves:  $\alpha_b = \alpha_b(\mathbf{q})$ ,  $L_b = L_b(\mathbf{q})$ .

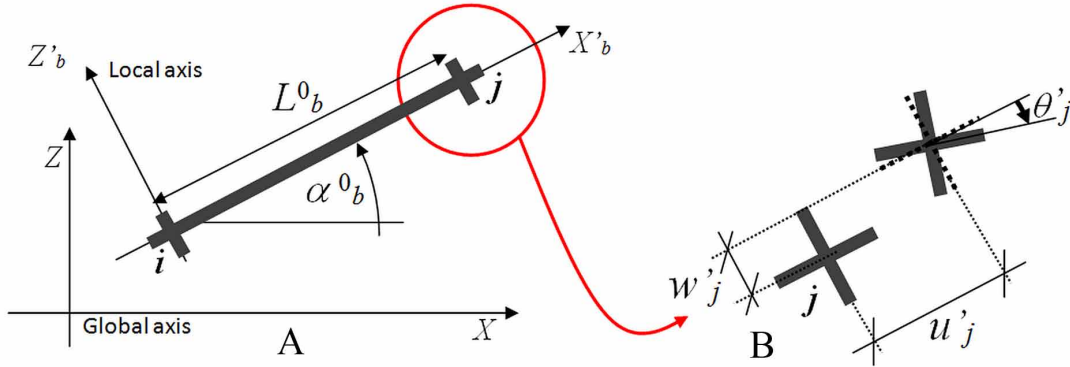
A set of local coordinate axes  $X'_b Z'_b$  is also introduced; its origin is fixed at the end  $i$  of the element and the axis  $X'_b$  is "glued" to the cord  $i$ - $j$  (see Figure 4).

The nodal displacements can also be expressed in local coordinate axes:  $\{\mathbf{q}'\}_b^t = (u'_i, w'_i, \theta'_i, u'_j, w'_j, \theta'_j)$  (see Figure 4a). Both sets of displacements,  $\{\mathbf{q}'\}_b$  and  $\{\mathbf{q}\}_b$  are related by the following expressions:

$$u'_i = u_i \cos \alpha_b + w_i \sin \alpha_b; \omega'_i = -u_i \sin \alpha_b + w_i \cos \alpha_b; \theta'_i = \theta_i;$$

$$u'_j = u_j \cos \alpha_b + w_j \sin \alpha_b; \omega'_j = -u_j \sin \alpha_b + w_j \cos \alpha_b; \theta'_j = \theta_j \quad (3.1.4)$$

Figure 4. a) Local coordinate axes b) Displacements in the local coordinate axes



Equation (3.1.4) is based on the well-known relationship between the components of a vector in two different coordinate systems. In matrix notation, Equation (3.1.4) can be written as:

$$\{\mathbf{q}'\}_b = [T]_b \{\mathbf{q}\}_b; [T]_b = \begin{bmatrix} \cos \alpha_b & \sin \alpha_b & 0 & 0 & 0 & 0 \\ -\sin \alpha_b & \cos \alpha_b & 0 & 0 & 0 & 0 \\ 0 & 0 & 1 & 0 & 0 & 0 \\ 0 & 0 & 0 & \cos \alpha_b & \sin \alpha_b & 0 \\ 0 & 0 & 0 & -\sin \alpha_b & \cos \alpha_b & 0 \\ 0 & 0 & 0 & 0 & 0 & 1 \end{bmatrix} \quad (3.1.5)$$

$[T]$  is called geometrical transformation matrix.

The relationships between displacements and deformations are easily obtained in the local-coordinate axes. Consider an infinitesimal increment of displacement of the node  $i$  in the direction of the axis  $X'$ ,  $du'_i$ , as indicated in Figure 5a. Notice that there are no increments of relative rotations, only modification of the cord length. Therefore, the following infinitesimal deformations are obtained from this displacement:

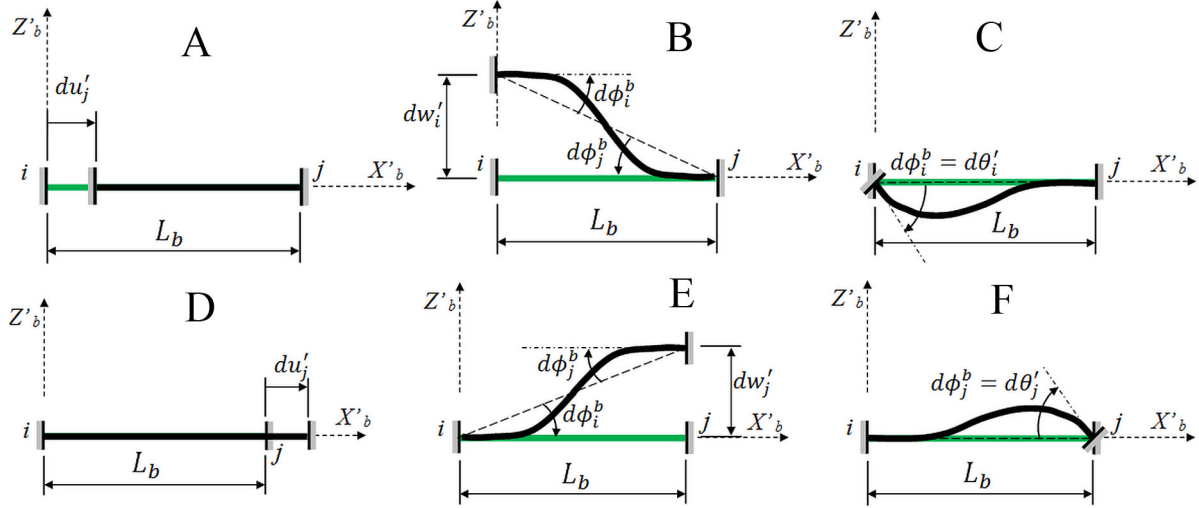
$$d\phi_i^b = 0; d\phi_j^b = 0; d\delta_b = -du'_i \quad (3.1.6)$$

An infinitesimal displacement  $dw'_i$  (Figure 5b) produces relative rotations of the cross-sections at  $i$  and  $j$  with respect to the cord but no modification of its length; thus, the corresponding deformations are:

$$d\phi_i^b = d\phi_j^b = -\frac{dw'_i}{L_b}; d\delta_b = 0 \quad (3.1.7)$$

## Elastic Frames

Figure 5. Increment of deformations due to infinitesimal displacements at the node  $i$  and  $j$  a) Displacement of node  $i$  in the  $X'_b$  axis b) Displacement of node  $i$  in the  $Z'_b$  axis c) Rotation of node  $i$  d) Displacement of node  $j$  in the  $X'_b$  direction e) Displacement of node  $j$  in the  $Z'_b$  direction f) Rotation of node  $j$ .



An infinitesimal rotation  $d\theta'_i$  (Figure 5c) produces only an increment of the relative rotation at the end  $i$  of the element:

$$d\phi_i^b = d\theta'_i; d\phi_j^b = 0; d\delta_b = 0 \quad (3.1.8)$$

Considering infinitesimal displacements  $du'_i$ ,  $dw'_i$  and  $d\theta'_i$  too (Figures 5d, 5e, 5f) and adding all the deformation terms, it is obtained the following kinematic relationships:

$$d\phi_i^b = -\frac{dw'_i}{L_b} + d\theta'_i + \frac{dw'_j}{L_b}$$

$$d\phi_j^b = -\frac{dw'_i}{L_b} + \frac{dw'_j}{L_b} + d\theta'_j \quad (3.1.9)$$

$$d\delta_b = -du'_i + du'_j$$

Substitution of (3.1.4) into (3.1.9) gives the kinematic equations in the global coordinate axes; these equations can be expressed in matrix form:

$$\{d\Phi\} = [\mathbf{B}(\mathbf{q})]\{d\mathbf{q}\}; [\mathbf{B}(\mathbf{q})] = \begin{bmatrix} \frac{\sin \alpha_b}{L_b} & -\frac{\cos \alpha_b}{L_b} & 1 & -\frac{\sin \alpha_b}{L_b} & \frac{\cos \alpha_b}{L_b} & 0 \\ \frac{\sin \alpha_b}{L_b} & -\frac{\cos \alpha_b}{L_b} & 0 & -\frac{\sin \alpha_b}{L_b} & \frac{\cos \alpha_b}{L_b} & 1 \\ -\cos \alpha_b & -\sin \alpha_b & 0 & \cos \alpha_b & \sin \alpha_b & 0 \end{bmatrix} \quad (3.1.10)$$

The matrix  $[\mathbf{B}]_b$  is called kinematic transformation matrix of the element  $b$ . Equation (3.1.10) is nonlinear in the general case; however in many engineering problems, the structure is so rigid that the modifications of length and orientation of the elements during the frame movement are small and can be neglected when computing the transformation matrix. In these cases, the kinematic relationship can be approximated by the following linear expression:

$$\alpha_b \cong \alpha_b^0; L_b \cong L_b^0; \{\Phi\}_b \cong [\mathbf{B}^0]_b \{\mathbf{q}\}_b \quad (3.1.11)$$

where  $[\mathbf{B}^0]_b$  is the kinematic transformation matrix in the initial configuration of the frame.

The kinematic equation can also be written in terms of the displacement matrix of the frame instead of the element displacements:

$$\{d\Phi\}_b \cong [\mathbf{B}_E(\mathbf{U})]_b \{d\mathbf{U}\}; \text{ or } \{\Phi\}_b \cong [\mathbf{B}_E^0]_b \{\mathbf{U}\} \quad (3.1.12)$$

Where  $[\mathbf{B}_E(\mathbf{q})]_b$  is denoted enlarged transformation matrix and it is built by adding columns of zeros in the positions that do not correspond to the displacements of the element, i.e.:

$$[\mathbf{B}_E(\mathbf{q})]_b = \begin{bmatrix} 0 & 0 & \dots & \frac{\sin \alpha_b}{L_b} & -\frac{\cos \alpha_b}{L_b} & 1 & 0 & \dots & -\frac{\sin \alpha_b}{L_b} & \frac{\cos \alpha_b}{L_b} & 0 & \dots \\ 0 & 0 & \dots & \frac{\sin \alpha_b}{L_b} & -\frac{\cos \alpha_b}{L_b} & 0 & 0 & \dots & -\frac{\sin \alpha_b}{L_b} & \frac{\cos \alpha_b}{L_b} & 1 & \dots \\ 0 & 0 & \dots & -\cos \alpha_b & -\sin \alpha_b & 0 & 0 & \dots & \cos \alpha_b & \sin \alpha_b & 0 & \dots \\ u_1 & w_1 & \dots & u_i & w_i & \theta_i & u_{i+1} & \dots & u_j & w_j & \theta_j & \dots \end{bmatrix} \quad (3.1.13)$$

Equation (3.1.12) is used for a formal presentation of the equilibrium equations (section 3.2) and the direct stiffness method (section 4.1). An example of application of the kinematic equations is presented in the section 3.7.1.

### 3.1.5 Simplified Analysis of Deformations: Story Drift Ratio

Consider a frame composed exclusively of horizontal beams and vertical columns as the one shown in Figure 6a. Assume that beams are very rigid (they often are linked to plates) so that their deformation can be neglected; axial deformations of the columns are also neglected; then movement of the frame under lateral loadings (that represent, for instance, earthquake loads) is similar to the one shown in Fig 6b.

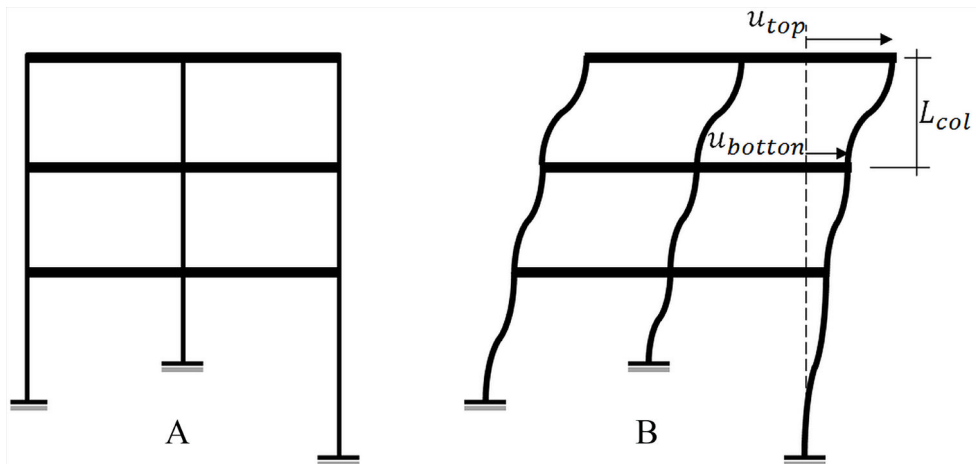
The generalized deformation matrices of all the columns in a single floor are equal and can be obtained by the kinematic equation (3.1.11b) with  $\alpha_b = \pi/2$ ,  $L_b = L_{col}$ ,  $w_i = w_j = \theta_i = \theta_j = 0$ ,  $u_i = u_{bottom}$ ,  $u_j = u_{top}$ . It is then obtained the following expression:

$$\{\Phi\}_{col} = \begin{bmatrix} \phi_{bottom}^{col} \\ \phi_{top}^{col} \\ \delta_b \end{bmatrix} = \begin{bmatrix} \frac{(u_{top} - u_{bottom})}{L_{col}} \\ (u_{top} - u_{bottom}) \\ \frac{L_{col}}{0} \end{bmatrix} \quad (3.1.14)$$

The deformation  $\Delta = \left| \phi_{bottom}^{col} \right| - \left| \phi_{top}^{col} \right|$  in Equation (3.1.14) is called story drift ratio. It is used in a failure criterion for frame columns: the column deformation or drift ratio must not exceed some normative limit, otherwise severe damage of the columns or the other components of the structure such as brick walls can be expected; typical values of maximum allowed drift ratio for reinforced concrete columns varies between 0.010 and 0.025 depending on the use and type of the structure.

If the frame is not regular or the beams are not stiff enough, the drift notion must be substituted by the more general concept of generalized deformation.

Figure 6. a) Regular frame b) Movement under lateral loading



## 3.2 DYNAMICS OF PLANAR FRAMES

### 3.2.1 Deformation Work of a Frame and Generalized Stress Matrix of a Frame Element

According to the principle of virtual work formulated in chapter 2 (section 2.2.1), a structure in dynamic equilibrium verifies the equation:

$$W_{def}^* + W_{ine}^* = W_{ext}^* \forall \{\mathbf{U}^*\} \quad (3.2.1)$$

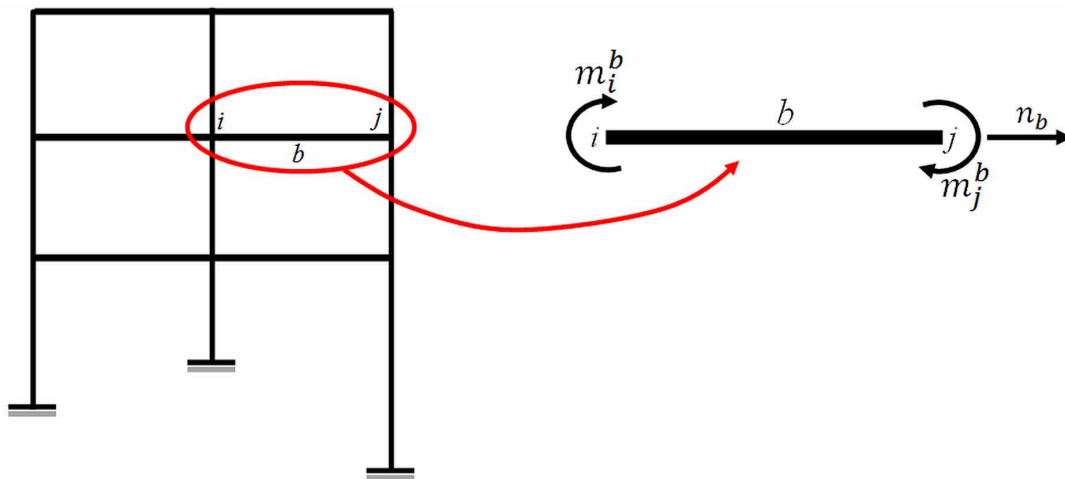
Taking into account the characteristics of the deformation matrix  $\{\Phi\}_b$ , the following generalized stress matrix  $\{\mathbf{M}\}_b$  is introduced in order to obtain the expression of the deformation work of a frame element:

$$\{\mathbf{M}\}_b = \begin{bmatrix} m_i^b \\ m_j^b \\ n_b \end{bmatrix} \quad (3.2.2)$$

where  $m_i^b$  is the bending moment at the  $i$  end of the element,  $m_j^b$  is the bending moment at the end  $j$  and  $n_b$  is average axial force on the element, as shown in Figure 7. In the continuum mechanics literature, it is said that stresses and deformations are conjugated variables; where the stresses are the driving force of the element deformations.

The deformation work of a frame is then given by:

Figure 7. Generalized stresses on a frame element



## Elastic Frames

$$W_{def}^* = \sum_{b=1}^m \{\Phi^*\}_b^t \{M\}_b \quad (3.2.3)$$

where  $\{\Phi^*\}_b$  is a virtual, i.e. arbitrary and infinitesimal, deformation matrix.

As in the case of generalized deformations, the stress components are also used in failure criteria. In the engineering practice, the failure criterion of a beam column element is usually presented in graphical form: the interaction diagram. An interaction diagram describes a surface in the moment axial force space (see for instance Figure 8) and depends on the element material (reinforced concrete, steel, etc.) and cross-section. If any of the two points that represent the stress state of the element at each end, i.e.  $(m_i^b, n_b)$  and  $(m_j^b, n_b)$ , are outside the surface, failure of the element can be expected.

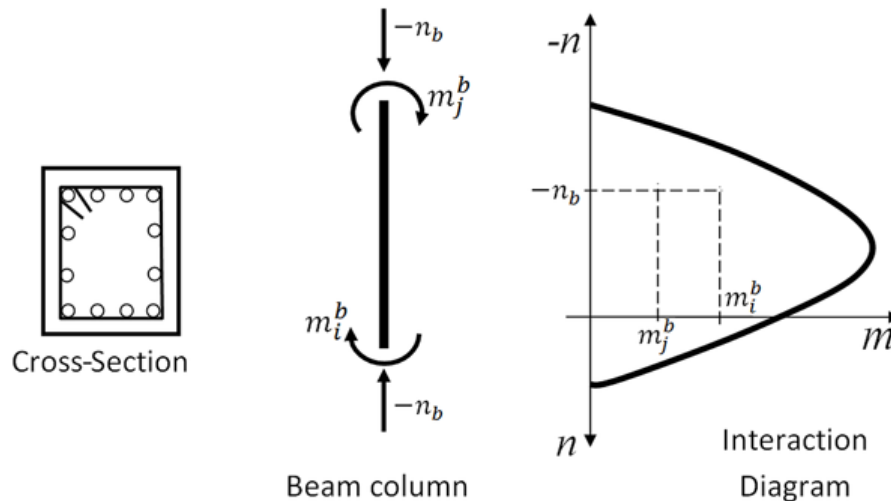
The determination of interaction diagrams is described in chapter 6.

### 3.2.2 Inertia Work of a Frame and Matrix of Masses

Let  $Mass_b$  be the mass of the element  $b$  of a frame. The matrix of masses of the element is defined as follows:

$$[Mass]_b = \begin{bmatrix} Mass_b/2 & 0 & 0 & 0 & 0 & 0 \\ 0 & Mass_b/2 & 0 & 0 & 0 & 0 \\ 0 & 0 & 0 & 0 & 0 & 0 \\ 0 & 0 & 0 & Mass_b/2 & 0 & 0 \\ 0 & 0 & 0 & 0 & Mass_b/2 & 0 \\ 0 & 0 & 0 & 0 & 0 & 0 \end{bmatrix} \quad (3.2.4)$$

Figure 8. Interaction diagram for a reinforced concrete column with a rectangular cross-section





The inertia force on an element  $b$  of the frame is given by  $[\mathbf{Mass}]_b \{\ddot{\mathbf{q}}\}$ , where  $\{\ddot{\mathbf{q}}\} = \left\{ \frac{d^2 \mathbf{q}}{dt^2} \right\}$  is the generalized acceleration matrix of the element. Alternatively, the inertial work of the element can be expressed as a function of the generalized acceleration matrix of the frame by using the enlarged mass matrix of the element:  $[\mathbf{Mass}_E]_b \{\ddot{\mathbf{U}}\}$ . This matrix is built adding rows and columns of zeros in the positions that do not correspond to the displacements of the element, in the same way as the enlarged transformation matrix described in section 3.1.4.

The inertial work is now defined in the following way:

$$W_{inc}^* = \{\mathbf{U}^*\}^t \sum_{b=1}^m [\mathbf{Mass}_E]_b \{\ddot{\mathbf{U}}\} = \{\mathbf{U}^*\}^t [\mathbf{Mass}] \{\ddot{\mathbf{U}}\} \quad (3.2.5)$$

where  $[\mathbf{Mass}] = \sum_{b=1}^m [\mathbf{Mass}_E]_b$  is the matrix of masses of the frame. The mass of each element of the frame must be included in the data of the problem.

### 3.2.3 External work of a Frame and Matrix of Generalized External Forces

In the engineering practice, two kinds of external forces are considered. The first one corresponds to forces or moments directly applied on the nodes, the second class represents forces distributed over the elements (see Figure 9).

On the other hand, the movement of the frame is characterized by the matrix  $\{\mathbf{U}\}$  that includes only nodal displacements; therefore, forces distributed on the elements must be taken into account through equivalent nodal forces. The external work is then defined as follows:

$$W_{ext}^* = \{\mathbf{U}^*\}^t \{\mathbf{P}\} \quad (3.2.6)$$

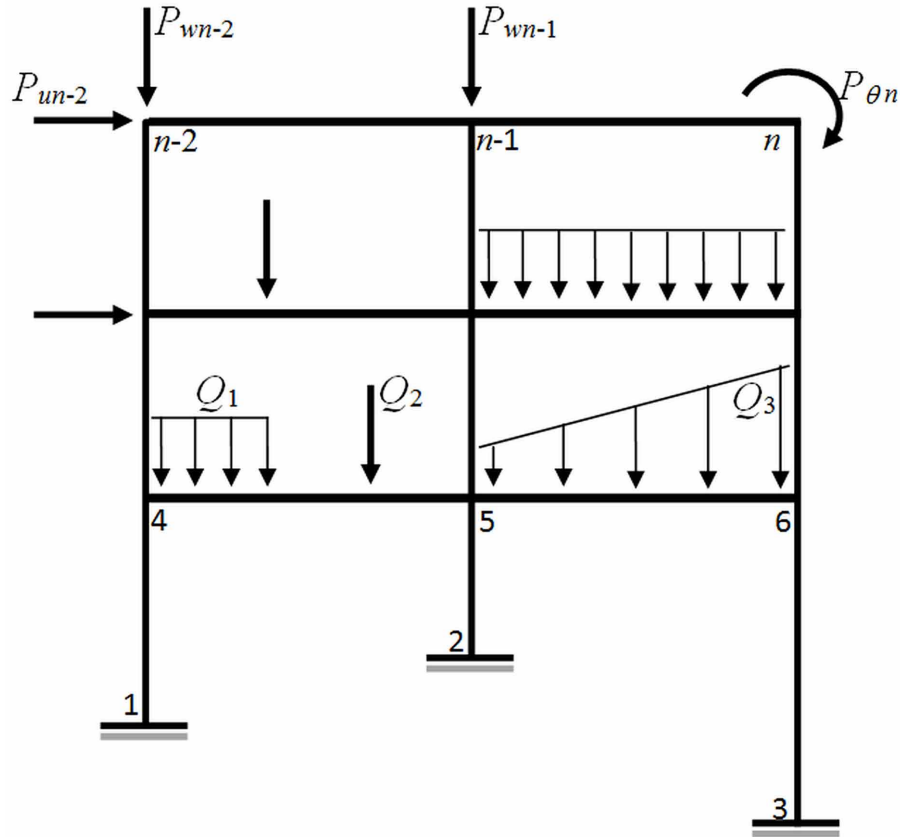
where  $\{\mathbf{P}\}$  is the matrix of generalized external forces:

$$\{\mathbf{P}\} = \begin{bmatrix} p_{u1} \\ p_{w1} \\ p_{\theta1} \\ p_{u2} \\ \vdots \\ \vdots \\ p_{un} \\ p_{\theta n} \end{bmatrix} \quad (3.2.7)$$

The term  $p_{ui}$  is the force that corresponds to the displacement  $u_i$ , i.e. a force on the node  $i$  and in the  $X$  direction,  $p_{\theta i}$  is the moment on the node  $i$ , and so on.

**Elastic Frames**

Figure 9. External forces on a frame



The external forces applied on the nodes can be classified into two categories. Those that correspond to the free displacements of the frame are data that must be supplied by the analyst. The forces that correspond to the restricted displacements are called reactions and are computed during the analysis (see the example 3.7.2).

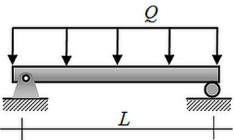

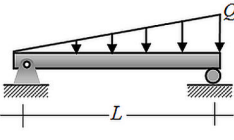
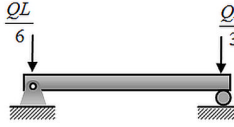
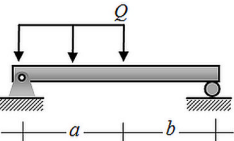
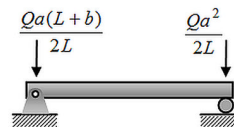
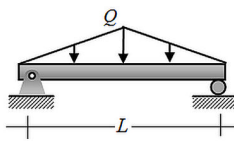
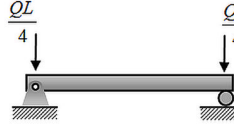
The forces applied on the nodes of the frame can be included directly in the matrix of external forces. The nodal static forces equivalent of the distributed forces are obtained using the expressions indicated in Table 2.

Therefore, the matrix of external forces can be split into two terms; one with the forces applied directly on the nodes and another with the equivalent forces:

$$\{\mathbf{P}\} = \{\mathbf{P}^n\} + \{\mathbf{P}^{eq}\} \quad (3.2.8)$$

The last variables that must be computed during an elastic analysis are the reaction forces and reaction moments.

Table 2. Nodal equivalent forces for some cases of forces distributed on the elements

Solicitation	Nodal equivalent forces	Solicitation	Nodal equivalent forces
			
			

### 3.2.4 Dynamic and Quasi-Static Equilibrium Equations

The principle of virtual work (3.2.1) states that:

$$\sum_{b=1}^m \{\Phi^*\}_b^t \{\mathbf{M}\}_b + \{\mathbf{U}^*\}^t [\mathbf{Mass}] \{\ddot{\mathbf{U}}\} = \{\mathbf{U}^*\}^t \{\mathbf{P}\} \forall \{\mathbf{U}^*\} \quad (3.2.9)$$

Taking into account the kinematic equation (3.1.12), the principle of virtual work leads to:

$$\{\mathbf{U}^*\}^t \left( \sum_{b=1}^m [\mathbf{B}_E]_b^t \{\mathbf{M}\}_b + [\mathbf{Mass}] \{\ddot{\mathbf{U}}\} - \{\mathbf{P}\} \right) = 0 \forall \{\mathbf{U}^*\} \quad (3.2.10)$$

Considering that this expression is verified for any virtual displacement matrix, then the term into the parenthesis must be again nil, and the following dynamic equilibrium equation is obtained:

$$\sum_{b=1}^m [\mathbf{B}_E]_b^t \{\mathbf{M}\}_b + [\mathbf{Mass}] \{\ddot{\mathbf{U}}\} = \{\mathbf{P}\} \quad (3.2.11)$$

This equation depends on the actual displacements of the structure as the kinematic transformation matrices  $[\mathbf{B}_E]_b^t$  so do. If displacements are small, the current transformation matrices can be substituted by the initial ones and the following linear expression is obtained:

$$\sum_{b=1}^m [\mathbf{B}_E^0]_b^t \{\mathbf{M}\}_b + [\mathbf{Mass}] \{\ddot{\mathbf{U}}\} = \{\mathbf{P}\} \quad (3.2.12)$$

**Elastic Frames**

If inertial forces are neglected (quasi-static analysis) the equilibrium equations for, respectively linear and nonlinear cases, become:

$$\sum_{b=1}^m [\mathbf{B}_E^0]_b^t \{\mathbf{M}\}_b = \{\mathbf{P}\} \tag{3.2.13}$$

$$\sum_{b=1}^m [\mathbf{B}_E]_b^t \{\mathbf{M}\}_b = \{\mathbf{P}\} \tag{3.2.14}$$

An application example of the equilibrium equations is presented in section 3.7.2.

**3.3 CONSTITUTIVE EQUATIONS FOR A SLENDER FRAME MEMBER**

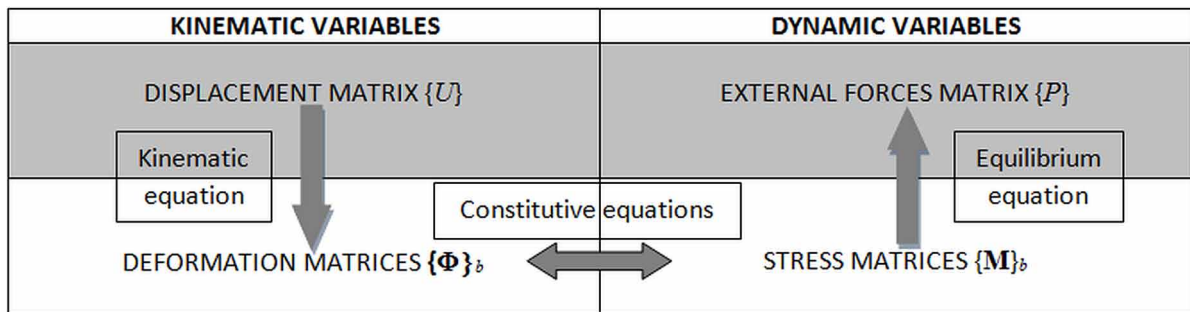
**3.3.1 Summary of Variables and Equations in an Elastic Analysis**

As aforementioned, the variables and equations of the elastic problem can be summarized as shown in Figure 10.

There are  $6n$  ( $n$  number of nodes in the frame) plus  $6m$  variables ( $m$  number of elements); i.e.  $3n$  displacements,  $3n$  external forces,  $3m$  deformations and  $3m$  stresses.  $3n$  of these variables are part of the data of the problem (the restricted displacements and known external forces); the remaining  $3n$  (free displacements and reaction forces) and  $6m$  variables are unknowns of the problem.

So far,  $3m$  kinematic equations (represented by the descending arrow in Figure 10) and  $3m$  equilibrium equations (represented by the ascending arrow in Figure 10) have been defined. The former group allows the computation of the deformations from displacements, the latter permits the calculation of the external forces from stresses and, if the problem is nonlinear, displacements. Clearly, there is still a deficit of  $3m$  equations; these relate deformations and stresses and are called constitutive equations. They are represented by the horizontal double arrow in Figure 10.

Figure 10. Summary of variables and equations for an elastic structure



### 3.3.2 Constitutive Equations Based on the Theory of Euler-Bernoulli Beams

The nonlinear terms in the kinematic and equilibrium equations can be, in some practical problems (tall buildings for instance), very important. This is not the case of the elastic constitutive equations which have nonlinear terms that are, in almost all cases of practical interest, very small. Therefore, only the linear cases are analyzed in this chapter. It is also assumed that the material of the cross-section and properties are constant along the element.

Consider a frame element  $b$  between nodes  $i$  and  $j$ . Again, the local set of local coordinate axes  $X'_b$ ,  $Z'_b$  is introduced (See Figure 11).

According to the Euler-Bernoulli beam theory (see section 2.4), the behavior of a frame element is defined by the following equations:

$$\text{a) } \frac{d^2 M_b(x_b)}{dx_b^2} = Q_b(x_b); \text{ b) } \frac{d^2 \omega_b(x_b)}{dx_b^2} = \frac{M_b(x_b)}{EI_b}; \text{ c) } n_b = EA_b \frac{du_b(x_b)}{dx_b} \quad (3.3.1)$$

Where  $M_b(x_b)$  is the bending moment distribution on the element,  $Q_b(x_b)$  represents the distributed external forces,  $\omega_b(x_b)$  is the deflection,  $EI_b$  is the elasticity modulus multiplied by the inertia moment of the cross-section,  $n_b$  is the axial force,  $A_b$  is the area of the cross-section and  $u_b(x_b)$  is the displacement in the direction of the cord. The cross-section and material properties ( $EI_b$  and  $A_b$ ) are considered data of the problem. The bending and axial effects are assumed uncoupled. The Euler-Bernoulli beam theory does not take into account shear deformations, which makes it only valid for slender frame members where those deformations are indeed small.

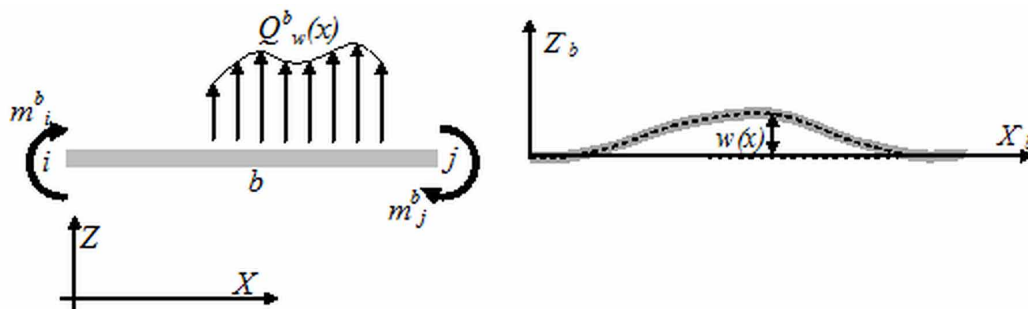
The general solution of (3.3.1a) is:

$$M_b(x_b) = Q2(x_b) + C_1 x_b + C_2; \text{ where } Q2(x_b) = \int_0^x \int_0^x Q(x_b) dx_b dx_b \quad (3.3.2)$$

If stresses  $\{\mathbf{M}\}_b$  are applied, the constants  $C_1$  and  $C_2$  can be computed by the boundary conditions:

$m_i^b = M_b(0)$  and  $m_j^b = -M_b(L_b)$ . The general solution to (3.3.1b) is:

Figure 11. Forces and deflections on an element  $b$  in the coordinate axes



## Elastic Frames

$$EI_b \omega(x_b) = Q4(x_b) + C_1 \frac{x_b^3}{6} + C_2 \frac{x_b^2}{2} + C_3 x_b + C_4; \text{ where } Q4(x_b) = \int_0^x \int_0^x \int_0^x \int_0^x Q(x_b) dx dx dx dx \quad (3.3.3)$$

The constants  $C_3$  and  $C_4$  can be computed by the boundary conditions  $\omega(0) = 0$  and  $\omega(L_b) = 0$ . The constitutive equation for the deformation  $\phi_i^b$  is then given by:

$$\phi_i^b = -\frac{d\omega_b(0)}{dx_b} = \frac{L_b}{3EI_b} m_i^b - \frac{L_b}{6EI_b} m_j^b + \phi_i^0; \text{ where} \quad (3.3.4)$$

$$\begin{aligned} \phi_i^0 &= \frac{1}{EI_b} \left( -\frac{L_b Q2(0)}{3} - \frac{L_b Q2(L_b)}{6} - Q3(0) - \frac{Q4(0)}{L_b} + \frac{Q4(L_b)}{L_b} \right); Q3(x_b) \\ &= \int_0^x \int_0^x \int_0^x Q(x_b) dx dx dx \end{aligned} \quad (3.3.5)$$

The constitutive equation for the deformation  $\phi_j^b$  is:

$$\phi_j^b = -\frac{d\omega_b(L_b)}{dx_b} = -\frac{L_b}{6EI_b} m_i^b + \frac{L_b}{3EI_b} m_j^b + \phi_j^0; \text{ where} \quad (3.3.6)$$

$$\phi_j^0 = \frac{1}{EI_b} \left( \frac{L_b Q2(0)}{6} + \frac{L_b Q2(L_b)}{3} - Q3(L_b) - \frac{Q4(0)}{L_b} + \frac{Q4(L_b)}{L_b} \right) \quad (3.3.7)$$

The resolution of the differential equation (3.3.1c) with the boundary conditions  $u_b(0) = 0$  and  $u_b(L_b) = \delta_b$  gives the constitutive equation for the axial force:

$$n_b = \frac{AE_b}{L_b} \delta_b \quad (3.3.8)$$

Writing the constitutive equations in matrix form gives:

$$\{\Phi\}_b = [F_f]_b \{M\}_b + \{\Phi^0\}_b; \text{ where } [F_f]_b = \begin{bmatrix} \frac{L_b}{3EI_b} & -\frac{L_b}{6EI_b} & 0 \\ -\frac{L_b}{6EI_b} & \frac{L_b}{3EI_b} & 0 \\ 0 & 0 & \frac{L_b}{AE_b} \end{bmatrix}; \{\Phi^0\}_b = \begin{bmatrix} \phi_i^0 \\ \phi_j^0 \\ 0 \end{bmatrix} \quad (3.3.9)$$

$[\mathbf{F}]_b$  is denoted flexibility matrix of the element  $b$  and  $\{\Phi^0\}_b$  is the matrix of initial deformations. Alternatively, the constitutive equation can be expressed in terms of stresses as a function of deformations:

$$\{\mathbf{M}\}_b = [\mathbf{E}]_b \{\Phi\}_b + \{\mathbf{M}^0\}_b; \text{ where} \quad (3.3.10)$$

$$[\mathbf{E}]_b = [\mathbf{F}]_b^{-1} = \begin{bmatrix} \frac{4EI_b}{L_b} & \frac{2EI_b}{L_b} & 0 \\ \frac{2EI_b}{L_b} & \frac{4EI_b}{L_b} & 0 \\ 0 & 0 & \frac{AE_b}{L_b} \end{bmatrix} \text{ and } \{\mathbf{M}^0\}_b = -[\mathbf{E}]_b \{\Phi^0\}_b \quad (3.3.11)$$

$[\mathbf{E}]_b$  is called elasticity matrix of the element  $b$  and  $\{\mathbf{M}^0\}_b$  is the matrix of initial stresses. Table 3 shows the expressions of the initial stresses and deformations computed with Equations (3.3.5-3.3.7 and 3.3.11, for the most common cases.

An example of application of these constitutive equations is presented in section 3.7.3.

## 3.4 CONSTITUTIVE EQUATIONS FOR FRAME MEMBERS OF ANY ASPECT RATIO

### 3.4.1 Dual Structures

In chapter 2, it was shown (see example 2.7.3) that Euler-Bernoulli beam theory is not valid for squat structural elements. In that case, shear deformations are significant and are not taken into account in this theory.

In the engineering practice, it is common the use of dual structures, as the one represented in Figure 12, that include slender frame elements and walls sometimes connected by very short beams.

The constitutive equations formulated in the previous section do not represent adequately the behavior of the walls and the short elements. A more general constitutive equation valid for all the elements, no matter its aspect ratio, is then needed. The new constitutive equations are based on the modified Timoshenko beam theory instead of Euler-Bernoulli beam theory. This is the subject of the next section.

### 3.4.2 Constitutive Equations Based on the Theory of Modified Timoshenko Beams

Consider again a frame element  $b$  between nodes  $i$  and  $j$ . It is introduced the same local set of coordinate axes  $X'_b-Z'_b$  (see Figure 11).

According to the modified Timoshenko beam theory, the behavior of a frame element is defined by the following equations:

### Elastic Frames

Table 3. Initial stresses and deformations for some cases of forces on the elements

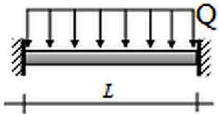
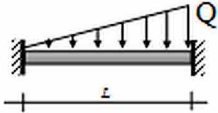
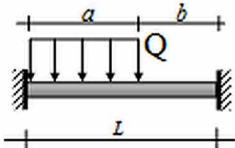
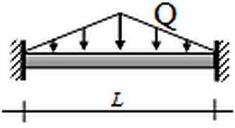
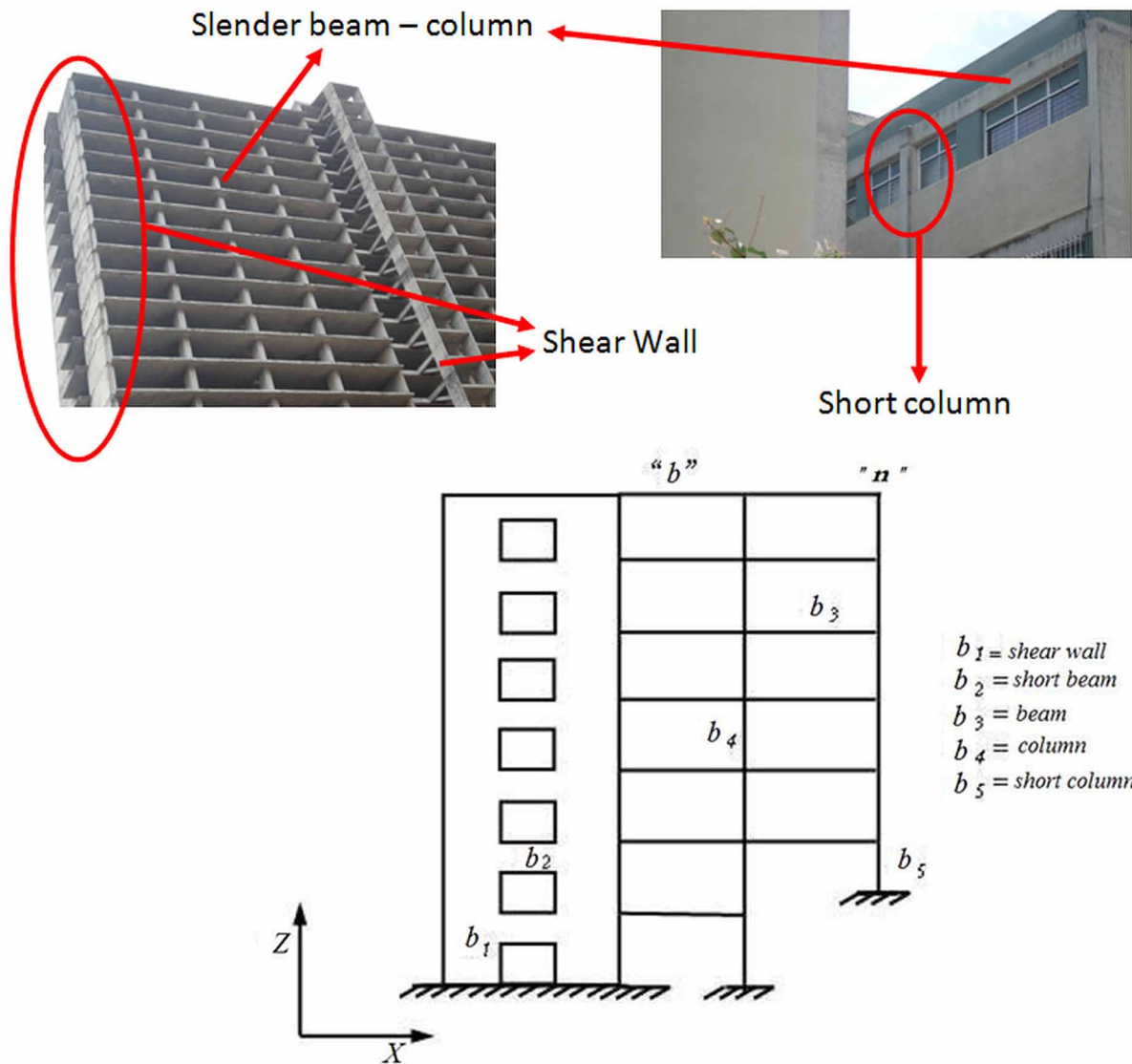
Loading condition	Initial deformations	Initial stresses
	$\{\Phi^0\}_b = \begin{bmatrix} \frac{QL^3}{24EI} \\ -\frac{QL^3}{24EI} \\ 0 \end{bmatrix}$	$\{M^0\}_b = \begin{bmatrix} -\frac{QL^2}{12} \\ \frac{QL^2}{12} \\ 0 \end{bmatrix}$
	$\{\Phi^0\}_b = \begin{bmatrix} \frac{7QL^3}{360EI} \\ -\frac{QL^3}{45EI} \\ 0 \end{bmatrix}$	$\{M^0\}_b = \begin{bmatrix} -\frac{QL^2}{30} \\ \frac{QL^2}{20} \\ 0 \end{bmatrix}$
	$\{\Phi^0\}_b = \begin{bmatrix} \frac{Qa^2(-4aL+4L^2+a^2)}{24LEI} \\ -\frac{2QL^2a^2-Qa^4}{24LEI} \\ 0 \end{bmatrix}$	$\{M^0\}_b = \begin{bmatrix} -\frac{Qa^2(-8aL+6L^2+3a^2)}{12L^2} \\ \frac{Qa^3(4L-3a)}{12L^2} \\ 0 \end{bmatrix}$
	$\{\Phi^0\}_b = \begin{bmatrix} \frac{5QL^3}{192EI} \\ -\frac{5QL^3}{192EI} \\ 0 \end{bmatrix}$	$\{M^0\}_b = \begin{bmatrix} -\frac{5QL^2}{96} \\ \frac{5QL^2}{96} \\ 0 \end{bmatrix}$



Figure 12. Dual structures



$$\frac{dV_b(x_b)}{dx_b} = Q_b(x_b); \frac{dM_b(x_b)}{dx_b} = V_b(x_b); \quad (3.4.1)$$

$$M_b(x_b) = EI_b \frac{d\beta_b(x_b)}{dx_b}; V_b(x_b) = GA_b \left( \beta_b(x_b) - \frac{d\omega_b(x_b)}{dx_b} \right) \quad (3.4.2)$$

### Elastic Frames

$$n_b = EA_b \frac{du_b(x_b)}{dx_b} \quad (3.4.3)$$

where  $V_b$  is the shear force on the element,  $\beta_b$  is the rotation of the cross-section and  $G$  is the transverse elastic modulus. The remaining variables have the meaning indicated in the previous section.

The solution of the differential equations 3.4.1 is:

$$V_b(x_b) = Q1(x_b) + C_1; \text{ where } Q1(x_b) = \int_0^x Q(x_b)dx; \quad (3.4.4)$$

$$M_b(x_b) = Q2(x_b) + C_1x_b + C_2 \quad (3.4.4)$$

The constants  $C_1$  and  $C_2$  can be computed by the same boundary conditions indicated in the previous section ( $m_i^b = M_b(0)$  and  $m_j^b = -M_b(L_b)$ ). The general solutions of the differential equations (3.4.2) are:

$$EI_b\beta_b(x_b) = Q3(x_b) + C_1 \frac{x_b^2}{2} + C_2x_b + C_3; \quad (3.4.5)$$

$$GA_b\omega_b(x_b) = -Q2(x_b) - C_1x_b + \frac{GA_b}{EI_b} \left( Q4(x_b) + C_1 \frac{x_b^3}{6} + C_2 \frac{x_b^2}{2} + C_3x_b \right) + C_4 \quad (3.4.6)$$

Constants  $C_3$  and  $C_4$  can be computed, again, by the boundary conditions indicated in the previous section ( $\omega(0) = 0$  and  $\omega(L_b) = 0$ ). The constitutive equation for deformations  $\phi_i^b$  and  $\phi_j^b$  are then given by:

$$\phi_i^b = -\beta_b(0) = \left( \frac{L_b}{3EI_b} m_i^b - \frac{L_b}{6EI_b} m_j^b \right) + \left( \frac{m_i^b}{L_bGA_b} + \frac{m_j^b}{L_bGA_b} \right) + \phi_i^0; \quad (3.4.7)$$

$$\phi_j^b = -\beta_b(L_b) = \left( -\frac{L_b}{6EI_b} m_i^b + \frac{L_b}{3EI_b} m_j^b \right) + \left( \frac{m_i^b}{L_bGA_b} + \frac{m_j^b}{L_bGA_b} \right) + \phi_j^0$$

where the initial deformations  $\phi_i^0$  and  $\phi_j^0$  have the same expressions of the previous section, i.e. Equations (3.3.5) and (3.3.7). The constitutive equation for the elongation is the same in both theories, that is, Equation (3.3.8). Writing the constitutive equations in matrix form gives:

$$\{\Phi\}_b = ([\mathbf{F}_f]_b + [\mathbf{F}_s]_b)\{\mathbf{M}\}_b + \{\Phi^0\}_b; \text{ where} \quad (3.4.8)$$

$$[\mathbf{F}_f]_b = \begin{bmatrix} \frac{L_b}{3EI_b} & -\frac{L_b}{6EI_b} & 0 \\ -\frac{L_b}{6EI_b} & \frac{L_b}{3EI_b} & 0 \\ 0 & 0 & \frac{L_b}{AE_b} \end{bmatrix}; [\mathbf{F}_s]_b = \begin{bmatrix} \frac{1}{L_b GA_b} & \frac{1}{L_b GA_b} & 0 \\ \frac{1}{L_b GA_b} & \frac{1}{L_b GA_b} & 0 \\ 0 & 0 & 0 \end{bmatrix} \quad (3.4.9)$$

Notice that the matrix  $[\mathbf{F}_f]_b$  has the same expression obtained in the previous section for the flexibility matrix, Equation (3.3.9). Thus, the only difference between the constitutive equation based on the Euler-Bernoulli theory and the one derived from the modified Timoshenko theory is the shear flexibility matrix  $[\mathbf{F}_s]_b$ . For slender frame elements, that is with large aspect ratios, the shear flexibility matrix  $[\mathbf{F}_s]_b$  becomes very small with respect to the flexure flexibility term  $[\mathbf{F}_f]_b$  and the additional shear deformations  $[\mathbf{F}_s]_b\{\mathbf{M}\}_b$  can indeed be neglected. For short or squat elements this is not the case and both flexibility matrices should be taken into account.

Again, the constitutive equation can also be expressed in terms of stresses as a function of deformations:

$$\{\mathbf{M}\}_b = [\mathbf{E}]_b\{\Phi\}_b + \{\mathbf{M}^0\}_b; \text{ where} \quad (3.4.10)$$

$$[\mathbf{E}]_b = \left( [\mathbf{F}_f]_b + [\mathbf{F}_s]_b \right)^{-1} = \begin{bmatrix} \frac{4(L_b^2 GA_b + 3EI_b)EI_b}{L_b(L_b^2 GA_b + 12EI_b)} & \frac{2(L_b^2 GA_b - 6EI_b)EI_b}{L_b(L_b^2 GA_b + 12EI_b)} & 0 \\ \frac{2(L_b^2 GA_b - 6EI_b)EI_b}{L_b(L_b^2 GA_b + 12EI_b)} & \frac{4(L_b^2 GA_b + 3EI_b)EI_b}{L_b(L_b^2 GA_b + 12EI_b)} & 0 \\ 0 & 0 & \frac{AE_b}{L_b} \end{bmatrix} \quad (3.4.11)$$

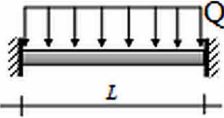
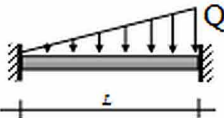
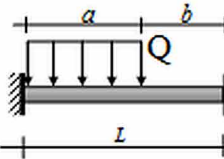
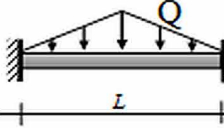
$$\{\mathbf{M}^0\}_b = -[\mathbf{E}]_b\{\Phi^0\}_b \quad (3.4.12)$$

Notice that even if the initial deformations are the same for both theories, the initial stresses may be different. Table 4 shows the expressions of the initial stresses for some frequent cases.

An example of application of these constitutive equations is presented in example 3.7.4.

**Elastic Frames**

Table 4. Initial stresses for some cases of forces on the elements

Loading condition	Initial stresses
	$\{M^0\}_b = \begin{bmatrix} -\frac{QL^2}{12} \\ \frac{QL^2}{12} \\ 0 \end{bmatrix}$
	$\{M^0\}_b = \begin{bmatrix} -\frac{QL^2(L^2GA + 15EI)}{30(L^2GA + 12EI)} \\ \frac{QL^2(L^2GA + 10EI)}{20(L^2GA + 12EI)} \\ 0 \end{bmatrix}$
	$\{M^0\}_b = \begin{bmatrix} -\frac{Qa^2(-8L^2GAa + 6L^3GA + 3LGAa^2 - 24EIa + 36LEI)}{12L(L^2GA + 12EI)} \\ \frac{Qa^2(4L^2GAa - 3LGAa^2 - 24EIa + 36LEI)}{12L(L^2GA + 12EI)} \\ 0 \end{bmatrix}$
	$\{M^0\}_b = \begin{bmatrix} -\frac{5QL^2}{96} \\ \frac{5QL^2}{96} \\ 0 \end{bmatrix}$

### 3.5 TRIDIMENSIONAL ELASTIC FRAMES

#### 3.5.1 Kinematic of Tridimensional Frames

As mentioned in section 3.1.1, structures can be analyzed as two-dimensional or tridimensional frames. The former option, although simpler, neglects some significant effects. In some important practical cases, such as irregular buildings or structures, the tridimensional effects should not be ignored. This is the subject of the present section.

Consider a tridimensional frame as the one shown in Figure 13. It is introduced a set of coordinate axes  $X Y Z$ . The movement of a node  $i$  of the frame is now characterized by six values. They are the displacements  $u_i, v_i, w_i$  in the directions of the three coordinate axes and the corresponding rotations  $\varphi_i, \theta_i, \zeta_i$ . The matrix of generalized displacements of an element  $b$  is now:

$$\{\mathbf{q}\}_b^t = (u_i, v_i, w_i, \varphi_i, \theta_i, \zeta_i, u_j, v_j, w_j, \varphi_j, \theta_j, \zeta_j) \quad (3.5.1)$$

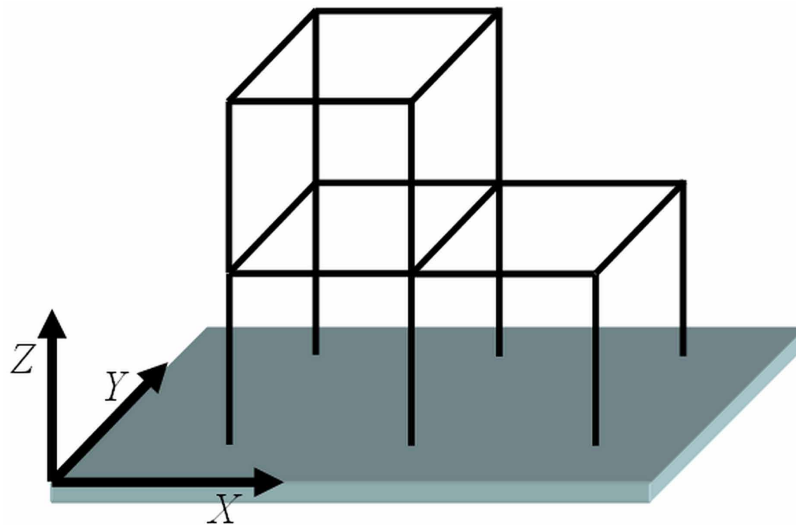
The matrix of generalized displacements of the frame is also obtained including the displacements and rotations of all nodes; thus, it has now  $6n$  components.

In order to define the matrix of generalized deformations of a tridimensional element, a set of local coordinate axes  $X'_b, Y'_b, Z'_b$  is also introduced; the origin of the local axes is fixed on the node  $i$  of the element and the axis  $X'_b$  remains adhered to the element's cord; the axes  $Y'_b, Z'_b$  coincide with the principal axes of the cross-section.

The matrix of generalized deformations of a tridimensional frame element is:

$$\{\Phi\}_b^t = (\phi_{iy}^b, \phi_{jy}^b, \delta_b, \phi_{iz}^b, \phi_{jz}^b, \phi_x^b) \quad (3.5.2)$$

Figure 13. Generalized displacements of a node in a tridimensional frame



## Elastic Frames

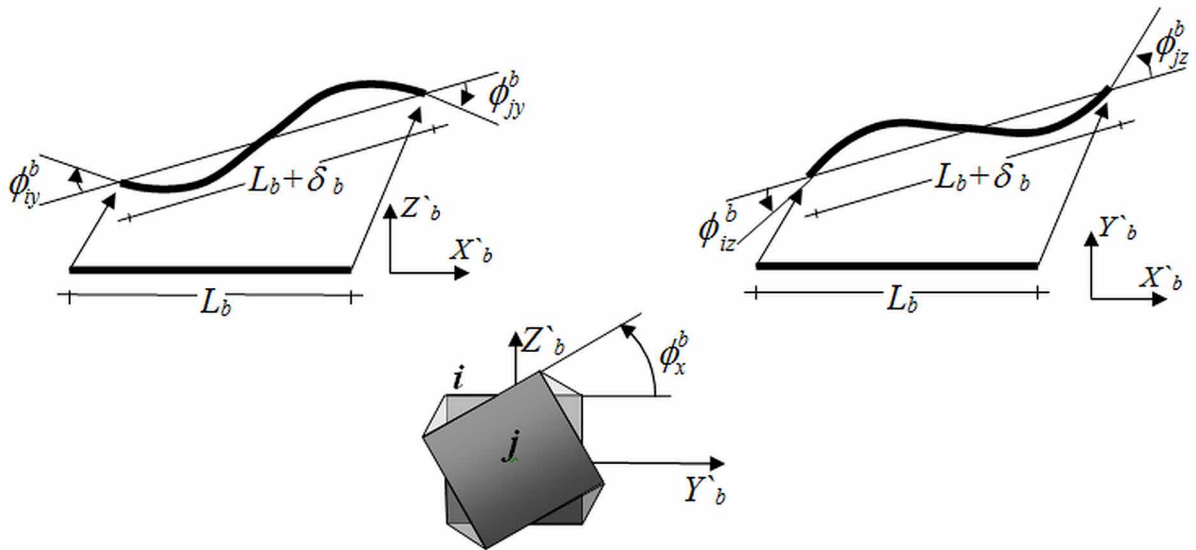
where  $\phi_{iy}^b$  and  $\phi_{jy}^b$  are the rotations relative to the cord around the local axis  $Y'_b$ , i.e. the same as in the two dimensional case;  $\delta_b$  is again the cord's elongation;  $\phi_{iz}^b$  and  $\phi_{jz}^b$  are the relative rotations around the local axis  $Z'_b$ ; finally,  $\phi_x^b$  is the torsion deformation of the element, see Figure 14.

The kinematic equation has the same general form, but with the following kinematic transformation matrix:

$$\{d\Phi\}_b = [\mathbf{B}]_b \{dq\}_b \quad (3.5.3)$$

$$[\mathbf{B}]_b = \begin{bmatrix} \frac{m_x^b}{L_b} & -\frac{m_y^b}{L_b} & -\frac{m_z^b}{L_b} & n_x^b & n_y^b & n_z^b & \frac{m_x^b}{L_b} & \frac{m_y^b}{L_b} & \frac{m_z^b}{L_b} & 0 & 0 & 0 \\ -\frac{m_x^b}{L_b} & \frac{m_y^b}{L_b} & -\frac{m_z^b}{L_b} & 0 & 0 & 0 & \frac{m_x^b}{L_b} & \frac{m_y^b}{L_b} & \frac{m_z^b}{L_b} & n_x^b & n_y^b & n_z^b \\ -t_x^b & -t_y^b & -t_z^b & 0 & 0 & 0 & t_x^b & t_y^b & t_z^b & 0 & 0 & 0 \\ \frac{n_x^b}{L_b} & \frac{n_y^b}{L_b} & \frac{n_z^b}{L_b} & m_x^b & m_y^b & m_z^b & -\frac{n_x^b}{L_b} & -\frac{n_y^b}{L_b} & -\frac{n_z^b}{L_b} & 0 & 0 & 0 \\ \frac{n_x^b}{L_b} & \frac{n_y^b}{L_b} & \frac{n_z^b}{L_b} & 0 & 0 & 0 & -\frac{n_x^b}{L_b} & -\frac{n_y^b}{L_b} & -\frac{n_z^b}{L_b} & m_x^b & m_y^b & m_z^b \\ 0 & 0 & 0 & -t_x^b & -t_y^b & -t_z^b & 0 & 0 & 0 & t_x^b & t_y^b & t_z^b \end{bmatrix} \quad (3.5.4)$$

Figure 14. Generalized deformations in a tridimensional frame element



where  $\{\mathbf{t}\}_b^t = (t_x^b, t_y^b, t_z^b)$ ,  $\{\mathbf{n}\}_b^t = (n_x^b, n_y^b, n_z^b)$ ;  $\{\mathbf{m}\}_b^t = (m_x^b, m_y^b, m_z^b)$  are, respectively, unit vectors in the directions of the local coordinate axes  $X'_b, Y'_b, Z'_b$ ; the components of these vectors are expressed with respect to the coordinate global axes. The demonstration of (3.5.4) is given in the next section.

### 3.5.2 Kinematic Transformation Matrix in the Tridimensional Case

Consider a frame element in the local coordinates as shown in Figure 15. Let  $\{\mathbf{q}'\}_b$  be the matrix of generalized displacements with respect to the local coordinate system:

$$\{\mathbf{q}'\}_b^t = (u'_i, v'_i, w'_i, \varphi'_i, \theta'_i, \zeta'_i, u'_j, v'_j, w'_j, \varphi'_j, \theta'_j, \zeta'_j) \quad (3.5.5)$$

The generalized displacements in the local coordinates and the global coordinates are related by the following expressions:

$$\{\mathbf{q}'\}_b = [\mathbf{T}]_b \{\mathbf{q}\}_b; \text{ where } [\mathbf{T}]_b = \begin{bmatrix} \mathbf{t}_b & \mathbf{0} & \mathbf{0} & \mathbf{0} \\ \mathbf{0} & \mathbf{t}_b & \mathbf{0} & \mathbf{0} \\ \mathbf{0} & \mathbf{0} & \mathbf{t}_b & \mathbf{0} \\ \mathbf{0} & \mathbf{0} & \mathbf{0} & \mathbf{t}_b \end{bmatrix}; \mathbf{t}_b = \begin{bmatrix} t_x & t_y & t_z \\ n_x & n_y & n_z \\ m_x & m_y & m_z \end{bmatrix}; \mathbf{0} = \begin{bmatrix} 0 & 0 & 0 \\ 0 & 0 & 0 \\ 0 & 0 & 0 \end{bmatrix} \quad (3.5.6)$$

Again, Equation (3.5.6) is based on the well-known relationship between the components of a vector in two different coordinate systems.

The kinematic equations for the generalized deformations in the coordinate local axes can be obtained by simple inspection of the diagrams included in Figure 15; they are:

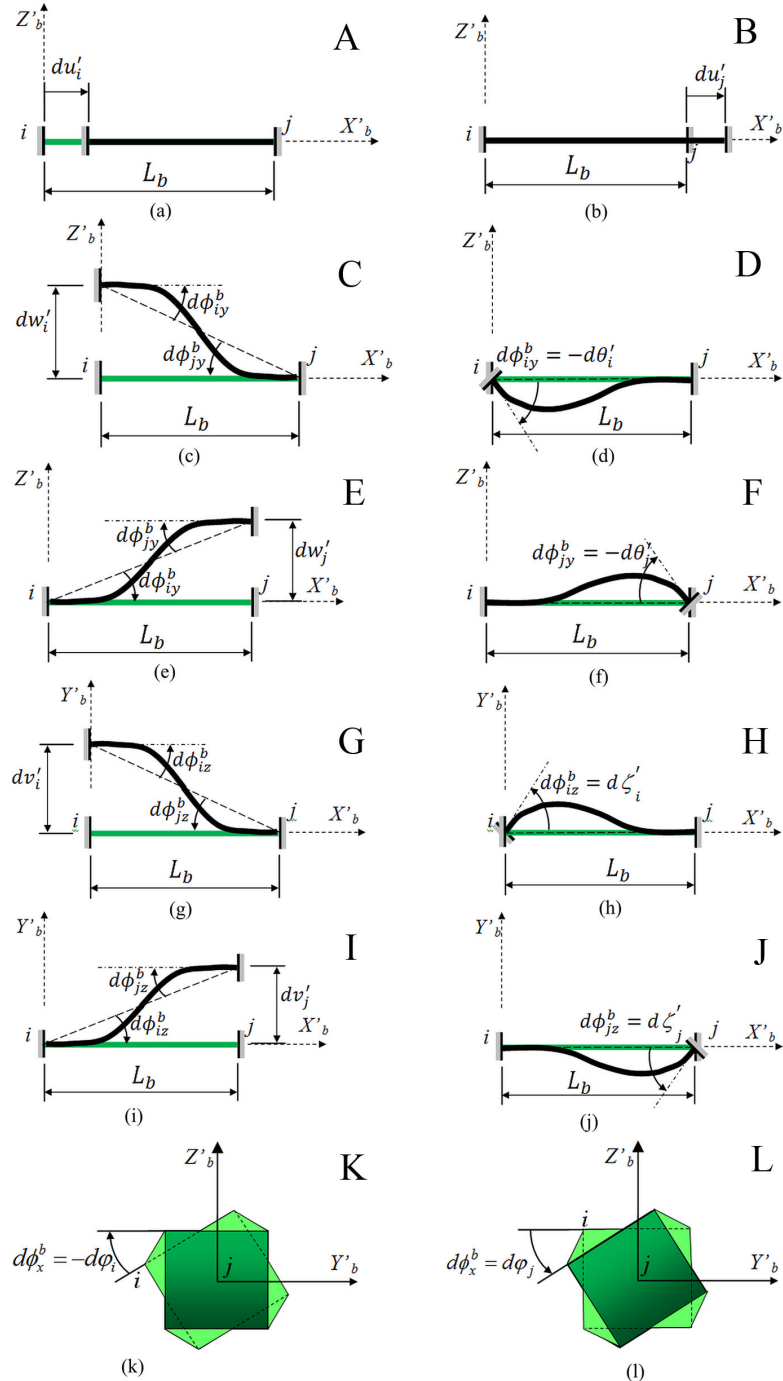
$$\begin{aligned} d\phi_{iy}^b &= -\frac{dw'_i}{L_b} + \frac{dw'_j}{L_b} + d\theta'_i; d\phi_{jy}^b = -\frac{dw'_i}{L_b} + \frac{dw'_j}{L_b} + d\theta'_j; d\delta_b = -du'_i + du'_j; \\ d\phi_{iz}^b &= \frac{dv'_i}{L_b} - \frac{dv'_j}{L_b} + d\zeta'_i; d\phi_{jz}^b = \frac{dv'_i}{L_b} - \frac{dv'_j}{L_b} + d\zeta'_j; d\phi_x^b = -d\varphi'_i + d\varphi'_j \end{aligned} \quad (3.5.7)$$

In matrix notation, the kinematic equations are written as:

$$\{d\Phi\}_b = [\mathbf{B}' ]_b \{d\mathbf{q}'\}_b;$$

**Elastic Frames**

Figure 15. Kinematic equations in local coordinates: a-b) Displacement of node i and j in the  $X'_b$  local axis. c-d) Displacement in the  $Z'_b$  local axis and relative rotation around the  $Y'_b$  local axis of node i. e-f) Displacement in the  $Z'_b$  direction and relative rotation around the  $Y'_b$  local axis of node j. g-h) Displacement in the  $Y'_b$  local axis and relative rotation around the  $Z'_b$  local axis of node i. i-j) Displacement in the  $Y'_b$  direction and relative rotation around the  $Z'_b$  local axis of node j. k-l) Relative rotation around the  $X'_b$  local axis of node i and j





$$[\mathbf{B}']_b = \begin{bmatrix} 0 & 0 & -\frac{1}{L_b} & 0 & 1 & 0 & 0 & 0 & \frac{1}{L_b} & 0 & 0 & 0 \\ 0 & 0 & -\frac{1}{L_b} & 0 & 0 & 0 & 0 & 0 & \frac{1}{L_b} & 0 & 1 & 0 \\ -1 & 0 & 0 & 0 & 0 & 0 & 1 & 0 & 0 & 0 & 0 & 0 \\ 0 & \frac{1}{L_b} & 0 & 0 & 0 & 1 & 0 & -\frac{1}{L_b} & 0 & 0 & 0 & 0 \\ 0 & \frac{1}{L_b} & 0 & 0 & 0 & 0 & 0 & -\frac{1}{L_b} & 0 & 0 & 0 & 1 \\ 0 & 0 & 0 & -1 & 0 & 0 & 0 & 0 & 0 & 1 & 0 & 0 \end{bmatrix} \quad (3.5.8)$$

The substitution of (3.5.6) into (3.5.8) leads to the kinematic Equation (3.5.3) with  $[\mathbf{B}]_b = [\mathbf{B}']_b [\mathbf{T}]_b$ ; it can be verified that the latter equation gives, indeed, expression (3.5.4).

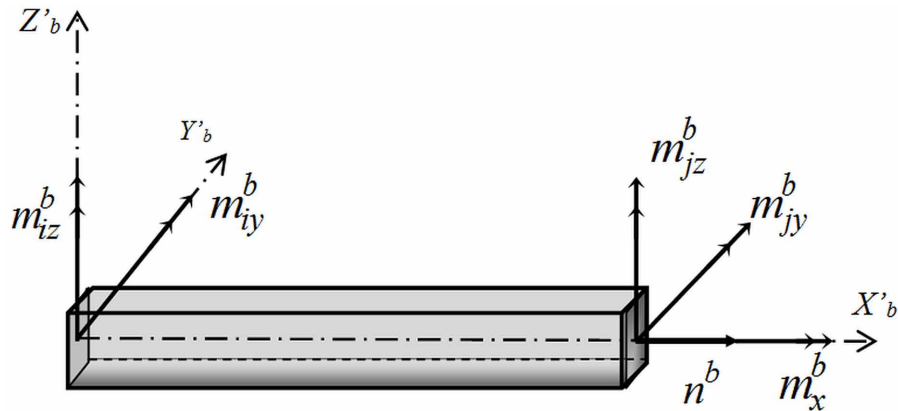
### 3.5.3 Dynamic of Tridimensional Frames

The matrix of generalized stresses conjugated to the deformations introduced in the previous section is:

$$\{\mathbf{M}\}_b^t = (m_{iy}^b, m_{jy}^b, n_b, m_{iz}^b, m_{jz}^b, m_x^b) \quad (3.5.9)$$

where  $m_{iy}^b$  and  $m_{jy}^b$  are the flexural moments around the local axis  $Y'_b$ , i.e. the same of the two dimensional case;  $n_b$  is again the average axial force;  $m_{iz}^b$  and  $m_{jz}^b$  are the flexural moments around the local axis  $Z'_b$ ;  $m_x^b$  is the average torque (see Figure 16).

Figure 16. Generalized stresses in a tridimensional frame element



## Elastic Frames

The matrix of generalized external forces is composed, as in the planar case, with forces and moments that correspond to the generalized displacements introduced in the previous section:

$$\{\mathbf{P}\}^t = (p_{u1}, p_{v1}, p_{w1}, p_{\varphi1}, p_{\theta1}, p_{\zeta1}, \dots, p_{\theta n}, p_{\zeta n}) \quad (3.5.10)$$

Thus, the general form of the equilibrium equation does not change:

$$\sum_{b=1}^m [\mathbf{B}_E]_b^t \{\mathbf{M}\}_b + [\mathbf{Mass}] \{\ddot{\mathbf{U}}\} = \{\mathbf{P}\} \quad (3.5.11)$$

Where the mass matrix has now the following expression:

$$[\mathbf{Mass}]_b = [\mathbf{T}]_b^t \begin{bmatrix} \text{Mass}_b/2 & 0 & 0 & 0 & 0 & 0 & 0 & 0 & 0 & 0 & 0 \\ 0 & \text{Mass}_b/2 & 0 & 0 & 0 & 0 & 0 & 0 & 0 & 0 & 0 \\ 0 & 0 & \text{Mass}_b/2 & 0 & 0 & 0 & 0 & 0 & 0 & 0 & 0 \\ 0 & 0 & 0 & \text{Mass}_b J_b / 2A & 0 & 0 & 0 & 0 & 0 & 0 & 0 \\ 0 & 0 & 0 & 0 & 0 & 0 & 0 & 0 & 0 & 0 & 0 \\ 0 & 0 & 0 & 0 & 0 & 0 & \text{Mass}_b/2 & 0 & 0 & 0 & 0 \\ 0 & 0 & 0 & 0 & 0 & 0 & 0 & \text{Mass}_b/2 & 0 & 0 & 0 \\ 0 & 0 & 0 & 0 & 0 & 0 & 0 & 0 & \text{Mass}_b/2 & 0 & 0 \\ 0 & 0 & 0 & 0 & 0 & 0 & 0 & 0 & 0 & \text{Mass}_b J_b / 2A & 0 \\ 0 & 0 & 0 & 0 & 0 & 0 & 0 & 0 & 0 & 0 & 0 \\ 0 & 0 & 0 & 0 & 0 & 0 & 0 & 0 & 0 & 0 & 0 \end{bmatrix} [\mathbf{T}]_b \quad (3.5.12)$$

where  $J_b$  is the polar moment of inertia and  $[\mathbf{T}]_b^t$  is the geometric transformation matrix of the element  $b$  (3.5.6).

### 3.5.4 Constitutive Equations for Tridimensional Frame Element

The procedure for the determination of the constitutive equations does not change in the tridimensional case. For instance if the shear deformations are neglected, the constitutive equation is:

$$\{\mathbf{M}\}_b = \{\mathbf{M}_0\}_b + [\mathbf{E}]_b \{\Phi\}_b \quad (3.5.13)$$

With

$$[\mathbf{E}] = \begin{bmatrix} \frac{4EI_y^b}{L_b} & \frac{2EI_y^b}{L_b} & 0 & 0 & 0 & 0 \\ \frac{2EI_y^b}{L_b} & \frac{4EI_y^b}{L_b} & 0 & 0 & 0 & 0 \\ 0 & 0 & \frac{AE_b}{L_b} & 0 & 0 & 0 \\ 0 & 0 & 0 & \frac{4EI_z^b}{L_b} & \frac{2EI_z^b}{L_b} & 0 \\ 0 & 0 & 0 & \frac{2EI_z^b}{L_b} & \frac{4EI_z^b}{L_b} & 0 \\ 0 & 0 & 0 & 0 & 0 & \frac{GJ_b}{L_b} \end{bmatrix} \quad (3.5.14)$$

where  $I_y^b$  is the moment of inertia of the element's cross-section around the local axis  $Y'_b$ ;  $I_z^b$  is the moment of inertia around the axis  $Y'_b$ ;  $GJ_b$  is torsional rigidity of the cross-section.

### 3.6. SUMMARY AND EQUATIONS QUICK REFERENCE

The kinematic of frames is defined by the matrix of displacements and m deformation matrices, one for each element of the frame. Statics of frames is described by the external forces matrix and m generalized stresses matrices. There is a kinematic equation for each frame element that relates the corresponding deformation matrix with displacements. The equilibrium equation permits the computation of the external forces from the generalized stresses. Finally, the elastic constitutive equation relates stresses with deformation or vice versa. All these equations have been defined for planar frames, tridimensional frames and dual systems. External forces can be applied directly on the nodes or along the elements. The algorithms for including both kind of external actions are discussed in the chapter. Set of external displacements have to be imposed in the analysis in order to ensure the stability of the structure (See Table 5).

## Elastic Frames

Table 5.

<b>KINEMATICS OF PLANAR FRAMES</b>	
<i>Generalized Displacements of a Planar Frame</i>	
Generalized displacement matrix of the frame	
$\{\mathbf{U}\} = \begin{bmatrix} u_1 \\ w_1 \\ \theta_1 \\ \vdots \\ u_n \\ w_n \\ \theta_n \end{bmatrix} \quad (3.1.1)$	
<p> <math>u_1</math> = displacement in the direction X of the node 1.  <math>w_1</math> = displacement in the direction Z of the node 1.  <math>\theta_1</math> = rotation of the node 1.  <math>\vdots</math>  <math>u_n</math> = displacement in the direction X of the node n.  <math>w_n</math> = displacement in the direction Z of the node n.  <math>\theta_n</math> = rotation of the node n.                 </p>	
Generalized displacement matrix of a frame element b between nodes i and j	
$\{\mathbf{q}\}_b = \begin{bmatrix} u_i \\ w_i \\ \theta_i \\ u_j \\ w_j \\ \theta_j \end{bmatrix} \quad (3.1.2)$	
<p> <math>u_i</math> = displacement in the direction X of the node i.  <math>w_i</math> = displacement in the direction Z of the node i.  <math>\theta_i</math> = rotation of the node i.  <math>u_j</math> = displacement in the direction X of the node j.  <math>w_j</math> = displacement in the direction Z of the node j.  <math>\theta_j</math> = rotation of the node j.                 </p>	
<i>Generalized Deformation Matrix</i>	
Generalized deformation matrix of the frame element b	
$\{\mathbf{\Phi}\}_b = \begin{bmatrix} \phi_i^b \\ \phi_j^b \\ \delta_b \end{bmatrix} \quad (3.1.3)$	
<p> <math>\phi_i^b</math> = angle between the cord i-j and the normal to the cross-section at the end i.  <math>\phi_j^b</math> = angle between the cord i-j and the normal to the cross-section at the end j.  <math>\delta_b</math> = elongation of the cord.                 </p>	

continued on following page

Table 5. Continued

<i>Kinematic Equations</i>	
Nodal displacement in local coordinate axes	$\{\mathbf{q}'\}_b^t = (u'_i, w'_i, \theta'_i, u'_j, w'_j, \theta'_j)$
<p>Relationship between <math>\{\mathbf{q}'\}_b</math> and <math>\{\mathbf{q}\}_b</math></p> <p><math>\{\mathbf{q}'\}_b = [T]_b \{\mathbf{q}\}_b</math>; (3.1.5)</p> $[T]_b = \begin{bmatrix} \cos \alpha_b & \sin \alpha_b & 0 & 0 & 0 & 0 \\ -\sin \alpha_b & \cos \alpha_b & 0 & 0 & 0 & 0 \\ 0 & 0 & 1 & 0 & 0 & 0 \\ 0 & 0 & 0 & \cos \alpha_b & \sin \alpha_b & 0 \\ 0 & 0 & 0 & -\sin \alpha_b & \cos \alpha_b & 0 \\ 0 & 0 & 0 & 0 & 0 & 1 \end{bmatrix}$ <p>[T]<sub>b</sub>: geometrical transformation matrix</p>	
<p>Kinematic equations</p> <p>For <math>\alpha_b = \alpha_b(\mathbf{q})</math>, <math>L_b = L_b(\mathbf{q})</math></p> $\{d\Phi\} = [\mathbf{B}(\mathbf{q})]\{d\mathbf{q}\}; [\mathbf{B}(\mathbf{q})] = \begin{bmatrix} \frac{\sin \alpha_b}{L_b} & -\frac{\cos \alpha_b}{L_b} & 1 & -\frac{\sin \alpha_b}{L_b} & \frac{\cos \alpha_b}{L_b} & 0 \\ \frac{\sin \alpha_b}{L_b} & -\frac{\cos \alpha_b}{L_b} & 0 & -\frac{\sin \alpha_b}{L_b} & \frac{\cos \alpha_b}{L_b} & 1 \\ -\cos \alpha_b & -\sin \alpha_b & 0 & \cos \alpha_b & \sin \alpha_b & 0 \end{bmatrix}; \quad (3.1.10)$ <p><math>[\mathbf{B}]_b</math> is called kinematic transformation matrix of the element b</p> <p>For <math>\alpha_b \cong \alpha_b^0; L_b \cong L_b^0; \{\Phi\}_b \cong [\mathbf{B}^0]_b \{\mathbf{q}\}_b</math> (3.1.11)</p> <p><math>[\mathbf{B}^0]_b</math> is the kinematic transformation matrix</p>	
<p><math>\{d\Phi\}_b \cong [\mathbf{B}_E(\mathbf{U})]_b \{d\mathbf{U}\}</math>; or <math>\{\Phi\}_b \cong [\mathbf{B}_E^0]_b \{\mathbf{U}\}</math>; (3.1.12)</p> <p><math>[\mathbf{B}_E(\mathbf{q})]_b</math> is denoted enlarged transformation matrix</p>	

continued on following page

**Elastic Frames**

Table 5. Continued

$[\mathbf{B}_E(\mathbf{q})]_b = \begin{bmatrix} 0 & 0 & \dots & \frac{\sin \alpha_b}{L_b} & -\frac{\cos \alpha_b}{L_b} & 1 & 0 & \dots & -\frac{\sin \alpha_b}{L_b} & \frac{\cos \alpha_b}{L_b} & 0 & \dots \\ 0 & 0 & \dots & \frac{\sin \alpha_b}{L_b} & -\frac{\cos \alpha_b}{L_b} & 0 & 0 & \dots & -\frac{\sin \alpha_b}{L_b} & \frac{\cos \alpha_b}{L_b} & 1 & \dots \\ 0 & 0 & \dots & -\cos \alpha_b & -\sin \alpha_b & 0 & 0 & \dots & \cos \alpha_b & \sin \alpha_b & 0 & \dots \\ u_1 & w_1 & \dots & u_i & w_i & \theta_i & u_{i+1} & \dots & u_j & w_j & \theta_j & \dots \end{bmatrix}$ <p>(3.1.13)</p>
<b>Simplified Analysis of Deformations: Story Drift Ratio</b>
<p>Kinematic equation</p> $\{\Phi\}_{col} = \begin{bmatrix} \phi_{bottom}^{col} \\ \phi_{top}^{col} \\ \delta_b \end{bmatrix} = \begin{bmatrix} \frac{(u_{top} - u_{bottom})}{L_{col}} \\ \frac{(u_{top} - u_{bottom})}{L_{col}} \\ 0 \end{bmatrix}$ <p style="text-align: right;">(3.1.14)</p> $\Delta = \left  \phi_{bottom}^{col} \right  = \left  \phi_{top}^{col} \right $ <p style="text-align: center;">: story drift ratio</p>
<b>DYNAMICS OF PLANAR FRAMES</b>
<b>Deformation Work of a Frame and Generalized Stress Matrix of a Frame Element</b>
<p>A structure in dynamic equilibrium verifies the equation:</p> $W_{def}^* + W_{ine}^* = W_{ext}^* \quad \forall \quad \{\mathbf{U}^*\} \quad (3.2.1)$
<p>Generalized stress matrix:</p> $\{\mathbf{M}\}_b = \begin{bmatrix} m_i^b \\ m_j^b \\ n_b \end{bmatrix} \quad (3.2.2)$ <p style="margin-left: 40px;"><math>m_i^b</math> : bending moment at the i end of the element b,</p> <p style="margin-left: 40px;"><math>m_j^b</math> : bending moment at the end j</p> <p style="margin-left: 40px;">nb: average axial force on the element b</p>
<p>Deformation work of a frame:</p> $W_{def}^* = \sum_{b=1}^m \{\Phi^*\}_b^t \{\mathbf{M}\}_b \quad (3.2.3)$ <p><math>\{\Phi^*\}_b</math> : a virtual, i.e. arbitrary and infinitesimal, deformation matrix</p>

*continued on following page*

Table 5. Continued

<i>Inertia Work of a Frame and Matrix of Masses</i>	
The matrix of masses of the element b	
$[\mathbf{Mass}]_b =$	$\begin{bmatrix} Mass_b/2 & 0 & 0 & 0 & 0 & 0 \\ 0 & Mass_b/2 & 0 & 0 & 0 & 0 \\ 0 & 0 & 0 & 0 & 0 & 0 \\ 0 & 0 & 0 & Mass_b/2 & 0 & 0 \\ 0 & 0 & 0 & 0 & Mass_b/2 & 0 \\ 0 & 0 & 0 & 0 & 0 & 0 \end{bmatrix} \quad (3.2.4)$
Mass <sub>b</sub> : mass of the element b	
$[\mathbf{Mass}]_b \{\ddot{\mathbf{q}}\}$ : inertia force on an element b	
$\{\ddot{\mathbf{q}}\} = \left\{ \frac{d^2 \mathbf{q}}{dt^2} \right\}$ : generalized acceleration matrix of element b the	
Inertia work	
$W_{ine}^* = \{\mathbf{U}^*\}^t \sum_{b=1}^m [\mathbf{Mass}_E]_b \{\ddot{\mathbf{U}}\} = \{\mathbf{U}^*\}^t [\mathbf{Mass}] \{\ddot{\mathbf{U}}\} \quad (3.2.5)$	
$[\mathbf{Mass}] = \sum_{b=1}^m [\mathbf{Mass}_E]_b$	
is the matrix of masses of the frame	
<i>External Work of a Frame and Matrix of Generalized External Forces</i>	
External work:	
$W_{ext}^* = \{\mathbf{U}^*\}^t \{\mathbf{P}\} \quad (3.2.6)$	
Generalized external forces matrix of a frame:	
$\{\mathbf{P}\} =$	$\begin{bmatrix} p_{u1} \\ p_{w1} \\ p_{\theta1} \\ p_{u2} \\ \vdots \\ \vdots \\ p_{wn} \\ p_{\theta n} \end{bmatrix} \quad (3.2.7)$
<p><math>p_{u1}</math> = external force in direction X on the node 1.  <math>p_{w1}</math> = external force in direction Z on the node 1.  <math>p_{\theta1}</math> = external bending moment on the node 1.</p> <p>⋮</p> <p><math>p_{wn}</math> = external force in direction Z on the node n.  <math>p_{\theta n}</math> = external bending moment on the node n.</p>	

continued on following page

**Elastic Frames**

Table 5. Continued

Matrix of external forces	$\{\mathbf{P}\} = \{\mathbf{P}^n\} + \{\mathbf{P}^{eq}\}$ (3.2.8)
<b>Dynamic and Quasi Static Equilibrium Equations</b>	
The principle of virtual work (3.2.1) states that:	
$\sum_{b=1}^m \{\Phi^*\}_b^t \{\mathbf{M}\}_b + \{\mathbf{U}^*\}^t [\mathbf{Mass}] \{\ddot{\mathbf{U}}\} = \{\mathbf{U}^*\}^t \{\mathbf{P}\} \forall \{\mathbf{U}^*\}$ <span style="float: right;">(3.2.9)</span>	
The principle of virtual work leads to:	
$\{\mathbf{U}^*\}^t \left( \sum_{b=1}^m [\mathbf{B}_E]_b^t \{\mathbf{M}\}_b + [\mathbf{Mass}] \{\ddot{\mathbf{U}}\} - \{\mathbf{P}\} \right) = 0 \forall \{\mathbf{U}^*\}$ <span style="float: right;">(3.2.10)</span>	
Dynamic equilibrium equation	
For $\alpha_b = \alpha_b(\mathbf{q}); L_b = L_b(\mathbf{q})$ ;	
$\sum_{b=1}^m [\mathbf{B}_E]_b^t \{\mathbf{M}\}_b + [\mathbf{Mass}] \{\ddot{\mathbf{U}}\} = \{\mathbf{P}\}$ <span style="float: right;">(3.2.11)</span>	
For $\alpha_b \cong \alpha_b^0; L_b \cong L_b^0$ ;	
$\sum_{b=1}^m [\mathbf{B}_E^0]_b^t \{\mathbf{M}\}_b + [\mathbf{Mass}] \{\ddot{\mathbf{U}}\} = \{\mathbf{P}\}$ <span style="float: right;">(3.2.12)</span>	
Quasi static equilibrium equations	
For $\alpha_b = \alpha_b(\mathbf{q}); L_b = L_b(\mathbf{q})$ ;	
$\sum_{b=1}^m [\mathbf{B}_E^0]_b^t \{\mathbf{M}\}_b = \{\mathbf{P}\}$ <span style="float: right;">(3.2.13)</span>	
For $\alpha_b \cong \alpha_b^0; L_b \cong L_b^0$ ;	
$\sum_{b=1}^m [\mathbf{B}_E]_b^t \{\mathbf{M}\}_b = \{\mathbf{P}\}$ <span style="float: right;">(3.2.14)</span>	
<b>CONSTITUTIVE EQUATIONS FOR A SLENDER FRAME MEMBER</b>	
<i>Summary of Variables and Equations in an Elastic Analysis</i>	
<pre> graph TD     subgraph Kinematic_Variables [KINEMATIC VARIABLES]         U[DISPLACEMENT MATRIX {U}]     end     subgraph Dynamic_Variables [DYNAMIC VARIABLES]         P[EXTERNAL FORCES MATRIX {P}]     end     U -- Kinematic equation --&gt; Phi[DEFORMATION MATRICES {Phi}_b]     P -- Equilibrium equation --&gt; M[STRESS MATRICES {M}_b]     Phi &lt;--&gt;  Constitutive equations  M     </pre>	

continued on following page



Table 5. Continued

<i>Constitutive Equations Based on the Theory of Euler-Bernoulli Beams</i>	
Constitutive equations	
$\frac{d^2 M_b(x_b)}{dx_b^2} = Q_b(x_b) \quad ; \quad \frac{d^2 \omega_b(x_b)}{dx_b^2} = \frac{M_b(x_b)}{EI_b} \quad ; \quad n_b = EA_b \frac{du_b(x_b)}{dx_b} \quad (3.3.1)$	
<p>Mb(xb): bending moment distribution on the element Qb(xb): distributed external forces,            ωb(xb): deflection            EIb: elasticity modulus multiplied by the inertia moment of the cross-section            nb: axial force            Ab: area of the cross-section            ub(xb): displacement in the direction of the cord</p>	
The general solution of (3.3.1a) is:	
$M_b(x_b) = Q2(x_b) + C_1 x_b + C_2 \quad ; \quad \text{where} \quad Q2(x_b) = \int_0^x \int_0^x Q(x_b) dx dx \quad (3.3.2)$	
The constants C1 and C2 can be computed by the boundary conditions: $m_i^b = M_b(0)$ and $m_j^b = -M_b(L_b)$ .	
The general solution to (3.3.1b) is:	
$EI_b \omega_b(x_b) = Q4(x_b) + C_1 \frac{x_b^3}{6} + C_2 \frac{x_b^2}{2} + C_3 x_b + C_4 \quad ; \quad \text{where} \quad Q4(x_b) = \int_0^x \int_0^x \int_0^x \int_0^x Q(x_b) dx dx dx dx \quad (3.3.3)$	
The constants C3 and C4 can be computed by the boundary conditions $\omega(0) = 0$ and $\omega(L_b) = 0$ .	
The constitutive equation for the deformation $\phi_i^b$ is then given by:	
$\phi_i^b = -\frac{d\omega_b(0)}{dx_b} = \frac{L_b}{3EI_b} m_i^b - \frac{L_b}{6EI_b} m_j^b + \phi_i^0 \quad ; \quad (3.3.4)$	
where	
$\phi_i^0 = \frac{1}{EI_b} \left( -\frac{L_b Q2(0)}{3} - \frac{L_b Q2(L_b)}{6} - Q3(0) - \frac{Q4(0)}{L_b} + \frac{Q4(L_b)}{L_b} \right) \quad ; \quad Q3(x_b) = \int_0^x \int_0^x \int_0^x Q(x_b) dx dx dx \quad (3.3.5)$	
The constitutive equation for the deformation $\phi_j^b$ is:	
$\phi_j^b = -\frac{d\omega_b(L_b)}{dx_b} = -\frac{L_b}{6EI_b} m_i^b + \frac{L_b}{3EI_b} m_j^b + \phi_j^0 \quad ; \quad (3.3.6)$	
where	
$\phi_j^0 = \frac{1}{EI_b} \left( \frac{L_b Q2(0)}{6} + \frac{L_b Q2(L_b)}{3} - Q3(L_b) - \frac{Q4(0)}{L_b} + \frac{Q4(L_b)}{L_b} \right) \quad (3.3.7)$	
The constitutive equation for the axial force:	
$n_b = \frac{AE_b}{L_b} \delta_b \quad (3.3.8)$	

continued on following page

## Elastic Frames

Table 5. Continued

Constitutive equations in matrix form	
$\{\Phi\}_b = [F_f]_b \{M\}_b + \{\Phi^0\}_b \quad \text{where}$	$[F_f]_b = \begin{bmatrix} \frac{L_b}{3EI_b} & -\frac{L_b}{6EI_b} & 0 \\ -\frac{L_b}{6EI_b} & \frac{L_b}{3EI_b} & 0 \\ 0 & 0 & \frac{L_b}{AE_b} \end{bmatrix}; \quad (3.3.9)$
$\{\Phi^0\}_b = \begin{bmatrix} \phi_i^0 \\ \phi_j^0 \\ 0 \end{bmatrix}$	
$[F_f]_b$ : flexibility matrix of the element b $\{\Phi^0\}_b$ : matrix of initial deformations	
Constitutive equations, expressed in terms of stresses as a function of deformations, in matrix form:	
$\{M\}_b = [E]_b \{\Phi\}_b + \{M^0\}_b \quad (3.3.10)$	
$[E]_b = [F_f]_b^{-1} = \begin{bmatrix} \frac{4EI_b}{L_b} & \frac{2EI_b}{L_b} & 0 \\ \frac{2EI_b}{L_b} & \frac{4EI_b}{L_b} & 0 \\ 0 & 0 & \frac{AE_b}{L_b} \end{bmatrix}$	$\text{and } \{M^0\}_b = -[E]_b \{\Phi^0\}_b \quad (3.3.11)$
$[E]_b$ : elasticity matrix of the element b $\{M^0\}_b$ : matrix of initial stresses.	
<b>CONSTITUTIVE EQUATIONS FOR FRAME MEMBERS OF ANY ASPECT RATIO</b>	
<i>Constitutive Equations Based on the Theory of Modified Timoshenko Beams</i>	
Constitutive equations:	
$\frac{dV_b(x_b)}{dx_b} = Q_b(x_b); \quad \frac{dM_b(x_b)}{dx_b} = V_b(x_b) \quad (3.4.1)$	
$M_b(x_b) = EI_b \frac{d\beta_b(x_b)}{dx_b}; \quad V_b(x_b) = GA_b \left( \beta_b(x_b) - \frac{d\omega_b(x_b)}{dx_b} \right) \quad (3.4.2)$	
$n_b = EA_b \frac{du_b(x_b)}{dx_b} \quad (3.4.3)$	
Vb: shear force on the element βb: rotation of the cross-section G: transverse elastic modulus	

continued on following page

Table 5. Continued

$V_b(x_b) = Q1(x_b) + C_1; \text{ where } Q1(x_b) = \int_0^x Q(x_b)dx$ $(3.4.4)$ $M_b(x_b) = Q2(x_b) + C_1x_b + C_2$
<p>The general solutions of the differential equations (3.4.2) are:</p> $EI_b\beta_b(x_b) = Q3(x_b) + C_1\frac{x_b^2}{2} + C_2x_b + C_3 \quad ; (3.4.5)$ $GA_b\omega_b(x_b) = -Q2(x_b) - C_1x_b + \frac{GA_b}{EI_b}\left(Q4(x_b) + C_1\frac{x_b^3}{6} + C_2\frac{x_b^2}{2} + C_3x_b\right) + C_4 \quad (3.4.6)$ <p>The constitutive equation for deformations <math>\phi_i^b</math> and <math>\phi_j^b</math> are:</p> $\phi_i^b = -\beta_b(0) = \left(\frac{L_b}{3EI_b}m_i^b - \frac{L_b}{6EI_b}m_j^b\right) + \left(\frac{m_i^b}{L_bGA_b} + \frac{m_j^b}{L_bGA_b}\right) + \phi_i^0$ $(3.4.7)$ $\phi_j^b = -\beta_b(L_b) = \left(-\frac{L_b}{6EI_b}m_i^b + \frac{L_b}{3EI_b}m_j^b\right) + \left(\frac{m_i^b}{L_bGA_b} + \frac{m_j^b}{L_bGA_b}\right) + \phi_j^0$
<p>Constitutive equations in matrix form</p> $\{\Phi\}_b = ([F_f]_b + [F_s]_b)\{M\}_b + \{\Phi^0\}_b \quad (3.4.8)$ <p>where</p> $[F_f]_b = \begin{bmatrix} \frac{L_b}{3EI_b} & -\frac{L_b}{6EI_b} & 0 \\ -\frac{L_b}{6EI_b} & \frac{L_b}{3EI_b} & 0 \\ 0 & 0 & \frac{L_b}{AE_b} \end{bmatrix}; [F_s]_b = \begin{bmatrix} \frac{1}{L_bGA_b} & \frac{1}{L_bGA_b} & 0 \\ \frac{1}{L_bGA_b} & \frac{1}{L_bGA_b} & 0 \\ 0 & 0 & 0 \end{bmatrix} \quad (3.4.9)$ <p><math>[F_f]_b</math> : flexibility matrix of the element b  <math>[F_s]_b</math> : shear flexibility matrix of the element b</p>
<p>Constitutive equations in matrix form:</p> $\{M\}_b = [E]_b\{\Phi\}_b + \{M^0\}_b \quad (3.4.10)$

continued on following page

**Elastic Frames**

Table 5. Continued

$[\mathbf{E}]_b = \left( [\mathbf{F}_f]_b + [\mathbf{F}_s]_b \right)^{-1} = \begin{bmatrix} \frac{4(L_b^2 GA_b + 3EI_b)EI_b}{L_b(L_b^2 GA_b + 12EI_b)} & \frac{2(L_b^2 GA_b - 6EI_b)EI_b}{L_b(L_b^2 GA_b + 12EI_b)} & 0 \\ \frac{2(L_b^2 GA_b - 6EI_b)EI_b}{L_b(L_b^2 GA_b + 12EI_b)} & \frac{4(L_b^2 GA_b + 3EI_b)EI_b}{L_b(L_b^2 GA_b + 12EI_b)} & 0 \\ 0 & 0 & \frac{AE_b}{L_b} \end{bmatrix} \quad (3.4.11)$
$\{\mathbf{M}^0\}_b = -[\mathbf{E}]_b \{\Phi^0\}_b \quad (3.4.12)$
$\{\mathbf{M}^0\}_b = \text{matrix of initial stresses by modified Timoshenko beam theory.}$
<b>TRIDIMENSIONAL ELASTIC FRAMES</b>
<i>Kinematic of Tridimensional Frames</i>
<p>Generalized displacement matrix of a frame element b</p> $\{\mathbf{q}\}_b^t = (u_i, v_i, w_i, \varphi_i, \theta_i, \zeta_i, u_j, v_j, w_j, \varphi_j, \theta_j, \zeta_j) \quad (3.5.1)$ <p> <math>u_i, v_i, w_i</math> = displacements in directions X, Y, Z at the end i.  <math>\varphi_i, \theta_i, \zeta_i</math> = rotations around the X, Y, Z axes at the end i.  <math>u_j, v_j, w_j</math> = displacements in directions X, Y, Z at the end j.  <math>\varphi_j, \theta_j, \zeta_j</math> = rotation around the X, Y, Z axes at the end j.         </p>
<p>Generalized deformation matrix of a frame element b</p> $\{\Phi\}_b^t = (\phi_{iy}^b, \phi_{jy}^b, \delta_b, \phi_{iz}^b, \phi_{jz}^b, \phi_x^b) \quad 3.5.2)$ <p> <math>\phi_{iy}^b, \phi_{jy}^b</math> = relative rotations to the cord around the local axis Y'b.  <math>\delta_b</math> = cord's elongation.  <math>\phi_{iz}^b, \phi_{jz}^b</math> = relative rotations to the cord around the local axis Z'b.  <math>\phi_x^b</math> = torsion deformation.         </p>

*continued on following page*

Table 5. Continued

Kinematic equation		
$\{d\Phi\}_b = [\mathbf{B}]_b \{d\mathbf{q}\}_b$ (3.5.3)		
$[\mathbf{B}]_b =$	$\begin{bmatrix} \frac{m_x^b}{L_b} & \frac{m_y^b}{L_b} & \frac{m_z^b}{L_b} & n_x^b & n_y^b & n_z^b & \frac{m_x^b}{L_b} & \frac{m_y^b}{L_b} & \frac{m_z^b}{L_b} & 0 & 0 & 0 \\ \frac{m_x^b}{L_b} & \frac{m_y^b}{L_b} & \frac{m_z^b}{L_b} & 0 & 0 & 0 & \frac{m_x^b}{L_b} & \frac{m_y^b}{L_b} & \frac{m_z^b}{L_b} & n_x^b & n_y^b & n_z^b \\ -t_x^b & -t_y^b & -t_z^b & 0 & 0 & 0 & t_x^b & t_y^b & t_z^b & 0 & 0 & 0 \\ \frac{n_x^b}{L_b} & \frac{n_y^b}{L_b} & \frac{n_z^b}{L_b} & m_x^b & m_y^b & m_z^b & -\frac{n_x^b}{L_b} & -\frac{n_y^b}{L_b} & -\frac{n_z^b}{L_b} & 0 & 0 & 0 \\ \frac{n_x^b}{L_b} & \frac{n_y^b}{L_b} & \frac{n_z^b}{L_b} & 0 & 0 & 0 & -\frac{n_x^b}{L_b} & -\frac{n_y^b}{L_b} & -\frac{n_z^b}{L_b} & m_x^b & m_y^b & m_z^b \\ 0 & 0 & 0 & -t_x^b & -t_y^b & -t_z^b & 0 & 0 & 0 & t_x^b & t_y^b & t_z^b \end{bmatrix}$	
(3.5.4)		
$\{\mathbf{t}\}_b^t = (t_x^b, t_y^b, t_z^b)$ = unit vector in the direction of the local coordinate axis X <sup>b</sup> .		
$\{\mathbf{n}\}_b^t = (n_x^b, n_y^b, n_z^b)$ = unit vector in the direction of the local coordinate axis Y <sup>b</sup> .		
$\{\mathbf{m}\}_b^t = (m_x^b, m_y^b, m_z^b)$ = unit vector in the direction of the local coordinate axis Z <sup>b</sup> .		
<b>Kinematic Transformation Matrix in the Tridimensional Case</b>		
Matrix of generalized displacements with respect to the local coordinate system		
$\{\mathbf{q}'\}_b^t = (u'_i, v'_i, w'_i, \varphi'_i, \theta'_i, \zeta'_i, u'_j, v'_j, w'_j, \varphi'_j, \theta'_j, \zeta'_j)$ (3.5.5)		
Relationship between $\{\mathbf{q}'\}_b$ and $\{\mathbf{q}\}_b$		
$\{\mathbf{q}'\}_b = [\mathbf{T}]_b \{\mathbf{q}\}_b$ , where	$[\mathbf{T}]_b = \begin{bmatrix} \mathbf{t}_b & \mathbf{0} & \mathbf{0} & \mathbf{0} \\ \mathbf{0} & \mathbf{t}_b & \mathbf{0} & \mathbf{0} \\ \mathbf{0} & \mathbf{0} & \mathbf{t}_b & \mathbf{0} \\ \mathbf{0} & \mathbf{0} & \mathbf{0} & \mathbf{t}_b \end{bmatrix}; \quad \mathbf{t}_b = \begin{bmatrix} t_x & t_y & t_z \\ n_x & n_y & n_z \\ m_x & m_y & m_z \end{bmatrix}$	
(3.5.6)		
Kinematic equations for the generalized deformations in the local coordinate axes:		
$d\phi_{iy}^b = -\frac{dw'_i}{L_b} + \frac{dw'_j}{L_b} + d\theta'_i; \quad d\phi_{jy}^b = -\frac{dw'_i}{L_b} + \frac{dw'_j}{L_b} + d\theta'_j; \quad d\delta_b = -du'_i + du'_j$		
(3.5.7)		
$d\phi_{iz}^b = \frac{dv'_i}{L_b} - \frac{dv'_j}{L_b} + d\zeta'_i; \quad d\phi_{iz}^b = \frac{dv'_i}{L_b} - \frac{dv'_j}{L_b} + d\zeta'_i; \quad d\phi_x^b = -d\varphi'_i + d\varphi'_j$		

continued on following page

**Elastic Frames**

Table 5. Continued

<p>Constitutive equations in matrix form</p> $\{d\Phi\}_b = [B^1]_b \{dq^1\}_b; (3.5.8)$ $[B^1]_b = \begin{bmatrix} 0 & 0 & -\frac{1}{L_b} & 0 & 1 & 0 & 0 & 0 & \frac{1}{L_b} & 0 & 0 & 0 \\ 0 & 0 & -\frac{1}{L_b} & 0 & 0 & 0 & 0 & 0 & \frac{1}{L_b} & 0 & 1 & 0 \\ -1 & 0 & 0 & 0 & 0 & 0 & 1 & 0 & 0 & 0 & 0 & 0 \\ 0 & \frac{1}{L_b} & 0 & 0 & 0 & 1 & 0 & -\frac{1}{L_b} & 0 & 0 & 0 & 0 \\ 0 & \frac{1}{L_b} & 0 & 0 & 0 & 0 & 0 & -\frac{1}{L_b} & 0 & 0 & 0 & 1 \\ 0 & 0 & 0 & -1 & 0 & 0 & 0 & 0 & 0 & 1 & 0 & 0 \end{bmatrix}$
<b>Dynamic of Tridimensional Frames</b>
<p>Generalized stress matrix of a frame element b</p> $\{M\}_b^t = (m_{iy}^b, m_{jy}^b, n_b, m_{iz}^b, m_{jz}^b, m_x^b) (3.5.9)$ <p><math>m_{iy}^b, m_{jy}^b</math> = flexural moments around the local axis Y'b.  <math>n_b</math> = average axial force.</p> <p><math>m_{iz}^b, m_{jz}^b</math> = flexural moment around the local axis Z'b.  <math>m_x^b</math> = average torsion moment.</p>
<p>Generalized external forces matrix</p> $\{P\}^t = (p_{u1}, p_{v1}, p_{w1}, p_{\varphi1}, p_{\theta1}, p_{\zeta1}, \dots, p_{\theta n}, p_{\zeta n}) (3.5.10)$ <p><math>P_{u1}, P_{v1}, P_{w1}</math> = external forces in direction X, Y, Z global axes on the node 1.  <math>P_{\varphi1}, P_{\theta1}, P_{\zeta1}</math> = external bending moments around of X, Y, Z global axes on the node 1.</p> <p><math>P_{u1}, P_{v1}, P_{w1}</math> = external forces in direction of X, Y, Z global axes on the node n.  <math>P_{\varphi1}, P_{\theta1}, P_{\zeta1}</math> = external bending moments around of X, Y, Z global axes on the node n.</p>

*continued on following page*

Table 5. Continued

Equilibrium equation $\sum_{b=1}^m [\mathbf{B}_E]_b^t \{\mathbf{M}\}_b + [\mathbf{Mass}] \{\ddot{\mathbf{U}}\} = \{\mathbf{P}\} \quad (3.5.11)$										
$[\mathbf{Mass}]_b = [\mathbf{T}]_b^t$	$\begin{bmatrix} Mass_b/2 & 0 & 0 & 0 & 0 & 0 & 0 & 0 & 0 & 0 \\ 0 & Mass_b/2 & 0 & 0 & 0 & 0 & 0 & 0 & 0 & 0 \\ 0 & 0 & Mass_b/2 & 0 & 0 & 0 & 0 & 0 & 0 & 0 \\ 0 & 0 & 0 & Mass_b J_b / 2A & 0 & 0 & 0 & 0 & 0 & 0 \\ 0 & 0 & 0 & 0 & 0 & 0 & 0 & 0 & 0 & 0 \\ 0 & 0 & 0 & 0 & 0 & 0 & 0 & 0 & 0 & 0 \\ 0 & 0 & 0 & 0 & 0 & 0 & Mass_b/2 & 0 & 0 & 0 \\ 0 & 0 & 0 & 0 & 0 & 0 & 0 & Mass_b/2 & 0 & 0 \\ 0 & 0 & 0 & 0 & 0 & 0 & 0 & 0 & Mass_b/2 & 0 \\ 0 & 0 & 0 & 0 & 0 & 0 & 0 & 0 & 0 & Mass_b J_b / 2A \\ 0 & 0 & 0 & 0 & 0 & 0 & 0 & 0 & 0 & 0 \\ 0 & 0 & 0 & 0 & 0 & 0 & 0 & 0 & 0 & 0 \end{bmatrix} [\mathbf{T}]_b$									
(3.5.12) $J_b$ : polar moment of inertia $[\mathbf{T}]_b^t$ is the geometric transformation matrix of the element b										
<b>Constitutive Equations for Tridimensional Frame Element</b>										
Constitutive equations $\{\mathbf{M}\}_b = \{\mathbf{M}_0\}_b + [\mathbf{E}]_b \{\Phi\}_b \quad (3.5.13)$										
$[\mathbf{E}] =$	$\begin{bmatrix} \frac{4EI_y^b}{L_b} & \frac{2EI_y^b}{L_b} & 0 & 0 & 0 & 0 \\ \frac{2EI_y^b}{L_b} & \frac{4EI_y^b}{L_b} & 0 & 0 & 0 & 0 \\ 0 & 0 & \frac{AE_b}{L_b} & 0 & 0 & 0 \\ 0 & 0 & 0 & \frac{4EI_z^b}{L_b} & \frac{2EI_z^b}{L_b} & 0 \\ 0 & 0 & 0 & \frac{2EI_z^b}{L_b} & \frac{4EI_z^b}{L_b} & 0 \\ 0 & 0 & 0 & 0 & 0 & \frac{GJ_b}{L_b} \end{bmatrix}$									
$I_y^b$ = moment of inertia of the element's cross-section around the local axis Y'b. $I_z^b$ = moment of inertia of the element's cross-section around the local axis Z'b. $J_b$ = polar moment of inertia of the cross-section.										

### 3.7. EXAMPLES

#### 3.7.1 Kinematic Equations of a Two Span Continuous Beam

In this example, the kinematic equations for the beam shown in Figure 17 are written considering small displacements.

The structure has only 2 elements and 3 free displacements: the horizontal displacement ( $u_2$ ), the vertical one ( $w_2$ ) and the rotation ( $\theta_2$ ) at the node 2. The remaining six displacements are all restricted and correspond to the fixed supports at nodes 1 and 3.

For the element 1 between nodes 1 and 2 ( $L = 0.75$  m and  $\alpha = 0$ ), the linear kinematic equation  $\{\Phi\}_1 = [\mathbf{B}^0]_1 \{\mathbf{q}\}_1$  can be written as:

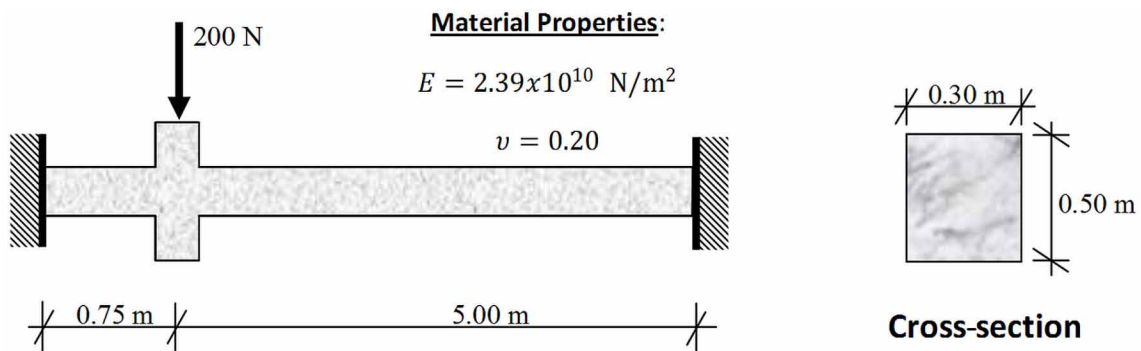
$$\begin{bmatrix} \phi_1^1 \\ \phi_2^1 \\ \delta_1 \end{bmatrix} = \begin{bmatrix} 0 & -1.333 & 1 & 0 & 1.333 & 0 \\ 0 & -1.333 & 0 & 0 & 1.333 & 1 \\ -1 & 0 & 0 & 1 & 0 & 0 \end{bmatrix} \begin{bmatrix} 0 \\ 0 \\ 0 \\ u_2 \\ w_2 \\ \theta_2 \end{bmatrix} \quad (3.7.1)$$

i.e.:

$$\phi_1^1 = 1.333 w_2; \phi_2^1 = 1.333 w_2 + \theta_2; \delta_1 = u_2 \quad (3.7.2)$$

For the element 2 between nodes 2 and 3 ( $L = 5$  m and  $\alpha = 0$ ), the kinematic equation  $\{\Phi\}_2 = [\mathbf{B}^0]_2 \{\mathbf{q}\}_2$  can be written as:

Figure 17. Two span beam





$$\begin{bmatrix} \phi_2^2 \\ \phi_3^2 \\ \delta_2 \end{bmatrix} = \begin{bmatrix} 0 & -0.20 & 1 & 0 & 0.20 & 0 \\ 0 & -0.20 & 0 & 0 & 0.20 & 1 \\ -1 & 0 & 0 & 1 & 0 & 0 \end{bmatrix} \begin{bmatrix} u_2 \\ \omega_2 \\ \theta_2 \\ 0 \\ 0 \\ 0 \end{bmatrix} \quad (3.7.3)$$

That is:

$$\phi_2^2 = -0.20w_2 + \theta_2; \phi_3^2 = 0.20w_2; \delta_2 = -u_2 \quad (3.7.4)$$

### 3.7.2 Equilibrium Equations of a Two Span Continuous Beam

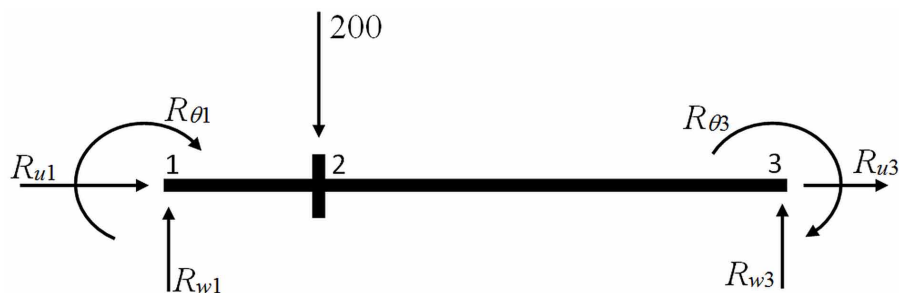
Consider again the structure in Figure 17; in the case of quasi-static analysis, the equilibrium equation is written as:

$$[\mathbf{B}_E^0]_1^t \{\mathbf{M}\}_1 + [\mathbf{B}_E^0]_2^t \{\mathbf{M}\}_2 = \{\mathbf{P}\} \quad (3.7.5)$$

where the generalized external forces matrix is (see Figure 18):

$$\{\mathbf{P}\} = \begin{bmatrix} R_{u1} \\ R_{w1} \\ R_{\theta1} \\ 0 \\ -200 \\ 0 \\ R_{u3} \\ R_{w3} \\ R_{\theta3} \end{bmatrix} \quad (3.7.6)$$

Figure 18. External nodal forces



## Elastic Frames

For the element 1, the enlarged transformation matrix is obtained from the expression (3.7.1):

$$[\mathbf{B}_E]_1 = \begin{bmatrix} 0 & -1.333 & 1 & 0 & 1.333 & 0 & 0 & 0 & 0 \\ 0 & -1.333 & 0 & 0 & 1.333 & 1 & 0 & 0 & 0 \\ -1 & 0 & 0 & 1 & 0 & 0 & 0 & 0 & 0 \end{bmatrix} \quad (3.7.7)$$

And the generalized stress matrix is:

$$\{\mathbf{M}\}_1 = \begin{bmatrix} m_1^1 \\ m_2^1 \\ n_1 \end{bmatrix} \quad (3.7.8)$$

For element 2, the enlarged transformation matrix is obtained from the expression (3.7.3):

$$[\mathbf{B}_E]_2 = \begin{bmatrix} 0 & 0 & 0 & 0 & -0.2 & 1 & 0 & 0.2 & 0 \\ 0 & 0 & 0 & 0 & -0.2 & 0 & 0 & 0.2 & 1 \\ 0 & 0 & 0 & -1 & 0 & 0 & 1 & 0 & 0 \end{bmatrix} \quad (3.7.9)$$

And the generalized stress matrix is:

$$\{\mathbf{M}\}_2 = \begin{bmatrix} m_2^2 \\ m_3^2 \\ n_2 \end{bmatrix} \quad (3.7.10)$$

In explicit form, Eq. (3.7.5) gives the following equilibrium equations:

$$\begin{aligned} R_{u_1} &= -n_1; R_{w_1} = -1.333(m_{11} + m_{21}); R_{\theta_1} = m_{11}; \\ n_1 &= n_2; 1.333(m_{11} + m_{21}) - 0.20(m_{22} + m_{32}) = -200; m_{21} = -m_{22} \\ R_{u_3} &= n_2; R_{w_3} = 0.20(m_{22} + m_{32}); R_{\theta_3} = m_{32} \end{aligned} \quad (3.7.11)$$

### 3.7.3 Constitutive Equations of a Two Span Continuous Beam using Euler-Bernoulli Theory

Consider again the beam that is shown in Figure 17. The initial stresses and deformations in the constitutive equation (3.3.10) for this case are nil because there are not forces on the two elements:  $\{\mathbf{M}\}_b = [\mathbf{E}]_b \{\Phi\}_b$  for  $b=1, 2$ .

The elasticity matrices for elements 1 and 2 obtained from Eq. (3.3.11), with an elasticity modulus of  $2.39 \times 10^4$  MPa, are:

$$[\mathbf{E}]_1 = \begin{bmatrix} 3.983 \times 10^8 & 1.992 \times 10^8 & 0 \\ 1.992 \times 10^8 & 3.983 \times 10^8 & 0 \\ 0 & 0 & 4.780 \times 10^9 \end{bmatrix} \quad (3.7.12)$$

$$[\mathbf{E}]_2 = \begin{bmatrix} 5.975 \times 10^7 & 2.988 \times 10^7 & 0 \\ 2.988 \times 10^7 & 5.975 \times 10^7 & 0 \\ 0 & 0 & 7.170 \times 10^8 \end{bmatrix} \quad (3.7.13)$$

Then the expressions of generalized stresses, in function of the generalized deformations, are for element 1:

$$m_1^1 = 3.983 \times 10^8 \phi_1^1 + 1.992 \times 10^8 \phi_2^1; m_2^1 = 1.992 \times 10^8 \phi_1^1 + 3.983 \times 10^8 \phi_2^1; n_1 = 4.780 \times 10^9 \delta_1 \quad (3.7.14)$$

and for element 2:

$$m_2^2 = 5.975 \times 10^7 \phi_2^2 + 2.988 \times 10^7 \phi_3^2; m_3^2 = 2.988 \times 10^7 \phi_2^2 + 5.975 \times 10^7 \phi_3^2; n_2 = 7.170 \times 10^8 \delta_2 \quad (3.7.15)$$

### 3.7.4 Constitutive Equations of a Two Span Continuous Beam using Modified Timoshenko Theory

In this case, the constitutive equations for the elements of the beam shown in Figure 17 are obtained using the Eq. (3.3.10) with the elasticity matrices given in (3.4.11) and considering  $\nu = 0.20$ .

$$[\mathbf{E}]_1 = \begin{bmatrix} 2.441 \times 10^8 & 4.497 \times 10^7 & 0 \\ 4.497 \times 10^7 & 2.441 \times 10^8 & 0 \\ 0 & 0 & 4.780 \times 10^9 \end{bmatrix} \quad (3.7.16)$$

### Elastic Frames

$$[\mathbf{E}]_2 = \begin{bmatrix} 5.870x10^7 & 2.882x10^7 & 0 \\ 2.882x10^7 & 5.870x10^7 & 0 \\ 0 & 0 & 7.170x10^8 \end{bmatrix} \quad (3.7.17)$$

Therefore, the expressions of generalized stresses, in function of the generalized deformations, for element 1 are:

$$m_1^1 = 2.441x10^8 \phi_1^1 + 4.497x10^7 \phi_2^1; m_2^1 = 4.497x10^7 \phi_1^1 + 2.441x10^8 \phi_2^1; n_1 = 4.780x10^9 \delta_1 \quad (3.7.18)$$

and for element 2, they are:

$$m_2^2 = 5.870x10^7 \phi_2^2 + 2.882x10^7 \phi_3^2; m_3^2 = 2.882x10^7 \phi_2^2 + 5.870x10^7 \phi_3^2; n_2 = 7.170x10^8 \delta_2 \quad (3.7.19)$$

Notice that there is a small difference between in the elasticity matrices (3.7.13) and (3.7.17) corresponding to the largest element and there is a big difference between the matrices (3.7.12) and (3.7.16).

### 3.7.5 Initial Deformations and Initial Stresses Computations for a Fixed Beam under Constant Loading using Euler-Bernoulli Theory

The initial deformations for the beam shown in Figure 19 are determined using Equations (3.3.5 and 3.3.7 that are, respectively,

$$\phi_i^0 = \frac{1}{EI_b} \left( -\frac{L_b Q2(0)}{3} - \frac{L_b Q2(L)}{6} - Q3(0) - \frac{Q4(0)}{L_b} + \frac{Q4(L)}{L_b} \right)$$

$$\phi_j^0 = \frac{1}{EI_b} \left( \frac{L_b Q2(0)}{6} + \frac{L_b Q2(L)}{3} - Q3(L) - \frac{Q4(0)}{L_b} + \frac{Q4(L)}{L_b} \right)$$

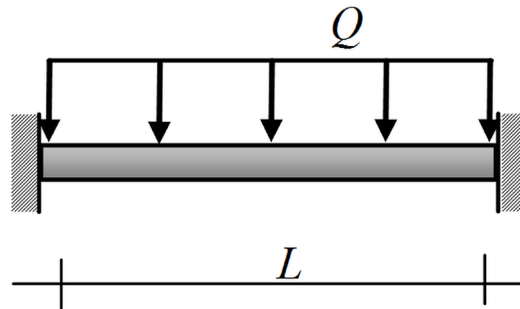
For the beam shown in Figure 19 the load can be written as:

$$Q(x_b) = -Q \quad (3.7.20)$$

Then,

$$Q2(x_b) = -\frac{Qx^2}{2}, Q3(x_b) = -\frac{Qx^3}{6}, \text{ and } Q4(x_b) = -\frac{Qx^4}{24} \quad (3.7.21)$$

Figure 19. Fixed beam subjected to a uniform load



The following expressions of initial deformations are obtained after the evaluation of these integrals for  $x = 0$  and  $x = L$ :

$$\phi_i^0 = \frac{QL^3}{24EI_b}; \phi_j^0 = -\frac{QL^3}{24EI_b} \quad (3.7.22)$$

Therefore, the initial deformation matrix is:

$$\{\Phi^0\}_b = \begin{bmatrix} \frac{QL^3}{24EI_b} \\ \frac{QL^3}{24EI_b} \\ 0 \end{bmatrix} \quad (3.7.23)$$

The initial stresses are computed using Eq. (3.3.11):  $\{M^0\}_b = -[E]_b \{\Phi^0\}_b$ . Then, the initial stresses are obtained multiplying the elasticity matrix (3.3.11) and the computed initial deformations (3.7.23).

$$m_i^0 = -\frac{QL^2}{12}; m_j^0 = \frac{QL^2}{12} \quad (3.7.24)$$

Thus, the initial stresses matrix is:

$$\{M^0\}_b = \begin{bmatrix} -\frac{QL^2}{12} \\ \frac{QL^2}{12} \\ 0 \end{bmatrix} \quad (3.7.25)$$

### 3.7.6 Initial Stresses Computation for a Fixed Beam under Constant Loading using Modified Timoshenko Theory

The initial deformations are the same in both theories; then, the expressions obtained in the former example are valid in this case too. The initial stresses are computed using again the expression (3.4.12) but this time, the expression for the elasticity matrix (3.4.11).

The initial stresses are obtained by the multiplication of the elasticity matrix and the initial deformations,

$$m_i^0 = -\frac{QL^2}{12}; m_j^0 = \frac{QL^2}{12} \quad (3.7.26)$$

Notice that these expressions are identical to the ones computed in the former example.

### 3.7.7 Initial deformations and Initial Stresses Computations for a Fixed Beam under a Partial Constant Loading using Euler-Bernoulli Theory

The initial deformations for the beam shown in Figure 20 are determined using Equations (3.3.5 and 3.3.7 in the same way as in the example 3.7.5,

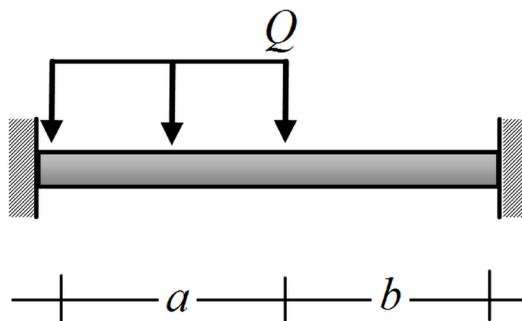
For the beam shown in Figure 20, the load can be expressed as:

$$Q(x_b) = \begin{cases} -Q & \text{if } x \leq a \\ 0 & \text{otherwise} \end{cases} \quad (3.7.27)$$

A Heaviside step function is used in order to obtain only one expression to define the load along the beam. This function is defined as:

$$Heaviside(x) = \begin{cases} 0 & \text{if } x < 0 \\ \text{undefined} & \text{if } x = 0 \\ 1 & \text{if } x > 0 \end{cases} \quad (3.7.28)$$

Figure 20. Fixed beam subjected to a partial uniform load



Then, the load expression is:

$$Q(x_b) = -Q + Q\text{Heaviside}(x - a) \quad (3.7.29)$$

Using an algebraic manipulating program in order to obtain the terms indicated in (3.3.2b), (3.3.5b), (3.3.3b) give

$$\begin{aligned} Q2(0) = 0; Q2(L) = Qa\left(\frac{a}{2} - L\right); Q3(0) = 0; Q3(L) = -\frac{1}{6}Qa^3 + \frac{1}{2}Qa^2L - \frac{1}{2}QaL^2 \\ Q4(0) = 0; Q4(L) = \frac{1}{24}Qa^4 - \frac{1}{6}Qa^3L + \frac{1}{4}Qa^2L^2 - \frac{1}{6}QaL^3 \end{aligned} \quad (3.7.30)$$

Finally the substitution of (3.7.30) in (3.3.5a and 3.3.7a), gives:

$$\phi_i^0 = \frac{Qa^2(-4aL + 4L^2 + a^2)}{24LEI}; \phi_j^0 = -\frac{2QL^2a^2 - Qa^4}{24LEI} \quad (3.7.31)$$

Therefore, the initial deformation matrix is:

$$\{\Phi^0\}_b = \begin{bmatrix} \frac{Qa^2(-4aL + 4L^2 + a^2)}{24LEI} \\ -\frac{2QL^2a^2 - Qa^4}{24LEI} \\ 0 \end{bmatrix} \quad (3.7.32)$$

The initial stresses matrix is obtained by the multiplication of the elasticity matrix (3.3.11) and the initial deformation matrix (3.7.32):

$$\{\mathbf{M}^0\}_b = \begin{bmatrix} -\frac{Qa^2(-8aL + 6L^2 + 3a^2)}{12L^2} \\ \frac{Qa^3(4L - 3a)}{12L^2} \\ 0 \end{bmatrix} \quad (3.7.33)$$

### 3.7.8 Initial Stresses Computation for a Fixed Beam under a Partial Constant Loading using Modified Timoshenko Theory

In this case, the initial stresses are defined by the multiplication of the elasticity matrix (3.4.11) and the initial deformation matrix (3.7.32). Thus, the initial stresses matrix is:

$$\{M^0\}_b = \begin{bmatrix} \frac{Qa^2(-8L^2GAa + 6L^3GA + 3LGAa^2 - 24EIa + 36LEI)}{12L(L^2GA + 12EI)} \\ \frac{Qa^2(4L^2GAa - 3LGAa^2 - 24EIa + 36LEI)}{12L(L^2GA + 12EI)} \\ 0 \end{bmatrix} \quad (3.7.34)$$

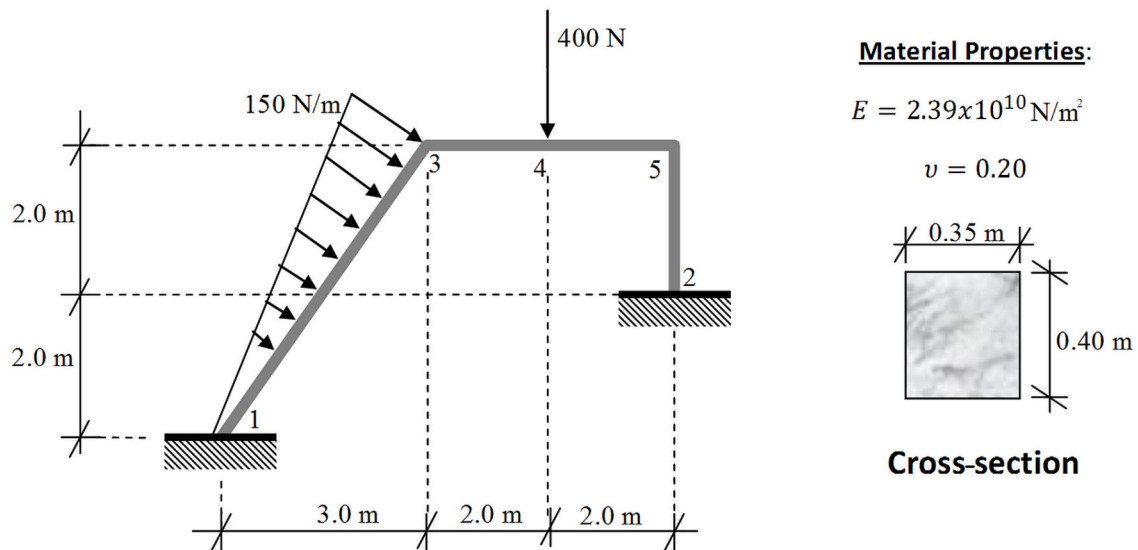
Notice that if the loading is not symmetric, the initial stresses are different in the two theories.

## 3.8. PROBLEMS

3.8.1 Define the Kinematic, Equilibrium and Constitutive Equations for the Planar Frame Shown in Figure 21 Using Modified Timoshenko Theory and Euler-Bernoulli Theory

3.8.2 Compute Initial Deformations and Initial Stresses for the Beam Shown in Figure 22 Using Euler-Bernoulli Theory and Modified Timoshenko Theory

Figure 21. Planar frame





**3.8.3 Compute the Initial Deformations and Stresses for the Beam Shown in Figure 23 Using Euler-Bernoulli Theory and Modified Timoshenko Theory**

**3.8.4 Demonstrate That Both Theories Give Different the Initial Stresses If the Loading on a Beam Is Unsymmetrical**

**3.8.5 In Section 3.4.2, the Constitutive Equations Were Developed for the Case of a Planar Element with Any Aspect Ratio**

Generalize the formulation to the case of a tridimensional frame element.

Figure 22. Fixed beam subjected to a triangular central load

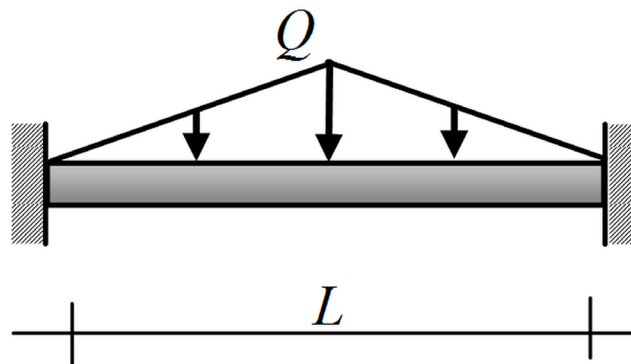
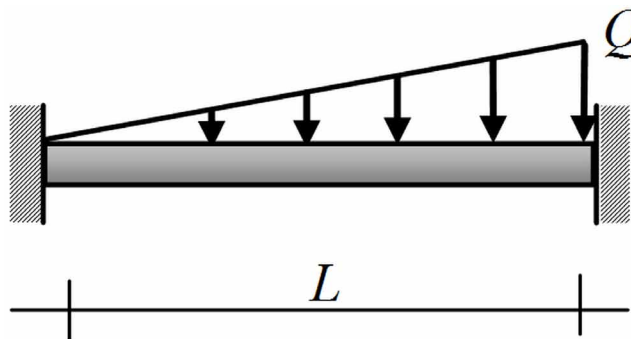


Figure 23. A fixed beam subjected to a triangular load



## REFERENCES

- Batoz, J. L., & Dhatt, G. (1992). *Modélisation des structures par éléments finis: Poutres et plaques* (Vol. 2). Paris, France: Éditions Hermès.
- Cipollina, A., López-Inojosa, A., & Flórez-López, J. (1995). A simplified damage mechanics approach to nonlinear analysis of frames. *Computers & Structures*, 54(6), 1113–1126. doi:10.1016/0045-7949(94)00394-I
- Marante, M. E., & Flórez-López, J. (2002). Model of damage for RC elements subjected to biaxial bending. *Engineering Structures*, 24(9), 1141–1152. doi:10.1016/S0141-0296(02)00044-5
- Ortiz, J., & Hernando, J. I. (2002). *Estructuras de edificación: Análisis lineal y no lineal*. Barcelona, Spain: Ariel.
- Perdomo, M. E., Picón, R., Marante, M. E., Hild, F., Roux, S., & Flórez-López, J. (2013). Experimental analysis and mathematical modeling of fracture in RC elements with any aspect ratio. *Engineering Structures*, 46, 407–416. doi:10.1016/j.engstruct.2012.07.005
- Powell, H. G. (1969). Theory for nonlinear elastic structures. *Journal of the Structural Division*, ST12, 2687–2701.

# Chapter 4

## Analysis of Elastic Frames

### ABSTRACT

*The formulation of a mathematical model that describes some physical phenomenon is just a first step; a second one, equally important, is the development of numerical procedures that transform this model into a potentially predictive tool with practical engineering applications; no computer software can be developed without robust numerical algorithms. This chapter describes some of these procedures in the case of elastic frames. First, it considers the direct stiffness method that permits the analysis of linear elastic and quasi static structures (Section 4.1); then, the procedure is extended to the more complex cases of nonlinear structures (Section 4.2) and dynamic loading (Section 4.3).*

### 4.1 THE DIRECT STIFFNESS METHOD

#### 4.1.1 Stiffness Matrix of a Frame and Matrix of Total Forces

Consider the particular case of a structure under quasi-static loading; assume that nonlinear terms can be neglected. Then, the problem is formulated as follows:

1. **Compute:** The free displacements, reaction forces, deformations and stresses.
2. **With the Following Data:** the initial configuration of the structure, the restricted displacements, the external forces corresponding to the free displacements and those applied over the elements; finally, the material and cross-section properties ( $E, \nu, I, A$ ).
3. Such that they verify:
  - a. The Kinematic Equation:  $\{\Phi\}_b = [\mathbf{B}_E^0]_b \{\mathbf{U}\}$
  - b. The Equilibrium Equation:  $\sum_{b=1}^m [\mathbf{B}_E^0]^t \{\mathbf{M}\}_b = \{\mathbf{P}^n\} + \{\mathbf{P}^{eq}\}$  (4.1.1)
  - c. The Constitutive Equation:  $\{\mathbf{M}\}_b = [\mathbf{E}]_b \{\Phi\}_b + \{\mathbf{M}^0\}_b$

The problem can now be resolved as follows; the combination of Equations (4.1.1) leads to:

## Analysis of Elastic Frames

$$[\mathbf{K}]\{\mathbf{U}\} = \{\mathbf{F}\} \quad (4.1.2)$$

where

$$[\mathbf{K}] = \sum_{b=1}^m [\mathbf{B}_E^0]_b^t [\mathbf{E}]_b [\mathbf{B}_E^0]_b; \text{ or } [\mathbf{K}] = \sum_{b=1}^m [\mathbf{k}_E]_b; [\mathbf{k}_E]_b = [\mathbf{B}_E^0]_b^t [\mathbf{E}]_b [\mathbf{B}_E^0]_b; \quad (4.1.3)$$

$$\{\mathbf{F}\} = \{\mathbf{P}^n\} + \{\mathbf{P}^e\}; \{\mathbf{P}^e\} = \{\mathbf{P}^{eq}\} - \sum_{b=1}^m [\mathbf{B}_E^0]_b^t \{\mathbf{M}^0\}_b \quad (4.1.4)$$

The matrix  $[\mathbf{K}]$  is called stiffness matrix of the structure;  $[\mathbf{k}_E]_b$  is denoted expanded stiffness matrix of element  $b$ . The elasticity matrix  $[\mathbf{E}]_b$  used for the computation of the stiffness matrix of the element  $b$  can be based on the Euler-Bernoulli beam theory (Equation 3.3.11), if the element is slender, or on the Timoshenko theory (Equation 3.4.11) in all cases.

The term  $\{\mathbf{F}\}$  is called matrix of total forces. It is decomposed into two terms; the first one,  $\{\mathbf{P}^n\}$ , includes external forces applied directly on the nodes; the second matrix,  $\{\mathbf{P}^e\}$ , depends exclusively on the external forces distributed over the element. The terms  $\{\mathbf{P}^n\}$  and  $\{\mathbf{P}^{eq}\}$  were defined in the previous chapter (section 3.2.3).

Notice that (4.1.2) is again an equilibrium equation but this time it is expressed in function of displacements instead of stresses; the left hand term gives the internal forces, the right hand one includes the external forces.

The resolution of the linear equation (4.1.2), by any conventional method, gives the values of the unknown displacements and reaction forces. Then, element deformations can be computed by the kinematic equation (4.1.1a), finally the element stresses are calculated by the constitutive law (4.1.1c); (see examples 4.4.1 and 4.4.2).

### 4.1.2 Assemblage of the Stiffness Matrix of the Structure.

The expanded stiffness matrices are square, symmetric and of the same size as the frame's stiffness matrix, however they are mainly composed of zeros; for instance in a planar frame, the expanded stiffness matrices are  $3n \times 3n$  ( $n$  is the number of nodes) but only  $6 \times 6$  terms can be non nil. In academic examples with few elements the use of expanded matrices is the best option; they define clearly the total stiffness of the structure as the sum of the contributions of each element. In the engineering practice, with structures that may have hundreds or thousands of elements, these matrices are not computed; instead, the non-expanded stiffness matrices  $[\mathbf{k}]_b$  are calculated:

$$[\mathbf{k}]_b = [\mathbf{B}_E^0]_b^t [\mathbf{E}]_b [\mathbf{B}_E^0]_b \quad (4.1.5)$$

Notice the use of the non-expanded transformation matrix instead of the expanded in (4.1.5). The terms  $[\mathbf{k}]_b$  include all the possibly non nil components of the expanded stiffness matrices; its dimensions

are 6\*6 for planar frames and 12\*12 for tridimensional ones. As opposed to the expanded stiffness matrices, they cannot be added directly since they are related to different generalized displacements; instead they are processed using the so called assemblage algorithm that is shown in Figure 2 (see example 4.4.3 too).

In the assemblage algorithm, the stiffness matrix of an element is decomposed into four blocks as shown in Figure 1 for the case of planar frames. The block 1 is constituted by positions with rows and columns corresponding to node  $i$ ; the block 2 includes positions whose rows still correspond to node  $i$  but the columns are related to node  $j$  and so forth.

Let  $(f_L, c_L)$  be the position of a component of the stiffness matrix  $[k]_b$  of the element; if this position corresponds to one of the block 1 (node  $i$ -node  $i$ ), then this component must be added to the component in the position  $(f_G, c_G)$  of the structure stiffness matrix  $[K]$ , where:

$$f_G = 3i + (f_L - 3); c_G = 3i + (c_L - 3); \quad (4.1.6)$$

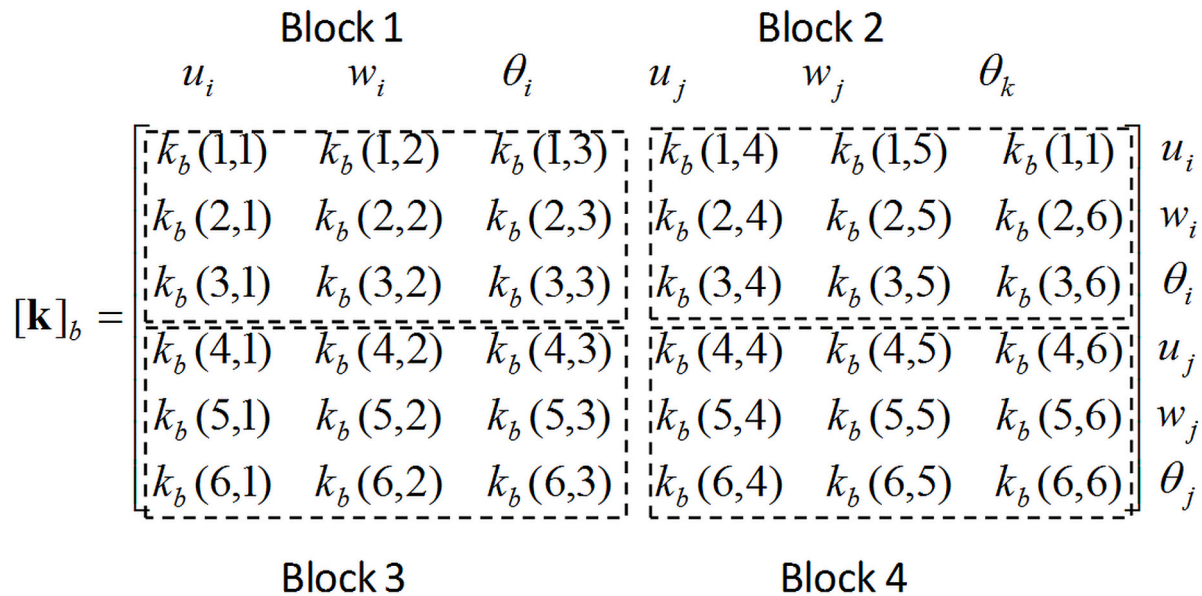
For the positions of block 2 (node  $i$ -node  $j$ ):

$$f_G = 3i + (f_L - 3); c_G = 3j + (c_L - 6); \quad (4.1.7)$$

In the block 3 (node  $j$ -node  $i$ ):

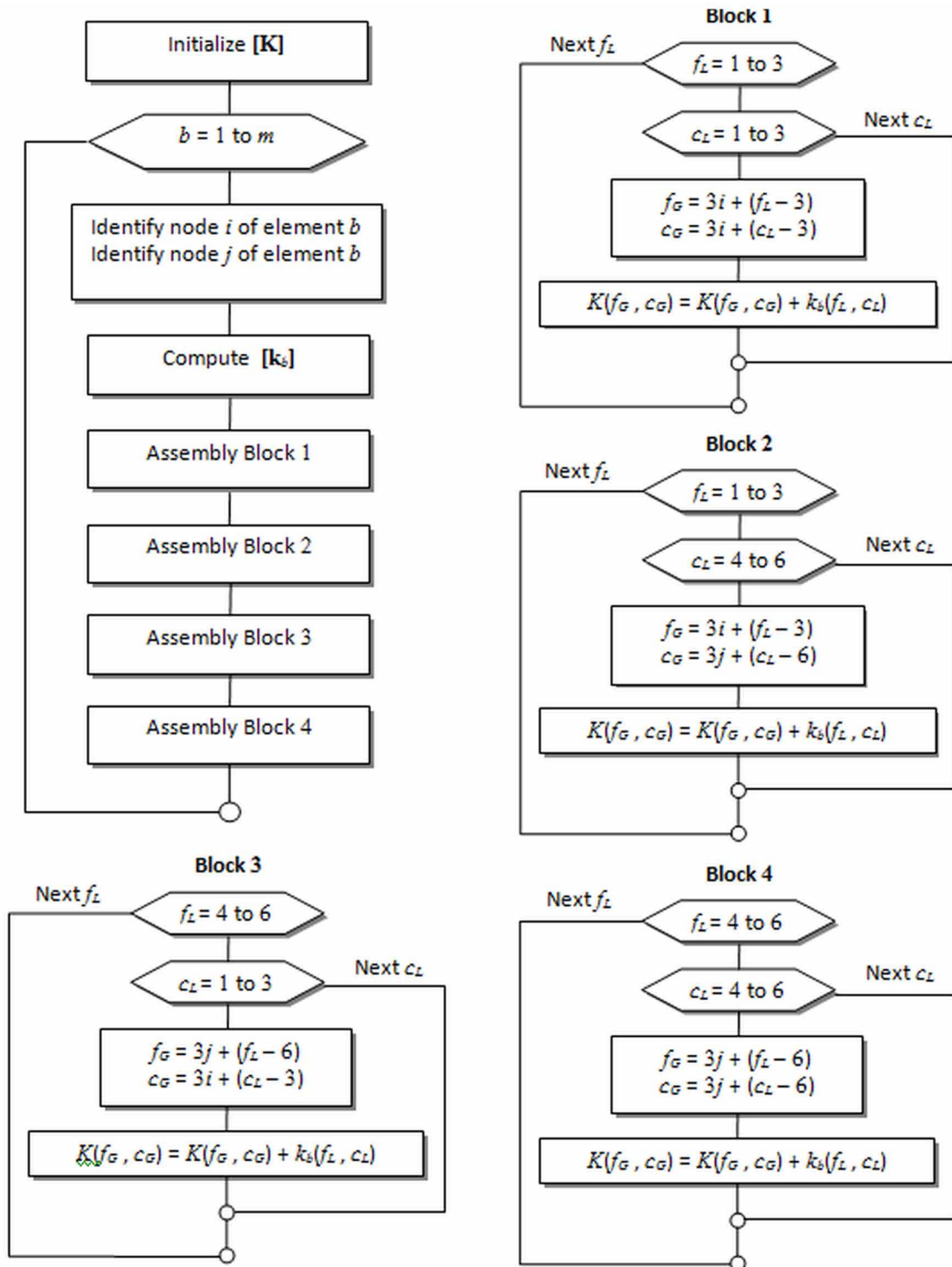
$$f_G = 3j + (f_L - 6); c_G = 3i + (c_L - 3); \quad (4.1.8)$$

Figure 1. Decomposition of the stiffness matrix of an element



## Analysis of Elastic Frames

Figure 2. Assemblage algorithm for the stiffness matrix for a planar frame



Finally, for the block 4 (node  $j$ -node  $j$ ):

$$f_G = 3j + (f_L - 6); c_G = 3j + (c_L - 6) \quad (4.1.9)$$

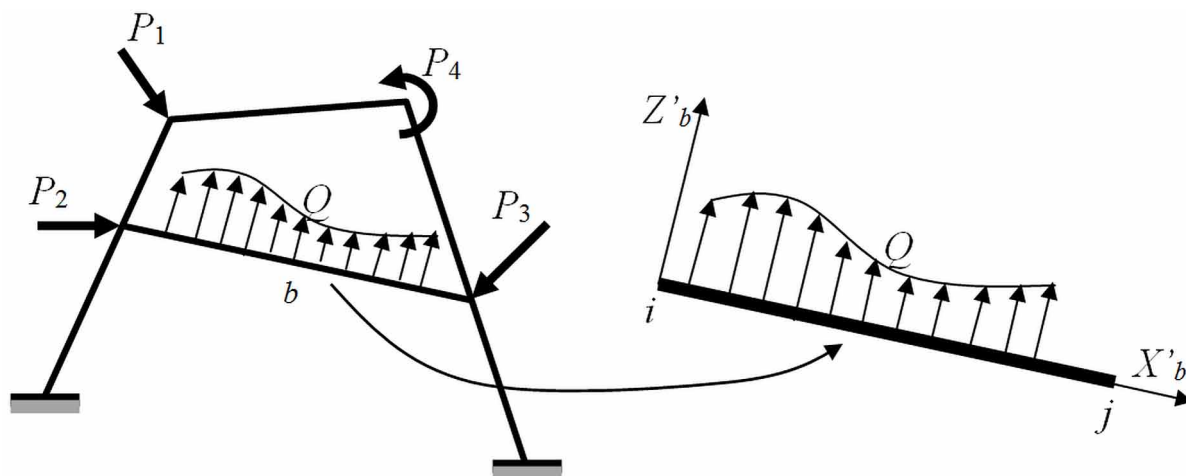
Notice that it is not necessary the assemblage of the entire matrix, specially the block 3, since stiffness matrices are symmetric. The stiffness matrix of the structure has also a special configuration: it is a band matrix; this means that the non-zero components of the matrix are confined to a diagonal band. Thus, it is not necessary neither the computation nor the storage of all its values, only those within the upper part of the band. In general finite element analysis, where structures with millions of elements are not uncommon, the consideration of these properties is very important; in framed structures, where tens of thousands elements are rare, this aspect of the numerical implementation is not so crucial.

### 4.1.3 Assemblage of the Matrix of Total Forces

Consider a frame element in the local coordinate system of reference as shown in Figure 3. Let  $\{\mathbf{p}^{le}\}_b$  be the non-expanded contribution of this element to the matrix of total forces in the local system of reference:

$$\{\mathbf{p}^{le}\}_b = \{\mathbf{p}^{leq}\}_b - [\mathbf{B}'^0]_b^t \{\mathbf{M}^0\}_b = \begin{bmatrix} p'_{wi} \\ p'_{wi} \\ p'_{\theta i} \\ p'_{wj} \\ p'_{wj} \\ p'_{\theta j} \end{bmatrix} \quad (4.1.10)$$

Figure 3. Frame element subjected to distributed forces

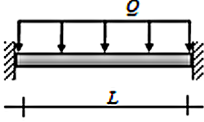
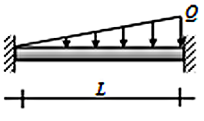
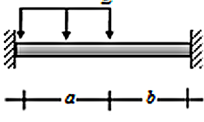
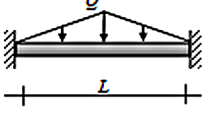


## Analysis of Elastic Frames

The components of the matrix  $\{\mathbf{p}'^e\}$  can be pre-computed for the most frequent types of distributed forces; they are included in Table 1 for the particular case of planar frames.

As aforementioned, the forces and moments in  $\{\mathbf{p}'^e\}_b$  are expressed in the local system of reference; in the global system, they are given by:

Table 1. Contributions to the total force matrix for typical cases of distributed forces on an element in a planar frame

Loading condition	Euler-Bernoulli Beams {P' <sup>e</sup> }	Timoshenko Beams {P' <sup>e</sup> }
	$\begin{bmatrix} 0 \\ -\frac{QL}{2} \\ \frac{QL}{2} \\ 0 \\ -\frac{QL}{2} \\ -\frac{QL}{2} \end{bmatrix}$	$\begin{bmatrix} 0 \\ -\frac{QL}{2} \\ \frac{QL}{2} \\ 0 \\ -\frac{QL}{2} \\ -\frac{QL}{2} \end{bmatrix}$
	$\begin{bmatrix} 0 \\ -\frac{QL}{6} \\ \frac{QL^2}{30} \\ 0 \\ -\frac{QL}{3} \\ -\frac{QL^2}{20} \end{bmatrix}$	$\begin{bmatrix} 0 \\ -\frac{QL}{6} \\ \frac{QL^2(L^2GA+15EI)}{30(L^2GA+12EI)} \\ 0 \\ -\frac{QL}{3} \\ -\frac{QL^2(L^2GA+10EI)}{20(L^2GA+12EI)} \end{bmatrix}$
	$\begin{bmatrix} 0 \\ -\frac{Q(L+b)}{2L} \\ \frac{Qa^2(-3aL+6L^2+3a^2)}{12L^2} \\ 0 \\ -\frac{Qa^2}{2L} \\ -\frac{Qa^2(4L-3a)}{12L^2} \end{bmatrix}$	$\begin{bmatrix} 0 \\ -\frac{Q(L+b)}{2L} \\ \frac{Qa^2(-3L^2GA+6L^2GA+3LGAa^2-24EIa+36LEI)}{12L(L^2GA+12EI)} \\ 0 \\ -\frac{Qa^2}{2L} \\ \frac{Qa^2(4L^2GA-3LGAa^2-24EIa+36LEI)}{12L(L^2GA+12EI)} \end{bmatrix}$
	$\begin{bmatrix} 0 \\ -\frac{QL}{4} \\ \frac{5QL^2}{96} \\ 0 \\ -\frac{QL}{4} \\ -\frac{5QL^2}{96} \end{bmatrix}$	$\begin{bmatrix} 0 \\ -\frac{QL}{4} \\ \frac{5QL^2}{96} \\ 0 \\ -\frac{QL}{4} \\ -\frac{5QL^2}{96} \end{bmatrix}$



$$\{\mathbf{p}^e\}_b = [\mathbf{T}]_b^t \{\mathbf{p}^{1e}\}_b \quad (4.1.11)$$

where  $[\mathbf{T}]_b$  is the geometrical transformation matrix introduced in chapter 3: Equation(3.1.5) for the planar case and Equation (3.5.6) for the tridimensional one.

This local contribution can be included into the matrix of total forces using the algorithm indicated in Figure 5 (see also example 4.5.4); in it, the matrix of the element forces is decomposed into two blocks, the first one includes the forces on node  $i$ , the second block those applied on node  $j$  (see Figure 4).

Let  $NL$  be the position of a component of the matrix  $\{\mathbf{p}^e\}_b$ ; if this position corresponds to one of the block 1 (node  $i$ ), then this component must be added to the component  $NG$  of the matrix of total forces  $\{\mathbf{F}\}$ , where:

$$NG = 3i + (NL - 3) \quad (4.1.12)$$

For the positions of block 2 (node  $j$ ):

$$NG = 3j + (NL - 6) \quad (4.1.13)$$

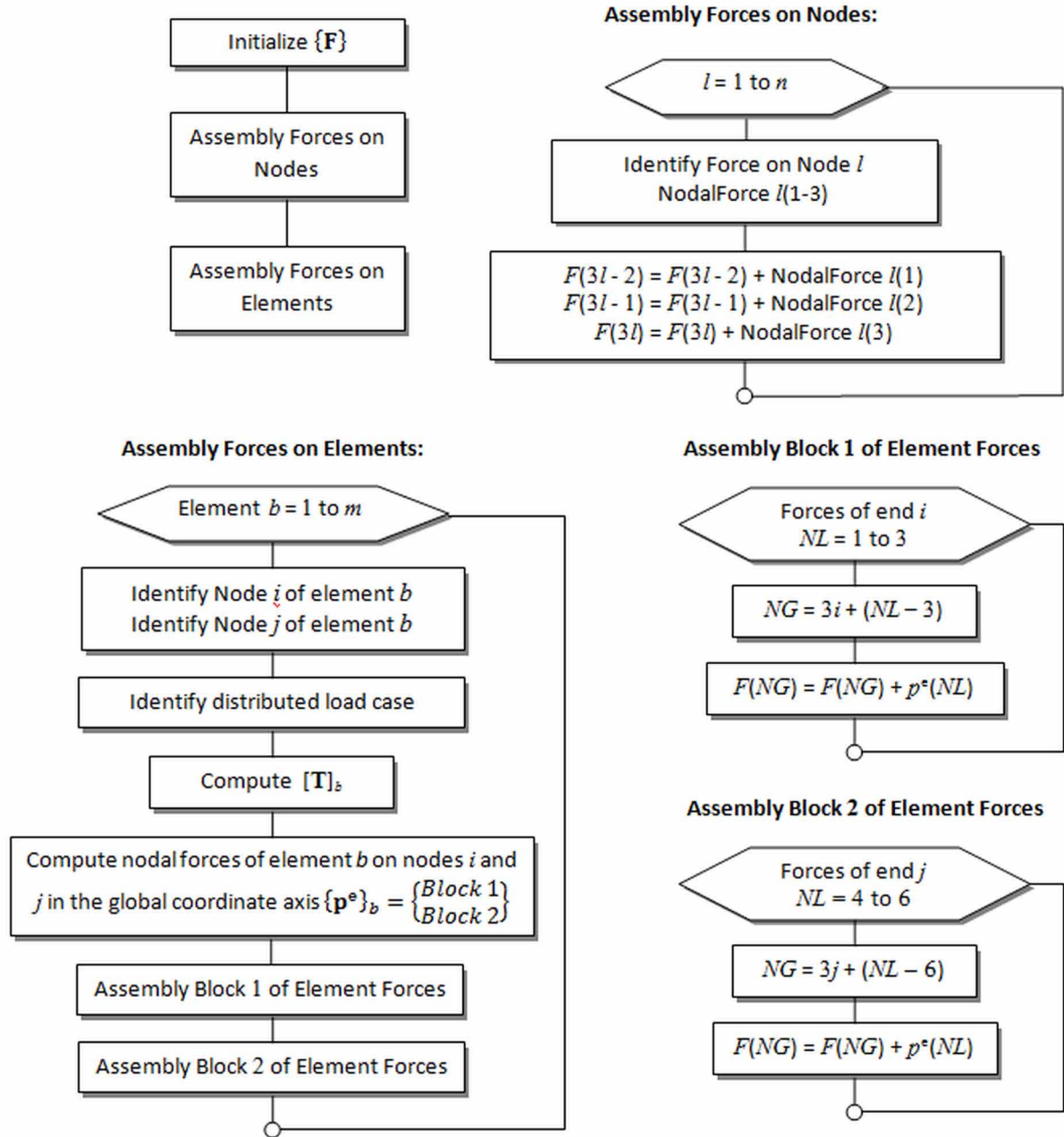
#### 4.1.4 Penalization Algorithm

In the conventional numerical analysis, there are several methods to solve linear system of equations in the form  $[\mathbf{A}]\{\mathbf{X}\} = \{\mathbf{B}\}$  if all the unknown are in the matrix  $\{\mathbf{X}\}$ . However the equations obtained by the direct stiffness method are not in this form since both, the matrix of generalized displacements and the matrix of generalized forces, include unknowns: respectively the free displacements and the reaction forces. In order to use the standards algorithms and routines to solve the frame problem, it is therefore necessary to transform the equilibrium equation  $[\mathbf{K}]\{\mathbf{U}\} = \{\mathbf{F}\}$  into the standard form. The simplest method to do so is the penalization algorithm.

Figure 4. Decomposition of the matrix of forces of an element

$$\{\mathbf{p}^e\}_b = \begin{array}{l} \left[ \begin{array}{l} p_b^e(1) \\ p_b^e(2) \\ p_b^e(3) \end{array} \right] \begin{array}{l} u_i \\ w_i \\ \theta_i \end{array} \\ \left[ \begin{array}{l} p_b^e(4) \\ p_b^e(5) \\ p_b^e(6) \end{array} \right] \begin{array}{l} u_j \\ w_j \\ \theta_j \end{array} \end{array} \quad \begin{array}{l} \text{Block 1} \\ \text{Block 2} \end{array}$$

Figure 5. Assemblage algorithm for the external forces



Be  $G$  a very large number and  $\bar{u}_i$  the imposed displacement in a support. This algorithm consists in modifying the stiffness matrix and force matrix in the following form:

$$\begin{bmatrix} K_{11} & \cdots & K_{1i} & \cdots & K_{1l} \\ \vdots & & \vdots & & \vdots \\ K_{i1} & \cdots & K_{ii} + G & \cdots & K_{il} \\ \vdots & & \vdots & & \vdots \\ K_{n1} & \cdots & K_{ni} & \cdots & K_{nl} \end{bmatrix} \begin{Bmatrix} u_1 \\ \vdots \\ u_i \\ \vdots \\ \theta_l \end{Bmatrix} = \begin{Bmatrix} F_{u1} \\ \vdots \\ \bar{u}_i G \\ \vdots \\ F_{\theta l} \end{Bmatrix} \quad (4.1.14)$$

This manipulation of the system must be repeated for each one of the restricted displacements. Now, solving  $u_i$  when  $G$  tends to infinite gives:

$$u_i = \lim_{G \rightarrow \infty} \frac{\bar{u}_i G - K_{i1}u_1 - \dots - K_{il}\theta_l}{K_{ii} + G} = \bar{u}_i \quad (4.1.15)$$

In practice it is sufficient to choose a value for  $G$  very large, typically  $G = 10^{4-10} K_{ii}$ .

Once the unknown displacements have been obtained, the reactions can be computed with the unmodified equilibrium equation.

## 4.2 STATIC ANALYSIS OF NONLINEAR ELASTIC FRAMES

### 4.2.1 Step by Step Procedures

Structures are subjected to external actions that are not constant in time. For instance, a building may be subjected first to service loads, then to the actions of an unusually strong wind and after that, to seismic forces.

In this section, the problem is again formulated in terms of the same variables but, unlike section 4.1, they are now considered as functions of time; in this way it is possible to consider the variations of the external actions in a single analysis. The variables are defined in a time interval that is arbitrarily fixed between zero and a final instant  $T$ :

$$\begin{aligned} \{\mathbf{U}\} &= \{\mathbf{U}(t)\}; \{\Phi\}_b = \{\Phi(t)\}_b; \{\mathbf{P}\} = \{\mathbf{P}(t)\}; \{\mathbf{M}\}_b = \{\mathbf{M}(t)\}_b; \\ \text{for } 0 \leq t \leq T; \{\Phi\}_b &= \{\Phi(t)\}_b \end{aligned} \quad (4.2.1)$$

It is postulated that the values of the free displacements, deformations, reaction forces and stresses are known at the time  $t = 0$ .

The kinematic equations, equilibrium equations and constitutive law are now written in the more general nonlinear form:

$$\{d\Phi\}_b = [\mathbf{B}_E(\mathbf{U})]_b \{d\mathbf{U}\}$$

## Analysis of Elastic Frames

$$\sum_{b=1}^m [\mathbf{B}(\mathbf{U})_E]_b^t \{\mathbf{M}\}_b = \{\mathbf{P}\}$$

$$\{\mathbf{M}\}_b = [\mathbf{E}]_b \{\Phi\}_b + \{\mathbf{M}^0\}_b \quad (4.2.2)$$

This problem can be solved using a step by step procedure; this means that the continuum time interval  $[0, T]$  is substituted by a set of particular instants chosen by the analyst:  $(0, t_1, t_2, \dots, t_r, \dots, T)$ . Then, instead of computing the functions (4.2.1), only the values of the variables for these particular instants are calculated. This algorithm is called step by step because the values are computed sequentially; that is, the unknowns are first calculated at the instant  $t_1$ , then at  $t_2$  and so on until that the final time  $T$  is reached.

The kinematic equation (4.2.2a) is discretized using a finite difference scheme, i.e. this differential equation is substituted by the following algebraic one:

$$\{\Delta\Phi\}_b = \{\Phi_{t=t_r} - \Phi_{t=t_{r-1}}\} \cong [\mathbf{B}_E(\mathbf{U}_{t=t_r})]_b \{\Delta\mathbf{U}\} \quad (4.2.3)$$

In this expression the terms at the instant  $t_{r-1}$  are known, they were computed at the precedent step, and only the values at the instant  $t_r$  have to be calculated. Notice that the kinematic transformation matrix is not known since it depends on the unknown displacements; in the numerical analysis textbooks, this kind of procedure is called implicit.

Notice that the approximation (4.2.3) improves as the size of the time step ( $\Delta t = t_r - t_{r-1}$ ) decreases; i.e. for tiny time steps, the differential equation (4.2.2a) and the algebraic one (4.2.3) give almost the same results; on the other hand, large time steps may produce significant differences between both expressions. The analyst must find a satisfactory compromise between precision and computer cost for each specific application.

### 4.2.2 The Nonlinear Incremental Equilibrium Equation in Displacements

In most practical applications, distributed forces on the elements represent the so called service loads; they are used to characterize the dead weight and the live loads of the structure. Exceptional overloads such as earthquake forces (in the static equivalent method), settlement of foundations, explosions, wind loads, and so on, are frequently represented as nodal forces or displacements. Usually, a structure under service loads only does not need nonlinear analysis; on the other hand, overloads may represent a significant demand on the structure that may require not only nonlinear but inelastic analyses as well.

Starting from this section and in the rest of the book, the distributed forces are assumed to be relatively small, applied in the first step and kept constant throughout the rest of the analysis. For the subsequent steps, the constitutive law (4.2.2c) can be written as:

$$\{\Delta\mathbf{M}\}_b = \{\mathbf{M}_{t=t_r} - \mathbf{M}_{t=t_{r-1}}\} \cong [\mathbf{E}]_b \{\Delta\Phi\}_b \cong [\mathbf{E}]_b [\mathbf{B}_E(\mathbf{U}_{t=t_r})]_b \{\Delta\mathbf{U}\}; \text{ for } r > 1 \quad (4.2.4)$$

Substitution of (4.2.4) into (4.2.2b) gives:

$$[\mathbf{K}(\mathbf{U}_{t=t_r})]\{\Delta\mathbf{U}\} = \{\Delta\mathbf{F}(\mathbf{U}_{t=t_r})\} \quad (4.2.5)$$

where

$$[\mathbf{K}(\mathbf{U}_{t=t_r})] = \sum_{b=1}^m [\mathbf{B}(\mathbf{U}_{t=t_r})_E]_b^t [\mathbf{E}]_b [\mathbf{B}(\mathbf{U}_{t=t_r})_E]_b^t; \{\Delta\mathbf{F}\} = \{\mathbf{P}_{t=t_r}\} - \sum_{b=1}^m [\mathbf{B}(\mathbf{U}_{t=t_r})_E]_b^t \{\mathbf{M}_{t=t_{r-1}}\}_b ;$$

Notice that Equation (4.2.5) is quite similar to its equivalent in the direct stiffness method except that the stiffness matrix and the increment of total forces cannot be computed directly since they depend on the unknown displacements.

### 4.2.3 Resolution of the Nonlinear Equilibrium Equation by the Direct Iteration Method

The direct iteration method is a well-known algorithm for solving nonlinear equations. First, a provisional or trial solution  $\{\mathbf{U}_p\}$  is chosen by some adequate criterion. Then, approximations of the stiffness matrices and the increment of total forces are computed using the same assemblage algorithms described in section (4.1). Next, an improved solution  $\{\mathbf{U}_I\}$  is obtained by solving the following linear approximation of (4.2.5):

$$[\mathbf{K}(\mathbf{U}_p)]\{\mathbf{U}_I - \mathbf{U}_{t=t_{r-1}}\} = \{\Delta\mathbf{F}(\mathbf{U}_p)\} \quad (4.2.6)$$

This process must be repeated using as provisional solution the improved solution of the previous iteration. The process can be stopped when improved and provisional solutions are indistinguishable; when this happens, it is said that the process has converged. Possible convergence criteria can be:

$$\{\mathbf{U}_I\} - \{\mathbf{U}_p\} \cong 0; \text{ and/or } [\mathbf{K}(\mathbf{U}_I)]\{\mathbf{U}_I - \mathbf{U}_{t=t_{r-1}}\} - \{\Delta\mathbf{F}(\mathbf{U}_I)\} \cong 0 ; \quad (4.2.7)$$

The left hand term in the second expression in (4.2.7) is called residual forces and corresponds to the difference between internal and external forces. The exact solution has been found when the residual forces are equal to zero. Again, the acceptable difference between both solutions in (4.2.7a) and/or the tolerable values in the residual forces (4.2.7b) must be decided by the user for each specific application.

A flux diagram of this algorithm is shown in Figure 7. See also example 4.5.5.

A graphical interpretation in the case of a structure with only one displacement and without distributed forces is included in Figure 6. In this figure two iterations are presented. In the first one (Figure 6a) a trial displacement  $U_p$  far away from the solution is chosen, then the slope  $K(U_p)$  is computed and the improved displacement  $U_I$  is obtained. Notice that the improved displacement is closer to the solution than the trial displacement. In the second iteration (Figure 6b), the new trial displacement is the improved one obtained in the precedent iteration. A new slope is computed and a new improved displacement is obtained and so on.

## Analysis of Elastic Frames

Figure 6. Graphical interpretation of the direct iteration method

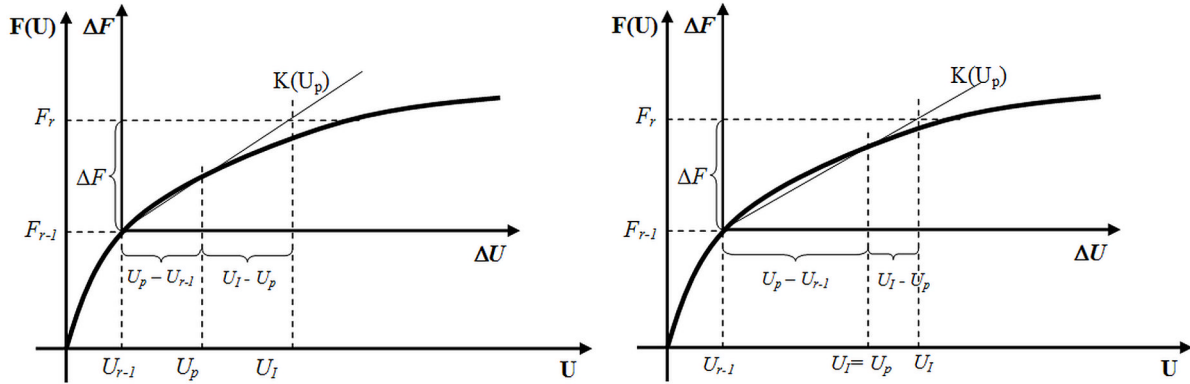
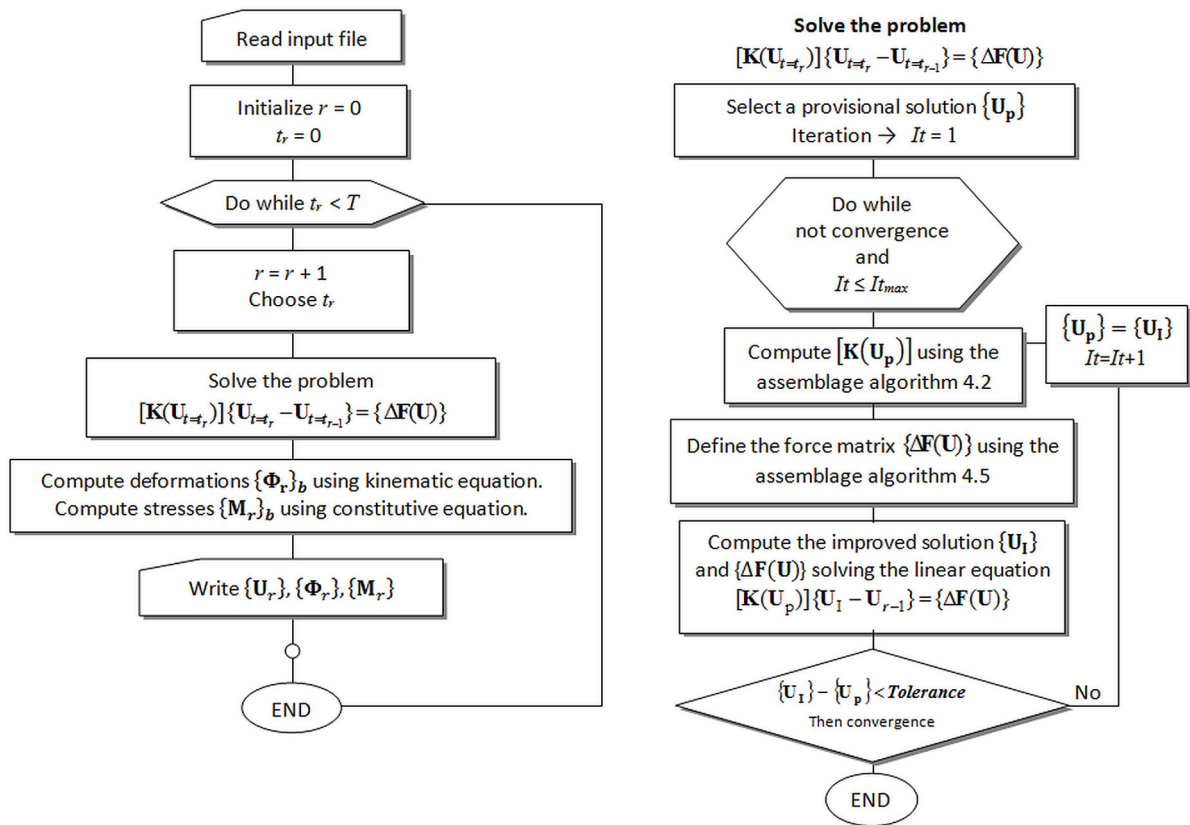


Figure 7. Flux diagram of the direct iteration method



This procedure is not always convergent; i.e. not always “improved” displacements are closer to the solution than the provisional ones. This may be the case if the size of the time steps ( $t_r - t_{r-1}$ ) is too large. Thus, the analyst must establish a maximum number of iterations in order to avoid an infinite loop. If this limit is reached, it is necessary to restart the process with a smaller time step. Instead of asking the user

for a new time step, computer programs for nonlinear analysis of structures should have implemented this process automatically. That is, if the iteration process fails to converge, then the program should reduce automatically the time step and it should try to solve the incremental equilibrium equation again. The user can control this process by fixing the reduction percentage of the time step. This process of time step reduction must be repeated until convergence is achieved. Again, the analyst must establish a maximum number of time step reductions in order to avoid another infinite loop; if that limit is reached the program should renounce solving the problem and so inform the analyst. Very often failure of convergence is due to errors in the data of the problem.

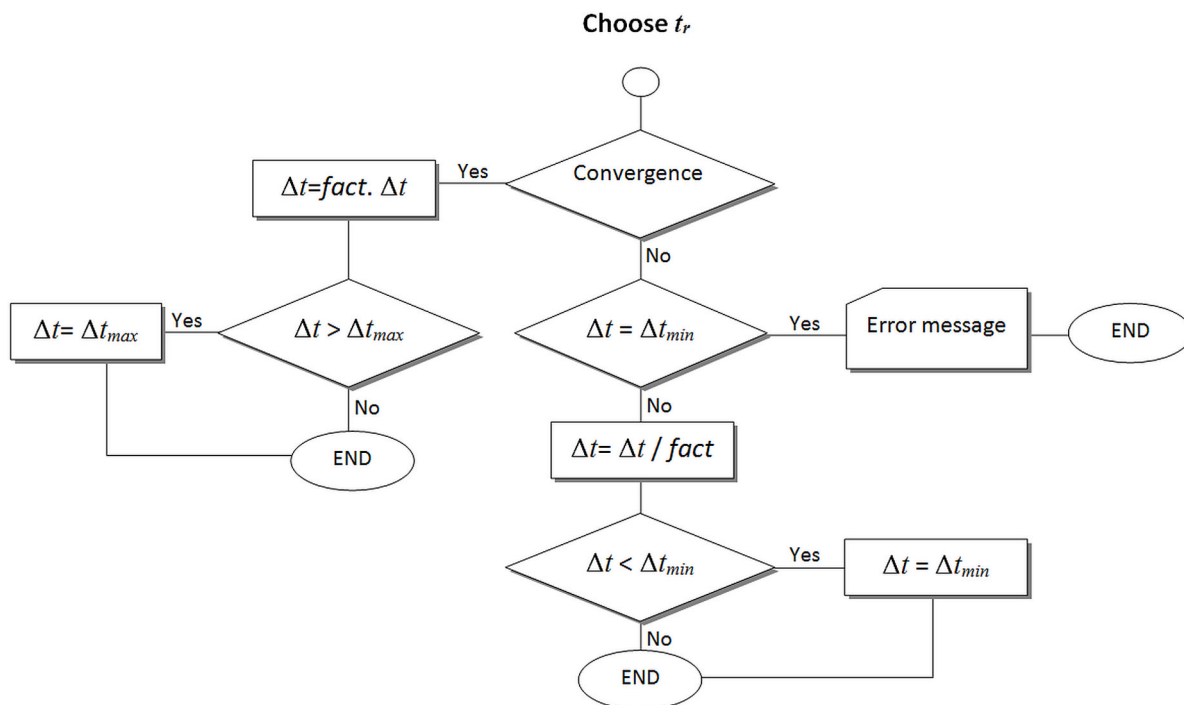
If the algorithm converges adequately after a time step reduction, then the program should automatically augment progressively the step sizes until the original value chosen by the analyst is reached. An algorithm of time steps adjustment is shown in Figure 8. In this figure,  $fact$  is the factor of increment or reduction of the time increment step; naturally  $fact > 1$ .  $\Delta t_{max}$  and  $\Delta t_{min}$  are the limits established by the user for admissible time step sizes.

#### 4.2.4 Criteria for Selecting Provisional Solutions

Notice that the first action in the flux diagram of Figure 7b is choosing the first provisional solution; there are several possibilities for that. The simplest criterion is to choose the last convergent solution; i.e. let  $r$  be the current time step, then:  $\{U_p\} = \{U_{t=t_{r-1}}\}$ .

A better option is to use a quadratic predictor from the three last steps. Let  $w_i^p$  be any component of the first provisional solution at the instant  $t_r$ , then:

Figure 8. Flux diagram of time steps adjustments



## Analysis of Elastic Frames

$$w_i^p = a.t_r^2 + b.t_r + c \quad (4.2.8)$$

where the parameters  $a$ ,  $b$ , and  $c$  are computed by the resolution of the following system of linear equations:

$$\begin{aligned} w_i(t_{r-1}) &= a.t_{r-1}^2 + b.t_{r-1} + c \\ w_i(t_{r-2}) &= a.t_{r-2}^2 + b.t_{r-2} + c; \text{ i.e.} \\ w_i(t_{r-3}) &= a.t_{r-3}^2 + b.t_{r-3} + c \end{aligned} \quad \begin{bmatrix} a \\ b \\ c \end{bmatrix} = \begin{bmatrix} t_{r-1}^2 & t_{r-1} & 1 \\ t_{r-2}^2 & t_{r-2} & 1 \\ t_{r-3}^2 & t_{r-3} & 1 \end{bmatrix}^{-1} \begin{bmatrix} w_i(t_{r-1}) \\ w_i(t_{r-2}) \\ w_i(t_{r-3}) \end{bmatrix} \quad (4.2.9)$$

Remember that the precedent values of displacement at times  $t_{r-1}$ ,  $t_{r-2}$  and  $t_{r-3}$  are already known when the first provisional solution  $\{\mathbf{U}_p\}$  at time  $t_r$  is needed. In the three first steps of the analysis, where three previous values of displacements are not available, a linear predictor or the last result can be used.

### 4.2.5 The Newton-Raphson method

The Newton-Raphson method is another well-known iterative algorithm for solving nonlinear equations. Consider again the equilibrium equation at the instant  $t_r$ :

$$\{\mathbf{L}(\mathbf{U}_{t=t_r})\} = \{\mathbf{P}_{t=t_r}\}; \text{ where } \{\mathbf{L}(\mathbf{U}_{t=t_r})\} = \sum_{b=1}^m [\mathbf{B}(\mathbf{U}_{t=t_r})_E]_b^t \{\mathbf{M}(\mathbf{U}_{t=t_r})\}_b \quad (4.2.10)$$

Notice that, as shown in the precedent sections, the internal forces  $\{\mathbf{L}(\mathbf{U})\}$  in the left hand term of (4.2.10) can be expressed as a function of the displacements. In the Newton-Raphson method, the internal forces  $\{\mathbf{L}(\mathbf{U})\}$  are linearized around the provisional solution; i.e. they are approximated by the closest linear function of displacements:

$$\{\mathbf{L}(\mathbf{U})\} \cong \left[ \frac{\partial \mathbf{L}}{\partial \mathbf{U}} \right]_{U=U_p} \{\mathbf{U} - \mathbf{U}_p\} \quad (4.2.11)$$

Then the improved solution  $\{\mathbf{U}_I\}$  is obtained by solving the linear approximation of Equation (4.2.10):

$$\{\mathbf{L}(\mathbf{U})\} \cong \left[ \frac{\partial \mathbf{L}}{\partial \mathbf{U}} \right]_{U=U_p} \{\mathbf{U}_I - \mathbf{U}_p\} = \{\mathbf{P}\} \Rightarrow \{\mathbf{U}_I\} = \left[ \frac{\partial \mathbf{L}}{\partial \mathbf{U}} \right]_{U=U_p}^{-1} \{\mathbf{P}\} + \{\mathbf{U}_p\} \quad (4.2.12)$$

The term  $\left[ \frac{\partial \mathbf{L}}{\partial \mathbf{U}} \right]$  is the tangent stiffness matrix of the structure and its computation is described in the next section; in mathematics textbook, this kind of matrix is called the Jacobian of the operator  $\{\mathbf{L}(\mathbf{U})\}$ . Notice that in the linear case, the Jacobian is equal to the stiffness matrix  $[\mathbf{K}]$ . A flux diagram of this algorithm is shown in Figure 9 and a graphical interpretation in Figure 10.



### 4.2.6 Computation of the Tangent Stiffness Matrix

The contribution of a single element to the internal forces  $\{\mathbf{L}(\mathbf{U})\}$  in the non-expanded form is given by:

$$\{\mathbf{Q}(\mathbf{q})\}_b = [\mathbf{B}(\mathbf{q})]_b^t \{\mathbf{M}(\mathbf{q})\}_b \quad (4.2.13)$$

Figure 9. Flux diagram of the NewtonRaphson method

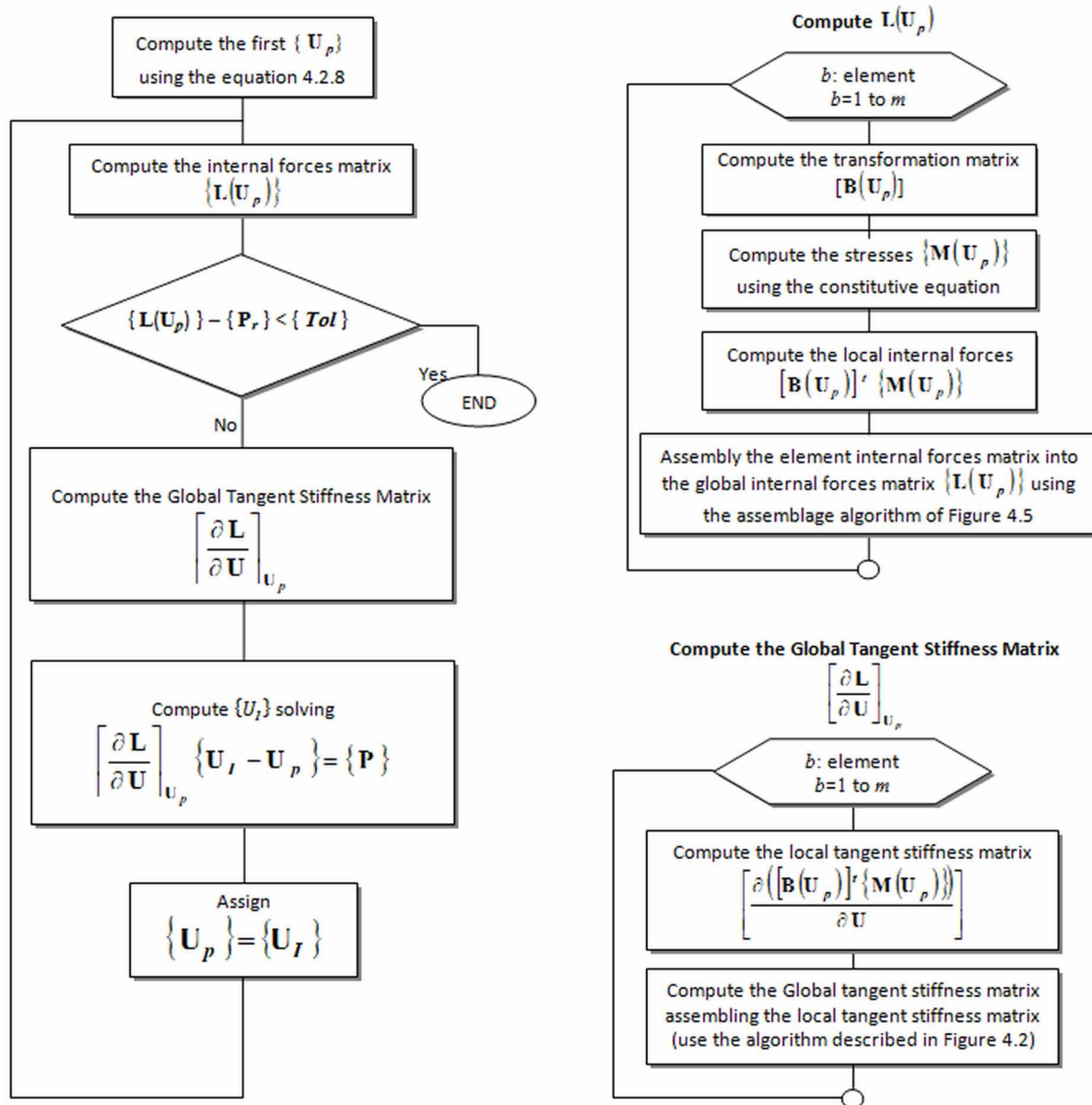
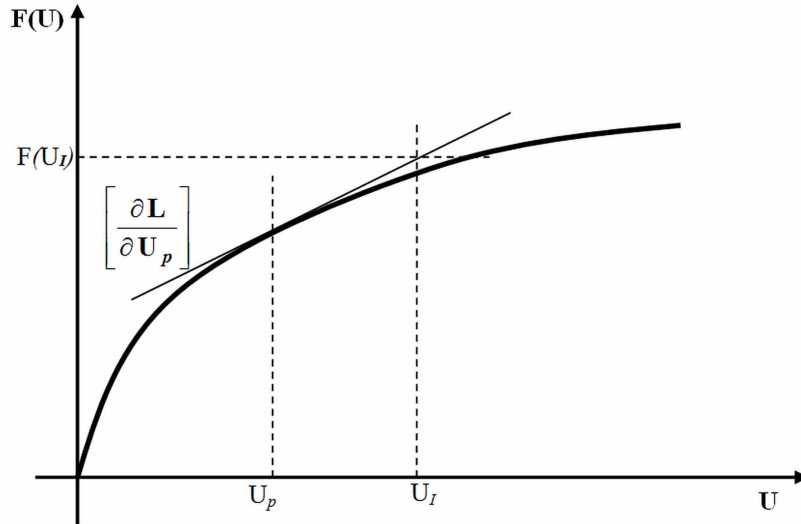


Figure 10. Graphical interpretation of the NewtonRaphson method



where the column matrix  $\{\mathbf{Q}(\mathbf{q})\}_b$  has six components for a planar frame member and twelve for a tri-dimensional one. Therefore, the contribution of the element to the Jacobian in non-expanded form is:  $\left[ \frac{\partial \mathbf{Q}}{\partial \mathbf{q}} \right]_b$ . This matrix is called tangent stiffness matrix of element  $b$ . The simplest procedure for its computation is to use a finite difference approximation; let  $Q_{ui}$  be any component of the matrix  $\{\mathbf{Q}(\mathbf{q})\}_b$  and  $w_j$  any displacement of the matrix  $\{\mathbf{q}\}_b$ , then:

$$\frac{\partial Q_{ui}}{\partial w_j} \cong \frac{Q_{ui}(u_i, \dots, w_j + \Delta w, \dots) - Q_{ui}(\mathbf{q})}{\Delta w} \quad (4.2.14)$$

where  $\Delta w$  is any “small” increment of displacement. Good values for  $\Delta w$  are  $10^{-3}$  or  $10^{-4}$  times any typical displacement of the frame.

Once the local tangent stiffness matrix has been computed, it can be assembled into the Jacobian using the algorithm described in section 4.1.2.

The local tangent stiffness matrix can also be determined in an exact way by carrying out analytically the derivatives  $\left[ \frac{\partial \mathbf{Q}}{\partial \mathbf{q}} \right]_b$ .

### 4.3 DYNAMIC ANALYSIS OF ELASTIC FRAMES

In the case of structures subjected to earthquake loadings, impacts or explosions on a structure, the external actions are of dynamical nature; this means that the inertial forces are no longer negligible and must also be taken into consideration. In this case the problem is formulated as follows:

$$\{d\Phi\}_b = [\mathbf{B}_E(\mathbf{U})]_b \{d\mathbf{U}\}$$

$$\sum_{b=1}^m [\mathbf{B}_E]_b^t \{\mathbf{M}\}_b + [\mathbf{Mass}] \{\ddot{\mathbf{U}}\} = \{\mathbf{P}\}$$

$$\{\mathbf{M}\}_b = [\mathbf{E}]_b \{\Phi\}_b + \{\mathbf{M}^0\}_b \tag{4.3.1}$$

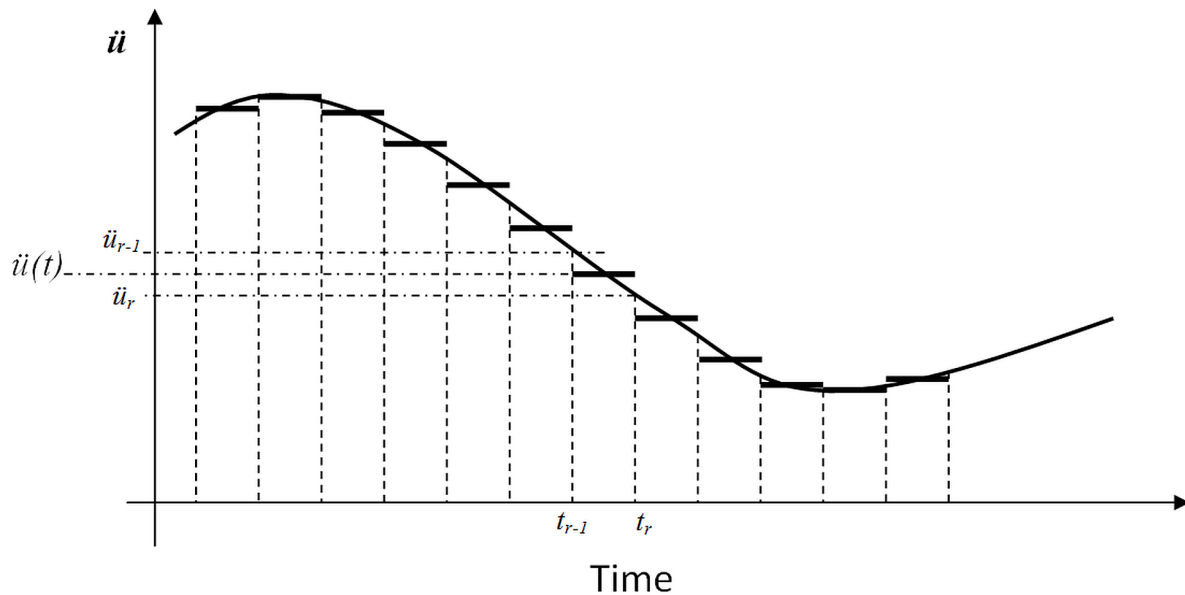
The problem is solved using again a step by step procedure. The kinematic equation is also discretized as described in section 4.2.1 (Equation 4.2.3); but now the equilibrium equation includes the generalized acceleration matrix  $\{\ddot{\mathbf{U}}\}$ . This equation can be discretized using the Constant Average Acceleration algorithm that is described next.

Consider a component  $\ddot{u}$  of the generalized acceleration matrix; the history of acceleration is approximate by a piecewise constant function as shown in Figure 11. Each value of the function is computed as the average of the values at the ends of the actual acceleration function:

$$\ddot{u}(t) \cong \frac{\ddot{u}_{t=t_r} + \ddot{u}_{t=t_{r-1}}}{2}; \quad t_{r-1} < t < t_r \tag{4.3.2}$$

Thus, the velocity and displacement at the end of the interval  $t_{r-1} < t < t_r$  can be computed after integration in time of (4.3.2) by:

Figure 11. Approximation of an acceleration history by a piecewise constant function



### **Analysis of Elastic Frames**

$$\begin{aligned} \dot{u}_{t_r} &\cong \dot{u}_{t_{r-1}} + \frac{\Delta t}{2} (\ddot{u}_{t_r} + \ddot{u}_{t_{r-1}}); \text{ where } \Delta t = t_r - t_{r-1}; u_{t_r} \cong u_{t_{r-1}} + \Delta t \dot{u}_{t_{r-1}} \\ &+ \frac{\Delta t^2}{4} (\ddot{u}_{t_r} + \ddot{u}_{t_{r-1}}) \end{aligned} \quad (4.3.3)$$

The acceleration at the end of the interval can be obtained from the second equation of (4.3.3):

$$\ddot{u}_{t_r} \cong \frac{4}{\Delta t^2} (u_{t_r} - u_{t_{r-1}}) - \frac{4\dot{u}_{t_{r-1}}}{\Delta t} - \ddot{u}_{t_{r-1}} \quad (4.3.4)$$

Taking into account the nature of the step by step procedure, all the quantities at the instant of time  $t_{r-1}$  have already been computed when the structure is analyzed at the instant  $t_r$ ; thus, the acceleration matrix at that instant can be expressed as a function of the displacement at  $t_r$  by the use of (4.3.4) for each component of the matrix. Therefore, the discretized form of the equilibrium equation does not depend on the acceleration but only on the displacements, stresses and external forces at the instant  $t_r$ :

$$\{\mathbf{L}(\mathbf{U}_{t_r})\} = \{\mathbf{P}_{t_r}\} \text{ where } \{\mathbf{L}(\mathbf{U}_{t_r})\} = \sum_{b=1}^m [\mathbf{B}(\mathbf{U}_{t_r})_E]_b^t \{\mathbf{M}(\mathbf{U}_{t_r})\}_b + [\mathbf{Mass}] \{\ddot{\mathbf{U}}(\mathbf{U}_{t_r})\} \quad (4.3.5)$$

Notice that the left hand term of (4.3.5) corresponds now to the internal plus the inertia forces. This nonlinear equation can be solved using the Newton-Raphson method again; the Jacobian matrix does not correspond to the tangent stiffness in this case because an additional term related to the inertia forces has to be included. This supplementary term is a diagonal matrix whose components can be computed easily by the analytical determination of the corresponding derivatives.

Notice that the intervals  $[t_{r-1}, t_r]$  should be chosen sufficiently small because of the approximations made to discretize the kinematic and equilibrium equations.

## **4.4 SUMMARY AND EQUATIONS QUICK REFERENCE**

The method of the direct stiffness is obtained by the combination of the linear versions of the kinematic, equilibrium and constitutive equations. As a result, it is obtained a stiffness matrix and a external forces matrix. The generalized displacements and reactions can be computed by the resolution of this linear matrix equation.

A more precise analysis derives from the use of the nonlinear version of kinematic and equilibrium equations. If such is the case, some numerical algorithm such as the direct iteration or the Newton-Raphson methods have to be used.

In the case of nonlinear dynamic analysis, a step by step procedure is needed. Then, accelerations are approximated using values of displacements at the beginning and the end of each step. Again the Newton-Raphson method is needed to solve the problem (See Table 2).

Table 2.

<b>THE DIRECT STIFFNESS METHOD</b>	
<i>Stiffness Matrix of a Frame and Matrix of Total Forces</i>	
Kinematic equation $\{\Phi\}_b = [B_E^0]_b \{U\}$ (4.1.1 a)	
Equilibrium equation $\sum_{b=1}^m [B_E^0]_b^t \{M\}_b = \{P^n\} + \{P^{eq}\}$ (4.1.1 b)	
Constitutive equation $\{M\}_b = [E]_b \{\Phi\}_b + \{M^0\}_b$ (4.1.1 c)	
<p>Problem to solve:</p> <p><math>\{U\}</math> : displacements matrix</p> <p><math>[K]</math> : stiffness matrix of the structure</p> <p><math>[k_E]_b</math> : stiffness matrix of element <math>b</math></p> <p><math>[E]_b</math> : elasticity matrix of the element <math>b</math></p> <p><math>\{F\}</math> : matrix of total forces</p> <p><math>\{P^n\}</math> : external forces applied directly on the nodes;</p> <p><math>\{P^e\}</math> : external forces distributed over the element</p>	<p><math>[K]\{U\} = \{F\}</math> (4.1.2)</p> <p><math>[K] = \sum_{b=1}^m [B_E^0]_b^t [E]_b [B_E^0]_b = \sum_{b=1}^m [k_E]_b</math> (4.1.3 a -b)</p> <p><math>[k_E]_b = [B_E^0]_b^t [E]_b [B_E^0]_b</math> (4.1.3 c)</p> <p><math>\{F\} = \{P^n\} + \{P^e\}</math> (4.1.4 a)</p> <p><math>\{P^e\} = \{P^{eq}\} - \sum_{b=1}^m [B_E^0]_b^t \{M^0\}_b</math> (4.1.4 b)</p> <p>The terms <math>\{P^n\}</math> and <math>\{P^{eq}\}</math> were defined in the previous chapter (section 3.2.3)</p>
<i>Assemblage of the Stiffness Matrix of the Structure</i>	
<p><math>[k]_b</math> : non-expanded stiffness matrix</p> <p><math>[k]_b = [B^0]_b^t [E]_b [B^0]_b</math> (4.1.5)</p>	
<i>Assemblage of the Matrix of Total Forces</i>	
<p><math>\{P^{le}\}_b</math> : non-expanded contribution of this element to the matrix of total forces in the local system of reference</p> <p><math>\{P^e\}_b</math> : non-expanded contribution of this element to the matrix of total forces in the global system of reference</p> <p><math>[T]_b</math> : geometry transformation matrix</p>	<p><math>\{P^{le}\}_b = \{P^{leq}\}_b - [B^{l0}]_b^t \{M^0\}_b = \begin{bmatrix} p'_{ui} \\ p'_{wi} \\ p'_{\theta i} \\ p'_{uj} \\ p'_{wj} \\ p'_{\theta j} \end{bmatrix}</math> (4.1.10)</p> <p><math>\{P^e\}_b = [T]_b^t \{P^{le}\}_b</math> (4.1.11)</p>

continued on following page

## Analysis of Elastic Frames

Table 2. Continued

STATIC ANALYSIS OF NONLINEAR ELASTIC FRAME	
<i>Step by Step Procedures</i>	
Variables expressed as functions of time $\{\mathbf{U}\} = \{\mathbf{U}(t)\}; \{\Phi\}_b = \{\Phi(t)\}_b$ (4.2.1) $\{\mathbf{P}\} = \{\mathbf{P}(t)\}; \{\mathbf{M}\}_b = \{\mathbf{M}(t)\}_b$ for $0 \leq t \leq T$	
Kinematic equation $\{d\Phi\}_b = [\mathbf{B}_E(\mathbf{U})]_b \{d\mathbf{U}\}$ (4.2.2 a)	
Equilibrium equation $\sum_{b=1}^m [\mathbf{B}(\mathbf{U})_E]_b^t \{\mathbf{M}\}_b = \{\mathbf{P}\}$ (4.2.2 b)	
Constitutive Law $\{\mathbf{M}\}_b = [\mathbf{E}]_b \{\Phi\}_b + \{\mathbf{M}^0\}_b$ (4.2.2 c)	
Kinematic equation discretized using a finite difference scheme $\{\Delta\Phi\}_b = \{\Phi_{t=t_r} - \Phi_{t=t_{r-1}}\} \cong [\mathbf{B}_E(\mathbf{U}_{t=t_r})]_b \{\Delta\mathbf{U}\}$ (4.2.3)	
<i>The Nonlinear Incremental Equilibrium Equation in Displacements</i>	
Constitutive law $\{\Delta\mathbf{M}\}_b = \{\mathbf{M}_{t=t_r} - \mathbf{M}_{t=t_{r-1}}\} \cong [\mathbf{E}]_b \{\Delta\Phi\}_b \cong [\mathbf{E}]_b [\mathbf{B}_E(\mathbf{U}_{t=t_r})]_b \{\Delta\mathbf{U}\}$ ; for $r > 1$ (4.2.4)	
Equation to solve $[\mathbf{K}(\mathbf{U}_{t=t_r})] \{\Delta\mathbf{U}\} = \{\Delta\mathbf{F}(\mathbf{U}_{t=t_r})\}$ (4.2.5) where: $[\mathbf{K}(\mathbf{U}_{t=t_r})] = \sum_{b=1}^m [\mathbf{B}(\mathbf{U}_{t=t_r})_E]_b^t [\mathbf{E}]_b [\mathbf{B}(\mathbf{U}_{t=t_r})_E]_b; \{\Delta\mathbf{F}\} = \{\mathbf{P}_{t=t_r}\} - \sum_{b=1}^m [\mathbf{B}(\mathbf{U}_{t=t_r})_E]_b^t \{\mathbf{M}_{t=t_{r-1}}\}_b$ ;	
<i>Resolution of the Nonlinear Equilibrium Equation by The Direct Iteration Method</i>	
4) Choose a provisional solution $\{\mathbf{U}_P\}$ . Compute approximations of stiffness matrices and total forces.  5) Determination of an improved solution $\{\mathbf{U}_I\}$ solving: 6) Repeat this procedure using the convergence criteria:	$[\mathbf{K}(\mathbf{U}_p)] \{\mathbf{U}_I - \mathbf{U}_{t=t_{r-1}}\} = \{\Delta\mathbf{F}(\mathbf{U}_p)\}$ (4.2.6) $[\mathbf{K}(\mathbf{U}_I)] \{\mathbf{U}_I - \mathbf{U}_{t=t_{r-1}}\} - \{\Delta\mathbf{F}(\mathbf{U}_I)\} \cong 0$ (4.2.7b) $\{\mathbf{U}_I\} - \{\mathbf{U}_P\} \cong 0$ (4.2.7a)
<i>Criteria for Selecting Provisional Solutions</i>	
Criterion 1: Choose a first trial solution to use the last convergent solution $\{\mathbf{U}_P\} = \{\mathbf{U}_{t=t_{r-1}}\}$	
Criterion 2: Use a quadratic predictor from the three last steps.	

continued on following page

Table 2. Continued

<p><math>w_i^p</math> = any component of the first provisional solution at the instant <math>t_r</math></p> $w_i^p = a.t_r^2 + b.t_r + c \quad (4.2.8)$
<p>The parameters a, b, and c are computed by the resolution of:</p> $\begin{matrix} w_i(t_{r-1}) = a.t_{r-1}^2 + b.t_{r-1} + c \\ w_i(t_{r-2}) = a.t_{r-2}^2 + b.t_{r-2} + c; \text{ i.e.} \\ w_i(t_{r-3}) = a.t_{r-3}^2 + b.t_{r-3} + c \end{matrix} \quad \begin{bmatrix} a \\ b \\ c \end{bmatrix} = \begin{bmatrix} t_{r-1}^2 & t_{r-1} & 1 \\ t_{r-2}^2 & t_{r-2} & 1 \\ t_{r-3}^2 & t_{r-3} & 1 \end{bmatrix}^{-1} \begin{bmatrix} w_i(t_{r-1}) \\ w_i(t_{r-2}) \\ w_i(t_{r-3}) \end{bmatrix} \quad (4.2.9)$ <p><math>t_{r-1}</math>, <math>t_{r-2}</math> and <math>t_{r-3}</math> are known</p>
<b>The Newton-Raphson Method</b>
<p>Equilibrium equation at the instant <math>t_r</math></p> $\{\mathbf{L}(\mathbf{U}_{t=t_r})\} = \{\mathbf{P}_{t=t_r}\}; \text{ where } \{\mathbf{L}(\mathbf{U}_{t=t_r})\} = \sum_{b=1}^m [\mathbf{B}(\mathbf{U}_{t=t_r})_E]_b^t \{\mathbf{M}(\mathbf{U}_{t=t_r})\}_b \quad ; (4.2.10)$
<p>Internal Forces</p> $\{\mathbf{L}(\mathbf{U})\} \cong \left[ \frac{\partial \mathbf{L}}{\partial \mathbf{U}} \right]_{U=U_p} \{\mathbf{U} - \mathbf{U}_p\} \quad (4.2.11)$
$\{\mathbf{L}(\mathbf{U})\} \cong \left[ \frac{\partial \mathbf{L}}{\partial \mathbf{U}} \right]_{U=U_p} \{\mathbf{U}_I - \mathbf{U}_p\} = \{\mathbf{P}\} \Rightarrow \{\mathbf{U}_I\} = \left[ \frac{\partial \mathbf{L}}{\partial \mathbf{U}} \right]_{U=U_p}^{-1} \{\mathbf{P}\} + \{\mathbf{U}_p\} \quad ; (4.2.12)$ <p><math>\{\mathbf{U}_I\}</math> : Improved solution <math>\left[ \frac{\partial \mathbf{L}}{\partial \mathbf{U}} \right]</math> : tangent stiffness matrix</p>
<b>Computation of the Tangent Stiffness Matrix</b>
<p>Internal forces in the non-expanded form</p> $\{\mathbf{Q}(\mathbf{q})\}_b = [\mathbf{B}(\mathbf{q})]_b^t \{\mathbf{M}(\mathbf{q})\}_b \quad (4.2.13)$
$\frac{\partial Q_{ui}}{\partial w_j} \cong \frac{Q_{ui}(u_i, \dots, w_j + \Delta w, \dots) - Q_{ui}(\mathbf{q})}{\Delta w} \quad (4.2.14)$ <p><math>Q_{ui}</math> = any component of matrix <math>\{\mathbf{Q}(\mathbf{q})\}_b</math></p> <p><math>w_j</math> = any displacement of matrix <math>\{\mathbf{q}\}_b</math></p> <p><math>\Delta w</math> = any small increment of displacement (<math>10^{-3}</math> or <math>10^{-4}</math> times any typical displacement of the frame).</p> <p><math>\left[ \frac{\partial \mathbf{L}}{\partial \mathbf{U}} \right]</math> is obtained by the assemblage of <math>\left[ \frac{\partial \mathbf{Q}}{\partial \mathbf{q}} \right]_b</math></p> <p><math>\left[ \frac{\partial \mathbf{Q}}{\partial \mathbf{q}} \right]_b</math> : Tangent stiffness matrix of element <math>b</math> (contribution of the element <math>b</math> to the jacobian in non-expanded form)</p>

continued on following page

## Analysis of Elastic Frames

Table 2. Continued

DYNAMIC ANALYSIS OF ELASTIC FRAMES
<p>Kinematic equation formulated in the nonlinear form</p> $\{d\Phi\}_b = [\mathbf{B}_E(\mathbf{U})]_b \{d\mathbf{U}\}$ $\sum_{b=1}^m [\mathbf{B}_E]_b^t \{\mathbf{M}\}_b + [\mathbf{Mass}] \{\ddot{\mathbf{U}}\} = \{\mathbf{P}\} \quad (4.3.1)$ $\{\mathbf{M}\}_b = [\mathbf{E}]_b \{\Phi\}_b + \{\mathbf{M}^0\}_b$ <p>Inertial forces = <math>[\mathbf{Mass}] \{\ddot{\mathbf{U}}\}</math>;  <math>\{\ddot{\mathbf{U}}\}</math> = generalized acceleration matrix</p>
<p>Discretization using the Constant Average Acceleration algorithm</p> $\ddot{u}(t) \cong \frac{\ddot{u}_{t=t_r} + \ddot{u}_{t=t_{r-1}}}{2}; \quad t_{r-1} < t < t_r \quad (4.3.2)$
<p>Velocity and displacement at the end of the interval <math>t_{r-1} &lt; t &lt; t_r</math></p> $\dot{u}_{t=t_r} \cong \dot{u}_{t=t_{r-1}} + \frac{\Delta t}{2} (\ddot{u}_{t=t_r} + \ddot{u}_{t=t_{r-1}}); \text{ where } \Delta t = t_r - t_{r-1}; u_{t=t_r} \cong u_{t=t_{r-1}} + \Delta t \dot{u}_{t=t_{r-1}} + \frac{\Delta t^2}{4} (\ddot{u}_{t=t_r} + \ddot{u}_{t=t_{r-1}})$ <p>(4.3.3)</p>
<p>Acceleration at the end of the interval</p> $\ddot{u}_{t=t_r} \cong \frac{4}{\Delta t^2} (u_{t=t_r} - u_{t=t_{r-1}}) - \frac{4\dot{u}_{t=t_{r-1}}}{\Delta t} - \ddot{u}_{t=t_{r-1}} \quad (4.3.4)$
<p>The problem is solve by a step by step procedure:  All the quantities at the instant <math>t_{r-1}</math> are known when the structure is analyzed at the instant <math>t_r</math>.  Discretized form of the equilibrium equation:</p> $\{\mathbf{L}(\mathbf{U}_{t=t_r})\} = \{\mathbf{P}_{t=t_r}\}$ <p>(4.3.5)</p> $\{\mathbf{L}(\mathbf{U}_{t=t_r})\} = \sum_{b=1}^m [\mathbf{B}(\mathbf{U}_{t=t_r})_E]_b^t \{\mathbf{M}(\mathbf{U}_{t=t_r})\}_b + [\mathbf{Mass}] \{\ddot{\mathbf{U}}(\mathbf{U}_{t=t_r})\}$

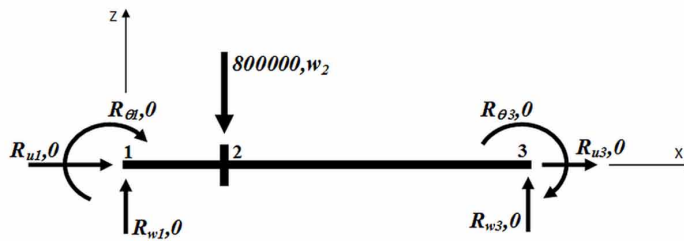
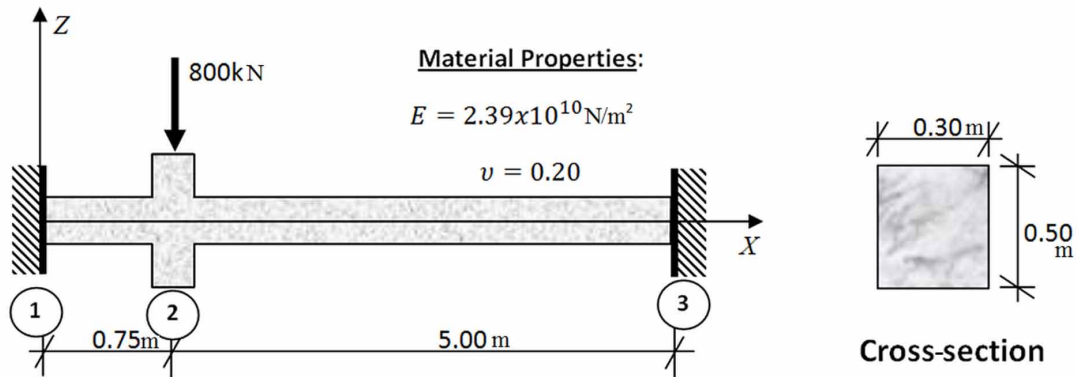
## 4.5 EXAMPLES

### 4.5.1 Analysis of a Two Span Continuous Euler-Bernoulli Beam Shown in Figure 12 using the Direct Stiffness Method

The matrices of generalized displacements and nodal forces are, respectively,



Figure 12. Two-span beam



$$\{\mathbf{U}\} = \begin{Bmatrix} 0 \\ 0 \\ 0 \\ u_2 \\ w_2 \\ \theta_2 \\ 0 \\ 0 \\ 0 \\ 0 \end{Bmatrix}; \{\mathbf{F}\} = \begin{Bmatrix} R_{u1} \\ R_{w1} \\ R_{\theta1} \\ 0 \\ -800000 \\ 0 \\ R_{u3} \\ R_{w3} \\ R_{\theta3} \end{Bmatrix} \quad (4.5.1)$$

where  $u_2$ ,  $w_2$  are the horizontal and vertical displacements at the node 2 and  $\theta_2$  is the rotation of the same node;  $R_{u1}$ ,  $R_{w1}$ ,  $R_{\theta1}$ ,  $R_{u3}$ ,  $R_{w3}$  and  $R_{\theta3}$  are the reaction forces at the ends 1 and 3. Notice that in this case there are no forces over the element, then  $\{\mathbf{F}\} = \{\mathbf{P}^n\}$ .

For element 1 between nodes 1 and 2, the expanded transformation matrix is computed by Equation (3.1.13):

$$\left[ \mathbf{B}_E^0 \right]_1 = \begin{bmatrix} 0 & -1.333 & 1 & 0 & 1.333 & 0 & 0 & 0 & 0 \\ 0 & -1.333 & 0 & 0 & 1.333 & 1 & 0 & 0 & 0 \\ -1 & 0 & 0 & 1 & 0 & 0 & 0 & 0 & 0 \end{bmatrix} \quad (4.5.2)$$

### Analysis of Elastic Frames

And the elasticity matrix is calculated using Equation (3.3.11):

$$[\mathbf{E}]_1 = \begin{bmatrix} 3.983x10^8 & 1.992x10^8 & 0 \\ 1.992x10^8 & 3.983x10^8 & 0 \\ 0 & 0 & 4.780x10^9 \end{bmatrix} \quad (4.5.3)$$

Using Equation (4.1.3c):  $[\mathbf{k}_E]_b = [\mathbf{B}_E^0]^t [\mathbf{E}] [\mathbf{B}_E^0]_b$ , it is obtained the expanded stiffness matrix for element 1

$$[\mathbf{k}_E]_1 = \begin{bmatrix} 4.78x10^9 & 0 & 0 & -4.78 x10^9 & 0 & 0 & 0 & 0 & 0 \\ 0 & 2.12x10^9 & -7.97x10^8 & 0 & -2.12x10^9 & -7.97x10^8 & 0 & 0 & 0 \\ 0 & -7.97x10^8 & 3.98x10^8 & 0 & 7.97x10^8 & 1.99x10^8 & 0 & 0 & 0 \\ -4.78 10^9 & 0 & 0 & 4.78 x10^9 & 0 & 0 & 0 & 0 & 0 \\ 0 & -2.12x10^9 & 7.97x10^8 & 0 & 2.12x10^9 & 7.97x10^8 & 0 & 0 & 0 \\ 0 & -7.97x10^8 & 1.99x10^8 & 0 & 7.97x10^8 & 3.98x10^8 & 0 & 0 & 0 \\ 0 & 0 & 0 & 0 & 0 & 0 & 0 & 0 & 0 \\ 0 & 0 & 0 & 0 & 0 & 0 & 0 & 0 & 0 \\ 0 & 0 & 0 & 0 & 0 & 0 & 0 & 0 & 0 \end{bmatrix} \quad (4.5.4)$$

For element 2 between nodes 2 and 3, the expanded transformation matrix is:

$$[\mathbf{B}_E^0]_2 = \begin{bmatrix} 0 & 0 & 0 & 0 & -0.2 & 1 & 0 & 0.2 & 0 \\ 0 & 0 & 0 & 0 & -0.2 & 0 & 0 & 0.2 & 1 \\ 0 & 0 & 0 & -1 & 0 & 0 & 1 & 0 & 0 \end{bmatrix} \quad (4.5.5)$$

And the elasticity matrix is:

$$[\mathbf{E}]_2 = \begin{bmatrix} 5.975x10^7 & 2.988x10^7 & 0 \\ 2.988x10^7 & 5.975x10^7 & 0 \\ 0 & 0 & 7.170x10^8 \end{bmatrix} \quad (4.5.6)$$

Using Equation (4.1.3c), it is obtained the expanded stiffness matrix of the element 2:

$$[\mathbf{k}_E]_2 = \begin{bmatrix} 0 & 0 & 0 & 0 & 0 & 0 & 0 & 0 & 0 \\ 0 & 0 & 0 & 0 & 0 & 0 & 0 & 0 & 0 \\ 0 & 0 & 0 & 0 & 0 & 0 & 0 & 0 & 0 \\ 0 & 0 & 0 & 7.17 \cdot 10^8 & 0 & 0 & -7.17 \cdot 10^8 & 0 & 0 \\ 0 & 0 & 0 & 0 & 7.17 \cdot 10^6 & -1.79 \cdot 10^7 & 0 & -7.17 \cdot 10^6 & -1.79 \cdot 10^7 \\ 0 & 0 & 0 & 0 & -1.79 \cdot 10^7 & 5.97 \cdot 10^7 & 0 & 1.79 \cdot 10^7 & 2.99 \cdot 10^7 \\ 0 & 0 & 0 & -7.17 \cdot 10^8 & 0 & 0 & 7.17 \cdot 10^8 & 0 & 0 \\ 0 & 0 & 0 & 0 & -7.17 \cdot 10^6 & 1.79 \cdot 10^7 & 0 & 7.17 \cdot 10^6 & 1.79 \cdot 10^7 \\ 0 & 0 & 0 & 0 & -1.79 \cdot 10^7 & 2.99 \cdot 10^7 & 0 & 1.79 \cdot 10^7 & 5.97 \cdot 10^7 \end{bmatrix} \quad (4.5.7)$$

The stiffness matrix of the structure is obtained as the sum of  $[\mathbf{k}_E]_1$  and  $[\mathbf{k}_E]_2$ ,

$$[\mathbf{K}] = \begin{bmatrix} 4.78 \cdot 10^9 & 0 & 0 & -4.78 \cdot 10^9 & 0 & 0 & 0 & 0 & 0 \\ 0 & 2.12 \cdot 10^9 & -7.97 \cdot 10^8 & 0 & -2.12 \cdot 10^9 & -7.97 \cdot 10^8 & 0 & 0 & 0 \\ 0 & -7.97 \cdot 10^8 & 3.98 \cdot 10^8 & 0 & 7.97 \cdot 10^8 & 1.99 \cdot 10^8 & 0 & 0 & 0 \\ -4.78 \cdot 10^9 & 0 & 0 & 5.5 \cdot 10^9 & 0 & 0 & -7.17 \cdot 10^8 & 0 & 0 \\ 0 & -2.12 \cdot 10^9 & 7.97 \cdot 10^8 & 0 & 2.13 \cdot 10^9 & 7.79 \cdot 10^8 & 0 & -7.17 \cdot 10^6 & -1.79 \cdot 10^7 \\ 0 & -7.97 \cdot 10^8 & 1.99 \cdot 10^8 & 0 & 7.79 \cdot 10^8 & 4.58 \cdot 10^8 & 0 & 1.79 \cdot 10^7 & 2.99 \cdot 10^7 \\ 0 & 0 & 0 & -7.17 \cdot 10^8 & 0 & 0 & 7.17 \cdot 10^8 & 0 & 0 \\ 0 & 0 & 0 & 0 & -7.17 \cdot 10^6 & 1.79 \cdot 10^7 & 0 & 7.17 \cdot 10^6 & 1.79 \cdot 10^7 \\ 0 & 0 & 0 & 0 & -1.79 \cdot 10^7 & 2.99 \cdot 10^7 & 0 & 1.79 \cdot 10^7 & 5.98 \cdot 10^7 \end{bmatrix} \quad (4.5.8)$$

Free displacements and reactions forces are obtained solving Equation (4.1.2)  $[\mathbf{K}]\{\mathbf{U}\} = \{\mathbf{F}\}$

$$u_2 = 0, \quad w_2 = -9.9040 \cdot 10^{-4} \text{ m}, \quad \theta_2 = 1.6837 \cdot 10^{-3} \text{ rad}$$

$$R_{u1} = 0, \quad R_{w1} = 7.6272 \cdot 10^5 \text{ N}, \quad R_{\theta1} = -4.5369 \cdot 10^5 \text{ N.m},$$

$$R_{u3} = 0, \quad R_{w3} = 3.7281 \cdot 10^4 \text{ N}, \quad R_{\theta3} = 6.8053 \cdot 10^4 \text{ N.m} \quad (4.5.9)$$

Now, the generalized deformation matrices are computed using Equation (3.1.12):  $\{\Phi\}_b = [\mathbf{B}_E^0]_b \{\mathbf{U}\}$  and the generalized stress matrices by Equation (3.3.10):  $\{\mathbf{M}\}_b = [\mathbf{E}]_b \{\Phi\}_b$ :

## Analysis of Elastic Frames

$$\{\Phi\}_1 = \begin{bmatrix} -0.001320 \\ 0.00036 \\ 0 \end{bmatrix}; \{\mathbf{M}\}_1 = \begin{bmatrix} -4.5369 \times 10^5 \\ -1.1835 \times 10^5 \\ 0 \end{bmatrix}; \{\Phi\}_2 = \begin{bmatrix} 0.00188 \\ 0.00020 \\ 0 \end{bmatrix}; \{\mathbf{M}\}_2 = \begin{bmatrix} 1.1835 \times 10^5 \\ 0.6805 \times 10^5 \\ 0 \end{bmatrix} \quad (4.5.10)$$

In Figure 13, it is shown the vertical displacement along the beam length. In Figure 14a, it is shown the moment diagram which is drawn in the side of the beam subjected to tension and in Figure 14b, the shear forces diagram. The shear forces are computed by considering static equilibrium of the element subjected to moments  $m_i^b$  and  $m_j^b$ .

$$V_i^b = V_j^b = V^b = \frac{m_i^b + m_j^b}{L_b} \quad (4.5.11)$$

### 4.5.2 Analysis of a Two Span Continuous Timoshenko Beam Shown in Figure 12 using the Direct Stiffness Method

The matrices of the generalized displacements and nodal forces matrices are the same of the previous example (see Equation 4.5.1). The expanded transformation matrices of elements 1 and 2,  $[\mathbf{B}_E^0]_1$  and  $[\mathbf{B}_E^0]_2$ , are the ones shown in Equations (4.5.2) and (4.5.5).

For element 1, the elasticity matrix is computed using Equation (3.4.11):

Figure 13. Vertical displacements (along the beam length)

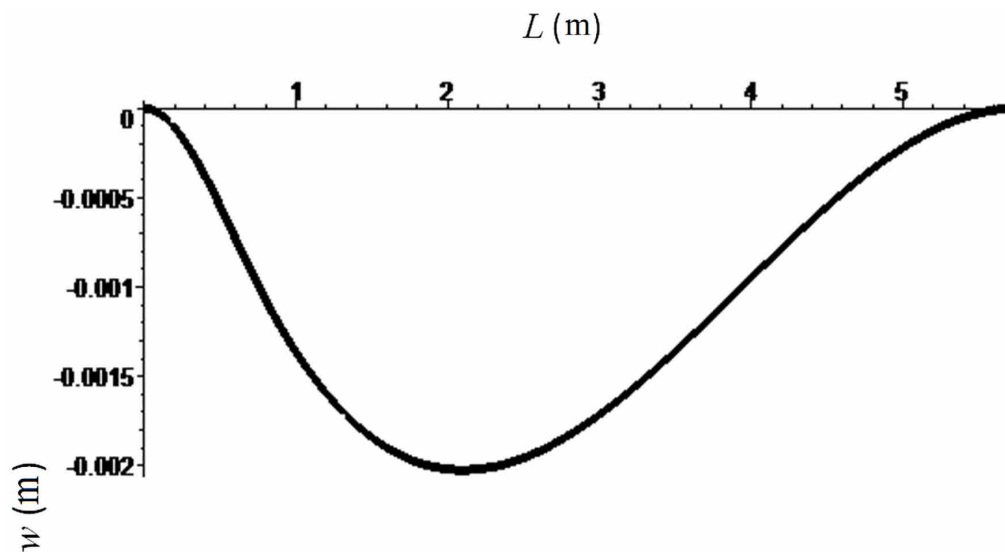
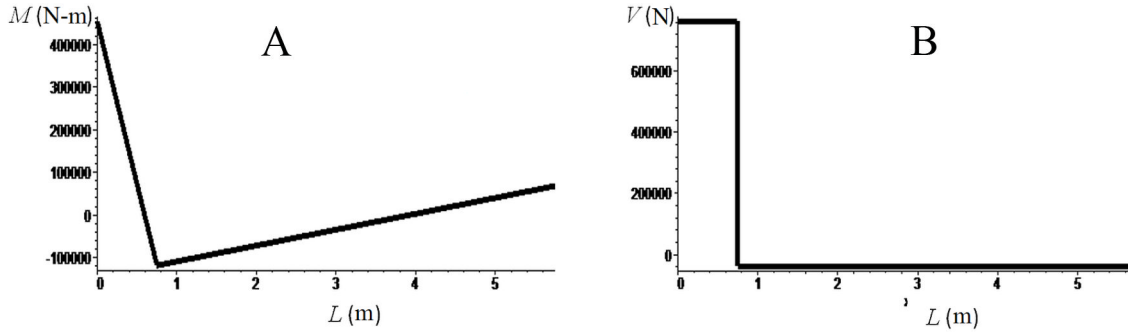


Figure 14. (a) Moment diagram (b) Shear forces diagram



$$[\mathbf{E}]_1 = \begin{bmatrix} 2.441 \times 10^8 & 4.497 \times 10^7 & 0 \\ 4.497 \times 10^7 & 2.441 \times 10^8 & 0 \\ 0 & 0 & 4.780 \times 10^9 \end{bmatrix} \quad (4.5.12)$$

The expanded stiffness matrix is obtained by the Equation (4.1.3c) using the expanded transformation matrix (4.5.2)

$$[\mathbf{k}_e]_1 = \begin{bmatrix} 4.78 \times 10^9 & 0 & 0 & -4.78 \times 10^9 & 0 & 0 & 0 & 0 & 0 \\ 0 & 1.03 \times 10^9 & -3.85 \times 10^8 & 0 & -1.03 \times 10^9 & -3.85 \times 10^8 & 0 & 0 & 0 \\ 0 & -3.85 \times 10^8 & 2.44 \times 10^8 & 0 & 3.85 \times 10^8 & 4.50 \times 10^7 & 0 & 0 & 0 \\ -4.78 \times 10^9 & 0 & 0 & 4.78 \times 10^9 & 0 & 0 & 0 & 0 & 0 \\ 0 & -1.03 \times 10^9 & 3.85 \times 10^8 & 0 & 1.03 \times 10^9 & 3.85 \times 10^8 & 0 & 0 & 0 \\ 0 & -3.85 \times 10^8 & 4.50 \times 10^7 & 0 & 3.85 \times 10^8 & 2.44 \times 10^8 & 0 & 0 & 0 \\ 0 & 0 & 0 & 0 & 0 & 0 & 0 & 0 & 0 \\ 0 & 0 & 0 & 0 & 0 & 0 & 0 & 0 & 0 \\ 0 & 0 & 0 & 0 & 0 & 0 & 0 & 0 & 0 \end{bmatrix} \quad (4.5.13)$$

For element 2, the elasticity matrix is:

$$[\mathbf{E}]_2 = \begin{bmatrix} 5.870 \times 10^8 & 2.882 \times 10^7 & 0 \\ 2.882 \times 10^7 & 5.870 \times 10^8 & 0 \\ 0 & 0 & 7.17 \times 10^8 \end{bmatrix} \quad (4.5.14)$$

And the expanded stiffness matrix is obtained from Equation (4.1.3c) using the expanded transformation matrix (4.5.5)

### Analysis of Elastic Frames

$$[\mathbf{k}_E]_2 = \begin{bmatrix} 0 & 0 & 0 & 0 & 0 & 0 & 0 & 0 & 0 \\ 0 & 0 & 0 & 0 & 0 & 0 & 0 & 0 & 0 \\ 0 & 0 & 0 & 0 & 0 & 0 & 0 & 0 & 0 \\ 0 & 0 & 0 & 7.17 \cdot 10^8 & 0 & 0 & -7.17 \cdot 10^8 & 0 & 0 \\ 0 & 0 & 0 & 0 & 7.00 \cdot 10^6 & -1.75 \cdot 10^7 & 0 & -7.00 \cdot 10^6 & -1.75 \cdot 10^7 \\ 0 & 0 & 0 & 0 & -1.75 \cdot 10^7 & 5.87 \cdot 10^7 & 0 & 1.75 \cdot 10^7 & 2.88 \cdot 10^7 \\ 0 & 0 & 0 & -7.17 \cdot 10^8 & 0 & 0 & 7.17 \cdot 10^8 & 0 & 0 \\ 0 & 0 & 0 & 0 & -7.00 \cdot 10^6 & 1.75 \cdot 10^7 & 0 & 7.00 \cdot 10^6 & 1.75 \cdot 10^7 \\ 0 & 0 & 0 & 0 & -1.75 \cdot 10^7 & 2.88 \cdot 10^7 & 0 & 1.75 \cdot 10^7 & 5.87 \cdot 10^7 \end{bmatrix} \quad (4.5.15)$$

Then, the stiffness matrix of the structure is  $[\mathbf{K}] = [\mathbf{k}_E]_1 + [\mathbf{k}_E]_2$ :

$$[\mathbf{K}] = \begin{bmatrix} 4.78 \cdot 10^9 & 0 & 0 & -4.78 \cdot 10^9 & 0 & 0 & 0 & 0 & 0 \\ 0 & 1.03 \cdot 10^9 & -3.85 \cdot 10^8 & 0 & -1.03 \cdot 10^9 & -3.85 \cdot 10^8 & 0 & 0 & 0 \\ 0 & -3.85 \cdot 10^8 & 2.44 \cdot 10^8 & 0 & 3.85 \cdot 10^8 & 4.50 \cdot 10^7 & 0 & 0 & 0 \\ -4.78 \cdot 10^9 & 0 & 0 & 5.5 \cdot 10^9 & 0 & 0 & -7.17 \cdot 10^8 & 0 & 0 \\ 0 & -1.03 \cdot 10^9 & 3.85 \cdot 10^8 & 0 & 1.03 \cdot 10^9 & 3.68 \cdot 10^8 & 0 & -7.00 \cdot 10^6 & -1.75 \cdot 10^7 \\ 0 & -3.85 \cdot 10^8 & 4.50 \cdot 10^7 & 0 & 3.68 \cdot 10^8 & 3.03 \cdot 10^8 & 0 & 1.75 \cdot 10^7 & 2.88 \cdot 10^7 \\ 0 & 0 & 0 & -7.17 \cdot 10^8 & 0 & 0 & 7.17 \cdot 10^8 & 0 & 0 \\ 0 & 0 & 0 & 0 & -7.00 \cdot 10^6 & 1.75 \cdot 10^7 & 0 & 7.00 \cdot 10^6 & 1.75 \cdot 10^7 \\ 0 & 0 & 0 & 0 & -1.75 \cdot 10^7 & 2.88 \cdot 10^7 & 0 & 1.75 \cdot 10^7 & 5.87 \cdot 10^7 \end{bmatrix} \quad (4.5.16)$$

Solving Equation (4.1.2):  $[\mathbf{K}]\{\mathbf{U}\} = \{\mathbf{F}\}$  the displacements and reaction forces are obtained:

$$u_2 = 0, \quad w_2 = -1.361 \cdot 10^{-3} \text{ m}, \quad \theta_2 = 1.6537 \cdot 10^{-3} \text{ rad}$$

$$R_{u1} = 0, \quad R_{w1} = 7.6152 \cdot 10^5 \text{ N}, \quad R_{\theta1} = -4.5025 \cdot 10^5 \text{ N.m}$$

$$R_{u3} = 0, \quad R_{w3} = 3.8476 \cdot 10^4 \text{ N}, \quad R_{\theta3} = 7.1490 \cdot 10^4 \text{ N.m} \quad (4.5.17)$$

The matrices of generalized deformations and generalized stresses are:

$$\{\Phi\}_1 = \begin{bmatrix} -0.00181 \\ -0.00016 \\ 0 \end{bmatrix}; \{M\}_1 = \begin{bmatrix} -4.5025 \times 10^5 \\ -1.2089 \times 10^5 \\ 0 \end{bmatrix}; \{\Phi\}_2 = \begin{bmatrix} 0.00193 \\ 0.00027 \\ 0 \end{bmatrix}; \{M\}_2 = \begin{bmatrix} 1.2089 \times 10^5 \\ 0.7149 \times 10^5 \\ 0 \end{bmatrix} \quad (4.5.18)$$

In Figure 15 it is shown the vertical displacement along the beam length, in Figure 16a the diagram of moments and in Figure 16b the corresponding shear force one.

Notice that the vertical displacement of node 2 is larger with the Timoshenko model (37%). However, the differences in the diagrams of moments and shear forces do not exceed 1%.

### 4.5.3 Assemblage of the Stiffness Matrix for the Frame Shown in Figure 17 using Timoshenko Theory

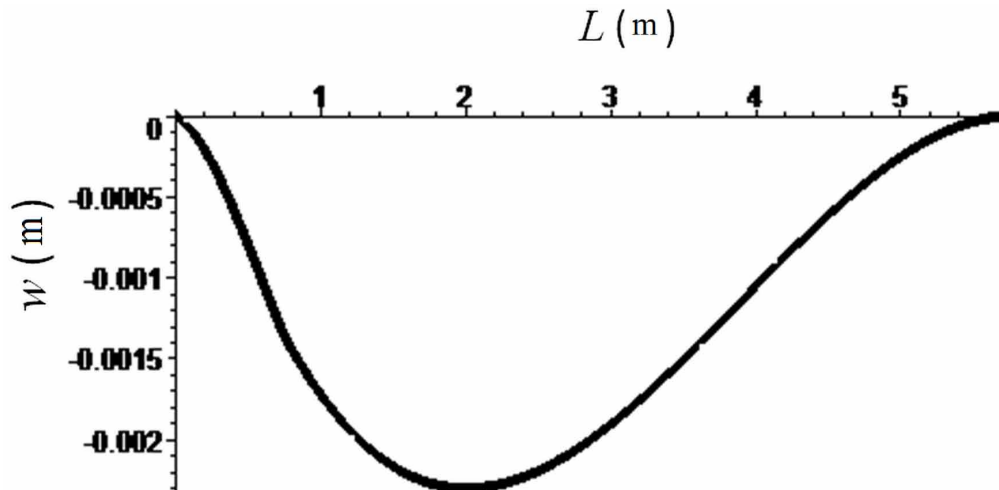
For element 1 between nodes 1 and 3 the non-expanded transformation matrix is:

$$[B^0]_1 = \begin{bmatrix} 0.16 & -0.12 & 1 & -0.16 & 0.12 & 0 \\ 0.16 & -0.12 & 0 & -0.16 & 0.12 & 1 \\ -0.6 & -0.8 & 0 & 0.6 & 0.8 & 0 \end{bmatrix} \quad (4.5.19)$$

The elasticity matrix is computed using Equation (3.4.11):

$$[E]_1 = \begin{bmatrix} 5.84 \times 10^7 & 2.88 \times 10^7 & 0 \\ 2.88 \times 10^7 & 5.84 \times 10^7 & 0 \\ 0 & 0 & 7.16 \times 10^8 \end{bmatrix} \quad (4.5.20)$$

Figure 15. Vertical displacements ( $w$ ) along the beam length



**Analysis of Elastic Frames**

Figure 16. a) Moment diagram; (b) Shear forces diagram

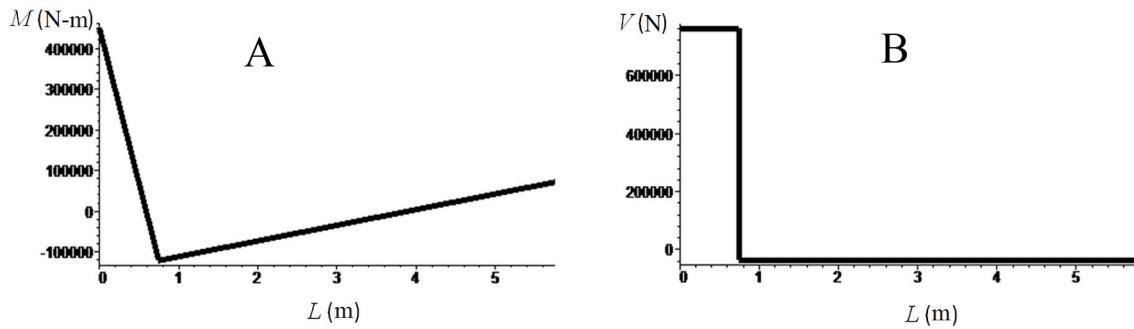
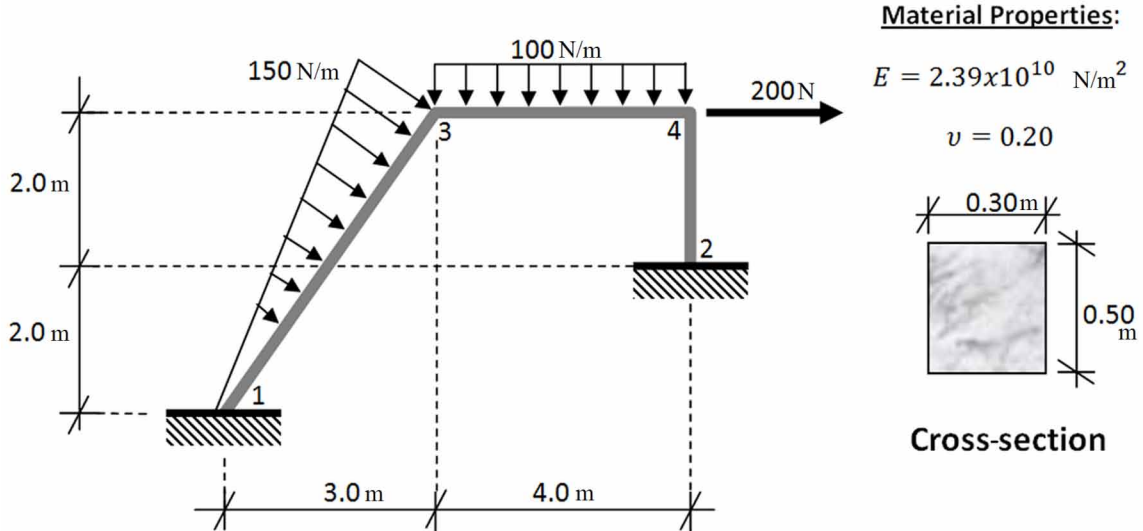


Figure 17. Planar Frame subjected to several external loads



The stiffness matrix is:

$$\left[ \mathbf{k} \right]_1 = \begin{bmatrix} 2.62 \times 10^8 & 3.41 \times 10^8 & 1.40 \times 10^7 & -2.62 \times 10^8 & -3.41 \times 10^8 & 1.40 \times 10^7 \\ 3.41 \times 10^8 & 4.62 \times 10^8 & -1.05 \times 10^7 & -3.41 \times 10^8 & -4.62 \times 10^8 & -1.05 \times 10^7 \\ 1.40 \times 10^7 & -1.05 \times 10^7 & 5.87 \times 10^7 & -1.40 \times 10^7 & 1.05 \times 10^7 & 2.88 \times 10^7 \\ -2.62 \times 10^8 & -3.41 \times 10^8 & -1.40 \times 10^7 & 2.62 \times 10^8 & 3.41 \times 10^8 & -1.40 \times 10^7 \\ -3.41 \times 10^8 & -4.62 \times 10^8 & 1.05 \times 10^7 & 3.41 \times 10^8 & 4.62 \times 10^8 & 1.05 \times 10^7 \\ 1.40 \times 10^7 & -1.05 \times 10^7 & 2.88 \times 10^7 & -1.40 \times 10^7 & 1.05 \times 10^7 & 5.87 \times 10^7 \end{bmatrix} \quad (4.5.21)$$

The assemblage of the matrix  $\left[ \mathbf{k} \right]_1$  in the stiffness matrix of the structure  $\left[ \mathbf{K} \right]$  results in:



$$\mathbf{[K]} = \begin{bmatrix}
 2.62x10^8 & 3.41x10^8 & 1.40x10^7 & 0 & 0 & 0 & -2.62x10^8 & -3.41x10^8 & 1.40x10^7 & 0 & 0 & 0 \\
 3.41x10^8 & 4.62x10^8 & -1.05x10^7 & 0 & 0 & 0 & -3.41x10^8 & -4.62x10^8 & -1.05x10^7 & 0 & 0 & 0 \\
 1.40x10^7 & -1.05x10^7 & 5.87x10^7 & 0 & 0 & 0 & -1.40x10^7 & 1.05x10^7 & 2.88x10^7 & 0 & 0 & 0 \\
 0 & 0 & 0 & 0 & 0 & 0 & 0 & 0 & 0 & 0 & 0 & 0 \\
 0 & 0 & 0 & 0 & 0 & 0 & 0 & 0 & 0 & 0 & 0 & 0 \\
 0 & 0 & 0 & 0 & 0 & 0 & 0 & 0 & 0 & 0 & 0 & 0 \\
 -2.62x10^8 & -3.41x10^8 & -1.40x10^7 & 0 & 0 & 0 & 2.62x10^8 & 3.41x10^8 & -1.40x10^7 & 0 & 0 & 0 \\
 -3.41x10^8 & -4.62x10^8 & 1.05x10^7 & 0 & 0 & 0 & 3.41x10^8 & 4.62x10^8 & 1.05x10^7 & 0 & 0 & 0 \\
 1.40x10^7 & -1.05x10^7 & 2.88x10^7 & 0 & 0 & 0 & -1.40x10^7 & 1.05x10^7 & 5.87x10^7 & 0 & 0 & 0 \\
 0 & 0 & 0 & 0 & 0 & 0 & 0 & 0 & 0 & 0 & 0 & 0 \\
 0 & 0 & 0 & 0 & 0 & 0 & 0 & 0 & 0 & 0 & 0 & 0
 \end{bmatrix} \quad (4.5.22)$$

For element 2 between nodes 2 and 4 the transformation matrix is:

$$\mathbf{[B^0]}_2 = \begin{bmatrix}
 0.5 & 0 & 1 & -0.5 & 0 & 0 \\
 0.5 & 0 & 0 & -0.5 & 0 & 1 \\
 0 & -1 & 0 & 0 & 1 & 0
 \end{bmatrix} \quad (4.5.23)$$

The elasticity matrix is computed using Equation (3.4.11):

$$\mathbf{[E]}_2 = \begin{bmatrix}
 1.35x10^8 & 6.00x10^7 & 0 \\
 6.00x10^7 & 1.35x10^8 & 0 \\
 0 & 0 & 1.79x10^9
 \end{bmatrix} \quad (4.5.24)$$

The stiffness matrix is:

$$\mathbf{[k]}_2 = \begin{bmatrix}
 9.76x10^7 & 0 & 9.75x10^7 & -9.76x10^7 & 0 & 9.75x10^7 \\
 0 & 1.79x10^9 & 0 & 0 & -1.79x10^9 & 0 \\
 9.75x10^7 & 0 & 1.35x10^8 & -9.75x10^7 & 0 & 6.01x10^7 \\
 -9.76x10^7 & 0 & -9.75x10^7 & 9.76x10^7 & 0 & -9.75x10^7 \\
 0 & -1.79x10^9 & 0 & 0 & 1.79x10^9 & 0 \\
 9.75x10^7 & 0 & 6.01x10^7 & -9.75x10^7 & 0 & 1.35x10^8
 \end{bmatrix} \quad (4.5.25)$$

The assemblage of the matrix  $\mathbf{[k]}_2$  in the stiffness matrix of the structure  $\mathbf{[K]}$  results in (See Box 1):

For element 3 between nodes 3 and 4 the transformation matrix is:

Box 1.

$$\begin{bmatrix}
 2.62x10^8 & 3.41x10^8 & 1.40x10^7 & 0 & 0 & -2.62x10^8 & -3.41x10^8 & 1.40x10^7 & 0 & 0 & 0 \\
 3.41x10^8 & 4.62x10^8 & -1.05x10^7 & 0 & 0 & -3.41x10^8 & -4.62x10^8 & -1.05x10^7 & 0 & 0 & 0 \\
 1.40x10^7 & -1.05x10^7 & 5.87x10^7 & 0 & 0 & -1.40x10^7 & 1.05x10^7 & 2.88x10^7 & 0 & 0 & 0 \\
 0 & 0 & 9.74x10^7 & 0 & 9.74x10^7 & 0 & 0 & 0 & -9.74x10^7 & 0 & 9.74x10^7 \\
 0 & 0 & 0 & 1.79x10^9 & 0 & 0 & 0 & 0 & 0 & -1.79x10^9 & 0 \\
 0 & 0 & 9.74x10^7 & 0 & 1.35x10^8 & 0 & 0 & 0 & -9.74x10^7 & 0 & 6.01x10^7 \\
 -2.62x10^8 & -3.41x10^8 & -1.40x10^7 & 0 & 0 & 2.62x10^8 & 3.41x10^8 & -1.40x10^7 & 0 & 0 & 0 \\
 -3.41x10^8 & -4.62x10^8 & 1.05x10^7 & 0 & 0 & 3.41x10^8 & 4.62x10^8 & 1.05x10^7 & 0 & 0 & 0 \\
 1.40x10^7 & -1.05x10^7 & 2.88x10^7 & 0 & 0 & -1.40x10^7 & 1.05x10^7 & 5.87x10^7 & 0 & 0 & 0 \\
 0 & 0 & -9.74x10^7 & 0 & -9.74x10^7 & 0 & 0 & 0 & 9.74x10^7 & 0 & -9.74x10^7 \\
 0 & 0 & 0 & -1.79x10^9 & 0 & 0 & 0 & 0 & 0 & 1.79x10^9 & 0 \\
 0 & 0 & 9.74x10^7 & 0 & 6.01x10^7 & 0 & 0 & 0 & -9.74x10^7 & 0 & 1.35x10^8
 \end{bmatrix}$$

$[\mathbf{K}] =$

(4.5.26)

$$[\mathbf{B}^0]_3 = \begin{bmatrix} 0 & -0.25 & 1 & 0 & 0.25 & 0 \\ 0 & -0.25 & 0 & 0 & 0.25 & 1 \\ -1 & 0 & 0 & 1 & 0 & 0 \end{bmatrix} \quad (4.5.27)$$

The elasticity matrix is:

$$[\mathbf{E}]_3 = \begin{bmatrix} 7.24x10^7 & 3.54x10^7 & 0 \\ 3.54x10^7 & 7.24x10^7 & 0 \\ 0 & 0 & 8.95x10^8 \end{bmatrix} \quad (4.5.28)$$

The stiffness matrix is:

$$[\mathbf{k}]_3 = \begin{bmatrix} 8.95x10^8 & 0 & 0 & -8.95x10^8 & 0 & 0 \\ 0 & 1.35x10^7 & -2.70x10^7 & 0 & -1.35x10^7 & -2.70x10^7 \\ 0 & -2.70x10^7 & 7.24x10^7 & 0 & 2.70x10^7 & 3.54x10^7 \\ -8.95x10^8 & 0 & 0 & 8.95x10^8 & 0 & 0 \\ 0 & -1.35x10^7 & 2.70x10^7 & 0 & 1.35x10^7 & 2.70x10^7 \\ 0 & -2.70x10^7 & 3.54x10^7 & 0 & 2.70x10^7 & 7.24x10^7 \end{bmatrix} \quad (4.5.29)$$

The assemblage of the matrix  $[\mathbf{k}]_3$  in the stiffness matrix of the structure  $[\mathbf{K}]$  results in (See Box 2):

#### 4.5.4 Analysis of the Frame Shown in Figure 17 using Timoshenko Theory and the Direct Stiffness Method

The matrices of generalized displacements and nodal forces for the frame are, respectively,

$$\{\mathbf{U}\} = \begin{bmatrix} 0 \\ 0 \\ 0 \\ 0 \\ 0 \\ 0 \\ u_3 \\ w_3 \\ \theta_3 \\ u_4 \\ w_4 \\ \theta_4 \end{bmatrix}; \{\mathbf{P}^n\} = \begin{bmatrix} R_{u1} \\ R_{w1} \\ R_{\theta1} \\ R_{u2} \\ R_{w2} \\ R_{\theta2} \\ 0 \\ 0 \\ 0 \\ 200 \\ 0 \\ 0 \end{bmatrix} \quad (4.5.31)$$

Box 2.

$$\begin{bmatrix}
 2.62x10^8 & 3.41x10^8 & 1.40x10^7 & 0 & 0 & 0 & -2.62x10^8 & -3.41x10^8 & 1.40x10^7 & 0 & 0 & 0 \\
 3.41x10^8 & 4.62x10^8 & -1.05x10^7 & 0 & 0 & 0 & -3.41x10^8 & -4.62x10^8 & -1.05x10^7 & 0 & 0 & 0 \\
 1.40x10^7 & -1.05x10^7 & 5.87x10^7 & 0 & 0 & 0 & -1.40x10^7 & 1.05x10^7 & 2.88x10^7 & 0 & 0 & 0 \\
 0 & 0 & 9.74x10^7 & 9.74x10^7 & 0 & 9.74x10^7 & 0 & 0 & 0 & -9.74x10^7 & 0 & 9.74x10^7 \\
 0 & 0 & 0 & 0 & 1.79x10^9 & 0 & 0 & 0 & 0 & 0 & -1.79x10^9 & 0 \\
 0 & 0 & 9.74x10^7 & 9.74x10^7 & 0 & 1.35x10^8 & 0 & 0 & 0 & -9.74x10^7 & 0 & 6.01x10^7 \\
 -2.62x10^8 & -3.41x10^8 & -1.40x10^7 & 0 & 0 & 0 & 1.16x10^9 & 3.41x10^8 & -1.40x10^7 & -8.96x10^8 & 0 & 0 \\
 -3.41x10^8 & -4.62x10^8 & 1.05x10^7 & 0 & 0 & 0 & 3.41x10^8 & 4.74x10^8 & -1.65x10^7 & 0 & -1.35x10^7 & -2.70x10^7 \\
 1.40x10^7 & -1.05x10^7 & 2.88x10^7 & 0 & 0 & 0 & -1.40x10^7 & -1.65x10^7 & 1.31x10^8 & 0 & 2.70x10^7 & 3.53x10^7 \\
 0 & 0 & 0 & -9.74x10^7 & 0 & -9.74x10^7 & -8.96x10^8 & 0 & 0 & 9.93x10^8 & 0 & -9.74x10^7 \\
 0 & 0 & 0 & 0 & -1.79x10^9 & 0 & 0 & -1.35x10^7 & 2.70x10^7 & 0 & 1.79x10^9 & 2.70x10^7 \\
 0 & 0 & 0 & 9.74x10^7 & 0 & 6.01x10^7 & 0 & -2.70x10^7 & 3.53x10^7 & -9.74x10^7 & 2.70x10^7 & 2.08x10^8
 \end{bmatrix} = \mathbf{[K]} \tag{4.5.30}$$

Note that there are distributed-loads along the elements 1 and 3 thus, it is necessary the computation of equivalent nodal forces and moments. The nodal equivalent forces in local coordinates are calculated using Table 1, then for element 1 between nodes 1 and 3 it is obtained:

$$\{\mathbf{p}^{le}\}_1 = \begin{bmatrix} 0 \\ -112.793 \\ 125.732 \\ 0 \\ -262.207 \\ -186.768 \end{bmatrix} \quad (4.5.32)$$

To transform  $\{\mathbf{p}^{le}\}_1$  to the global coordinate system, it is used the Equation (4.1.11). The geometrical transformation matrix for this element is computed using Equation (3.1.5):

$$[\mathbf{T}]_1 = \begin{bmatrix} 0.6 & 0.8 & 0 & 0 & 0 & 0 \\ -0.8 & 0.6 & 0 & 0 & 0 & 0 \\ 0 & 0 & 1 & 0 & 0 & 0 \\ 0 & 0 & 0 & 0.6 & 0.8 & 0 \\ 0 & 0 & 0 & -0.8 & 0.6 & 0 \\ 0 & 0 & 0 & 0 & 0 & 1 \end{bmatrix} \quad (4.5.33)$$

Then, the equivalent nodal forces expressed in global coordinates are:

$$\{\mathbf{p}^e\}_1 = \begin{bmatrix} 90.234 \\ -67.676 \\ 125.732 \\ 209.766 \\ -157.324 \\ -186.768 \end{bmatrix} \quad (4.5.34)$$

The expanded equivalent nodal forces matrix is:

**Analysis of Elastic Frames**

$$\{\mathbf{P}^e\}_1 = \begin{bmatrix} 90.234 \\ -67.676 \\ 125.732 \\ 0 \\ 0 \\ 0 \\ 209.766 \\ -157.324 \\ -186.768 \\ 0 \\ 0 \\ 0 \end{bmatrix} \quad (4.5.35)$$

For element 3, between nodes 3 and 4 the equivalent nodal forces are:

$$\{\mathbf{P}^e\}_3 = \begin{bmatrix} 0 \\ -200 \\ 133.333 \\ 0 \\ -200 \\ -133.333 \end{bmatrix} \quad (4.5.36)$$

The expanded equivalent nodal forces matrix is:

$$\{\mathbf{P}^e\}_1 = \begin{bmatrix} 0 \\ 0 \\ 0 \\ 0 \\ 0 \\ 0 \\ 0 \\ -200 \\ 133.333 \\ 0 \\ -200 \\ -133.333 \end{bmatrix} \quad (4.5.37)$$

For this element, the local coordinate system coincides with the global one, thus:  $\{\mathbf{p}^e\}_3 = \{\mathbf{p}'^e\}_3$

The nodal forces  $\{\mathbf{F}\}$  are:

$$\{\mathbf{F}\} = \{\mathbf{P}^n\} + \{\mathbf{P}^e\}_1 + \{\mathbf{P}^e\}_3 = \begin{bmatrix} R_{u1} + 90.234 \\ R_{w1} - 67.676 \\ R_{\theta1} + 125.732 \\ R_{u2} \\ R_{w2} \\ R_{\theta2} \\ 209.766 \\ -357.324 \\ -53.434 \\ 200 \\ -200 \\ -133.333 \end{bmatrix} \quad (4.5.38)$$

Solving Equation (4.1.2):  $[\mathbf{K}]\{\mathbf{U}\} = \{\mathbf{F}\}$ , where  $[\mathbf{K}]$  has the expression (4.4.31), the following displacements and reaction forces are obtained:

$$u_3 = 7.4616 \times 10^{-6} \text{ m}, \quad w_3 = -6.0237 \times 10^{-6} \text{ m}, \quad \theta_3 = -8.9667 \times 10^{-7} \text{ rad},$$

$$u_4 = 7.1372 \times 10^{-6} \text{ m}, \quad w_4 = -1.7376 \times 10^{-7} \text{ m}, \quad \theta_4 = 2.1006 \times 10^{-6} \text{ rad}$$

$$R_{u1} = -9.336 \text{ N}, \quad R_{w1} = 313.5388 \text{ N}, \quad R_{\theta1} = -319.3363 \text{ N.m},$$

$$R_{u2} = -490.6639 \text{ N}, \quad R_{w2} = 311.4611 \text{ N}, \quad R_{\theta2} = -569.1077 \text{ N.m} \quad (4.5.39)$$

Now, the generalized deformation matrices are computed using Equation (3.1.11):  $\{\Phi\} = [\mathbf{B}^0]_b \{\mathbf{q}\}_b$ , where  $[\mathbf{B}^0]_1$ ,  $[\mathbf{B}^0]_2$ ,  $[\mathbf{B}^0]_3$  have, respectively, the expressions (4.5.19), (4.5.23) and (4.5.27);  $\{\mathbf{q}\}_1$ ,  $\{\mathbf{q}\}_2$ ,  $\{\mathbf{q}\}_3$  are the displacement matrices for elements 1, 2 and 3.

$$\{\Phi\}_1 = \begin{bmatrix} -1.917 \times 10^{-6} \\ -2.813 \times 10^{-6} \\ -3.420 \times 10^{-7} \end{bmatrix}; \{\Phi\}_2 = \begin{bmatrix} -3.569 \times 10^{-6} \\ -1.468 \times 10^{-6} \\ -1.738 \times 10^{-7} \end{bmatrix}; \{\Phi\}_3 = \begin{bmatrix} 5.658 \times 10^{-7} \\ 3.563 \times 10^{-6} \\ -3.243 \times 10^{-7} \end{bmatrix} \quad (4.5.40)$$

## Analysis of Elastic Frames

The matrices of generalized stresses are obtained by Equation (3.3.10):  $\{M\}_b = [E]_b \{\Phi\}$  where  $[E]_1$ ,  $[E]_2$ ,  $[E]_3$  have, respectively, the expressions (4.5.20), (4.5.24) and (4.5.28):

$$\{M\}_1 = \begin{bmatrix} -319.3363 \\ -33.6245 \\ -245.229 \end{bmatrix}; \{M\}_2 = \begin{bmatrix} -569.1077 \\ -412.2201 \\ -311.4611 \end{bmatrix}; \{M\}_3 = \begin{bmatrix} 33.6245 \\ 412.2201 \\ -290.6639 \end{bmatrix} \quad (4.5.41)$$

In Figure 18 it is shown the deformed shape of the frame.

In Figure 19 it is shown the shear forces diagram and in Figure 20 the moment diagram.

### 4.5.5 Analysis of the Cantilever Column Shown in Figure 21 Including Nonlinear Effects using the Direct Iteration Method

The problem is solved using two steps with increments of force equal to 50 kN each one. It is supposed that at  $t = 0$  the free displacements, deformations, reaction forces and stresses are nil.

In the first step, the increments of the generalized displacements and nodal forces of the element are, respectively,

Figure 18. Deformed frame

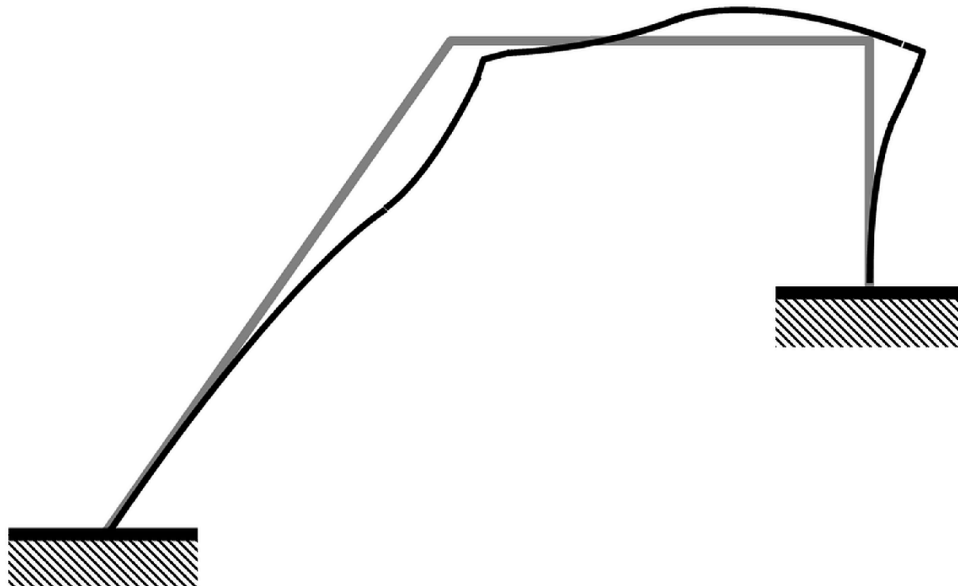




Figure 19. Shear forces diagram

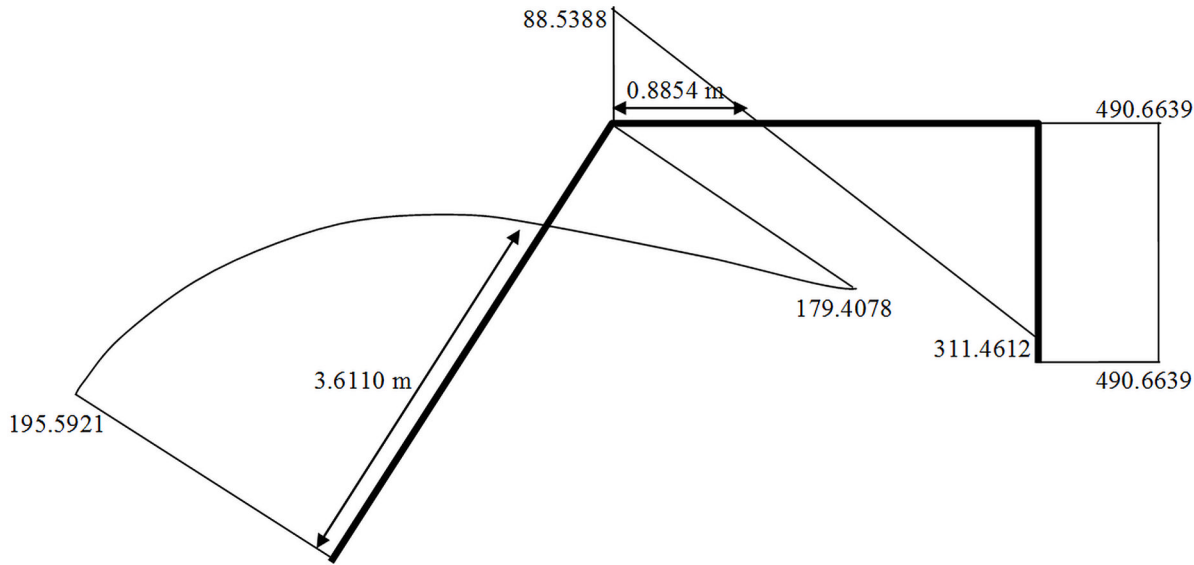
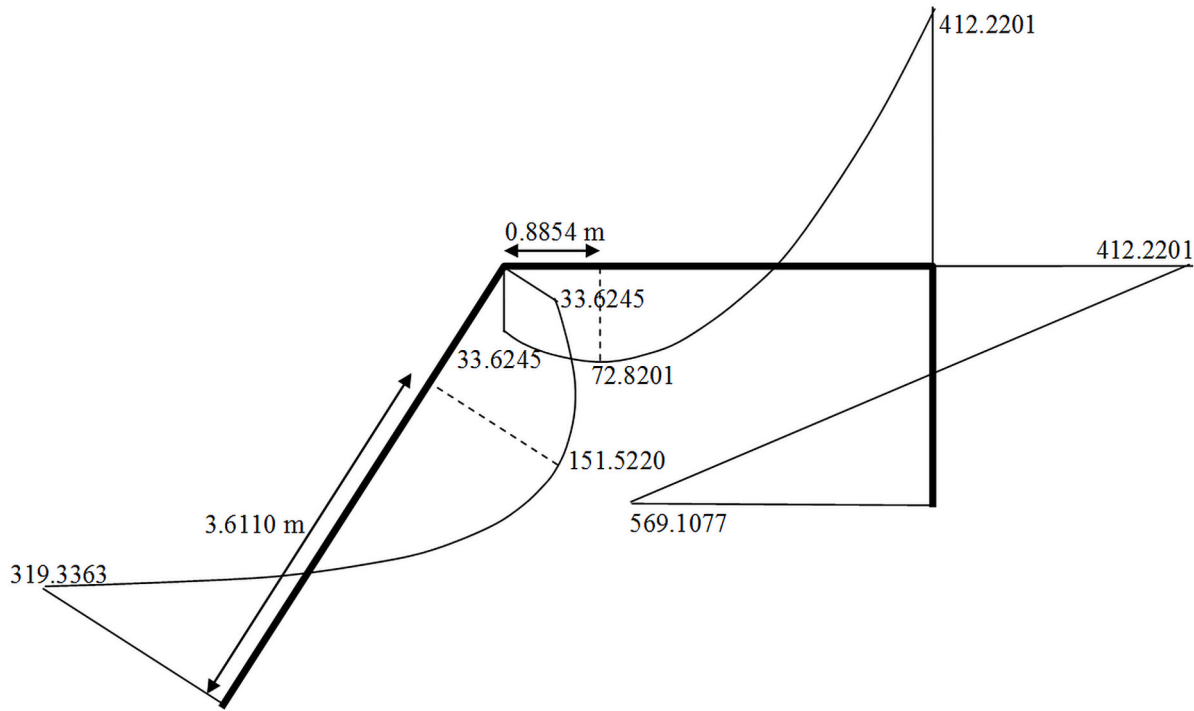
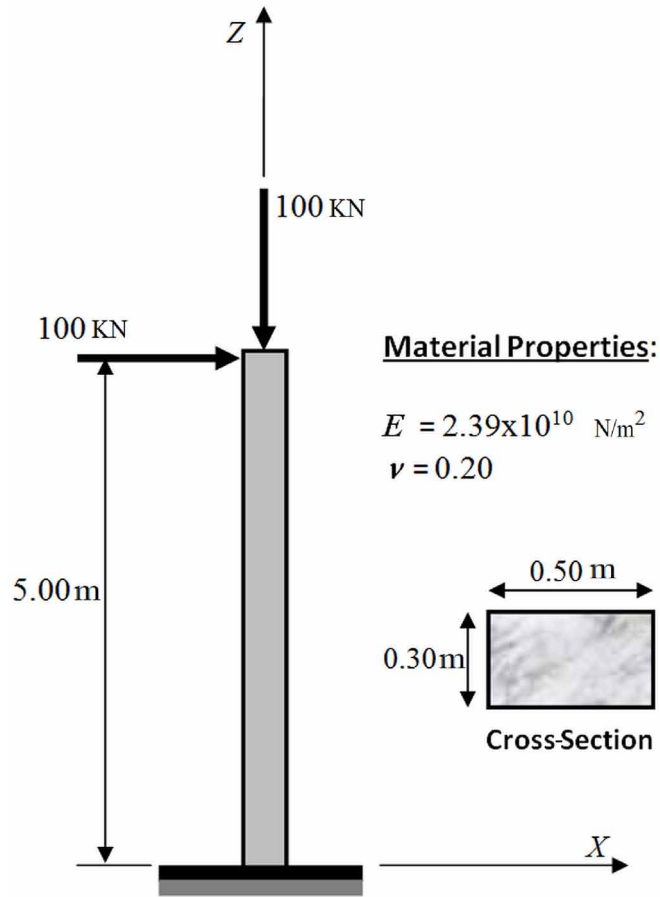


Figure 20. Moment diagram



**Analysis of Elastic Frames**

Figure 21. Cantilever column



$$\{\Delta \mathbf{U}\} = \begin{bmatrix} 0 \\ 0 \\ 0 \\ \Delta u \\ \Delta w \\ \Delta \theta \end{bmatrix}; \{\Delta \mathbf{F}\} = \{\mathbf{P}_{t_1}\} - [\mathbf{B}(\mathbf{U}_{t_1})]^t \{\mathbf{M}_{t_0}\} = \begin{bmatrix} R_{u_{t_1}} \\ R_{w_{t_1}} \\ R_{\theta_{t_1}} \\ 50000 \\ -50000 \\ 0 \end{bmatrix} \quad (4.5.42)$$

It is chosen the provisional solution:

$$\{\mathbf{U}_p\} = \begin{bmatrix} 0 \\ 0 \\ 0 \\ u_p \\ w_p \\ \theta_p \end{bmatrix} = \begin{bmatrix} 0 \\ 0 \\ 0 \\ 0 \\ 0 \\ 0 \end{bmatrix}; \quad (4.5.43)$$

In order to consider the nonlinear effects, the element length and the sine and cosine are computed as:

$$L = \sqrt{u_p^2 + (5 + w_p)^2} = 5 : \sin \alpha = \frac{5 + w_p}{L} = 1; \cos \alpha = \frac{u_p}{L} = 0 \quad (4.5.44)$$

Then, the transformation matrix is:

$$[\mathbf{B}(\mathbf{U}_{t_1})] = \begin{bmatrix} 0.2 & 0 & 1 & -0.2 & 0 & 0 \\ 0.2 & 0 & 0 & -0.2 & 0 & 1 \\ 0 & -1 & 0 & 0 & 1 & 0 \end{bmatrix} \quad (4.5.45)$$

And the elasticity matrix using Euler-Bernoulli theory is:

$$[\mathbf{E}] = \begin{bmatrix} 5.97500 \times 10^7 & 2.98750 \times 10^7 & 0 \\ 2.98750 \times 10^7 & 5.97500 \times 10^7 & 0 \\ 0 & 0 & 7.17000 \times 10^8 \end{bmatrix} \quad (4.5.46)$$

The stiffness matrix of the structure is computed as  $[\mathbf{K}(\mathbf{U}_{t_1})] = [\mathbf{B}(\mathbf{U}_{t_1})]^t [\mathbf{E}] [\mathbf{B}(\mathbf{U}_{t_1})]$  (See Box 3)

The displacements and reaction forces are obtained solving Equation (4.2.5)  $[\mathbf{K}(\mathbf{U}_{t_1})] \{\Delta \mathbf{U}\} = \{\Delta \mathbf{F}(\mathbf{U}_{t_1})\}$ , where  $\{\Delta \mathbf{F}(\mathbf{U}_{t_1})\}$  is (4.5.42b).

$$\Delta u = 0.027894 \text{ m}, \Delta w = -0.00006973 \text{ m}, \Delta \theta = 0.008368 \text{ rad}$$

$$R_{u_{t_1}} = -50000 \text{ N}, R_{w_{t_1}} = 50000 \text{ N}, R_{\theta_{t_1}} = -250000 \text{ N.m} \quad (4.5.48)$$

The actualization of the displacements gives:

**Analysis of Elastic Frames**

Box 3.

$$[\mathbf{K}(\mathbf{U}_{t_1})] = \begin{bmatrix} 0.7172x10^7 & 0 & 0.1793x10^8 & -0.7172x10^7 & 0 & 0.1793x10^8 \\ 0 & 0.7170x10^9 & 0 & 0 & -0.7170x10^9 & 0 \\ 0.1793x10^8 & 0 & 0.5975x10^8 & -0.1793x10^8 & 0 & 0.2988x10^8 \\ -0.7172x10^7 & 0 & -0.1793x10^8 & 0.7172x10^7 & 0 & -0.1793x10^8 \\ 0 & -0.7170x10^9 & 0 & 0 & 0.7170x10^9 & 0 \\ 0.1793x10^8 & 0 & 0.2988x10^8 & -0.1793x10^8 & 0 & 0.5975x10^8 \end{bmatrix} \quad (4.5.47)$$

$$\{\mathbf{U}_{t_1}\} = \{\mathbf{U}_{t_0}\} + \{\Delta\mathbf{U}\} = \begin{bmatrix} 0 \\ 0 \\ 0 \\ u_{t_1} \\ w_{t_1} \\ \theta_{t_1} \end{bmatrix} = \begin{bmatrix} 0 \\ 0 \\ 0 \\ 0 \\ 0 \\ 0 \end{bmatrix} + \begin{bmatrix} 0 \\ 0 \\ 0 \\ 0.02789 \\ -0.00006973 \\ 0.008368 \end{bmatrix} = \begin{bmatrix} 0 \\ 0 \\ 0 \\ 0.02789 \\ -0.00006973 \\ 0.008368 \end{bmatrix} \quad (4.5.49)$$

The convergence criterion used is:

$$\left| \frac{u_t - u_p}{u_t} \right| \leq 10^{-3}; \left| \frac{w_t - w_p}{w_t} \right| \leq 10^{-3} \text{ and } \left| \frac{\theta_t - \theta_p}{\theta_t} \right| \leq 10^{-3} \quad (4.5.50)$$

In this first iteration, it is obtained  $\left| \frac{u_{t_1} - u_p}{u_{t_1}} \right| = \left| \frac{w_{t_1} - w_p}{w_{t_1}} \right| = \left| \frac{\theta_{t_1} - \theta_p}{\theta_{t_1}} \right| = 1.00 > 10^{-3}$ .

All these values are larger than the tolerance; then, it is necessary continue with the iterations in order to obtain an accurate result. For the second iteration, it is chosen as provisional solution the values obtained in the first one, thus:

$$\{\mathbf{U}_p\} = \begin{bmatrix} 0 \\ 0 \\ 0 \\ 0.02789 \\ -0.00006973 \\ 0.008368 \end{bmatrix} \quad (4.5.51)$$

For this iteration:

$$L = 5.000008 \text{ m}, \sin \alpha = 0.99998, \cos \alpha = 0.005578 \quad (4.5.52)$$

with the new values for  $L$ ,  $\sin \alpha$  and  $\cos \alpha$ , the transformation matrix is:

$$[\mathbf{B}(\mathbf{U}_{t_1})] = \begin{bmatrix} 2.00x10^{-1} & -1.11x10^{-3} & 1.00 & -2.00x10^{-1} & 1.11x10^{-3} & 0 \\ 2.00x10^{-1} & -1.11x10^{-3} & 0 & -2.00x10^{-1} & 1.11x10^{-3} & 1.00 \\ -5.58x10^{-3} & -1.00 & 0 & 5.58x10^{-3} & 1.00 & 0 \end{bmatrix} \quad (4.5.53)$$

The stiffness matrix of the structure is:

$$[\mathbf{K}(\mathbf{U}_{t_1})] = \begin{bmatrix} 0.7192x10^7 & 0.3960x10^7 & 0.1792x10^8 & -0.7192x10^7 & -0.3960x10^7 & 0.1792x10^8 \\ 0.3960x10^7 & 0.7170x10^9 & -9.9999x10^4 & -0.3960x10^7 & -0.7170x10^9 & -9.9999x10^4 \\ 0.1792x10^8 & -9.9999x10^4 & 0.5975x10^8 & -0.1792x10^8 & 9.9999x10^4 & 0.2988x10^8 \\ -0.7192x10^7 & -0.3960x10^7 & -0.1792x10^8 & 0.7192x10^7 & 0.3960x10^7 & -0.1792x10^8 \\ -0.3960x10^7 & -0.7170x10^9 & 9.9999x10^4 & 0.3960x10^7 & 0.7170x10^9 & 9.9999x10^4 \\ 0.1792x10^8 & -9.9999x10^4 & 0.2988x10^8 & -0.1792x10^8 & 9.9999x10^4 & 0.5975x10^8 \end{bmatrix} \quad (4.5.54)$$

The following displacements and reaction forces are obtained solving Equation (4.2.5):

$$\Delta u = 0.02804845076 \text{ m}, \Delta w = -0.0002258248590 \text{ m}, \Delta \theta = 0.008414768649 \text{ rad}$$

$$R_{u_{t_1}} = -50000 \text{ N}, R_{w_{t_1}} = 50000 \text{ N}, R_{\theta_{t_1}} = -251391.2134 \text{ N.m} \quad (4.5.55)$$

The resultant displacements are:

$$\{\mathbf{U}_{t_1}\} = \{\mathbf{U}_{t_0}\} + \{\Delta \mathbf{U}\} = \begin{bmatrix} 0 \\ 0 \\ 0 \\ u_{t_1} \\ w_{t_1} \\ \theta_{t_1} \end{bmatrix} = \begin{bmatrix} 0 \\ 0 \\ 0 \\ 0 \\ 0 \\ 0 \end{bmatrix} + \begin{bmatrix} 0 \\ 0 \\ 0 \\ 0.02804845076 \\ -0.0002258248590 \\ 0.008414768649 \end{bmatrix} = \begin{bmatrix} 0 \\ 0 \\ 0 \\ 0.02804845076 \\ -0.0002258248590 \\ 0.008414768649 \end{bmatrix} \quad (4.5.56)$$

The convergence criterion checking, gives:

### Analysis of Elastic Frames

$$\left| \frac{u_{t_1} - u_p}{u_{t_1}} \right| = 5.51x10^{-3} > 10^{-3}; \left| \frac{w_{t_1} - w_p}{w_{t_1}} \right| = 0.69 > 10^{-3}; \left| \frac{\theta_{t_1} - \theta_p}{\theta_{t_1}} \right| = 0.55x10^{-2} < 10^{-3} \quad (4.5.57)$$

Thus, the iterations must continue. For the third iteration, it is chosen as provisional solution the values obtained in the second one,

$$\{ \mathbf{U}_p \} = \begin{bmatrix} 0 \\ 0 \\ 0 \\ 0.02804845076 \\ -0.0002258248590 \\ 0.008414768649 \end{bmatrix} \quad (4.5.58)$$

In this case:

$$L = 4.99985 \text{ m}, \sin \alpha = 0.999984, \cos \alpha = 0.0056099 \quad (4.5.59)$$

The transformation matrix is:

$$[\mathbf{B}(\mathbf{U}_{t_1})] = \begin{bmatrix} 2.00x10^{-1} & -1.12x10^{-3} & 1.00 & -2.00x10^{-1} & 1.11x10^{-3} & 0 \\ 2.00x10^{-1} & -1.12x10^{-3} & 0 & -2.00x10^{-1} & 1.11x10^{-3} & 1.00 \\ -5.61x10^{-3} & -1.00 & 0 & 5.61x10^{-3} & 1.00 & 0 \end{bmatrix} \quad (4.5.60)$$

The stiffness matrix is:

$$[\mathbf{K}(\mathbf{U}_{t_1})] = \begin{bmatrix} 0.7193x10^7 & 0.3982x10^7 & 0.1792x10^8 & -0.7193x10^7 & -0.3982x10^7 & 0.1792x10^8 \\ 0.3982x10^7 & 0.7170x10^9 & -10.0560x10^4 & -0.3982x10^7 & -0.7170x10^9 & -10.0560x10^4 \\ 0.1792x10^8 & -10.0560x10^4 & 0.5975x10^8 & -0.1792x10^8 & 10.0560x10^4 & 0.2988x10^8 \\ -0.7193x10^7 & -0.3982x10^7 & -0.1792x10^8 & 0.7193x10^7 & 0.3982x10^7 & -0.1792x10^8 \\ -0.3982x10^7 & -0.7170x10^9 & 10.0560x10^4 & 0.3982x10^7 & 0.7170x10^9 & 10.0560x10^4 \\ 0.1793x10^8 & -10.0560x10^4 & 0.2988x10^8 & -0.1792x10^8 & 10.0560x10^4 & 0.5975x10^8 \end{bmatrix} \quad (4.5.61)$$

Solving Equation (4.2.5), the following displacements and reaction forces are obtained:

$$\Delta u = 0.0280 \text{ m}, \Delta w = -0.0002267 \text{ m}, \Delta \theta = 0.008415 \text{ rad}$$

$$R_{u_{t_1}} = -50000 \text{ N}, R_{w_{t_1}} = 50000 \text{ N}, R_{\theta_{t_1}} = -251391.1317 \text{ N.m} \quad (4.5.62)$$

Then,

$$\{\mathbf{U}_{t_1}\} = \{\mathbf{U}_{t_0}\} + \{\Delta\mathbf{U}\} = \begin{bmatrix} 0 \\ 0 \\ 0 \\ u_{t_1} \\ w_{t_1} \\ \theta_{t_1} \end{bmatrix} = \begin{bmatrix} 0 \\ 0 \\ 0 \\ 0 \\ 0 \\ 0 \end{bmatrix} + \begin{bmatrix} 0 \\ 0 \\ 0 \\ 0.02805 \\ -0.0002267 \\ 0.008415 \end{bmatrix} = \begin{bmatrix} 0 \\ 0 \\ 0 \\ 0.02805 \\ -0.0002267 \\ 0.008415 \end{bmatrix} \quad (4.5.63)$$

The convergence criterion checking, gives:

$$\left| \frac{u_{t_1} - u_p}{u_{t_1}} \right| = 3.16x10^{-5} < 10^{-3}; \left| \frac{w_{t_1} - w_p}{w_{t_1}} \right| = 3.81x10^{-3} > 10^{-3}; \left| \frac{\theta_{t_1} - \theta_p}{\theta_{t_1}} \right| = -3.25x10^{-7} < 10^{-3} \quad (4.5.64)$$

In order to improve the value of the vertical displacement, the process is repeated once again. For the fourth iteration, the provisional solution is:

$$\{\mathbf{U}_p\} = \begin{bmatrix} 0 \\ 0 \\ 0 \\ 0.02805 \\ -0.0002267 \\ 0.008415 \end{bmatrix} \quad (4.5.65)$$

In this case

$$L = 4.99985 \text{ m}, \sin \alpha = 0.999984, \cos \alpha = 0.0056097 \quad (4.5.66)$$

The transformation matrix is:

$$[\mathbf{B}(\mathbf{U}_{t_1})] = \begin{bmatrix} 2.00x10^{-1} & -1.12x10^{-3} & 1.00 & -2.00x10^{-1} & 1.12x10^{-3} & 0 \\ 2.00x10^{-1} & -1.12x10^{-3} & 0 & -2.00x10^{-1} & 1.12x10^{-3} & 1.00 \\ -5.61x10^{-3} & -1.00 & 0 & 5.61x10^{-3} & 1.00 & 0 \end{bmatrix} \quad (4.5.67)$$

## Analysis of Elastic Frames

The stiffness matrix of the structure:

$$[\mathbf{K}(\mathbf{U}_{t_1})] = \begin{bmatrix} 0.7193x10^7 & 0.3982x10^7 & 0.1792x10^8 & -0.7193x10^7 & -0.3982x10^7 & 0.1792x10^8 \\ 0.3982x10^7 & 0.7170x10^9 & -10.0560x10^4 & -0.3982x10^7 & -0.7170x10^9 & -10.0560x10^4 \\ 0.1792x10^8 & -10.0560x10^4 & 0.5975x10^8 & -0.1792x10^8 & 10.0560x10^4 & 0.2988x10^8 \\ -0.7193x10^7 & -0.3982x10^7 & -0.1792x10^8 & 0.7193x10^7 & 0.3982x10^7 & -0.1792x10^8 \\ -0.3982x10^7 & -0.7170x10^9 & 10.0560x10^4 & 0.3982x10^7 & 0.7170x10^9 & 10.0560x10^4 \\ 0.1793x10^8 & -10.0560x10^4 & 0.2988x10^8 & -0.1792x10^8 & 10.0560x10^4 & 0.5975x10^8 \end{bmatrix} \quad (4.5.68)$$

Solving Equation (4.2.5), the following displacements and reaction forces are obtained:

$$\Delta u = 0.02804754924 \text{ m}, \Delta w = -0.0002266840291 \text{ m}, \Delta \theta = 0.008414762972 \text{ rad}$$

$$R_{u_{t_1}} = -50000 \text{ N}, R_{w_{t_1}} = 50000 \text{ N}, R_{\theta_{t_1}} = -251391.0438 \text{ N.m} \quad (4.5.69)$$

The resultant displacements are:

$$\{\mathbf{U}_{t_1}\} = \{\mathbf{U}_{t_0}\} + \{\Delta\mathbf{U}\} = \begin{bmatrix} 0 \\ 0 \\ 0 \\ u_{t_1} \\ w_{t_1} \\ \theta_{t_1} \end{bmatrix} = \begin{bmatrix} 0 \\ 0 \\ 0 \\ 0 \\ 0 \\ 0 \end{bmatrix} + \begin{bmatrix} 0 \\ 0 \\ 0 \\ 0.02804754924 \\ -0.0002266840291 \\ 0.008414762972 \end{bmatrix} = \begin{bmatrix} 0 \\ 0 \\ 0 \\ 0.02804754924 \\ -0.0002266840291 \\ 0.008414762972 \end{bmatrix} \quad (4.5.70)$$

The convergence criterion is checked again:

$$\left| \frac{u_{t_1} - u_p}{u_{t_1}} \right| = 5.22x10^{-7} < 10^{-3}; \left| \frac{w_{t_1} - w_p}{w_{t_1}} \right| = 2.21x10^{-5} < 10^{-3}; \left| \frac{\theta_{t_1} - \theta_p}{\theta_{t_1}} \right| = -3.50x10^{-7} < 10^{-3} \quad (4.5.71)$$

It is not necessary to continue with the process since the three displacements satisfy the convergence criterion.

The displacements and reactions at the final of the first step are:



$$\{\mathbf{U}_{t_1}\} = \{\mathbf{U}_{t_0}\} + \{\Delta\mathbf{U}\} = \begin{bmatrix} 0 \\ 0 \\ 0 \\ 0.02804754924 \\ -0.0002266840291 \\ 0.008414762972 \end{bmatrix}; \{\mathbf{F}\} = \begin{bmatrix} -50000 \\ 50000 \\ -251391.0438 \\ 50000 \\ -50000 \\ 0 \end{bmatrix} \quad (4.5.72)$$

The deformations and stresses at the final of the step are:

$$\{\Phi_{t_1}\} = [\mathbf{B}(\mathbf{U}_{t_1})] \{\mathbf{U}_{t_1}\} = \begin{bmatrix} -0.00560984 \\ 0.00280492 \\ -0.00006934 \end{bmatrix}; \{\mathbf{M}_{t_1}\} = [\mathbf{E}] \{\Phi_{t_1}\} = \begin{bmatrix} -251391.0438 \\ 0.00000 \\ -49718.72938 \end{bmatrix} \quad (4.5.73)$$

In the second step, the increments of the generalized displacements and nodal forces of the element are, respectively,

$$\{\Delta\mathbf{U}\} = \begin{bmatrix} 0 \\ 0 \\ 0 \\ \Delta u \\ \Delta w \\ \Delta\theta \end{bmatrix}; \{\Delta\mathbf{F}\} = \{\mathbf{P}_{t_2}\} - [\mathbf{B}(\mathbf{U}_{t_1})]^t \{\mathbf{M}_{t_1}\} = \begin{bmatrix} R_{u_{t_2}} \\ R_{w_{t_2}} \\ R_{\theta_{t_2}} \\ 100000 \\ -100000 \\ 0 \end{bmatrix} - [\mathbf{B}(\mathbf{U}_{t_1})]^t \begin{bmatrix} -251391.0438 \\ 0.00000 \\ -49718.72938 \end{bmatrix} \quad (4.5.74)$$

As provisional solution it is chosen the displacements obtained at the final of the step 1.

$$\{\mathbf{U}_p\} = \begin{bmatrix} 0 \\ 0 \\ 0 \\ 0.02804754924 \\ -0.0002266840291 \\ 0.008414762972 \end{bmatrix} \quad (4.5.75)$$

In this case

$$L = 4.99985 \text{ m}, \sin \alpha = 0.999984, \cos \alpha = 0.0056097 \quad (4.5.76)$$

The transformation matrix is:

**Analysis of Elastic Frames**

$$[\mathbf{B}(\mathbf{U}_{t_2})] = \begin{bmatrix} 2.00x10^{-1} & -1.12x10^{-3} & 1.00 & -2.00x10^{-1} & 1.12x10^{-3} & 0 \\ 2.00x10^{-1} & -1.12x10^{-3} & 0 & -2.00x10^{-1} & 1.12x10^{-3} & 1.00 \\ -5.61x10^{-3} & -1.00 & 0 & 5.61x10^{-3} & 1.00 & 0 \end{bmatrix} \quad (4.5.77)$$

The stiffness matrix of the structure is computed as  $[\mathbf{K}(\mathbf{U}_{t_2})] = [\mathbf{B}(\mathbf{U}_{t_2})]^t [\mathbf{E}] [\mathbf{B}(\mathbf{U}_{t_2})]$

$$[\mathbf{K}(\mathbf{U}_{t_2})] = \begin{bmatrix} 0.7193x10^7 & 0.3982x10^7 & 0.1792x10^8 & -0.7193x10^7 & -0.3982x10^7 & 0.1792x10^8 \\ 0.3982x10^7 & 0.7170x10^9 & -10.0560x10^4 & -0.3982x10^7 & -0.7170x10^9 & -10.0560x10^4 \\ 0.1792x10^8 & -10.0560x10^4 & 0.5975x10^8 & -0.1792x10^8 & 10.0560x10^4 & 0.2988x10^8 \\ -0.7193x10^7 & -0.3982x10^7 & -0.1792x10^8 & 0.7193x10^7 & 0.3982x10^7 & -0.1792x10^8 \\ -0.3982x10^7 & -0.7170x10^9 & 10.0560x10^4 & 0.3982x10^7 & 0.7170x10^9 & 10.0560x10^4 \\ 0.1793x10^8 & -10.0560x10^4 & 0.2988x10^8 & -0.1792x10^8 & 10.0560x10^4 & 0.5975x10^8 \end{bmatrix} \quad (4.5.78)$$

and the increment of the forces  $\{\Delta\mathbf{F}\}$  is

$$\{\Delta\mathbf{F}\} = \{\mathbf{P}_{t_2}\} - [\mathbf{B}(\mathbf{U}_{t_2})]^t \{\mathbf{M}_{t_1}\} = \begin{bmatrix} R_{ut_2} \\ R_{wt_2} \\ R_{\theta t_2} \\ 100000 \\ -100000 \\ 0 \end{bmatrix} - [\mathbf{B}(\mathbf{U}_{t_2})]^t \begin{bmatrix} -251391.0438 \\ 0.00000 \\ -49718.72938 \end{bmatrix} = \begin{bmatrix} R_{ut_2} + 50000.00008 \\ R_{wt_2} - 49999.99989 \\ R_{\theta t_2} + 251391.0438 \\ 49999.99992 \\ -50000.00011 \\ 0 \end{bmatrix} \quad (4.5.79)$$

The following displacements and reaction forces are obtained with the resolution of Equation (4.2.5):

$$\Delta u = 0.02804754917 \text{ m}; \Delta w = -0.0002266839468 \text{ m}; \Delta \theta = 0.008414762941 \text{ rad}$$

$$R_{ut_2} = -100000 \text{ N}, R_{wt_2} = 100000 \text{ N}, R_{\theta t_2} = -502782.0867 \text{ N.m} \quad (4.5.80)$$

The displacements are:

$$\{\mathbf{U}_{t_2}\} = \{\mathbf{U}_{t_1}\} + \{\Delta\mathbf{U}\} = \begin{bmatrix} 0 \\ 0 \\ 0 \\ u_{t_2} \\ w_{t_2} \\ \theta_{t_2} \end{bmatrix} = \begin{bmatrix} 0 \\ 0 \\ 0 \\ 0.02804754924 \\ -0.0002266840291 \\ 0.008414762972 \end{bmatrix} + \begin{bmatrix} 0 \\ 0 \\ 0 \\ 0.02804754917 \\ -0.0002266839468 \\ 0.008414762941 \end{bmatrix} = \begin{bmatrix} 0 \\ 0 \\ 0 \\ 0.05609509841 \\ -0.0004533679759 \\ 0.01682952591 \end{bmatrix} \quad (4.5.81)$$

The convergence criterion checking, gives:

$$\left| \frac{u_{t_1} - u_p}{u_{t_1}} \right| = 0.49999 > 10^{-3}; \left| \frac{w_{t_1} - w_p}{w_{t_1}} \right| = 0.49999 > 10^{-3}; \left| \frac{\theta_{t_1} - \theta_p}{\theta_{t_1}} \right| = 0.49999 > 10^{-3} \quad (4.5.82)$$

Thus, it is necessary to continue with the iterations. Taking the final displacements of the first iteration as provisional solution:

$$\{\mathbf{U}_p\} = \begin{bmatrix} 0 \\ 0 \\ 0 \\ 0.02789400279 \\ -0.00006973500697 \\ 0.008368200837 \end{bmatrix} \quad (4.5.83)$$

The new length,  $\sin\alpha$  and  $\cos\alpha$  are computed:

$$L = 4.999861317 \text{ m}, \sin\alpha = 0.9999370613, \cos\alpha = 0.01121933087 \quad (4.5.84)$$

With these values, the transformation matrix is:

$$[\mathbf{B}(\mathbf{U}_{t_2})] = \begin{bmatrix} 2.00x10^{-1} & -2.24x10^{-3} & 1.00 & -2.00x10^{-1} & 2.24x10^{-3} & 0 \\ 2.00x10^{-1} & -2.24x10^{-3} & 0 & -2.00x10^{-1} & 2.24x10^{-3} & 1.00 \\ -1.12x10^{-2} & -1.00 & 0 & 1.12x10^{-2} & 1.00 & 0 \end{bmatrix} \quad (4.5.85)$$

The stiffness matrix of the structure is:

### Analysis of Elastic Frames

$$[\mathbf{K}(\mathbf{U}_{t_2})] = \begin{bmatrix} 0.7260x10^7 & 0.7963x10^7 & 0.1792x10^8 & -0.7260x10^7 & -0.7963x10^7 & 0.1792x10^8 \\ 0.7963x10^7 & 0.7169x10^9 & -20.1112x10^4 & -0.7963x10^7 & -0.7169x10^9 & -20.1112x10^4 \\ 0.1792x10^8 & -20.1112x10^4 & 0.5975x10^8 & -0.1792x10^8 & 20.1112x10^4 & 0.2988x10^8 \\ -0.7260x10^7 & -0.7963x10^7 & -0.1792x10^8 & 0.7260x10^7 & 0.7963x10^7 & -0.1792x10^8 \\ -0.7963x10^7 & -0.7169x10^9 & 20.1112x10^4 & 0.7963x10^7 & 0.7169x10^9 & 20.1112x10^4 \\ 0.1792x10^8 & -20.1112x10^4 & 0.2988x10^8 & -0.1792x10^8 & 20.1112x10^4 & 0.5975x10^8 \end{bmatrix} \quad (4.5.86)$$

The increments of the forces are:

$$\{\Delta \mathbf{F}\} = \begin{bmatrix} R_{u_{t_2}} + 49718.62794 \\ R_{w_{t_2}} - 50279.70366 \\ R_{\theta_{t_2}} + 251391.0438 \\ 50281.37206 \\ -49720.29634 \\ 0 \end{bmatrix} \quad (4.5.87)$$

Solving Equation (4.2.5), the following displacements and reaction forces are obtained:

$$\Delta u = 0.02835628328 \text{ m}, \Delta w = -0.0003867166206 \text{ m}, \Delta \theta = 0.008507887161 \text{ rad}$$

$$R_{u_{t_2}} = -100000 \text{ N}, R_{w_{t_2}} = 100000 \text{ N}, R_{\theta_{t_2}} = -505564.1727 \text{ N.m} \quad (4.5.88)$$

The resultant displacements are:

$$\{\mathbf{U}_{t_2}\} = \{\mathbf{U}_{t_1}\} + \{\Delta \mathbf{U}\} = \begin{bmatrix} 0 \\ 0 \\ 0 \\ 0.05640383252 \\ -0.0006134006497 \\ 0.01692265013 \end{bmatrix} \quad (4.5.89)$$

The convergence criterion checking, gives:

$$\left| \frac{u_{t_1} - u_p}{u_{t_1}} \right| = 5.474x10^{-3} > 10^{-3}; \left| \frac{w_{t_1} - w_p}{w_{t_1}} \right| = 0.2609 > 10^{-3}; \left| \frac{\theta_{t_1} - \theta_p}{\theta_{t_1}} \right| = 0.5503 x10^{-2} < 10^{-3} \quad (4.5.90)$$

Therefore, it is required to continue with the iterations again. For the third iteration, it is chosen as provisional solution the values obtained in the second one, then

$$\{ \mathbf{U}_p \} = \begin{bmatrix} 0 \\ 0 \\ 0 \\ 0.05640383252 \\ -0.0006134006497 \\ 0.01692265013 \end{bmatrix} \quad (4.5.91)$$

The new length,  $\sin\alpha$  and  $\cos\alpha$  are computed:

$$L = 4.999704767 \text{ m}, \sin\alpha = 0.9999363626, \cos\alpha = 0.01128143263 \quad (4.5.92)$$

With these values, the transformation matrix is:

$$[\mathbf{B}(\mathbf{U}_{t_2})] = \begin{bmatrix} 2.00x10^{-1} & -2.23x10^{-3} & 1.00 & -2.00x10^{-1} & 2.23x10^{-3} & 0 \\ 2.00x10^{-1} & -2.23x10^{-3} & 0 & -2.00x10^{-1} & 2.23x10^{-3} & 1.00 \\ -1.12x10^{-2} & -1.00 & 0 & 1.13x10^{-2} & 1.00 & 0 \end{bmatrix} \quad (4.5.93)$$

The stiffness matrix of the structure is:

$$[\mathbf{K}(\mathbf{U}_{t_2})] = \begin{bmatrix} 0.7261x10^7 & 0.8007x10^7 & 0.1792x10^8 & -0.7261x10^7 & -0.8007x10^7 & 0.1792x10^8 \\ 0.8007x10^7 & 0.7169x10^9 & -20.2231x10^4 & -0.8007x10^7 & -0.7169x10^9 & -20.2231x10^4 \\ 0.1792x10^8 & -20.2231x10^4 & 0.5975x10^8 & -0.1792x10^8 & 20.2231x10^4 & 0.2988x10^8 \\ -0.7261x10^7 & -0.8007x10^7 & -0.1792x10^8 & 0.7261x10^7 & 0.8007x10^7 & -0.1792x10^8 \\ -0.8007x10^7 & -0.7169x10^9 & 20.2231x10^4 & 0.8007x10^7 & 0.7169x10^9 & 20.2231x10^4 \\ 0.1792x10^8 & -20.2231x10^4 & 0.2988x10^8 & -0.1792x10^8 & 20.2231x10^4 & 0.5975x10^8 \end{bmatrix} \quad (4.5.94)$$

The increments of the forces are:

**Analysis of Elastic Frames**

$$\{\Delta \mathbf{F}\} = \begin{bmatrix} R_{u_{t_2}} + 49717.07943 \\ R_{w_{t_2}} - 50282.80913 \\ R_{\theta_{t_2}} + 251391.0438 \\ 50282.92057 \\ -49717.19087 \\ 0 \end{bmatrix} \quad (4.5.95)$$

Solving Equation (4.2.5), the following displacements and reaction forces are obtained:

$$\Delta u = 0.02835703041 \text{ m}, \Delta w = -0.0003884776480 \text{ m}, \Delta \theta = 0.008508384923 \text{ rad}$$

$$R_{u_{t_2}} = -100000 \text{ N}, R_{w_{t_2}} = 100000 \text{ N}, R_{\theta_{t_2}} = -505579.0434 \text{ N.m} \quad (4.5.96)$$

The resultant displacements are:

$$\{\mathbf{U}_{t_2}\} = \{\mathbf{U}_{t_1}\} + \{\Delta \mathbf{U}\} = \begin{bmatrix} 0 \\ 0 \\ 0 \\ 0.05640457965 \\ -0.0006151616771 \\ 0.01692314790 \end{bmatrix} \quad (4.5.97)$$

The convergence criterion checking, gives:

$$\left| \frac{u_{t_1} - u_p}{u_{t_1}} \right| = 1.325 \times 10^{-5} > 10^{-3}; \left| \frac{w_{t_1} - w_p}{w_{t_1}} \right| = 2.863 \times 10^{-3} > 10^{-3}; \left| \frac{\theta_{t_1} - \theta_p}{\theta_{t_1}} \right| = 2.941 \times 10^{-5} < 10^{-3} \quad (4.5.98)$$

In order to improve the vertical displacement, other iteration is required. Again, it is chosen as provisional solution, the values obtained in the former iteration, thus

$$\{\mathbf{U}_p\} = \begin{bmatrix} 0 \\ 0 \\ 0 \\ 0.05640457965 \\ -0.0006151616771 \\ 0.01692314790 \end{bmatrix} \quad (4.5.99)$$

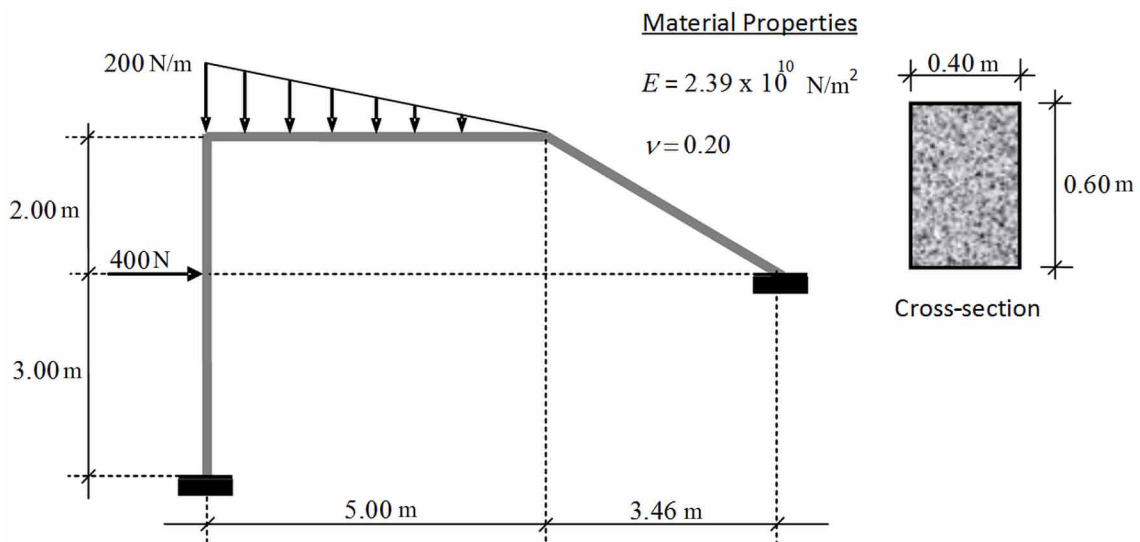
The new length,  $\sin\alpha$  and  $\cos\alpha$  are computed:

$$L = 4.999703015 \text{ m}, \sin\alpha = 0.9999363608, \cos\alpha = 0.01128158602 \quad (4.5.100)$$

With these values, the transformation matrix is:

$$[\mathbf{B}(\mathbf{U}_{t_2})] = \begin{bmatrix} 2.00 \times 10^{-1} & -2.26 \times 10^{-3} & 1.00 & -2.00 \times 10^{-1} & 2.26 \times 10^{-3} & 0 \\ 2.00 \times 10^{-1} & -2.26 \times 10^{-3} & 0 & -2.00 \times 10^{-1} & 2.26 \times 10^{-3} & 1.00 \\ -1.13 \times 10^{-2} & -1.00 & 0 & 1.13 \times 10^{-2} & 1.00 & 0 \end{bmatrix} \quad (4.5.101)$$

Figure 22. Planar frame



## Analysis of Elastic Frames

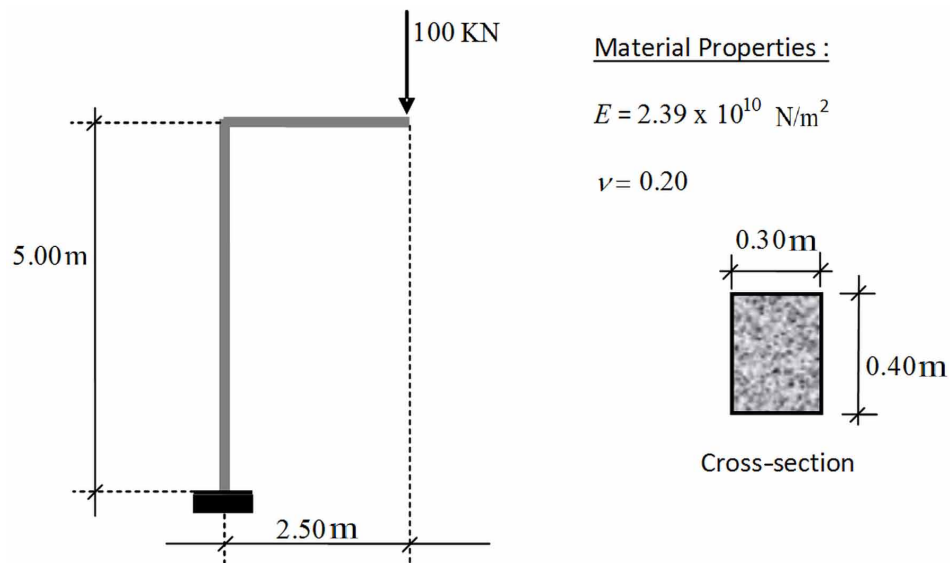
The stiffness matrix of the structure is:

$$[\mathbf{K}(\mathbf{U}_{t_2})] = \begin{bmatrix} 0.7261 \times 10^7 & 0.8007 \times 10^7 & 0.1792 \times 10^8 & -0.7261 \times 10^7 & -0.8007 \times 10^7 & 0.1792 \times 10^8 \\ 0.8007 \times 10^7 & 0.7169 \times 10^9 & -20.2234 \times 10^4 & -0.8007 \times 10^7 & -0.7169 \times 10^9 & -20.2234 \times 10^4 \\ 0.1792 \times 10^8 & -20.2234 \times 10^4 & 0.5975 \times 10^8 & -0.1792 \times 10^8 & 20.2234 \times 10^4 & 0.2988 \times 10^8 \\ -0.7261 \times 10^7 & -0.8007 \times 10^7 & -0.1792 \times 10^8 & 0.7261 \times 10^7 & 0.8007 \times 10^7 & -0.1792 \times 10^8 \\ -0.8007 \times 10^7 & -0.7169 \times 10^9 & 20.2234 \times 10^4 & 0.8007 \times 10^7 & 0.7169 \times 10^9 & 20.2234 \times 10^4 \\ 0.1792 \times 10^8 & -20.2234 \times 10^4 & 0.2988 \times 10^8 & -0.1792 \times 10^8 & 20.2234 \times 10^4 & 0.5975 \times 10^8 \end{bmatrix} \quad (4.5.102)$$

The increments of the forces are:

$$\{\Delta \mathbf{F}\} = \begin{bmatrix} R_{u_{t_2}} + 49717.08933 \\ R_{w_{t_2}} - 50282.81695 \\ R_{\theta_{t_2}} + 251391.0438 \\ 50282.91067 \\ -49717.18305 \\ 0 \end{bmatrix} \quad (4.5.103)$$

Figure 23. Planar frame





Solving Equation (4.2.5), the following displacements and reaction forces are obtained:

$$\Delta u = 0.02835700909 \text{ m}, \Delta w = -0.0003884817364 \text{ m}, \Delta \theta = 0.008508381520 \text{ rad}$$

$$R_{u_{t_2}} = -100000 \text{ N}, R_{w_{t_2}} = 100000 \text{ N}, R_{\theta_{t_2}} = -505579.0434 \text{ N.m} \quad (4.5.104)$$

The resultant displacements are:

$$\{\mathbf{U}_{t_2}\} = \{\mathbf{U}_{t_1}\} + \{\Delta \mathbf{U}\} = \begin{bmatrix} 0 \\ 0 \\ 0 \\ 0.05640455833 \\ -0.0006151657655 \\ 0.01692314449 \end{bmatrix} \quad (4.5.105)$$

The convergence criterion checking, gives:

$$\left| \frac{u_{t_1} - u_p}{u_{t_1}} \right| = -0.377 \times 10^{-7} < 10^{-3}; \left| \frac{w_{t_1} - w_p}{w_{t_1}} \right| = 0.665 \times 10^{-5} < 10^{-3}; \left| \frac{\theta_{t_1} - \theta_p}{\theta_{t_1}} \right| = -0.201 \times 10^{-6} < 10^{-3} \quad (4.5.106)$$

Therefore, the final displacements and nodal forces are:

$$\{\mathbf{U}\} = \{\mathbf{U}_{t_2}\} = \begin{bmatrix} 0 \\ 0 \\ 0 \\ 0.05640455833 \\ -0.0006151657655 \\ 0.01692314449 \end{bmatrix}; \{\mathbf{F}\} = \begin{bmatrix} -100000 \\ 100000 \\ -505579.0434 \\ 100000 \\ -100000 \\ 0 \end{bmatrix} \quad (4.5.107)$$

And the final deformations and stresses are:

$$\{\Phi_{t_2}\} = [\mathbf{B}(\mathbf{U}_{t_2})] \{\mathbf{U}_{t_2}\} = \begin{bmatrix} -0.01128225190 \\ 0.00564089259 \\ -0.0000212062599 \end{bmatrix}; \{\mathbf{M}_{t_2}\} = [\mathbf{E}] \{\Phi_{t_2}\} = \begin{bmatrix} -505592.8849 \\ -13.9432 \\ 15204.88835 \end{bmatrix} \quad (4.5.108)$$

As shown, the bending moment at the free end has a value of -13.9432 with is negligible compared with 505592.8849.

## **4.6 PROBLEMS**

### **4.6.1 Planar Frame Subjected to Several Force**

Solve the frame shown in Figure 22 using Timoshenko theory and the direct stiffness method.

### **4.6.2 Assemblage of the Stiffness and the Total Forces Matrices**

For the frame shown in Figure 22, assemble the stiffness matrix and total forces.

### **4.6.3 Analysis of a Cantilever Column**

Solve the cantilever column shown in Figure 19 using the Newton-Raphson method.

### **4.6.4 Analysis of a Planar Frame Considering Nonlinear Effects**

Solve the frame shown in Figure 23 by the direct iteration method, using any algebraic manipulation program.

### **4.6.5 Analysis of a Planar Frame Considering Nonlinear Effects**

Solve the frame shown in Figure 23 by the Newton-Raphson method using any algebraic manipulation program.

### **4.6.6 Tridimensional Stiffness Matrix**

Deduce the stiffness matrix corresponding to the tridimensional case using any algebraic manipulation program.

### **4.6.7 Algorithms of Assemblage**

Generalize the algorithms for the assemblage of the stiffness and total forces matrices (sections: 4.1.2 and 4.1.3) to the tridimensional case.

## **4.7 PROJECTS**

**4.7.1 Write a Program Based on the Direct Stiffness Algorithm Using Any Computer Programming Language (Fortran, Visual Basic, Matlab, Maple, Pascal, Python, Etc.)**

**4.7.2 Generalize the Program Written in Section 4.7.1 including the Analysis of Nonlinear Frames Using the Direct Iteration Method**

**4.7.3 Generalize the Program Written in Section 4.7.1 including the Analysis of Nonlinear Frames Using the Newton-Raphson Method**

**4.7.4 Generalize the Program Written in Section 4.7.3 to the Tridimensional Case**

## **REFERENCES**

- Atkinson, K. E. (1989). *An introduction to numerical analysis*. New York, NY: John Wiley & Sons.
- Bathe, J. (1996). *Finite element procedures in engineering analysis*. Prentice Hall.
- Batoz, J. L., & Dhatt, G. (1992). *Modélisation des structures par éléments finis: Solides élastiques* (Vol. 1). Paris, France: Hermès.
- Carnahan, B., Luther, H., & Wilkes, J. (1969). *Applied numerical methods*. New York, NY: John Wiley & Sons.
- Clough, R. W., & Penzien, J. (1993). *Dynamics of structures*. New York, NY: McGraw-Hill.
- Craig, R. R. (1981). *Structural dynamics-An introduction to computer methods*. New York, NY: John Wiley & Sons.
- McGuire, W., Gallagher, R. H., & Ziemian, R. D. (1979). *Matrix structural analysis*. New York, NY: John Wiley & Sons.
- Paz, M. (1997). *Structural dynamics-Theory and computation*. Boston, MA: Springer. doi:10.1007/978-1-4684-0018-2
- Powell, G. H. (1969). Theory for nonlinear elastic structures. *Journal of the Structural Division, ST12*, 2687–2701.
- Powell, G. H. (1969). Theory of nonlinear elastic structures. *Structural Division Journal, 95*, 2687–2701.

# Chapter 5

## Fundamental Concepts of Plasticity

### ABSTRACT

*This chapter introduces some fundamental concepts of plasticity that are used in Chapter 6 to formulate the concept of plastic hinge and in Chapter 7 to describe elasto-plastic models for frames; in the present one, only the uniaxial behavior of the material is considered. In this chapter, the key concepts of perfect plasticity, yield function, and plastic hardening are introduced. The two alternative formulations for plastic hardening, isotropic and kinematic, are discussed in detail. Plasticity is presented as a way to mathematically represent the experimental behavior of ductile materials; the limits of plasticity for describing reality are also established.*

### 5.1 EXPERIMENTAL BEHAVIOR OF DUCTILE MATERIALS

Consider again the example of the paper clip used in chapter 1. The loading process consists in imposed displacements that represent the actions of the paper sheets on the clip (see Figure 1). If a limited number of pages is used, the clip recovers its initial form once they are removed. If the clip is used with an excessive number of sheets, it will not recuperate its original shape. It is evident that a computer analysis that does not predict structural modifications or deterioration of the clip, no matter how many paper sheets are used, is not very useful. That would be the case if only elastic analyses of the paper clip are carried out: no permanent deformations can be predicted in that case.

Elastic models as the ones described in chapter 3 should be used with extreme precautions and always with some elastic limit criterion at hand. If that limit is exceeded, then more sophisticated models are needed. This chapter describes a step in that direction; the elasto-plastic models differ from the elastic ones because they consider the possibility of permanent deformations, as the ones that occur when an excessive number of pages are held together.

Figure 2 shows the experimental response of a metallic specimen during a tension test with unloading: the specimen is stretched in a testing machine so that the material is subjected to the strain history shown

DOI: 10.4018/978-1-4666-6379-4.ch005

Figure 1. Paper clip as a structure

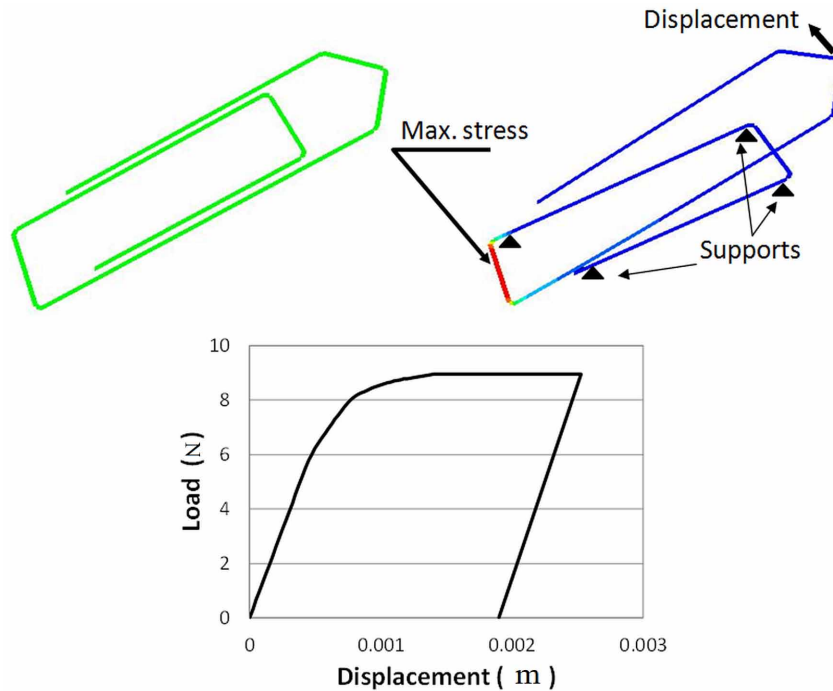
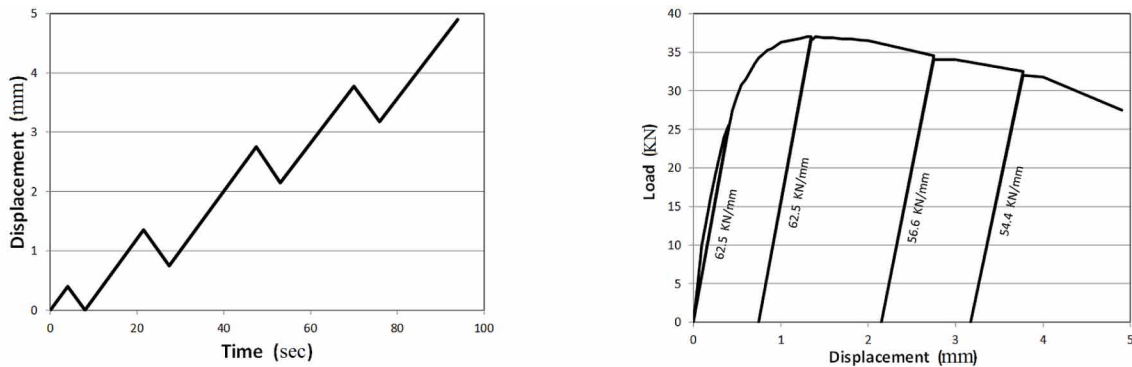


Figure 2. Experimental behavior of a metallic specimen in a mono-sign test



in Figure 2a. This kind of tests is called mono-sign traction test in this book. Notice that the number and the instant of the unloadings are arbitrarily fixed by the experimenter. The behavior of metallic materials observed in these tests is summarized in table 1.

Notice that during the test, the material behavior changes with the loading: first, it is elastic and then permanent strains appear; this is called plastic behavior. The strength to plasticity grows with permanent strains and then decreases; the material stiffness is first constant and then starts to decrease with large plastic strains.

## Fundamental Concepts of Plasticity

Table 1. Phenomena observed during mono-sign tests

a)	Existence of a zone that can be characterized as linear elastic
b)	Presence of plastic strains; i.e. strains that do not disappear after unloading if a limit in stress is reached
c)	Zone of constant elasticity modulus
d)	Zone of plastic hardening, which is an increase in the elastic limit with plastic strain
e)	Existence of an ultimate or maximum stress
f)	Zone of plastic softening or strength degradation; i.e. a decrease in the elastic limit with plastic strain
g)	Zone of stiffness degradation; i.e. a decrease of the elastic modulus with plastic strain
h)	Existence of a maximum or failure strain

The goal of plasticity theory is to model some of these behaviors, specifically phenomena “a” to “e”. The rest of them are taken into account in the framework of the theory of damage mechanics described in chapter 9.

## 5.2 ELASTO-PERFECT PLASTIC CONSTITUTIVE MODEL

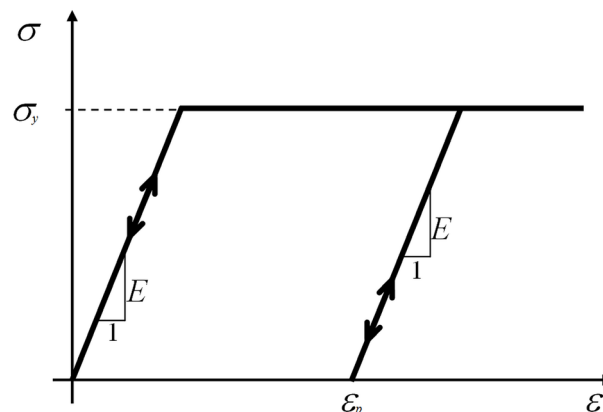
### 5.2.1 Idealization of the Mono-Sign Test

The elasto-perfect plastic model idealizes the behavior of metallic specimens in mono sign tests as shown in Figure 3. This idealization takes into account only phenomena “a”, “b”, “c” and “e” in Table 1.

In this model, there is a zone of elastic behavior while the stress does not reach the elastic limit  $\sigma_y$ ; i.e. strains are reversible in that case. When the stress reaches the elastic limit  $\sigma_y$ , the material starts yielding with constant stress; i.e. permanent strains appear. The value  $\sigma_y$  is called yield stress.

During any elastic unloading, stress and strain decrease following straight lines of slope  $E$ . The remaining strain for a  $\sigma$  equal to zero is the plastic strain value  $\epsilon_p$ . If a reloading process follows the unloading,

Figure 3. Elasto-perfect plastic model



the strain stress points continue in the same straight line until the elastic limit  $\sigma_y$  is reached again, then the material starts yielding once more.

### 5.2.2 Elasticity Law

It is now necessary to express the behavior represented in Figure 3 in mathematical language. Notice that a single mathematical relationship such as  $\sigma = \sigma(\varepsilon)$  cannot describe it since an indefinite number of stresses can correspond to a given strain value: one for each elastic unloading. As aforementioned, during a mono-sign test, the number and occurrence of elastic unloadings is arbitrary; therefore, in plasticity, stress does not depend on the current strain value exclusively (as in elasticity) but on the history of strain. An elasto-plastic constitutive equation must describe this relationship.

In this chapter, a general procedure called “method of the local state” is used to describe constitutive equations that involve strain or deformation histories. This method assumes that the effects of the history of strains on the material can be registered in a set of additional parameters, called internal variables; these are a record of the modifications experienced by the material. The values of the internal variables indicate how the material will react to future loading. The state of the material is characterized by the current values of the strain and the internal variables. Thus, instead of using the history of strain, the constitutive equations are written in terms of the current values of stress, strain, internal variables, and its increments.

A first step in the method of the local state is the introduction of the internal variables that define unambiguously the current value of stress; i.e. the set conformed by strain and the internal variables must be related to a unique value of stress. The equation that relates those variables is called elasticity law. The elasticity law describes the equation of the branches of unloading/reloading shown in Figure 3.

In order to characterize a straight line, only two parameters are needed, one is the slope of the line which in this case is the constant elastic modulus; the second one is its intersection with the horizontal axis which in this case is variable: the plastic strain. Plastic strain is, therefore, the first internal variable in plasticity and the corresponding elasticity law is:

$$\sigma = E(\varepsilon - \varepsilon_p) \tag{5.2.1}$$

However, the elasticity law does not represent by itself a constitutive equation since the current values of the internal variables are not a priori known. New equations that complement the elasticity law are thus needed; they are called evolution laws of internal variables and, usually, they are expressed as differential equations.

### 5.2.3 Plastic Strain Evolution Law and Yield Function

The perfectly plastic model states that there is no plastic strain if the stress is less than the yield stress. In mathematical language this can be expressed as:

$$\begin{cases} d\varepsilon_p = 0 & \text{if } f(\sigma) < 0 \text{ (elastic behavior)} \\ f(\sigma) = 0 & \text{if } d\varepsilon_p \neq 0 \text{ (plastic behavior)} \end{cases} \tag{5.2.2}$$

## Fundamental Concepts of Plasticity

where

$$f(\sigma) = |\sigma| - \sigma_y \leq 0 \quad (5.2.3)$$

Equation (5.2.2) is the plastic strain evolution law, the term  $f(\sigma)$  in (5.2.3) is called yield function. The yield function can only be negative or nil since the stress value cannot exceed the yield stress in the perfectly plastic model. The first line in Equation (5.2.2) indicates that there is no increment of the plastic strain if the absolute value of the stress is less than the yield stress; the absolute value of the stress is used because plasticity can appear in compression as well as in traction. This first line corresponds to an elastic behavior of the material. The second line in (5.2.2) states that stress, in absolute value, has to be equal to the yield stress if there are increments of the plastic strain; this line corresponds to a plastic behavior of the material.

The elasticity law (5.2.1), the plastic strain evolution law (5.2.2) and the yield function (5.2.3) form the constitutive equations of the perfectly plastic model; i.e. this set of equations defines a unique relationship between the stress value and the history of strain. The elastic modulus and yield stress are properties of the material and are considered data of the problem.

### 5.2.4 Example

Consider the strain history that is shown in Figure 4; it can be considered as a loading history chosen by an experimenter for the test. The goal of this example is to obtain the corresponding stress history according to the perfectly plastic constitutive equations.

The strain history consists, first, in a loading with constant strain velocity  $m$  up to the time  $t_i$ ; the instant  $t_a$  corresponds to the first time when the material experiences plasticity; then an elastic unloading, at constant velocity  $m$  too, is carried out until zero stress is reached at the instant  $t_b$ ; a second and final loading, with the same velocity, ends at the instant  $t_c$ ; during this interval, the material experiences plasticity again at some instant  $t_c$ .

The analysis is carried out step by step. The first step corresponds to the time interval  $0 \leq t < t_a$ . In this step, the material behaves elastically; thus, the first line of Equation (5.2.2) applies:

$$d\varepsilon_p = 0 \Rightarrow \varepsilon_p = 0 \quad (5.2.4)$$

The elasticity law (5.2.1) gives now the value of the stress:

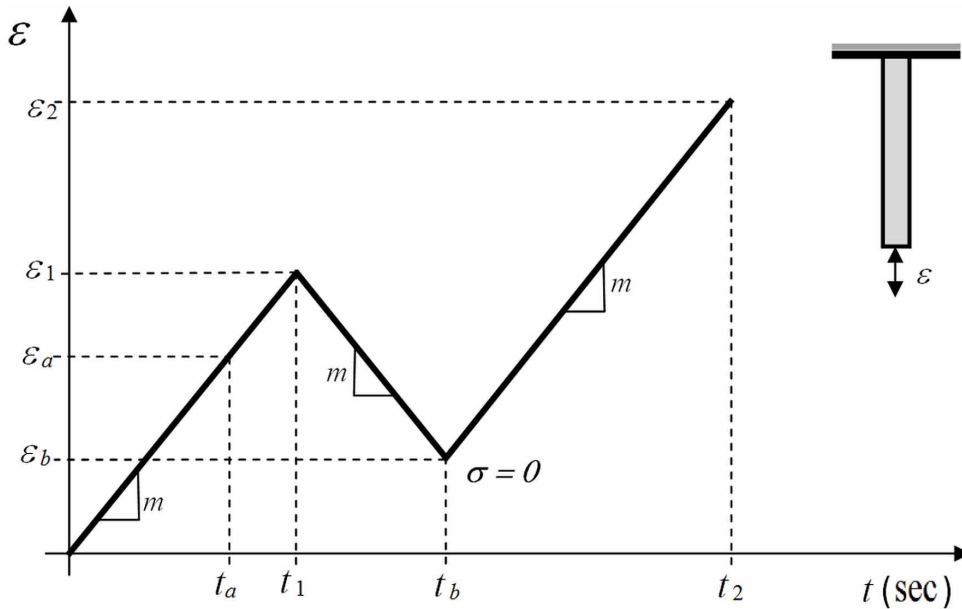
$$\sigma = E\varepsilon = Emt \quad (5.2.5)$$

The behavior remains elastic while the yield function is negative. Thus, this step ends when:

$$f(\sigma) = \sigma - \sigma_y = 0 \text{ for } t=t_a; \text{ therefore } t_a = \frac{\sigma_y}{E.m}; \quad (5.2.6)$$



Figure 4. History of strain



The histories of stress and plastic strain defined by expressions (5.2.4) and (5.2.5) are shown in Figure 5a.

The second step corresponds to the interval  $t_a \leq t < t_1$ . It is assumed that the behavior in this step is plastic; thus the second line in the evolution law (5.2.2) applies:

$$f(\sigma) = 0 \Rightarrow \sigma = \sigma_y \quad (5.2.7)$$

The elasticity law (5.2.1) can now be used to compute the plastic strain:

$$\varepsilon_p = \varepsilon - \frac{\sigma}{E} = mt - \frac{\sigma_y}{E} \quad (5.2.8)$$

The histories of stress and plastic strain of the first and second steps are shown in Figure 5b.

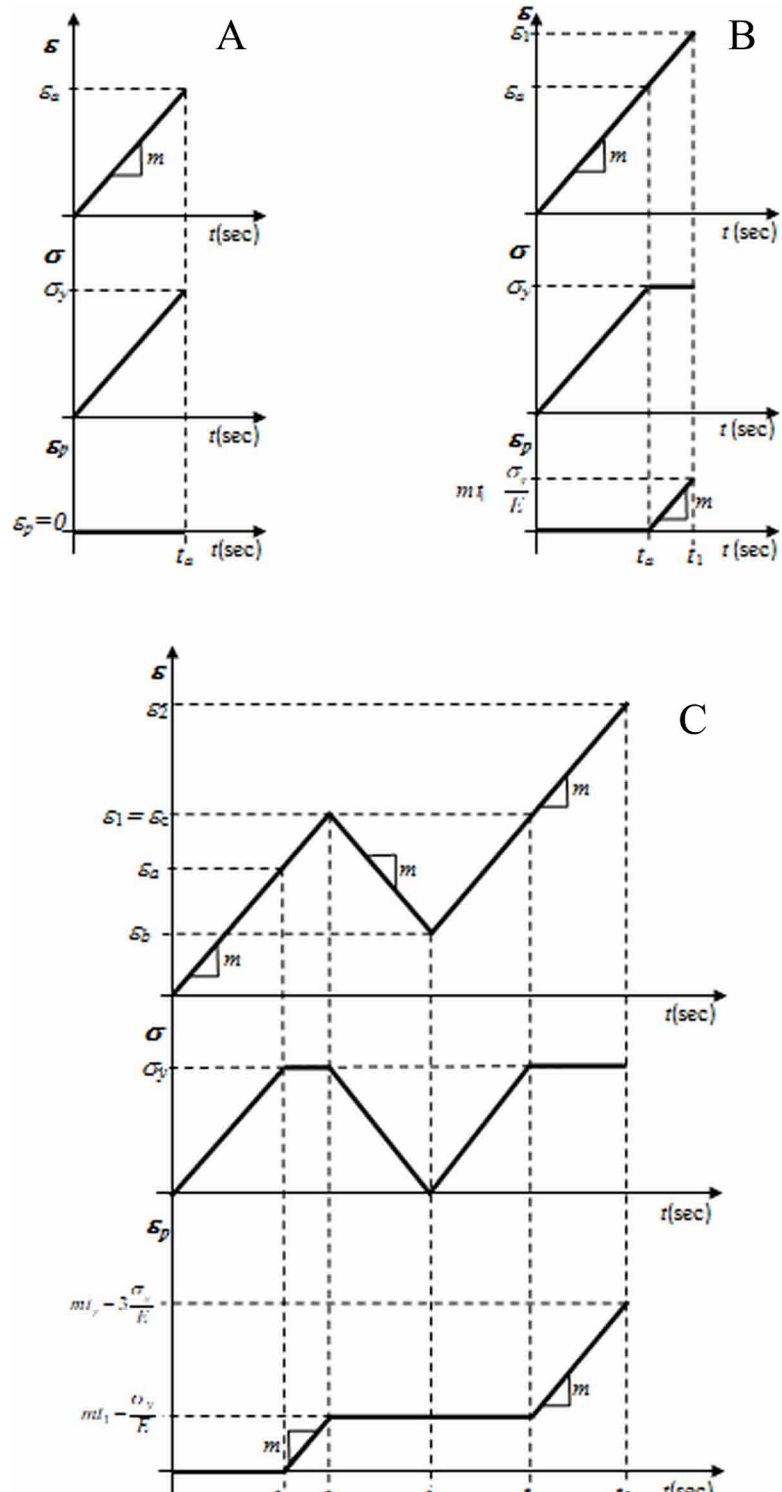
The third step corresponds to the interval  $t_1 \leq t < t_b$ . Since this is an unloading, it is assumed that the behavior in this step is elastic; thus the first line in the evolution law (5.2.2) applies:

$$d\varepsilon_p = 0 \Rightarrow \varepsilon_p = mt_1 - \frac{\sigma_y}{E} \quad (5.2.9)$$

And the elasticity law (5.2.1) can be used to compute the stress:

**Fundamental Concepts of Plasticity**

Figure 5. a) History of strains, stresses and plastic strains for  $0 \leq t < t_a$  b) History of strains, stresses and plastic strains for  $0 \leq t < t_1$  c) Total history of strains, stresses and plastic strains



$$\sigma = E(\varepsilon - \varepsilon_p) = E(-mt + \varepsilon_1 + \frac{\sigma_y}{E}) \quad (5.2.10)$$

The third step ends with the total unloading of the specimen ( $\sigma = 0$ ); thus, the instant  $t_b$  is:

$$\sigma = E(-mt + \varepsilon_1 + \frac{\sigma_y}{E}) = 0 \text{ for } t = t_b; \text{ therefore } t_b = \frac{\varepsilon_1}{m} + \frac{\sigma_y}{E.m}; \quad (5.2.11)$$

The histories of stress and plastic strain (5.2.9) and (5.2.10) are shown in Figure 5c.

The fourth step ( $t_b \leq t < t_c$ ) corresponds to the elastic reloading, thus the first line of the evolution law and the elasticity law give again:

$$d\varepsilon_p = 0 \Rightarrow \varepsilon_p = m.t_1 - \frac{\sigma_y}{E}; \sigma = E(\varepsilon - \varepsilon_p) = E(m.t - \varepsilon_1) - \sigma_y \quad (5.2.12)$$

This elastic part of the reloading ends when the yield function is equal to zero:

$$f(\sigma) = \sigma - \sigma_y = 0 \text{ for } t = t_c; \text{ therefore, } t_c = \frac{\varepsilon_1}{m} + \frac{2\sigma_y}{E.m} \quad (5.2.13)$$

The histories of strains, stresses and plastic strains in this interval are shown in Figure 5c.

The last step is the plastic part of the reloading ( $t_c \leq t < t_2$ ); the second line of the evolution law and the elasticity law lead to:

$$f(\sigma) = 0 \Rightarrow \sigma = \sigma_y; \varepsilon_p = \varepsilon - \frac{\sigma}{E} = mt - 3\frac{\sigma_y}{E} \quad (5.2.14)$$

At time  $t_2$  the history of the variables ends.

Notice that the adequate choice of the evolution law line allows for the computation of one variable: the plastic strain if the behavior is elastic or the stress if the behavior is plastic; the elasticity law gives the remaining variable. The set composed by the elasticity law (5.2.1), evolution law of the plastic strain (5.2.2) and the yield function (5.2.3) represent, indeed, a constitutive equation.

The combination of the strain and stress histories shown in Figures 5c permits the construction of the stress as a function of strain curve that is shown in Figure 6; notice that, in fact, it corresponds to the perfect plastic idealization.

### 5.3 ELASTO-PLASTIC MODEL WITH LINEAR ISOTROPIC HARDENING

#### 5.3.1 Idealization of the Mono-Sign Test

As aforementioned, the perfect plasticity model considers only some of the phenomena listed in Table 1. In this section, a new plasticity model that takes into account the plastic hardening effect is presented. In the case of the so called linear hardening, the experimental behavior in a mono-sign test is idealized as shown in Figure 7.

#### 5.3.2 Constitutive Equations

Notice that this new model does not change the representation of branches of the elastic unloading/reloading; therefore the same elasticity law applies in this case. The general form of the plastic strain evolution law is also kept unmodified. However in the perfect plastic model, the elastic limit is constant and equal to the yield stress. This cannot be the case anymore; in the new model the elastic limit augments with the plastic strain. As the transition from the elastic behavior to the plastic one depends on the yield function, this has to be modified. The new model has the following general form:

$$\sigma = E(\varepsilon - \varepsilon_p); \begin{cases} d\varepsilon_p = 0 & \text{if } f(\sigma, p) < 0 \text{ (elastic behavior)} \\ f(\sigma, p) = 0 & \text{if } d\varepsilon_p \neq 0 \text{ (plastic behavior)} \end{cases} \quad (5.3.1)$$

with the yield function:

$$f(\sigma, p) = |\sigma| - (\sigma_y + c.p) \leq 0 \quad (5.3.2)$$

Figure 6. Stress as a function of strain in the example

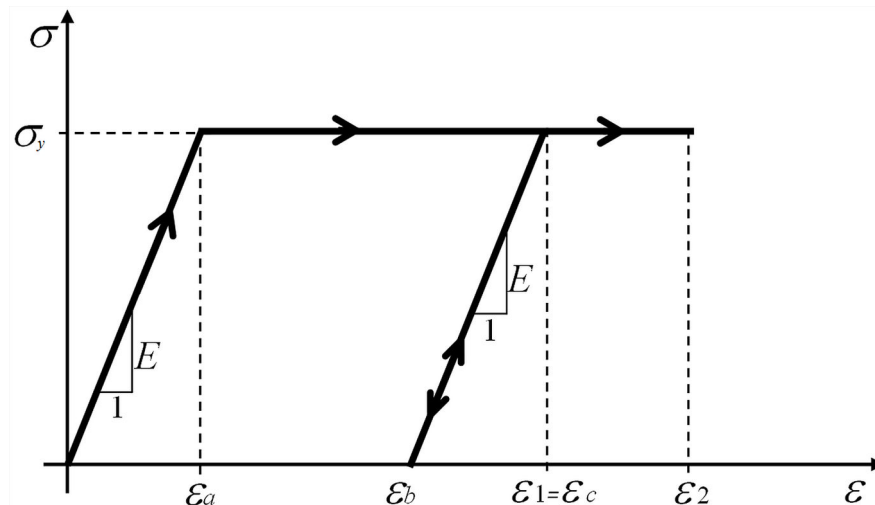
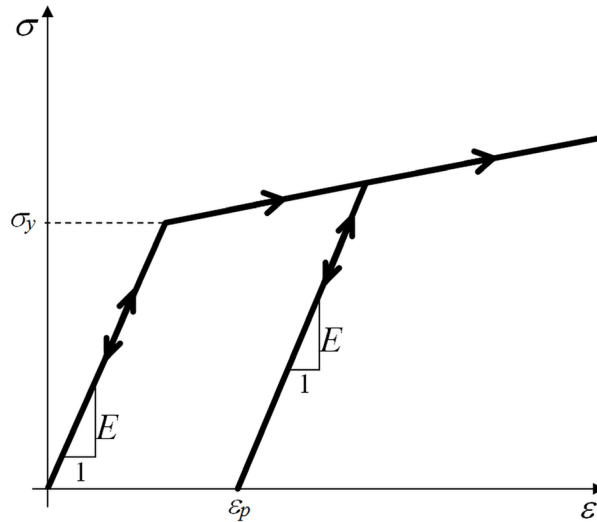


Figure 7. Elasto-plastic model with linear hardening



In this yield function, the elastic limit corresponds to the term  $(\sigma_y + c.p)$  where  $c$  is a material parameter (as it is the yield stress or the elastic modulus) constant and positive; and  $p$  is a variable that measures the total amount of plasticity experienced by the material. The variable  $p$  can be defined in two different ways. The first one is the accumulated plastic strain that can be interpreted as a “plastic odometer”. The new evolution law for  $p$  is in this case:

$$dp = |d\varepsilon_p| \tag{5.3.3}$$

Notice the variable  $p$  always increases with plasticity no matter the sign of the plastic strain, in the same way as the mileage in an odometer can only increase regardless driving northward or southward.

A second alternative is the use of the maximum plastic strain; the corresponding evolution law for  $p$  is in this case:

$$\begin{cases} dp = 0 \text{ if } |\varepsilon_p| < p \\ |\varepsilon_p| = p \text{ if } dp \neq 0 \end{cases}; \text{ or } p = \text{Max} |\varepsilon_p| \tag{5.3.4}$$

Equation (5.3.4a) indicates that the variable  $p$  does not increase if the plastic strain is less than the current value of  $p$ ; and  $p$  cannot be less than the plastic strain. A much simpler way to describe this evolution law is indicated in Equation (5.3.4b): the variable  $p$  at a time  $t$  is equal to the maximum absolute value of the plastic strain during its history up to that instant.

The variable  $p$  has to be always positive since in uniaxial compression as well as in uniaxial tension tests, the hardening represents an increase in the elastic limit.

## Fundamental Concepts of Plasticity

Thus, in this model, a new internal variable was introduced: the accumulated plastic strain or the maximum plastic strain. Although  $p$  is not included in the elasticity law, it is an internal variable since it is necessary to define the nature of the material behavior: elastic or plastic.

Notice that even if the stress can now have larger values than the yield stress, the yield function is still negative or nil.

Consider, as an example, a monotonic loading; i.e. a history of constantly increasing values of strains from zero to some final value and no unloading. During the elastic part of the behavior:

$$\varepsilon_p = 0 \text{ and } \sigma = E\varepsilon \quad (5.3.5)$$

In the plastic part:

$$p = \varepsilon_p \Rightarrow \sigma = \sigma_y + c.\varepsilon_p; \varepsilon_p = \varepsilon - \frac{\sigma}{E} \Rightarrow \sigma = \frac{c.E}{E+c} \varepsilon + \frac{E.\sigma_y}{E+c} \quad (5.3.6)$$

Equations (5.3.5-5.3.6) give the stress as a function of strain that is represented in Figure 8; this curve is called envelope of the model. The model (5.3.1)-(5.3.2) is indeed a mathematical representation of the idealization of Figure 7. The model is said to have linear isotropic hardening because the strength increment over the yield stress, i.e. the hardening term  $Q(p)=c.p$ , is a linear function of  $p$ .

## 5.4 ELASTO-PLASTIC MODEL WITH NONLINEAR ISOTROPIC HARDENING

### 5.4.1 Constitutive Equations

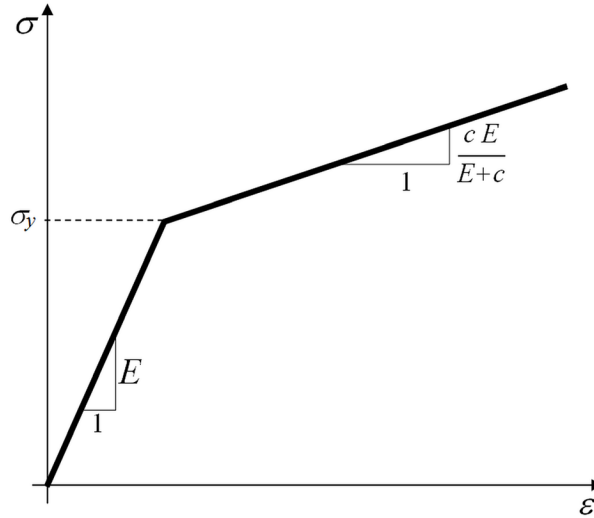
On one hand, the model described in the previous section represents an improvement with respect to the perfect plastic one because it takes into account plastic hardening; on the other hand, it loses the capacity to establish an ultimate stress value: the plastic branch increases the stress indefinitely. The goal of the model in this section is to improve the preceding ones taking into account phenomena “a”, “b”, “c”, “d” and “e” of Table 1 simultaneously; i.e. it will include plastic hardening and the existence of an ultimate stress resistance as well.

In this model the same elasticity law (5.3.1a), the same two internal variables ( $\varepsilon_p$  and  $p$ ) and internal variable evolution laws (5.3.1.b and 5.3.3 or 5.3.4) are used; however the yield function is now modified in the following way:

$$f(\sigma, p) = |\sigma| - (\sigma_y + Q(p)) \leq 0 \text{ where } Q(p) = (\sigma_u - \sigma_y)(1 - e^{-\alpha p}) \quad (5.4.1)$$

The new elastic limit is the term  $(\sigma_y + (\sigma_u - \sigma_y)(1 - e^{-\alpha p}))$ ; where  $\sigma_u$  and  $\alpha$  are constant and positive material parameters, specifically  $\sigma_u$  is the ultimate stress or last strength of the material.

Figure 8. Envelope of the elasto-plastic model with linear isotropic hardening



### 5.4.2 Identification of the Material Parameters

Notice that the elastic limit in this model is equal to the yield stress at the beginning of a plasticity process ( $p = 0$ ) and tends exponentially to the ultimate stress  $\sigma_u$  when the plastic strain tends to infinity. The rapidity of the transition between  $\sigma_y$  and  $\sigma_u$  depends on the value of parameter  $\alpha$ . The envelope of this model is shown in Figure 9a.

Another interpretation of the parameter  $\alpha$  can be given as follows. Consider the part of a monotonic loading with plastic deformation, then:

$$f = \sigma - \left( \sigma_y + (\sigma_u - \sigma_y)(1 - e^{-\alpha \varepsilon_p}) \right) = 0 \Rightarrow \frac{\sigma_u - \sigma}{\sigma_u - \sigma_y} = e^{-\alpha \varepsilon_p} \quad (5.4.2)$$

Taking logarithms in both sides of Equation (5.4.2b) leads to:

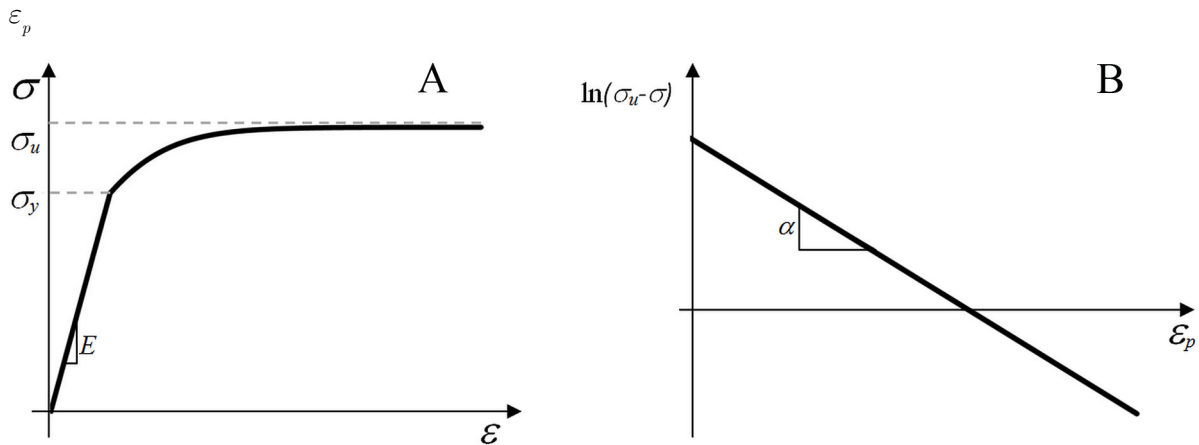
$$\ln(\sigma_u - \sigma) = -\alpha \varepsilon_p + \ln(\sigma_u - \sigma_y) \quad (5.4.3)$$

Therefore, the parameter  $\alpha$  is the slope of the resulting line in a graph of  $\ln(\sigma_u - \sigma)$  vs.  $\varepsilon_p$  as shown in Figure 9b.

The material parameters can be easily identified in a mono-sign test. Notice that the parameter  $\alpha$  is related to the hardening velocity as it is shown in Figure 10.

The example 5.9.1 shows how to plot a curve strain vs. stress using this model and a spreadsheet.

Figure 9. a) Envelope of the elasto-plastic model with nonlinear isotropic hardening b)  $\ln(\sigma_u - \sigma)$  vs.



## 5.5 ELASTO-PLASTIC MODEL WITH LINEAR KINEMATIC HARDENING

### 5.5.1 The Bauschinger Effect

Reversal of loading often has a devastating effect on structures as, for example, in earthquakes; thus the study of the behavior of materials under such conditions is very important. The most significant test for this purpose is the cyclic test in which the specimens are subjected to traction and compression successively, usually the maximum and minimum strain of each cycle increases. Figure 11 shows a typical result for a metallic specimen in a cyclic test.

In the first cycle, as in mono-sign tests, a zone of plastic behavior with hardening follows to an elastic one; when the load is reversed and stress changes the sign, the same sequence is observed but the elastic limit appears to be significantly lower. Then, the process of plastic hardening restarts and the elastic limit recovers its initial value and even increases it. If the loading is reversed again, the same events repeat: elastic unloading, elastic reloading and plastic behavior with hardening; but once more, the elastic limit is much lower than the previous one. This phenomenon: decrease of elastic limit in compression when there has been a plastic hardening in traction, and vice versa, is called Bauschinger effect.

The perfect plastic model cannot describe this effect since the elastic limit is always constant; nor can the models with isotropic hardening because once the elastic limit increases in traction the same effect appears in compression and vice versa (see Figure 12).

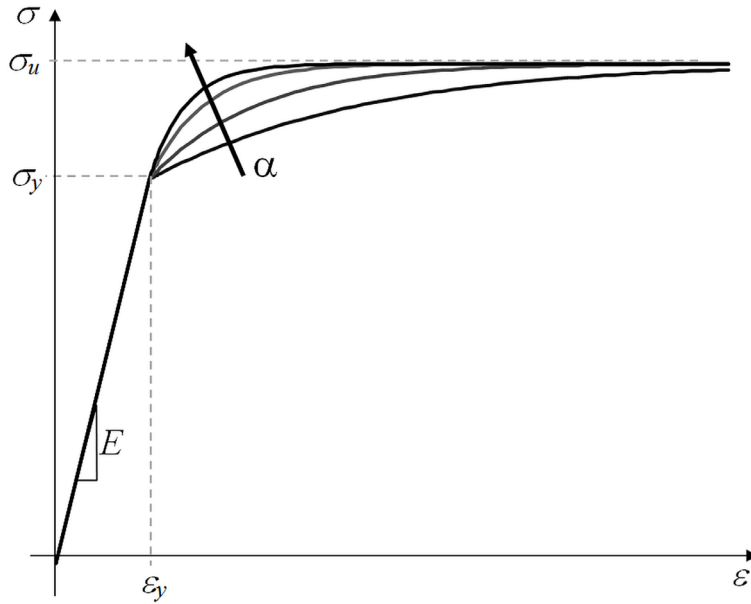
### 5.5.2 The Elastic Domain

The elastic domain of a material is defined as the set of stress values such that the material behavior is elastic. In mathematical language this is written as:

$$\sigma \mid f < 0 \tag{5.5.1}$$



Figure 10. Increase of hardening velocity with parameter  $\alpha$



Equation (5.5.1) is read as follows: the elastic domain is the set of stress values so that the yield function is strictly negative.

In the theory of plasticity, it is said that the elastic domain is always an open convex set. In the uniaxial case, this means that the elastic domain can be expressed as a single open interval in the stress axis, i.e.:

$$\sigma \mid L_{\text{inf}} < \sigma < L_{\text{sup}} \quad (5.5.2)$$

where  $L_{\text{inf}}$  is the inferior limit of the elastic interval and  $L_{\text{sup}}$  is the superior limit. For instance, in the perfect plastic model the elastic domain is given by:  $\sigma \mid -\sigma_y < \sigma < \sigma_y$  since for any stress value greater than minus the yield stress and less than the yield stress, the yield function is negative.

In the case of perfect plasticity, the elastic domain is invariant; that is its inferior and superior limits are unvarying because the yield stress is constant.

In the models with isotropic hardening the elastic domain is:  $\sigma \mid -(\sigma_y + Q(p)) < \sigma < (\sigma_y + Q(p))$ ; where  $Q(p) = c.p$  in the case of linear hardening and  $Q(p) = (\sigma_u - \sigma_y)(1 - e^{-\alpha p})$  for nonlinear hardening. In this case, the elastic domain is not invariant: it depends on the amount of plasticity experienced by the material, but the interval can only increase its boundaries.

The size of the elastic domain  $Sz$ , is defined as the difference between the maximum and minimum limits of the elastic domain:

$$Sz = L_{\text{sup}} - L_{\text{inf}} \quad (5.5.3)$$

**Fundamental Concepts of Plasticity**

Figure 11. Stress vs. strain in a cyclic test on a steel specimen

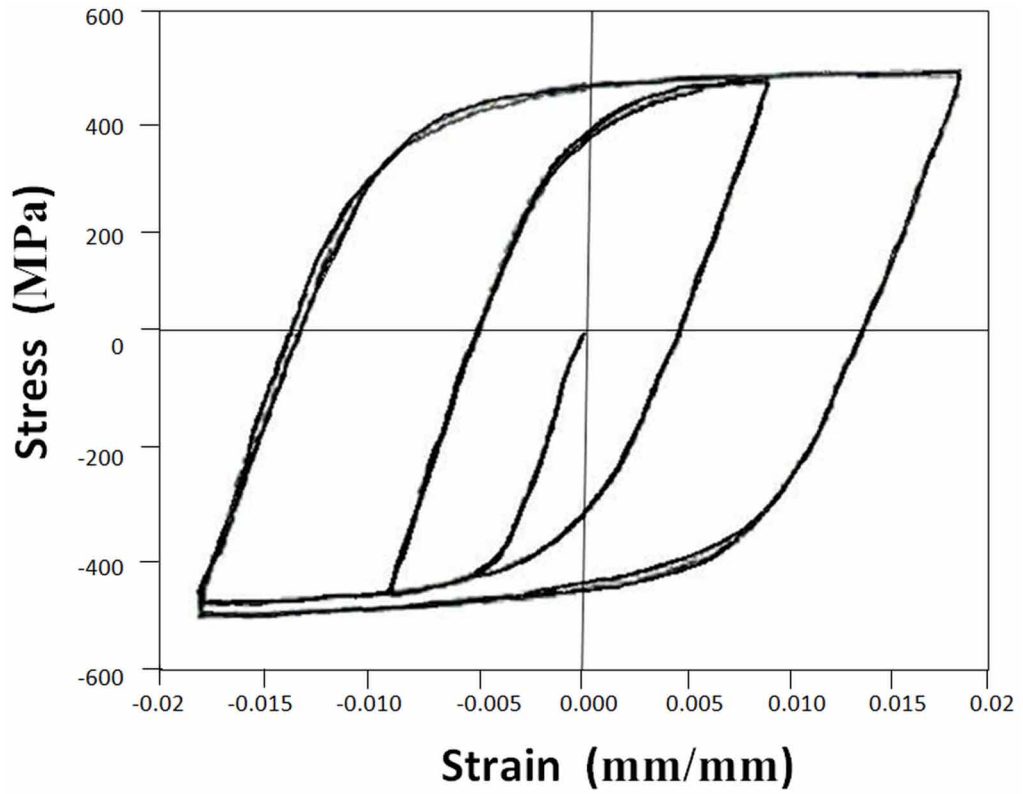
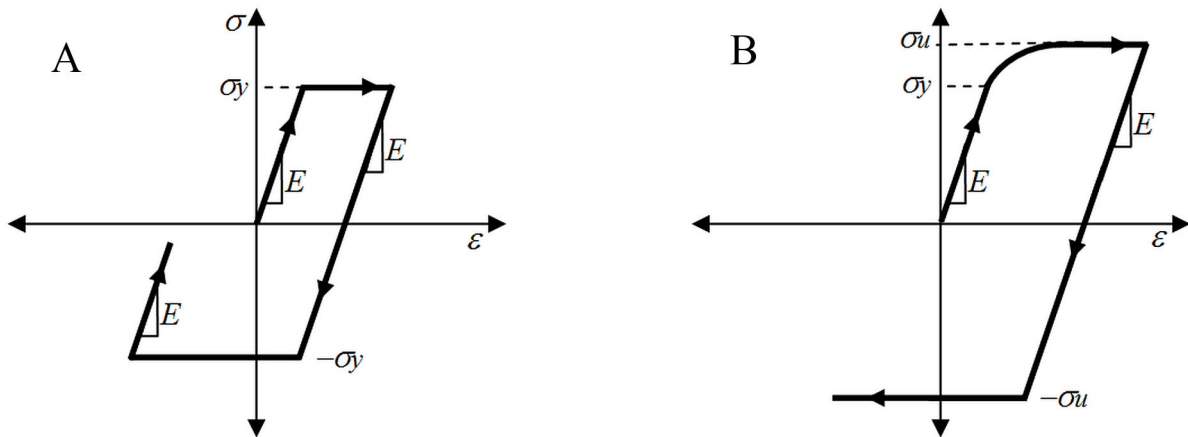


Figure 12. a) Simulation of a cyclic test with the perfect plastic model b) Simulation of a cyclic test with the model of plasticity with nonlinear isotropic hardening



For instance, in the perfectly plastic model, the size of the elastic domain is:  $Sz = 2.\sigma_y$ , which is constant. In models with isotropic hardening, the size of the elastic domain is not constant and it can only increase:  $Sz = 2.(\sigma_y + Q(p))$ .

The center of the elastic domain,  $Ct$ , corresponds to the mid-point of the interval:  $\sigma / L_{inf} < \sigma < L_{sup}$  and it is given by:

$$Ct = \frac{L_{sup} + L_{inf}}{2} \quad (5.5.4)$$

In all the models described so far the center of the elastic domain is always constant and equal to zero:  $Ct = 0$ ; i.e. even if the elastic domain is growing up, its center does not move across the stress axis.

The Bauschinger effect can now be explained in a very simple way: it corresponds to displacements (instead of growth) of the elastic domain in the stress space; when the elastic domain moves in the positive direction of the stress axis, there is an increment in the tensile elastic limit and simultaneously a reduction of the compression one; if the elastic domain displaces in the negative direction, the opposite effects are observed.

The goal of the models with kinematic hardening is the characterization of this movement.

### 5.5.3 Constitutive Equations

The elasticity law is not related with the characteristics of the elastic domain, only with the elastic branches of unloading/reloading; thus, the expression (5.2.1) is still used. The general form of the evolution law of the plastic strain is also the same, except that the yield function depends now on the plastic strain directly, instead of the variable  $p$ :

$$\sigma = E(\varepsilon - \varepsilon_p); \begin{cases} d\varepsilon_p = 0 \text{ if } f(\sigma, \varepsilon_p) < 0 \text{ (elastic behavior)} \\ f(\sigma, \varepsilon_p) = 0 \text{ if } d\varepsilon_p \neq 0 \text{ (plastic behavior)} \end{cases} \quad (5.5.5)$$

with the following expression for the yield function:

$$f(\sigma, \varepsilon_p) = |\sigma - c.\varepsilon_p| - \sigma_y \leq 0 \quad (5.5.6)$$

where  $c$  is a material parameter as in the model of isotropic hardening.

Notice that the new elastic domain is now given by:  $\sigma | -\sigma_y + c.\varepsilon_p < \sigma < \sigma_y + c.\varepsilon_p$ ; its size is  $Sz = 2.\sigma_y$ , as in the perfectly plastic model, but its center is not longer equal to zero:  $Ct = c.\varepsilon_p$ . Therefore, for positive plastic strains, the elastic domain displaces in the positive direction of the stress axis and vice-versa. The simulation of a cyclic test with this model is presented in Figure 13.

## Fundamental Concepts of Plasticity

Notice that isotropic hardening is obtained by including a term  $Q$  outside the absolute value in the yield function; for kinematic hardening, the additional term is placed inside the absolute value; i.e. an additional term within the absolute value modifies the position of the elastic domain center; an outside term changes its size.

### 5.6 ELASTO-PLASTIC MODEL WITH NONLINEAR KINEMATIC HARDENING

The drawback of the model described in the previous section is the same as in the model with linear isotropic hardening: it loses the description of the effect “e” in table 1 (the ultimate stress resistance). A model that includes the phenomena “a” to “e” and the Bauschinger effect is:

$$\sigma = E(\varepsilon - \varepsilon_p); \begin{cases} d\varepsilon_p = 0 & \text{if } f(\sigma, x) < 0 \text{ (elastic behavior)} \\ f(\sigma, x) = 0 & \text{if } d\varepsilon_p \neq 0 \text{ (plastic behavior)} \end{cases} \quad (5.6.1)$$

where

$$f(\sigma) = |\sigma - x| - \sigma_y \leq 0 \quad (5.6.2)$$

The new internal variable  $x$  is called kinematic hardening stress or back stress. The evolution law of the back stress is given by:

$$dx = \alpha \left( (\sigma_u - \sigma_y) d\varepsilon_p - x \cdot |d\varepsilon_p| \right) \quad (5.6.3)$$

Notice that for  $x$  equal to zero, the position of the elastic domain center displaces in the positive direction of the stress axis if the plastic strain increments are positive and vice versa. For positive plastic strain augmentations, the back stress increments tend to zero as this variable tends to  $(\sigma_u - \sigma_y)$ ; therefore the total stress  $\sigma$  can never be greater than  $\sigma_u$ . For negative plastic strain, the back stress increments tend to zero as  $x$  tends to  $-(\sigma_u - \sigma_y)$ , therefore the stress  $\sigma$  can never be less than  $-\sigma_u$ .

A cycle using the plastic model with nonlinear kinematic hardening gives the behavior indicated in Figure 14.

The improvement in the representation of the material behavior requires an increment of the complexity of the models as can be noticed comparing Figures 14 and 13 with 11.

The example 5.9.2 shows how to plot a curve strain vs. stress using an algebraic manipulation program and a spreadsheet.

An analogy between mathematical modeling of physical phenomena and art can also be noticed; the models can be seen as “paintings” of the material behavior observed in the experimental tests. In structural analysis, mathematical language is used to describe a physical phenomenon in a way not too different as painting or sculpture is used to represent a person, landscape or object. A model is just a representation and never an exact explanation of the actual phenomenon which is infinitely complex.

Figure 13. Material behavior according to the elasto-plastic model with linear kinematic hardening

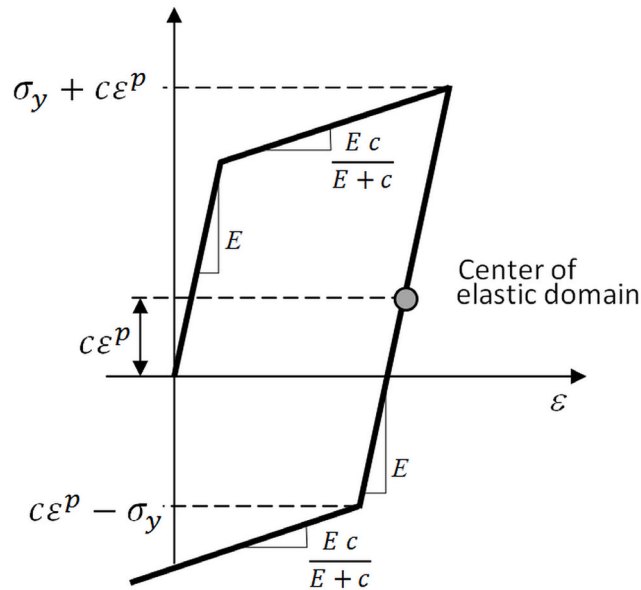
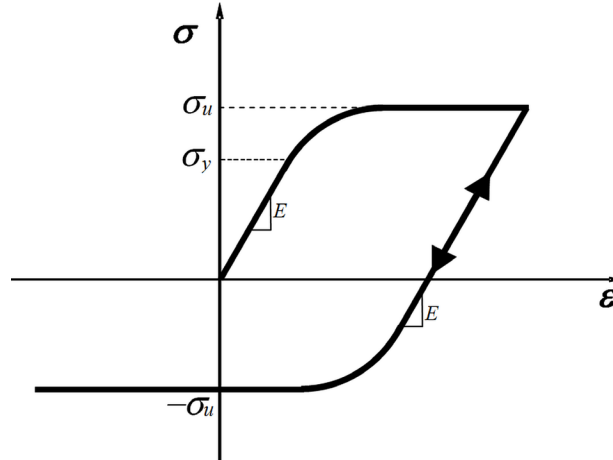


Figure 14. Material behavior according to the elasto-plastic model with nonlinear kinematic hardening



## 5.7 ELASTO-PLASTIC SHEAR STRESS-STRAIN RELATIONSHIP

Consider a thin walled cylindrical tube of average radius,  $R$  and thickness  $e$  subjected to torsion as shown in Figure 15. This can be considered as an isostatic problem; i.e. its stress distribution does not depend on the material behavior. The shear stress in the structure is approximately constant and can be computed by considering equilibrium of moments around the axis of the tube; the angular shear strain in the solid elements of the tube is also constant and can be determined from kinematic considerations (see section 2.5). They can be computed as a function of the moment and torsion rotation as:

**Fundamental Concepts of Plasticity**

Figure 15. Thin walled cylindrical tube subjected to torque force  $T$

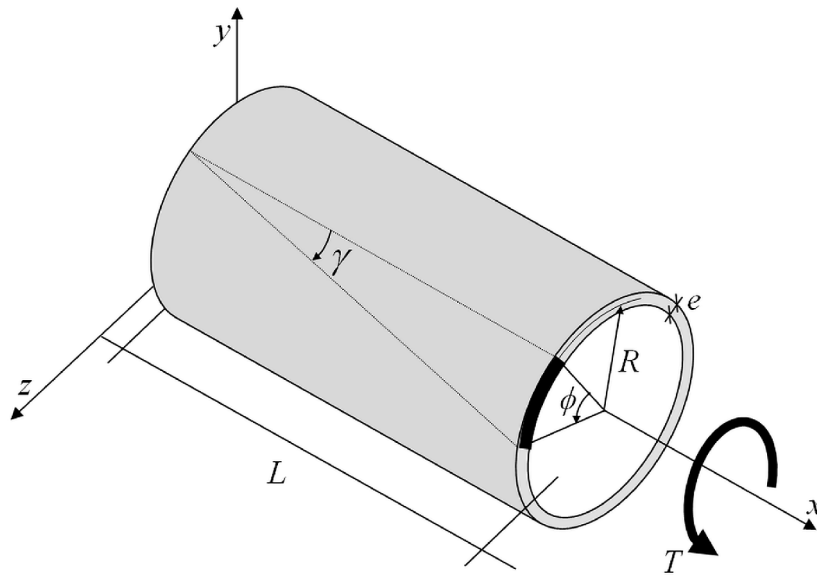
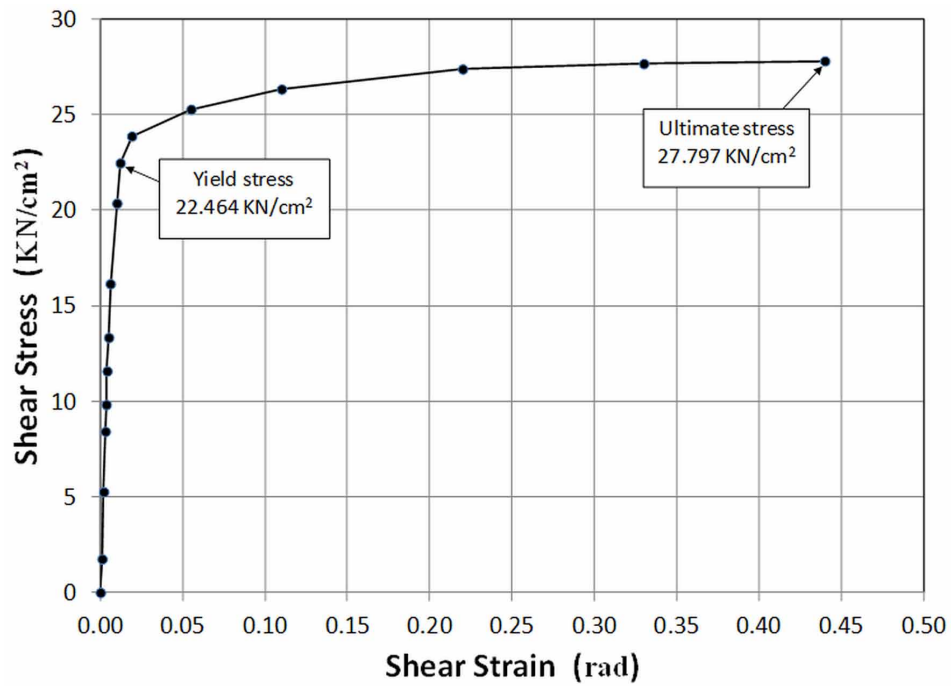


Figure 16. Shear stress vs. angular shear strain in aluminum



$$\tau = \frac{T}{2e\pi R^2}; \gamma = \frac{R\phi}{L} \quad (5.7.1)$$

where  $\tau$  is the shear stress,  $\gamma$  is the angular shear strain or distortion;  $T$  is the torque,  $\phi$  is the angle of twist and  $L$  is the length of the element (see Figure 15).

Thus, the experimental behavior of a material subjected to shear effects can be observed and measured in a test with this kind of specimens. Figure 16 shows the experimental results corresponding to an aluminum specimen represented in a graph of distortion vs. shear stress.

Notice that this is the same kind of behavior observed in the tension tests; thus, similar models can be used to describe the behavior under shear stresses:

$$\tau = G(\gamma - \gamma_p); \begin{cases} d\gamma_p = 0 & \text{if } f_s(\tau, p_s, x_s) < 0 \text{ (elastic behavior)} \\ f_s(\tau, p_s, x_s) = 0 & \text{if } d\gamma_p \neq 0 \text{ (plastic behavior)} \end{cases} \quad (5.7.2)$$

where  $\gamma_p$  is the plastic angular strain and  $G$  is again the transverse elastic modulus. The shear yield function  $f_s$  may have isotropic and/or kinematic hardening terms:

$$f_s(\tau, p_s, x_s) = |\tau - x_s| - (\tau_y + Q(p_s)) \leq 0 \quad (5.7.3)$$

where  $\tau_y$  is the yield shear stress, that is assumed to be a material property and the hardening terms  $x_s$  and  $Q(p_s)$  may have the linear or nonlinear expressions already defined. The material parameters have not the same values in the  $\sigma$ - $\epsilon$  relationship than in the  $\tau$ - $\gamma$  one.

## 5.8 SUMMARY AND EQUATIONS QUICK REFERENCE

The most important inelastic phenomena in ductile materials can be identified in uniaxial tests. Those are: presence of permanent strains, plastic hardening, stiffness degradation and plastic softening or strength degradation.

In order to model the inelastic behavior, the equations relate histories of displacements and generalized deformations with histories of external forces and generalized stresses. The simplest way to describe this kind of relationship is introducing internal variables that describe the modification of the state of the material. Next, the constitutive equations are divided into two sets of relationships: the elasticity law and the evolution law of the internal variables.

The simplest model is called perfectly plastic. In this model only one internal variable is introduced: the plastic strain. The evolution law is defined using a yield function. The perfectly plastic model is characterized by a maximum constant stress.

In order to describe those inelastic phenomena two concepts were introduced: the size of the elastic domain and its position. The subsequent models describe the hardening process. They are denoted as elasto-plastic models with isotropic and kinematic hardening. In the first one the size of the elastic domain increases with plastic strains. The kinematic hardening model displaces of the elastic domain.

Finally, the elasto-plastic shear stress-strain relationship is presented (See Table 2).

## Fundamental Concepts of Plasticity

Table 2.

<b>ELASTO-PERFECT PLASTIC CONSTITUTIVE MODEL</b>	
<i>Idealization of the Mono Sign Test</i>	
Elasticity law	$\sigma = E(\varepsilon - \varepsilon_p)$ (5.2.1)
<i>Plastic Strain Evolution Law and Yield Function</i>	
Plastic strain evolution law	$\begin{cases} d\varepsilon_p = 0 & \text{if } f(\sigma) < 0 \text{ (elastic behavior)} \\ f(\sigma) = 0 & \text{if } d\varepsilon_p \neq 0 \text{ (plastic behavior)} \end{cases}$ (5.2.2)
Yield function	$f(\sigma) =  \sigma  - \sigma_y \leq 0$ (5.2.3)
<b>ELASTO-PLASTIC MODEL WITH LINEAR ISOTROPIC HARDENING</b>	
<i>Idealization of the Mono Sign Test</i>	
<i>Constitutive Equations</i>	
Elasticity law	$\sigma = E(\varepsilon - \varepsilon_p)$ (5.3.1a)
Plastic strain evolution law	$\begin{cases} d\varepsilon_p = 0 & \text{if } f(\sigma, p) < 0 \text{ (elastic behavior)} \\ f(\sigma, p) = 0 & \text{if } d\varepsilon_p \neq 0 \text{ (plastic behavior)} \end{cases}$ (5.3.1b)
Yield function	$f(\sigma, p) =  \sigma  - (\sigma_y + c.p) \leq 0$ (5.3.2)
Evolution law for $p$ , the accumulated plastic strain	$dp =  d\varepsilon_p $ (5.3.3)
Evolution law for $p$ , the maximum plastic strain	$\begin{cases} dp = 0 & \text{if }  \varepsilon_p  < p \\  \varepsilon_p  = p & \text{if } dp \neq 0 \end{cases} \quad \text{or} \quad p = \text{Max}  \varepsilon_p $ (5.3.4)
Envelope of the elasto-plastic model with linear isotropic hardening with a monotonic loading: During the elastic part of the behavior	$\varepsilon_p = 0$ and $\sigma = E\varepsilon$ (5.3.5)
In the plastic part	$p = \varepsilon_p \Rightarrow \sigma = \sigma_y + c.\varepsilon_p; \varepsilon_p = \varepsilon - \frac{\sigma}{E} \Rightarrow \sigma = \frac{c.E}{E+c}\varepsilon + \frac{E.\sigma_y}{E+c}$ (5.3.6)

continued on following page



Table 2. Continued

ELASTO-PLASTIC MODEL WITH NONLINEAR ISOTROPIC HARDENING
<i>Constitutive Equations</i>
Elasticity law $\sigma = E(\varepsilon - \varepsilon_p) \quad (5.2.1, 5.3.1a)$
Plastic strain evolution law $\begin{cases} d\varepsilon_p = 0 & \text{if } f(\sigma, p) < 0 \text{ (elastic behavior)} \\ f(\sigma, p) = 0 & \text{if } d\varepsilon_p \neq 0 \text{ (plastic behavior)} \end{cases} \quad (5.3.1b)$
Evolution law for $p$ , the accumulated plastic strain $dp =  d\varepsilon_p  \quad (5.3.3)$
Evolution law for $p$ , the maximum plastic strain $\begin{cases} dp = 0 & \text{if }  \varepsilon_p  < p \\  \varepsilon_p  = p & \text{if } dp \neq 0 \end{cases} \quad \text{or} \quad p = \text{Max}  \varepsilon_p  \quad (5.3.4)$
Yield function $f(\sigma, p) =  \sigma  - (\sigma_y + Q(p)) \leq 0 \quad Q(p) = (\sigma_u - \sigma_y)(1 - e^{-\alpha p}) \quad (5.4.1)$
<i>Identification of the Material Parameters</i>
The rapidity of the transition between $\sigma_y$ and $\sigma_u$ depends on the value of parameter $\alpha$ . From the yield function $f = \sigma - (\sigma_y + (\sigma_u - \sigma_y)(1 - e^{-\alpha\varepsilon_p})) = 0 \Rightarrow \frac{\sigma_u - \sigma}{\sigma_u - \sigma_y} = e^{-\alpha\varepsilon_p} \quad (5.4.2)$
$\ln(\sigma_u - \sigma) = -\alpha\varepsilon_p + \ln(\sigma_u - \sigma_y) \quad (5.4.3)$ Parameter $\alpha$ is the slope of the resulting line in a graph of $\ln(\sigma_u - \sigma) \quad \text{vs.} \quad \varepsilon_p.$
<b>Elasto-plastic model with kinematic hardening</b> The Bauschinger effect can be explained in a very simple way: when the elastic domain moves in the positive direction of the stress axis, the elastic limit increases in traction and, simultaneously, decreases in compression; if the elastic domain displaces in the negative direction the opposite effects are observed.
<i>The Elastic Domain</i>
Elastic domain of a material $\sigma \mid f < 0 \quad (5.5.1)$
$\sigma \mid L_{\text{inf}} < \sigma < L_{\text{sup}} \quad (5.5.2)$ $L_{\text{inf}}$ : inferior limit of the elastic interval $L_{\text{sup}}$ is the superior limit
Size of the elastic domain, Sz $SZ = L_{\text{sup}} - L_{\text{inf}} \quad (5.5.3)$

continued on following page

## Fundamental Concepts of Plasticity

Table 2. Continued

Center of the elastic domain, Ct $Ct = \frac{L_{sup} + L_{inf}}{2} \quad (5.5.4)$
<b>Constitutive Equations</b>
Elasticity law $\sigma = E(\varepsilon - \varepsilon_p) \quad (5.5.5 \text{ a})$
Plastic strain evolution law $\begin{cases} d\varepsilon_p = 0 & \text{if } f(\sigma, \varepsilon_p) < 0 \text{ (elastic behavior)} \\ f(\sigma, \varepsilon_p) = 0 & \text{if } d\varepsilon_p \neq 0 \text{ (plastic behavior)} \end{cases} \quad (5.5.5 \text{ b})$
Yield function $f(\sigma, \varepsilon_p) =  \sigma - c\varepsilon_p  - \sigma_y \leq 0 \quad (5.5.6)$ <i>c</i> : material parameter
<b>ELASTO-PLASTIC MODEL WITH NONLINEAR KINEMATIC HARDENING</b>
Elasticity law $\sigma = E(\varepsilon - \varepsilon_p) \quad (5.6.1 \text{ a})$
Plastic strain evolution law $\begin{cases} d\varepsilon_p = 0 & \text{if } f(\sigma, x) < 0 \text{ (elastic behavior)} \\ f(\sigma, x) = 0 & \text{if } d\varepsilon_p \neq 0 \text{ (plastic behavior)} \end{cases} \quad (5.6.1 \text{ b})$
Yield function $f(\sigma) =  \sigma - x  - \sigma_y \leq 0 \quad (5.6.2)$ <i>x</i> : kinematic hardening stress or back stress
The back stress evolution law $dx = \alpha \left( (\sigma_u - \sigma_y) d\varepsilon_p - x \cdot  d\varepsilon_p  \right) \quad (5.6.3)$
<b>ELASTO-PLASTIC SHEAR STRESS STRAIN RELATIONSHIP</b>
Shear stress ( $\tau$ ) $\tau = \frac{T}{2\varepsilon\pi R^2} \quad (5.7.1a)$
Angular shear strain ( $\gamma$ ) $\gamma = \frac{R\phi}{L} \quad (5.7.1)$
Elasticity law of elasto-plastic shear model $\tau = G(\gamma - \gamma_p) \quad (5.7.2 \text{ a})$ <i>G</i> : transverse elastic modulus $\gamma_p$ : plastic angular strain

continued on following page

Table 2. Continued

Plastic angular strain evolution law	
$\begin{cases} d\gamma_p = 0 & \text{if } f_s(\tau, p_s, x_s) < 0 \text{ (elastic behavior)} \\ f_s(\tau, p_s, x_s) = 0 & \text{if } d\gamma_p \neq 0 \text{ (plastic behavior)} \end{cases}$	(5.7.2 b)
$f_s$ : shear yield function	
Shear yield function with isotropic and kinematic hardening	
$f_s(\tau, p_s, x_s) =  \tau - x_s  - (\tau_y + Q(p_s)) \leq 0$	(5.7.3)
$\tau_y$ is the yield shear stress	

## 5.9 EXAMPLES

### 5.9.1 Plot the Stress Strain Curve for a Material with Nonlinear Isotropic Hardening Using an Elastic Modulus $E = 100000 \text{ MPa}$ , Yield Stress $\sigma_y = 900 \text{ MPa}$ , Ultimate Stress $\sigma_u = 1200 \text{ MPa}$ and $\alpha = 100$ , for a Monotonic Loading Using a Spreadsheet

The best way to solve this problem is to choose the plastic strain as the independent variable. In Figure 17 it is shown the way as this problem is programmed in a spreadsheet. In column A several values for the plastic strain were chosen, then the variable  $p$  is computed using Equation (5.3.3), the hardening term is determined using Equation (5.4.1). The stress is obtained making the yield function equal to zero and the strain is computed by the elasticity law (5.2.1).

In Figure 18 the values obtained for the example are shown and Figure 19 presents the resulting stress strain curve. Notice that first there is an elastic behavior and then a plastic one.

Figure 17. Equations programmed in the spreadsheet

	A	B	C	D	E	F	G	H	I
1	$\epsilon_p$	$p$	$Q(p)$ (Mpa)	$\sigma$ (Mpa)	$\epsilon$				
2	0	=A2		0	=D2/\$H\$3+A2	Start Step 1 (Elastic behavior)			
3	0	=A3	=(H\$5-H\$4)*(1-EXP(-H\$6*B3))	=\$H\$4+C3	=D3/\$H\$3+A3	End Step 1 (Elastic behavior)	E = 100000	Mpa	
4	=A3+0.001	=A4	=(H\$5-H\$4)*(1-EXP(-H\$6*B4))	=\$H\$4+C4	=D4/\$H\$3+A4	Start Step 2 (Plastic behavior)	$\sigma_y = 900$	Mpa	
5	=A4+0.001	=A5	=(H\$5-H\$4)*(1-EXP(-H\$6*B5))	=\$H\$4+C5	=D5/\$H\$3+A5		$\sigma_u = 1200$	Mpa	
6	=A5+0.001	=A6	=(H\$5-H\$4)*(1-EXP(-H\$6*B6))	=\$H\$4+C6	=D6/\$H\$3+A6		$\alpha = 100$		
7	=A6+0.001	=A7	=(H\$5-H\$4)*(1-EXP(-H\$6*B7))	=\$H\$4+C7	=D7/\$H\$3+A7				
8	=A7+0.001	=A8	=(H\$5-H\$4)*(1-EXP(-H\$6*B8))	=\$H\$4+C8	=D8/\$H\$3+A8				
9	=A8+0.001	=A9	=(H\$5-H\$4)*(1-EXP(-H\$6*B9))	=\$H\$4+C9	=D9/\$H\$3+A9				
10	=A9+0.001	=A10	=(H\$5-H\$4)*(1-EXP(-H\$6*B10))	=\$H\$4+C10	=D10/\$H\$3+A10				
11	=A10+0.001	=A11	=(H\$5-H\$4)*(1-EXP(-H\$6*B11))	=\$H\$4+C11	=D11/\$H\$3+A11				
12	=A11+0.001	=A12	=(H\$5-H\$4)*(1-EXP(-H\$6*B12))	=\$H\$4+C12	=D12/\$H\$3+A12				
13	=A12+0.001	=A13	=(H\$5-H\$4)*(1-EXP(-H\$6*B13))	=\$H\$4+C13	=D13/\$H\$3+A13				
14	=A13+0.001	=A14	=(H\$5-H\$4)*(1-EXP(-H\$6*B14))	=\$H\$4+C14	=D14/\$H\$3+A14				
15	=A14+0.001	=A15	=(H\$5-H\$4)*(1-EXP(-H\$6*B15))	=\$H\$4+C15	=D15/\$H\$3+A15				

## Fundamental Concepts of Plasticity

Figure 18. Stresses and strains computed with the spreadsheet

	A	B	C	D	E	F	G	H	I
1	$\epsilon_p$	p	Q(p) (Mpa)	$\sigma$ (Mpa)	$\epsilon$				
2	0	0		0	0	Start Step 1 (Elastic behavior)			
3	0	0	0	900	0.009	End Step 1 (Elastic behavior)	E =	100000	Mpa
4	0.001	0.001	28.54877459	928.5487746	0.010285488	Start Step 2 (Plastic behavior)	$\sigma_y =$	900	Mpa
5	0.002	0.002	54.38077408	954.3807741	0.011543808		$\sigma_u =$	1200	Mpa
6	0.003	0.003	77.75453338	977.7545338	0.012777545		$\alpha =$	100	
7	0.004	0.004	98.90398619	998.9039862	0.01398904				
8	0.005	0.005	118.0408021	1018.040802	0.015180408				
9	0.006	0.006	135.3565092	1035.356509	0.016353565				
10	0.007	0.007	151.0244089	1051.024409	0.017510244				
11	0.008	0.008	165.2013108	1065.201311	0.018652013				
12	0.009	0.009	178.0291021	1078.029102	0.019780291				
13	0.01	0.01	189.6361676	1089.636168	0.020896362				
14	0.011	0.011	200.1386749	1100.138675	0.022001387				
15	0.012	0.012	209.6417364	1109.641736	0.023096417				

Figure 19. Stress strain curve

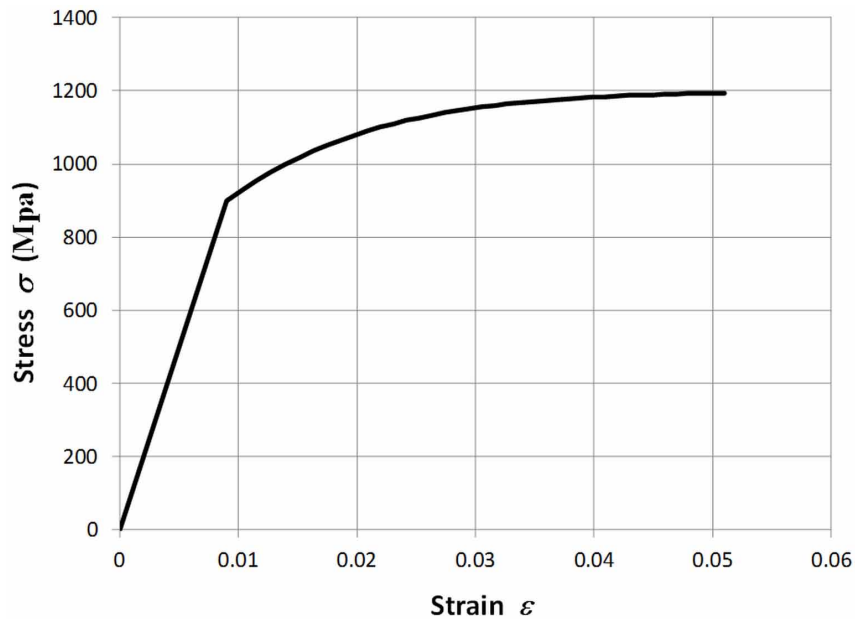
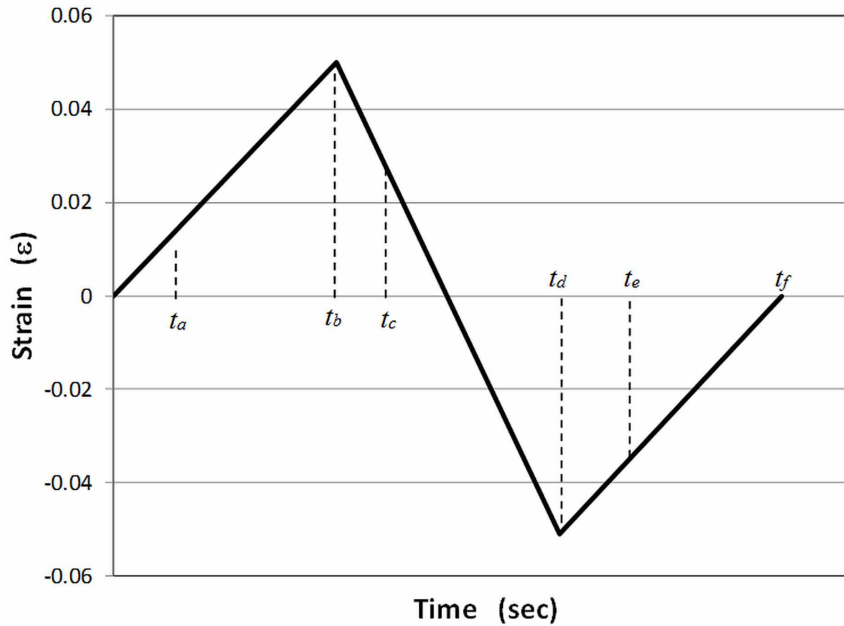


Figure 20. Strain history



**5.9.2 Plot the Stress Strain Curve for a Material with Nonlinear Kinematic Hardening for the Loading Path That Is Shown in Figure 20 with  $E = 100000$  Mpa, , Yield Stress  $\sigma_y = 900$  MPa, Ultimate Stress  $\sigma_u = 1200$  and  $\alpha = 100$ , Using an Algebraic Manipulation Program to Solve the Differential Equation and a Spreadsheet to Plot the Curve.**

The problem is solved using a step by step procedure. The first step corresponds to the interval  $0 \leq t < t_a$  where the material behaves elastically; the strain is computed using the elasticity law with plastic strain equal to zero. The strain at the last elastic point is:

$$\sigma = E(\varepsilon - \varepsilon_p) \Rightarrow \varepsilon = \frac{900}{100000} = 0.009 \tag{5.9.1}$$

Therefore, the corresponding point  $(\varepsilon, \sigma)$  in the stress strain curve is  $(0.009, 900)$ .

The second step corresponds to the interval  $t_a \leq t < t_b$  where it is assumed that the material behaves plastically; thus the second line of the evolution law (5.6.1b) applies:

$$f(\sigma) = 0 \Rightarrow \sigma = \sigma_y + x; \tag{5.9.2}$$

In order to obtain the expression for the hardening term  $x$ , the Equation (5.6.3) is integrated, using an algebraic manipulation program. It is considered that the hardening term,  $x$  is nil for a plastic strain equal to zero. The procedure is shown in Figure 21.

## Fundamental Concepts of Plasticity

This expression for  $x$  is used to compute the stress using the Equation (5.9.2). This computation was performed using a spreadsheet as it is shown in Figure 22.

The values obtained are shown in Figure 23.

This step ends at  $t_b$  that corresponds to a strain equal to 0.05. Notice that an approximate value of 0.049932888 was obtained for a stress equal to 1193.2887668. (See Figure 26).

The third step corresponds to the unloading in the interval  $t_b \leq t < t_c$ . It is assumed that the behavior in this step is elastic; thus the first line in the evolution law (5.2.2) applies. In this step the plastic strain

Figure 21. Computation of the hardening term, for the first positive yielding, using an algebraic manipulation program

```

> restart;
> eq1 := diff(x(ε_p), ε_p) = alpha * (σ_u - σ_y) - alpha * x(ε_p);
                                eq1 := d/dε_p x(ε_p) = α (σ_u - σ_y) - α x(ε_p) (1)
> ic := x(0) = 0;
                                ic := x(0) = 0 (2)
> dsolve({eq1, ic});
                                x(ε_p) = σ_u - σ_y + e^{-α ε_p} (-σ_u + σ_y) (3)

```

Figure 22. Equations programmed in spreadsheet for the first positive yielding of the material

	A	B	C	D	E	F	G	H	I
1	$\epsilon_p$		$X(\epsilon_p)$ (Mpa)	$\sigma$ (Mpa)	$\epsilon$				
2				0	0	Start Step 1 (Elastic behavior)			
3	0		$=\$H\$5-\$H\$4+EXP(-\$H\$6*A3)*(-\$H\$5+\$H\$4)$	$=\$H\$4+C3$	$=D3/\$H\$3+A3$	End Step 1 (Elastic behavior)	E = 100000	Mpa	
4	$=A3+0.001$		$=\$H\$5-\$H\$4+EXP(-\$H\$6*A4)*(-\$H\$5+\$H\$4)$	$=\$H\$4+C4$	$=D4/\$H\$3+A4$	Start Step 2 (Nonlinear behavior)	$\sigma_y = 900$	Mpa	
5	$=A4+0.001$		$=\$H\$5-\$H\$4+EXP(-\$H\$6*A5)*(-\$H\$5+\$H\$4)$	$=\$H\$4+C5$	$=D5/\$H\$3+A5$		$\sigma_u = 1200$	Mpa	
6	$=A5+0.001$		$=\$H\$5-\$H\$4+EXP(-\$H\$6*A6)*(-\$H\$5+\$H\$4)$	$=\$H\$4+C6$	$=D6/\$H\$3+A6$		$\alpha = 100$		
7	$=A6+0.001$		$=\$H\$5-\$H\$4+EXP(-\$H\$6*A7)*(-\$H\$5+\$H\$4)$	$=\$H\$4+C7$	$=D7/\$H\$3+A7$				
8	$=A7+0.001$		$=\$H\$5-\$H\$4+EXP(-\$H\$6*A8)*(-\$H\$5+\$H\$4)$	$=\$H\$4+C8$	$=D8/\$H\$3+A8$				
9	$=A8+0.001$		$=\$H\$5-\$H\$4+EXP(-\$H\$6*A9)*(-\$H\$5+\$H\$4)$	$=\$H\$4+C9$	$=D9/\$H\$3+A9$				

Figure 23. Stresses and strains computed for the first positive yielding of the material

	A	B	C	D	E	F	G	H	I
1	$\epsilon_p$		$X(\epsilon_p)$ (Mpa)	$\sigma$ (Mpa)	$\epsilon$				
2				0	0	Start Step 1 (Elastic behavior)			
3	0		0	900	0.009	End Step 1 (Elastic behavior)	E = 100000	Mpa	
4	0.001		28.54877459	928.5487746	0.010285488	Start Step 2 (Nonlinear behavior)	$\sigma_y = 900.0000$	Mpa	
5	0.002		54.38077408	954.3807741	0.011543808		$\sigma_u = 1200.0000$	Mpa	
6	0.003		77.7545338	977.7545338	0.012777545		$\alpha = 100.0000$		
7	0.004		98.90398619	998.9039862	0.01398904				
8	0.005		118.0408021	1018.040802	0.015180408				
9	0.006		135.3565092	1035.356509	0.016353565				

Figure 24. Hardening term computation for the negative yielding using an algebraic manipulation program

```

> restart;
> eq2 := diff(x(εp), εp) = alpha · (σu - σy) + alpha · x(εp);
                                eq2 :=  $\frac{d}{d\varepsilon_p} x(\varepsilon_p) = \alpha (\sigma_u - \sigma_y) + \alpha x(\varepsilon_p)$  (4)
> ic2 := x(0.038) = 293.2887684;
                                ic2 := x(0.038) = 293.2887684 (5)
> dsolve({eq2, ic2});
                                 $x(\varepsilon_p) = -\sigma_u + \sigma_y - \frac{e^{\alpha \varepsilon_p} \left( -\frac{733221921}{2500000} - \sigma_u + \sigma_y \right)}{e^{\frac{19}{500} \alpha}}$  (6)
    
```

Figure 25. Equations programmed in spreadsheet for the negative yielding of the material

	A	B	C	D	E	F
1	ε <sub>p</sub>		X(ε <sub>p</sub> ) (Mpa)	σ (Mpa)	ε	
41	=A40+0.001		=H\$5-\$H\$4+EXP(-H\$6*A41)*(-H\$5+H\$4)	=H\$4+C41	=D41/H\$3+A41	End Step 2 - Start Step 3
42	0.038		=H\$5+H\$4-EXP(H\$6*A42)*(-733221921/2500000-H\$5+H\$4)/EXP((19/500)*H\$6)	=H\$4+C42	=D42/H\$3+A42	End Step 3 (Elastic behavior - Unloading)
43	=A42-0.001		=H\$5+H\$4-EXP(H\$6*A43)*(-733221921/2500000-H\$5+H\$4)/EXP((19/500)*H\$6)	=H\$4+C43	=D43/H\$3+A43	Start Step 4 (Nonlinear behavior)
44	=A43-0.001		=H\$5+H\$4-EXP(H\$6*A44)*(-733221921/2500000-H\$5+H\$4)/EXP((19/500)*H\$6)	=H\$4+C44	=D44/H\$3+A44	
45	=A44-0.001		=H\$5+H\$4-EXP(H\$6*A45)*(-733221921/2500000-H\$5+H\$4)/EXP((19/500)*H\$6)	=H\$4+C45	=D45/H\$3+A45	
46	=A45-0.001		=H\$5+H\$4-EXP(H\$6*A46)*(-733221921/2500000-H\$5+H\$4)/EXP((19/500)*H\$6)	=H\$4+C46	=D46/H\$3+A46	
47	=A46-0.001		=H\$5+H\$4-EXP(H\$6*A47)*(-733221921/2500000-H\$5+H\$4)/EXP((19/500)*H\$6)	=H\$4+C47	=D47/H\$3+A47	
48	=A47-0.001		=H\$5+H\$4-EXP(H\$6*A48)*(-733221921/2500000-H\$5+H\$4)/EXP((19/500)*H\$6)	=H\$4+C48	=D48/H\$3+A48	
49	=A48-0.001		=H\$5+H\$4-EXP(H\$6*A49)*(-733221921/2500000-H\$5+H\$4)/EXP((19/500)*H\$6)	=H\$4+C49	=D49/H\$3+A49	
50	=A49-0.001		=H\$5+H\$4-EXP(H\$6*A50)*(-733221921/2500000-H\$5+H\$4)/EXP((19/500)*H\$6)	=H\$4+C50	=D50/H\$3+A50	
51	=A50-0.001		=H\$5+H\$4-EXP(H\$6*A51)*(-733221921/2500000-H\$5+H\$4)/EXP((19/500)*H\$6)	=H\$4+C51	=D51/H\$3+A51	

Figure 26. Stresses and strains computed for the negative yielding of the material

	A	B	C	D	E	F	G
1	ε <sub>p</sub>		X(ε <sub>p</sub> ) (Mpa)	σ (Mpa)	ε		
41	0.038		293.2887684	1193.288768	0.049932888	End Step 2 - Start Step 3	
42	0.038		293.2887684	-606.7112316	0.031932888	End Step 3 (Elastic behavior - Unloading)	
43	0.037		236.8298773	-663.1701227	0.030368299	Start Step 4 (Nonlinear behavior)	
44	0.036		185.7437601	-714.2562399	0.028857438		
45	0.035		139.5191298	-760.4808702	0.027395191		
46	0.034		97.69335455	-802.3066455	0.025976934		
47	0.033		59.8478281	-840.1521719	0.024598478		
48	0.032		25.60377966	-874.3962203	0.023256038		
49	0.031		-5.381516708	-905.3815167	0.021946185		
50	0.03		-33.41817227	-933.4181723	0.020665818		
51	0.029		-58.7867873	-958.7867873	0.019412132		

## Fundamental Concepts of Plasticity

is constant and equal to the value at  $t_b$ , i.e.  $\varepsilon_p = 0.038$ .  $t_c$  corresponds to the beginning of the plastic behavior of the material (see Figure 26).

The fourth step ( $t_c \leq t < t_d$ ) corresponds to a negative yielding of the material. Again, the yield function is equal to zero and the stress is computed by Equation (5.5.8):

$$f(\sigma) = 0 \Rightarrow \sigma = x - \sigma_y; \quad (5.9.3)$$

The hardening term  $x$ , is obtained through the integration of Equation (5.6.3) considering that the hardening term  $x$  is equal to 293.2887684 for a plastic strain equal to 0.038. The equations are shown in Figure 24.

The expression of the hardening term is used to compute the stress using Equation (5.9.3). This calculation is shown in Figure 25.

The corresponding values are shown in Figure 26.

This step ends at  $t_d$  that corresponds to a strain equal to -0.05.

The fifth step ( $t_d \leq t < t_e$ ) corresponds to the elastic reloading; thus, the plastic strain is kept constant and equal to -0.039 (see Figure 29). This step finishes at  $t_e$  when the positive yielding initiates (sixth

Figure 27. Hardening term computation for the second positive yielding using an algebraic manipulation program

```

> restart;
> eq3 := diff(x(εp), εp) = alpha · (σu - σy) - alpha · x(εp);
                                eq3 :=  $\frac{d}{d\varepsilon_p} x(\varepsilon_p) = \alpha (\sigma_u - \sigma_y) - \alpha x(\varepsilon_p)$  (7)
> ic3 := x(-0.039) = -299.7313427;
                                ic3 := x(-0.039) = -299.7313427 (8)
> dsolve({eq3, ic3});
                                 $x(\varepsilon_p) = \sigma_u - \sigma_y - \frac{e^{-\alpha \varepsilon_p} \left( \frac{2997313427}{10000000} + \sigma_u - \sigma_y \right)}{\frac{39}{1000} \alpha}$  (9)

```

Figure 28. Equations programmed in spreadsheet for the second positive yielding of the material

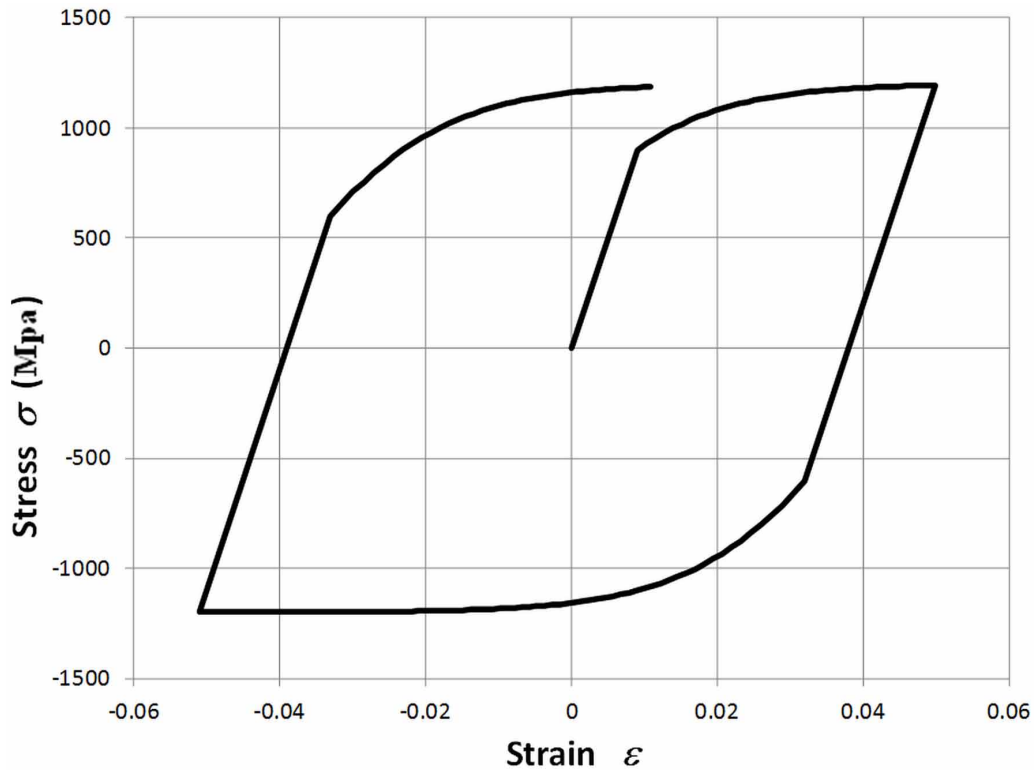
	A	B	C	D	E	F
1	$\varepsilon_p$		$X(\varepsilon_p)$ (Mpa)	$\sigma$ (Mpa)	$\varepsilon$	
119	=A118-0.001	=\$H\$5+\$H\$4-EXP(\$H\$6*A119)*(-733221921/2500000+\$H\$5+\$H\$4)/EXP((19/500)*\$H\$6)	=\$H\$4+C119	=D119/\$H\$3+A119		End Step 4 - Start Step 5
120	=-0.039	=\$H\$5-\$H\$4-EXP(-\$H\$6*A120)*(2997313427/10000000+\$H\$5-\$H\$4)/EXP((39/1000)*\$H\$6)	=\$H\$4+C120	=D120/\$H\$3+A120		End Step 5 (Elastic behavior - Unloading)
121	=A120+0.001	=\$H\$5-\$H\$4-EXP(-\$H\$6*A121)*(2997313427/10000000+\$H\$5-\$H\$4)/EXP((39/1000)*\$H\$6)	=\$H\$4+C121	=D121/\$H\$3+A121		Start Step 6 (Nonlinear behavior)
122	=A121+0.001	=\$H\$5-\$H\$4-EXP(-\$H\$6*A122)*(2997313427/10000000+\$H\$5-\$H\$4)/EXP((39/1000)*\$H\$6)	=\$H\$4+C122	=D122/\$H\$3+A122		
123	=A122+0.001	=\$H\$5-\$H\$4-EXP(-\$H\$6*A123)*(2997313427/10000000+\$H\$5-\$H\$4)/EXP((39/1000)*\$H\$6)	=\$H\$4+C123	=D123/\$H\$3+A123		
124	=A123+0.001	=\$H\$5-\$H\$4-EXP(-\$H\$6*A124)*(2997313427/10000000+\$H\$5-\$H\$4)/EXP((39/1000)*\$H\$6)	=\$H\$4+C124	=D124/\$H\$3+A124		
125	=A124+0.001	=\$H\$5-\$H\$4-EXP(-\$H\$6*A125)*(2997313427/10000000+\$H\$5-\$H\$4)/EXP((39/1000)*\$H\$6)	=\$H\$4+C125	=D125/\$H\$3+A125		
126	=A125+0.001	=\$H\$5-\$H\$4-EXP(-\$H\$6*A126)*(2997313427/10000000+\$H\$5-\$H\$4)/EXP((39/1000)*\$H\$6)	=\$H\$4+C126	=D126/\$H\$3+A126		
127	=A126+0.001	=\$H\$5-\$H\$4-EXP(-\$H\$6*A127)*(2997313427/10000000+\$H\$5-\$H\$4)/EXP((39/1000)*\$H\$6)	=\$H\$4+C127	=D127/\$H\$3+A127		
128	=A127+0.001	=\$H\$5-\$H\$4-EXP(-\$H\$6*A128)*(2997313427/10000000+\$H\$5-\$H\$4)/EXP((39/1000)*\$H\$6)	=\$H\$4+C128	=D128/\$H\$3+A128		
129	=A128+0.001	=\$H\$5-\$H\$4-EXP(-\$H\$6*A129)*(2997313427/10000000+\$H\$5-\$H\$4)/EXP((39/1000)*\$H\$6)	=\$H\$4+C129	=D129/\$H\$3+A129		
130	=A129+0.001	=\$H\$5-\$H\$4-EXP(-\$H\$6*A130)*(2997313427/10000000+\$H\$5-\$H\$4)/EXP((39/1000)*\$H\$6)	=\$H\$4+C130	=D130/\$H\$3+A130		



Figure 29. Stresses and strains computed for the second positive yielding of the material

	A	B	C	D	E	F
1	$\epsilon_p$		$\chi(\epsilon_p)$ (Mpa)	$\sigma$ (Mpa)	$\epsilon$	
119	-0.039		-299.7313427	-1199.731343	-0.050997313	End Step 4 - Start Step 5
120	-0.039		-299.7313427	600.2686573	-0.032997313	End Step 5 (Elastic behavior - Unloading)
121	-0.038		-242.6593596	657.3406404	-0.031426594	Start Step 6 (Nonlinear behavior)
122	-0.037		-191.0184939	708.9815061	-0.029910185	
123	-0.036		-144.2919062	755.7080938	-0.028442919	
124	-0.035		-102.0119412	797.9880588	-0.027020119	
125	-0.034		-63.75544694	836.2445531	-0.025637554	
126	-0.033		-29.1395394	870.8604606	-0.024291395	
127	-0.032		2.182228992	902.182229	-0.022978178	
128	-0.031		30.52333704	930.523337	-0.021694767	
129	-0.03		56.16743206	956.1674321	-0.020438326	
130	-0.029		79.37116879	979.3711688	-0.019206288	

Figure 30. Stress strain curve



## **Fundamental Concepts of Plasticity**

step, ( $t_e \leq t < t_f$ )). In order to determine  $t_e$ , the yield function is made equal to zero and the stress is computed using again Equation (5.9.2), i.e.  $\sigma = \sigma_y + x$ . For the determination of the hardening term the Equation (5.6.3) is integrated considering  $x$  equal to -299.7313427 for a plastic strain equal to -0.039. (See Figure 27). The formulation is shown in Figure 28 and the corresponding values in Figure 29.

Figure 30 shows the resulting stress-strain curve.

## **5.10 PROBLEMS**

**5.10.1 Repeat the Example 5.2.4 Using the Strain History That Is Indicated in the Example 5.9.2**

**5.10.2 Propose a Plasticity Model with Both, Linear Isotropic and Kinematic Hardening**

**5.10.3 Plot the Stress-Strain Curve of the Model Proposed in the Problem 5.10.2 Using the History of Strain of the Problem 5.2.4**

**5.10.4 Plot the Stress-Strain Curve of the Model Proposed in the Problem 5.10.2 Using the History of Strain of the Problem 5.9.2**

**5.10.5 Propose a Model with Both, Nonlinear Isotropic and Kinematic Hardening**

**5.10.6 Plot the Stress-Strain Curve of the Model Proposed in the Problem 5.10.5 Using the History of Strain of the Problem 5.2.4**

**5.10.7 Plot the Stress-Strain Curve of the Model Proposed in the Problem 5.10.5 Using the History of Strain of the Problem 5.9.2**

## **REFERENCE**

Lemaitre, J., & Chaboche, J. L. (1985). *Mécanique des matériaux solides*. Paris, France: Dunod Bordas.

# Chapter 6

## The Plastic Hinge

### ABSTRACT

*The plastic hinge is a key concept of the theory of frames that differentiates this theory from the remaining models for structural analysis. This chapter is exclusively dedicated to define this concept and describe the different models of plastic hinges. It also discusses the differences of implementation between plastic hinges in steel frames (Sections 6.1-6.4) and those in reinforced concrete structures (Sections 6.5-6.6). This chapter is based on the ideas presented in Chapter 5 and it allows formulating the models for elasto-plastic frames that are introduced in the next chapter.*

### 6.1 ELASTO-PLASTIC MOMENT VS. CURVATURE RELATIONSHIP

Consider a simply supported beam, as the one shown in Figure 1a, subjected to a concentrated force at its mid-section; the force is monotonically increased until total collapse of the structure. The beam has a symmetric cross-section of height  $h$ , it is homogeneous and its material follows the elasto-perfect plastic constitutive model described in section 5.2. The bending moment distribution along the beam and the stress and strain distributions in the mid-section B (the most loaded) are shown in Figures 1b, 1c and 1d.

According to the fundamental hypothesis of the beam theory, the strain distribution in the cross-section is always linear, even if the behavior is not elastic:

$$\varepsilon = \chi \cdot z \tag{6.1.1}$$

where  $\chi$  is the curvature and  $z$  is the coordinate of the fiber under consideration as shown Figure 1b (see chapter 2). The elastic relationship between moment and curvature is:

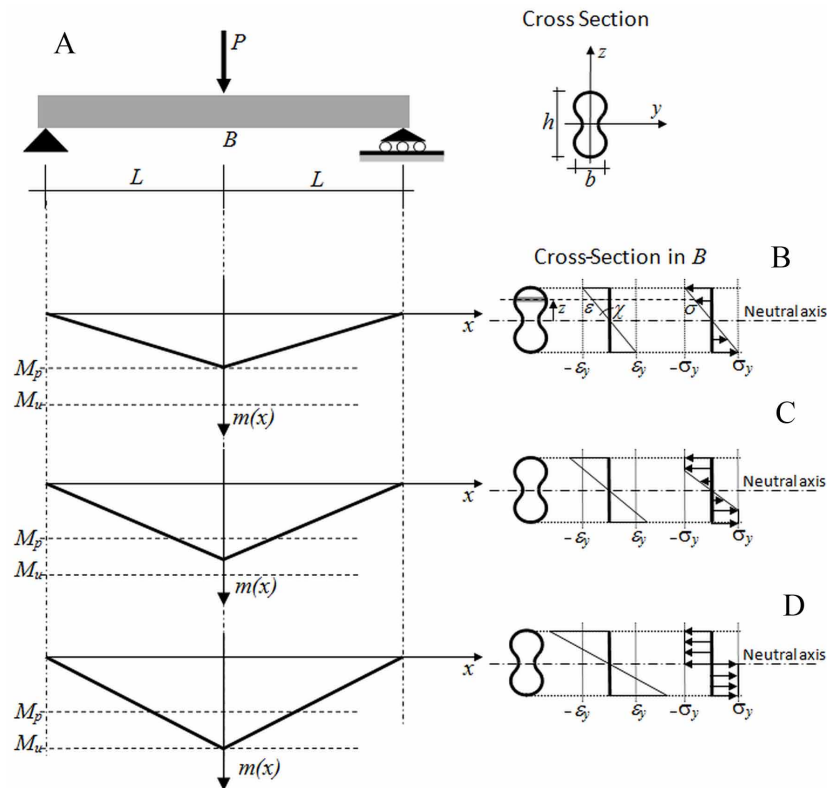
$$m = EI\chi \tag{6.1.2}$$

This last expression does not apply if the behavior is elasto-plastic. Elastic behavior in the beam ends when the maximum stress at the mid-section is equal to the yield stress as shown in Figure 1b. The normal stress distribution is still linear at this instant, and according to the Hooke's law, it is propor-

DOI: 10.4018/978-1-4666-6379-4.ch006

## The Plastic Hinge

Figure 1. a) Simply supported beam; Flexural moment distribution along the beam, strain distribution in the mid-cross-section and stress distribution at: b) Last elastic stress, c) Elasto-plastic stress, d) Ultimate stress



tional to the strain values:  $\sigma = E \cdot \chi \cdot z$ . The bending moment in the section corresponding to this load is called first plastic moment  $M_p$ :

$$M_p = S \cdot \sigma_y; \text{ where } S = \frac{2I}{h} \quad (6.1.3)$$

$S$  is called elastic section modulus. For larger values of the force (Figure 1c), some of the fibers in the cross-section begin yielding at constant stress. As the force and curvature increase, more and more fibers yield. As the curvature tends to infinity the bending moment tends to the ultimate bending strength of the section; this value is called ultimate moment  $M_u$  and can be computed assuming that all the fibers in the cross-section have plastic behavior (Figure 1d):

$$M_u = \sigma_y H_f; \text{ where } H_f = 2 \int_0^{h/2} b(z) z dz \quad (6.1.4)$$

$H_f$  is called plastic section modulus. Examples of computation of the first plastic moment and the ultimate one for different cross-sections are presented in section 6.8.

The moment curvature relationship in the mid-section of the beam is shown in Figure 2.

The mid-section of the beam is not the only one that may experience plastic strains. According to the moment-curvature relationship depicted in Figure 2, any section subjected to bending moments larger than  $M_p$  is partially plasticized (Figure 3b); the curvature distribution along the beam is indicated in Figure 3c.

Notice that the maximum curvature value in Figure 3c rapidly tends to infinite as the load tends to  $\frac{2M_u}{L}$ .

## 6.2 THE PERFECT PLASTIC HINGE

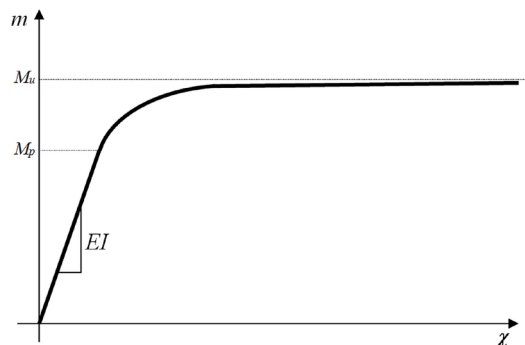
The structure analyzed in the previous section is one of the simplest examples of a problem in plasticity solved in the framework of the beam theory; in more complex cases, hyperstatic beams for instance, the analyses have to be carried out using structural analysis computer programs. The determination of the plastic zone requires the discretization of the beam in short fibers, in two or three dimensions. In large frames, this is a process complex, time consuming and unnecessary. The goal of this section is to introduce the fundamental concept for a simplified analysis in plasticity of beams and frames: the plastic hinge.

Consider again the moment-curvature relationship indicated in Figure 2, the first step for a simplified analysis is the substitution of the exact solution by an approximate one that has the two branches of the elastic perfect plastic model such as it is shown in Figure 4.

The value  $M_y$  is called yield moment. The yield moment can be made equal to the ultimate moment of the cross-section  $M_u$  or, for a more conservative analysis, it can be chosen equal to the first plastic moment  $M_p$ .

Assume that  $M_y$  is the ultimate moment and consider again the simply supported beam of Figure 1a; suppose now that the moment at the mid-section has reached its ultimate value as it is shown in Figure 1d; the perfectly plastic approximation (Figure 4) would result in the curvature distribution indicated in Figure 5 b.

Figure 2. Moment-curvature relationship at the mid-section of the beam



### The Plastic Hinge

Figure 3. a) Distribution of bending moment along the beam b) Plastic zone in the beam c) Curvature distribution along the beam

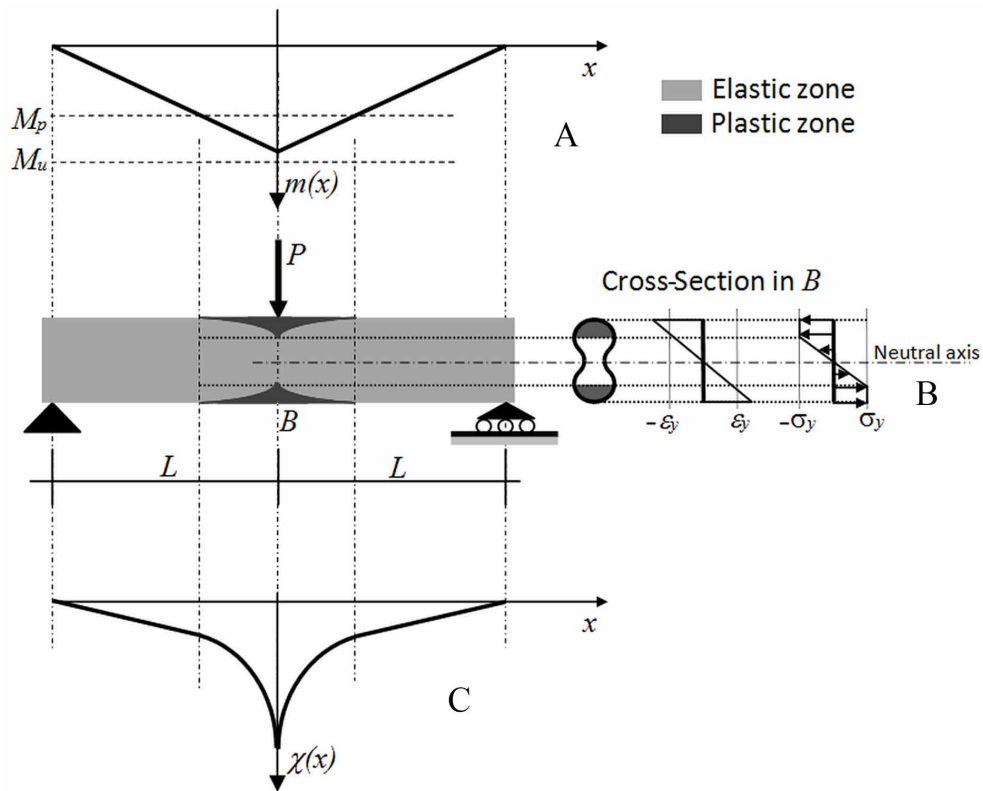
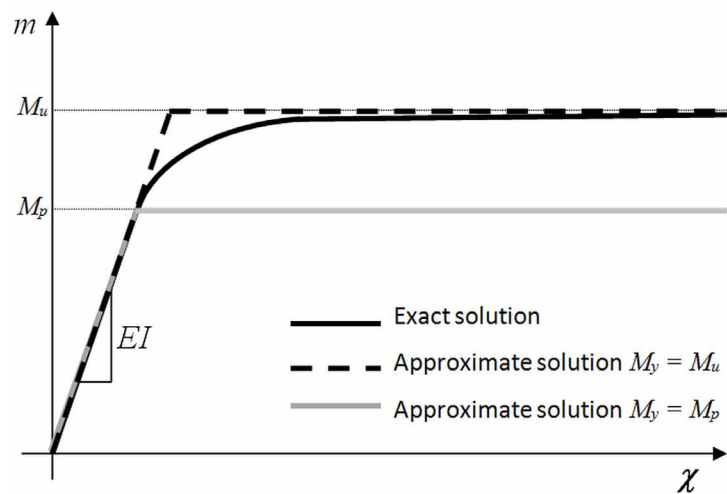


Figure 4. Elasto-perfect plastic idealization of the moment curvature relationship



The curvature in all the sections of the beam, except the mid-one, is equal to  $M/EI$ , as in the elastic curvature distribution. In the mid-section there is a discontinuity; at this point the curvature is indeterminate. In mathematical language, it is said that the curvature at the unique plasticized section of the beam can be represented by a Dirac delta function multiplied by a term denoted plastic rotation  $\phi^p$ . The plastic rotation is the value of the hatched area in the exact curvature distribution that is indicated in Figure 5a. The mathematical expressions of the bending moment distribution that is shown in Figure 1d and the curvature distribution that is shown in Figure 5b are:

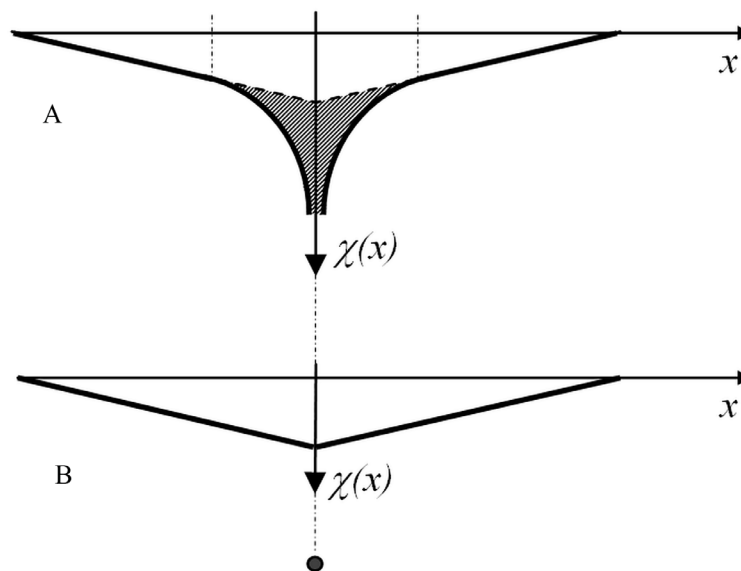
$$m = M_y \left( 1 - \frac{|x|}{L} \right) \Rightarrow \chi = \frac{M_y}{EI} \left( 1 - \frac{|x|}{L} \right) + Dirac(x)\phi^p \quad (6.2.1)$$

where the Dirac delta function is defined as (see a textbook on theory of distributions, for instance the one included in the bibliography of this chapter):

$$Dirac(x) = \begin{cases} +\infty & \text{if } x = 0 \\ 0 & \text{if } x \neq 0 \end{cases}; \int_{-\infty}^{\infty} Dirac(x) dx = 1 \quad (6.2.2)$$

As aforementioned in section 2.3, the kinematic equation of the beam theory that relates curvature and rotation is:

Figure 5. Curvature distribution along a simply supported beam a) Exact distribution b) Approximate distribution



### The Plastic Hinge

$$\chi = -\frac{d\beta}{dx} \quad (6.2.3)$$

Integration of Equation (6.2.3), considering Equation (6.2.1b), gives the relative rotation between both ends of the beam  $\beta_{i-j}$ .

$$\beta_{i-j} = -\int_{x=-L}^{x=L} \chi dx = -\int_{x=-L}^{x=L} \frac{M_y}{EI} \left(1 - \frac{|x|}{L}\right) dx - \phi^p \int_{x=-L}^{x=L} Dirac(x) dx \quad (6.2.4)$$

Taking into account that  $\int_{-L}^L Dirac(x) dx = 1$ , it is obtained:

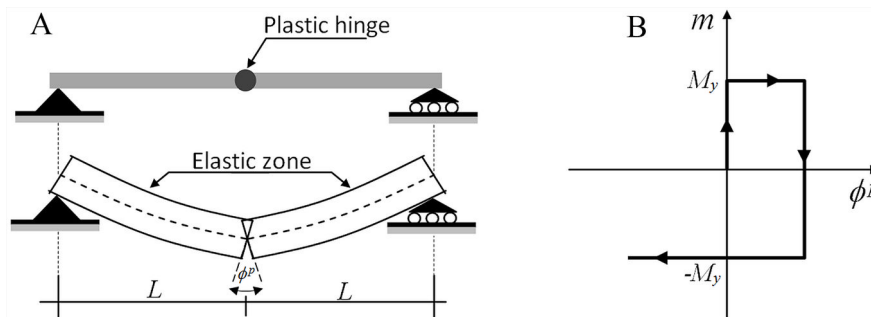
$$\beta_{i-j} = -\frac{M_y L}{EI} - \phi^p \quad (6.2.5)$$

A physical interpretation of the plastic rotation can be given by considering the structure as represented by two elastic elements connected by a sort of flexural plastic spring, as shown in Figure 6a. This rotational spring is called plastic hinge and, initially, it has zero length. The angle between both ends of the plastic hinge is the plastic rotation ( $\phi^p$ ). The first term in Equation (6.2.5) is the relative rotation due to the elastic bending of the two elements adjacent to the plastic hinge. The behavior of the plastic hinge is characterized in terms of moment vs. plastic rotation as indicated in Figure 6b.

A plastic hinge can be imagined as a rusty hinge of a door. If the door is pushed just slightly, a moment on the hinge is generated but the door will not open. The door has to be pushed hard enough so that the moment on the hinge equals the yield moment  $M_y$ . At this point, the door will open at a uniform rate as far as the moment is kept constant; if the force decreases, the hinge will lock again and the door would not open or close anymore.

In mathematical terms, the constitutive equation of the perfect plastic hinge has the same general form of the evolution law of the plastic strain that is described in chapter 5.

Figure 6. a) Plastic hinge connecting two elastic elements b) Moment vs. plastic rotation in a perfect plastic hinge





$$\begin{cases} d\phi^p = 0 & \text{if } f(m) < 0 \text{ (locked hinge)} \\ f(m) = 0 & \text{if } d\phi^p \neq 0 \text{ (active hinge)} \end{cases} \quad (6.2.6)$$

where

$$f(m) = |m| - M_y \leq 0 \quad (6.2.7)$$

The term  $f(m)$  is the yield function of the plastic hinge. An example of the analysis of a hyperstatic beam using plastic hinges is analyzed in chapter 8.

The plastic hinge approximation is a good one if the loads applied on the structure are mainly due to concentrated forces. In this case, the plastic zones have small areas compared with the dimensions of the structure. Otherwise, the procedure based on beam theory has to be used; however this is a more cumbersome and time-consuming alternative.

## 6.3 PLASTIC HINGE WITH HARDENING

### 6.3.1 Plastic Hinge with Isotropic Hardening

A better approximation to the exact solution can be obtained by introducing hardening terms into the yield function of the plastic hinge. For instance, a plastic hinge with isotropic hardening is characterized by:

$$\begin{cases} d\phi^p = 0 & \text{if } f(m, p) < 0 \text{ (locked hinge)} \\ f(m, p) = 0 & \text{if } d\phi^p \neq 0 \text{ (active hinge)} \end{cases} ; f(m, p) = |m| - (M_p + Q(p)) \leq 0 \quad (6.3.1)$$

where  $p$  can be the accumulated plastic rotation:

$$dp = |d\phi^p| \quad (6.3.2)$$

or the maximum plastic rotation:

$$p = \text{Max} |\phi^p| \quad (6.3.3)$$

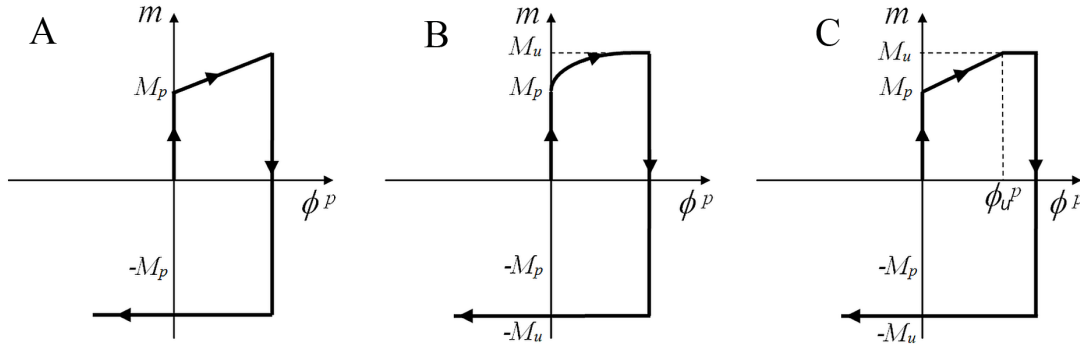
The isotropic term can be linear (see Figure 7a):

$$Q(p) = c.p \quad (6.3.4)$$

where  $c$  is, again, a member-dependent constant. The isotropic term can also be nonlinear (see Figure 7b):

## The Plastic Hinge

Figure 7. Moment vs. plastic rotation in plastic hinge with isotropic hardening a) Linear hardening b) Nonlinear hardening c) Multi-linear hardening with two plastic segments



$$Q(p) = (M_u - M_p)(1 - e^{-\alpha p}) \quad (6.3.5)$$

where  $\alpha$  is also a member-dependent parameter that characterizes the transition from the first plastic moment to the ultimate moment of the cross-section.

This approximation represents a behavior that is very close to the exact one (Figure 2) because, unlike the perfect plastic hinge, it includes the first plastic moment and ultimate moment in the behavior; additionally, it is much simpler to compute than the exact approach.

Another kind of nonlinear hardening that is frequently used in practice is the so-called “multi-linear” models; in this case, the behavior is approximated by several straight lines as shown in Figure 7c. For instance, in the case of two plastic segments, the model is given by:

$$Q(p) = \begin{cases} \frac{(M_u - M_p)}{\phi_u^p} p & \text{if } 0 \leq p \leq \phi_u^p \\ M_u - M_p & \text{if } p > \phi_u^p \end{cases} \quad (6.3.6)$$

The constant  $\phi_u^p$  is a member-dependent property that is denoted ultimate plastic rotation; notice that it has the same role of  $\alpha$  in Equation (6.3.5), i.e. it is related to the velocity of the transition between the first plastic moment and the ultimate moment.

### 6.3.2 Plastic Hinge with Kinematic Hardening

The Bauschinger effect is also observed in the case of cyclic loading on a beam or column; plastic hinges with kinematic hardening can represent this phenomenon; they are defined by the evolution law:

$$\begin{cases} d\phi^p = 0 & \text{if } f(m, x) < 0 \text{ (locked hinge)} \\ f(m, x) = 0 & \text{if } d\phi^p \neq 0 \text{ (active hinge)} \end{cases}; f(m, x) = |m - x| - M_p \leq 0 \quad (6.3.7)$$

Where the kinematic hardening term or back moment  $x$  can be a linear function or a nonlinear function of the plastic rotation. In the linear kinematic hardening case (see Figure 8a):

$$x = c.\phi^p \quad (6.3.8)$$

The evolution law of nonlinear kinematic hardening is defined by:

$$dx = \alpha \left( (M_u - M_p) d\phi^p - x \cdot |d\phi^p| \right) \quad (6.3.9)$$

and the resulting response is indicated in Figure 8b. Alternatively, nonlinear kinematic hardening can also be given by the following multi-linear model (see Figure 8c):

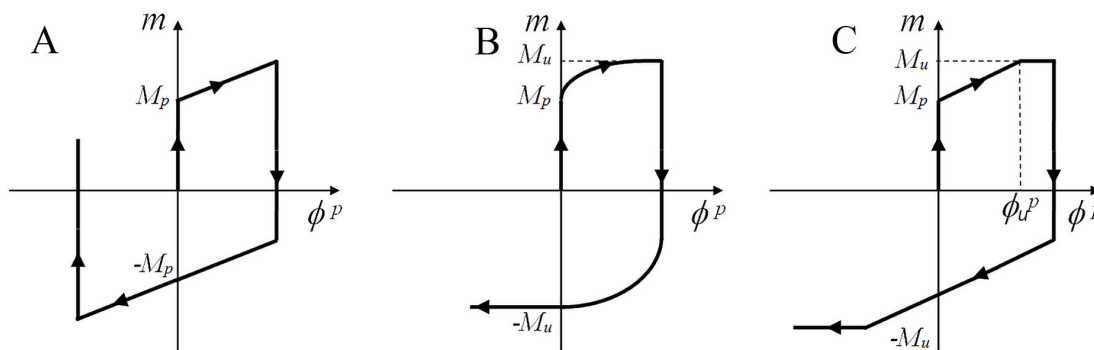
$$dx = \begin{cases} \frac{(M_u - M_p)}{\phi_u^p} d\phi^p & \text{if } |m| < M_u \\ 0 & \text{if } |m| = M_u \end{cases} \quad (6.3.10)$$

### 6.3.3 Kinematic and Isotropic Nonlinear Hardening Simultaneously

In most cases, particularly in reinforced concrete and steel frame elements, displacement and growth of the elastic domain are observed simultaneously. This behavior can be modeled by introducing both hardening variables into the yield function:

$$f = |m - x| - (M_p + Q) \leq 0 \quad (6.3.11)$$

Figure 8. Moment vs. plastic rotation in a plastic hinge with kinematic hardening: a) Linear hardening b) Nonlinear hardening c) Multi linear hardening with two segments



### The Plastic Hinge

As aforementioned, the total amount of hardening is:  $M_u - M_p$ . This quantity must be split into the two mechanisms. Assuming that there is a constant ratio between isotropic hardening and kinematic hardening, the corresponding evolution laws are given by:

$$Q = (1 - r)(M_u - M_p)(1 - e^{-\alpha p}); dx = \alpha \left( r(M_u - M_p) d\phi^p - x \cdot |d\phi^p| \right); 0 \leq r \leq 1 \quad (6.3.12)$$

The value  $r = 0$  represents isotropic hardening only,  $r = 1$  kinematic hardening exclusively; intermediate values give combined hardening. The parameter  $r$  must be chosen so that the best approximation of experimental results is observed; for instance, in the case of reinforced concrete elements  $r$  takes values around 0.7. The same approach can be followed in the formulation of a plastic hinge with kinematic and isotropic hardening that could be linear or multi-linear.

## 6.4 PERFECTLY PLASTIC HINGE SUBJECTED TO BENDING AND AXIAL FORCES

### 6.4.1 Simply Supported Beam-Column Subjected to Bending and Axial Force

Consider a simply supported beam-column with a rectangular cross-section of height  $h$  and base  $b$  as the one shown in Figure 9; the beam-column is subjected to a concentrated force  $P$  at its mid-section and an axial force  $n$ . Its material follows the elastic-perfectly plastic model that is described in section 5.2.

The elastic stress distribution at the mid-section is obtained by adding the one resulting from bending plus the other that depends on the axial force. Notice that there is an arbitrary number of stress distribution that reach the elastic limit, unlike the example presented in section 6.1, there is an arbitrary number of stress distributions that reach the elastic limit; all these distributions depend on the distance,  $z_0$ , between the fibers with zero stress (neutral axis) and the centroid of the cross-section (centroidal axis) (see Figure 10a). Similarly, the cross-section can be fully plasticized in an infinity number of ways; each one of them is in equilibrium with a different combination of bending moment and axial force (see Figure 10c). These values can be expressed as a function of  $z_0$  decomposing the stress distribution into two parts, one that only generates axial force and another related to the bending moment as shown in Figure 10c.

In a beam theory analysis, the cross-section shows a gradual evolution from an elastic stress distribution to a fully plastic one passing through intermediate states such as the one shown in Figure 10b. In a frame analysis with perfectly plastic hinges, this process will be ignored and it is assumed that the cross-section becomes fully plastic without passing through any intermediate state. In the beam analysis there is a plastic zone that covers not only the mid-section but also the adjacent ones. In the frame analysis, a plastic hinge is generated in the mid-section and the rest of the structure remains elastic as in the case of the beam without axial force; however, the behavior of the plastic hinge is not exactly the same. As shown in Figure 11b, the plastic hinge presents now two different deformations: a plastic rotation  $\phi^p$  and a plastic elongation  $\delta_p$ .

Figure 9. a) Simply supported beam subjected to bending and axial forces b) Bending moment distribution c) Axial force distribution

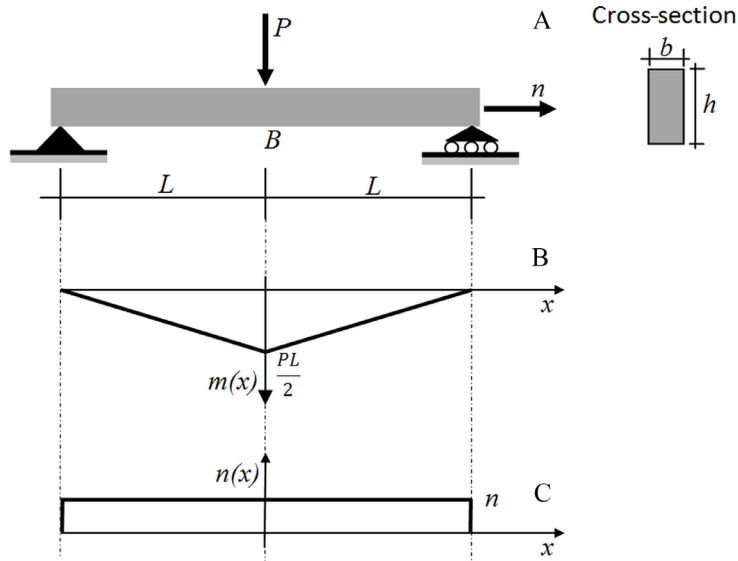
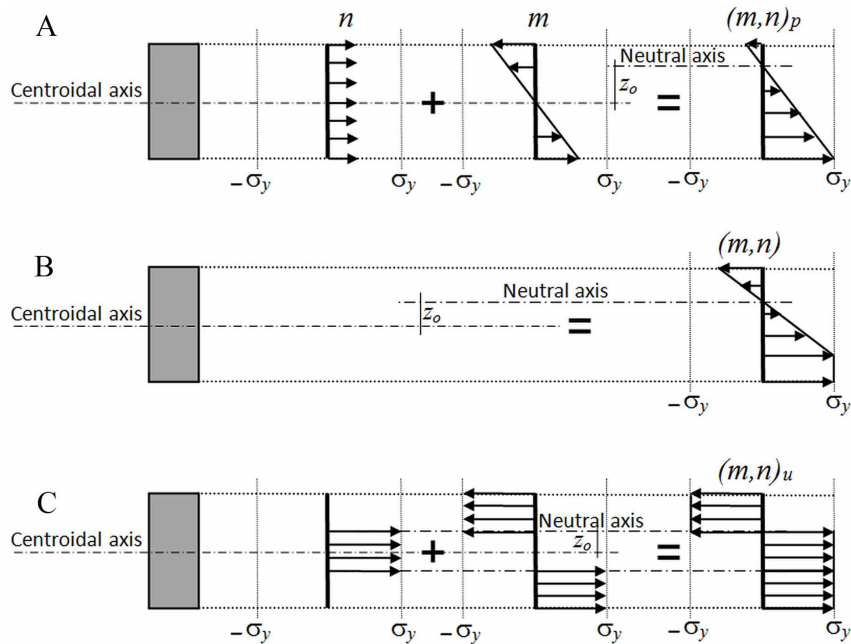


Figure 10. Stress distributions in a beam subjected to bending and axial force a) First elasto-plastic stress distribution b) Intermediate elasto-plastic stress distribution c) Fully plastic stress distribution



## The Plastic Hinge

### 6.4.2 Yield Function of a Plastic Hinge Subjected to Bending and Axial Force

According to the stress distribution shown in Figure 10c, the moment and the axial forces are given by:

$$m = 2\sigma_y \int_{z_o}^{h/2} z.b.dz = 2\sigma_y b \left( \frac{h^2}{8} - \frac{z_o^2}{2} \right); n = 2\sigma_y \int_0^{z_o} b.dz = 2\sigma_y b.z_o \quad (6.4.1)$$

Obtaining the expression of  $z_o$  from Equation (6.4.1b) and introducing it into (6.4.1a) gives:

$$\frac{|m|}{M_y} + \left( \frac{n}{N_y} \right)^2 - 1 = 0; \text{ where } M_y = \frac{\sigma_y b.h^2}{4}; N_y = \sigma_y b.h \quad (6.4.2)$$

Notice that  $M_y$  is the yield moment of the cross-section without axial forces and  $N_y$  produces the total plasticization of the element when there is no bending moments. Equation (6.4.2) describes a surface (see Figure 12) in the  $m$ - $n$  space that encloses the elastic domain of the plastic hinge; i.e. any combination of axial force and bending moment that represents a stress point inside the surface, corresponds to an elastic state. A plastic hinge appears or becomes active only if the stress point lies on the surface; a stress point outside the surface cannot be withstood by the beam according to the perfectly plastic model. The yield function of a perfectly plastic hinge corresponding to a rectangular cross-section is therefore given by:

$$f(m, n) = \frac{|m|}{M_y} + \left( \frac{n}{N_y} \right)^2 - 1 \leq 0 \quad (6.4.3)$$

Figure 11. a) Plastic hinge subjected to bending b) Plastic hinge subjected to bending and axial force

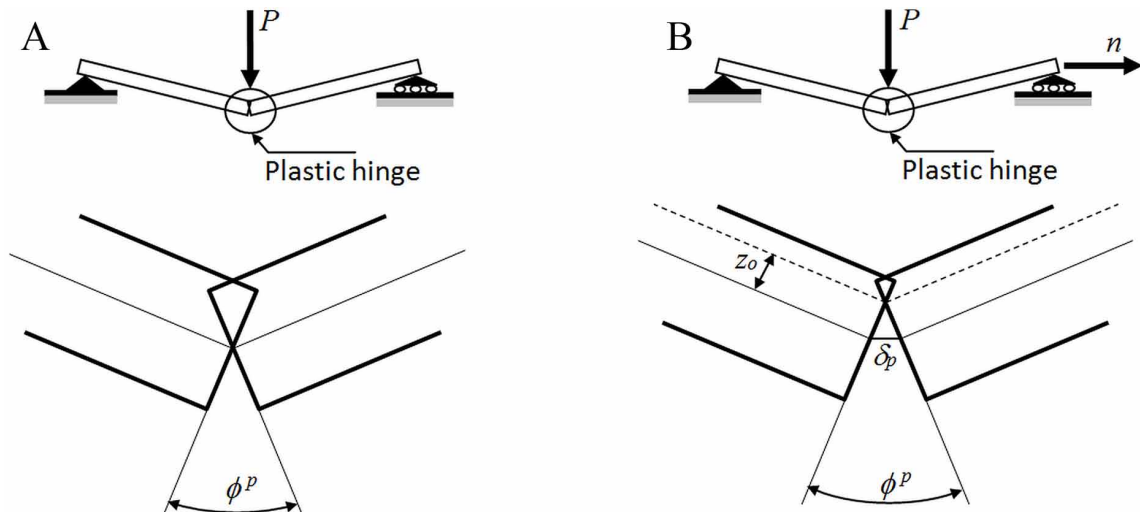
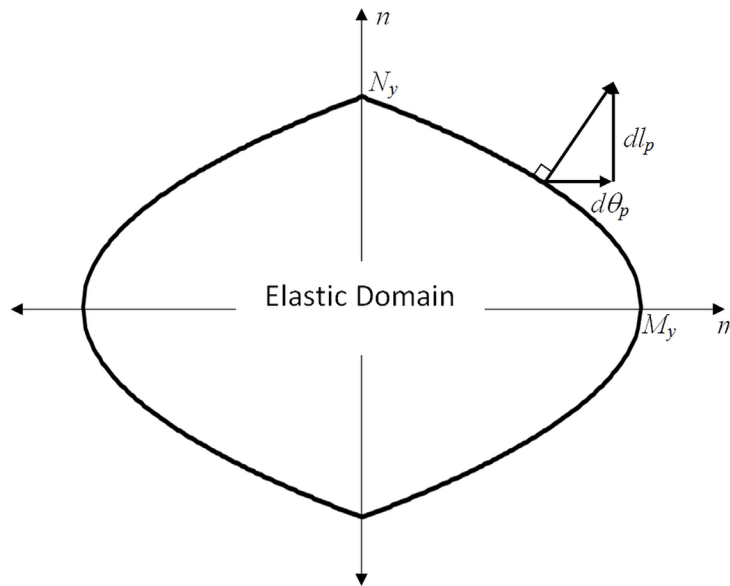


Figure 12. Yield surface, elastic domain and normality rule for a rectangular cross-section



The elastic domain is defined as:

$$(m, n) \Big| f < 0 \tag{6.4.4}$$

The border of the elastic domain is also called yield surface; in the reinforced concrete structures and steel structures textbooks it is named interaction diagram.

The yield functions,  $f = f(m, n) \leq 0$ , of different cross-sections can be obtained using the same procedure.

Alternatively, approximate expressions of the yield function are postulated instead of computed exactly; this is often the procedure followed for the design of steel structural frames. For instance, an empirical expression for any symmetric cross-section is:

$$f(m, n) = \left( \frac{n}{N_y} \right)^{\nu_1} + \left( \frac{m}{M_y} \right)^{\nu_2} - 1 \tag{6.4.5}$$

Often the coefficients  $\nu_1$  and  $\nu_2$  are chosen equal to 2 and the elastic domain becomes an ellipse in the  $m$ - $n$  space.

### 6.4.3 The Normality Rule

The yield function (6.4.3) indicates again if the plastic hinge is locked or active; however it does not determines which plastic state is happening in the hinge. As opposed to the case of bending only, now

### The Plastic Hinge

plasticity is represented by two different components as shown in Figure 11b: plastic rotation and plastic elongation; the yield function does not establish their relative contributions. Intuition suggests that in an element with large axial forces and low bending moments, the plastic elongation should be dominant in the hinge and vice-versa, small axial forces and large bending moments should lead to relatively larger plastic rotations. This general idea can be formulated precisely by introducing an additional equation called normality rule. This expression completes the mathematical description of the behavior of a plastic hinge. The normality rule is stated as follows:

$$d\phi^p = d\lambda \frac{\partial f}{\partial m}; d\delta_p = d\lambda \frac{\partial f}{\partial n} \quad (6.4.6)$$

The new variable  $\lambda$  is called plastic multiplier and it is defined as:

$$\begin{cases} d\lambda = 0 & \text{if } f(m, n) < 0 \text{ (locked hinge)} \\ f(m, n) = 0 & \text{if } d\lambda > 0 \text{ (active hinge)} \end{cases} \quad (6.4.7)$$

In the case of a perfect plastic hinge in a rectangular cross-section, the normality rule can be formally proved. According to the yield function (6.4.3), the normality rule gives:

$$d\phi^p = d\lambda \frac{1 \cdot \text{sign}(m)}{M_y} = d\lambda \frac{4 \cdot \text{sign}(m)}{\sigma_y b \cdot h^2}; d\delta_p = d\lambda \frac{n}{N_y^2} = d\lambda \frac{4z_o}{\sigma_y b \cdot h^2} \quad (6.4.8)$$

The elimination of the plastic multiplier by combining expressions (6.4.8) gives:

$$d\delta_p = \text{sign}(m) z_o d\phi^p \quad (6.4.9)$$

It can be verified by inspection of Figure 11b that this is indeed the relationship between the plastic rotation and the plastic elongation in the hinge.

The normality rule cannot be proved in the general case of cross-sections of arbitrary shape and elasto-plastic constitutive equations with hardening; however, it is assumed that expressions (6.4.5) are always valid: the normality rule becomes the normality law.

Equations (6.4.5) are called normality rule or normality law because similar expressions correspond to the components of a vector normal to a surface; i.e. be  $f(x,y)=0$  a curve in the  $x - y$  plane, a vector of components  $\left( \frac{\partial f}{\partial x}, \frac{\partial f}{\partial y} \right)$  is perpendicular to the curve at the point of coordinates  $(x,y)$  (see any calculus

textbook). Note, that although  $d\lambda \left( \frac{\partial f}{\partial m}, \frac{\partial f}{\partial n} \right)$  is not a vector (the components do not even have the same units), the plastic deformation matrix  $(d\phi^p, d\delta_p)$  can be imagined, by analogy, as a vector normal to the yield surface at the point  $(m,n)$  that activates the plastic hinge (see Figure 12). The rapport between the derivatives gives the direction of this plastic “vector”. For instance, in the case of a rectangular cross-



section, this vector is horizontal if there is no axial force; i.e. there is no plastic elongation of the hinge only rotation; for negative axial forces, the normal vector is inclined downward: the plastic elongation component is negative, and so on. The plastic multiplier is related to the “size” of the plastic “vector”; that is, it characterizes the amount of deformation experienced by the plastic hinge. Note that the plastic multiplier can only be positive and always increases when the plastic hinge is active.

#### 6.4.4 Perfect Plastic Hinge Subjected to Biaxial Bending Moments and Axial Force

Consider now a tridimensional frame element. Be  $Y$  and  $Z$  the principal axes of the cross-section; a plastic hinge in this case presents three plastic deformations:

$$(\phi_y^p, \phi_z^p, \delta_p) \quad (6.4.10)$$

where  $\phi_y^p$  is the plastic rotation around the local axis  $Y$  and  $\phi_z^p$  is the component around the local axis  $Z$ . The behavior of a plastic hinge in this condition can be easily generalized from the case discussed in the precedent sections; the normality law is:

$$d\phi_y^p = d\lambda \frac{\partial f}{\partial m_y}; d\phi_z^p = d\lambda \frac{\partial f}{\partial m_z}; d\delta_p = d\lambda \frac{\partial f}{\partial n} \quad (6.4.11)$$

$$\begin{cases} d\lambda = 0 & \text{if } f(m_y, m_z, n) < 0 \text{ (locked hinge)} \\ f(m_y, m_z, n) = 0 & \text{if } d\lambda > 0 \text{ (active hinge)} \end{cases} \quad (6.4.12)$$

In practical cases, the explicit form of the yield function is postulated instead of computed exactly for each particular cross-section; for instance, the expression (6.4.5) can be generalized as:

$$f(m_y, m_z, n) = \left( \frac{n}{N_u} \right)^{\nu_1} + \left( \frac{m_y}{M_{uy}} \right)^{\nu_2} + \left( \frac{m_z}{M_{uz}} \right)^{\nu_3} - 1 \quad (6.4.13)$$

Again  $\nu_1$ ,  $\nu_2$  and  $\nu_3$  can be chosen equal to 2 and the elastic domain becomes an ellipsoid.

## 6.5 PLASTIC HINGES IN REINFORCED CONCRETE ELEMENTS

### 6.5.1 Typical Geometry of a Reinforced Concrete Cross-Section

In the previous sections only structures composed by a unique material were considered; for instance, this is the case of steel frames. In the civil engineering practice, reinforced concrete (RC) structures

## The Plastic Hinge

are a very important construction alternative. In these structures, the elements are composed by two materials: concrete and steel bars.

Rectangular shapes are the most common cross-sections used in the design of reinforced concrete elements. The sections are reinforced with at least two layers of longitudinal steel. They are placed very near the opposite faces of the sections as it is shown in Figure 13;  $A_s$  and  $A'_s$  are the areas of reinforcement at the opposed faces of the cross-section. The longitudinal steel is kept in place through transversal reinforcement. The design hypothesis states that compression forces are mainly supported by concrete, the longitudinal reinforcement is in charge of tension stresses and the transversal one resists the shear forces.

### 6.5.2 Behavior of the Materials

The compressive strength of concrete is obtained experimentally; for this purpose, cylinders with a specific height/diameter ratio, made and cured in accordance with standardized procedures, are subjected to longitudinal loads at a slow strain rate until they reach the maximum stress in a compression testing machine. The compressive strength is obtained by the division of the failure load over the cross-section area and reported in units of megapascals (MPa) in SI units or pound force per square inch (psi) in the US customary units. A test result is the average of at least two specimens made from the same concrete and tested at the same age. The strength of concrete at an age of 28 days is denoted  $f'_c$ . This value can vary from 17 MPa (2500 psi) to 28 MPa (4000 psi). The strength can even reach and exceed 70 MPa (10000 psi) for some special applications.

It is assumed that the concrete behavior is described by a nonlinear elastic model; one of the most cited was proposed by Hognestad and it is shown in Figure 14. In this figure  $f_c = -\sigma$  is the compression stress in the concrete and  $\varepsilon_c = -\varepsilon$  is the compression strain.  $f''_c$  is the maximum stress reached in the concrete; in this model, it is assumed that this value may differ from the cylinder strength  $f'_c$  because of the difference in size and shape of the compressed concrete;  $f''_c$  may be taken as  $0.85f'_c$ . The behavior is almost linear until half the concrete resistance and then it is assumed parabolic. The strain

Figure 13. Typical cross-section of a RC element

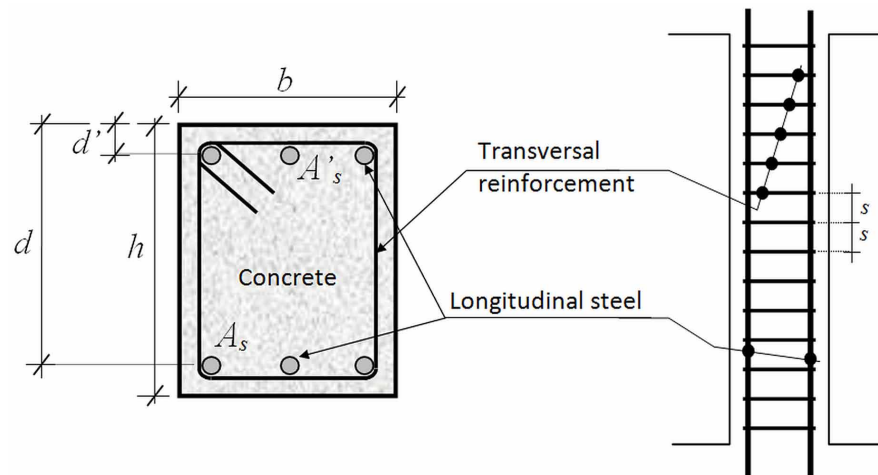
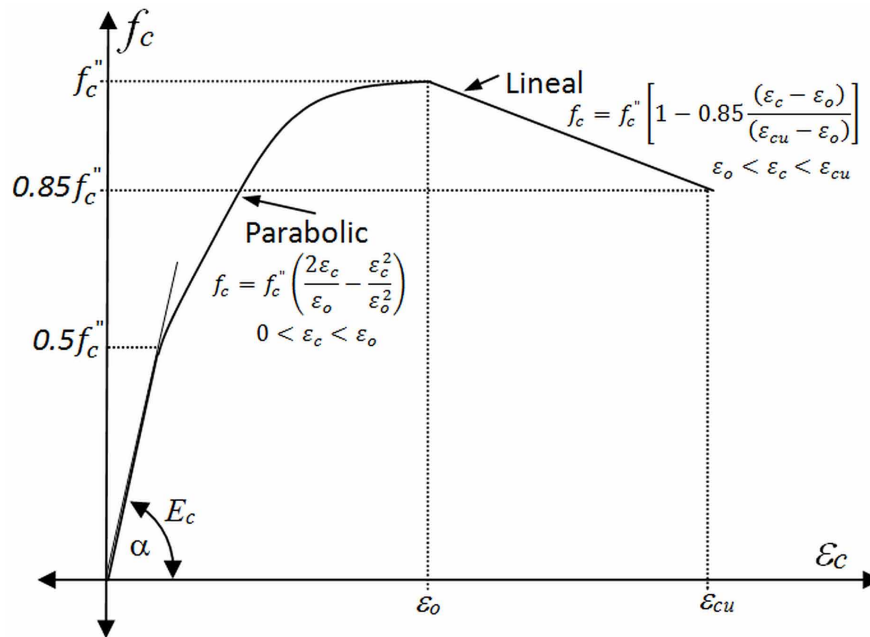


Figure 14. Stress-Strain curve proposed by Hognestad



corresponding to the maximum stress is called  $\epsilon_o$ ; unlike the strength, this value is approximately constant for any kind of concrete; many codes state that this strain is equal to 0.002. The failure deformation of the concrete fibers is denoted  $\epsilon_{cu}$  and can vary from 0.003 to 0.004 depending on the concrete resistance, for lower values of strength, larger  $\epsilon_{cu}$  can be observed; as a result, the peak of the curve is relatively sharp for high resistance concrete and plane for low resistance one.

The modulus of elasticity, i.e. the slope of the initial straight part in the curve of stress vs. strain increases with the concrete strength. The ACI (American Concrete Institute) proposes the following empirical expressions:

$$E_c = w^{1.5} 33\sqrt{f'_c} \text{ (psi)} = w^{1.5} 0.043\sqrt{f'_c} \text{ (MPa)} \quad (6.5.1)$$

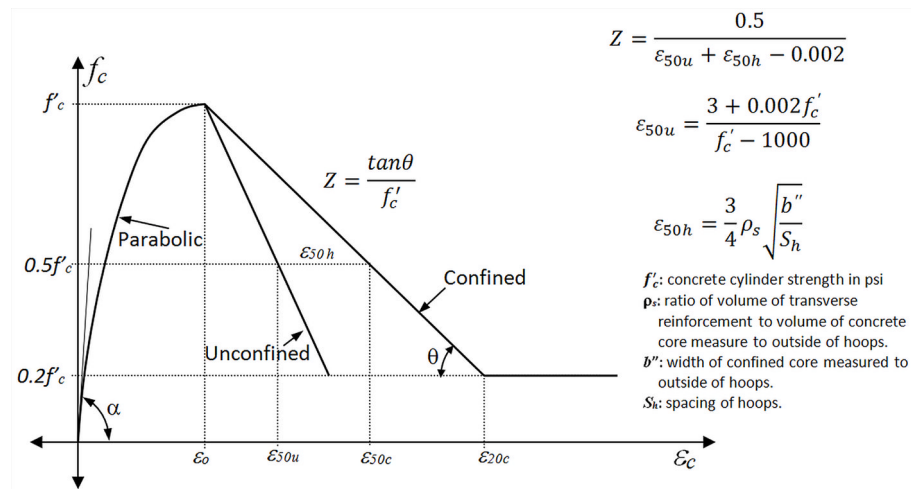
for concretes of unit weight  $w$  between 90 and 160 lb/ft<sup>3</sup> and, for normal weight concrete, the modulus of elasticity can be taken as

$$E_c = 57000\sqrt{f'_c} \text{ (psi)} = 4700\sqrt{f'_c} \text{ (MPa)} \quad (6.5.2)$$

In practice, the concrete is confined by lateral reinforcement. The uniaxial behavior of the concrete is different in the confined and non confined cases. For confined concretes, many researchers have proposed a modification of the Hognestad model. One of the most used curves is the model proposed by Kent and Park that is shown in Figure 15. Notice that in this model the maximum stress reached by the concrete does correspond to  $f'_c$ . The concrete resistance in tension is neglected

## The Plastic Hinge

Figure 15. Stress vs. Strain curve proposed by Kent and Park (1971).



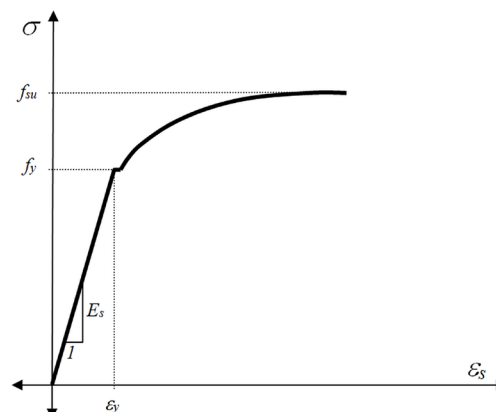
The steel bars used as longitudinal reinforcement for the concrete elements have an elasto-plastic behavior with nonlinear hardening as the one shown in Figure 16.

In the RC theory, the yield stress of the reinforcement is denoted as  $f_y$  and the ultimate one  $f_{su}$ ; the strain that corresponds to the yield stress is called yield strain  $\epsilon_y$ .

### 6.5.3 Plastic Hinge in RC Planar Frame Elements

All the models described in sections 6.2 and 6.3 can be used for reinforced concrete elements. However, in this case, the plastic elongations are usually neglected; therefore, unlike steel frames, these models can be used even in the presence of high compressive axial forces. The only modification of the model presented in those sections is that the properties  $M_p$ ,  $M_u$  and  $\phi_u^p$  are functions of the axial force. For instance, a plastic hinge in a reinforced concrete element subjected to planar forces may be characterized by the following expressions:

Figure 16. Behavior curve of steel bar



$$\begin{cases} d\phi^p = 0 \text{ if } f < 0 \text{ (locked hinge)} \\ f = 0 \text{ if } d\phi^p \neq 0 \text{ (active hinge)} \end{cases}; f = |m - x| - M_p(n) \leq 0; \delta^p = 0 \quad (6.5.3)$$

$$dx = \begin{cases} \frac{(M_u(n) - M_p(n))}{\phi_u^p(n)} d\phi^p \text{ if } |m| < M_u(n) \\ 0 \text{ if } |m| = M_u(n) \end{cases} \quad (6.5.4)$$

The functions  $M_u(n)$ ,  $M_p(n)$  and  $\phi_u^p(n)$  are usually presented graphically and this representation is denoted interaction diagrams.

### 6.5.4 Computation of the Interaction Diagram for the First Plastic Moment $M_p$ of a RC Cross-Section

An interaction diagram is defined by at least the following conditions:

1. Pure compression
2. Pure tension
3. Pure bending
4. Maximum bending resistance, which is called, balanced condition.

The interaction diagram can have as many additional points as decided by the analyst. All these points may be joined by straight lines as shown in Figure 17.

#### Pure Compression Point

The axial force in the pure compression condition is computed as it is illustrated in the Figure 18. Notice that there is a constant strain distribution across the section equal to the yield strain  $\varepsilon_y$ ; therefore the axial force is:

$$N_p \cong C'_s + C_c + C_s, \text{ where } C'_s = -f_y A'_s, C_c = -f_c (b * h - A'_s - A_s) \text{ and } C_s = -f_y A_s \quad (6.5.5)$$

$f_c$  is the maximum stress in the concrete. For this point of the iteration diagram, it is assumed that reinforcement bars yield in compression at the same time as concrete reaches its maximum strength.

#### Pure Tension Point

In this case, the axial force in plastic condition is shown in the Figure 19. Note that it is assumed that the strain at the reinforcement bars is  $\varepsilon_y$ ; therefore the axial force is equal to:

## The Plastic Hinge

Figure 17. Interaction diagram

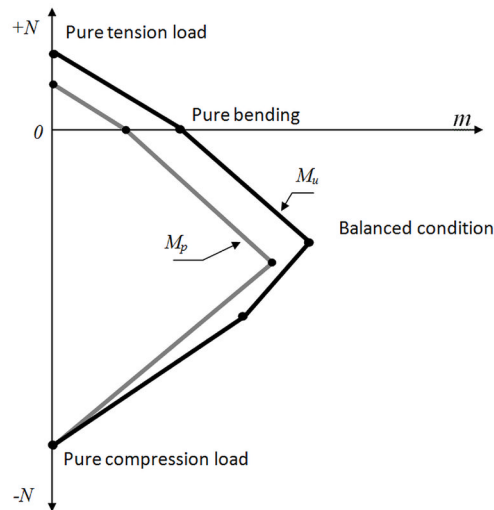
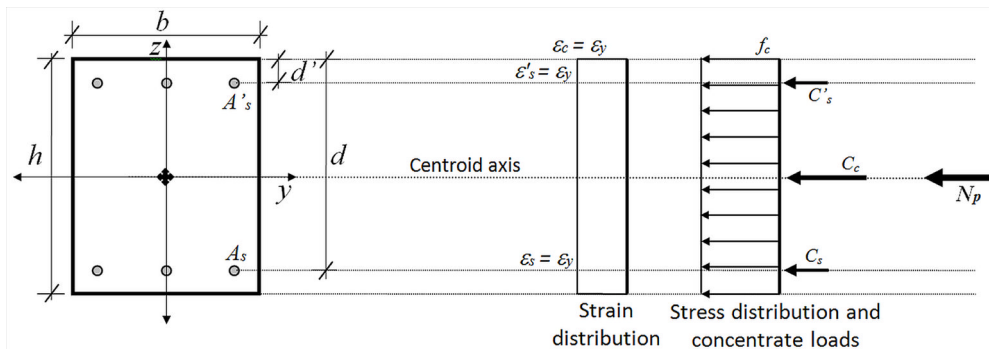


Figure 18. Strain and Stress distributions in a RC cross-section subjected axial force of pure compression for plastic condition



$$N_p \cong T'_s + T_s, \text{ where } T'_s = f_y A'_s \text{ and } T_s = f_y A_s \quad (6.5.6)$$

Notice that, as aforementioned, the strength of the concrete in tension is neglected.

## Pure Bending Point

The general theory of bending for reinforced concrete sections is based on the Euler- Bernoulli theory that is described in section 2.4. This assumption implies a linear distribution of the strain.

In the case of pure bending (see Figure 20), the following equilibrium equation must be satisfied in order to determine the location of the neutral axis assuming that the strain in the tension reinforcement is  $\epsilon_y$ :

Figure 19. Strain and concentrated loads distributions in a RC cross-section subjected to pure tension for plastic condition

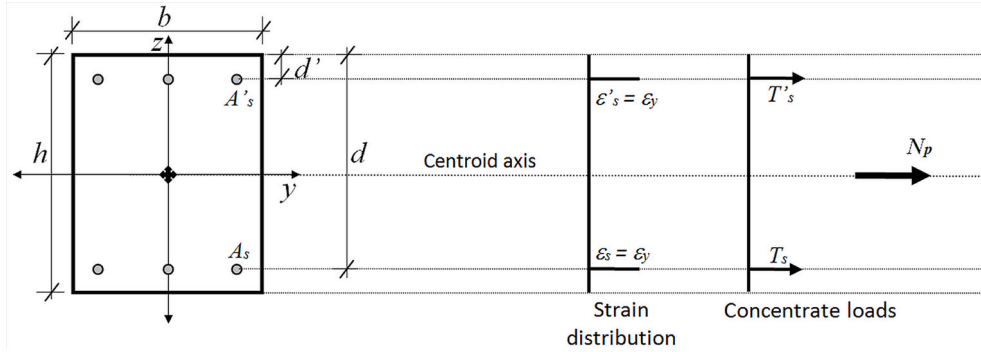
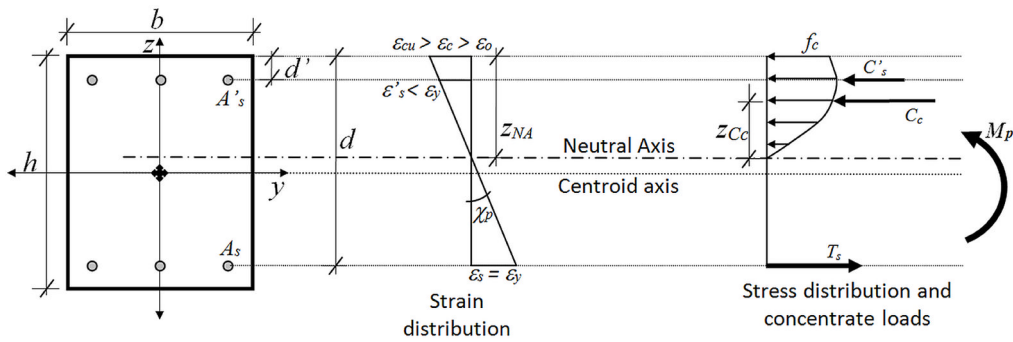


Figure 20. Strain and Stress distributions in a RC cross-section subjected pure bending for plastic condition



$$N_p = C'_s + C_c + T_s = 0, \text{ where } C'_s = -f_s A'_s, C_c = -b \int_0^{z_{NA}} f_c dz \text{ and } T_s = f_y A_s \quad (6.5.7)$$

$M_p$  is determined computing the moment around the centroidal axis of the cross-section as:

$$M_p = C_c \left( \frac{h}{2} - (z_{NA} - z_{C_c}) \right) + C'_s \left( \frac{h}{2} - d' \right) + T_s \left( d - \frac{h}{2} \right) \quad (6.5.8)$$

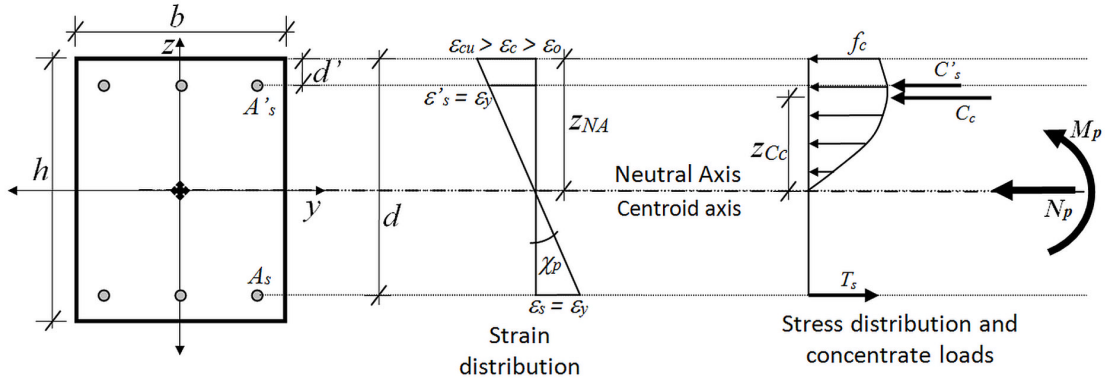
where  $z_{C_c}$  is the location of the force in the concrete (see Figure 20).

### Maximum Bending Resistance Point (Balanced Condition)

In this case, it is assumed that the tension and compression reinforcements yield simultaneously (see Figure 21); thus, the neutral axis depth is obtained as:

## The Plastic Hinge

Figure 21. Strain and Stress distributions in a RC cross-section subjected to bending and axial force in an element subjected to the maximum bending resistance (balanced condition)



$$z_{NA} = \frac{d + d'}{2} \quad (6.5.9)$$

Therefore, the strain at the extreme compression fiber can be determined and the loads  $C'_s$ ,  $C_c$  and  $T_s$  computed. The balanced load  $N_p$  is obtained by the equilibrium equation:

$$N_p = C'_s + C_c + T_s, \text{ where } C'_s = -f_y A'_s, C_c = -b \int_0^{z_{NA}} f_c dz \text{ and } T_s = A_s f_y \quad (6.5.10)$$

$f_c$  is the stress in the extreme compression fiber on the concrete. The bending moment is:

$$M_p = C_c \left( \frac{h}{2} - (z_{NA} - z_{Cc}) \right) + C'_s \left( \frac{h}{2} - d' \right) + T_s \left( d - \frac{h}{2} \right) \quad (6.5.11)$$

An example of the computation of interaction diagram of  $M_p$  is presented in section 6.8. For unsymmetrically reinforced elements, the procedure so far described has to be slightly modified as indicated in the bibliography indicated at the final of the chapter.

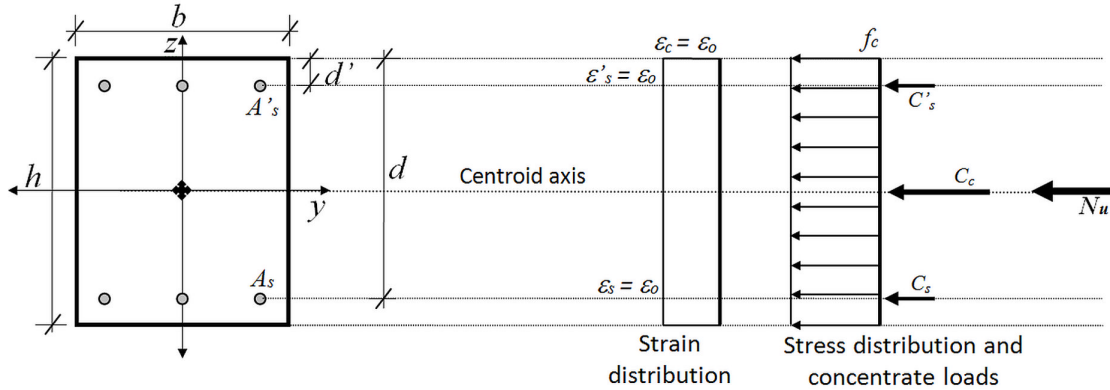
### 6.5.5 Computation of the Interaction Diagram for the Ultimate Moment of a RC Cross-Section

For the ultimate condition, the interaction diagram points can be computed as:

*Pure compression point:* In this condition, it is assumed that the ultimate axial force and the first plastic axial force are approximately the same (see Figure 22):



Figure 22. Strain and Stress distributions in a RC cross-section subjected axial force of pure compression for ultimate condition



$$N_u \cong N_p = C'_s + C_c + C_s, \text{ where } C'_s = -f_y A'_s, \quad (6.5.12)$$

$$C_c = -f_c (b * h - A'_s - A_s) \text{ and } C_s = -f_y A_s$$

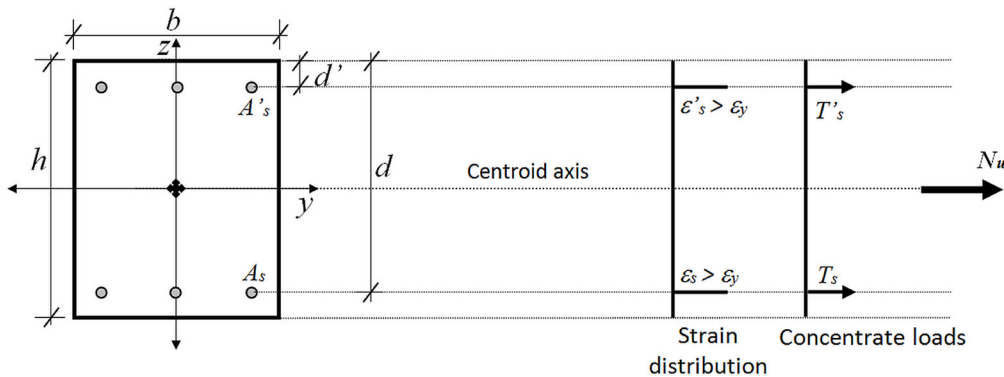
$f_c$  is the maximum stress in the concrete.

*Pure tension point:* In this case it is taken into account the hardening of the steel reinforcement bars; thus, the ultimate tension resistance is given by (see Figure 23):

$$N_u \cong T'_s + T_s, \text{ where } T'_s = f_{su} A'_s \text{ and } T_s = f_{su} A_s \quad (6.5.13).$$

*Pure bending point:* In the case of pure bending, it is assumed that the strain in the extreme compression fiber is equal to  $\epsilon_{cu}$ ; thus, the following equilibrium equation gives the location of the neutral axis  $Z_{NA}$ :

Figure 23. Strain and Concentrate loads distribution in a RC cross-section subjected axial force of pure tension for ultimate condition



### The Plastic Hinge

$$N_u = C'_s + C_c + T_s = 0, \text{ where } C'_s = -A'_s f'_s, \\ C_c = -b \int_0^{z_{NA}} f_c dz \text{ and } T_s = A_s f_s \quad (6.5.14)$$

The moment for pure bending condition can be computed as:

$$M_u = C_c \left( \frac{h}{2} - (z_{NA} - z_{C_c}) \right) + C'_s \left( \frac{h}{2} - d' \right) + T_s \left( d - \frac{h}{2} \right) \quad (6.5.15)$$

where  $z_{C_c}$  is the location of the force in the concrete (see Figure 24).

*Maximum bending resistance point (balanced condition):* For balanced condition point, it is considered that the strain in the extreme compression fiber is equal to  $\varepsilon_{cu}$  and the strain in the reinforcement steel in tension is equal to  $\varepsilon_y$  (see Figure 25). The neutral axis depth is obtained as:

$$z_{NA} = \frac{\varepsilon_{cu}}{\varepsilon_{cu} + \varepsilon_y} d \quad (6.5.16)$$

Now, the strain at the extreme compression fiber can be determined and the loads  $C'_s$ ,  $C_c$ , and  $T_s$  computed. The ultimate load  $N_u$  is obtained by the equilibrium equation:

$$N_u = C'_s + C_c + T_s, \text{ where } C'_s = -A'_s f'_s, C_c = -b \int_0^{z_{NA}} f_c dz \text{ and } T_s = A_s f_y \quad (6.5.17)$$

Then, the bending moment for this case can be computed as:

$$M_u = C_c \left( \frac{h}{2} - (z_{NA} - z_{C_c}) \right) + C'_s \left( \frac{h}{2} - d' \right) + T_s \left( d - \frac{h}{2} \right) \quad (6.5.18)$$

An example of the computation of the interaction diagram of  $M_u$  is presented in section 6.8. As aforementioned, for an unsymmetrically reinforced element all the moments must be computed around plastic centroid of the cross-section.

### 6.5.6 Computation of the Interaction Diagram for the Ultimate Plastic Rotation of a RC Cross-Section

The ultimate plastic rotation can be defined as:

Figure 24. Strain and Stress distributions in a RC cross-section subjected pure bending ultimate condition

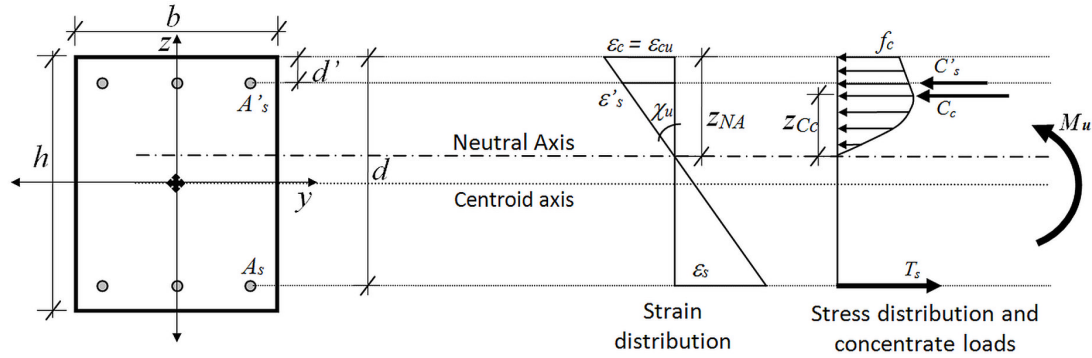
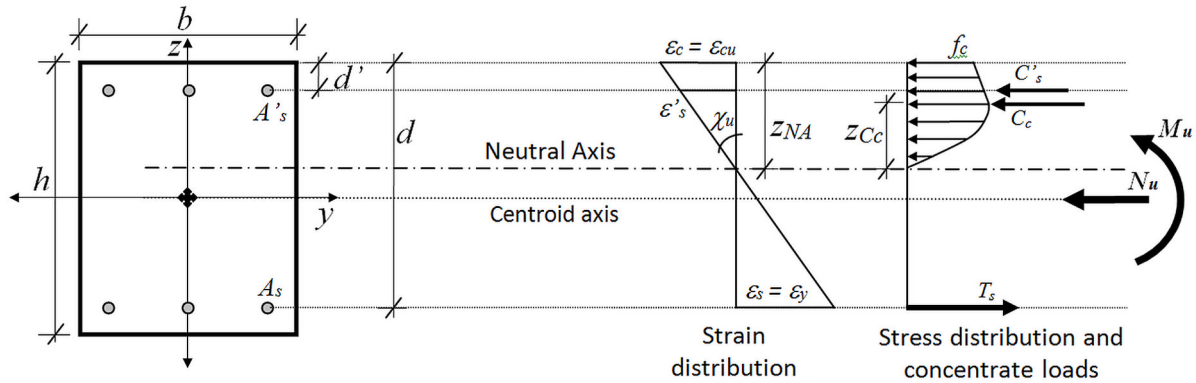


Figure 25. Strain and Stress distributions in a RC cross-section subjected to bending and axial force for an element subjected to the ultimate moment (balanced condition)



$$\phi_u^p = (\chi_u(n) - \chi_p(n))L_p; \chi_u(n) = \frac{\epsilon_{cu}}{z_{NA}(n)}; \chi_p(n) = \frac{\epsilon_y}{d - z_{NA}(n)} \quad (6.5.19)$$

where  $\chi_u$  is the ultimate curvature and  $\chi_p$  is the plastic curvature (see Figures 24, 25, 20 and 21). The term  $(\chi_u - \chi_p)$  is called ultimate plastic curvature.

$L_p$  is called “plastic hinge length” in the reinforced concrete literature and it represents a measure of the zone where the reinforcement bars that are subjected to plastic deformations. Usually, the plastic hinge length is computed using empirical expressions; the simplest of them is:

$$L_p = 0.5d + 0.05x_{cs} \quad (6.5.20)$$

$x_{cs}$  is the distance from the critical section to the point of inflection. The interaction diagram of the ultimate plastic rotation can be computed as:

## The Plastic Hinge

1. For pure compression and pure tension conditions the curvatures are nil; thus, for these two points only the axial forces are computed.
2. For the pure bending and balanced conditions, the ultimate plastic rotation are determined with Equation (6.5.19) using the corresponding curvatures as it is shown in the example 6.8.4.

The interaction diagram of the ultimate plastic rotation has the shape shown in Figure 26. An example of the computation of the  $\phi_u^p$  interaction diagram is presented in section 6.8.

### 6.5.7 Plastic Hinges in RC Frame Elements Subject to Biaxial Bending

Consider again a tridimensional beam-column. Neglecting plastic elongations as customary in reinforced concrete elements, the deformations of the plastic hinge are given by

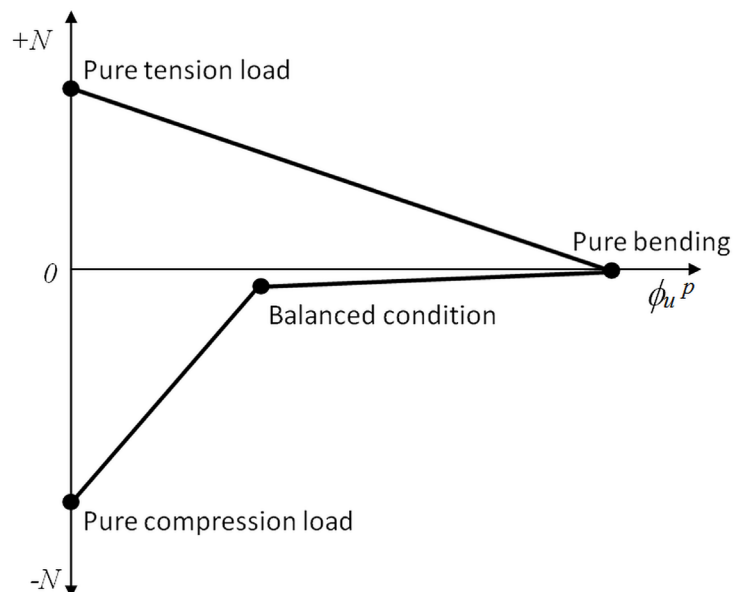
$$d\phi_y^p = d\lambda \frac{\partial f}{\partial m_y}; d\phi_z^p = d\lambda \frac{\partial f}{\partial m_z}; \delta_p \cong 0 \quad (6.5.21)$$

The evolution law of the plastic multiplier remains unchanged.

$$\begin{cases} d\lambda = 0 & \text{if } f < 0 \text{ (locked hinge)} \\ f = 0 & \text{if } d\lambda > 0 \text{ (active hinge)} \end{cases} \quad (6.5.22)$$

An expression of the yield function for a RC plastic hinge is:

Figure 26. Typical ultimate plastic rotation interaction diagram



$$f = \left| \frac{m_y}{M_{uy}(n)} \right|^2 + \left| \frac{m_z}{M_{uz}(n)} \right|^2 - 1 \leq 0 \quad (6.5.23)$$

$M_{uy}$  and  $M_{uz}$  are the ultimate resistant moments with respect to the principal axes of the cross-section. These properties can be computed using twice the same procedure described in section 6.5.5. It is also possible the introduction of hardening terms into the yield function. For example:

$$f = \left| \frac{m_y - x_y}{M_{py}(n)} \right|^2 + \left| \frac{m_z - x_z}{M_{pz}(n)} \right|^2 - 1 \leq 0 \quad (6.5.24)$$

where  $M_{py}$  and  $M_{pz}$  are first plastic moments with respect to the principal axes of the cross-section. These properties can also be computed using twice the same procedure describe in section 6.5.4.  $x_y$  and  $x_z$  are the components of the back moment. The corresponding evolution laws are:

$$\begin{aligned} dx_y &= \begin{cases} \frac{M_{uy}(n) - M_{py}(n)}{\phi_{uy}^p(n)} d\phi_y^p & \text{if } |m_y| < M_{uy}(n) \\ 0 & \text{if } |m_y| = M_{uy}(n) \end{cases} ; \\ dx_z &= \begin{cases} \frac{M_{uz}(n) - M_{pz}(n)}{\phi_{uz}^p(n)} d\phi_z^p & \text{if } |m_z| < M_{uz}(n) \\ 0 & \text{if } |m_z| = M_{uz}(n) \end{cases} \end{aligned} \quad (6.5.25)$$

## 6.6 PLASTIC HINGE WITH PINCHING EFFECT DUE TO SLIP

### 6.6.1 Slip of Steel Reinforcement in a RC Beam-Column Joint

The inelastic response of RC structures to cyclic loading, like during an earthquake, is a very complex phenomenon that is influenced by many parameters of the material and the structure. Besides the Bauschinger effect, another phenomenon that may appear is the pinching of the load-deformation hysteretic loops (see Figure 27b); the so called pinching is the constriction of the cycles observed in that figure. This effect is mainly due to cyclic bond deterioration between reinforcing steel and concrete. This type of behavior is not always present in RC structures but it is typical in connections of wide-beam to column (Figure 27a).

In these connections a significant part of the longitudinal reinforcement of the beam passes outside the column core thus originating bond condition poorer than for normal beam connections.

Figure 28 depicts an interior joint between a wide-beam and a column with a low level of axial load on the column and a high level of lateral load. In this case, the lower reinforcement is subjected to tractions on the right hand side and to compressions on the left one. In this situation, for low values of the beam bending moment, the compression stresses on the interface between concrete and reinforcement in the beam are very low and so is the slip resistance. Additionally, the beam hoops are not contribut-

## The Plastic Hinge

Figure 27. a) Connection of an interior wide-beam to a column. b) Experimental behavior curve of interior joint of reinforced concrete

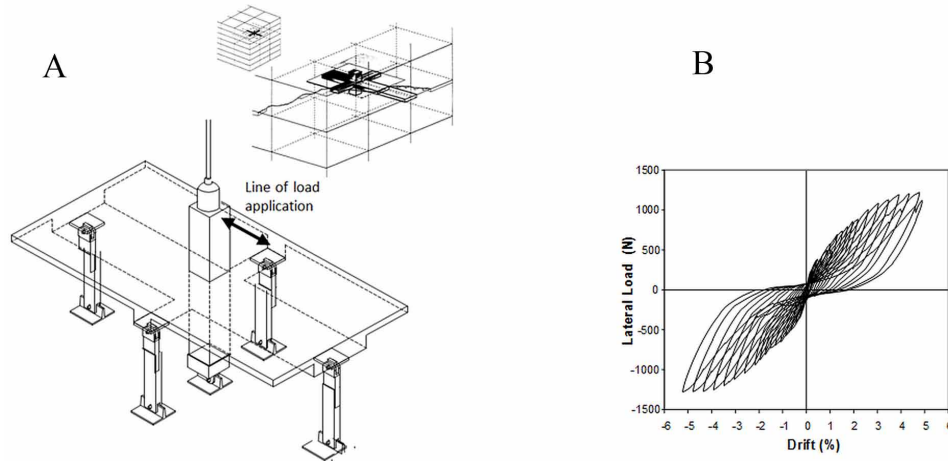
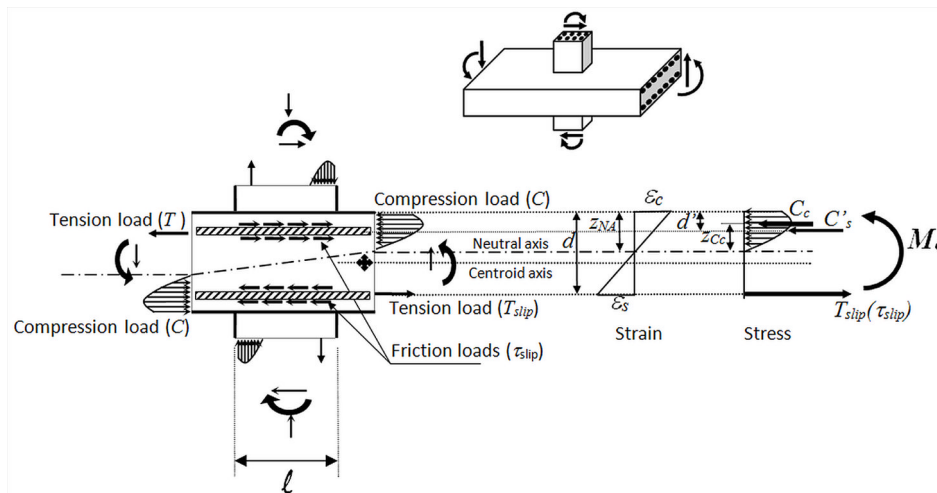


Figure 28. Stress distribution in a connection of an interior wide-beam and a column subjected to lateral load



ing yet to the confinement of the concrete due to the little volumetric strains in the material; therefore, small traction forces can produce slip of the reinforcement. For higher values of the moment, the hoops start to confine the concrete around the reinforcement and the compression stresses on the interface increase rapidly. The slip resistance grows faster than the tractions on the reinforcement and eventually, slip stops. Notice that in the case of an interior connection of a wide beam and a column, the parts of the beam at the sides of the column do not have the column axial compression at all; thus, the phenomenon described above applies entirely.

The hypothesis of plastic hinge can be used again to model bond deterioration between concrete and steel reinforcement. This particular kind of plastic hinge is called slip hinge. A slip hinge permits

only permanent deformations by slipping between concrete and steel reinforcement. Beams can present permanent strains by steel yielding and by slipping between both materials, while the columns can only present permanent strains by yielding of the steel (Figure 29).

### 6.6.2 Interfaces with Coulomb Friction Plasticity

Consider an interface between two different continua as shown in the Figure 30a. Let  $\sigma$  and  $\tau$  be the normal and shear stresses on the interface. If the surface is characterized by a Coulomb friction criterion, the relative horizontal displacement  $h$  between the blocks obeys the following law:

$$\begin{cases} dh > 0 & \text{if } |\tau| - \tau_{slip}(\sigma) = 0 \\ dh = 0 & \text{if } |\tau| - \tau_{slip}(\sigma) < 0 \end{cases} \quad (6.6.1)$$

where the term  $\tau_{slip}$  is the slip resistance that depends on the normal stress: larger values of  $\sigma$  implies higher slip resistances. The domain of non-slip, assuming an arbitrary resistance, is represented as a shaded area in the Figure 30b; slip occurs when the shear stress reaches the value of the slip resistance.

Figure 29. a) Interior wide-beam and a column with slipping real zone. b) Model of slip hinges

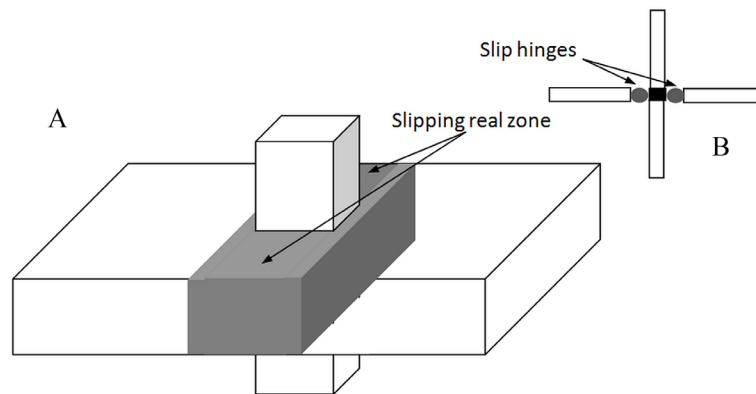
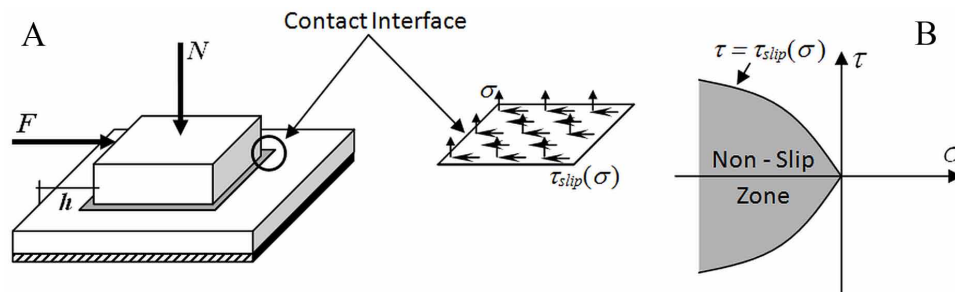


Figure 30. a) Interface between two media b) Non-slip domain



## The Plastic Hinge

The Coulomb theory can be used to describe the behavior of the interface between concrete and reinforcing steel in RC elements (see Figure 31). The term  $T_{slip}$  in that figure represents the force needed to produce slip in the bar.

### 6.6.3 Slip Function of a Plastic Hinge

A slip hinge is defined as follows:

$$f^{slip} = |m| - k_{slip} \leq 0; \begin{cases} d\phi^p = 0 & \text{if } f^{slip} < 0 \text{ (no slip: locked hinge)} \\ f(m, x) = 0 & \text{if } d\phi^p \neq 0 \text{ (slip: active hinge)} \end{cases} \quad (6.6.2)$$

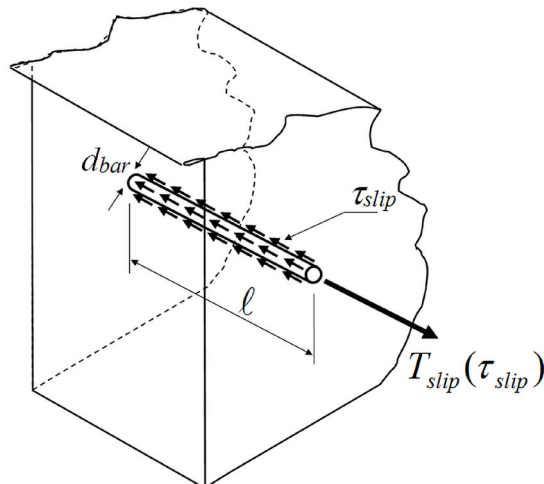
The expression (6.6.2) must be interpreted as follows: there are increments of the plastic rotations due to slip of the reinforcement if the moment in the hinge reaches the critical value  $k_{slip}$ , otherwise these increments are nil.

In the case of plasticity of Coulomb friction, it is accepted that the slip critical value depends on the normal stress on the interface. For a slip hinge it is assumed that the critical value,  $k_{slip}$ , corresponds to a hardening function. An appropriate expression for  $k_{slip}$  is:

$$k_{slip} = M_o e^{(\text{sign}(m)\eta\phi^p)} \quad (6.6.3)$$

An exponential function of the plastic rotation has been chosen so that the typical pinched curves are obtained when slip is present in the hinge. The term  $M_o$  is called “slip resistance” and it is a concept similar to the yield moment in plasticity, i.e.,  $M_o$  is the moment that produces slip when no plastic rotations have occurred yet; the parameter  $\eta$  characterizes the recovery velocity of the slip resistance. The computation of the parameters  $M_o$  and  $\eta$  is discussed in, respectively, sections 6.6.5 and 6.6.6. The behavior of this slip hinge is shown in the Figure 32.

Figure 31. Contact interface between concrete and the reinforcement steel bar





### 6.6.4 The Plasticity Criterion in a Plastic Hinge with Slip or Yielding

A yield function with kinematic hardening, such as Equation (6.5.3), describes the plasticity criterion of a plastic hinge whose physical mechanism is the yield of the reinforcement. The slip function (Equations 6.6.2 and 6.6.3) corresponds to a plasticity criterion of a plastic hinge whose rotations are due to slipping reinforcement. However, in a RC element both mechanisms are possible and may occur one after the other (the physical evidence indicates that they do not occur at the same time); therefore, the following evolution law for the rotations of a plastic hinge that integrates both phenomena is:

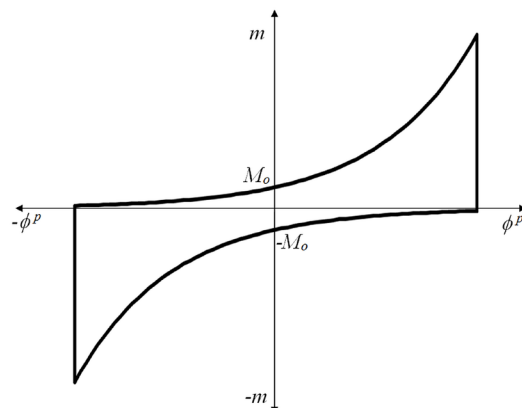
$$\begin{cases} d\phi^p = 0 & \text{if } f < 0 \\ f = 0 & \text{if } d\phi^p \neq 0 \end{cases}; \text{ where } f = \text{Max}(f^y, f^{\text{slip}}) \quad (6.6.4)$$

Note that the new criterion of plasticity determines what mechanism of plastic rotations is active, yield or slip, by the evaluation of the maximum value of both inelastic functions. If the maximum value is that of the yielding function  $f^y$ , the plastic behavior will obey the kinematic hardening function defined by Equation(6.5.3 and 6.5.4. On the other hand, if the maximum value is that of the slip function  $f^{\text{slip}}$ , the behavior will follow the exponential hardening function Equation(6.6.3). This criterion automatically changes from one mechanism to the other as a function of the value of the moment, the plastic rotation and the specific properties of the cross-section. Figure 33 shows the behavior of a plastic hinge changing from slip to yielding.

### 6.6.5 Determination of the Slip Resistance $M_o$

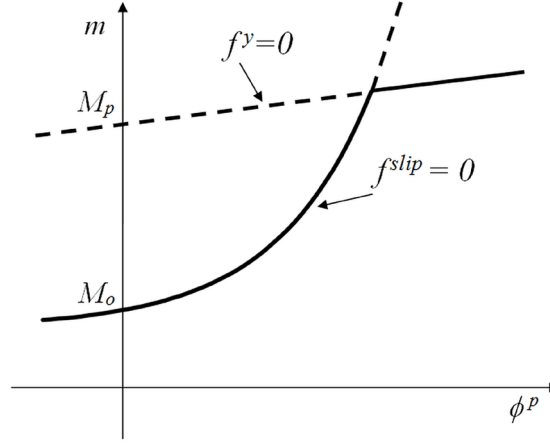
Consider again the beam-column joint of Figure 28. The strain distribution in the cross-section of the beam is assumed to follow the conventional linear one. The stress distribution also follows the usual parabolic diagram. Assuming that the reinforcement in tension is subjected for the first time to the force  $T_{\text{slip}}$  that produces slip and that no previous yielding has happened, the following equilibrium equation gives the location of the neutral axis ( $z_{NA}$ ):

Figure 32. Behavior of a slip hinge



## The Plastic Hinge

Figure 33. Behavior of an inelastic hinge with slip and yielding



$$C_c + C'_s - T_{slip} = 0 \quad (6.6.5)$$

where  $C_c = b \int_0^{z_{NA}} f_c dz$ ,  $C'_s$  is the compression force in  $A'_s$  and  $T_{slip}$  is the maximum load by sliding of the steel bars that depends on the average bond stress and contact area.  $T_{slip}$  can be computed as:

$$T_{slip} = \frac{\tau_{slip} \pi \cdot \ell}{2} \sum_{bar=1}^{nb} d_{bar} \quad (6.6.6)$$

where  $\tau_{slip}$  is the average slip stress,  $nb$  is the number of bars,  $d_{bar}$  is the diameter of the bar and  $\ell$  the slip length. The slip resistance  $M_o$  can now be computed by the following expression:

$$M_o = T_{slip} \left( d - \frac{h}{2} \right) + C_c \left( \frac{h}{2} - z_{NA} + z_{C_c} \right) + C'_s \left( \frac{h}{2} - d' \right) \quad (6.6.7)$$

where  $z_{C_c}$  is the location of the force in the concrete. An example of computation of  $M_o$  is presented in section 6.7.

### 6.6.6 Determination of Parameter $\eta$

The other parameter of the slip model is  $\eta$ . This parameter determines the point of intersection between the curves of slip (Equation 6.6.2) and yielding (Equation 6.5.3), see Figure 33.

$$f^y = f^{slip} = 0 \quad (6.6.8)$$

As a result, the term  $\eta$  can be obtained from Equation (6.6.8):

$$\eta = \frac{\ln \left( \frac{r^{slip} M_u - r^{slip} M_p + M_p}{M_o} \right)}{r^{slip} \phi_u^p} \quad (6.6.9)$$

where  $r^{slip}$  is again a parameter that can take values between 0 and 1; a good value for  $r^{slip}$  is 0.4. A hysteretic loop of an inelastic hinge with slip and yielding effects is shown in the Figure 34.

Figure 35 shows hysteresis loops for several ratios  $M_o/M_p$  with  $r^{slip}$  equal to 0.40. Notice that the pinching effect decreases when  $M_o$  tends to  $M_p$ . If  $M_o$  is greater than  $M_p$  then there is no pinching at all.

An example of computation of  $\eta$  is presented in section 6.8.

Figure 34. Hysteretic loop of an inelastic hinge with slip and yielding

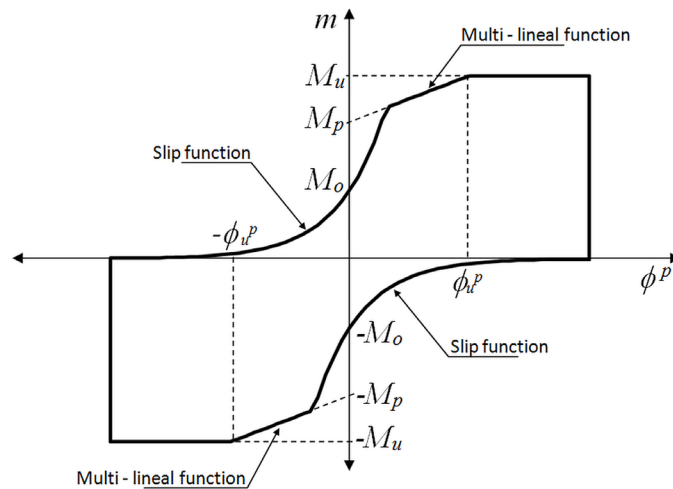
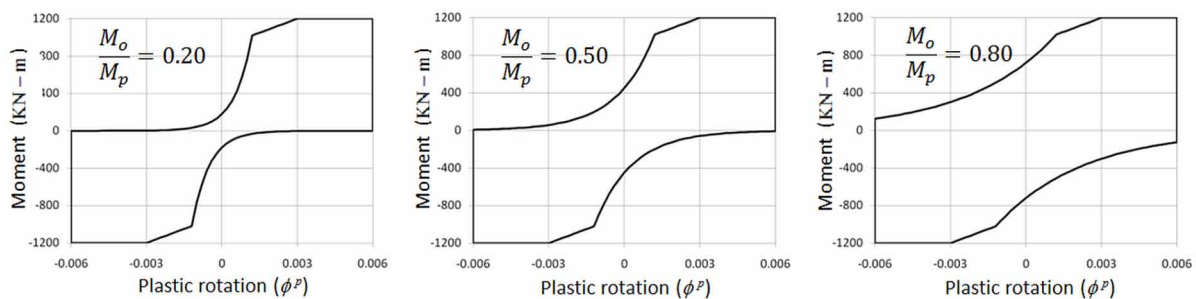


Figure 35. Hysteresis loops of an inelastic hinge with slip and yielding



## 6.7 SUMMARY AND EQUATIONS QUICK REFERENCE

The concepts of plasticity that were presented in the previous chapters can be used for the analysis of frame structures in two different ways. The first one characterizes the theory of elasto-plastic beams and combines the plasticity concepts with the fundamental hypothesis of beams. The second alternative is based on the concept of plastic hinge and characterizes the theory of elasto-plastic frames. A plastic hinge represents an approximation of the moment-curvature relationship. It can be shown that plastic hinge requires the introduction of the concept of the plastic rotation. A plastic hinge is defined by the yield function and the evolution law of the plastic rotation. Several kinds of plastic rotations can be defined: perfectly plastic, and with kinematic or isotropic hardening.

In the case of steel columns, axial forces generate plastic contractions that cannot be neglected. Therefore the concept of plastic hinge is generalized including a second deformation: the plastic elongation. In this case the plastic hinge is defined by the yield function, the normality rule and the plastic multiplier evolution law. The normality law establishes that plastic deformations represent a vector that is normal to the elastic domain in the space of bending moments and axial forces.

For RC structures the same concepts of plastic hinge can be used. However the determination of the elastic domain for interaction curves requires the use of special techniques: the classic RC theory.

Plastic hinges in tridimensional frames need the introduction of an additional deformation. Plastic rotation has components in the two principal planes of the frame element. Mathematically, the plastic hinge is defined in the same way; i.e. with a yield function, normality rules and evolution laws of the plastic multipliers.

RC wide-beams constitute a particular case. Plastic rotations can be produced by two different mechanisms: yield or slip of the reinforcement. This phenomenon is taken into account by a modification of the yield function of the plastic hinge (See Table 1).

*Table 1.*

ELASTIC PLASTIC MOMENT VS. CURVATURE RELATIONSHIP
The strain distribution in the cross-section $\varepsilon = \chi \cdot z$ (6.1.1) $\chi$ : curvature $z$ : coordinate of the fiber under consideration
The elastic relationship $m$ vs. $\chi$ $m = EI\chi$ (6.1.2)
First plastic moment $M_p$ $M_p = S\sigma_y; S = \frac{2I}{h}$ (6.1.3) $S$ : elastic section modulus
Ultimate moment $M_u$ $M_u = \sigma_y H_f; H_f = 2 \int_0^{h/2} b(z) z dz$ (6.1.4) $H_f$ : plastic section modulus

*continued on following page*

Table 1. Continued

<b>The Perfect Plastic Hinge</b>
<p>Evolution law of the plastic rotation <math>\phi^p</math></p> $\begin{cases} d\phi^p = 0 & \text{if } f(m) < 0 \text{ (locked hinge)} \\ f(m) = 0 & \text{if } d\phi^p \neq 0 \text{ (active hinge)} \end{cases} \quad (6.2.6)$
<p>Yield function <math>f(m)</math></p> $f(m) =  m  - M_y \leq 0 \quad (6.2.7)$ <p><math>M_y</math>: yield moment of the section</p>
<b>Plastic Hinge with Hardening</b>
<b>Plastic Hinge with Isotropic Hardening</b>
<p>Evolution law of the plastic rotation <math>\phi^p</math></p> $\begin{cases} d\phi^p = 0 & \text{if } f(m, p) < 0 \text{ (locked hinge)} \\ f(m, p) = 0 & \text{if } d\phi^p \neq 0 \text{ (active hinge)} \end{cases}; f(m, p) =  m  - (M_p + Q(p)) \leq 0 \quad (6.3.1)$
<p>Cumulated plastic rotation <math>p</math></p> $dp =  d\phi^p  \quad (6.3.2)$
<p>Maximum plastic rotation <math>p</math></p> $p = \text{Max}  \phi^p  \quad (6.3.3)$
<p>Linear isotropic term</p> $Q(p) = c \cdot p \quad (6.3.4)$ <p><math>c</math>: member dependent constant</p>
<p>Nonlinear isotropic term</p> $Q(p) = (M_u - M_p)(1 - e^{-\alpha p}) \quad (6.3.5)$ <p><math>\alpha</math>: member dependent parameter</p>
<p>Multilinear isotropic term</p> $Q(p) = \begin{cases} \frac{(M_u - M_p)}{\phi_u^p} p & \text{if } 0 \leq p \leq \phi_u^p \\ M_u - M_p & \text{if } p > \phi_u^p \end{cases} \quad (6.3.6)$ <p><math>\phi_u^p</math> is a member dependent property</p>

continued on following page

## The Plastic Hinge

Table 1. Continued

<b>Plastic Hinge with Kinematic Hardening</b>	
Evolution law of the plastic rotation	
$\begin{cases} d\phi^p = 0 & \text{if } f(m, x) < 0 \text{ (locked hinge)} \\ f(m, x) = 0 & \text{if } d\phi^p \neq 0 \text{ (active hinge)} \end{cases}; f(m, x) =  m - x  - M_p \leq 0$ <p style="text-align: right;">(6.3.7)</p>	
Linear kinematic term	
$x = c \cdot \phi^p \quad (6.3.8)$	
Nonlinear kinematic term	
$dx = \alpha \left( (M_u - M_p) d\phi^p - x  d\phi^p  \right) \quad (6.3.9)$	
Multi-linear kinematic term	
$dx = \begin{cases} \frac{(M_u - M_p)}{\phi_u^p} d\phi^p & \text{if }  m  < M_u \\ 0 & \text{if }  m  = M_u \end{cases} \quad (6.3.10)$ <p><math>\phi_u^p</math> : ultimate plastic rotation (member dependent property)</p>	
<b>Kinematic and Isotropic Nonlinear Hardening Simultaneously</b>	
Yield function $f(m)$	
$f(m) =  m - x  - (M_p + Q) \leq 0 \quad (6.3.11)$	
Evolution laws of $x$ and $p$	
$Q = (1 - r)(M_u - M_p)(1 - e^{-\alpha p}); dx = \alpha \left( r(M_u - M_p) d\phi^p - x  d\phi^p  \right); 0 \leq r \leq 1 \quad (6.3.12)$ <p>If <math>r=0</math> represents isotropic hardening only, <math>r=1</math> kinematic hardening exclusively. The <math>r</math> value can be 0.70 for RC elements.</p>	
<b>Perfect Plastic Hinge Subjected to Bending and Axial Forces</b>	
Plastic deformations	
$\phi^p$ : plastic rotation; $\delta^p$ : plastic elongation	
<b>Yield Function of a Plastic Hinge Subjected to Bending and Axial Force</b>	
Moment and axial force (rectangular cross-section)	
$m = 2\sigma_y \int_{z_o}^{h/2} z \cdot b \cdot dz = 2\sigma_y b \left( \frac{h^2}{8} - \frac{z_o^2}{2} \right); n = 2\sigma_y \int_0^{z_o} b \cdot dz = 2\sigma_y b \cdot z_o$ <p style="text-align: right;">(6.4.1)</p>	
Elastic domain of the plastic hinge	
$\frac{ m }{M_y} + \left( \frac{n}{N_y} \right)^2 - 1 = 0; M_y = \frac{\sigma_y b \cdot h^2}{4}; N_y = \sigma_y b \cdot h$ <p style="text-align: right;">(6.4.2)</p> <p><math>M_y</math> : yield moment of the cross-section without axial forces  <math>N_y</math> : axial force that produces the total plasticization of the element when there is no bending moments</p>	

continued on following page

Table 1. Continued

Yield function corresponding to a rectangular cross-section	
$f(m, n) = \frac{ m }{M_y} + \left(\frac{n}{N_y}\right)^2 - 1 \leq 0 \quad (6.4.3)$	
Elastic domain	
$(m, n) \mid f \leq 0 \quad (6.4.4)$	
Yield function for any symmetric cross-section	
$f(m, n) = \left(\frac{n}{N_y}\right)^{\nu_1} + \left(\frac{m}{M_y}\right)^{\nu_2} - 1 \quad (6.4.5)$	
Often the coefficients $\nu_1$ and $\nu_2$ are chosen equal to 2	
<b>The Normality Rule</b>	
Normality rule	
$d\phi^p = d\lambda \frac{\partial f}{\partial m}; d\delta_p = d\lambda \frac{\partial f}{\partial n} \quad (6.4.6)$	
$\lambda$ : plastic multiplier	
Plastic multiplier $\lambda$ evolution law	
$\begin{cases} d\lambda = 0 & \text{if } f(m, n) < 0 \text{ (locked hinge)} \\ f(m, n) = 0 & \text{if } d\lambda \neq 0 \text{ (active hinge)} \end{cases} \quad (6.4.7)$	
Normality rule of a perfect plastic hinge in a rectangular cross-section	
$d\phi^p = d\lambda \frac{1 \cdot \text{sign}(m)}{M_y} = d\lambda \frac{4 \cdot \text{sign}(m)}{\sigma_y b h^2}; d\delta_p = d\lambda \frac{n}{N_y^2} = d\lambda \frac{4z_0}{\sigma_y b h^2} \quad (6.4.8)$	
$d\delta_p = \text{sign}(m) z_0 d\phi^p \quad (6.4.9)$	
<b>Perfect Plastic Hinge Subjected to Biaxial Bending Moments and Axial Force</b>	
Plastic deformations	$\phi_y^p$ : plastic rotation around the local axis Y $\phi_z^p$ : plastic rotation around the local axis Z (6.4.10) $\delta_p$ : plastic elongation
Normality rule	
$d\phi_y^p = d\lambda \frac{\partial f}{\partial m_y}; d\phi_z^p = d\lambda \frac{\partial f}{\partial m_z}; d\delta_p = d\lambda \frac{\partial f}{\partial n} \quad (6.4.11)$	
Evolution law of plastic multiplier $\lambda$	
$\begin{cases} d\lambda = 0 & \text{if } f(m_y, m_z, n) < 0 \text{ (locked hinge)} \\ f(m_y, m_z, n) = 0 & \text{if } d\lambda > 0 \text{ (active hinge)} \end{cases} \quad (6.4.12)$	

continued on following page

## The Plastic Hinge

Table 1. Continued

Yield function	
$f(m_y, m_z, n) = \left(\frac{n}{N_u}\right)^{\nu_1} + \left(\frac{m_y}{M_{uy}}\right)^{\nu_2} + \left(\frac{m_z}{M_{uz}}\right)^{\nu_3} - 1 \quad (6.4.13)$	
$\nu_1, \nu_2$ and $\nu_3$ can be chosen equal to 2	
<b>Plastic Hinges in Reinforced Concrete Elements</b>	
<b>Behavior of the Materials</b>	
Modulus of elasticity of the concrete for concretes of unit weight $w$ between 90 and 160 lb/ft <sup>3</sup>	
$E_c = w^{1.5} 33\sqrt{f'_c} \text{ (psi)} = w^{1.5} 0.043\sqrt{f'_c} \text{ (MPa)} \quad (6.5.1)$	
Modulus of elasticity of the concrete for normal weight concrete	
$E_c = 57000\sqrt{f'_c} \text{ (psi)} = 4700\sqrt{f'_c} \text{ (MPa)} \quad (6.5.2)$	
<b>Plastic Hinge in RC Planar Frame Elements</b>	
Plastic deformations	$\phi^p$ is the plastic rotation; $\delta_p = 0$
Properties of element	$M_p(n)$ : first plastic moment $M_u(n)$ : ultimate moment $\phi_u^p(n)$ : ultimate plastic rotation
Plastic deformation evolution law	
$\begin{cases} d\phi^p = 0 & \text{if } f < 0 \text{ (locked hinge)} \\ f = 0 & \text{if } d\phi^p \neq 0 \text{ (active hinge)} \end{cases}; f =  m - x  - M_p(n) \leq 0 \quad (6.5.3)$	
Kinematic hardening term evolution law	
$dx = \begin{cases} \frac{(M_u(n) - M_p(n))}{\phi_u^p(n)} d\phi^p & \text{if }  m  < M_u(n) \\ 0 & \text{if }  m  = M_u(n) \end{cases} \quad (6.5.4)$	

continued on following page



Table 1. Continued

Computation of the Interaction Diagram for the First Plastic Moment ( $M_p$ ) of a RC Cross-Section	
<p>e) Pure compression point</p> <p><math>N_p \cong C'_s + C_c + C_s</math>, where <math>C'_s = -f_y A'_s</math>, <math>C_c = -f_c (b * h - A'_s - A_s)</math> and <math>C_s = -f_y A_s</math> (6.5.5)</p> <p><math>f_c</math> : maximum stress in the concrete  <math>f_y</math>: yield stress of steel bars  <math>M_p = 0</math></p>	
<p>f) Pure tension point</p> <p><math>N_p \cong T'_s + T_s</math>, where <math>T'_s = f_y A'_s</math> and <math>T_s = f_y A_s</math> (6.5.6)</p> <p><math>M_p = 0</math></p>	
<p>g) Pure bending point:</p> <p>Location of the neutral axis</p> <p><math>N_p = C'_s + C_c + T_s = 0</math>, where <math>C'_s = -f_s A'_s</math>, <math>C_c = -b \int_0^{z_{NA}} f_c dz</math> and <math>T_s = f_y A_s</math> (6.5.7)</p> <p><math>f_s</math> : stress in the compression reinforcement  <math>f_c</math> : stress in the extreme compression fiber on the concrete</p>	

continued on following page

## The Plastic Hinge

Table 1. Continued

<p>Plastic moment</p> $M_p = C_c \left( \frac{h}{2} - (z_{NA} - z_{C_c}) \right) + C'_s \left( \frac{h}{2} - d' \right) + T_s \left( d - \frac{h}{2} \right) \quad (6.5.8)$ <p><math>z_{C_c}</math> is the location of the force in the concrete</p>
<p>h) Maximum bending resistance point (balanced condition)</p>
<p>Neutral axis depth</p> $z_{NA} = \frac{d + d'}{2} \quad (6.5.9)$
<p>Balanced load <math>N_p</math></p> $N_p = C'_s + C_c + T_s, \text{ where } C'_s = -f_y A'_s, C_c = -b \int_0^{z_{NA}} f_c dz \text{ and } T_s = A_s f_y \quad (6.5.10)$ <p><math>f_c</math>: stress in the extreme compression fiber on the concrete  <math>f_y</math>: yield stress of steel bars</p>
<p>Bending moment</p> $M_p = C_c \left( \frac{h}{2} - (z_{NA} - z_{C_c}) \right) + C'_s \left( \frac{h}{2} - d' \right) + T_s \left( d - \frac{h}{2} \right) \quad (6.5.11)$
<p><b>Computation of the Interaction Diagram for the Ultimate Moment of a RC Cross-Section</b></p>

continued on following page

Table 1. Continued

<p>a) Pure compression point</p> $N_u \cong N_p = C'_s + C_c + C_s, \text{ where } C'_s = -f_y A'_s \quad (6.5.12)$ $C_c = -f_c (b * h - A'_s - A_s), \text{ and } C_s = -f_y A_s$ <p><math>f_c</math>: maximum stress in the concrete  <math>f_y</math>: yield stress of steel bars</p> $M_u = 0$
<p>b) Pure tension point:</p> $N_u \cong T'_s + T_s, \text{ where } T'_s = f_{su} A'_s \text{ and } T_s = f_{su} A_s \quad (6.5.13)$ <p><math>f_{su}</math>: ultimate stress of reinforcement steel</p> $M_u = 0$
<p>c) Pure bending point:            Location of the neutral axis <math>Z_{NA}</math></p> $N_u = C'_s + C_c + T_s = 0, \text{ where } C'_s = -A'_s f'_s, C_c = -b \int_0^{z_{NA}} f_c dz \text{ and } T_s = A_s f_s \quad (6.5.14)$
<p>Ultimate moment</p> $M_u = C_c \left( \frac{h}{2} - (z_{NA} - z_{C_c}) \right) + C'_s \left( \frac{h}{2} - d' \right) + T_s \left( d - \frac{h}{2} \right) \quad (6.5.15)$ <p><math>z_{C_c}</math> is the location of the force in the concrete</p>
<p>d) Maximum bending resistance point (balanced condition):            Location of the neutral axis depth</p> $z_{NA} = \frac{\epsilon_{cu}}{\epsilon_{cu} + \epsilon_y} d \quad (6.5.16)$
<p>Ultimate load</p> $N_u = C'_s + C_c + T_s, \text{ where } C'_s = -A'_s f'_s, C_c = -b \int_0^{z_{NA}} f_c dz \text{ and } T_s = A_s f_s \quad (6.5.17)$
<p>Ultimate bending moment</p> $M_u = C_c \left( \frac{h}{2} - (z_{NA} - z_{C_c}) \right) + C'_s \left( \frac{h}{2} - d' \right) + T_s \left( d - \frac{h}{2} \right) \quad (6.5.18)$

continued on following page

## The Plastic Hinge

Table 1. Continued

<i>Computation of the Interaction Diagram for the Ultimate Plastic Rotation of a RC Cross-Section</i>	
Ultimate plastic rotation	$\phi_u^p = (\chi_u(n) - \chi_p(n))L_p; \chi_u(n) = \frac{\varepsilon_{cu}}{z_{NA}(n)}; \chi_p(n) = \frac{\varepsilon_y}{d - z_{NA}(n)} \quad (6.5.19)$ <p> <math>\chi_u</math> : ultimate curvature  <math>\chi_p</math> : plastic curvature (see Figures 6.24, 6.25, 6.20 and 6.21).  <math>(\chi_u - \chi_p)</math> : ultimate plastic curvature.  <math>L_p</math> : plastic hinge length         </p>
Plastic hinge length	$L_p = 0.5d + 0.05x_{cs} \quad (6.5.20)$ <p> <math>x_{cs}</math> : distance from the critical section to the point of inflection         </p>
c) Pure compression point Axial load	$N_u \cong N_p = C'_s + C_c + C_s, \text{ where } C'_s = -f_y A'_s, C_c = -f_c (b * h - A'_s - A_s) \text{ and } C_s = -f_y A_s \quad (6.5.12)$ <p> <math>f_c</math> : maximum stress in the concrete  <math>f_y</math> : yield stress of steel bars         </p> <p>Ultimate plastic rotation <math>\phi_u^p = 0</math></p>
d) Pure tension point Axial load	$N_u \cong T'_s + T_s, \text{ where } T'_s = f_{su} A'_s \text{ and } T_s = f_{su} A_s \quad (6.5.13)$ <p> <math>f_{su}</math> : ultimate stress of reinforcement steel         </p> <p>Ultimate plastic rotation <math>\phi_u^p = 0</math></p>

continued on following page

Table 1. Continued

<p>c) Pure bending point</p> <p>Axial load <math>N_u = 0</math></p> <p>Ultimate plastic rotation</p> $\phi_u^p = (\chi_u(n) - \chi_p(n))L_p; \chi_u(n) = \frac{\varepsilon_{cu}}{z_{NA}(n)}; \chi_p(n) = \frac{\varepsilon_y}{d - z_{NA}(n)} \quad (6.5.19)$ <p><math>\chi_u</math>: ultimate curvature</p> <p><math>\chi_p</math>: plastic curvature (see Figures 6.24, 6.25, 6.20 and 6.21).</p> <p><math>(\chi_u - \chi_p)</math>: ultimate plastic curvature.</p> <p><math>L_p</math>: plastic hinge length</p> <p>Plastic hinge length</p> $L_p = 0.5d + 0.05x_{cs} \quad (6.5.20)$ <p><math>x_{cs}</math>: distance from the critical section to the point of inflection</p>
<p>e) Balanced condition point</p> <p>Neutral axis depth</p> $z_{NA} = \frac{\varepsilon_{cu}}{\varepsilon_{cu} + \varepsilon_y} d \quad (6.5.16)$ <p>Ultimate load</p> $N_u = C'_s + C_c + T_s, \text{ where } C'_s = -A'_s f'_s, C_c = -b \int_0^{z_{NA}} f_c dz \text{ and } T_s = A_s f_y \quad (6.5.17)$ <p>Ultimate curvature</p> $\phi_u^p = (\chi_u(n) - \chi_p(n))L_p; \chi_u(n) = \frac{\varepsilon_{cu}}{z_{NA}(n)}; \chi_p(n) = \frac{\varepsilon_y}{d - z_{NA}(n)} \quad (6.5.19)$ <p><math>\chi_u</math>: ultimate curvature</p> <p><math>\chi_p</math>: plastic curvature (see Figures 6.24, 6.25, 6.20 and 6.21).</p> <p><math>(\chi_u - \chi_p)</math>: ultimate plastic curvature.</p> <p><math>L_p</math>: plastic hinge length</p> <p>Plastic hinge length</p> $L_p = 0.5d + 0.05x_{cs} \quad (6.5.20)$ <p><math>x_{cs}</math>: distance from the critical section to the point of inflection</p>

continued on following page

## The Plastic Hinge

Table 1. Continued

<b>Plastic Hinges in RC Frame Elements Subject to Biaxial Bending</b>	
Deformations in the plastic hinge	
$d\phi_y^p = d\lambda \frac{\partial f}{\partial m_y}; d\phi_z^p = d\lambda \frac{\partial f}{\partial m_z}; \delta_p \cong 0$ <p style="text-align: right;">(6.5.21)</p>	
Plastic multiplier evolution law	
$\begin{cases} d\lambda = 0 & \text{if } f < 0 \text{ (locked hinge)} \\ f = 0 & \text{if } d\lambda > 0 \text{ (active hinge)} \end{cases}$ <p style="text-align: right;">(6.5.22)</p>	
Yield function of perfect plastic hinge	
$f = \left  \frac{m_y}{M_{uy}(n)} \right ^2 + \left  \frac{m_z}{M_{uz}(n)} \right ^2 - 1 \leq 0$ <p style="text-align: right;">(6.5.23)</p> <p><math>M_{uy}</math> and <math>M_{uz}</math>: ultimate resistant moments with respect to the principal axes of the cross-section.</p>	
Yield function of plastic hinge with multi linear kinematic hardening	
$f = \left  \frac{m_y - x_y}{M_{py}(n)} \right ^2 + \left  \frac{m_z - x_z}{M_{pz}(n)} \right ^2 - 1 \leq 0$ <p style="text-align: right;">(6.5.24)</p> <p><math>M_{py}</math> and <math>M_{pz}</math>: first plastic moments with respect to the principal axes of the cross-section.  <math>x_y</math> and <math>x_z</math>: components of the back moment</p>	
Evolution laws	
$dx_y = \begin{cases} \frac{M_{uy}(n) - M_{py}(n)}{\phi_{uy}^p(n)} d\phi_y^p & \text{if }  m_y  < M_{uy}(n) \\ 0 & \text{if }  m_y  = M_{uy}(n) \end{cases}$ $dx_z = \begin{cases} \frac{M_{uz}(n) - M_{pz}(n)}{\phi_{uz}^p(n)} d\phi_z^p & \text{if }  m_z  < M_{uz}(n) \\ 0 & \text{if }  m_z  = M_{uz}(n) \end{cases}$ <p style="text-align: right;">(6.5.25)</p>	
<b>Plastic Hinge with Pinching Effect due to Slip</b>	
<b>Interfaces with Coulomb Friction Plasticity (<math>\tau</math>: Shear Stress)</b>	
Evolution law relative displacement between two blocks	
$\begin{cases} dh > 0 & \text{if }  \tau  - \tau_{slip}(\sigma) = 0 \\ dh = 0 & \text{if }  \tau  - \tau_{slip}(\sigma) < 0 \end{cases}$ <p style="text-align: right;">; <math>\tau_{slip}</math>: slip resistance (6.6.1)</p>	
<i>Slip Function of a Plastic Hinge</i>	
Slip function	
$f^{slip} =  m  - k_{slip} \leq 0 \quad \begin{cases} d\phi^p = 0 & \text{if } f^{slip} < 0 \text{ (no slip: locked hinge)} \\ f(m, x) = 0 & \text{if } d\phi^p \neq 0 \text{ (slip: active hinge)} \end{cases}$ <p style="text-align: right;">(6.6.2)</p>	

*continued on following page*

Table 1. Continued

<p>Slip critical value</p> $k_{slip} = M_o e^{(sign(m)\eta\phi^p)} \quad (6.6.3)$ <p><math>M_o</math> and <math>\eta</math> are parameters of cross-section of element  <math>M_o</math> is slip resistance  <math>\eta</math> characterizes the recovery velocity of the slip resistance</p>
<p><b>The Plasticity Criterion in an in a Plastic Hinge with Slip or Yielding</b></p>
<p>Evolution law of plastic hinge with slip or yielding</p> $\begin{cases} d\phi^p = 0 & \text{if } f < 0 \\ f = 0 & \text{if } d\phi^p \neq 0 \end{cases}, \text{ where } f = \text{Max}(f^y, f^{slip}) \quad (6.6.4)$
<p><b>Determination of the Slip Resistance <math>M_o</math></b></p>
<p>Location of the neutral axis <math>z_{NA}</math></p> $C_c + C'_s - T_{slip} = 0 \quad \epsilon_c < \epsilon_o \text{ and } \epsilon_s < \epsilon_y \quad (6.6.5)$ $C_c = b \int_0^{z_{NA}} f_c dz$ <p>where <math>C'_s</math>: compression force in <math>A'_s</math>  <math>T_{slip}</math>: maximum load by sliding of the steel bars</p>
<p>The maximum load by sliding</p> $T_{slip} = \frac{\tau_{slip} \pi \cdot \ell}{2} \sum_{bar=1}^n d_{bar} \quad (6.6.6)$ <p><math>\tau_{slip}</math> is the average slip stress  <math>n</math> is the number of bars  <math>d_{bar}</math> is the diameter of the bar  <math>\ell</math> the slip length</p>
<p>Slip resistance <math>M_o</math></p> $M_o = T_{slip} \left(d - \frac{h}{2}\right) + C_c \left(\frac{h}{2} - z_{NA} + z_{C_c}\right) + C'_s \left(\frac{h}{2} - d'\right) \quad (6.6.7)$ <p>where <math>z_{C_c}</math> is the location of the force in the concrete</p>
<p><b>Determination of Parameter <math>\eta</math></b></p>
<p>Point of intersection between the slip and yielding curves <math>\eta</math></p> $f^y = f^{slip} = 0 \quad (6.6.8)$
<p>Parameter <math>\eta</math></p> $\eta = \frac{\ln \left( \frac{r^{slip} M_u - r^{slip} M_p + M_p}{M_o} \right)}{r^{slip} \phi_u^p} \quad ; (6.6.9)$ <p><math>0 \leq r^{slip} \leq 1</math>; a good value for <math>r^{slip}</math> is 0.4</p>

## 6.8 EXAMPLES

### 6.8.1 Compute the Expressions of the First Plastic and Ultimate Moments for the H-Shaped Cross-Section with Respect to the Horizontal Axis (Figure 36)

The first plastic moment can be computed using Equation (6.1.3a); since the cross-section is symmetric, the locations of the elastic and plastic neutral axes correspond to the symmetry axis of the cross-section. The elastic section modulus is given by:

$$S = \frac{2I}{h} \quad (6.8.1)$$

The expression of moment of inertia  $I$  is:

$$I = \frac{2b_f t_f^3}{3} + \frac{b_f t_f h^2}{2} - b_f t_f^2 h + \frac{t_w h^3}{12} - \frac{t_w h^2 t_f}{2} + t_w h t_f^2 - \frac{2t_w t_f^3}{3} \quad (6.8.2)$$

The first plastic moment is (see Figure 37a):

$$M_p = \frac{8b_f t_f^3 + 6b_f t_f h^2 - 12b_f t_f^2 h + t_w h^3 - 6t_w h^2 t_f + 12t_w h t_f^2 - 8t_w t_f^3}{6h} \sigma_y \quad (6.8.3)$$

The ultimate moment is computed as the moment produced by the forces on the flanges and web (see Figure 37b), thus:

$$M_u = \sigma_y \left[ 2b_f t_f \left( \frac{h}{2} - \frac{t_f}{2} \right) + t_w \left( \frac{h}{2} - t_f \right)^2 \right] \quad (6.8.4)$$

Figure 36. Homogeneous H-shape cross-section

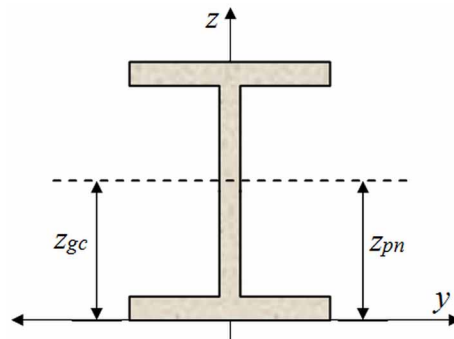
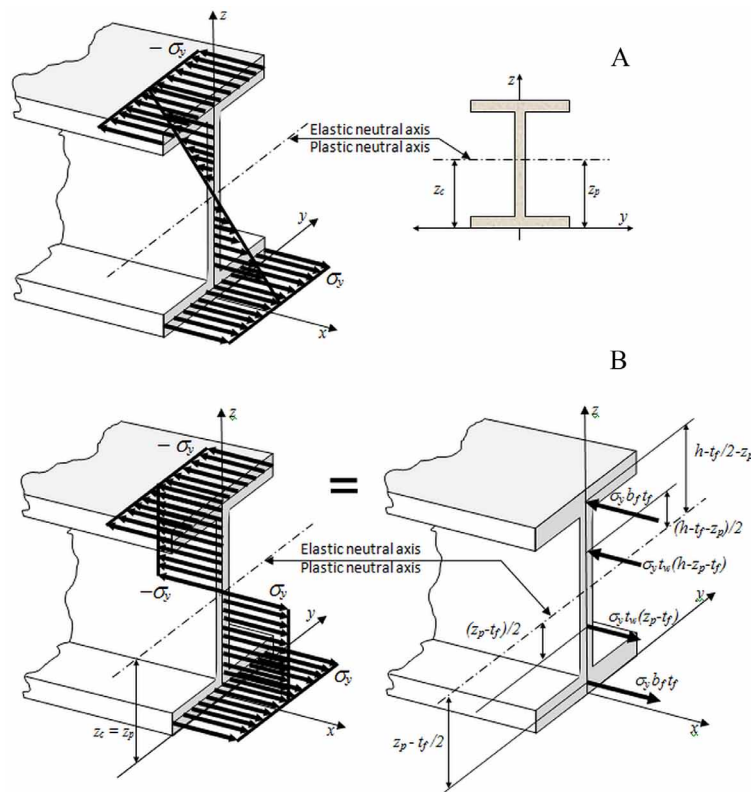




Figure 37. a) Stress distribution for the first plastic moment b) Stress distribution for the ultimate moment



### 6.8.2 Compute the Expressions of the First Plastic and Ultimate Moments with Respect to the Horizontal Axis of the Hollow Circular Cross-Section (Figure 38)

In this case, the location of the elastic and plastic neutral axes corresponds to the symmetry axis of the cross-section. The moment of inertia for this cross-section is:

$$I = \frac{\pi(R^4 - r^4)}{4} \tag{6.8.5}$$

The first plastic moment is obtained with the Equations (6.1.3) (see Figure 39a):

$$M_p = \frac{1}{4} \frac{\sigma_y \pi(R^4 - r^4)}{R} \tag{6.8.6}$$

The semi area of the cross-section is:

$$\frac{A}{2} = \frac{1}{2} \pi(R^2 - r^2) \tag{6.8.7}$$

**The Plastic Hinge**

Figure 38. Homogeneous hollow circular cross-section

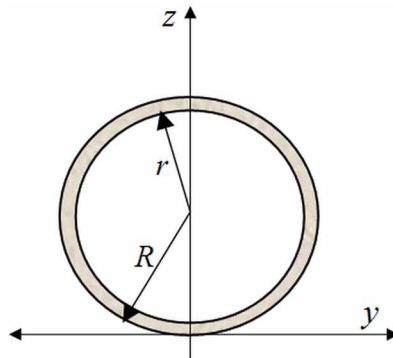
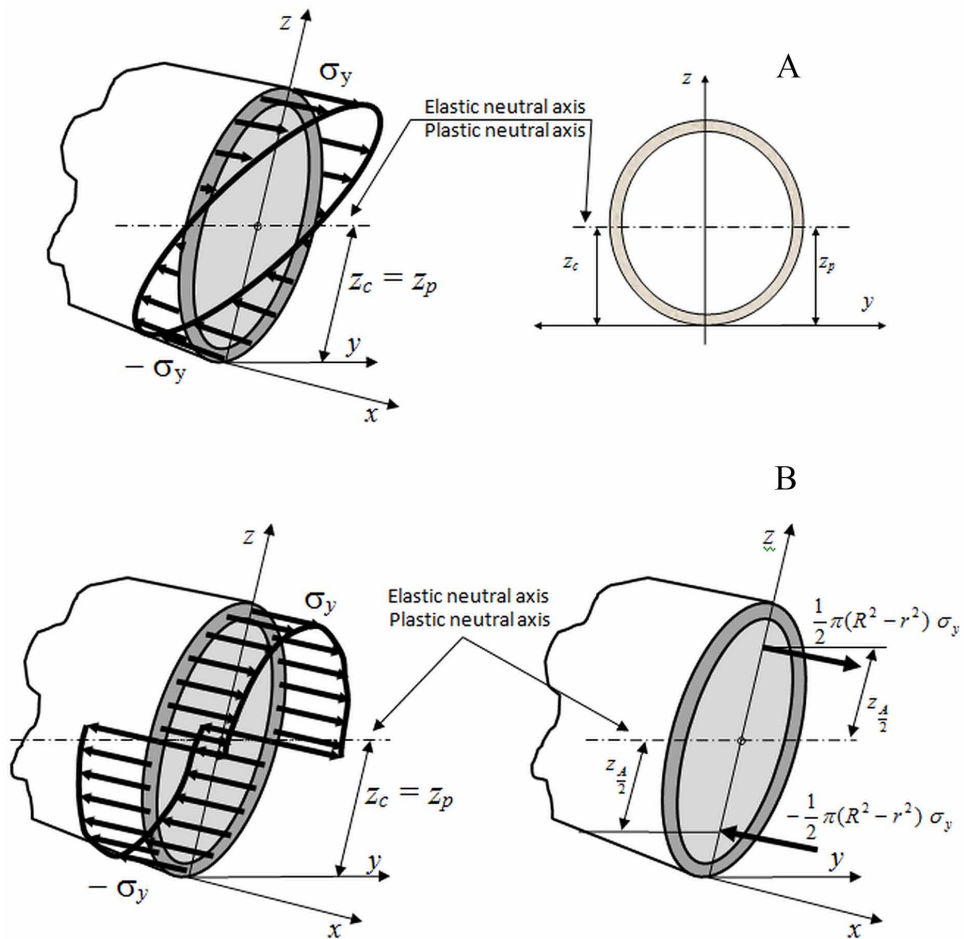


Figure 39. a) Stress distribution for the first plastic moment b) Stress distribution for the ultimate moment



And the centroid of this semi area is:

$$z_{\frac{A}{2}} = \frac{4}{3} \frac{R^2 + Rr + r^2}{(R + r)\pi} \quad (6.8.8)$$

Then the ultimate moment is:

$$M_u = \sigma_y \left( \frac{4R^3}{3} - \frac{4r^3}{3} \right) \quad (6.8.9)$$

### 6.8.3 Compute the Expressions of the First Plastic and Ultimate Moments with Respect to the Horizontal Axis of the T Cross-Section (Figure 40)

In this case, the cross-section is asymmetric; therefore, neither the elastic nor plastic neutral axis are located at  $\frac{h}{2}$ . The location of the elastic neutral axis corresponds to the centroid of the cross-section (see Figure 41a) which is:

$$z_c = \frac{b_f t_f \left( h - \frac{t_f}{2} \right) + \frac{t_w (h - t_f)^2}{2}}{b_f t_f + t_w (h - t_f)} \quad (6.8.10)$$

The moment of inertia is (Box 1):

As shown in Figure 41a the first fibers that reach the yield stress are the bottom ones. The elastic section modulus is:

Box 1.

$$I = \frac{b_f t_f^3}{12} + b_f t_f \left( h - \frac{t_f}{2} - \frac{b_f t_f \left( h - \frac{t_f}{2} \right) + \frac{t_w (h - t_f)^2}{2}}{b_f t_f + t_w (h - t_f)} \right)^2 + \frac{t_w (h - t_f)^3}{12} + t_w (h - t_f) \left( \frac{b_f t_f \left( h - \frac{t_f}{2} \right) + \frac{t_w (h - t_f)^2}{2}}{b_f t_f + t_w (h - t_f)} - \frac{h}{2} + \frac{t_f}{2} \right)^2 \quad (6.8.11)$$

**The Plastic Hinge**

Figure 40. Homogeneous T cross-section

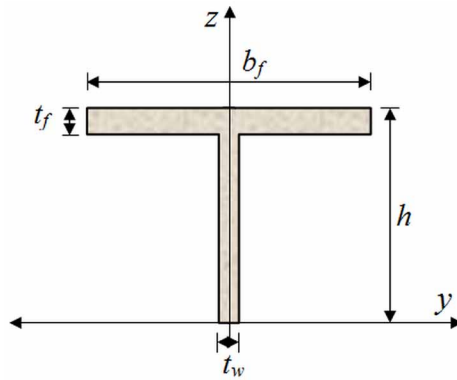
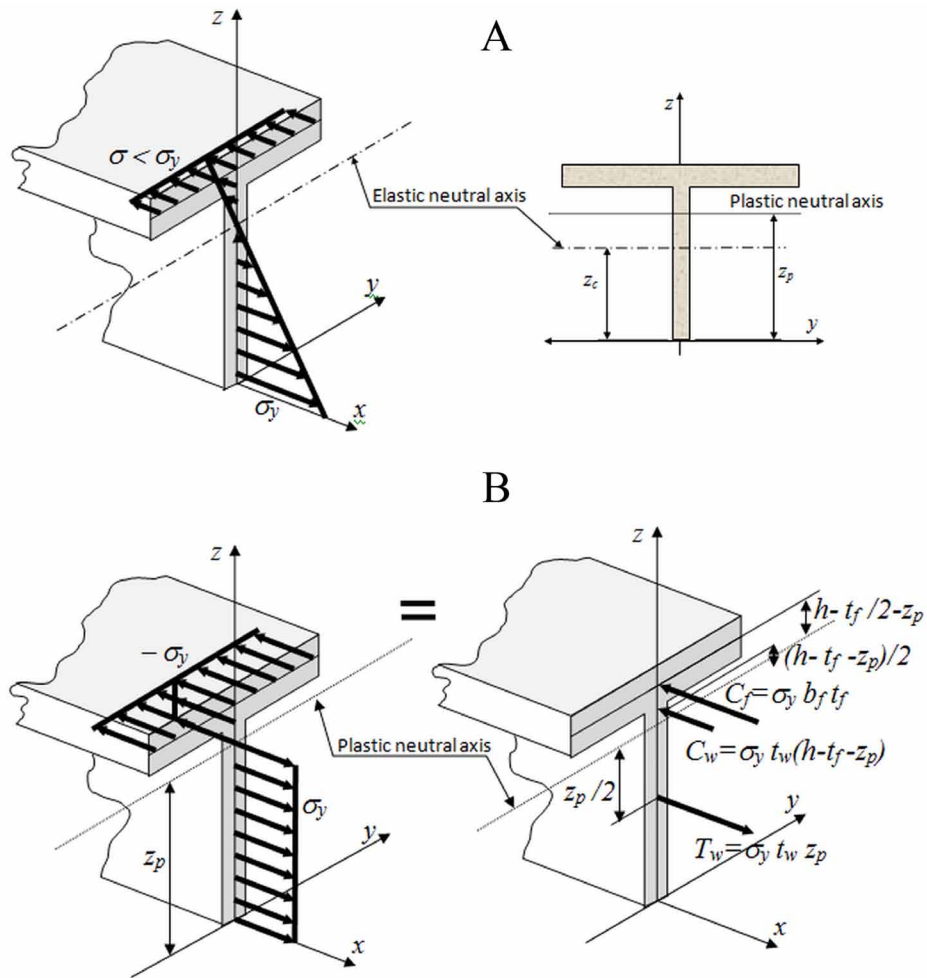


Figure 41. a) Stress distribution for the first plastic moment b) Stress distribution for the ultimate moment



$$S = \frac{I}{z_c} \quad (6.8.12)$$

and the first plastic moment can be computed as:

$$M_p = \sigma_y S \quad (6.8.13)$$

The plastic neutral axis does not coincide with the elastic one as can be observed in Figure 41a; this axis divides the cross-section in two equal areas. Assuming that the plastic neutral axis is located in the web of the beam:

$$b_f t_f + t_w (h - t_f - z_p) = t_w z_p, \text{ therefore } z_p = \frac{b_f t_f + t_w h - t_w t_f}{2 t_w} \quad (6.8.14)$$

The ultimate moment is computed as (see Figure 41b)

$$M_u = C_f \left( h - \frac{t_f}{2} - z_p \right) + C_w \left( \frac{h - t_f - z_p}{2} \right) + T_w \frac{z_p}{2} \quad (6.8.15)$$

#### 6.8.4 Compute the Interaction Diagram for the First Plastic Moment for the Cross-Section Shown in Figure 42; Consider Unconfined Concrete

For the first plastic moment, four points corresponding to the pure compression, pure tension, pure bending and balanced conditions are computed.

1. For the case of pure compression, it is used Equation (6.5.5) in order to obtain the axial force. Thus,

$$\begin{aligned} N_p &\cong -0.85 f'_c (b * h - A'_s - A_s) - f_y (A'_s + A_s) \\ N_p &\cong -0.85 * 2070 * (30 * 60 - 18.00 - 18.00) - 40000 * (18.00 + 18.00) \\ N_p &\cong -4543.76 \text{ KN} \end{aligned} \quad (6.8.16)$$

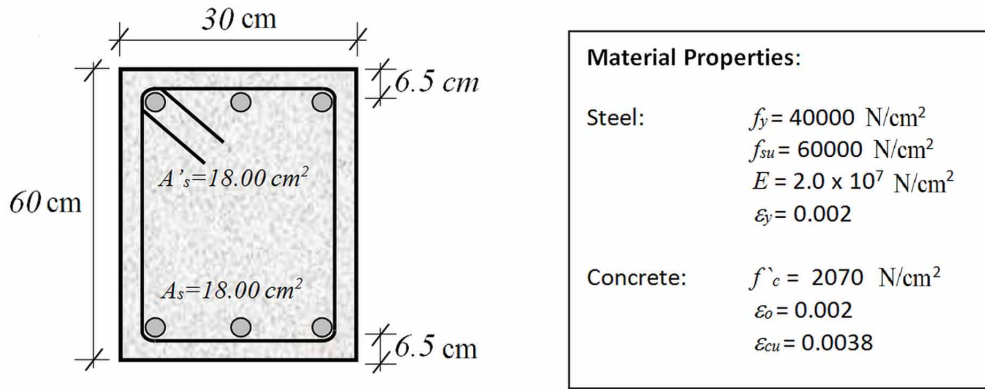
2. For the case of pure tension, it is used Equation (6.5.6):

$$N_p \cong f_y (A'_s + A_s) = 40000 * (18.00 + 18.00) \quad N_p \cong 1440.00 \text{ KN} \quad (6.8.17)$$

3. For pure bending, an iterative procedure has to be carried out in order to obtain the neutral axis location. Thus, the strain in the tension reinforcement level is fixed to  $\epsilon_y = 0.002$  and the equilibrium of forces is satisfied when the neutral axis is located at 19.10 cm from the most compressed fiber; the resulting forces in the concrete and steel are:

## The Plastic Hinge

Figure 42. Unconfined typical concrete cross-section



$$C_c = 456.24 \text{ KN}; C_s = 263.76 \text{ KN}; T = 720.00 \text{ KN} \quad (6.8.18)$$

The position of the force in the concrete is  $z_{C_c} = 12.37 \text{ cm}$  from the neutral axis. Then, the bending moment computed with the Equation (6.5.8) results in:

$$M_p = C_c \left( \frac{h}{2} - (z_{NA} - z_{C_c}) \right) + C_s \left( \frac{h}{2} - d' \right) + T \left( d - \frac{h}{2} \right) = 33735688.94 = 337.36 \text{ KN.m} \quad (6.8.19)$$

4. For the balanced condition, it is necessary to carry out an iterative procedure, but in this case the strains at the level of both steel areas ( $A_s$  and  $A'_s$ ) are fixed to a value  $\epsilon_y$ . Thus, in order to satisfy the equilibrium of forces the neutral axis must be located at a depth  $z_{NA} = 29.88 \text{ cm}$ . The resulting forces are:

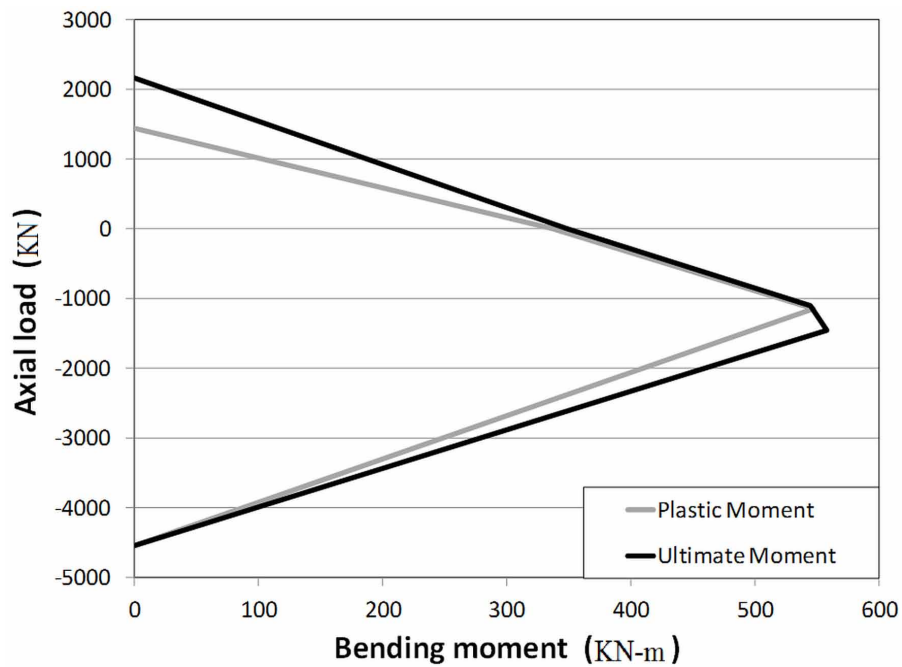
$$C_c = 1154.44 \text{ KN}; C_s = 712.79 \text{ KN}; T = 720 \text{ KN} \Rightarrow N_p = 1147.23 \text{ KN} \quad (6.8.20)$$

The location of the compression force in the concrete is  $z_{C_c} = 18.13 \text{ cm}$  from the neutral axis. The bending moment is computed using Equation (6.5.10):

$$M_p = C_c \left( \frac{h}{2} - (z_{NA} - z_{C_c}) \right) + C_s \left( \frac{h}{2} - d' \right) + T \left( d - \frac{h}{2} \right) = 54731936.40 \text{ N.cm} = 547.32 \text{ KN.m} \quad (6.8.21)$$

The resulting interaction diagram is shown in Figure 43.

Figure 43. Interaction diagram for plastic and ultimate moment



### 6.8.5 Compute the Interaction Diagram of the Ultimate Moment for the Cross-Section Shown in Figure 42; Consider Unconfined Concrete

The following points are computed:

1. The first point, i.e. pure compression, is the same of the first plastic moment. Thus, the axial force is equal to:

$$N_u \cong -4543.76 \text{ KN} \quad (6.8.22)$$

2. For the case of pure tension, it is used Equation (6.5.12):

$$N_u \cong f_{su} (A'_s + A_s) = 60000 * (18.00 + 18.00); N_u \cong 2160.00 \text{ KN} \quad (6.8.23)$$

3. For the pure bending condition, the strain in the extreme compression fiber is fixed to  $\epsilon_{cu} = 0.0038$ . The neutral axis is located at 8.77 cm from the extreme compression fiber; the resulting forces in the concrete and steel are:

$$C_c = 365.44 \text{ KN}; C_s = 354.56 \text{ KN}; T = 720.00 \text{ KN} \quad (6.8.24)$$

### The Plastic Hinge

The location of the force in the concrete is  $z_{C_c} = 5.03$  cm from the neutral axis. Thus, the bending moment computed with Equation (6.5.14) results in:

$$M_u = C_c \left( \frac{h}{2} - (z_{NA} - z_{C_c}) \right) + C_s \left( \frac{h}{2} - d' \right) + T \left( d - \frac{h}{2} \right) = 34848205.10 \text{ N} \cdot \text{cm} = 348.48 \text{ KN} \cdot \text{m} \quad (6.8.25)$$

4. As aforementioned, for the balanced condition the strain in the most compressed fiber is equal to  $\epsilon_{cu}$  and the strain in the reinforcement steel in tension is equal to  $\epsilon_y$ . Thus, to satisfy the equilibrium of forces, the neutral axis must be located at a depth  $z_{NA} = 35.05$  cm. The resulting forces are:

$$C_c = 1459.76 \text{ KN}; C_s = 720.00 \text{ KN}; T = 720.00 \text{ KN} \Rightarrow N_u = 1459.76 \text{ KN} \quad (6.8.26)$$

The location of the compression force in the concrete is  $z_{C_c} = 20.11$  cm from the neutral axis. The bending moment is computed using Equation (6.5.16):

$$M_u = C_c \left( \frac{h}{2} - (z_{NA} - z_{C_c}) \right) + C_s \left( \frac{h}{2} - d' \right) + T \left( d - \frac{h}{2} \right) = 55818409.76 \text{ N} \cdot \text{cm} = 558.18 \text{ KN} \cdot \text{m} \quad (6.8.27)$$

5. Additional points can be computed considering that the strain in the most compressed fiber is equal to  $\epsilon_{cu}$  and that the axial force takes different values larger than the balanced one. For example, considering  $N_u = 1100.00$  KN the neutral axis is located at 26.41 cm from the extreme compression fiber and the forces in the concrete and steel are:

$$C_c = 1100.00 \text{ KN}; C_s = 720.00 \text{ KN}; T = 720.00 \text{ KN} \quad (6.8.28)$$

The location of compression force in the concrete is  $z_{C_c} = 15.15$  cm from the neutral axis. The corresponding bending moment is:

$$M_u = C_c \left( \frac{h}{2} - (z_{NA} - z_{C_c}) \right) + C_s \left( \frac{h}{2} - d' \right) + T \left( d - \frac{h}{2} \right) = 544.52 \text{ KN} \cdot \text{m} \quad (6.8.29)$$

The interaction diagram is presented in Figure 43.



### 6.8.6. Compute the Interaction Diagram of the Ultimate Plastic Curvature for the Cross-Section Shown in Figure 42; Consider Unconfined Concrete

The ultimate plastic curvature is determined by  $(\chi_u - \chi_p)$ , where  $\chi_u = \frac{\varepsilon_{cu}}{x}$  and  $\chi_p = \frac{\varepsilon_y}{d-x}$  (Equations 6.5.19b y c). For pure compression and pure tension the curvatures are nil; the ultimate and plastic curvatures for pure bending condition are shown in Box 2.

For the balanced condition they are shown in Box 3.

The interaction diagram is shown in Figure 44.

Box 2.

$$\chi_p = \frac{\varepsilon_y}{d-x} = \frac{0.002}{53.5 - 19.10} = 5.81 \times 10^{-5} \text{ 1/cm} \quad \text{and} \quad \chi_u = \frac{\varepsilon_{cu}}{x} = \frac{0.0038}{8.77} = 4.33 \times 10^{-4} \text{ 1/cm}$$

$$\text{then } (\chi_u - \chi_p) = \frac{\phi_u^p}{L_p} = 3.75 \times 10^{-4} \text{ 1/cm}$$

(6.8.30)

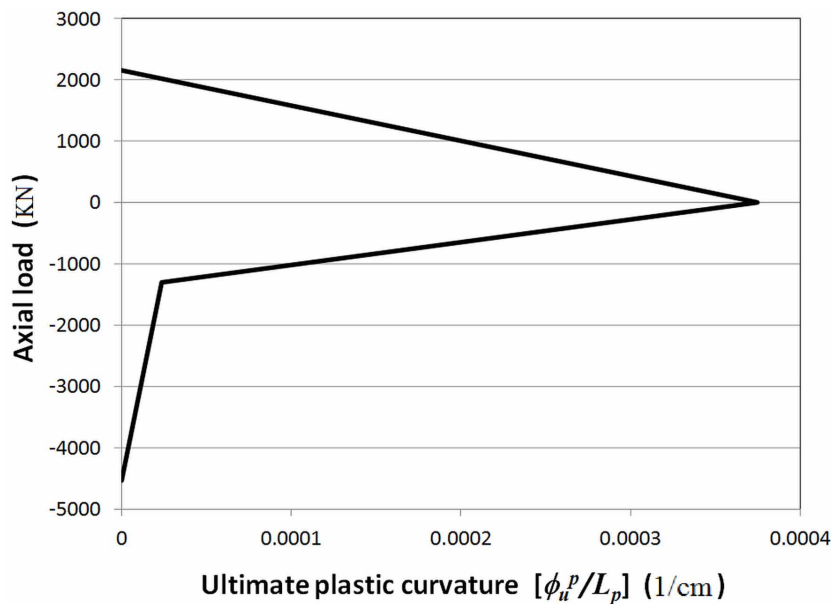
Box 3.

$$\chi_p = \frac{\varepsilon_y}{d-x} = \frac{0.002}{53.5 - 29.88} = 8.47 \times 10^{-5} \text{ 1/cm} \quad \text{and} \quad \chi_u = \frac{\varepsilon_{cu}}{x} = \frac{0.0038}{35.04} = 1.08 \times 10^{-4} \text{ 1/cm}$$

$$\text{then } (\chi_u - \chi_p) = \frac{\phi_u^p}{L_p} = 2.37 \times 10^{-5} \text{ 1/cm}$$

(6.8.31)

Figure 44. Interaction diagram for ultimate plastic curvature



### The Plastic Hinge

#### 6.8.7. Compute the Plastic Length of the Hinge for the Bending Moment Diagram Shown in the Figure 45 and the Cross-Section Presented in Figure 42

From the Figure 45 it is obtained  $x_{cs}$  that is the distance from the critical section to the point of inflection.

$$x_{cs} = \frac{3L}{5} \quad (6.8.32)$$

The plastic hinge length  $L_p$  is computed with the Equation (6.5.20)

$$L_p = 0.5d + 0.05x_{cs} = 0.5(53.5) + 0.05\left(\frac{3L}{5}\right) = 26.75 + 0.03L \quad (6.8.33)$$

#### 6.8.8. Compute the Slip Resistance $M_o$ and the Parameter $\eta$ for the Beam-Column Joint Shown in Figure 46

Following the same procedure used in the previous examples, the properties of the wide-beam shown in Figure 46 are obtained. The properties for pure bending condition are:

$$M_p = 219.68 \text{ KN} \cdot \text{m}; M_u = 227.62 \text{ KN} \cdot \text{m}; \quad (6.8.34)$$

For this joint,  $l$  = slip length = column width = 40 cm,  $\tau_{slip}$  = the average slip stress = 303.60 N/cm<sup>2</sup>,  $d_{bar} = 3/4'' \approx 1.905$  cm, thus:

Figure 45. Bending moment diagram

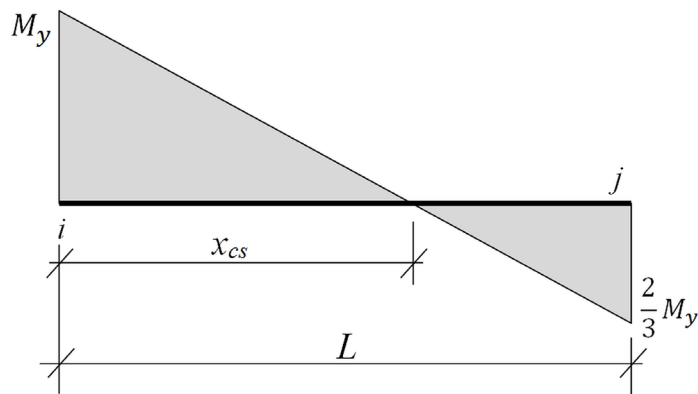
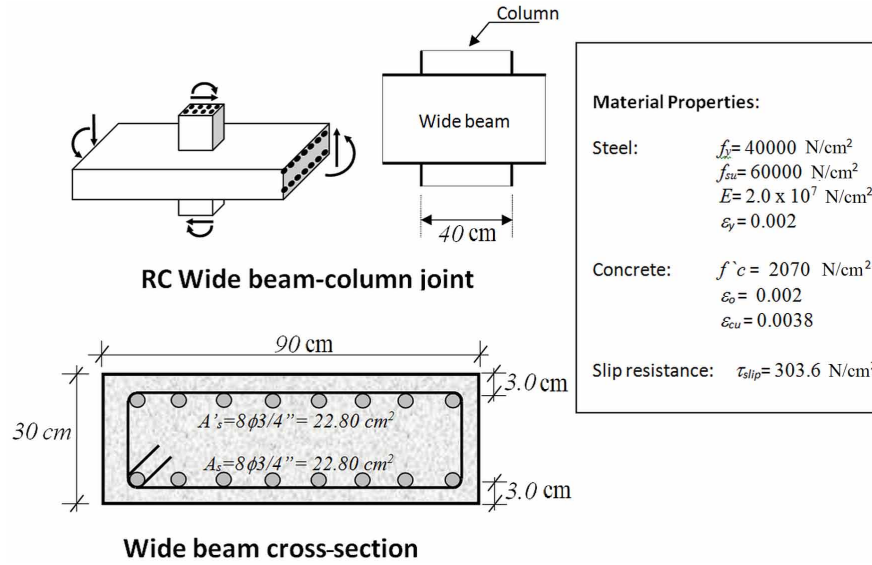


Figure 46. RC wide-beam-column joint; wide-beam cross-section



$$T_{slip} = \frac{\tau_{slip} \pi \cdot \ell}{2} \sum_{bar=1}^n d_{bar} = \frac{303.82 \pi \cdot 40}{2} 8 (1.905) = 290925.10 \text{ N} = 290.93 \text{ KN} \quad (6.8.35)$$

Solving Equation (6.6.5)  $C_c + C_s - T_{slip} = 0$ , it is obtained the neutral axis depth  $z_{NA} = 7.98 \text{ cm}$  and the location of compression force in the concrete  $z_{C_c} = 5.29 \text{ cm}$ . Then, the slip resistance  $M_o$  is computed as:

$$M_o = T_{slip} \left(d - \frac{h}{2}\right) + C_c \left(\frac{h}{2} - z_{NA} + z_{C_c}\right) + C_s \left(\frac{h}{2} - d\right)$$

$$M_o = 290925.10 (27 - 15) + 214514.33 (15 - 7.98 + 5.29) + 76200.11 (15 - 3) = 7046173.92 \text{ N} \cdot \text{cm}$$

$$M_o = 70.46 \text{ KN} \cdot \text{m} \quad (6.8.36)$$

The parameter  $\eta$  is computed with a value of  $r = 0.4$  as:

$$\eta = \frac{\ln \left( \frac{rM_u - rM_p + M_p}{M_o} \right)}{r\phi_u^p} = \frac{\ln \left( \frac{0.4 \times 227.68 - 0.4 \times 219.68 + 219.68}{70.46} \right)}{0.4\phi_u^p} = \frac{2.88}{\phi_u^p} \quad (6.8.37)$$

## 6.9 PROBLEMS

6.9.1 Plot the Elastic Domains and Develop the Normality Rules for a Rectangular Cross-Section Using the Exact Solution Equation (6.4.5) and the Approximated One Equation (6.4.13) with  $\nu_1 = \nu_2 = 2$  and  $\nu_1 = \nu_2 = 2/2$

6.9.2 Compute the First Plastic and Ultimate Moments for a Homogeneous T Cross-Section Assuming That the Plastic Neutral Axis Is Located in the Flange of the Beam

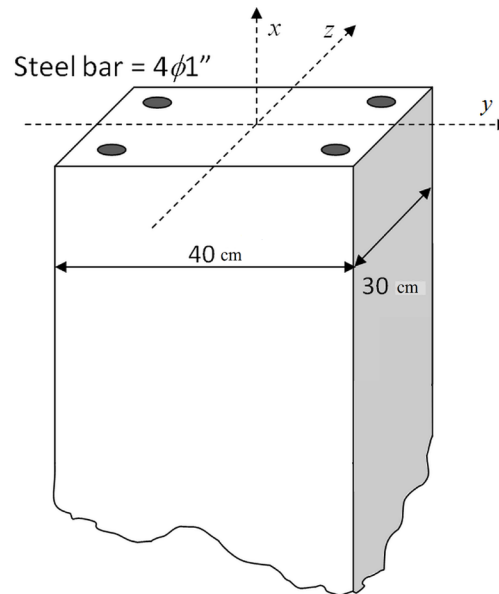
6.9.3 Compute the First Plastic and Ultimate Moments for a Homogeneous Equilateral Triangle Cross-Section

6.9.4 For the Column Shown in Figure 47 Compute the Properties Considering the Biaxial Effects.

6.9.5 Propose a Model for a RC Plastic Hinge with Multi-Linear Isotropic Hardening

6.9.6 Propose a Model for a RC Plastic Hinge with Multi-Linear Kinematic and Isotropic Hardening

Figure 47. RC Column element



## REFERENCES

- Chen, W. F., & Sohal, I. (1995). *Plastic design and second-order analysis of steel frames*. New York, NY: Springer-Verlag. doi:10.1007/978-1-4613-8428-1
- Friedlander, F. G., & Joshi, M. S. (1998). *Introduction to the theory of distributions*. Cambridge, UK: University Press.
- Hsu, T. C., & Mo, Y. L. (2010). *Unified theory of concrete structures*. West Sussex, UK: John Wiley and Sons. doi:10.1002/9780470688892
- Kent, D. C., & Park, R. (1971). Flexural members with confined concrete. *Journal of the Structural Division*, 97, 1960–1990.
- Li, G. Q., & Li, J. J. (2007). *Advanced analysis and design of steel frames*. John Wiley & Sons. doi:10.1002/9780470319949
- Park, R., & Paulay, T. (1975). *Reinforced concrete structures*. New York, NY: John Wiley and Sons. doi:10.1002/9780470172834
- Picon-Rodriguez, R., Quintero-Febres, C., & Florez-Lopez, J. (2007). Modeling of cyclic bond deterioration in RC beam-column connections. *Structural Engineering & Mechanics*, 26(5), 569–589. doi:10.12989/sem.2007.26.5.569

# Chapter 7

## Elasto–Plastic Frames

### ABSTRACT

*The goal of this chapter is to describe how the concepts presented in Chapters 5 and 6 can be included in the mathematical models for the elastic plastic analysis of frame structures. The numerical implementation of such an analysis is described in Chapter 8. The models presented in this chapter cover applications for reinforced concrete frames, shear walls, wide beams, and dual systems, as well as steel structures. Both cases, planar and tridimensional analyses, are considered. However, this chapter does not yet describe the numerical and computational analysis of elasto-plastic structures; this is the subject of the next chapter.*

### 7.1 ELASTO-PLASTIC CONSTITUTIVE MODEL FOR A SLENDER ELEMENT OF A PLANAR FRAME

Buildings in seismic zones must be designed so that there is no structural damage at all under service loads or earthquakes of small intensity; the latter are defined as those events that may occur frequently during the life time of the structure. In mathematical terms, no structural damage means that the structures must behave elastically under such conditions. In the case of earthquakes of intermediate intensity, i.e. those that are expected to occur at most once or twice during the life time of the structure, it is allowed some structural damage provided that it is repairable. In mathematical terms, repairable structural damage means a limited amount of plastic deformations or, the formation of a small number of plastic hinges in the structure. Taking into account that an earthquake of intermediate intensity is considered an event of high probability during the expected life time of the structure, a plastic analysis of such kind of structures should be mandatory.

Earthquake loading is the main cause of structural damage in the practice; however, frame structures may also enter into the plastic range in the case of other kind of overloads. For instance, those due to displacements of its supports (because of the failure of the soil underneath) or impacts or explosions.

### 7.1.1 Lumped Plasticity Model

As mentioned in Chapter 4, distributed forces on the elements are used to characterize service loads; they are assumed to be small compared with exceptional overloads such as earthquake forces, settlement of foundations, explosions or others; these exceptional overloads can be represented as nodal forces or displacements. As aforementioned, a structure only under service loads does not need inelastic analysis; it is therefore assumed that nodal forces are the main cause of plastic deformations in the elements. Typically, the moment distribution in these cases (small distributed forces and relatively large nodal forces) presents maximums at the ends of the elements such as indicated in Figure 1.

The simplest way to consider the presence of plasticity in a frame structure under these conditions is the lumped plasticity model that consists in assuming that a slender frame element can be represented as the assemblage of an elastic beam-column and two plastic hinges at the ends  $i$  and  $j$  such as shown in Figure 2.

In the lumped plasticity model, the deformations of a frame member can be decomposed into two terms:

$$\{\Phi\}_b = \{\Phi^{bc}\}_b + \{\Phi^p\}_b \quad (7.1.1)$$

where  $\{\Phi^{bc}\}_b$  is the matrix of generalized deformations of the elastic beam-column and  $\{\Phi^p\}_b$  is called matrix of plastic deformations; the latter contains the rotations and elongations of the plastic hinges:

$$\{\Phi^p\}_b = \begin{bmatrix} \phi_i^p \\ \phi_j^p \\ \delta^p \end{bmatrix} \quad (7.1.2)$$

Figure 1. Typical distribution of moments in a frame with large nodal forces and small distributed forces on the elements

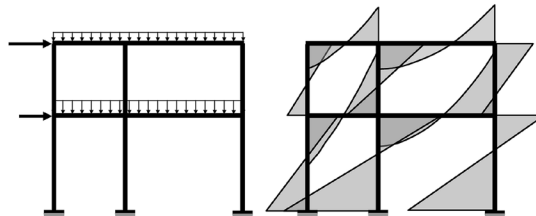
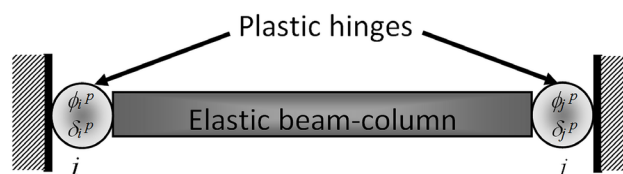


Figure 2. Lumped plasticity model of a slender frame member



## Elasto-Plastic Frames

The terms  $\phi_i^p$ ,  $\phi_j^p$  correspond, respectively, to the rotation of plastic hinges  $i$  and  $j$ ;  $\delta^p$  is the plastic elongation of the element chord; the latter is equal to the sum of the plastic elongations of each hinge:

$$\delta^p = \delta_i^p + \delta_j^p \quad (7.1.3)$$

### 7.1.2 Elasticity law

The lumped plasticity model is the basis of all the models for slender frame elements that are presented in this chapter. The elasticity law of an elasto-plastic frame element can be obtained as follows. Introducing the constitutive equation of the elastic beam-column (Equation 3.3.9a) into (7.1.1) gives:

$$\{\Phi\}_b = [\mathbf{F}]_b \{\mathbf{M}\}_b + \{\Phi^0\}_b + \{\Phi^p\}_b \quad (7.1.4)$$

The terms  $[\mathbf{F}]_b$ ,  $\{\mathbf{M}\}_b$ ,  $\{\Phi^0\}_b$  are, of course, the flexibility matrix, the generalized stresses and the initial deformations such as defined in chapter 3 (Equations 3.3.9b, 3.2.2 and Table 3 in Chapter 3); Equation (7.1.4) can also be written as:

$$\{\mathbf{M}\}_b = [\mathbf{E}]_b \{\Phi - \Phi^p\}_b + \{\mathbf{M}^0\}_b \quad (7.1.5)$$

where  $[\mathbf{E}]_b = [\mathbf{F}]_b^{-1}$  is the same elasticity matrix defined in chapter 3 and  $\{\mathbf{M}^0\}_b = -[\mathbf{E}]_b \{\Phi^0\}_b$  is the matrix of initial stresses (Equation 3.3.11b and Table 3 in Chapter 3). The expression (7.1.5), or (7.1.4), is the elasticity law of a slender elasto-plastic frame element.

The constitutive equations of this kind of elements can now be defined by combining this elasticity law with one of the plastic hinges introduced in chapter 6. The sections 7.1.4-7 describe the different models obtained in this way.

### 7.1.3 Selection of the Rigidity Term $EI$ in the Elasticity Law

For frame elements made of homogenous materials, like aluminum or steel, the moment of inertia of the cross-section is computed as is presented in the textbooks of strength of materials; the elastic modulus is identified in a simple tension test, as the slope of the initial linear part of the stress-strain curve.

In the case of reinforced concrete elements, the issue is more complicated due to the presence of two materials and the nonlinear behavior of the concrete. In compression, the initial behavior of the concrete is approximately linear elastic but it changes to a parabolic relation rapidly. Thus, it is not easy to identify a unique slope for the initial stress-strain curve. The ACI (American Concrete Institute) has proposed empirical expressions for the elastic modulus (Equations 6.5.1 and 6.5.2) for the initial linear stage but the use of these values conduces to a stiffness much larger than the values observed in experimental tests on RC elements. The simplest solution to obtain results near the values observed experimentally is the use of the following expression:



$$E_c = \frac{f_c'}{\varepsilon_0} \quad (7.1.6)$$

where  $\varepsilon_0 = 0.002$  is the strain in the concrete when the stress is equal to  $f_c'$ . For this material the moment of inertia is computed using the total area of the cross-section, making no deductions for the presence of the steel bars.

### 7.1.4 Elastic Perfectly Plastic Constitutive Model

In the case of perfect plasticity, the evolution laws of the plastic deformations are obtained by introducing the constitutive equations of the plastic hinges  $i$  and  $j$ , such as defined in the section 6.2. Let  $f_i$  and  $f_j$  be the yield functions of, respectively, plastic hinges at the ends  $i$  and  $j$ :

$$f_i = f_i(m_i, n) \leq 0; f_j = f_j(m_j, n) \leq 0 \quad (7.1.7)$$

The model of a slender elastic perfectly plastic frame element is given by the elasticity law (7.1.5) or (7.1.4), the normality rule:

$$d\phi_i^p = d\lambda_i \frac{\partial f_i}{\partial m_i}; d\phi_j^p = d\lambda_j \frac{\partial f_j}{\partial m_j}; d\delta_p = d\lambda_i \frac{\partial f_i}{\partial n} + d\lambda_j \frac{\partial f_j}{\partial n} \quad (7.1.8)$$

and the plastic multipliers evolution laws:

$$\left\{ \begin{array}{l} d\lambda_i = 0 \text{ if } f_i(m_i, n) < 0 \text{ (hinge } i \text{ is locked)} \\ f_i(m_i, n) = 0 \text{ if } d\lambda_i \neq 0 \text{ (hinge } i \text{ is active)} \end{array} \right\}; \left\{ \begin{array}{l} d\lambda_j = 0 \text{ if } f_j(m_j, n) < 0 \\ f_j(m_j, n) = 0 \text{ if } d\lambda_j \neq 0 \end{array} \right\} \quad (7.1.9)$$

$\lambda_i$  and  $\lambda_j$  are the plastic multipliers of hinges  $i$  and  $j$ . The yield functions  $f_i(m_i, n)$  and  $f_j(m_j, n)$  depend, of course, on the cross-section of the element and may be computed by any of the procedures described in the precedent chapter.

### 7.1.5 Elastic Perfectly Plastic Constitutive Model Neglecting Plastic Elongations

In the cases where plastic elongations can be neglected, typically in reinforced concrete frames, the constitutive equation is composed by the same elasticity law (7.1.5) or (7.1.4) and the following simplified evolution laws:

$$\left\{ \begin{array}{l} d\phi_i^p = 0 \text{ if } f_i(m_i) < 0 \text{ (hinge } i \text{ locked)} \\ f_i(m_i) = 0 \text{ if } d\phi_i^p \neq 0 \text{ (hinge } i \text{ active)} \end{array} \right\}; f_i(m_i) = |m_i| - M_{yi} \leq 0;$$

## Elasto-Plastic Frames

$$\delta_p = 0$$

$$\begin{cases} d\phi_j^p = 0 \text{ if } f_j(m_j) < 0 \text{ (hinge } j \text{ locked)} \\ f_j(m_j) = 0 \text{ if } d\phi_j^p \neq 0 \text{ (hinge } j \text{ active)} \end{cases}; f_j(m_j) = |m_j| - M_{yj} \leq 0; \quad (7.1.10)$$

Notice that, for the sake of generality, different yield moments  $M_{yi}$  and  $M_{yj}$  are introduced in the model; this might be the case of RC frame elements since the reinforcement can be dissimilar at its ends. The ultimate moment of the cross-section  $M_u$ , or the first plastic one  $M_p$ , can be used as yield moments in (7.1.10). Frequently, the yield moment is assumed to be constant; however, a better model is obtained if a function of the axial force is selected such as described in the previous chapter.

### 7.1.6 Elasto-Plastic Constitutive Model with Hardening

A more accurate model that includes both values,  $M_p$  and  $M_u$ , can be obtained by using plastic hinges with hardening. In this case, the same elasticity law (7.1.5) or (7.1.4) is combined with the plastic deformation evolution laws derived from the yield functions presented in section 6.3.3:

$$\begin{cases} d\phi_i^p = 0 \text{ if } f_i(m_i, p_i, x_i) < 0 \text{ (hinge } i \text{ locked)} \\ f_i(m_i, p_i, x_i) = 0 \text{ if } d\phi_i^p \neq 0 \text{ (hinge } i \text{ active)} \end{cases}$$

$$\delta_p = 0$$

$$\begin{cases} d\phi_j^p = 0 \text{ if } f_j(m_j, p_j, x_j) < 0 \text{ (hinge } j \text{ locked)} \\ f_j(m_j, p_j, x_j) = 0 \text{ if } d\phi_j^p \neq 0 \text{ (hinge } j \text{ active)} \end{cases} \quad (7.1.11)$$

$$f_i(m_i, p_i, x_i) = |m_i - x_i| - (M_{pi} + Q(p_i)) \leq 0; f_j(m_j, p_j, x_j) = |m_j - x_j| - (M_{pj} + Q(p_j)) \leq 0 \quad (7.1.12)$$

where  $p_i$  and  $p_j$  can be the accumulated plastic rotations of, respectively, hinges  $i$  and  $j$  as defined in the Equation (6.3.2) of the precedent chapter:

$$dp_i = |d\phi_i^p| \text{ and } dp_j = |d\phi_j^p| \quad (7.1.13)$$

Alternatively,  $p_i$  and  $p_j$  may represent the maximum plastic rotations as in (6.3.3):

$$p_i = \text{Max} |\phi_i^p| \text{ and } p_j = \text{Max} |\phi_j^p| \quad (7.1.14)$$

The isotropic hardening term  $Q$  can be nonlinear (7.1.15a), multilinear (7.1.15b) or linear (7.1.15c):

$$Q(p_i) = (1 - r)(M_{ui} - M_{pi})(1 - e^{-\alpha_i p_i})$$

$$Q(p_i) = \begin{cases} \frac{(1 - r)(M_{ui} - M_{pi})}{\phi_{ui}^p} p_i & \text{if } 0 \leq p_i \leq \phi_{ui}^p \\ (1 - r)(M_{ui} - M_{pi}) & \text{if } p_i > \phi_{ui}^p \end{cases}$$

$$Q(p_i) = (1 - r)c_i p_i \tag{7.1.15}$$

with the same choices for the kinematic hardening term:

$$dx_i = \alpha \left( r(M_{ui} - M_{pi})d\phi_i^p - x_i |d\phi_i^p| \right)$$

$$dx_i = \begin{cases} \frac{r(M_{ui} - M_{pi})}{\phi_{ui}^p} d\phi_i^p & \text{if } |m_i| < M_{ui} \\ 0 & \text{if } |m_i| = M_{ui} \end{cases}$$

$$x_i = r c_i \phi_i^p \tag{7.1.16}$$

The values of  $r$  were discussed in section 6.3.3. The expressions for the isotropic and kinematic hardening terms corresponding to the hinge  $j$  can be written in the same way changing only the subscript  $i$  by  $j$ .

### 7.1.7 Constitutive Equations for Inelastic Hinges with Slip in RC Wide Beam-Column Connections

As discussed in section 6.6, some RC structures subjected to cyclic loads can show pinching of the loops. The pinching is mainly due to cyclic bond deterioration between longitudinal reinforcing steel and concrete. This type of behavior is typical in wide beam-to-column connections but it is not always relevant in RC structures.

A model with slip hinge includes the “slip resistance”,  $M_o$ . This model combines the elasticity law (7.1.5) or (7.1.4) with the plastic deformation evolution laws derived from slip functions presented in the section 6.6.3:

$$\begin{cases} d\phi_i^p = 0 & \text{if } f_i^{slip} < 0 \text{ (hinge } i \text{ locked)} \\ f_i^{slip} = 0 & \text{if } d\phi_i^p \neq 0 \text{ (hinge } i \text{ active)} \end{cases}$$

### Elasto-Plastic Frames

$$\delta_p = 0$$

$$\begin{cases} d\phi_j^p = 0 & \text{if } f_j^{slip} < 0 \text{ (hinge } j \text{ locked)} \\ f_j^{slip} = 0 & \text{if } d\phi_j^p \neq 0 \text{ (hinge } j \text{ active)} \end{cases} \quad (7.1.17)$$

$$f_i^{slip} = |m_i| - M_{oi} e^{(\text{sign}(m_i)\eta_i\varphi_i^p)} \leq 0; f_j^{slip} = |m_j| - M_{oj} e^{(\text{sign}(m_j)\eta_j\varphi_j^p)} \leq 0 \quad (7.1.18)$$

where the parameters  $\eta_i$  and  $\eta_j$  can be computed using the Equation (6.6.9) of precedent chapter:

$$\eta_i = \frac{\ln\left(\frac{0.4M_{ui} - 0.4M_{pi} + M_{pi}}{M_{oi}}\right)}{0.4\phi_{ui}^p}; \eta_j = \frac{\ln\left(\frac{0.4M_{uj} - 0.4M_{pj} + M_{pj}}{M_{oj}}\right)}{0.4\phi_{uj}^p} \quad (7.1.19)$$

A more complex model that combines the slip and yielding mechanisms can be obtained by the same elasticity laws (7.1.5) or (7.1.4), the plastic deformation evolution laws (7.1.11) and (7.1.17). Both mechanisms are possible and may occur one after the other in RC structures. Then, the following evolution laws for the plastic deformations in plastic hinges with yielding and slip for RC elements can be written as:

$$\begin{cases} d\phi_i^p = 0 & \text{if } f_i < 0 \text{ (hinge } i \text{ locked)} \\ f_i = 0 & \text{if } d\phi_i^p \neq 0 \text{ (hinge } i \text{ active)} \end{cases}$$

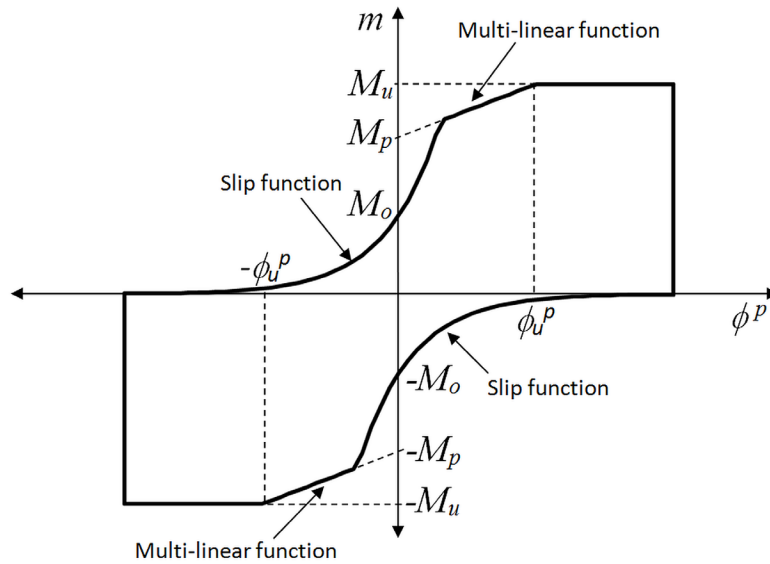
$$\delta_p = 0$$

$$\begin{cases} d\phi_j^p = 0 & \text{if } f_j < 0 \text{ (hinge } j \text{ locked)} \\ f_j = 0 & \text{if } d\phi_j^p \neq 0 \text{ (hinge } j \text{ active)} \end{cases} \quad (7.1.20)$$

$$f_i = \text{Max}(f_i^y, f_i^{slip}); f_j = \text{Max}(f_j^y, f_j^{slip}) \quad (7.1.21)$$

where  $f_i^y$  and  $f_j^y$  are respectively, the yield functions in the hinges  $i$  and  $j$  (Equations 7.1.12a and 7.1.12b).  $f_i^{slip}$  and  $f_j^{slip}$  are respectively, the slip functions in the hinges  $i$  and  $j$  (Equations 7.1.18a and 7.1.18b). A behavior curve that represents this complex model is shown in Figure 3.

Figure 3. Plastic behavior curve of a inelastic hinge with slip and yielding



## 7.2 ELASTO-PLASTIC CONSTITUTIVE MODEL FOR SQUAT RC ELEMENTS

### 7.2.1 Elasticity Law

In chapter 4, slender frame elements were defined as those with high aspect ratio; in these cases, deformations due to shear forces are negligible when compared with the bending ones. Under this condition, the constitutive law derived from the Euler-Bernoulli theory of beams is accurate enough and a considerably simpler alternative. Plasticity in slender frame elements is only due to bending and can be lumped at plastic hinges as discussed in the precedent section.

On the other hand, squat reinforced concrete elements are defined as those with a very low aspect ratio. These elements need elasticity equations based on the Timoshenko beam theory as the one introduced in section 3.4. Examples of squat elements are RC walls and very short columns.

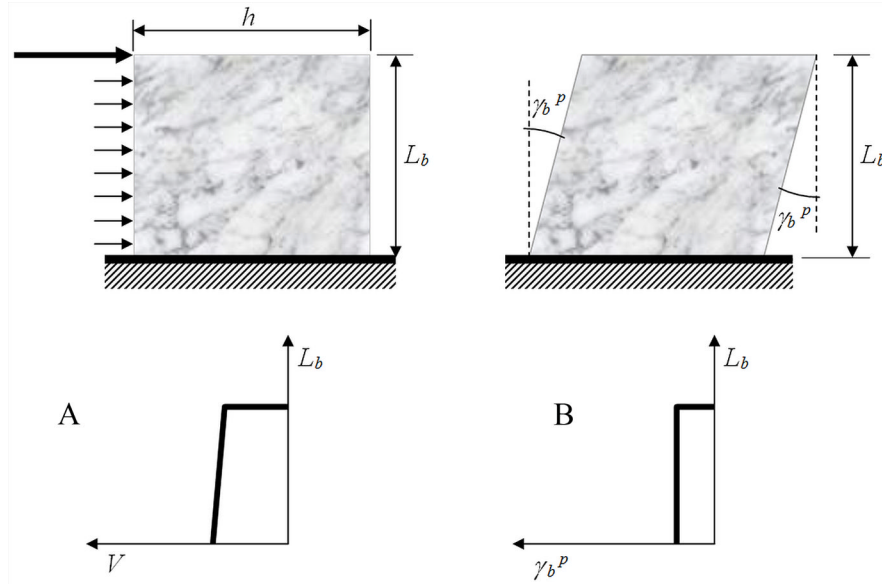
As in the previous section, it is assumed that distributed forces on the element are small compared with the nodal forces. Shear forces and distortions are, therefore, approximately constants along the element as shown in Figure 4a. Assume that the state of plastic deformation in a squat element under this condition is represented as in Figure 4b.

Mathematically, this state of deformation is characterized by the following matrix of plastic deformations:

$$\{\gamma^p\}_b = \begin{bmatrix} \gamma_b^p \\ \gamma_b^p \\ 0 \end{bmatrix} \quad (7.2.1)$$

## Elasto-Plastic Frames

Figure 4. a) Distribution of shear forces in a squat element under low distributed forces b) Approximate plastic deformation state in a squat element under low distributed forces



The elasticity law for a squat element with plasticity can be obtained by modification of the constitutive equation (3.4.8): the total deformations are now obtained adding the plastic deformation matrix to this equation:

$$\{\Phi\}_b = ([\mathbf{F}_f]_b + [\mathbf{F}_s]_b)\{\mathbf{M}\}_b + \{\Phi^0\}_b + \{\gamma^p\}_b \quad (7.2.2)$$

where the flexibility matrices  $[\mathbf{F}_f]_b$  and  $[\mathbf{F}_s]_b$  are the same that were introduced in section 3.4.2 (Equation 3.4.9). Alternatively, the elasticity law can also be written as:

$$\{\mathbf{M}\}_b = [\mathbf{E}]_b\{\Phi - \gamma^p\}_b + \{\mathbf{M}^0\}_b \quad (7.2.3)$$

where  $[\mathbf{E}]_b$  and  $\{\mathbf{M}^0\}_b$  are the same elasticity matrix and initial stresses introduced in section 3.3.2 (Equations 3.3.11a and 3.3.11b).

### 7.2.2 Evolution Law of Plastic Distortion

The same evolution law of plastic distortion introduced in section 5.7 (Equation 5.7.2) can be used in this case; the integration of the yield function over the cross-section of the element completes the evolution law:

$$\begin{cases} d\gamma^p = 0 & \text{if } f_s(V, p_s, x_s) < 0 \text{ (elastic behavior)} \\ f_s(V, p_s, x_s) = 0 & \text{if } d\gamma^p \neq 0 \text{ (plastic behavior)} \end{cases}; f_s(V, p_s, x_s) = |V - x_s| - (V_p + Q(p_s)) \leq 0 \quad (7.2.4)$$

where the shear force  $V$  is approximated as:

$$V \cong \frac{m_i^b + m_j^b}{L_b} \quad (7.2.5)$$

Again, there are at least two options for the variable  $p_s$ , the accumulated plastic distortion as defined in (7.2.6a) or the maximum plastic distortion as in (7.2.6b):

$$dp_s = |d\gamma^p| \text{ or } p_s = \text{Max}|\gamma^p| \quad (7.2.6)$$

As in the previous case, the shear yield function  $f_s$  can have isotropic and/or kinematic hardening terms; those terms can be nonlinear, multilinear or linear:

$$Q(p_s) = (1 - r_s)(V_u - V_p)(1 - e^{-\alpha_s p_s})$$

$$Q(p_s) = \begin{cases} \frac{(1 - r_s)(V_u - V_p)}{\gamma_u^p} p_s & \text{if } 0 \leq p_s \leq \gamma_u^p \\ (1 - r_s)(V_u - V_p) & \text{if } p_s > \gamma_u^p \end{cases}$$

$$Q(p_s) = (1 - r_s)c_s p_s \quad (7.2.7)$$

$$dx_s = \alpha \left( r_s (V_u - V_p) d\gamma^p - x_s \cdot |d\gamma^p| \right)$$

$$dx_s = \begin{cases} \frac{r_s (V_u - V_p)}{\gamma_u^p} d\gamma^p & \text{if } |x_s| < r_s (V_u - V_p) \\ 0 & \text{if } |x_s| = r_s (V_u - V_p) \end{cases}$$

$$x_s = r_s \cdot c_s \cdot \gamma^p \quad (7.2.8)$$

In the case of shear plasticity in RC elements, the recommended value of  $r_s$  is 0.6.

### 7.3 SHEAR PROPERTIES OF RC ELEMENTS

Consider the squat RC elements shown in Figure 5; in it, the geometrical characteristics, the longitudinal and transversal reinforcement are detailed.

## Elasto-Plastic Frames

The shear properties of a squat RC element needed for the elasto-plastic analysis of squat element are the first plastic shear force, the ultimate shear force and the ultimate plastic distortion that are indicated in Figure 6.

The first plastic shear force  $V_p$  is defined as the level of force that initiates yielding of the stirrups or ties in the element. This parameter can be computed using a simplified design method called “Strut-and-Tie Model”. The description of this method is outside the scope of this book and the interested reader should consult, for instance, the references indicated in the bibliography of this chapter. A simple equation that gives the value of the plastic shear force is:

$$V_p = k_p \frac{A_{sh} f_{yh} [\cot(\theta) + \cot(\beta)] \text{sen}(\beta)}{s} d \quad (7.3.1)$$

where  $A_{sh}$  is the area of stirrups,  $f_{yh}$  is the yield strength of the stirrups and the meaning of the terms  $s$  and  $d$  is indicated in Figure 5.  $\beta$  is the angle between the transversal and longitudinal reinforcement.  $\theta$  is the angle of inclination of the compression strut in the concrete that can be computed approximately assuming cracking patterns as the ones shown in Figure 7.  $k_p$  is a dimensionless coefficient that considers the efficiency of transversal reinforcement; it takes values between 0.40 for  $\beta = 90^\circ$  and 0.70 for  $\beta = 45^\circ$ . As it can be observed in this figure, in the case of a beam-column element  $\theta = 45^\circ$  and for a wall element this angle can be computed as:

$$\cot(\theta) = \frac{a}{d} \quad (7.3.2)$$

where  $a$  is the shear span, i.e., for a cantilever element  $a = L$  and for a doubled fixed element  $a = \frac{L}{2}$ .

For the most frequent case,  $\beta = 90^\circ$ , the plastic shear force becomes:

$$V_p = k_p \frac{A_{sh} f_{yh} [\cot(\theta)]}{s} d \quad (7.3.3)$$

A possibility for obtaining the ultimate shear force consists in using the following semi-empirical expression:

$$V_u = k_u \frac{A_{sh} \cdot f_{yh} \cdot d}{s} + k_u \left( \frac{0.5\sqrt{f'_c}}{a/d} \sqrt{1 + \frac{n}{0.5\sqrt{f'_c} A}} \right) 0.8A \quad (7.3.4)$$

$K_u$  is a dimensionless coefficient that takes the value of 1 for elements with aspect ratio less than 5 and 0.7 otherwise. Notice that, in (7.2.12), the ultimate shear force depends on the axial force  $n$  and the



Figure 5. Reinforcement and geometrical details in squat elements: a) wall b) beam-column

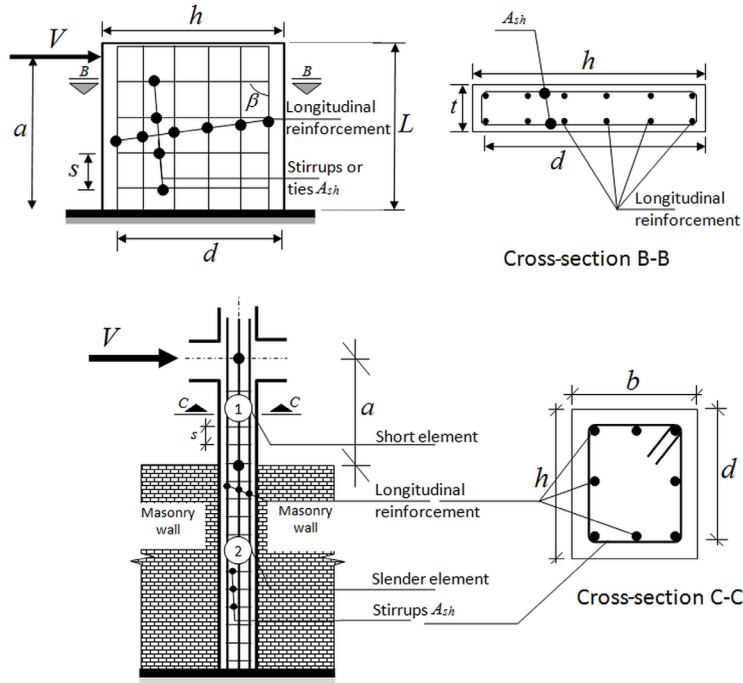
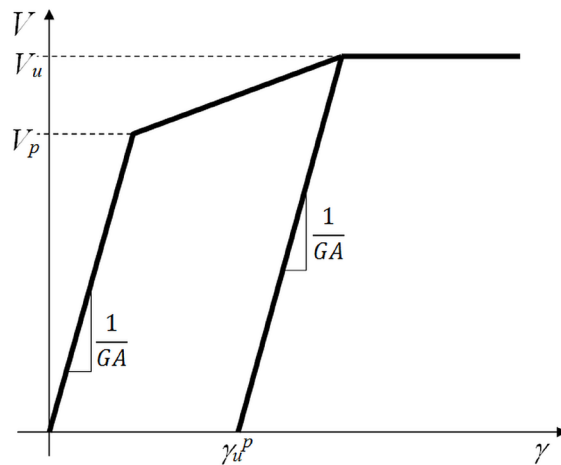


Figure 6. Shear force vs. angular deformation

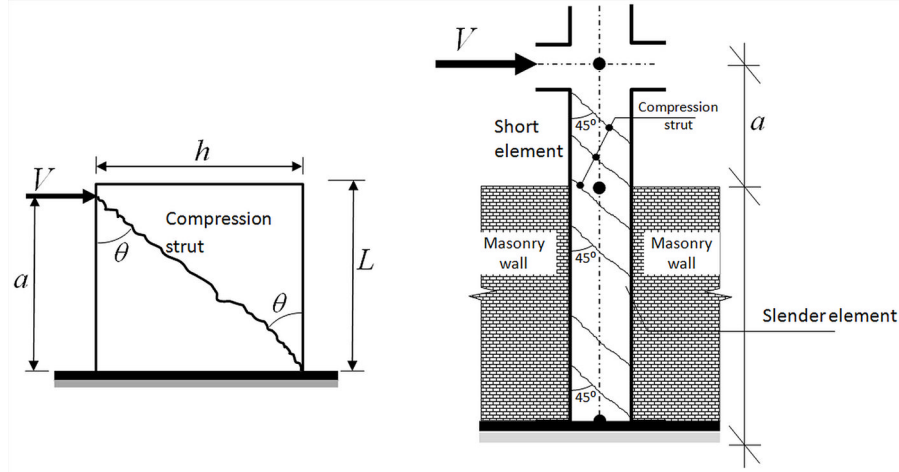


aspect ratio  $a/d$ ;  $f'_c$  is, as usual, the strength of the concrete cylinder in compression in MPa; notice that the term  $0.5\sqrt{f'_c}$  is expressed in terms of force over area, i.e. 0.5 is not dimensionless;  $A$  is the total area of the cross-section.

The ultimate plastic shear distortion can be computed by the expression:

## Elasto-Plastic Frames

Figure 7. Inclination of the compression strut in the concrete for: a) a wall element b) a beam-column element



$$\gamma_u^P = \frac{d}{L_{ps}} \left[ \left( \frac{f_{suh}}{E_s} + \frac{\varepsilon_{cu}}{\sin^2 \theta} \right) - \left( \frac{1}{\rho_{sh}} + \frac{2E_s}{E_c \sin^2 \theta} \right) \frac{f_{yh} A_{sh}}{E_s b s} \right] \quad (7.3.5)$$

where  $L_{ps}$  is a coefficient that can take values between  $0.1L$  to  $L$ ; a simple rule to choose an adequate value is using  $L_{ps} = 0.25L$  for high aspect ratios (i.e. larger than 5) and  $L_{ps} = L$  for low aspect ratios.  $f_{suh}$  is the ultimate strength of the transversal reinforcement;  $E_s$  and  $E_c$  are, respectively, the elasticity modulus of steel and concrete;  $\varepsilon_{cu}$  is the ultimate strain in the concrete ( $\varepsilon_{cu} = 0.004$  for non-confined concrete and  $\varepsilon_{cu} = 0.0084$  for confined concrete),  $\rho_{sh}$  is the volumetric ratio between transversal reinforcement and the concrete (see examples 7.7.1 and 7.7.2).

## 7.4 AN ELASTO-PLASTIC CONSTITUTIVE MODEL FOR ELEMENTS OF ANY ASPECT RATIO

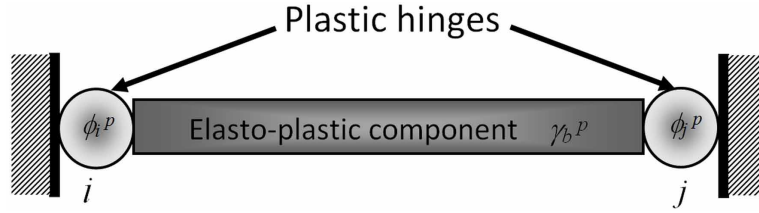
RC elements with an aspect ratio less than 2.5 can be classified as squat; for aspect ratios larger than 6.5 they are slender; between those limits, plastic hinges and shear plasticity may appear simultaneously. In this section it is presented a model that includes the previous ones as particular cases.

The elasticity law is now obtained on the basis of the lumped/distributed plasticity model shown in Figure 8. The frame element is therefore assumed to be the assemblage of an elasto-plastic component with shear plasticity and two plastic hinges at the ends of the element.

The frame deformations can be decomposed as:

$$\{\Phi\}_b = \{\Phi^{bcw}\}_b + \{\Phi^p\}_b \quad (7.4.1)$$

Figure 8. Lumped/distributed plasticity model



where  $\{\Phi^{bcw}\}_b$  is the matrix of generalized deformations of the elasto-plastic component and  $\{\Phi^p\}_b$  is the matrix of rotations of the plastic hinges neglecting plastic elongation. In the lumped/distributed plasticity model, the elasto-plastic component obeys the Equation (7.2.2); thus, the elasticity law derived from (7.3.1) is:

$$\{\Phi\}_b = ([\mathbf{F}_f]_b + [\mathbf{F}_s]_b)\{\mathbf{M}\}_b + \{\Phi^0\}_b + \{\gamma^p\}_b + \{\Phi^p\}_b \quad (7.4.2)$$

Alternatively:

$$\{\mathbf{M}\}_b = [\mathbf{E}]_b \{\Phi - \Phi^p - \gamma^p\}_b + \{\mathbf{M}^0\}_b; \text{ where } [\mathbf{E}]_b = ([\mathbf{F}_f]_b + [\mathbf{F}_s]_b)^{-1} \quad (7.4.3)$$

The evolution laws of the plastic deformations, those of the hinges and the one due to shear, are exactly the same that were introduced in the two previous sections, that is (7.1.9-16) and (7.2.4-8).

The behavior described by this constitutive equation is shown in the examples 7.6.4 and 7.6.5.

## 7.5 TRIDIMENSIONAL ELASTO-PLASTIC FRAMES

### 7.5.1 Constitutive Equations

Consider a tridimensional frame composed by slender elements; the generalized deformations and stresses are now defined as in (3.5.2) and (3.5.9):

$$\{\Phi\}_b^t = (\phi_{iy}^b, \phi_{jy}^b, \delta_b, \phi_{iz}^b, \phi_{jz}^b, \phi_x^b); \{\mathbf{M}\}_b^t = (m_{iy}^b, m_{jy}^b, n_b, m_{iz}^b, m_{jz}^b, m_x^b) \quad (7.5.1)$$

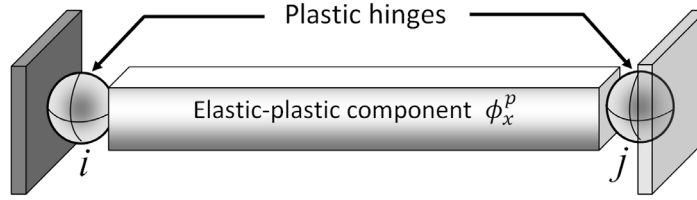
The elasticity law in this case is based on a lumped/distributed model similar to the one used in section 7.3 except that in this case, it is the plastic deformation due to torsion the one that is assumed as uniformly distributed along the element. A consequence of this simplifying assumption is the uncoupling between torsion and bending.

The elasticity law is now given by:

$$\{\mathbf{M}\}_b = [\mathbf{E}]_b \{\Phi - \Phi^p\}_b + \{\mathbf{M}^0\}_b; \{\Phi^p\}_b^t = (\phi_{iy}^p, \phi_{jy}^p, \delta_p, \phi_{iz}^p, \phi_{jz}^p, \phi_x^p) \quad (7.5.2)$$

## Elasto-Plastic Frames

Figure 9. Lumped/distributed model of a tridimensional frame element



Where the elasticity matrix  $[\mathbf{E}]_b$  has the same expression introduced in chapter 3 (3.5.14). The evolution laws of the plastic deformations are based again on three yield functions, one for plastic hinge  $i$ :  $f_i(m_{yi}^b, m_{zi}^b, n_b) \leq 0$ , another for plastic hinge  $j$ :  $f_j(m_{yj}^b, m_{zj}^b, n_b) \leq 0$  and a third one for plastic torsion:  $f_x(m_x^b) \leq 0$ . The yield functions of the plastic hinges may have the same expressions introduced in sections 6.4.4 or 6.5.7. The simplest form of the yield function for plastic torsion is:

$$f_x(m_x) = |m_x| - M_{ux} \leq 0 \quad (7.5.3)$$

where  $M_{ux}$  is the ultimate torque of the cross-section of the element.

The evolution laws of plastic deformations are now formulated as described in chapter 6:

$$d\phi_{yi}^p = d\lambda_i \frac{\partial f_i}{\partial m_{yi}}; d\phi_{yj}^p = d\lambda_j \frac{\partial f_j}{\partial m_{yj}}; d\phi_{zi}^p = d\lambda_i \frac{\partial f_i}{\partial m_{zi}}; d\phi_{zj}^p = d\lambda_j \frac{\partial f_j}{\partial m_{zj}}$$

$$d\delta_p = d\lambda_i \frac{\partial f_i}{\partial n} + d\lambda_j \frac{\partial f_j}{\partial n}$$

$$\begin{cases} d\lambda_i = 0 \text{ if } f_i(m_i, n) < 0 \\ f_i(m_i, n) = 0 \text{ if } d\lambda_i > 0 \end{cases}; \begin{cases} d\lambda_j = 0 \text{ if } f_j(m_j, n) < 0 \\ f_j(m_j, n) = 0 \text{ if } d\lambda_j > 0 \end{cases}; \begin{cases} d\phi_x^p = 0 \text{ if } f_x(m_x) < 0 \\ f_x(m_x) = 0 \text{ if } d\phi_x^p > 0 \end{cases} \quad (7.5.4)$$

Every one of the already described variations is, of course, possible. For instance, in the case of RC elements, plastic elongations can be neglected; the three yield functions can also be modified including isotropic and kinematic terms.

### 7.5.2 Computation of the Ultimate Plastic Torque for Thin-Walled Steel Elements

In section 5.7 it was indicated that thin-walled tubes with hollow circular shapes subjected to torsion can be considered as an isostatic problem. In fact, any thin-walled tube no matter the form of the cross-

section can also be considered as isostatic; shear stresses are approximately constant across the walls and they point in the direction tangent to them as shown in Figure 10.

The magnitude of the shear stresses can now be computed considering an equilibrium equation between torque and shear stress. It is thus obtained:

$$\tau = \frac{T}{2Ae} \quad (7.5.5)$$

where  $e$  is in this case the wall width and  $A$  is the mean of the areas enclosed by the outer and the inner boundaries of the cross-section of the tube (see Figure 10). If the steel hardening is considered, the ultimate torque  $T_u$  can be computed as:

$$T_u = 2\tau_u Ae \quad (7.5.6)$$

where  $\tau_u$  is the ultimate shear stress that can be experimentally identify as is shown in Figure 16 in Chapter 5. Alternatively  $\tau_u$  can be computed as:  $\tau_u = \frac{\sigma_u}{\sqrt{3}}$ .

### 7.5.3 Computation of the Ultimate Torque for Reinforced Concrete Elements

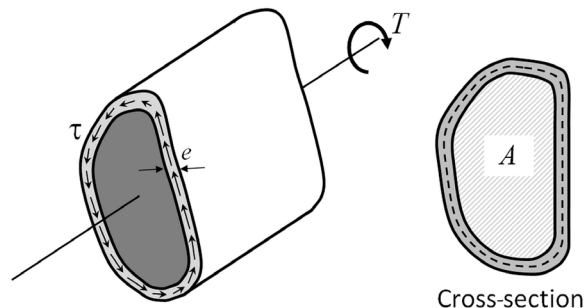
Figure 11 a shows a concrete element with rectangular cross-section subjected to a torque  $T$ .

The ultimate torque of a rectangular cross-section can be calculated based on the strut-and-tie model:

$$T_u = 2A_o \sqrt{\frac{\sum A_l f_{yl}}{p} \frac{A_s f_{yh}}{s}} \quad (7.5.7)$$

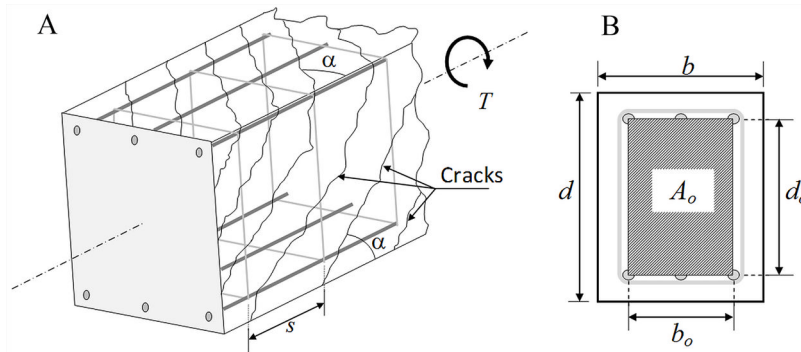
where  $A_o$  is the area enclosed by the line connecting the longitudinal corner bars ( $b_o$   $d_o$ ),  $p$  is the perimeter of  $A_o$  ( $2b_o + 2d_o$ ),  $s$  is the spacing of hoops (stirrups or ties),  $A_s f_{yh}$  is the yield force of one hoop,  $\sum A_l f_{yl}$  is the yield force of all longitudinal steel in a symmetrically reinforced section.

Figure 10. Shear stresses in a thin-walled tube



## Elasto-Plastic Frames

Figure 11. a) RC member subjected to a torque  $T$ . b) Definition of  $A_o$



## 7.6 SUMMARY AND EQUATIONS QUICK REFERENCE

Plasticity models for frame elements are based on the lumped plasticity hypothesis that consist in assuming that a slender frame element can be represented as the assemblage of an elastic beam-column and two plastic hinges at the ends of the element. A family of models can be obtained combining the lumped plasticity model with the plastic hinges described in chapter 6.

In dual systems, the elastic beam-column is substituted by an elasto-plastic component based on the theory of Timoshenko.

Models for tridimensional frame elements are obtained in the same way except that the elasto-plastic component describe torsion plasticity instead of shear plasticity (See Table 1).

Table 1.

ELASTO-PLASTIC CONSTITUTIVE MODEL FOR A SLENDER ELEMENT OF A PLANAR FRAME
<i>Lumped Plasticity Model</i>
Deformations of a frame member $\{\Phi\}_b = \{\Phi^{bc}\}_b + \{\Phi^p\}_b \quad (7.1.1)$ $\{\Phi^{bc}\}_b$ : matrix of generalized deformations of the elastic beam-column $\{\Phi^p\}_b$ : matrix of plastic deformations
Matrix of plastic deformations $\{\Phi^p\}_b = \begin{bmatrix} \phi_i^p \\ \phi_j^p \\ \delta^p \end{bmatrix} \quad (7.1.2)$ $\phi_i^p$ : rotation of plastic hinges $i$ $\phi_j^p$ : rotation of plastic hinges $j$ $\delta^p$ : plastic elongation of the element chord

continued on following page

Table 1. Continued

<p>Plastic elongation of the element</p> $\delta^p = \delta_i^p + \delta_j^p \quad (7.1.3)$
<p><b>Elasticity Law</b></p>
$\{\Phi\}_b = [F_f]_b \{M\}_b + \{\Phi^0\}_b + \{\Phi^p\}_b \quad (7.1.4)$ $\{M\}_b = [E]_b \{\Phi - \Phi^p\}_b + \{M^0\}_b \quad (7.1.5)$ <p><math>[F_f]_b</math> : flexibility matrix  <math>\{M\}_b</math> : generalized stresses matrix  <math>\{\Phi^0\}_b</math> : initial deformations matrix  <math>[E]_b = [F_f]_b^{-1}</math> : elasticity matrix  <math>\{M^0\}_b = -[E]_b \{\Phi^0\}_b</math> : matrix of initial stresses</p>
<p><b>Selection of the Rigidity Term EI in the Elasticity Law</b></p>
<p>Elastic modulus of concrete</p> $E_c = \frac{f'_c}{\epsilon_0} \quad (7.1.6)$ <p><math>f'_c</math> : maximum strength of concrete  <math>\epsilon_0 = 0.002</math> : strain in the concrete when the stress is <math>f'_c</math></p>
<p><b>Perfectly Plastic Constitutive Model</b></p>
<p>Elasticity law</p> $\{\Phi\}_b = [F_f]_b \{M\}_b + \{\Phi^0\}_b + \{\Phi^p\}_b \quad (7.1.4)$ $\{M\}_b = [E]_b \{\Phi - \Phi^p\}_b + \{M^0\}_b \quad (7.1.5)$
<p>Yield functions plastic hinges at the ends <math>i</math> and <math>j</math></p> $f_i = f_i(m_i, n) \leq 0; f_j = f_j(m_j, n) \leq 0 \quad (7.1.7)$
<p>Normality rule</p> $d\phi_i^p = d\lambda_i \frac{\partial f_i}{\partial m_i}; d\phi_j^p = d\lambda_j \frac{\partial f_j}{\partial m_j}; d\delta_p = d\lambda_i \frac{\partial f_i}{\partial n} + d\lambda_j \frac{\partial f_j}{\partial n} \quad (7.1.8)$
<p>Plastic multipliers evolution laws</p> $\left\{ \begin{array}{l} d\lambda_i = 0 \text{ if } f_i(m_i, n) < 0 \text{ (hinge } i \text{ is locked)} \\ f_i(m_i, n) = 0 \text{ if } d\lambda_i \neq 0 \text{ (hinge } i \text{ is active)} \end{array} \right\}; \left\{ \begin{array}{l} d\lambda_j = 0 \text{ if } f_j(m_j, n) < 0 \\ f_j(m_j, n) = 0 \text{ if } d\lambda_j \neq 0 \end{array} \right\} \quad (7.1.9)$ <p>where <math>\lambda_i</math> and <math>\lambda_j</math> are plastic multipliers of hinges <math>i</math> and <math>j</math></p>

continued on following page

## Elasto-Plastic Frames

Table 1. Continued

<i>Elastic Perfect Plastic Constitutive Model Neglecting Plastic Elongations</i>	
Elasticity law	$\{\Phi\}_b = [\mathbf{F}_f]_b \{\mathbf{M}\}_b + \{\Phi^0\}_b + \{\Phi^p\}_b$ (7.1.4)
	$\{\mathbf{M}\}_b = [\mathbf{E}]_b \{\Phi - \Phi^p\}_b + \{\mathbf{M}^0\}_b$ (7.1.5)
Evolution law	$\begin{cases} d\phi_i^p = 0 \text{ if } f_i(m_i) < 0 \text{ (hinge } i \text{ locked)} \\ f_i(m_i) = 0 \text{ if } d\phi_i^p \neq 0 \text{ (hinge } i \text{ active)} \end{cases}; f_i(m_i) =  m_i  - M_{yi} \leq 0$ $\delta_p = 0 \begin{cases} d\phi_j^p = 0 \text{ if } f_j(m_j) < 0 \text{ (hinge } j \text{ locked)} \\ f_j(m_j) = 0 \text{ if } d\phi_j^p \neq 0 \text{ (hinge } j \text{ active)} \end{cases}; f_j(m_j) =  m_j  - M_{yj} \leq 0$ <span style="float: right;">(7.1.10)</span>
<i>Elasto-Plastic Constitutive Model with Hardening</i>	
Elasticity law	$\{\Phi\}_b = [\mathbf{F}_f]_b \{\mathbf{M}\}_b + \{\Phi^0\}_b + \{\Phi^p\}_b$ (7.1.4)
	$\{\mathbf{M}\}_b = [\mathbf{E}]_b \{\Phi - \Phi^p\}_b + \{\mathbf{M}^0\}_b$ (7.1.5)
Evolution laws	$\begin{cases} d\phi_i^p = 0 \text{ if } f_i(m_i, p_i, x_i) < 0 \text{ (hinge } i \text{ locked)} \\ f_i(m_i, p_i, x_i) = 0 \text{ if } d\phi_i^p \neq 0 \text{ (hinge } i \text{ active)} \end{cases}$ $\delta_p = 0 \begin{cases} d\phi_j^p = 0 \text{ if } f_j(m_j, p_j, x_j) < 0 \text{ (hinge } j \text{ locked)} \\ f_j(m_j, p_j, x_j) = 0 \text{ if } d\phi_j^p \neq 0 \text{ (hinge } j \text{ active)} \end{cases}$ <span style="float: right;">(7.1.11)</span>
Yield functions	$f_i(m_i, p_i, x_i) =  m_i - x_i  - (M_{pi} + Q(p_i)) \leq 0; f_j(m_j, p_j, x_j) =  m_j - x_j  - (M_{pj} + Q(p_j)) \leq 0$ (7.1.12) $p_i$ and $p_j$ : accumulated plastic rotations or maximum plastic rotations
The accumulated plastic rotations	$dp_i =  d\phi_i^p ; dp_j =  d\phi_j^p $ (7.1.13)
Maximum plastic rotations	$p_i = \text{Max}  \phi_i^p ; p_j = \text{Max}  \phi_j^p $ (7.1.14)
Isotropic hardening terms	<p>Nonlinear: <math>Q(p_i) = (1 - r)(M_{ui} - M_{pi})(1 - e^{-\alpha p_i})</math></p> $Q(p_i) = \begin{cases} \frac{(1 - r)(M_{ui} - M_{pi})}{\phi_{ui}^p} p_i & \text{if } 0 \leq p_i \leq \phi_{ui}^p \\ (1 - r)(M_{ui} - M_{pi}) & \text{if } p_i > \phi_{ui}^p \end{cases}$ <p>Multilinear: <span style="float: right;">(7.1.15)</span></p> <p>Linear: <math>Q(p_i) = (1 - r)c_i \cdot p_i</math></p>

continued on following page



Table 1. Continued

Kinematic hardening terms	
Nonlinear:	$dx_i = \alpha \left( r(M_{ui} - M_{pi})d\phi_i^p - x_i \left  d\phi_i^p \right  \right)$
Multilinear:	$dx_i = \begin{cases} \frac{r(M_{ui} - M_{pi})}{\phi_{ui}^p} d\phi_i^p & \text{if }  m_i  < M_{ui} \\ 0 & \text{if }  m_i  = M_{ui} \end{cases} \quad (7.1.16)$
Linear:	$x_i = r c_i \phi_i^p$
<b>Constitutive Equations for Inelastic Hinges with Slip in RC Wide Beam-Column Connection</b>	
<b>Model with Slip Hinges</b>	
Elasticity law	
$\{\Phi\}_b = [F_f]_b \{M\}_b + \{\Phi^0\}_b + \{\Phi^p\}_b \quad (7.1.4)$	
$\{M\}_b = [E]_b \{\Phi - \Phi^p\}_b + \{M^0\}_b \quad (7.1.5)$	
Evolution laws	
$\begin{cases} d\phi_i^p = 0 & \text{if } f_i^{slip} < 0 \text{ (hinge } i \text{ locked)} \\ f_i^{slip} = 0 & \text{if } d\phi_i^p \neq 0 \text{ (hinge } i \text{ active)} \end{cases}$	
$\delta_p = 0$	
$\begin{cases} d\phi_j^p = 0 & \text{if } f_j^{slip} < 0 \text{ (hinge } j \text{ locked)} \\ f_j^{slip} = 0 & \text{if } d\phi_j^p \neq 0 \text{ (hinge } j \text{ active)} \end{cases} \quad (7.1.17)$	
Slip functions	
$f_i^{slip} =  m_i  - M_{oi} e^{(sign(m_i)\eta_i\phi_i^p)} \leq 0; f_j^{slip} =  m_j  - M_{oj} e^{(sign(m_j)\eta_j\phi_j^p)} \leq 0 \quad (7.1.18)$	
Parameters $\eta_i$ and $\eta_j$	
$\eta_i = \frac{\ln \left( \frac{0.4M_{ui} - 0.4M_{pi} + M_{pi}}{M_{oi}} \right)}{0.4\phi_{ui}^p}; \eta_j = \frac{\ln \left( \frac{0.4M_{uj} - 0.4M_{pj} + M_{pj}}{M_{oj}} \right)}{0.4\phi_{uj}^p} \quad (7.1.19)$	
Model that combines the slip and yielding mechanisms	
Elasticity law	
$\{\Phi\}_b = [F_f]_b \{M\}_b + \{\Phi^0\}_b + \{\Phi^p\}_b \quad (7.1.4)$	
$\{M\}_b = [E]_b \{\Phi - \Phi^p\}_b + \{M^0\}_b \quad (7.1.5)$	

continued on following page

## Elasto-Plastic Frames

Table 1. Continued

<p>Evolution laws</p> $\begin{cases} d\phi_i^p = 0 \text{ if } f_i < 0 \text{ (hinge } i \text{ locked)} \\ f_i = 0 \text{ if } d\phi_i^p \neq 0 \text{ (hinge } i \text{ active)} \end{cases}$ $\delta_p = 0$ $\begin{cases} d\phi_j^p = 0 \text{ if } f_j < 0 \text{ (hinge } j \text{ locked)} \\ f_j = 0 \text{ if } d\phi_j^p \neq 0 \text{ (hinge } j \text{ active)} \end{cases} \quad (7.1.20)$
<p>Inelastic functions</p> $f_i = \text{Max}(f_i^y, f_i^{\text{slip}}); f_j = \text{Max}(f_j^y, f_j^{\text{slip}}) \quad (7.1.21)$ <p><math>f_i^y</math> and <math>f_j^y</math> : yield functions in the hinges <math>i</math> and <math>j</math>  <math>f_i^{\text{slip}}</math> and <math>f_j^{\text{slip}}</math> : slip functions in the hinges <math>i</math> and <math>j</math></p>
<b>ELASTO-PLASTIC CONSTITUTIVE MODEL FOR SQUAT RC ELEMENTS</b>
<i>Elasticity Law</i>
<p>Matrix of plastic deformations</p> $\{\gamma^p\}_b = \begin{bmatrix} \gamma_b^p \\ \gamma_b^p \\ 0 \end{bmatrix} \quad (7.2.1)$ <p><math>\gamma_b^p</math> : plastic distortion or plastic angular strain</p>
<p>Elasticity law</p> $\{\Phi\}_b = ([\mathbf{F}]_b + [\mathbf{F}_s]_b)\{\mathbf{M}\}_b + \{\Phi^0\}_b + \{\gamma^p\}_b \quad (7.2.2)$ $\{\mathbf{M}\}_b = [\mathbf{E}]_b\{\Phi - \gamma^p\}_b + \{\mathbf{M}^0\}_b \quad (7.2.3)$ <p><math>[\mathbf{F}]_b</math> : flexure flexibility matrix  <math>[\mathbf{F}_s]_b</math> : shear flexibility matrix  <math>\{\Phi^0\}_b</math> : matrix of initial deformations  <math>[\mathbf{E}]_b</math> : elasticity matrix  <math>\{\mathbf{M}^0\}_b</math> : matrix of initial stresses</p>

continued on following page

Table 1. Continued

<i>Evolution Law of Plastic Distortion</i>	
Evolution law $\begin{cases} d\gamma_p = 0 & \text{if } f_s(V, p_s, x_s) < 0 \text{ (elastic behavior)} \\ f_s(V, p_s, x_s) = 0 & \text{if } d\gamma_p \neq 0 \text{ (plastic behavior)} \end{cases}$ $f_s(V, p_s, x_s) =  V - x_s  - (V_p + Q(p_s)) \leq 0 \quad (7.2.4)$	
Shear force $V \cong \frac{m_i^b + m_j^b}{L_b} \quad (7.2.5)$	
Accumulated plastic distortion $dp_s =  d\gamma^p  \quad (7.2.6a)$	
Maximum plastic distortion $p_s = \text{Max}  \gamma^p  \quad (7.2.6b)$	
Isotropic hardening terms Nonlinear: $Q(p_s) = (1 - r_s)(V_u - V_p)(1 - e^{-\alpha_s p_s})$ $Q(p_s) = \begin{cases} \frac{(1 - r_s)(V_u - V_p)}{\gamma_u^p} p_s & \text{if } 0 \leq p_s \leq \gamma_u^p \\ (1 - r_s)V_u - V_p & \text{if } p_s > \gamma_u^p \end{cases} \quad (7.2.7)$ Multilinear: Linear: $Q(p_s) = (1 - r_s)c_s p_s$	
Kinematic hardening terms Nonlinear: $dx_s = \alpha \left( r_s (V_u - V_p) d\gamma^p - x_s \cdot  d\gamma^p  \right)$ $dx_s = \begin{cases} \frac{r_s (V_u - V_p)}{\gamma_u^p} d\gamma^p & \text{if }  x_s  < r_s (V_u - V_p) \\ 0 & \text{if }  x_s  = r_s (V_u - V_p) \end{cases} \quad (7.2.8)$ Multilinear: Linear: $x_s = r_s \cdot c_s \cdot \gamma^p$ The recommended value of $r_s$ is 0.6	

continued on following page

## Elasto-Plastic Frames

Table 1. Continued

SHEAR PROPERTIES OF RC ELEMENTS	
<p>First plastic shear</p> $V_p = k_p \frac{A_{sh} f_{yh} [\cot(\theta) + \cot(\beta)] \sin(\beta)}{s} d \quad (7.3.1)$ <p> <math>A_{sh}</math>: area of stirrups  <math>f_{yh}</math>: yield strength of the stirrups  <math>s</math>: center-to-center spacing of transverse reinforcement  <math>d</math>: distance from extreme compression fiber to centroid of longitudinal tension reinforcement  <math>\beta</math> is the angle between the transversal and longitudinal reinforcement  <math>k_p</math>: dimensionless coefficient = 0.40 for <math>\beta = 90^\circ</math> and 0.70 for <math>\beta = 45^\circ</math>.  <math>\theta</math>: of inclination of the compression strut in the concrete. For a beam-column element <math>\theta = 45^\circ</math>, for a wall element: </p> $\cot(\theta) = \frac{a}{d} \quad (7.3.2)$ <p>           If <math>\beta = 90^\circ</math> <math display="block">V_p = k_p \frac{A_{sh} f_{yh} [\cot(\theta)]}{s} d \quad (7.3.3)</math> </p>	
<p>Ultimate shear</p> $V_u = k_u \frac{A_{sh} \cdot f_{yh} \cdot d}{s} + k_u \left( \frac{0.5\sqrt{f'_c}}{a/d} \sqrt{1 + \frac{n}{0.5\sqrt{f'_c} A}} \right) 0.8A \quad (7.3.4)$ <p> <math>A</math>: total area of the cross-section  <math>a/d</math>: aspect ratio  <math>K_u</math>: dimensionless coefficient = 1 for elements with <math>a/d &lt; 5</math> and 0.7 otherwise.  <math>f'_c</math>: strength of the concrete cylinder in compression in MPa  <math>n</math>: axial force. </p>	
<p>The ultimate plastic shear distortion</p> $\gamma_u^P = \frac{d}{L_{ps}} \left[ \left( \frac{f_{sub}}{E_s} + \frac{\varepsilon_{cu}}{\sin^2 \theta} \right) - \left( \frac{1}{\rho_{sh}} + \frac{2E_s}{E_c \sin^2 \theta} \right) \frac{f_{yh} A_{sh}}{E_s b s} \right] \quad (7.3.5)$ <p> <math>L_{ps}</math>: coefficient that can take values between <math>0.1L</math> to <math>L</math>.  <math>(L_{ps} = 0.25L</math> for <math>a/d \geq 5</math>, <math>L_{ps} = L</math> for <math>a/d &lt; 5</math>).  <math>f_{sub}</math>: ultimate strength of the transversal reinforcement  <math>E_s</math>: elasticity modulus of steel  <math>E_c</math>: elasticity modulus of the concrete  <math>\rho_{sh}</math>: volumetric ratio between transversal reinforcement and the concrete  <math>\varepsilon_{cu}</math>: ultimate strain in the concrete  <math>(\varepsilon_{cu} = 0.004</math> for non-confined concrete)  <math>(\varepsilon_{cu} = 0.0084</math> for confined concrete) </p>	

continued on following page

Table 1. Continued

AN ELASTO-PLASTIC CONSTITUTIVE MODEL FOR ELEMENTS OF ANY ASPECT RATIO
<i>Lumped/Distributed Plasticity Model</i>
<p>Frame deformations</p> $\{\Phi\}_b = \{\Phi^{bcw}\}_b + \{\Phi^p\}_b \quad (7.4.1)$ <p><math>\{\Phi^{bcw}\}_b</math> : matrix of generalized deformations of the elastic beam-column-wall</p> <p><math>\{\Phi^p\}_b</math> : matrix of rotations of the plastic hinges neglecting plastic elongation</p>
<p>Elasticity law</p> $\{\Phi\}_b = ([F_f]_b + [F_s]_b)\{M\}_b + \{\Phi^0\}_b + \{\gamma^p\}_b + \{\Phi^p\}_b \quad (7.4.2)$ $\{M\}_b = [E]_b\{\Phi - \Phi^p - \gamma^p\}_b + \{M^0\}_b \quad (7.4.3)$ $[E]_b = ([F_f]_b + [F_s]_b)^{-1}$
TRIDIMENSIONAL ELASTO-PLASTIC FRAMES
<i>Constitutive Equations</i>
<p>Generalized deformations</p> $\{\Phi\}_b^t = (\phi_{iy}^b, \phi_{jy}^b, \delta_b, \phi_{iz}^b, \phi_{jz}^b, \phi_x^b) \quad 7.5.1a$
<p>Generalized stress</p> $\{M\}_b^t = (m_{iy}^b, m_{jy}^b, n_b, m_{iz}^b, m_{jz}^b, m_x^b) \quad (7.5.1b)$
<p>Elasticity law</p> $\{M\}_b = [E]_b\{\Phi - \Phi^p\}_b + \{M^0\}_b \quad (7.5.2a)$
<p>Generalized plastic deformations</p> $\{\Phi^p\}_b^t = (\phi_{iy}^p, \phi_{jy}^p, \delta_p, \phi_{iz}^p, \phi_{jz}^p, \phi_x^p) \quad (7.5.2b)$
<p>Yield function for plastic hinge <i>i</i></p> $f_i(m_{yi}^b, m_{zi}^b, n_b) \leq 0 \quad (\text{see chapter 6})$
<p>Yield function for plastic hinge <i>j</i></p> $f_j(m_{yj}^b, m_{zj}^b, n_b) \leq 0 \quad (\text{see chapter 6})$
<p>The yield function for plastic torsion</p> $f_x(m_x) =  m_x  - M_{ux} \leq 0 \quad (7.5.3)$ <p><math>M_{ux}</math> : ultimate torque of the element cross-section</p>

continued on following page

**Elasto-Plastic Frames**

Table 1. Continued

<p>The plastic deformation evolution laws</p> $d\phi_{yi}^p = d\lambda_i \frac{\partial f_i}{\partial m_{yi}} \quad d\phi_{yj}^p = d\lambda_j \frac{\partial f_j}{\partial m_{yj}} \quad d\phi_{zi}^p = d\lambda_i \frac{\partial f_i}{\partial m_{zi}} \quad d\phi_{zj}^p = d\lambda_j \frac{\partial f_j}{\partial m_{zj}}$ $d\delta_p = d\lambda_i \frac{\partial f_i}{\partial n} + d\lambda_j \frac{\partial f_j}{\partial n} \quad (7.5.4)$ $\begin{cases} d\lambda_i = 0 & \text{if } f_i(m_i, n) < 0 \\ f_i(m_i, n) = 0 & \text{if } d\lambda_i > 0 \end{cases} ; \begin{cases} d\lambda_j = 0 & \text{if } f_j(m_j, n) < 0 \\ f_j(m_j, n) = 0 & \text{if } d\lambda_j > 0 \end{cases}$ $\begin{cases} d\phi_x^p = 0 & \text{if } f_x(m_x) < 0 \\ f_x(m_x) = 0 & \text{if } d\phi_x^p > 0 \end{cases}$
<p><b>Computation of the Ultimate Plastic Torque for Thin-Walled Steel Elements</b></p>
<p>Shear stress</p> $\tau = \frac{T}{2Ae} \quad (7.5.5)$ <p><i>e</i>: wall width  <i>A</i>: mean of the areas enclosed by the outer and the inner boundaries of the cross-section of the tube</p>
<p>Ultimate torque <math>T_u</math></p> $T_u = 2\tau_u Ae \quad (7.5.6)$ <p><math>\tau_u</math>: ultimate shear stress</p> $\tau_u = \frac{\sigma_u}{\sqrt{3}}$ <p>(It can be experimentally identify or computed as:</p>
<p><b>Computation of the Ultimate Torque for Reinforced Concrete Elements</b></p>
<p>Ultimate torque of a rectangular section</p> $T_u = 2A_o \sqrt{\frac{\sum A_l f_{yl}}{p} \frac{A_s f_{yh}}{s}} \quad (7.5.7)$ <p><math>A_o</math>: area enclosed by the line connecting the longitudinal corner bars (<math>b_o \quad d_o</math>)  <i>p</i>: perimeter of <math>A_o</math> (<math>2b_o + 2d_o</math>)  <i>s</i>: spacing of hoops (stirrups or ties)  <math>A_s f_{yh}</math>: yield force of one hoop  <math>\sum A_l f_{yl}</math>: yield force of all longitudinal steel in a symmetrically reinforced section</p>

## 7.7 EXAMPLES

### 7.7.1 Compute the Shear Properties of the Element Shown in Figure 12. Consider an Aspect Ratio Equal to 1.26, a Non-Confined Concrete and Nil Axial Force.

The first plastic shear is computed using Equation (7.2.11). The aspect ratio is  $a / d = \cot(\theta) = 1.26$ ,  $k_p = 0.4$  and as it can be observed in the Figure 12,  $A_{sh} = 1.42 \times 10^{-4} \text{ m}^2$ ,  $s = 0.30 \text{ m}$ , and  $d = 0.475 \text{ m}$ , thus,

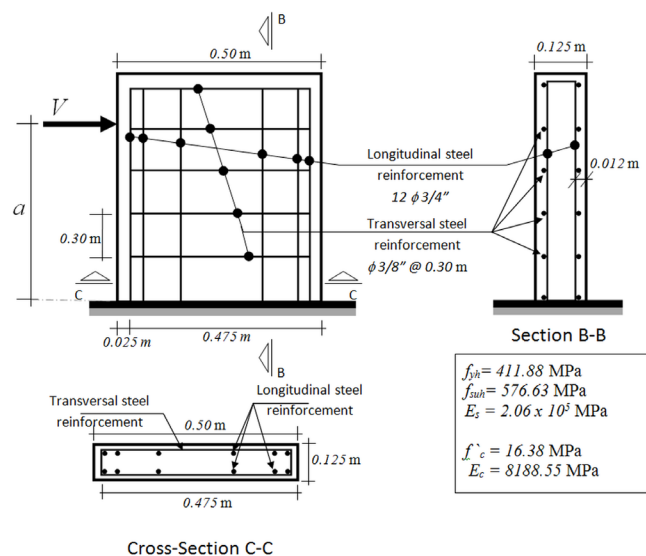
$$V_p = k_p \frac{A_{sh} f_{yh} [\cot(\theta)]}{s} d = 46.673 \text{ KN} \quad (7.7.1)$$

The ultimate shear force is computed by Equation (7.2.12) with  $A = b \cdot h = 0.5 \times 0.125 = 0.0625 \text{ m}^2$ ,  $k_u = 1$  and  $n = 0$ . Therefore:

$$V_u = k_u \frac{A_{sh} \cdot f_{yh} \cdot d}{s} + k \left( \frac{0.5 \sqrt{f'_c}}{a / d} \sqrt{1 + \frac{n}{0.5 \sqrt{f'_c} A}} \right) 0.8A = 172.906 \text{ KN} \quad (7.7.2)$$

The last shear property is the ultimate plastic shear distortion. It can be computed using Equation (7.2.13), where  $\varepsilon_{cu} = 0.004$  for non-confined concrete,  $\theta = \tan^{-1}(d / a) = 0.671 \text{ rad}$ , the volumetric ratio between transversal reinforcement and concrete is computed as:

Figure 12. RC wall element



### Elasto-Plastic Frames

$$\rho_{sh} = \frac{Vol_s}{Vol_c} = \frac{A_{sh} / 2 x L_{stirrup}}{b h s} = \frac{0.71 x 10^{-4} x 1.154}{0.125 x 0.5 x 0.30} = 0.00437 \quad (7.7.3)$$

where  $L_{stirrups} = 2 [0.125 - 2(0.012)] + 2 [0.5 - 2(0.012)] = 1.154$  m Therefore:

$$\gamma_u^P = \frac{d}{L_{ps}} \left[ \left( \frac{f_{suh}}{E_s} + \frac{\epsilon_{cu}}{\sin^2 \theta} \right) - \left( \frac{1}{\rho_{sh}} + \frac{2E_s}{E_c \sin^2 \theta} \right) \frac{f_{yh} A_{sh}}{E_s b s} \right] = 0.00827612 \text{ rad} \quad (7.7.4)$$

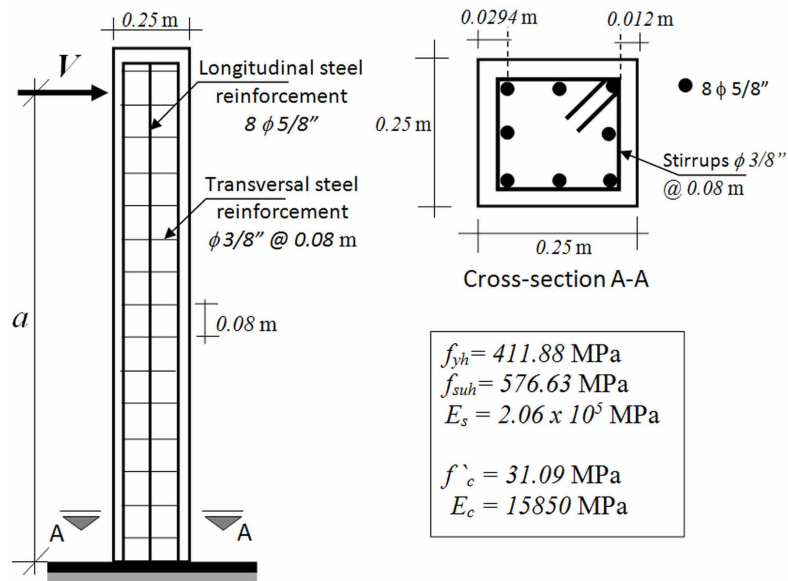
where  $L_{ps} = L = a = 1.26 x 0.475 = 0.5985$  m

### 7.7.2 Compute the Shear Properties of the Element Shown in Figure 13. Consider an Aspect Ratio Equal to 7.11, Confined Concrete and Nil Axial Force.

Again, the first plastic shear is computed using Equation (7.2.11), but in the case,  $\theta = 45^\circ$  because it is a slender element,  $A_{sh} = 1.42 x 10^{-4} \text{ m}^2$ ,  $k_p = 0.4$ ,  $s = 0.08$  m and  $d = 0.225$  m, then,

$$V_p = k_p \frac{A_{sh} f_{yh} [\cot(\theta)]}{s} d = 65.798 \text{ KN} \quad (7.7.5)$$

Figure 13. RC beam-column element





The ultimate shear force is computed by Equation (7.2.12), where  $A = b \cdot h = 0.25 \times 0.25 = 0.0625 \text{ m}^2$ ,  $k_u = 0.7$  and  $n = 0$ .

$$V_u = k_u \frac{A_{sh} \cdot f_{yh} \cdot d}{s} + k_u \left( \frac{0.5\sqrt{f'_c}}{a/d} \sqrt{1 + \frac{n}{0.5\sqrt{f'_c} A}} \right) 0.8A = 128.870 \text{ KN} \quad (7.7.6)$$

The ultimate plastic shear distortion can be computed using Equation (7.2.13), where  $\varepsilon_{cu} = 0.008$  for confined concrete,  $\theta = \tan^{-1} \left( \frac{\pi}{4} \right) = 0.7854 \text{ rad}$ ; the volumetric ratio between transversal reinforcement and concrete is computed as:

$$\rho_{sh} = \frac{Vol_s}{Vol_c} = \frac{A_{sh} / 2 \times L_{stirrup}}{b h s} = \frac{0.71 \times 10^{-4} \times 0.904}{0.25 \times 0.25 \times 0.08} = 0.01284 \quad (7.7.7)$$

where  $L_{stirrups} = 4(0.25 - 2(0.012)) = 0.904 \text{ m}$

$$\gamma_u^P = \frac{d}{L_{ps}} \left[ \left( \frac{f_{suh}}{E_s} + \frac{\varepsilon_{cu}}{\sin^2 \theta} \right) - \left( \frac{1}{\rho_{sh}} + \frac{2E_s}{E_c \sin^2 \theta} \right) \frac{f_{yh} A_{sh}}{E_s b s} \right] = 9.539 \text{ E} - 03 \text{ rad} \quad (7.7.8)$$

where  $L_{ps} = 0.25L = 0.25 a = 0.25 \times (7.11 \times 0.225) = 0.3999375 \text{ m}$

### 7.7.3 Compute the Ultimate Plastic Torque for the Element Shown in Figure 13

In this case,  $b_o = d_o = 0.1912 \text{ m}$ ,  $A_o = 0.0366 \text{ m}^2$ ,  $A_l = 8 (1.979 \times 10^{-4}) = 15.832 \times 10^{-4} \text{ m}^2$ ,  $A_s = 0.713 \times 10^{-4} \text{ m}^2$ ,  $f_{yl} = f_{yh} = 411.88 \times 10^6 \text{ N/m}^2$ ,  $p = 0.7648 \text{ m}$  and  $s = 0.08 \text{ m}$ . Thus,

$$T_u = 2A_o \sqrt{\frac{A_l f_{yl}}{p} \frac{A_s f_{yh}}{s}}$$

$$T_u = 2 (0.0366) \sqrt{\frac{15.832 \times 10^{-4} \times 411.88 \times 10^6}{0.7648} \frac{0.713 \times 10^{-4} \times 411.88 \times 10^6}{0.08}} = 40952 .04 \text{ Nm} \quad (7.7.9)$$

**7.7.4 Obtain the Force-Displacement Curve for the RC Wall Element Shown in Figure 12 using the Multi-Linear Elasto-Plastic Model Described in Section 7.3. Neglect Kinematic Hardening, Consider Aspect Ratios a/d Equal to 1.26, 1.68 and 2.11 and nil axial force.**

First, the bending properties  $M_p$ ,  $M_u$  and  $\phi_u^p$  are computed according to the procedures described in section 6.5.4; next, the shear ones,  $V_p$ ,  $V_u$  and  $\gamma_u^p$ , are determined as it is described in section 7.2.3. These values are presented in Table 2.

The problem is then solved considering a monotonic lateral load that increase from 0 to  $V_u$ , each 1.25 KN. For any load level, the corresponding displacement ( $u$ ) is computed as:

$$u = \phi_i a \tag{7.7.10}$$

$\phi_i$  is calculated with the first term of the elasticity law (7.3.2), where  $\phi_i^0$  is equal to zero because there are no loads along the element. Thus,

$$\phi_i = \left( \frac{L_b}{3EI_b} + \frac{1}{L_b GA_b} \right) m_i + \gamma^p + \phi_i^p \tag{7.7.11}$$

where  $L_b = a$ ,  $I_b = \frac{0.125 \times 0.5^3}{12} = 0.00130208 \text{ m}^4$ ,  $A_b = 0.125 \times 0.5 = 0.0625 \text{ m}^2$  and  $m_i = Va$ .

The plastic rotation  $\phi_i^p$  is computed with the plastic deformation evolution laws (7.1.1), the yield function (7.1.12), the isotropic hardening term (7.1.15) and the maximum plastic rotation (7.1.14) without considering the kinematic hardening term:

$$\begin{cases} d\phi_i^p = 0 \text{ if } f_i(m_i, p_i) < 0 \text{ (hinge } i \text{ locked)} \\ f_i(m_i, p_i) = 0 \text{ if } d\phi_i^p \neq 0 \text{ (hinge } i \text{ active)} \end{cases}; f_i(m_i, p_i) = |m_i| - (M_{pi} + Q(p_i)) \leq 0;$$

$$Q(p_i) = \begin{cases} \frac{(M_{ui} - M_{pi})}{\phi_{ui}^p} p_i \text{ if } 0 \leq p_i \leq \phi_{ui}^p; p_i = \text{Max} |\phi_i^p|; \\ M_{ui} - M_{pi} \text{ if } p_i > \phi_{ui}^p \end{cases}; \tag{7.7.12}$$

Table 2. Bending and shear properties for the walls with aspect ratios a/d equal to 1.26, 1.68 and 2.11.

a/d	$M_p$ (KN m)	$M_u$ (KN m)	$\phi_u^p$	$V_p$ (KN)	$V_u$ (KN)	$\gamma_u^p$
1.26	208.00	212.00	0.046	46.673	172.906	8.276E-03
1.68	208.00	212.00	0.046	62.230	152.831	8.869E-03
2.11	208.00	212.00	0.046	78.158	140.557	9.857 E-03

The plastic distortion  $\gamma^p$  is computed with the shear distortion evolution laws (7.2.4), the isotropic hardening term (7.2.7b) and the maximum plastic distortion as in (7.2.6b); again, it is not considered the kinematic hardening term:

$$\begin{cases} d\gamma_p = 0 \text{ if } f_s(V, p_s) < 0 \text{ (elastic behavior)} \\ f_s(V, p_s) = 0 \text{ if } d\gamma_p \neq 0 \text{ (plastic behavior)} \end{cases}; f_s(V, p_s) = |V| - (V_p + Q(p_s)) \leq 0 \quad ;$$

$$f_s(V, p_s) = |V| - (V_p + Q(p_s)) \leq 0$$

$$Q(p_s) = \begin{cases} \frac{(V_u - V_p)}{\gamma_u^p} p_s \text{ if } 0 \leq p_s \leq \gamma_u^p; p_s = \text{Max}|\gamma^p| \\ V_u - V_p \text{ if } p_s > \gamma_u^p \end{cases} \quad (7.7.13)$$

Tables 3, 4 and 5 show the spreadsheet used for the solution with an aspect ratio equal to 1.26. Column A presents the chosen lateral loads. Columns B and C show respectively, the computed maximum plastic shear distortion and the maximum plastic rotation. In columns D and E, the shear and bending yield functions are presented. In column F and G, the rotation and the resultant displacement are shown. Notice that in the first steps, while both yield functions are negative, the maximum plastic shear distortion and maximum plastic rotation are nil and the rotation is computed with the first term of the Equation (7.6.11).

This procedure continues until the shear yield function become positive for a  $V = 47.50$  KN (see Table 4). After that, the maximum plastic distortion  $p_s$  is computed as follows:

$$f_s(V, p_s) = |V| - (V_p + Q(p_s)) = 0; Q(p_s) = \frac{(V_u - V_p)}{\gamma_u^p} p_s; \text{resulting } p_s = \gamma^p = \frac{(|V| - V_p) \gamma_u^p}{(V_u - V_p)} \quad (7.7.14)$$

Thus, the rotation is computed with Equation (7.6.11) and the displacement with Equation (7.6.10).

This procedure continues until  $V_u$  is reached (see Table 5). Then the behavior is represented by a horizontal line as it is shown in Figure 14.

The force displacement curves corresponding to aspect ratios equal to 1.68 and 2.11 were computed following the same procedure. Table 6 shows the first steps of the computation with an aspect ratio equal to 1.68.

The shear yield function become positive, for a  $V = 62.23$  KN; from this instant, the maximum plastic distortion  $p_s$  is computed with Equation (7.6.13) as it is shown in Table 7.

Table 8. includes the steps when  $V_u$  is reached.

Table 9 presents the first steps of the computation with an aspect ratio equal to 2.11.

The shear yield function become positive, for a  $V = 78.16$  KN and, again, from this instant, the maximum plastic distortion  $p_s$  is computed with Equation (7.6.13) as it is shown in Table 10.

Table 11 includes the steps when  $V_u$  is reached.

Figure 14. shows the force-displacement curves for the three aspect ratios. Figure 15 presents the plastic distortion and plastic rotation evolution for the three aspect ratios.

## Elasto-Plastic Frames

Table 3. First steps of the solution of the wall with an aspect ratio equal to 1.26

A	B	C	D	E	F	G
V (KN)	$\gamma^p$	$\phi_i^p$	$f_s$ (KN)	$f_i$ (KN-m)	$\phi_i$	$u$ (m)
0.000	0.000	0.000	-46.670	-208.000	0.000E+00	0.000E+00
1.250	0.000	0.000	-45.420	-207.252	1.791E-05	1.072E-05
2.500	0.000	0.000	-44.170	-206.504	3.581E-05	2.143E-05

Table 4. Steps near the instant when the shear yield function becomes zero with an aspect ratio equal to 1.26

A	B	C	D	E	F	G
V (KN)	$\gamma^p$	$\phi_i^p$	$f_s$ (KN)	$f_i$ (KN-m)	$\phi_i$	$u$ (m)
45.000	0.000E+00	0.000	-1.670	-181.068	6.446E-04	3.858E-04
46.250	0.000E+00	0.000	-0.420	-180.319	6.625E-04	3.965E-04
47.500	5.442E-05	0.000	0.000	-179.571	7.347E-04	4.397E-04
48.750	1.364E-04	0.000	0.000	-178.823	8.344E-04	4.994E-04

Table 5. Final part of the solution with an aspect ratio equal to 1.26

A	B	C	D	E	F	G
V (KN)	$\gamma^p$	$\phi_i^p$	$f_s$ (KN)	$f_i$ (KN-m)	$\phi_i$	$u$ (m)
171.250	8.168E-03	0.000	0.000	-109.507	1.062E-02	6.356E-03
172.500	8.250E-03	0.000	0.000	-108.759	1.072E-02	6.416E-03
172.906	8.276E-03	0.000	0.000	-108.516	1.075E-02	6.436E-03
172.906	1.423E-02	0.000	0.000	-108.516	1.671E-02	1.000E-02

### 7.7.5 Obtain the Force- Displacement Curve for the RC Element Shown in Figure 13 Using the Multi-Linear Elasto-Plastic Model Described in Section 7.3. Neglect Kinematic Hardening and Consider Aspect Ratios a/d Equal to 1.78, 3.55 and 7.11.

First, the bending properties  $M_p$ ,  $M_u$  and  $\phi_u^p$  are computed according to the procedures described in section 6.5.4; the shear ones,  $V_p$ ,  $V_u$  and  $\gamma_u^p$ , are determined as described in section 7.2.3. These values are presented in Table 12.

In the present case, the problem is solved in a similar way than in the former example using Equations (7.7.10 to 7.7.13) again; a monotonic lateral loading is applied with increments of 1.25 KN.

Figure 14. Force-displacement curves with aspect ratios equal to 1.26, 1.68 and 2.11

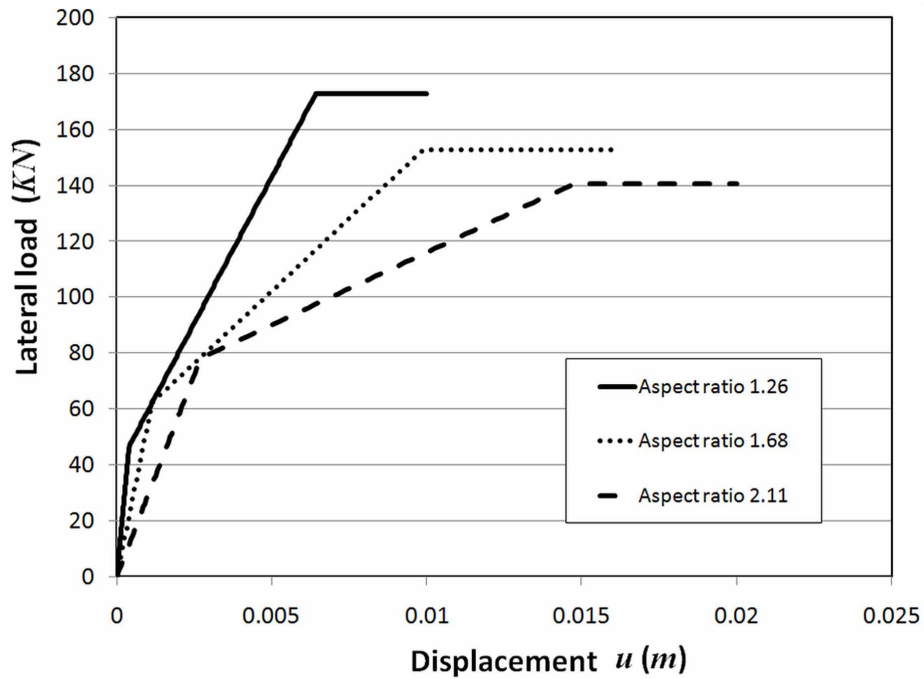


Table 6. First steps of the solution with an aspect ratio equal to 1.68

A	B	C	D	E	F	G
V (kN)	$\gamma^p$	$\phi_i^p$	$f_s$ (kN)	$f_i$ (kN-m)	$\phi_i$	$u$ (m)
0.000	0.000	0.000	-62.230	-208.000	0.000E+00	0.000E+00
1.250	0.000	0.000	-60.980	-207.003	2.879E-05	2.298E-05
2.500	0.000	0.000	-59.730	-206.005	5.759E-05	4.595E-05

Table 7. Steps when the shear yield function becomes zero with an aspect ratio equal to 1.68

A	B	C	D	E	F	G
V (kN)	$\gamma^p$	$\phi_i^p$	$f_s$ (kN)	$f_i$ (kN-m)	$\phi_i$	$u$ (m)
60.000	0.000	0.000	-2.230	-160.120	1.382E-03	1.103E-03
61.250	0.000	0.000	-0.980	-159.123	1.411E-03	1.126E-03
62.500	2.643E-05	0.000	0.000	-158.125	1.466E-03	1.170E-03
63.750	1.488E-04	0.000	0.000	-157.128	1.617E-03	1.291E-03

## Elasto-Plastic Frames

Table 8. Final part of the solution with an aspect ratio equal to 1.68

A	B	C	D	E	F	G
V (KN)	$\gamma^p$	$\phi_i^p$	$f_s$ (KN)	$f_i$ (KN-m)	$\phi_i$	$u$ (m)
151.250	8.714E-03	0.000	0.000	-87.303	1.220E-02	9.734E-03
152.500	8.837E-03	0.000	0.000	-86.305	1.235E-02	9.855E-03
152.830	8.869E-03	0.000	0.000	-86.041	1.239E-02	9.887E-03
152.830	1.653E-02	0.000	0.000	-86.041	2.005E-02	1.600E-02

Table 9. First steps of the solution with an aspect ratio equal to 2.11

A	B	C	D	E	F	G
V (KN)	$\gamma^p$	$\phi_i^p$	$f_s$ (KN)	$f_i$ (KN-m)	$\phi_i$	$u$ (m)
0.000	0.000	0.000	-78.158	-208.000	0.000E+00	0.000E+00
1.250	0.000	0.000	-76.908	-206.747	4.316E-05	4.326E-05
2.500	0.000	0.000	-75.658	-205.494	8.633E-05	8.652E-05

Table 10. Steps when the shear yield function becomes zero with an aspect ratio equal to 2.11

A	B	C	D	E	F	G
V (KN)	$\gamma^p$	$\phi_i^p$	$f_s$ (KN)	$f_i$ (KN-m)	$\phi_i$	$u$ (m)
76.250	0.000	0.000	-1.908	-131.578	2.633E-03	2.639E-03
77.500	0.000	0.000	-0.658	-130.326	2.676E-03	2.682E-03
78.750	9.352E-05	0.000	0.000	-129.073	2.813E-03	2.819E-03
80.000	2.910E-04	0.000	0.000	-127.820	3.053E-03	3.060E-03

Table 11. Final part of the solution with an aspect ratio equal to 2.11

A	B	C	D	E	F	G
V (KN)	$\gamma^p$	$\phi_i^p$	$f_s$ (KN)	$f_i$ (KN-m)	$\phi_i$	$u$ (m)
138.750	9.571E-03	0.000	0.000	-68.938	1.436E-02	1.439E-02
140.000	9.769E-03	0.000	0.000	-67.685	1.460E-02	1.464E-02
140.560	9.857E-03	0.000	0.000	-67.127	1.471E-02	1.474E-02
140.560	1.510E-02	0.000	0.000	-67.127	1.996E-02	2.000E-02

Tables 13 to 15 present the solution with an aspect ratio equal to 1.78. In the first steps, the bending and shear yield function are negative and the  $\gamma^p$  and  $\phi_i^p$  are nil, thus the behavior is elastic.

This procedure continues until the shear yield function become positive, for a  $V = 65.798 \text{ KN}$ . From this instant, the maximum plastic distortion  $p_s$  is computed with Equation (7.7.13), the rotation with Equation (7.7.11) and the corresponding displacement with Equation (7.7.10). Table 14 shows the steps near the instant when the shear yield function becomes equal to zero.

When the bending yield function changes to zero, the plastic rotation starts to evolve. Notice that the plastic shear distortion keeps increasing; see Table 15.

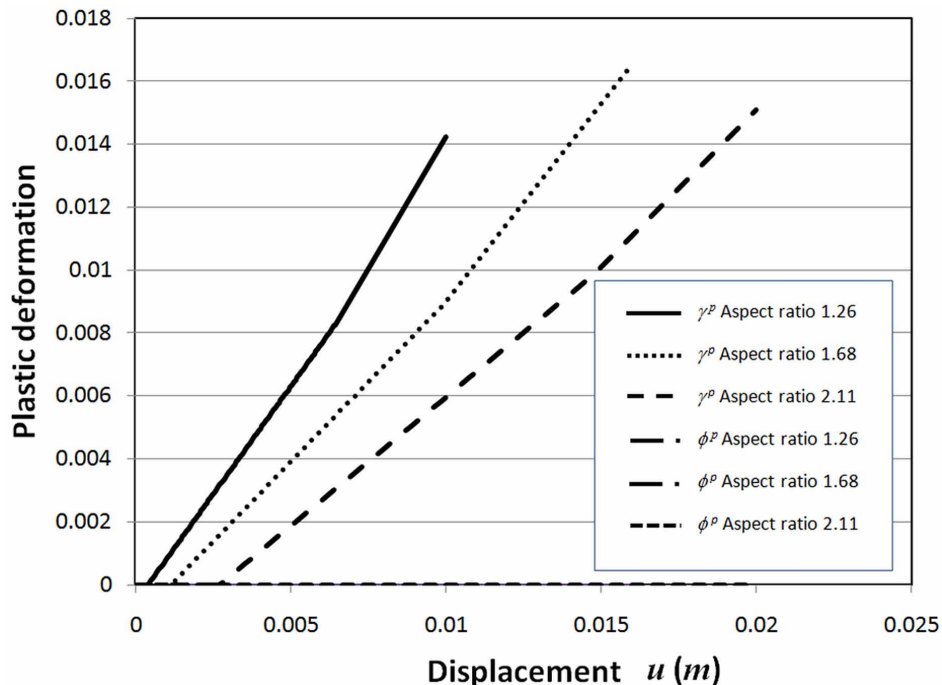
Finally, Table 16 presents the steps when  $V_u$  is reached. Notice that the element failed by shear because  $V_u$  is less than  $M_u/a$ :

$$V = \frac{M_u}{a} = 220.474 \text{ KN} > V_u = 169.965 \text{ KN} \tag{7.7.15}$$

Tables 17 to 19 present the solution for the element with an aspect ratio equal to 3.55 and Tables 19 to 21 show the results corresponding to an aspect ratio equal to 7.11.

Notice that this element failed by bending effect because the force that corresponds to  $M_u$  is smaller than  $V_u$ , i.e.,  $V = \frac{M_u}{a} = 110.548 \text{ KN} < V_u = 142.633 \text{ KN}$ .

Figure 15. Plastic distortion and plastic rotation evolution with aspect ratios equal to 1.26, 1.68 and 2.11



## Elasto-Plastic Frames

Table 12. Bending and shear properties for the beam-column with aspect ratios  $a/d$  equal to 1.78, 3.55 and 7.11

$a/d$	$M_p$ (KN m)	$M_u$ (KN m)	$\phi_u^p$	$V_p$ (KN)	$V_u$ (KN)	$\gamma_u^p$
1.78	53.400	88.300	8.010E-02	65.798	169.965	9.525E-03
3.55	53.400	88.300	8.010E-02	65.798	142.633	4.776E-03
7.11	53.400	88.300	8.010E-02	65.798	128.870	9.539E-03

Table 13. First steps of the solution with an aspect ratio equal to 1.78

A	B	C	D	E	F	G
$V$ (KN)	$\gamma^p$	$\phi_i^p$	$f_s$ (KN)	$f_i$ (KN m)	$\phi_i$	$u$ (m)
0.000	0.000E+00	0.000E+00	-65.798	-53.400	0.000E+00	0.000E+00
1.250	0.000E+00	0.000E+00	-64.548	-52.899	1.497E-04	5.996E-05
2.500	0.000E+00	0.000E+00	-63.298	-52.399	2.994E-04	1.199E-04

Table 14. Steps near the instant when the shear yield function becomes equal to zero with an aspect ratio equal to 1.78

A	B	C	D	E	F	G
$V$ (KN)	$\gamma^p$	$\phi_i^p$	$f_s$ (KN)	$f_i$ (KN m)	$\phi_i$	$u$ (m)
63.750	0.000E+00	0.000E+00	-2.048	-27.868	7.636E-03	3.058E-03
65.000	0.000E+00	0.000E+00	-0.798	-27.368	7.786E-03	3.118E-03
66.250	4.135E-05	0.000E+00	0.000	-26.867	7.977E-03	3.195E-03
67.500	1.557E-04	0.000E+00	0.000	-26.366	8.241E-03	3.300E-03

Table 15. Steps when the bending yield function becomes nil for the element with an aspect ratio equal to 1.78

A	B	C	D	E	F	G
$V$ (KN)	$\gamma^p$	$\phi_i^p$	$f_s$ (KN)	$f_i$ (KN m)	$\phi_i$	$u$ (m)
131.250	5.985E-03	0.000E+00	0.000	-0.834	2.171E-02	8.693E-03
132.500	6.100E-03	0.000E+00	0.000	-0.334	2.197E-02	8.799E-03
133.750	6.214E-03	3.830E-04	0.000	0.000	2.262E-02	9.058E-03
135.000	6.328E-03	1.532E-03	0.000	0.000	2.403E-02	9.624E-03



Again this element failed by bending effects. Figure 16 shows the force-displacement curves for the three aspect ratios. Figure 17 presents the plastic distortion and plastic rotation evolution for the three aspect ratios.

**7.7.6 Obtain the Force Displacement Curve for the RC Element Shown in Figure 18a. Consider the Variable Axial Loading Presented in Figure 18b. Use the Multi-Linear Elasto-Plastic Model Described in Section 7.4. Neglect Kinematic Hardening. The Interaction Diagrams are Indicated in Figure 18c.**

According to section 7.4, if the aspect ratio  $a/d$  is equal to 8 bending dominates the behavior; therefore in the solution of the problem, shear effects are going to be neglected. The bending properties  $M_p$ ,  $M_u$  and  $\phi_u^p$  of the element for the different levels of axial force are shown in Table 23; they were obtained from Figure 18c.

In this case, a monotonic lateral load is applied with increments of 1.00 KN. The Equations (7.7.10 to 7.7.12) are used for the solution (see Tables 24 to 27). Column A shows the lateral loads. Columns B and C present, respectively, the plastic rotation and maximum plastic rotation. Column D includes bending yield function. Column E presents the rotation and finally, column F shows the resultant displacement. Initially the axial force is equal to zero, then, the first line of the Table 22 is used for the analysis.

Table 16. Instant when  $V_u$  is reached for the element with an aspect ratio equal to 1.78

A	B	C	D	E	F	G
V (KN)	$\gamma^p$	$\phi_i^p$	$f_s$ (KN)	$f_i$ (KN m)	$\phi_i$	$u$ (m)
167.500	9.300E-03	3.141E-02	0.000	0.000	6.077E-02	2.434E-02
168.750	9.414E-03	3.255E-02	0.000	0.000	6.218E-02	2.490E-02
169.965	9.525E-03	3.367E-02	0.000	0.000	6.356E-02	2.545E-02
169.965	3.205E-01	3.367E-02	0.000	0.000	3.745E-01	1.500E-01

Table 17. First steps of the solution for the element with an aspect ratio equal to 3.55

A	B	C	D	E	F	G
V (KN)	$\gamma^p$	$\phi_i^p$	$f_s$ (KN)	$f_i$ (KN m)	$\phi_i$	$u$ (m)
0.000	0.000E+00	0.000E+00	-65.798	-53.400	0.000E+00	0.000E+00
1.250	0.000E+00	0.000E+00	-64.548	-52.402	5.354E-04	4.277E-04
2.500	0.000E+00	0.000E+00	-63.298	-51.403	1.071E-03	8.553E-04

## Elasto-Plastic Frames

Table 18. Steps when the shear and bending yield functions become equal to zero for an aspect ratio equal to 3.55

A	B	C	D	E	F	G
V (KN)	$\gamma^p$	$\phi_i^p$	$f_s$ (KN)	$f_i$ (KN m)	$\phi_i$	$u$ (m)
63.750	0.000E+00	0.000E+00	-2.048	-2.480	2.731E-02	2.181E-02
65.000	0.000E+00	0.000E+00	-0.798	-1.481	2.784E-02	2.224E-02
66.250	2.811E-05	0.000E+00	0.000	-0.483	2.841E-02	2.269E-02
67.500	1.058E-04	1.477E-03	0.000	0.000	3.050E-02	2.436E-02
68.750	1.835E-04	4.338E-03	0.000	0.000	3.397E-02	2.713E-02

Table 19. Steps near the instant when  $V_u$  is reached for an aspect ratio equal to 3.55

A	B	C	D	E	F	G
V (KN)	$\gamma^p$	$\phi_i^p$	$f_s$ (KN)	$f_i$ (KN m)	$\phi_i$	$u$ (m)
108.750	2.670E-03	9.589E-02	0.000	0.000	1.451E-01	1.159E-01
110.000	2.748E-03	9.875E-02	0.000	0.000	1.486E-01	1.187E-01
110.548	2.782E-03	1.000E-01	0.000	0.000	1.501E-01	1.199E-01
110.548	2.782E-03	2.629E-01	0.000	0.000	3.130E-01	2.500E-01

Figure 16. Force-displacement curves for aspect ratios equal to 1.78, 3.55 and 7.11

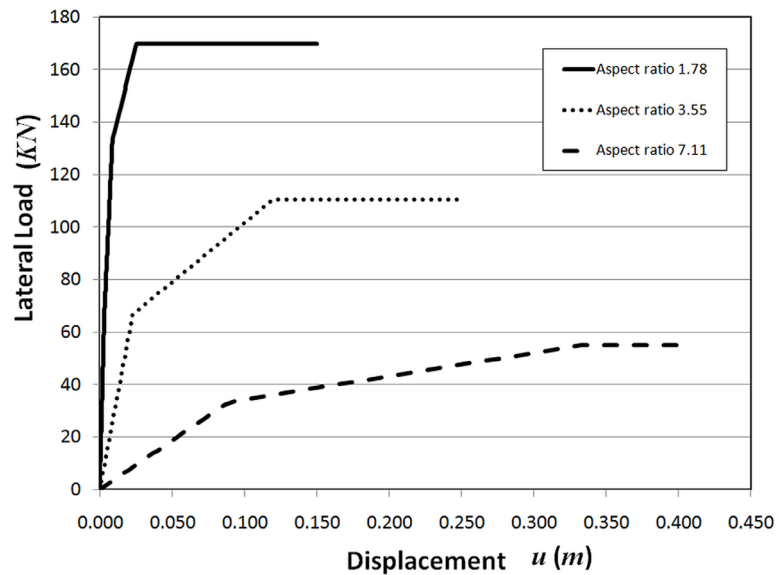


Figure 17. a) Plastic distortion and b) plastic rotation evolution for aspect ratios equal to 1.78, 3.55 and 7.11

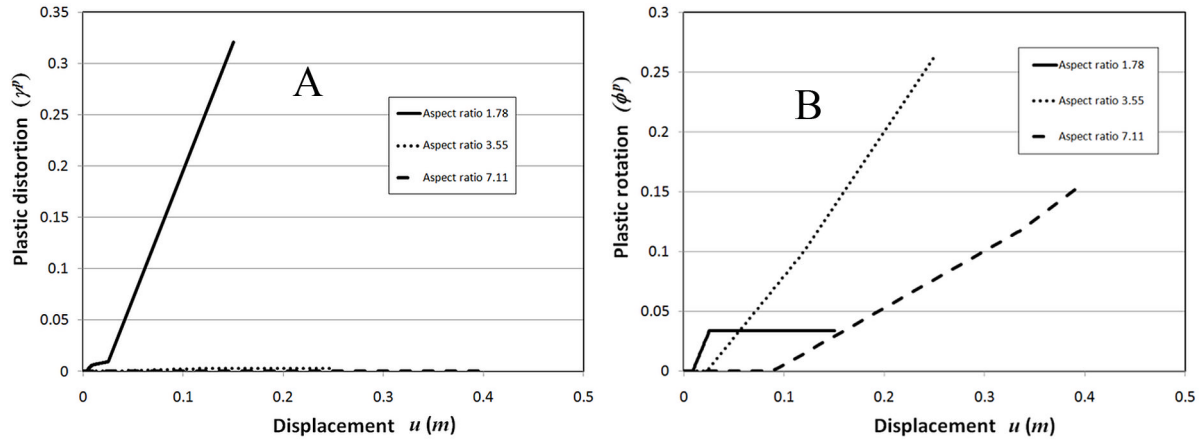


Table 20. First steps of the solution for an aspect ratio equal to 7.11

A	B	C	D	E	F	G
V (KN)	$\gamma^p$	$\phi_i^p$	$f_s$ (KN)	$f_i$ (KN m)	$\phi_i$	$u$ (m)
0.000	0.000E+00	0.000E+00	-65.798	-53.400	0.000E+00	0.000E+00
1.250	0.000E+00	0.000E+00	-64.548	-51.400	2.087E-03	3.339E-03
2.500	0.000E+00	0.000E+00	-63.298	-49.401	4.174E-03	6.677E-03

Table 21. Steps near the bending yield function becomes equal to zero for an aspect ratio equal to 7.11

A	B	C	D	E	F	G
V (KN)	$\gamma^p$	$\phi_i^p$	$f_s$ (KN)	$f_i$ (KN m)	$\phi_i$	$u$ (m)
31.250	0.000E+00	0.000E+00	-34.548	-3.408	5.217E-02	8.346E-02
32.500	0.000E+00	0.000E+00	-33.298	-1.408	5.426E-02	8.680E-02
33.750	0.000E+00	1.985E-03	-32.048	0.000	5.833E-02	9.332E-02
35.000	0.000E+00	8.694E-03	-30.798	0.000	6.713E-02	1.074E-01

Table 22. Steps when  $V_u$  is reached for an aspect ratio equal to 7.11

A	B	C	D	E	F	G
V (KN)	$\gamma^p$	$\phi_i^p$	$f_s$ (KN)	$f_i$ (KN-m)	$\phi_i$	$u$ (m)
53.750	0.000E+00	1.093E-01	-12.048	0.000	1.991E-01	3.185E-01
55.000	0.000E+00	1.160E-01	-10.798	0.000	2.079E-01	3.325E-01
55.196	0.000E+00	1.171E-01	-10.602	0.000	2.093E-01	3.348E-01
55.196	0.000E+00	1.579E-01	-10.602	0.000	2.500E-01	4.000E-01

## Elasto-Plastic Frames

The plastic moment is reached for a  $V = 42.315$  KN and the yield function become zero; from this instant, the plastic rotation starts to evolve (see Table 23).

When the displacement reaches the value of 0.05 m the axial load changes to -300 KN and the parameters must be modified in the Equation (7.7.12) to the corresponding values presented in Table 22. As it can be observed, once the parameters change, the yield function becomes negative again and the plastic rotation evolution, stops. When the force takes the value of 54.949 KN the plasticization process continues as it can be observed in Table 26.

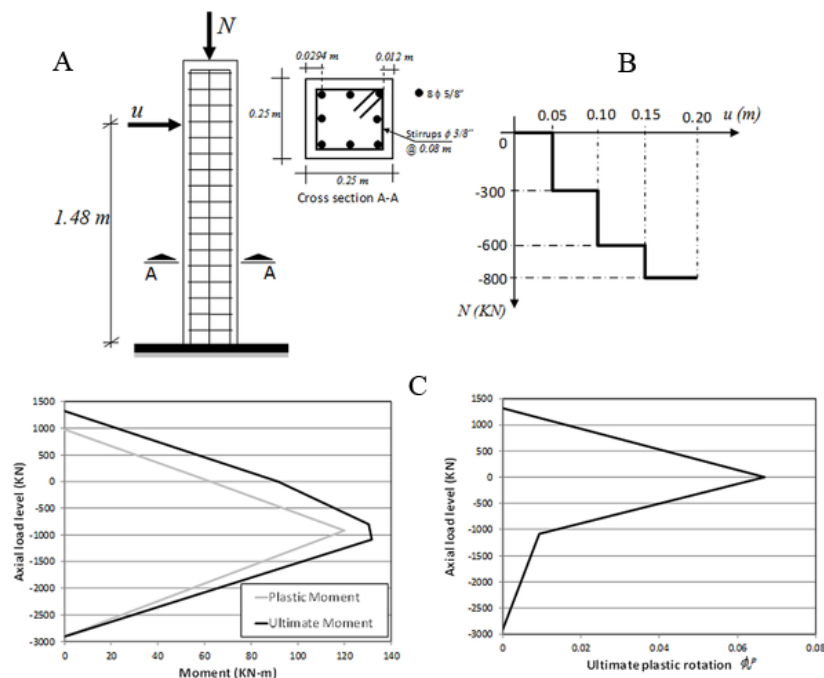
The force continues evolving until the displacement is equal to 0.10 m; then the parameters must be modified again because the axial load changes to -600 KN. After that, the evolution of the plastic rotation stops, until the force reaches the value of 67.583 KN; when that force is reached, the plasticization initiates once again as it can be noticed in Table 27.

When the displacement reaches the value of 0.15 m with a force of 79.33 KN, the parameters are changed for the corresponding to an axial force of -800 KN. As it can be noticed in Table 28, the plastic rotation continues evolving despite the new parameters until the final displacement of 0.20 m is reached.

Notice that the ultimate moment is reached for a displacement of 1.898E-01 m; then, displacement evolution does not produce increments of the lateral force. Figure 19 presents all force-displacement curves for constant axial forces (0 KN, -300 KN, -600 KN and -800 KN) and variable ones.

Figure 20 and Figure 21 show, respectively, the plastic rotation and displacement evolution during the analysis.

Figure 18. a) RC beam-column element, b) Displacement-axial load path, c) Interaction diagrams of plastic and ultimate moments and ultimate plastic rotation



*Table 23. Bending properties*

<b>n(KN)</b>	$M_p$ (KN m)	$M_u$ (KN m)	$\phi_u^p$
0.00	62.626	91.603	0.067
-300.00	81.325	106.099	0.051
-600.00	100.024	120.595	0.035
-800.00	112.489	130.259	0.024

*Table 24. First steps of the analysis*

<b>A</b>	<b>B</b>	<b>C</b>	<b>D</b>	<b>E</b>	<b>F</b>
$V$ (KN)	$\phi_i^p$	$p$	$f_i$ (KN m)	$\phi_i$	$u$ (m)
0.000	0.000E+00	0.000E+00	-62.626	0.000E+00	0.000E+00
1.000	0.000E+00	0.000E+00	-61.146	2.804E-04	4.149E-04
2.000	0.000E+00	0.000E+00	-59.666	5.607E-04	8.299E-04

*Table 25. Steps near the instant when the plastic rotation starts to evolve*

<b>A</b>	<b>B</b>	<b>C</b>	<b>D</b>	<b>E</b>	<b>F</b>
$V$ (KN)	$\phi_i^p$	$p$	$f_i$ (KN m)	$\phi_i$	$u$ (m)
41.000	0.000E+00	0.000E+00	-1.946	1.150E-02	1.701E-02
42.000	0.000E+00	0.000E+00	-0.466	1.178E-02	1.743E-02
43.000	2.641E-03	2.641E-03	0.000	1.440E-02	2.131E-02
44.000	5.754E-03	5.754E-03	0.000	1.809E-02	2.677E-02

*Table 26. Steps near the instant when plastic rotation evolution stops and starts again*

<b>A</b>	<b>B</b>	<b>C</b>	<b>D</b>	<b>E</b>	<b>F</b>
$V$ (KN)	$\phi_i^p$	$p$	$f_i$ (KN m)	$\phi_i$	$u$ (m)
48.247	2.026E-02	2.026E-02	0	3.378E-02	5.000E-02
49.247	0.000E+00	2.026E-02	-8.44E+00	3.406E-02	5.041E-02
50.247	0.000E+00	2.026E-02	-6.96E+00	3.434E-02	5.083E-02
51.247	0.000E+00	2.026E-02	-5.48E+00	3.462E-02	5.124E-02
52.247	0.000E+00	2.026E-02	-4.00E+00	3.491E-02	5.166E-02
53.247	0.000E+00	2.026E-02	-2.52E+00	3.519E-02	5.207E-02
54.247	0.000E+00	2.026E-02	-1.04E+00	3.547E-02	5.249E-02
55.247	9.067E-04	2.116E-02	0.00E+00	3.665E-02	5.425E-02
56.247	3.951E-03	2.421E-02	0.00E+00	3.998E-02	5.917E-02

## 7.8. PROBLEMS

**7.8.1. Compute and Plot the Force-Displacement Curve for the Thin Walled Steel Beam Shown in Figure 22. Consider an Elasto-Plastic Model with Nonlinear Isotropic Hardening.**

**7.8.2. Compute and Plot the Torque-Twist Angle Curve for the RC Element Shown in Figure 23**

**7.8.3. Compute and Plot the Force-Displacement Curve for the Element Shown in Figure 12 Considering an Axial Force Equal to 100 KN**

**7.8.4. Compute and Plot the Force-Displacement Curve for the Element Shown in Figure 12 Considering the Axial Loading Path Shown in Figure 24**

**7.8.5. Compute and Plot the Force-Displacement Curve for the Element Shown in Figure 13. Consider Axial Loads Equal to 0.25Pb, 0.5Pb and the Variable Axial Load History Shown in Figure 25**

Table 27. Steps when plastic rotation evolution stops and starts again

A	B	C	D	E	F
V (KN)	$\phi_i^p$	p	$f_i$ (KN m)	$\phi_i$	u (m)
64.546	2.921E-02	4.947E-02	0.00E+00	6.757E-02	1.000E-01
65.546	0.000E+00	4.947E-02	-3.02E+00	6.785E-02	1.004E-01
66.546	0.000E+00	4.947E-02	-1.54E+00	6.813E-02	1.008E-01
67.546	0.000E+00	4.947E-02	-5.62E-02	6.841E-02	1.012E-01
68.546	2.427E-03	5.190E-02	0.00E+00	7.111E-02	1.052E-01
69.546	4.949E-03	5.442E-02	0.00E+00	7.392E-02	1.094E-01

Table 28. Final part of the analysis

A	B	C	D	E	F
V (KN)	$\phi_i^p$	p	$f_i$ (KN m)	$\phi_i$	u (m)
79.334	2.964E-02	7.911E-02	0.00E+00	1.014E-01	1.500E-01
80.334	8.816E-03	8.792E-02	0.00E+00	1.104E-01	1.635E-01
81.334	1.085E-02	8.996E-02	0.00E+00	1.128E-01	1.669E-01
82.334	1.289E-02	9.200E-02	0.00E+00	1.151E-01	1.703E-01
83.334	1.493E-02	9.404E-02	0.00E+00	1.174E-01	1.738E-01
84.334	1.697E-02	9.607E-02	0.00E+00	1.197E-01	1.772E-01
85.334	1.900E-02	9.811E-02	0.00E+00	1.220E-01	1.806E-01
86.334	2.104E-02	1.001E-01	0.00E+00	1.244E-01	1.840E-01
87.334	2.308E-02	1.022E-01	0.00E+00	1.267E-01	1.875E-01
88.013	2.446E-02	1.036E-01	0.00E+00	1.282E-01	1.898E-01
88.013	1.105E-01	1.105E-01	0.000E+00	1.351E-01	2.000E-01

Figure 19. Force-displacement curve

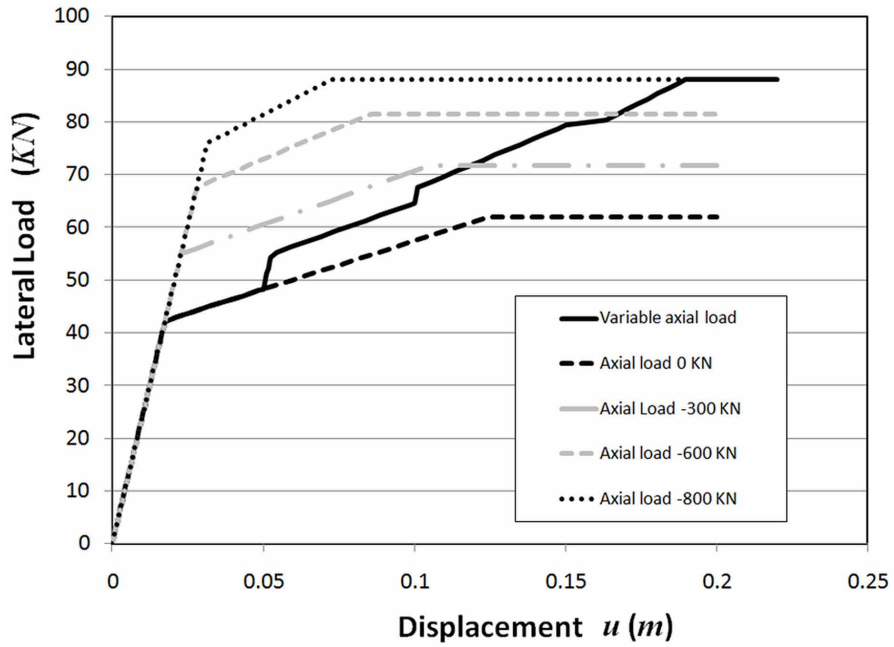
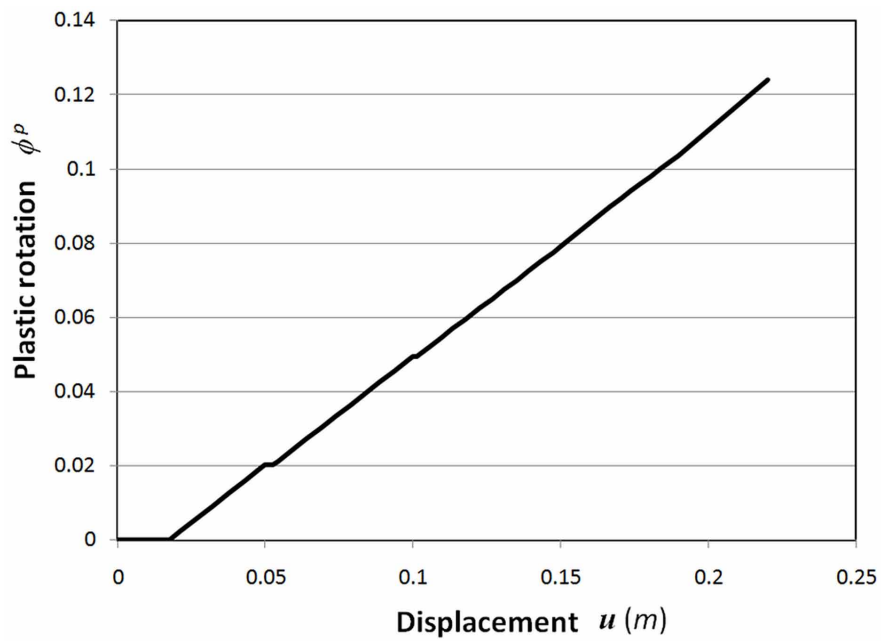


Figure 20. Plastic rotation evolution



## Elasto-Plastic Frames

Figure 21. Displacement evolution

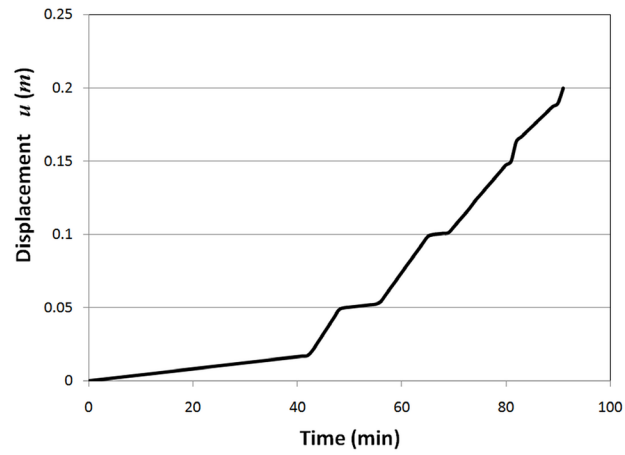


Figure 22. Thin walled steel beam

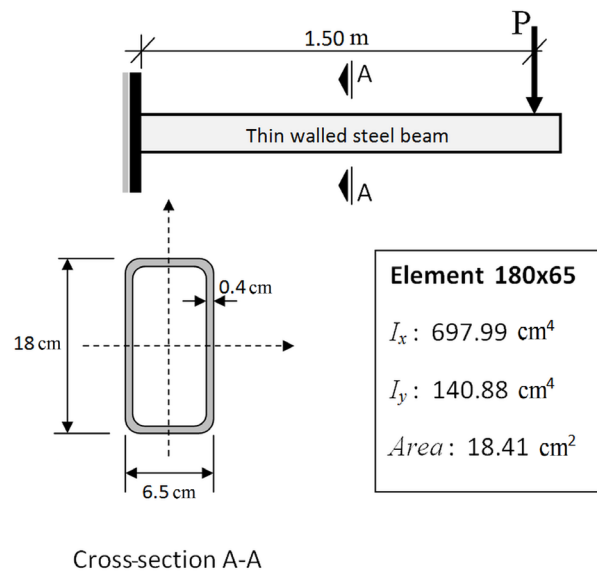




Figure 23. RC element subjected to torsion effect

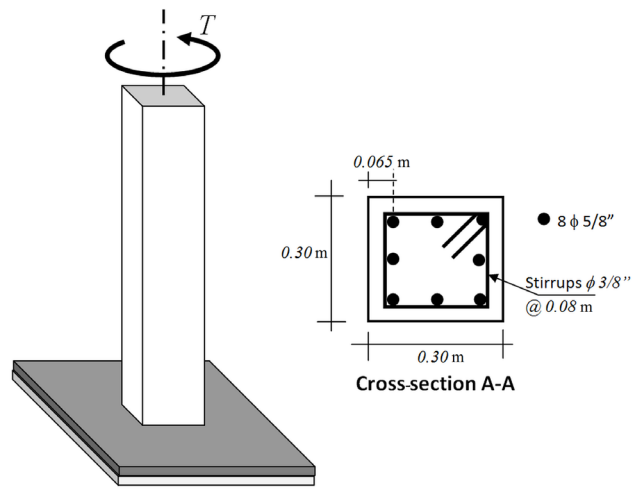


Figure 24. Axial loading path

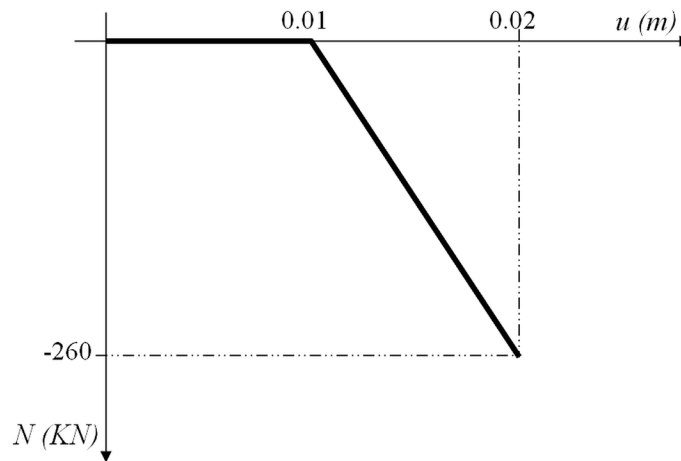
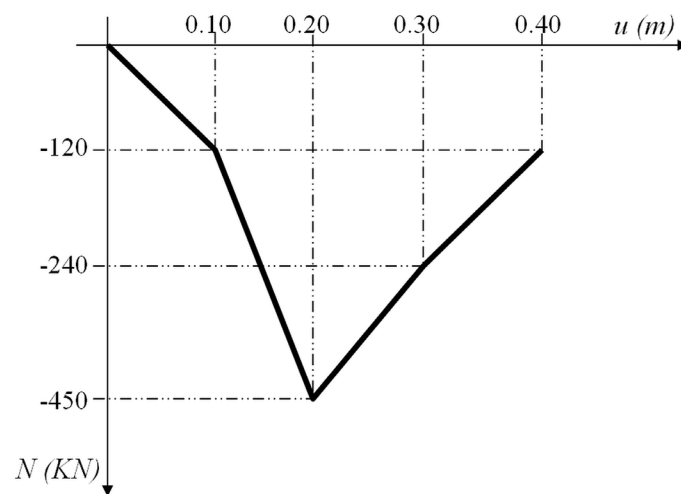


Figure 25. Axial loading path



## **REFERENCES**

ACI Committee. American Concrete Institute, & International Organization for Standardization. (2005). Building code requirements for structural concrete (ACI 318-05) and commentary. American Concrete Institute.

Hsu, T. (1984). *Torsion of reinforced concrete members*. New York, NY: Van Nostrand Reinhold.

Lampert, P., & Collins, M.P. (1972). Torsion, bending and confusion – An attempt to establish the facts. *ACI Journal*, 69-45, 500-504.

Priestley, M. J. N., Verma, R., & Xiao, Y. (1994). Seismic shear strength of reinforced concrete columns. *ASCE Journal of Structural Engineering*, 120(8), 2310–2329.

Sezen, H., & Moehle, J. P. (2004). Shear strength model for lightly reinforced columns. *Journal of Structural Engineering*, 130(11), 1692–1703.

Sezen, H., & Moehle, J. P. (2007). Seismic test of concrete columns with light transverse reinforcement. *ACI Structural Journal*, 133(11), 864–870.

Von Ramin, M., & Matamoros, A. (2006). Shear strength of reinforced concrete members subjected to monotonic loads. *ACI Structural Journal*, 103(1), 83–92.

# Chapter 8

## Analysis of Elasto– Plastic Frames

### ABSTRACT

*This chapter, as well as Chapter 4, deals with the algorithms for the analysis of frames; specifically, it shows how the models for elasto-plastic elements presented in Chapter 7 can be used in a structural analysis. In the first section, a particularly efficient algorithm is presented: the hinge-by-hinge method; in this case, the analysis of an elasto-plastic frame can be treated as a sequence of linear problems; this analysis also allows for an estimation of the ultimate resistance forces of the structure; on the other hand, the hinge-by-hinge procedure can only be used in very particular cases. A general procedure for the analysis of any kind of elasto-plastic frames under quasi-static forces is presented in Sections 8.2 and 8.3; this method is based on an algorithm called elastic predictor-plastic corrector that is a key concept for most of the inelastic structural analyses, even for the damage and fracture models that are described in the next chapters. The same algorithm can also be used for the dynamic analysis of elasto-plastic frames as discussed in Section 8.3.4.*

### 8.1 THE HINGE-BY-HINGE METHOD FOR PERFECTLY PLASTIC FRAMES

#### 8.1.1 Formulation of the Problem

Consider a perfectly plastic two dimensional frame, the generalized deformation and generalized stress measures are thus given by (3.1.3) and (3.2.2); the elements of the frame are slender, the plastic elongations are neglected and nonlinear geometrical effects are not considered.

The structure is subjected to the following loading system: first, a set of distributed loads is applied for a time  $t$  that is arbitrarily defined as zero; it is assumed that these loads do not produce plastic deformations of the frame elements and, as it is usual, that they remain constant for the subsequent steps; these forces generate the matrix  $\{\mathbf{P}^{eq}\}$ . Then, a second set of concentrated loads on the frame nodes is applied; it is assumed that these forces can be written as:  $l(t)\{\mathbf{P}_{ref}\}$ ; where  $\{\mathbf{P}_{ref}\}$  is a matrix of reference forces and  $l(t)$  is a loading parameter; the reference forces matrix may have non zero terms only in the

DOI: 10.4018/978-1-4666-6379-4.ch008

## Analysis of Elasto-Plastic Frames

locations corresponding to the free displacements and these terms are constant during the entire analysis. The term  $l(t)$  represents a monotonically increasing function of time; that is: for a  $t_2 > t_1$  then  $l(t_2) > l(t_1)$ ; the loading parameter takes the value zero for  $t = 0$ ; next, it increases until collapse of the structure is achieved. All these external forces produce reactions that will be grouped into a matrix denoted  $\{\mathbf{R}\}$ .

Therefore, the problem to be solved can be defined as:

1. **Compute:** the free displacements, reaction forces, generalized deformations, plastic rotations and stresses.
2. **With the Following Data:** the initial configuration of the structure, the restricted displacements, the reference forces  $\{\mathbf{P}_{ref}\}$  and those applied over the elements  $\{\mathbf{P}^{eq}\}$  and, finally, the material and cross-section properties ( $E, I, A, M_y$ ).
3. Such that they verify:
  - a. The linear kinematic equation:  $\{\Phi\}_b = [\mathbf{B}_E^0]_b \{\mathbf{U}\}$
  - b. The linear equilibrium equation:  $\sum_{b=1}^m [\mathbf{B}_E^0]^t \{\mathbf{M}\}_b = \{\mathbf{P}^{eq}\} + l\{\mathbf{P}_{ref}\} + \{\mathbf{R}\}$
  - c. The elasticity law:

$$\{\Phi - \Phi^p\}_b = [\mathbf{F}_f]_b \{\mathbf{M}\}_b + \{\Phi^0\}_b \quad (8.1.1)$$

- d. The plastic rotations evolution laws: 
$$\begin{cases} d\phi_i^p = 0 & \text{if } f_i(m_i) < 0 \text{ (hinge locked)} \\ f_i(m_i) = 0 & \text{if } d\phi_i^p \neq 0 \text{ (active hinge)} \end{cases}$$

$$\begin{cases} d\phi_j^p = 0 & \text{if } f_j(m_j) < 0 \text{ (hinge locked)} \\ f_j(m_j) = 0 & \text{if } d\phi_j^p \neq 0 \text{ (active hinge)} \end{cases}$$

- e. The yield functions:  $f_i(m_i) = |m_i| - M_{iy} \leq 0$ ;  $f_j(m_j) = |m_j| - M_{jy} \leq 0$ ;

### 8.1.2 Formulation of the Problem in Incremental Form

As in the case of the nonlinear elastic problems, the analysis of elasto-plastic frames is carried out incrementally; however in the former case, the size of each step is fixed and the instants  $t_1, t_2, \dots, T$  are chosen by the analyst; in the hinge-by-hinge method the end of each step, after the first one, is not fixed; it corresponds to the appearance of a new plastic hinge.

The first step determines the state of the structure after the application of the distributed forces on the elements; as this problem is linear and elastic, it can be solved by the direct stiffness method described in chapter 4 (section 4.1). For the subsequent steps, the increments of the variables can be expressed as:

$$\{\Delta\Phi\}_b = [\mathbf{B}_E^0]_b \{\Delta\mathbf{U}\} \quad (8.1.2)$$

$$\sum_{b=1}^m [\mathbf{B}_E^0]^t \{\Delta\mathbf{M}\}_b = \Delta l \{\mathbf{P}^R\}; \text{ where } \{\mathbf{P}^R\} = \{\mathbf{P}_{ref}\} + \frac{1}{\Delta l} \{\Delta\mathbf{R}\} \quad (8.1.3)$$

$$\{\Delta\Phi - \Delta\Phi^p\}_b = [\mathbf{F}_f]_b \{\Delta\mathbf{M}\}_b$$

$$\begin{cases} \Delta\phi_i^p = 0 \text{ if hinge } i \text{ is locked} \\ \Delta m_i^b = 0 \text{ if hinge } i \text{ is active} \end{cases}; \begin{cases} \Delta\phi_j^p = 0 \text{ if hinge } j \text{ is locked} \\ \Delta m_j^b = 0 \text{ if hinge } j \text{ is active} \end{cases} \quad (8.1.4)$$

Once a plastic hinge has been formed, it remains active since only increasing of external forces are considered. Thus, the evolution laws of the plastic rotations (8.1.4b-c) can be written in this particular case as:

$$\begin{cases} \phi_i^p = 0 \text{ if } |m_i^b| < M_{iy} \\ \Delta m_i^b = 0 \text{ if } |m_i^b| = M_{iy} \end{cases}; \begin{cases} \phi_j^p = 0 \text{ if } |m_j^b| < M_{jy} \\ \Delta m_j^b = 0 \text{ if } |m_j^b| = M_{jy} \end{cases} \quad (8.1.5)$$

### 8.1.3 Tangent Elasticity Matrix of a Frame Element

The elasticity law (8.1.4a) in explicit form is:

$$\Delta\phi_i^b - \Delta\phi_i^p = \frac{L_b}{3EI_b} \Delta m_i^b - \frac{L_b}{6EI_b} \Delta m_j^b$$

$$\Delta\phi_j^b - \Delta\phi_j^p = -\frac{L_b}{6EI_b} \Delta m_i^b + \frac{L_b}{3EI_b} \Delta m_j^b$$

$$\Delta\delta_b = \frac{L_b}{EA_b} \Delta n_b \quad (8.1.6)$$

In an element with two plastic hinges ( $\Delta m_i^b = 0, \Delta m_j^b = 0$ ), the elasticity law (8.1.6) becomes:

$$\{\Delta\mathbf{M}\}_b = [\mathbf{S}_2]_b \{\Delta\Phi\}_b; [\mathbf{S}_2]_b = \begin{bmatrix} 0 & 0 & 0 \\ 0 & 0 & 0 \\ 0 & 0 & \frac{AE_b}{L_b} \end{bmatrix}; \Delta\phi_i^p = \Delta\phi_i^b; \Delta\phi_j^p = \Delta\phi_j^b \quad (8.1.7)$$

If there is only one plastic hinge at the end  $i$  of the element ( $\Delta m_i^b = 0, \phi_j^p = 0$ ), the Equations (8.1.6) give:

**Analysis of Elasto-Plastic Frames**

$$\{\Delta \mathbf{M}\}_b = [\mathbf{S}_{1i}]_b \{\Delta \Phi\}_b; [\mathbf{S}_{1i}]_b = \begin{bmatrix} 0 & 0 & 0 \\ 0 & \frac{3EI_b}{L_b} & 0 \\ 0 & 0 & \frac{AE_b}{L_b} \end{bmatrix}; \Delta \phi_i^P = \Delta \phi_i^b + \frac{1}{2} \Delta \phi_j^b; \phi_j^P = 0 \quad (8.1.8)$$

If there is one plastic hinge, but this time at the end  $j$  ( $\Delta m_j^b = 0, \phi_i^P = 0$ ), then:

$$\{\Delta \mathbf{M}\}_b = [\mathbf{S}_{1j}]_b \{\Delta \Phi\}_b; [\mathbf{S}_{1j}]_b = \begin{bmatrix} \frac{3EI_b}{L_b} & 0 & 0 \\ 0 & 0 & 0 \\ 0 & 0 & \frac{AE_b}{L_b} \end{bmatrix}; \Delta \phi_j^P = \Delta \phi_j^b + \frac{1}{2} \Delta \phi_i^b; \phi_i^P = 0 \quad (8.1.9)$$

Finally, if there are no plastic hinges,

$$\{\Delta \mathbf{M}\}_b = [\mathbf{S}_0]_b \{\Delta \Phi\}_b; [\mathbf{S}_0]_b = \begin{bmatrix} \frac{4EI_b}{L_b} & \frac{2EI_b}{L_b} & 0 \\ \frac{2EI_b}{L_b} & \frac{4EI_b}{L_b} & 0 \\ 0 & 0 & \frac{AE_b}{L_b} \end{bmatrix}; \phi_i^P = 0; \phi_j^P = 0 \quad (8.1.10)$$

Equations (8.1.7-10) can be summarized as:

$$\{\Delta \mathbf{M}\}_b = [\mathbf{S}]_b \{\Delta \Phi\}_b \quad (8.1.11)$$

Where the tangent elasticity matrix  $[\mathbf{S}]_b$  is equal to:

$$[\mathbf{S}]_b = \begin{cases} [\mathbf{S}_0]_b & \text{if there are no plastic hinges} \\ [\mathbf{S}_{1i}]_b & \text{if there is a plastic hinge at the end } i \\ [\mathbf{S}_{1j}]_b & \text{if there is a plastic hinge at the end } j \\ [\mathbf{S}_2]_b & \text{if there are two plastic hinges} \end{cases} \quad (8.1.12)$$

### 8.1.4 The Hinge-by-Hinge Algorithm

The combination of Equation (8.1.2-3) and Equation (8.1.11) gives the following expression:

$$\left( \sum_{b=1}^m [\mathbf{B}_E^0]^t_b [\mathbf{S}]_b [\mathbf{B}_E^0]_b \right) \{ \Delta \mathbf{U} / \Delta l \} = \{ \mathbf{P}^R \} \quad (8.1.13)$$

This expression can be written in a similar way to the direct stiffness Equation (4.1.2):

$$[\mathbf{K}_t] \{ \mathbf{V} \} = \{ \mathbf{P}^R \}; \text{ where } [\mathbf{K}_t] = \sum_{b=1}^m [\mathbf{B}_E^0]^t_b [\mathbf{S}]_b [\mathbf{B}_E^0]_b; \{ \mathbf{V} \} = \frac{1}{\Delta l} \{ \Delta \mathbf{U} \} \quad (8.1.14)$$

Thus, the assemblage algorithm described in sections 4.1.2 and 4.1.3 can also be used.

As aforementioned, the known components of the matrix  $\{ \mathbf{P}^R \}$  remain constant during the entire analysis; on the other hand, the tangent stiffness matrix  $[\mathbf{K}_t]$  changes at each step.

The hinge-by-hinge algorithm is described in Figure 1. The first step consists in the determination of the state of the structure under the distributed forces. This state is defined by:  $\{ \mathbf{U} \}_{t=0} = \{ \mathbf{U}_0 \}$ ,  $\{ \Phi \}_{t=0} = \{ \Phi_0 \}$ ,  $\{ \mathbf{M} \}_{t=0} = \{ \mathbf{M}_0 \}$  with  $l(0) = 0$ .

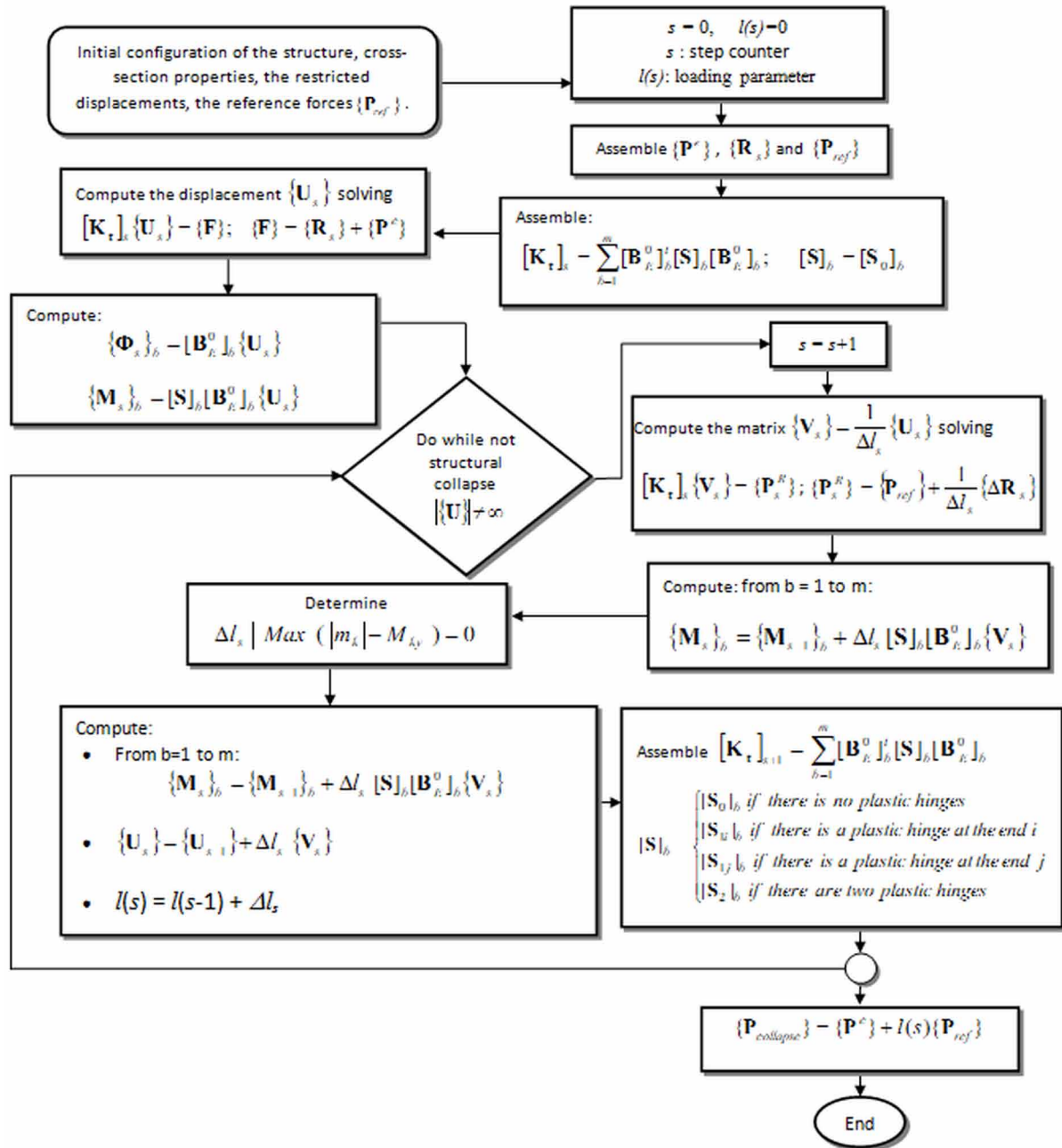
In the second step, the equation (8.1.14) is solved by the direct stiffness method. The tangent stiffness matrix  $[\mathbf{K}_t]$  is computed considering that there are no plastic hinges in the structure. Displacements, strains and stresses in this step are given by:

$$\begin{aligned} \{ \mathbf{U}_1 \} &= \{ \mathbf{U}_0 \} + \Delta l_1 \{ \mathbf{V}_1 \}; \\ \{ \Phi_1 \}_b &= \{ \Phi_0 \}_b + \Delta l_1 [\mathbf{B}_E^0]_b \{ \mathbf{V}_1 \} \\ \{ \mathbf{M} \}_b &= \{ \mathbf{M}_{t=0} \}_b + \Delta l [\mathbf{S}]_b [\mathbf{B}_E^0]_b \{ \mathbf{V}_1 \} \end{aligned} \quad (8.1.15)$$

This second step ends with the appearance of the first plastic hinge. The location of the first plastic hinge to become active is determined subtracting the yield moment from the corresponding absolute value of the moment on all the hinges of the structure and searching for their maximum; when this value is equal to zero, this plastic hinge is unlocked. The value of the loading parameter at the end of the second step is computed solving the Equation (8.1.16):

$$Max ( |m_k(\Delta l)| - M_{ky} ) = 0 \quad (8.1.16)$$

Figure 1. Hinge-by-hinge algorithm





In the third step, the Equation (8.1.14) is solved again taking into account the plastic hinge, or hinges, that appeared at the end of the second step. In the fourth step, there are at least two plastic hinges and so on for any subsequent step  $s$ .

Notice that the global tangent stiffness of the structure decreases with each step; eventually, the displacements tend to infinite: this is a mathematical definition of structural collapse.

The example 8.5.1 shows a practical application of hinge-by-hinge method.

### 8.1.5 Tangent Stiffness Matrix of a Frame Element

Each step of the hinge-by-hinge method can be solved by the direct stiffness method; only the tangent stiffness matrix has to be changed. It is therefore convenient to precompute the four possible expressions for the tangent stiffness matrix of an element; that is:

$$[\mathbf{k}_t] = [\mathbf{B}^0]_b^T [\mathbf{S}]_b [\mathbf{B}^0]_b \quad (8.1.17)$$

where  $[\mathbf{B}^0]_b$  is the non expanded kinematic transformation matrix defined in section 3.1.4.

For  $[\mathbf{S}]_b = [\mathbf{S}_0]_b$ , the tangent stiffness matrix is:

$$[\mathbf{k}_t] = \begin{bmatrix} \frac{12EI}{L^3} s^2 + \frac{EA}{L} c^2 & \left( -\frac{12EI}{L^3} + \frac{EA}{L} \right) sc & \frac{6EI}{L^2} s & -\frac{12EI}{L^3} s^2 - \frac{EA}{L} c^2 & \left( \frac{12EI}{L^3} - \frac{EA}{L} \right) sc & \frac{6EI}{L^2} s \\ \left( -\frac{12EI}{L^3} + \frac{EA}{L} \right) sc & \frac{12EI}{L^3} c^2 + \frac{EA}{L} s^2 & -\frac{6EI}{L^2} c & \left( \frac{12EI}{L^3} - \frac{EA}{L} \right) sc & -\frac{12EI}{L^3} c^2 - \frac{EA}{L} s^2 & -\frac{6EI}{L^2} c \\ \frac{6EI}{L^2} s & -\frac{6EI}{L^2} c & \frac{4EI}{L} & -\frac{6EI}{L^2} s & \frac{6EI}{L^2} c & \frac{2EI}{L} \\ -\frac{12EI}{L^3} s^2 - \frac{EA}{L} c^2 & \left( \frac{12EI}{L^3} - \frac{EA}{L} \right) sc & -\frac{6EI}{L^2} s & \frac{12EI}{L^3} s^2 + \frac{EA}{L} c^2 & \left( -\frac{12EI}{L^3} + \frac{EA}{L} \right) sc & -\frac{6EI}{L^2} s \\ \left( \frac{12EI}{L^3} - \frac{EA}{L} \right) sc & -\frac{12EI}{L^3} c^2 - \frac{EA}{L} s^2 & \frac{6EI}{L^2} c & \left( -\frac{12EI}{L^3} + \frac{EA}{L} \right) sc & \frac{12EI}{L^3} c^2 + \frac{EA}{L} s^2 & \frac{6EI}{L^2} c \\ \frac{6EI}{L^2} s & -\frac{6EI}{L^2} c & \frac{2EI}{L} & -\frac{6EI}{L^2} s & \frac{6EI}{L^2} c & \frac{4EI}{L} \end{bmatrix} \quad (8.1.18)$$

where  $s = \sin \alpha_b$  and  $c = \cos \alpha_b$ ;  $\alpha_b$  is the angle of the chord with respect the global axis  $X$ .

For  $[\mathbf{S}]_b = [\mathbf{S}_{1i}]_b$ :

**Analysis of Elasto-Plastic Frames**

$$\left[ \mathbf{k}_t \right] = \begin{bmatrix} \frac{3EI}{L^3} s^2 + \frac{EA}{L} c^2 & \left( -\frac{3EI}{L^3} + \frac{EA}{L} \right) sc & 0 & -\frac{3EI}{L^3} s^2 - \frac{EA}{L} c^2 & \left( \frac{3EI}{L^3} - \frac{EA}{L} \right) sc & \frac{3EI}{L^2} s \\ \left( -\frac{3EI}{L^3} + \frac{EA}{L} \right) sc & \frac{3EI}{L^3} c^2 + \frac{EA}{L} s^2 & 0 & \left( \frac{3EI}{L^3} - \frac{EA}{L} \right) sc & -\frac{3EI}{L^3} c^2 - \frac{EA}{L} s^2 & -\frac{3EI}{L^2} c \\ 0 & 0 & 0 & 0 & 0 & 0 \\ -\frac{3EI}{L^3} s^2 - \frac{EA}{L} c^2 & \left( \frac{3EI}{L^3} - \frac{EA}{L} \right) sc & 0 & \frac{3EI}{L^3} s^2 + \frac{EA}{L} c^2 & \left( -\frac{3EI}{L^3} + \frac{EA}{L} \right) sc & -\frac{3EI}{L^2} s \\ \left( \frac{3EI}{L^3} - \frac{EA}{L} \right) sc & -\frac{3EI}{L^3} c^2 - \frac{EA}{L} s^2 & 0 & \left( -\frac{3EI}{L^3} + \frac{EA}{L} \right) sc & \frac{3EI}{L^3} c^2 + \frac{EA}{L} s^2 & \frac{3EI}{L^2} c \\ \frac{3EI}{L^2} s & -\frac{3EI}{L^2} c & 0 & -\frac{3EI}{L^2} s & \frac{3EI}{L^2} c & \frac{3EI}{L} \end{bmatrix} \quad (8.1.19)$$

For  $[\mathbf{S}]_b = [\mathbf{S}_{1j}]_b$ :

$$\left[ \mathbf{k}_t \right] = \begin{bmatrix} \frac{3EI}{L^3} s^2 + \frac{EA}{L} c^2 & \left( -\frac{3EI}{L^3} + \frac{EA}{L} \right) sc & \frac{3EI}{L^2} s & -\frac{3EI}{L^3} s^2 - \frac{EA}{L} c^2 & \left( \frac{3EI}{L^3} - \frac{EA}{L} \right) sc & 0 \\ \left( -\frac{3EI}{L^3} + \frac{EA}{L} \right) sc & \frac{3EI}{L^3} c^2 + \frac{EA}{L} s^2 & -\frac{3EI}{L^2} c & \left( \frac{3EI}{L^3} - \frac{EA}{L} \right) sc & -\frac{3EI}{L^3} c^2 - \frac{EA}{L} s^2 & 0 \\ \frac{3EI}{L^2} s & -\frac{3EI}{L^2} c & \frac{3EI}{L} & -\frac{3EI}{L^2} s & \frac{3EI}{L^2} c & 0 \\ -\frac{3EI}{L^3} s^2 - \frac{EA}{L} c^2 & \left( \frac{3EI}{L^3} - \frac{EA}{L} \right) sc & -\frac{3EI}{L^2} s & \frac{3EI}{L^3} s^2 + \frac{EA}{L} c^2 & \left( -\frac{3EI}{L^3} + \frac{EA}{L} \right) sc & 0 \\ \left( \frac{3EI}{L^3} - \frac{EA}{L} \right) sc & -\frac{3EI}{L^3} c^2 - \frac{EA}{L} s^2 & \frac{3EI}{L^2} c & \left( -\frac{3EI}{L^3} + \frac{EA}{L} \right) sc & \frac{3EI}{L^3} c^2 + \frac{EA}{L} s^2 & 0 \\ 0 & 0 & 0 & 0 & 0 & 0 \end{bmatrix} \quad (8.1.20)$$

Finally, for  $[\mathbf{S}]_b = [\mathbf{S}_2]_b$ :

$$\left[ \mathbf{k}_t \right] = \begin{bmatrix} \frac{EA}{L} c^2 & \frac{EA}{L} sc & 0 & -\frac{EA}{L} c^2 & -\frac{EA}{L} sc & 0 \\ \frac{EA}{L} sc & \frac{EA}{L} s^2 & 0 & -\frac{EA}{L} sc & -\frac{EA}{L} s^2 & 0 \\ 0 & 0 & 0 & 0 & 0 & 0 \\ -\frac{EA}{L} c^2 & -\frac{EA}{L} sc & 0 & \frac{EA}{L} c^2 & \frac{EA}{L} sc & 0 \\ -\frac{EA}{L} sc & -\frac{EA}{L} s^2 & 0 & \frac{EA}{L} sc & \frac{EA}{L} s^2 & 0 \\ 0 & 0 & 0 & 0 & 0 & 0 \end{bmatrix} \quad (8.1.21)$$

## 8.2 ELASTIC PREDICTOR - PLASTIC CORRECTOR ALGORITHM

### 8.2.1 Formulation of the Problem

In more general cases, the hinge-by-hinge algorithm is no longer valid; more complex procedures are needed. As an example, consider the case of an elastic perfectly plastic structure, still geometrically linear, but including plastic elongations. Therefore, the problem is now defined as:

1. Compute: the free displacements, reaction forces, deformations, plastic deformations and stresses.
2. With the following data: the initial configuration of the structure, the restricted displacements, the nodal forces corresponding to the free displacements and those applied over the elements, the material and cross-section properties and yield functions.
3. Such that they verify:
  - a. The linear kinematic equation:  $\{\Phi\}_b = [\mathbf{B}_E^0]_b \{\mathbf{U}\}$
  - b. The linear equilibrium equation:

$$\sum_{b=1}^m [\mathbf{B}_E^0]_b^t \{\mathbf{M}\}_b = \{\mathbf{P}\} \quad (8.2.1)$$

- c. The elasticity law:  $\{\mathbf{M}\}_b = [\mathbf{E}]_b \{\Phi - \Phi^p\}_b + \{\mathbf{M}^0\}_b$
- d. The normality laws:  $d\phi_i^p = d\lambda_i \frac{\partial f_i}{\partial m_i}$ ;  $d\phi_j^p = d\lambda_j \frac{\partial f_j}{\partial m_j}$ ;  $d\delta_p = d\lambda_i \frac{\partial f_i}{\partial n} + d\lambda_j \frac{\partial f_j}{\partial n}$ ;
- e. The plastic multipliers evolution laws:
 
$$\begin{cases} d\lambda_i = 0 & \text{if } f_i(m_i, n) < 0 \\ f_i(m_i, n) = 0 & \text{if } d\lambda_i \neq 0 \end{cases} ;$$

$$\begin{cases} d\lambda_j = 0 & \text{if } f_j(m_j, n) < 0 \\ f_j(m_j, n) = 0 & \text{if } d\lambda_j \neq 0 \end{cases}$$

### 8.2.2 Global and Local Problems

The analysis is still carried out step by step, however as in the case of nonlinear elastic frames, and unlike the hinge-by-hinge algorithm, the size of the steps is chosen by the analyst.

## Analysis of Elasto-Plastic Frames

At any time  $t_r$ , the equations (8.2.1) are separated into two groups, the kinematic and constitutive equations on one hand and the equilibrium equation on the other. These two sets of equations will be solved separately; the equilibrium equation and its boundary conditions are called “global problem” because it involves all the elements of the frame; the kinematic and constitutive equations are called “local problem for the element  $b$ ” because they relate variables of only one element  $b$ .

Specifically, a local problem is formulated as follows:

1. Compute: the generalized deformations, plastic deformations and stresses of an element  $b$  at the time  $t_r$ .
2. With the following data: the displacements of the element and the forces applied over the elements at the time  $t_r$ ; the material and cross-section properties and yield functions.
3. Such that they verify:
  - a. The linear kinematic equation:  $\{\Phi_{t=tr}\}_b = [\mathbf{B}_E^0]_b \{\mathbf{U}_{t=tr}\}$
  - b. The elasticity law:  $\{\mathbf{M}_{t=tr}\}_b = [\mathbf{E}]_b \{\Phi_{t=tr} - \Phi_{t=tr}^p\}_b + \{\mathbf{M}^0\}_b$
  - c. The normality laws:  $\Delta\phi_i^p = \Delta\lambda_i \left. \frac{\partial f_i}{\partial m_i} \right|_{t=tr}$ ;  $\Delta\phi_j^p = \Delta\lambda_j \left. \frac{\partial f_j}{\partial m_j} \right|_{t=tr}$ ;  $\Delta\delta_p = \Delta\lambda_i \left. \frac{\partial f_i}{\partial n} \right|_{t=tr} + \Delta\lambda_j \left. \frac{\partial f_j}{\partial n} \right|_{t=tr}$
  - d. The plastic multipliers evolution laws:

$$\begin{cases} \Delta\lambda_i = 0 & \text{if } f_i|_{t=tr} < 0 \\ f_i|_{t=tr} = 0 & \text{if } \Delta\lambda_i \neq 0 \end{cases} ; \quad \begin{cases} \Delta\lambda_j = 0 & \text{if } f_j|_{t=tr} < 0 \\ f_j|_{t=tr} = 0 & \text{if } \Delta\lambda_j \neq 0 \end{cases} \quad (8.2.2)$$

Notice that, implicitly, the resolution of the local problems relates the stresses at the end of the step with the displacements:  $\{\mathbf{M}_{t=tr}\}_b = \{\mathbf{M}(\mathbf{U}_{t=tr})\}_b$ , therefore the equilibrium equation can be written as in the case of nonlinear elastic frames:

$$\{\mathbf{L}(\mathbf{U}_{t=tr})\} = \{\mathbf{P}_{t=tr}\}; \{\mathbf{L}(\mathbf{U}_{t=tr})\} = \sum_{b=1}^m [\mathbf{B}(\mathbf{U}_{t=tr})_E]_b^t \{\mathbf{M}(\mathbf{U}_{t=tr})\}_b \quad (8.2.3)$$

This is the global problem that can be solved using the Newton-Raphson algorithm that is described in section 4.2.5. For each iteration of the Newton-Raphson procedure, it is needed the resolution of the  $m$  local problems, one for each element of the frame. An algorithm for solving the local problems is described in the next section.

### 8.2.3 Numerical Resolution of the Local Problem

The local problem may be solved using an algorithm called elastic predictor - plastic corrector that is shown in Figure 2(a-e).

The main difficulty for solving the local problem is to know which one plastic hinge is active. It is first assumed that none is active: this is the elastic predictor phase of the algorithm; therefore a provisional stress matrix  $\{\mathbf{M}^{prov}\}_b$  is given by:

$$\{\Phi_{t=tr}\}_b = [\mathbf{B}_E^0]_b \{\mathbf{U}_{t=tr}\}; \{\mathbf{M}^{prov}\}_b = [\mathbf{E}]_b \{\Phi_{t=tr} - \Phi_{t=tr-1}^p\}_b + \{\mathbf{M}^0\}_b \quad (8.2.4)$$

Notice that the provisional stresses at the end of the step are computed using the plastic deformations at the end of the precedent step. The elastic assumption can now be verified; this is carried out computing the provisional value of the yield functions with the provisional stress matrix:

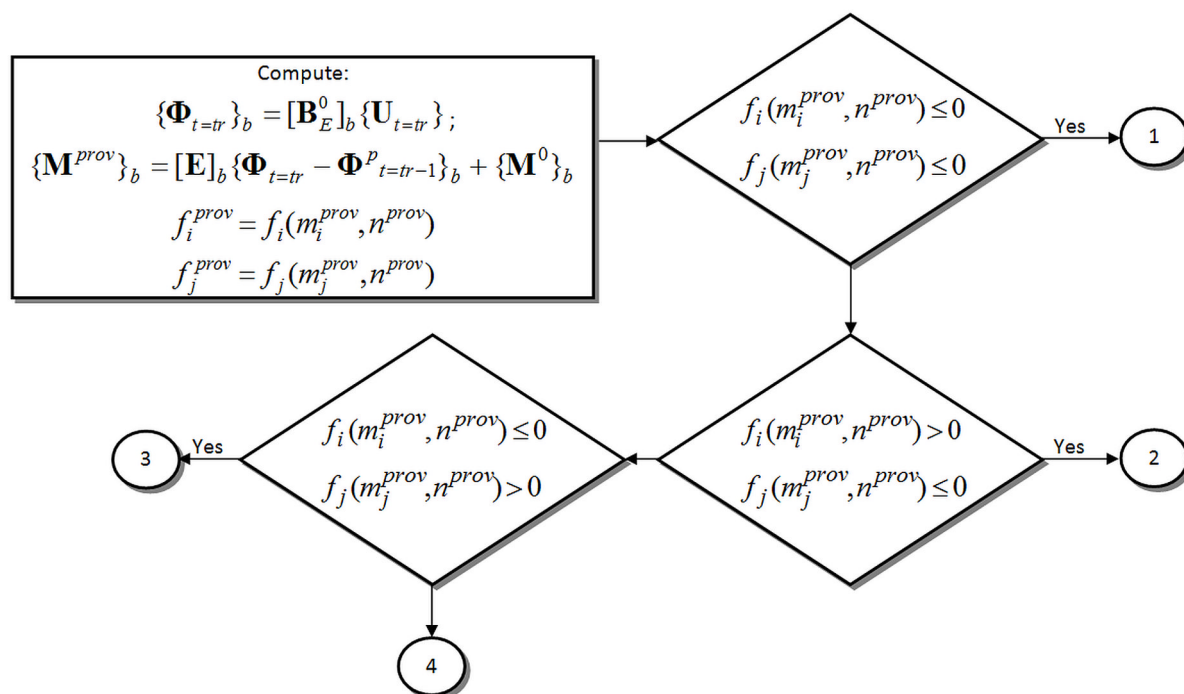
$$f_i^{prov} = f_i(m_i^{prov}, n^{prov}); f_j^{prov} = f_j(m_j^{prov}, n^{prov}) \quad (8.2.5)$$

If both yield functions are negative or zero, then the local problem is indeed elastic and the provisional stresses are the solution of the local problem:

$$\{\mathbf{M}_{t=tr}\}_b = \{\mathbf{M}^{prov}\}_b \quad (8.2.6)$$

If one or all yield functions are positive then a plastic correction is needed (remember that yield functions are negative or nil by definition). There are three different kinds of plastic corrections possible: one with the plastic hinge  $i$  active, another with the plastic hinge  $j$  active and, finally, a plastic correction

Figure 2a. Elastic predictor - plastic corrector algorithm



### Analysis of Elasto-Plastic Frames

where both plastic hinges are active. The appropriate plastic correction is chosen considering the sign of the values of the functions. For instance, if  $f_i^{prov} > 0$  and  $f_j^{prov} \leq 0$  then, a new provisional stress matrix is obtained solving:

$$\begin{aligned} \{\mathbf{M}^{prov}\}_b &= [\mathbf{E}]_b \{\Phi_{t=tr} - \Phi_{prov}^p\}_b + \{\mathbf{M}^0\}_b; f_i^{prov} = 0; \\ \Delta\phi_i^p &= \Delta\lambda_i \left. \frac{\partial f_i}{\partial m_i} \right|_{prov}; \Delta\delta_p = \Delta\lambda_i \left. \frac{\partial f_i}{\partial n} \right|_{prov}; \Delta\phi_j^p \Big|_{prov} = 0 \end{aligned} \quad (8.2.7)$$

This new provisional solution should also be verified. This is carried out by computing the new value of the yield function  $j$  and the increment of the plastic multiplier  $i$ . If they are, respectively, negative and positive ( $f_j^{prov} \leq 0$  and  $\Delta\lambda_i \Big|_{prov} \geq 0$ ) then, the new provisional stresses are indeed the solution of the local problem.

The second possible correction consists in assuming an active plastic hinge at the end  $j$ ; this is the case if  $f_i^{prov} \leq 0$  and  $f_j^{prov} > 0$ , therefore:

$$\begin{aligned} \{\mathbf{M}^{prov}\}_b &= [\mathbf{E}]_b \{\Phi_{t=tr} - \Phi_{prov}^p\}_b + \{\mathbf{M}^0\}_b; f_i^{prov} = 0; \\ \Delta\phi_i^p \Big|_{prov} &= 0; \Delta\phi_j^p = \Delta\lambda_j \left. \frac{\partial f_j}{\partial m_j} \right|_{prov}; \Delta\delta_p = \Delta\lambda_j \left. \frac{\partial f_j}{\partial n} \right|_{prov} \end{aligned} \quad (8.2.8)$$

And the corresponding verification is:  $f_i^{prov} \leq 0$  and  $\Delta\lambda_j \Big|_{prov} \geq 0$ .

The last possible plastic correction consists in assuming that both plastic hinges are active:

$$\begin{aligned} \{\mathbf{M}^{prov}\}_b &= [\mathbf{E}]_b \{\Phi_{t=tr} - \Phi_{prov}^p\}_b + \{\mathbf{M}^0\}_b; f_i^{prov} = 0; f_j^{prov} = 0; \\ \Delta\phi_i^p &= \Delta\lambda_i \left. \frac{\partial f_i}{\partial m_i} \right|_{prov}; \Delta\phi_j^p = \Delta\lambda_j \left. \frac{\partial f_j}{\partial m_j} \right|_{prov}; \Delta\delta_p = \Delta\lambda_i \left. \frac{\partial f_i}{\partial n} \right|_{prov} + \Delta\lambda_j \left. \frac{\partial f_j}{\partial n} \right|_{prov} \end{aligned} \quad (8.2.9)$$

In this case, the verification is:  $\Delta\lambda_i \Big|_{prov} \geq 0$  and  $\Delta\lambda_j \Big|_{prov} \geq 0$ .

Notice that plastic corrections are, in most cases, nonlinear problems; they can be solved by any conventional method; for instance, the Newton-Raphson method but at the local level. The verifications can be carried out after convergence of the plastic correction or even after a local iteration. An example of resolution of a local problem using this algorithm is presented in the section 8.5.2.

Figure 2b. Elastic predictor - plastic corrector algorithm: elastic behavior

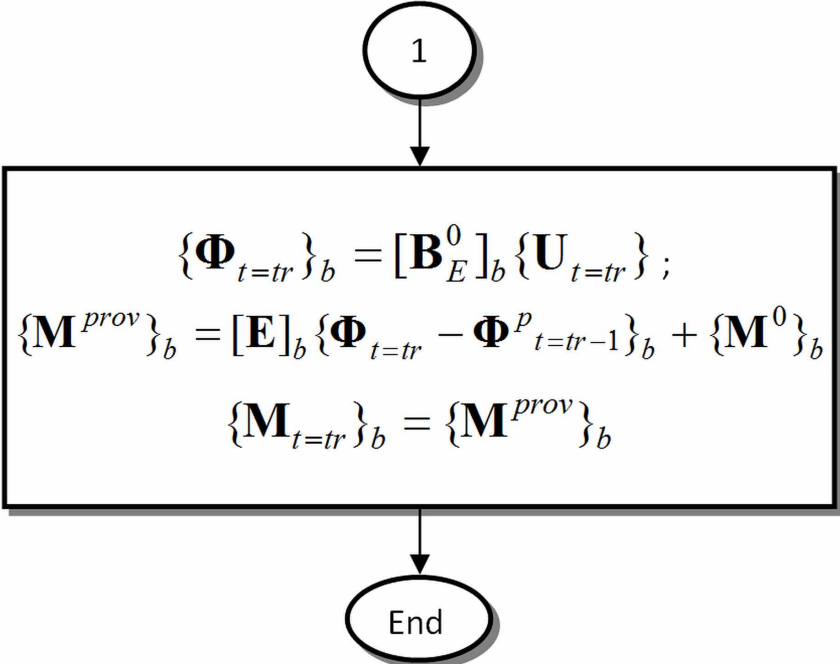
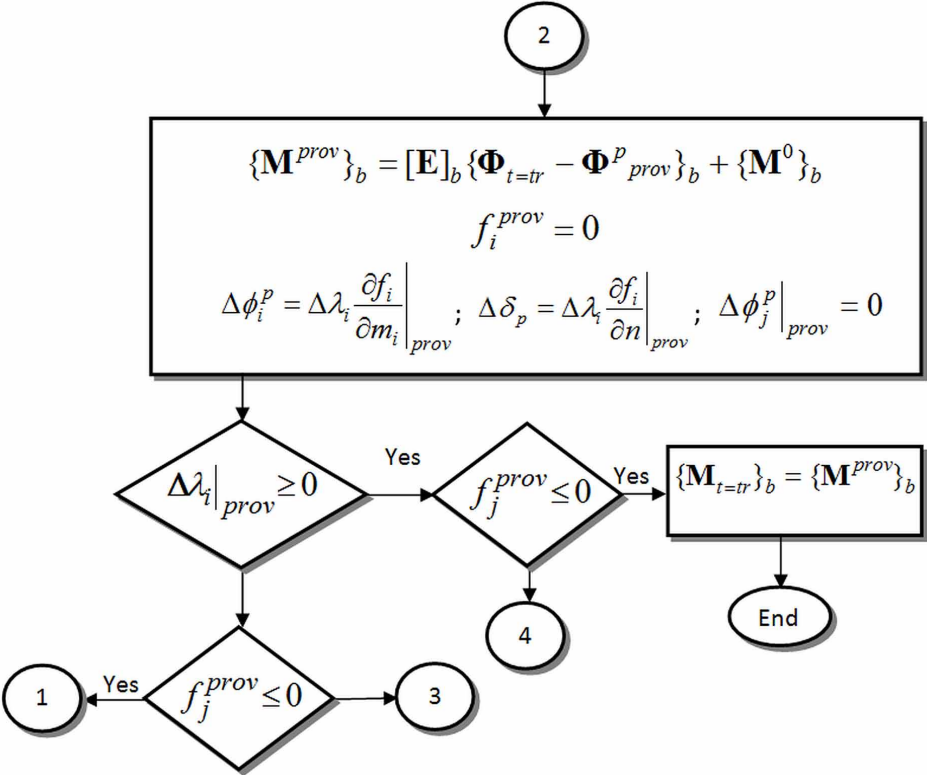


Figure 2c. Elastic predictor - plastic corrector algorithm: inelastic behavior at hinge i



**Analysis of Elasto-Plastic Frames**

Figure 2d. Elastic predictor - plastic corrector algorithm: inelastic behavior at hinge j

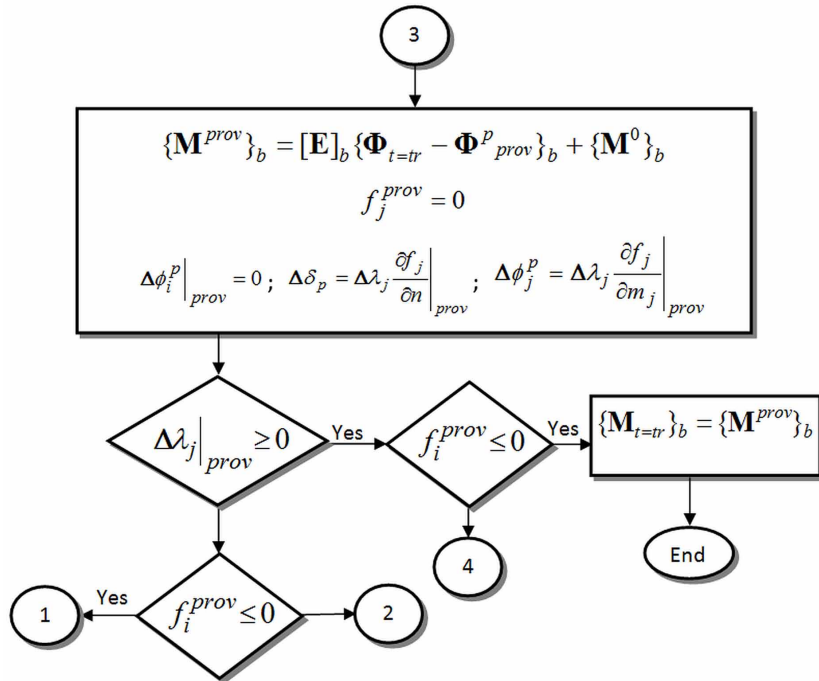
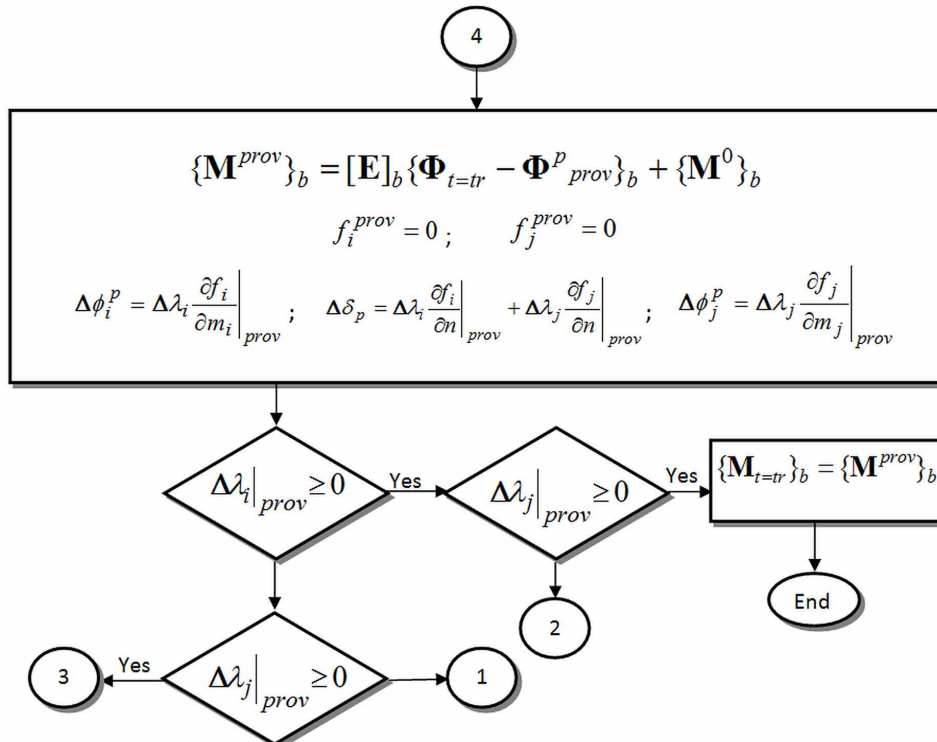


Figure 2e. Elastic predictor - plastic corrector algorithm: inelastic behavior at hinges i and j





## 8.3 GENERAL ANALYSIS OF ELASTO-PLASTIC FRAMES

### 8.3.1 Formulation of the Quasi-Static Problem

Consider now a more general case that includes geometrically nonlinear effects and/or plastic hardening. The problem is solved, again, step by step using a generalized form of the elastic predictor - plastic corrector algorithm. The kinematic and equilibrium equations at a time  $t_r$  are:

$$\begin{aligned} \{\Delta \Phi\}_b &= [\mathbf{B}_E(\mathbf{U}_{t=tr})]_b \{\Delta \mathbf{U}\}; \\ \{\mathbf{L}(\mathbf{U}_{t=tr})\} &= \{\mathbf{P}_{t=tr}\}; \{\mathbf{L}(\mathbf{U}_{t=tr})\} = \sum_{b=1}^m [\mathbf{B}(\mathbf{U}_{t=tr})_E]_b^t \{\mathbf{M}(\mathbf{U}_{t=tr})\}_b \end{aligned} \quad (8.3.1)$$

The constitutive equations will now be written in a somewhat abstract way that has the advantage of including, as particular cases, all the models presented in chapter 7, as well as the tridimensional ones and those with shear plasticity. The variables of the local problems will be grouped into four sets: the generalized deformations  $\{\Phi_{t=tr}\}_b$ , the stresses  $\{\mathbf{M}_{t=tr}\}_b$ , a set of internal variables with yield functions that are denoted  $VWf_1|_{t=tr}$ ,  $VWf_2|_{t=tr}$ , ...,  $VWf_k|_{t=tr}$ , and a matrix of internal variables without yield functions  $\{\mathbf{VW}\mathbf{o}_{t=tr}\}_b$ ; the examples 8.5.3 and 8.5.4 show how specific plasticity models fit into this general framework. The elasticity law is presented in abstract way as:

$$\{\mathbf{EL}(\Phi, \mathbf{M}, VWf_1, \dots, VWf_k, \mathbf{VW}\mathbf{o})\}|_{t=tr} = 0 \quad (8.3.2)$$

The yield functions are:

$$Yf_1(\mathbf{M}, VWf_1, \dots, VWf_k, \mathbf{VW}\mathbf{o})|_{t=tr} \leq 0 \quad \dots \quad Yf_k(\mathbf{M}, VWf_1, \dots, VWf_k, \mathbf{VW}\mathbf{o})|_{t=tr} \leq 0 \quad (8.3.3)$$

Finally, the normality laws and remaining equations of the model are written as:

$$\{\mathbf{RM}(\mathbf{M}, VWf_1, \dots, VWf_k, \mathbf{VW}\mathbf{o})\}|_{t=tr} = 0 \quad (8.3.4)$$

### 8.3.2 Elastic Predictor and Plastic Correctors

The global problem is again defined by the nonlinear equilibrium equation and it is solved by the Newton method. The elastic predictor - plastic corrector algorithm is generalized as follows:

Elastic predictor phase:

$$\begin{aligned} \{\mathbf{EL}(\Phi_{t=tr}, \mathbf{M}^{prov}, VWf_1|_{t=tr-1}, \dots, VWf_k|_{t=tr-1}, \mathbf{VW}\mathbf{o}_{t=tr-1})\} &= 0; \\ Yf_k^{prov} &= Yf_k(\mathbf{M}^{prov}, VWf_1|_{t=tr-1}, \dots, VWf_k|_{t=tr-1}, \mathbf{VW}\mathbf{o}_{t=tr-1}) \end{aligned} \quad (8.3.5)$$

## Analysis of Elasto-Plastic Frames

The plastic correction phase:

$$\begin{aligned} \{\mathbf{EL}(\Phi, \mathbf{M}, VWf_1, \dots, VWf_k, \mathbf{VW}\mathbf{o})\}\Big|_{t=tr} &= 0 \\ \begin{cases} Yf_k(\mathbf{M}, VWf_1, \dots, VWf_k, \mathbf{VW}\mathbf{o})\Big|_{t=tr} = 0 & \text{if } Yf_k^{prov} > 0 \\ \Delta VWf_1, \dots, \Delta VWf_k = 0 & \text{otherwise} \end{cases} \\ \{\mathbf{RM}(\mathbf{M}, VWf_1, \dots, VWf_k, \mathbf{VW}\mathbf{o})\}\Big|_{t=tr} &= 0 \end{aligned} \quad (8.3.6)$$

### 8.3.3 Verification Phase

The verifications depend on which line of (8.3.6b) is being actually used. If the increment of the internal variable  $VWf_k$  is zero, then it must be verified that the corresponding yield function is indeed negative:

$$\text{If } \Delta VWf_1, \dots, \Delta VWf_k = 0 \text{ verify } Yf_k(\mathbf{M}, VWf_1, \dots, VWf_k, \mathbf{VW}\mathbf{o})\Big|_{t=tr} \leq 0 \quad (8.3.7)$$

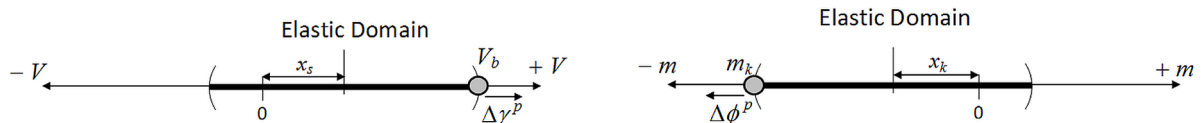
Notice that the set of variables  $VWf_k$  includes plastic multipliers and/or isolated plastic rotations. In the former case, i.e.,  $VWf_k$  is a plastic multiplier; its increments have to be positive since the plastic vector is always pointing outward the elastic domain (see Figure 12 in Chapter 6):

$$\text{If } \Delta \lambda_k \neq 0 \text{ verify } \Delta \lambda_k > 0 \quad (8.3.8)$$

Consider now the case of an isolated plastic rotation as for instance a plastic hinge without plastic elongation or shear plasticity. The elastic domain is in that case an open interval (see Figure 3). Notice that, according to the normality law, if the generalized stress point lies on the right end of the interval, then the increment of the corresponding plastic deformation has to be positive; if it is on the left one the increment should be negative; thus:

$$\begin{aligned} \text{If } \Delta \phi_k^p \neq 0 \text{ verify } (m_k - x_k) \Delta \phi_k^p > 0; \\ \text{If } \Delta \gamma^p \neq 0 \text{ verify } (V - x_s) \Delta \gamma^p > 0 \end{aligned} \quad (8.3.9)$$

Figure 3. Elastic domain and plastic increments in the case of a single plastic deformation according to the normality law



### 8.3.4 Dynamic Analysis of Elasto-Plastic Frames

If the inertia forces cannot be neglected, the constant average acceleration method described in section 4.3 can be used for the discretization of the equilibrium equation; therefore, the global problem can be written as in the case of nonlinear elastic frames subjected to dynamic forces:

$$\{\mathbf{L}(\mathbf{U}_{t=tr})\} = \{\mathbf{P}_{t=tr}\} \text{ where } \{\mathbf{L}(\mathbf{U}_{t=tr})\} = \sum_{b=1}^m [\mathbf{B}(\mathbf{U}_{t=tr})_E]_b^T \{\mathbf{M}(\mathbf{U}_{t=tr})\}_b + [\mathbf{Mass}] \{\ddot{\mathbf{U}}(\mathbf{U}_{t=tr})\} \quad (8.3.10)$$

The global problem can also be solved by the Newton method; the local problems remain unmodified.

### 8.4 SUMMARY AND EQUATIONS QUICK REFERENCE

This chapter presents two methods for the elasto-plastic analysis of frame structures. The first one is called hinge-by-hinge method. It consists in the resolution of a sequence of linear problems; however, it can only be used in the simplest case of plasticity. The second one is based on the elastic predictor – plastic corrector algorithm. In this case, the equations are separated into two groups. These two sets of equations are solved separately: the global problem and the local problem; both of them could be nonlinear. Therefore, they are solved using an iterative method. The local problem requires also the use of the elastic predictor – plastic corrector algorithm. This algorithm represents a systematic procedure to determine which plastic hinges are active at any step (See Table 1).

Table 1.

THE HINGE-BY-HINGE METHOD FOR PERFECT PLASTIC FRAMES	
<i>Formulation of the Problem</i>	
Variables to determine: <ul style="list-style-type: none"> <li>• Free displacements</li> <li>• Reaction forces</li> <li>• Generalized deformations</li> <li>• Plastic rotations</li> <li>• Stresses</li> </ul>	Data: <ul style="list-style-type: none"> <li>• Initial configuration of the structure</li> <li>• Restricted displacements</li> </ul> Reference forces $\{\mathbf{P}_{ref}\}$  Forces applied over the elements $\{\mathbf{P}^{eq}\}$ <ul style="list-style-type: none"> <li>• Material and cross-section properties (<math>E, I, A, M_y</math>)</li> </ul>
The structure is subjected to:  Set of distributed loads that not produce plastic deformations: $\{\mathbf{P}^e\}$  Set of concentrated loads on the frame: $l(t)\{\mathbf{P}_{ref}\}$ <ul style="list-style-type: none"> <li>• <math>l(t)</math>: loading parameter (monotonically strict increasing function of time)</li> <li>• <math>\{\mathbf{P}_{ref}\}</math> : references forces that remain constant during the entire analysis</li> <li>•</li> </ul>	

*continued on following page*

## Analysis of Elasto-Plastic Frames

Table 1. Continued

<p>Linear kinematic equation</p> $\{\Phi\}_b = [\mathbf{B}_E^0]_b \{\mathbf{U}\} \quad (8.1.1 \text{ a})$
<p>Linear equilibrium equation</p> $\sum_{b=1}^m [\mathbf{B}_E^0]_b^t \{\mathbf{M}\}_b = \{\mathbf{P}^{eq}\} + l\{\mathbf{P}_{ref}\} + \{\mathbf{R}\} \quad (8.1.1 \text{ b})$
<p>Elasticity law</p> $\{\Phi - \Phi^p\}_b = [\mathbf{F}_f]_b \{\mathbf{M}\}_b + \{\Phi^0\}_b \quad (8.1.1 \text{ c})$
<p>Plastic rotations evolution laws</p> $\left\{ \begin{array}{l} d\phi_i^p = 0 \text{ if } f_i(m_i) < 0 \text{ (hinge locked)} \\ f_i(m_i) = 0 \text{ if } d\phi_i^p \neq 0 \text{ (active hinge)} \end{array} \right\}; \quad (8.1.1 \text{ d})$ $\left\{ \begin{array}{l} d\phi_j^p = 0 \text{ if } f_j(m_j) < 0 \text{ (hinge locked)} \\ f_j(m_j) = 0 \text{ if } d\phi_j^p \neq 0 \text{ (active hinge)} \end{array} \right\}$
<p>Yield functions</p> $f_i(m_i) =  m_i  - M_{iy} \leq 0; f_j(m_j) =  m_j  - M_{jy} \leq 0 \quad (8.1.1 \text{ e})$
<p><b>Formulation of the Problem in Incremental Form</b></p>
<p>Linear kinematic equation</p> $\{\Delta\Phi\}_b = [\mathbf{B}_E^0]_b \{\Delta\mathbf{U}\} \quad (8.1.2)$
<p>Linear equilibrium equation</p> $\sum_{b=1}^m [\mathbf{B}_E^0]_b^t \{\Delta\mathbf{M}\}_b = \Delta l\{\mathbf{P}^R\}; \text{ where } \{\mathbf{P}^R\} = \{\mathbf{P}_{ref}\} + \frac{1}{\Delta l}\{\Delta\mathbf{R}\} \quad (8.1.3)$
<p>Elasticity law</p> $\{\Delta\Phi - \Delta\Phi^p\}_b = [\mathbf{F}_f]_b \{\Delta\mathbf{M}\}_b \quad (8.1.4 \text{ a})$ $\left\{ \begin{array}{l} \Delta\phi_i^p = 0 \text{ if hinge } i \text{ is locked} \\ \Delta m_i^b = 0 \text{ if hinge } i \text{ is active} \end{array} \right\}; \left\{ \begin{array}{l} \Delta\phi_j^p = 0 \text{ if hinge } j \text{ is locked} \\ \Delta m_j^b = 0 \text{ if hinge } j \text{ is active} \end{array} \right\}$
<p>Plastic rotations evolution laws</p> $\left\{ \begin{array}{l} \phi_i^p = 0 \text{ if }  m_i^b  < M_{iy} \\ \Delta m_i^b = 0 \text{ if }  m_i^b  = M_{iy} \end{array} \right\}; \left\{ \begin{array}{l} \phi_j^p = 0 \text{ if }  m_j^b  < M_{jy} \\ \Delta m_j^b = 0 \text{ if }  m_j^b  = M_{jy} \end{array} \right\} \quad (8.1.5)$

continued on following page

Table 1. Continued

<i>Tangent Elasticity Matrix of a Frame Element</i>	
Elasticity law	$\Delta\phi_i^b - \Delta\phi_i^P = \frac{L_b}{3EI_b} \Delta m_i^b - \frac{L_b}{6EI_b} \Delta m_j^b$ $\Delta\phi_j^b - \Delta\phi_j^P = -\frac{L_b}{6EI_b} \Delta m_i^b + \frac{L_b}{3EI_b} \Delta m_j^b$ $\Delta\delta_b = \frac{L_b}{AE_b} \Delta n_b \quad (8.1.6)$
Element with two plastic hinges ( $\Delta m_i^b = 0, \Delta m_j^b = 0$ )	$\{\Delta\mathbf{M}\}_b = [\mathbf{S}_2]_b \{\Delta\Phi\}_b; [\mathbf{S}_2]_b = \begin{bmatrix} 0 & 0 & 0 \\ 0 & 0 & 0 \\ 0 & 0 & \frac{AE_b}{L_b} \end{bmatrix}; \Delta\phi_i^P = \Delta\phi_i^b; \Delta\phi_j^P = \Delta\phi_j^b \quad (8.1.7)$
Element with plastic hinge at the end $i$ ( $\Delta m_i^b = 0, \phi_j^P = 0$ )	$\{\Delta\mathbf{M}\}_b = [\mathbf{S}_{1i}]_b \{\Delta\Phi\}_b; [\mathbf{S}_{1i}]_b = \begin{bmatrix} 0 & 0 & 0 \\ 0 & \frac{3EI_b}{L_b} & 0 \\ 0 & 0 & \frac{AE_b}{L_b} \end{bmatrix}; \Delta\phi_i^P = \Delta\phi_i^b + \frac{1}{2} \Delta\phi_j^b; \phi_j^P = 0 \quad (8.1.8)$
Element with plastic hinge at the end $j$ ( $\Delta m_j^b = 0, \phi_i^P = 0$ )	$\{\Delta\mathbf{M}\}_b = [\mathbf{S}_{1j}]_b \{\Delta\Phi\}_b; [\mathbf{S}_{1j}]_b = \begin{bmatrix} \frac{3EI_b}{L_b} & 0 & 0 \\ 0 & 0 & 0 \\ 0 & 0 & \frac{AE_b}{L_b} \end{bmatrix}; \Delta\phi_j^P = \Delta\phi_j^b + \frac{1}{2} \Delta\phi_i^b; \phi_i^P = 0 \quad (8.1.9)$

*continued on following page*

*Table 1. Continued*

<p>Element without plastic hinges</p> $\{\Delta \mathbf{M}\}_b = [\mathbf{S}_0]_b \{\Delta \Phi\}_b; [\mathbf{S}_0]_b = \begin{bmatrix} \frac{4EI_b}{L_b} & \frac{2EI_b}{L_b} & 0 \\ \frac{2EI_b}{L_b} & \frac{4EI_b}{L_b} & 0 \\ 0 & 0 & \frac{AE_b}{L_b} \end{bmatrix}; \phi_i^P = 0; \phi_j^P = 0$ <p style="text-align: right;">(8.1.10)</p>
<p>Equations (8.1.7-10) can be summarized as:</p> $\{\Delta \mathbf{M}\}_b = [\mathbf{S}]_b \{\Delta \Phi\}_b \quad (8.1.11)$ $[\mathbf{S}]_b = \begin{cases} \begin{bmatrix} [\mathbf{S}_0]_b \\ [\mathbf{S}_{1i}]_b \\ [\mathbf{S}_{1j}]_b \end{bmatrix} & \begin{array}{l} \text{if there are no plastic hinges} \\ \text{if there is a plastic hinge at the end i} \\ \text{if there is a plastic hinge at the end j} \end{array} \\ \begin{bmatrix} [\mathbf{S}_2]_b \end{bmatrix} & \text{if there are two plastic hinges} \end{cases} \quad (8.1.12)$
<b>The Hinge-by-Hinge Algorithm</b>
<p>Stiffness matrix</p> $\left( \sum_{b=1}^m [\mathbf{B}_E^0]_b^t [\mathbf{S}]_b [\mathbf{B}_E^0]_b \right) \{\Delta \mathbf{U} / \Delta l\} = \{\mathbf{P}^R\} \quad (8.1.13)$ $[\mathbf{K}_t] \{\mathbf{V}\} = \{\mathbf{P}^R\}; \text{ where } [\mathbf{K}_t] = \sum_{b=1}^m [\mathbf{B}_E^0]_b^t [\mathbf{S}]_b [\mathbf{B}_E^0]_b; \{\mathbf{V}\} = \frac{1}{\Delta l} \{\Delta \mathbf{U}\} \quad (8.1.14)$
<p>Displacements, strains and stresses</p> $\{\mathbf{U}\} = \{\mathbf{U}\}_{t=0} + \Delta l \{\mathbf{V}\}$ $\{\Phi\}_b = \{\Phi_{t=0}\}_b + \Delta l [\mathbf{B}_E^0]_b \{\mathbf{V}\} \quad (8.1.15)$ $\{\mathbf{M}\}_b = \{\mathbf{M}_{t=0}\}_b + \Delta l [\mathbf{S}]_b [\mathbf{B}_E^0]_b \{\mathbf{V}\}$
<p>Resolution of the hinge-by-hinge method</p> <p>First step: Determination of the state of the structure under the distributed forces</p> $\{\mathbf{U}\}_{t=0} = \{\mathbf{U}_0\}, \{\Phi\}_{t=0} = \{\Phi_0\}, \{\mathbf{M}\}_{t=0} = \{\mathbf{M}_0\} \text{ with } l(0) = 0$ <p>Second step: equation <math>[\mathbf{K}_t] \{\mathbf{V}\} = \{\mathbf{P}^R\}</math> is solved by the direct stiffness method</p> $[\mathbf{K}_t] = \sum_{b=1}^m [\mathbf{B}_E^0]_b^t [\mathbf{S}_0]_b [\mathbf{B}_E^0]_b; \{\mathbf{V}\} = \frac{1}{\Delta l} \{\Delta \mathbf{U}\}$ <p>Plastic hinge is unlocked, second step is therefore computed solving</p> $\text{Max } (  m_k  - M_{ky} ) = 0 \quad (8.1.16)$

*continued on following page*

Table 1. Continued

<i>Tangent Stiffness Matrix of a Frame Element</i>	
Tangent stiffness matrix of an element	
$[\mathbf{k}_t] = [\mathbf{B}^0]^t [\mathbf{S}]_b [\mathbf{B}^0]_b$ (8.1.17)	
$[\mathbf{B}^0]_b$ : non expanded kinematic transformation matrix	
For $[\mathbf{S}]_b = [\mathbf{S}_0]_b$ : tangent stiffness matrix	
$[\mathbf{k}_t] =$	$\begin{bmatrix} \frac{12EI}{L^3} s^2 + \frac{EA}{L} c^2 & \left(-\frac{12EI}{L^3} + \frac{EA}{L}\right) sc & \frac{6EI}{L^2} s & -\frac{12EI}{L^3} s^2 - \frac{EA}{L} c^2 & \left(\frac{12EI}{L^3} - \frac{EA}{L}\right) sc & \frac{6EI}{L^2} s \\ \left(-\frac{12EI}{L^3} + \frac{EA}{L}\right) sc & \frac{12EI}{L^3} c^2 + \frac{EA}{L} s^2 & -\frac{6EI}{L^2} c & \left(\frac{12EI}{L^3} - \frac{EA}{L}\right) sc & -\frac{12EI}{L^3} c^2 - \frac{EA}{L} s^2 & -\frac{6EI}{L^2} c \\ \frac{6EI}{L^2} s & -\frac{6EI}{L^2} c & \frac{4EI}{L} & -\frac{6EI}{L^2} s & \frac{6EI}{L^2} c & \frac{2EI}{L} \\ -\frac{12EI}{L^3} s^2 - \frac{EA}{L} c^2 & \left(\frac{12EI}{L^3} - \frac{EA}{L}\right) sc & -\frac{6EI}{L^2} s & \frac{12EI}{L^3} s^2 + \frac{EA}{L} c^2 & \left(-\frac{12EI}{L^3} + \frac{EA}{L}\right) sc & -\frac{6EI}{L^2} s \\ \left(\frac{12EI}{L^3} - \frac{EA}{L}\right) sc & -\frac{12EI}{L^3} c^2 - \frac{EA}{L} s^2 & \frac{6EI}{L^2} c & \left(-\frac{12EI}{L^3} + \frac{EA}{L}\right) sc & \frac{12EI}{L^3} c^2 + \frac{EA}{L} s^2 & \frac{6EI}{L^2} c \\ \frac{6EI}{L^2} s & -\frac{6EI}{L^2} c & \frac{2EI}{L} & -\frac{6EI}{L^2} s & \frac{6EI}{L^2} c & \frac{4EI}{L} \end{bmatrix}$
(8.1.18)	
$s = \sin \alpha_b$ ; $c = \cos \alpha_b$ ; $\alpha_b$ is the angle with respect the global axis $X$	
For $[\mathbf{S}]_b = [\mathbf{S}_{1i}]_b$	
$[\mathbf{k}_t] =$	$\begin{bmatrix} \frac{3EI}{L^3} s^2 + \frac{EA}{L} c^2 & \left(-\frac{3EI}{L^3} + \frac{EA}{L}\right) sc & 0 & -\frac{3EI}{L^3} s^2 - \frac{EA}{L} c^2 & \left(\frac{3EI}{L^3} - \frac{EA}{L}\right) sc & \frac{3EI}{L^2} s \\ \left(-\frac{3EI}{L^3} + \frac{EA}{L}\right) sc & \frac{3EI}{L^3} c^2 + \frac{EA}{L} s^2 & 0 & \left(\frac{3EI}{L^3} - \frac{EA}{L}\right) sc & -\frac{3EI}{L^3} c^2 - \frac{EA}{L} s^2 & -\frac{3EI}{L^2} c \\ 0 & 0 & 0 & 0 & 0 & 0 \\ -\frac{3EI}{L^3} s^2 - \frac{EA}{L} c^2 & \left(\frac{3EI}{L^3} - \frac{EA}{L}\right) sc & 0 & \frac{3EI}{L^3} s^2 + \frac{EA}{L} c^2 & \left(-\frac{3EI}{L^3} + \frac{EA}{L}\right) sc & -\frac{3EI}{L^2} s \\ \left(\frac{3EI}{L^3} - \frac{EA}{L}\right) sc & -\frac{3EI}{L^3} c^2 - \frac{EA}{L} s^2 & 0 & \left(-\frac{3EI}{L^3} + \frac{EA}{L}\right) sc & \frac{3EI}{L^3} c^2 + \frac{EA}{L} s^2 & \frac{3EI}{L^2} c \\ \frac{3EI}{L^2} s & -\frac{3EI}{L^2} c & 0 & -\frac{3EI}{L^2} s & \frac{3EI}{L^2} c & \frac{3EI}{L} \end{bmatrix}$
(8.1.19)	

continued on following page

**Analysis of Elasto-Plastic Frames**

Table 1. Continued

<p>For <math>[\mathbf{S}]_b = [\mathbf{S}_{1j}]_b</math></p> $[\mathbf{k}_t] = \begin{bmatrix} \frac{3EI}{L^3} s^2 + \frac{EA}{L} c^2 & \left(-\frac{3EI}{L^3} + \frac{EA}{L}\right) sc & \frac{3EI}{L^2} s & -\frac{3EI}{L^3} s^2 - \frac{EA}{L} c^2 & \left(\frac{3EI}{L^3} - \frac{EA}{L}\right) sc & 0 \\ \left(-\frac{3EI}{L^3} + \frac{EA}{L}\right) sc & \frac{3EI}{L^3} c^2 + \frac{EA}{L} s^2 & -\frac{3EI}{L^2} c & \left(\frac{3EI}{L^3} - \frac{EA}{L}\right) sc & -\frac{3EI}{L^3} c^2 - \frac{EA}{L} s^2 & 0 \\ \frac{3EI}{L^2} s & -\frac{3EI}{L^2} c & \frac{3EI}{L} & -\frac{3EI}{L^2} s & \frac{3EI}{L^2} c & 0 \\ -\frac{3EI}{L^3} s^2 - \frac{EA}{L} c^2 & \left(\frac{3EI}{L^3} - \frac{EA}{L}\right) sc & -\frac{3EI}{L^2} s & \frac{3EI}{L^3} s^2 + \frac{EA}{L} c^2 & \left(-\frac{3EI}{L^3} + \frac{EA}{L}\right) sc & 0 \\ \left(\frac{3EI}{L^3} - \frac{EA}{L}\right) sc & -\frac{3EI}{L^3} c^2 - \frac{EA}{L} s^2 & \frac{3EI}{L^2} c & \left(-\frac{3EI}{L^3} + \frac{EA}{L}\right) sc & \frac{3EI}{L^3} c^2 + \frac{EA}{L} s^2 & 0 \\ 0 & 0 & 0 & 0 & 0 & 0 \end{bmatrix} \quad (8.1.20)$	
<p>For <math>[\mathbf{S}]_b = [\mathbf{S}_2]_b</math></p> $[\mathbf{k}_t] = \begin{bmatrix} \frac{EA}{L} c^2 & \frac{EA}{L} sc & 0 & -\frac{EA}{L} c^2 & -\frac{EA}{L} sc & 0 \\ \frac{EA}{L} sc & \frac{EA}{L} s^2 & 0 & -\frac{EA}{L} sc & -\frac{EA}{L} s^2 & 0 \\ 0 & 0 & 0 & 0 & 0 & 0 \\ -\frac{EA}{L} c^2 & -\frac{EA}{L} sc & 0 & \frac{EA}{L} c^2 & \frac{EA}{L} sc & 0 \\ -\frac{EA}{L} sc & -\frac{EA}{L} s^2 & 0 & \frac{EA}{L} sc & \frac{EA}{L} s^2 & 0 \\ 0 & 0 & 0 & 0 & 0 & 0 \end{bmatrix} \quad (8.1.21)$	
<b>ELASTIC PREDICTOR - PLASTIC CORRECTOR ALGORITHM</b>	
<i>Formulation of the Problem</i>	
<p>Variables to determine:</p> <ul style="list-style-type: none"> <li>• Free displacements,</li> <li>• Reaction forces</li> <li>• Generalized deformations</li> <li>• Plastic rotations</li> <li>• Stresses</li> </ul>	<p>Data:</p> <ul style="list-style-type: none"> <li>• Initial configuration of the structure</li> <li>• Restricted displacements</li> </ul> <p>Forces applied over the elements <math>\{\mathbf{P}^{eq}\}</math></p> <ul style="list-style-type: none"> <li>• Material and cross-section properties (<math>E, I, A, M_y</math>)</li> <li>• Yield functions</li> </ul>
<p>Linear kinematic equation</p> $\{\Phi\}_b = [\mathbf{B}_E^0]_b \{\mathbf{U}\} \quad (8.2.1 a)$	
<p>Linear equilibrium equation</p> $\sum_{b=1}^m [\mathbf{B}_E^0]_b^t \{\mathbf{M}\}_b = \{\mathbf{P}\} \quad (8.2.1 b)$	

*continued on following page*



Table 1. Continued

Elasticity law $\{\mathbf{M}\}_b = [\mathbf{E}]_b \{\Phi - \Phi^p\}_b + \{\mathbf{M}^0\}_b \quad (8.2.1 \text{ c})$	
The normality laws $d\phi_i^p = d\lambda_i \frac{\partial f_i}{\partial m_i}; d\phi_j^p = d\lambda_j \frac{\partial f_j}{\partial m_j}; d\delta_p = d\lambda_i \frac{\partial f_i}{\partial n} + d\lambda_j \frac{\partial f_j}{\partial n} \quad (8.2.1 \text{ d})$	
Evolution laws of plastic multipliers $\begin{cases} d\lambda_i = 0 \text{ if } f_i(m_i, n) < 0 \\ f_i(m_i, n) = 0 \text{ if } d\lambda_i \neq 0 \end{cases}; \begin{cases} d\lambda_j = 0 \text{ if } f_j(m_j, n) < 0 \\ f_j(m_j, n) = 0 \text{ if } d\lambda_j \neq 0 \end{cases} \quad (8.2.1 \text{ e})$	
<b>Global and Local Problems</b>	
<b>Global Problem:</b> Resolution of the equilibrium equation and its boundary conditions (it involves all the elements of the frame) <b>Local Problem:</b> Resolution of the kinematic and constitutive equations (they relate variables of only one element b)	
<b>Formulation of the Local Problem (At Any Time <math>t_r</math>)</b>	
Variables to determine: <ul style="list-style-type: none"> <li>• Generalized deformations</li> <li>• Plastic rotations</li> <li>• Stresses</li> </ul>	Data: <ul style="list-style-type: none"> <li>• Displacements of the element</li> <li>• Forces applied over the elements at time <math>t_r</math></li> <li>• Material and cross-section properties (<math>E, I, A, M_y</math>)</li> <li>• Yield functions</li> </ul>
Linear kinematic equation $\{\Phi_{t=tr}\}_b = [\mathbf{B}_E^0]_b \{\mathbf{U}_{t=tr}\} \quad (8.2.2 \text{ a})$	
Elasticity law $\{\mathbf{M}_{t=tr}\}_b = [\mathbf{E}]_b \{\Phi_{t=tr} - \Phi_{t=tr}^p\}_b + \{\mathbf{M}^0\}_b \quad (8.2.2 \text{ b})$	
Normality laws $\Delta\phi_i^p = \Delta\lambda_i \left. \frac{\partial f_i}{\partial m_i} \right _{t=tr}; \Delta\phi_j^p = \Delta\lambda_j \left. \frac{\partial f_j}{\partial m_j} \right _{t=tr}; \Delta\delta_p = \Delta\lambda_i \left. \frac{\partial f_i}{\partial n} \right _{t=tr} + \Delta\lambda_j \left. \frac{\partial f_j}{\partial n} \right _{t=tr} \quad (8.2.2 \text{ c})$	
Plastic multipliers evolution laws $\begin{cases} \Delta\lambda_i = 0 \text{ if } f_i _{t=tr} < 0 \\ f_i _{t=tr} = 0 \text{ if } \Delta\lambda_i \neq 0 \end{cases}; \begin{cases} \Delta\lambda_j = 0 \text{ if } f_j _{t=tr} < 0 \\ f_j _{t=tr} = 0 \text{ if } \Delta\lambda_j \neq 0 \end{cases} \quad (8.2.2 \text{ d})$	
<b>Formulation of the Global Problem (At Any Time <math>t_r</math>)</b>	
Equilibrium equation Newton-Raphson algorithm $\{\mathbf{L}(\mathbf{U}_{t=tr})\} = \{\mathbf{P}_{t=tr}\}; \{\mathbf{L}(\mathbf{U}_{t=tr})\} = \sum_{b=1}^m [\mathbf{B}(\mathbf{U}_{t=tr})_E]_b^T \{\mathbf{M}(\mathbf{U}_{t=tr})\}_b; \{\mathbf{L}(\mathbf{U}_{t=tr})\} = \{\mathbf{P}_{t=tr}\} \quad (8.2.3)$	
<b>Numerical Resolution of the Local Problem</b>	
Provisional stress matrix $\{\Phi_{t=tr}\}_b = [\mathbf{B}_E^0]_b \{\mathbf{U}_{t=tr}\}; \{\mathbf{M}^{prov}\}_b = [\mathbf{E}]_b \{\Phi_{t=tr} - \Phi_{t=tr-1}^p\}_b + \{\mathbf{M}^0\}_b \quad (8.2.4)$	

continued on following page

*Table 1. Continued*

<p>Yield functions  <math>f_i^{prov} = f_i(m_i^{prov}, n^{prov}); f_j^{prov} = f_j(m_j^{prov}, n^{prov})</math> (8.2.5)</p> <p>If both yield functions are negative or zero  <math>\{\mathbf{M}_{t=tr}\}_b = \{\mathbf{M}^{prov}\}_b</math> (8.2.6)</p>	
<p>If <math>f_i^{prov} &gt; 0</math> and <math>f_j^{prov} \leq 0</math>  <math>\{\mathbf{M}^{prov}\}_b = [\mathbf{E}]_b \{\Phi_{t=tr} - \Phi_{prov}^p\}_b + \{\mathbf{M}^0\}_b; f_i^{prov} = 0;</math>  <math>\Delta\phi_i^p = \Delta\lambda_i \left. \frac{\partial f_i}{\partial m_i} \right _{prov}; \Delta\delta_p = \Delta\lambda_i \left. \frac{\partial f_i}{\partial n} \right _{prov}; \Delta\phi_j^p _{prov} = 0</math> (8.2.7)</p>	
<p>If <math>f_i^{prov} \leq 0</math> and <math>f_j^{prov} &gt; 0</math>  <math>\{\mathbf{M}^{prov}\}_b = [\mathbf{E}]_b \{\Phi_{t=tr} - \Phi_{prov}^p\}_b + \{\mathbf{M}^0\}_b; f_j^{prov} = 0;</math>  <math>\Delta\phi_i^p _{prov} = 0; \Delta\phi_j^p = \Delta\lambda_j \left. \frac{\partial f_j}{\partial m_j} \right _{prov}; \Delta\delta_p = \Delta\lambda_j \left. \frac{\partial f_j}{\partial n} \right _{prov}</math> (8.2.8)</p> <p>The corresponding verification is: <math>f_i^{prov} \leq 0</math> and <math>\Delta\lambda_j _{prov} \geq 0</math></p>	
<p>If <math>f_i^{prov} &gt; 0</math> and <math>f_j^{prov} &gt; 0</math>  <math>\{\mathbf{M}^{prov}\}_b = [\mathbf{E}]_b \{\Phi_{t=tr} - \Phi_{prov}^p\}_b + \{\mathbf{M}^0\}_b; f_i^{prov} = 0; f_j^{prov} = 0;</math>  <math>\Delta\phi_i^p = \Delta\lambda_i \left. \frac{\partial f_i}{\partial m_i} \right _{prov}; \Delta\phi_j^p = \Delta\lambda_j \left. \frac{\partial f_j}{\partial m_j} \right _{prov}; \Delta\delta_p = \Delta\lambda_i \left. \frac{\partial f_i}{\partial n} \right _{prov} + \Delta\lambda_j \left. \frac{\partial f_j}{\partial n} \right _{prov}</math> (8.2.9)</p> <p>The verification is: <math>\Delta\lambda_i _{prov} \geq 0</math> and <math>\Delta\lambda_j _{prov} \geq 0</math>.</p>	
<b>GENERAL ANALYSIS OF ELASTIC PLASTIC FRAMES</b>	
<i>Formulation of the Quasi-Static Problem</i>	
Variables	<p>Generalized deformations <math>\{\Phi_{t=tr}\}_b</math></p> <p>Generalized stresses <math>\{\mathbf{M}_{t=tr}\}_b</math></p> <ul style="list-style-type: none"> <li>• Set of internal variables with yield functions:  <math>VWf_{j_1} _{t=tr}, VWf_{j_2} _{t=tr}, \dots, VWf_{j_k} _{t=tr}</math></li> <li>• A matrix of internal variables without yield function  <math>\{\mathbf{VW}\mathbf{o}_{t=tr}\}_b</math></li> </ul>

*continued on following page*

Table 1. Continued

Linear kinematic equation $\{\Delta \Phi\}_b = [\mathbf{B}_E(\mathbf{U}_{t=tr})]_b \{\Delta \mathbf{U}\}; \{\mathbf{L}(\mathbf{U}_{t=tr})\} = \{\mathbf{P}_{t=tr}\}; \{\mathbf{L}(\mathbf{U}_{t=tr})\} = \sum_{b=1}^m [\mathbf{B}(\mathbf{U}_{t=tr})_E]_b^t \{\mathbf{M}(\mathbf{U}_{t=tr})\}_b \quad (8.3.1)$
Elasticity law is presented in abstract way $\{\mathbf{E}\mathbf{L}(\Phi, \mathbf{M}, VWf_1, \dots, VWf_k, \mathbf{V}\mathbf{W}\mathbf{o})\}_{t=tr} = 0 \quad (8.3.2)$
Yield functions $Yf_1(\mathbf{M}, VWf_1, \dots, VWf_k, \mathbf{V}\mathbf{W}\mathbf{o})\Big _{t=tr} \leq 0 \quad \dots \quad Yf_k(\mathbf{M}, VWf_1, \dots, VWf_k, \mathbf{V}\mathbf{W}\mathbf{o})\Big _{t=tr} \leq 0 \quad (8.3.3)$
Normality laws $\{\mathbf{R}\mathbf{M}(\mathbf{M}, VWf_1, \dots, VWf_k, \mathbf{V}\mathbf{W}\mathbf{o})\}_{t=tr} = 0 \quad (8.3.4)$
<b>Elastic Predictor and Plastic Correctors</b>
Elastic predictor phase $\{\mathbf{E}\mathbf{L}(\Phi_{t=tr}, \mathbf{M}^{prov}, VWf_1\Big _{t=tr-1}, \dots, VWf_k\Big _{t=tr-1}, \mathbf{V}\mathbf{W}\mathbf{o}_{t=tr-1})\} = 0 \quad (8.3.5)$ $Yf_k^{prov} = Yf_k(\mathbf{M}^{prov}, VWf_1\Big _{t=tr-1}, \dots, VWf_k\Big _{t=tr-1}, \mathbf{V}\mathbf{W}\mathbf{o}_{t=tr-1})$
Plastic correction phase $\{\mathbf{E}\mathbf{L}(\Phi, \mathbf{M}, VWf_1, \dots, VWf_k, \mathbf{V}\mathbf{W}\mathbf{o})\}_{t=tr} = 0;$ $\begin{cases} Yf_k(\mathbf{M}, VWf_1, \dots, VWf_k, \mathbf{V}\mathbf{W}\mathbf{o})\Big _{t=tr} = 0 & \text{if } Yf_k^{prov} > 0; \\ \Delta VWf_1, \dots, \Delta VWf_k = 0 & \text{otherwise} \end{cases};$ $\{\mathbf{R}\mathbf{M}(\mathbf{M}, VWf_1, \dots, VWf_k, \mathbf{V}\mathbf{W}\mathbf{o})\}_{t=tr} = 0 \quad (8.3.6)$
<b>Verification Phase</b>
Yield functions If $\Delta VWf_1, \dots, \Delta VWf_k = 0$ verify $Yf_k(\mathbf{M}, VWf_1, \dots, VWf_k, \mathbf{V}\mathbf{W}\mathbf{o})\Big _{t=tr} \leq 0 \quad (8.3.7)$
Plastic multiplier If $\Delta \lambda_k \neq 0$ verify $\Delta \lambda_k > 0 \quad (8.3.8)$
Elastic domain If $\Delta \phi_k^p \neq 0$ verify $(m_k - x_k) \Delta \phi_k^p > 0$ ; If $\Delta \gamma^p \neq 0$ verify $(V - x_s) \Delta \gamma^p > 0 \quad (8.3.9)$
<b>Dynamic Analysis of Elasto-Plastic Frames</b>
Equilibrium equation $\{\mathbf{L}(\mathbf{U}_{t=tr})\} = \{\mathbf{P}_{t=tr}\} \text{ where } \{\mathbf{L}(\mathbf{U}_{t=tr})\} = \sum_{b=1}^m [\mathbf{B}(\mathbf{U}_{t=tr})_E]_b^t \{\mathbf{M}(\mathbf{U}_{t=tr})\}_b + [\mathbf{Mass}] \{\ddot{\mathbf{U}}(\mathbf{U}_{t=tr})\} \quad (8.3.10)$

## 8.5 EXAMPLES

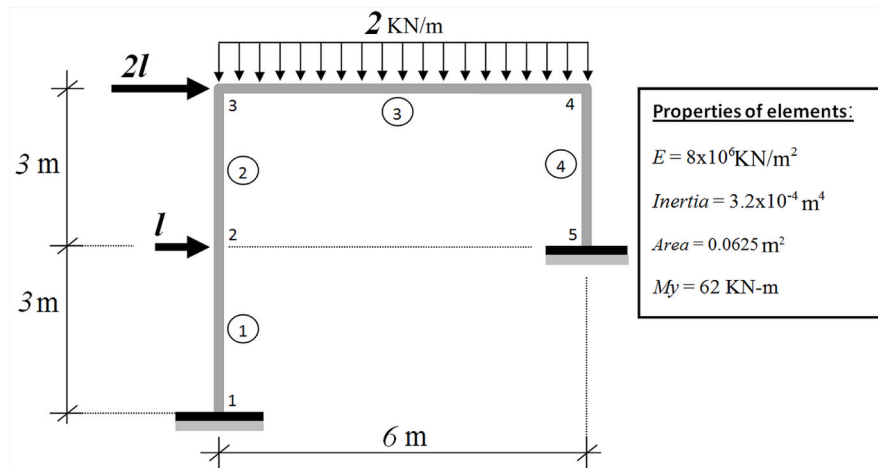
### 8.5.1. Analyze the Frame Shown in Figure 4 Using the Hinge-by-Hinge Method

The structure is analyzed following the procedure presented in section 8.1.4.

- **First Step:** (state of the structure after the application of the distributed forces on the elements)  
 $s = 0, l(0)=0$ .

$$\begin{Bmatrix} 0 \\ 0 \\ 0 \\ u_{02} \\ w_{02} \\ \theta_{02} \\ u_{03} \\ w_{03} \\ \theta_{03} \\ u_{04} \\ w_{04} \\ \theta_{04} \\ 0 \\ 0 \\ 0 \end{Bmatrix}; \begin{Bmatrix} \mathbf{P}^e \end{Bmatrix} = \begin{Bmatrix} 0 \\ 0 \\ 0 \\ -6 \\ 6 \\ 0 \\ 0 \\ 0 \\ 0 \\ -6 \\ -6 \\ 0 \\ 0 \\ 0 \end{Bmatrix}; \begin{Bmatrix} \mathbf{R}_0 \end{Bmatrix} = \begin{Bmatrix} R_{0u1} \\ R_{0w1} \\ R_{0\theta1} \\ 0 \\ 0 \\ 0 \\ 0 \\ 0 \\ 0 \\ 0 \\ 0 \\ 0 \\ R_{0u5} \\ R_{0w5} \\ R_{0\theta5} \end{Bmatrix}; \begin{Bmatrix} \mathbf{P}_{ref} \end{Bmatrix} = \begin{Bmatrix} 0 \\ 0 \\ 0 \\ 1 \\ 0 \\ 0 \\ 2 \\ 0 \\ 0 \\ 0 \\ 0 \\ 0 \\ 0 \\ 0 \\ 0 \end{Bmatrix} \quad (8.5.1)$$

Figure 4. RC frame subjected to horizontal and vertical loads



Computation of the tangent elasticity matrices:  
 Element 1 between nodes 1 and 2:

$$\left[ \mathbf{B}_E^0 \right]_1 = \begin{bmatrix} 0.33 & 0 & 1 & -0.33 & 0 & 0 & 0 & 0 & 0 & 0 & 0 & 0 & 0 & 0 & 0 \\ 0.33 & 0 & 0 & -0.33 & 0 & 1 & 0 & 0 & 0 & 0 & 0 & 0 & 0 & 0 & 0 \\ 0 & -1 & 0 & 0 & 1 & 0 & 0 & 0 & 0 & 0 & 0 & 0 & 0 & 0 & 0 \end{bmatrix} \tag{8.5.2}$$

$$\left[ \mathbf{S}_0 \right]_1 = \begin{bmatrix} 3472.00 & 1736.00 & 0 \\ 1736.00 & 3472.00 & 0 \\ 0 & 0 & 1.667 \times 10^5 \end{bmatrix} \tag{8.5.3}$$

$$\left[ \mathbf{k}_{tE} \right]_1 = \begin{bmatrix} 1157.33 & 0 & 1736.00 & -1157.33 & 0 & 1736.00 & 0 & 0 & 0 & 0 & 0 & 0 & 0 & 0 & 0 \\ 0 & 1.67 \times 10^5 & 0 & 0 & -1.67 \times 10^5 & 0 & 0 & 0 & 0 & 0 & 0 & 0 & 0 & 0 & 0 \\ 1736.00 & 0 & 3472.00 & -1736.00 & 0 & 1736.00 & 0 & 0 & 0 & 0 & 0 & 0 & 0 & 0 & 0 \\ -1157.33 & 0 & -1736.00 & 1157.33 & 0 & -1736.00 & 0 & 0 & 0 & 0 & 0 & 0 & 0 & 0 & 0 \\ 0 & -1.67 \times 10^5 & 0 & 0 & 1.67 \times 10^5 & 0 & 0 & 0 & 0 & 0 & 0 & 0 & 0 & 0 & 0 \\ 1736.00 & 0 & 1736.00 & -1736.00 & 0 & 3472.00 & 0 & 0 & 0 & 0 & 0 & 0 & 0 & 0 & 0 \\ 0 & 0 & 0 & 0 & 0 & 0 & 0 & 0 & 0 & 0 & 0 & 0 & 0 & 0 & 0 \\ 0 & 0 & 0 & 0 & 0 & 0 & 0 & 0 & 0 & 0 & 0 & 0 & 0 & 0 & 0 \\ 0 & 0 & 0 & 0 & 0 & 0 & 0 & 0 & 0 & 0 & 0 & 0 & 0 & 0 & 0 \\ 0 & 0 & 0 & 0 & 0 & 0 & 0 & 0 & 0 & 0 & 0 & 0 & 0 & 0 & 0 \\ 0 & 0 & 0 & 0 & 0 & 0 & 0 & 0 & 0 & 0 & 0 & 0 & 0 & 0 & 0 \\ 0 & 0 & 0 & 0 & 0 & 0 & 0 & 0 & 0 & 0 & 0 & 0 & 0 & 0 & 0 \\ 0 & 0 & 0 & 0 & 0 & 0 & 0 & 0 & 0 & 0 & 0 & 0 & 0 & 0 & 0 \\ 0 & 0 & 0 & 0 & 0 & 0 & 0 & 0 & 0 & 0 & 0 & 0 & 0 & 0 & 0 \end{bmatrix} \tag{8.5.4}$$

Element 2 between nodes 2 and 3:

$$\left[ \mathbf{B}_E^0 \right]_2 = \begin{bmatrix} 0 & 0 & 0 & 0.33 & 0 & 1 & -0.33 & 0 & 0 & 0 & 0 & 0 & 0 & 0 & 0 \\ 0 & 0 & 0 & 0.33 & 0 & 0 & -0.33 & 0 & 1 & 0 & 0 & 0 & 0 & 0 & 0 \\ 0 & 0 & 0 & 0 & -1 & 0 & 0 & 1 & 0 & 0 & 0 & 0 & 0 & 0 & 0 \end{bmatrix} \tag{8.5.5}$$

**Analysis of Elasto-Plastic Frames**

$$[\mathbf{S}_0]_2 = \begin{bmatrix} 3472.00 & 1736.00 & 0 \\ 1736.00 & 3472.00 & 0 \\ 0 & 0 & 1.667 \times 10^5 \end{bmatrix} \quad (8.5.6)$$

$$[\mathbf{k}_{tE}]_2 = \begin{bmatrix} 0 & 0 & 0 & 0 & 0 & 0 & 0 & 0 & 0 & 0 & 0 & 0 & 0 & 0 & 0 \\ 0 & 0 & 0 & 0 & 0 & 0 & 0 & 0 & 0 & 0 & 0 & 0 & 0 & 0 & 0 \\ 0 & 0 & 0 & 0 & 0 & 0 & 0 & 0 & 0 & 0 & 0 & 0 & 0 & 0 & 0 \\ 0 & 0 & 0 & 1157.33 & 0 & 1736.00 & -1157.33 & 0 & 1736.00 & 0 & 0 & 0 & 0 & 0 & 0 \\ 0 & 0 & 0 & 0 & 1.67 \times 10^5 & 0 & 0 & -1.67 \times 10^5 & 0 & 0 & 0 & 0 & 0 & 0 & 0 \\ 0 & 0 & 0 & 1736.00 & 0 & 3472.00 & -1736.00 & 0 & 1736.00 & 0 & 0 & 0 & 0 & 0 & 0 \\ 0 & 0 & 0 & -1157.33 & 0 & -1736.00 & 1157.33 & 0 & -1736.00 & 0 & 0 & 0 & 0 & 0 & 0 \\ 0 & 0 & 0 & 0 & -1.67 \times 10^5 & 0 & 0 & 1.67 \times 10^5 & 0 & 0 & 0 & 0 & 0 & 0 & 0 \\ 0 & 0 & 0 & 1736.00 & 0 & 1736.00 & -1736.00 & 0 & 3472.00 & 0 & 0 & 0 & 0 & 0 & 0 \\ 0 & 0 & 0 & 0 & 0 & 0 & 0 & 0 & 0 & 0 & 0 & 0 & 0 & 0 & 0 \\ 0 & 0 & 0 & 0 & 0 & 0 & 0 & 0 & 0 & 0 & 0 & 0 & 0 & 0 & 0 \\ 0 & 0 & 0 & 0 & 0 & 0 & 0 & 0 & 0 & 0 & 0 & 0 & 0 & 0 & 0 \\ 0 & 0 & 0 & 0 & 0 & 0 & 0 & 0 & 0 & 0 & 0 & 0 & 0 & 0 & 0 \\ 0 & 0 & 0 & 0 & 0 & 0 & 0 & 0 & 0 & 0 & 0 & 0 & 0 & 0 & 0 \\ 0 & 0 & 0 & 0 & 0 & 0 & 0 & 0 & 0 & 0 & 0 & 0 & 0 & 0 & 0 \end{bmatrix} \quad (8.5.7)$$

Element 3 between nodes 3 and 4:

$$[\mathbf{B}_E^0]_3 = \begin{bmatrix} 0 & 0 & 0 & 0 & 0 & 0 & 0 & -0.167 & 1 & 0 & 0.167 & 0 & 0 & 0 & 0 \\ 0 & 0 & 0 & 0 & 0 & 0 & 0 & -0.167 & 0 & 0 & 0.167 & 1 & 0 & 0 & 0 \\ 0 & 0 & 0 & 0 & 0 & 0 & -1 & 0 & 0 & 1 & 0 & 0 & 0 & 0 & 0 \end{bmatrix} \quad (8.5.8)$$

$$[\mathbf{S}_0]_3 = \begin{bmatrix} 1736.00 & 868.00 & 0 \\ 868.00 & 1736.00 & 0 \\ 0 & 0 & 83333.33 \end{bmatrix} \quad (8.5.9)$$

$$\left[ \mathbf{k}_{tE} \right]_3 = \begin{bmatrix}
 0 & 0 & 0 & 0 & 0 & 0 & 0 & 0 & 0 & 0 & 0 & 0 & 0 & 0 & 0 & 0 \\
 0 & 0 & 0 & 0 & 0 & 0 & 0 & 0 & 0 & 0 & 0 & 0 & 0 & 0 & 0 & 0 \\
 0 & 0 & 0 & 0 & 0 & 0 & 0 & 0 & 0 & 0 & 0 & 0 & 0 & 0 & 0 & 0 \\
 0 & 0 & 0 & 0 & 0 & 0 & 0 & 0 & 0 & 0 & 0 & 0 & 0 & 0 & 0 & 0 \\
 0 & 0 & 0 & 0 & 0 & 0 & 0 & 0 & 0 & 0 & 0 & 0 & 0 & 0 & 0 & 0 \\
 0 & 0 & 0 & 0 & 0 & 0 & 0 & 0 & 0 & 0 & 0 & 0 & 0 & 0 & 0 & 0 \\
 0 & 0 & 0 & 0 & 0 & 0 & 83333.33 & 0 & 0 & -83333.33 & 0 & 0 & 0 & 0 & 0 & 0 \\
 0 & 0 & 0 & 0 & 0 & 0 & 0 & 144.67 & -434.00 & 0 & -144.67 & -434.00 & 0 & 0 & 0 & 0 \\
 0 & 0 & 0 & 0 & 0 & 0 & 0 & -434.00 & 1736.00 & 0 & 434.00 & 868.00 & 0 & 0 & 0 & 0 \\
 0 & 0 & 0 & 0 & 0 & 0 & -83333.33 & 0 & 0 & 83333.33 & 0 & 0 & 0 & 0 & 0 & 0 \\
 0 & 0 & 0 & 0 & 0 & 0 & 0 & -144.67 & 434.00 & 0 & 144.67 & 434.00 & 0 & 0 & 0 & 0 \\
 0 & 0 & 0 & 0 & 0 & 0 & 0 & -434.00 & 868.00 & 0 & 434.00 & 1736.00 & 0 & 0 & 0 & 0 \\
 0 & 0 & 0 & 0 & 0 & 0 & 0 & 0 & 0 & 0 & 0 & 0 & 0 & 0 & 0 & 0 \\
 0 & 0 & 0 & 0 & 0 & 0 & 0 & 0 & 0 & 0 & 0 & 0 & 0 & 0 & 0 & 0 \\
 0 & 0 & 0 & 0 & 0 & 0 & 0 & 0 & 0 & 0 & 0 & 0 & 0 & 0 & 0 & 0
 \end{bmatrix}$$

(8.5.10)

Element 4 between nodes 4 and 5:

$$\left[ \mathbf{B}_E^0 \right]_4 = \begin{bmatrix}
 0 & 0 & 0 & 0 & 0 & 0 & 0 & 0 & 0 & -0.33 & 0 & 1 & 0.33 & 0 & 0 \\
 0 & 0 & 0 & 0 & 0 & 0 & 0 & 0 & 0 & -0.33 & 0 & 0 & 0.33 & 0 & 1 \\
 0 & 0 & 0 & 0 & 0 & 0 & 0 & 0 & 0 & 0 & 1 & 0 & 0 & -1 & 0
 \end{bmatrix}$$

(8.5.11)

$$\left[ \mathbf{S}_0 \right]_4 = \begin{bmatrix}
 3472.00 & 1736.00 & 0 \\
 1736.00 & 3472.00 & 0 \\
 0 & 0 & 1.67 \times 10^5
 \end{bmatrix}$$

(8.5.12)

**Analysis of Elasto-Plastic Frames**

$$\left[ \mathbf{k}_{tE} \right]_4 = \begin{bmatrix}
 0 & 0 & 0 & 0 & 0 & 0 & 0 & 0 & 0 & 0 & 0 & 0 & 0 & 0 & 0 & 0 \\
 0 & 0 & 0 & 0 & 0 & 0 & 0 & 0 & 0 & 0 & 0 & 0 & 0 & 0 & 0 & 0 \\
 0 & 0 & 0 & 0 & 0 & 0 & 0 & 0 & 0 & 0 & 0 & 0 & 0 & 0 & 0 & 0 \\
 0 & 0 & 0 & 0 & 0 & 0 & 0 & 0 & 0 & 0 & 0 & 0 & 0 & 0 & 0 & 0 \\
 0 & 0 & 0 & 0 & 0 & 0 & 0 & 0 & 0 & 0 & 0 & 0 & 0 & 0 & 0 & 0 \\
 0 & 0 & 0 & 0 & 0 & 0 & 0 & 0 & 0 & 0 & 0 & 0 & 0 & 0 & 0 & 0 \\
 0 & 0 & 0 & 0 & 0 & 0 & 0 & 0 & 0 & 0 & 0 & 0 & 0 & 0 & 0 & 0 \\
 0 & 0 & 0 & 0 & 0 & 0 & 0 & 0 & 0 & 0 & 0 & 0 & 0 & 0 & 0 & 0 \\
 0 & 0 & 0 & 0 & 0 & 0 & 0 & 0 & 0 & 0 & 0 & 0 & 0 & 0 & 0 & 0 \\
 0 & 0 & 0 & 0 & 0 & 0 & 0 & 0 & 0 & 1157.33 & 0.00 & -1736.00 & -1157.33 & 0.00 & -1736.00 & 0.00 \\
 0 & 0 & 0 & 0 & 0 & 0 & 0 & 0 & 0 & 0.00 & 1.67 \times 10^5 & 0.00 & 0.00 & -1.67 \times 10^5 & 0.00 & 0.00 \\
 0 & 0 & 0 & 0 & 0 & 0 & 0 & 0 & 0 & -1736.00 & 0.00 & 3472.00 & 1736.00 & 0.00 & 1736.00 & 0.00 \\
 0 & 0 & 0 & 0 & 0 & 0 & 0 & 0 & 0 & -1157.33 & 0.00 & 1736.00 & 1157.33 & 0.00 & 1736.00 & 0.00 \\
 0 & 0 & 0 & 0 & 0 & 0 & 0 & 0 & 0 & 0.00 & -1.67 \times 10^5 & 0.00 & 0.00 & 1.67 \times 10^5 & 0.00 & 0.00 \\
 0 & 0 & 0 & 0 & 0 & 0 & 0 & 0 & 0 & -1736.00 & 0.00 & 1736.00 & 1736.00 & 0.00 & 3472.00 & 0.00
 \end{bmatrix} \tag{8.5.13}$$

The tangent stiffness matrix of the structure is (See Box 1):  $[\mathbf{K}_t]_0 = [\mathbf{k}_{tE}]_1 + [\mathbf{k}_{tE}]_2 + [\mathbf{k}_{tE}]_3 + [\mathbf{k}_{tE}]_4$

The structure is solved by the direct stiffness method; therefore, solving the expression  $[\mathbf{K}_t]_0 \{\mathbf{U}_0\} = \{\mathbf{F}\} = \{\mathbf{P}^e\} + \{\mathbf{R}_0\}$ , the free displacements and reaction forces are obtained:



Box 1.

$$\begin{bmatrix}
 1157.33 & 0 & 1736.00 & -1157.33 & 0 & 1736.00 & 0 & 0 & 0 & 0 & 0 & 0 & 0 & 0 & 0 & 0 & 0 & 0 & 0 & 0 \\
 0 & 1.67 \times 10^5 & 0 & 0 & -1.67 \times 10^5 & 0 & 0 & 0 & 0 & 0 & 0 & 0 & 0 & 0 & 0 & 0 & 0 & 0 & 0 & 0 \\
 1736.00 & 0 & 3472.00 & -1736.00 & 0 & 1736.00 & 0 & 0 & 0 & 0 & 0 & 0 & 0 & 0 & 0 & 0 & 0 & 0 & 0 & 0 \\
 -1157.33 & 0 & -1736.00 & 2314.67 & 0 & 0 & -1157.33 & 0 & 1736.00 & 0 & 0 & 0 & 0 & 0 & 0 & 0 & 0 & 0 & 0 & 0 \\
 0 & -1.67 \times 10^5 & 0 & 0 & 3.33 \times 10^5 & 0 & 0 & 0 & -1.67 \times 10^5 & 0 & 0 & 0 & 0 & 0 & 0 & 0 & 0 & 0 & 0 & 0 \\
 1736.00 & 0 & 1736.00 & 0 & 0 & 6944.00 & -1736.00 & 0 & 1736.00 & 0 & 0 & 0 & 0 & 0 & 0 & 0 & 0 & 0 & 0 & 0 \\
 0 & 0 & 0 & -1157.33 & 0 & -1736.00 & 8.45 \times 10^4 & 0 & -1736.00 & -8.33 \times 10^4 & 0 & 0 & 0 & 0 & 0 & 0 & 0 & 0 & 0 & 0 \\
 0 & 0 & 0 & 0 & -1.67 \times 10^5 & 0 & 0 & 1.67 \times 10^5 & -434.00 & 0 & -144.67 & -434.00 & 0 & 0 & 0 & 0 & 0 & 0 & 0 & 0 \\
 0 & 0 & 0 & 1736.00 & 0 & 1736.00 & -1736.00 & -434.00 & -434.00 & 5208.00 & 434.00 & 868.00 & 0 & 0 & 0 & 0 & 0 & 0 & 0 & 0 \\
 0 & 0 & 0 & 0 & 0 & 0 & -8.33 \times 10^4 & 0 & 8.45 \times 10^4 & 0 & 0 & -1736.00 & -1157.33 & 0 & 0 & 0 & 0 & 0 & 0 & -1736.00 \\
 0 & 0 & 0 & 0 & 0 & 0 & 0 & 0 & 0 & 0 & 1.67 \times 10^5 & 434.00 & 0 & -1.67 \times 10^5 & 0 & 0 & 0 & 0 & 0 & 0 \\
 0 & 0 & 0 & 0 & 0 & 0 & 0 & -434.00 & 808.00 & -1736.00 & 434.00 & 5208.00 & 1736.00 & 0 & 1736.00 & 0 & 0 & 0 & 0 & 1736.00 \\
 0 & 0 & 0 & 0 & 0 & 0 & 0 & 0 & 0 & 0 & 0 & 1736.00 & 1157.33 & 0 & 1736.00 & 0 & 0 & 0 & 0 & 1736.00 \\
 0 & 0 & 0 & 0 & 0 & 0 & 0 & 0 & 0 & 0 & -1.67 \times 10^5 & 0 & 0 & 1.67 \times 10^5 & 0 & 0 & 0 & 0 & 0 & 0 \\
 0 & 0 & 0 & 0 & 0 & 0 & 0 & 0 & 0 & 0 & 0 & 0 & 1736.00 & 1736.00 & 0 & 0 & 0 & 0 & 0 & 3472.00
 \end{bmatrix}$$

(8.5.14)

**Analysis of Elasto-Plastic Frames**

$$\{\mathbf{U}_0\} = \begin{bmatrix} 0 \\ 0 \\ 0 \\ -2.679x10^{-3} \\ -3.670x10^{-5} \\ -1.090x10^{-3} \\ -2.361x10^{-3} \\ -7.340x10^{-5} \\ 1.998x10^{-3} \\ -2.376x10^{-3} \\ -3.523x10^{-5} \\ -2.28x10^{-3} \\ 0 \\ 0 \\ 0 \end{bmatrix}; \{\mathbf{R}_0\} = \begin{bmatrix} 1.209 \\ 6.117 \\ 2.759 \\ 0 \\ 0 \\ 0 \\ 0 \\ 0 \\ 0 \\ 0 \\ 0 \\ 0 \\ -1.209 \\ 5.883 \\ 0.166 \end{bmatrix} \quad (8.5.15)$$

The generalized deformation matrices are computed by  $\{\Phi_0\}_b = [\mathbf{B}_E^0]_b \{\mathbf{U}_0\}$  and the generalized stress matrices by  $\{\mathbf{M}_0\}_b = [\mathbf{S}]_b [\mathbf{B}_E^0]_b \{\mathbf{U}_0\}$ :

$$\{\Phi_0\}_1 = \begin{bmatrix} 8.931x10^{-4} \\ -1.968x10^{-4} \\ -3.670x10^{-5} \end{bmatrix}; \{\Phi_0\}_2 = \begin{bmatrix} -1.196 x 10^{-3} \\ 1.892 x 10^{-3} \\ -3.670x10^{-5} \end{bmatrix}; \{\Phi_0\}_3 = \begin{bmatrix} 2.004x10^{-3} \\ -2.274x10^{-3} \\ -1.451x10^{-5} \end{bmatrix}; \{\Phi_0\}_4 = \begin{bmatrix} -1.488 x 10^{-3} \\ 7.919 x 10^{-4} \\ -3.530x10^{-5} \end{bmatrix}$$

$$\{\mathbf{M}_0\}_1 = \begin{bmatrix} 2.759 \\ 0.867 \\ -6.117 \end{bmatrix}; \{\mathbf{M}_0\}_2 = \begin{bmatrix} -0.867 \\ 4.494 \\ -6.117 \end{bmatrix}; \{\mathbf{M}_0\}_3 = \begin{bmatrix} -4.494 \\ 3.792 \\ -1.209 \end{bmatrix}; \{\mathbf{M}_0\}_4 = \begin{bmatrix} -3.792 \\ 0.166 \\ -5.883 \end{bmatrix} \quad (8.5.16)$$

• **Second Step:  $s = 1$**

In this step, the following equation is solved:

$$[\mathbf{K}_t]_1 \{\mathbf{V}_1\} = \{\mathbf{P}_1^R\} \quad (8.5.17)$$

where  $[\mathbf{K}_t]_1 = [\mathbf{K}_t]_0$  assuming that there are no active plastic hinges in the structure,

$$\{\mathbf{V}_1\} = \frac{1}{\Delta l_1} \{\Delta \mathbf{U}_1\} \quad (8.5.18)$$

and

$$\{\mathbf{P}_1^R\} = \{\mathbf{P}_{ref}\} + \frac{1}{\Delta l_1} \{\Delta \mathbf{R}_1\} = \begin{bmatrix} \Delta R_{1u1} / \Delta l_1 \\ \Delta R_{1w1} / \Delta l_1 \\ \Delta R_{1\theta1} / \Delta l_1 \\ 1 \\ 0 \\ 0 \\ 2 \\ 0 \\ 0 \\ 0 \\ 0 \\ 0 \\ 0 \\ \Delta R_{1u5} / \Delta l_1 \\ \Delta R_{1w5} / \Delta l_1 \\ \Delta R_{1\theta5} / \Delta l_1 \end{bmatrix} \tag{8.5.19}$$

After the resolution, the following increments of the displacements and reactions are obtained:

$$\{\Delta \mathbf{U}_1\} = \begin{bmatrix} 0 \\ 0 \\ 0 \\ 2.217x10^{-3} \Delta l_1 \\ 2.823x10^{-6} \Delta l_1 \\ 8.836x10^{-4} \Delta l_1 \\ 3.462x10^{-3} \Delta l_1 \\ 5.647x10^{-6} \Delta l_1 \\ -7.189x10^{-5} \Delta l_1 \\ 3.434x10^{-3} \Delta l_1 \\ -2.823x10^{-6} \Delta l_1 \\ 1.159x10^{-3} \Delta l_1 \\ 0 \\ 0 \\ 0 \end{bmatrix} ; \{\Delta \mathbf{R}_1\} = \begin{bmatrix} -1.032\Delta l_1 \\ -0.470\Delta l_1 \\ -2.315\Delta l_1 \\ 0 \\ 0 \\ 0 \\ 0 \\ 0 \\ 0 \\ 0 \\ 0 \\ 0 \\ -1.968\Delta l_1 \\ 0.470\Delta l_1 \\ -3.958\Delta l_1 \end{bmatrix} \tag{8.5.20}$$

### Analysis of Elasto-Plastic Frames

The stresses in the elements are computed by:

$$\{\mathbf{M}_1\}_b = \{\mathbf{M}_0\}_b + \Delta l_1 [\mathbf{S}_0]_b [\mathbf{B}_E^0]_b \{\mathbf{V}_1\} \quad (8.5.21)$$

$\Delta l_1$  is obtained from the maximum moment that occurs in the hinge  $j$  of the element 4; therefore, this is the location of the first plastic hinge that becomes active. For this element:

$$\{\mathbf{M}\}_4 = \begin{bmatrix} -3.792 \\ 0.166 \\ -5.883 \end{bmatrix} + \begin{bmatrix} -1.946\Delta l_1 \\ -3.958\Delta l_1 \\ -0.470\Delta l_1 \end{bmatrix} \quad (8.5.22)$$

Then,  $\Delta l_1$  is computed solving Equation (8.1.16):  $Max (|m_k| - M_{ky}) = 0$ , resulting:

$$|0.166 - 3.958\Delta l_1| - 62 = 0 \Rightarrow \Delta l_1 = 15.707 \text{ or } \Delta l_1 = -15.623 \quad (8.5.23)$$

The positive value is chosen. The maximum moment is not always easy to determine; therefore, it could be easier the computation of the expression (8.5.23) for all hinges and the selection of the smallest value of  $\Delta l$ . At the end of the second step, the stresses in the elements are:

$$\{\mathbf{M}_1\}_1 = \begin{bmatrix} -33.604 \\ -11.403 \\ 1.274 \end{bmatrix}; \{\mathbf{M}_1\}_2 = \begin{bmatrix} 11.403 \\ -9.289 \\ 1.274 \end{bmatrix}; \{\mathbf{M}_1\}_3 = \begin{bmatrix} 9.289 \\ 34.356 \\ -32.119 \end{bmatrix}; \{\mathbf{M}_1\}_4 = \begin{bmatrix} -34.356 \\ -62.000 \\ -13.274 \end{bmatrix} \quad (8.5.24)$$

and the displacements:

$$\{U_1\} = \{U_0\} + \Delta l_1 \{V_1\} = \begin{bmatrix} 0 \\ 0 \\ 0 \\ 3.214 \times 10^{-2} \\ 7.646 \times 10^{-6} \\ 1.279 \times 10^{-2} \\ 5.202 \times 10^{-2} \\ 1.529 \times 10^{-5} \\ 8.690 \times 10^{-4} \\ 5.164 \times 10^{-2} \\ -7.964 \times 10^{-5} \\ 1.592 \times 10^{-2} \\ 0 \\ 0 \\ 0 \end{bmatrix} \quad (8.5.25)$$

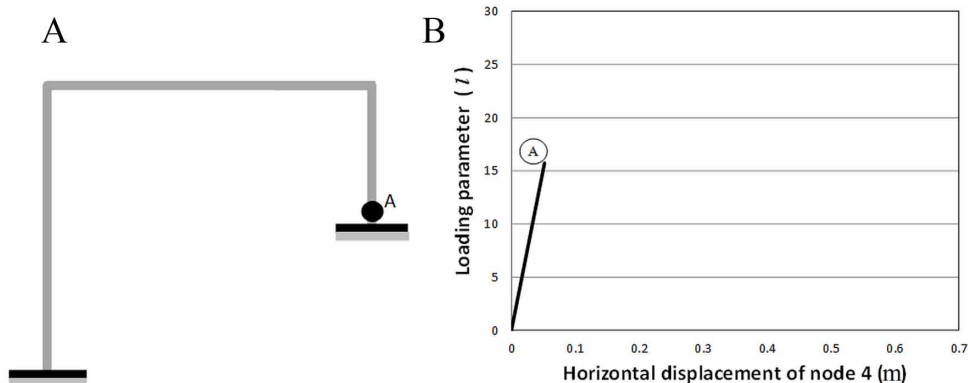
The loading parameter is:

$$l(1) = l(0) + \Delta l_1 = 15.701 \quad (8.5.26)$$

Figure 5 shows the structural configuration after the first plastic hinge and the plot of horizontal displacements at nodes 4 vs. loading parameter.

The new tangent stiffness matrix of the structure for the next step is computed changing the matrix corresponding to the element 4 that now must be calculated as  $[k_{tE}]_4 = [B_E^0]_4^t [S_{1j}]_4 [B_E^0]_4$ , where:

Figure 5. a) Location of the first plastic hinge in the RC frame; b) Plot of horizontal displacements at nodes 4 vs. loading parameter



**Analysis of Elasto-Plastic Frames**

$$[\mathbf{S}_{1j}]_4 = \begin{bmatrix} 2604.00 & 0 & 0 \\ 0 & 0 & 0 \\ 0 & 0 & 1.67 \times 10^5 \end{bmatrix} \quad (8.5.27)$$

then,

$$[\mathbf{k}_{tE}]_4 = \begin{bmatrix} 0 & 0 & 0 & 0 & 0 & 0 & 0 & 0 & 0 & 0 & 0 & 0 & 0 & 0 & 0 \\ 0 & 0 & 0 & 0 & 0 & 0 & 0 & 0 & 0 & 0 & 0 & 0 & 0 & 0 & 0 \\ 0 & 0 & 0 & 0 & 0 & 0 & 0 & 0 & 0 & 0 & 0 & 0 & 0 & 0 & 0 \\ 0 & 0 & 0 & 0 & 0 & 0 & 0 & 0 & 0 & 0 & 0 & 0 & 0 & 0 & 0 \\ 0 & 0 & 0 & 0 & 0 & 0 & 0 & 0 & 0 & 0 & 0 & 0 & 0 & 0 & 0 \\ 0 & 0 & 0 & 0 & 0 & 0 & 0 & 0 & 0 & 0 & 0 & 0 & 0 & 0 & 0 \\ 0 & 0 & 0 & 0 & 0 & 0 & 0 & 0 & 0 & 0 & 0 & 0 & 0 & 0 & 0 \\ 0 & 0 & 0 & 0 & 0 & 0 & 0 & 0 & 0 & 0 & 0 & 0 & 0 & 0 & 0 \\ 0 & 0 & 0 & 0 & 0 & 0 & 0 & 0 & 0 & 0 & 0 & 0 & 0 & 0 & 0 \\ 0 & 0 & 0 & 0 & 0 & 0 & 0 & 0 & 0 & 289.33 & 0 & -868.00 & -289.33 & 0 & 0 \\ 0 & 0 & 0 & 0 & 0 & 0 & 0 & 0 & 0 & 0 & 1.67 \times 10^5 & 0 & 0 & -1.67 \times 10^5 & 0 \\ 0 & 0 & 0 & 0 & 0 & 0 & 0 & 0 & 0 & -868.00 & 0 & 2604.00 & 868.00 & 0 & 0 \\ 0 & 0 & 0 & 0 & 0 & 0 & 0 & 0 & 0 & -289.33 & 0 & 868.00 & 289.33 & 0 & 0 \\ 0 & 0 & 0 & 0 & 0 & 0 & 0 & 0 & 0 & 0 & -1.67 \times 10^5 & 0 & 0 & 1.67 \times 10^5 & 0 \\ 0 & 0 & 0 & 0 & 0 & 0 & 0 & 0 & 0 & 0 & 0 & 0 & 0 & 0 & 0 \end{bmatrix} \quad (8.5.28)$$

and the tangent stiffness matrix of the structure for the next step is (Box 2):

• **Third Step:**  $s = 2$

This analysis starts with solving the expression:

$$[\mathbf{K}_t]_2 \{ \mathbf{V}_2 \} = \{ \mathbf{P}_2^R \} \quad (8.5.30)$$

where, as aforementioned,  $[\mathbf{K}_t]_2$  considers that the hinge  $j$  of the element 4 is active,

$$\{ \mathbf{V}_2 \} = \frac{1}{\Delta l_2} \{ \Delta \mathbf{U}_2 \} \quad (8.5.31)$$

and

Box 2.

$$\begin{bmatrix}
 1157.33 & 0 & 1736.00 & -1157.33 & 0 & 1736.00 & 0 & 0 & 0 & 0 & 0 & 0 & 0 & 0 & 0 & 0 & 0 & 0 & 0 & 0 & 0 \\
 0 & 1.67 \times 10^5 & 0 & 0 & -1.67 \times 10^5 & 0 & 0 & 0 & 0 & 0 & 0 & 0 & 0 & 0 & 0 & 0 & 0 & 0 & 0 & 0 & 0 \\
 1736.00 & 0 & 3472.00 & -1736.00 & 0 & 1736.00 & 0 & 0 & 0 & 0 & 0 & 0 & 0 & 0 & 0 & 0 & 0 & 0 & 0 & 0 & 0 \\
 -1157.33 & 0 & -1736.00 & 2314.67 & 0 & 0 & -1157.33 & 0 & 1736.00 & 0 & 0 & 0 & 0 & 0 & 0 & 0 & 0 & 0 & 0 & 0 & 0 \\
 0 & -1.67 \times 10^5 & 0 & 0 & 3.33 \times 10^5 & 0 & 0 & -1.67 \times 10^5 & 0 & 0 & 0 & 0 & 0 & 0 & 0 & 0 & 0 & 0 & 0 & 0 & 0 \\
 1736.00 & 0 & 1736.00 & 0 & 0 & 6944.00 & -1736.00 & 0 & 1736.00 & 0 & 1736.00 & 0 & 0 & 0 & 0 & 0 & 0 & 0 & 0 & 0 & 0 \\
 0 & 0 & 0 & -1157.33 & 0 & -1736.00 & 8.45 \times 10^4 & 0 & -1736.00 & -8.33 \times 10^4 & 0 & 0 & 0 & 0 & 0 & 0 & 0 & 0 & 0 & 0 & 0 \\
 0 & 0 & 0 & 0 & -1.67 \times 10^5 & 0 & 0 & 1.67 \times 10^5 & -434.00 & 0 & -144.67 & -434.00 & 0 & 0 & 0 & 0 & 0 & 0 & 0 & 0 & 0 \\
 0 & 0 & 0 & 1736.00 & 0 & 1736.00 & -1736.00 & -434.00 & 5208.00 & 0 & 434.00 & 868.00 & 0 & 0 & 0 & 0 & 0 & 0 & 0 & 0 & 0 \\
 0 & 0 & 0 & 0 & 0 & 0 & -8.33 \times 10^4 & 0 & 0 & 8.33 \times 10^4 & 0 & -868.00 & -289.33 & 0 & 0 & 0 & 0 & 0 & 0 & 0 & 0 \\
 0 & 0 & 0 & 0 & 0 & 0 & 0 & -144.67 & 434.00 & 0 & 1.67 \times 10^5 & 434.00 & 0 & -1.67 \times 10^5 & 0 & 0 & 0 & 0 & 0 & 0 & 0 \\
 0 & 0 & 0 & 0 & 0 & 0 & 0 & -434.00 & 868.00 & -868.00 & 434.00 & 4340.00 & 868.00 & 0 & 0 & 0 & 0 & 0 & 0 & 0 & 0 \\
 0 & 0 & 0 & 0 & 0 & 0 & 0 & 0 & 0 & -289.33 & 0 & 868.00 & 289.33 & 0 & 0 & 0 & 0 & 0 & 0 & 0 & 0 \\
 0 & 0 & 0 & 0 & 0 & 0 & 0 & 0 & 0 & 0 & -1.67 \times 10^5 & 0 & 0 & 1.67 \times 10^5 & 0 & 0 & 0 & 0 & 0 & 0 & 0 \\
 0 & 0
 \end{bmatrix}$$

$[\mathbf{K}]_{t-2} =$

(8.5.29)

**Analysis of Elasto-Plastic Frames**

$$\{\mathbf{P}_2^R\} = \{\mathbf{P}_{ref}\} + \frac{1}{\Delta l_2} \{\Delta \mathbf{R}_2\} = \begin{bmatrix} \Delta R_{2w1} / \Delta l_2 \\ \Delta R_{2w1} / \Delta l_2 \\ \Delta R_{2\theta1} / \Delta l_2 \\ 1 \\ 0 \\ 0 \\ 2 \\ 0 \\ 0 \\ 0 \\ 0 \\ 0 \\ 0 \\ \Delta R_{2u5} / \Delta l_2 \\ \Delta R_{2w5} / \Delta l_2 \\ \Delta R_{2\theta5} / \Delta l_2 \end{bmatrix} \quad (8.5.32)$$

Once Equation (8.5.30) is solved, the increments of the displacements and reactions can be written as:

$$\{\Delta \mathbf{U}_2\} = \begin{bmatrix} 0 \\ 0 \\ 0 \\ 5.094x10^{-3} \Delta l_2 \\ 6.498x10^{-6} \Delta l_2 \\ 2.403x10^{-3} \Delta l_2 \\ 1.019x10^{-2} \Delta l_2 \\ 1.299x10^{-5} \Delta l_2 \\ 5.803x10^{-4} \Delta l_2 \\ 1.018x10^{-2} \Delta l_2 \\ -6.498x10^{-6} \Delta l_2 \\ 1.922x10^{-3} \Delta l_2 \\ 0 \\ 0 \\ 0 \end{bmatrix}; \{\Delta \mathbf{R}_2\} = \begin{bmatrix} -1.723\Delta l_2 \\ -1.083\Delta l_2 \\ -4.671\Delta l_2 \\ 0 \\ 0 \\ 0 \\ 0 \\ 0 \\ 0 \\ 0 \\ 0 \\ 0 \\ 0 \\ -1.277\Delta l_2 \\ 1.083\Delta l_2 \\ 0 \end{bmatrix} \quad (8.5.33)$$

$\Delta l_2$  is computed from the maximum moment of the structure. It occurs in the hinge  $i$  of the element 1; therefore, this is the location of the second plastic hinge that becomes active. For this element:



$$\{\mathbf{M}\}_1 = \begin{bmatrix} -33.604 \\ -11.403 \\ 1.274 \end{bmatrix} + \begin{bmatrix} -4.671\Delta l_2 \\ -0.498\Delta l_2 \\ 1.083\Delta l_2 \end{bmatrix} \quad (8.5.34)$$

then,  $\Delta l_2$  is computed by solving:

$$|-33.604 - 4.671\Delta l_2| - 62 = 0 \Rightarrow \Delta l_2 = 6.08 \text{ or } \Delta l_2 = -20.469 \quad (8.5.35)$$

It is chosen again the positive value. At the end of the third step, the stresses in the elements are:

$$\{\mathbf{M}_2\}_1 = \begin{bmatrix} -62.000 \\ -14.432 \\ 7.859 \end{bmatrix}; \{\mathbf{M}_2\}_2 = \begin{bmatrix} 14.432 \\ -25.503 \\ 7.859 \end{bmatrix}; \{\mathbf{M}_2\}_3 = \begin{bmatrix} 25.503 \\ 57.649 \\ -39.883 \end{bmatrix}; \{\mathbf{M}_2\}_4 = \begin{bmatrix} -57.649 \\ -62.000 \\ -19.859 \end{bmatrix} \quad (8.5.36)$$

and the displacements:

$$\{\mathbf{U}_2\} = \{\mathbf{U}_1\} + \Delta l_2 \{\mathbf{V}_2\} = \begin{bmatrix} 0 \\ 0 \\ 0 \\ 6.311x10^{-2} \\ 4.715x10^{-5} \\ 2.740x10^{-2} \\ 1.140x10^{-1} \\ 9.430x10^{-5} \\ 4.397x10^{-3} \\ 1.135x10^{-1} \\ -1.191x10^{-4} \\ 2.761x10^{-2} \\ 0 \\ 0 \\ 0 \end{bmatrix} \quad (8.5.37)$$

The loading parameter is:

$$l(2) = l(1) + \Delta l_2 = 21.787 \quad (8.5.38)$$

**Analysis of Elasto-Plastic Frames**

Figure 6. a) Location of the plastic hinges in the RC frame; b) Horizontal displacements at nodes 4 vs. loading parameter graph

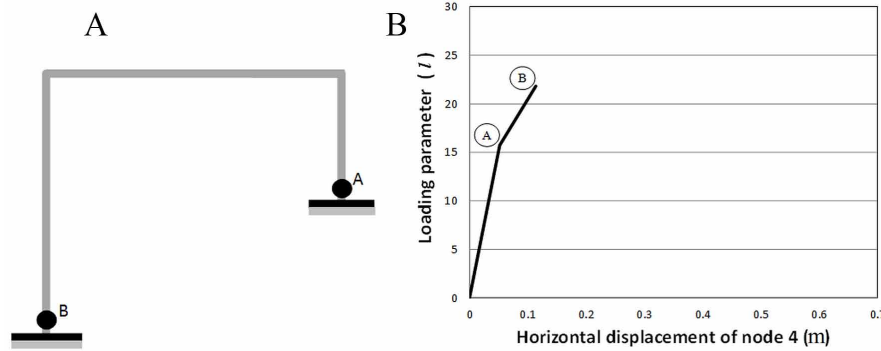


Figure 6 shows the location of the plastic hinges in the frame and the plot of horizontal displacements at nodes 4 vs. loading parameter.

The tangent stiffness matrix of the structure is computed after changing the matrix corresponding to the element 1. It must be computed as  $[k_{tE}]_1 = [B_E^0]_1^t [S_{1i}]_1 [B_E^0]_1$ , where:

$$[S_{1i}]_1 = \begin{bmatrix} 0 & 0 & 0 \\ 0 & 2604.00 & 0 \\ 0 & 0 & 1.67 \times 10^5 \end{bmatrix} \quad (8.5.39)$$

then,

$$[k_{tE}]_1 = \begin{bmatrix} 289.33 & 0 & 0 & -289.33 & 0 & 868.00 & 0 & 0 & 0 & 0 & 0 & 0 & 0 & 0 & 0 \\ 0 & 1.67 \times 10^5 & 0 & 0 & -1.67 \times 10^5 & 0 & 0 & 0 & 0 & 0 & 0 & 0 & 0 & 0 & 0 \\ 0 & 0 & 0 & 0 & 0 & 0 & 0 & 0 & 0 & 0 & 0 & 0 & 0 & 0 & 0 \\ -289.33 & 0 & 0 & 289.33 & 0 & -868.00 & 0 & 0 & 0 & 0 & 0 & 0 & 0 & 0 & 0 \\ 0 & -1.67 \times 10^5 & 0 & 0 & 1.67 \times 10^5 & 0 & 0 & 0 & 0 & 0 & 0 & 0 & 0 & 0 & 0 \\ 868.00 & 0 & 0 & -868.00 & 0 & 2604.00 & 0 & 0 & 0 & 0 & 0 & 0 & 0 & 0 & 0 \\ 0 & 0 & 0 & 0 & 0 & 0 & 0 & 0 & 0 & 0 & 0 & 0 & 0 & 0 & 0 \\ 0 & 0 & 0 & 0 & 0 & 0 & 0 & 0 & 0 & 0 & 0 & 0 & 0 & 0 & 0 \\ 0 & 0 & 0 & 0 & 0 & 0 & 0 & 0 & 0 & 0 & 0 & 0 & 0 & 0 & 0 \\ 0 & 0 & 0 & 0 & 0 & 0 & 0 & 0 & 0 & 0 & 0 & 0 & 0 & 0 & 0 \\ 0 & 0 & 0 & 0 & 0 & 0 & 0 & 0 & 0 & 0 & 0 & 0 & 0 & 0 & 0 \\ 0 & 0 & 0 & 0 & 0 & 0 & 0 & 0 & 0 & 0 & 0 & 0 & 0 & 0 & 0 \\ 0 & 0 & 0 & 0 & 0 & 0 & 0 & 0 & 0 & 0 & 0 & 0 & 0 & 0 & 0 \\ 0 & 0 & 0 & 0 & 0 & 0 & 0 & 0 & 0 & 0 & 0 & 0 & 0 & 0 & 0 \end{bmatrix} \quad (8.5.40)$$

and the tangent stiffness matrix of the structure is (Box 3):

- **Fourth step:**  $s = 3$

This step starts solving the expression:

$$[\mathbf{K}_t]_3 \{ \mathbf{V}_3 \} = \{ \mathbf{P}_3^R \} \tag{8.5.42}$$

where  $[\mathbf{K}_t]_3$  considers that the hinge  $i$  of the element 1 and the hinge  $j$  of the element 4 are active.

$$\{ \mathbf{V}_3 \} = \frac{1}{\Delta l_3} \{ \Delta \mathbf{U}_3 \} \tag{8.5.43}$$

and

$$\{ \mathbf{P}_3^R \} = \{ \mathbf{P}_{ref} \} + \frac{1}{\Delta l_3} \left\{ \begin{array}{c} \Delta R_{3u1} / \Delta l_3 \\ \Delta R_{3w1} / \Delta l_3 \\ \Delta R_{3\theta1} / \Delta l_3 \\ 1 \\ 0 \\ 0 \\ 2 \\ 0 \\ 0 \\ 0 \\ 0 \\ 0 \\ 0 \\ \Delta R_{3u5} / \Delta l_3 \\ \Delta R_{3w5} / \Delta l_3 \\ \Delta R_{3\theta5} / \Delta l_3 \end{array} \right\} \tag{8.5.44}$$

After solving Equation (8.5.42), the increments of the displacements and reactions are:

Box 3.

$$\begin{bmatrix}
 289.33 & 0 & 0 & -289.33 & 0 & 868.00 & 0 & 0 & 0 & 0 & 0 & 0 & 0 & 0 & 0 & 0 \\
 0 & 1.67x10^5 & 0 & 0 & -1.67x10^5 & 0 & 0 & 0 & 0 & 0 & 0 & 0 & 0 & 0 & 0 & 0 \\
 0 & 0 & 0 & 0 & 0 & 0 & 0 & 0 & 0 & 0 & 0 & 0 & 0 & 0 & 0 & 0 \\
 -289.33 & 0 & 0 & 1446.67 & 0 & 868.00 & -1157.33 & 0 & 1736.00 & 0 & 0 & 0 & 0 & 0 & 0 & 0 \\
 0 & -1.67x10^5 & 0 & 0 & 3.33x10^5 & 0 & 0 & -1.67x10^5 & 0 & 0 & 0 & 0 & 0 & 0 & 0 & 0 \\
 868.00 & 0 & 0 & 868.00 & 0 & 6076.00 & -1736.00 & 0 & 1736.00 & 0 & 0 & 0 & 0 & 0 & 0 & 0 \\
 0 & 0 & 0 & -1157.33 & 0 & -1736.00 & 8.45x10^4 & 0 & -1736.00 & -8.33x10^4 & 0 & 0 & 0 & 0 & 0 & 0 \\
 \mathbf{K_t} & = & 0 & 0 & 0 & 0 & 0 & 1.67x10^5 & -434.00 & 0 & -144.67 & -434.00 & 0 & 0 & 0 & 0 \\
 0 & 0 & 0 & 1736.00 & 0 & 1736.00 & -1736.00 & -434.00 & 5208.00 & 0 & 434.00 & 868.00 & 0 & 0 & 0 & 0 \\
 0 & 0 & 0 & 0 & 0 & 0 & -8.33x10^4 & 0 & 0 & 8.33x10^4 & 0 & -868.00 & -289.33 & 0 & 0 & 0 \\
 0 & 0 & 0 & 0 & 0 & 0 & 0 & -144.67 & 434.00 & 0 & 1.67x10^5 & 434.00 & 0 & -1.67x10^5 & 0 & 0 \\
 0 & 0 & 0 & 0 & 0 & 0 & 0 & -434.00 & 868.00 & -868.00 & 434.00 & 4340.00 & 868.00 & 0 & 0 & 0 \\
 0 & 0 & 0 & 0 & 0 & 0 & 0 & 0 & 0 & -289.33 & 0 & 868.00 & 289.33 & 0 & 0 & 0 \\
 0 & 0 & 0 & 0 & 0 & 0 & 0 & 0 & 0 & 0 & -1.67x10^5 & 0 & 0 & 1.67x10^5 & 0 & 0 \\
 0 & 0 & 0 & 0 & 0 & 0 & 0 & 0 & 0 & 0 & 0 & 0 & 0 & 0 & 0 & 0
 \end{bmatrix}$$

(8.5.41)

$$\{\Delta \mathbf{U}_3\} = \begin{bmatrix} 0 \\ 0 \\ 0 \\ 1.305x10^{-2} \Delta l_3 \\ 8.935x10^{-6} \Delta l_3 \\ 3.224x10^{-3} \Delta l_3 \\ 1.769x10^{-2} \Delta l_3 \\ 1.787x10^{-5} \Delta l_3 \\ -1.200x10^{-4} \Delta l_3 \\ 1.767x10^{-2} \Delta l_3 \\ -8.935x10^{-6} \Delta l_3 \\ 3.560x10^{-3} \Delta l_3 \\ 0 \\ 0 \\ 0 \end{bmatrix}; \{\Delta \mathbf{R}_3\} = \begin{bmatrix} -0.978 \Delta l_3 \\ -1.489 \Delta l_3 \\ 0 \\ 0 \\ 0 \\ 0 \\ 0 \\ 0 \\ 0 \\ 0 \\ 0 \\ 0 \\ -2.022 \Delta l_3 \\ 1.489 \Delta l_3 \\ 0 \end{bmatrix} \quad (8.5.45)$$

The maximum moments occur simultaneously at the hinge  $j$  of the element 3 and hinge  $i$  of element 4; therefore, these are the locations of the third and fourth plastic hinges that become active. For these elements:

$$\{\mathbf{M}\}_3 = \begin{bmatrix} 25.503 \\ 57.649 \\ -39.883 \end{bmatrix} + \begin{bmatrix} 2.870 \Delta l_3 \\ 6.065 \Delta l_3 \\ -2.022 \Delta l_3 \end{bmatrix}; \{\mathbf{M}\}_4 = \begin{bmatrix} -57.649 \\ -62.00 \\ -19.859 \end{bmatrix} + \begin{bmatrix} -6.065 \Delta l_3 \\ 0 \\ -1.489 \Delta l_3 \end{bmatrix} \quad (8.5.46)$$

$\Delta l_3$  is computed by solving:

$$|57.649 + 6.065 \Delta l_3| - 62 = 0 \Rightarrow \Delta l_3 = 0.717 \quad (8.5.47)$$

At the end of the fourth step, the stresses in the elements are:

$$\{\mathbf{M}_3\}_{j_1} = \begin{bmatrix} -62.000 \\ -16.537 \\ 8.927 \end{bmatrix}; \{\mathbf{M}_3\}_{j_2} = \begin{bmatrix} 16.537 \\ -27.562 \\ 8.927 \end{bmatrix}; \{\mathbf{M}_3\}_{j_3} = \begin{bmatrix} 27.562 \\ 62.000 \\ -41.333 \end{bmatrix}; \{\mathbf{M}_3\}_{j_4} = \begin{bmatrix} -62.000 \\ -62.000 \\ -20.927 \end{bmatrix} \quad (8.5.48)$$

and the displacements are:

**Analysis of Elasto-Plastic Frames**

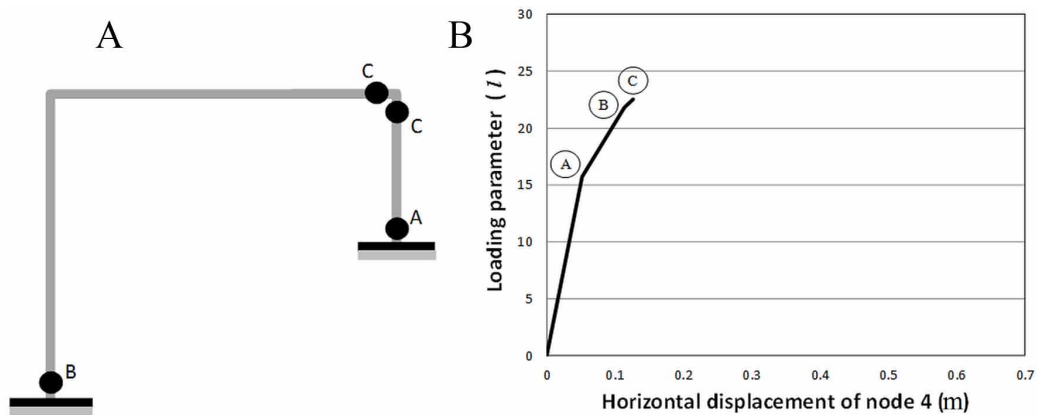
$$\{U_3\} = \{U_2\} + \Delta l_3 \{V_3\} = \begin{bmatrix} 0 \\ 0 \\ 0 \\ 7.25 \times 10^{-2} \\ 5.356 \times 10^{-5} \\ 2.971 \times 10^{-2} \\ 1.267 \times 10^{-1} \\ 1.071 \times 10^{-4} \\ 4.311 \times 10^{-3} \\ 1.262 \times 10^{-1} \\ -1.256 \times 10^{-4} \\ 3.016 \times 10^{-2} \\ 0 \\ 0 \\ 0 \end{bmatrix} \quad (8.5.49)$$

The loading parameter is:

$$l(3) = l(2) + \Delta l_3 = 22.504 \quad (8.5.50)$$

Figure 7 shows the location of the plastic hinges in the frame and the plot of horizontal displacements at nodes 4 vs. loading parameter.

Figure 7. a) Location of the plastic hinges in the RC frame; b) Plot of horizontal displacement at node 4 vs. loading parameter



The tangent stiffness matrix of the structure is computed after changing the matrices corresponding to the elements 3 and 4. They must be computed, respectively, as  $[k_{tE}]_3 = [B_E^0]_3^t [S_{1j}]_3 [B_E^0]_3$  .and

$[k_{tE}]_4 = [B_E^0]_4^t [S_2]_4 [B_E^0]_4$ , where:

$$[S_{1j}]_3 = \begin{bmatrix} 1302.00 & 0 & 0 \\ 0 & 0 & 0 \\ 0 & 0 & 8.33x10^4 \end{bmatrix} \tag{8.5.51}$$

then,

$$[k_{tE}]_3 = \begin{bmatrix} 0 & 0 & 0 & 0 & 0 & 0 & 0 & 0 & 0 & 0 & 0 & 0 & 0 & 0 & 0 \\ 0 & 0 & 0 & 0 & 0 & 0 & 0 & 0 & 0 & 0 & 0 & 0 & 0 & 0 & 0 \\ 0 & 0 & 0 & 0 & 0 & 0 & 0 & 0 & 0 & 0 & 0 & 0 & 0 & 0 & 0 \\ 0 & 0 & 0 & 0 & 0 & 0 & 0 & 0 & 0 & 0 & 0 & 0 & 0 & 0 & 0 \\ 0 & 0 & 0 & 0 & 0 & 0 & 0 & 0 & 0 & 0 & 0 & 0 & 0 & 0 & 0 \\ 0 & 0 & 0 & 0 & 0 & 0 & 0 & 0 & 0 & 0 & 0 & 0 & 0 & 0 & 0 \\ 0 & 0 & 0 & 0 & 0 & 0 & 83333.33 & 0 & 0 & -83333.33 & 0 & 0 & 0 & 0 & 0 \\ 0 & 0 & 0 & 0 & 0 & 0 & 0 & 36.17 & -217.00 & 0 & -36.17 & 0 & 0 & 0 & 0 \\ 0 & 0 & 0 & 0 & 0 & 0 & 0 & -217.00 & 1302.00 & 0 & 217.00 & 0 & 0 & 0 & 0 \\ 0 & 0 & 0 & 0 & 0 & 0 & -83333.33 & 0 & 0 & 83333.33 & 0 & 0 & 0 & 0 & 0 \\ 0 & 0 & 0 & 0 & 0 & 0 & 0 & -36.17 & 217.00 & 0 & 36.17 & 0 & 0 & 0 & 0 \\ 0 & 0 & 0 & 0 & 0 & 0 & 0 & 0 & 0 & 0 & 0 & 0 & 0 & 0 & 0 \\ 0 & 0 & 0 & 0 & 0 & 0 & 0 & 0 & 0 & 0 & 0 & 0 & 0 & 0 & 0 \\ 0 & 0 & 0 & 0 & 0 & 0 & 0 & 0 & 0 & 0 & 0 & 0 & 0 & 0 & 0 \\ 0 & 0 & 0 & 0 & 0 & 0 & 0 & 0 & 0 & 0 & 0 & 0 & 0 & 0 & 0 \end{bmatrix} \tag{8.5.52}$$

$$[S_2]_4 = \begin{bmatrix} 0 & 0 & 0 \\ 0 & 0 & 0 \\ 0 & 0 & 1.67x10^5 \end{bmatrix} \tag{8.5.53}$$

so,

**Analysis of Elasto-Plastic Frames**

$$\left[ \mathbf{k}_{tE} \right]_4 = \begin{bmatrix}
 0 & 0 & 0 & 0 & 0 & 0 & 0 & 0 & 0 & 0 & 0 & 0 & 0 & 0 & 0 \\
 0 & 0 & 0 & 0 & 0 & 0 & 0 & 0 & 0 & 0 & 0 & 0 & 0 & 0 & 0 \\
 0 & 0 & 0 & 0 & 0 & 0 & 0 & 0 & 0 & 0 & 0 & 0 & 0 & 0 & 0 \\
 0 & 0 & 0 & 0 & 0 & 0 & 0 & 0 & 0 & 0 & 0 & 0 & 0 & 0 & 0 \\
 0 & 0 & 0 & 0 & 0 & 0 & 0 & 0 & 0 & 0 & 0 & 0 & 0 & 0 & 0 \\
 0 & 0 & 0 & 0 & 0 & 0 & 0 & 0 & 0 & 0 & 0 & 0 & 0 & 0 & 0 \\
 0 & 0 & 0 & 0 & 0 & 0 & 0 & 0 & 0 & 0 & 0 & 0 & 0 & 0 & 0 \\
 0 & 0 & 0 & 0 & 0 & 0 & 0 & 0 & 0 & 0 & 0 & 0 & 0 & 0 & 0 \\
 0 & 0 & 0 & 0 & 0 & 0 & 0 & 0 & 0 & 0 & 0 & 0 & 0 & 0 & 0 \\
 0 & 0 & 0 & 0 & 0 & 0 & 0 & 0 & 0 & 0 & 0 & 0 & 0 & 0 & 0 \\
 0 & 0 & 0 & 0 & 0 & 0 & 0 & 0 & 0 & 0 & 0 & 0 & 0 & 0 & 0 \\
 0 & 0 & 0 & 0 & 0 & 0 & 0 & 0 & 0 & 0 & 0 & 0 & 0 & 0 & 0 \\
 0 & 0 & 0 & 0 & 0 & 0 & 0 & 0 & 0 & 0 & 0 & 0 & 0 & 0 & 0 \\
 0 & 0 & 0 & 0 & 0 & 0 & 0 & 0 & 0 & 0 & 0 & 0 & 0 & 0 & 0 \\
 0 & 0 & 0 & 0 & 0 & 0 & 0 & 0 & 0 & 0 & 0 & 0 & 0 & 0 & 0 \\
 0 & 0 & 0 & 0 & 0 & 0 & 0 & 0 & 0 & 0 & 0 & 0 & 0 & 0 & 0 \\
 0 & 0 & 0 & 0 & 0 & 0 & 0 & 0 & 0 & 0 & 1.67x10^5 & 0 & 0 & -1.67x10^5 & 0 \\
 0 & 0 & 0 & 0 & 0 & 0 & 0 & 0 & 0 & 0 & 0 & 0 & 0 & 0 & 0 \\
 0 & 0 & 0 & 0 & 0 & 0 & 0 & 0 & 0 & 0 & 0 & 0 & 0 & 0 & 0 \\
 0 & 0 & 0 & 0 & 0 & 0 & 0 & 0 & 0 & 0 & -1.67x10^5 & 0 & 0 & 1.67x10^5 & 0 \\
 0 & 0 & 0 & 0 & 0 & 0 & 0 & 0 & 0 & 0 & 0 & 0 & 0 & 0 & 0
 \end{bmatrix} \quad (8.5.54)$$

And the tangent stiffness matrix of the structure is (Box 4):

- **Fifth step:**  $s = 4$

This step starts solving the expression:

$$\left[ \mathbf{K}_t \right]_4 \{ \mathbf{V}_4 \} = \{ \mathbf{P}_4^R \} \quad (8.5.56)$$

where  $\left[ \mathbf{K}_t \right]_4$  was computed considering that the hinge  $i$  of the element 1, the hinge  $j$  of the element 3 and the hinges  $i$  and  $j$  of the element 4 are active.

$$\{ \mathbf{V}_4 \} = \frac{1}{\Delta l_4} \{ \Delta \mathbf{U}_4 \} \quad (8.5.57)$$

and



Box 4.

$$\begin{bmatrix}
 289.33 & 0 & 0 & -289.33 & 0 & 868.00 & 0 & 0 & 0 & 0 & 0 & 0 & 0 & 0 & 0 \\
 0 & 1.67 \times 10^5 & 0 & 0 & -1.67 \times 10^5 & 0 & 0 & 0 & 0 & 0 & 0 & 0 & 0 & 0 & 0 \\
 0 & 0 & 0 & 0 & 0 & 0 & 0 & 0 & 0 & 0 & 0 & 0 & 0 & 0 & 0 \\
 -289.33 & 0 & 0 & 1446.67 & 0 & 868.00 & -1157.33 & 0 & 1736.00 & 0 & 0 & 0 & 0 & 0 & 0 \\
 0 & -1.67 \times 10^5 & 0 & 0 & 3.33 \times 10^5 & 0 & 0 & -1.67 \times 10^5 & 0 & 0 & 0 & 0 & 0 & 0 & 0 \\
 868.00 & 0 & 0 & 868.00 & 0 & 6076.00 & -1736.00 & 0 & 1736.00 & 0 & 0 & 0 & 0 & 0 & 0 \\
 0 & 0 & 0 & -1157.33 & 0 & -1736.00 & 8.45 \times 10^4 & 0 & -1736.00 & -8.33 \times 10^4 & 0 & 0 & 0 & 0 & 0 \\
 \mathbf{[K]_t}_4 = & 0 & 0 & 0 & 0 & -1.67 \times 10^5 & 0 & 1.67 \times 10^5 & -217.00 & 0 & -36.17 & 0 & 0 & 0 & 0 \\
 0 & 0 & 0 & 1736.00 & 0 & 1736.00 & -1736.00 & -217.00 & 4774.00 & 0 & 217.00 & 0 & 0 & 0 & 0 \\
 0 & 0 & 0 & 0 & 0 & 0 & -8.33 \times 10^4 & 0 & 0 & 8.33 \times 10^4 & 0 & 0 & 0 & 0 & 0 \\
 0 & 0 & 0 & 0 & 0 & 0 & 0 & -36.16 & 217.00 & 0 & 1.67 \times 10^5 & 0 & 0 & -1.67 \times 10^5 & 0 \\
 0 & 0 & 0 & 0 & 0 & 0 & 0 & 0 & 0 & 0 & 0 & 0 & 0 & 0 & 0 \\
 0 & 0 & 0 & 0 & 0 & 0 & 0 & 0 & 0 & 0 & 0 & 0 & 0 & 0 & 0 \\
 0 & 0 & 0 & 0 & 0 & 0 & 0 & 0 & 0 & 0 & -1.67 \times 10^5 & 0 & 0 & 1.67 \times 10^5 & 0 \\
 0 & 0 & 0 & 0 & 0 & 0 & 0 & 0 & 0 & 0 & 0 & 0 & 0 & 0 & 0
 \end{bmatrix}$$

(8.5.55)

**Analysis of Elasto-Plastic Frames**

$$\{\mathbf{P}_4^R\} = \{\mathbf{P}_{ref}\} + \frac{1}{\Delta l_4} \{\Delta \mathbf{R}_4\} = \begin{bmatrix} \Delta R_{4w1} / \Delta l_4 \\ \Delta R_{4w1} / \Delta l_4 \\ \Delta R_{4\theta 1} / \Delta l_4 \\ 1 \\ 0 \\ 0 \\ 2 \\ 0 \\ 0 \\ 0 \\ 0 \\ 0 \\ 0 \\ \Delta R_{4w5} / \Delta l_4 \\ \Delta R_{4w5} / \Delta l_4 \\ \Delta R_{4\theta 5} / \Delta l_4 \end{bmatrix} \quad (8.5.58)$$

The increments of the displacements and reactions are:

$$\{\Delta \mathbf{U}_4\} = \begin{bmatrix} 0 \\ 0 \\ 0 \\ 8.643x10^{-2} \Delta l_4 \\ 1.500x10^{-5} \Delta l_4 \\ 2.535x10^{-2} \Delta l_4 \\ 1.435x10^{-1} \Delta l_4 \\ 3.000x10^{-5} \Delta l_4 \\ 1.153x10^{-2} \Delta l_4 \\ 1.435x10^{-1} \Delta l_4 \\ -1.500x10^{-5} \Delta l_4 \\ \Delta \theta_4 \\ 0 \\ 0 \\ 0 \end{bmatrix}; \{\Delta \mathbf{R}_4\} = \begin{bmatrix} -3.000 \Delta l_4 \\ -2.500 \Delta l_4 \\ 0 \\ 0 \\ 0 \\ 0 \\ 0 \\ 0 \\ 0 \\ 0 \\ 0 \\ 0 \\ 0 \\ 0 \\ 2.500 \Delta l_4 \\ 0 \end{bmatrix} \quad (8.5.59)$$

The maximum moments occur simultaneously in the hinge  $j$  of the element 2 and in the hinge  $i$  of the element 3; therefore, these are the locations of the fifth and sixth plastic hinges that become active. For these elements:

$$\{\mathbf{M}\}_2 = \begin{bmatrix} 16.537 \\ -27.562 \\ 8.927 \end{bmatrix} + \begin{bmatrix} 9.000\Delta l_4 \\ -15.000\Delta l_4 \\ 2.500\Delta l_4 \end{bmatrix}; \{\mathbf{M}\}_3 = \begin{bmatrix} 27.562 \\ 62.000 \\ -41.333 \end{bmatrix} + \begin{bmatrix} 15.000\Delta l_4 \\ 0 \\ 0 \end{bmatrix} \quad (8.5.60)$$

$\Delta l_4$  is computed by solving:

$$|27.562 + 15.000\Delta l_4| - 62 = 0 \Rightarrow \Delta l_4 = 2.296 \quad (8.5.61)$$

At the end of the fifth step, the stresses in the elements are:

$$\{\mathbf{M}_4\}_1 = \begin{bmatrix} -62.000 \\ -37.200 \\ 14.667 \end{bmatrix}; \{\mathbf{M}_4\}_2 = \begin{bmatrix} 37.200 \\ -62.000 \\ 14.667 \end{bmatrix}; \{\mathbf{M}_4\}_3 = \begin{bmatrix} 62.000 \\ 62.000 \\ -41.333 \end{bmatrix}; \{\mathbf{M}_4\}_4 = \begin{bmatrix} -62.000 \\ -62.000 \\ -26.667 \end{bmatrix} \quad (8.5.62)$$

and the displacements are:

$$\{\mathbf{U}_4\} = \{\mathbf{U}_3\} + \Delta l_4 \{\mathbf{V}_4\} = \begin{bmatrix} 0 \\ 0 \\ 0 \\ 2.709x10^{-1} \\ 8.800x10^{-5} \\ 8.792x10^{-2} \\ 4.561x10^{-1} \\ 1.760x10^{-4} \\ 3.078x10^{-2} \\ 4.556x10^{-1} \\ -1.600x10^{-4} \\ 3.016x10^{-2} + \Delta\theta_4 \\ 0 \\ 0 \\ 0 \end{bmatrix} \quad (8.5.63)$$

The loading parameter is:

$$l(4) = l(3) + \Delta l_4 = 24.800 \quad (8.5.64)$$

## Analysis of Elasto-Plastic Frames

In Figure 8a it is shown the localization of the plastic hinges in the frame and in Figure 8b the plot horizontal displacement of the node 4 vs. the loading parameter. In the later, it can be observed the change of the tangent stiffness with the progressive plasticization of the frame.

### 8.5.2. Solve the Local Problem for the Column Shown in Figure 6a Considering the Interaction Diagram of Figure 6b

The displacement matrix of the element is:

$$\{\mathbf{U}_{t=1}\} = \begin{bmatrix} 0 \\ 0 \\ 0 \\ 0.024 \\ -0.00042 \\ 0.03 \end{bmatrix} \quad (8.5.65)$$

Based on Figure 6b the yield function is defined as:For

$$|n| \leq 0.1N_y, f = \frac{|m|}{M_y} - 1; 0.1N_y < |n| \leq N_y; f = 0.9 \frac{|m|}{M_y} + \frac{|n|}{N_y} - 1 \quad (8.5.66)$$

- Elastic predictor phase: It is assumed that none of the plastic hinges is active. The generalized deformations are obtained by the kinematic equation:

$$\{\Phi_{t=1}\}_1 = [\mathbf{B}_E^0]_1 \{\mathbf{U}_{t=1}\} = \begin{bmatrix} 0.33 & 0 & 1 & -0.33 & 0 & 0 \\ 0.33 & 0 & 0 & -0.33 & 0 & 1 \\ 0 & -1 & 0 & 0 & 1 & 0 \end{bmatrix} \begin{bmatrix} 0 \\ 0 \\ 0 \\ 0.024 \\ -0.00042 \\ 0.03 \end{bmatrix} = \begin{bmatrix} -0.008 \\ 0.022 \\ -0.00042 \end{bmatrix} \quad (8.5.67)$$

The provisional stress matrix is computed as:

$$\{\mathbf{M}^{prov}\}_1 = [\mathbf{E}]_1 \{\Phi_{t=1} - \Phi_{t=0}^p\}_b = \begin{bmatrix} 3472 & 1736 & 0 \\ 1736 & 3472 & 0 \\ 0 & 0 & 1.67 \times 10^5 \end{bmatrix} \begin{bmatrix} -0.008 \\ 0.022 \\ -0.00042 \end{bmatrix} = \begin{bmatrix} 10.416 \\ 62.496 \\ -70.000 \end{bmatrix} \quad (8.5.68)$$

Figure 8. a) Location of then plastic hinges in the RC frame; b) Plot of horizontal displacement at node 4 vs. loading parameter

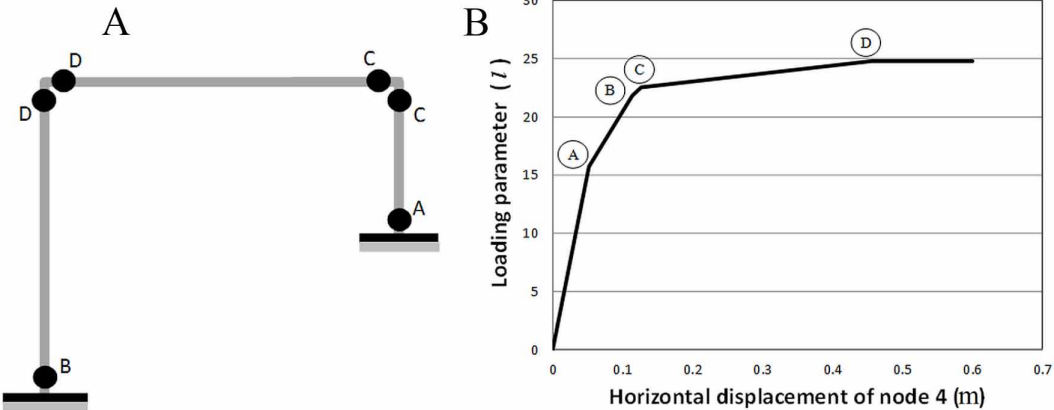
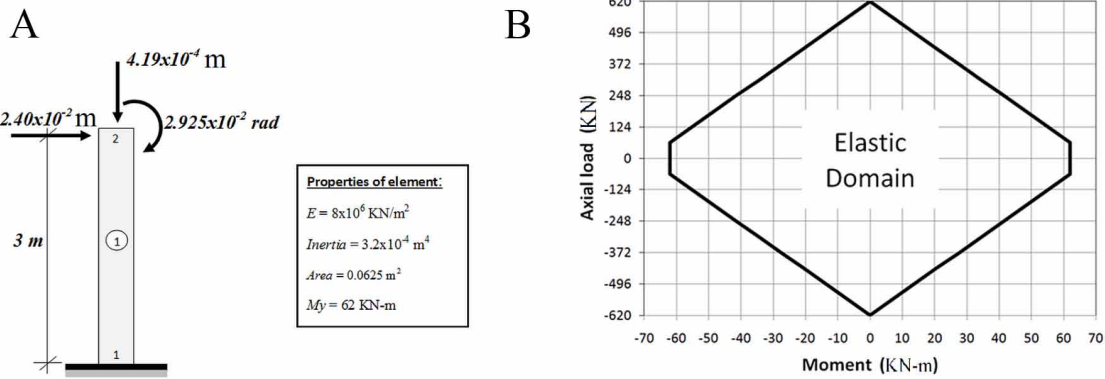


Figure 9. a) RC element subjected to displacements; b) Elastic domain of the element cross-section



In order to verify the elastic assumption, the yield functions (8.5.66) are computed:

$$n = -70KN > N_y \Rightarrow f = 0.9 \frac{|m|}{M_y} + \frac{|n|}{N_y} - 1 \Rightarrow \begin{cases} f_1^{prov} = 0.9 \frac{|10.416|}{62} + \frac{|70|}{620} - 1 = -0.7359 \\ f_2^{prov} = 0.9 \frac{|62.496|}{62} + \frac{|70|}{620} - 1 = 0.0201 \end{cases} \quad (8.5.69)$$

As the yield function at node 2 is positive, a plastic correction is needed.

- Plastic correction

The provisional plastic deformation matrix is:

### Analysis of Elasto-Plastic Frames

$$\{\Phi_{prov}^p\}_1 = \begin{bmatrix} 0 \\ \phi_2^p \\ \delta_p \end{bmatrix} \quad (8.5.70)$$

and the provisional stress matrix is:

$$\{\mathbf{M}^{prov}\}_1 = [\mathbf{E}]_1 \{\Phi_{t=0} - \Phi_{prov}^p\}_1 = \begin{bmatrix} m_1 \\ m_2 \\ n \end{bmatrix} \quad (8.5.71)$$

$$\{\mathbf{M}^{prov}\}_1 = \begin{bmatrix} 3472 & 1736 & 0 \\ 1736 & 3472 & 0 \\ 0 & 0 & 1.67 \times 10^5 \end{bmatrix} \begin{bmatrix} -0.008 \\ 0.022 - \phi_2^p \\ -0.00042 - \delta_p \end{bmatrix} = \begin{bmatrix} m_1 - 10.416 + 1736 \phi_2^p \\ m_2 - 62.496 + 3472 \phi_2^p \\ n + 70 + 1.67 \times 10^5 \delta_p \end{bmatrix} \quad (8.5.72)$$

The provisional yield functions are defined as:

$$f_1^{prov} = 0.9 \frac{|m_1|}{62} + \frac{|n|}{620} - 1; f_2^{prov} = 0.9 \frac{|m_2|}{62} + \frac{|n|}{620} - 1 = 0 \quad (8.5.73)$$

And the provisional normality rule is:

$$\Delta \phi_1^p \Big|_{prov} = 0; \Delta \phi_j^p = \Delta \lambda_2 \frac{\partial f_2}{\partial m_2} \Big|_{prov} = 0.01452 \Delta \lambda_2; \Delta \delta_p = \Delta \lambda_2 \frac{\partial f_2}{\partial n} \Big|_{prov} = -0.001613 \Delta \lambda_2 \quad (8.5.74)$$

Solving the set of equations conformed by Equation (8.5.73) and (8.5.74), it is obtained the following solution:

$$\{\mathbf{M}^{prov}\}_1 = \begin{bmatrix} 9.9812 \\ 61.6264 \\ -65.3620 \end{bmatrix}; \{\Phi_{prov}^p\}_1 = \begin{bmatrix} 0 \\ 0.00025045 \\ -0.00002783 \end{bmatrix}; \Delta \lambda_2 = 0.017253 \quad (8.5.75)$$

The necessary verifications are:

$$f_1^{prov} = 0.9 \frac{|9.9812|}{62} + \frac{|-65.3620|}{620} - 1 \cong -0.7497 < 0; \Delta \lambda_2 = 0.017253 > 0 \quad (8.5.76)$$

Therefore, it can be concluded that the provisional values obtained in the plastic correction are the definitive ones.

### 8.5.3. Adjust the Model for Elements of any Aspect Ratio of Section 7.4 to the General Formulation for the Analysis of Elasto-Plastic Frames

1. The variables are:

a. Generalized displacements:  $\{\mathbf{U}_{t=tr}\}_b = \begin{bmatrix} u_1 \\ w_1 \\ \theta_1 \\ u_2 \\ \vdots \\ \vdots \\ w_n \\ \theta_n \end{bmatrix}$

b. Generalized stresses:  $\{\mathbf{M}_{t=tr}\}_b = \begin{bmatrix} m_i^b \\ m_j^b \\ n_b \end{bmatrix}$

c. Generalized deformations:  $\{\Phi_{t=tr}\}_b = \begin{bmatrix} \phi_i^b \\ \phi_j^b \\ \delta_b \end{bmatrix}$

d. Internal variables with yield functions:  $VWf_1|_{t=tr} = \gamma^p, VWf_2|_{t=tr} = \phi_i^p, VWf_3|_{t=tr} = \phi_j^p$

e. Internal variables without yield functions:  $\{\mathbf{VW}\mathbf{o}_{t=tr}\}_b : \{x_s, x_i, x_j\}$

2. The equations are:

a. Kinematic equations:  $\{\Delta\Phi\}_b = [\mathbf{B}_E(\mathbf{U}_{t=tr})]_b \{\Delta\mathbf{U}\}$

b. Equilibrium equations:  $\{\mathbf{L}(\mathbf{U}_{t=tr})\} = \{\mathbf{P}_{t=tr}\}; \{\mathbf{L}(\mathbf{U}_{t=tr})\} = \sum_{b=1}^m [\mathbf{B}(\mathbf{U}_{t=tr})_E]_b^t \{\mathbf{M}(\mathbf{U}_{t=tr})\}_b ;$

i. Elasticity laws:

$$\{\mathbf{E}\mathbf{L}(\Phi, \mathbf{M}, VWf_1, \dots, VWf_k, \mathbf{VW}\mathbf{o})\}_{t=tr} = \{\Phi\}_b - ([\mathbf{F}_f]_b + [\mathbf{F}_s]_b) \{\mathbf{M}\}_b - \{\Phi^0\}_b - \{\gamma^p\}_b - \{\Phi^p\}_b = 0$$

ii. Yield functions:

$$Yf_1(\mathbf{M}, VWf_1, \dots, VWf_k, \mathbf{VW}\mathbf{o})|_{t=tr} = f_s(m_i^b, m_j^b, x_s) = \left| \frac{m_i^b + m_j^b}{L_b} - x_s \right| - V_p \leq 0$$

$$Yf_2(\mathbf{M}, VWf_1, \dots, VWf_k, \mathbf{VW}\mathbf{o})|_{t=tr} = f_i(m_i^b, x_i) = |m_i^b - x_i| - M_{pi} \leq 0$$

### Analysis of Elasto-Plastic Frames

$$Yf_3(\mathbf{M}, VWf_1, \dots, VWf_k, \mathbf{VW}\mathbf{o}) \Big|_{t=tr} = f_j(m_j^b, x_j) = |m_j^b - x_j| - M_{pj} \leq 0$$

iii. Remaining equations:

$$\{\mathbf{R}\mathbf{M}(\mathbf{M}, VWf_1, \dots, VWf_k, \mathbf{VW}\mathbf{o})\} \Big|_{t=tr} = \begin{bmatrix} x_s - r_s \cdot c_s \cdot \gamma^p \\ x_i - r c_i \phi_i^p \\ x_j - r c_j \phi_j^p \end{bmatrix} = 0$$

### 8.5.4. Adjust the Tridimensional Model of Section 7.5 to the General Formulation for the Analysis of Elasto-Plastic Frames

1. The variables are:

- a. Generalized displacements:  $\{\mathbf{U}\}_b^t = (u_i, v_i, w_i, \varphi_i, \theta_i, \zeta_i, \dots, u_n, v_n, w_n, \varphi_n, \theta_n, \zeta_n)$
- b. Generalized stresses:  $\{\mathbf{M}\}_b^t = (m_{iy}^b, m_{jy}^b, n_b, m_{iz}^b, m_{jz}^b, m_x^b)$
- c. Generalized deformations:  $\{\Phi_{t=tr}\}_b^t = (\phi_{iy}, \phi_{jy}, \delta_p, \phi_{iz}, \phi_{jz}, \phi_x)$
- d. Internal variables with yield functions:  $VWf_1 \Big|_{t=tr} = \phi_x^p, VWf_2 \Big|_{t=tr} = \lambda_i, VWf_3 \Big|_{t=tr} = \lambda_j$
- e. Internal variables without yield functions:  $\{\mathbf{VW}\mathbf{o}_{t=tr}\}_b^t = (\phi_{iy}^p, \phi_{jy}^p, \delta_p, \phi_{iz}^p, \phi_{jz}^p)$

2. The equations are:

- a. Kinematic equations:  $\{\Delta\Phi\}_b = [\mathbf{B}_E(\mathbf{U}_{t=tr})]_b \{\Delta\mathbf{U}\}$
- b. Equilibrium equations:  $\{\mathbf{L}(\mathbf{U}_{t=tr})\} = \{\mathbf{P}_{t=tr}\}; \{\mathbf{L}(\mathbf{U}_{t=tr})\} = \sum_{b=1}^m [\mathbf{B}(\mathbf{U}_{t=tr})_E]_b^t \{\mathbf{M}(\mathbf{U}_{t=tr})\}_b$ 
  - i. Elasticity laws:

$$\{\mathbf{E}\mathbf{L}(\Phi, \mathbf{M}, VWf_1, \dots, VWf_k, \mathbf{VW}\mathbf{o})\} \Big|_{t=tr} = \{\mathbf{M}\}_b - [\mathbf{E}]_b \{\Phi - \Phi^p\}_b - \{\mathbf{M}^0\}_b = 0$$

ii. Yield functions:

$$Yf_1(\mathbf{M}, VWf_1, \dots, VWf_k, \mathbf{VW}\mathbf{o}) \Big|_{t=tr} = f_i = \left(\frac{n}{N_u}\right)^{\nu_1} + \left(\frac{m_{iy}}{M_{uy}}\right)^{\nu_2} + \left(\frac{m_{iz}}{M_{uz}}\right)^{\nu_3} - 1 \leq 0$$

$$Yf_2(\mathbf{M}, VWf_1, \dots, VWf_k, \mathbf{VW}\mathbf{o}) \Big|_{t=tr} = f_j = \left(\frac{n}{N_u}\right)^{\nu_1} + \left(\frac{m_{jy}}{M_{uy}}\right)^{\nu_2} + \left(\frac{m_{jz}}{M_{uz}}\right)^{\nu_3} - 1 \leq 0$$

$$Yf_3(\mathbf{M}, VWf_1, \dots, VWf_k, \mathbf{VW}\mathbf{o}) \Big|_{t=tr} = f_x(m_x) = |m_x| - M_{ux} \leq 0$$



iii. Remaining equations:

$$\{\mathbf{RM}(\mathbf{M}, VWf_1, \dots, VWf_k, \mathbf{VW}\mathbf{o})\}_{t=tr} = \begin{bmatrix} d\phi_{yi}^p - d\lambda_i \frac{\partial f_i}{\partial m_{yi}} \\ d\phi_{yj}^p - d\lambda_j \frac{\partial f_j}{\partial m_{yj}} \\ d\phi_{zi}^p - d\lambda_i \frac{\partial f_i}{\partial m_{zi}} \\ d\phi_{zj}^p - d\lambda_j \frac{\partial f_j}{\partial m_{zj}} \\ d\delta_p - d\lambda_i \frac{\partial f_i}{\partial n} - d\lambda_j \frac{\partial f_j}{\partial n} \end{bmatrix} = 0$$

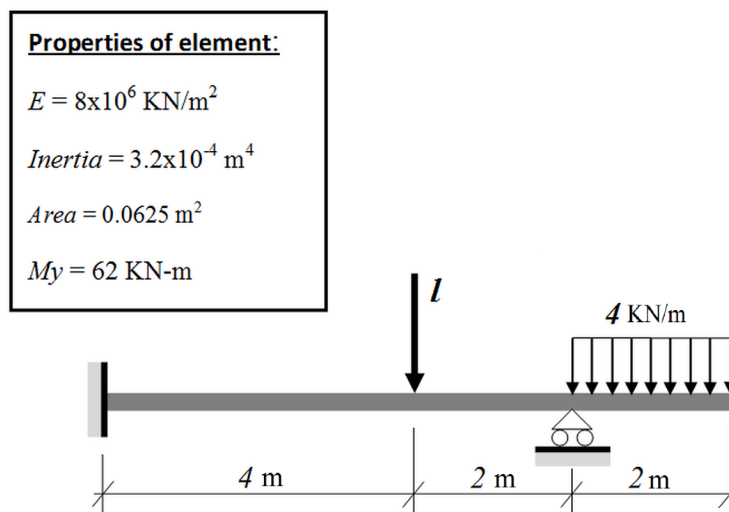
## 8.6 PROBLEMS

8.6.1 Analyze the Frame Shown in Figure 10 Using the Hinge-by-Hinge Method

8.6.2 Solve the Local and Global Problems for the Column Shown in Figure 11 Using the Displacement History and Constant Axial Load

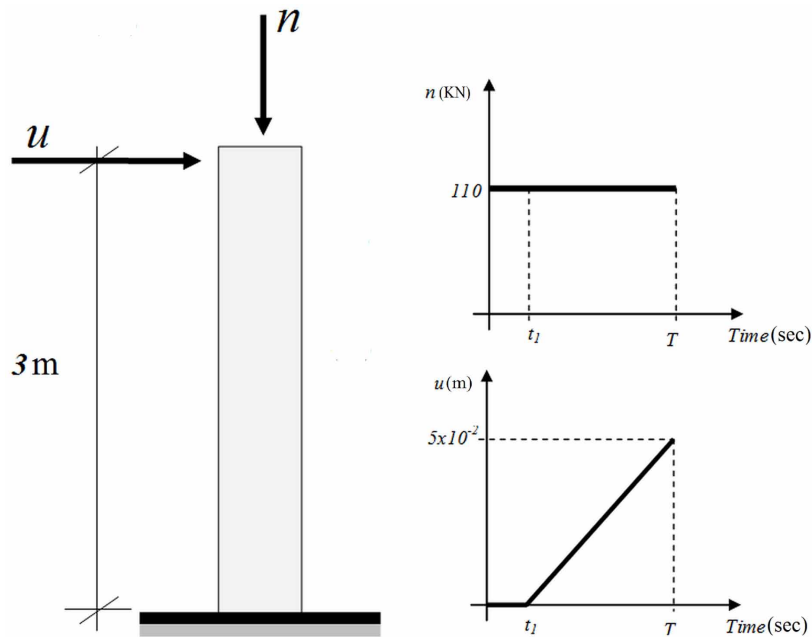
8.6.3 Adjust the Model for Elements of Any Aspect Ratio to the General Formulation. Consider Multi-Linear Isotropic and Kinematic Terms.

Figure 10. Beam subjected to transversal loads



## Analysis of Elasto-Plastic Frames

Figure 11. Column subjected to constant axial load and variable lateral displacements



## 8.7 PROJECTS

8.7.1 Generalize the Program Written in Project 4.7.1 including a Hinge-by-Hinge Analysis

8.7.2 Generalize the Program Written in Project 4.7.3 to the Case of Elasto-Plastic Frames

8.7.3 Generalize the Program Written in Project 4.7.4 to the Case of Elasto-Plastic Frames

## REFERENCES

Chen, W. F., & Sohal, I. (1995). *Plastic design and second-order analysis of steel frames*. New York: Springer-Verlag. doi:10.1007/978-1-4613-8428-1

Corradi, L., De Donato, O., & Maier, G. (1974). Inelastic analysis of reinforced concrete frames. *Journal of the Structural Division*, 100(9), 1925–1942.

Simo, J. C., Kennedy, J. G., & Govindjee, S. (1988). Non-smooth multisurface plasticity and viscoplasticity: Loading/unloading conditions and numerical algorithms. *International Journal for Numerical Methods in Engineering*, 26(10), 2161–2185. doi:10.1002/nme.1620261003

## Chapter 9

# Fundamental Concepts of Fracture and Continuum Damage Mechanics

### ABSTRACT

*Some fundamental concepts of fracture mechanics, those needed for the description of concrete cracking in framed structures, are presented in a simplified way in the first section of this chapter. The second section introduces the fundamentals of continuum damage mechanics. The third section describes a physical phenomenon called localization; this is a very important effect during the process of structural collapse. In this section, it is shown that damage mechanics can lead to ill-posed mathematical problems. Finally, the relationship between localization and ill-posedness is discussed. In this chapter, fracture and damage mechanics or localization concepts are not yet applied to the analysis of framed structures; that is the subject of the following chapters.*

### 9.1 GRIFFITH CRITERION AND FRACTURE MECHANICS

In the theories of elasticity and plasticity, it is assumed that the boundaries of the solid are fixed and non-modifiable; they cannot be changed during an analysis. This simplifying hypothesis eliminates the possibility of representing crack propagation in solids; however, this phenomenon is one of the main causes of structural failure. Fracture mechanics differs from the aforementioned theories because it does not discard the possibility of modifications in the boundaries of a solid due to cracks propagation. Specifically, the primary goal of fracture mechanics is the determination of conditions for crack propagation in elastic or elasto-plastic solids.

### 9.1.1 Stress Concentration Factors in Solids

It is often necessary to drill holes in structural components. When the structural modifications occur in this way (see Figure 1), the local stresses are increased. The ratio of the local maximum stress and the average stress in the structure is called “stress concentration factors”  $SCF$ :

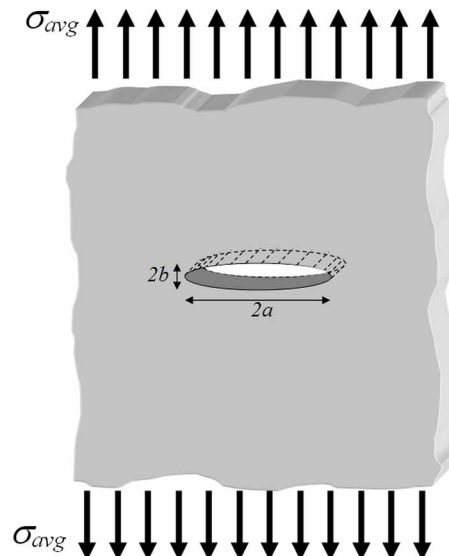
$$SCF = \frac{\sigma_{\max}}{\sigma_{\text{avg}}}, \text{ i.e. } \sigma_{\max} = SCF\sigma_{\text{avg}} \quad (9.1.1)$$

An important subject of the theories of elasticity and strength of materials is the determination of these factors for changes in the cross-section, structures with holes and other discontinuities. A particularly relevant case in fracture mechanics is the one shown in Fig 1: Consider an infinite plate of thickness  $t$  with an elliptic hole of mayor diameter  $2a$  and minor diameter  $2b$  in its center; the plate is subjected to constant stresses  $\sigma_{\text{avg}}$  far away from the hole as shown in Figure 1. It can be shown that the stress concentration factor in a linear elastic case is given by:

$$SCF = \frac{\sigma_{\max}}{\sigma_{\text{avg}}} \quad (9.1.2)$$

Mathematically, a crack can be defined as an infinitesimally narrow ellipse; notice that the local maximum stress tends to infinite when the shorter semi-axis  $b$  tends to zero, regardless of the magnitude of the tensile force applied to the plate. It can also be shown that this is always the case at any crack tip for any kind of structure.

*Figure 1. Infinite plate with elliptical hole*



Therefore, even if the stress concentration factors are a common and useful concept in the design of structural components, they cannot be used as a condition for crack propagation. Furthermore, it must now be explained why there are cracks in brittle solids that do not propagate at all if elastic stresses at the crack tips tend to infinite; the answer to this question can be found in an energy balance as presented in the following sections.

### 9.1.2 Energy Balance in a Cracked Structure

The potential energy  $PE$  of a force  $P$  is given by:

$$PE = -P \Delta \quad (9.1.3)$$

where  $\Delta$  is the displacement of the force. Consider, for instance, a rigid solid of mass  $M$ ; the gravitational force of the solid is:  $-M.g$  (positive direction upwards), where  $g$  is the acceleration of gravity; if the body is elevated a distance  $\Delta$  the potential energy is given by:  $M g \Delta$ ; that is  $PE = -P \Delta$ .

Consider now an elastic solid of stiffness  $S$  subjected to the force  $P$ . This force induce elongations in the solid denoted by  $\Delta$ :

$$P = S.\Delta \quad (9.1.4)$$

The total work done to deform the structure is stored in the solid; this new term of energy is called the “deformation energy”  $U$  (see Figure 2):

$$U = \int_0^{\Delta} P d\Delta = \frac{1}{2} S.\Delta^2 = \frac{1}{2} P.\Delta \quad (9.1.5)$$

Another area can be appreciated in the curve of force vs. elongation of Figure 2; this corresponds to the so called “complementary deformation energy”  $W$ :

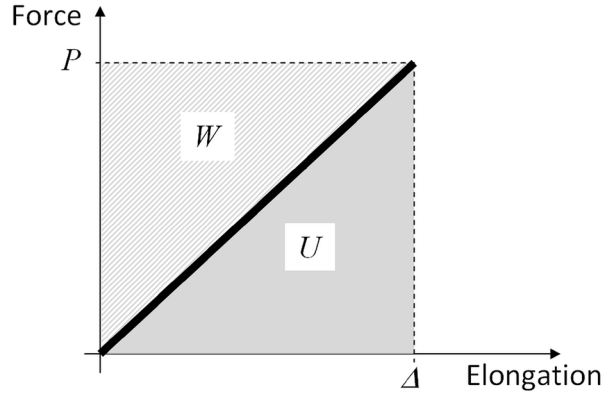
$$W = \int_0^P \Delta dP = \frac{1}{2S} P^2 = \frac{1}{2} FP^2 \quad (9.1.6)$$

where  $F = \frac{1}{S}$  is the flexibility of the solid. In a linear elastic solid, the two energy terms are equal.

The total energy  $TE$  in an elastic solid is now defined as the sum of the potential energy plus the deformation energy:

$$TE = U + PE \quad (9.1.7)$$

Figure 2. Deformation energy in a solid subjected to a force  $P$



Consider an elastic solid with a crack area equal to  $4a.t$ ; a new energy term must now be considered; this is called the surface energy  $SE$  and it is assumed to be proportional to the surface of the crack; thus, the surface energy increases with crack propagation:

$$SE = 4\Gamma_{sup} a.t \quad (9.1.8)$$

where  $\Gamma_{sup}$  is the surface energy per unit area.

The total energy of an elastic solid with a crack is therefore given by:

$$TE = U + PE + SE \quad (9.1.9)$$

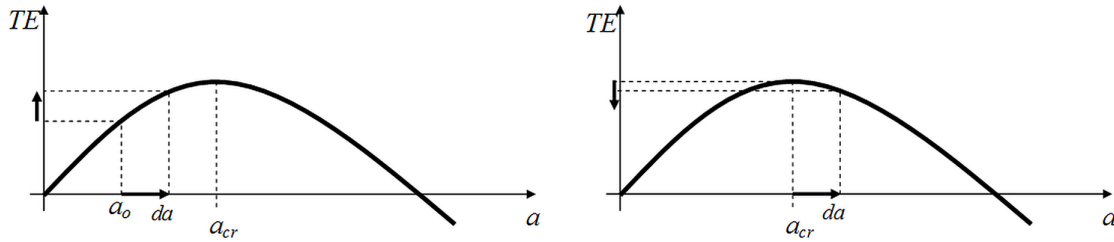
### 9.1.3 The Energy Release Rate and the Griffith Criterion

Consider again the infinite plate of section 9.1.1; it can be shown that the total energy is given by:

$$TE = U + PE + SE = U_0 - \frac{\pi\sigma_{avg}^2}{E} a^2 + 4\Gamma_{sup} a \quad (9.1.10)$$

where  $U_0$  is the deformation energy of a similar plate but without the crack. Notice that the curve of total energy vs. crack length corresponds to a concave parabola (see Figure 3). This curve explains why there are cracks that do not propagate, even if the stress concentration factor tends to infinite. Consider the case of a “small crack”  $a_0$ , i.e. a crack whose length is at the left of the peak in the curve in Figure 3. Suppose that this crack propagates, that is, its length increases from  $a_0$  to  $a_0+da$ . The total energy should also increase; however, this process is physically impossible since the external forces represented by the term  $\sigma_{avg}$  are constant in this analysis. Therefore, no additional work is being added to the structure; no matter how high the stress concentration factor is, crack propagation cannot occur under such conditions.

Figure 3. Total energy as a function of the crack length



Consider now the case of a “large crack”  $a_{cr}$ , i.e. a crack whose length corresponds to the peak of the curve. If the crack propagates, and its length increases to  $a_{cr}+da$ , then the total energy decreases this time. This process is physically possible; the excess of energy can be transformed, for instance, into kinetic energy as the structure breaks. If crack propagation is energetically possible, then it will occur since the stress concentration factor tends to infinite.

This analysis indicates that there is a critical crack length for each set of the external forces: shorter cracks do not grow up; larger cracks propagate

If the structure is not an infinite plate or if the loading is not the indicated in section 9.1.1, then Equation (9.1.10) is no longer valid; however, the reasoning is still applicable; the total energy is a concave function of the crack length and it presents a maximum for a critical value. Thus, in the general case, crack propagation is possible only if the derivative of the total energy with respect to the crack length is equal to zero:

$$G = R; \text{ where } G = -\frac{d}{da}(U + PE) \text{ and } R = \frac{d}{da}(SE) \quad (9.1.11)$$

The term  $G$  is called “energy release rate” or “crack driving force” and  $R$  is denoted “crack resistance”. If the crack driving force is less than the crack resistance, the crack cannot propagate; the propagation can occur only if Equation (9.1.11) holds; this is the “Griffith criterion”. The energy release rate can be computed in a structural analysis; the crack resistance can be measured in the course of an experimental analysis.

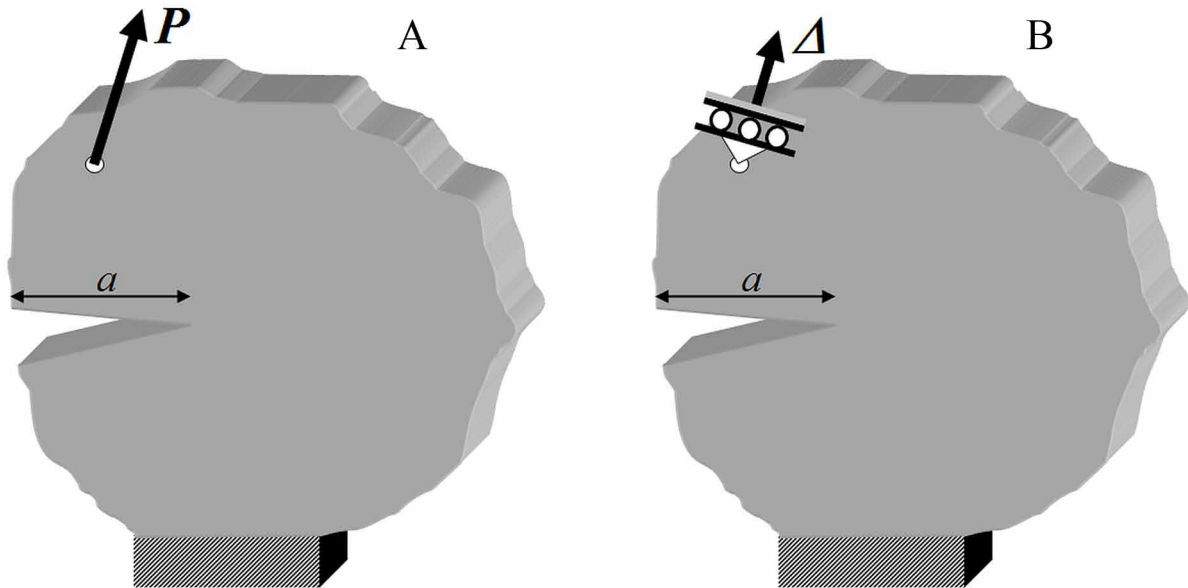
### 9.1.4 Energy Release Rate Expression in Terms of Stiffness or Flexibility

Consider a structure with a crack subjected to an external force  $P$  (see Figure 4a). The flexibility of the structure depends on the crack length and, therefore, the resulting displacement too. The energy release rate is in this case:

$$G = -\frac{d}{da}(U + PE) = -\frac{d}{da}\left(\frac{1}{2}P\Delta(a) - P\Delta(a)\right) = \frac{1}{2}\frac{dF(a)}{da}P^2 \quad (9.1.12)$$

If the structure is subjected to an imposed displacement (see Figure 4b), then:

Figure 4. a) Structure subjected to a concentrated force b) Structure subjected to a displacement  $\Delta$



$$G = -\frac{d}{da}(U + PE) = -\frac{d}{da}\left(\frac{1}{2}P(a)\Delta\right) = \frac{1}{2}\frac{dS(a)}{da}\Delta^2 \quad (9.1.13)$$

Notice that both expressions of the energy release rate are equivalent: the substitution of  $F = 1/S$  and Equation (9.1.4) into (9.1.12) leads to (9.1.13) and vice versa. These equations show that the energy release rate can be computed if the dependence of the structural stiffness, or flexibility, on the crack length is known.

Chapters 10, 11 and 12 present simple expressions for the energy release rate and crack resistance for RC frame members.

## 9.2 UNIAXIAL DAMAGE MECHANICS MODELS

Fracture mechanics is a powerful tool for structural vulnerability assessment; however, it presents some limitations. Fracture mechanics analyses are computationally expensive; therefore, its methods are not convenient in the cases of massive distributions of cracks propagating simultaneously. Additionally, even if it describes global structural degradation by modification of boundaries, it still assumes an elastic or elasto-plastic behavior of the material; however, it has been observed that an extensive local degradation usually precedes crack propagation; this local degradation is not considered in elasticity or plasticity. Continuum damage mechanics is a different theory that deals in a very efficient way with these two issues.



### 9.2.1 The Damage Variable

The mechanical degradation of materials takes the form of micro cracks and/or micro voids. The goal of continuum damage mechanics is to describe the evolution of these micro defects in structures subjected to thermo-mechanical loadings, which was not considered at all in the analysis of section 9.1 or in the elastic, neither the elastic plastic models of chapters 2 and 5.

Consider a damaged element as the one shown in Figure 5. Be  $A$  de total cross-section area of the element and  $A_d$  the area of micro defects. The damage of the bar is defined as:

$$\omega = \frac{A_d}{A} \quad (9.2.1)$$

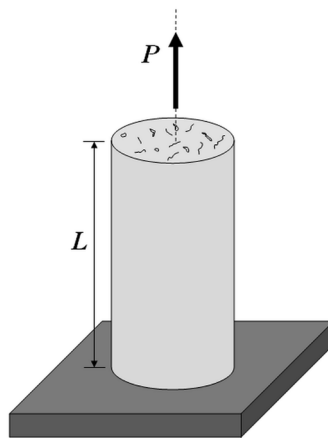
Notice that  $\omega$  can take values between zero (intact material) and one (a broken bar).

### 9.2.2 The Equivalent Stress and the Hypothesis of Equivalence in Deformation

In order to carry out the computation of the damage, it is necessary the introduction of this variable into the constitutive equations. One of simplest and most effective ways to do so is the use of an additional stress measure called “equivalent stress”. Consider again the damaged bar subjected to an axial force  $P$  as shown in Figure 5; the average normal stress  $\sigma$  in the bar is given by:  $\sigma = P / A$ . The effective stress  $\bar{\sigma}$  in the bar is defined as:

$$\bar{\sigma} = \frac{P}{A - A_d} \quad (9.2.2)$$

Figure 5. Damaged bar



## Fundamental Concepts of Fracture and Continuum Damage Mechanics

Notice that in the computation of the effective stress, the effective resistance area  $\bar{A} = A - A_d$  is used instead of the total area.

A relationship between the effective stress and the conventional normal stress is obtained by introducing the damage definition (9.2.1) into (9.2.2):

$$\bar{\sigma} = \frac{P}{A - \omega A} = \frac{\sigma}{1 - \omega} \quad (9.2.3)$$

Notice that the effective stress is equal to the normal stress for an intact material and that it tends to infinite when the damage tends to one.

The hypothesis of equivalence in strains states that the behavior of a damaged material can be described by the same equations of the intact one, if the normal stress measure  $\sigma$  is substituted by the effective one  $\bar{\sigma}$ . Therefore, according to the hypothesis of equivalence in deformations, the elasticity law for a damage material is given by:

$$\bar{\sigma} = E\varepsilon \Rightarrow \sigma = (1 - \omega)E\varepsilon \quad (9.2.4)$$

Notice that damage decreases the effective stiffness  $\bar{E} = (1 - \omega)E$  of the material.

The elasticity law (9.2.4) can be written also in terms of flexibility:

$$\varepsilon = \frac{1}{(1 - \omega)E} \sigma \quad (9.2.5)$$

An alternative way of writing the elasticity law (9.2.5) is described next; this alternative is very useful in the formulation of models for frame members. The strain  $\varepsilon$  is split into two terms, an elastic one and an additional damage related term defined as follows:

$$\varepsilon = \varepsilon^e + \varepsilon^d, \text{ where } \varepsilon^e = \frac{1}{E} \sigma \text{ and } \varepsilon^d = \frac{\omega}{E(1 - \omega)} \sigma \quad (9.2.6)$$

Notice that (9.2.5) and (9.2.6) are indeed equivalent. The elasticity law can now be interpreted as follows: the material presents an initial flexibility  $1/E$ ; the degradation process induces an increase in the flexibility of the material  $\frac{\omega}{E(1 - \omega)}$  that results in an additional strain term  $\varepsilon^d$  denoted “damage strain”.

If the material is elasto-plastic, as in metallic materials, the elasticity law is:

$$\bar{\sigma} = E(\varepsilon - \varepsilon^p) \Rightarrow \sigma = (1 - \omega)E(\varepsilon - \varepsilon^p) \quad (9.2.7)$$

or in terms of flexibility:

$$\varepsilon = \varepsilon^e + \varepsilon^d + \varepsilon^p \text{ where } \varepsilon^e = \frac{1}{E}\sigma; \text{ and } \varepsilon^d = \frac{\omega}{E(1-\omega)}\sigma \quad (9.2.8)$$

That is, the total strain can be decomposed into an elastic term that obeys the Hooke law, a damage strain and the plastic one.

The yield functions can also be modified in the same way, for instance an elastic perfectly plastic yield function becomes:

$$f = \left| \frac{\sigma}{1-\omega} \right| - \sigma_y \leq 0 \quad (9.2.9)$$

### 9.2.3 Brittle Damage Model

In brittle materials, the damage takes the form of micro cracks, therefore, the elasticity law (9.2.4) or (9.2.7) can be accompanied by a damage evolution law derived from the Griffith criterion introduced in section 9.1.

Consider again a solid differential element subjected to a normal stress  $\sigma$ . The strain energy of the element is defined as:

$$U = \frac{1}{2}\sigma\varepsilon \quad (9.2.10)$$

According to the elasticity law (9.2.4), the strain energy of a damaged material is given by:

$$U = \frac{1}{2}\sigma\varepsilon = \frac{1}{2}(1-\omega)E\varepsilon^2 \quad (9.2.11)$$

A generalized form of the Griffith criterion is:

$$G_m - R_m \leq 0; \text{ where } G_m = -\frac{dU}{d\omega} = \frac{1}{2}E\varepsilon^2 \quad (9.2.12)$$

$G_m$  is the energy release rate of a damaged element and  $R_m$  is the “damage resistance function”. Notice that the energy release rate of a damaged element can also be expressed in an alternative way. Be  $W$  the complementary strain energy defined as:

$$W = \frac{1}{2}\sigma.\varepsilon = \frac{1}{2}\frac{\sigma^2}{E(1-\omega)} \quad (9.2.13)$$

where the elasticity law is expressed in terms of flexibility, i.e. Equation (9.2.5), instead of stiffness. Thus, as in the case of fracture mechanics:

$$G_m = \frac{\partial W}{\partial \omega} = -\frac{\partial U}{\partial \omega} = \frac{1}{2} \frac{\sigma^2}{E(1-\omega)^2} = \frac{1}{2} E \varepsilon^2 \quad (9.2.14)$$

### 9.2.4 A Damage Mechanics Model for Concrete

As described in section 6.5.2, the strength of the concrete fibers in tension can be neglected and, in compression, the behavior can be represented by a second-degree parabola. This kind of behavior can be described by the following elasticity law:

$$\sigma = (1 - \omega)E \langle \varepsilon \rangle_- \quad (9.2.15)$$

where the term  $\langle \varepsilon \rangle_-$  is called “negative part of the strain” and it is defined as:

$$\langle \varepsilon \rangle_- = \begin{cases} \varepsilon & \text{if } \varepsilon \leq 0 \\ 0 & \text{otherwise} \end{cases} \quad (9.2.16)$$

The hypothesis of zero tension strength can be specified using the negative part of the strain; i.e., for any positive value of the strain, the stress is equal to zero according to the elasticity law (9.2.15).

Damage evolution in compression is described by the Griffith criterion:

$$\begin{cases} d\omega = 0 & \text{if } G_m < R_m \\ G_m = R_m & \text{if } d\omega > 0 \end{cases} \quad (9.2.17)$$

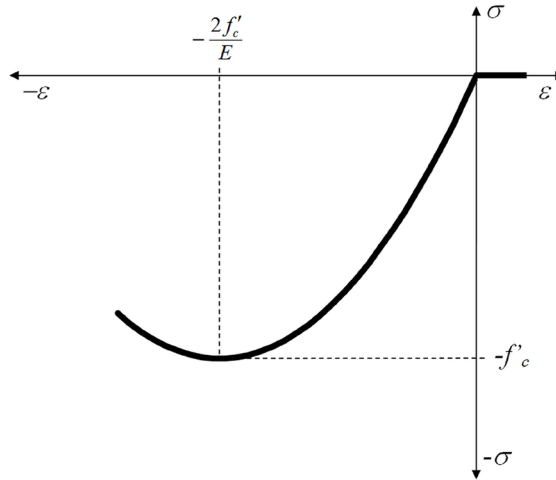
The term  $R_m$  is a constant in perfect brittle materials, but other models can be derived assuming that the micro-crack resistance is a function of the damage. For instance a second-degree parabola in the stress strain curve is obtained using the following crack resistance function:

$$R_m = \frac{8(f'_c)^2}{E} \omega^2 \quad (9.2.18)$$

where  $f'_c$  is the concrete resistance in compression. This model gives the behavior shown in Figure 6.

The stress vs. strain curve reaches a maximum for a strain value of  $\frac{2f'_c}{E}$  and this stress is indeed equal to  $f'_c$ ; the demonstration is given in the example 9.5.1. For larger values of strain, the stress decreases and tends to zero; this is called the softening stage of the material behavior.

Figure 6. A damage mechanics model for concrete



### 9.2.5 Ductile Damage Model

Consider now an elasto-plastic material; as aforementioned, the elasticity law is in this case given by:

$$\sigma = (1 - \omega)E(\varepsilon - \varepsilon^p) \quad (9.2.19)$$

If plastic hardening effects are neglected, the plastic strain evolution law is:

$$\begin{cases} d\varepsilon_p = 0 & \text{if } f < 0 \\ f = 0 & \text{if } d\varepsilon_p \neq 0 \end{cases}; f = \left| \frac{\sigma}{1 - \omega} \right| - \sigma_y \leq 0 \quad (9.2.20)$$

In metallic materials, micro-defects consist, mainly, in micro-voids that may reproduce and grow; therefore the Griffith criterion is not an adequate approach in this case. It has been observed experimentally that micro-voids or damage evolution depends on the plastic strain; therefore, a simple and effective model is given by:

$$\omega = \kappa \langle p - p_{cr} \rangle_+ \quad (9.2.21)$$

where  $\kappa$  and  $p_{cr}$  are material constants, the term  $\langle p \rangle_+$  is called “the positive part of the variable  $p$ ” and it is defined as:

$$\langle p \rangle_+ = \begin{cases} p & \text{if } p \geq 0 \\ 0 & \text{otherwise} \end{cases} \quad (9.2.22)$$

The variable  $p$  is, again, the accumulated plastic strain as defined in section 5.3:

$$dp = |d\varepsilon_p| \tag{9.2.23}$$

$p_{cr}$  represents a critical value of the plastic strain that triggers the damage evolution. The behavior described by this model is shown in Figure 7 (see also example 9.5.2).

Consider again Table 1 of chapter 5; notice that with this damage model all these phenomena, with the exception of effect d, are represented, at least qualitatively. The plastic hardening can, of course, also be included by modifying the yield function, for instance:

$$f(\sigma) = \left| \frac{\sigma}{1-\omega} - x \right| - \sigma_y \leq 0; dx = \alpha \left( (\sigma_u - \sigma_y) d\varepsilon_p - x \cdot |d\varepsilon_p| \right) \tag{9.2.24}$$

In this way, all the phenomena listed in chapter 5 are described in this last model.

### 9.2.6 Unilateral Damage

Consider again a brittle material, but this time subjected to cyclic loading; two sets of independent micro-cracks appear in the element; one of them emerges under traction stresses, the other is associated to compressions (see Figure 8). When the load is reversed, say from compression to traction, the cracks of compression tend to close while new traction cracks appear; thus, as most of them are closed, compression cracks do not have a significant influence in the material behavior in traction; the opposite effect occurs when the load changes its sign from traction to compression. This phenomenon is called “unilateral behavior” because a particular kind of micro-cracks has an influence on the material behavior only for loadings of a specific sign.

In order to model unilateral behavior, two different damage variables are introduced:  $\omega^+$  and  $\omega^-$ . The former variable represents micro-defects due to positive stresses (tractions) and the latter is related to damage due to negative (compression) stresses. The variable  $\omega^+$  is called “positive damage” and the term  $\omega^-$  is the “negative damage”. The effective stress can now be generalized as follows:

Figure 7. A damage mechanics model for ductile materials

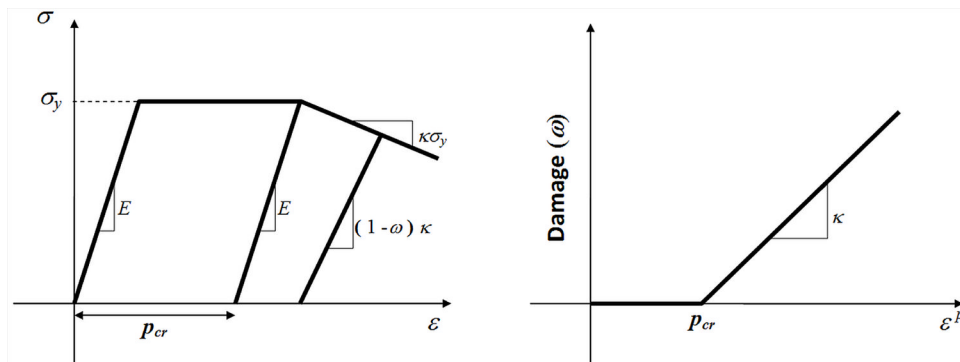
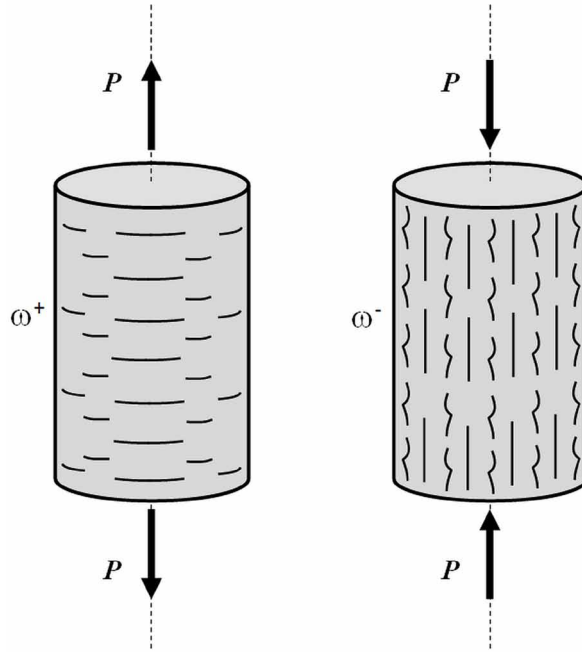


Figure 8. Unilateral cracks



$$\bar{\sigma} = \begin{cases} \frac{\sigma}{1 - \omega^+} & \text{if } \sigma > 0 \\ 0 & \text{if } \sigma = 0 \\ \frac{\sigma}{1 - \omega^-} & \text{if } \sigma < 0 \end{cases} \quad (9.2.25)$$

The application of the hypothesis of equivalence in strain for a brittle material gives the following elasticity law:

$$\varepsilon = \frac{\bar{\sigma}}{E}, \text{ i.e. } \varepsilon = \frac{\langle \sigma \rangle_+}{E(1 - \omega^+)} + \frac{\langle \sigma \rangle_-}{E(1 - \omega^-)} \quad (9.2.26)$$

where the terms  $\langle \sigma \rangle_+$  and  $\langle \sigma \rangle_-$  are, respectively, the positive and negative part of the normal stress. Notice that for a positive stress, the negative part of sigma is zero and the elastic modulus is reduced only by the positive damage and vice versa.

The complementary strain energy is given by:

$$W = \frac{1}{2} \sigma \varepsilon(\sigma, \omega) = \frac{1}{2} \frac{\sigma \langle \sigma \rangle_+}{E(1 - \omega^+)} + \frac{1}{2} \frac{\sigma \langle \sigma \rangle_-}{E(1 - \omega^-)} = \frac{1}{2} \frac{\langle \sigma \rangle_+^2}{E(1 - \omega^+)} + \frac{1}{2} \frac{\langle \sigma \rangle_-^2}{E(1 - \omega^-)} \quad (9.2.27)$$

Two different energy release rates can now be defined: the energy release rate for positive damage and the energy release rate for negative damage:

$$G_m^+ = \frac{\partial W}{\partial \omega^+} = \frac{1}{2} \frac{\langle \sigma \rangle_+^2}{E(1 - \omega^+)^2}; G_m^- = \frac{\partial W}{\partial \omega^-} = \frac{1}{2} \frac{\langle \sigma \rangle_-^2}{E(1 - \omega^-)^2} \quad (9.2.28)$$

Two damage evolution laws are needed in this case, they are given by:

$$\left\{ \begin{array}{l} d\omega^+ = 0 \text{ if } G_m^+ < R_m^+ \\ G_m^+ = R_m^+ \text{ if } d\omega^+ > 0 \end{array} \right\}; \left\{ \begin{array}{l} d\omega^- = 0 \text{ if } G_m^- < R_m^- \\ G_m^- = R_m^- \text{ if } d\omega^- > 0 \end{array} \right\} \quad (9.2.29)$$

where  $R_m^+$  and  $R_m^-$  are, respectively, the resistance function for positive and negative damage.

A better model for concrete can be obtained by using different damage resistance functions for positive and negative damage:

$$R_m^- = \frac{8(f_c^t)^2}{E} (\omega^-)^2; R_m^+ = \frac{A}{(B - \omega^+)^2} \quad (9.2.30)$$

where  $A$  and  $B$  are material parameters. This model gives the curve stress vs. strain that is shown in Figure 9 (see also the example 9.5.4).

The constants  $A$  and  $B$  can be computed so that positive damage and the softening behavior start simultaneously for a tension strength  $f_t$ ; and the stress tends to zero for a given strain value  $\varepsilon_u$  (see the demonstration in the example 9.5.3):

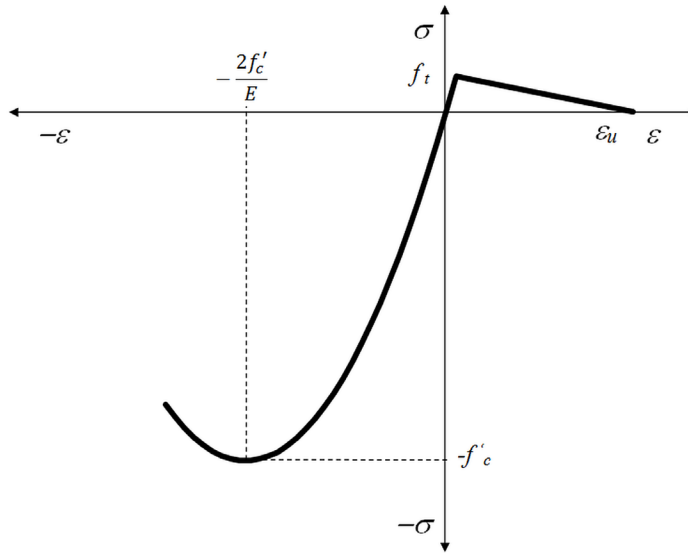
$$A = \frac{E(f_t)^2 \varepsilon_u^2}{2(E\varepsilon_u - f_t)^2}; B = \frac{E\varepsilon_u}{E\varepsilon_u - f_t} \quad (9.2.31)$$

### 9.3 STRAIN AND DAMAGE LOCALIZATION

As any other theory, continuum damage mechanics also presents limitations and drawbacks; an especially serious one is that it may lead to ill-posed mathematical problems, i.e. in some cases, an infinite number of solutions may verify the equations of the damage mechanics theory; paradoxically, in practical terms this means that the problem has not yet been fully solved: new concepts and ideas are needed in order to choose the right solution. This mathematical feature is related to a physical phenomenon called localization. Strain localization is another important failure mechanism in materials and structures. It has been observed that previous to total structural collapse, often, strains tend to concentrate in some narrow bands; this process accelerates structural failure.



Figure 9. A model of unilateral damage for concrete



Consider a bar divided into two elements of the same cross-section  $A$  and same material but with lengths  $L_1$  and  $L_2$  as shown in Figure 10. The lower end of the structure is blocked and the upper one is subjected to a displacement  $\Delta$  that is a linear function of time as shown in the same figure.

The material behavior of the elements is described by the damage model presented in section 9.2.4. The equilibrium equations give:

$$\sigma_1 = \sigma_2 = \frac{n}{A} \tag{9.3.1}$$

where  $\sigma_1$  and  $\sigma_2$  are the normal stress in the first and second element respectively;  $n$  is the axial force which is constant along the bar. The kinematic equations of the two elements give:

$$\varepsilon_1 L_1 + \varepsilon_2 L_2 = \Delta \tag{9.3.2}$$

where  $\varepsilon_1$  and  $\varepsilon_2$  are the strains in the first and second element respectively. The equilibrium and constitutive equations of this problem are represented in Figure 11; the former is the horizontal line that indicates equal stresses in both elements, the latter are two parabolas as indicated in section 9.2.4. Thus, the state of the structure at an instant  $t$  is represented by two points on both parabolas that lie on the same horizontal line.

Suppose that the points at the beginning of a step are at the left of the peak as shown in Figure 12a. Consider an increment of the displacement so that the strain in the first element follows the loading branch of the constitutive law. In that case, only one solution verifies the constitutive equation of the second element and the equilibrium equation of the bar at the same time, and this solution imposes a strain equal to that of the first element. This case shows identical stresses, strains and damage in both elements.

Figure 10. a) Bar divided into two elements subjected to an imposed displacement b) Displacement history

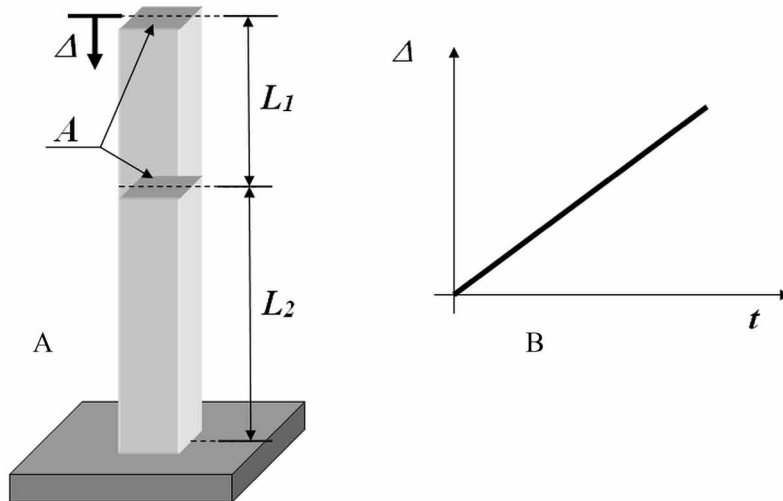
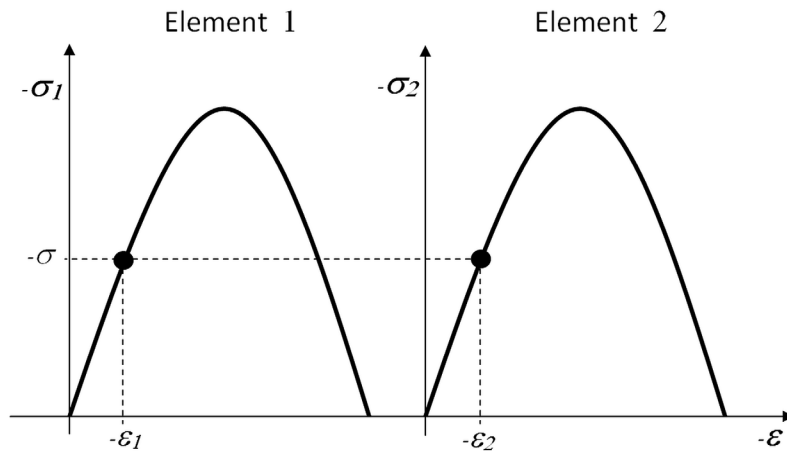
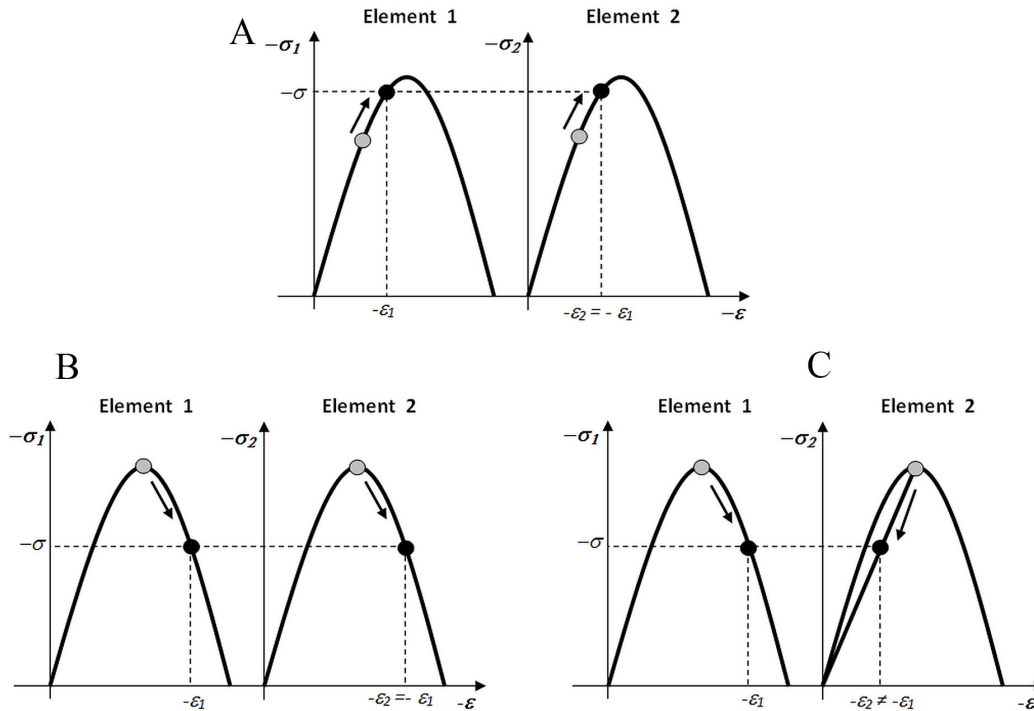


Figure 11. Equilibrium and constitutive equations



Suppose now that the points at the beginning of the step are at the peak of the constitutive curves or at its right (see Figure 12 b and c). Consider again an increment of displacement with an increment in the strain of the first element too. As this element is entering in the softening phase there must be a reduction in the stress of the second element as well. Notice that now there are two ways to verify the equilibrium equation; in the first one, the state in both elements follows the loading branch with damage increment (see Figure 12b). In this solution, strains and damage in both elements are still the same; this is called “homogeneous solution”. In the second one (see Figure 12c), the point of the second element follows the elastic unloading branch. In this alternative solution there is a reduction of the strain of the second element even if the total displacement of the bar is increased. This second option is called “localized solution” because strain and damage tend to concentrate only in a part of the bar (element 1) while there is an elastic unloading in the remaining fraction (element 2).

Figure 12. a) Unique solution before the peak b) Homogeneous solution after the peak c) Localized solution after the peak



The curve force  $P$  vs. displacement  $\Delta$  for both solutions is shown in Figure 13. Observe that in the homogeneous solution the displacement tends to a maximum value of  $\frac{4f'_c}{E}L$  while in the localized solution this last displacement is  $\frac{4f'_c}{E}L_1$ . Notice too, that the lengths of the elements are arbitrary; the bar can be divided into two elements of any length as long as their sum is equal to  $L$ . Thus, for each value of  $L_1$  a different localized solution is obtained; the problem presents an infinite number of different solutions. The real solution, the one that effectively is observed experimentally, is always a localized one with a given length  $L_1$  that depends on the material. This length is called “width of the localization band”. This phenomenon, the localization, appears not only in uniaxial problems but in any kind of structure. Figure 14 shows the appearance of a localization bands in a sand specimen subjected to a plane strain state.

When damage mechanics models are used to predict structural collapse, it is therefore necessary to choose some criterion that allows selecting the most significant solution from the physical point of view. The model of damage presented in chapter 10 assumes that the width of localization bands in a frame element subjected to bending is so small, as compared to the length of the element, so that the damage can be concentrated in the plastic hinges with zero length. This is the regularization criterion used in the case of damage models for framed structures.

Figure 13. Force vs. displacement curves

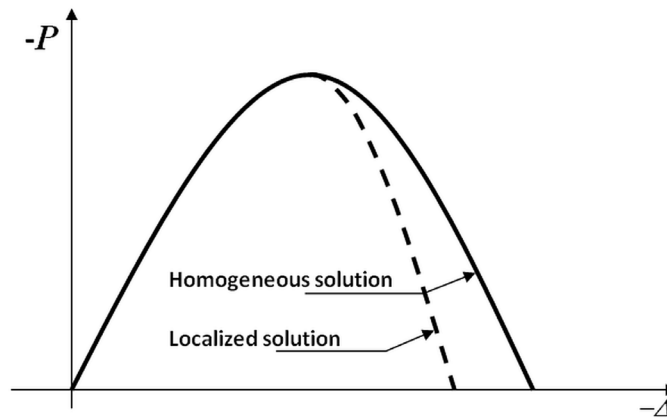
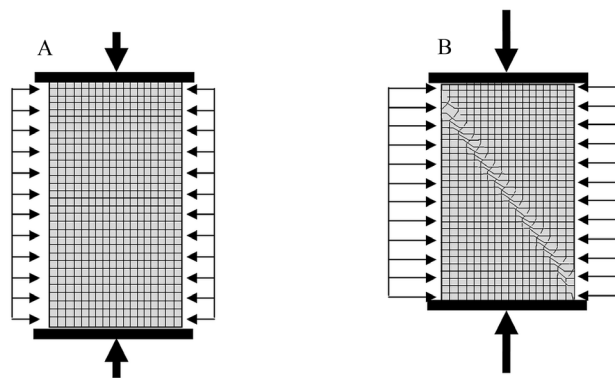


Figure 14. Schematic representation of a triaxial test a) Before the localization, b) After the localization



## 9.4 SUMMARY AND EQUATIONS QUICK REFERENCE

The fundamental goal of fracture mechanics is the determination of conditions for crack propagation. The Griffith criterion is one of these conditions and is based on an energy balance. This criterion introduces two essential concepts: the energy release rate (or crack driving force) and crack resistance. The energy release rate can be computed as a function of the derivative of stiffness or flexibility with respect to the crack length. The crack resistance might be a function of the crack extension and must be identified from experimental results.

Continuum damage mechanics is a theory that describes the evolution of micro-defects in a material. This theory is based on the introduction of four concepts: the continuum damage variable, the effective stress, the hypothesis of equivalence in deformations and the unilateral damage. Within this framework it is possible to develop model of damage for many kinds of materials; specifically, this chapter describes models for concrete and steel.

The term localization may refer to a mathematical condition related to damage models and to a physical phenomenon. In the first case, it corresponds to the emergence of an infinite number of solutions for the problem. In the second case, it refers to the appearance of a band where strain and damage are

concentrated while the rest of the solid unloads elastically. In fact, both, infinite solutions and concentration of damage are related. After localization, the damage analysis of a solid requires the introduction of some regularization procedure. Plastic hinges are used to regularize damage problems in the following chapters (See Table 1).

*Table 1.*

GRIFFITH CRITERION AND FRACTURE MECHANICS
<i>Stress Concentration Factors in Solids</i>
Stress concentration factors $SCF = \frac{\sigma_{\max}}{\sigma_{\text{avg}}} \text{ i.e. } \sigma_{\max} = SCF \sigma_{\text{avg}} \quad (9.1.1)$
Stress concentration factor in a linear elastic case $SCF = \frac{\sigma_{\max}}{\sigma_{\text{avg}}} \quad (9.1.2)$
<i>Energy Balance in a Cracked Structure</i>
Potential energy of a force $PE = -P \Delta \quad (9.1.3)$ <i>P</i> : force $\Delta$ : displacement of the force
Stiffness of an elastic solid $P = S \Delta \quad (9.1.4)$ <i>S</i> : stiffness of an elastic solid
Deformation energy <i>U</i> $U = \int_0^{\Delta} p d\delta = \frac{1}{2} S \Delta^2 = \frac{1}{2} P \Delta \quad (9.1.5)$
Complementary deformation energy <i>W</i> $W = \int_0^P \delta dp = \frac{1}{2S} P^2 = \frac{1}{2} F P^2 \quad (9.1.6)$ $F = \frac{1}{S} \text{ :flexibility of the solid}$
Total energy $TE = U + PE \quad (9.1.7)$
Surface energy $SE = 4\Gamma_{\text{sup}} a.t \quad (9.1.8)$ $\Gamma_{\text{sup}}$ : surface energy per unit area <i>a.t</i> : crack area

*continued on following page*

*Table 2. Continued*

Total energy of an elastic solid with a crack $TE = U + PE + SE$ (9.1.9)
<b>The Energy Release Rate and the Griffith Criterion</b>
Total energy of infinite plate $TE = U + PE + SE = U_0 - \frac{\pi\sigma_{avg}^2}{E} a^2 + 4\Gamma_{sup} a$ (9.1.10) $U_0$ : deformation energy
Energy release rate $G$ and crack resistance $R$ $G = R$ $G = -\frac{d}{da}(U + PE)$ $R = \frac{d}{da}(SE)$ (9.1.11)
<b>Energy Release Rate Expression in Terms of Stiffness or Flexibility</b>
Energy release rate $G = -\frac{d}{da}(U + PE) = -\frac{d}{da}\left(\frac{1}{2}P\Delta(a) - P\Delta(a)\right) = \frac{1}{2}\frac{dF(a)}{da}P^2$ (9.1.12) $G = -\frac{d}{da}(U + PE) = -\frac{d}{da}\left(\frac{1}{2}P(a)\Delta\right) = \frac{1}{2}\frac{dS(a)}{da}\Delta^2$ (9.1.13)
<b>UNIAXIAL DAMAGE MECHANICS MODELS</b>
<b>The Damage Variable</b>
Damage $\omega$ $\omega = \frac{A_d}{A}$ (9.2.1) $A$ : Total Area $A_d$ : Area of micro defects
<b>The Equivalent Stress and the Hypothesis of Equivalence in Deformation</b>
Effective stress $\bar{\sigma}$ $\bar{\sigma} = \frac{P}{A - A_d}$ (9.2.2) $\bar{\sigma} = \frac{P}{A - \omega A} = \frac{\sigma}{1 - \omega}$ (9.2.3)
Elasticity law for a damage material $\bar{\sigma} = E\varepsilon \Rightarrow \sigma = (1 - \omega)E\varepsilon$ (9.2.4)
Elasticity law in terms of flexibility $\varepsilon = \frac{1}{(1 - \omega)E}\sigma$ (9.2.5)

*continued on following page*

*Table 2. Continued*

<p>Strain <math>\varepsilon</math></p> $\varepsilon = \varepsilon^e + \varepsilon^d; \varepsilon^e = \frac{1}{E} \sigma; \varepsilon^d = \frac{1}{E} \sigma \quad (9.2.6)$ <p><math>\varepsilon^e</math> :elastic strain  <math>\varepsilon^d</math> : damage related term</p>
<p>Elastic plastic material</p> $\bar{\sigma} = E(\varepsilon - \varepsilon^p) \Rightarrow \sigma = (1 - \omega)E(\varepsilon - \varepsilon^p) \quad (9.2.7)$
<p>Strain <math>\varepsilon</math> in elastic plastic material</p> $\varepsilon = \varepsilon^e + \varepsilon^d + \varepsilon^p; \varepsilon^e = \frac{1}{E} \sigma; \varepsilon^d = \frac{\omega}{E(1 - \omega)} \sigma \quad (9.2.8)$
<p>Elastic perfect plastic yield function</p> $f = \left  \sigma \right  - \sigma_y = \left  \frac{\sigma}{1 - \omega} \right  - \sigma_y \leq 0 \quad (9.2.9)$
<b>Brittle Damage Model</b>
<p>Strain energy of the element <math>U</math></p> $U = \frac{1}{2} \sigma \varepsilon \quad (9.2.10)$ $U = \frac{1}{2} \sigma \varepsilon = \frac{1}{2} (1 - \omega) E \varepsilon^2 \quad (9.2.11)$
<p>Generalized Griffith criterion</p> $G_m - R_m \leq 0; G_m = -\frac{dU}{d\omega} = \frac{1}{2} E \varepsilon^2 \quad (9.2.12)$ <p><math>G_m</math> : Energy release rate  <math>R_m</math> : Damage resistance function</p>
<p>Complementary strain energy</p> $W = \frac{1}{2} \sigma \cdot \varepsilon = \frac{1}{2} \frac{\sigma^2}{E(1 - \omega)} \quad (9.2.13)$
<p>Energy release rate</p> $G_m = \frac{\partial W}{\partial \omega} = -\frac{\partial U}{\partial \omega} = \frac{1}{2} \frac{\sigma^2}{E(1 - \omega)^2} = \frac{1}{2} E \varepsilon^2 \quad (9.2.14)$
<b>A Damage Mechanics Model for Concrete</b>
<p>Elasticity law</p> $\sigma = (1 - \omega) E \langle \varepsilon \rangle_- \quad (9.2.15)$ $\langle \varepsilon \rangle_- = \begin{cases} \varepsilon & \text{if } \varepsilon \leq 0 \\ 0 & \text{otherwise} \end{cases} \quad (9.2.16)$

*continued on following page*

*Table 2. Continued*

<p>Damage evolution in compression</p> $\begin{cases} d\omega = 0 & \text{if } G_m < R_m \\ G_m = R_m & \text{if } d\omega > 0 \end{cases} \quad (9.2.17)$ <p><math>R_m</math> : crack resistance function</p>
<p>Crack resistance function</p> $R_m = \frac{8(f_c')^2}{E} \omega^2 \quad (9.2.18)$ <p><math>f_c'</math> is the strength resistance in compression</p>
<p><b>Ductile Damage Model</b></p>
<p>Elasticity law</p> $\sigma = (1 - \omega)E(\varepsilon - \varepsilon^p) \quad (9.2.19)$
<p>Plastic strain evolution law</p> $\begin{cases} d\varepsilon_p = 0 & \text{if } f < 0 \\ f = 0 & \text{if } d\varepsilon_p \neq 0; f = \left  \frac{\sigma}{1 - \omega} \right  - \sigma_y \leq 0 \end{cases} ; (9.2.20)$
<p>Damage evolution</p> $\omega = \kappa \langle p - p_{cr} \rangle_+ \quad (9.2.21)$ $\langle p \rangle_+ = \begin{cases} p & \text{if } p \geq 0 \\ 0 & \text{otherwise} \end{cases} \quad (9.2.22)$ <p><math>\kappa, p_{cr}</math> : material constants  <math>\langle p \rangle_+</math> : positive part of the variable <math>p</math></p>
<p>Cumulated plastic strain</p> $dp =  d\varepsilon_p  \quad (9.2.23)$
<p>Yield function</p> $f(\sigma) = \left  \frac{\sigma}{1 - \omega} - x \right  - \sigma_y \leq 0; dx = \alpha \left( (\sigma_u - \sigma_y) d\varepsilon_p - x \cdot  d\varepsilon_p  \right) \quad (9.2.24)$
<p><b>Unilateral Damage</b></p>
<p>Effective stress</p> $\bar{\sigma} = \begin{cases} \frac{\sigma}{1 - \omega^+} & \text{if } \sigma > 0 \\ 0 & \text{if } \sigma = 0 \\ \frac{\sigma}{1 - \omega^-} & \text{if } \sigma < 0 \end{cases} \quad (9.2.25)$

*continued on following page*



Table 2. Continued

<p>Elasticity law</p> $\varepsilon = \frac{\bar{\sigma}}{E}; \varepsilon = \frac{\langle \sigma \rangle_+}{E(1 - \omega^+)} + \frac{\langle \sigma \rangle_-}{E(1 - \omega^-)} \quad (9.2.26)$ <p><math>\langle \sigma \rangle_+</math> : positive part of the normal stress  <math>\langle \sigma \rangle_-</math> : negative part of the normal stress</p>
<p>Complementary strain energy</p> $W = \frac{1}{2} \sigma \cdot \varepsilon(\sigma, \omega) = \frac{1}{2} \frac{\sigma \langle \sigma \rangle_+}{E(1 - \omega^+)} + \frac{1}{2} \frac{\sigma \langle \sigma \rangle_-}{E(1 - \omega^-)} = \frac{1}{2} \frac{\langle \sigma \rangle_+^2}{E(1 - \omega^+)} + \frac{1}{2} \frac{\langle \sigma \rangle_-^2}{E(1 - \omega^-)} \quad (9.2.27)$
<p>Energy release rate for positive damage</p> $G_m^+ = \frac{\partial W}{\partial \omega^+} = \frac{1}{2} \frac{\langle \sigma \rangle_+^2}{E(1 - \omega^+)^2} \quad (9.2.28a)$ <p>Energy release rate for negative damage</p> $G_m^- = \frac{\partial W}{\partial \omega^-} = \frac{1}{2} \frac{\langle \sigma \rangle_-^2}{E(1 - \omega^-)^2} \quad (9.2.28b)$
<p>Damage evolution law: (9.2.29)</p> $\begin{cases} d\omega^+ = 0 & \text{if } G_m^+ < R_m^+ \\ G_m^+ = R_m^+ & \text{if } d\omega^+ > 0 \end{cases}; \begin{cases} d\omega^- = 0 & \text{if } G_m^- < R_m^- \\ G_m^- = R_m^- & \text{if } d\omega^- > 0 \end{cases} \quad (9.2.29)$ <p><math>R_m^+</math> : resistance function for positive damage  <math>R_m^-</math> : resistance function for negative damage</p>
<p>Crack resistances for concrete</p> $R_m^- = \frac{8(f_c^t)^2}{E} (\omega^-)^2; R_m^+ = \frac{A}{(B - \omega^+)^2} \quad (9.2.30)$ <p>A and B are material parameters</p> $A = \frac{E(f_t)^2 \varepsilon_u^2}{2(E\varepsilon_u - f_t)^2}, B = \frac{E\varepsilon_u}{E\varepsilon_u - f_t} \quad (9.2.31)$

## 9.5 EXAMPLES

### 9.5.1. Plot Stress as a Function of the Strain for the Model Described in Section 9.2.4. Consider $f'_c = 30$ MPa and $E = 28000$ MPa

The energy release rate is defined by Equation (9.2.12):  $G_m = \frac{1}{2} E \varepsilon^2$ . Considering the crack resistance proposed by Equation (9.2.18):  $R_m = \frac{8(f'_c)^2}{E} \omega^2$ , the Griffith criterion results in:

$$G_m - R_m = \frac{E \varepsilon^2}{2} - \frac{8(f'_c)^2}{E} \omega^2 = 0 \quad (9.5.1)$$

The expression of the damage variable is obtained from (9.5.1):

$$\omega = \frac{E \varepsilon}{4f'_c} \text{ and } \omega = -\frac{E \varepsilon}{4f'_c} \quad (9.5.2)$$

(9.5.2b) is chosen since damage is always positive and  $\varepsilon$  is negative. Substituting  $\omega$  in the elasticity law (9.2.15), the relationship between stresses and strains is:

$$\sigma = \left( 1 + \frac{E \varepsilon}{4f'_c} \right) E \varepsilon \quad (9.5.3)$$

Plotting this expression, the curve shown in Figure 15 is obtained.

As aforementioned, the maximum stress corresponds to a strain equal to  $\frac{2f'_c}{E}$  since:

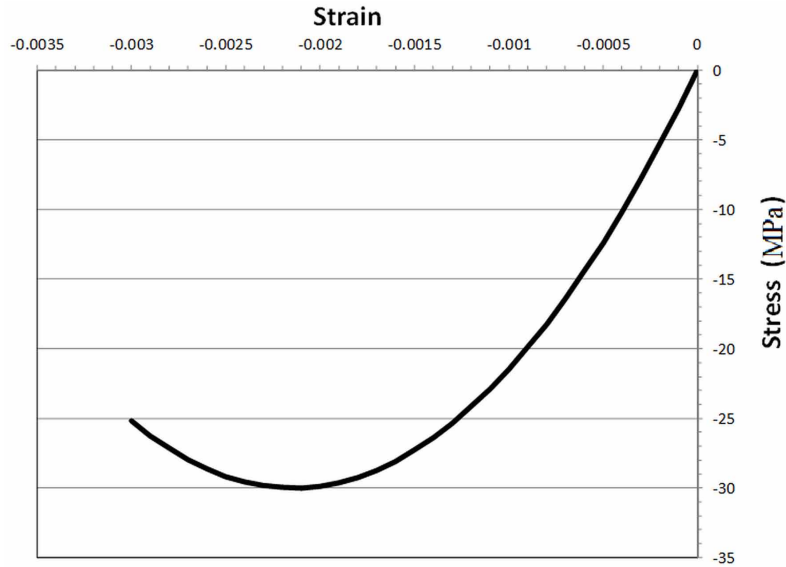
$$\frac{d\sigma}{d\varepsilon} = -\frac{E(E\varepsilon - 2f'_c)}{2f'_c} = 0 \Rightarrow \varepsilon = \frac{2f'_c}{E} \quad (9.5.4)$$

### 9.5.2. Plot Stress as a Function of the Strain for the Model Described in Section 9.2.5. Consider $\sigma_y = 420$ MPa, $E = 210000$ MPa, $p_{cr} = 0.005$ and $\kappa = 130$

The behavior of a ductile material is described considering three phases; first, an elastic behavior, then a plastic one and finally a damage phase. The elastic part is defined by Equation (9.2.19) with  $\omega = 0$  and  $\varepsilon^p = 0$  thus:

$$\sigma = E \varepsilon = 210000 \varepsilon \quad (9.5.5)$$

Figure 15. Stress vs. strain curve for a brittle material



This part finishes when the yield function is equal to zero (Equation 9.2.20b) and the plastic strain starts growing; at this instant:

$$\sigma = \sigma_y = 420 \text{ MPa} \quad (9.5.6)$$

The plastic stage lasts until the plastic strain reaches the critical value  $p_{cr}$ . At this time, the value of the total strain can be computed with Equation (9.2.19) considering still  $\omega = 0$  and

$$\varepsilon^p = p_{cr} : \varepsilon = p_{cr} + \frac{\sigma_y}{E} = 0.007 \quad (9.5.7)$$

After this instant, damage starts evolving. The introduction of Equations (9.2.21).and (9.5.7) into the yield function (Equation 9.2.20b) gives the relationship between stress and strain for the last part of the behavior:

$$\sigma = -\kappa\sigma_y \varepsilon + \sigma_y \left( 1 + \kappa \left( \frac{\sigma_y}{E} + p_{cr} \right) \right) = -54600\varepsilon + 802.2 \quad (9.5.8)$$

Finally, the behavior for a ductile material can be described as:

$$\sigma = E\varepsilon \text{ for } 0 \leq \varepsilon \leq \frac{\sigma_y}{E}$$

$$\sigma = \sigma_y \text{ for } \frac{\sigma_y}{E} \leq \varepsilon \leq \frac{\sigma_y}{E} + p_{cr}$$

$$\sigma = -\kappa\sigma_y\varepsilon + \sigma_y \left( 1 + \kappa \left( \frac{\sigma_y}{E} + p_{cr} \right) \right) \text{ for } \varepsilon \geq \frac{\sigma_y}{E} + p_{cr} \quad (9.5.9)$$

Expression (9.5.9) is plotted in Figure 16.

### 9.5.3 Deduct the Expressions (9.2.31)

The tension branch ( $\langle \sigma \rangle_- = 0$ ) can be described considering two phases: first, an elastic behavior, then, a damaged phase. The elastic part is defined by Equation (9.2.26) with  $\omega^+ = 0$  thus:

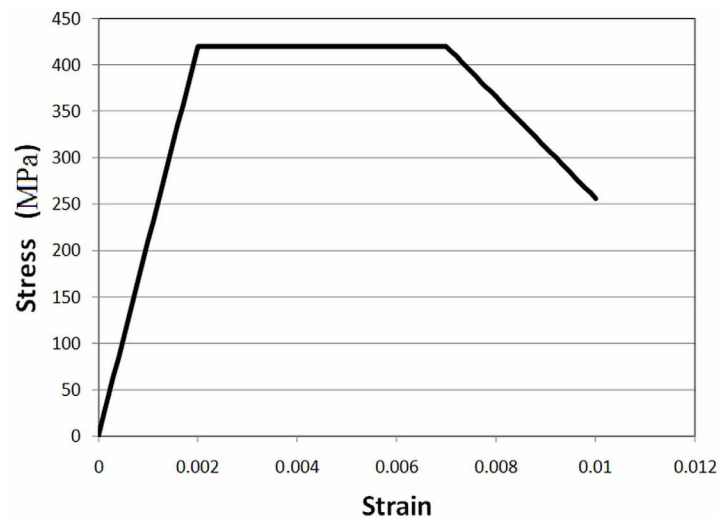
$$\langle \sigma \rangle_+ = E\varepsilon \quad (9.5.10)$$

This part finishes when the material reaches the tension strength  $f_t$ , thus, the strain is:

$$\varepsilon_t = \frac{f_t}{E} \quad (9.5.11)$$

At this instant, the damage in the material starts evolving. The stress tends to zero for a strain value of  $\varepsilon_u$ . The equation of the line that describes this behavior is:

*Figure 16. Stress vs. strain curve for a ductile material*



$$\langle \sigma \rangle_+ = f_t \left( 1 - \frac{1}{\varepsilon_u - \frac{f_t}{E}} \left( \varepsilon - \frac{f_t}{E} \right) \right) \quad (9.5.12)$$

Introducing Equation (9.2.26)  $\varepsilon = \frac{\langle \sigma \rangle_+}{E(1 - \omega^+)}$  into (9.5.12), it is obtained the stress:

$$\sigma = \frac{f_t + \frac{f_t^2 / E}{\varepsilon_u - f_t / E}}{1 + \frac{f_t}{(\varepsilon_u - f_t / E) E(1 - \omega^+)}} \quad (9.5.13)$$

Substituting (9.5.13) into the energy release rate (9.2.28a) and applying the Griffith criterion:

$$G_m^+ = \frac{E \varepsilon_u^2 f_t^2}{2(E \varepsilon_u - f_t)^2 \left( \frac{E \varepsilon_u}{(E \varepsilon_u - f_t)} - \omega^+ \right)^2} = R_m^+ \quad (9.5.14)$$

Or:

$$R_m^+ = \frac{A}{(B - \omega^+)^2}, \text{ where } A = \frac{E(f_t)^2 \varepsilon_u^2}{2(E \varepsilon_u - f_t)^2}; B = \frac{E \varepsilon_u}{E \varepsilon_u - f_t} \quad (9.5.15)$$

### 9.5.4 Plot Stress as a Function of Strain for the Model Described in Section

**9.2.6. Consider**  $f'_c = 30$  MPa,  $f_t = 3$  MPa,  $\varepsilon_u = 0.002$  **and**  $E = 28000$  MPa

The negative phase was described in example (9.5.1). As aforementioned, the tension part has two phases. The elastic part is described with Equation (9.5.10) resulting in:

$$\sigma = 28000\varepsilon \quad (9.5.16)$$

The last point of this phase corresponds to a stress equal to  $f_t = 3$  MPa and to a strain equal to:

$$\varepsilon = \frac{f_t}{E} = \frac{3}{28000} = 0.00010714 \quad (9.5.17)$$

The damage phase is described by Equation (9.5.12)

$$\sigma = f_t \left( 1 - \frac{1}{\varepsilon_u - \frac{f_t}{E}} \left( \varepsilon - \frac{f_t}{E} \right) \right) = 3.17 - 1584.93 \varepsilon \quad (9.5.18)$$

Figure 17 shows the unilateral behavior.

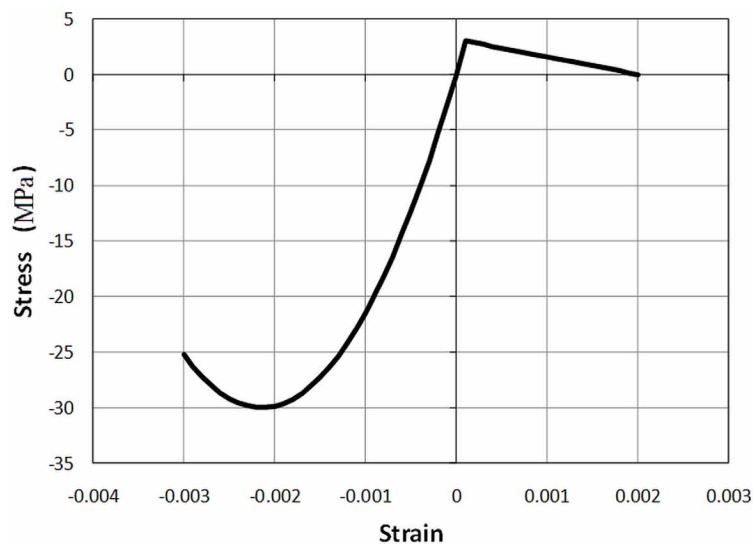
## 9.6 PROBLEMS

### 9.6.1 Plot Stress as a Function of the Strain for the Model Described by the Equations

- **Elasticity Law:**  $\sigma = (1 - \omega)E\varepsilon$
- **Energy Release Rate:**  $G_m = \frac{1}{2} \frac{\sigma^2}{E(1 - \omega)^2}$
- **Crack Resistance:**  $R_m = \frac{1}{2} \frac{A}{(1 - \omega)}$

Consider that the behavior can be described considering two phases: first, an elastic one, then, a damaged phase that starts at the point  $\left( \frac{f_t}{E}, f_t \right)$ . Use the following numerical values  $f_t = 5$  MPa and  $E = 5000$  MPa.

Figure 17. Stress vs. strain curve for a ductile material



**9.6.2 Plot Stress as a Function of the Strain for the Model Described by the Equations**

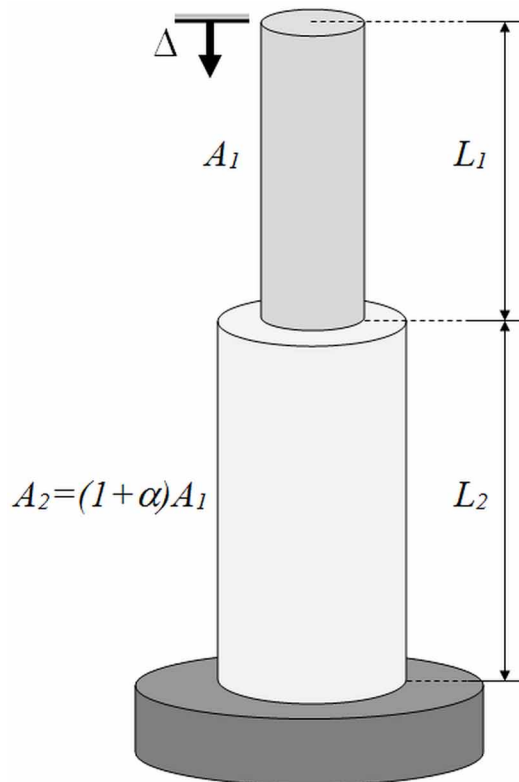
- **Elasticity Law:**  $\sigma = (1 - \omega)E(\varepsilon - \varepsilon^p)$
- **Plastic Strain Evolution Law:**  $\begin{cases} d\varepsilon_p = 0 & \text{if } f < 0 \\ f = 0 & \text{if } d\varepsilon_p \neq 0 \end{cases}; f = \left| \frac{\sigma}{1 - \omega} \right| - \tilde{A}_y \leq 0$
- **Damage Evolution:**  $\omega = 1 - e^{-c\langle p - p_{cr} \rangle_+}; \langle p \rangle_+ = \begin{cases} p & \text{if } p \geq 0 \\ 0 & \text{otherwise} \end{cases}; dp = |d\varepsilon_p|$

Consider  $p_{cr} = 0.005$ ,  $c = 5$ ,  $\sigma_y = 420$  MPa, and  $E = 210000$  MPa.

**9.6.3 Plot the Force vs. Displacement Curve for the Two-Bar Structure Shown in Figure 18. Use the Constitutive Law Described in Section 9.2.4. Consider  $E = 28000$  MPa,  $f'_c = 30$  MPa,  $A_1 = 0.05$  m<sup>2</sup>,  $L_1 = L_2 = 1.0$  m. Discuss What Happens When  $\alpha$  Tends to Zero.**

**9.6.4 Plot the Force vs. Displacement Curve for the Two-Bar Structure Shown in Figure 18. Use the Constitutive Law Described in Section 9.2.5. Consider  $\sigma_y = 420$  MPa,  $E = 210000$  MPa;  $p_{cr} = 0.005$ ,  $\kappa = 130$ ,  $A_1 = 18.65 \times 10^{-4}$  m<sup>2</sup> and  $L_1 = L_2 = 1.0$  m.**

Figure 18. Two-bar element ( $\alpha > 0$ )



## REFERENCES

- Anderson, T. L. (2005). *Fracture mechanics: Fundamentals and applications*. CRC Press.
- Broek, D. (1986). *Elementary engineering fracture mechanics*. The Hague, The Netherlands: Martinus Nijhoff Publishers; doi:10.1007/978-94-009-4333-9
- Leckie, F. A., & Bello, D. J. (2009). *Strength and stiffness of engineering systems*. New York, NY: Springer.
- Lemaitre, J. (1992). *A course on damage mechanics*. Springer-Verlag. doi:10.1007/978-3-662-02761-5
- Lemaitre, J., & Chaboche, J. L. (1985). *Mécanique des matériaux solides*. Paris, France: Dunod Bordas.
- Lemaitre, J., & Desmorat, R. (2005). *Engineering damage mechanics, ductile, creep, fatigue and brittle failures*. Berlin: Springer.
- Marante, M. E., Benallal, A., & Flórez-López, J. (2007). Análisis de falla de sólidos inelásticos mediante la teoría de localización. *Acta Científica Venezolana*, 58(2), 43–51.
- Marante, M. E., & Flórez-López, J. (2004). Plastic localization revisited. *Journal of Applied Mechanics*, 71(2), 283–284. doi:10.1115/1.1636790
- Whittaker, B. N., Singh, R. N., & Sun, G. (1992). *Rock fracture mechanics: Principles, design, and applications*. Amsterdam: Elsevier.



## Chapter 10

# Lumped Damage Mechanics: Reinforced Concrete Frames

### ABSTRACT

*As aforementioned, buildings in seismic zones must be designed to behave elastically under service loads or earthquakes of small intensity, and they can enter in the plastic range for events of intermediate intensity. Severe earthquakes are defined as those that are improbable but not impossible to happen during the lifetime of the structure. In these cases, structural damage, even damage that cannot be repaired, is allowed as long as there is no structural collapse. In order to design or certify safe structures, it is necessary to have computational tools that allow for the quantification of structural damage and that are able to describe structural behavior accurately near collapse. The elasto-plastic models present serious limitations in this sense. Damage and fracture mechanics represent a more rational option. The goal of this chapter is to describe how the concepts presented in Chapter 9 can be included in the mathematical models for the analysis of framed structures and its numerical implementation in structural analysis programs.*

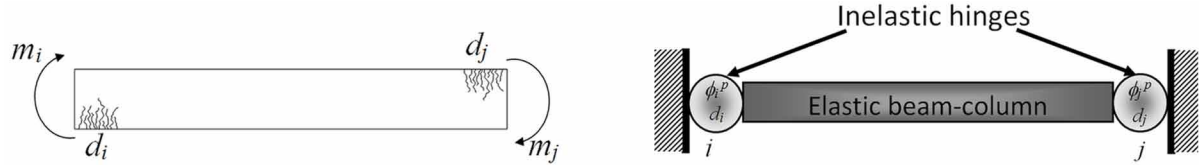
### 10.1 THE LUMPED DAMAGE MODEL

Consider a slender RC frame element in the planar case. It is assumed that not only yielding of the reinforcement, but concrete cracks are also localized at the extremes of the element. The lumped plasticity model that is described in section 7.1.1 is modified by assuming that concrete cracks can be lumped at the plastic hinges as well: plastic hinges become inelastic hinges and the “lumped plasticity model” develops into the “lumped damage model”. In this and the following chapters, the terms “inelastic hinge” or “plastic hinge with damage” are used indistinctly. In order to represent the appearance and propagation of these cracks, a new set of internal variables  $(\mathbf{D})_b = (d_i, d_j)$  is introduced. The term  $(\mathbf{D})_b$  is denoted “damage array” of the element  $b$ . The variables  $d_i$  and  $d_j$  are damage parameters that take values between zero and one; however, they represent densities of macroscopic cracks, as in fracture mechanics, instead of micro defects (see Figure 1a). The first variable in  $(\mathbf{D})_b$  characterizes the crack density that can be lumped at the inelastic hinge  $i$  while the second one is related to cracking lumped at inelastic hinge  $j$  (see Figure 1b).

DOI: 10.4018/978-1-4666-6379-4.ch010

## Lumped Damage Mechanics

Figure 1. a) Cracks at the end of a frame member b) Lumped damage model



The hypothesis of equivalence in deformation described in section 9.2.2, Equation (9.2.8) can be written in the case of a frame element as:

$$\{\Phi\}_b = \{\Phi^{bc}\}_b + \{\Phi^p\}_b + \{\Phi^d\}_b \quad (10.1.1)$$

where  $\{\Phi^{bc}\}_b$  is, again, the matrix of generalized deformations of the elastic beam-column.  $\{\Phi^p\}_b$  is the matrix of plastic deformations; the plastic elongations are neglected as it is usual in RC elements, thus  $\{\Phi^p\}_b^t = (\phi_i^p, \phi_j^p, 0)$ . The last matrix,  $\{\Phi^d\}_b$ , contains the damage rotations; i.e. the additional rotations due to concrete cracking.

The deformations of the elastic beam-column can be expressed as a function of the generalized stresses using (Equation 3.3.9):

$$\{\Phi^{bc}\}_b = [\mathbf{F}_f]_b \{\mathbf{M}\}_b + \{\Phi^0\}_b \quad (10.1.2)$$

The terms  $[\mathbf{F}_f]_b$ ,  $\{\mathbf{M}\}_b$ ,  $\{\Phi^0\}_b$  are, again, the flexibility matrix of a slender element, the generalized stresses and the initial deformations such as defined in chapter 3 (Equation 3.3.9, 3.2.2 and Table 3).

According to the hypothesis of equivalence in deformations (Equation 9.2.8c), the damage deformation matrix can be written as:

$$\{\Phi^d\}_b = [\mathbf{C}(\mathbf{D})]_b \{\mathbf{M}\}_b; \text{ where } [\mathbf{C}(\mathbf{D})]_b = \begin{bmatrix} \frac{d_i}{1-d_i} F_{11}^e & 0 & 0 \\ 0 & \frac{d_j}{1-d_j} F_{22}^e & 0 \\ 0 & 0 & 0 \end{bmatrix} \quad (10.1.3)$$

The term  $[\mathbf{C}(\mathbf{D})]_b$  is a matrix of additional flexibility due to concrete cracking and  $F_{ij}^e$  represents the  $(i,j)$  component of the elastic flexibility matrix. Substitution of (10.1.2-3) into (10.1.1) gives the elastic-law, in terms of flexibility, of a damaged frame element:

$$\{\Phi - \Phi^p\}_b = [\mathbf{F}(\mathbf{D})]_b \{\mathbf{M}\}_b + \{\Phi^0\}_b \quad \text{where } [\mathbf{F}(\mathbf{D})] = [\mathbf{F}_f] + [\mathbf{C}(\mathbf{D})] = \begin{bmatrix} \frac{F_{11}^e}{1-d_i} & F_{12}^e & 0 \\ F_{21}^e & \frac{F_{22}^e}{1-d_j} & 0 \\ 0 & 0 & F_{33}^e \end{bmatrix} \quad (10.1.4)$$

$[\mathbf{F}(\mathbf{D})]$  is the flexibility matrix of a damaged frame member. Notice that there is no additional flexibility if there is no concrete cracking, and that the diagonal components of the flexibility matrix tend to infinity if the damage parameters tend to one.

The elasticity law in terms of stiffness is:

$$\{\mathbf{M}\}_b = [\mathbf{E}(\mathbf{D})]_b \{\Phi - \Phi^p\}_b + \{\mathbf{M}^0(\mathbf{D})\}_b \quad (10.1.5)$$

where  $[\mathbf{E}(\mathbf{D})]_b = [\mathbf{F}(\mathbf{D})]_b^{-1}$  is the elasticity matrix of a damaged frame element:

$$[\mathbf{E}(\mathbf{D})]_b = k \begin{bmatrix} 12(1-d_i) & 6(1-d_i)(1-d_j) & 0 \\ 6(1-d_i)(1-d_j) & 12(1-d_j) & 0 \\ 0 & 0 & \frac{EA_b}{kL_b} \end{bmatrix}; k = \frac{1}{4 - (1-d_i)(1-d_j)} \frac{EI_b}{L_b} \quad (10.1.6)$$

$$\text{and } \{\mathbf{M}^0(\mathbf{D})\}_b = -[\mathbf{E}(\mathbf{D})]_b \{\Phi^0\}_b$$

Notice that the matrix  $\{\mathbf{M}^0(\mathbf{D})\}_b$  tends to zero as the damage variables tend to one. As the distributed forces are assumed small compared with the nodal forces, even for the uncracked stiffness, this term can be neglected in many applications of structural analysis.

## 10.2 GENERALIZED GRIFFITH CRITERION FOR AN INELASTIC HINGE

As indicated in the previous section, damage in a RC element characterizes cracks in the concrete. Thus, damage evolution can be described using the Griffith criterion presented in sections 9.1.3-4 of the previous chapter. The complementary deformation energy of a damaged frame element is given by:

$$W_b = \frac{1}{2} \{\mathbf{M}\}_b^t \{\Phi - \Phi^p\}_b = \frac{1}{2} \{\mathbf{M}\}_b^t [\mathbf{F}(\mathbf{D})]_b \{\mathbf{M}\}_b + \frac{1}{2} \{\mathbf{M}\}_b^t \{\Phi^0\}_b \quad (10.2.1)$$

Therefore, the energy release rates, or “damage driving moments”,  $G_i$  and  $G_j$  of, respectively, hinges  $i$  and  $j$  are defined as:

### Lumped Damage Mechanics

$$G_i = \frac{\partial W}{\partial d_i} = \frac{F_{11}^0 m_i^2}{2(1-d_i)^2}; G_j = \frac{\partial W}{\partial d_j} = \frac{F_{22}^0 m_j^2}{2(1-d_j)^2} \quad (10.2.2)$$

And the damage evolution laws based on the Griffith criterion are:

$$\left\{ \begin{array}{l} \Delta d_i = 0 \text{ if } G_i < R_i \\ G_i = R_i \text{ if } \Delta d_i > 0 \end{array} \right\}; \left\{ \begin{array}{l} \Delta d_j = 0 \text{ if } G_j < R_j \\ G_j = R_j \text{ if } \Delta d_j > 0 \end{array} \right\} \quad (10.2.3)$$

The terms  $R_i$  and  $R_j$  are the crack resistance functions of, respectively, inelastic hinges  $i$  and  $j$ .

## 10.3 CRACK RESISTANCE FUNCTION OF AN INELASTIC HINGE

### 10.3.1 Experimental Measure of the Damage in a Plastic Hinge

As indicated in the previous chapter (section 9.1.3), the crack resistance function must be identified with an experimental analysis. Fracture mechanics introduces a straightforward variable: the crack length; therefore its measurement is a direct procedure; the damage in a plastic hinge is a more ambiguous concept. In this section it is described a method for the experimental determination of the damage of a plastic hinge; this procedure is called “method of the stiffness variation”.

The specimen shown in Figure 2b represents a beam-column joint subjected to bending. Mono-sign displacements are imposed to the column as it is indicated in Figure 2c. The experimental response of the specimen is represented in the curve of force vs. displacement (see Figure 3d).

Consider now the mechanical representation of the test that is shown in Figure 2e. The specimen is modeled as a two-element structure. A symmetric behavior is assumed, at least up the peak of the curve of force vs. displacement. The second line of the elasticity law (Equation 10.1.4) for the first element is:

$$\phi_2 - \phi_2^p = -\frac{L}{6EI} m_1 + \frac{L}{3EI(1-d_2)} m_2 \quad (10.3.1)$$

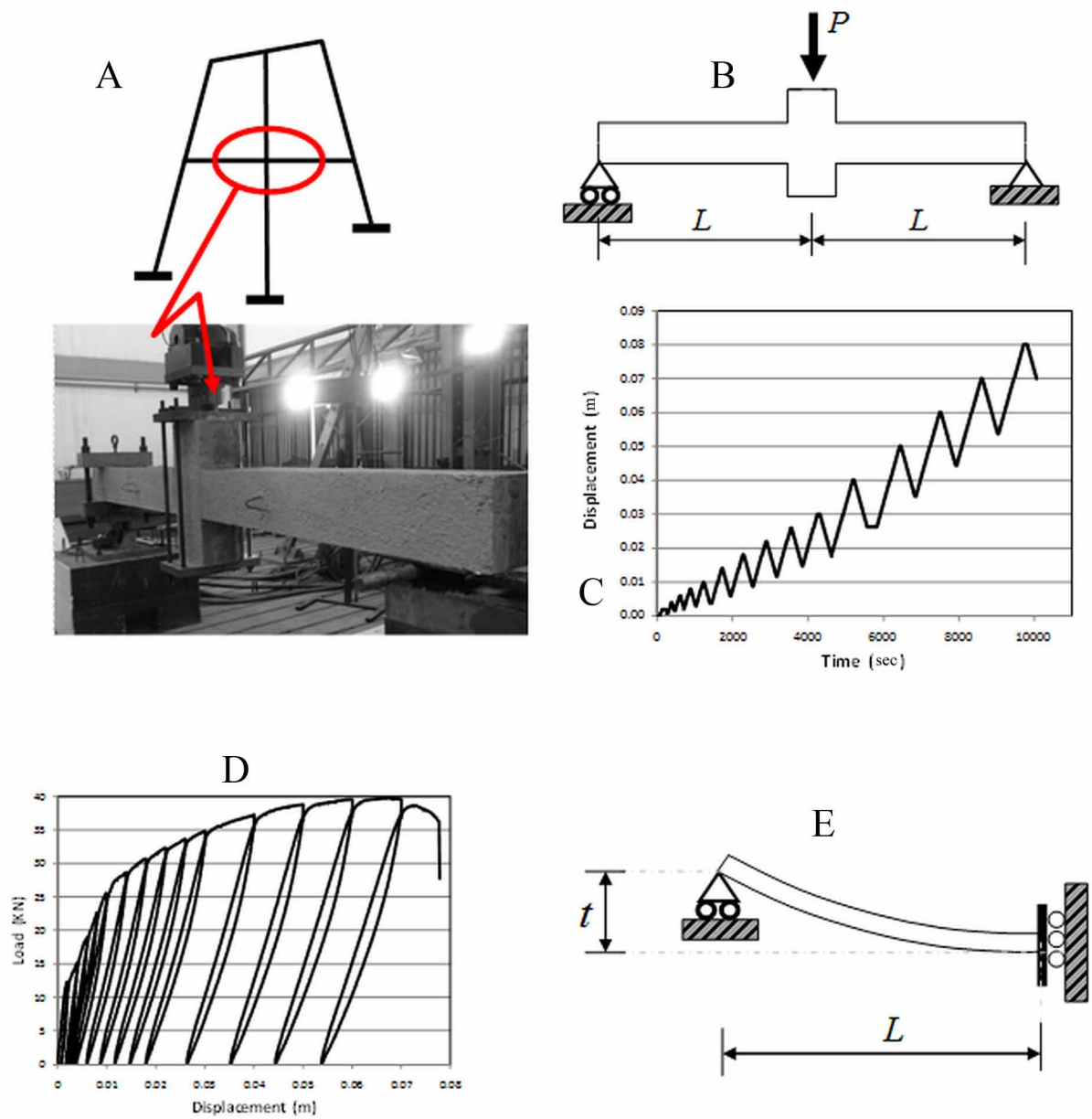
The equilibrium and boundary conditions give:

$$m_1 = 0; m_2 = \frac{P.L}{2} \quad (10.3.2)$$

and the kinematic equation (Equation 3.1.11):

$$\phi_2 = \frac{t}{L} \quad (10.3.3)$$

Figure 2. a) Planar frame b) Specimen representing a beam-column joint c) Loading history d) Experimental response e) Mechanical representation of the test

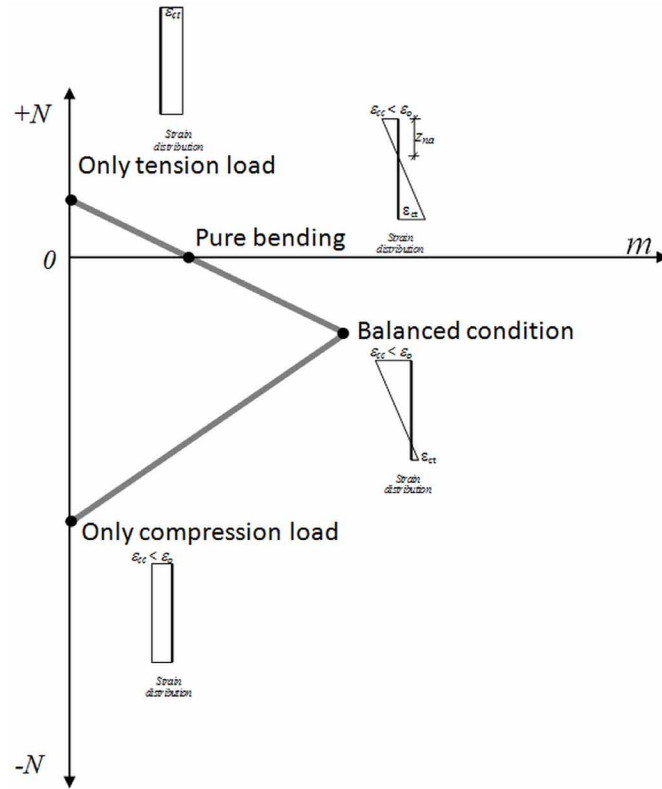


The combination of Equation (10.3.1-3) lead to:

$$P = Z(d)(t - t_p); \text{ where } d = d_2; Z(d) = (1 - d)Z_0; Z_0 = \frac{6EI}{L^3} \text{ and } t_p = \phi_2^p L \quad (10.3.4)$$

**Lumped Damage Mechanics**

Figure 3. a) Measurement of  $Z_0$  b) Measurement of  $Z(d)$



Notice that this expression represents a straight line in the force-displacement space; the line has a slope  $Z(d)$  and crosses the horizontal axis for  $t = t_p$ . Thus, this equation is a mathematical representation of any elastic unloading/re-loadings shown in Figure 3a. The initial (undamaged) slope corresponds to the value  $Z_0$ . Therefore this constant can be measured experimentally as shown in Figure 3a. The experimental results indicate a reduction in the stiffness of the structure that can be appreciated in the successive elastic unloading/re-loadings. The value of the damaged slopes  $Z(d)$  can also be measured experimentally (see Figure 3b).

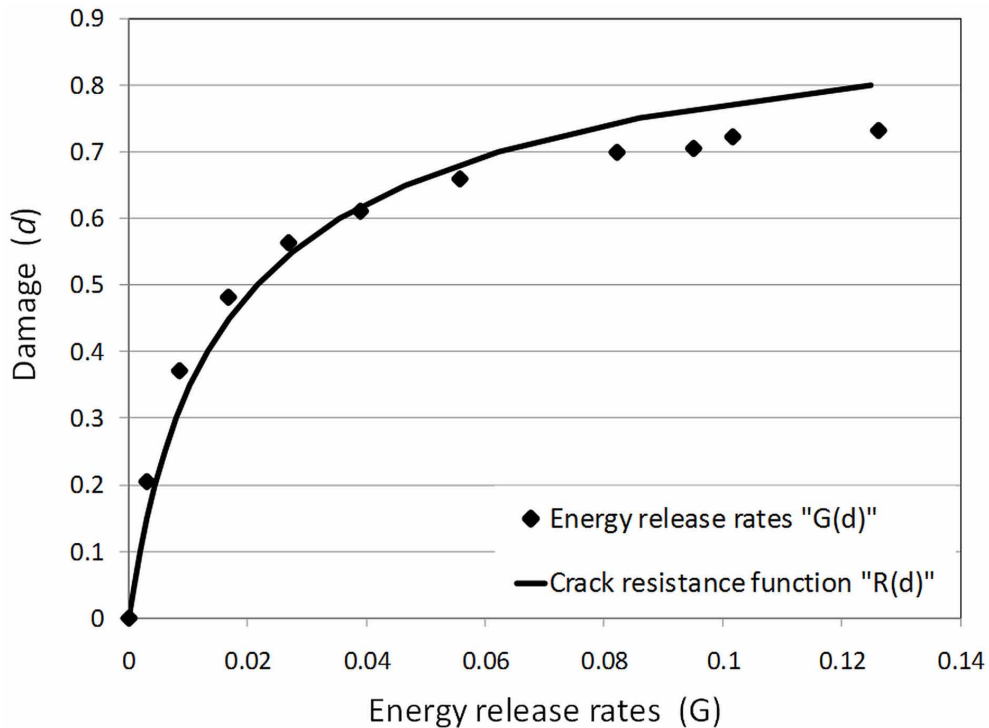
Therefore, the value of damage that corresponds to the force  $P$ , or moment  $m_2$ , that is reached just before the start of the elastic unloading, can be obtained as:

$$d = 1 - \frac{Z(d)}{Z_0} \tag{10.3.5}$$

**10.3.2 Experimental Identification of the Crack Resistance Function**

The plot of energy release rate vs. damage of Figure 4 can be obtained with the values of damage and moments measured experimentally using the procedures described in the previous section.

Figure 4. Energy release rate as a function of damage in a RC specimen



The energy release rates are computed with values of force during a stage of damage propagation; thus, according to the Griffith criterion, they are equal to the values of the crack resistance function  $R$ . Therefore, the graph of Figure 4 is also a plot of  $R$  vs.  $d$ ; this graph allows choosing a mathematical expression that describes approximately these results. This approach to obtain the crack resistance function is sometimes called “phenomenological”. A good alternative for the crack resistance function consists in using the following expression:

$$R(d) = R_0 + q \frac{\ln(1-d)}{1-d} \quad (10.3.6)$$

where  $R_0$  and  $q$  are parameters that depend on the characteristics of the element. Note that this function includes an initial crack resistance  $R_0$  (for  $d = 0$ ) and a hardening term ( $q \ln(1-d) / (1-d)$ ). Physically, hardening in the crack resistance is due to presence of the steel reinforcement that blocks crack propagation in the concrete; thus, significant increments of moment are needed in order to pursue cracking evolution in the plastic hinge region.

### 10.3.3 Computation of the parameters $R_0$ and $q$

One advantage of the elasto-plastic models is that their parameters have a well-defined meaning in the conventional theory of reinforced concrete theory; this is not the case of  $R_0$  and  $q$ . This section describes

### Lumped Damage Mechanics

a procedure that permits the computation of these terms as a function of the first cracking moment  $M_{cr}$  and the ultimate moment  $M_u$ . These parameters are well established concepts in the RC theory.

Consider a monotonic loading on a RC element; during damage propagation the Griffith criterion states that:

$$G = R, \text{ i.e. } \frac{F^0 m^2}{2(1-d)^2} = R_0 + q \frac{\ln(1-d)}{1-d} \quad (10.3.7)$$

Thus, Equation (10.3.7) relates moment and damage (see also Figure 5):

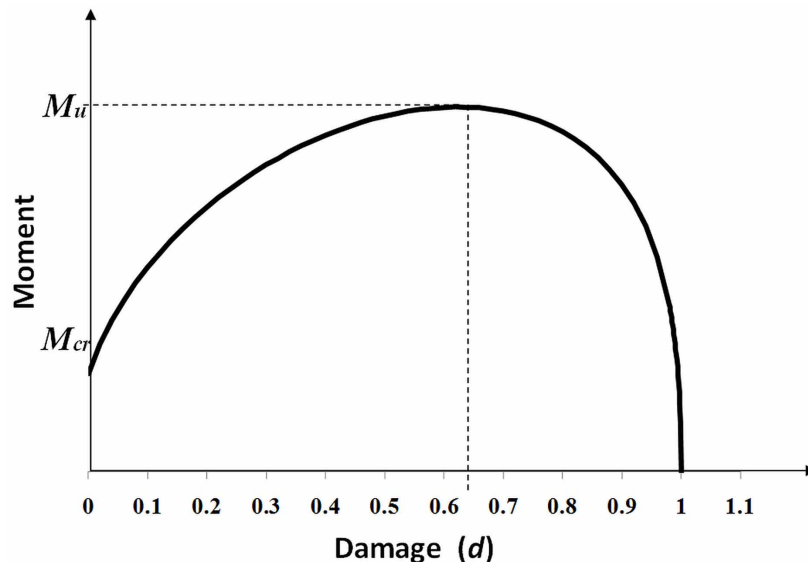
$$m^2 = \frac{2(1-d)^2}{F^0} R_0 + \frac{2q}{F^0} (1-d) \ln(1-d) \quad (10.3.8)$$

According to the conventional RC theory, cracking starts when the moment reaches a value called first cracking moment (see next section), thus:

$$M_{cr}^2 = \frac{2}{F^0} R_0 \quad (10.3.9)$$

This equation allows for the computation of the initial crack resistance  $R_0$ . The RC theory establishes that the first cracking moment depends on the axial force on the element; thus  $R_0$  is in fact a function of this force too. Therefore, the analysis of damaged RC columns requires the interaction diagram of the first cracking moment.

Figure 5. Moment as a function of damage as stated in the Griffith criterion





As shown in Figure 5, the moment reaches a maximum for a specific value of damage,  $d_u$ , called “ultimate damage” because it corresponds to the ultimate moment  $M_u$  (and not because it is the largest possible value of damage). The computation of the ultimate moment of a RC cross-section is described in section 6.5.5. When the variable  $d$  takes the value of the ultimate damage, the derivative of Equation (10.3.6) with respect to the damage is equal to zero:

$$2R_0(1 - d_u) + q(\ln(1 - d_u) + 1) = 0 \quad (10.3.10)$$

For  $d$  equal to  $d_u$ , the moment is equal to the ultimate moment  $M_u$ , thus:

$$M_u^2 = \frac{2(1 - d_u)^2}{F^0} R_0 + \frac{2q}{F^0} (1 - d_u) \ln(1 - d_u) \quad (10.3.11)$$

The expressions (10.3.10-11) constitute a system of two equations with two unknown variables whose resolution gives the values of  $q$  and  $d_u$ . Thus, the computation of the parameter  $q$  for a RC column requires an interaction diagram of the ultimate moment too.

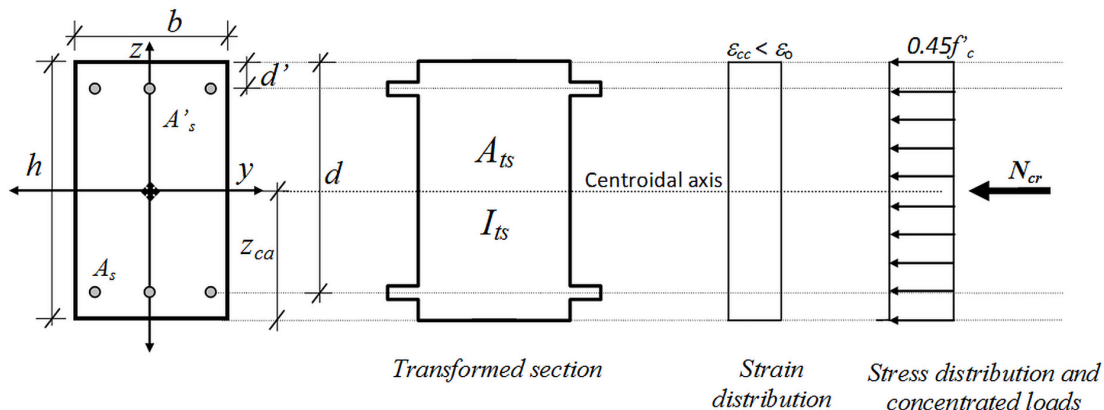
An example of application of these procedures is presented in the section 10.9.1.

It is important to underline that the value of  $d_u$  varies in a small interval for common RC cross-sections: in the majority of applications  $d_u$  is within the interval [0.6 - 0.65].

### 10.3.4 Computation of the Interaction Diagram for the First Cracking Moment

As in the case of the interaction diagram for the first plastic moment (see section 6.5), the interaction diagram of the first cracking moment can be defined by the pure compression, pure tension, pure bending and balanced conditions. The transformed section concept, well known in the strength of materials theory, is used. This notion consists in the substitution of the steel area into an equivalent concrete one (see Figure 6).

Figure 6. Transformed section, strain and stress distributions in pure compression condition for first cracking



**Lumped Damage Mechanics**

*Pure compression point:* The axial force is computed as indicated in Figure 6. Notice that there is a constant strain and stress distributions across the section. As it was described in section 6.5.2, it is supposed that the concrete behavior is almost linear until near the half of the concrete resistance. Assuming that this loss of linearity is due to concrete cracking, the corresponding axial force is:

$$N_{cr} = -A_{ts} * 0.45f'_c \tag{10.3.12}$$

where  $A_{ts}$  is the area of the transformed section.

*Pure tension point:* In this case, the axial force is computed as shown in Figure 7; notice that there are constant distributions of strain and stress again. Assuming that cracking starts when the stress reaches the value of the tension strength  $f_t$ , the corresponding axial force is equal to:

Figure 7. Transformed section, strain and stress distributions in pure tension condition for first cracking

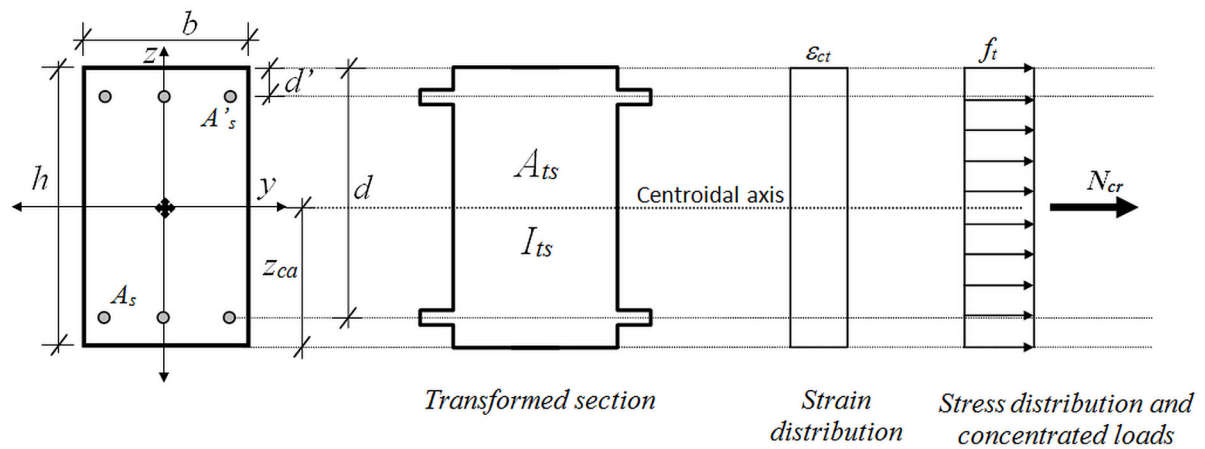
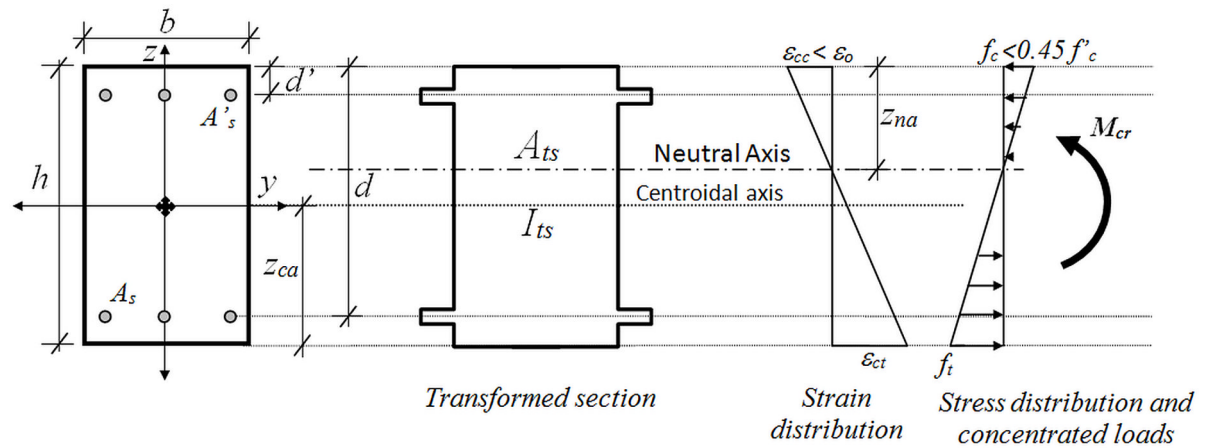


Figure 8. Transformed section, strain and stress distributions in pure bending condition for first cracking



$$N_{cr} = A_{ts} * f_t \tag{10.3.13}$$

*Pure bending point:* It is used the Euler-Bernoulli theory that is described in section 2.4; therefore, linear distributions of stress and strain are assumed (see Figure 8).

The first cracking bending moment is obtained considering that maximum tension stress is equal to  $f_t$ :

$$f_t = \frac{M_{cr} z_{ca}}{I_{ts}} \Rightarrow M_{cr} = \frac{f_t I_{ts}}{z_{ca}} \tag{10.3.14}$$

where  $z_{ca}$  is the distance between the extreme tension fiber and the centroidal axis,  $I_{ts}$  is the moment of inertia of the transformed section.

*Balanced condition point:* In this case, it is assumed that a compression stress of  $0.45f'_c$  and a tension stress equal to  $f_t$  are reached simultaneously at the extreme fibers as shown in Figure 9.

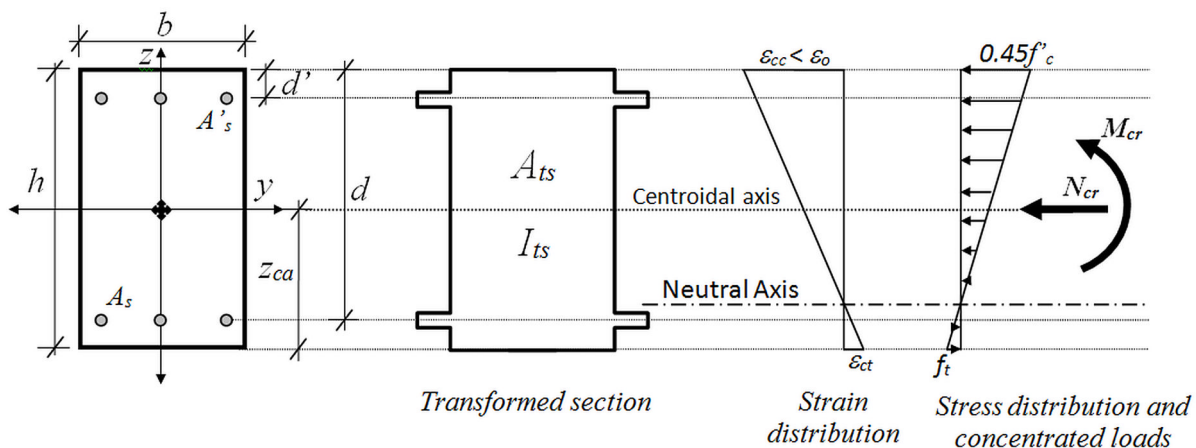
This linear stress distribution is described by Equation (10.3.15):

$$f = \frac{M_{cr} z}{I_{ts}} + \frac{N_{cr}}{A_{ts}} \tag{10.3.15}$$

where  $z$  is the distance between the centroidal axis and the fiber under consideration.

The bending moment and the axial force are computed taking into account that the maximum compressive stress is equal to  $f'_c$  and the maximum tension stress is equal to  $f_t$ .

Figure 9. Transformed section, strain and stress distributions in the balanced condition for first cracking



### Lumped Damage Mechanics

$$0.45f'_c = \frac{M_{cr}(h - z_{ca})}{I_{ts}} + \frac{N_{cr}}{A_{ts}} \quad (10.3.16)$$

$$f_t = \frac{M_{cr} z_{ca}}{I_{ts}} - \frac{N_{cr}}{A_{ts}}$$

Solving the system of equations for the bending moment and the axial force gives:

$$N_{cr} = \frac{z_{ca}(0.45f'_c + f_t) - h f_t}{h} A_{ts}; M_{cr} = \frac{0.45f'_c + f_t}{h} I_{ts} \quad (10.3.17)$$

## 10.4 YIELD FUNCTION OF A DAMAGED PLASTIC HINGE

### 10.4.1 Plastic Deformation Evolution Law

An evolution law for the plastic deformation must be added in order to complete the damage model. Again, it is used the hypothesis of equivalence in deformation. The equivalent moment on a plastic hinge  $i$  can be defined as:

$$\bar{m}_i = \frac{m_i}{1 - d_i} \quad (10.4.1)$$

The yield function of a damaged plastic hinge can now be obtained after modification of a function with linear kinematic hardening via the hypothesis of equivalence in deformations:

$$f_i = \left| \bar{m}_i - c_i \phi_i^p \right| - k_{0i} = \left| \frac{m_i}{1 - d_i} - c_i \phi_i^p \right| - k_{0i} \leq 0 \quad (10.4.2)$$

where  $c_i$  and  $k_{0i}$  are parameters that depends on the characteristics of the element. Therefore, the plastic deformation evolution laws are:

$$\begin{cases} d\phi_i^p = 0 & \text{if } f_i < 0 \\ f_i = 0 & \text{if } d\phi_i^p \neq 0 \end{cases}; \begin{cases} d\phi_j^p = 0 & \text{if } f_j < 0 \\ f_j = 0 & \text{if } d\phi_j^p \neq 0 \end{cases}; f_j = \left| \frac{m_j}{1 - d_j} - c_j \phi_j^p \right| - k_{0j} \leq 0 \quad (10.4.3)$$

### 10.4.2 Computation of the Parameters $c$ and $k_0$

Consider again a monotonic loading on a RC element; thus, Equation (10.3.11) relates the moment on a plastic hinge  $i$  with its damage. It is assumed that the first plastic moment  $M_p$  is larger than the first

cracking moment  $M_{cr}$ ; thus the value of damage  $d_p$  that corresponds to the former moment can be computed by the resolution of the following equation:

$$M_p^2 = \frac{2(1-d_p)^2}{F^0} R_0 + \frac{2q}{F^0} (1-d_p) \ln(1-d_p) \quad (10.4.4)$$

The value  $d_p$  represents the cracking state that corresponds to the first yielding of the reinforcement. In most applications, this value is in the interval (0.3 – 0.4).

At this stage, the yield function is equal to zero with nil plastic rotation; thus, the parameter  $k_0$  is in fact the effective plastic moment:

$$k_0 = \frac{M_p}{1-d_p} = \bar{M}_p \quad (10.4.5)$$

The yield function is also equal to zero when the moment reaches its ultimate value, thus, the last parameter  $c$  can be computed as:

$$c = \frac{1}{\phi_u^p} \left( \frac{M_u}{1-d_u} - k_0 \right) = \frac{\bar{M}_u - \bar{M}_p}{\phi_u^p} \quad (10.4.6)$$

where  $\phi_u^p$  is the ultimate plastic rotation that is introduced in chapter 6 (section 6.5.6). Notice that  $c$  is equal to the difference between effective moments divided by the ultimate plastic rotation.

The use of concepts of fracture and damage mechanics in the analysis of framed structures does not require the use of very advanced concepts of the theory of reinforced concrete; just the conventional procedures for the computation of the first cracking moment, first plastic moment, ultimate moment and ultimate plastic rotation are sufficient in any application.

## **10.5 SOME NUMERICAL SIMULATIONS WITH THE DAMAGE MODEL**

### **10.5.1 Numerical Simulation of the Test that is Shown in Figure 10 Using Experimentally Measured Parameters**

This section presents the results of two simulations of *the identification test shown in Figure 10*.

This section presents the results of two simulations of the identification test that is shown in Figure 10.

The first simulation is carried out with the elasto-plastic constitutive equations presented in section (7.1.6). In the second simulation, it is used the damage model described in this chapter. The following values of the parameters are taken from the experimental results:  $EI = 1025.373 \text{ KN.m}^2$ ,  $M_{cr} = 4.004 \text{ KN.m}$ ,  $M_p = 24.220 \text{ KN.m}$ ,  $M_u = 29.034 \text{ KN.m}$  and  $\phi_u^p = 0.095$ . The experimental and the numerical results with the elasto-plastic model are presented in Figure 11a; and the ones using the damage model in Figure 11b.

## Lumped Damage Mechanics

Figure 10. RC beam tested and material properties

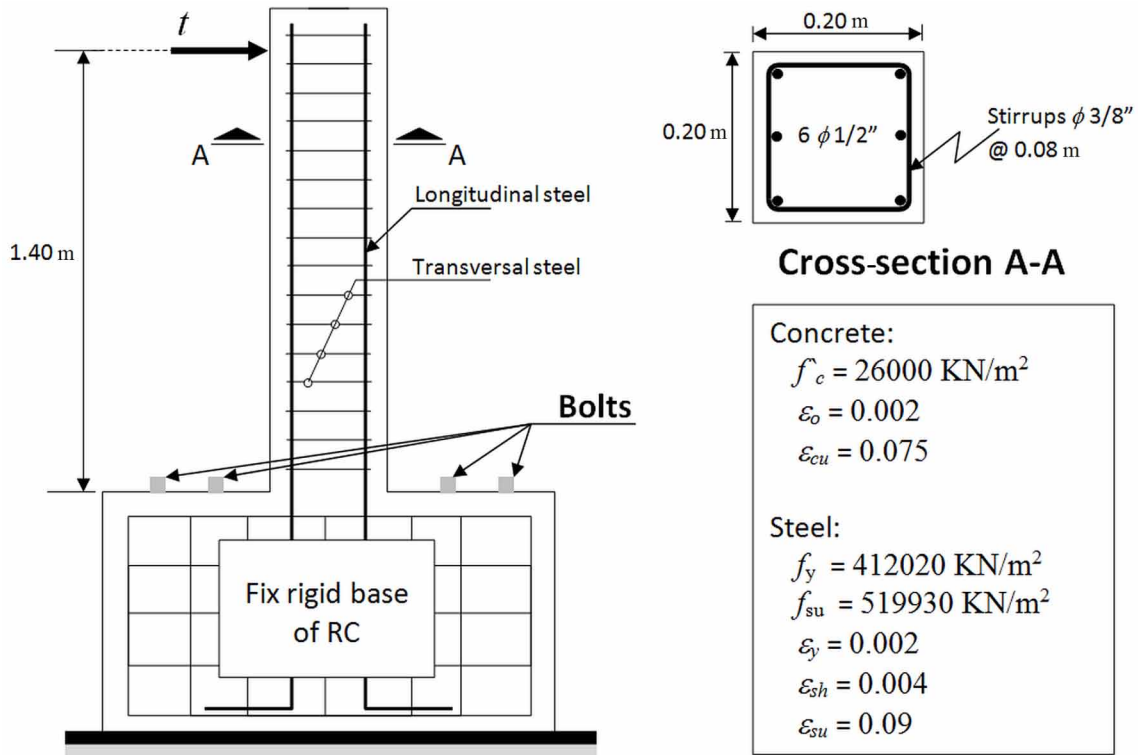
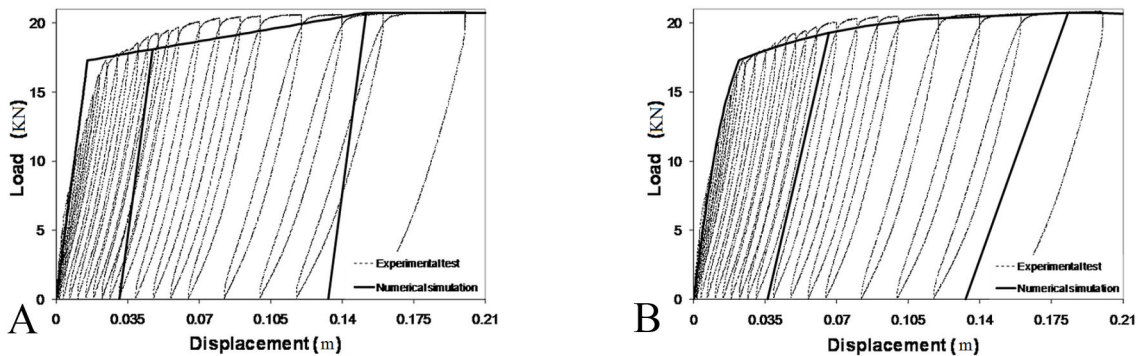


Figure 11. a) Comparison of the elasto-plastic model with experimental results b) Comparison of the damage model with experimental results



As the parameters were chosen to give the best results, the differences between theoretical and experimental results are due only to deficiencies of the model. The examples 10.10.2 and 10.10.3 show the procedures used to obtain the curve that was plotted in Figure 11b.

Notice that the damage model used for the simulation presented in Figure 11b is essentially the elasto-plastic of Figure 11a modified by the hypothesis of equivalence in deformations, adding the Griffith criterion. There are no significant differences in the envelopes of both simulations, only a slight improvement with the damage model. The main difference lays in the description of the stiffness degradation and in the fact that the later model gives a rational measure of structural damage as well.

Plastic models can also be modified including empirical rules of stiffness degradation as a function of the plastic rotation in the hinges and adding the so called “damage indexes”. The latter are parameters computed by postprocessors (that is, after the simulation was concluded without considering damage) as a function of the plastic rotations again, the expressions for the determination of the damage indexes are of semi empirical nature as well. The bibliography of this chapter includes some important references in this field.

### 10.5.2 Numerical Simulation of the Test Described in Figure 10 with Parameters Calculated Analytically

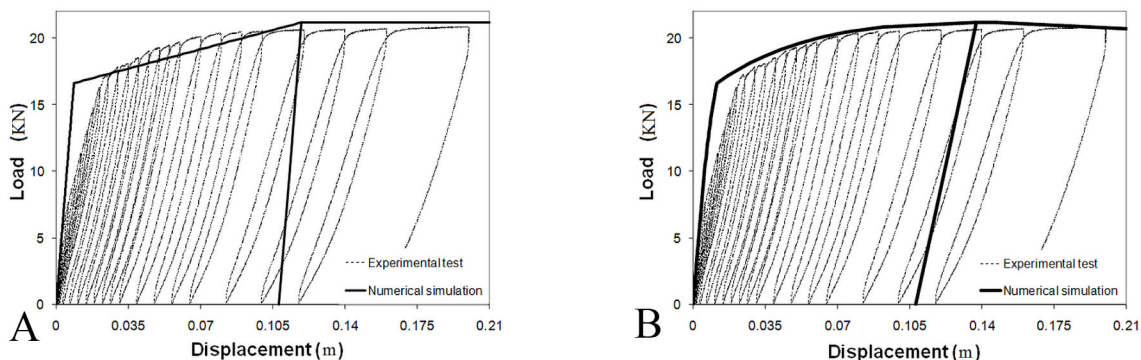
In a standard engineering application, the model parameters cannot be measured from experimental results; they must be computed using RC theory. Thus, additionally to the deficiencies of the model, the errors due to the simplifying assumptions of that theory must be added. In the simulations presented in this section, the analysis was carried out as follows. First, the parameters are computed using the procedures described in the sections 10.3.4, 6.5 and the properties for concrete and steel presented in Figure 10; the following values were obtained:  $EI = 1765.80 \text{ KN.m}^2$ ,  $M_{cr} = 6.288 \text{ KN.m}$ ,  $M_p = 23.250 \text{ KN.m}$ ,  $M_u = 29.626 \text{ KN.m}$  and  $\phi_u^p = 0.0771$ ; next, the analytical determination of the response is obtained using the procedures described in the examples 10.10.2 and 10.10.3. The results are shown in Figure 12.

Notice that the main difference between the computed values and the best ones lies in the stiffness modulus EI. The RC theory predicts a beam seventy two percent stiffer than the experimentally measured value. The computed value of the ultimate plastic rotation is only eighty one percent of the observed one. On the other hand, the theory gave very good estimates of the first plastic moment and ultimate moment for this example.

### 10.5.3 Behavior of a RC Element under Different Axial Forces

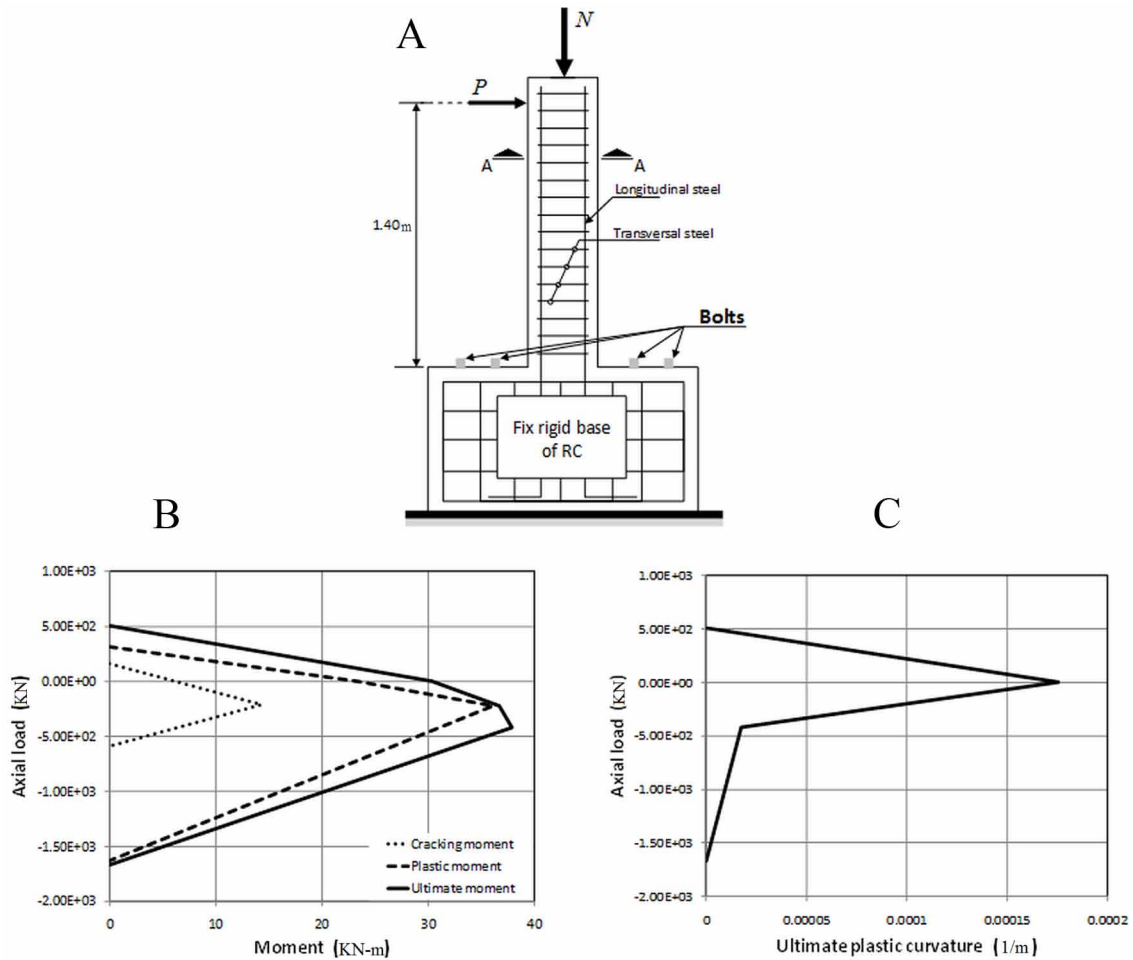
Consider again the column in cantilever (Figure 10a) subjected to axial loads and lateral displacements, as it is shown in Figure 13a. The interaction diagrams are presented in Figures 13b-c. Five loading histories are considered; in four of the simulations, the loadings are applied in two steps: first (interval  $0 - t_1$ ) a monotonic axial load is imposed and then (interval  $t_1 - t_2$ ) a monotonic lateral displacement according

Figure 12. a) Comparison of the elasto-plastic model with experimental results b) Comparison of the damage model with experimental results



## Lumped Damage Mechanics

Figure 13. a) Column subjected to an axial load and a lateral displacement b) Interaction diagram of moments c) Interaction diagram of the ultimate plastic rotation

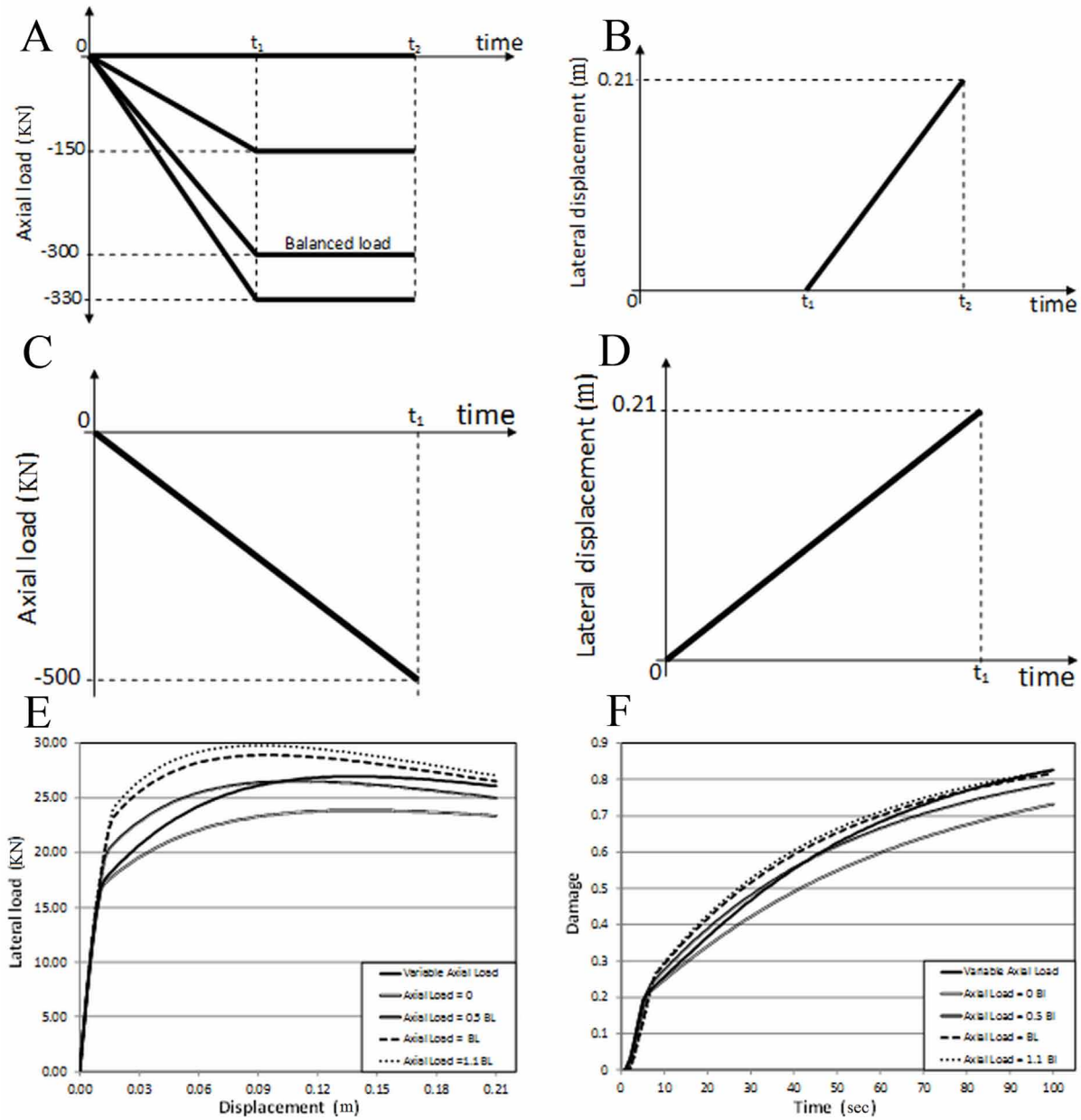


to the histories shown in Figure 14a. In the last simulation, axial force and lateral displacement histories are applied simultaneously as it is shown in Figure 14b. The behaviors of the column are presented in Figure 14c. The histories of damage of the five simulations are shown in Figure 14d.

Notice that the history of axial forces modifies in a significant way the behavior of the column. This is consequence of changes in ductility and strength at the critical sections. This phenomenon has been observed experimentally and its consideration is fundamental for any realistic representation of the behavior of frames subjected to severe lateral forces since they imply variations of the axial forces in the columns.

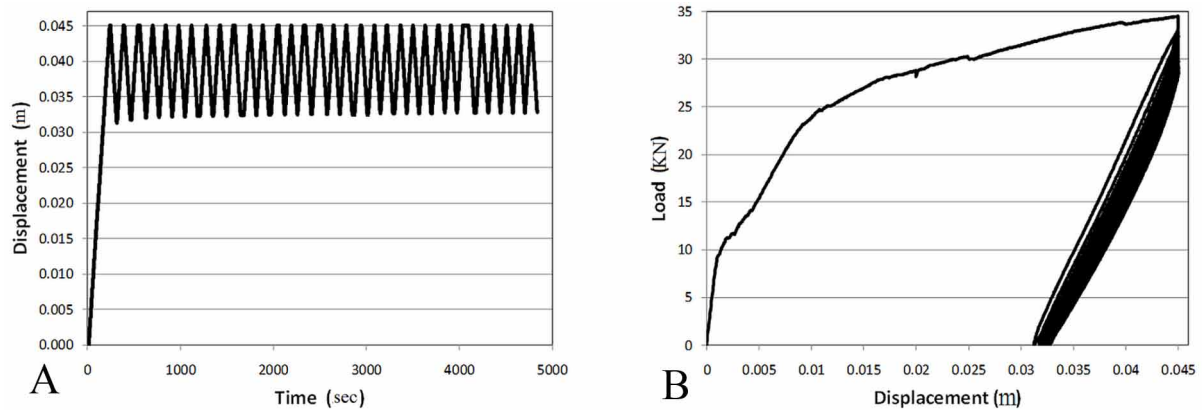


Figure 14. a) Loading histories in two steps: axial forces and lateral displacements b) Loading histories in one step: axial forces and lateral displacements c) Force vs. displacement responses d) Damage histories



## Lumped Damage Mechanics

Figure 15. a) Ultra-low cycle fatigue loading in displacements b) Force vs. displacement curve



## 10.6 A MODEL OF DAMAGE FOR RC ELEMENTS CONSIDERING ULTRA-LOW CYCLE FATIGUE EFFECTS

### 10.6.1 The Ultra-Low Cycle Fatigue Effect

Consider again a specimen like the one used for the numerical identification of the crack resistance function (Figure 2b); but now a different kind of mono-sign loading was applied (see Figure 15a and compare with Figure 2c); imposed displacements are chosen but, unlike the test in Figure 2, the maximum displacement of each cycle remains constant. It can be observed in the experimental response (Figure 15b) that even without increments of the loading, the stiffness and strength of the specimen decreases after each cycle. In section 10.1.3 it is explained that these stiffness and strength degradations are caused by crack propagation; therefore, there is damage evolution during each cycle even without increasing their maximum solicitation. This phenomenon is called “ultra-low cycle fatigue effect”.

It has been observed experimentally that the ultra-low cycle fatigue effect is magnified by the current state of damage: for reduced cracking, the fatigue effect can hardly be appreciated; for high cracking densities, the damage increment after each cycle is considerable.

### 10.6.2 Modified Griffith Criterion

The Griffith criterion is unable to represent the ultra-low-cycle fatigue effects; in this criterion, cracking extension is assumed to be a function of the maximum value of the energy release rate. Thus, in fatigue tests with constant maximum force or displacement, the damage keeps the value reached at the end of the first cycle.

This section describes a modification of the Griffith criterion that presents the following characteristics:

1. No additional variables are introduced.
2. The model relates damage evolution to energy release rate.
3. During a monotonic loading it gives the same response as the classic Griffith criterion.
4. It includes the Griffith criterion (without fatigue effects) as a particular case.

5. It assumes that there is no damage evolution during elastic unloading.
6. The damage increment is possible during loading phases even if the energy release rate is less than the actual crack resistance; i.e. the damage evolution due to fatigue effects is described.
7. It includes only one additional parameter.

Consider the Griffith criterion during a phase of crack propagation:

$$\text{if } \Delta d_i > 0; G_i = R(d_i); \text{ or } G_i^{\alpha+1} = R(d_i)^{\alpha+1} \text{ for } \alpha \geq 0 \quad (10.6.1)$$

The differentiation of (10.6.1b) gives the modified Griffith criterion:

$$\begin{cases} \Delta d_i = 0 & \text{if } G_i < R_0 \\ \Delta d_i = \frac{1}{\partial R / \partial d_i} \left( \frac{G_i}{R} \right)^\alpha \langle \Delta G_i \rangle_+ & \text{otherwise} \end{cases} \quad (10.6.2)$$

where  $\alpha$  is the additional parameter.

During a monotonic loading, this evolution law and the Griffith criterion (10.2.3) predict the same behavior regardless what value of  $\alpha$  is used. In other cases, both laws may differ since with the modified law, there is evolution of the damage even if the energy release rate has not yet reached the crack resistance. Notice that the fatigue law tends to the Griffith criterion for high values of  $\alpha$ ; the term  $\left( \frac{G_i}{R} \right)^\alpha$  tends to zero when  $\alpha$  tends to infinite, unless  $G_i = R$ ; in that case both evolution laws give identical results. The constant  $\alpha$  can be considered as a “fatigue brake”, the maximum effect of fatigue is obtained for  $\alpha = 0$  and there is no fatigue, at all, for  $\alpha = \infty$ . The experimental results show that a value of  $\alpha = 2$  is a good choice for any RC element. Figure 16 shows the numerical simulation of the test described in section 10.6.1.

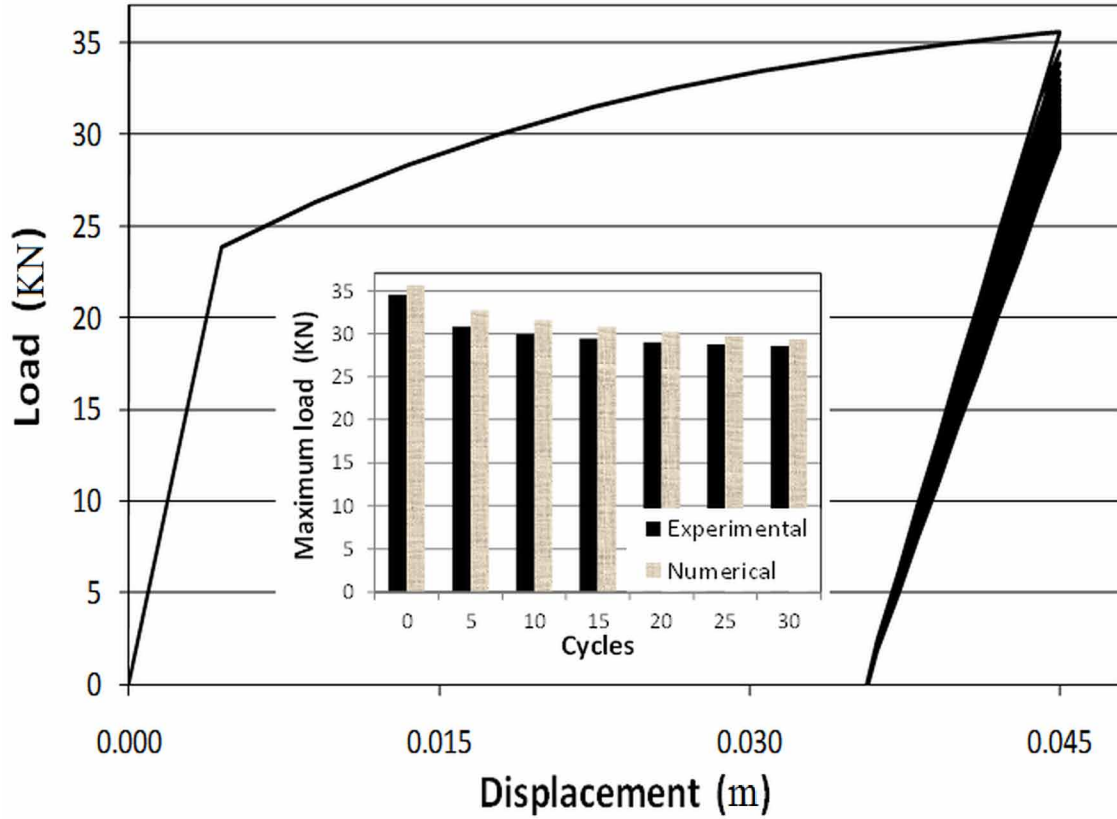
## 10.7 ANALYSIS OF DAMAGED FRAMES

### 10.7.1 Formulation of the problem

Consider a planar frame subjected to a mono-sign loading. The problem is defined as:

- **Compute:** The free displacements, reaction forces, stresses, deformations, plastic deformations and damages.
- **With the Following Data:** The initial configuration of the structure, the restricted displacements, the nodal forces corresponding to the free displacements and those applied over the elements, the material properties, cross-section properties and the yield functions.
- Such that they verify the nonlinear kinematic and equilibrium equations:

Figure 16. Numerical simulation of the experimental test described in section 10.6.1



- $\{\Delta\Phi\}_b = [\mathbf{B}_E(\mathbf{U}_{t=tr})]_b \{\Delta\mathbf{U}\}$
- $\{\mathbf{L}_{t=tr}\} = \{\mathbf{P}_{t=tr}\}; \{\mathbf{L}_{t=tr}\} = \sum_{b=1}^m [\mathbf{B}(\mathbf{U}_{t=tr})_E]_b^t \{\mathbf{M}_{t=tr}\}_b$  (10.7.1)
- The elasticity law:  $\{\mathbf{M}\}_b = [\mathbf{E}(\mathbf{D})]_b \{\Phi - \Phi^p\}_b + \{\mathbf{M}_0\}_b$
- The plastic deformation evolution laws:
  - $\begin{cases} d\phi_i^p = 0 & \text{if } f_i < 0 \\ d\phi_j^p = 0 & \text{if } f_j < 0 \\ f_i = 0 & \text{if } d\phi_i^p \neq 0 \\ f_j = 0 & \text{if } d\phi_j^p \neq 0 \end{cases}$
- With the yield functions:
  - $f_i = \left| \frac{m_i}{1-d_i} - c_i \phi_i^p \right| - k_{0i} \leq 0; f_j = \left| \frac{m_j}{1-d_j} - c_j \phi_j^p \right| - k_{0j} \leq 0$
- And the damage evolution laws:

$$\circ \quad \begin{cases} \Delta d_i = 0 \text{ if } G_i < R_{0i} \\ \Delta d_i = \frac{1}{\partial R_i / \partial d_i} \left( \frac{G_i}{R_i} \right)^2 \langle \Delta G_i \rangle_+ \text{ otherwise} \end{cases} ;$$

$$\begin{cases} \Delta d_j = 0 \text{ if } G_j < R_{0j} \\ \Delta d_j = \frac{1}{\partial R_j / \partial d_j} \left( \frac{G_j}{R_j} \right)^2 \langle \Delta G_j \rangle_+ \text{ otherwise} \end{cases}$$

Notice that the damage constitutive law can be included in the framework described in section 8.3.1 with:

$$VWf_1 = \phi_i^p; VWf_2 = \phi_j^p; \{\mathbf{VW}\mathbf{o}\}_b = \{d_i, d_j\} \quad (10.7.2)$$

Therefore the numerical algorithm in that section for elasto-plastic models can also be used with the damage model. The problem can be analyzed step-by-step and at each step, it can be decomposed in a global problem and local problems for each element; both kinds of problems are solved using the Newton method. However, damage problems present a higher degree of nonlinearity as compared with elasto-plastic ones and more serious convergence difficulties. The algorithms described in section 8.3.1 can be improved using the procedure that is described in the next section.

### 10.7.2 The Multi-Steps Version of the Step-By-Step Algorithm

The main drawback of the damage models in practical applications is the heavy computational costs that they imply. This cost is due to convergence requirements that often impose tiny time steps during the step-by-step resolution. Occasionally, the programs simply do not converge without apparent causes.

The conventional step-by-step algorithm can be modified and the performances of the programs be improved noticeably; this modification is called “multi-steps version”. The idea of the multi-steps procedure is very simple: the step size of the global problem and those of the local ones do not necessarily have to be the same.

As aforementioned, the global problem and local problems using damage models does not differ of those formulated with elasto-plastic or nonlinear elastic ones; the global problem in the quasi-static case is:

$$\{\mathbf{L}(\mathbf{U}_{t=tr})\} = \{\mathbf{P}_{t=tr}\} \quad (10.7.3)$$

where  $\{\mathbf{L}(\mathbf{U}_{t=tr})\}$  is the matrix of internal forces and  $\{\mathbf{P}_{t=tr}\}$  are the external nodal forces for the global problem. The local problems can be formulated as

$$\{\mathbf{M}\}_b = \{\mathbf{M}(\mathbf{U}_{t=tr})\}_b \text{ for } b = 1 \text{ to } m \quad (10.7.4)$$

Therefore, there is a total of  $m + 1$  nonlinear problems to be solved by the Newton method, where  $m$  is the number of elements of the structure. The convergence of the algorithm depends on “how close”

### **Lumped Damage Mechanics**

is the first provisional displacement matrix  $\{U_p\}$  with respect to the exact solution. As indicated in section 4.2.4, the provisional displacement matrix is derived from the displacements at the precedent step. Therefore, the convergence of the method depends, amongst other things, on the size of the global step.

In the standard procedure, the global step is also used for the local problem. Thus this step must satisfy the convergence requirements of the global problem and the  $m$  local problems. Therefore, if any one of these  $m+1$  problems fails to converge, the size of the time step must be reduced for all of them.

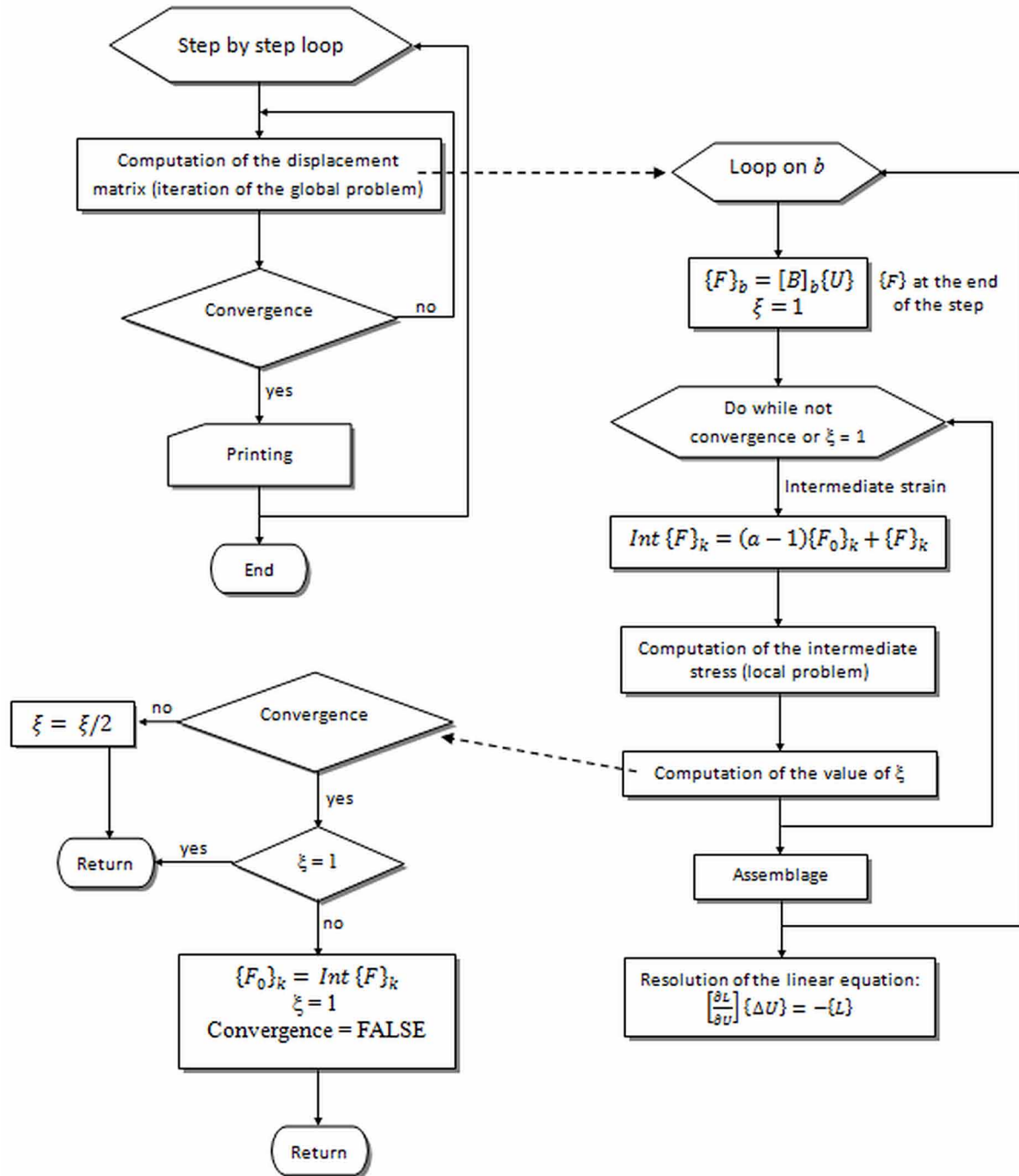
The conventional method would be optimum if the local problems had similar or softer convergence requirements than the global one. However, for the damage models this is not the case. In general, the local problems can be classified into two groups. The first one corresponds to the elements whose behavior is elastic or inelastic but with convergence requirements equal or less strict than the global problem. In the cases of severe overloads this group has 70%-95% of the local problems. The second group includes the elements where damage effects concentrate. It has been observed that for these local problems, the convergence requirements can be much stricter than that of the global problem. Often, they are needed time steps 10, 100, 1000 or even 10000 times smaller than that of the minimum needed for the global problem. With the conventional algorithm, all the  $m+1$  problems for a given instant,  $t_r$ , must be solved with the smaller step needed: that of the most difficult problem. Therefore, it appears that the standard algorithm is highly inefficient.

One possible modification of the step-by-step procedure is shown in Figure 17. In this algorithm, the initial local step of any element is chosen equal to the global step. If the local problem is successfully solved then the program continues with the next local problem. If the Newton procedure fails to find the solution, the local step size is divided by two, this is simply done by reducing accordingly of the total deformation matrix of the element. An intermediate local problem is subsequently solved, if convergence is still not achieved, the local step is halved again. This process is repeated until a local time step is found so that an intermediate problem can be solved or until that some limit fixed by the user is reached; in the latter case, there is no choice but reduce the global time step and to try again. If finally an intermediate local problem is successfully solved, then the final local problem, i.e. the stresses at the time  $t_r$ , is again try by using as initial provisional solution the one corresponding to the intermediate problem; this is because the possibility of convergence has increased since the intermediate solution is closer to the final one. Of course, convergence is not guaranteed even using an intermediate solution as a starting point; if, in spite of the more favorable conditions, there is no success, a second intermediate problem between the first one and the final local problem is attempted. This sequence of intermediate local problems/ final local problems can be repeated as many times as allowed by the programmer.

Two simulations, one static and other dynamic, of a RC tridimensional building were carried out in order to show the advantages of the use of multi-step modification. The building has four frames of six levels in each orthogonal direction as it is shown in Figure 18. The geometry of the elements is presented in the figure. Rigid diaphragms were considered at each story. The structure was analyzed using the tridimensional damage model that is described in Chapter 12. Each simulation was performed twice; one using the multi-step modification and the second one allowing changes only in the sizes of the global steps.

For the static simulations, a displacement of 70 cms in the direction X was applied at the top of the building. When the multi-step modification was used, only 32 of the 456 elements of the structure required changes of its local size due to convergence problems.

Figure 17. The multi-step version of the step-by-step algorithm



**Lumped Damage Mechanics**

Figure 18. a) Plan view b) Frames A, B, C, D, 1, 2, 3, 4 c) Cross-section of all elements and material properties d) Acceleration record: El Centro earthquake

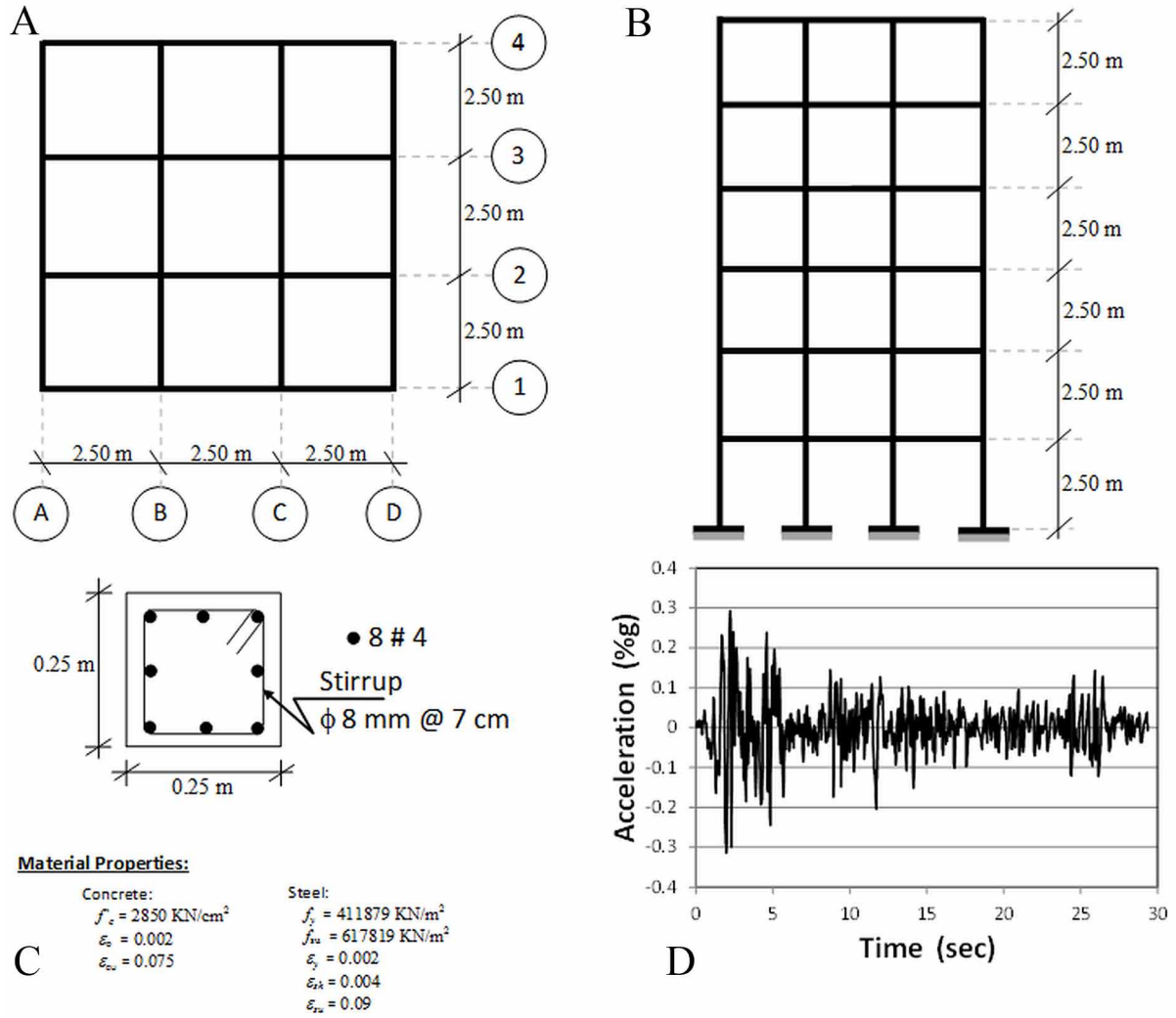
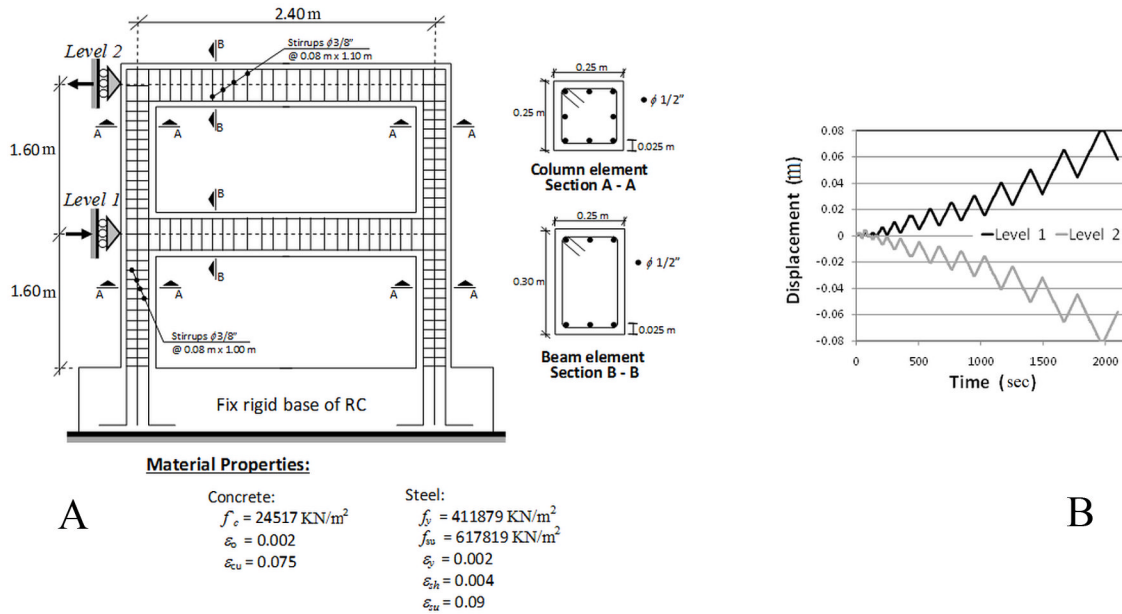


Table 1. Comparison of computational effort for solving two damage problems

Simulation Type	Step Algorithm	CPU Time Sec.	Number of Steps	Total Number of Iterations Global Problems	Max Number of Iterations in a Step
Static	Multi	230	10	28	3
Static	Unique	962	66	109	4
Dynamic	Multi	4413	524	1012	7
Dynamic	Unique	20376	3664	4127	3



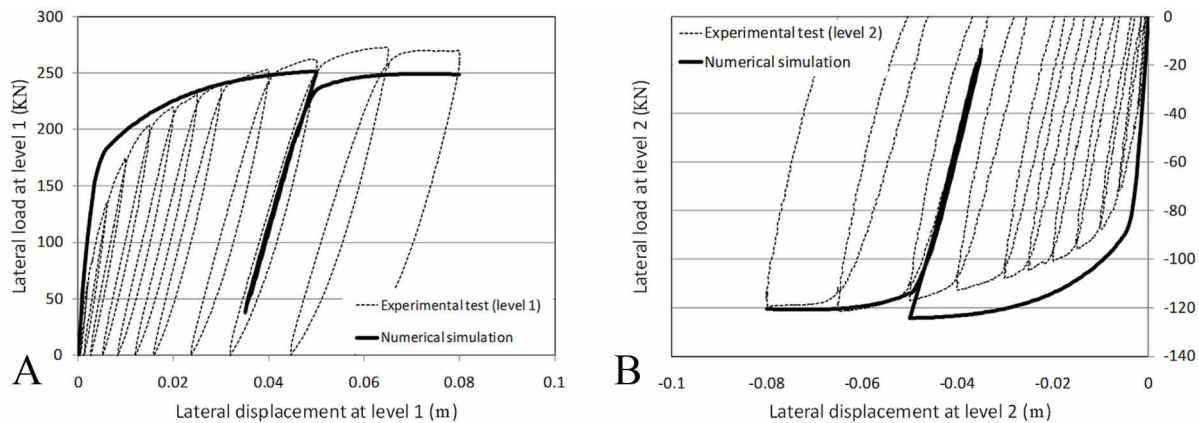
Figure 19. a) Two stories frame b) Displacement histories applied to the frame



For the dynamic analyses an acceleration record corresponding to the El Centro earthquake was imposed in the base of the building (see Figure 18d). The first dynamic analysis was developed satisfactorily but when only changes of global sizes were considered, the structure could be analyzed only in the first 7 sec of the record due to convergence problems.

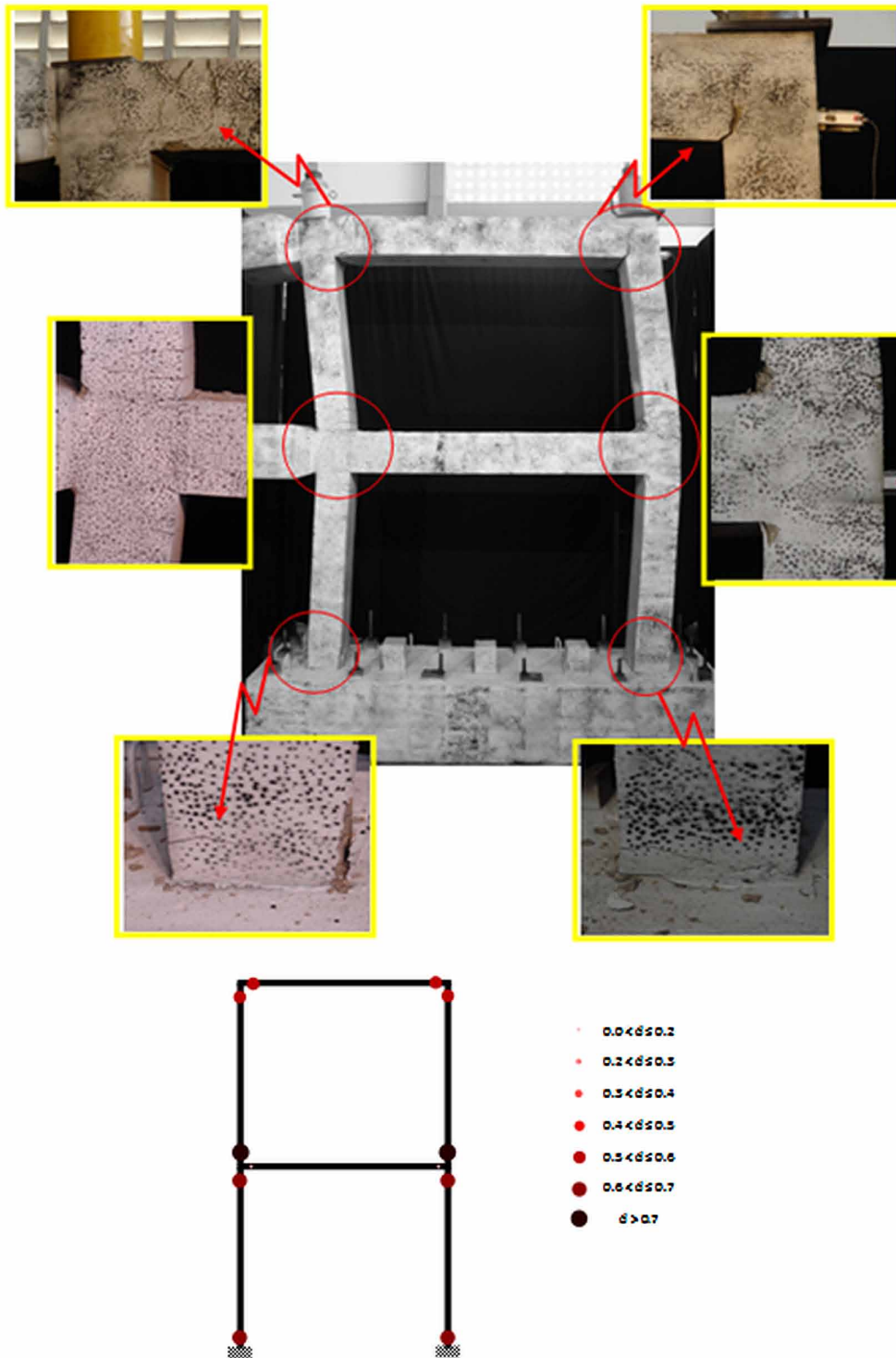
In Table 1 it is presented the comparison of the computational effort required for the solutions of the static analyses and the first 7 sec of the dynamic analyses. As it can be appreciated, the CPU times required for the static and dynamics analyses are, respectively, 24% and 22% smaller when the multi-step modification is used.

Figure 20. Experimental and numerical force-displacement curves a) at level 1 b) at level 2



**Lumped Damage Mechanics**

*Figure 21. Experimental and numerical test results*



In almost all the applications, the multi-step modification improves the efficiency of the program.

It is important to underline that in some situations, the global problem has no possible solution because the external forces  $\{P\}$  are higher than the maximum possible internal forces that the structure can generate. If that is the case, no algorithm can, of course, converge. This absence of solution can be interpreted as structural collapse.

### **10.7.3 Numerical Simulation of a Two Stories Framed Structure**

The two stories frame that is shown in Figure 19a was experimentally tested and analyzed with the described procedure. The frame was subjected to the displacement histories shown in Figure 19b. As it can be appreciated in this figure, at the first level the frame was pushed and at the second one it was pulled with mono-signs displacements. In Figure 20 are shown the experimental and numerical force-displacement curves corresponding to the points where the loading was applied.

Figure 21 shows the damage in the frame at the final of the test and the damage map of the numerical simulation. It can be appreciated how the size and color of the balls in the damage map clearly represent the magnitude of the damage experimented by the elements of the frame.

## **10.8 LIMITATIONS OF THE DAMAGE MECHANICS MODEL**

The model presented in this chapter describes in a simplified way three phenomena taking place in a RC element: elastic deformations, plastic rotations due to yielding of the longitudinal reinforcement and concrete cracking. The model also describes some interactions between these effects. The quantitative accuracy of the model when compared with the experimental curves of force vs. displacement is quite good for engineering applications.

However, some significant phenomena were not taken into account. One of them is that the model only considers one kind of damage: bending cracking that may be lumped at the plastic hinges. In some important engineering applications, a second damage mechanism, shear cracking, is a significant phenomenon. This effect is considered in the next chapter.

Another damage mechanism that has not been taken into account is the buckling of the longitudinal reinforcement. This phenomenon can be observed when there is a so severe state of cracking that lumps of concrete fall down leaving the longitudinal reinforced without any confinement; consequently, steel bars buckle when they are subjected to compression (see Figure 22).

This effect accelerates the stiffness and strength degradation of the element and, of course, cannot be described by the Griffith criterion. It has been observed that this phenomenon does not yet occur when the moment on the plastic hinges reaches its ultimate value  $M_u$ ; thus for values of damage less than or equal to  $d_u$  this effect has not yet started. As aforementioned,  $d_u$  is slightly larger than 0.6 in any common application. The experimental observations indicate that the model can be used for damage values up to 0.65, after that, it may underestimate significantly the damage state of the plastic hinge. Modeling of damage for buckling of the reinforcement is not considered in this book and probably is not very important from the point of view of engineering applications.

## Lumped Damage Mechanics

Figure 22. Buckling of the longitudinal reinforcement in a RC element (Courtesy of NISEE-PEER, University of California, Berkeley)



10.22 Steinbrugge, Karl V. (1960) Retrieved January, 29 2014 from <http://nisee.berkeley.edu/elibrary/Image/S1686>.



## 10.9 SUMMARY AND EQUATIONS QUICK REFERENCE

This chapter describes how the concepts of fracture and damage mechanics can be used for modeling the behavior of RC structures. It is introduced a new internal variable for each hinge: the damage. Thus, plastic hinges become inelastic hinges; the plastic rotations are not the only deformation on the hinge, a second term related to concrete cracking is introduced. The elasticity and plasticity laws are obtained based on the hypothesis of equivalence on deformations. The damage law is a generalized Griffith criterion. It is deduced the energy release rate of an inelastic hinge and the crack resistance function of an RC element is obtained experimentally. The parameters of the model can be computed using concepts of the conventional RC theory. Griffith criterion can be modified to include ultra-low cycle fatigue effect. The numerical analysis of damaged structures is similar to the one used for elasto-plastic structures. However, as degree of nonlinearity of the problem increases one modification was introduced: the multi-step algorithm. Essentially, it consists in using different time steps for the local and global problems (See Table 2).

Table 2.

THE LUMPED DAMAGE MODEL	
	
<p>Hypothesis of equivalence in deformation</p> $\{\Phi\}_b = \{\Phi^{bc}\}_b + \{\Phi^p\}_b + \{\Phi^d\}_b \quad (10.1.1)$ <p><math>\{\Phi^{bc}\}_b</math> : matrix of generalized deformations of the elastic beam column.  <math>\{\Phi^p\}</math> : matrix of plastic deformations.  <math>\{\Phi^d\}_b</math> : damage rotations matrix.</p>	
<p>Matrix of generalized deformations of the elastic beam column:</p> $\{\Phi^{bc}\}_b = [\mathbf{F}_f]_b \{\mathbf{M}\}_b + \{\Phi^0\}_b \quad (10.1.2)$ <p><math>[\mathbf{F}_f]_b</math> : flexibility matrix of a slender element.  <math>\{\mathbf{M}\}_b</math> : generalized stresses matrix.  <math>\{\Phi^0\}_b</math> : the initial deformations matrix.</p>	
<p>Damage deformation matrix</p> $\{\Phi^d\}_b = [\mathbf{C}(\mathbf{D})]_b \{\mathbf{M}\}_b \quad (10.1.3)$ $[\mathbf{C}(\mathbf{D})]_b = \begin{bmatrix} \frac{d_i}{1-d_i} F_{11}^e & 0 & 0 \\ 0 & \frac{d_j}{1-d_j} F_{22}^e & 0 \\ 0 & 0 & 0 \end{bmatrix}$ <p><math>[\mathbf{C}(\mathbf{D})]_b</math> : matrix of additional flexibility due to concrete cracking.  <math>F_{ij}^e</math> represents the <math>(i,j)</math> component of the elastic flexibility matrix.</p>	

continued on following page

## Lumped Damage Mechanics

Table 2. Continued

<p>Elasticity law in terms of flexibility</p> $\{\Phi - \Phi^p\}_b = [\mathbf{F}(\mathbf{D})]_b \{\mathbf{M}\}_b + \{\Phi^0\}_b \quad (10.1.4)$ <p><math>[\mathbf{F}(\mathbf{D})]</math>: flexibility matrix of a damaged frame member.</p> $[\mathbf{F}(\mathbf{D})] = [\mathbf{F}_f] + [\mathbf{C}(\mathbf{D})] = \begin{bmatrix} \frac{F_{11}^e}{1-d_i} & F_{12}^e & 0 \\ F_{21}^e & \frac{F_{22}^e}{1-d_j} & 0 \\ 0 & 0 & F_{33}^e \end{bmatrix}$
<p>Elasticity law in terms of stiffness</p> $\{\mathbf{M}\}_b = [\mathbf{E}(\mathbf{D})]_b \{\Phi - \Phi^p\}_b + \{\mathbf{M}^0(\mathbf{D})\}_b \quad (10.1.5)$ <p><math>[\mathbf{E}(\mathbf{D})]_b = [\mathbf{F}(\mathbf{D})]_b^{-1}</math>: elasticity matrix of a damaged frame element.</p> $\{\mathbf{M}^0(\mathbf{D})\}_b = -[\mathbf{E}(\mathbf{D})]_b \{\Phi^0\}_b$
<p>Elasticity matrix of a damaged frame element.</p> $[\mathbf{E}(\mathbf{D})]_b = k \begin{bmatrix} 12(1-d_i) & 6(1-d_i)(1-d_j) & 0 \\ 6(1-d_i)(1-d_j) & 12(1-d_j) & 0 \\ 0 & 0 & \frac{EA_b}{kL_b} \end{bmatrix} \quad (10.1.6)$ $k = \frac{1}{4 - (1-d_i)(1-d_j)} \frac{EI_b}{L_b}$
<b>GENERALIZED GRIFFITH CRITERION FOR AN INELASTIC HINGE</b>
<i>Complementary Deformation Energy of a Damaged Frame Element</i>
$W_b = \frac{1}{2} \{\mathbf{M}\}_b^t \{\Phi - \Phi^p\}_b = \frac{1}{2} \{\mathbf{M}\}_b^t [\mathbf{F}(\mathbf{D})]_b \{\mathbf{M}\}_b + \frac{1}{2} \{\mathbf{M}\}_b^t \{\Phi^0\}_b \quad (10.2.1)$
<p>Energy release rates of hinges <math>i</math> and <math>j</math></p> $G_i = \frac{\partial W}{\partial d_i} = \frac{F_{11}^0 m_i^2}{2(1-d_i)^2}; \quad G_j = \frac{\partial W}{\partial d_j} = \frac{F_{22}^0 m_j^2}{2(1-d_j)^2} \quad (10.2.2)$ <p><math>G_i</math> and <math>G_j</math>: energy release rates, or "damage driving moments"</p>

continued on following page

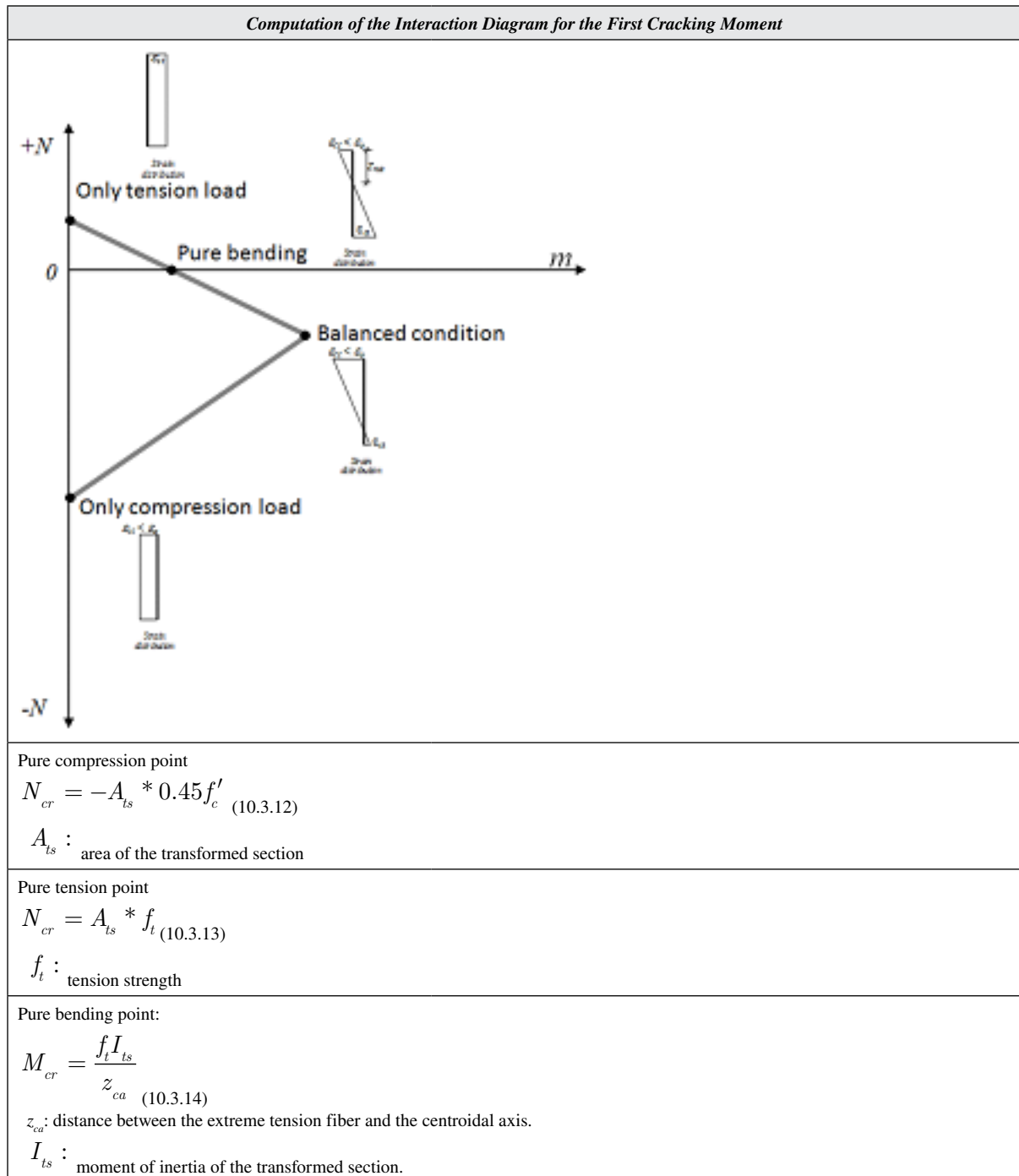
*Table 2. Continued*

<p>Damage evolution laws</p> $\begin{cases} \Delta d_i = 0 & \text{if } G_i < R_i \\ G_i = R_i & \text{if } \Delta d_i > 0 \end{cases}; \begin{cases} \Delta d_j = 0 & \text{if } G_j < R_j \\ G_j = R_j & \text{if } \Delta d_j > 0 \end{cases} \quad (10.2.3)$ <p><math>R_i</math> and <math>R_j</math> are the crack resistance functions of, respectively, inelastic hinges <math>i</math> and <math>j</math>.</p>
<b>CRACK RESISTANCE FUNCTION OF AN INELASTIC HINGE</b>
<i>Experimental Measure of the Damage in a Plastic Hinge</i>
<p>Experimental damage</p> $d = 1 - \frac{Z(d)}{Z_0} \quad (10.3.5)$ <p><math>Z(d)</math>: slope of an elastic unloading/re-loading  <math>Z_0</math>: initial undamaged slope.</p>
<i>Experimental Identification of the Crack Resistance Function</i>
<p>Crack resistance function</p> $R(d) = R_0 + q \frac{\ln(1-d)}{1-d} \quad (10.3.6)$ <p><math>R_0, q</math>: member dependent parameters</p>
<p>Determination of <math>R_0</math></p> $M_{cr}^2 = \frac{2}{F^0} R_0 \quad (10.3.9)$ <p><math>M_{cr}</math> : first cracking moment</p>
<p>Determination of <math>q</math> and <math>d_u</math>: (solving the system of equations)</p> $2R_0(1-d_u) + q(\ln(1-d_u) + 1) = 0 \quad (10.3.10)$ $M_u^2 = \frac{2(1-d_u)^2}{F^0} R_0 + \frac{2q}{F^0} (1-d_u) \ln(1-d_u) \quad (10.3.11)$

*continued on following page*

**Lumped Damage Mechanics**

Table 2. Continued



continued on following page



Table 2. Continued

<p>Balanced condition point</p> $N_{cr} = \frac{z_{ca}(0.45f'_c + f_t) - h f_t}{h} A_{ts}$ <p>(10.3.17)</p> $M_{cr} = \frac{0.45f'_c + f_t}{h} I_{ts}$
<b>YIELD FUNCTION OF A DAMAGED PLASTIC HINGE</b>
<i>Plastic Deformation Evolution Law</i>
<p>Equivalent moment on a plastic hinge <math>i</math></p> $\bar{m}_i = \frac{m_i}{1 - d_i} \quad (10.4.1)$
<p>Yield function of a damaged plastic hinge:</p> $f_i = \left  \bar{m}_i - c_i \phi_i^p \right  - k_{0i} = \left  \frac{m_i}{1 - d_i} - c_i \phi_i^p \right  - k_{0i} \leq 0 \quad (10.4.2)$ <p><math>c_i, k_{0i}</math>: member dependent parameters</p>
<p>Plastic deformation evolution laws</p> $\begin{cases} d\phi_i^p = 0 \text{ if } f_i < 0 \\ f_i = 0 \text{ if } d\phi_i^p \neq 0 \end{cases} ; \begin{cases} d\phi_j^p = 0 \text{ if } f_j < 0 \\ f_j = 0 \text{ if } d\phi_j^p \neq 0 \end{cases} ; f_j = \left  \frac{m_j}{1 - d_j} - c_j \phi_j^p \right  - k_{0j} \leq 0 \quad (10.4.3)$
<b>Computation of the Parameters <math>c</math> and <math>k_0</math></b>
<p>First plastic moment <math>M_p</math></p> $M_p^2 = \frac{2(1 - d_p)^2}{F^0} R_0 + \frac{2q}{F^0} (1 - d_p) \ln(1 - d_p) \quad (10.4.4)$ <p><math>M_p</math>: first plastic moment.</p> <p><math>d_p</math>: value of damage that corresponds to <math>M_p</math></p>
<p>Effective plastic moment <math>k_0</math></p> $k_0 = \frac{M_p}{1 - d_p} = \bar{M}_p \quad (10.4.5)$
<p>Parameter <math>c</math></p> $c = \frac{1}{\phi_u^p} \left( \frac{M_u}{1 - d_u} - k_0 \right) = \frac{\bar{M}_u - \bar{M}_p}{\phi_u^p} \quad (10.4.6)$ <p><math>\phi_u^p</math>: the ultimate plastic rotation</p>

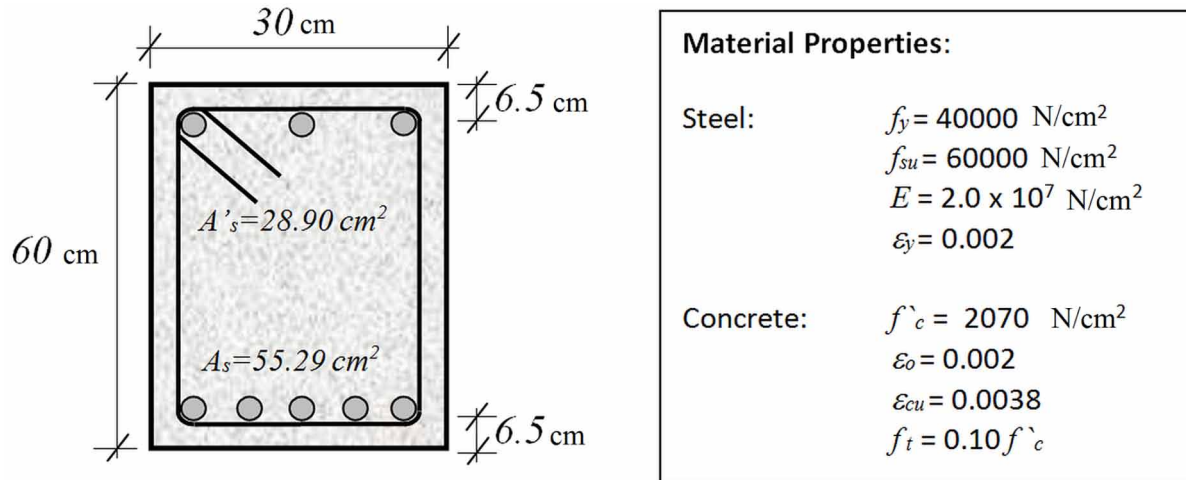
continued on following page

## Lumped Damage Mechanics

Table 2. Continued

A MODEL OF DAMAGE FOR RC ELEMENTS CONSIDERING ULTRA-LOW-CYCLE FATIGUE EFFECTS	
<i>Modified Griffith Criterion</i>	
Griffith criterion during a phase of cracking propagation: if $\Delta d_i > 0; G_i = R(d_i)$ or $G_i^{\alpha+1} = R(d_i)^{\alpha+1}$ for $\alpha \geq 0$ (10.6.1)	
Modified Griffith criterion: $\begin{cases} \Delta d_i = 0 & \text{if } G_i < R_0 \\ \Delta d_i = \frac{1}{\partial R / \partial d_i} \left( \frac{G_i}{R} \right)^\alpha \langle \Delta G_i \rangle_+ & \text{otherwise} \end{cases}$ (10.6.2) $\alpha$ : constant	
ANALYSIS OF DAMAGED FRAMES	
<i>Formulation of the Problem</i>	
Variables to determine: <ul style="list-style-type: none"> <li>• Free displacements,</li> <li>• Reaction forces</li> <li>• Generalized deformations</li> <li>• Plastic rotations</li> <li>• Stresses</li> <li>• Damages</li> </ul>	Data: <ul style="list-style-type: none"> <li>• Initial configuration of the structure</li> <li>• Restricted displacements</li> <li>• Nodal forces</li> <li>• Forces applied over the elements</li> <li>• Material and cross-section properties</li> <li>• Yield functions.</li> </ul>
Equations to verify: (10.7.1) <ul style="list-style-type: none"> <li>• The nonlinear kinematic equation  <math display="block">\{\Delta \Phi\}_b = [\mathbf{B}_E(\mathbf{U}_{t=tr})]_b \{\Delta \mathbf{U}\}</math></li> <li>• The equilibrium equations  <math display="block">\{\mathbf{L}_{t=tr}\} = \{\mathbf{P}_{t=tr}\}; \{\mathbf{L}_{t=tr}\} = \sum_{b=1}^m [\mathbf{B}(\mathbf{U}_{t=tr})_E]_b^t \{\mathbf{M}_{t=tr}\}_b</math></li> <li>• The elasticity law  <math display="block">\{\mathbf{M}\}_b = [\mathbf{E}(\mathbf{D})]_b \{\Phi - \Phi^p\}_b + \{\mathbf{M}_0\}_b</math></li> <li>• The plastic deformation evolution laws  <math display="block">\begin{cases} d\phi_i^p = 0 &amp; \text{if } f_i &lt; 0 \\ f_i = 0 &amp; \text{if } d\phi_i^p \neq 0 \end{cases}; \begin{cases} d\phi_j^p = 0 &amp; \text{if } f_j &lt; 0 \\ f_j = 0 &amp; \text{if } d\phi_j^p \neq 0 \end{cases}</math></li> <li>• The yield functions  <math display="block">f_i = \left  \frac{m_i}{1-d_i} - c_i \phi_i^p \right  - k_{0i} \leq 0; f_j = \left  \frac{m_j}{1-d_j} - c_j \phi_j^p \right  - k_{0j} \leq 0</math></li> <li>• The damage evolution laws  <math display="block">\begin{cases} \Delta d_i = 0 &amp; \text{if } G_i &lt; R_{0i} \\ \Delta d_i = \frac{1}{\partial R_i / \partial d_i} \left( \frac{G_i}{R_i} \right)^2 \langle \Delta G_i \rangle_+ &amp; \text{otherwise} \end{cases}; \begin{cases} \Delta d_j = 0 &amp; \text{if } G_j &lt; R_{0j} \\ \Delta d_j = \frac{1}{\partial R_j / \partial d_j} \left( \frac{G_j}{R_j} \right)^2 \langle \Delta G_j \rangle_+ &amp; \text{otherwise} \end{cases}</math></li> </ul>	

Figure 23. Unconfined typical concrete cross-section



## 10.10 EXAMPLES

### 10.10.1 Determination of the Interaction Diagram of the First Cracking Moment for the Following Cross-Section

For the first cracking moment, four points corresponding to the pure compression, pure tension, pure bending and balanced conditions are computed.

1. For the case of pure compression, it is used Equation (10.3.12):  $N_{cr} = -A_{ts} * 0.45 f'_c$ . Thus,

$$A_{ts} = bh + (n - 1)(A'_s + A_s) \Rightarrow n = \frac{E_s}{E_c} \quad (10.10.1)$$

$$E_c = \frac{f'_c}{\epsilon_o} = \frac{2070}{0.002} = 1035000 \text{ N/cm}^2 \Rightarrow n = \frac{E_s}{E_c} = 19.3237 \quad (10.10.2)$$

$$A_{ts} = bh + (n - 1)(A'_s + A_s) = (30)60 + (19.3237 - 1)(28.90 + 55.29) = 3342.67 \text{ cm}^2 \quad (10.10.3)$$

$$N_{cr} = -A_{ts} * 0.45 * f'_c = -3342.67 * 0.45 * 2070 = -3113.697 \times 10^3 \text{ N} = -3113.697 \text{ KN} \quad (10.10.4)$$

### Lumped Damage Mechanics

2. For the case of pure tension it is used Equation (10.3.13):

$$N_{cr} = A_{ts} * f_t = 3342.67 * 207 = 691.933 \times 10^3 \text{ N} = 691.933 \text{ KN} \quad (10.10.5)$$

3. For pure bending, the first cracking moment is computed using Equation (10.3.14)

$$z_{ca} = \frac{\frac{bh^2}{2} + (n-1)A'_s(h - rec) + (n-1)A_s(rec)}{A_{ts}};$$

$$z_{ca} = \frac{\frac{30 * 60^2}{2} + (19.3237 - 1) * 28.90 * (60 - 6.5) + (19.3237 - 1) * 55.29 * 6.5}{3342.67} = 26.6004 \text{ cm} \quad (10.10.6)$$

$$I_{ts} = \frac{bh^3}{12} + bh\left(\frac{h}{2} - z_{ca}\right)^2 + (n-1)A'_s(h - rec - z_{ca})^2 + (n-1)A_s(z_{ca} - rec)^2;$$

$$I_{ts} = \frac{30 * 60^3}{12} + 30 * 60 * \left(\frac{60}{2} - 26.6004\right)^2 + (19.3237 - 1) * 28.90 * (60 - 6.5 - 26.6004)^2 + (19.3237 - 1) * 55.29 * (26.6004 - 6.5)^2 = 1353308 \text{ cm}^4 \quad (10.10.7)$$

$$M_{cr} = \frac{f_t I_{ts}}{z_{ca}} = \frac{207 * 135308}{26.6004} = 10531223.44 \text{ N.cm} = 105.312 \text{ KN.m} \quad (10.10.8)$$

4. For the balanced condition, the axial force and bending moment are obtaining using Equation (10.3.17):

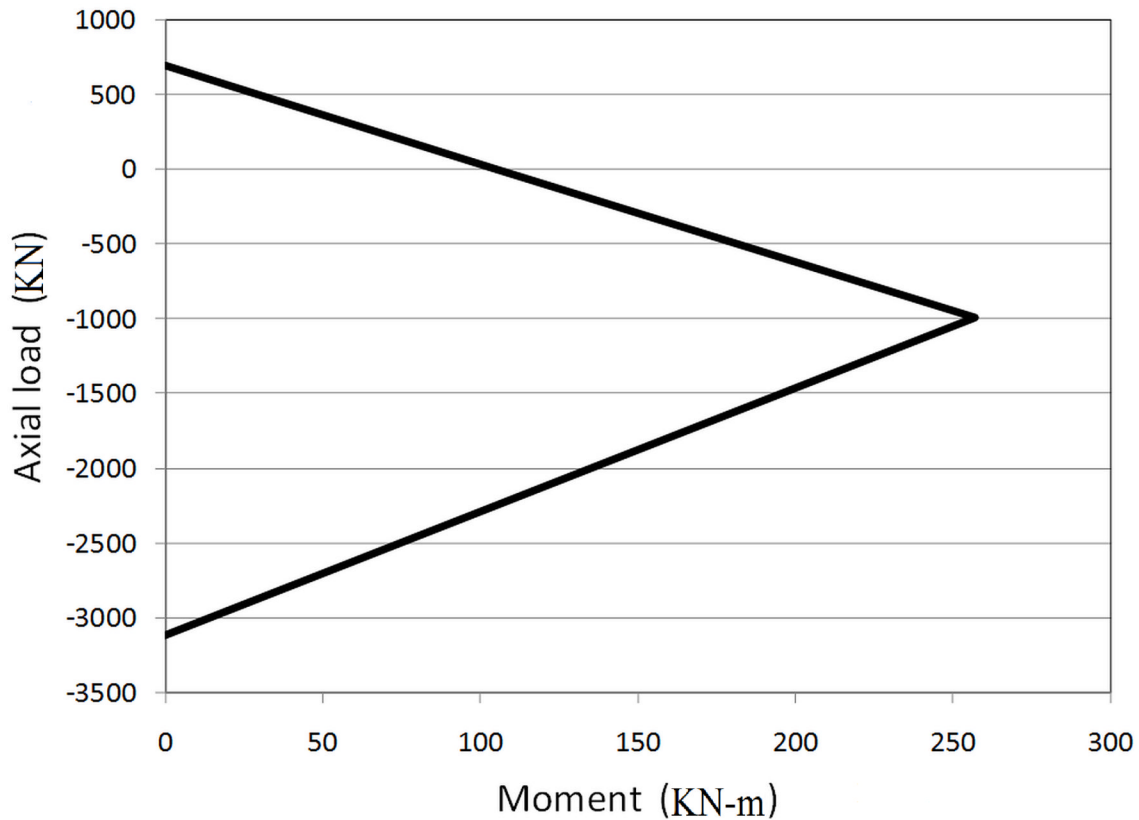
$$P_{cr} = -\frac{z_{ca}(0.45f'_c + f_t) - hf_t}{h} A_{ts}$$

$$= -\frac{26.6004 * (0.45 * 2070 + 207) - 60 * 207}{60} 3342.67 = -995255.22 \text{ N} = -995.26 \text{ KN} \quad (10.10.9)$$

$$M_{cr} = \frac{0.45 * f'_c + f_t}{h} I_{ts} = \frac{0.45 * 2070 + 207}{60} 1353308 = 25670019.3 \text{ N.cm} = 256.79 \text{ KN.m} \quad (10.10.10)$$

The resulting interaction diagram is shown in Figure 24.

Figure 24. Interaction diagram of the first cracking moment



### 10.10.2 Obtain the Equations for the Numerical Simulation Presented in Figure 11a

The numerical simulation corresponds to the cantilever beam that in Figure 10. The element is subjected to a history of mono-sign lateral force.

The problem is simulated using the elasto-plastic constitutive model with a multi-linear isotropic hardening that is described in section 7.1.

The section properties  $M_p$ ,  $M_u$  and  $\phi_u^p$  are obtained from the experimental curve presented in Figure 11a.

Using kinematic equation (3.1.12),  $\{d\Phi\} = [\mathbf{B}(q)]\{dq\}$ , it is obtained:

**Lumped Damage Mechanics**

$$\begin{bmatrix} \phi_1 \\ \phi_2 \\ \delta \end{bmatrix} = \begin{bmatrix} 1/L_b & 0 & 1 & -1/L_b & 0 & 0 \\ 1/L_b & 0 & 0 & -1/L_b & 0 & 1 \\ 0 & -1 & 0 & 0 & 1 & 0 \end{bmatrix} \begin{bmatrix} 0 \\ 0 \\ 0 \\ u_2 \\ \omega_2 \\ \theta_2 \end{bmatrix} \quad (10.10.11)$$

Resulting:

$$\phi_1 = -\frac{u_2}{L_b}; \phi_2 = -\frac{u_2}{L_b} + \theta_2; \delta = \omega_2 \quad (10.10.12)$$

Applying the equilibrium equation (3.2.13),  $\sum_{b=1}^m [\mathbf{B}_E^0]^t \{\mathbf{M}\}_b = \{\mathbf{P}\}$ , it is obtained:

$$\begin{bmatrix} P_{u1} \\ P_{w1} \\ P_{\theta1} \\ P_{u2} = P \\ P_{w2} = 0 \\ P_{\theta2} = 0 \end{bmatrix} = \begin{bmatrix} 1/L_b & 1/L_b & 0 \\ 0 & 0 & -1 \\ 1 & 0 & 0 \\ -1/L_b & -1/L_b & 0 \\ 0 & 0 & 1 \\ 0 & 1 & 0 \end{bmatrix} \begin{bmatrix} m_1 \\ m_2 \\ n \end{bmatrix} \quad (10.10.13)$$

That is:

$$\begin{aligned} P_{w2} = 0 = n; P_{\theta2} = 0 = m_2; P_{u2} = P = -\frac{m_1}{L_b}; \\ P_{u1} = -\frac{m_1}{L_b} + \frac{m_2}{L_b} = -\frac{m_1}{L_b}; P_{w1} = -n = 0; P_{\theta1} = m_1 \end{aligned} \quad (10.10.14)$$

The elasticity law for the elasto-plastic element is:

$$\begin{bmatrix} \phi_1 \\ \phi_2 \\ \delta \end{bmatrix} = \begin{bmatrix} \frac{L_b}{3EI_b} & -\frac{L_b}{6EI_b} & 0 \\ -\frac{L_b}{6EI_b} & \frac{L_b}{3EI_b} & 0 \\ 0 & 0 & \frac{L_b}{AE_b} \end{bmatrix} \begin{bmatrix} m_1 \\ m_2 \\ n \end{bmatrix} + \begin{bmatrix} \phi_1^p \\ \phi_2^p \\ \delta^p \end{bmatrix} \quad (10.10.15)$$

Resulting:

$$\phi_1 = \frac{L_b}{3EI_b} m_1 + \phi_1^p \quad (10.10.16)$$

Introducing (10.10.12a) and (10.10.14c) into (10.10.16) it is obtained a relation between the force  $P$  and the lateral displacement  $t$ :

$$P = Z_0(t - t_p); \text{ where } Z_0 = \frac{3EI_b}{L_b^3}; t = u_2; \phi_i^p = -\frac{t_p}{L_b} \quad (10.10.17)$$

In the plastic phase of the element behavior, the plastic rotation evolution law gives:

$$\begin{cases} P = \frac{M_u - M_p}{\phi_u^p} \frac{t_p}{L^2} - \frac{M_p}{L^2} \text{ if } P < \frac{M_u}{L} \\ P = \frac{M_p}{L} \text{ otherwise} \end{cases} \quad (10.10.18)$$

Combination of Equation (10.10.17-18) gives:

$$P = \frac{Z_0(M_u - M_p)}{L_b^2 Z_0 \phi_u^p + M_u - M_p} t + \frac{Z_0 M_p L_b \phi_u^p}{L_b^2 Z_0 \phi_u^p + M_u - M_p} \quad (10.10.19)$$

Plotting this equation it is obtained the curve:

### 10.10.3 Plot the Curve Force vs. Displacement Using the Damage Model for the Cantilever Beam that is Shown in Figure 10 and a Spreadsheet

The first step is the computation of the model parameters  $R_0$ ,  $q$ ,  $c$  and  $k_0$  using the procedures described in sections 10.3.3 and 10.4.2. Considering the experimental values:  $EI = 1025.373$  KN.m<sup>2</sup>,  $M_{cr} = 4.004$  KN.m,  $M_p = 24.220$  KN.m,  $M_u = 29.034$  KN.m and  $\varphi_u^p = 0.09$ , the parameters  $R_0 = 0.003648$ ,  $q = -0.52$ ,  $c = 459.31$  and  $k_0 = 34.88$  were obtained.

The analysis starts assuming several damage values between 0 and a value slightly higher than  $d_u \approx 0.64$ . With these damage values, the bending moment  $m_1$  is computed with the Griffith criterion (10.3.8) (see Table 3).

$$m_1^2 = \frac{2(1 - d_1)^2}{F^0} R_0 + \frac{2q}{F^0} (1 - d_1) \ln(1 - d_1) \quad (10.10.20)$$

### Lumped Damage Mechanics

Table 3. Force vs. displacement curve values in the case of imposed damage values

$d_1$	$m_1$ (KN m)	$\phi_1^p$	$\phi_1$	$t$ (m)	$P$ (KN)
0.00	0.0000	0.0000	0.0000	0.0000	0.0000
0.00	4.0039	0.0000	0.0018	0.0026	2.8599
0.05	11.2169	0.0000	0.0054	0.0075	8.0121
0.10	15.1548	0.0000	0.0077	0.0107	10.8249
0.15	18.0901	0.0000	0.0097	0.0136	12.9215
0.20	20.4496	0.0000	0.0116	0.0163	14.6069
0.25	22.4066	0.0000	0.0136	0.0190	16.0047
0.30	24.0496	0.0000	0.0156	0.0219	17.1783
0.35	25.4288	0.0092	0.0270	0.0379	18.1634
0.40	26.5734	0.0205	0.0406	0.0569	18.9810
0.45	27.4994	0.0329	0.0557	0.0779	19.6424
0.50	28.2129	0.0469	0.0726	0.1016	20.1521
0.55	28.7115	0.0630	0.0920	0.1288	20.5082
0.60	28.9844	0.0818	0.1148	0.1607	20.7031
0.65	29.0103	0.1045	0.1422	0.1991	20.7217

The damage values and the corresponding bending moments are used to compute the plastic rotation with the yield function (10.4.2):  $f_1 = \left| \bar{m}_1 - c\phi_1^p \right| - k_0 = \left| \frac{m_1}{1-d_1} - c\phi_1^p \right| - k_0 \leq 0$ .

Then, the total deformations are determined with the elasticity law (Equation 10.1.4):

$$\phi_1 = \frac{L_b}{3EI_b} \frac{m_1}{(1-d_1)} + \phi_1^p \quad (10.10.21)$$

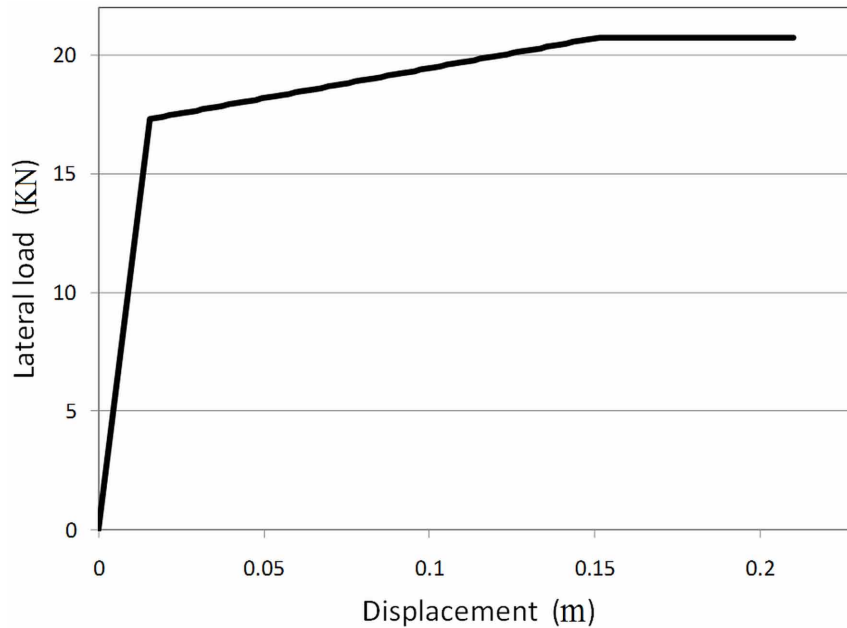
The displacement in the node 2 is computed with the kinematic Equation (3.1.1):

$$\phi_1 = -\frac{t}{L_b} \text{ for } t = u_2 \quad (10.10.22)$$

Finally the force  $P$  is obtained with the equilibrium Equation (3.2.13):



Figure 25. Force vs. displacement curve



$$P = -\frac{m_1}{L_b} \quad (10.10.23)$$

The resulting curve is shown in Figure 26.

#### 10.10.4 Solve Problem 10.10.3 Imposing Forces Instead of Damage

The values of force are increased until the ultimate moment is reached. Using the equilibrium Equation (3.2.13), the bending moment is computed as:

$$m_1 = -PL_b \quad (10.10.24)$$

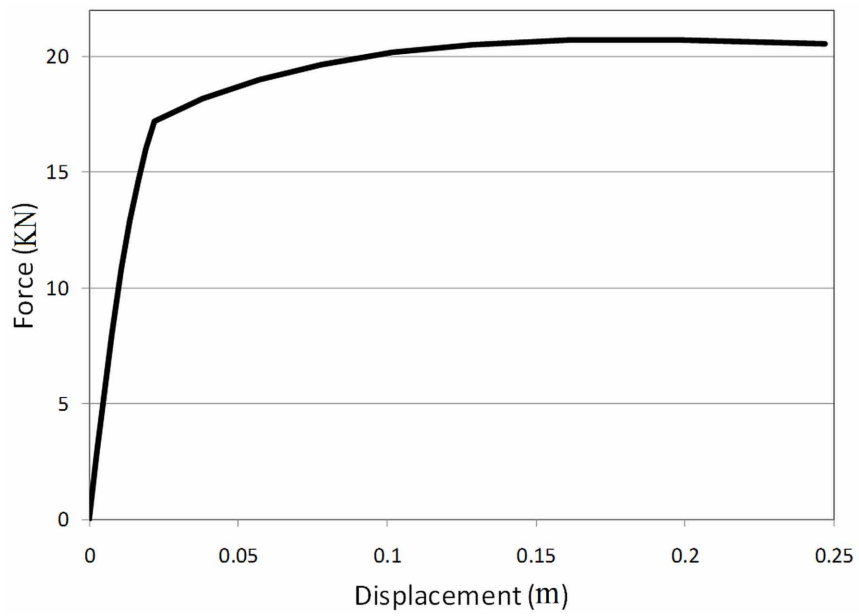
With the Griffith criterion (Equation 10.3.8), the corresponding damage values are obtained:

$$\frac{F^0 m_1^2}{2(1-d_1)^2} = R_0 + q \frac{\ln(1-d_1)}{1-d_1} \quad (10.10.25)$$

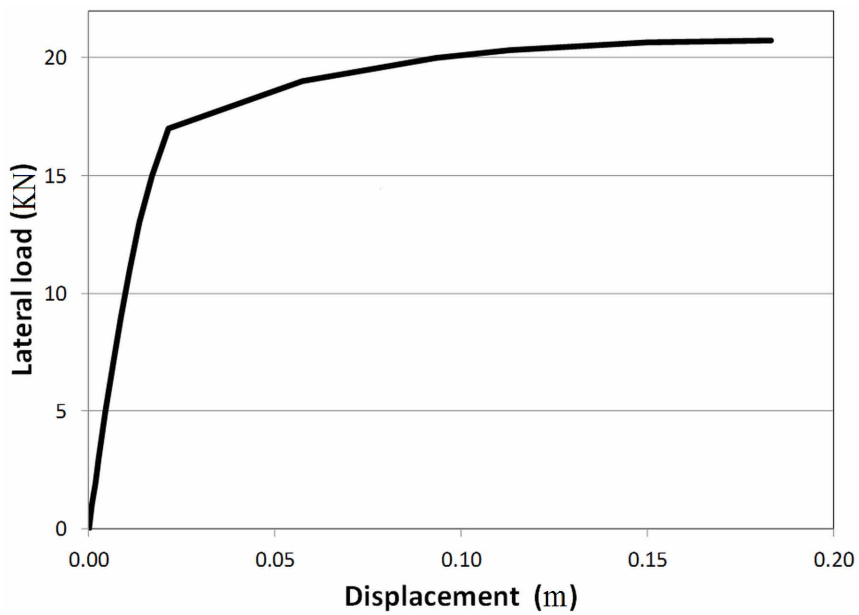
As in the former example, the plastic deformation is computed with the yield function (Equation 10.4.2), the total deformations with the elasticity law (Equation 10.1.4) and the displacement at the node 2 with the kinematic Equation (3.1.1). The resultant curve of force vs. displacement is shown in Figure 27.

**Lumped Damage Mechanics**

*Figure 26. Force vs. displacement curve*



*Figure 27. Force vs. displacement curve*



### 10.10.5 Develop a Model for a Frame Member Made out of a Brittle Material without Plastic Deformation

In this case the elasticity law is written as:

$$\{\Phi\}_b = [\mathbf{F}(\mathbf{D})]_b \{\mathbf{M}\}_b + \{\Phi^0\}_b \quad (10.10.26)$$

where  $[\mathbf{F}(\mathbf{D})]$  is the flexibility matrix of a damaged frame member (Equation 10.1.4),  $\{\mathbf{M}\}_b$  and  $\{\Phi^0\}_b$  are the generalized stresses and the initial deformations such as defined in chapter 3 (Equation 3.2.2 and Table 3).

As it can be observed, this equation do not consider the plastic deformation term. Therefore, no yield function is needed.

The Griffith criterion ( $G(d) = R(d)$ ) can be used as damage evolution law. The energy release rates  $G_i$  and  $G_j$  can be written like in Equation (10.2.2) and the crack resistance is a function of damage  $R(d)$ . Therefore, damage evolution is express as in Equation (10.2.3).

Therefore, a model for a frame member made out of a brittle material is composed by:

1. **The Kinematic Equation:**  $\{\Phi\}_b = [\mathbf{B}_E^0]_b \{\mathbf{U}\}$
2. **The Equilibrium Equation:**

$$\sum_{b=1}^m [\mathbf{B}_E^0]_b^t \{\mathbf{M}\}_b = \{\mathbf{P}^n\} + \{\mathbf{P}^{eq}\} \quad (10.10.27)$$

3. **The Constitutive Equation:**  $\{\Phi\}_b = [\mathbf{F}(\mathbf{D})]_b \{\mathbf{M}\}_b + \{\Phi^0\}_b$
4. **Damage Evolution Laws:**

$$\begin{cases} \Delta d_i = 0 & \text{if } G_i < R_i \\ G_i = R_i & \text{if } \Delta d_i > 0 \end{cases};$$

$$\begin{cases} \Delta d_j = 0 & \text{if } G_j < R_j \\ G_j = R_j & \text{if } \Delta d_j > 0 \end{cases}$$

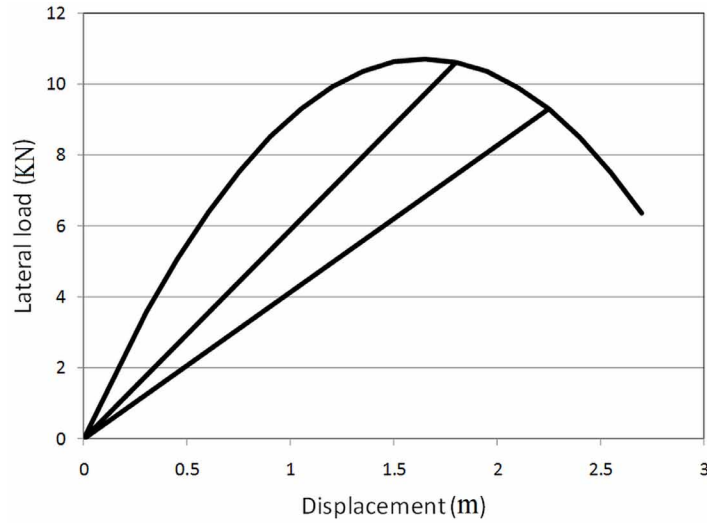
### 10.10.6 Obtain a Crack Resistance Function for the Model of the Example 10.10.4 so that there is a Parabolic Relationship between Moment and Damage as Shown in Figure 28

In order to obtain a parabolic relationship between moment and damage, it is proposed the following equation:

$$M = a + b * d + c * d^2 \quad (10.10.28)$$

## Lumped Damage Mechanics

Figure 28. Lateral load vs. displacement curve



where  $a$ ,  $b$  and  $c$  are parameters that are computed with the element properties  $M_{cr}$  and  $M_u$ , by the consideration of the following conditions:

1. For  $M = M_{cr}, d = 0$
2. For

$$M = M_u, d = d_u \quad (10.10.29)$$

3. For  $M = M_u; \frac{dM}{dd} = 0$
4. For  $d = 1, M = 0$

The resultant expressions of the parameters are:

$$a = M_{cr}; b = -2 \left( M_{cr} - M_u - \sqrt{M_u (M_u - M_{cr})} \right); \quad (10.10.30)$$

$$c = M_{cr} - 2M_u - 2\sqrt{M_u (M_u - M_{cr})}; du = \frac{-b}{2c} = \frac{M_{cr} - M_u + \sqrt{M_u (M_u - M_{cr})}}{M_{cr} - 2M_u + 2\sqrt{M_u (M_u - M_{cr})}}$$

Applying the Griffith criterion, the crack resistant function results in:

$$R(d) = \frac{1}{2} \frac{(a + b * d + c * d^2)^2 * F^0}{(1 - d)^2} \quad (10.10.31)$$

The curve of force vs. displacement for a cantilever beam element made out of a brittle material with  $M_{cr} = 3.92 \text{ KNm}$ ,  $L = 1 \text{ m}$ ,  $EI = 5.23 \text{ KNm}^2$  and  $M_u = 11.77 \text{ KNm}$ , is:

**10.10.7 Plot the Curve Force vs. Displacement Using the Damage Model of Section 10.6 for the Cantilever Beam That Is Shown in Figure 29a and a Spreadsheet. Consider  $\alpha$  Values of 2, 0.5 and 10.**

For this problem were chosen the parameters:  $R_0 = 0.003648$ ,  $q = -0.52$ ,  $c = 459.31$  and  $k_0 = 34.88$ , computed from experimental results (section 10.10.3). The beam is subjected to the displacement history that is shown in Figure 29b. The analysis is done considering three phases: the first one, where the beam is subjected to a monotonic displacement; the second one where the specimen is unloaded and the last phase where the beam is reloaded to the same displacement of the first step. In order to observe the ultra-low cycle fatigue effect, the second and third phases are repeated several times. The procedure used for the computation of the first cycle considering  $\alpha = 2$  is described below and the values needed for the curve of force vs. displacement are presented in Table 4.

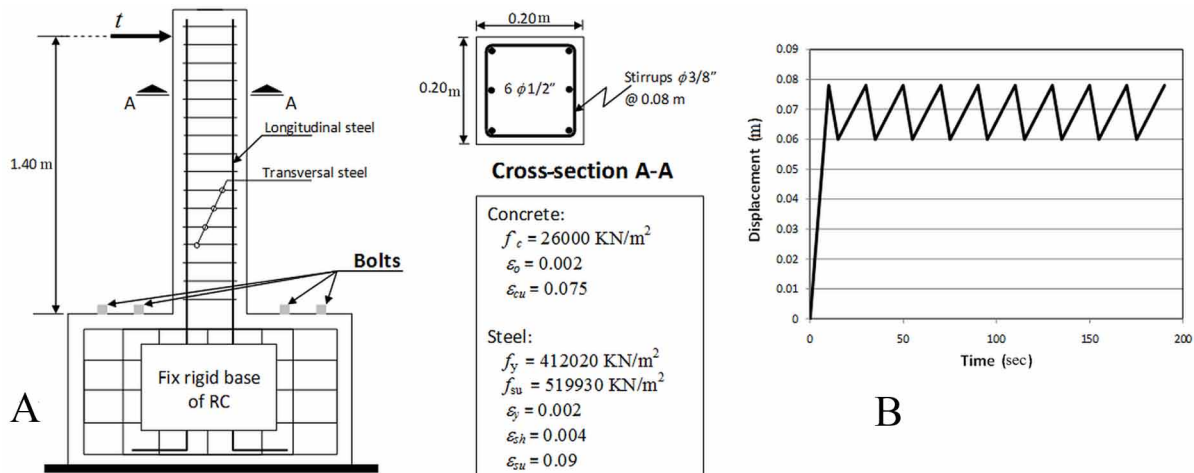
The monotonic phase is solved in the same way that the problem 10.10.3. Then an elastic unload is applied (phase 2). In this stage, the damage value and the plastic rotation remain constant and a displacement equal to 0.06 is imposed (see displacement history). The total deformation is computed by the kinematic equation (10.10.22):

$$\phi_1 = -\frac{t}{L_b}$$

for  $t = u_2$  and the bending moment with the elasticity law (10.10.21):

$$m_1 = (\phi_1 - \phi_1^p) \frac{3EI_b}{L_b} (1 - d_1).$$

Figure 29. a) Beam subjected to ultra-low cycle fatigue analysis b) Displacement history



### Lumped Damage Mechanics

Table 4. Force vs. displacement curve values in the case of imposed forces

P (KN)	$m_1$ (KN m)	$d_1$	$\phi_1^p$	$\phi_1$	$t$ (m)
0.0000	0.0000	0.00	0.0000	0.0000	0.0000
1.0000	1.4000	0.00	0.0000	0.0006	0.0009
2.0000	2.8000	0.00	0.0000	0.0013	0.0018
3.0000	4.2000	0.00	0.0000	0.0019	0.0027
5.0000	7.0000	0.01	0.0000	0.0032	0.0045
7.0000	9.8000	0.04	0.0000	0.0046	0.0065
9.0000	12.6000	0.07	0.0000	0.0061	0.0086
11.0000	15.4000	0.10	0.0000	0.0078	0.0109
13.0000	18.2000	0.15	0.0000	0.0098	0.0137
15.0000	21.0000	0.21	0.0000	0.0121	0.0170
17.0000	23.8000	0.29	0.0000	0.0153	0.0214
19.0000	26.6000	0.40	0.0208	0.0410	0.0574
20.0000	28.0000	0.48	0.0420	0.0667	0.0934
20.3300	28.4620	0.52	0.0537	0.0808	0.1131
20.6600	28.9240	0.58	0.0753	0.1069	0.1497
20.7387	29.0342	0.63	0.0950	0.1307	0.1830

Finally the force  $P$  is obtained with the equilibrium equation (10.10.23):

$$P = -\frac{m_1}{L_b}.$$

In the last phase of the first cycle, the displacement is increased from 0.06 to 0.078 m in three steps. The total deformation and the bending moment are computed again, respectively, with the kinematic equation (10.10.22) and elasticity law (10.10.21). The damage is computed with the modified Griffith criterion (10.6.2) (See Table 5):

$$\Delta d_i = \frac{1}{\partial R / \partial d_i} \left( \frac{G_i}{R} \right)^\alpha \langle \Delta G_i \rangle_+.$$

*Table 5. First cycle of the curve of force vs. displacement values considering ultra-low cycle fatigue with  $\alpha = 2$*

$d_1$	$m_1$ (KN m)	$\phi_1^p$	$\phi_1$	$t$ (m)	$P$ (KN)	Phase
0.000	0.000	0.000	0.000	0.000	0.000	1
0.000	4.004	0.000	0.002	0.003	2.860	1
0.050	11.218	0.000	0.005	0.008	8.013	1
0.100	15.156	0.000	0.008	0.011	10.826	1
0.150	18.092	0.000	0.010	0.014	12.923	1
0.200	20.452	0.000	0.012	0.016	14.608	1
0.250	22.409	0.000	0.014	0.019	16.006	1
0.300	24.052	0.000	0.016	0.022	17.180	1
0.350	25.431	0.009	0.027	0.038	18.165	1
0.400	26.576	0.020	0.041	0.057	18.983	1
0.450	27.502	0.033	0.056	0.078	19.644	1
0.450	11.964	0.033	0.043	0.060	8.546	2
0.456	16.965	0.033	0.047	0.066	12.118	3
0.473	21.385	0.033	0.051	0.072	15.275	3
0.505	24.764	0.033	0.056	0.078	17.689	3

Another eight cycles were computed following the described procedure and the resultant force vs. displacement curve is shown in Figure 30. As it can be observe, even if the maximum displacement is kept constant, there is evolution of the damage.

The curve of force vs. displacement corresponding, respectively, to  $\alpha = 0.5$  and  $\alpha = 10$ , are presented in Figure 31a and b.

Notice that the lower values of the parameter  $\alpha$  accelerates the strength degradation.

## **10.11 PROBLEMS**

**10.11.1 For the Structure Shown in Figure 32 Compute the Properties of the Cross-Section and Carry out the Numerical Simulation. Neglect the Influence of the Axial Load.**

## Lumped Damage Mechanics

Figure 30. Force vs. displacement curve for  $\alpha = 2$

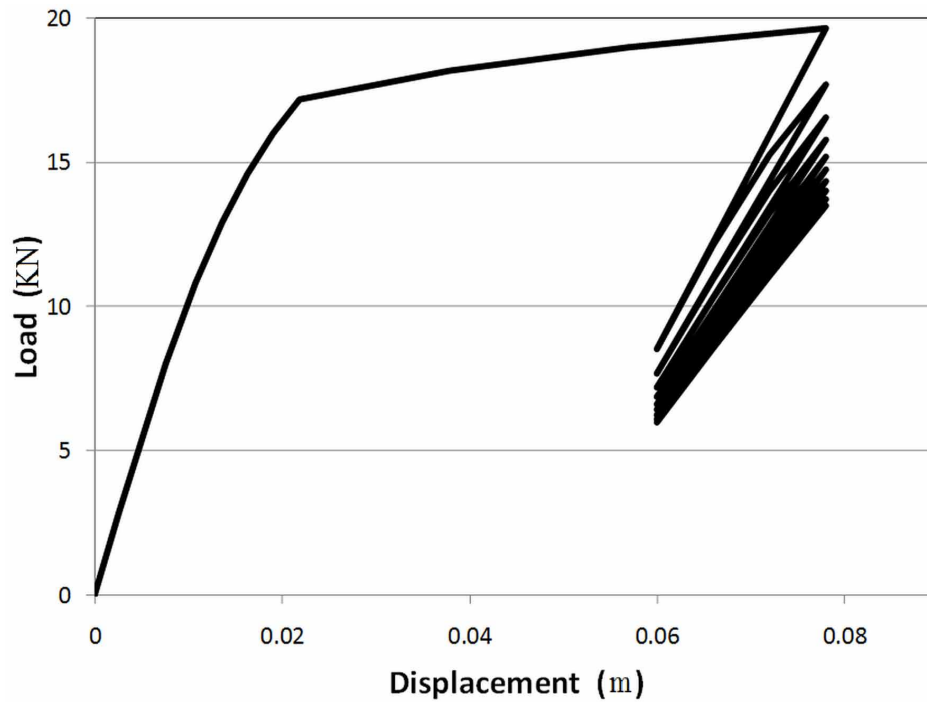
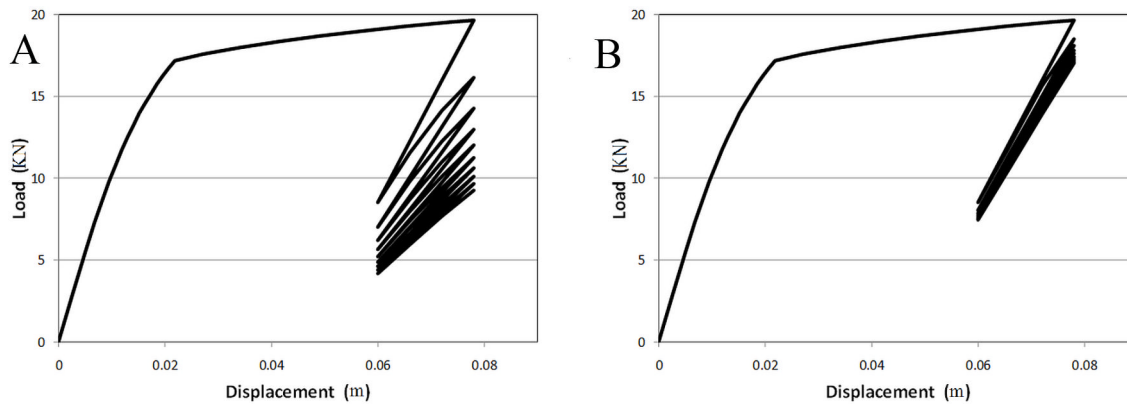


Figure 31. Force vs. displacement curves for a)  $\alpha = 0.5$  b)  $\alpha = 10$



## 10.12 PROJECTS

**10.12.1 Write a Program for the Analysis of RC Elements Using the Lumped Damage Model. i.e.**

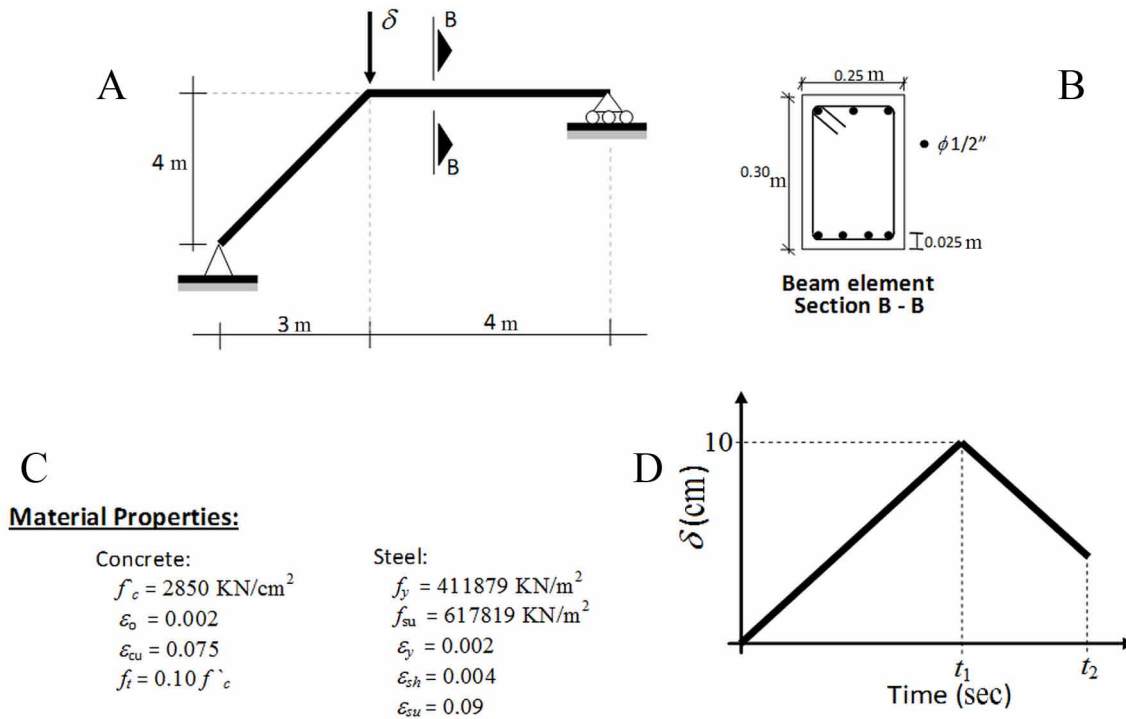
**Generalize the Program Written in Project 8.7.2 including Damage Effects**

**10.12.2 Include the Ultra-Low Cycle Fatigue Effects in the Project 10.12.1**

**10.12.3 Generalize the Program Written in Project 8.7.3 including Damage Effects**



Figure 32. a) Geometry of the structure b) Cross-section c) Material properties d) Displacement history



## REFERENCES

- Alarcón, E., Recuero, A., Perera, R., López, C., Gutiérrez, J. P., & De Diego, A. et al. (2001). A reparability index for reinforced concrete members based on fracture mechanics. *Engineering Structures*, 23(6), 687–697. doi:10.1016/S0141-0296(00)00075-4
- Alva, G. M. S., & El Debs, A. L. H. C. (2010). Application of lumped dissipation model in nonlinear analysis of reinforced concrete structures. *Engineering Structures*, 32(4), 974–981. doi:10.1016/j.eng-struct.2009.12.024
- Araujo, F., & Proença, S. P. B. (2008). Application of a lumped dissipation model to reinforced concrete structures with the consideration of residual strains and cycles of hysteresis. *Journal of Mechanics of Materials and Structures*, 3(5), 1011–1031. doi:10.2140/jomms.2008.3.1011
- Avon, D. T., Marante, M. E., & Flórez-López, J. (2002). El doble paso de INTEGRACIÓN: Un algoritmo computacional para mejorar la convergencia en problemas altamente no lineales. In *Proceedings of the Conference CIMENICS, Numerical Methods in Engineering and Applied Sciences (TM1-TM8)*. Caracas, Venezuela: SVMNI.
- Cipollina, A., López-Inojosa, A., & Flórez-López, J. (1995). A simplified damage mechanics approach to nonlinear analysis of frames. *Computers & Structures*, 54(6), 1113–1126. doi:10.1016/0045-7949(94)00394-I

### **Lumped Damage Mechanics**

- Colombo, A., & Negro, P. (2005). A damage index of generalized applicability. *Engineering Structures*, 27(8), 1164–1174. doi:10.1016/j.engstruct.2005.02.014
- Cosenza, E., & Manfredi, G. (2000). Damage indices and damage measures. *Progress in Structural Engineering and Materials*, 2(1), 50–59. doi:10.1002/(SICI)1528-2716(200001/03)2:1<50::AID-PSE7>3.0.CO;2-S
- Faleiro, J., Oller, S., & Barbat, A. H. (2010). Plastic-damage analysis of reinforced concrete frames. *Engineering Computations*, 27(1), 57–83. doi:10.1108/02644401011008522
- Kappos, A. J. (1997). Seismic damage indices for RC buildings: Evaluation of concepts and procedures. *Progress in Structural Engineering and Materials*, 1(1), 78–87. doi:10.1002/pse.2260010113
- Lemaitre, J., & Chaboche, J. L. (1985). *Mécanique des matériaux solides*. Paris, France: Dunod Bordas.
- Liu, Y. B., & Liu, J. B. (2004). A damage beam element model for nonlinear analysis of reinforced concrete member. *Earthquake Engineering and Engineering Vibration-Chinese Edition*, 24(2), 95-100.
- Marante, M. E., & Flórez-López, J. (2003). Three dimensional analysis of reinforced concrete frames based on lumped damage mechanics. *International Journal of Solids and Structures*, 40(19), 5109–5123. doi:10.1016/S0020-7683(03)00258-0
- Padilla, D., & Rodriguez, M. (2009). A damage index for the seismic analysis of reinforced concrete members. *Journal of Earthquake Engineering*, 13(3), 364–383. doi:10.1080/13632460802597893
- Park, Y. J., & Ang, A. H. S. (1985). Mechanistic seismic damage model for reinforced concrete. *Journal of Structural Engineering*, 111(4), 722–739. doi:10.1061/(ASCE)0733-9445(1985)111:4(722)
- Rajasankar, J., Iyer, N. R., & Prasad, A. P. (2009). Modelling inelastic hinges using CDM for nonlinear analysis of reinforced concrete frame structures. *Computers and Concrete*, 6(4), 319–341. doi:10.12989/cac.2009.6.4.319
- Shi, Z. (2009). *Crack analysis in structural concrete: Theory and applications*. Burlington, MA: Butterworth-Heinemann.
- Sinha, R., & Shiradhonkar, S. R. (2012). Seismic damage index for classification of structural damage – Closing the loop. In *Proceedings of the 15th World Conference on Earthquake Engineering*. Lisboa, Portugal: Academic Press.
- Tang, X. S., Zhang, J. R., Li, C. X., Xu, F. H., & Pan, J. (2005). Damage analysis and numerical simulation for failure process of a reinforced concrete arch structure. *Computers & Structures*, 83(31), 2609–2631. doi:10.1016/j.compstruc.2005.03.017
- Yang, T. S., & Wang, J. L. (2010). Damage analysis of three-dimensional frame structure suffering from impact. *Journal of Vibration and Shock*, 29(12), 177–180.
- Williams, M. S., & Sexsmith, R. G. (1995). Seismic damage indices for concrete structures: A state-of-the-art. *Earthquake Spectra*, 11(2), 740–757. doi:10.1193/1.1585817

# Chapter 11

## Damage Mechanics of Dual Systems

### ABSTRACT

*This chapter begins with the presentation of some experimental results on RC specimens using a special technique called “digital image correlation.” Then, it describes a damage model for RC walls. Next, the model is generalized to include elements with any aspect ratio; finally, the analysis of dual system is described and some numerical simulations are presented. Notice that Section 3.4 described the elastic behavior of dual systems; in section 7.3 that model was extended to include plastic deformations. The goal of this chapter is to generalize that model, including cracking propagation described by the Griffith criterion or its modified version.*

### 11.1 EXPERIMENTAL ANALYSIS OF RC ELEMENTS OF VARIOUS ASPECT RATIOS

Dual systems are reinforced concrete structures composed by slender elements and walls. These systems are often used as a good structural alternative for buildings and facilities in earthquake-prone areas. Even in framed structures, short or intermediate columns and beams and, in general, RC elements of any aspect ratio may appear as a result of inadequate disposition of masonry walls or other non-structural components (see Figure 1).

#### 11.1.1 Digital Image Correlation

In the digital image correlation technique (DIC), the surface of the specimen to be tested is prepared in order to create a random texture. A first digital photo of reference is taken before the test (see Figure 2a). Next, further pictures are taking during the experiment while the chosen external forces are applied (see Figure 2b). A computer program analyzes first the reference digital image; the software divides this photo in small portions that may be imagined as small “finger prints”; subsequently, it identifies each

DOI: 10.4018/978-1-4666-6379-4.ch011

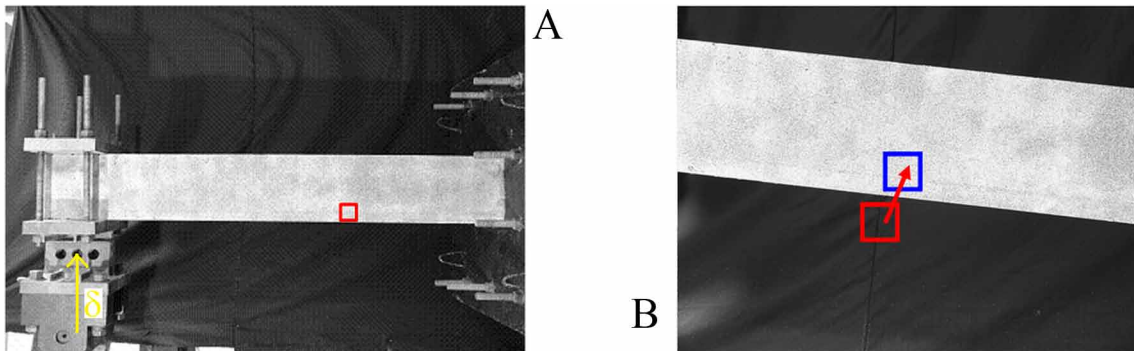
## Damage Mechanics of Dual Systems

Figure 1. Failure of a short column in a RC structure (Courtesy of Dr. Jürg Hammer, DRM Disaster Risk Management Switzerland SA)

11.1 Hammer, J. (2001). Retrieved February 28, 2014 from [http://www.drmonline.net/drmlibrary/peru\\_photos.htm](http://www.drmonline.net/drmlibrary/peru_photos.htm) DRM Disaster Risk Management Switzerland SA.



Figure 2. Representation of a displacement measurement with DIC a) Reference picture b) Deformed configuration



of them. Then, the program processes the following picture, looking for the same “finger prints” and determines their new position in the photo. This procedure gives the average displacement vector of each specific portion. The same procedure is followed sequentially with each digital photograph of the test.

With the displacements, the program computes the strain field using the conventional expressions. Cracks in the concrete appear as concentrations of strains.

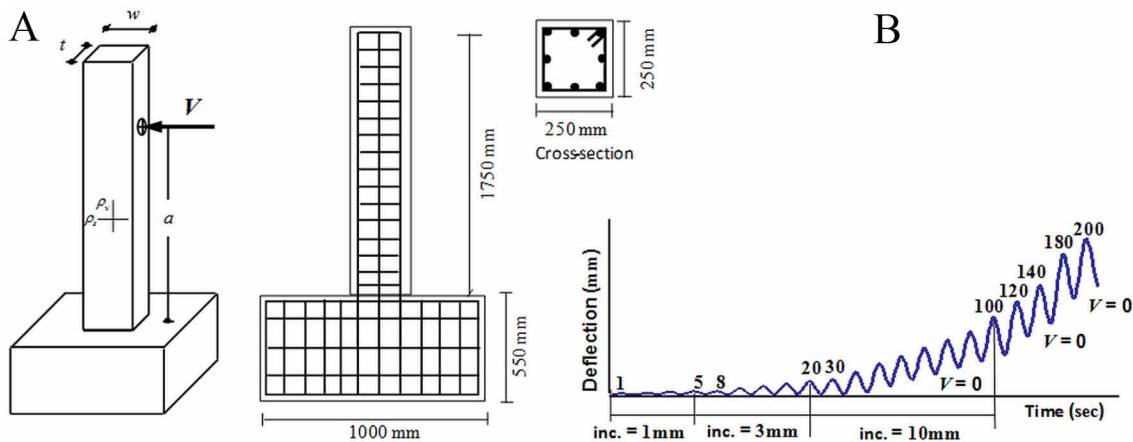
### 11.1.2 Experimental Analysis of Beams with Different Aspect Ratios

Four specimens that represent RC beams in cantilever with different aspect ratios are shown in Figure 3a and Table 1. The variation of the aspect ratio is achieved changing the height of the applied lateral force. The specimen labeled B4 in Figure 4 is a slender beam with an aspect ratio of 7.11 (see Figure 13 in Chapter 2 for a classification of beams in terms of the aspect ratio); the specimen B1 is a very short beam (aspect ratio 1.78); the specimens B2 and B3 represent intermediate beams with, respectively, aspect ratios of 3.56 and 5.36. The specimens are subjected to the mono-sign solicitation that is shown in Figure 3b. Figure 4 presents the results of the tests that show the variation of the cracking patterns and of the quantity of diagonal tension by shear with the aspect ratio.

Horizontal cracks in the lowest part of the specimens can be appreciated in the four beams. They are called flexural cracks because are located in the zone of the maximum bending moment. Diagonal cracks along the entire element appear in specimens B1 and B2. They are called diagonal tension cracks or shear cracks and are the result of the shear forces that in these tests are constant along the elements. Notice that DIC not only indicates the appearance of each kind of cracks but also indicates its intensity.

In slender beams, for instance specimen B4, only flexural cracks are concentrated in the plastic hinge zone. In squat beams, for instance specimen B1, diagonal tension cracks along the entire element are dominant. Notice that intermediate beams exhibit mixed cracking patterns. The transition from flexural dominant to shear dominant cracking with the aspect ratio appears to be progressive.

Figure 3. RC beam a) Geometry b) Loading history

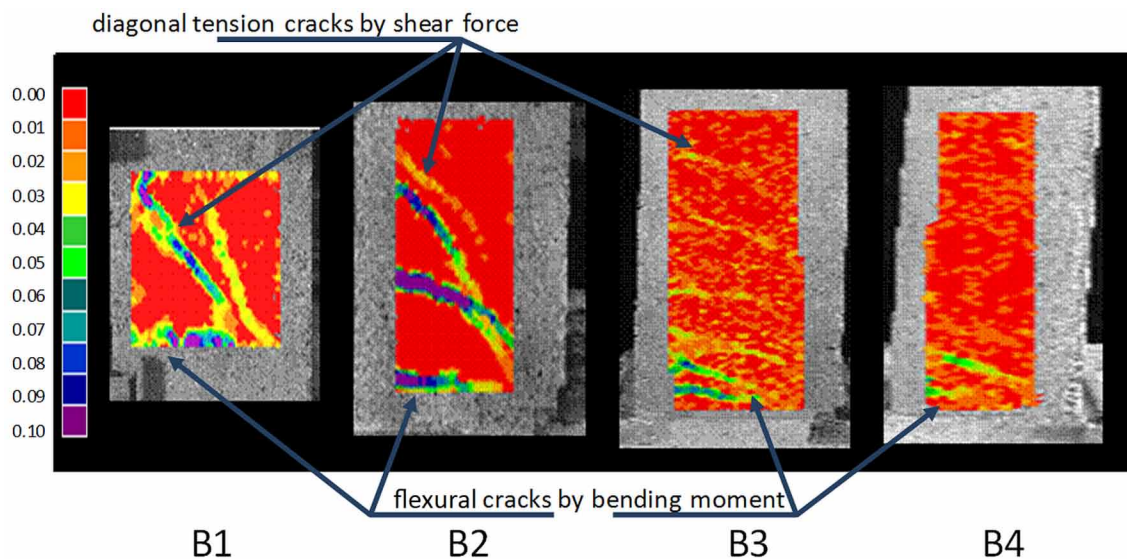


## Damage Mechanics of Dual Systems

Table 1. Properties of RC Beams

Specimen	$w$ (mm)	$t$ (mm)	$a$ (mm)	$d$ (mm)	$a/d$	$\rho_v$ (%)	$\rho_s$ (%)	$f'_c$ (Mpa)
B1	250	250	400	225	1.78	2.53	1.03	26.7
B2	250	250	800	225	3.56	2.53	1.03	26.7
B3	250	250	1200	225	5.36	2.53	1.03	26.7
B4	250	250	1600	225	7.11	2.53	1.03	26.7

Figure 4. Cracking patterns in beams with different aspect ratios and quantification of the diagonal tension



It is important to underline that structural failure due to shear cracking is a much more brittle and dangerous process than bending collapse. Therefore having a model that can differentiate and quantify the two cracking processes is very important for the structural safety assessment.

### 11.1.3 Experimental Analysis of RC Walls

Figure 5 shows a RC wall with an aspect ratio of 1.26. The longitudinal reinforcement is over dimensioned with the purpose of minimizing flexural damage as much as possible. The wall is subjected to a mono-sign loading without.

Figure 6 shows the evolution of the cracking pattern in the wall. Figure 6a presents the first manifestation of diagonal tension at the peak of the first cycle of the loading. In Figure 6b it is appreciated many shear cracks along the wall in the fifth cycle of loading. Finally Figure 6c shows the cracking pattern corresponding to the ultimate force of the wall. Notice that flexural cracks are not appreciated in the wall.

Figure 5. RC wall a) Geometry b) Loading history

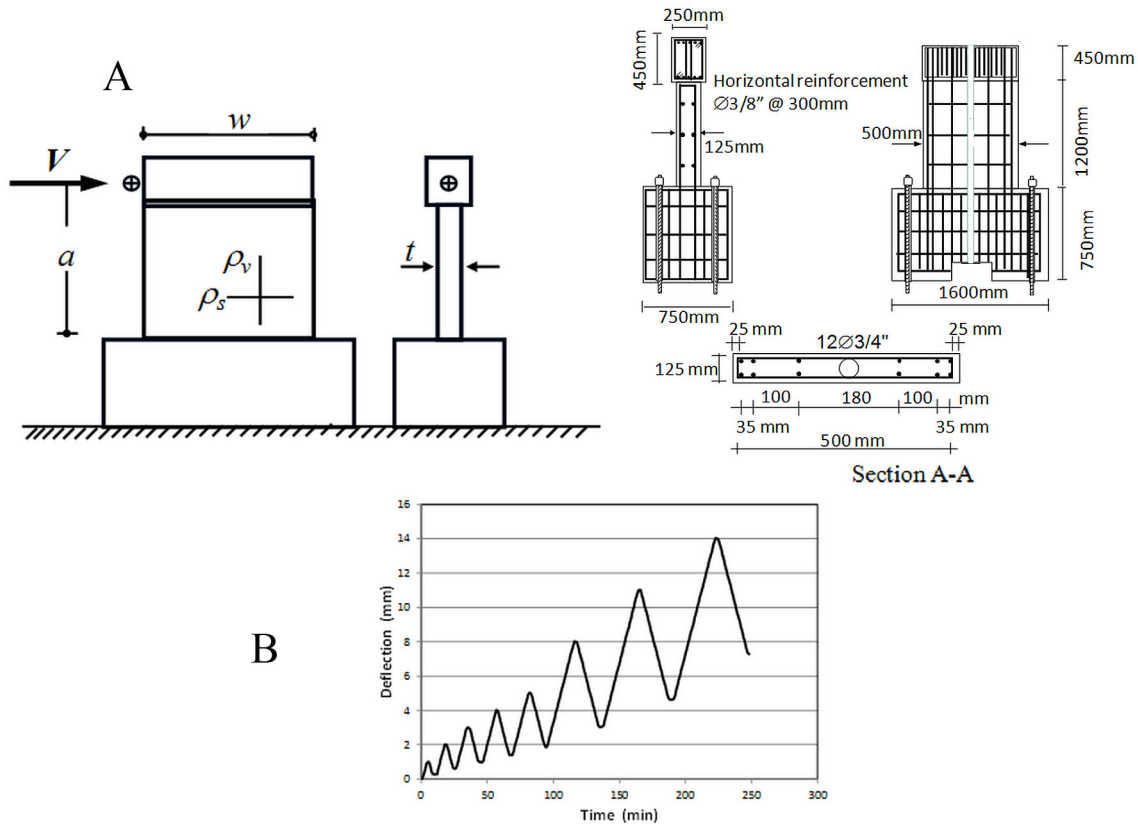


Figure 7 shows a RC wall with an aspect ratio equal to 1.26 subjected to lateral mono-sign loading and axial force. An axial force equal to 314 KN is first applied and then kept constant while sequence of lateral loading is applied. The axial force was applied using a post-tensioning technique.

Figure 8 presents evolution of the cracking pattern of the wall of Figure 7. Notice that the presence of axial force on the specimen does not modify significantly the cracking pattern, just alters slightly the orientation of the shear cracks.

### 11.1.4 Cracking Pattern in Short Columns

Figure 9 shows the reinforcement of a RC short column. Two levels of constant axial force (180 KN and 420 KN) are applied. Again the axial force is first applied and kept constant while it is applied the mono-sign lateral loading. Figure 10 shows the cracking pattern of the column subjected to 180 KN of axial force and Figure 11, the corresponding to the axial force equal to 420 KN.

Notice that in these cases flexural cracks appear simultaneously with the shear ones. The diagonal cracking pattern that is shown in Figure 10c is very similar to the one presented in Figure 11c; again, only the orientation of the shear cracks changes slightly.

Damage Mechanics of Dual Systems

Figure 6. Cracking evolution in a wall subjected to lateral loading

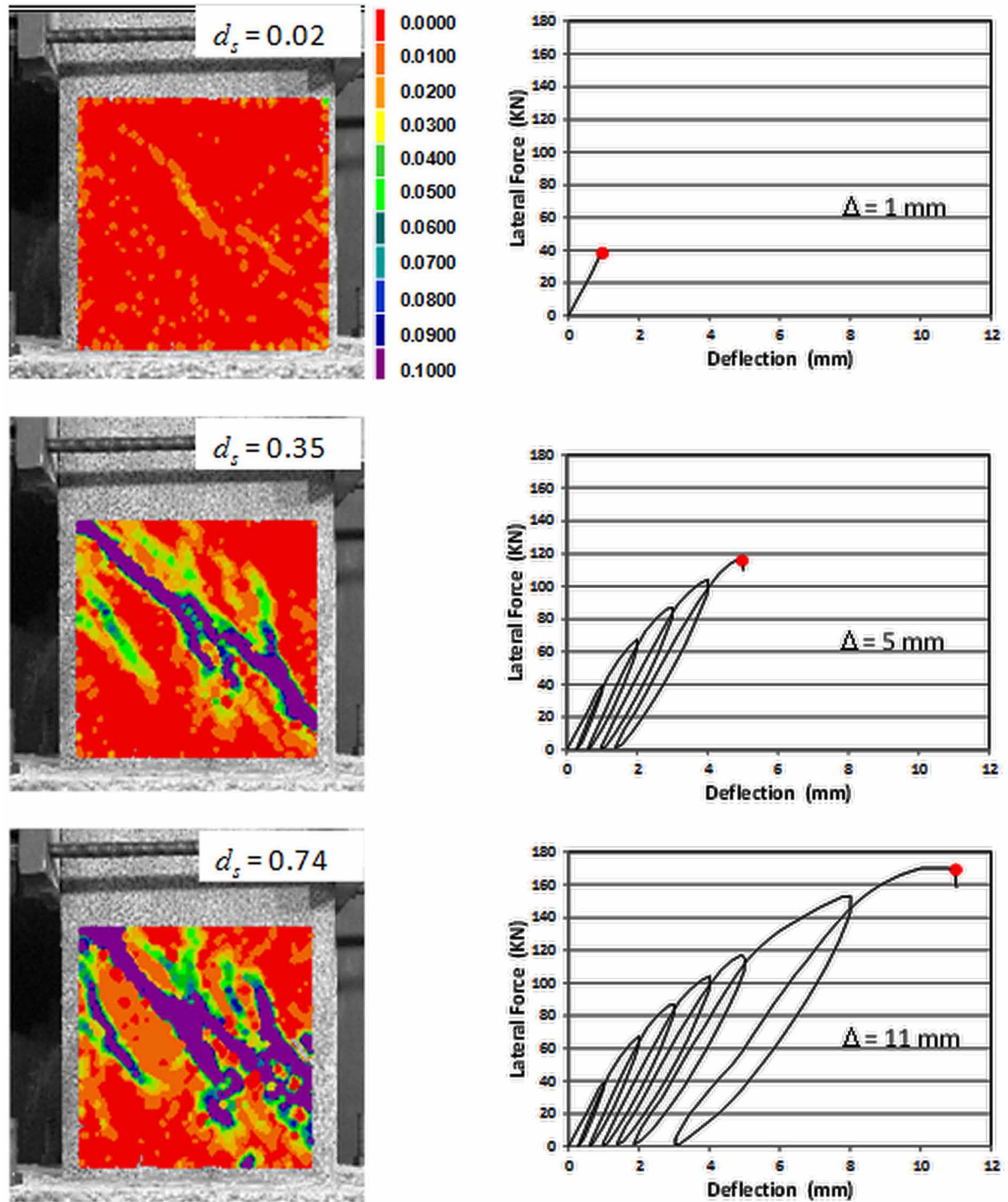
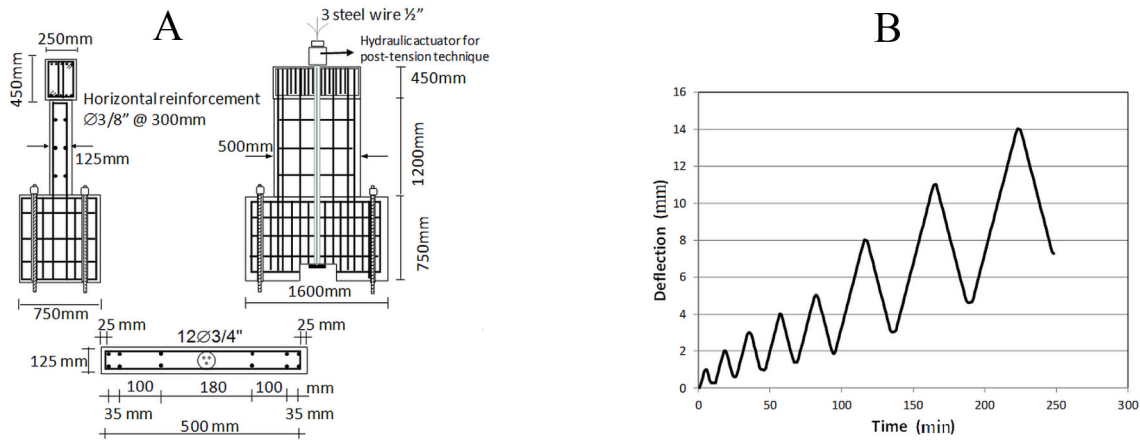




Figure 7. a) RC wall specimen with aspect ratio equal to 1.26 subjected to lateral loads and axial force  
 b) Lateral loading history



## 11.2 ELASTICITY LAW FOR FRAME MEMBERS OF ANY ASPECT RATIO

The experimental analysis described in the previous section indicates that the cracking pattern in RC elements can be schematized as follows:

1. There are two distinct sets of cracks that may be assumed to propagate independently.
2. One of them can be lumped at the plastic hinges because they are concentrated at the ends of the element; they are called flexural cracks; they are assumed to be the result of bending moments because they are present in specimens with high aspect ratios; i.e. with high levels of bending moments and relatively low values of shear forces.
3. The second one corresponds to the, so called, diagonal tension cracks or shear cracks. In squat elements, shear cracks almost cross the entire length of the element. They are assumed to be caused by shear forces because they are characteristic of elements with intermediate or low aspect ratios; i.e. with high levels of shear forces with respect to the bending moments.
4. In slender elements, shear cracks are scarce or non-existent.
5. The density of the shear cracking increases and may become predominant with respect to flexural cracking as the aspect ratio of the element is reduced.

The observations a-c can be represented in mathematical terms by choosing an adequate expression of the elasticity law; the remarks d-e can be characterized with the damage evolution laws that are the subject of the next section.

The physical phenomena that may take place in a RC element subjected to lateral loads can be summarized as follows:

**Damage Mechanics of Dual Systems**

*Figure 8. Cracking evolution in a wall subjected to lateral loading and axial force*

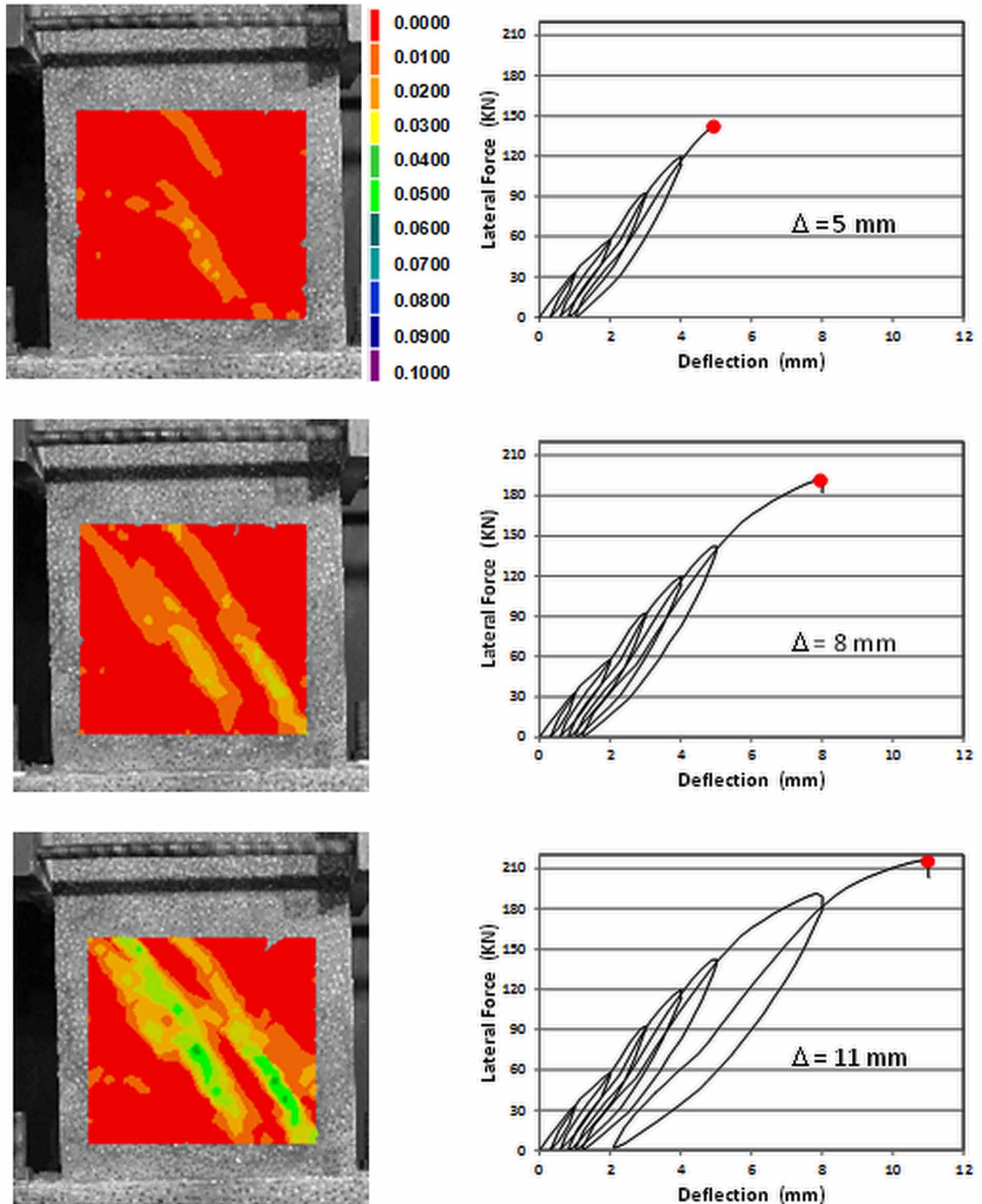
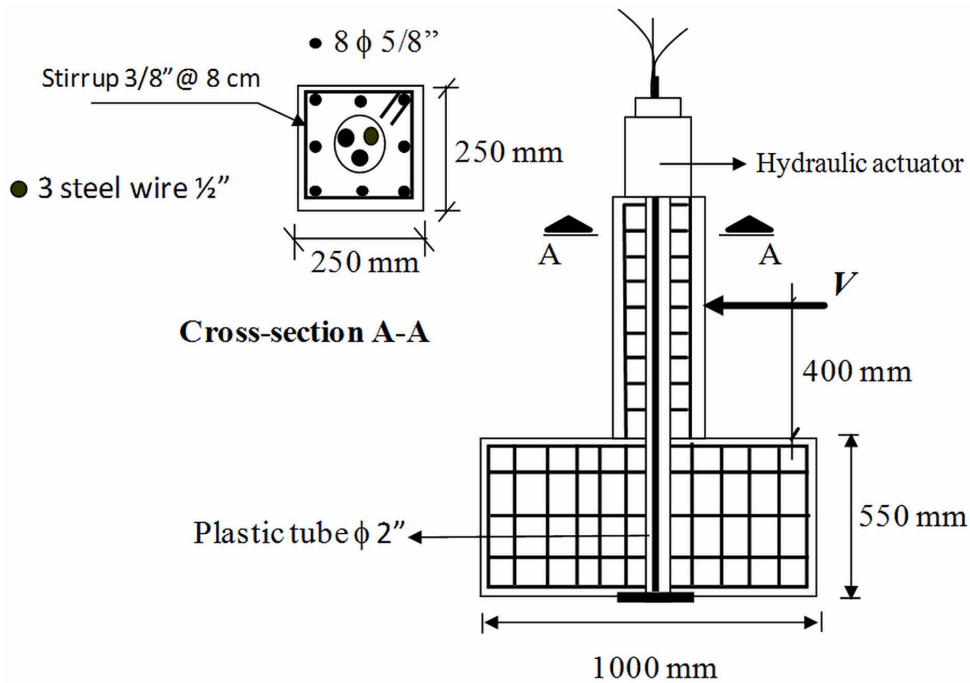


Figure 9. Short column



- Yield of the longitudinal reinforcement; this effect is represented by the matrix of plastic deformations  $\{\Phi^p\}_b$  that was introduced in chapter 7.
- Yield of the transverse reinforcement; this effect is represented by the plastic distortion  $\gamma^p$  that was introduced in the same chapter.
- Flexural cracks that can be lumped at the plastic hinges. They are represented by the damage set  $(\mathbf{D})_b$  that was introduced in chapter 10.
- Finally, shear cracks along the element. A new damage variable (i.e. that takes values between zero and one) denoted  $d_s$  is now introduced in order to represent this last inelastic phenomenon.

The lumped/ distributed plasticity model introduced in section 7.4 is used again as a basis for the formulation of the elasticity law but, this time, damage is also included. Thus a frame element is assumed to be the assemblage of an inelastic element with any aspect ratio and two plastic hinges with damage (see Figure 12).

Total deformations are again decomposed into a term corresponding to the elasto-plastic component  $\{\Phi^{bcw}\}_b$  and the deformations of the inelastic hinges  $\{\Phi^h\}_b$ ; the former term can be decomposed once more into an elastic deformation, a plastic one and a damage related to distortion; the term corresponding to the inelastic hinges can be decomposed, again, into a plastic deformations matrix and a damage matrix:

**Damage Mechanics of Dual Systems**

*Figure 10. Cracking evolution in a short column with axial force equal to 180 kN*

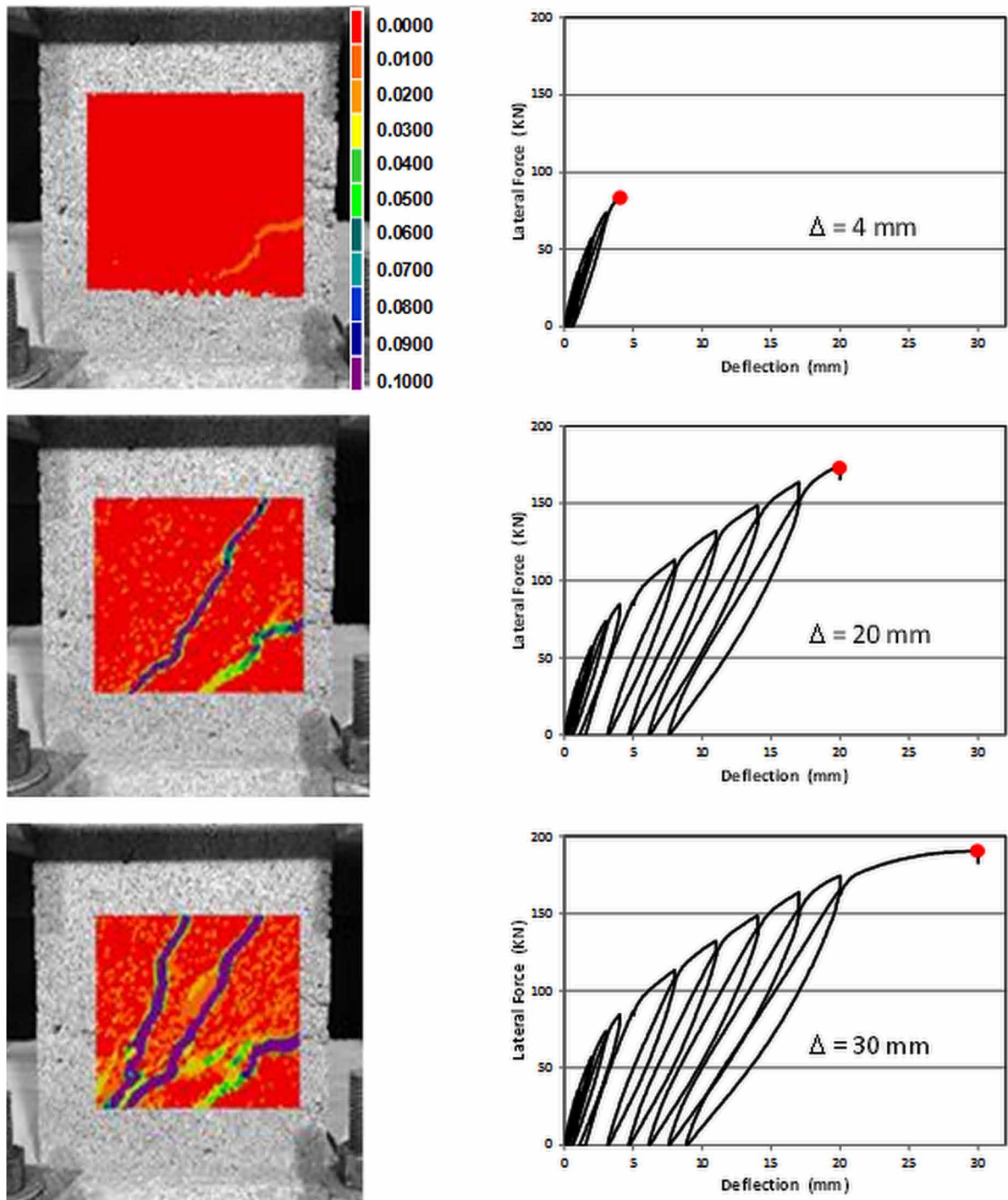


Figure 11. Cracking evolution in a short column with axial force equal to 420 KN

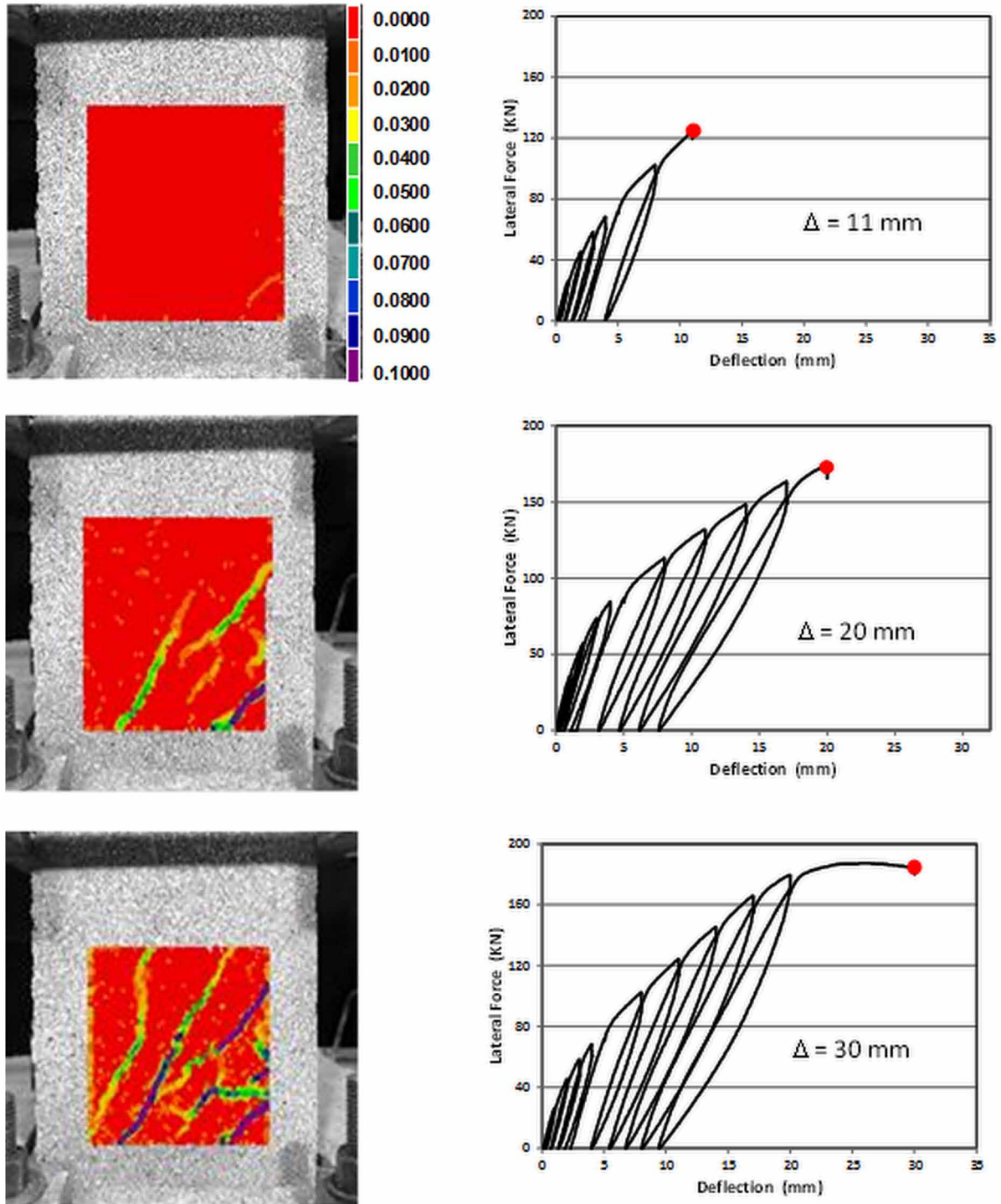
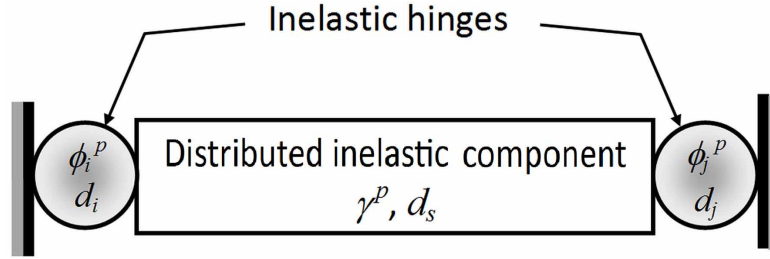


Figure 12. Lumped/distributed inelasticity model



$$\begin{aligned} \{\Phi\}_b &= \{\Phi^{bcw}\}_b + \{\Phi^h\}_b \\ \{\Phi\}_b &= \left( [\mathbf{F}_f]_b + [\mathbf{F}_s]_b \right) \{\mathbf{M}\}_b + \{\gamma^p\}_b + \{\gamma^d\}_b + \{\Phi^p\}_b + \{\Phi^d\}_b \end{aligned} \quad (11.2.1)$$

Notice that all these terms, with the exception of the damage related to distortion  $\{\gamma^d\}_b$ , were introduced in precedent chapters: Equation (3.4.8) for the elastic deformations, Equation (7.2.1) for the plastic distortions  $\{\gamma^p\}_b^t = (\gamma^p, \gamma^p, 0)$  and Equation (7.1.2) for the plastic rotations  $\{\Phi^p\}_b^t = (\phi_i^p, \phi_j^p, 0)$ . The damage deformations lumped at the inelastic hinges can be expressed as in section 10.1:  $\{\Phi^d\}_b = [\mathbf{C}(\mathbf{D})]_b \{\mathbf{M}\}_b$ . The application of the hypothesis of equivalence in deformation gives the following expression for the damage related to distortion:

$$\{\gamma^d\}_b = [\mathbf{C}_s(d_s)]_b \{\mathbf{M}\}_b; \text{ where } [\mathbf{C}_s(d_s)] = \frac{d_s}{1-d_s} \begin{bmatrix} \frac{1}{GA_b L_b} & \frac{1}{GA_b L_b} & 0 \\ \frac{1}{GA_b L_b} & \frac{1}{GA_b L_b} & 0 \\ 0 & 0 & 0 \end{bmatrix} \quad (11.2.2)$$

The combination of all these equations gives the elasticity law in terms of flexibility:

$$\begin{aligned} \{\Phi\}_b - \{\Phi^p\}_b - \{\gamma^p\}_b &= [\mathbf{F}(\mathbf{D}, d_s)] \{\mathbf{M}\}_b, \\ \text{where } [\mathbf{F}(\mathbf{D}, d_s)]_b &= [\mathbf{F}_f]_b + [\mathbf{F}_s]_b + [\mathbf{C}(\mathbf{D})]_b + [\mathbf{C}_s(d_s)]_b \end{aligned} \quad (11.2.3)$$

$$[\mathbf{F}(\mathbf{D}, d_s)] = \begin{bmatrix} \frac{L_b}{3EI_b (1-d_i)} + \frac{1}{GA_b L_b (1-d_s)} & -\frac{L_b}{6EI_b} + \frac{1}{GA_b L_b (1-d_s)} & 0 \\ -\frac{L_b}{6EI_b} + \frac{1}{GA_b L_b (1-d_s)} & \frac{L_b}{3EI_b (1-d_j)} + \frac{1}{GA_b L_b (1-d_s)} & 0 \\ 0 & 0 & \frac{L_b}{EA_b} \end{bmatrix} \quad (11.2.4)$$

The elasticity law can also be presented as:

$$\{\mathbf{M}\}_b = [\mathbf{E}(\mathbf{D}, d_s)] \{\Phi - \Phi^p - \gamma^p\}_b; \text{ where } [\mathbf{E}(\mathbf{D}, d_s)] = [\mathbf{F}(\mathbf{D}, d_s)]^{-1} \quad (11.2.5)$$

The term  $[\mathbf{E}(\mathbf{D}, d_s)]$  is the elasticity matrix of a RC element of any aspect ratio that may be experiencing flexural and shear cracking simultaneously.

## 11.3 DAMAGE EVOLUTION LAWS

### 11.3.1 Energy Release Rates

The complementary deformation energy of a damaged frame element with flexural and shear cracking is given by:

$$W_b = \frac{1}{2} \{\mathbf{M}\}_b^t \{\Phi - \Phi^p - \gamma^p\}_b = \frac{1}{2} \{\mathbf{M}\}_b^t [\mathbf{F}(\mathbf{D}, d_s)]_b \{\mathbf{M}\}_b \quad (11.3.1)$$

Therefore, the energy release rates corresponding to flexural cracking at the plastic hinge  $i$ , plastic hinge  $j$  and shear cracking are:

$$\frac{1}{2} \{\mathbf{M}\}_b^t \{\Phi - \Phi^p - \gamma^p\}_b = \frac{1}{2} \{\mathbf{M}\}_b^t [\mathbf{F}(\mathbf{D}, d_s)]_b \{\mathbf{M}\}_b \quad (11.3.2)$$

Notice that according to the Griffith theory, the flexural energy release rate depends indeed on the bending moment while the shear damage driving force depends on the shear force.

If any interaction between flexural and shear cracks is neglected, all damage evolution can be described by the successive application of the Griffith criterion:

$$\begin{cases} \Delta d_i = 0 & \text{if } G_i < R_i \\ G_i = R_i & \text{if } \Delta d_i > 0 \end{cases}; \quad \begin{cases} \Delta d_j = 0 & \text{if } G_j < R_j \\ G_j = R_j & \text{if } \Delta d_j > 0 \end{cases}; \quad (11.3.3)$$

$$\begin{cases} \Delta d_s = 0 & \text{if } G_s < R_s \\ G_s = R_s & \text{if } \Delta d_s > 0 \end{cases}$$

with the same flexural crack resistance function that was presented in section 10.3; the shear crack resistance expression is discussed in the next section.

### 11.3.2 Experimental Measurement of the Shear Damage $d_s$

The method of the stiffness variation described in section 10.3.1 can be used again for the experimental identification of the shear crack resistance function. The experimental results chosen for this identification correspond to the wall with a very low aspect ratio of section 11.3 (Figure 6). The cracking pattern obtained using DIC shows that flexural cracking in that test is minimal. Figure 13 shows the experimental results of that test in a curve of lateral force vs. deflection.

This test can be modeled using a single element in cantilever that is subjected to the displacements history of Figure 14.

Assume that flexural cracks are negligible and that the longitudinal reinforcement does not yield; then, the first line of the elasticity law (11.2.3) for this element is:

$$\phi_1 - \gamma^p = \left( \frac{L}{3EI} + \frac{1}{GAL(1-d_s)} \right) m_1 + \left( -\frac{L}{6EI} + \frac{1}{GAL(1-d_s)} \right) m_2 \quad (11.3.4)$$

The boundary conditions, the equilibrium equations and the kinematic equations for this problem are:

$$m_1 = P.L; m_2 = 0; \phi_1 = \frac{t}{L} \quad (11.3.5)$$

Figure 13. Experimental force vs. lateral displacement curve of the wall with aspect ratio equal to 1.26

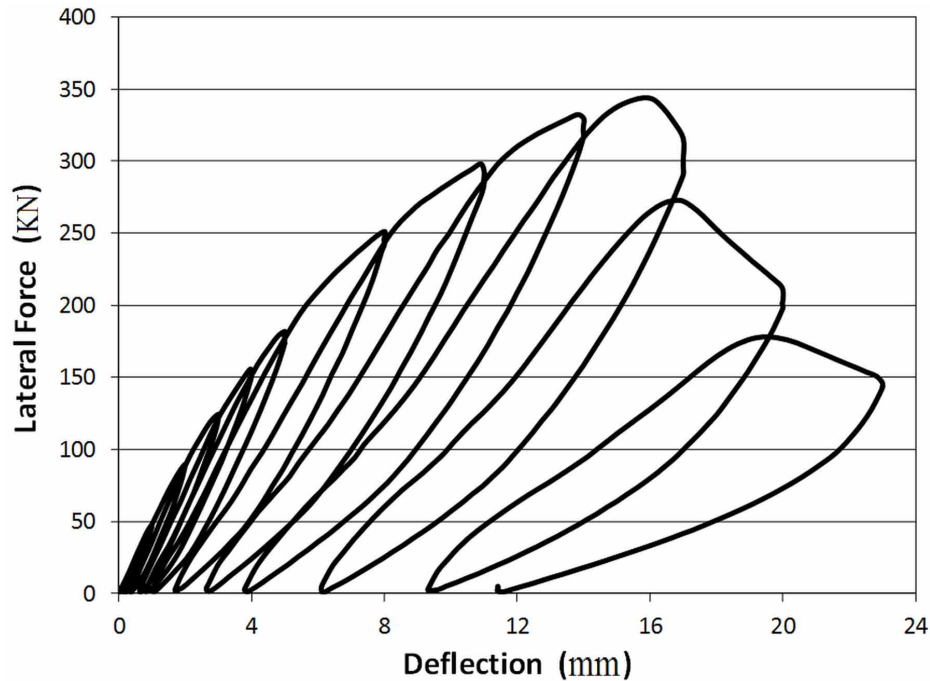
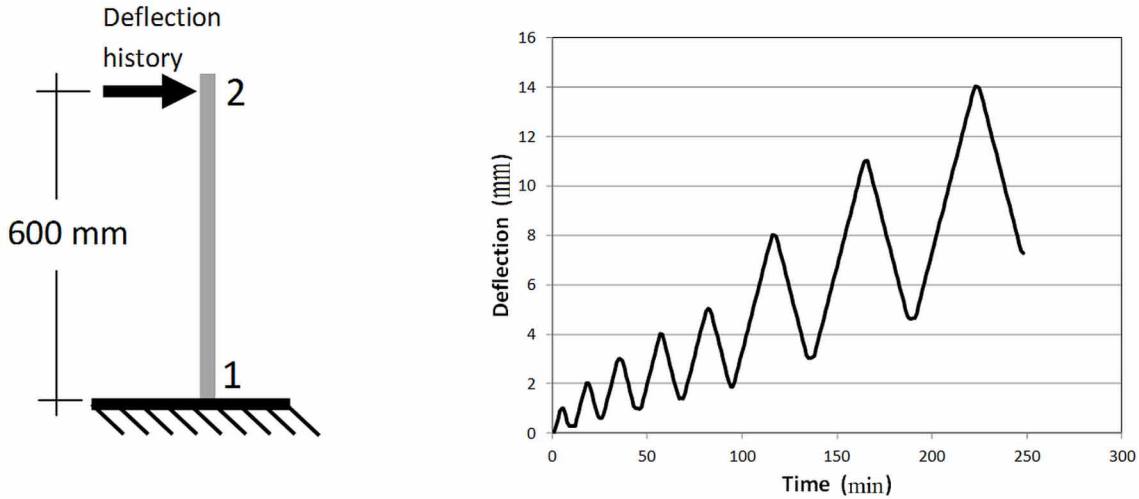




Figure 14. Modeling of the test presented in Figure 5



where  $P$  and  $t$  are, respectively, the force and lateral displacement on the node 2. The combination of (11.3.4-5) gives:

$$P = Z(d_s)(t - t_p); t_p = \gamma^p L; Z(d_s) = \frac{3EI GA(1 - d_s)}{L(L^2 GA - L^2 GA d_s + 3EI)} \quad (11.3.6)$$

Notice that Equation (11.3.6) is quite similar to the expression (10.2.7); only the equation for the slope  $Z$  is modified. Therefore, Equation (11.3.6a) represents again the straight lines of the elastic unloading/reloading in Figure 13. An expression for the determination of the shear damage variable  $d_s$  as a function of the dimensions of the specimen, the material properties and the slopes of the elastic unloading/reloading can be obtained from (11.3.6c):

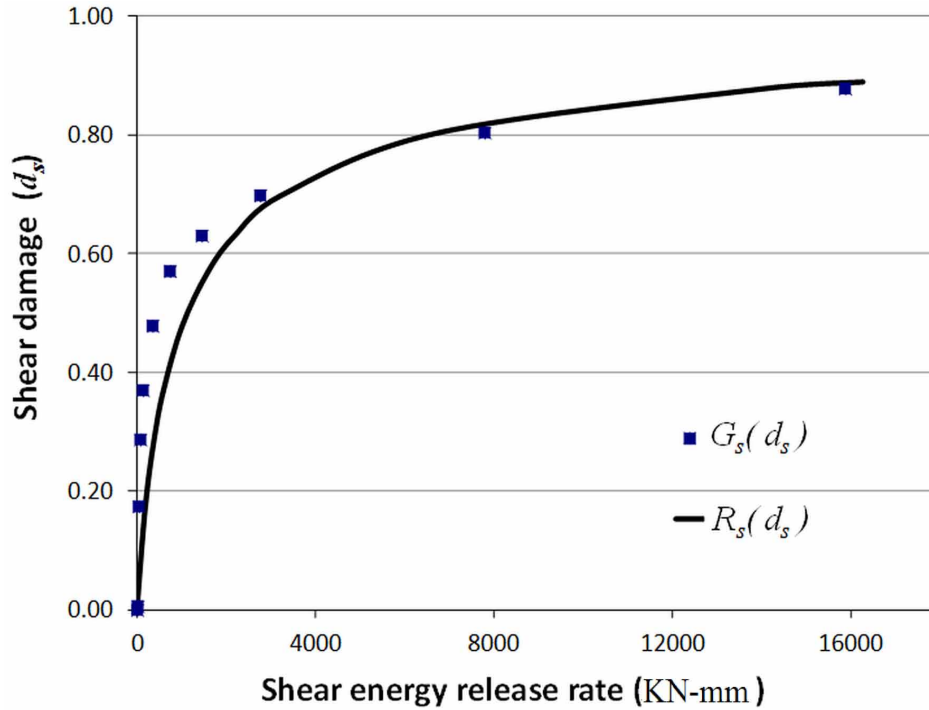
$$d_s = \frac{3GA EI - 3Z L EI - Z L^3 GA}{GA(3EI - L^3 Z)} \quad (11.3.7)$$

As the slope  $Z$  can be measured experimentally and the properties of the specimen can be determined with a reasonable degree of precision, the Equation (11.3.7) permits the quantification of the shear cracking density; it has been observed that the values of shear damage obtained in this way agrees, at least qualitatively, with the experimental observations via DIC. The values of the shear damage computed with Equation (11.3.7) can be compared with the cracking state determined via DIC in Figure 6.

### 11.3.3 Shear Crack Resistance Function

Figure 15. shows the plot of energy release rate, or shear crack resistance, as a function the damage variable obtained with the procedures described in the previous section.

Figure 15. Shear crack resistance as a function of shear damage in a RC specimen



The same general expression of the flexural crack resistance function presented in section 10.3.2 can be used to describe to experimental results of Figure 15; of course, with others element dependent parameters:

$$R(d_s) = R_{0s} + q_s \frac{\ln(1 - d_s)}{1 - d_s} \quad (11.3.8)$$

It appears that Equation (11.3.8) can be considered as a general expression for the crack resistance function in any of its manifestations: so far, shear cracks or flexural cracks.

### 11.3.4 Computation of the Parameters $R_{0s}$ and $q_s$

The computation of the parameters can be carried out using a procedure similar to the one described in section 10.3.3; but in this case the parameters are determined as a function of the first shear cracking force,  $V_{cr}$  and the ultimate shear force,  $V_u$ . The Griffith criterion states that:

$$\frac{LV^2}{2GA(1 - d_s)^2} = R_{0s} + q_s \frac{\ln(1 - d_s)}{1 - d_s}, \text{ i.e. } LV^2 = 2GA(1 - d_s)^2 \left( R_{0s} + q_s \frac{\ln(1 - d_s)}{1 - d_s} \right) \quad (11.3.9)$$

The condition of cracking initiation ( $d_s = 0$ ) for the first shear cracking force in (11.3.9) gives the value of the initial crack resistance function:

$$LV_{cr}^2 = 2GAR_{0s}; \text{ i.e. } R_{0s} = \frac{LV_{cr}^2}{2GA} \quad (11.3.10)$$

As in the case of flexural damage, the curve of shear force as a function of damage also presents a maximum; thus, it is necessary to take the derivative of the Equation (11.3.9b) with respect to shear damage. Then, it is made equal to zero:

$$2R_{0s}d_{su} - 2R_{0s} - q_s - q_s \ln(1 - d_{su}) = 0 \quad (11.3.11)$$

The relation between the ultimate shear force and the ultimate shear damage gives a second equation:

$$LV_u^2 = 2GA(1 - d_{su})^2 \left( R_{0s} + q_s \frac{\ln(1 - d_{su})}{1 - d_{su}} \right) \quad (11.3.12)$$

The numerical resolution of (11.3.11-12) gives the values of the ultimate shear damage and the parameter  $q_s$ . Again, only conventional concepts of the theory of reinforced concrete are needed for the prediction of the propagation of shear cracks: the ultimate shear force that was presented in section 7.3 and the first cracking shear force that is described in the next section.

### **11.3.5 Computation of the First Cracking Shear Force**

The first cracking shear force  $V_{cr}$  is defined as the least value of shear force that produces inclined cracking in the element. For members subjected to shear, bending and axial force, the first cracking shear force can be computed with the following expression:

$$V_{cr} = 0.17 \left( 1 + \frac{N}{14A_g} \right) \sqrt{f'_c} A_g \quad (11.3.13)$$

where  $N$  is the axial force in N,  $A_g$  is the gross area of the concrete section in mm<sup>2</sup> and  $f'_c$  is the strength of concrete in MPa.

### **11.3.6 Modified Griffith Criterion**

The substitution of the damage evolution laws (11.3.3) by the modified Griffith criterion described in section 10.6, allows for the consideration of the ultra-low cycle fatigue effects.

$$\begin{cases} \Delta d_i = 0 \text{ if } G_i < R_{0i} \\ \Delta d_i = \frac{1}{\partial R_i / \partial d_i} \left( \frac{G_i}{R_i} \right)^2 \langle \Delta G_i \rangle_+ \text{ otherwise} \\ \Delta d_j = 0 \text{ if } G_j < R_{0j} \\ \Delta d_j = \frac{1}{\partial R_j / \partial d_j} \left( \frac{G_j}{R_j} \right)^2 \langle \Delta G_j \rangle_+ \text{ otherwise} \\ \Delta d_s = 0 \text{ if } G_s < R_{0s} \\ \Delta d_s = \frac{1}{\partial R_s / \partial d_s} \left( \frac{G_s}{R_s} \right)^2 \langle \Delta G_s \rangle_+ \text{ otherwise} \end{cases} \quad (11.3.14)$$

## 11.4 PLASTIC DEFORMATIONS EVOLUTION LAWS

Assuming again the uncoupling of inelasticity by shear and bending, the evolution laws of the plastic rotations corresponding to the inelastic hinges remain as presented in section 10.4.1:

$$\begin{cases} d\phi_i^p = 0 \text{ if } f_i < 0 \\ f_i = 0 \text{ if } d\phi_i^p \neq 0 \end{cases}; \begin{cases} d\phi_j^p = 0 \text{ if } f_j < 0 \\ f_j = 0 \text{ if } d\phi_j^p \neq 0 \end{cases} \quad (11.4.1)$$

$$f_i = \left| \frac{m_i}{1-d_i} - c_i \phi_i^p \right| - k_{0i} \leq 0; f_j = \left| \frac{m_j}{1-d_j} - c_j \phi_j^p \right| - k_{0j} \leq 0$$

The computation of the parameters  $c_i$ ,  $c_j$ ,  $k_{0i}$  and  $k_{0j}$  is carried out using the same procedure presented in section 10.4.2.

The plastic distortion evolution law can be obtained with a similar process. First, the effective shear force can be defined as:

$$\bar{V} = \frac{V}{1-d_s} = \frac{m_i + m_j}{(1-d_s)L} \quad (11.4.2)$$

Next, the application of the hypothesis of equivalence in deformations is used to modify a yield function for plastic distortion with linear kinematic hardening:

$$f_s = \left| \bar{V} - c_s \gamma^p \right| - k_{os} = \left| \frac{m_i + m_j}{(1-d_s)L} - c_s \gamma^p \right| - k_{os} \leq 0 \quad (11.4.3)$$

The plastic distortion evolution law has the usual expression:

$$\begin{cases} d\gamma_p = 0 & \text{if } f_s < 0 \\ f_s = 0 & \text{if } d\gamma_p \neq 0 \end{cases} \quad (11.4.4)$$

The computation of the member dependent parameters,  $c_s$  and  $k_{0s}$ , is also similar to the one described in section 10.4.2 for bending effects as discussed in the following paragraphs.

Consider a monotonic loading on a RC element; The Equation (11.3.12) relates the shear force with shear damage. The value of damage  $d_{sp}$  that corresponds to the first plastic force is given by the following equation:

$$LV_p^2 = 2GA(1 - d_{sp})^2 \left( R_{0s} + q_s \frac{\ln(1 - d_{sp})}{1 - d_{sp}} \right) \quad (11.4.5)$$

The yield function is equal to zero for the plastic damage value  $d_{sp}$  with no plastic distortion; thus, the parameter,  $k_{0s}$ , is the effective plastic shear force:

$$k_{0s} = \frac{V_p}{1 - d_{sp}} \quad (11.4.6)$$

The yield function is also equal to zero when the shear force reaches its ultimate value, thus, the last parameter,  $c_s$ , can be computed as:

$$c_s = \frac{1}{\gamma_u^p} \left( \frac{V_u}{1 - d_{su}} - k_{0s} \right) \quad (11.4.7)$$

where  $\gamma_u^p$  is the ultimate plastic distortion (see section 7.3).

## **11.5 ANALYSIS OF DUAL SYSTEMS**

### **11.5.1 Formulation of the Problem**

Consider a planar frame subjected to an arbitrary mono-sign loading. The problem is defined as:

- Compute: the free displacements, reaction forces, stresses, deformations, plastic deformations and damages.
- With the following data: the initial configuration of the structure, the restricted displacements, the nodal forces corresponding to the free displacements and those applied over the elements, the material and cross-section properties and yield functions.
- Such that they verify the nonlinear kinematic and equilibrium equations:

## Damage Mechanics of Dual Systems

$$\begin{aligned} \{\Delta \Phi\}_b &= [\mathbf{B}_E(\mathbf{U}_{t=tr})]_b \{\Delta \mathbf{U}\}; \\ \circ \quad \{\mathbf{L}_{t=tr}\} &= \{\mathbf{P}_{t=tr}\}; \{\mathbf{L}_{t=tr}\} = \sum_{b=1}^m [\mathbf{B}(\mathbf{U}_{t=tr})_E]_b^t \{\mathbf{M}_{t=tr}\}_b \end{aligned}$$

- The Elasticity Law:

$$\begin{aligned} \{\Phi\}_b - \{\Phi^p\}_b - \{\gamma^p\}_b &= [\mathbf{F}(\mathbf{D}, d_s)] \{\mathbf{M}\}_b \quad \text{or} \\ \{\mathbf{M}\}_b &= [\mathbf{E}(\mathbf{D}, d_s)] \{\Phi - \Phi^p - \gamma^p\}_b \end{aligned} \quad (11.5.1)$$

- The Plastic Deformation Evolution Laws:

$$\begin{cases} d\phi_i^p = 0 \text{ if } f_i < 0 \\ f_i = 0 \text{ if } d\phi_i^p \neq 0 \end{cases}; \begin{cases} d\phi_j^p = 0 \text{ if } f_j < 0 \\ f_j = 0 \text{ if } d\phi_j^p \neq 0 \end{cases}; \begin{cases} d\gamma_p = 0 \text{ if } < 0 \\ f_s = 0 \text{ if } d\gamma_p \neq 0 \end{cases};$$

- With the Yield Functions:

$$f_j = \left| \frac{m_j}{1-d_j} - c_j \phi_j^p \right| - k_{0j} \leq 0; f_i = \left| \frac{m_i}{1-d_i} - c_i \phi_i^p \right| - k_{0i} \leq 0; f_s = \left| \frac{V}{1-d_s} - c_s \gamma^p \right| - k_{os} \leq 0$$

- And the damage evolution laws:

$$\begin{cases} \Delta d_j = 0 \text{ if } G_j < R_{0j} \\ \Delta d_j = \frac{1}{\partial R_j / \partial d_j} \left( \frac{G_j}{R_j} \right)^2 \langle \Delta G_j \rangle_+ \text{ otherwise} \end{cases}$$

$$\begin{cases} \Delta d_i = 0 \text{ if } G_i < R_{0i} \\ \Delta d_i = \frac{1}{\partial R_i / \partial d_i} \left( \frac{G_i}{R_i} \right)^2 \langle \Delta G_i \rangle_+ \text{ otherwise} \end{cases}$$

$$\begin{cases} \Delta d_s = 0 \text{ if } G_s < R_{0s} \\ \Delta d_s = \frac{1}{\partial R_s / \partial d_s} \left( \frac{G_s}{R_s} \right)^2 \langle \Delta G_s \rangle_+ \text{ otherwise} \end{cases}$$

These damage evolution laws can also be included in the framework described in section 8.3.1 with:

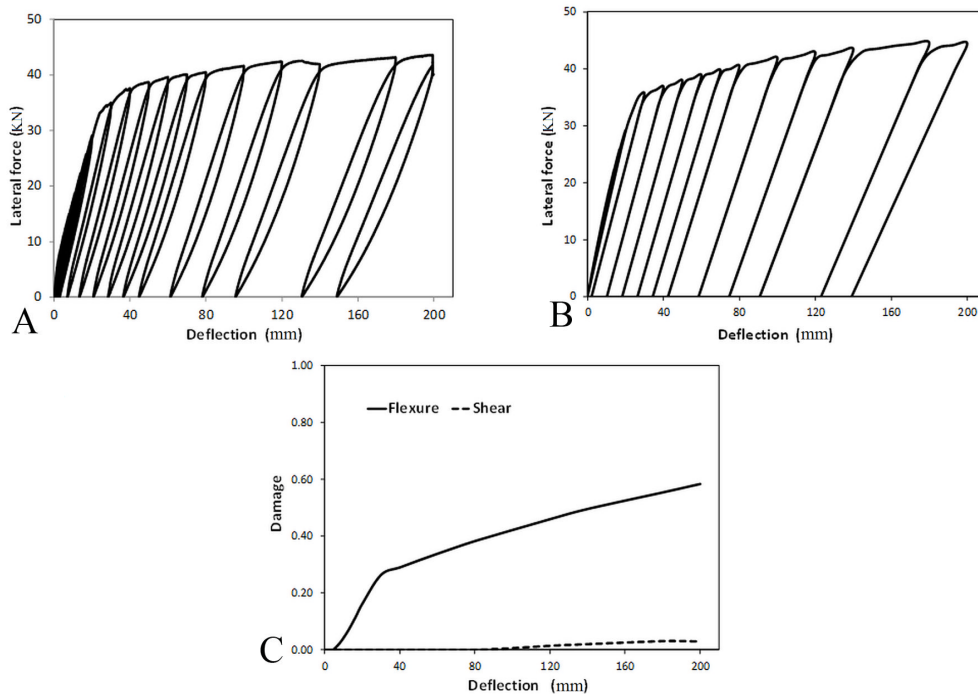
$$VWf_1 = \phi_i^p; VWf_2 = \phi_j^p; VWf_3 = \gamma^p; \{\mathbf{VW}\mathbf{o}\}_b = \{d_i, d_j, d_s\} \quad (11.5.2)$$

Therefore the conventional numerical algorithms can also be used to analyze dual systems. The problem can be solved with the multi-step version of the step-by-step method.

### 11.5.2 Numerical Simulation of the Tests Described in Section 11.1.2

The Figure 16a-b shows the experimental results and the numerical simulation of the slender column (specimen B4 of Figure 3-4) in a graph of deflection vs. lateral force; notice that the numerical results are very good. The Figure 16c indicates the histories of damage; the DIC analysis validates the large value of flexural damage (0.58) and the negligible shear damage (0.03) obtained in the simulation.

Figure 16. Behavior of a slender RC beam in cantilever a) Experimental deflection vs. lateral force b) Numerical deflection vs. lateral force c) Damage evolution



The Figure 17b shows the numerical simulation of the longer intermediate beam (specimen B3 in Figure 3-4). The results of the numerical simulation are also very good. The histories of damage now are different (Figure 17c); the final value of flexural damage is also very large (0.74) but shear damage is now not negligible (0.33). Again, DIC seems to validate this result (See specimen B3 in Figure 4).

The results for the shortest intermediate beam (specimen B2) are shown in Figure 18. The numerical simulation is good and now the relationship between flexural damage and shear damage are reversed, final values of 0.48 and 0.84 respectively. This is again true according to the DIC analysis (See specimen B2 in Figure 3-4).

The Figure 19 shows the results of the short beam (specimen B1). The numerical simulation is also good, with low flexural damage (final value of 0.31) and high shear damage (final value of 0.85). The DIC analysis perhaps indicates a more severe flexural damage than the one given by the model, but the mechanism of failure appears to be clearly one of shear.

### 11.5.3 Numerical Simulation of the Tests Described in Section 11.1.3

The Figure 20 and 21 show the numerical simulations of the shear walls subjected to mono-sign lateral loading and axial force equal to, respectively, 0 and 314 kN (Figure 5-8). In these walls, shear damage is the main mechanism of failure while flexural damage is small or even negligible.

**Damage Mechanics of Dual Systems**

Figure 17. Behavior of an intermediate RC beam in cantilever a) Experimental deflection vs. lateral force b) Numerical deflection vs. lateral force c) Damage evolution

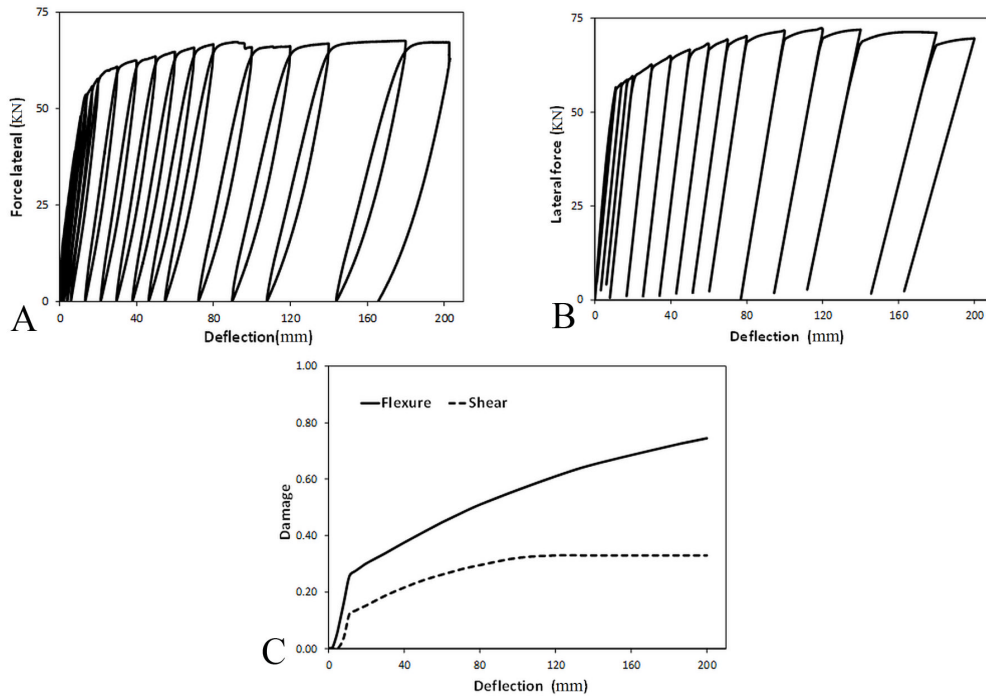


Figure 18. Behavior of an intermediate RC beam in cantilever a) Experimental deflection vs. lateral force b) Numerical deflection vs. lateral force c) Damage evolution

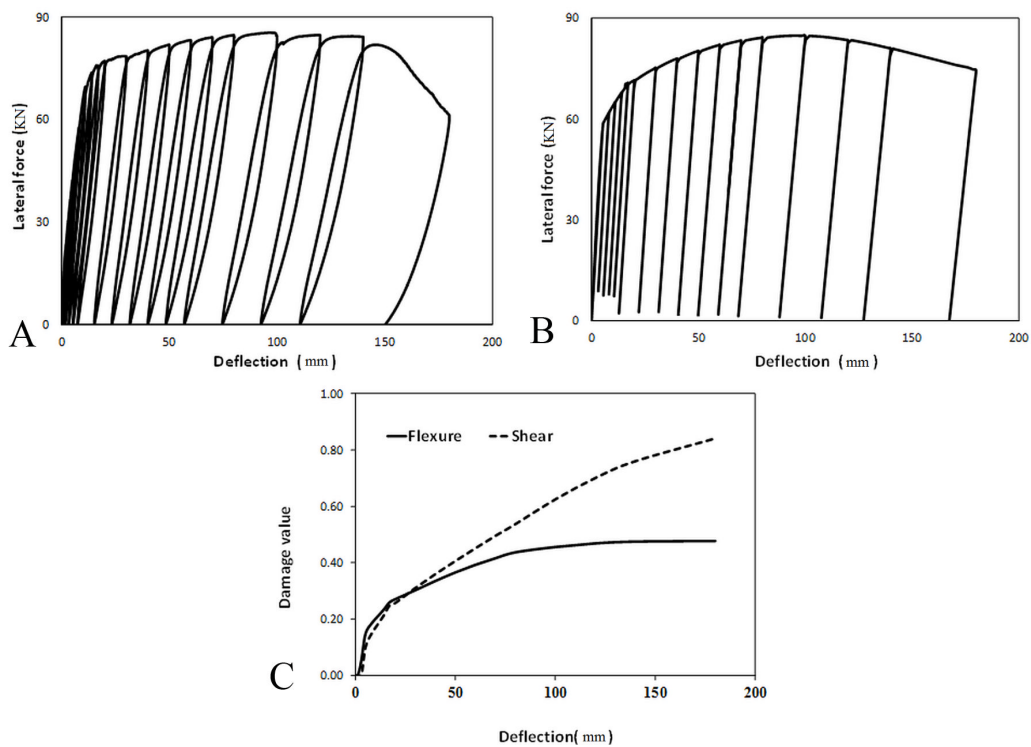




Figure 19. Behavior of a short RC beam in cantilever a) Experimental deflection vs. lateral force b) Numerical deflection vs. lateral force c) Damage evolution

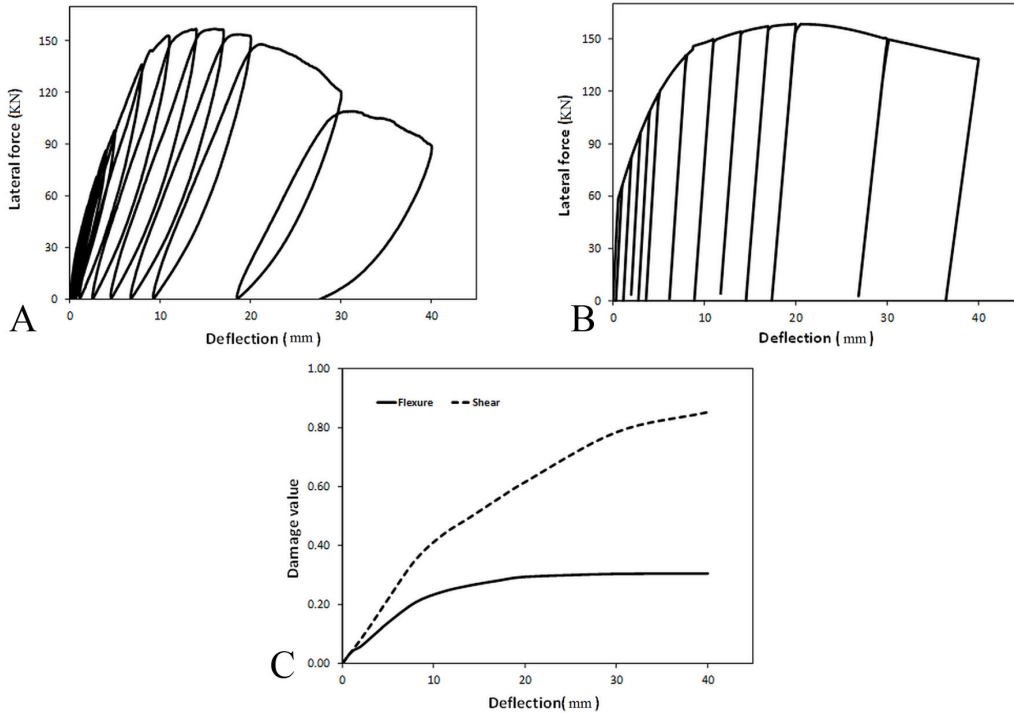
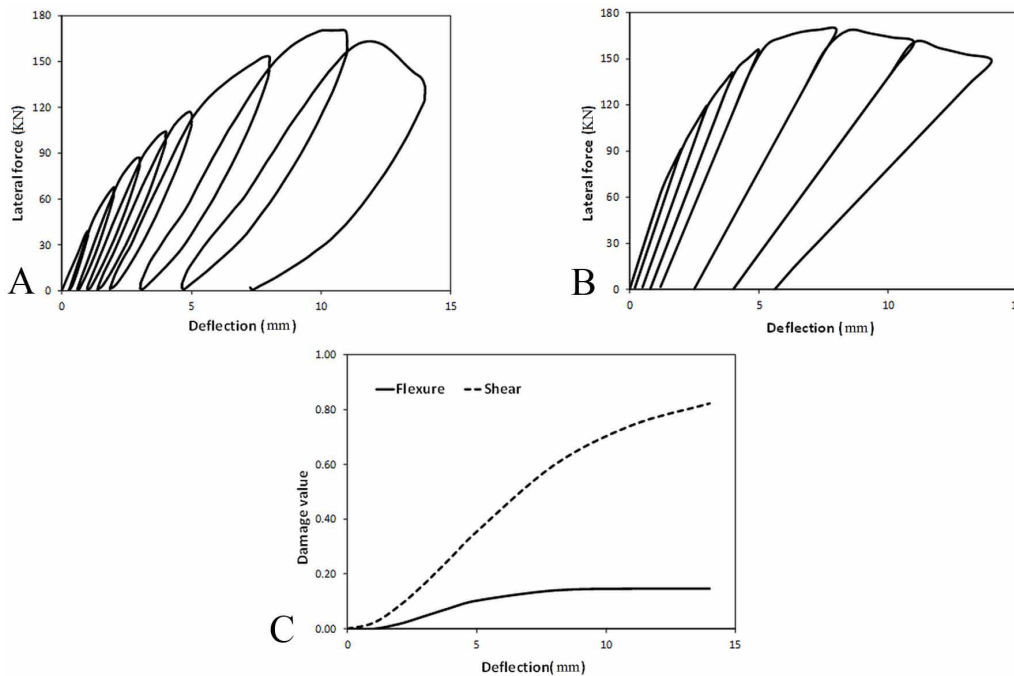
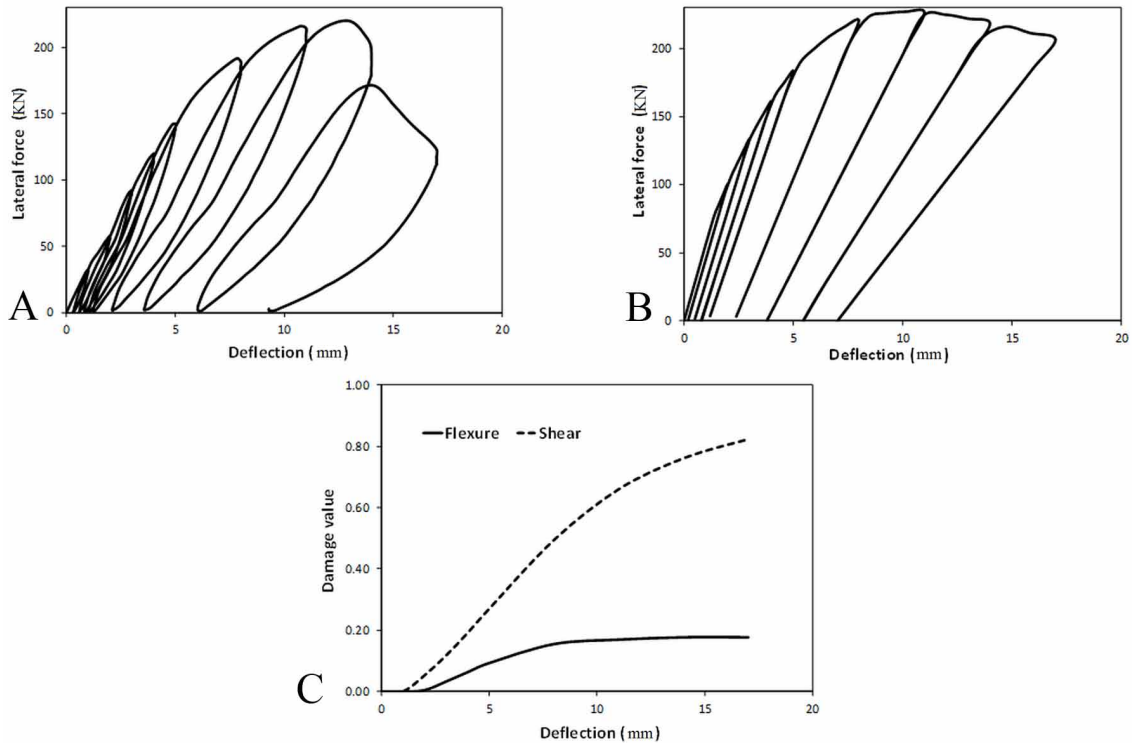


Figure 20. Behavior of a RC wall in cantilever subjected to lateral load without axial force a) Experimental deflection vs. lateral force b) Numerical deflection vs. lateral force c) Damage evolution



## Damage Mechanics of Dual Systems

Figure 21. Behavior of a RC wall in cantilever subjected to lateral load and an axial force equal to 340 KN  
a) Experimental deflection vs. lateral force b) Numerical deflection vs. lateral force c) Damage evolution



### 11.5.4 Numerical Simulation of the Tests Described in Section 11.1.4

The Figure 22 and 23 show the numerical simulations of RC short columns subjected to axial force equal to, respectively, 180 KN and 420 KN (Figure 9-11). It is important to underline that the axial force changes the values of the characteristic moments and shear forces: for first cracking, first yield and ultimate. Thus, although the model is the same, the procedure for the computation of its parameters is modified by the presence of the axial force. In the numerical simulation, the two damages reached very high values simultaneously.

### 11.5.5 Numerical Simulation of a Test on a Dual Structure

The last validation was carried out using the structure shown in Figure 24. This is a continuous beam of two elements, one short and one slender, separated by a chunk that represents a column; the beam is embedded at its ends in two heavy RC blocks that represent fixed supports. A mono-sign loading was applied at the column. The goal of this test is to reproduce the short element effect that is shown in Figure 1; and then to test the ability of the model to simulate it and recognize the different patterns of cracking in the structure.

Figure 22. Behavior of a short RC column in cantilever subjected to lateral loads and axial force equal to 180 KN a) Experimental deflection vs. lateral force b) Numerical deflection vs. lateral force c) Damage evolution

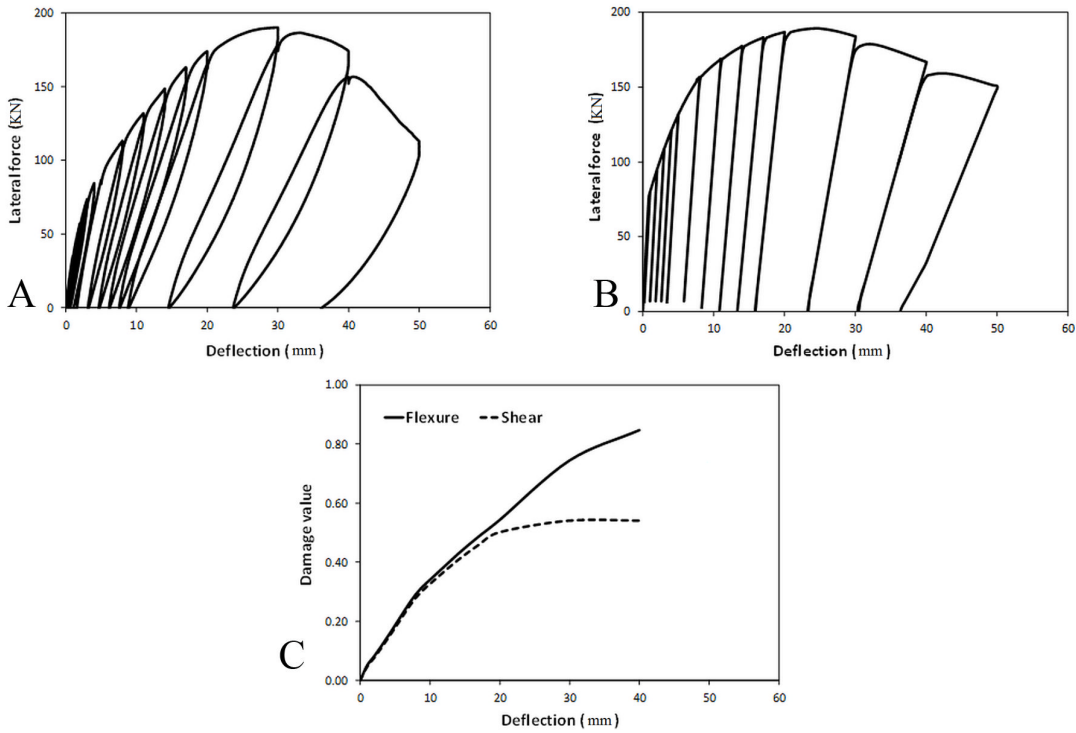
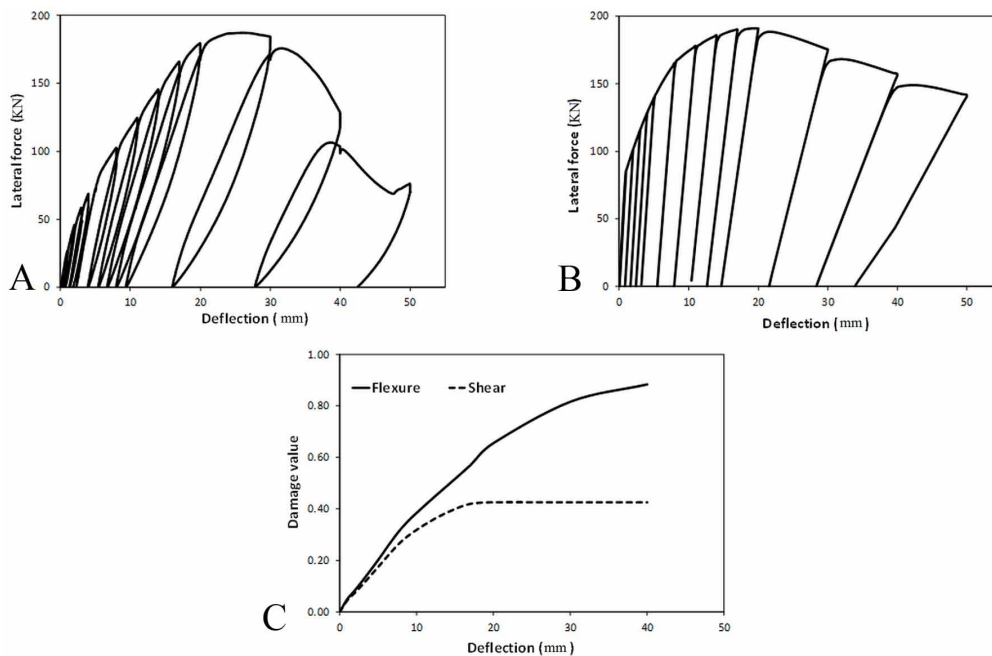
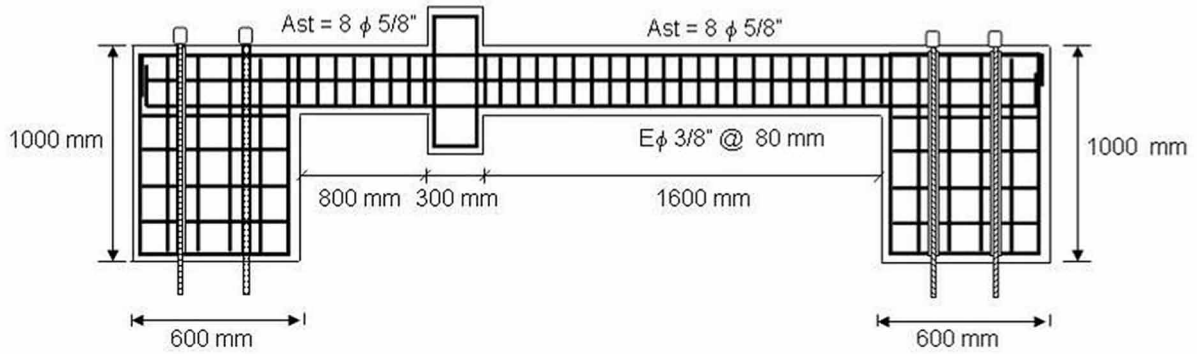


Figure 23. Behavior of a short RC column in cantilever subjected to lateral loads and axial force equal to 420 KN a) Experimental deflection vs. lateral force b) Numerical deflection vs. lateral force c) Damage evolution



## Damage Mechanics of Dual Systems

Figure 24. Continuous two element beam



As expected, the experimental results show moderate flexural damage in the plastic hinge regions of both elements and severe shear damage in the short beam. The quality of the numerical simulation can be evaluated in the graph of deflection vs. force for the column shown in Figure 25.

The histories of damage obtained numerically are presented in Figure 26. They can be compared with the cracking patterns observed in the test. Notice that the simulation is good and that the computed damage values seem to agree with the observed fracture state.

Figure 25. Deflection vs. force a) Experimental analysis b) Numerical simulation

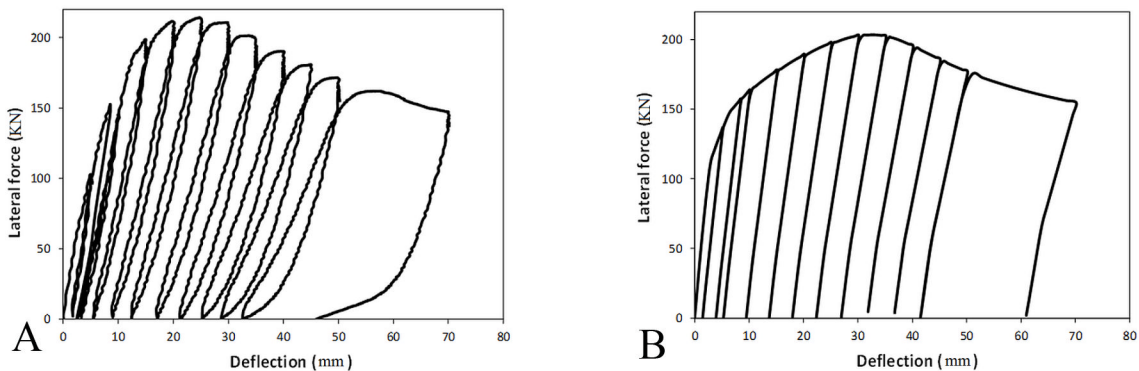
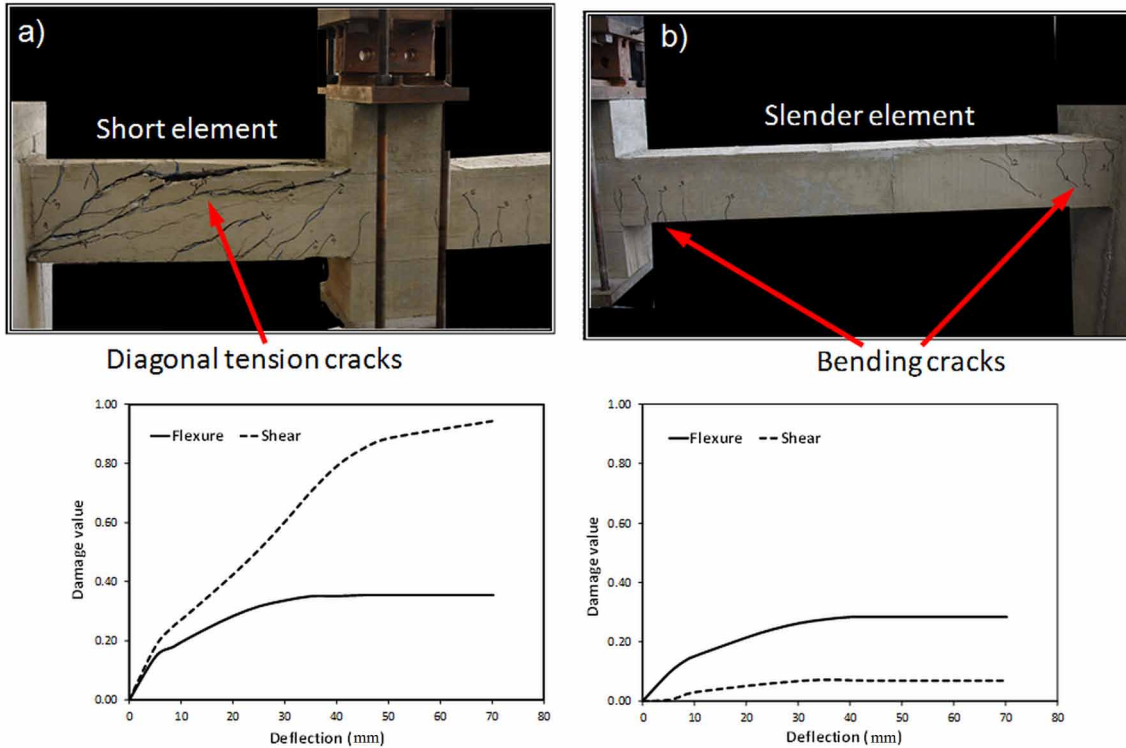


Figure 26. Cracking evolution in the continuous beam a) Short element and corresponding damage history b) Slender element and corresponding damage history



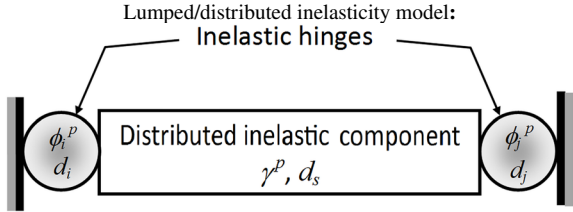
## 11.6 SUMMARY AND EQUATIONS QUICK REFERENCE

In this chapter, lumped damage mechanics was extended to the case of dual systems and, in general, RC structures with elements that have any aspect ratio. An experimental analysis using indicators indicates that two different sets of cracks appear in walls, squat elements or intermediate elements: one due to bending moments and another due to shear forces; the former were considered in the previous chapter.

It is important to underline that structural failure due to shear cracking is a much more brittle and dangerous process than bending collapse. Therefore having a model that can differentiate and quantify the two cracking processes is very important for the structural safety assessment.

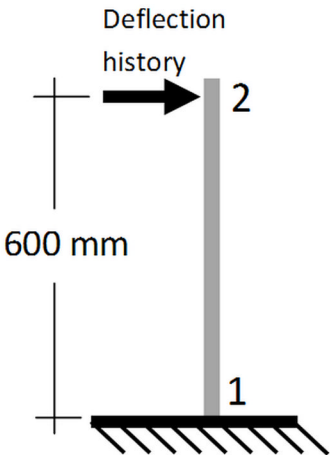
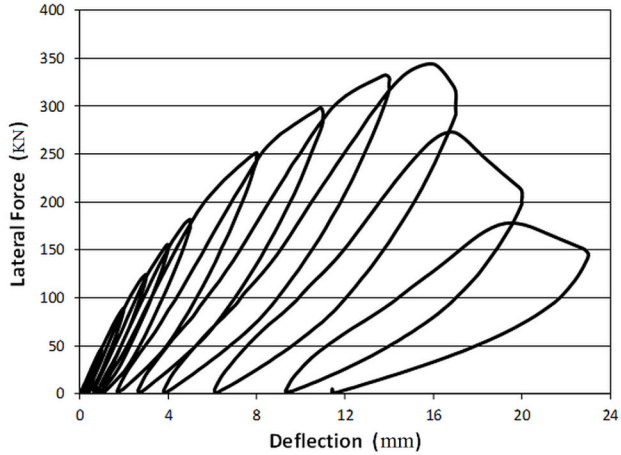
The generalization of the damage model was carried out by using the lumped/distributed plasticity assumption of chapter 7 with the techniques presented in chapter 10. The numerical simulations of test on elements with different aspect ratios prove that the new model describes the physical phenomena (See Table 2).

Table 2.

ELASTICITY LAW FOR FRAME MEMBERS OF ANY ASPECT RATIO	
<p>Lumped/distributed inelasticity model: Inelastic hinges</p> 	
<p>Elasticity law for frame members of any aspect ratio</p> $\{\Phi\}_b = \{\Phi^{bcw}\}_b + \{\Phi^h\}_b$ $\{\Phi\}_b = ([F_f]_b + [F_s]_b)\{M\}_b + \{\gamma^p\}_b + \{\gamma^d\}_b + \{\Phi^p\}_b + \{\Phi^d\}_b \quad (11.2.1)$ <p><math>\{\gamma^d\}_b</math> : damage related distortion</p>	
<p>Damage related distortion</p> $\{\gamma^d\}_b = [C_s(d_s)]_b \{M\}_b, \text{ where } [C_s(d_s)] = \frac{d_s}{1-d_s} \begin{bmatrix} \frac{1}{GA_b L_b} & \frac{1}{GA_b L_b} & 0 \\ \frac{1}{GA_b L_b} & \frac{1}{GA_b L_b} & 0 \\ 0 & 0 & 0 \end{bmatrix} \quad (11.2.2)$	
<p>Elasticity law in terms of flexibility</p> $\{\Phi\}_b - \{\Phi^p\}_b - \{\gamma^p\}_b = [F(D, d_s)] \{M\}_b \quad (11.2.3)$ $[F(D, d_s)]_b = [F_f]_b + [F_s]_b + [C(D)]_b + [C_s(d_s)]_b \quad (11.2.4)$ $[F(D, d_s)] = \begin{bmatrix} \frac{L_b}{3EI_b(1-d_i)} + \frac{1}{GA_b L_b(1-d_s)} & -\frac{L_b}{6EI_b} + \frac{1}{GA_b L_b(1-d_s)} & 0 \\ -\frac{L_b}{6EI_b} + \frac{1}{GA_b L_b(1-d_s)} & \frac{L_b}{3EI_b(1-d_j)} + \frac{1}{GA_b L_b(1-d_s)} & 0 \\ 0 & 0 & \frac{L_b}{EA_b} \end{bmatrix}$	
<p>Elasticity law in terms of stiffness</p> $\{M\}_b = [E(D, d_s)] \{\Phi - \Phi^p - \gamma^p\}_b, [E(D, d_s)] = [F(D, d_s)]^{-1} \quad (11.2.5)$ <p><math>[E(D, d_s)]</math> : elasticity matrix of a RC element of any aspect ratio</p>	

*continued on following page*

Table 2. Continued

DAMAGE EVOLUTION LAWS	
<i>Energy Release Rates</i>	
Complementary deformation energy	
$W_b = \frac{1}{2} \{ \mathbf{M} \}_b^t \{ \Phi - \Phi^p - \gamma^p \}_b = \frac{1}{2} \{ \mathbf{M} \}_b^t [ \mathbf{F}(\mathbf{D}, d_s) ]_b \{ \mathbf{M} \}_b \quad (11.3.1)$	
The energy release rates	
$G_i = \frac{\partial W}{\partial d_i} = \frac{L m_i^2}{6EI(1-d_i)^2}; \quad G_j = \frac{\partial W}{\partial d_j} = \frac{L m_j^2}{6EI(1-d_j)^2}; \quad G_s = \frac{\partial W}{\partial d_s} = \frac{LV^2}{2GA(1-d_s)^2} \quad (11.3.2)$	
$V = (m_i + m_j)/L$	
Damage evolution law by:	
$\left\{ \begin{array}{l} \Delta d_i = 0 \text{ if } G_i < R_i \\ G_i = R_i \text{ if } \Delta d_i > 0 \end{array} \right\}; \left\{ \begin{array}{l} \Delta d_j = 0 \text{ if } G_j < R_j \\ G_j = R_j \text{ if } \Delta d_j > 0 \end{array} \right\}; \left\{ \begin{array}{l} \Delta d_s = 0 \text{ if } G_s < R_s \\ G_s = R_s \text{ if } \Delta d_s > 0 \end{array} \right\} \quad (11.3.3)$	
<i>Experimental Measurement of the Shear Damage <math>d_s</math></i>	
	
First line of the elasticity law (11.2.3)	
$\phi_1 - \gamma^p = \left( \frac{L}{3EI} + \frac{1}{GAL(1-d_s)} \right) m_1 + \left( -\frac{L}{6EI} + \frac{1}{GAL(1-d_s)} \right) m_2 \quad (11.3.4)$	
Boundary conditions	
$m_1 = P.L; \quad m_2 = 0; \quad \phi_1 = \frac{t}{L} \quad (11.3.5)$	
$P$ : lateral force on node 2 $t$ : lateral displacement on the node 2	

continued on following page

## Damage Mechanics of Dual Systems

Table 2. Continued

<p>Shear damage</p> $P = Z(d_s)(t - t_p); t_p = \gamma^p L; Z(d_s) = \frac{3EI GA(1 - d_s)}{L(L^2 GA - L^2 GA d_s + 3EI)} \quad (11.3.6)$ $d_s = \frac{3GA EI - 3Z L EI - Z L^3 GA}{GA(3EI - L^3 Z)} \quad (11.3.7)$
<b>Shear Crack Resistance Function</b>
<p>General expression for the crack resistance function</p> $R(d_s) = R_{0s} + q_s \frac{\ln(1 - d_s)}{1 - d_s} \quad (11.3.8)$
<b>Computation of the Parameters <math>R_{0s}</math> and <math>q_s</math></b>
<p>Griffith criterion</p> $\frac{LV^2}{2GA(1 - d_s)^2} = R_{0s} + q_s \frac{\ln(1 - d_s)}{1 - d_s} \quad ; \text{i.e.} \quad LV^2 = 2GA(1 - d_s)^2 \left( R_{0s} + q_s \frac{\ln(1 - d_s)}{1 - d_s} \right) \quad (11.3.9)$
<p>Parameter <math>R_{0s}</math> The condition of cracking initiation (<math>d_s = 0</math>):</p> $LV_{cr}^2 = 2GAR_{0s}; \text{i.e.} \quad R_{0s} = \frac{LV_{cr}^2}{2GA} \quad (11.3.10)$
<p>Parameter <math>q_s</math> The numerical resolution of (11.3.11-12) gives: <math>q_s</math> and <math>d_{su}</math></p> $2R_{0s} d_{su} - 2R_{0s} - q_s - q_s \ln(1 - d_{su}) = 0 \quad (11.3.11)$ $LV_u^2 = 2GA(1 - d_{su})^2 \left( R_{0s} + q_s \frac{\ln(1 - d_{su})}{1 - d_{su}} \right) \quad (11.3.12)$
<b>Computation of The First Cracking Shear Force</b>
<p>Cracking shear force</p> $V_{cr} = 0.17 \left( 1 + \frac{N}{14A_g} \right) \sqrt{f'_c} A_g \quad (11.3.13)$ <p><math>N</math>: Axial Load in N.  <math>A_g</math>: gross area of the concrete section in mm<sup>2</sup>.  <math>f'_c</math>: strength of concrete in MPa.</p>

continued on following page



Table 2. Continued

<b>Modified Griffith Criteria</b>	
Modified Griffith criterion	
$\begin{cases} \Delta d_i = 0 & \text{if } G_i < R_{0i} \\ \Delta d_i = \frac{1}{\partial R_i / \partial d_i} \left( \frac{G_i}{R_i} \right)^2 \langle \Delta G_i \rangle_+ & \text{otherwise} \end{cases}$	
$\begin{cases} \Delta d_j = 0 & \text{if } G_j < R_{0j} \\ \Delta d_j = \frac{1}{\partial R_j / \partial d_j} \left( \frac{G_j}{R_j} \right)^2 \langle \Delta G_j \rangle_+ & \text{otherwise} \end{cases}$	(11.3.14)
$\begin{cases} \Delta d_s = 0 & \text{if } G_s < R_{0s} \\ \Delta d_s = \frac{1}{\partial R_s / \partial d_s} \left( \frac{G_s}{R_s} \right)^2 \langle \Delta G_s \rangle_+ & \text{otherwise} \end{cases}$	
<b>PLASTIC DEFORMATIONS EVOLUTION LAWS</b>	
The evolution laws of the plastic rotations corresponding to the inelastic hinges	
$\begin{cases} d\phi_i^p = 0 \text{ if } f_i < 0 \\ f_i = 0 \text{ if } d\phi_i^p \neq 0 \end{cases} \quad \begin{cases} d\phi_j^p = 0 \text{ if } f_j < 0 \\ f_j = 0 \text{ if } d\phi_j^p \neq 0 \end{cases}$	
(11.4.1)	
$f_i = \left  \frac{m_i}{1-d_i} - c_i \phi_i^p \right  - k_{0i} \leq 0 \quad f_j = \left  \frac{m_j}{1-d_j} - c_j \phi_j^p \right  - k_{0j} \leq 0$	
$c_i, c_j, k_{0i}$ and $k_{0j}$ parameters obtained using the same procedure presented in section 10.4.2.	
Effective shear force	
$\bar{V} = \frac{V}{1-d_s} = \frac{m_i + m_j}{(1-d_s)L} \quad (11.4.2)$	
Yield function for plastic distortion with linear kinematic hardening	
$f_s = \left  \bar{V} - c_s \gamma^p \right  - k_{os} = \left  \frac{m_i + m_j}{(1-d_s)L} - c_s \gamma^p \right  - k_{os} \leq 0 \quad (11.4.3)$	

continued on following page

## Damage Mechanics of Dual Systems

Table 2. Continued

<p>Plastic distortion evolution law</p> $\begin{cases} d\gamma_p = 0 & \text{if } f_s < 0 \\ f_s = 0 & \text{if } d\gamma_p \neq 0 \end{cases} \quad (11.4.4)$ <p><math>c_s</math> and <math>k_{0s}</math>: parameters obtained using the same procedure presented in section 10.4.2.</p>
<p>Value of damage <math>d_{sp}</math> that corresponds to <math>V=V_p</math></p> $L V_p^2 = 2GA(1 - d_{sp})^2 \left( R_{0s} + q_s \frac{\ln(1 - d_{sp})}{1 - d_{sp}} \right) \quad (11.4.5)$
<p>Parameter <math>k_{0s}</math></p> $k_{0s} = \frac{V_p}{1 - d_{sp}} \quad (11.4.6)$
<p>Parameter <math>c_s</math></p> $c_s = \frac{1}{\gamma_u^p} \left( \frac{V_u}{1 - d_{su}} - k_{0s} \right) \quad (11.4.7)$ <p><math>\gamma_u^p</math>: ultimate plastic distortion</p>
<p><b>ANALYSIS OF DUAL SYSTEMS</b></p>
<p><i>Formulation of the problem</i></p> <ul style="list-style-type: none"> <li>- Compute: the free displacements, reaction forces, stresses, deformations, plastic deformations and damages.</li> <li>- With the following data: the initial configuration of the structure, the restricted displacements, the nodal forces corresponding to the free displacements and those applied over the elements, the material and cross-section properties and yield functions.</li> </ul>
<p>Such that they verify the following equations (11.5.1):</p>
<p>Nonlinear kinematic and Equilibrium equations</p> $\{\Delta \Phi\}_b = [\mathbf{B}_E(\mathbf{U}_{t=tr})]_b \{\Delta \mathbf{U}\}$ $\{\mathbf{L}_{t=tr}\} = \{\mathbf{P}_{t=tr}\}; \quad \{\mathbf{L}_{t=tr}\} = \sum_{b=1}^m [\mathbf{B}(\mathbf{U}_{t=tr})_E]_b^T \{\mathbf{M}_{t=tr}\}_b$
<p>Elasticity law</p> $\{\Phi\}_b - \{\Phi^p\}_b - \{\gamma^p\}_b = [\mathbf{F}(\mathbf{D}, d_s)] \{\mathbf{M}\}_b; \text{ or } \{\mathbf{M}\}_b = [\mathbf{E}(\mathbf{D}, d_s)] \{\Phi - \Phi^p - \gamma^p\}_b$
<p>Plastic deformation evolution laws</p> $\begin{cases} d\phi_i^p = 0 \text{ if } f_i < 0 \\ f_i = 0 \text{ if } d\phi_i^p \neq 0 \end{cases}; \quad \begin{cases} d\phi_j^p = 0 \text{ if } f_j < 0 \\ f_j = 0 \text{ if } d\phi_j^p \neq 0 \end{cases}; \quad \begin{cases} d\gamma_p = 0 \text{ if } < 0 \\ f_s = 0 \text{ if } d\gamma_p \neq 0 \end{cases}$
<p>With the yield functions:</p> $f_j = \left  \frac{m_j}{1 - d_j} - c_j \phi_j^p \right  - k_{0j} \leq 0; \quad f_i = \left  \frac{m_i}{1 - d_i} - c_i \phi_i^p \right  - k_{0i} \leq 0; \quad f_s = \left  \frac{V}{1 - d_s} - c_s \gamma^p \right  - k_{0s} \leq 0$

continued on following page

Table 2. Continued

and the damage evolution laws:

$$\begin{cases} \Delta d_j = 0 & \text{if } G_j < R_{0j} \\ \Delta d_j = \frac{1}{\partial R_j / \partial d_j} \left( \frac{G_j}{R_j} \right)^2 \langle \Delta G_j \rangle_+ & \text{otherwise} \end{cases}$$

$$\begin{cases} \Delta d_i = 0 & \text{if } G_i < R_{0i} \\ \Delta d_i = \frac{1}{\partial R_i / \partial d_i} \left( \frac{G_i}{R_i} \right)^2 \langle \Delta G_i \rangle_+ & \text{otherwise} \end{cases}$$

$$\begin{cases} \Delta d_s = 0 & \text{if } G_s < R_{0s} \\ \Delta d_s = \frac{1}{\partial R_s / \partial d_s} \left( \frac{G_s}{R_s} \right)^2 \langle \Delta G_s \rangle_+ & \text{otherwise} \end{cases}$$

## 11.7 PROJECTS

### 11.7.1. Generalize the Program Developed in the Project 10.12.1 including the Case of RC Elements with Any Ratio Aspect

## REFERENCES

- Perdomo, M. E. (2010). *Fractura y daño en estructuras duales de concreto armado*. (Unpublished doctoral dissertation). University of Los Andes, Los Andes, Venezuela.
- Perdomo, M. E., Picón, R., Marante, M. E., Hild, F., Roux, S., & Flórez-López, J. (2013). Experimental analysis and mathematical modeling of fracture in RC elements with any aspect ratio. *Engineering Structures*, 46, 407–416. doi:10.1016/j.engstruct.2012.07.005
- Thomson, E. (2004). *Modelo simplificado para la evaluación del daño en muros estructurales bajos de concreto armado sujetos a cargas laterales*. (Unpublished doctoral dissertation). University of Los Andes, Los Andes, Venezuela.
- Thomson, E., Perdomo, M. E., Picón, R., Marante, M. E., & Flórez López, J. (2009). Simplified model for damage in squat RC shear wall. *Engineering Structures*, 31(10), 2215–2223. doi:10.1016/j.engstruct.2009.05.020

# Chapter 12

## Unilateral Damage in Reinforced Concrete Frames

### ABSTRACT

*One of the main applications of the lumped damage mechanics or the damage mechanics of dual systems is the earthquake vulnerability assessment of structures. This means not only the consideration of the inertia forces but, mainly, the adequate description of crack propagation under general cyclic loading. Chapter 9 described the concept of unilateral damage (i.e. the appearance of distinct and independent sets of cracks after loading reversals). This phenomenon can also be observed in RC structures, and the models presented in Chapters 10 and 11 do not describe it; thus, they should be used only in the cases of mono sign loadings. The first goal of this chapter is the generalization of the damage models, including unilateral effects; the next one consists of the development of lumped damage models for tridimensional analysis of RC frames. Finally, some guidelines for the use of the damage models in industrial applications are presented.*

### 12.1 ELASTICITY LAW UNDER CYCLIC LOADING

#### 12.1.1 Unilateral Damage in Reinforced Concrete Elements

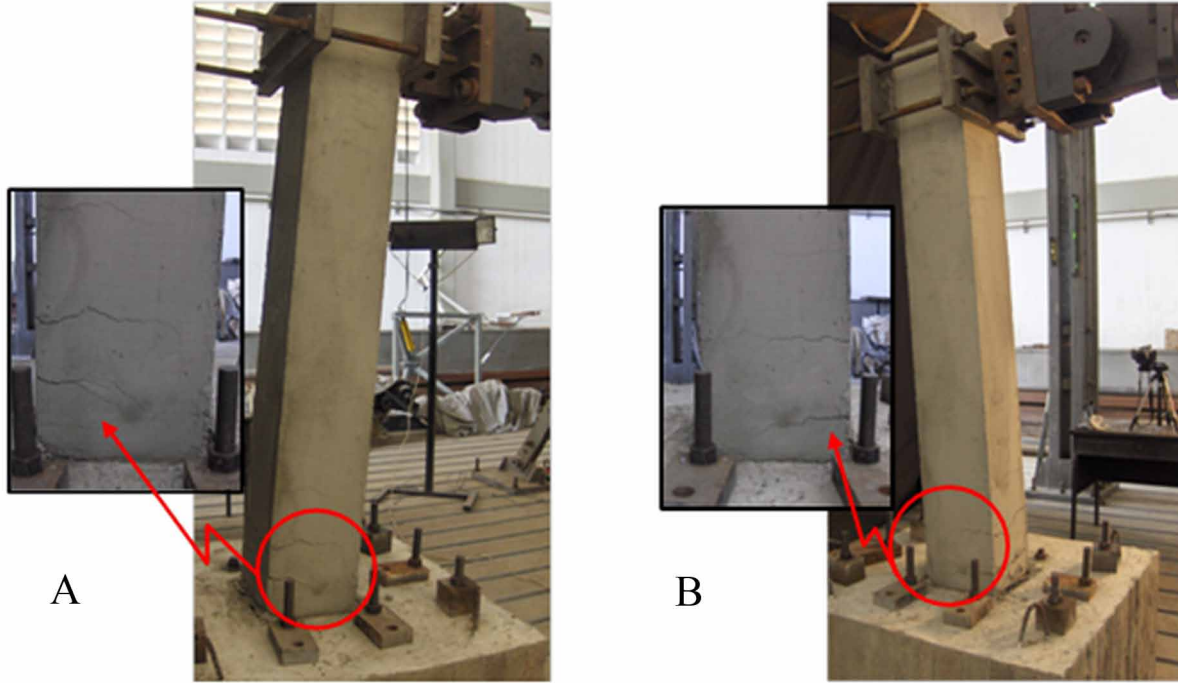
Figure 1 shows the sequence of cracking patterns in a slender RC specimen subjected to cyclic loading. The two images of the figure show the cracking pattern corresponding to external forces of different sign. It can be observed clearly the two distinct set of cracks.

Figure 2 shows the same phenomenon in a wall, the two sets of shear cracks can also be appreciated.

These damage mechanisms can be characterized using unilateral damage arrays as in continuum damage mechanics (see section 9.2.6):  $(\mathbf{D}^+)_b = (d_i^+, d_j^+), d_s^+$  and  $(\mathbf{D}^-)_b = (d_i^-, d_j^-), d_s^-$ ; the damage parameters  $d_i^+$  and  $d_j^+$  represent crack density due to positive bending moments. The variable  $d_s^+$  measures shear cracking caused by positive shear forces. The damage parameters  $d_i^-$ ,  $d_j^-$  and  $d_s^-$  represent, respectively, damage at plastic hinge  $i$  due to negative bending moments, flexure negative cracks lumped at plastic hinges  $j$  and shear crack density caused by negative shear forces (see Figure 3).

DOI: 10.4018/978-1-4666-6379-4.ch012

Figure 1. a) Cracking pattern in a slender frame element under negative lateral forces b) Cracking pattern after load reversal



### 12.1.2 Elasticity Law of a RC Element with Unilateral Damage

Consider again the elasticity law in the case of mono-sign loadings only (see section 11.2):  $\{\Phi\}_b - \{\Phi^p\}_b - \{\gamma^p\}_b = [\mathbf{F}(\mathbf{D}, d_s)] \{\mathbf{M}\}_b$ . The development of this matrix equation gives:

$$\phi_i - \phi_i^p - \gamma_s^p = \left( \frac{L_b}{3EI_b(1-d_i)} m_i - \frac{L_b}{6EI_b} m_j \right) + \frac{V}{GA_b(1-d_s)}$$

$$\delta = \frac{L_b}{AE_b} n$$

$$\phi_j - \phi_j^p - \gamma_s^p = \left( -\frac{L_b}{6EI_b} m_i + \frac{L_b}{3EI_b(1-d_j)} m_j \right) + \frac{V}{GA_b(1-d_s)} \quad (12.1.1)$$

where  $V = \frac{m_i + m_j}{L_b}$  is the shear force.

**Unilateral Damage in Reinforced Concrete Frames**

Figure 2. a) Shear cracks under positive, nil and negative lateral forces b) Shear cracks after of several cyclic loads

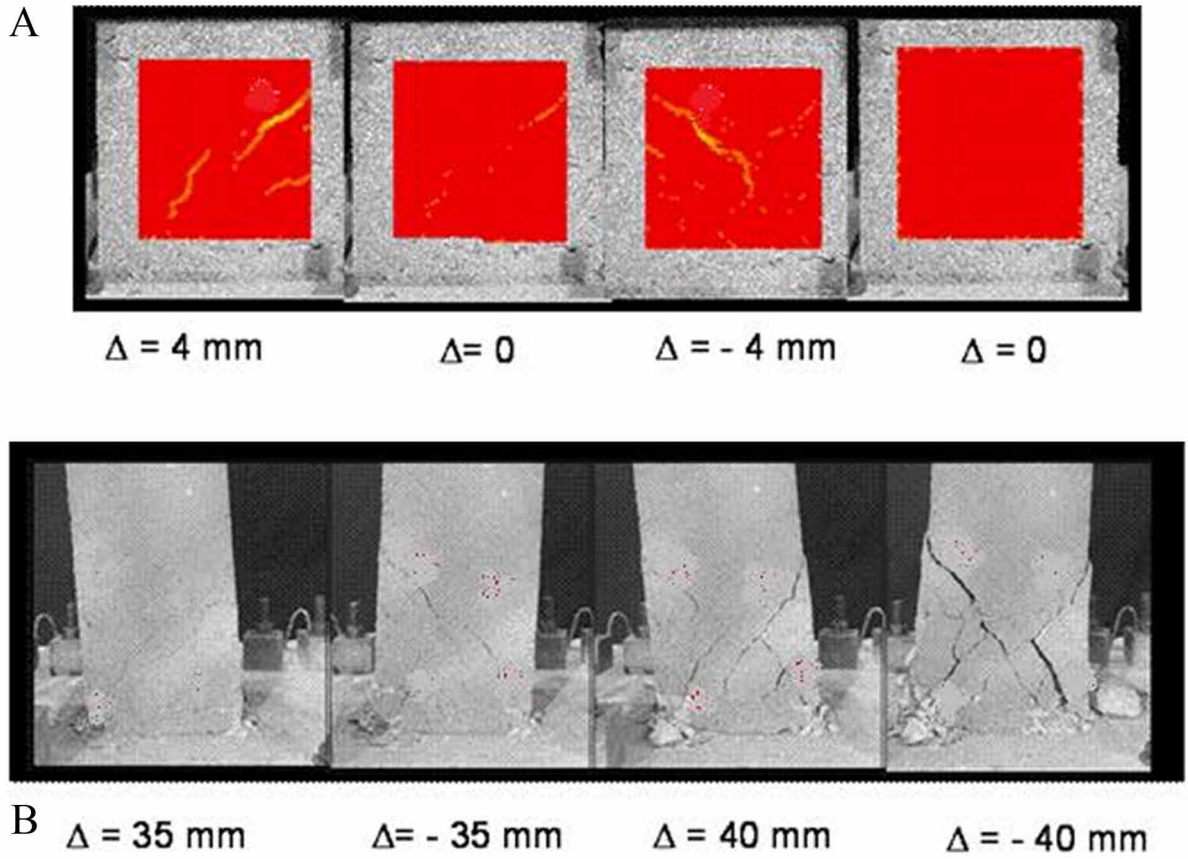
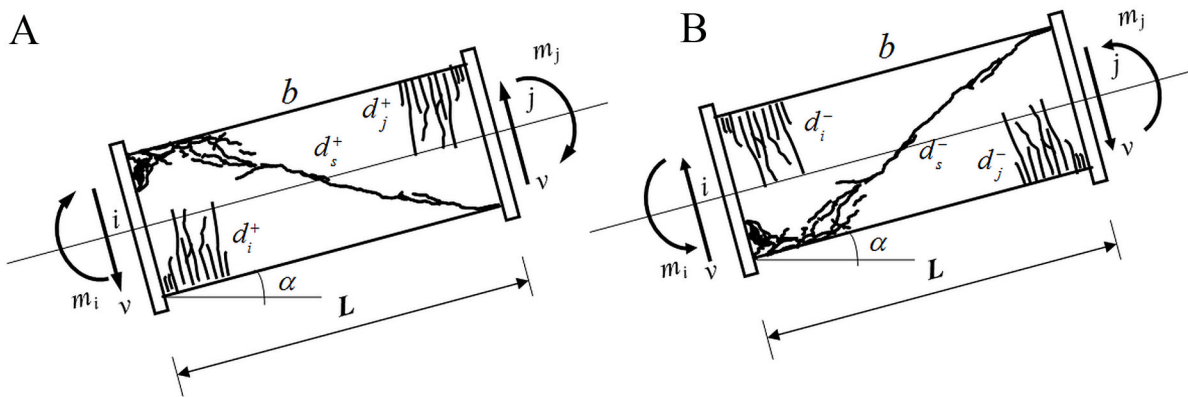


Figure 3. Unilateral damage in a RC frame element of any aspect ratio under a) positive actions b) negative actions



Following the same procedure described in section 9.2.6, the elasticity law of a damaged RC element of any aspect ratio under general cyclic loading is obtained by modifying (12.1.1) as follows:

$$\phi_i - \phi_i^p - \gamma_s^p = \left( \frac{L_b}{3EI_b(1-d_i^+)} \langle m_i \rangle_+ + \frac{L_b}{3EI_b(1-d_i^-)} \langle m_i \rangle_- - \frac{L_b}{6EI_b} m_j \right) + \frac{\langle V \rangle_+}{GA_b(1-d_s^+)} + \frac{\langle V \rangle_-}{GA_b(1-d_s^-)}$$

$$\delta = \frac{L_b}{AE_b} n$$

$$\phi_i - \phi_i^p - \gamma_s^p = \left( -\frac{L_i}{6EI_i} m_i + \frac{L_i}{3EI_i(1-d_i^+)} \langle m_i \rangle_+ + \frac{L_i}{3EI_i(1-d_i^-)} \langle m_i \rangle_- \right) + \frac{\langle V \rangle_+}{GA_i(1-d_s^+)} + \frac{\langle V \rangle_-}{GA_i(1-d_s^-)} \quad (12.1.2)$$

In matrix notation, the equations (12.1.2) can be written as:

$$\{\Phi\}_b - \{\Phi^p\}_b - \{\gamma^p\}_b = [\mathbf{F}_f(\mathbf{D}^+)] \langle \mathbf{M} \rangle_b^+ + [\mathbf{F}_f(\mathbf{D}^-)] \langle \mathbf{M} \rangle_b^- + \frac{1}{GA_b(1-d_s^+)} \langle \mathbf{V} \rangle_b^+ + \frac{1}{GA_b(1-d_s^-)} \langle \mathbf{V} \rangle_b^- \quad (12.1.3)$$

where  $[\mathbf{F}_f(\mathbf{D}^+)]$  and  $[\mathbf{F}_f(\mathbf{D}^-)]$  are matrices of elastic flexibility with damage but without shear effects; the terms  $\langle \mathbf{V} \rangle_b^+$  and  $\langle \mathbf{V} \rangle_b^-$  represent the positive and negative part of a shear matrix for element  $b$ :

$$[\mathbf{F}_f(\mathbf{D}^{+/-})] = \begin{bmatrix} \frac{L_b}{3EI_b(1-d_i^{+/-})} & -\frac{L_b}{6EI_b} & 0 \\ -\frac{L_b}{6EI_b} & \frac{L_b}{3EI_b(1-d_j^{+/-})} & 0 \\ 0 & 0 & \frac{L_b}{EA_b} \end{bmatrix}; \langle \mathbf{V} \rangle_b^{+/-} = \begin{bmatrix} \langle V \rangle_{+/-} \\ \langle V \rangle_{+/-} \\ 0 \end{bmatrix} \quad (12.1.4)$$

The Equation (12.1.2) is again based on the assumption that negative cracks are completely closed under positive stresses; thus, they have no influence at all on the behavior of the element and vice versa.

In the case of slender elements, where the shear terms can be neglected, the elasticity law becomes a much simpler expression:

$$\{\Phi\}_b - \{\Phi^p\}_b = [\mathbf{F}_f(\mathbf{D}^+)] \langle \mathbf{M} \rangle_b^+ + [\mathbf{F}_f(\mathbf{D}^-)] \langle \mathbf{M} \rangle_b^- \quad (12.1.5)$$

## 12.2 INTERNAL VARIABLES EVOLUTION LAWS UNDER CYCLIC LOADING

### 12.2.1 Damage Evolution Laws

The same procedure used in chapters 9, 10 and 11 can also be followed in this case; i.e. the complementary deformation energy is given by:

$$W = \frac{1}{2} \{\mathbf{M}\}_b^t \{\Phi - \Phi^p - \gamma^p\}_b = \frac{1}{2} \{\mathbf{M}\}_b^t [\mathbf{F}_f(\mathbf{D}^+)] \langle \mathbf{M} \rangle_b^+ + \frac{1}{2} \{\mathbf{M}\}_b^t [\mathbf{F}_f(\mathbf{D}^-)] \langle \mathbf{M} \rangle_b^- + \frac{1}{2GA_b(1-d_s^+)} \{\mathbf{M}\}_b^t \langle \mathbf{V} \rangle_b^+ + \frac{1}{2GA_b(1-d_s^-)} \{\mathbf{M}\}_b^t \langle \mathbf{V} \rangle_b^- \quad (12.2.1)$$

now the energy release rates can be obtained for the six different arrays of cracks defined so far:

$$G_{i/j}^{+/-} = \frac{\partial W}{\partial d_{i/j}^{+/-}} = \frac{L_b \langle m_{i/j} \rangle_{+/-}^2}{6EI_b(1-d_{i/j}^{+/-})^2}; G_s^{+/-} = \frac{\partial W}{\partial d_s^{+/-}} = \frac{L_b V_{+/-}^2}{2GA_b(1-d_s^{+/-})^2} \quad (12.2.2)$$

Assuming again that there is no coupling between the different cracking mechanisms, the damage evolution laws can be defined using six independent Griffith criteria, or their modified versions:

$$\begin{cases} \Delta d_{i/j/s}^{+/-} = 0 & \text{if } G_{i/j/s}^{+/-} < R_{i/j/s}^{+/-} \\ G_{i/j/s}^{+/-} = R_{i/j/s}^{+/-} & \text{if } \Delta d_{i/j/s}^{+/-} > 0 \end{cases}; \quad (12.2.3)$$

for the classic version, or

$$\begin{cases} \Delta d_{i/j/s}^{+/-} = 0 & \text{if } G_{i/j/s}^{+/-} < R_{0i/j/s}^{+/-} \\ \Delta d_{i/j/s}^{+/-} = \frac{1}{\left(\frac{\partial R_{i/j/s}^{+/-}}{\partial d_{i/j/s}^{+/-}}\right)} \left(\frac{G_{i/j/s}^{+/-}}{R_{i/j/s}^{+/-}}\right)^2 \langle \Delta G_{i/j/s}^{+/-} \rangle_+ & \text{otherwise} \end{cases} \quad (12.2.4)$$

for the modified one.

The parameters of the six functions of crack resistance can be computed by the repeated application of the procedures indicated in sections 10.3 and 11.3.; consequently, it is possible to introduce into the analysis different ultimate moments, under positive and negative actions. This is important in the case of beams, which often have an asymmetric cross-section or an asymmetric reinforcement distribution (see example 12.9.1).



### 12.2.2 Plastic Deformations Evolution Laws

Consider again the yield function of a plastic hinge in the case of mono-sign loadings only (Equation 10.4.2). Notice that the absolute value of a variable “ $Y$ ” can also be written in a more cumbersome but completely equivalent way by choosing the maximum between  $Y$  and  $-Y$ ; i.e. in mathematical notation:  $|Y| = \text{Max}(Y, -Y)$ ; therefore, the yield function (10.4.2) can also be written as:

$$f_i = \left| \frac{m_i}{1-d_i} - c_i \phi_i^p \right| - k_{0i} = \text{Max} \left( \frac{m_i}{1-d_i} - c_i \phi_i^p - k_{0i}, -\frac{m_i}{1-d_i} + c_i \phi_i^p - k_{0i} \right) \leq 0 \quad (12.2.5)$$

This expression can be modified so that unilateral damage is included in the following way:

$$f_i = \text{Max} \left( \frac{m_i}{1-d_i^+} - c_i^+ \phi_i^p - k_{0i}^+, -\frac{m_i}{1-d_i^-} + c_i^- \phi_i^p - k_{0i}^- \right) \leq 0 \quad (12.2.6)$$

The computation of the four parameters  $c_i^{+/-}$ ,  $k_{0i}^{+/-}$  can be carried out by applying twice the procedure described in section 10.4.2. Again, these different parameters allow for the consideration of beams with asymmetric cross section and different resistances under positive and negative bending moments.

Finally, in the Equation (12.2.6) only kinematic hardening is considered. However in section 7.1.6, it was indicated that there are two hardening mechanism: kinematic and isotropic. In a monotonic loading, any kind of hardening describes the same behavior; in a cyclic one, it is important establishing the percentages that correspond to each effect. In section 6.3.3, it was indicated that in the case of bending, about seventy percent can be assigned to kinematic hardening and the remaining thirty to the isotropic one; the proportion is sixty / forty for shear. Therefore, the yield function of a plastic hinge with damage and general cyclic moments is:

$$f_i = \text{Max} \left\{ \begin{array}{l} \frac{m_i}{1-d_i^+} - 0.7c_i^+ \phi_i^p - k_{0i}^+ - 0.3c_i^+ p_i \\ -\frac{m_i}{1-d_i^-} + 0.7c_i^- \phi_i^p - k_{0i}^- - 0.3c_i^- p_i \end{array} \right. \leq 0; p_i = \text{Max} |\phi_i^p| \quad (12.2.7)$$

Unlike cracking patterns, the number of plastic rotations does not change in the case of cyclic loading, there are still three of them: the plastic rotation of hinges  $i$  and  $j$  and the plastic distortion. Therefore, only three yield functions and evolution laws are needed:

$$\left\{ \begin{array}{l} d\phi_i^p = 0 \text{ if } f_i < 0 \\ f_i = 0 \text{ if } d\phi_i^p \neq 0 \end{array} \right\}; \left\{ \begin{array}{l} d\phi_j^p = 0 \text{ if } f_j < 0 \\ f_j = 0 \text{ if } d\phi_j^p \neq 0 \end{array} \right\}; \left\{ \begin{array}{l} d\gamma_s^p = 0 \text{ if } f_s < 0 \\ f_s = 0 \text{ if } d\gamma_s^p \neq 0 \end{array} \right\} \quad (12.2.8)$$

with yield functions for inelastic hinge  $j$  and shear similar to Equation (12.2.7):

## Unilateral Damage in Reinforced Concrete Frames

$$f_j = \text{Max} \left\{ \begin{array}{l} \frac{m_j}{1-d_j^+} - 0.7c_j^+ \phi_j^p - k_{0j}^+ - 0.3c_j^+ p_j \\ -\frac{m_j}{1-d_j^-} + 0.7c_j^- \phi_j^p - k_{0j}^- - 0.3c_j^- p_j \end{array} \leq 0; p_j = \text{Max} \left| \phi_j^p \right| \right. \quad (12.2.9)$$

$$f_s = \text{Max} \left\{ \begin{array}{l} \frac{V}{1-d_s^+} - 0.6c_s \gamma_s^p - k_{0s} - 0.4c_s p_s \\ -\frac{V}{1-d_s^-} + 0.6c_s \gamma_s^p - k_{0s} - 0.4c_s p_s \end{array} \leq 0; p_s = \text{Max} \left| \gamma_s^p \right| \right. \quad (12.2.10)$$

## 12.3 NUMERICAL SIMULATIONS OF THE BEHAVIOR OF RC ELEMENTS OF DIFFERENT ASPECT RATIOS

### 12.3.1 Analysis of Frames with Unilateral Damage

The damage model is therefore composed by the elasticity law (12.1.2), the six damage evolution laws (12.2.3) or (12.2.4) and the three plastic rotations evolution laws (12.2.7-10). This model also fits into the scheme described in section 8.3. If the modified Griffith criterion is used, the variables of the model are distributed as follows:

$$VWf_1 = \phi_i^p; VWf_2 = \phi_j^p; VWf_3 = p_i; VWf_4 = p_j; VWf_5 = \gamma_s^p; VWf_6 = p_s$$

$$\{\mathbf{VWo}\}_b^t = (d_i^+, d_i^-, d_j^+, d_j^-, d_s^+, d_s^-) \quad (12.3.1)$$

Therefore the step-by-step algorithm applied in plasticity, with the multi-step modification, can be used again in the numerical simulations. In the following sections, it is presented the comparison between model and some experimental results.

### 12.3.2 Numerical Simulation of a Wall Element

Figure 4 shows a wall with an aspect ratio equal to 1.27. The reinforcement and cross-section corresponds to typical configurations for this kind of element (see Figure 4a). The wall is subjected to the deflection history presented in Figure 4b. The graph of lateral displacement vs. force obtained experimentally is presented in Figure 5a and the corresponding numerical simulation in Figure 5b.

The histories of shear and flexural damages obtained in the analysis are presented in Figure 6a and 6b.

Figure 4. a) RC wall cross-section and reinforcement b) Deflection history

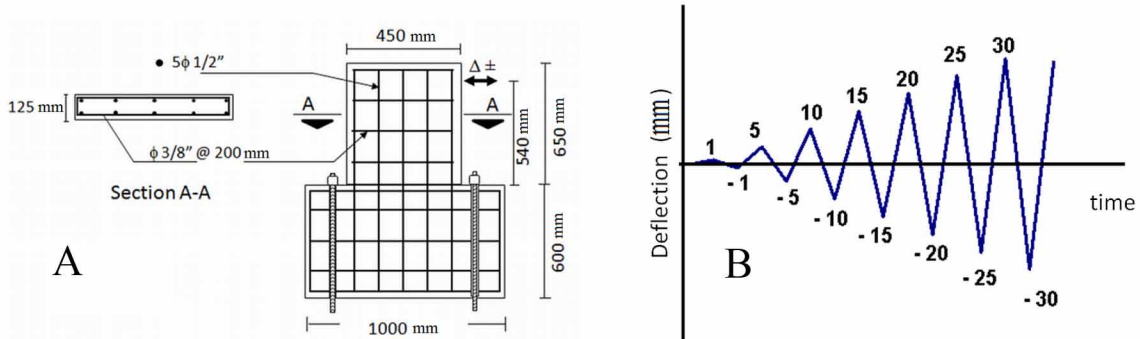


Figure 5. Deflection vs. lateral force in a RC wall a) experimental results b) numerical simulation

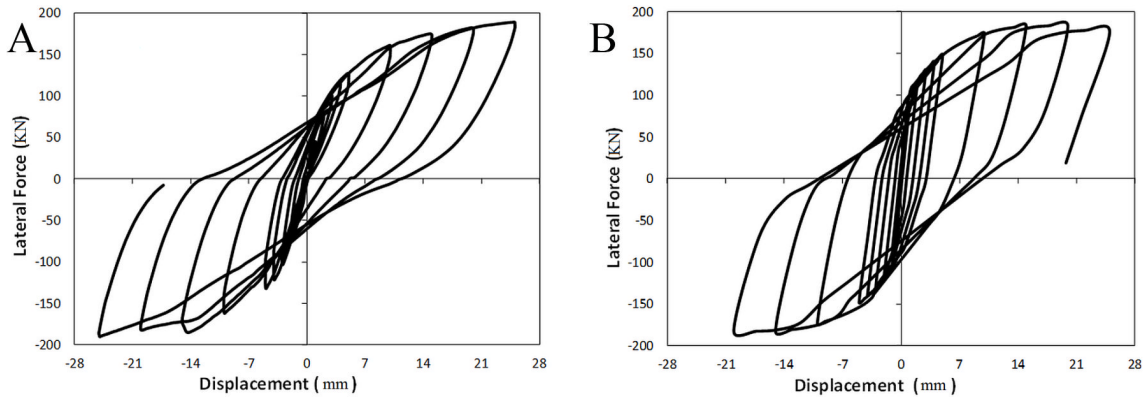
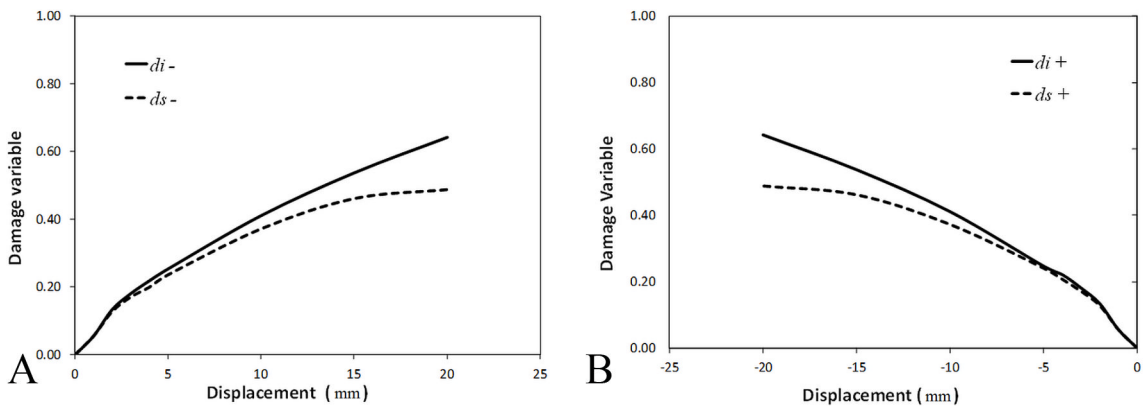


Figure 6. a) History of negative damages b) History of positive damages



### 12.3.3 Numerical Simulation of a Slender Column

Figure 7a shows a slender column with an aspect ratio equal to 7.11. The specimen was first subjected to an axial force of 250 kN and then to the cyclic lateral deflections history presented in Figure 7b; the axial force was kept constant during the second part of the test. The experimental curve of deflection vs. lateral force obtained is indicated in Figure 8a and the numerical simulation in Figure 8b.

The histories of shear and flexural damages are shown in Figure 9. As expected, small values of shear damage and very large flexural damages were obtained with the model.

### 12.3.4 Numerical Simulation of a RC Frame

The one span RC frame that is shown in Figure 10a was subjected to the lateral displacement history presented in Figure 10b.

The graph of displacement vs. lateral force obtained experimentally is shown in Figure 11a and the numerical simulation in Figure 11b.

The damage distribution at the final of the test is presented in Figure 12.

### 12.3.5 Numerical Simulation of a Four-Story RC Frame

Figure 13 shows a full-scale building that was subjected to pseudo-dynamic tests. The building consisted of three frames of two spans in the two orthogonal directions and four storeys (Figure 14); it was designed according to Eurocode 8.

Figure 7. a) RC slender column cross-section and reinforcement b) Deflection history

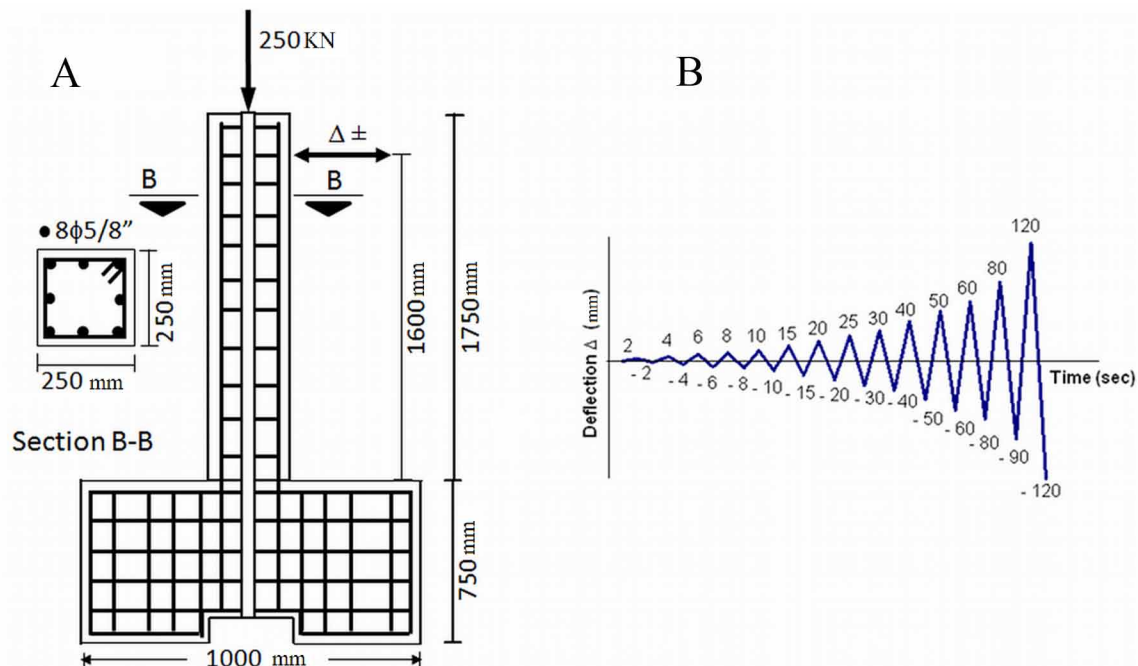


Figure 8. Deflection vs. lateral force curves a) Experimental b) Numerical simulation

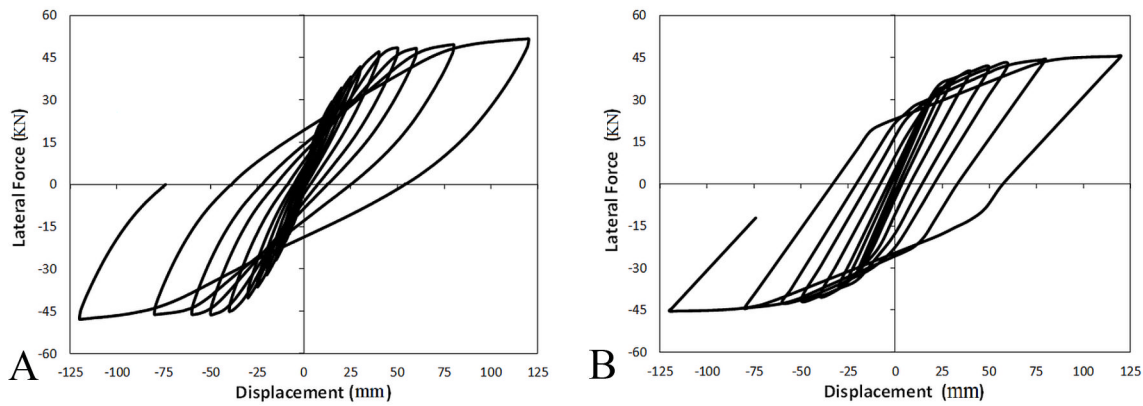
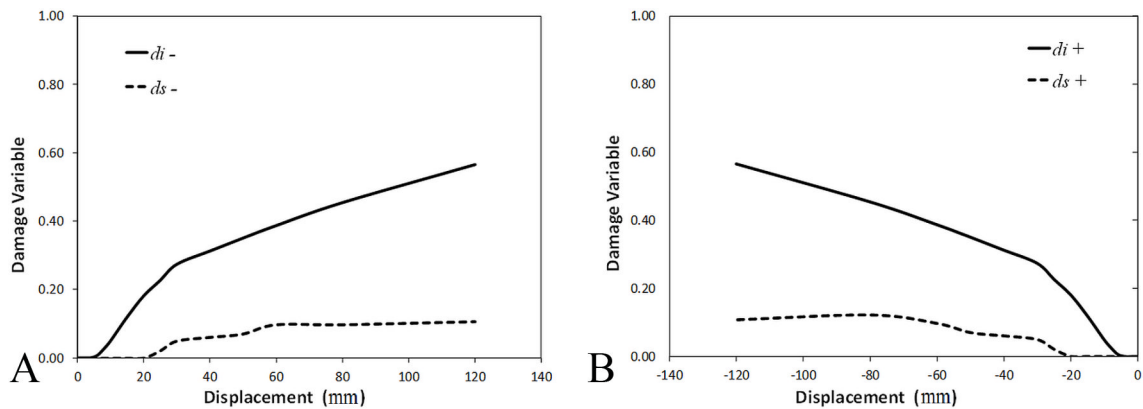


Figure 9. a) History of negative damages b) History of positive damages



The geometry of the structure and the reinforcement details of the elements are presented in Figures 14, 15, and 16.

The pseudo-dynamic tests were performed using an artificial accelerogram derived from the 1976 Friuli earthquake. The signal was generated to fit the elastic response spectrum of the Eurocode 8 with a peak acceleration of 0.3g. Two tests were performed; in the first one, called low level pseudo-dynamic test, it was used the reference signal multiplied by a factor of 0.4 and in the second one, the high level test, an intensity factor of 1.5 was used. The peak ground accelerations were then, respectively,  $0.4 \times 0.3 = 0.12$  g and  $1.5 \times 0.3 = 0.45$  g. The resulting displacements of each level for the low and high level tests are shown, respectively, in Figures 17 and 18.

The numerical simulations of the tests were performed using the model described in sections 12.1 and 12.2. Figure 19 shows the experimental and numerical histories of the base shear obtained for the low level test and Figure 20 the corresponding to the high level test.

The experimental and numerical base shear vs. top displacement diagrams for the low and high level tests are presented, respectively, in Figures 21 and 22.

**Unilateral Damage in Reinforced Concrete Frames**

Figure 10. a) RC frame b) Lateral displacement history

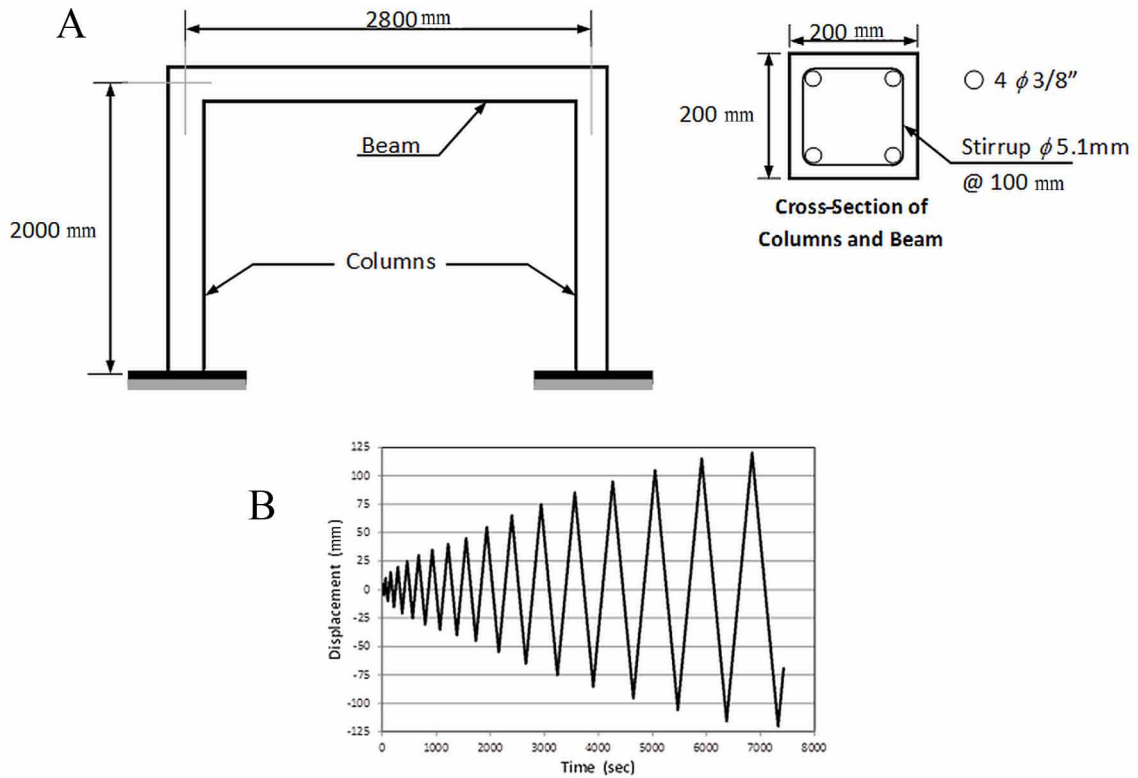


Figure 11. Displacement vs. lateral force curves a) Experimental b) Numerical simulation

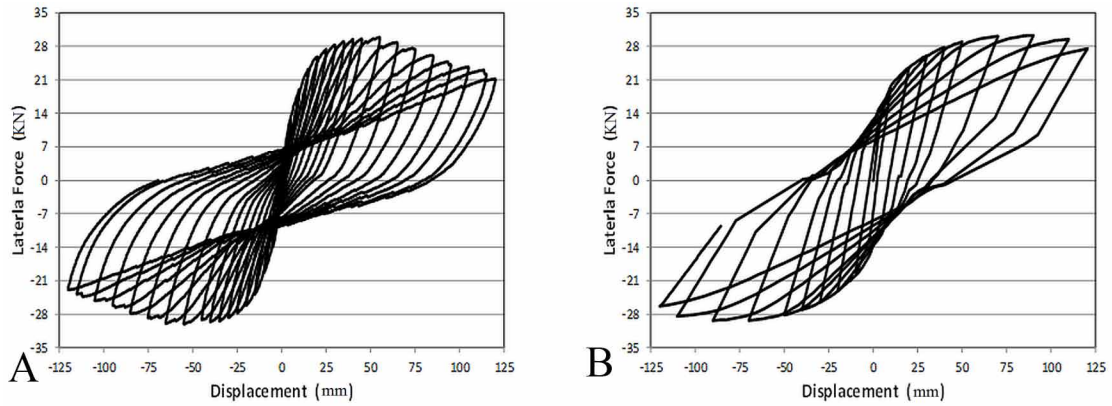


Figure 12. Damage distribution at the final of the test

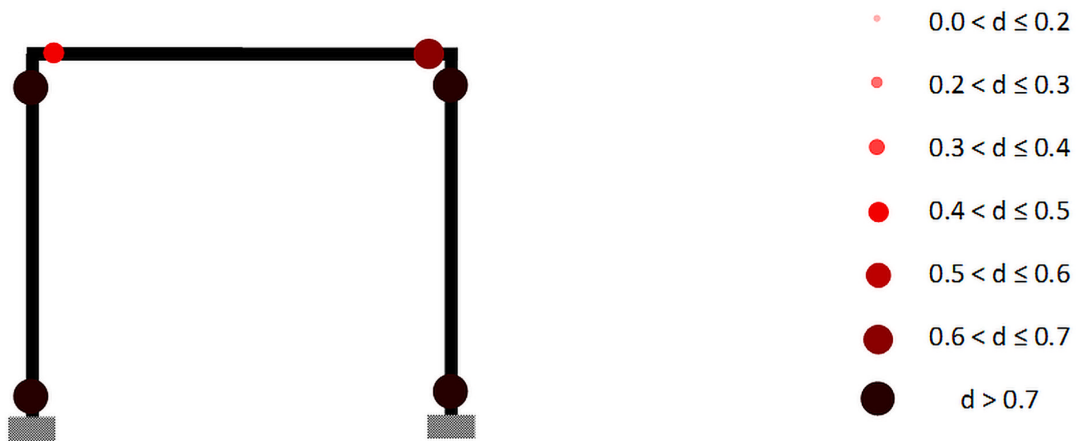


Figure 13. RC building tested at the ELSA Laboratory of the Joint Research Centre (copyright © European Union)

12.13. Negro, P.; Verzeletti, G.; Magonette, G.E., & Pinto, A.V. (1994). Retrieved January, 29 2014 from [https://lh4.ggpht.com/TMiJ0so-NTHNeqUKkFYuD21qdm5ULluxKnM-1eY\\_gxPPmtBqKU60LENYnYjkPiZs8s9Uw=s130](https://lh4.ggpht.com/TMiJ0so-NTHNeqUKkFYuD21qdm5ULluxKnM-1eY_gxPPmtBqKU60LENYnYjkPiZs8s9Uw=s130).



**Unilateral Damage in Reinforced Concrete Frames**

Figure 14. a) Geometry of the structure b) Reinforcement details of the elements

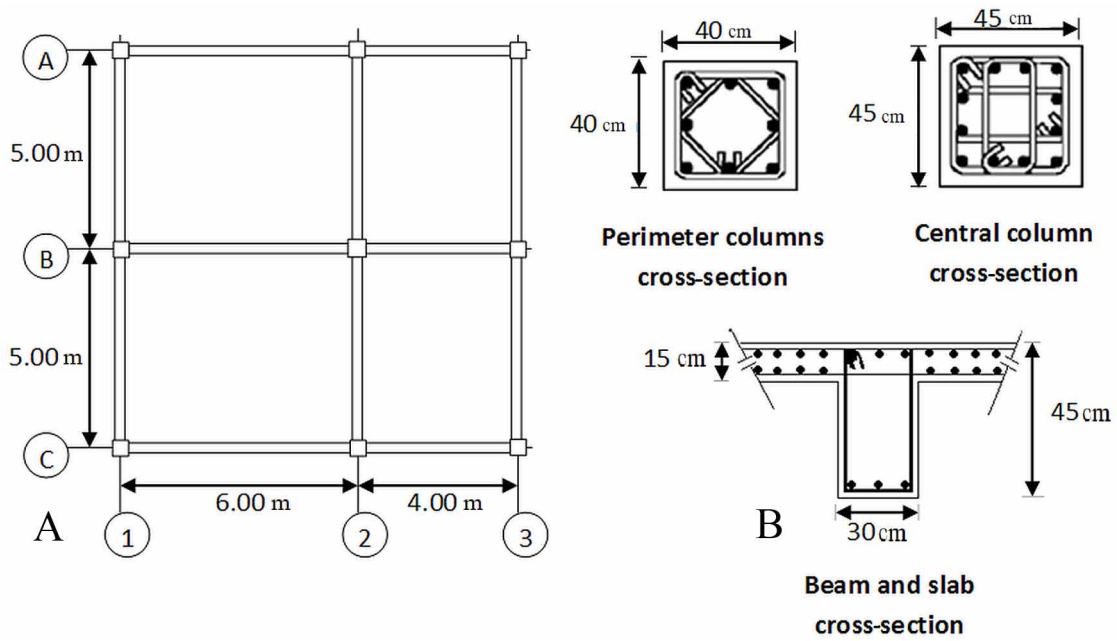


Figure 15. Longitudinal steel bar in columns of a) Frame B and b) Frames A and C

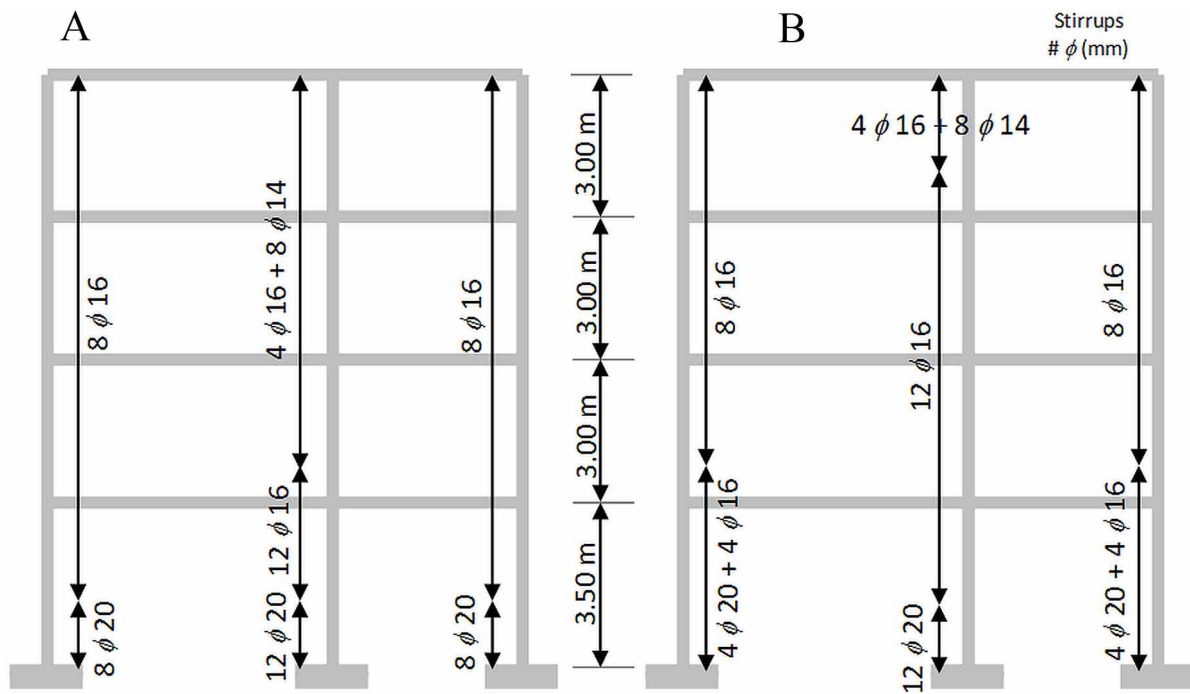




Figure 16. Longitudinal steel bar in beams of: a) Frame B and b) Frames A and C

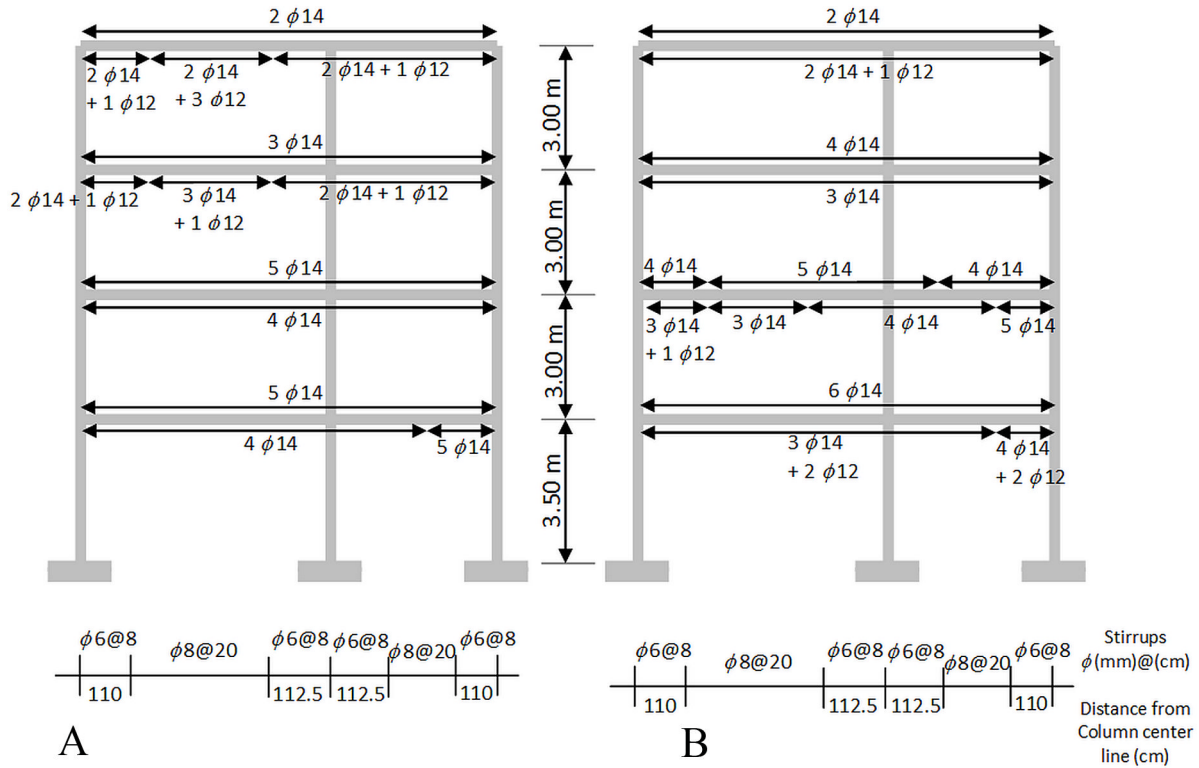
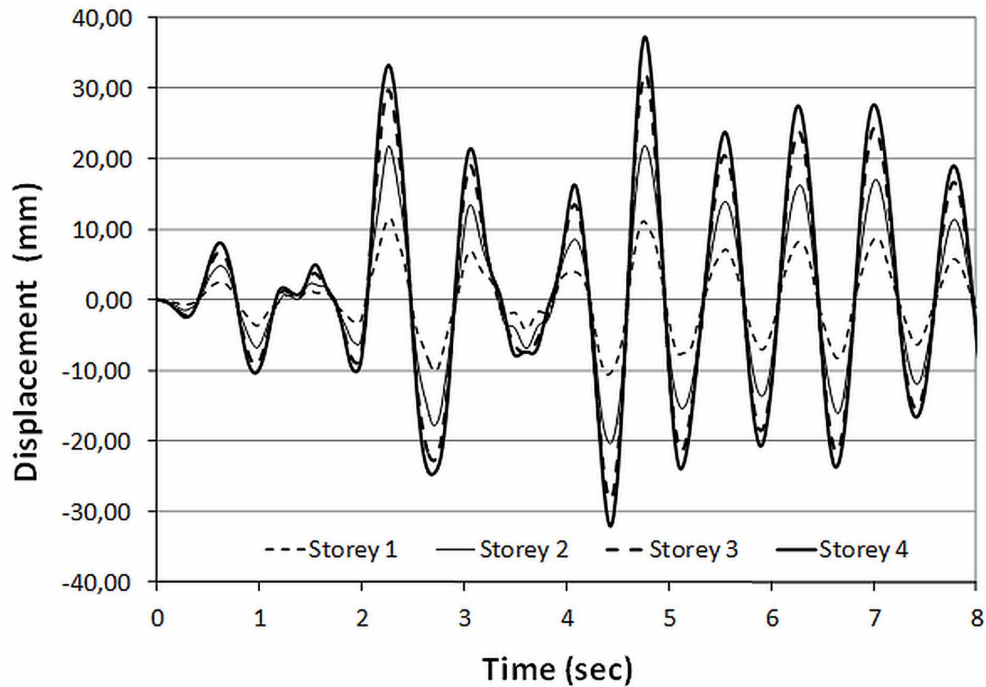


Figure 17. Displacement history applied at each level for the low level test



## Unilateral Damage in Reinforced Concrete Frames

Figure 18. Displacement history applied at each level for the high level test

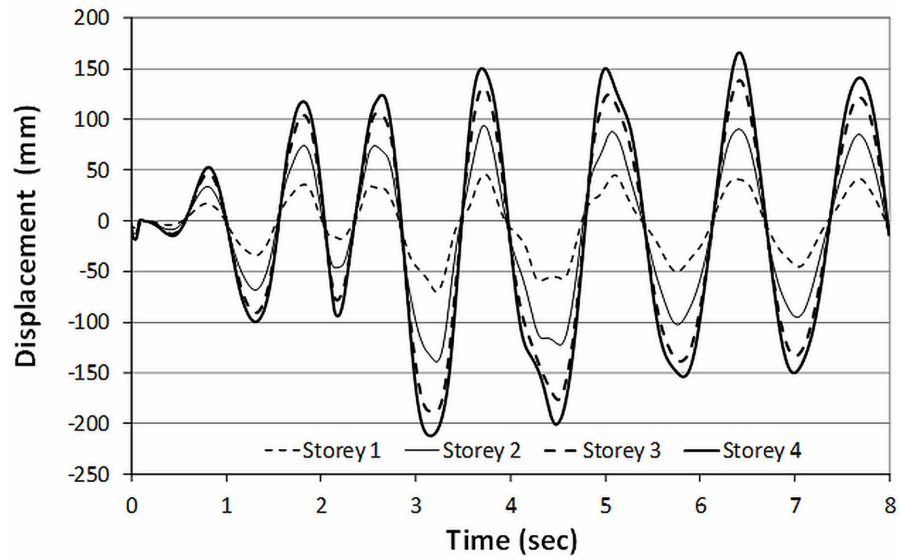


Figure 19. Low level test: base shear histories a) Experimental b) Numerical

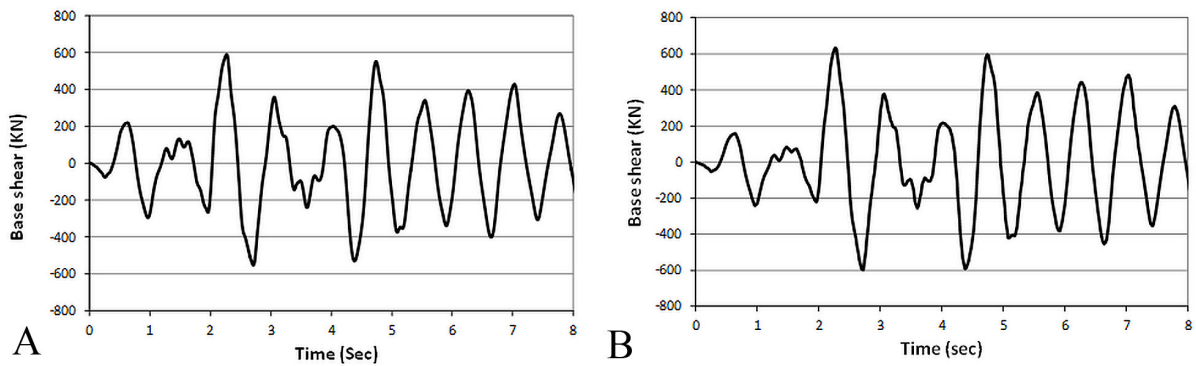


Figure 20. High level test: base shear histories a) Experimental b) Numerical

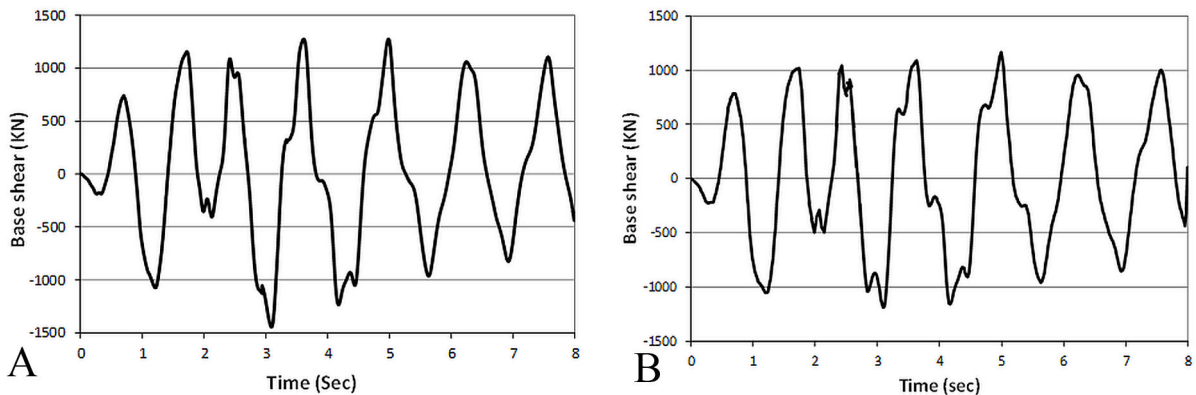


Figure 21. Low level test: base shear vs. top displacement diagrams: a) Experimental b) Numerical

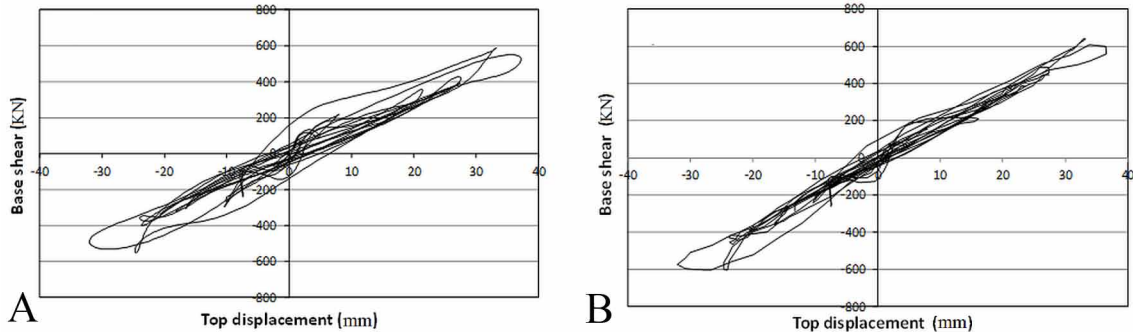
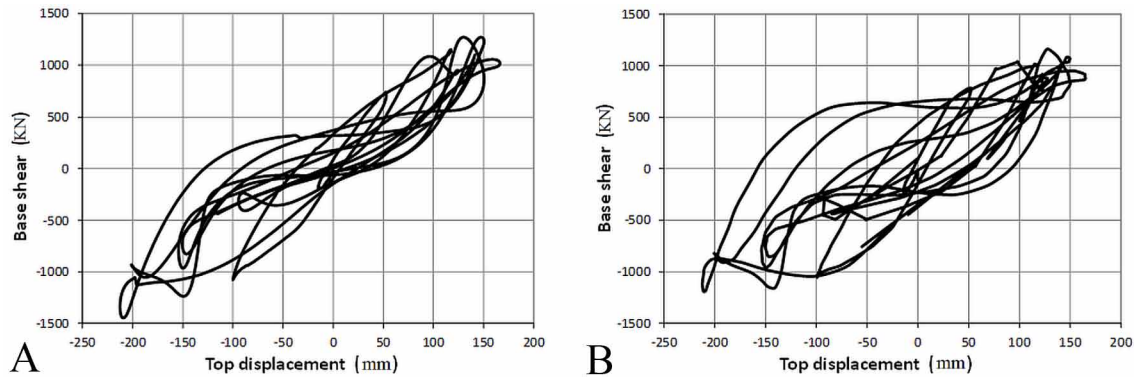


Figure 22. High level test: base shear vs. top displacement diagrams: a) Experimental b) Numerical



The damage distribution at the final of the low level test is presented in Figure 23 and the results for the high level test in Figure 24.

## 12.4 DAMAGE IN A RC WIDE BEAM-COLUMN JOINT

### 12.4.1 Constitutive Equations

Consider again the case of wide beams discussed in sections 6.6 and 7.1.7. In those previous sections only two inelastic phenomena were taken into account: yield and slip of the longitudinal reinforcement. In this section, the model presented in section 7.1.7 is generalized including of concrete cracking using the damage concepts already discussed.

The elasticity law of an element representing a wide beam is given by (12.1.5); i.e. shear deformations are neglected in this case. The damage evolution laws are also defined by the classic or modified Griffith's criteria (12.2.3) or (12.2.4).

The yield functions of hinges  $i$  and  $j$  are the ones described in section 7.1.7 except that they are modified using the hypotheses of equivalence in deformations and of unilateral damage:

**Unilateral Damage in Reinforced Concrete Frames**

Figure 23. Damage distribution at the final of the low level test a) Frame B b) Frames A and C

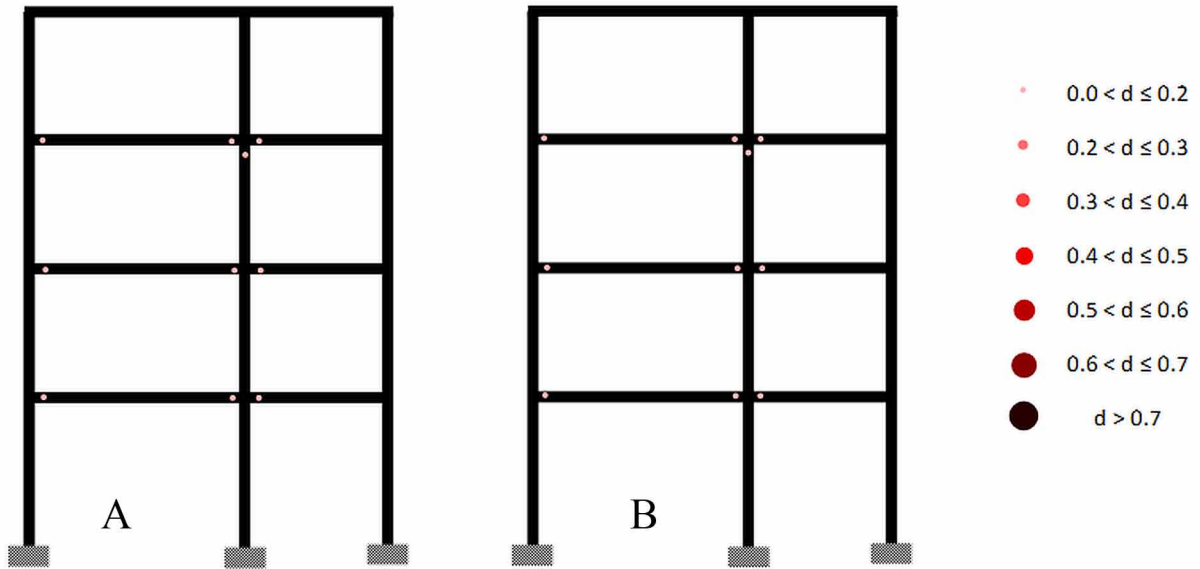
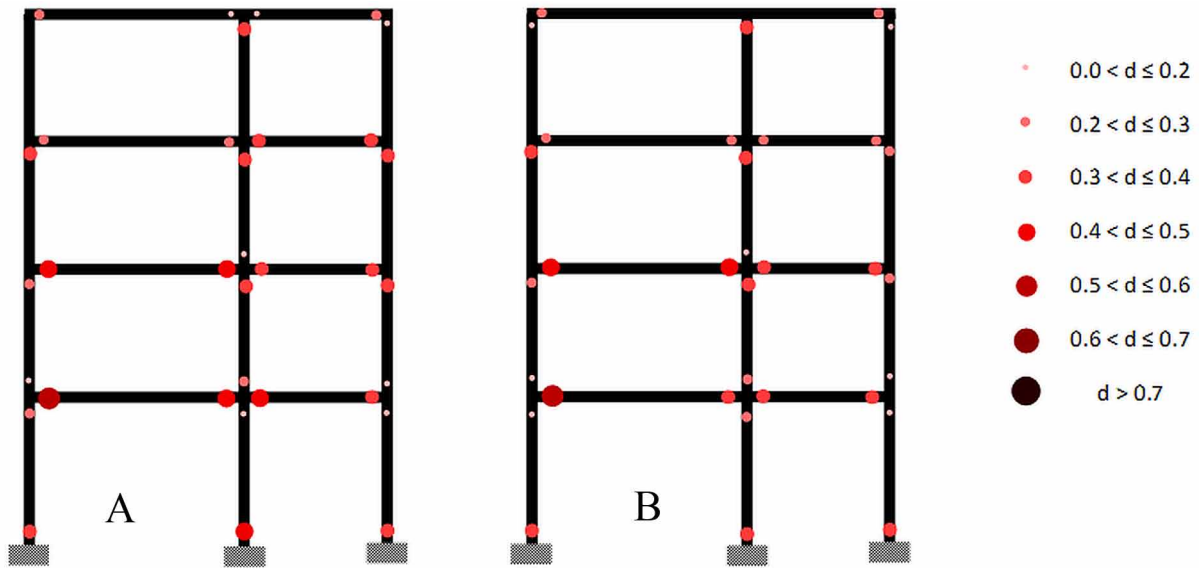


Figure 24. Damage distribution at the final of the high level test a) Frame B b) Frames A and C



$$f_i = \text{Max}(f_i^y, f_i^{\text{slip}}); f_j = \text{Max}(f_j^y, f_j^{\text{slip}}) \quad (12.4.1)$$

The yield functions  $f_i^y$  and  $f_j^y$  are identical to those presented in (12.2.7) and (12.2.9); and the slip functions with damage are derived from Equation (7.1.18) using again the concept of effective moment:

$$f_i^{slip} = Max \begin{cases} \frac{m_i}{1-d_i^+} - M_{0i}^+ e^{(\eta_i^+ \varphi_i^p)} \\ -\frac{m_i}{1-d_i^-} - M_{0i}^- e^{-(\eta_i^- \varphi_i^p)} \end{cases}; f_j^{slip} = Max \begin{cases} \frac{m_j}{1-d_j^+} - M_{0j}^+ e^{(\eta_j^+ \varphi_j^p)} \\ -\frac{m_j}{1-d_j^-} - M_{0j}^- e^{-(\eta_j^- \varphi_j^p)} \end{cases} \quad (12.4.2)$$

The four parameters  $\eta_{i/j}^{+/-}$  are determined assuming that concrete cracking evolution restarts only when the reinforcement no longer slips and starts yielding again. In mathematical terms, this hypothesis is stated as follows:

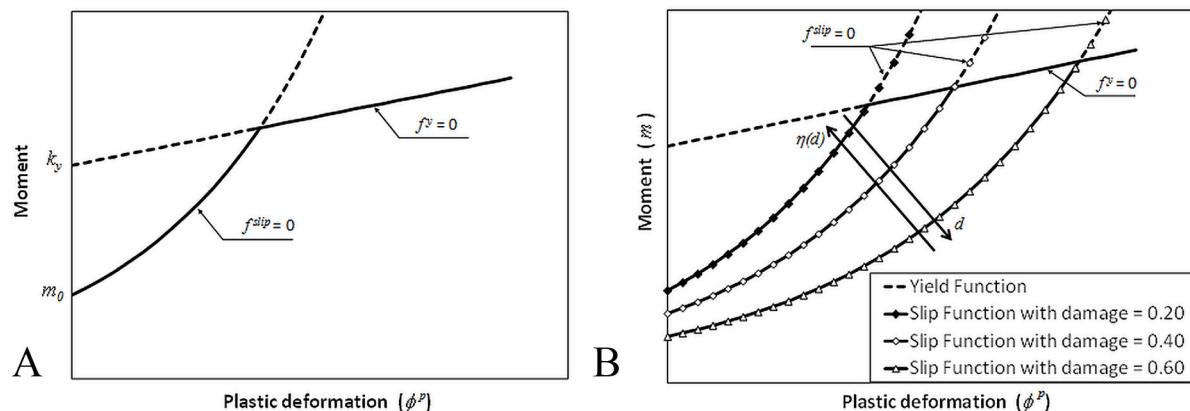
$$f^y = f^{slip} = 0 \text{ for } G = R(d) \quad (12.4.3)$$

This condition leads to the following expression:

$$\eta_{i/j}^{+/-}(d_{i/j}^{+/-}) = \frac{1}{2} \frac{c_{i/j}^{+/-}(1-d_{i/j}^{+/-}) \ln \left( 2 \frac{R(d_{i/j}^{+/-})}{(m_{0i/j}^{+/-})^2 F^0} \right)}{\sqrt{\frac{2R(d_{i/j}^{+/-})(1-d_{i/j}^{+/-})^2}{F^0} - k_{yi/j}^{+/-} + d_{i/j}^{+/-} k_{yi/j}^{+/-}}} \quad (12.4.4)$$

The parameter  $\eta$  determines the point of intersection between the slipping curve and the yielding: high values of  $\eta$  produce a more stiff behavior because slipping of the reinforcement stops faster (see Figure 25a). On the other hand,  $\eta$  decreases with damage (see Figure 25b); thus, according to the model, cracking of concrete produces an internal slipping of the reinforcement. That is, a slip hinge with damage shows a slower recovery of the slip resistance during the process of confinement of the reinforcement.

Figure 25. a) Behavior of an inelastic hinge with slip and yielding b) Influence of the parameter  $\eta$  and  $d$



### 12.4.2 Numerical Simulations of Interior Wide Beam-Column Connections

Figure 26 shows the geometry of two interior wide beam column joints called WB-1 and WB-4; the dimensions of the elements and the reinforcement are presented in Table 1. The boundary conditions and the applied drifts history are shown, respectively, in Figures 26b-c. Notice that the only difference between WB-1 and WB-4 is the beam width.

In Figure 27 are shown the experimental and numerical simulation drift vs. load curves of the joint WB-1 and the results of the WB-2 are presented in Figure 28. The damage distributions are presented in Figure 29.

### 12.4.3 Numerical Simulations of Interior Normal Beam-Column Connection

Figure 30 shows an interior beam-column connection. Notice that the beam has typical cross-section dimensions.

The experimental and numerical results of the test are presented in Figure 31. The damage distribution at the final of the test is shown in Figure 32.

Figure 26. a) Geometry of the wide beam-column connections b) Boundary conditions c) Applied drifts history

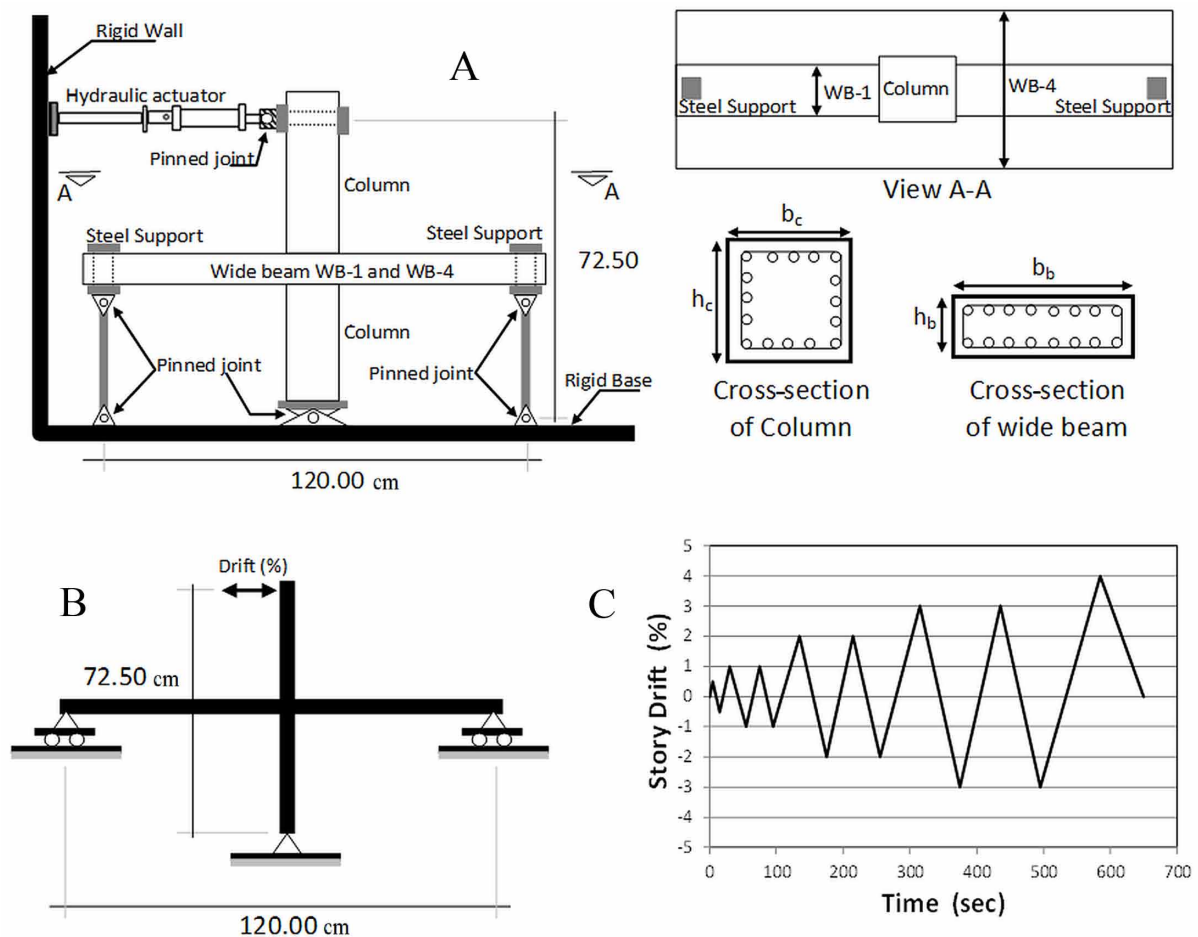


Figure 27. Drift vs. load curves of joint WB-1 a) Experimental b) Numerical

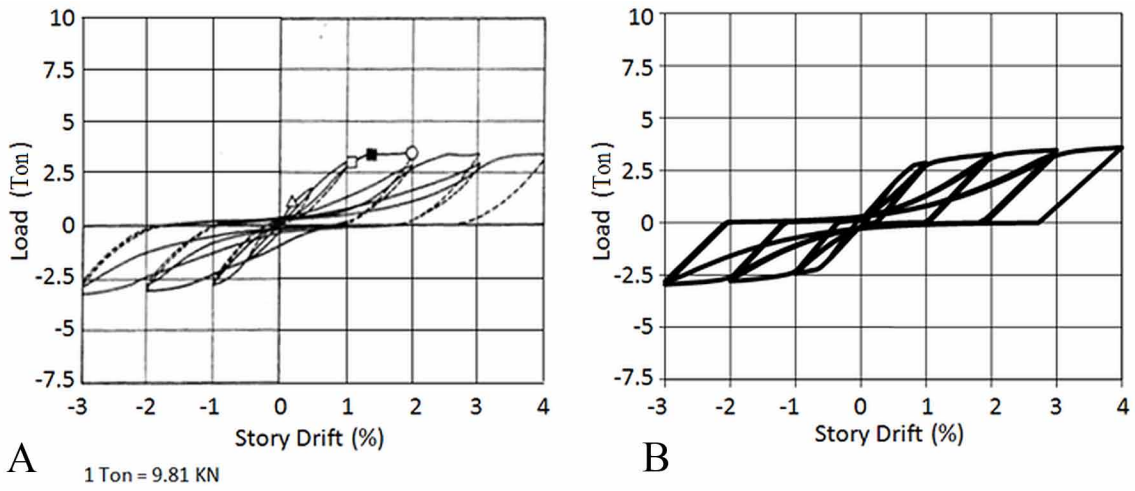


Figure 28. Drift vs. load curves of joint WB-2 a) Experimental b) Numerical

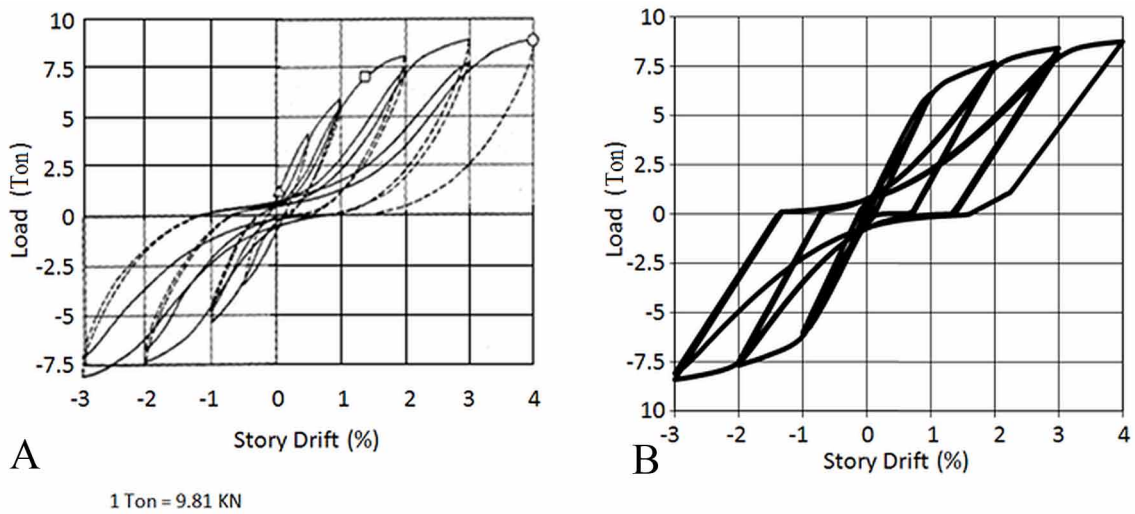
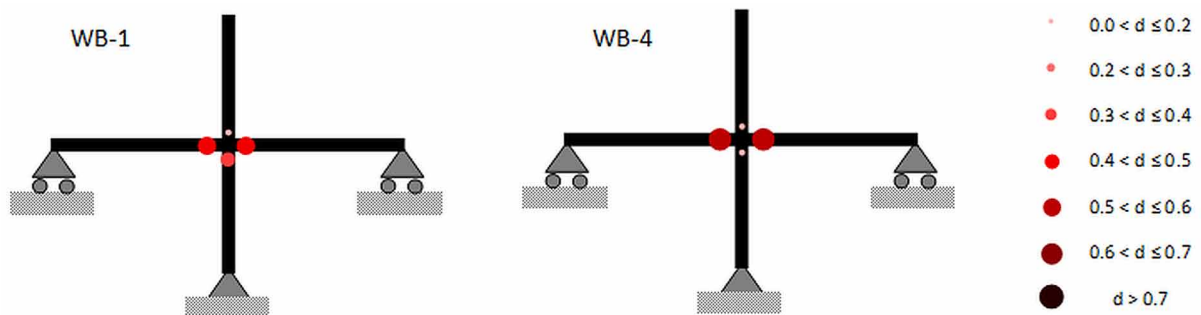


Figure 29. Damage distributions



**Unilateral Damage in Reinforced Concrete Frames**

Figure 30. a) Geometry of the normal beam-column connection. All dimensions are in cm. b) Boundary conditions c) Applied drifts history

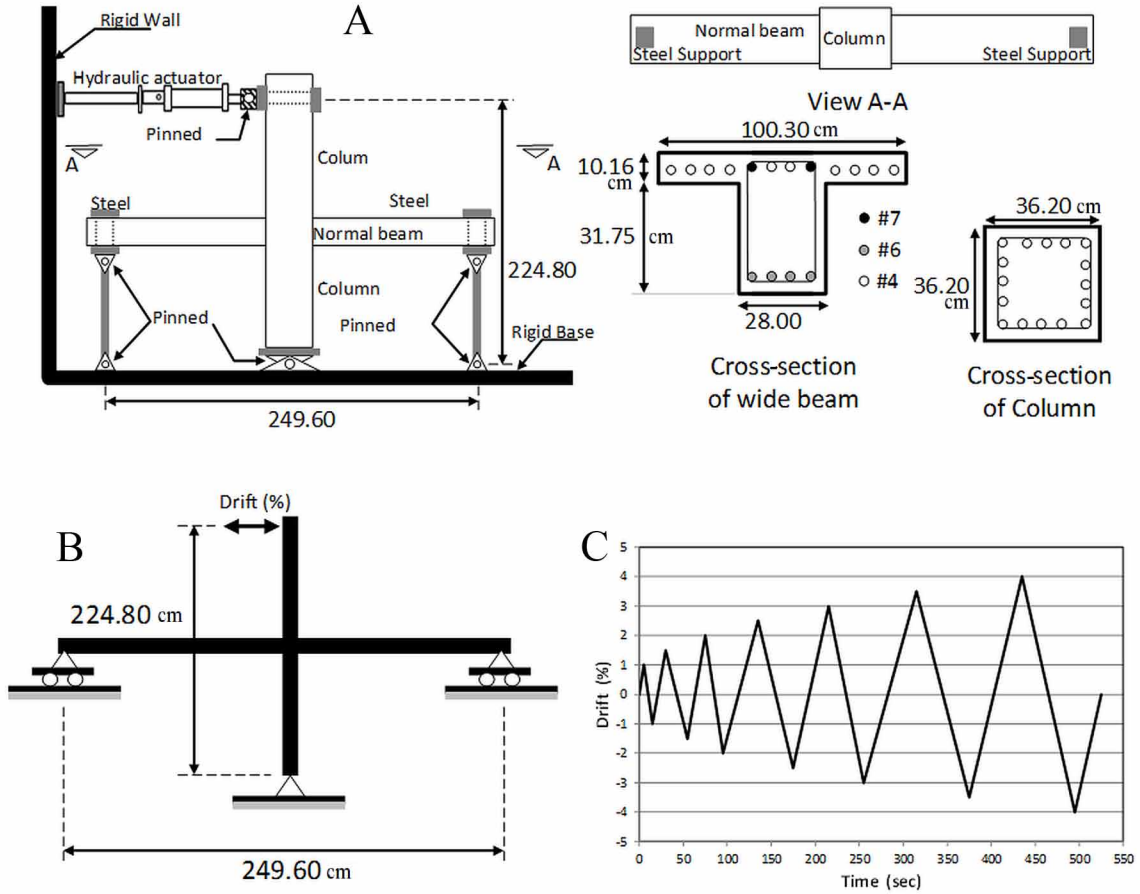


Figure 31. Drift vs. load curves of the normal beam-column connection a) Experimental b) Numerical

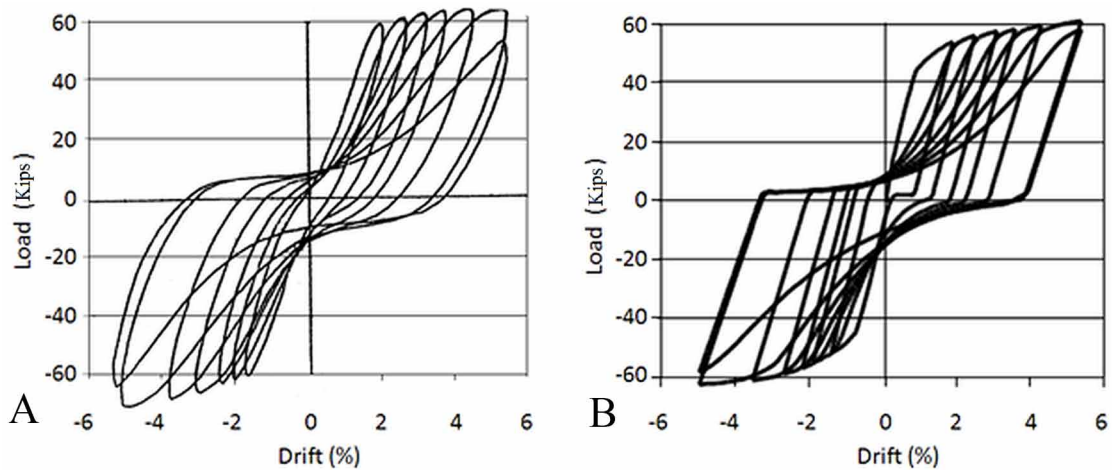
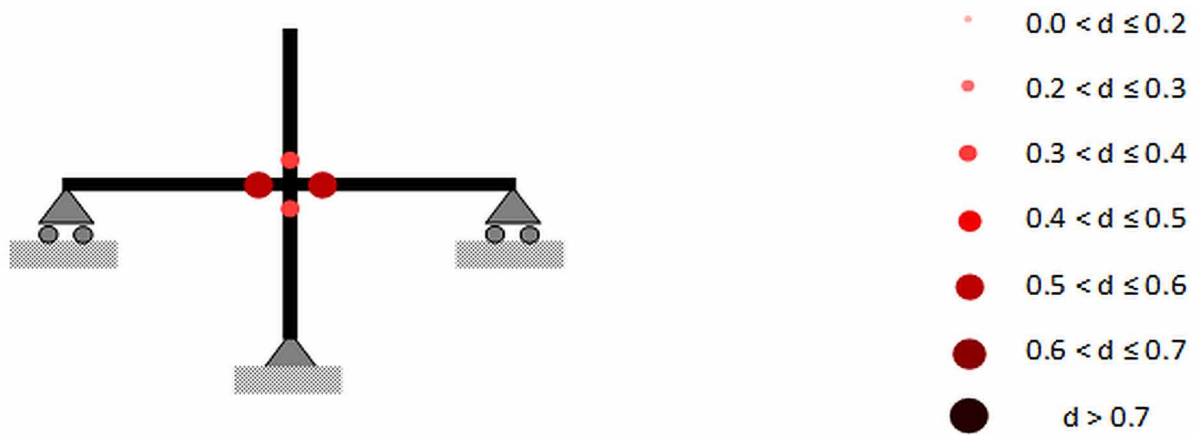




Table 1. Dimensions and reinforcement of interior joints WB-1 and WB-2

Label	Column		Wide Beam		Wide Beam Rebars		Column Rebars	
	$b_c$ (cm)	$h_c$ (cm)	$b_b$ (cm)	$h_b$ (cm)	Long. (mm)	Trans. (mm)	Long. (mm)	Trans. (mm)
WB-1	20.00	20.00	17.60	12.50	4-D10	2-D4@50	20-D10	2-D6
WB-4			71.94	12.50	16-D10	8-D4@50		

Figure 32. Damage distribution



#### 12.4.4 Numerical Simulations of Exterior Wide Beam-Column Connection

Figure 33a shows the geometry of an exterior wide beam-column joint. Figure 33b shows reinforcement details and in Figure 34 is presented the boundary conditions and the applied drifts history.

In Figure 35 are shown the experimental and numerical simulation drift vs. load curves and the damage distribution are presented in Figure 36.

### 12.5 TORSION DAMAGE

#### 12.5.1 Experimental Behavior of a RC Element under Mono-Sign Torsion

Figure 37 shows a square RC column built in cantilever and subjected to pure torsion. At the top of the column was built a rigid beam where the torque, shown in Figure 38, was applied. Notice that the pure torsion was generated by the application of opposite forces with the same magnitude on this beam.

Figure 39 shows the cracking pattern at the final of the test. Note that cracks with an inclination of 45 degrees are spread along the specimen in a uniform way.

## Unilateral Damage in Reinforced Concrete Frames

Figure 33. a) Geometry of the wide beam-column connections b) Reinforcement details. (All dimensions are in cm.)

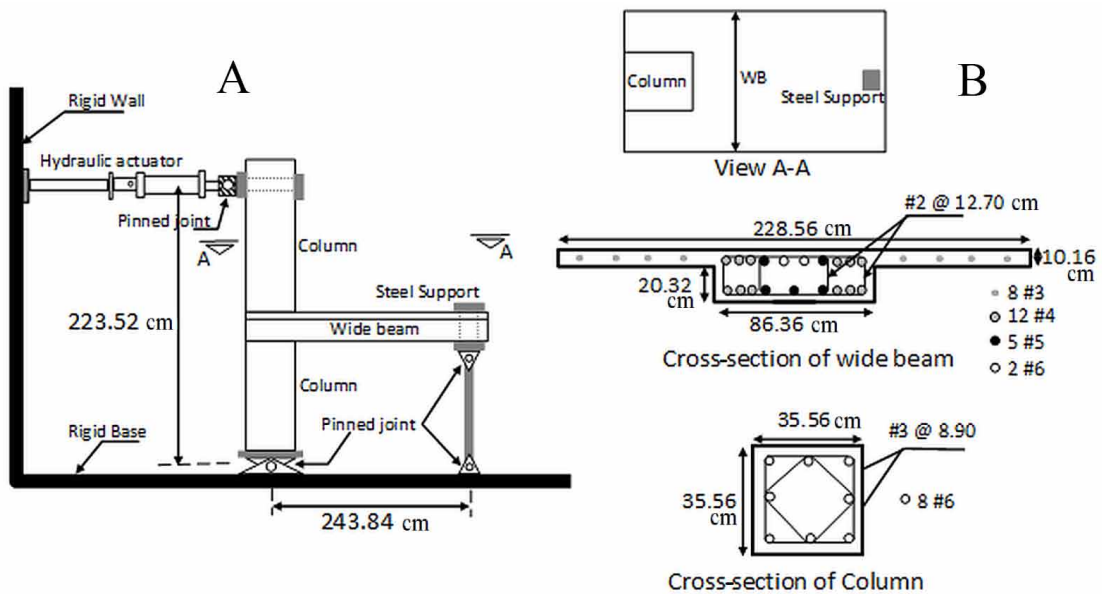
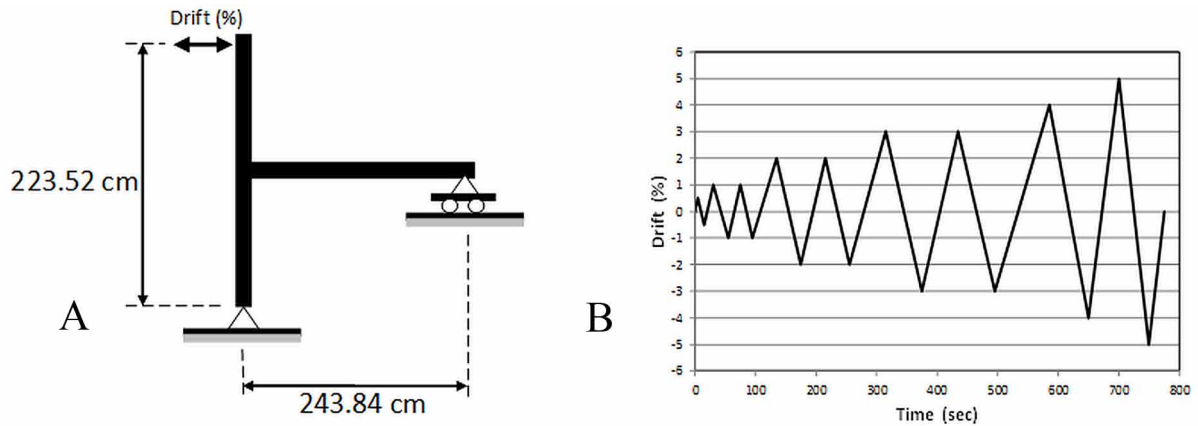


Figure 34. a) Boundary conditions b) Applied drifts history



## 12.5.2 Constitutive Equations for Mono-Sign Torsion

Following the conventional damage mechanics procedure, the angle of twist can be expressed as:

$$\phi_x = m_x \frac{L}{GJ} + \phi_x^d + \phi_x^p \quad (12.5.1)$$

Figure 35. Drift vs. force curves a) Experimental b) Numerical simulation

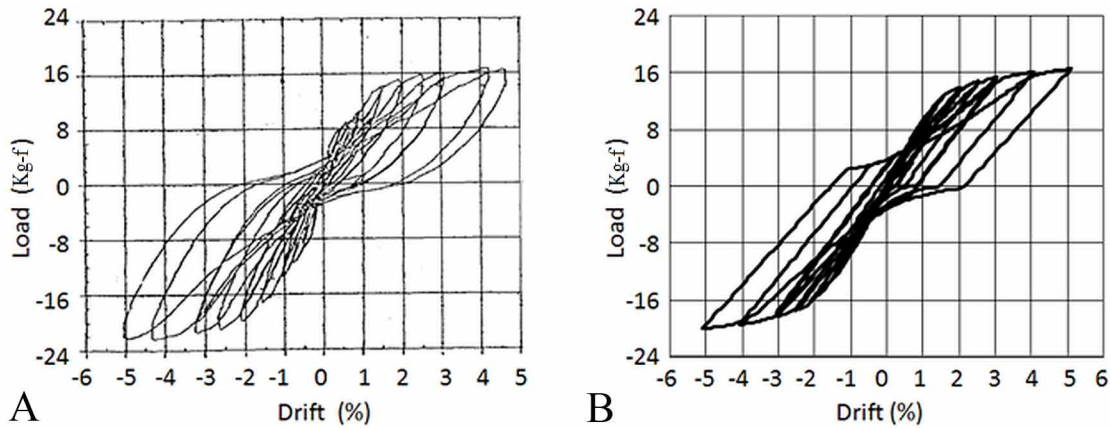
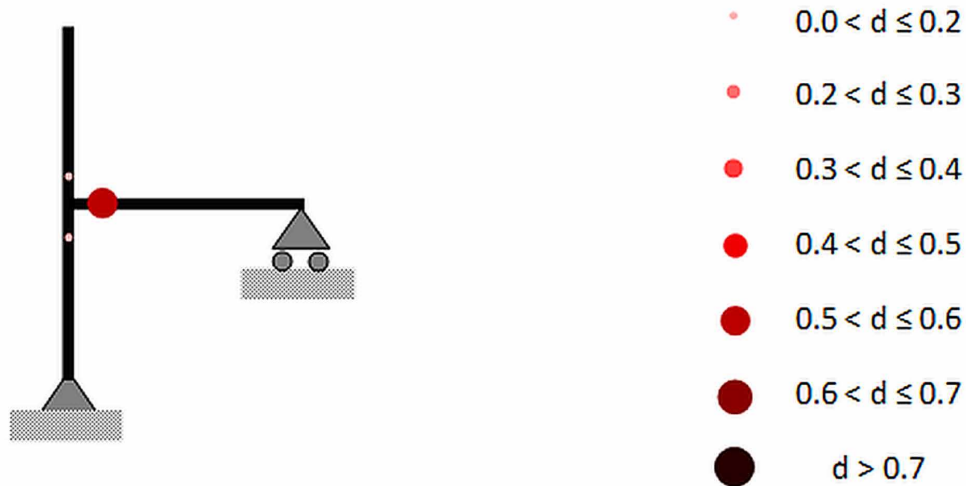


Figure 36. Damage distribution



where  $m_x \frac{L}{GJ}$  is the elastic rotation (see section 2.5),  $\phi_x^p$  is the plastic twist due to reinforcement yielding and  $\phi_x^d$  is the additional twist due to concrete cracking. If the distributed damage model is used and according to the hypothesis of equivalence in deformations, the latter term can be written as:

$$\phi_x^d = \frac{d_x L}{(1 - d_x)GJ} m_x \tag{12.5.2}$$

where  $d_x$  is the torsion damage. This variable takes values between zero and one as usual and represents concrete cracking that is assumed to be evenly distributed along the element. The elasticity law of a damaged RC element subjected to torsion only is therefore given by:

**Unilateral Damage in Reinforced Concrete Frames**

Figure 37. Square RC column built in cantilever and subjected to pure torsion

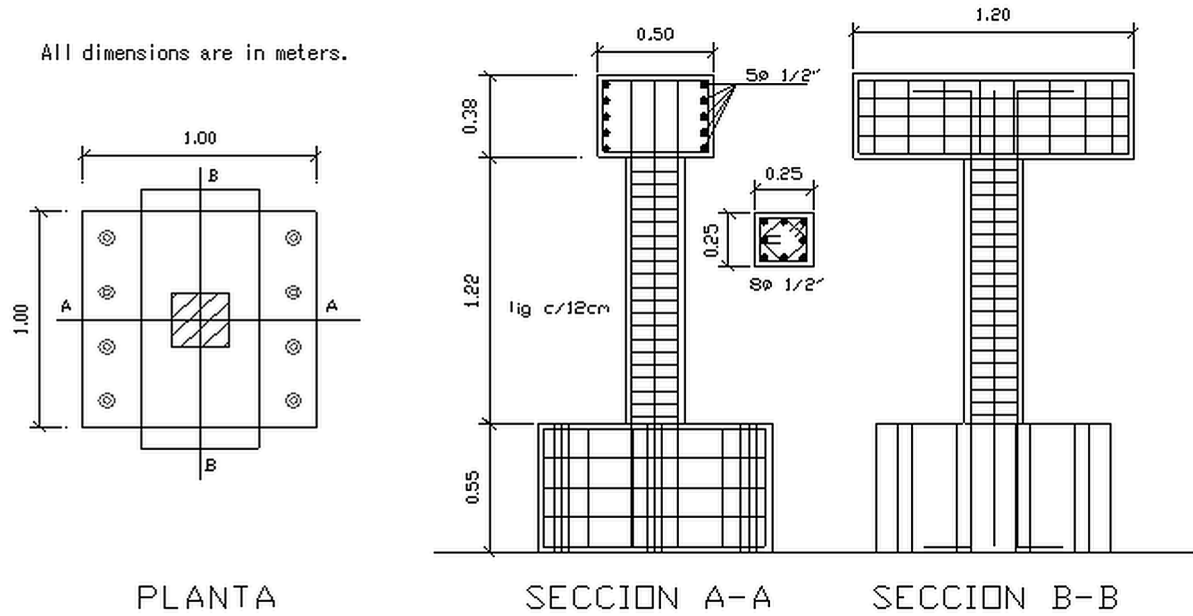
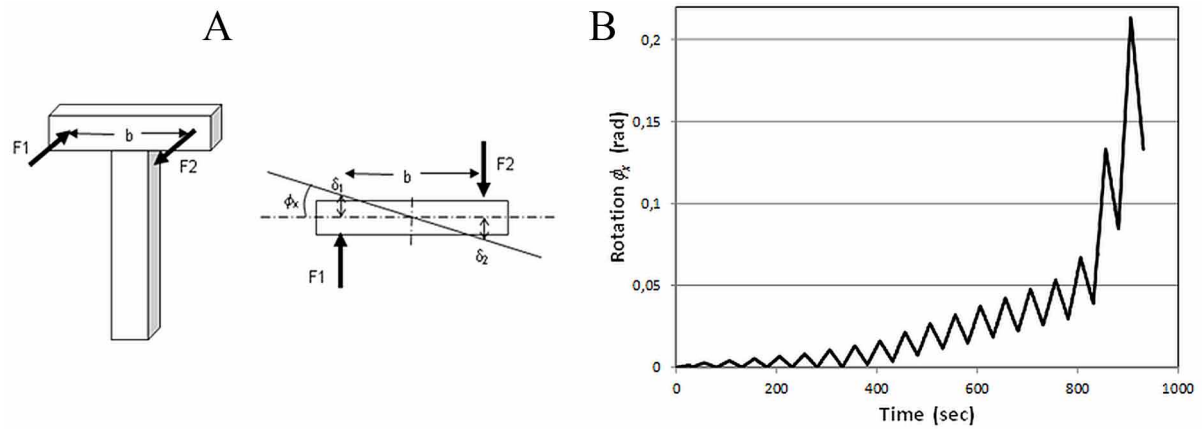


Figure 38. a) Loading application scheme b) loading paths

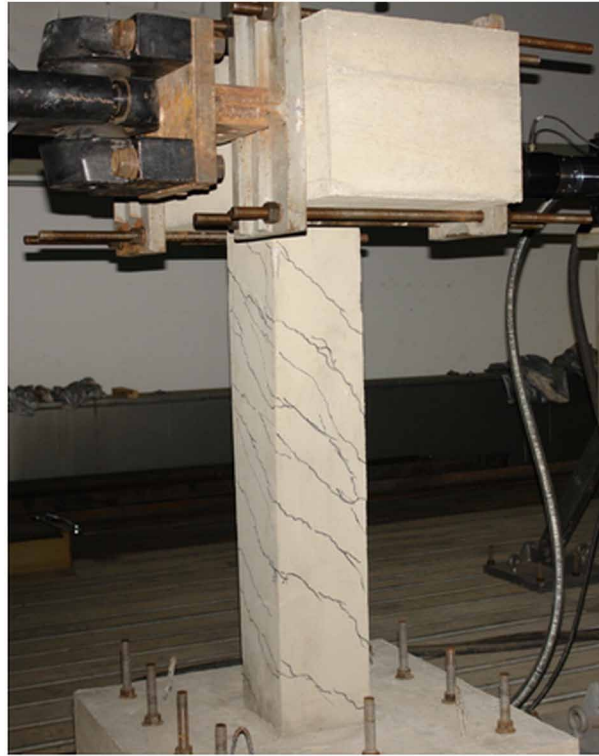


$$\phi_x - \phi_x^p = \frac{L}{(1 - d_x)GJ} m_x; \text{ or } m_x = (1 - d_x) \frac{GJ}{L} (\phi_x - \phi_x^p) \quad (12.5.3)$$

The deformation energy due to torsion is, therefore, given by:

$$W = \frac{1}{2} m_x (\phi_x - \phi_x^p) = \frac{1}{2} \frac{m_x^2 L}{(1 - d_x)GJ} \quad (12.5.4)$$

Figure 39. Cracking pattern at the final of the test



and the energy release rate due to torsion is:

$$G_x = \frac{\partial W}{\partial d_x} = \frac{1}{2} \frac{m_x^2 L}{(1 - d_x)^2 GJ} \quad (12.5.5)$$

The Griffith criterion for torsion cracks is then:

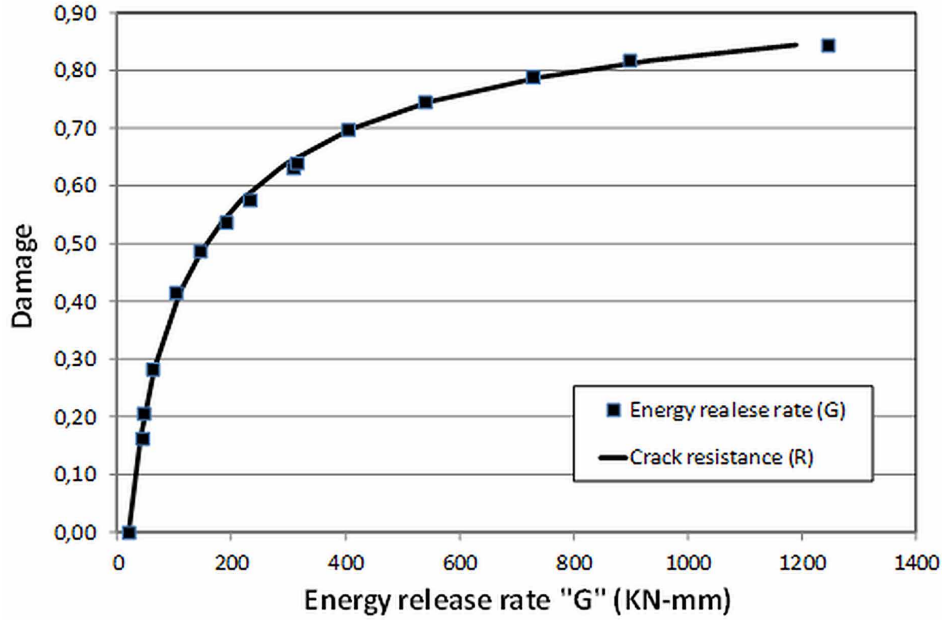
$$G_x \leq R(d_x) \quad (12.5.6)$$

where  $R(d_x)$  is, again, the crack resistance to torsion. Notice that the elasticity law (12.4.3) and the relationship between force and deflection in a simply supported beam subjected to a concentrated load (see section 10.3) are similar; therefore the method of stiffness variation can be used without modification. The resulting graph of crack resistance against damage is presented in Figure 40.

Notice that these experimental results are also similar to those obtained in bending and shear; therefore, the same general expression of the crack resistance can be used once more:

$$R(d_x) = R_{0x} + q_x \frac{\ln(1 - d_x)}{1 - d_x} \quad (12.5.7)$$

Figure 40. Torsion damage vs. Energy release rate



The yield function in torsion obtained from the hypothesis of equivalence in deformation is:

$$f = \left| \bar{m}_x - c_x \phi_x^p \right| - k_{0x} = \left| \frac{m_x}{1 - d_x} - c_x \phi_x^p \right| - k_{0x} \leq 0 \quad (12.5.8)$$

The parameters of the model ( $R_{0x}$ ,  $q_x$ ,  $c_x$  and  $k_{0x}$ ) can also be computed with the same procedures described in the cases of bending and shear (see sections 10.3.3 and 10.4.2); therefore, the values of the first cracking torque  $M_{crx}$ , ultimate torque  $M_{ux}$ , first plastic torque  $M_{px}$  torque and ultimate plastic rotation  $\phi_{ux}^p$  in torsion are needed.

The analysis of the ultimate plastic torque was already discussed in section 7.4.3. The determination of the interaction diagrams for the remaining properties of the cross-section is described in next sections

### 12.5.3 Determination of the First Cracking Torque

The first cracking torque  $M_{crx}$  is assumed to occur when the principal tensile stress reaches the value  $\sqrt{f'_c}$ . For members subjected to torsion and axial force, the first cracking shear force can be computed with the following expression:

$$M_{crx} = 0.33\sqrt{f'_c} \left( \frac{A_{cp}^2}{p_{cp}} \right) \sqrt{1 + \frac{N}{0.33A_g\sqrt{f'_c}}} \text{ N}\cdot\text{mm} \quad (12.5.9)$$

where  $N$  is the axial force in N,  $A_{cp}$  is the area enclosed by outside perimeter of concrete cross-section in mm<sup>2</sup>,  $p_{cp}$  is the outside perimeter of concrete cross section in mm,  $A_g$  is the gross area of the concrete section in mm<sup>2</sup> and  $f'_c$  is the strength of concrete in MPa.

#### **12.5.4 Determination of the First Plastic Torque**

The first plastic torque is defined as the level of torque that initiates yielding of the stirrups or ties in the element can be computed with the expression:

$$M_{px} = \Omega \ x^2 y \sqrt{f'_c} \text{ N} \cdot \text{mm} \quad (12.5.10)$$

where  $x$  and  $y$  are the dimensions of the cross-section (for  $x \leq y$ ), and  $\Omega$  varies from 0.166 for  $y/x = 1$  to 0.249 for  $y/x = \infty$ .

#### **12.5.5 Determination of the Ultimate Plastic Twist**

The ultimate plastic twist  $\phi_{ux}^p$  is computed as:

$$\phi_{ux}^p = \theta_{ux}^p L$$

$$\theta_{ux}^p = \theta_{ux} - \theta_{ex} = \frac{M_{ux}}{(GC)_u} - \frac{M_{ux}}{GJ}$$

$$(GC)_u = \frac{4E_s A_0^2 A_{cp}}{p_0 \left( \frac{16nA_{cp}}{p_0 t_d} + \frac{1}{\rho_l} + \frac{1}{\rho_t} \right)} \quad (12.5.11)$$

where  $(GC)_u$  is the ultimate torsional rigidity,  $GJ$  is the initial torsional rigidity,  $E_s$  is the modulus of elasticity of steel,  $A_{cp}$  is the area enclosed by outside perimeter of concrete cross-section,  $A_0$  is the area enclosed by the centerline of shear flow zone,  $p_0$  is the perimeter of the centerline of the shear flow zone,  $n = E_s / E_c$ ,  $t_d$  is the thickness of shear flow zone,  $\rho_l = A_l / A_{cp}$  is the total volumetric ratio of longitudinal steel,  $\rho_t = A_s t_p / A_{cp} s$  is the volumetric ratio of transverse hoop steel,  $\theta_{ux}^p$  is the ultimate plastic unitary twist,  $\theta_{ux}$  is the ultimate unitary twist and  $\theta_{ex}$  is the elastic unitary twist.

#### **12.5.6 Experimental Behavior of a RC Element under Cyclic Loading**

The column shown in Figure 37 was subjected to cyclic torsion loads. The loading path is presented in Figure 41.

## Unilateral Damage in Reinforced Concrete Frames

Figure 42 shows the cracking pattern at the final of the test. Notice that the cracks with an inclination of 45 degrees are distributed along the specimen in both directions.

### 12.5.7 General Constitutive Equations for Torsion Damage

The cracking patterns described in the previous section indicate the presence of the unilateral damage phenomenon; thus the conventional damage mechanics procedure can be used again. Therefore, the elasticity law with unilateral damage becomes:

$$\phi_x - \phi_x^p = \frac{L}{(1 - d_x^+)GJ} \langle m_x \rangle_+ + \frac{L}{(1 - d_x^-)GJ} \langle m_x \rangle_- \quad (12.5.12)$$

The energy release rates and the crack resistance functions for unilateral torsion cracks are:

$$G_x^{+/-} = \frac{1}{2} \frac{\langle m_x^2 \rangle_{+/-} L}{(1 - d_x^{+/-})^2 GJ}; R = R_{0x}^{+/-} + q_x^{+/-} \frac{\ln(1 - d_x^{+/-})}{1 - d_x^{+/-}} \quad (12.5.13)$$

The yield function is also similar to those used in bending and shear:

$$f_x = \text{Max} \begin{cases} \frac{m_x}{1 - d_x^+} - 0.8c_x^+ \phi_x^p - k_{0x}^+ - 0.2c_x^+ p_x \\ -\frac{m_x}{1 - d_x^-} + 0.8c_x^- \phi_x^p - k_{0x}^- - 0.2c_x^- p_x \end{cases} \leq 0; p_x = \text{Max} |\phi_x^p| \quad (12.5.14)$$

### 12.5.8 Numerical Simulations

The tests described in sections 12.4.1 and 12.4.7 were simulated using the described model. In Figure 43 are shown the experimental and corresponding numerical simulation of the specimen subjected to mono-sign loads and in Figure 44 the results of the column subjected to cyclic loads.

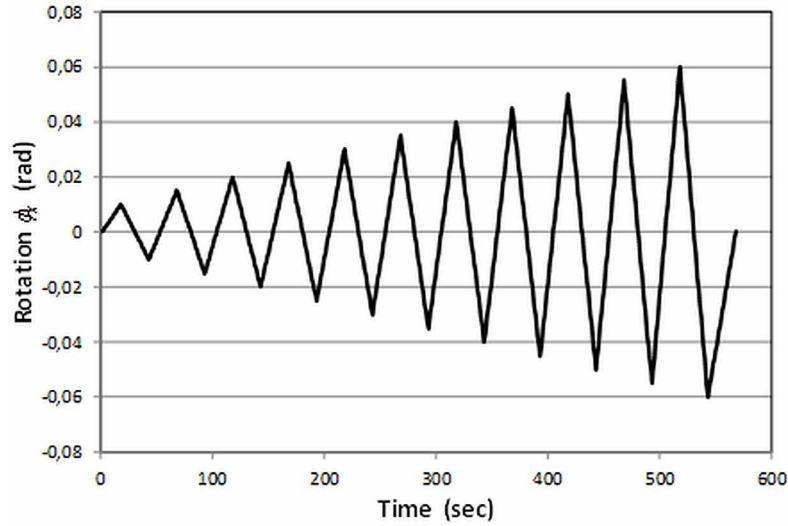
## 12.6 DAMAGE MODEL FOR TRIDIMENSIONAL FRAMES

### 12.6.1 Constitutive Equations

The tridimensional elasto-plastic model described in section 7.5 is generalized including concrete cracking. Consider a slender element; the same lumped/distributed inelasticity model introduced in that section is used again. Unilateral damage in the element can be characterized by the introduction of two sets of damage for the element:  $(\mathbf{D}^{+/-})_b$  as in the planar case. Each set includes a torsion damage variable and two bending damage measures for every plastic hinge; one due to moments around the local axis  $Y_b$  and the other related to bending around the axis  $Z_b$ :



Figure 41. Loading path



$$(\mathbf{D}^{+/-})_b = (d_{iy}^{+/-}, d_{jy}^{+/-}, d_{iz}^{+/-}, d_{jz}^{+/-}, d_x^{+/-})_b \quad (12.6.1)$$

where  $d_{iy}^{+/-}$  represents concrete cracking densities lumped at the plastic hinge  $i$  due to positive/negative bending moments around the local axis  $Y_b$ . The variables  $d_{jy}^{+/-}$ ,  $d_{iz}^{+/-}$ ,  $d_{jz}^{+/-}$  must be interpreted likewise (see Figure 45) and  $d_x^{+/-}$  are, again, torsion damages.

The elasticity law (12.1.5) may also be used to represent unilateral damage in this case, but with the stress and deformation variables employed in section 7.5 and the following flexibility matrices:

$$[\mathbf{F}(\mathbf{D}^{+/-})] = \begin{bmatrix} \frac{L_b}{3(1-d_{iy}^{+/-})EI_y^b} & \frac{-L_b}{6EI_y^b} & 0 & 0 & 0 & 0 \\ \frac{-L_b}{6EI_y^b} & \frac{L_b}{3(1-d_{jy}^{+/-})EI_y^b} & 0 & 0 & 0 & 0 \\ 0 & 0 & \frac{AE_b}{L_b} & 0 & 0 & 0 \\ 0 & 0 & 0 & \frac{L_b}{3(1-d_{iz}^{+/-})EI_z^b} & \frac{-L_b}{6EI_z^b} & 0 \\ 0 & 0 & 0 & \frac{-L_b}{6EI_z^b} & \frac{L_b}{3(1-d_{jz}^{+/-})EI_z^b} & 0 \\ 0 & 0 & 0 & 0 & 0 & \frac{GJ_b}{(1-d_x^{+/-})L_b} \end{bmatrix} \quad (12.6.2)$$

**Unilateral Damage in Reinforced Concrete Frames**

Figure 42. Cracking pattern in a square element subjected to cyclic loads



Figure 43. Torque vs. Angle of twist corresponding to the mono-sign loads a) Experimental b) Numerical simulation

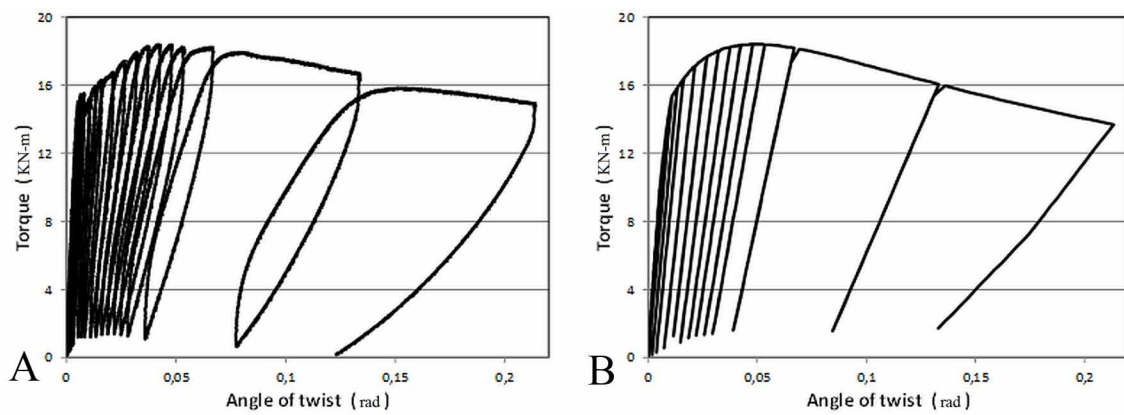


Figure 44. Torque vs. Angle of twist corresponding to the cyclic loads a) Experimental b) Numerical simulation

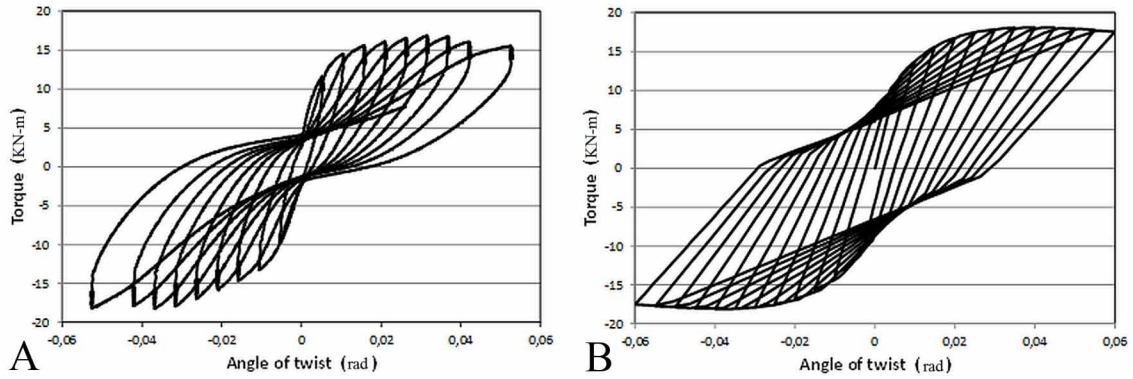
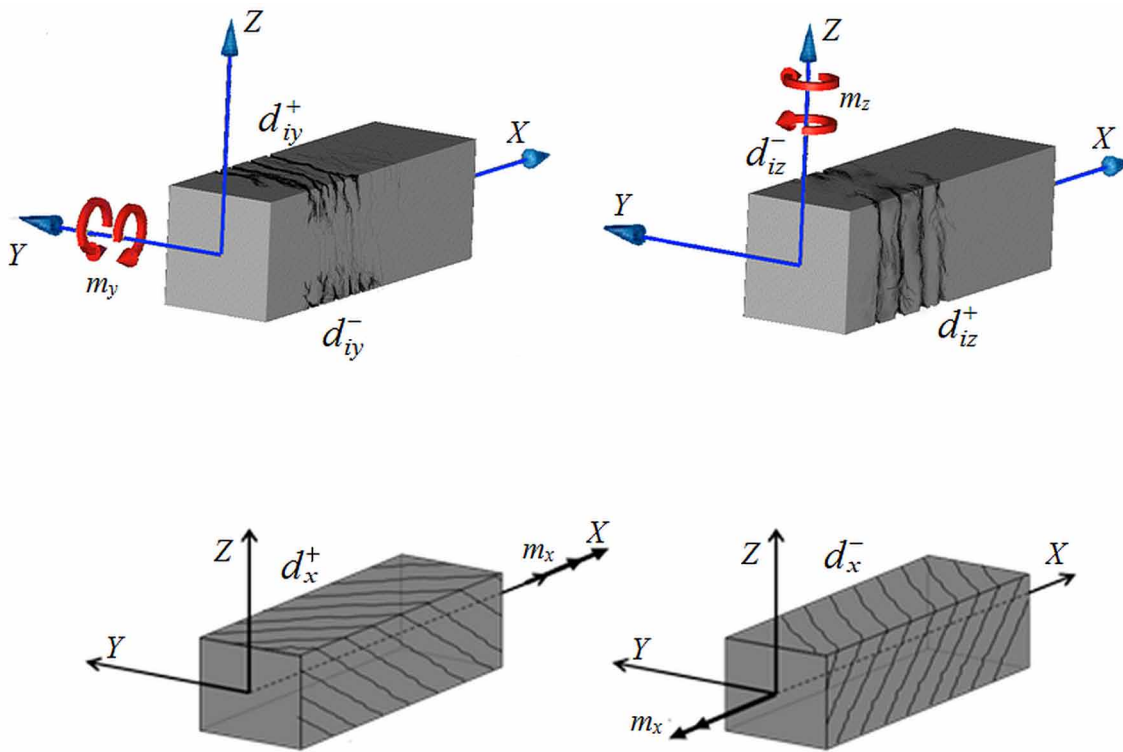


Figure 45. Damage variables in a tridimensional element



## Unilateral Damage in Reinforced Concrete Frames

The yield function of an inelastic hinge in a tridimensional frame is obtained by modifying the yield function (6.5.24) with the unilateral damage concept and the hypothesis of equivalence in deformations, therefore:

$$f_{i/j} = \left[ \text{Max} \left( \frac{1}{k_{0iy/jy}^+ (n, m_x)} \left\langle \frac{m_{iy/jy}}{1 - d_{iy/jy}^+} - c_{iy/jy}^+ (n, m_x) \phi_{iy/jy}^p \right\rangle ; \frac{1}{k_{0iy/jy}^- (n, m_x)} \left\langle \frac{-m_{iy/jy}}{1 - d_{iy/jy}^-} + c_{iy/jy}^- (n, m_x) \phi_{iy/jy}^p \right\rangle \right) \right]_+^\nu + \left[ \text{Max} \left( \frac{1}{k_{0iz/jz}^+ (n, m_x)} \left\langle \frac{m_{iz/jz}}{1 - d_{iz/jz}^+} - c_{iz/jz}^+ (n, m_x) \phi_{iz/jz}^p \right\rangle ; \frac{1}{k_{0iz/jz}^- (n, m_x)} \left\langle \frac{-m_{iz/jz}}{1 - d_{iz/jz}^-} + c_{iz/jz}^- (n, m_x) \phi_{iz/jz}^p \right\rangle \right) \right]_+^\nu - 1 \quad (12.6.3)$$

The Griffith criteria for a tridimensional inelastic hinge are:

$$G_{iy/jy}^{+/-} = R(d_{iy/jy}^{+/-}; n); G_{iz/jz}^{+/-} = R(d_{iz/jz}^{+/-}; n) \quad (12.6.4)$$

where the energy release rates, or “damage driving moments” are:

$$G_{iy/jy}^{+/-} = \frac{\partial W}{\partial d_{iy/jy}^{+/-}} = \frac{L_b \langle m_{iy/jy} \rangle_{+/-}^2}{6EI_b (1 - d_{iy/jy}^{+/-})^2}; G_{iz/jz}^{+/-} = \frac{\partial W}{\partial d_{iz/jz}^{+/-}} = \frac{L_b \langle m_{iz/jz} \rangle_{+/-}^2}{6EI_b (1 - d_{iz/jz}^{+/-})^2} \quad (12.6.5)$$

And the crack resistance functions:

$$R(d_{iy/jy}^{+/-}) = R_{0iy/jy}^{+/-} (n, m_x) + q_{iy/jy}^{+/-} (n, m_x) \frac{\ln(1 - d_{iy/jy}^{+/-})}{(1 - d_{iy/jy}^{+/-})}; \quad (12.6.6)$$

$$R(d_{iz/jz}^{+/-}) = R_{0iz/jz}^{+/-} (n, m_x) + q_{iz/jz}^{+/-} (n, m_x) \frac{\ln(1 - d_{iz/jz}^{+/-})}{(1 - d_{iz/jz}^{+/-})}$$

The torsion and bending effects can be assumed to be uncoupled.

### 12.6.2 Numerical Simulations

Figure 46 shows a square RC column built in cantilever. The specimen was subjected to displacement controlled in the  $Y$ -direction and force controlled in the  $Z$ -direction at the Joint Research Center in Ispra, Italy. The constant level of  $Z$ -force is gradually increased, while in the orthogonal direction the same set of three deflection cycles with linearly increasing amplitude is applied for each level of the  $Y$ -force. The loading path is indicated in Figure 47a.

Figure 46. Schematic representation of a RC column subjected to biaxial bending tested at the Joint Research Center in Ispra, Italy

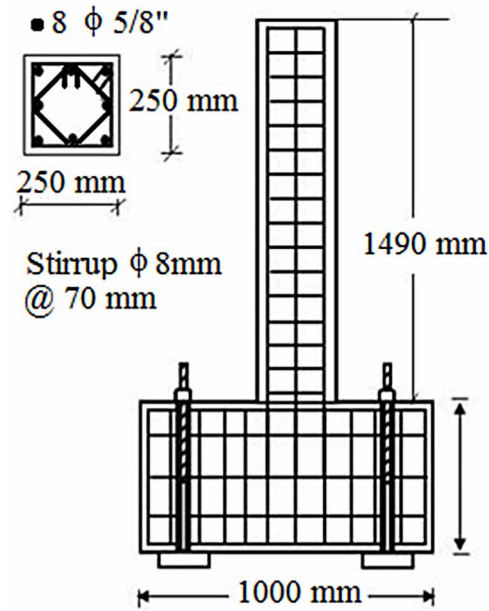
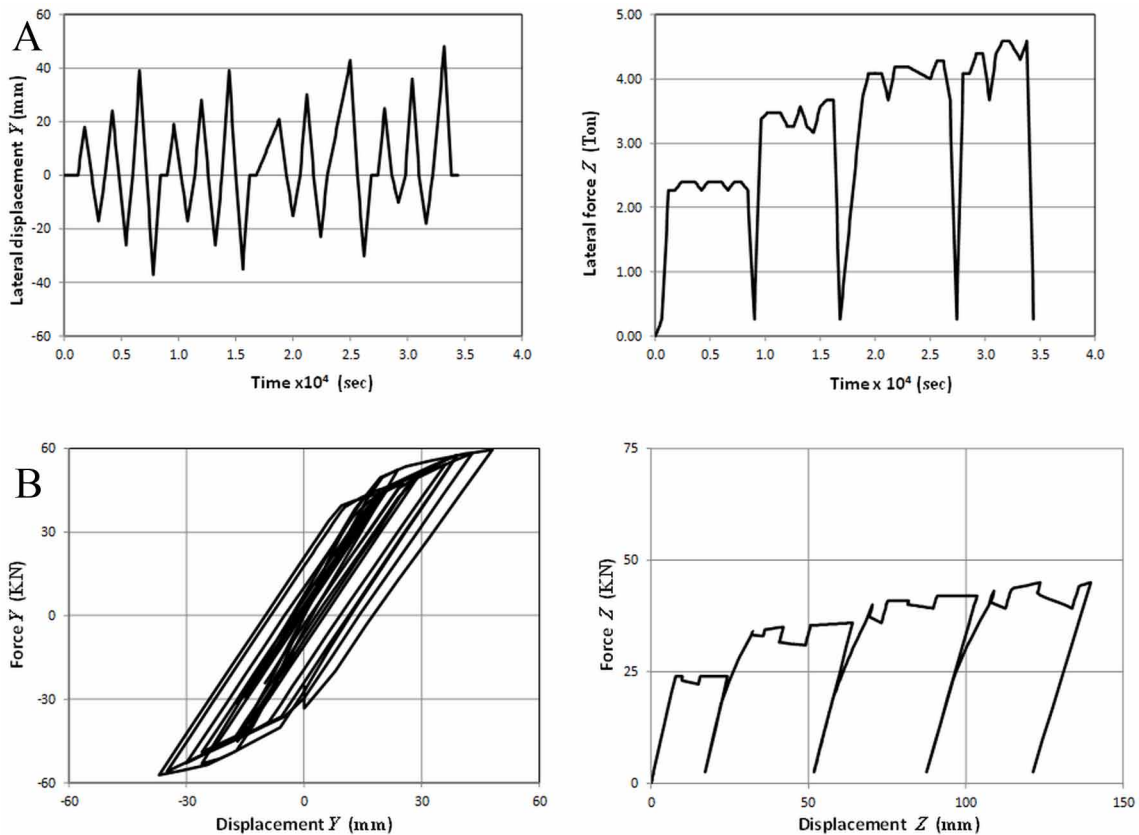


Figure 47. a) Loading path applied in Y-direction and Z-direction b) Numerical curves in the Y and Z directions



## Unilateral Damage in Reinforced Concrete Frames

In Figure 47b are presented the numerical responses. The experimental results can be found in the seventh reference of the bibliography included at the final of the chapter.

The second example consists in the numerical simulation of a test carried out at the University of California, Berkeley. The two-story framed structure represented in the Figure 48 was subjected several times to ground displacements histories derived from the Taft earthquake record. The structure was placed with an angle of  $25^\circ$  with respect to the axis of the shaking table motion. Thus, the structure was subjected to biaxial solicitations. First two low intensity shakes, with peak acceleration amplitude of 0.06 g, were applied on the structure. The goal of this loading was to induce minor cracking in the virgin frame to replicate the condition of a real structure which has seen service loading. Then the structure was subjected to a severe shaking with a peak acceleration of 0.685 g.

The beams and columns of the structure were represented with the model described in this section. Standard elastic plate elements (Kirchoff theory) were used to represent the first and second floor slabs. The numerical results obtained after the severe shake are shown in Figures 49 and 12.50. In the Figure 49, the experimental and computed displacements of the first floor are presented. Figure 50 shows the computed and observed local behavior of one of the columns of the first floor.

The damage state after the first low intensity shake can be observed in the Figure 51a. In this figure, the maximum values of damage of each hinge (there are four values per hinge) are shown. It can be noticed that no value exceeded 0.26. This corresponds indeed to minor cracking that does not need reparation. The Figure 51b indicates the final state of damage after the numerical simulation.

Figure 48. Frame structure subjected to earthquake loading Courtesy of NISEE-PEER, University of California, Berkeley

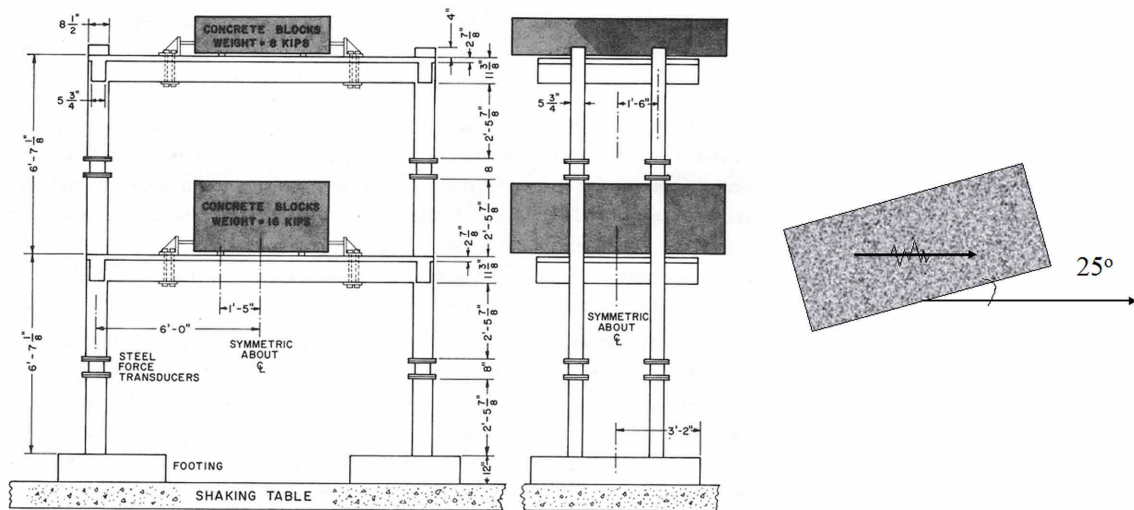


Figure 49. Displacements of the first floor: a) longitudinal direction, experimental b) longitudinal axes, numerical c) transversal axes, experimental d) transversal axes, numerical

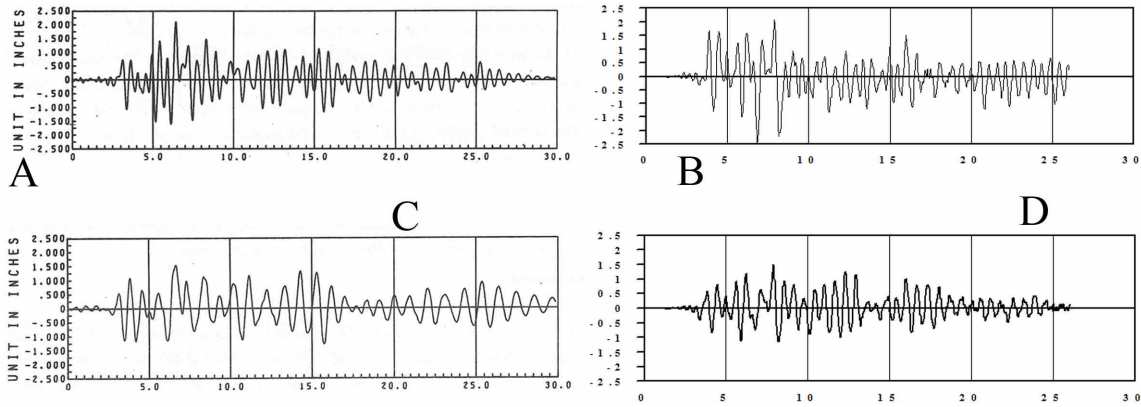
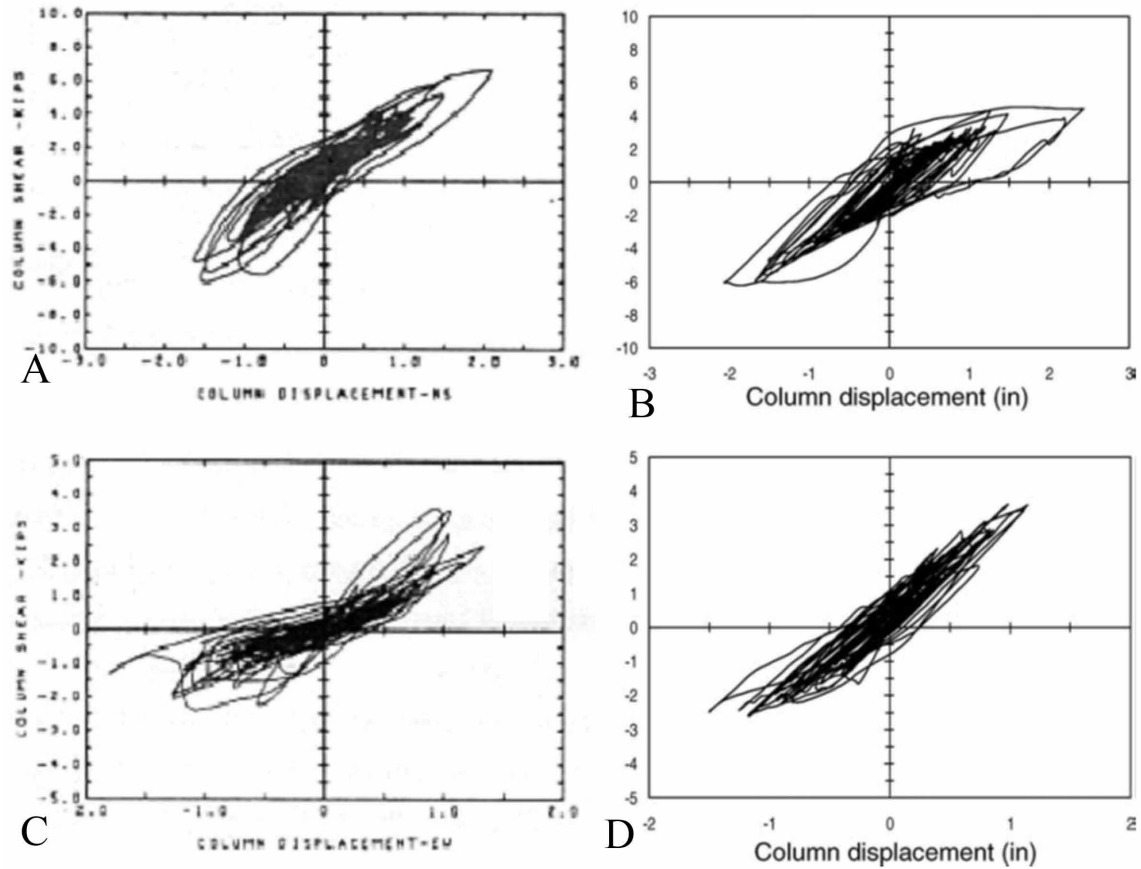
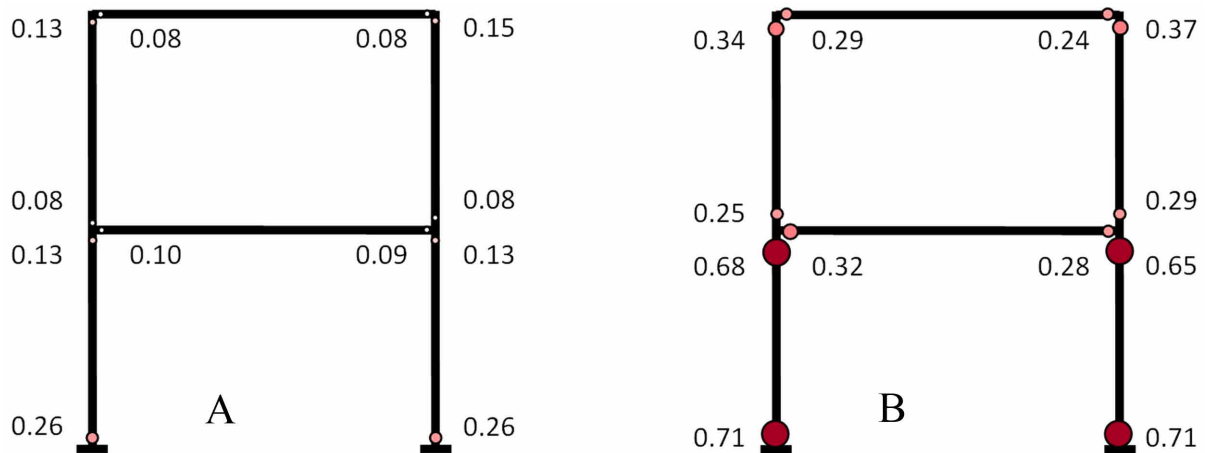


Figure 50. Local behavior of a first floor column: a) longitudinal axes, experimental b) longitudinal axes, numerical c) transversal axes, experimental d) transversal axes, numerical



## Unilateral Damage in Reinforced Concrete Frames

Figure 51. Damage distribution in the frame: a) after a low intensity shake b) after a severe shake



## 12.7 SUMMARY AND EQUATIONS QUICK REFERENCE

In this chapter, the unilateral damage concept was added to the procedures presented in chapters 10 and 11 in order to model the cyclic behavior of RC structures. As a result, models for planar frames, dual systems, torsion and tridimensional frames were developed. The numerical implementation of those models is the same to the one presented in sections 10.7 and 11.5 (See Table 2).

Table 2.

ELASTICITY LAW UNDER CYCLIC LOADING
<i>Unilateral Damage in Reinforced Concrete Elements</i>

continued on following page



Table 2. Continued

<p>Elasticity law in the case of mono sign loadings <math>\phi_i - \phi_i^p - \gamma_s^p = \left( \frac{L_b}{3EI_b(1-d_i)} m_i - \frac{L_b}{6EI_b} m_j \right) + \frac{V}{GA_b(1-d_s)}</math></p> $\delta = \frac{L_b}{AE_b} n \phi_j - \phi_j^p - \gamma_s^p = \left( -\frac{L_b}{6EI_b} m_i + \frac{L_b}{3EI_b(1-d_j)} m_j \right) + \frac{V}{GA_b(1-d_s)}$ $V = \frac{m_i + m_j}{L_b} \quad (12.1.1)$
<p>Elasticity law of a damaged RC element of any aspect ratio under general cyclic loading</p> $\phi_i - \phi_i^p - \gamma_s^p = \left( \frac{L_b}{3EI_b(1-d_i^+)} \langle m_i \rangle_+ + \frac{L_b}{3EI_b(1-d_i^-)} \langle m_i \rangle_- - \frac{L_b}{6EI_b} m_j \right) + \frac{\langle V \rangle_+}{GA_b(1-d_s^+)} + \frac{\langle V \rangle_-}{GA_b(1-d_s^-)}$ $\delta = \frac{L_b}{AE_b} n$ $\phi_j - \phi_j^p - \gamma_s^p = \left( -\frac{L_b}{6EI_b} m_i + \frac{L_b}{3EI_b(1-d_j^+)} \langle m_j \rangle_+ + \frac{L_b}{3EI_b(1-d_j^-)} \langle m_j \rangle_- \right) + \frac{\langle V \rangle_+}{GA_b(1-d_s^+)} + \frac{\langle V \rangle_-}{GA_b(1-d_s^-)}$ <p>(12.1.2)</p>
<p>Elasticity law of a damaged RC element of any aspect ratio under general cyclic loading</p> $\{\Phi\}_b - \{\Phi^p\}_b - \{\gamma^p\}_b = [\mathbf{F}_f(\mathbf{D}^+)] \langle \mathbf{M} \rangle_b^+ + [\mathbf{F}_f(\mathbf{D}^-)] \langle \mathbf{M} \rangle_b^- + \frac{1}{GA_b(1-d_s^+)} \langle \mathbf{V} \rangle_b^+ + \frac{1}{GA_b(1-d_s^-)} \langle \mathbf{V} \rangle_b^-$ <p>(12.1.3)</p> $[\mathbf{F}_f(\mathbf{D}^{+/-})] = \begin{bmatrix} \frac{L_b}{3EI_b(1-d_i^{+/-})} & -\frac{L_b}{6EI_b} & 0 \\ -\frac{L_b}{6EI_b} & \frac{L_b}{3EI_b(1-d_j^{+/-})} & 0 \\ 0 & 0 & \frac{L_b}{EA_b} \end{bmatrix}; \langle \mathbf{V} \rangle_b^{+/-} = \begin{bmatrix} \langle V \rangle_{+/-} \\ \langle V \rangle_{+/-} \\ 0 \end{bmatrix}$ <p style="text-align: right;">(12.1.4)</p>
<p>Elasticity law of slender RC elements</p> $\{\Phi\}_b - \{\Phi^p\}_b = [\mathbf{F}_f(\mathbf{D}^+)] \langle \mathbf{M} \rangle_b^+ + [\mathbf{F}_f(\mathbf{D}^-)] \langle \mathbf{M} \rangle_b^- \quad (12.1.5)$
<b>INTERNAL VARIABLES EVOLUTION LAWS UNDER CYCLIC LOADING</b>
<i>Damage Evolution Laws</i>
<p>Complementary deformation energy</p> $W = \frac{1}{2} \{\mathbf{M}\}_b^t \{\Phi - \Phi^p - \gamma^p\}_b =$ $= \frac{1}{2} \{\mathbf{M}\}_b^t [\mathbf{F}_f(\mathbf{D}^+)] \langle \mathbf{M} \rangle_b^+ + \frac{1}{2} \{\mathbf{M}\}_b^t [\mathbf{F}_f(\mathbf{D}^-)] \langle \mathbf{M} \rangle_b^- + \frac{1}{2GA_b(1-d_s^+)} \{\mathbf{M}\}_b^t \langle \mathbf{V} \rangle_b^+ + \frac{1}{2GA_b(1-d_s^-)} \{\mathbf{M}\}_b^t \langle \mathbf{V} \rangle_b^-$ <p>(12.2.1)</p>

continued on following page

## Unilateral Damage in Reinforced Concrete Frames

Table 2. Continued

<p>The energy release rates</p> $G_{i/j}^{+/-} = \frac{\partial W}{\partial d_{i/j}^{+/-}} = \frac{L_b \langle m_{i/j} \rangle_{+/-}^2}{6EI_b (1 - d_{i/j}^{+/-})^2}; \quad G_s^{+/-} = \frac{\partial W}{\partial d_s^{+/-}} = \frac{L_b V_{+/-}^2}{2GA_b (1 - d_s^{+/-})^2} \quad (12.2.2)$
<p>Damage evolution laws</p> $\begin{cases} \Delta d_{i/j/s}^{+/-} = 0 & \text{if } G_{i/j/s}^{+/-} < R_{i/j/s}^{+/-} \\ G_{i/j/s}^{+/-} = R_{i/j/s}^{+/-} & \text{if } \Delta d_{i/j/s}^{+/-} > 0 \end{cases}; \quad (12.2.3)$ <p>for the classic version, or</p> $\begin{cases} \Delta d_{i/j/s}^{+/-} = 0 & \text{if } G_{i/j/s}^{+/-} < R_{0i/j/s}^{+/-} \\ \Delta d_{i/j/s}^{+/-} = \frac{1}{\left(\frac{\partial R_{i/j/s}^{+/-}}{\partial d_{i/j/s}^{+/-}}\right)} \left(\frac{G_{i/j/s}^{+/-}}{R_{i/j/s}^{+/-}}\right)^2 \langle \Delta G_{i/j/s}^{+/-} \rangle_+ & \text{otherwise} \end{cases} \quad (12.2.4)$ <p>for the modified one</p>
<p><b>Plastic Deformations Evolution Laws</b></p>
<p>Yield function for mono sign loadings</p> $f_i = \left  \frac{m_i}{1 - d_i} - c_i \phi_i^p \right  - k_{0i} = \text{Max} \left( \frac{m_i}{1 - d_i} - c_i \phi_i^p - k_{0i}, -\frac{m_i}{1 - d_i} + c_i \phi_i^p - k_{0i} \right) \leq 0 \quad (12.2.5)$
<p>Yield function with unilateral damage</p> $f_i = \text{Max} \left( \frac{m_i}{1 - d_i^+} - c_i^+ \phi_i^p - k_{0i}^+, -\frac{m_i}{1 - d_i^-} + c_i^- \phi_i^p - k_{0i}^- \right) \leq 0 \quad (12.2.6)$
<p>Yield function of a plastic hinge with damage and general cyclic moments</p> $f_i = \text{Max} \begin{cases} \frac{m_i}{1 - d_i^+} - 0.7c_i^+ \phi_i^p - k_{0i}^+ - 0.3c_i^+ p_i \\ -\frac{m_i}{1 - d_i^-} + 0.7c_i^- \phi_i^p - k_{0i}^- - 0.3c_i^- p_i \end{cases} \leq 0; \quad p_i = \text{Max}  \phi_i^p  \quad (12.2.7)$
<p>Evolution laws in the case of cyclic loadings</p> $\begin{cases} d\phi_i^p = 0 \text{ if } f_i < 0 \\ f_i = 0 \text{ if } d\phi_i^p \neq 0 \end{cases}; \begin{cases} d\phi_j^p = 0 \text{ if } f_j < 0 \\ f_j = 0 \text{ if } d\phi_j^p \neq 0 \end{cases}; \begin{cases} d\gamma_s^p = 0 \text{ if } f_s < 0 \\ f_s = 0 \text{ if } d\gamma_s^p \neq 0 \end{cases} \quad (12.2.8)$

continued on following page



## Unilateral Damage in Reinforced Concrete Frames

Table 2. Continued

TORSION DAMAGE
<i>Constitutive Equations for Mono Sign Torsion</i>
<p>Angle of twist</p> $\phi_x = m_x \frac{L}{GJ} + \phi_x^d + \phi_x^p \quad (12.5.1)$ <p><math>m_x \frac{L}{GJ}</math> : elastic rotation</p> <p><math>\phi_x^p</math> : plastic twist due to reinforcement yielding</p> <p><math>\phi_x^d</math> : additional twist due to concrete cracking</p>
<p>Additional twist due to concrete cracking</p> $\phi_x^d = \frac{d_x L}{(1 - d_x)GJ} m_x \quad (12.5.2)$ <p><math>d_x</math>: torsion damage</p>
<p>Elasticity law of a damaged RC element subjected to torsion only</p> $\phi_x - \phi_x^p = \frac{L}{(1 - d_x)GJ} m_x \quad m_x = (1 - d_x) \frac{GJ}{L} (\phi_x - \phi_x^p) \quad (12.5.3)$ <p style="text-align: center;">; or</p>
<p>Deformation energy due to torsion</p> $W = \frac{1}{2} m_x (\phi_x - \phi_x^p) = \frac{1}{2} \frac{m_x^2 L}{(1 - d_x)GJ} \quad (12.5.4)$
<p>Energy release rate due to torsion</p> $G_x = \frac{\partial W}{\partial d_x} = \frac{1}{2} \frac{m_x^2 L}{(1 - d_x)^2 GJ} \quad (12.5.5)$
<p>Griffith criterion for torsion cracks</p> $G_x \leq R(d_x) \quad (12.5.6)$ <p><math>R(d_x)</math>: crack resistance to torsion</p>
<p>Crack resistance for torsion cracks</p> $R(d_x) = R_{0x} + q_x \frac{\ln(1 - d_x)}{1 - d_x} \quad (12.5.7)$
<p>Yield function in torsion</p> $f = \left  \bar{m}_x - c_x \phi_x^p \right  - k_{0x} = \left  \frac{m_x}{1 - d_x} - c_x \phi_x^p \right  - k_{0x} \leq 0 \quad (12.5.8)$ <p><math>R_{0x}</math>, <math>q_x</math>, <math>c_x</math> and <math>k_{0x}</math> can be computed with the same procedures described in the cases of bending and shear (see section 10.3.3 and 10.4.2).</p>

continued on following page

Table 2. Continued

<b>Determination of the First Cracking Torque</b>
First cracking torque $M_{crx} = 0.33\sqrt{f'_c} \left( \frac{A_{cp}^2}{p_{cp}} \right) \sqrt{1 + \frac{N}{0.33A_g\sqrt{f'_c}}} \text{N.mm} \quad (12.5.9)$
$N$ : Axial force in N $A_{cp}$ : area enclosed by outside perimeter of concrete cross section in mm <sup>2</sup> $p_{cp}$ : outside perimeter of concrete cross section in mm $A_g$ : gross area of the concrete section in mm <sup>2</sup> $f'_c$ : strength of concrete in MPa.
<b>Determination of the First Plastic Torque</b>
First plastic torque $M_{px} = \Omega x^2 y \sqrt{f'_c} \text{N.mm} \quad (12.5.10)$
$x$ and $y$ : dimensions of the cross-section (for $x \leq y$ ) $\Omega$ varies from 0.166 for $y/x = 1$ and 0.249 for $y/x = \infty$
<b>Determination of the Ultimate Plastic Twist</b>
Ultimate plastic twist $\phi_{ux}^p = \theta_{ux}^p L; \quad \theta_{ux}^p = \theta_{ux} - \theta_{cx} = \frac{M_{ux}}{(GC)_u} - \frac{M_{ux}}{GJ}; \quad (GC)_u = \frac{4E_s A_o^2 A_{cp}}{p_0 \left( \frac{16nA_{cp}}{p_0 t_d} + \frac{1}{\rho_l} + \frac{1}{\rho_t} \right)} \quad (12.5.11)$
$GJ$ : initial torsional rigidity $E_s$ : modulus of elasticity of steel $A_{cp}$ : area enclosed by outside perimeter of concrete cross section $A_o$ : area enclosed by the centerline of shear flow zone $p_0$ : perimeter of the centerline of the shear flow zone $n = E_s / E_c$ $t_d$ : thickness of shear flow zone $\rho_l = A_l / A_{cp}$ : total volumetric ratio of longitudinal steel $\rho_t = A_s t_p / A_{cp} s$ : volumetric ratio of transverse hoop steel
<b>General Constitutive Equations for Torsion Damage</b>
Elasticity law with unilateral damage $\phi_x - \phi_x^p = \frac{L}{(1 - d_x^+)GJ} \langle m_x \rangle_+ + \frac{L}{(1 - d_x^-)GJ} \langle m_x \rangle_- \quad (12.5.12)$

continued on following page

**Unilateral Damage in Reinforced Concrete Frames**

Table 2. Continued

Energy release rates and crack resistance functions for unilateral torsion cracks	
$G_x^{+/-} = \frac{1}{2} \frac{\langle m_x^2 \rangle_{+/-} L}{(1 - d_x^{+/-})^2 GJ}; \quad R = R_{0x}^{+/-} + q_x^{+/-} \frac{\ln(1 - d_x^{+/-})}{1 - d_x^{+/-}} \quad (12.5.13)$	
Yield function	
$f_x = Max \begin{cases} \frac{m_x}{1 - d_x^+} - 0.8c_x^+ \phi_x^p - k_{0x}^+ - 0.2c_x^+ p_x \\ -\frac{m_x}{1 - d_x^-} + 0.8c_x^- \phi_x^p - k_{0x}^- - 0.2c_x^- p_x \end{cases} \leq 0; \quad p_x = Max  \phi_x^p  \quad (12.5.14)$	
<b>DAMAGE MODEL FOR TRIDIMENSIONAL FRAMES</b>	
Unilateral damage	
$(\mathbf{D}^{+/-})_b = (d_{iy}^{+/-}, d_{jy}^{+/-}, d_{iz}^{+/-}, d_{jz}^{+/-}, d_x^{+/-})_b \quad (12.6.1)$	
$d_{iy}^{+/-}, d_{jy}^{+/-}$ : Concrete cracking densities lumped at the plastic hinge $i$ and $j$ due to positive/negative bending moments around the local axis $Y_b$ .	
$d_{iz}^{+/-}, d_{jz}^{+/-}$ : Concrete cracking densities lumped at the plastic hinge $i$ and $j$ due to positive/negative bending moments around the local axis $Z_b$ .	
$d_x^{+/-}$ : torsion damages.	
Flexibility matrices	
$[\mathbf{F}(\mathbf{D}^{+/-})] = \begin{bmatrix} \frac{L_b}{3(1 - d_{iy}^{+/-})EI_y^b} & \frac{-L_b}{6EI_y^b} & 0 & 0 & 0 & 0 \\ \frac{-L_b}{6EI_y^b} & \frac{L_b}{3(1 - d_{jy}^{+/-})EI_y^b} & 0 & 0 & 0 & 0 \\ 0 & 0 & \frac{AE_b}{L_b} & 0 & 0 & 0 \\ 0 & 0 & 0 & \frac{L_b}{3(1 - d_{iz}^{+/-})EI_z^b} & \frac{-L_b}{6EI_z^b} & 0 \\ 0 & 0 & 0 & \frac{-L_b}{6EI_z^b} & \frac{L_b}{3(1 - d_{jz}^{+/-})EI_z^b} & 0 \\ 0 & 0 & 0 & 0 & 0 & \frac{GJ_b}{(1 - d_x^{+/-})L_b} \end{bmatrix} \quad (12.6.2)$	

*continued on following page*

Table 2. Continued

<p>The yield functions on hinges <math>i</math> and <math>j</math>:</p> $f_{i/j} = \left[ \text{Max} \left( \frac{1}{k_{0iy/jy}^+ (n)} \left\langle \frac{m_{iy/jy}}{1 - d_{iy/jy}^+} - c_{iy/jy}^+ (n, m_x) \phi_{iy/jy}^p \right\rangle ; \frac{1}{k_{0iy/jy}^- (n)} \left\langle \frac{-m_{iy/jy}}{1 - d_{iy/jy}^-} + c_{iy/jy}^- (n, m_x) \phi_{iy/jy}^p \right\rangle \right) \right]_+^{\nu} + \left[ \text{Max} \left( \frac{1}{k_{0iz/jz}^+ (n)} \left\langle \frac{m_{iz/jz}}{1 - d_{iz/jz}^+} - c_{iz/jz}^+ (n, m_x) \phi_{iz/jz}^p \right\rangle ; \frac{1}{k_{0iz/jz}^- (n)} \left\langle \frac{-m_{iz/jz}}{1 - d_{iz/jz}^-} + c_{iz/jz}^- (n, m_x) \phi_{iz/jz}^p \right\rangle \right) \right]_+^{\nu} - 1 \quad (12.6.3)$
<p>The Griffith criteria for the tridimensional model</p> $G_{iy/jy}^{+/-} = R(d_{iy/jy}^{+/-}; n); \quad G_{iz/jz}^{+/-} = R(d_{iz/jz}^{+/-}; n) \quad (12.6.4)$ <p>where the energy release rates:</p> $G_{iy/jy}^{+/-} = \frac{\partial W}{\partial d_{iy/jy}^{+/-}} = \frac{L_b \langle m_{iy/jy} \rangle_{+/-}^2}{6EI_b (1 - d_{iy/jy}^{+/-})^2}; \quad G_{iz/jz}^{+/-} = \frac{\partial W}{\partial d_{iz/jz}^{+/-}} = \frac{L_b \langle m_{iz/jz} \rangle_{+/-}^2}{6EI_b (1 - d_{iz/jz}^{+/-})^2} \quad (12.6.5)$ <p>The crack resistance functions</p> $R(d_{iy/jy}^{+/-}) = R_{0iy/jy}^{+/-} (n, m_x) + q_{iy/jy}^{+/-} (n, m_x) \frac{\ln(1 - d_{iy/jy}^{+/-})}{(1 - d_{iy/jy}^{+/-})};$ $R(d_{iz/jz}^{+/-}) = R_{0iz/jz}^{+/-} (n, m_x) + q_{iz/jz}^{+/-} (n, m_x) \frac{\ln(1 - d_{iz/jz}^{+/-})}{(1 - d_{iz/jz}^{+/-})} \quad (12.6.6)$

## 12.8 EXAMPLES

### 12.8.1 For the Structure That Is Shown in Figure 52 Carry out the Numerical Simulation Using the Unilateral Damage Model

The aspect ratio of the element is:

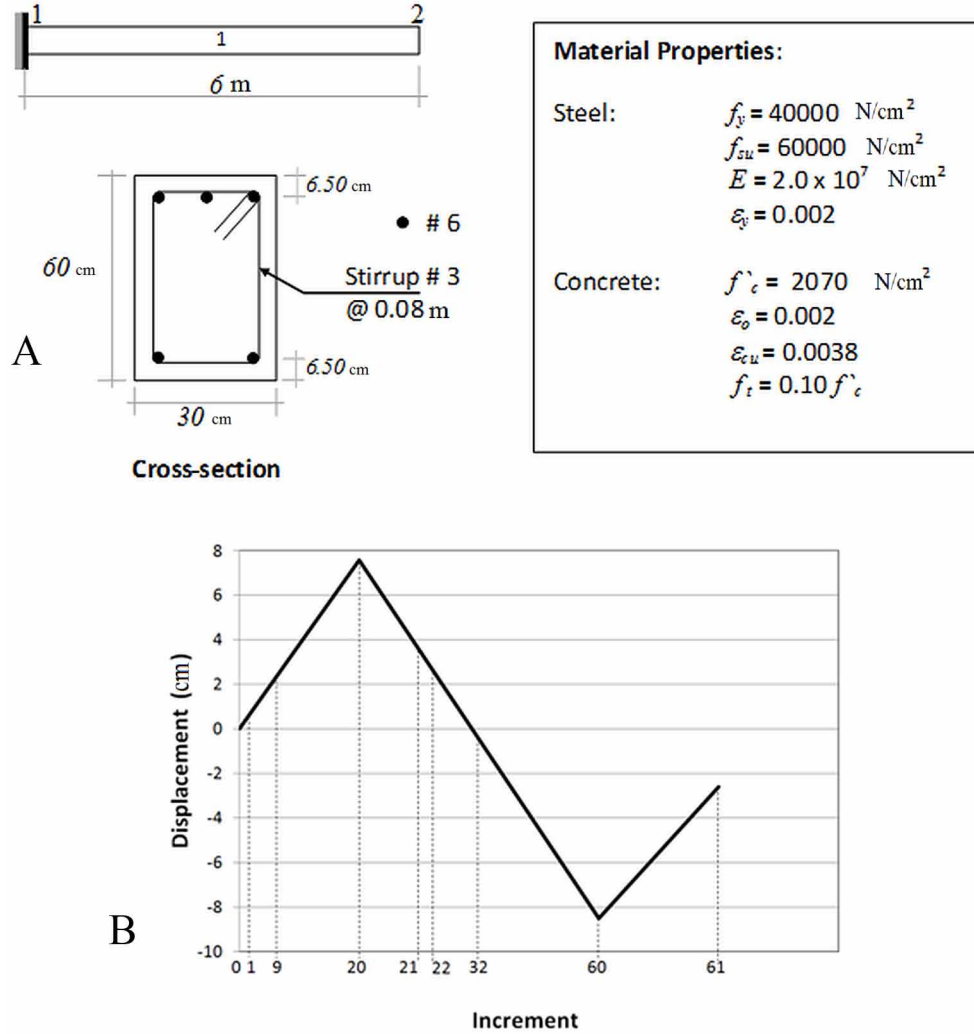
$$\frac{a}{d} = \frac{600}{53.5} = 11.21 > 6.5 \quad (12.8.1)$$

This beam can be classified as slender (see Chapter 2, section 2.7.3) then, shear effects are neglected.

Section properties  $M_{cr}^{+/-}$ ,  $M_p^{+/-}$ ,  $M_u^{+/-}$ , and  $\phi_u^{p+/-}$  are computed following the procedures described, respectively, in sections 10.3.4, 6.5.4, 6.5.5 and 6.5.6. As the beam is asymmetrically reinforced, these values are different for ends 1 and 2. These values are presented in Table 3. Positive properties at end 1 and negative at end 2 are computed considering  $A_s = 5.7 \text{ cm}^2$  and  $A'_s = 8.55 \text{ cm}^2$ ; the negative properties at end 1 and positive at end 2 are computed considering  $A_s = 8.55 \text{ cm}^2$  and  $A'_s = 5.7 \text{ cm}^2$ . The plastic hinge length is obtained with Equation (6.5.20) resulting a value  $L_p = 60 \text{ cm}$ .

## Unilateral Damage in Reinforced Concrete Frames

Figure 52. a) Structure geometry, section of element and material properties b) Displacement history applied at the free end of the beam (node 2)



With these properties, model parameters  $R_0^{+/-}$ ,  $q^{+/-}$ ,  $c^{+/-}$  and  $k_0^{+/-}$  are computed using the procedures described in sections 10.3.3 and 10.4.2. The model parameters are presented in Table 4.

The generalized displacements and nodal forces matrices for the beam are, respectively,

$$\{\mathbf{U}\} = \begin{bmatrix} 0 \\ 0 \\ 0 \\ u_{2_i} \\ w_{2_i} \\ \theta_{2_i} \end{bmatrix}; \{\mathbf{P}\} = \begin{bmatrix} R_{u_{1_i}} \\ R_{w_{1_i}} \\ R_{\theta_{1_i}} \\ 0 \\ R_{w_{2_i}} \\ 0 \end{bmatrix} \quad (12.8.2)$$



Table 3. Section properties of the cross-section

$M_{cr1}^+ = M_{cr2}^- = 4.62 \times 10^6 \text{ N.cm}$	$M_{cr2}^+ = M_{cr1}^- = 4.81 \times 10^6 \text{ N.cm}$
$M_{p1}^+ = M_{p2}^- = 1.11 \times 10^7 \text{ N.cm}$	$M_{p2}^+ = M_{p1}^- = 1.64 \times 10^7 \text{ N.cm}$
$M_{u1}^+ = M_{u2}^- = 1.17 \times 10^7 \text{ N.cm}$	$M_{u2}^+ = M_{u1}^- = 1.71 \times 10^7 \text{ N.cm}$
$\chi_{p1}^+ = \chi_{p2}^- = 4.87 \times 10^{-5} \text{ rad/cm}$	$\chi_{p2}^+ = \chi_{p1}^- = 5.26 \times 10^{-5} \text{ rad/cm}$
$\chi_{u1}^+ = \chi_{u2}^- = 6.12 \times 10^{-4} \text{ rad/cm}$	$\chi_{u2}^+ = \chi_{u1}^- = 5.28 \times 10^{-4} \text{ rad/cm}$
$\phi_{u1}^{p+} = \phi_{u2}^{p-} = 3.38 \text{E-02}$	$\phi_{u2}^{p+} = \phi_{u1}^{p-} = 2.85 \text{E-02}$

Table 4. Model parameters

$R_{01}^+ = R_{02}^- = 3022.77652$	$R_{02}^+ = R_{01}^- = 3272.56988$
$q_1^+ = q_2^- = -51549.7798$	$q_2^+ = q_1^- = -111167.51$
$c_1^+ = c_2^- = 571404636$	$c_2^+ = c_1^- = 1019721538$
$k_{01}^+ = k_{02}^- = 19446406.2$	$k_{02}^+ = k_{01}^- = 30484928.9$

The matrix of total deformation and stresses are:

$$\{\Phi\}_1 = \begin{bmatrix} \phi_{11_t} \\ \phi_{12_t} \\ \delta_{1_t} \end{bmatrix}; \{\mathbf{M}\}_1 = \langle \mathbf{M} \rangle_1^+ + \langle \mathbf{M} \rangle_1^- = \begin{bmatrix} m_{11_t} \\ m_{12_t} \\ n_{1_t} \end{bmatrix} \quad (12.8.3)$$

The stresses are divided into a positive and a negative part. In an algebraic manipulation program this can be carried out in the following way:

$$\langle \mathbf{M} \rangle_1^+ = \begin{bmatrix} \frac{1}{2} m_{11_t} + \frac{1}{2} |m_{11_t}| \\ \frac{1}{2} m_{12_t} + \frac{1}{2} |m_{12_t}| \\ \frac{1}{2} n_{1_t} + \frac{1}{2} |n_{1_t}| \end{bmatrix}; \langle \mathbf{M} \rangle_1^- = \begin{bmatrix} \frac{1}{2} m_{11_t} - \frac{1}{2} |m_{11_t}| \\ \frac{1}{2} m_{12_t} - \frac{1}{2} |m_{12_t}| \\ \frac{1}{2} n_{1_t} - \frac{1}{2} |n_{1_t}| \end{bmatrix} \quad (12.8.4)$$

**Unilateral Damage in Reinforced Concrete Frames**

The plastic deformation is given by:

$$\{\Phi^p\}_1 = \begin{bmatrix} \phi_{11_t}^p \\ 0 \\ 0 \end{bmatrix} \quad (12.8.5)$$

Two damages values are defined,  $d_{1_t}^+$  and  $d_{1_t}^-$ , for the hinge at the end 1.

$$(\mathbf{D}^+)_1 = (d_{1_t}^+, 0) \quad (\mathbf{D}^-)_1 = (d_{1_t}^-, 0) \quad (12.8.6)$$

The kinematic equation (3.1.12b) with  $\alpha = 0$ ,  $L = 600$  cm: is

$$\{d\Phi\} = [\mathbf{B}(q)]\{d\mathbf{q}\}; \begin{bmatrix} \phi_{11_t} \\ \phi_{12_t} \\ \delta_{1_t} \end{bmatrix} \cong \begin{bmatrix} \frac{\sin \alpha}{L} & -\frac{\cos \alpha}{L} & 1 & -\frac{\sin \alpha}{L} & \frac{\cos \alpha}{L} & 0 \\ \frac{\sin \alpha}{L} & -\frac{\cos \alpha}{L} & 0 & -\frac{\sin \alpha}{L} & \frac{\cos \alpha}{L} & 1 \\ -\cos \alpha & -\sin \alpha & 0 & \cos \alpha & \sin \alpha & 0 \end{bmatrix} \begin{bmatrix} 0 \\ 0 \\ 0 \\ u_{2_t} \\ w_{2_t} \\ \theta_{2_t} \end{bmatrix} \quad (12.8.7)$$

where

$$[\mathbf{B}_E^0] = \begin{bmatrix} 0 & -0.00167 & 1 & 0 & 0.00167 & 0 \\ 0 & -0.00167 & 0 & 0 & 0.00167 & 1 \\ -1 & 0 & 0 & 1 & 0 & 0 \end{bmatrix} \quad (12.8.8)$$

then

$$\{\Phi\}_1 = \begin{bmatrix} \phi_{11_t} \\ \phi_{12_t} \\ \delta_{1_t} \end{bmatrix} \cong \begin{bmatrix} 0.00167w_{2_t} \\ 0.00167w_{2_t} + \theta_{2_t} \\ u_{2_t} \end{bmatrix} \quad (12.8.9)$$

The equilibrium equation (3.2.13) results in:

$$\sum_{b=1}^m [\mathbf{B}_E^0]_b^t \{\mathbf{M}\}_b = \{\mathbf{P}\}; \quad \begin{bmatrix} \frac{\sin \alpha}{L} & \frac{\sin \alpha}{L} & -\cos \alpha \\ \frac{\cos \alpha}{L} & -\frac{\cos \alpha}{L} & -\sin \alpha \\ 1 & 0 & 0 \\ \frac{\sin \alpha}{L} & -\frac{\sin \alpha}{L} & \cos \alpha \\ \frac{\cos \alpha}{L} & \frac{\cos \alpha}{L} & \sin \alpha \\ 0 & 1 & 0 \end{bmatrix} \begin{bmatrix} m_{11_t} \\ m_{12_t} \\ n_{1_t} \end{bmatrix} = \begin{bmatrix} R_{u1_t} \\ R_{w1_t} \\ R_{\theta1_t} \\ 0 \\ R_{w2_t} \\ 0 \end{bmatrix}, \quad (12.8.10)$$

$$\begin{bmatrix} R_{u1_t} \\ R_{w1_t} \\ R_{\theta1_t} \\ 0 \\ R_{w2_t} \\ 0 \end{bmatrix} = \begin{bmatrix} -n_{1_t} \\ -0.00167m_{11_t} - 0.00167m_{12_t} \\ m_{11_t} \\ n_{1_t} \\ 0.00167m_{11_t} + 0.00167m_{12_t} \\ m_{12_t} \end{bmatrix} \quad (12.8.11)$$

The elasticity law (12.1.5) is

$$\{\Phi\}_b - \{\Phi^p\}_b = [\mathbf{F}_f(\mathbf{D}^+)] \langle \mathbf{M} \rangle_b^+ + [\mathbf{F}_f(\mathbf{D}^-)] \langle \mathbf{M} \rangle_b^- \quad (12.8.12)$$

where from Equation (10.1.4)

$$[\mathbf{F}_f(\mathbf{D}^+)] = \begin{bmatrix} \frac{L}{3EI(1-d_1^+)} & -\frac{L}{6EI} & 0 \\ -\frac{L}{6EI} & \frac{L}{3EI} & 0 \\ 0 & 0 & \frac{L}{AE} \end{bmatrix} = \begin{bmatrix} \frac{0.2827 \times 10^{-9}}{(1-d_1^+)} & -0.1414 \times 10^{-9} & 0 \\ -0.1414 \times 10^{-9} & 0.2827 \times 10^{-9} & 0 \\ 0 & 0 & 0.2813 \times 10^{-6} \end{bmatrix};$$

$$[\mathbf{F}_f(\mathbf{D}^-)] = \begin{bmatrix} \frac{L}{3EI(1-d_1^-)} & -\frac{L}{6EI} & 0 \\ -\frac{L}{6EI} & \frac{L}{3EI} & 0 \\ 0 & 0 & \frac{L}{AE} \end{bmatrix} = \begin{bmatrix} \frac{0.2827 \times 10^{-9}}{(1-d_1^-)} & -0.1414 \times 10^{-9} & 0 \\ -0.1414 \times 10^{-9} & 0.2827 \times 10^{-9} & 0 \\ 0 & 0 & 0.2813 \times 10^{-6} \end{bmatrix} \quad (12.8.13)$$

### Unilateral Damage in Reinforced Concrete Frames

$$\begin{bmatrix} \phi_{11_t} - \phi_{11_t}^p \\ \phi_{12_t} \\ \delta_{1_t} \end{bmatrix} = \begin{bmatrix} \frac{L}{3EI(1-d_{1_t}^+)} & -\frac{L}{6EI} & 0 \\ -\frac{L}{6EI} & \frac{L}{3EI} & 0 \\ 0 & 0 & \frac{L}{AE} \end{bmatrix} \begin{bmatrix} \frac{1}{2}m_{11_t} + \frac{1}{2}|m_{11_t}| \\ \frac{1}{2}m_{12_t} + \frac{1}{2}|m_{12_t}| \\ \frac{1}{2}n_{1_t} + \frac{1}{2}|n_{1_t}| \end{bmatrix} + \begin{bmatrix} \frac{L}{3EI(1-d_{1_t}^-)} & -\frac{L}{6EI} & 0 \\ -\frac{L}{6EI} & \frac{L}{3EI} & 0 \\ 0 & 0 & \frac{L}{AE} \end{bmatrix} \begin{bmatrix} \frac{1}{2}m_{11_t} - \frac{1}{2}|m_{11_t}| \\ \frac{1}{2}m_{12_t} - \frac{1}{2}|m_{12_t}| \\ \frac{1}{2}n_{1_t} - \frac{1}{2}|n_{1_t}| \end{bmatrix} \quad (12.8.14)$$

then

$$\begin{bmatrix} \phi_{11_t} - \phi_{11_t}^p \\ \phi_{12_t} \\ \delta_{1_t} \end{bmatrix} \cong \begin{bmatrix} \frac{0.2827x10^{-9} \left( \frac{1}{2}m_{11_t} + \frac{1}{2}|m_{11_t}| \right) - 0.1414x10^{-9}m_{12_t} + \frac{0.2827x10^{-9} \left( \frac{1}{2}m_{11_t} - \frac{1}{2}|m_{11_t}| \right)}{1-d_{1_t}^-}}{1-d_{1_t}^+} \\ -0.1414x10^{-9}m_{11_t} + 0.2827x10^{-9}m_{12_t} \\ 0.2813x10^{-6}n_{1_t} \end{bmatrix} \quad (12.8.15)$$

The problem is solved using a step-by-step procedure. Then, the solution is divided into 8 stages according to the type of structural behavior.

**Stage 1:** Interval:  $0 \leq t \leq 1$ , elastic behavior  $\Rightarrow \phi_{11_t}^p = 0, d_{1_t}^+ = d_{1_t}^- = 0$

This phase is completed in only one step and finishes when the cracking moment  $M_{cr1}^+$  is reached. Solving Equations (12.8.9), (12.8.11) and (12.8.15):

$$\begin{aligned} \{\mathbf{U}\} = \begin{bmatrix} 0 \\ 0 \\ 0 \\ w_{2_t} \\ w_{2_t} \\ \theta_{2_t} \end{bmatrix} &= \begin{bmatrix} 0 \\ 0 \\ 0 \\ 0 \\ w_{2_t} \\ -0.0025w_{2_t} \end{bmatrix}; \{\mathbf{P}\} = \begin{bmatrix} R_{w_{1_t}} \\ R_{w_{1_t}} \\ R_{\theta_{1_t}} \\ 0 \\ R_{w_{2_t}} \\ 0 \end{bmatrix} = \begin{bmatrix} 0 \\ -9824.8611w_{2_t} \\ 0.5894x10^7w_{2_t} \\ 0 \\ 9824.8611w_{2_t} \\ 0 \end{bmatrix}; \\ \{\Phi\}_1 = \begin{bmatrix} \phi_{11_t} \\ \phi_{12_t} \\ \delta_{1_t} \end{bmatrix} &\cong \begin{bmatrix} 0.00167w_{2_t} \\ -8.333x10^{-4}w_{2_t} \\ 0 \end{bmatrix}; \{\mathbf{M}\}_1 = \begin{bmatrix} m_{11_t} \\ m_{12_t} \\ n_{1_t} \end{bmatrix} = \begin{bmatrix} 0.5895x10^7w_{2_t} \\ 0 \\ 0 \end{bmatrix} \end{aligned} \quad (12.8.16)$$

At the end of this interval at  $t = 1$ ,  $m_{11_t} = M_{cr1}^+ = 4.62 \times 10^6$  N.cm and the displacement at the end 2 is:

$$w_{2_1} = 0.7844 \text{ cm} \quad (12.8.17)$$

The resulting force vs. displacement curve is presented in Figure 53a.

**Stage 2:** Interval:  $1 < t \leq 9$ , inelastic behavior  $\Rightarrow \phi_{11_t}^p = 0$ ,  $d_{1_t}^+ > 0$ ,  $d_{1_t}^- = 0$

As the behavior is nonlinear, this phase is carried out in several steps and finishes when the first plastic moment  $M_{p1}^+$  is reached. Solving Equations (12.8.9), (12.8.11) and (12.8.15) (See Table 5).

Notice that at the final of this interval at  $t = 9$ ,  $m_{11_t} = M_{p1}^+ = 1.11 \times 10^7$  N.cm and the displacement at the end 2 is:

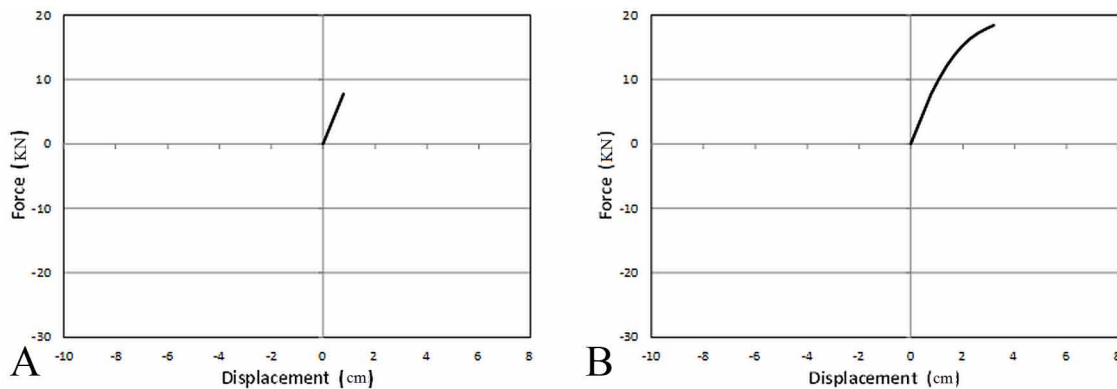
$$w_{2_1} = 3.18 \text{ cm} \quad (12.8.18)$$

The force vs. displacement curve is presented in Figure 53b.

**Stage 3:** Interval:  $9 < t \leq 20$ , inelastic behavior  $\Rightarrow \phi_{11_t}^p > 0$ ,  $d_{1_t}^+ > 0$ ,  $d_{1_t}^- = 0$

The structure behavior is still nonlinear, so this phase is carried out in several steps and finishes before the moment  $M_{u1}^+$  is reached. Solving Equations (12.8.9), (12.8.11) and (12.8.15) at each step gives (See Table 6).

Figure 53. Force vs. Displacement a) Stage 1:  $0 \leq t \leq 1$  b) Stage 2:  $1 < t \leq 9$



### Unilateral Damage in Reinforced Concrete Frames

Table 5. First plastic movement is reached

$t$	$w_{2_t}$	$\theta_{2_t}$	$R_{w1_t}$	$R_{\theta1_t}$	$R_{w2_t}$	$\phi_{11_t}$	$\phi_{12_t}$	$m_{11_t}$	$d_{1_t}^+$
	cm	Rad	N	N.cm	N			N.cm	
2	1.08	-2.67x10 <sup>-3</sup>	-1.01x10 <sup>4</sup>	6.08x10 <sup>6</sup>	10126.80	1.81x10 <sup>-3</sup>	-8.59x10 <sup>-4</sup>	6.08x10 <sup>6</sup>	4.95x10 <sup>-2</sup>
3	1.38	-3.34 x10 <sup>-3</sup>	-1.22x10 <sup>4</sup>	7.30x10 <sup>6</sup>	12173.00	2.31x10 <sup>-3</sup>	-1.03x10 <sup>-3</sup>	7.30x10 <sup>6</sup>	1.05x10 <sup>-1</sup>
4	1.68	-3.98x10 <sup>-3</sup>	-1.39x10 <sup>4</sup>	8.32x10 <sup>6</sup>	13860.00	2.81x10 <sup>-3</sup>	-1.18x10 <sup>-3</sup>	8.32x10 <sup>6</sup>	1.62x10 <sup>-1</sup>
5	1.98	-4.60x10 <sup>-3</sup>	-1.52x10 <sup>4</sup>	9.13x10 <sup>6</sup>	15225.70	3.31x10 <sup>-3</sup>	-1.29x10 <sup>-3</sup>	9.13x10 <sup>6</sup>	2.19x10 <sup>-1</sup>
6	2.28	-5.19x10 <sup>-3</sup>	-1.63x10 <sup>4</sup>	9.79x10 <sup>6</sup>	16315.90	3.81x10 <sup>-3</sup>	-1.38x10 <sup>-3</sup>	9.79x10 <sup>6</sup>	2.73x10 <sup>-1</sup>
7	2.58	-5.76x10 <sup>-3</sup>	-1.72x10 <sup>4</sup>	1.03x10 <sup>7</sup>	17176.20	4.31x10 <sup>-3</sup>	-1.46x10 <sup>-3</sup>	1.03x10 <sup>7</sup>	3.24x10 <sup>-1</sup>
8	2.88	-6.32x10 <sup>-3</sup>	-1.78x10 <sup>4</sup>	1.07x10 <sup>7</sup>	17847.30	4.81x10 <sup>-3</sup>	-1.51x10 <sup>-3</sup>	1.07x10 <sup>7</sup>	3.70x10 <sup>-1</sup>
9	3.18	-6.86x10 <sup>-3</sup>	-1.84x10 <sup>4</sup>	1.10x10 <sup>7</sup>	18364.10	5.31x10 <sup>-3</sup>	-1.56x10 <sup>-3</sup>	1.11x10 <sup>7</sup>	4.13x10 <sup>-1</sup>

Table 6.

$T$	$w_{2_t}$	$\theta_{2_t}$	$R_{w1_t}$	$R_{\theta1_t}$	$R_{w2_t}$	$\phi_{11_t}$	$\phi_{12_t}$	$m_{11_t}$	$d_{1_t}^+$	$\phi_{11_t}^p$
	cm	Rad	N	N.cm	N			N.cm		
10	3.58	-7.55x10 <sup>-3</sup>	-18579.20	1.11x10 <sup>7</sup>	18579.20	5.97x10 <sup>-3</sup>	-1.58x10 <sup>-3</sup>	1.11x10 <sup>7</sup>	0.43	4.10x10 <sup>-4</sup>
11	3.98	-8.22x10 <sup>-3</sup>	-18649.30	1.12x10 <sup>7</sup>	18649.30	6.64x10 <sup>-3</sup>	-1.58x10 <sup>-3</sup>	1.12x10 <sup>7</sup>	0.44	9.84x10 <sup>-4</sup>
12	4.38	-8.89x10 <sup>-3</sup>	-18715.80	1.12x10 <sup>7</sup>	18715.80	7.31x10 <sup>-3</sup>	-1.59x10 <sup>-3</sup>	1.12x10 <sup>7</sup>	0.45	1.56x10 <sup>-3</sup>
13	4.78	-9.57x10 <sup>-3</sup>	-18778.70	1.13x10 <sup>7</sup>	18778.70	7.97x10 <sup>-3</sup>	-1.59x10 <sup>-3</sup>	1.13x10 <sup>7</sup>	0.45	2.13x10 <sup>-3</sup>
14	5.18	-1.02x10 <sup>-2</sup>	-18838.10	1.13x10 <sup>7</sup>	18838.10	8.64x10 <sup>-3</sup>	-1.60x10 <sup>-3</sup>	1.13x10 <sup>7</sup>	0.46	2.71x10 <sup>-3</sup>
15	5.58	-1.09x10 <sup>-2</sup>	-18894.20	1.13x10 <sup>7</sup>	18894.20	9.31x10 <sup>-3</sup>	-1.60x10 <sup>-3</sup>	1.13x10 <sup>7</sup>	0.47	3.28x10 <sup>-3</sup>
16	5.98	-1.16x10 <sup>-2</sup>	-18947.20	1.14x10 <sup>7</sup>	18947.20	9.97x10 <sup>-3</sup>	-1.61x10 <sup>-3</sup>	1.14x10 <sup>7</sup>	0.47	3.85x10 <sup>-3</sup>
17	6.38	-1.23x10 <sup>-2</sup>	-18997.00	1.14x10 <sup>7</sup>	18997.00	1.06x10 <sup>-2</sup>	-1.61x10 <sup>-3</sup>	1.14x10 <sup>7</sup>	0.48	4.43x10 <sup>-3</sup>
18	6.78	-1.29x10 <sup>-2</sup>	-19044.00	1.14x10 <sup>7</sup>	19044.00	1.13x10 <sup>-2</sup>	-1.62x10 <sup>-3</sup>	1.14x10 <sup>7</sup>	0.49	5.00x10 <sup>-3</sup>
19	7.18	-1.36x10 <sup>-2</sup>	-19088.00	1.15x10 <sup>7</sup>	19088.00	1.20x10 <sup>-2</sup>	-1.62x10 <sup>-3</sup>	1.15x10 <sup>7</sup>	0.49	5.57x10 <sup>-3</sup>
20	7.58	-1.43x10 <sup>-2</sup>	-19129.40	1.15x10 <sup>7</sup>	19129.40	1.26x10 <sup>-2</sup>	-1.62x10 <sup>-3</sup>	1.15x10 <sup>7</sup>	0.50	6.15x10 <sup>-3</sup>

Notice that at the final of this interval at  $t = 20$ ,  $m_{11_t} = 1.15x10^7$  N cm and the displacement at the end 2 is:

$$w_{2_t} = 7.58 \text{ cm} \quad (12.8.19)$$

The force vs. displacement curve is presented in Figure 54.

**Stage 4:** Interval:  $20 < t \leq 21$ , corresponds to an unloading and the behavior is elastic, then

$$\phi_{11_{21}}^p = \phi_{11_{20}}^p = 1.26 \times 10^{-2}, \quad d_{1_{21}}^+ = d_{11_{20}}^+ = 0.5, \quad d_{1_{21}}^- = d_{1_{20}}^- = 0$$

This phase is completed in only one step and finishes when the force at end 1 is nil, i.e.,  $R_{w_{21}} = 0$ .

Solving Equations (12.8.9), (12.8.11) and (12.8.15) (See Table 7).

The force vs. displacement curve is presented in Figure 54.

**Stage 5:** Interval:  $21 < t \leq 22$ , elastic behavior  $\Rightarrow \phi_{11_{22}}^p = \phi_{11_{21}}^p = 6.15 \times 10^{-3}$ ,  $d_{1_{21}}^+ = d_{11_{20}}^+ = 0.5$ ,

$$d_{1_{21}}^- = d_{1_{20}}^- = 0$$

Solving Equations (12.8.9), (12.8.11) and (12.8.15):

Figure 54. Force vs. Displacement a) Stage 3:  $9 < t \leq 20$  b) Stage 4:  $20 < t \leq 21$

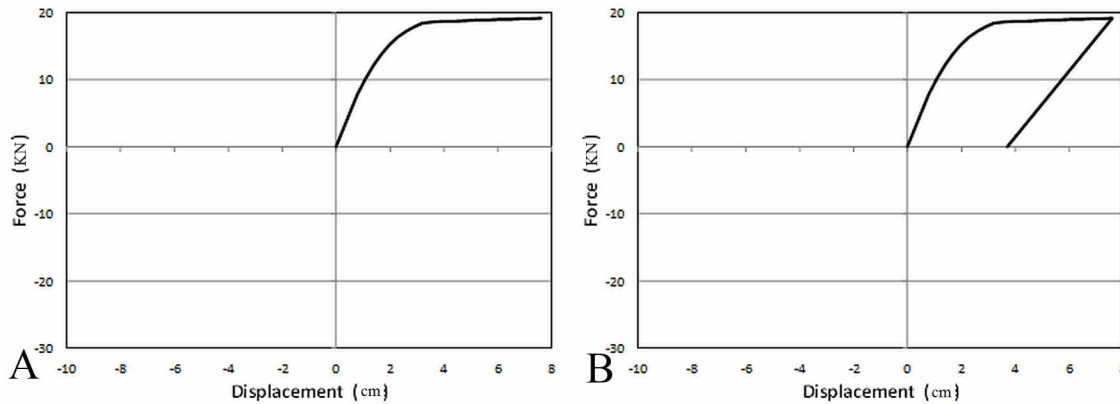


Table 7.

$t$	$w_{2_t}$	$\theta_{2_t}$	$R_{w_{1_t}}$	$R_{\theta_{1_t}}$	$R_{w_{2_t}}$	$\phi_{11_t}$	$\phi_{12_t}$	$m_{11_t}$	$d_{1_t}^+$	$\phi_{11_t}^p$
	cm	Rad	N	N.cm	N			N.cm		
21	3.69	$-6.15 \times 10^{-3}$	0.00	0.00	0.00	$6.15 \times 10^{-3}$	0.00	0.00	0.50	$6.15 \times 10^{-3}$

### Unilateral Damage in Reinforced Concrete Frames

$$\{\mathbf{U}\} = \begin{bmatrix} 0 \\ 0 \\ 0 \\ w_{2_t} \\ \theta_{2_t} \end{bmatrix} = \begin{bmatrix} 0 \\ 0 \\ 0 \\ 0 \\ w_{2_t} \\ -0.0025w_{2_t} + 3.07 \times 10^{-3} \end{bmatrix}; \{\mathbf{P}\} = \begin{bmatrix} R_{w_{1_t}} \\ R_{w_{1_t}} \\ R_{\theta_{1_t}} \\ 0 \\ R_{w_{2_t}} \\ 0 \end{bmatrix} = \begin{bmatrix} 0 \\ -9824.8611w_{2_t} + 36249.1488 \\ 0.5894 \times 10^7 w_{2_t} - 0.2174 \times 10^8 \\ 0 \\ 9824.8611w_{2_t} - 36249.1488 \\ 0 \end{bmatrix};$$

$$\{\Phi\}_1 = \begin{bmatrix} \phi_{11} \\ \phi_{12} \\ \delta_{1_1} \end{bmatrix} = \begin{bmatrix} 1.67 \times 10^{-3} w_{2_t} \\ -8.333 \times 10^{-4} w_{2_t} + 3.07 \times 10^{-3} \\ 0 \end{bmatrix}; \{\mathbf{M}\}_1 = \begin{bmatrix} m_{11} \\ m_{12} \\ n_{1_1} \end{bmatrix} = \begin{bmatrix} 0.5895 \times 10^7 w_{2_t} - 0.2175 \times 10^8 \\ 0 \\ 0 \end{bmatrix} \quad (12.8.20)$$

This phase is completed in only one step and finishes when the cracking moment  $M_{cr1}^-$  is reached. At the end of this interval, at  $t = 22$ ,  $m_{11} = 0.5895 \times 10^7 w_{2_t} - 0.2175 \times 10^8 = M_{cr1}^- = -4.81 \times 10^6 \text{ N.cm}$  and the resultant displacement at the end 2 is:

$$w_{2_1} = 2.87 \text{ cm} \quad (12.8.21)$$

The resulting force vs. displacement curve is presented in Figure 55a. Solving Equations (12.8.9), (12.8.11) and (12.8.15) (See Table 8). The force vs. displacement curve is presented in Figure 55b.

**Stage 6:** Interval:  $22 < t \leq 32$ , inelastic behavior  $\Rightarrow \phi_{11_{22}}^p = \phi_{11_{21}}^p = 6.15 \times 10^{-3}$ ,  $d_{1_{21}}^+ = d_{1_{20}}^+ = 0.5$ ,  $d_{1_t}^- > 0$

Figure 55. Force vs. Displacement a) Stage 5:  $21 < t \leq 22$  b) Stage 6:  $22 < t \leq 32$

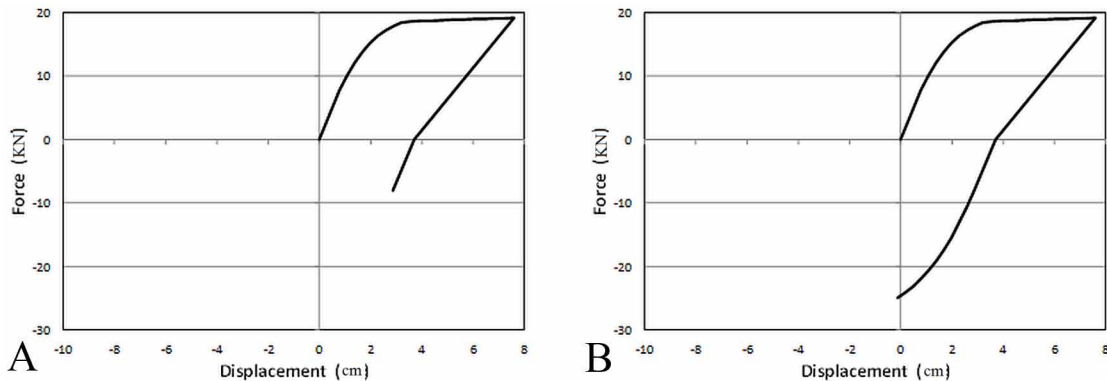




Table 8.

$t$	$w_{2_t}$	$\theta_{2_t}$	$R_{w1_t}$	$R_{\theta1_t}$	$R_{w2_t}$	$\phi_{11_t}$	$\phi_{12_t}$	$m_{11_t}$	$d_{1_t}^+$	$\phi_{11_t}^p$
	cm	Rad	N	N.cm	N			N.cm		
22	2.87	$-4.11 \times 10^{-3}$ $\times 10^{-4}$	8019.05	$-4.81 \times 10^6$	-8019.05	$4.79 \times 10^{-3}$	$6.80 \times 10^{-4}$	$-4.81 \times 10^6$	0.50	$6.15 \times 10^{-3}$

As the behavior is nonlinear, this phase is carried out in several steps and finishes when the first plastic moment  $M_{p1}^-$  is reached. Solving Equations (12.8.9), (12.8.11) and (12.8.15) at each step gives (See Table 9).

Notice that at the final of this interval at  $t = 23$ ,  $m_{11_t} = 1.50 \times 10^7$  N.cm That is very close to  $M_{p1}^-$ . The corresponding displacement at the end 2 is:

$$w_{2_1} = -0.13 \text{ cm} \tag{12.8.22}$$

The force vs. displacement curve is presented in Figure 55b.

**Stage 7:** Interval:  $32 < t \leq 60$ , inelastic behavior  $\Rightarrow \phi_{11_t}^p > 0, d_{1_t}^+ > 0, d_{1_t}^- > 0$

Table 9.

$t$	$w_{2_t}$	$\theta_{2_t}$	$R_{w1_t}$	$R_{\theta1_t}$	$R_{w2_t}$	$\phi_{11_t}$	$\phi_{12_t}$	$m_{11_t}$	$d_{1_t}^+$	$\phi_{11_t}^p$	$d_{1_t}^-$
	cm	Rad	N	N.cm	N			N.cm			
23	2.57	$-3.38 \times 10^{-3}$	10695.90	$-6.42 \times 10^6$	-10695.90	$4.29 \times 10^{-3}$	$9.07 \times 10^{-4}$	$-6.42 \times 10^6$	0.50	$6.15 \times 10^{-3}$	0.02
24	2.27	$-2.67 \times 10^{-3}$	13156.60	$-7.89 \times 10^6$	-13156.60	$3.79 \times 10^{-3}$	$1.12 \times 10^{-3}$	$-7.89 \times 10^6$	0.50	$6.15 \times 10^{-3}$	0.05
25	1.97	$-1.98 \times 10^{-3}$	15381.30	$-9.23 \times 10^6$	-15381.30	$3.29 \times 10^{-3}$	$1.30 \times 10^{-3}$	$-9.23 \times 10^6$	0.50	$6.15 \times 10^{-3}$	0.09
26	1.67	$-1.32 \times 10^{-3}$	17365.10	$-1.04 \times 10^7$	-17365.10	$2.79 \times 10^{-3}$	$1.47 \times 10^{-3}$	$-1.04 \times 10^7$	0.50	$6.15 \times 10^{-3}$	0.12
27	1.37	$-6.68 \times 10^{-4}$	19114.40	$-1.15 \times 10^7$	-19114.40	$2.29 \times 10^{-3}$	$1.62 \times 10^{-3}$	$-1.15 \times 10^7$	0.50	$6.15 \times 10^{-3}$	0.16
28	1.07	$-3.80 \times 10^{-5}$	20643.00	$-1.24 \times 10^7$	-20643.00	$1.79 \times 10^{-3}$	$1.75 \times 10^{-3}$	$-1.24 \times 10^7$	0.50	$6.15 \times 10^{-3}$	0.20
29	0.77	$5.74 \times 10^{-4}$	21968.80	$-1.32 \times 10^7$	-21968.80	$1.29 \times 10^{-3}$	$1.86 \times 10^{-3}$	$-1.32 \times 10^7$	0.50	$6.15 \times 10^{-3}$	0.23
30	0.47	$1.17 \times 10^{-3}$	23111.40	$-1.39 \times 10^7$	-23111.40	$7.89 \times 10^{-4}$	$1.96 \times 10^{-3}$	$-1.39 \times 10^7$	0.50	$6.15 \times 10^{-3}$	0.27
31	0.17	$1.75 \times 10^{-3}$	24090.80	$-1.45 \times 10^7$	-24090.80	$2.89 \times 10^{-4}$	$2.04 \times 10^{-3}$	$-1.45 \times 10^7$	0.50	$6.15 \times 10^{-3}$	0.30
32	-0.13	$2.33 \times 10^{-3}$	24925.90	$-1.50 \times 10^7$	-24925.90	$-2.11 \times 10^{-4}$	$2.11 \times 10^{-3}$	$-1.50 \times 10^7$	0.50	$6.15 \times 10^{-3}$	0.34

### Unilateral Damage in Reinforced Concrete Frames

Table 10.

$t$	$w_{2_t}$	$\theta_{2_t}$	$R_{w_{1_t}}$	$R_{\theta_{1_t}}$	$R_{w_{2_t}}$	$\phi_{11_t}$	$\phi_{12_t}$	$m_{11_t}$	$d_{1_t}^+$	$\phi_{11_t}^p$	$d_{1_t}^-$
	cm	Rad	N	N.cm	N			N.cm			
33	-0.43	$2.88 \times 10^{-3}$	25619.80	$-1.54 \times 10^7$	-25619.80	$-7.11 \times 10^{-4}$	$2.17 \times 10^{-3}$	$-1.54 \times 10^7$	0.50	$6.14 \times 10^{-3}$	0.37
34	-0.73	$3.40 \times 10^{-3}$	25763.20	$-1.55 \times 10^7$	-25763.20	$-1.21 \times 10^{-3}$	$2.19 \times 10^{-3}$	$-1.55 \times 10^7$	0.50	$5.75 \times 10^{-3}$	0.37
35	-1.03	$3.91 \times 10^{-3}$	25901.10	$-1.55 \times 10^7$	-25901.10	$-1.71 \times 10^{-3}$	$2.20 \times 10^{-3}$	$-1.55 \times 10^7$	0.50	$5.36 \times 10^{-3}$	0.38
36	-1.33	$4.42 \times 10^{-3}$	26033.80	$-1.56 \times 10^7$	-26033.80	$-2.21 \times 10^{-3}$	$2.21 \times 10^{-3}$	$-1.56 \times 10^7$	0.50	$4.97 \times 10^{-3}$	0.39
37	-1.63	$4.93 \times 10^{-3}$	26161.40	$-1.57 \times 10^7$	-26161.40	$-2.71 \times 10^{-3}$	$2.22 \times 10^{-3}$	$-1.57 \times 10^7$	0.50	$4.59 \times 10^{-3}$	0.39
38	-1.93	$5.44 \times 10^{-3}$	26284.00	$-1.58 \times 10^7$	-26284.00	$-3.21 \times 10^{-3}$	$2.23 \times 10^{-3}$	$-1.58 \times 10^7$	0.50	$4.20 \times 10^{-3}$	0.40
39	-2.23	$5.95 \times 10^{-3}$	26401.90	$-1.58 \times 10^7$	-26401.90	$-3.71 \times 10^{-3}$	$2.24 \times 10^{-3}$	$-1.58 \times 10^7$	0.50	$3.81 \times 10^{-3}$	0.40
40	-2.53	$6.46 \times 10^{-3}$	26515.20	$-1.59 \times 10^7$	-26515.20	$-4.21 \times 10^{-3}$	$2.25 \times 10^{-3}$	$-1.59 \times 10^7$	0.50	$3.42 \times 10^{-3}$	0.41
41	-2.83	$6.97 \times 10^{-3}$	26623.90	$-1.60 \times 10^7$	-26623.90	$-4.71 \times 10^{-3}$	$2.26 \times 10^{-3}$	$-1.60 \times 10^7$	0.50	$3.03 \times 10^{-3}$	0.42
42	-3.13	$7.48 \times 10^{-3}$	26728.30	$-1.60 \times 10^7$	-26728.30	$-5.21 \times 10^{-3}$	$2.27 \times 10^{-3}$	$-1.60 \times 10^7$	0.50	$2.65 \times 10^{-3}$	0.42
43	-3.43	$7.99 \times 10^{-3}$	26828.50	$-1.61 \times 10^7$	-26828.50	$-5.71 \times 10^{-3}$	$2.28 \times 10^{-3}$	$-1.61 \times 10^7$	0.50	$2.26 \times 10^{-3}$	0.43
44	-3.73	$8.49 \times 10^{-3}$	26924.60	$-1.62 \times 10^7$	-26924.60	$-6.21 \times 10^{-3}$	$2.28 \times 10^{-3}$	$-1.62 \times 10^7$	0.50	$1.87 \times 10^{-3}$	0.43
45	-4.03	$9.00 \times 10^{-3}$	27016.70	$-1.62 \times 10^7$	-27016.70	$-6.71 \times 10^{-3}$	$2.29 \times 10^{-3}$	$-1.62 \times 10^7$	0.50	$1.48 \times 10^{-3}$	0.44
46	-4.33	$9.51 \times 10^{-3}$	27105.00	$-1.63 \times 10^7$	-27105.00	$-7.21 \times 10^{-3}$	$2.30 \times 10^{-3}$	$-1.63 \times 10^7$	0.50	$1.09 \times 10^{-3}$	0.45
47	-4.63	$1.00 \times 10^{-2}$	27189.50	$-1.63 \times 10^7$	-27189.50	$-7.71 \times 10^{-3}$	$2.31 \times 10^{-3}$	$-1.63 \times 10^7$	0.50	$7.05 \times 10^{-4}$	0.45
48	-4.93	$1.05 \times 10^{-2}$	27270.40	$-1.64 \times 10^7$	-27270.40	$-8.21 \times 10^{-3}$	$2.31 \times 10^{-3}$	$-1.64 \times 10^7$	0.50	$3.17 \times 10^{-4}$	0.46
49	-5.23	$1.10 \times 10^{-2}$	27347.80	$-1.64 \times 10^7$	-27347.80	$-8.71 \times 10^{-3}$	$2.32 \times 10^{-3}$	$-1.64 \times 10^7$	0.50	$-7.15 \times 10^{-5}$	0.46
50	-5.53	$1.15 \times 10^{-2}$	27421.80	$-1.65 \times 10^7$	-27421.80	$-9.21 \times 10^{-3}$	$2.33 \times 10^{-3}$	$-1.65 \times 10^7$	0.50	$-4.60 \times 10^{-4}$	0.47
51	-5.83	$1.20 \times 10^{-2}$	27492.50	$-1.65 \times 10^7$	-27492.50	$-9.71 \times 10^{-3}$	$2.33 \times 10^{-3}$	$-1.65 \times 10^7$	0.50	$-8.48 \times 10^{-4}$	0.47
52	-6.13	$1.25 \times 10^{-2}$	27560.10	$-1.65 \times 10^7$	-27560.10	$-1.02 \times 10^{-2}$	$2.34 \times 10^{-3}$	$-1.65 \times 10^7$	0.50	$-1.24 \times 10^{-3}$	0.48
53	-6.43	$1.31 \times 10^{-2}$	27624.50	$-1.66 \times 10^7$	-27624.50	$-1.07 \times 10^{-2}$	$2.34 \times 10^{-3}$	$-1.66 \times 10^7$	0.50	$-1.62 \times 10^{-3}$	0.48
54	-6.73	$1.36 \times 10^{-2}$	27685.90	$-1.66 \times 10^7$	-27685.90	$-1.12 \times 10^{-2}$	$2.35 \times 10^{-3}$	$-1.66 \times 10^7$	0.50	$-2.01 \times 10^{-3}$	0.49
55	-7.03	$1.41 \times 10^{-2}$	27744.40	$-1.66 \times 10^7$	-27744.40	$-1.17 \times 10^{-2}$	$2.35 \times 10^{-3}$	$-1.66 \times 10^7$	0.50	$-2.40 \times 10^{-3}$	0.49
56	-7.33	$1.46 \times 10^{-2}$	27800.10	$-1.67 \times 10^7$	-27800.10	$-1.22 \times 10^{-2}$	$2.36 \times 10^{-3}$	$-1.67 \times 10^7$	0.50	$-2.79 \times 10^{-3}$	0.50
57	-7.63	$1.51 \times 10^{-2}$	27853.00	$-1.67 \times 10^7$	-27853.00	$-1.27 \times 10^{-2}$	$2.36 \times 10^{-3}$	$-1.67 \times 10^7$	0.50	$-3.18 \times 10^{-3}$	0.50
58	-7.93	$1.56 \times 10^{-2}$	27903.30	$-1.67 \times 10^7$	-27903.30	$-1.32 \times 10^{-2}$	$2.37 \times 10^{-3}$	$-1.67 \times 10^7$	0.50	$-3.56 \times 10^{-3}$	0.51
59	-8.23	$1.61 \times 10^{-2}$	27951.00	$-1.68 \times 10^7$	-27951.00	$-1.37 \times 10^{-2}$	$2.37 \times 10^{-3}$	$-1.68 \times 10^7$	0.50	$-3.95 \times 10^{-3}$	0.51
60	-8.53	$1.66 \times 10^{-2}$	27996.30	$-1.68 \times 10^7$	-27996.30	$-1.42 \times 10^{-2}$	$2.37 \times 10^{-3}$	$-1.68 \times 10^7$	0.50	$-4.34 \times 10^{-3}$	0.52

The structure behavior is nonlinear and so this phase is carried out in several steps and finishes at an instant close to the moment  $M_{u1}^-$  is reached. Solving Equations (12.8.9), (12.8.11) and (12.8.15) at each step gives (See Table 10).

Notice that at the final of this interval at  $t = 60$ ,  $m_{11_1} = -1.68 \times 10^7$  N cm and the displacement at the end 2 is:

$$w_{2_1} = -8.53 \text{ cm} \tag{12.8.23}$$

The force vs. displacement curve is presented in Figure 56a.

**Stage 8:** Interval:  $60 < t \leq 61$ , corresponds to an unloading and the behavior is elastic, then

$$\phi_{11_{21}}^p = \phi_{11_{20}}^p = -4.34 \times 10^{-3}, d_{1_{21}}^+ = d_{1_{20}}^+ = 0.5, d_{1_{21}}^- = d_{1_{20}}^- = 0.52$$

This phase is completed in only one step and finishes when the force at end 1 is nil, i.e.,  $R_{w_{2_1}} = 0$ .

Solving Equations (12.8.9), (12.8.11) and (12.8.15) (See Table 11):

The force vs. displacement curve at the final of the displacement history is presented in Figure 56b.

Figure 56. Force vs. Displacement a) Stage 7:  $32 < t \leq 60$  b) Stage 8:  $60 < t \leq 61$

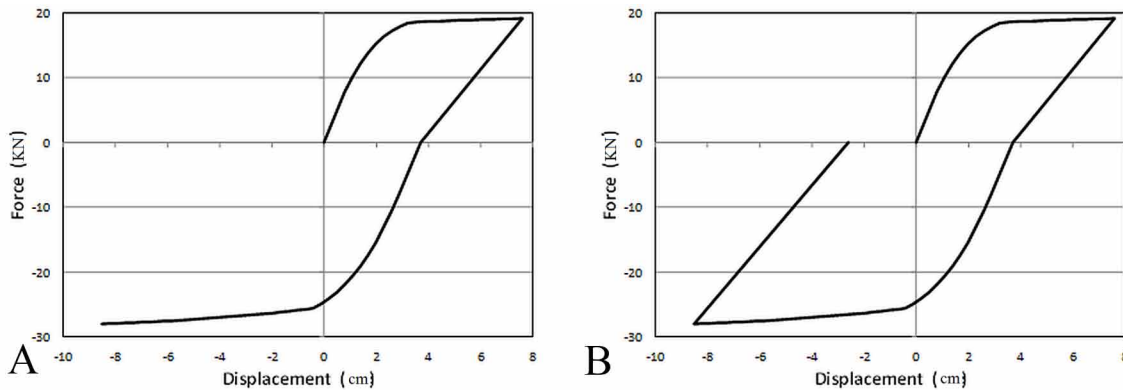


Table 11.

$t$	$w_{2_t}$	$\theta_{2_t}$	$R_{w_{1_t}}$	$R_{\theta_{1_t}}$	$R_{w_{2_t}}$	$\phi_{11_t}$	$\phi_{12_t}$	$m_{11_t}$	$d_{1_t}^+$	$\phi_{11_t}^p$	$d_{1_t}^-$
	cm	Rad	N	N.cm	N			N.cm			
61	-2.60	$4.34 \times 10^{-3}$	0	0	0	$-4.34 \times 10^{-3}$	0	0	0.50	$-4.34 \times 10^{-3}$	0.52

## 12.9 PROJECTS

**12.9.1 Generalize the Damage Model Developed in Project 10.12.1 including Unilateral Effects.**

**12.9.2 Generalize the Damage Model Developed in Project 10.12.2 including Unilateral Effects.**

**12.9.3 Generalize the Damage Model Developed in Project 11.7.1 including Unilateral Effects.**

**12.9.4 Generalize the Damage Model of Project 10.12.3 including Unilateral Flexural and Torsional Effects.**

## REFERENCES

ACI Committee, American Concrete Institute, & International Organization for Standardization. (2005). Building code requirements for structural concrete (ACI 318-05) and commentary. American Concrete Institute.

Alarcón, E., Recuero, A., Perera, R., López, C., Gutiérrez, J. P., & De Diego, A. et al. (2001). A repairability index for reinforced concrete members based on fracture mechanics. *Engineering Structures*, 23(6), 687–697.

Alva, G. M. S., & El Debs, A. L. H. C. (2010). Application of lumped dissipation model in nonlinear analysis of reinforced concrete structures. *Engineering Structures*, 32(4), 974–981. doi:10.1016/j.eng-struct.2009.12.024

Araujo, F., & Proença, S. P. B. (2008). Application of a lumped dissipation model to reinforced concrete structures with the consideration of residual strains and cycles of hysteresis. *Journal of Mechanics of Materials and Structures*, 3(5), 1011–1031. doi:10.2140/jomms.2008.3.1011

Avon, D., Marante, M. E., Picón, R., & Flórez-López, J. (2009). Modelo de daño para elementos de hormigón reforzado sometidos a torsión. In *Proceedings of the Numerical Methods in Engineering Congress* (pp. 1-11). Barcelona, Spain: SEMNI.

Avon, D., Marante, M. E., Picón, R., & Flórez-López, J. (2009). Modelo de daño para elementos de concreto armado sometidos a solicitaciones monotónicas de torsión. In *Proceedings of IX Venezuelan Congress on Seismology and Seismic Engineering*. Caracas, Venezuela: Academic Press.

Bousias, S. N., Verzeletti, G., Fardis, M. N., & Gutierrez, E. (1995). Load-path effects in column biaxial bending with axial force. *Journal of Engineering Mechanics*, 121(5), 596–605. doi:10.1061/(ASCE)0733-9399(1995)121:5(596)

Flórez-López, J. (1995). A simplified model of unilateral damage for RC frames. *Journal of Structural Engineering*, 121(12), 1765–1772. doi:10.1061/(ASCE)0733-9445(1995)121:12(1765)

Hsu, T. (1984). *Torsion of reinforced concrete members*. New York, NY: Van Nostrand Reinhold.

Marante, M. E., & Flórez-López, J. (2002). A model of damage for RC elements subjected to biaxial bending. *Engineering Structures*, 24(9), 1141–1152. doi:10.1016/S0141-0296(02)00044-5

Marante, M. E., & Flórez-López, J. (2003). Three-dimensional analysis of reinforced concrete frames based on lumped damage mechanics. *International Journal of Solids and Structures*, 40(19), 5109–5123. doi:10.1016/S0020-7683(03)00258-0

Negro, P., Verzeletti, G., Magonette, G. E., & Pinto, A. V. (1994). *Tests on a four-storey full-scale R/C frame designed according to Eurocodes 8 and 2: Preliminary report (EUR 15879EN)*. Ispra, Italy: ELSA Laboratory.

Oliva, M. G. (1980). *Shaking table testing of a reinforced concrete frame with biaxial response: Report No. EERC 80-28*. Berkeley, CA: Earthquake Engineering Research Center, University of California.

Oliva, M. G., & Clough, R. W. (1987). Biaxial seismic response of R/C frames. *Journal of Structural Engineering*, 113(6), 1264–1281. doi:10.1061/(ASCE)0733-9445(1987)113:6(1264)

Perdomo, M. E. (2010). *Fractura y daño en estructuras duales de concreto armado*. (Unpublished Doctoral Dissertation). University of Los Andes, Los Andes, Venezuela.

Perdomo, M. E., Picón, R., Marante, M. E., Hild, F., Roux, S., & Flórez-López, J. (2013). Experimental analysis and mathematical modeling of fracture in RC elements with any aspect ratio. *Engineering Structures*, 46, 407–416. doi:10.1016/j.engstruct.2012.07.005

Picón, R. (2004). *Modelo simplificado para el comportamiento dinámico de pórticos con vigas planar-columna de concreto armado considerando el deslizamiento entre el refuerzo y el concreto en las juntas*. (Unpublished Doctoral Dissertation). University of Los Andes, Los Andes, Venezuela.

Picón, R., Quintero, C., & Flórez-López, J. (2007). Modeling of cyclic bond deterioration in RC beam-column connections. *Structural Engineering & Mechanics*, 26(5), 569–589. doi:10.12989/sem.2007.26.5.569

Teng, T., & Teng, S. (2004). Effective torsional rigidity of reinforced concrete members. *ACI Structural Journal*, 101(2).

Thomson, E. (2004). *Modelo simplificado para la evaluación del daño en muros estructurales bajos de concreto armado sujetos a cargas laterales*. (Unpublished Doctoral Dissertation). University of Los Andes, Los Andes, Venezuela.

Thomson, E., Perdomo, M. E., Picón, R., Marante, M. E., & Flórez-López, J. (2009). Simplified model for damage in squat RC shear wall. *Engineering Structures*, 31(10), 2215–2223. doi:10.1016/j.engstruct.2009.05.020

# Chapter 13

## Industrial Applications

### ABSTRACT

*The application of structural analysis techniques to solve real engineering problems is an entirely independent discipline by itself that cannot be properly presented in a book of structural mechanics. However, it is important to give an overview of how mathematical models can help make engineering decisions. This is the subject of the current chapter. The context of the presentation is that of earthquake safety assessment. Of course, this is not the only industrial application of the fracture and damage mechanics of frames, but it is a very representative one and a good example of it. The chapter is organized as follows. First, the problem is presented and a protocol to solve it is described in Section 13.1. Then, an academic software that can be accessed via Internet is described in Section 13.2. This program is used to solve some examples of real structures in the last section of the chapter.*

### 13.1 ANALYSIS AND DIAGNOSIS OF VULNERABLE STRUCTURES

Any structure, for instance a building, can be evaluated using static or dynamic analyses. Besides, any of these studies may be performed considering linear or nonlinear behavior. The models, based on Damage and Fracture Mechanics, described in the former chapter may be used with any of the currently established nonlinear procedures for seismic structural assessment.

This chapter presents some industrial applications using nonlinear dynamic analysis. For this purpose, a mathematical model of a structure is subjected to an earthquake shaking represented by ground motion time histories corresponding to an earthquake hazard. Commonly seismic hazard is assessed from instrumental, historical and geological records. It varies from place to place because depends on the magnitudes of likely earthquakes, how often they occur and the properties of the soil through which the earthquake waves travel. In this chapter, three hazard levels are stated (see Table 1). They are defined through the probability of exceeding a certain amount of ground shaking in 50 years, how often they occurs (Mean Return Period) and a corresponding peak ground acceleration (PGA) that is defined as the maximum acceleration experienced by a particle during the course of the earthquake motion. PGA is expressed as a percentage of the acceleration of gravity ( $g$ ). The greater an earthquake magnitude, stronger is the ground motion it generates.

DOI: 10.4018/978-1-4666-6379-4.ch013

Table 1. Earthquake Hazard Levels

Earthquake	Probability of Exceedance (50 Years)	Mean Return Period (Years)	Percentage of Peak Ground Acceleration (% PGA)
Frequent	50%	72	0.4
Severe	20%	225	0.8
Rare	10%	474	1.0

Since the calculated response can be highly sensitive to the characteristic of the ground motion, it is recommendable the use of several ground motion records trying to cover all the potential shaking movements in the zone. When several real ground motions are not available, simulated time history data can be used. These records should have an equivalent duration and a spectral content corresponding to the zone where the structure is placed. These simulated time history data can be obtained from the general response spectrum, that is a plot of the peak acceleration, velocity or displacement of a series of oscillators of different natural frequency that are forced to move by the same base vibration. The description of the procedure for the calculation of simulated ground motions is out of the scope of this book but it can be easily found related information in the technical literature, some of them are cited in the references of this chapter. The analyses presented in the next sections were performed using only one simulated time history data.

Once the structures are analyzed, the results are checked using acceptance criteria. These conditions are stated using levels of damage that are indicative of the building condition after the event as it is described in Table 2.

In general, for the seismic vulnerability assessments, the following methodology can be used:

- The first step is the data collection. For this purpose it is necessary to determine the configuration of the structural system, type, detailing, the uniaxial behaviors of the materials, etc. This data can be obtained from the available drawings, specifications and any other documents. It would be very convenient the verification of this information by on-site investigations including non-destructive testing of the building materials. In order to determine the gravity loads and the lateral ones, it is necessary to determine the actual use of the building (residential, commercial, educational, etc.), the type and arrangement of existing structural elements and components. It is also very important to know the foundation configuration, soil characterization and geotechnical information.

Table 2. Performance Level for flexural damage

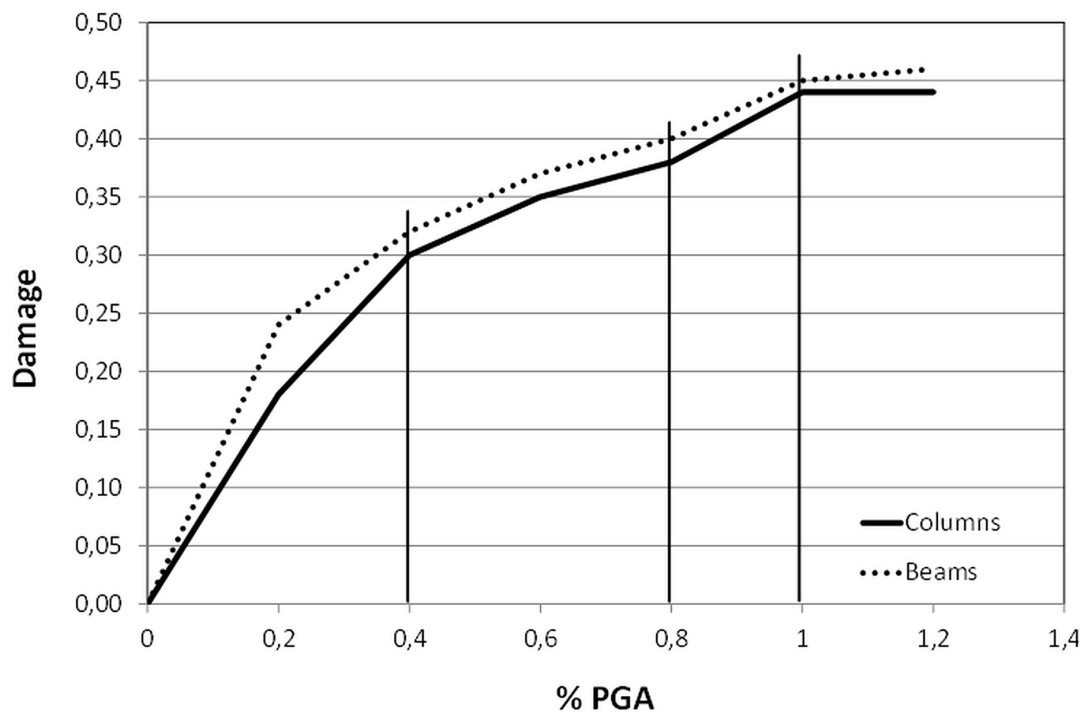
Performance Level	Max Expected Damage in Beams	Max Expected Damage in Columns	Description
1	$0.30 \approx d_p$	0.10	The elements do not require any intervention after the event.
2	0.40	$0.30 \approx d_p$	Some minor repairs may be needed.
3	0.50	0.40	The element requires reparation at reasonably costs.
4	$0.6 \approx d_u$	0.5	The structure requires a major rehabilitation process.
5	$> 0.7$	$> 0.6 \approx d_u$	Inacceptable structural behavior.

### Industrial Applications

- The second step corresponds to the digitalization of the structure and loading, i.e., the construction of the input file to be analyzed with the Finite Element (FE) program. This file contains the geometry of the structure, the properties and parameters for each element according to the model to use, the service loads and lateral ones to apply.
- The third step consists in the construction of the Dynamic Capacity Curve that is obtained by the following procedure:
  - Perform the dynamic analyses of the structure varying the peak ground acceleration (PGA) from zero up to the level corresponding to the no convergence of the analysis that is an indication of structural collapse.
  - For each level of acceleration, the maximum damage in beams and columns are plotted against the corresponding acceleration. An example of a Dynamic Capacity Curve is shown in Figure 1.
- Once the Dynamic Capacity Curve is obtained, the vulnerability of the structure can be assessed via the performance levels.

As it can be appreciated in Table 1, for each hazard level, a percentage of the PGA is specified. For each of these values, corresponding to frequent, severe or rare earthquakes, maximum damages in beams and columns can be determined from the Dynamic Capacity Curve. These values are used to determine the performance level of the structure according to Table 2. If the analyzed building corresponds, for

Figure 1. Dynamic Capacity Curve





example, to a residential use, for a rare earthquake it is expected a performance level of 4 or less; for a severe one, a performance level of 3 can be reasonable and for a frequent earthquake a level of 1 or 2 may be adequate. On the other hand, for an essential structure, considering the same hazards, performance levels of respectively, 3, 2 and 1 should be expected.

For example, consider the Dynamic Capacity Curve presented in Figure 1. For a frequent earthquake corresponding to a maximum acceleration of 0.4 PGA, damages values in respectively, beams and columns, of 0.32 and 0.30 are obtained. According to the Table 2, these results correspond to a performance level of 2. For a severe earthquake (0.8 PGA), the maximum damage in beams is 0.40 and in columns is 0.38. These results corresponds to a performance level of 3 and finally for a rare earthquake (1 PGA), a performance level of 4 is obtained with damage values in beams of 0.45 and 0.44 in columns. These performances are adequate for a residential building but are not satisfactory for a building with essential use.

## **13.2 PORTAL OF DAMAGE**

Portal of damage is a web-based dynamic nonlinear finite element program where the model described in section 12.1 for slender elements has been implemented. The portal can be accessed in the address <http://portalofdamage.ula.ve> using any commercial browser. It allows to:

1. Create an account in a server.
2. Make use of a semi-graphic pre-processor to create an input file with a digitized version of the structure.
3. Run a dynamic finite element program and monitor the state of the process
4. Download or upload input and output files in text format
5. Make use of a graphic post-processor.

The system has a data base, where the user has to register in the first visit. After registration, the user has access to the five links of the system: pre-processor, processor, post-processor, user manual and theory manual (see Figure 2).

Within the pre-processor, the user has different menus for the description of the frame geometry, the boundary conditions, the dimensions of the elements' cross-sections (only rectangular cross-sections are included so far), the amount and location of the longitudinal and transversal reinforcement, the uniaxial behavior of the concrete and the reinforcement and, finally, the loading. The user can impose distributed forces on the elements, and displacements, accelerations and/or forces on the nodes.

However, as indicated in section 6.5, the model needs interaction diagrams of the first cracking moment, first plastic moment, ultimate moment and ultimate plastic rotation. All these diagrams are computed by a Fortran program embedded into the pre-processor called diagram generator. The diagram generator uses as input the uniaxial behavior of the materials, the dimensions of the cross-section and the amount of the reinforcement. This process is carried out by using standard methods of the classic reinforced concrete theory for confined (Kent and Park model) or non-confined elements (Hognestad model). The details of these procedures were presented in sections 6.5 and 10.3. The user instructs the portal to perform the generation of the interaction diagrams in one of the menus of the pre-processor. The results of these computations are shown, graphically, in the portal (see Figure 3). Notice that a table with the coordinates of the diagrams is also created. The user can modify these values. This is useful

Figure 2. Main page of the Portal of Damage



for some special applications. Some errors can be expected in the diagrams calculated with the classical theory of reinforced concrete. In the case of very important structures, it can be convenient the execution of experimental tests on some typical elements of the frame. The experimental results can be inserted directly in the analysis by the modification of the diagram tables. Numerical results for single elements of other programs or procedures can also be used in this same way.

Two different kinds of data files are generated by the pre-processor. The first one has the raw data of the frame including the uniaxial behavior of the materials and details of the cross-section. A second data file is also generated; it has the values of the interaction diagrams of the model parameters instead of the element details. Only the second kind of data files can be processed by the FE program.

The second link of the portal gives access to a page called processor. In this page, the user may select a data file in her/his account and process it with the FE program. The user may also abort the analysis or monitor the process (see Figure 4).

When the process is successfully finished (see Figure 5), the user may download the results file in text format or may proceed to visualize them graphically with the third main link of the portal: the post-processor.

With the post-processor (see Figure 6), the user may plot histories of element variables (damage, generalized stresses or strains, plastic rotations) or node variables (forces, displacements, velocities, accelerations) and graphs of variable vs. variable. Damage distribution over the frame at any instant of the loading can also be plotted.

Figure 3. Diagrams of interaction computed by the pre-processor

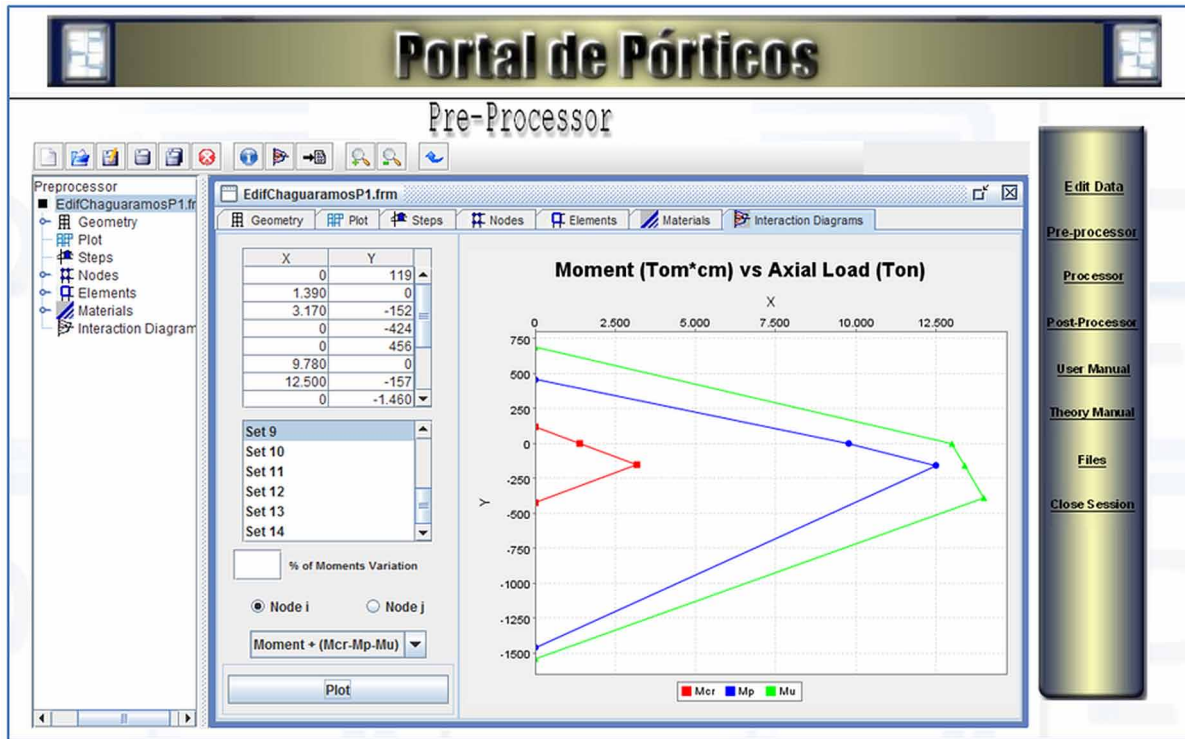


Figure 4. Analysis of a file in the portal

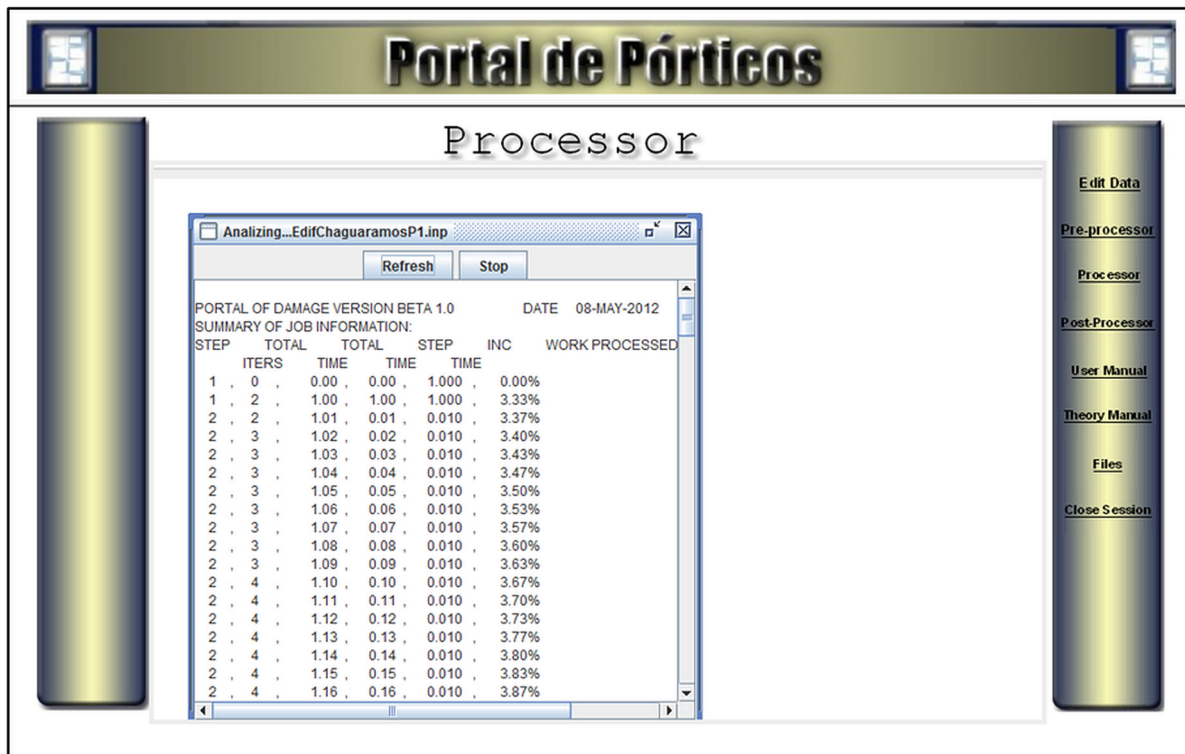
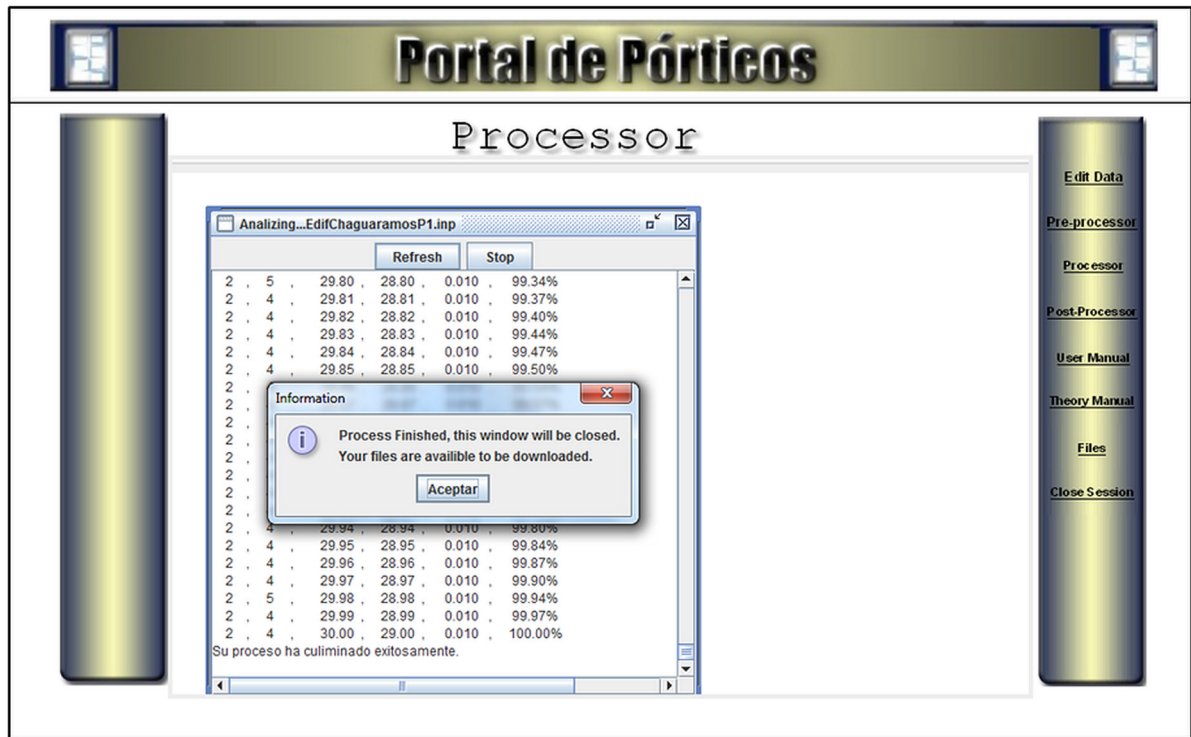


Figure 5. Monitoring of an analysis in the portal



### 13.3 INDUSTRIAL APPLICATIONS

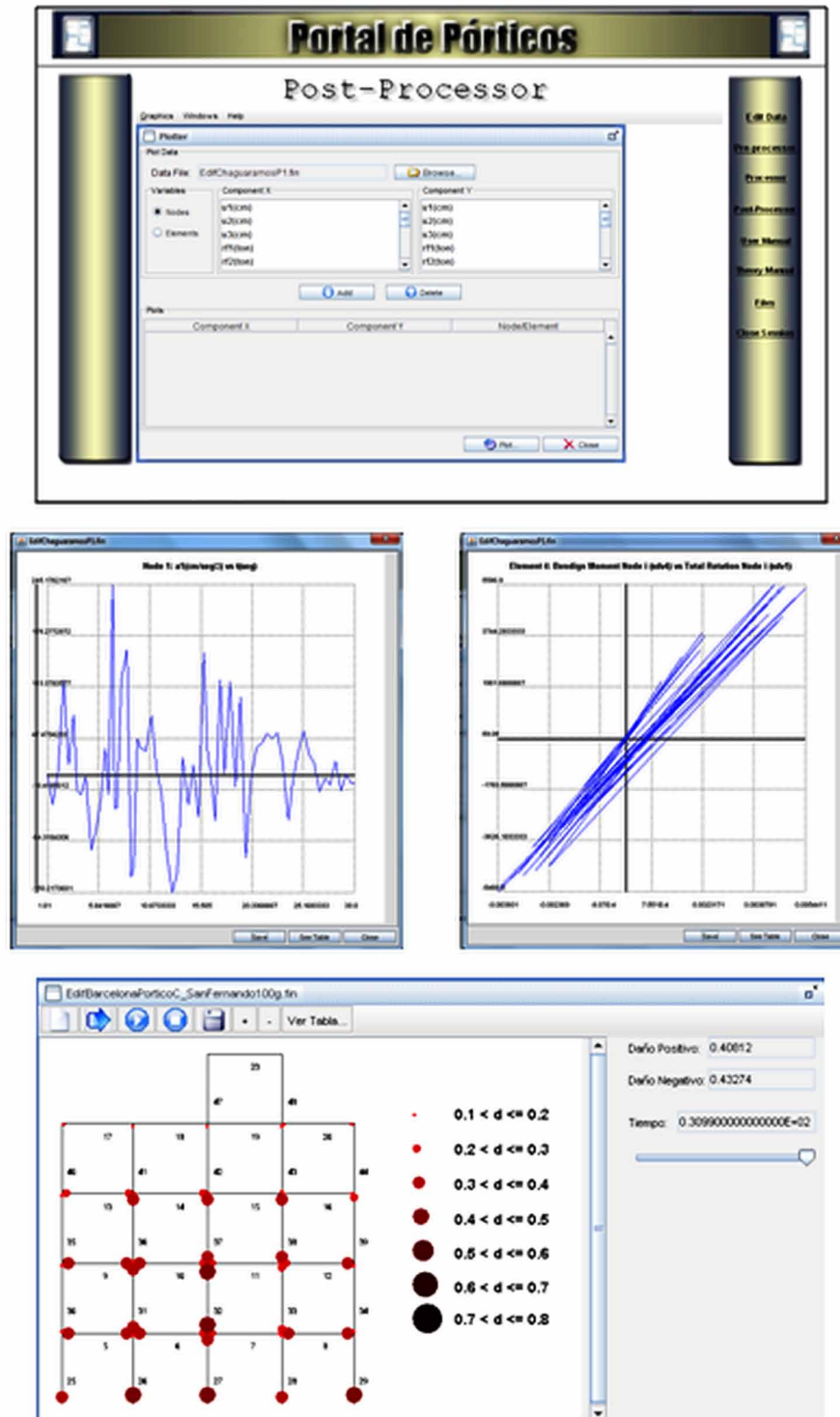
In this section two analyses are presented. The first one corresponds to a residential building and the second one to a structure of a school. For both structures, the dimensions of cross-sections of beams and columns are expressed in cm and the longitudinal reinforcement in cm<sup>2</sup>. The diameters of the transversal reinforcements are reported in mm and the separation in m.

#### 13.3.1 Residential Building

Figures 7 to 31 show the geometry and details of a seven-story residential building. The frames of the building were digitized and analyzed using the Portal of Damage. The loads applied on the frames are indicated in Tables 3 and 4; they were subjected to the artificial earthquake presented in Figure 32a and that was derived from the response spectrum of the Figure 32b.

As it can be appreciated in Figure 30b, the peak acceleration of the ground motion used in the analysis is 0.30g. This acceleration corresponds to a zone with high seismic risk. The damage distributions at the end of the event are presented in Figures 31 to 37.

Figure 6. Graphic post-processor



**Industrial Applications**

Figure 7. Residential building, floor geometry at level 0.00

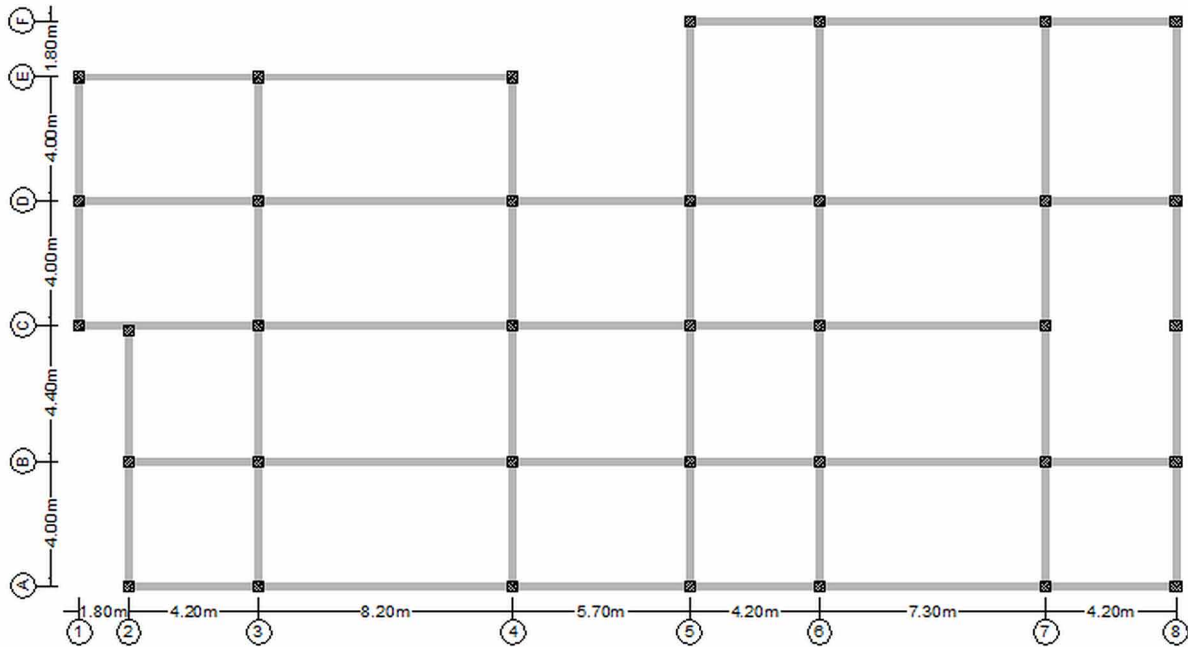


Figure 8. Residential building, geometry and reinforcement of frame 1 a) columns b) beams

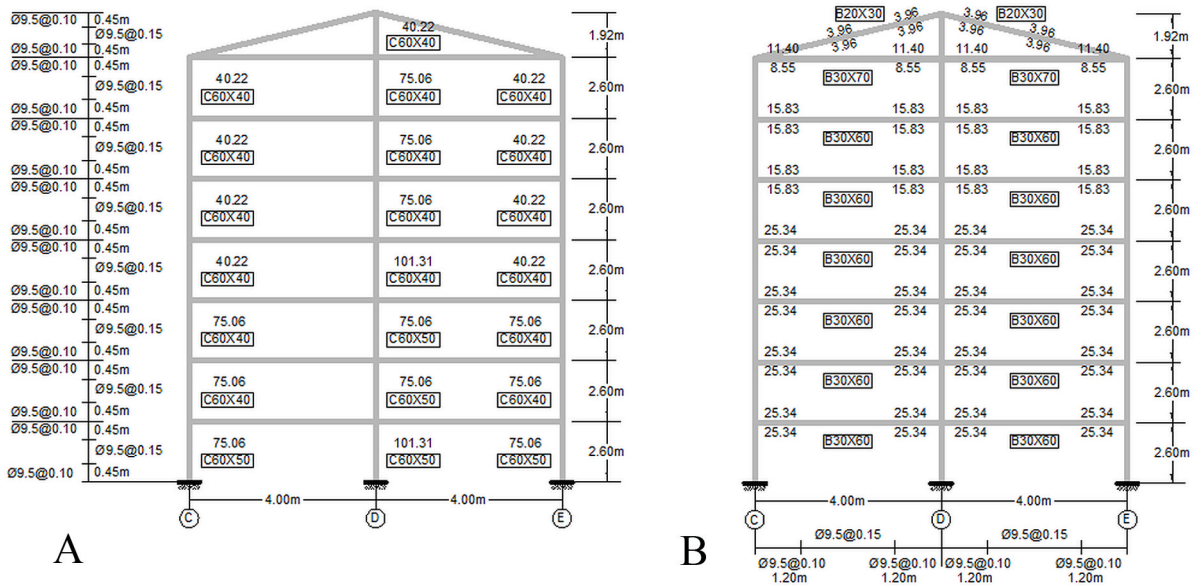


Figure 9. Residential building, geometry and reinforcement of frame 2 a) columns b) beams

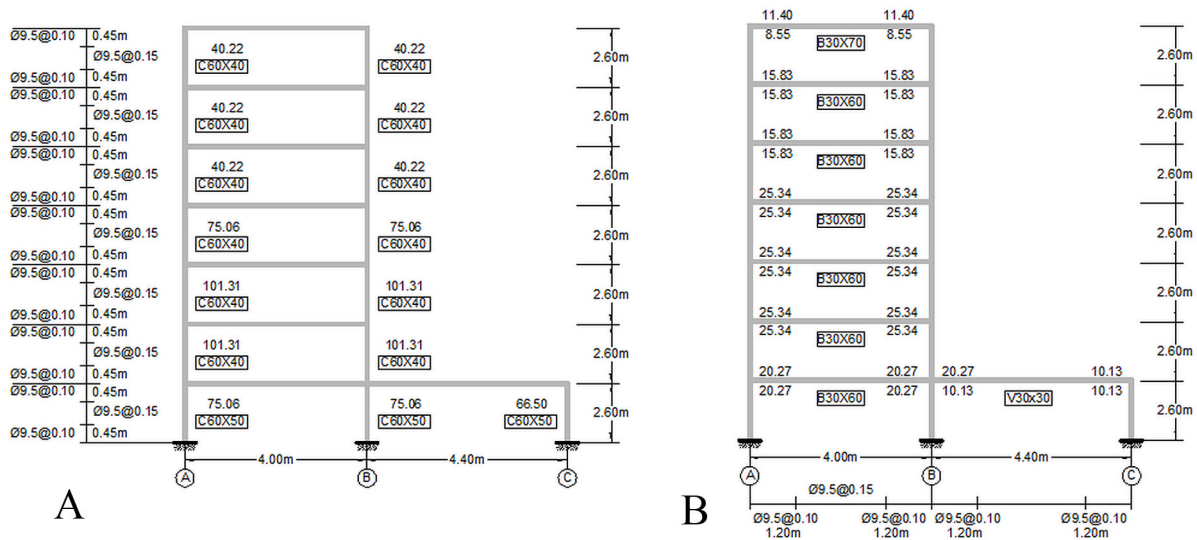
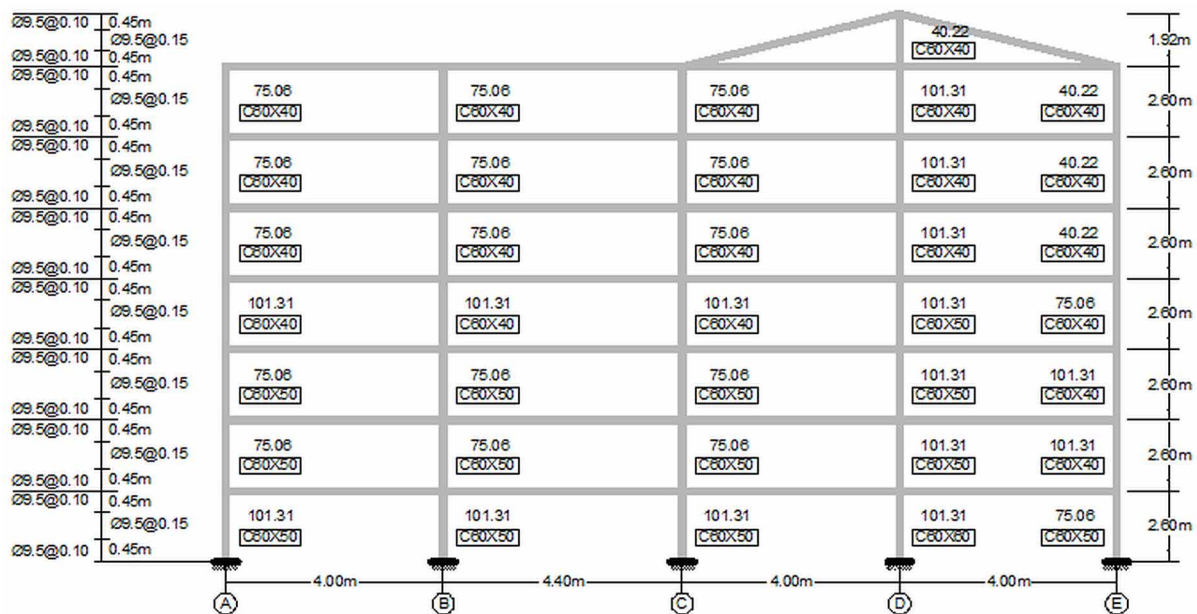


Figure 10. Residential building, geometry and reinforcement in columns of the frame 3



**Industrial Applications**

Figure 11. Residential building, geometry and reinforcement in beams of the frame 3

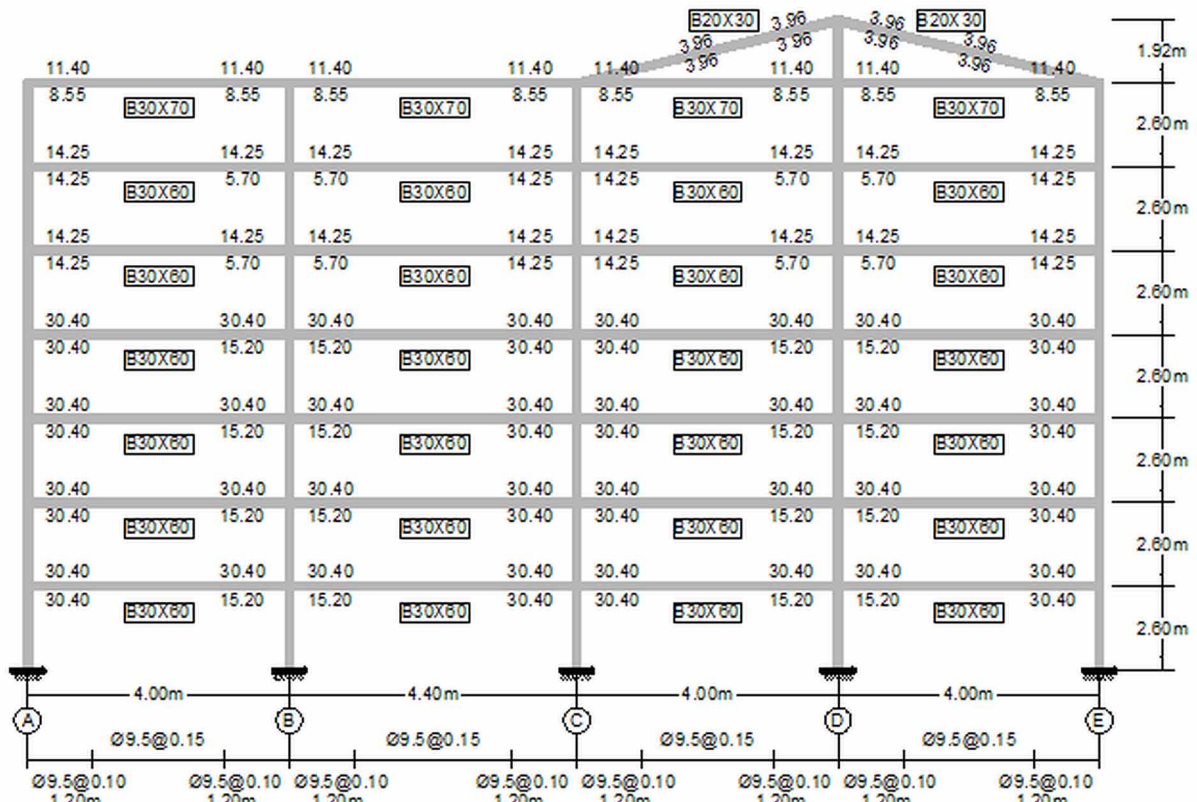


Figure 12. Residential building, geometry and reinforcement in columns of the frame 4

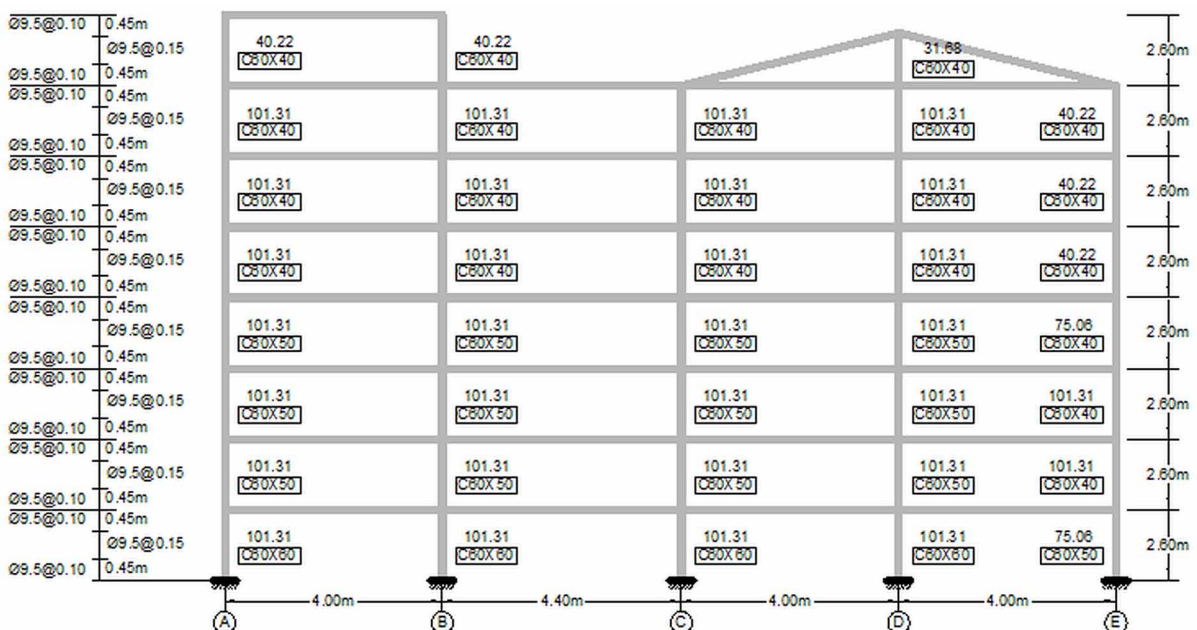




Figure 13. Residential building, geometry and reinforcement in beams of the frame 4

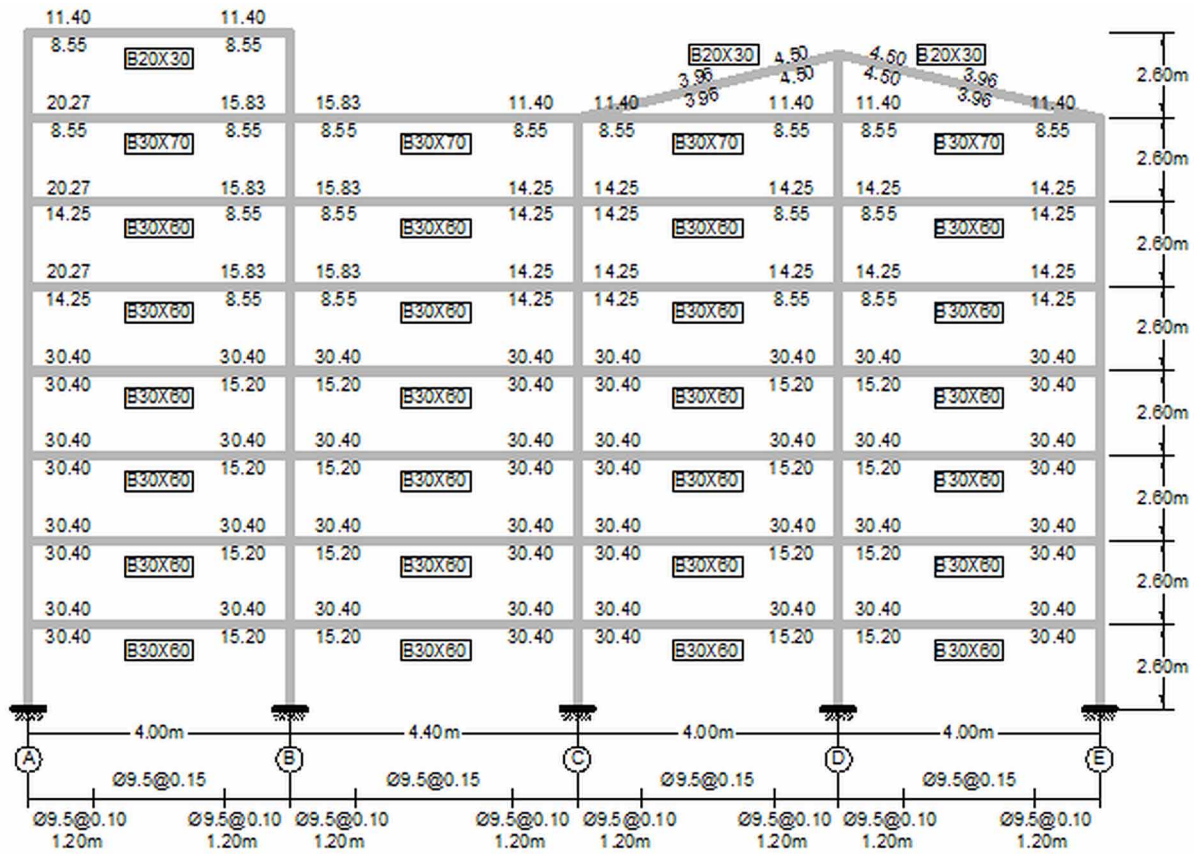
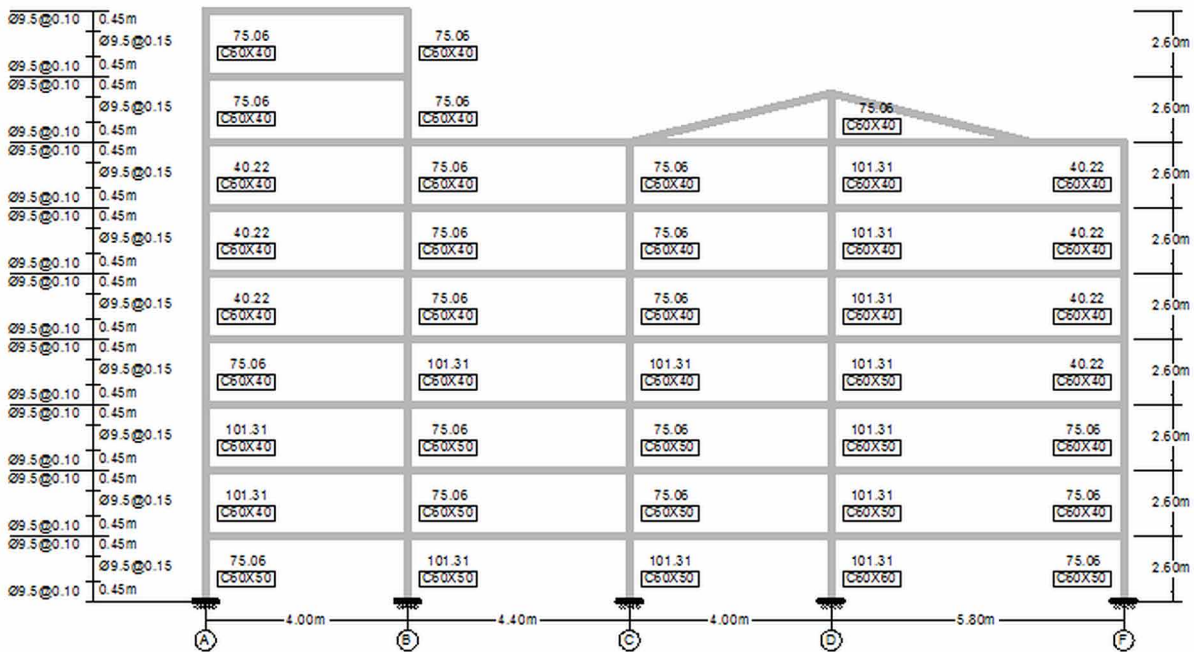


Figure 14. Residential building, geometry and reinforcement in columns of the frame 5



## Industrial Applications

Figure 15. Residential building, geometry and reinforcement in beams of the frame 5

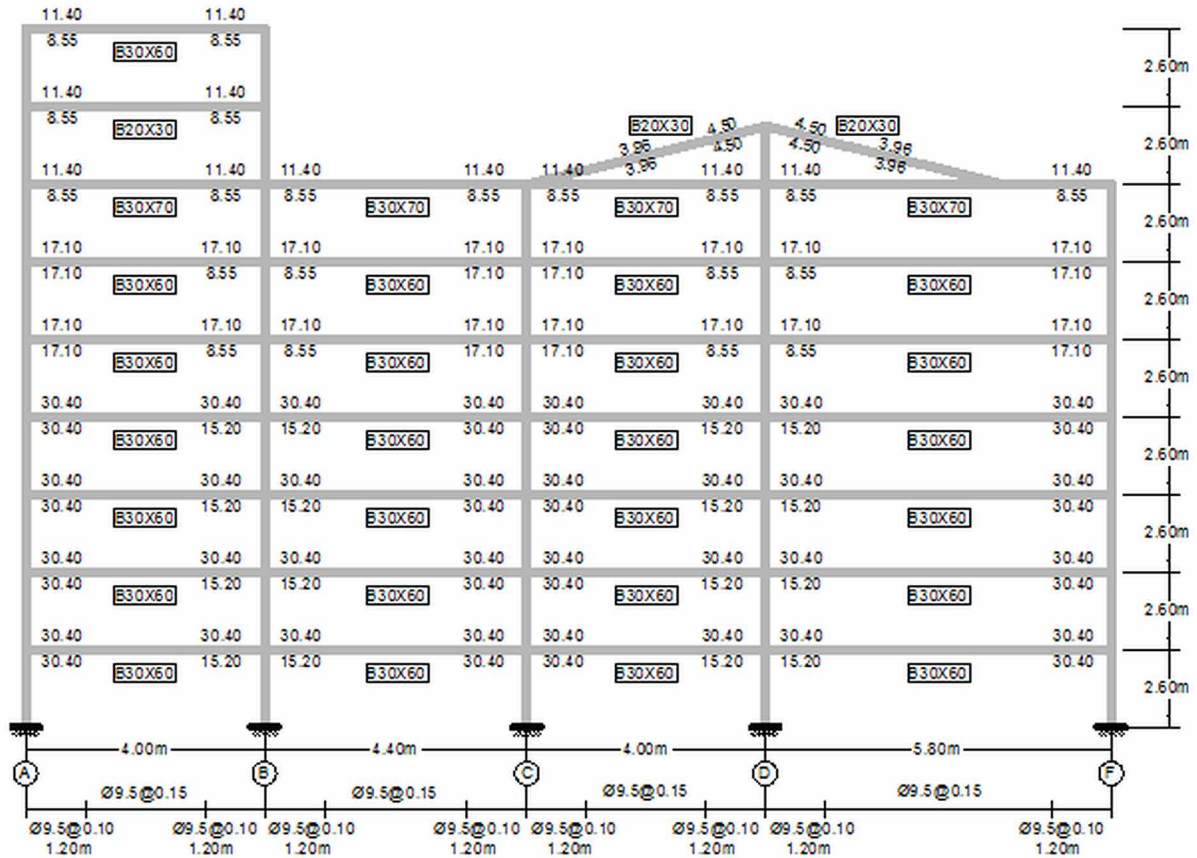


Figure 16. Residential building, geometry and reinforcement in columns of the frame 6

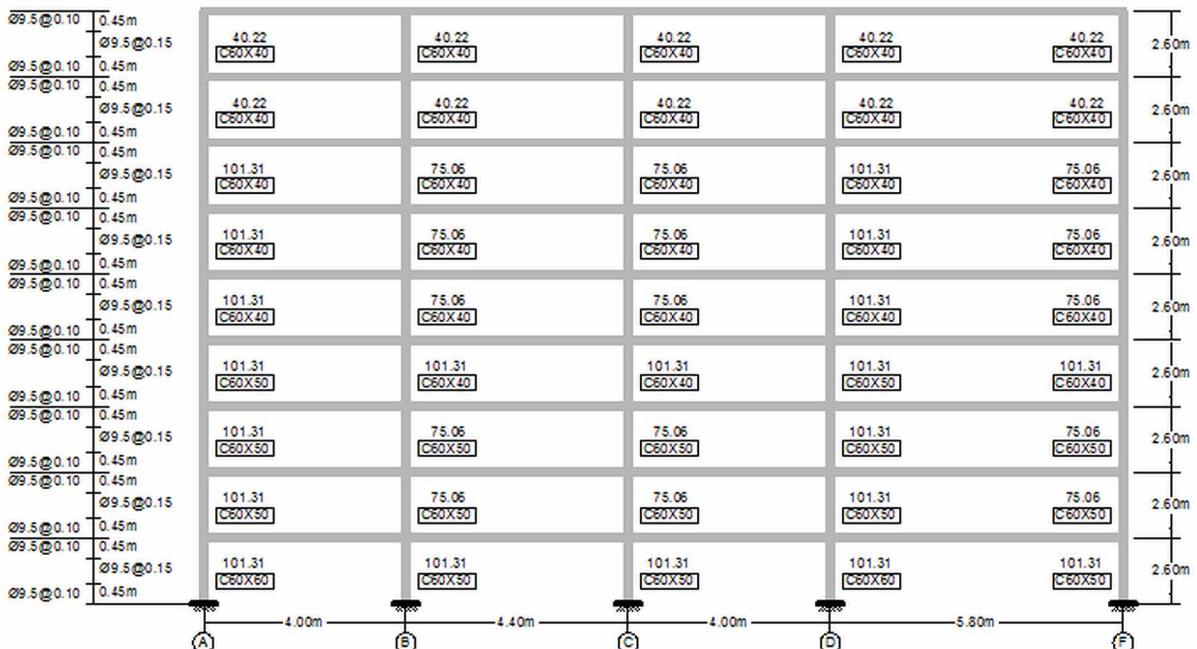


Figure 17. Residential building, geometry and reinforcement in beams of the frame 6

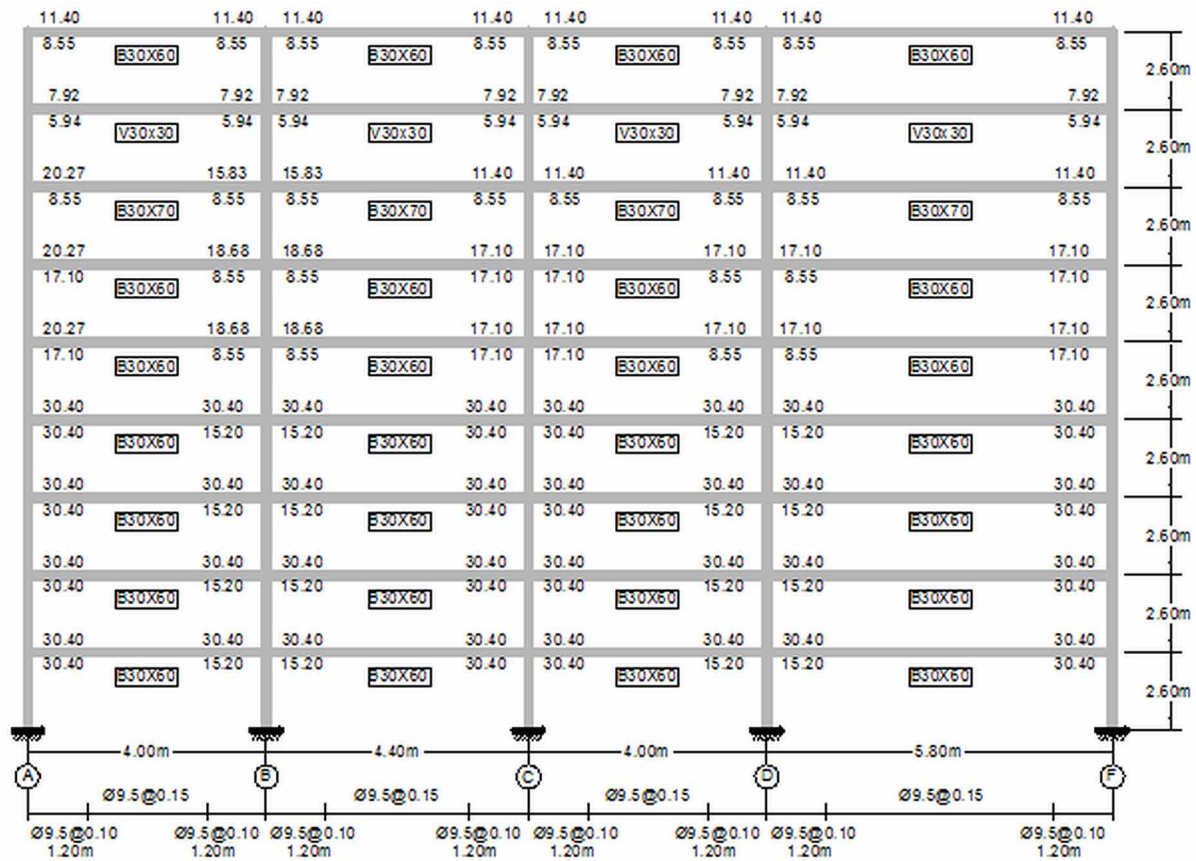
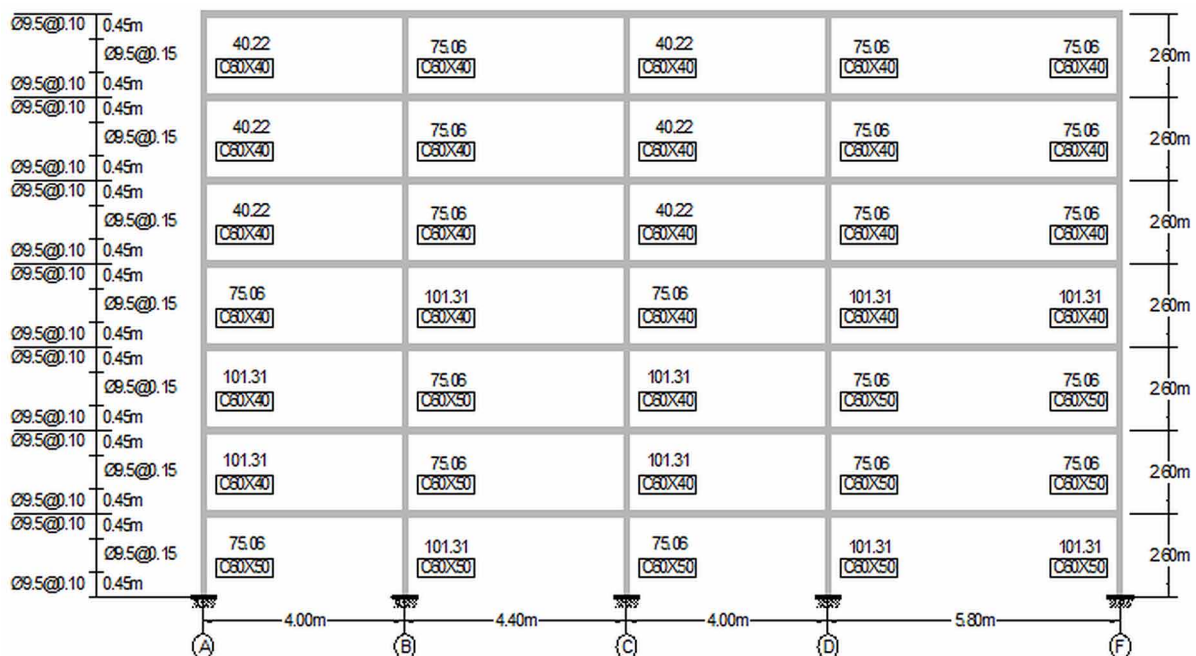


Figure 18. Residential building, geometry and reinforcement in columns of the frame 7



**Industrial Applications**

Figure 19. Residential building, geometry and reinforcement in beams of the frame 7

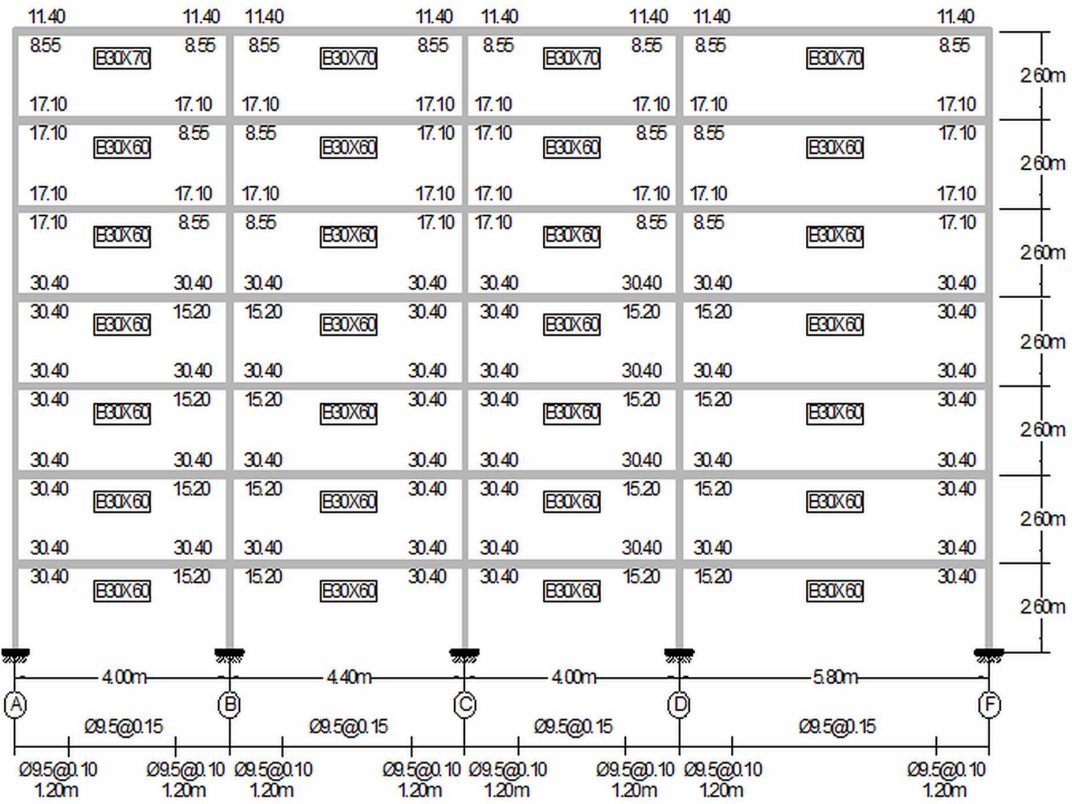


Figure 20. Residential building, geometry and reinforcement in columns of the frame 8

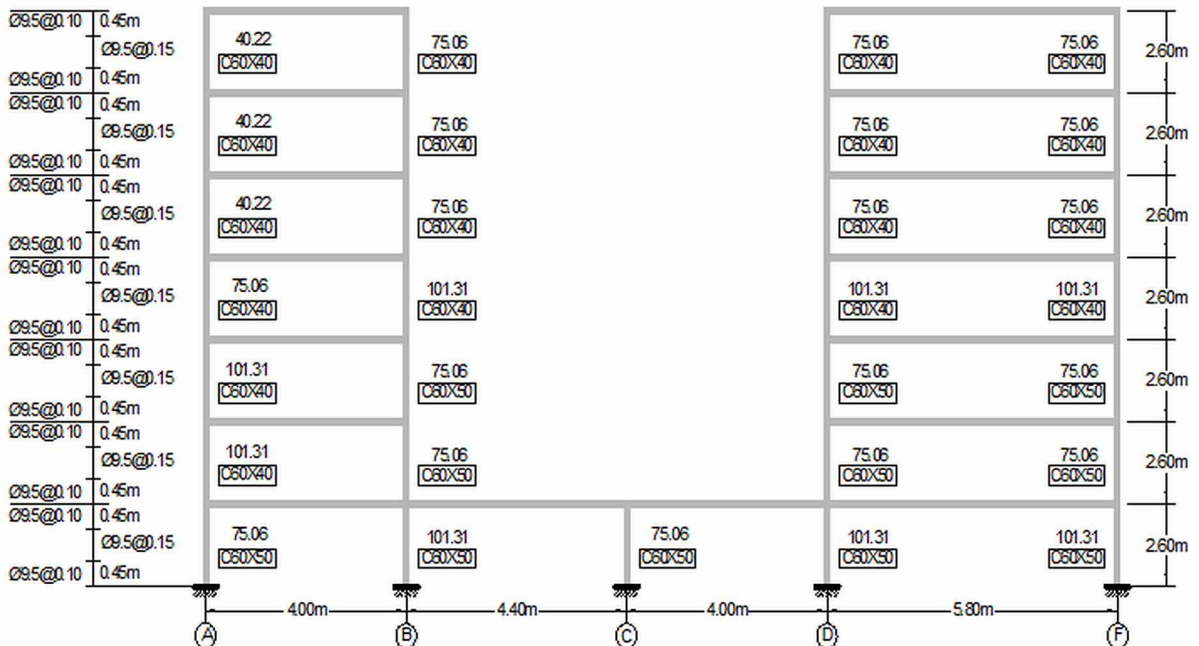


Figure 21. Residential building, geometry and reinforcement in beams of the frame 8

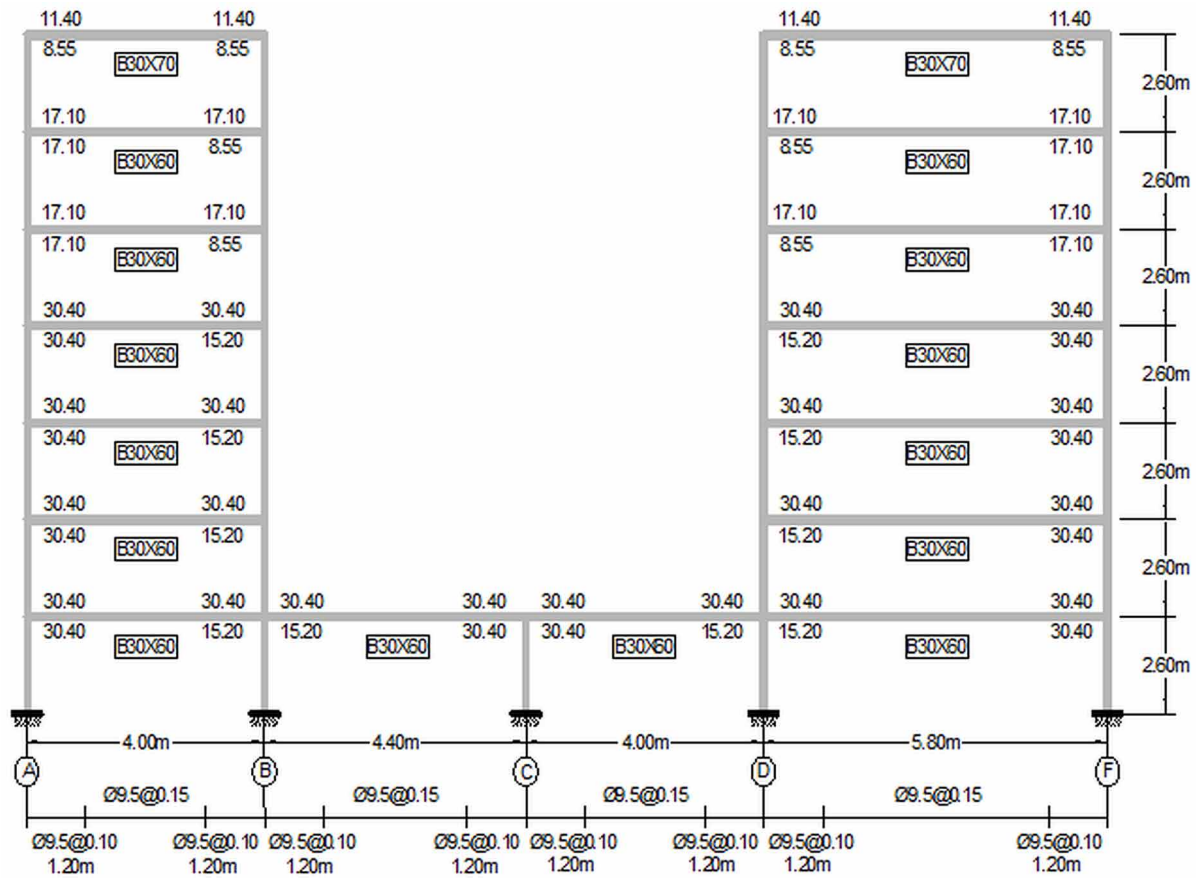
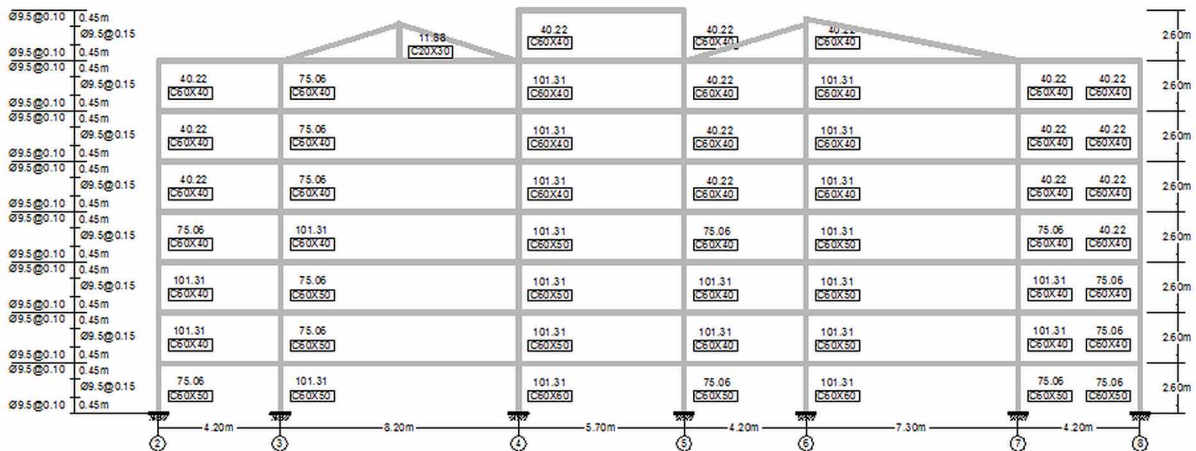


Figure 22. Residential building, geometry and reinforcement in columns of the frame A = frame B



## Industrial Applications

Figure 23. Residential building, geometry and reinforcement in beams of the frame A = frame B

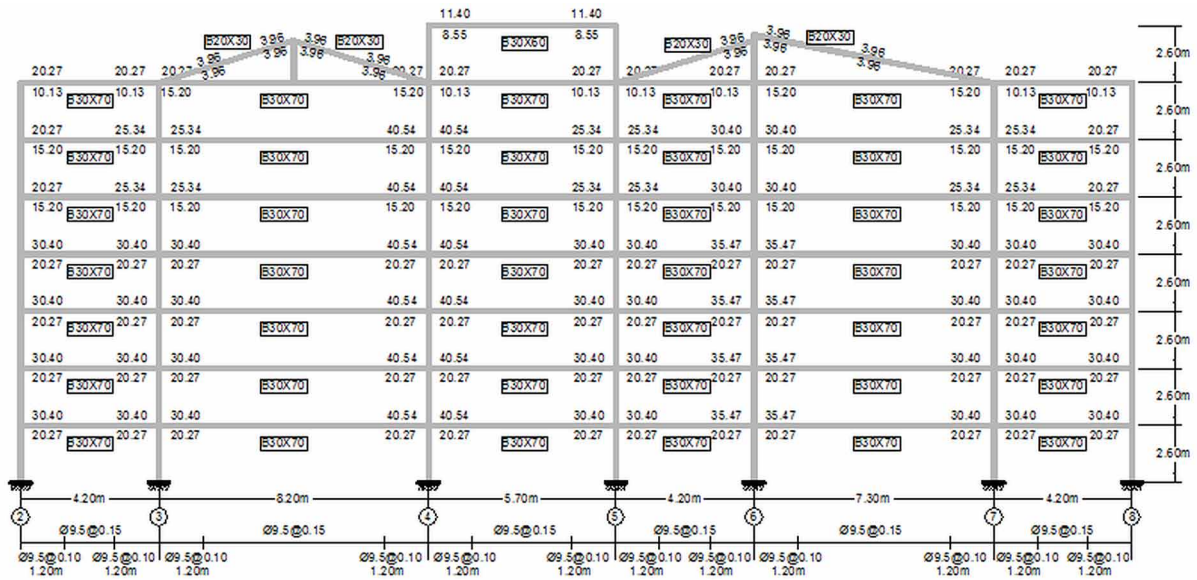


Figure 24. Residential building, geometry and reinforcement in columns of the frame C

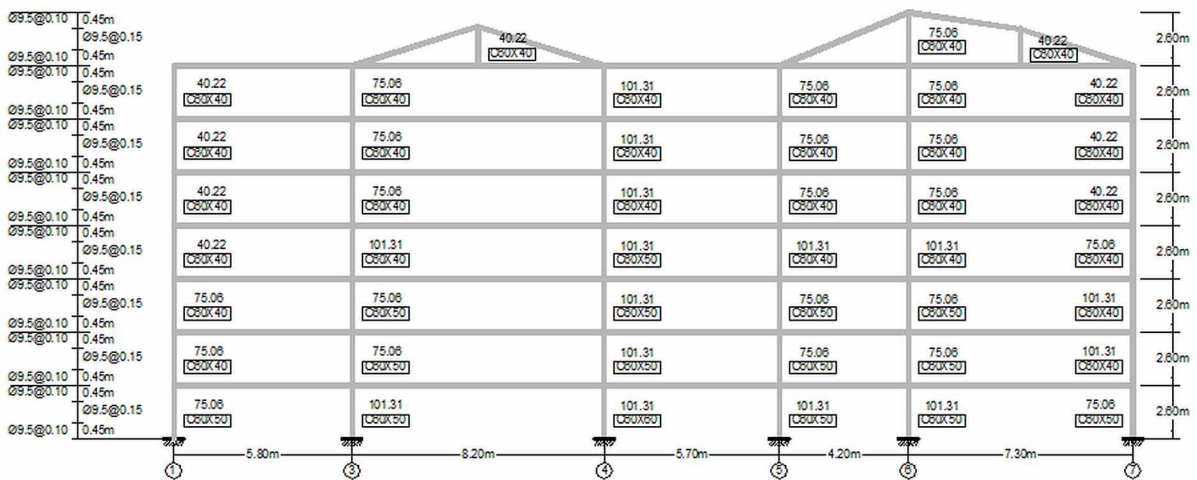


Figure 25. Residential building, geometry and reinforcement in beams of the frame C

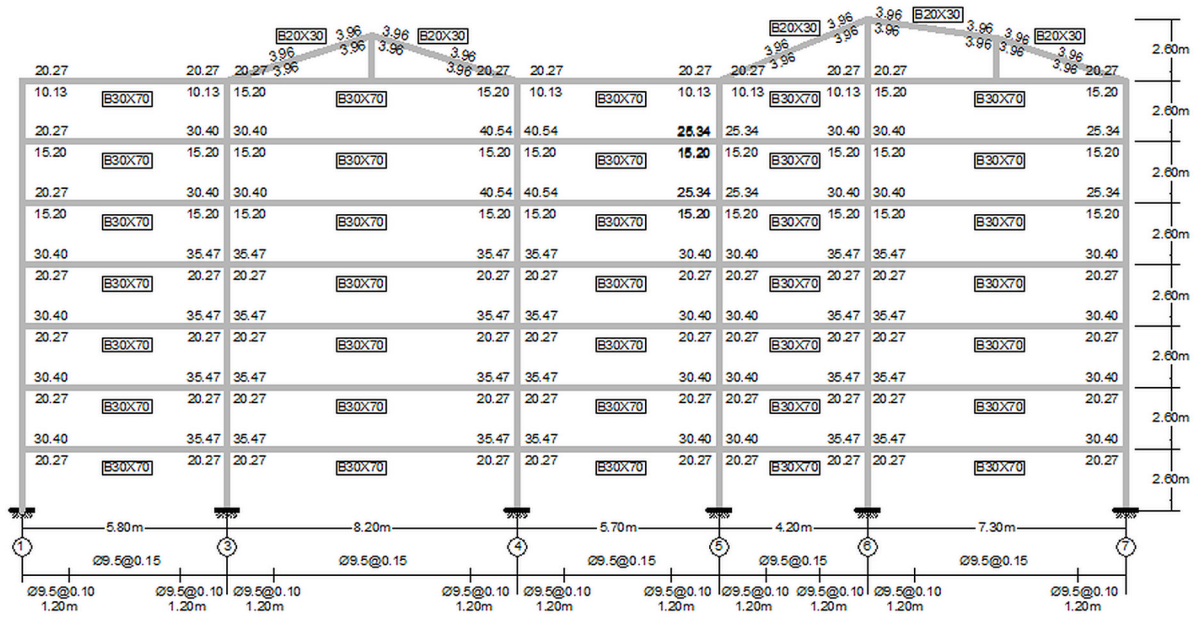
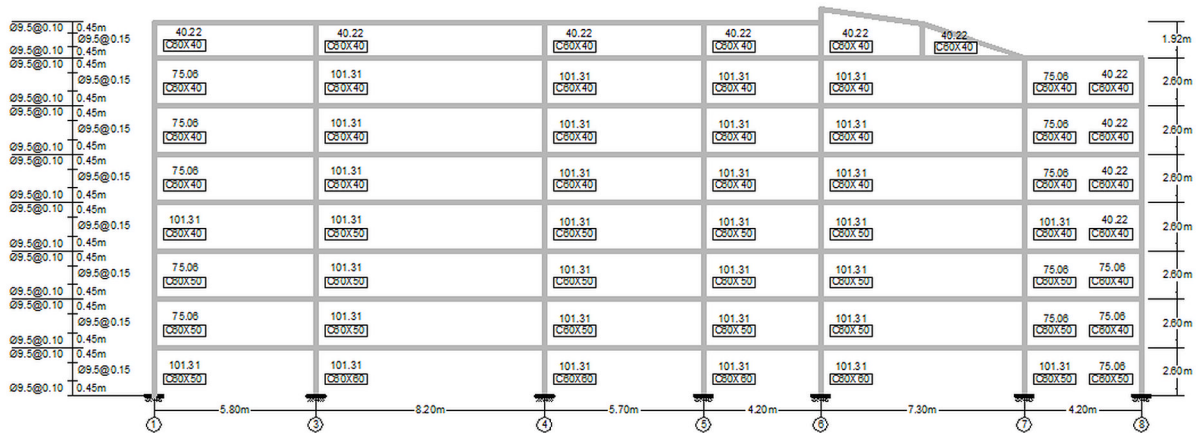
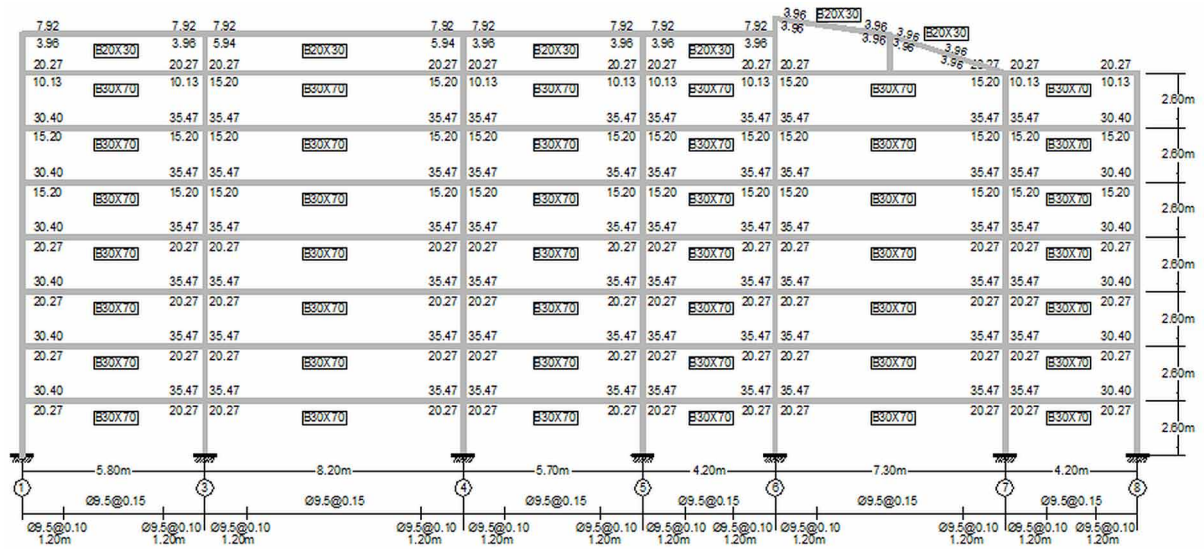


Figure 26. Residential building, geometry and reinforcement in columns of the frame D



**Industrial Applications**

*Figure 27. Residential building, geometry and reinforcement in beams of the frame D*



*Figure 28. Residential building, geometry and reinforcement of the frame E a) columns b) beams*

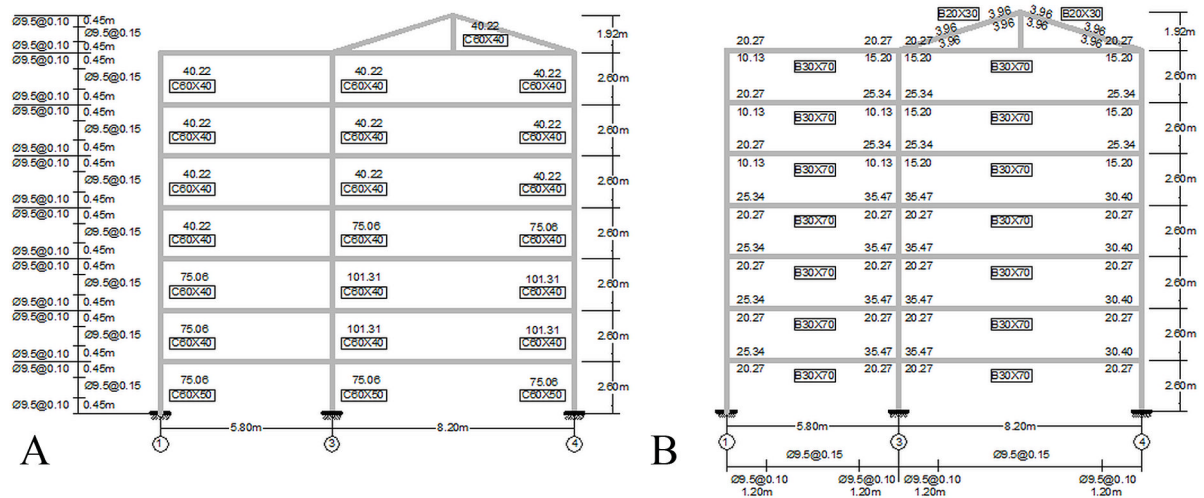
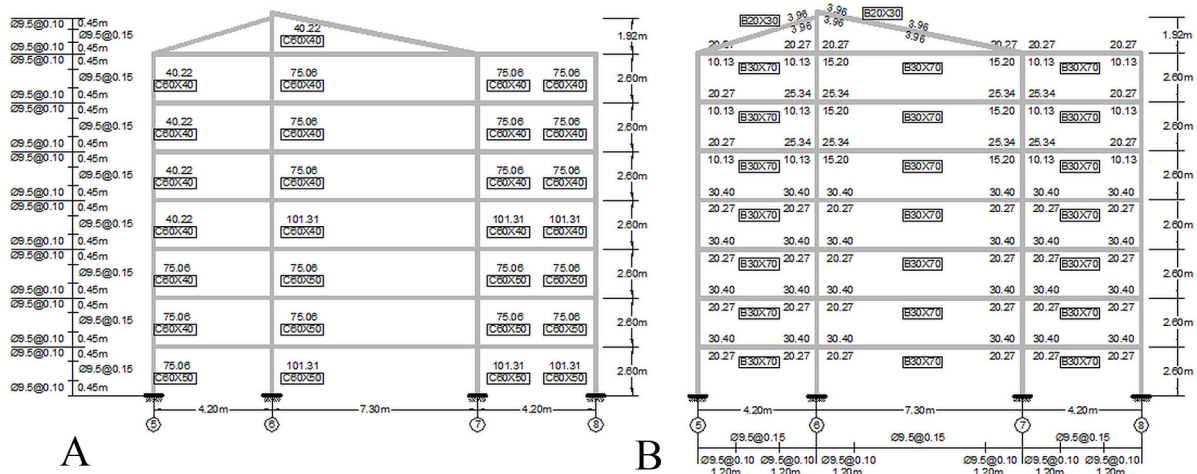




Table 3. Loads applied over the elements of frames 1 to 8

Frame	Level	Load on Span (KN/m)				
		A - B	B - C	C - D	D - E	E - F
1	1 - 7	-	-	40.18	40.18	-
	Roof	-	-	31.85	31.85	-
2	1	-	-	36.26	7.84	-
	2 - 6	-	-	36.26	-	-
	7	-	-	31.26	-	-
3	1 - 6	38.22	38.22	38.22	38.22	-
	7	36.26	36.26	36.26	36.26	-
	Roof	-	-	29.40	29.40	-
4	1 - 6	38.22	38.22	38.22	38.22	-
	7	38.22	33.32	38.22	38.22	-
	Roof	33.32	-	30.38	30.38	-
5	1 - 6	41.16	41.16	41.16	41.16	41.16
	7	37.24	37.24	37.24	37.24	37.24
	8 / Roof	34.30	-	33.32	33.32	-
	9	36.26	-	-	-	-
6	1 - 7	39.20	39.20	39.20	39.20	39.20
	8	34.30	34.30	34.30	34.30	34.30
	9	36.26	36.26	36.26	36.26	36.26
7	1 - 6	39.20	39.20	39.20	39.20	39.20
	7	35.28	35.28	35.28	35.28	35.28
8	1	35.28	35.28	35.28	35.28	35.28
	2 - 6	35.28	-	-	35.28	35.28
	7	31.36	-	-	31.36	31.36

Figure 29. Residential building, geometry and reinforcement of the frame F a) columns b) beams



## Industrial Applications

Table 4. Loads applied over the elements of frames A to F

Frame	Level	Load on Span (KN/m)						
		1-2	2-3	3-4	4-5	5-6	6-7	7-8
A=B	1 - 4	-	44.10	44.10	44.10	44.10	44.10	44.10
	5 - 6	-	43.12	43.12	43.12	43.12	43.12	43.12
	7	-	5.10	5.10	5.10	5.10	5.10	5.10
	Roof	-	-	1.47	4.410	1.47	1.47	-
C	1 - 6	41.16	41.16	41.16	41.16	41.16	41.16	-
	7	35.28	35.28	41.16	35.28	41.16	41.16	-
	Roof	-	-	1.47	-	1.47	1.47	-
D	1 - 4	40.18	40.18	40.18	40.18	40.18	40.18	40.18
	5 - 7	39.20	39.20	39.20	39.20	39.20	39.20	39.20
	Roof	0.98	0.98	0.98	0.98	1.47	1.47	-
E	1 - 6	38.22	38.22	38.22	-	-	-	-
	7	32.34	32.34	32.34	-	-	-	-
	Roof	-	-	29.40	-	-	-	-
F	1 - 6	-	-	-	-	37.24	37.24	37.24
	7	-	-	-	-	32.34	32.34	32.34
	Roof	-	-	-	-	1.96	1.96	-

Figure 30. a) Response spectrum used for the ground motion derivation b) Artificial earthquake used for the analysis

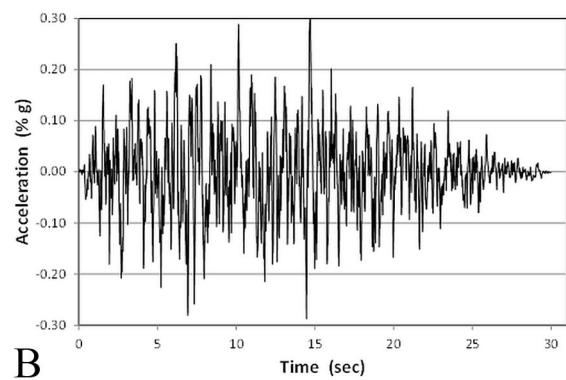
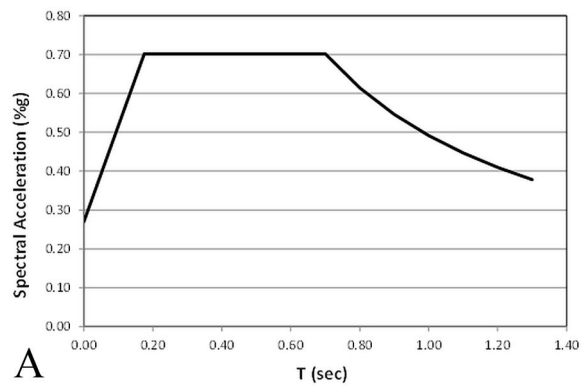


Figure 31. Damage distributions at the final of the event a) Frame 1 b) Frame 2

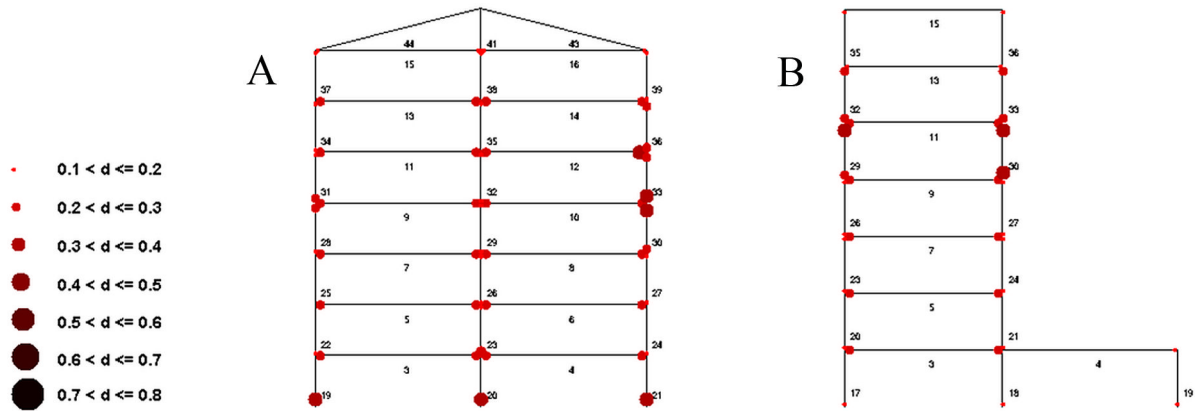
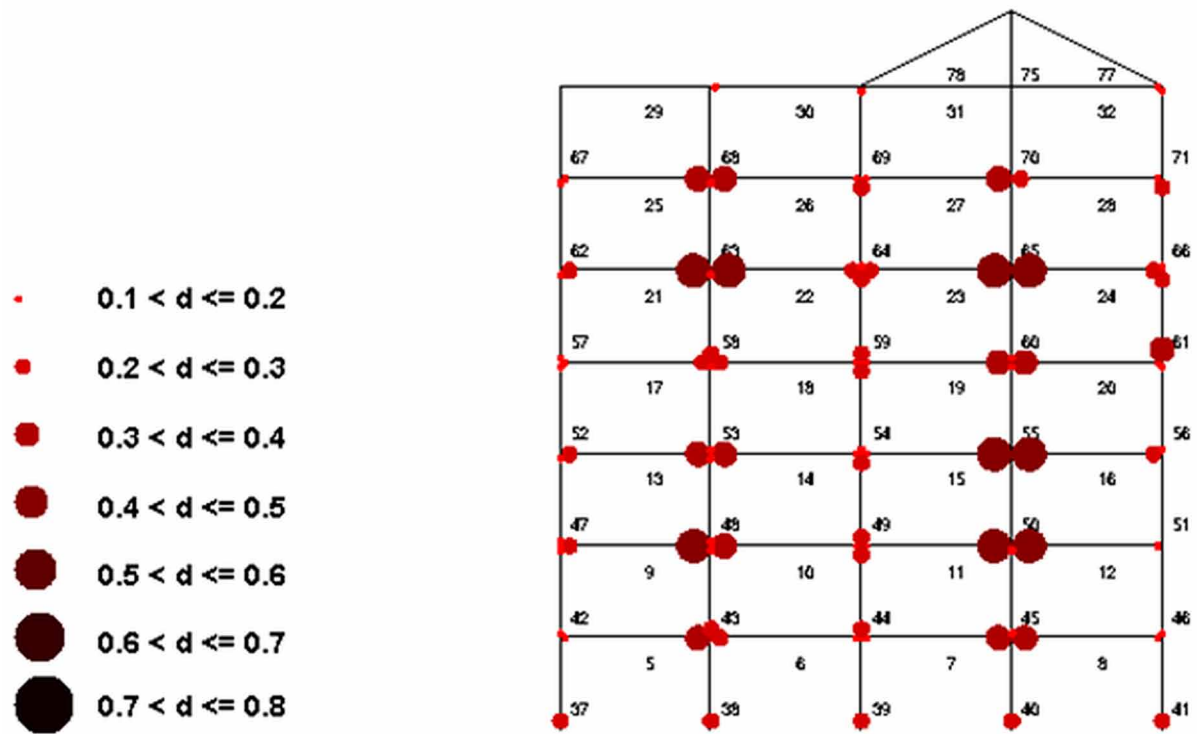


Figure 32. Damage distributions at the final of the event Frame 3



**Industrial Applications**

Figure 33. Damage distributions at the final of the event a) Frame 4 b) Frame 5

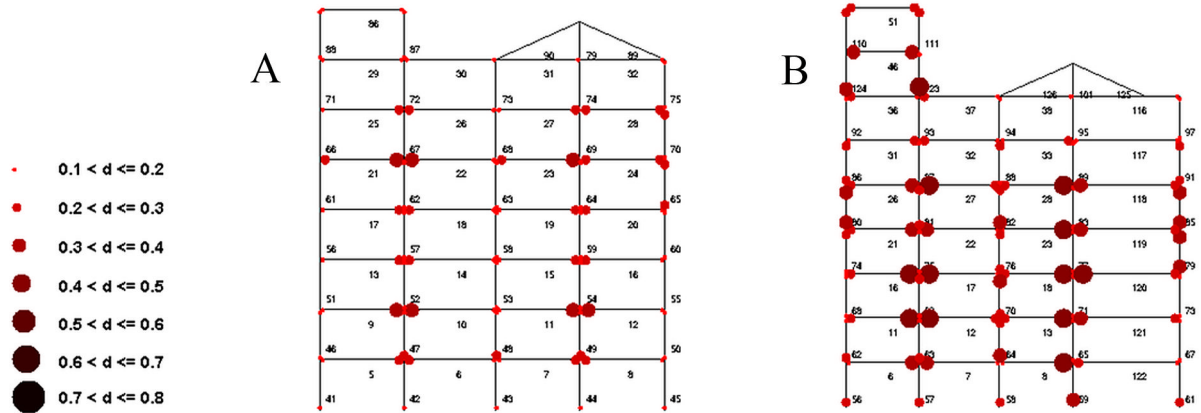


Figure 34. Damage distributions at the final of the event a) Frame 6 b) Frame 7

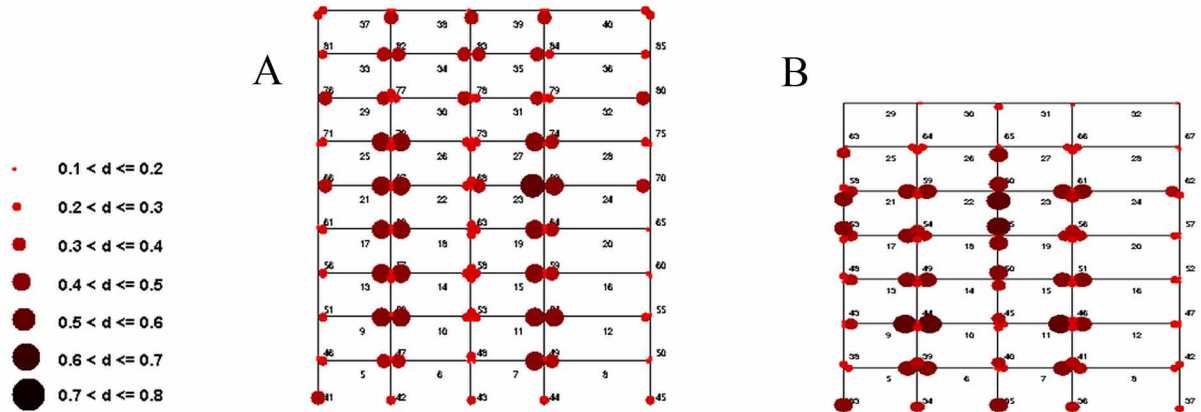
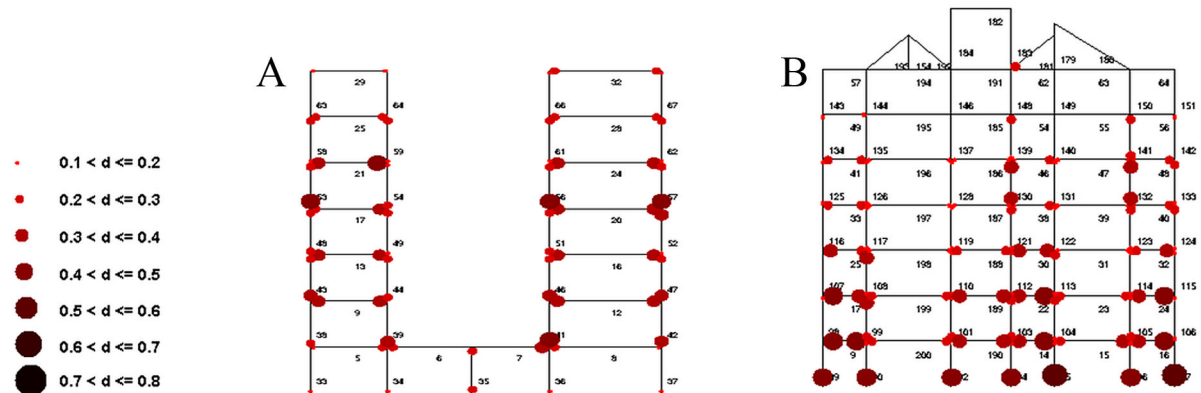


Figure 35. Damage distributions at the final of the event a) Frame 8 b) Frame A = B



As it can be appreciated the maximum damages occurred in the beams. This is in accordance with the recommendations prescribed in the standards of earthquake engineering. Frames 7 and A = B presented the largest damage values. The Dynamic Capacity Curve of the frame 7 is presented in Figure 38.

As can be appreciated in Figure 38 for a frequent earthquake (0.4 PGA) the maximum damage in beams and columns are, respectively, 0.263 and 0.32 that correspond to a performance level of 2. For a severe earthquake (0.8 PGA) are obtained damages in beams and columns of respectively, 0.422 and 0.497. This corresponds to a performance level of 3 and finally for a rare earthquake (1 PGA), the maximum damages obtained are 0.53 and 0.549 that corresponds to a performance level of 4. These results indicate that the structural behavior of the building is adequate.

### 13.3.2 Educational Facility

In Figure 39, it is presented the geometry of a typical edification built in Venezuela in the 60s. In Figures 40 to 58 it is presented the geometry and reinforcements details of beams and columns.

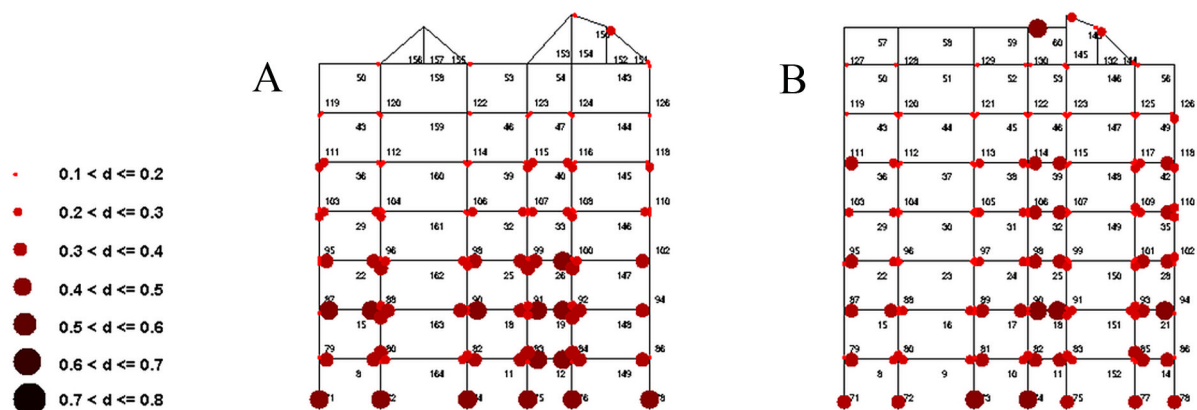
The loads applied on the frames are indicated in Tables 5 and 6; they were subjected to the artificial earthquake presented in Figure 59a that was derived from the response spectrum of the Figure 59b.

In this case (see Figure 59b), the peak acceleration of the ground motion is 0.40g. This acceleration corresponds to a zone with very high seismic risk. The frames were analyzed using the Portal of Damages but all the analyses stopped before finishing the earthquake record. The damage distributions at the end of each analysis are presented in Figures 60 to 65.

As it can be appreciated in Figures 60 to 65, the values of the damages in columns were between a value of 0.51 and 0.81 and in beams between 0.22 and 0.75, which are very high. In fact, collapse of frames A, C, D and F could be expected. This behavior is not acceptable for any edification especially for an essential one. This structure does not satisfy the criteria prescribed in the actual seismic codes.

After Cariaco Earthquake (Venezuela) in 1997, a school with this geometry collapsed as it is shown in Figure 56. As evidenced by the results presented, even when the influence of the masonry was not considered in the analyses, resulting behavior is similar to the real case.

Figure 36. Damage distributions at the final of the event a) Frame C b) Frame D



**Industrial Applications**

Figure 37. Damage distributions at the final of the event a) Frame E b) Frame F

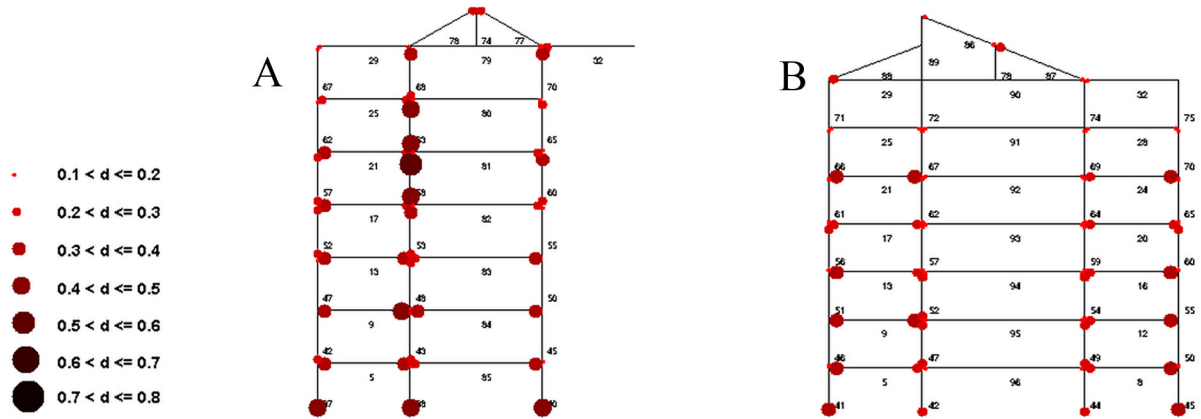


Figure 38. Dynamic Capacity Curve of the frame 7

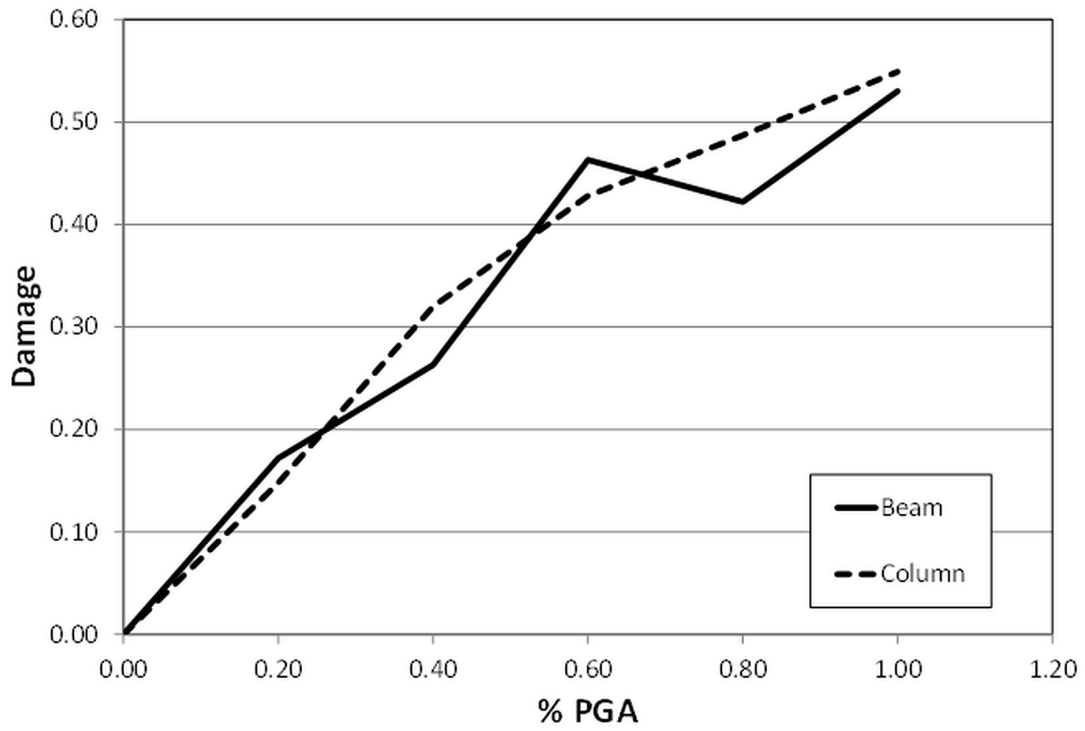


Figure 39. Educational facility, geometry of floor at level 0.00

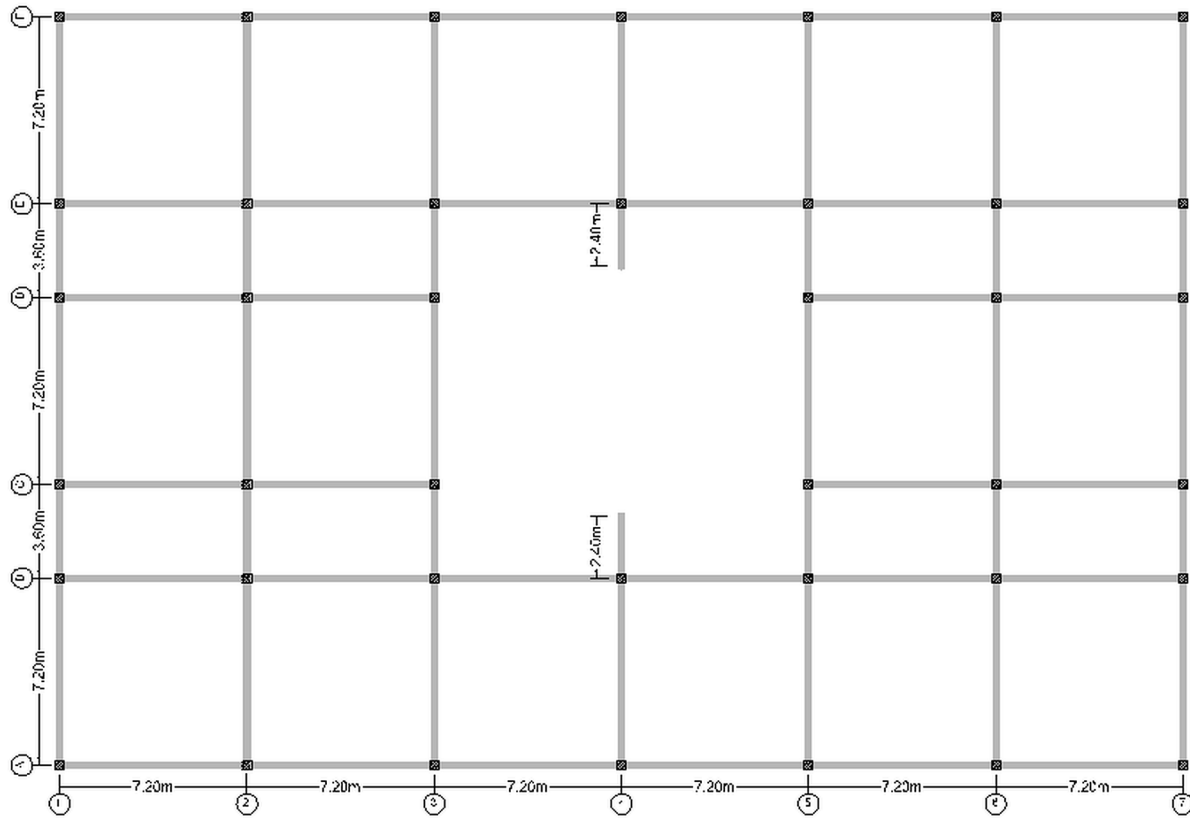


Figure 40. Educational facility, geometry and reinforcement in columns of Frame A = Frame B

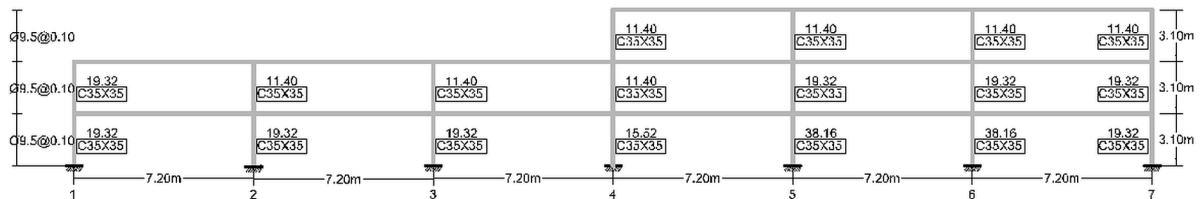
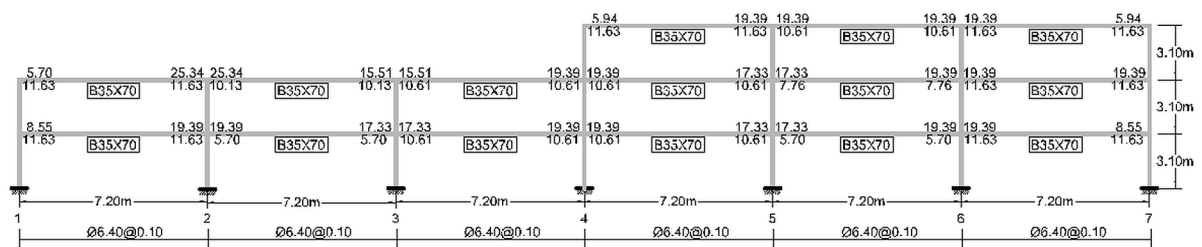


Figure 41. Educational facility, geometry and reinforcement in beams of Frame A = Frame B



**Industrial Applications**

Figure 42. Educational facility, geometry and reinforcement in columns of Frame B = Frame E

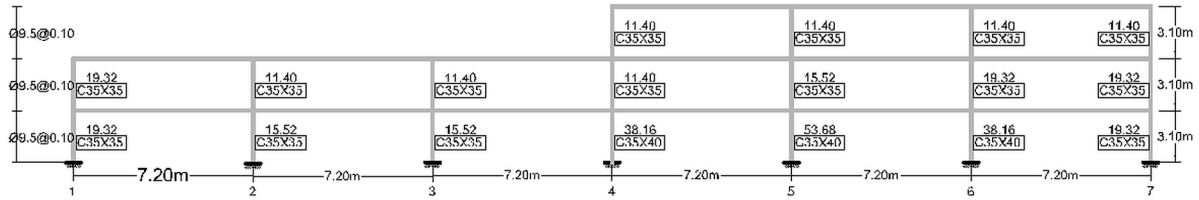


Figure 43. Educational facility, geometry and reinforcement in beams of Frame B = Frame E

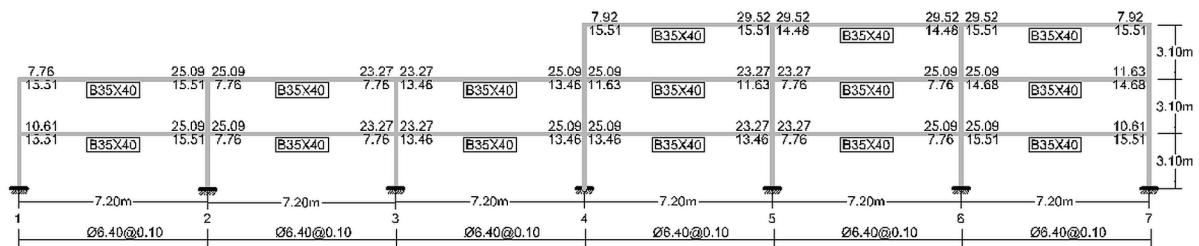


Figure 44. Educational facility, geometry and reinforcement of the Frame C (1-3)= Frame D (1-3) a) columns b) beams

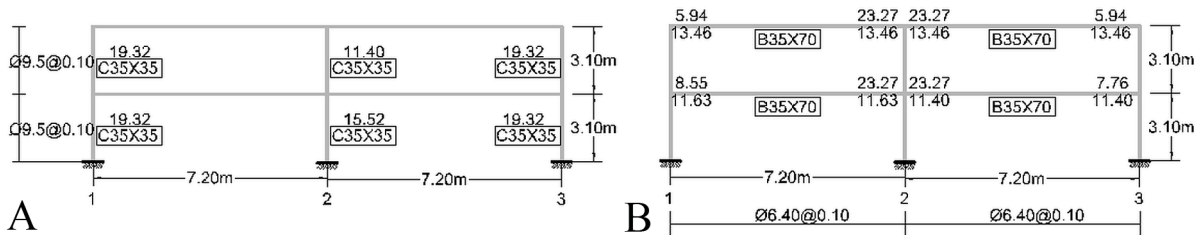


Figure 45. Educational facility, geometry and reinforcement of the Frame C (5-7)= Frame D (5-7) a) columns b) beams

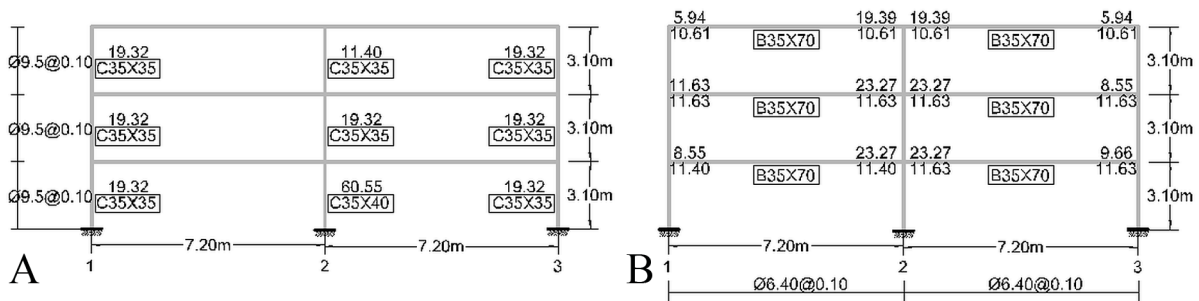




Figure 46. Educational facility, geometry and reinforcement in columns of the Frame 1

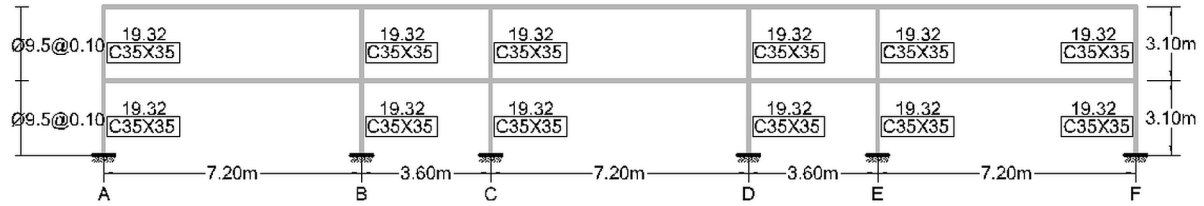


Figure 47. Educational facility, geometry and reinforcement in beams of the Frame 1

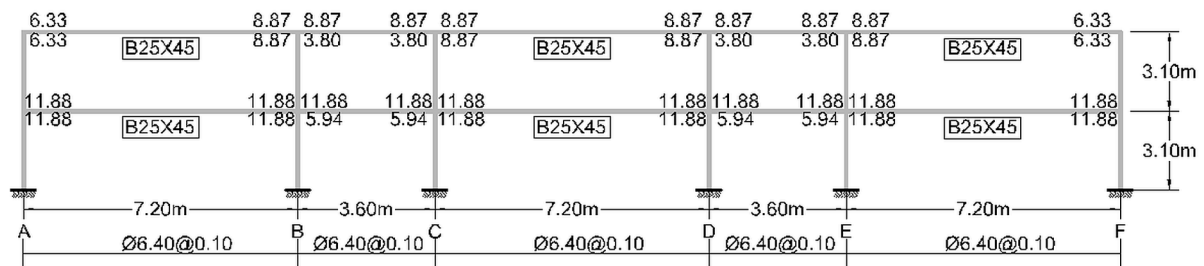


Figure 48. Educational facility, geometry and reinforcement in columns of the Frame 2

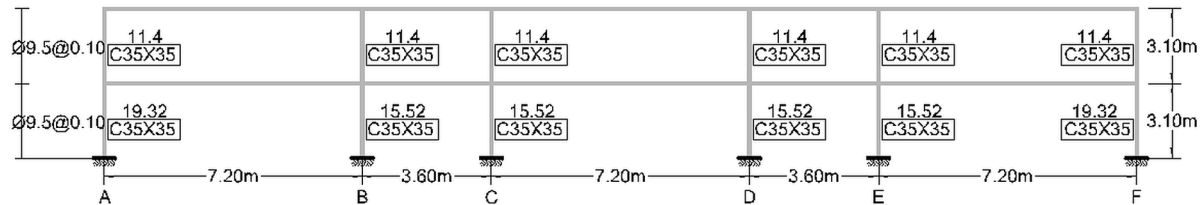
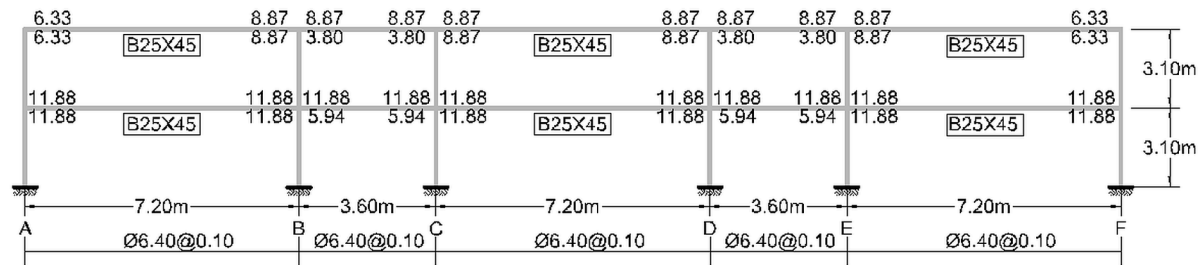


Figure 49. Educational facility, geometry and reinforcement in beams of the Frame 2



**Industrial Applications**

Figure 50. Educational facility, geometry and reinforcement in columns of the Frame 3

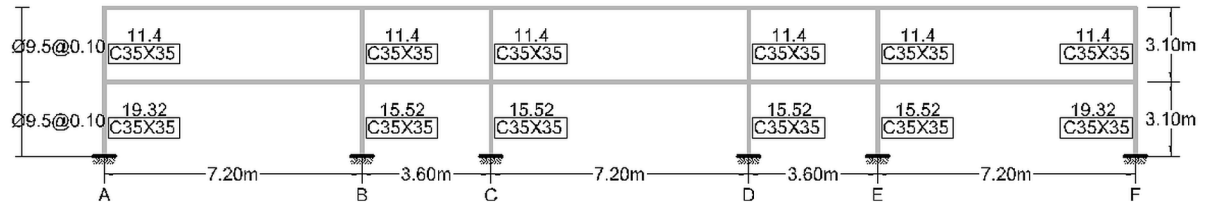


Figure 51. Educational facility, geometry and reinforcement in beams of the Frame 3

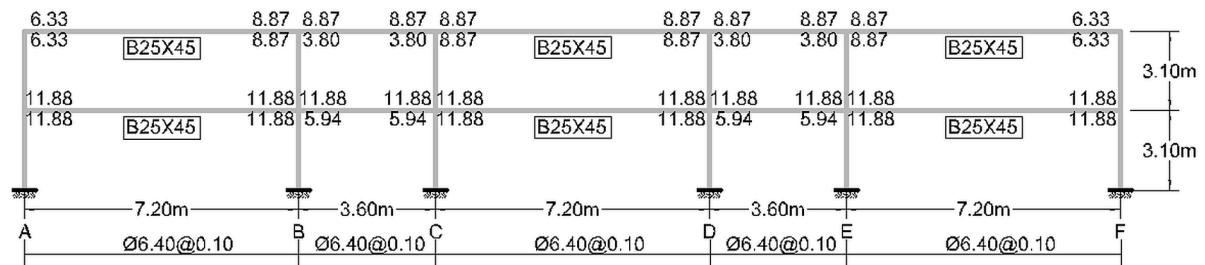


Figure 52. Educational facility, geometry and reinforcement of the Frame 4 (A-B)= Frame 4 (E-F) a) columns b) beams

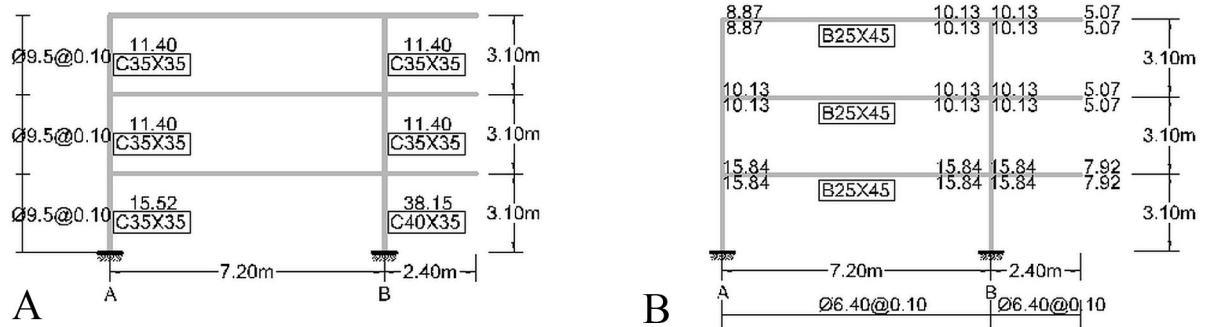


Figure 53. Educational facility, geometry and reinforcement in columns of the Frame 5

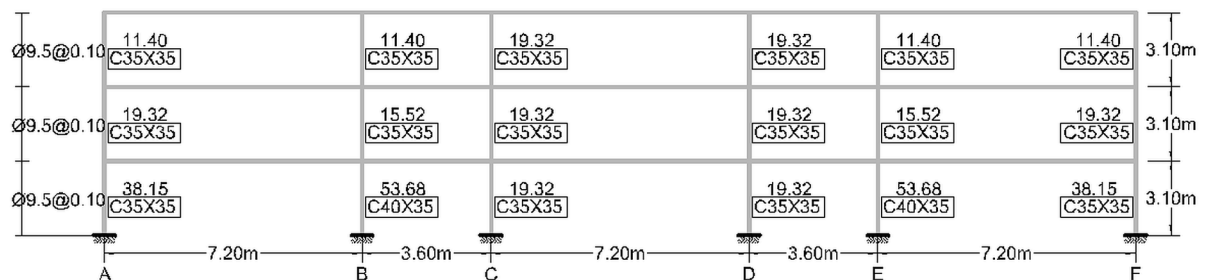


Figure 54. Educational facility, geometry and reinforcement in beams of the Frame 5

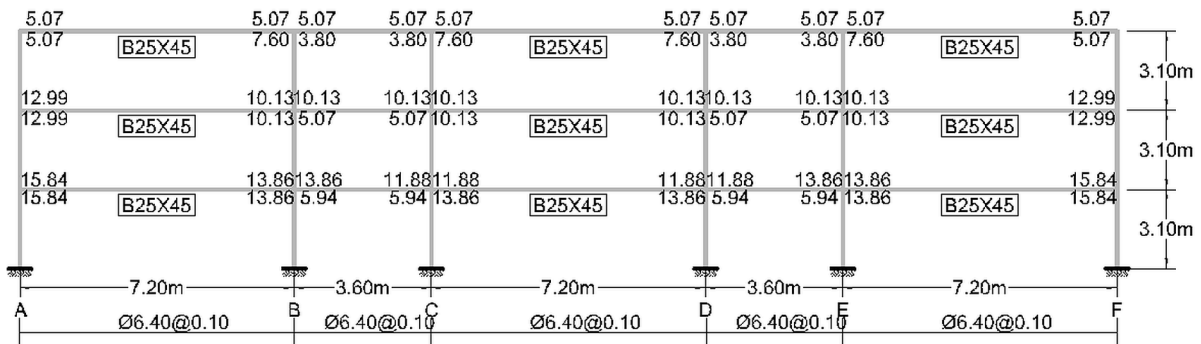


Figure 55. Educational facility, geometry and reinforcement in columns of the Frame 6

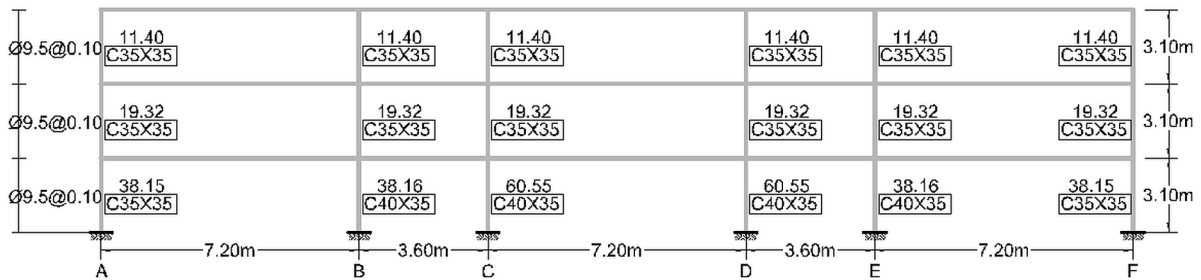


Figure 56. Educational facility, geometry and reinforcement in beams of the Frame 6

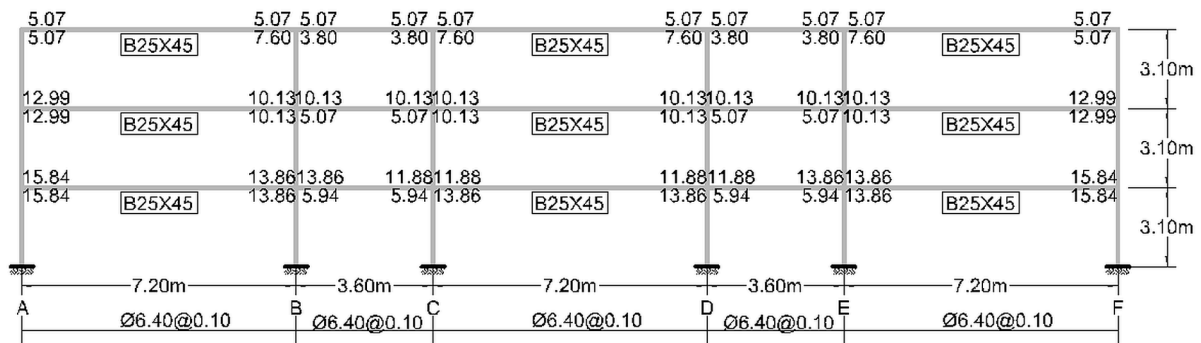
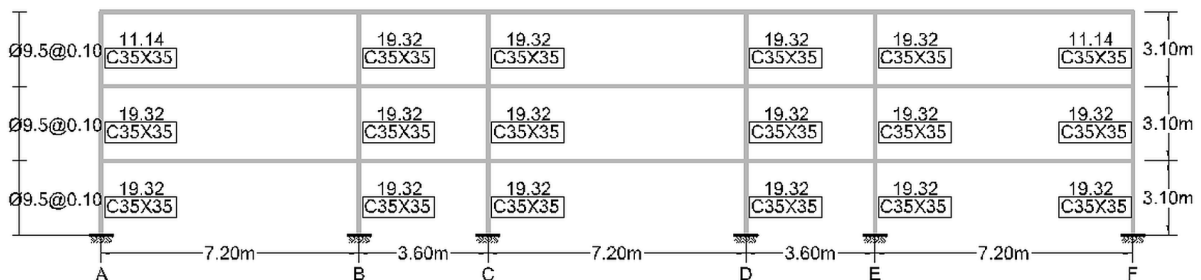


Figure 57. Educational facility, geometry and reinforcement in columns of the Frame 7



**Industrial Applications**

Figure 58. Educational facility, geometry and reinforcement in beams of the Frame 7

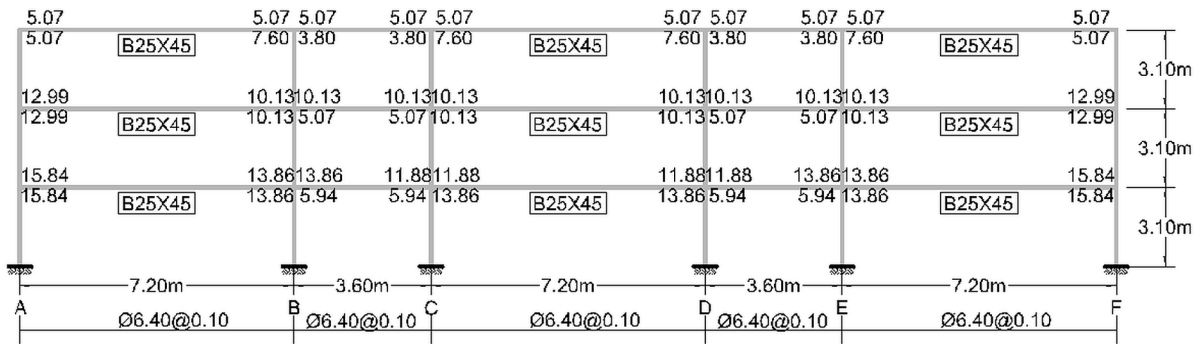


Figure 59. a) Response spectrum used for the ground motion derivation b) Artificial earthquake used for the analysis

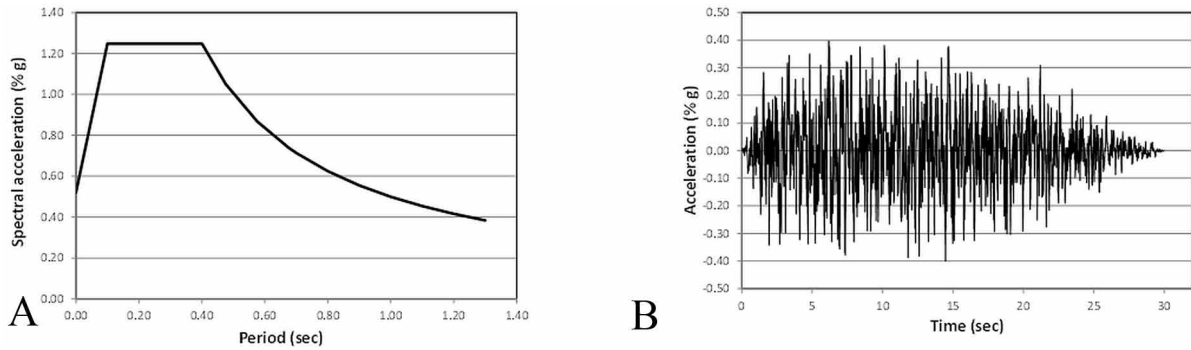


Table 5. Loads applied over the elements of frames 1 to 7

Frame	Level	Load on Span (KN/m)				
		A – B	B – C	C – D	D – E	E – F
1 = 2 = 3	1 – 2	5.20	5.20	5.20	5.20	5.20
4	1 – 3	5.20	-	-	-	5.20
5 = 6 = 7	1 – 3	5.20	5.20	5.20	5.20	5.20

**13.4 SUMMARY**

This chapter proposes a protocol for the seismic assessment of frame structures. The protocol is resumed in Tables 1, 2 and the concept of dynamic capacity curve. The first table summarizes the possible demands on the structure in terms of the peak ground acceleration or PGA; the second table characterizes the expected reparability state of the frame in terms of the damage values. The dynamic capacity curve

Table 6. Loads applied over the elements of frames A to F

Frame	Level	Load on Span (KN/m)					
		1 – 2	2 – 3	3 – 4	4 – 5	5 – 6	6 – 7
A = F	1 – 2	32.56	32.56	32.56	32.56	32.56	32.56
	3	-	-	-	27.46	27.46	27.46
B = E	1	45.82	45.82	45.82	45.82	45.82	45.82
	2	36.50	36.50	36.50	45.82	45.82	45.82
	3	-	-	-	36.50	36.50	36.50
D	1	45.82	45.82	-	-	45.82	45.82
	2	36.50	36.50	-	-	45.82	45.82
	3	-	-	-	-	36.50	36.50

Figure 60. Damage distributions at the final of the event a) Frame 1 b) Frame 2

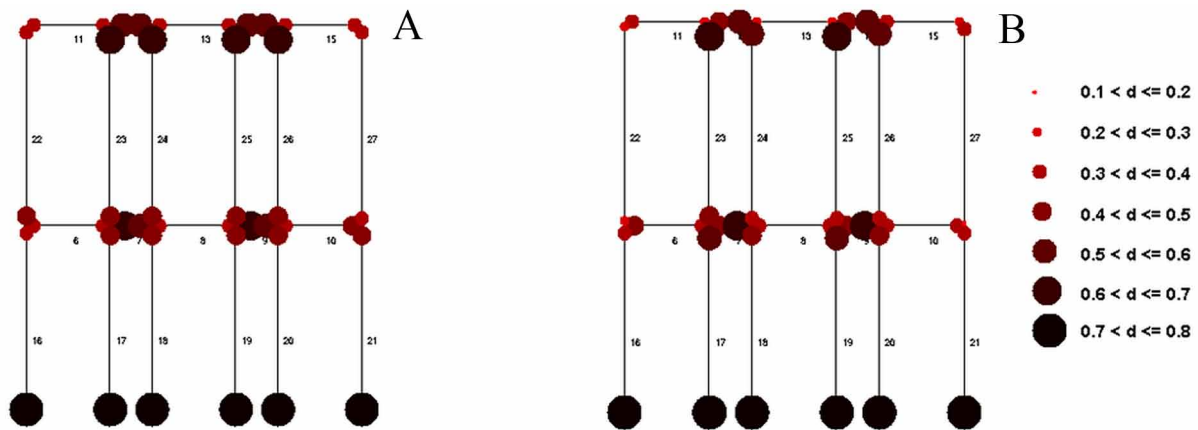
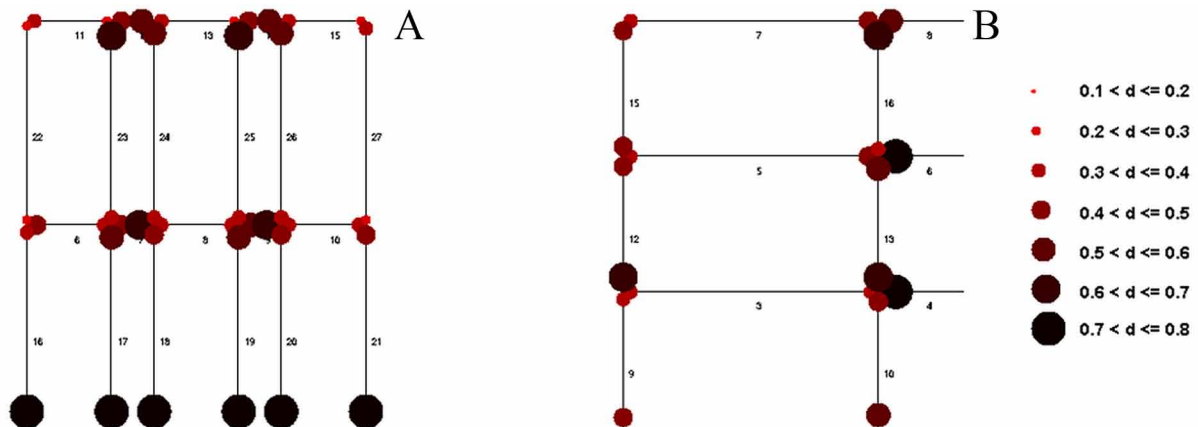


Figure 61. Damage distributions at the final of the event a) Frame 3 b) Frame 4(A-B)= 4(E-F)



**Industrial Applications**

Figure 62. Damage distributions at the final of the event a) Frame 5 b) Frame 6

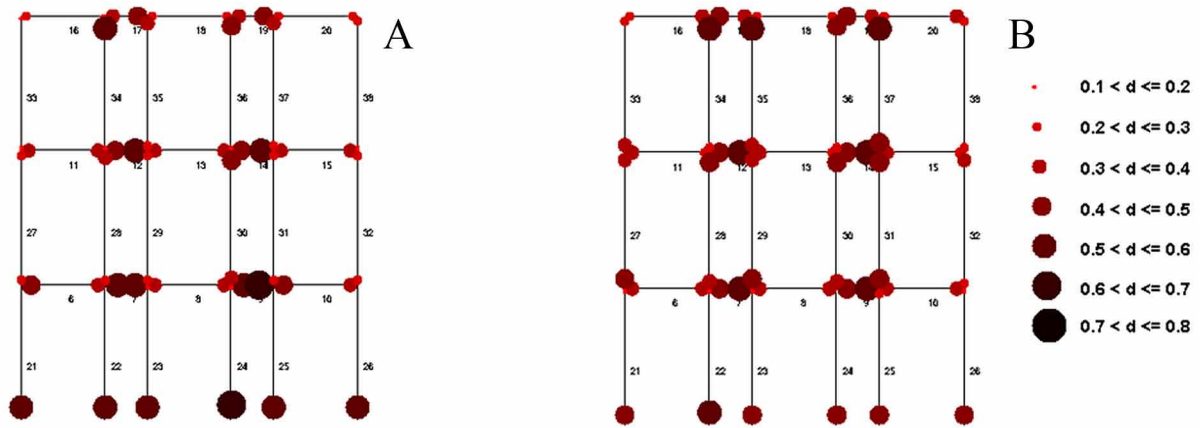


Figure 63. Damage distributions at the final of the event a) Frame 7 b) Frame A = F

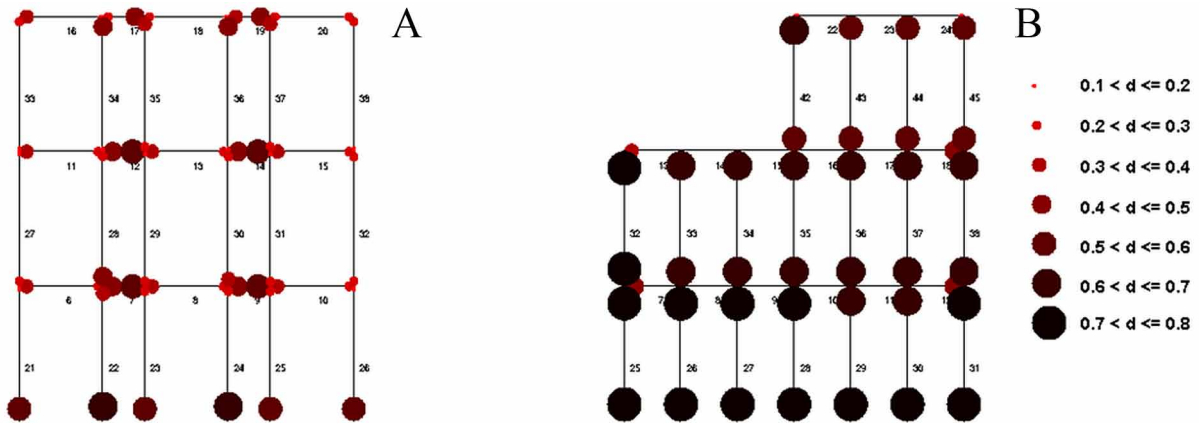


Figure 64. Damage distributions at the final of the event a) Frame C = D (1-3) b) Frame C = D (5-7)

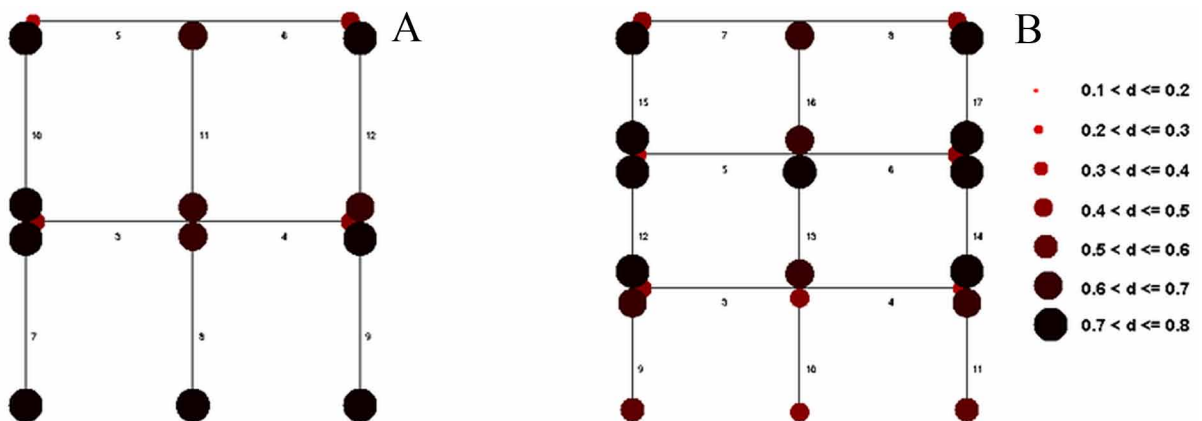


Figure 65. Damage distributions at the final of the event a) Frame B = E

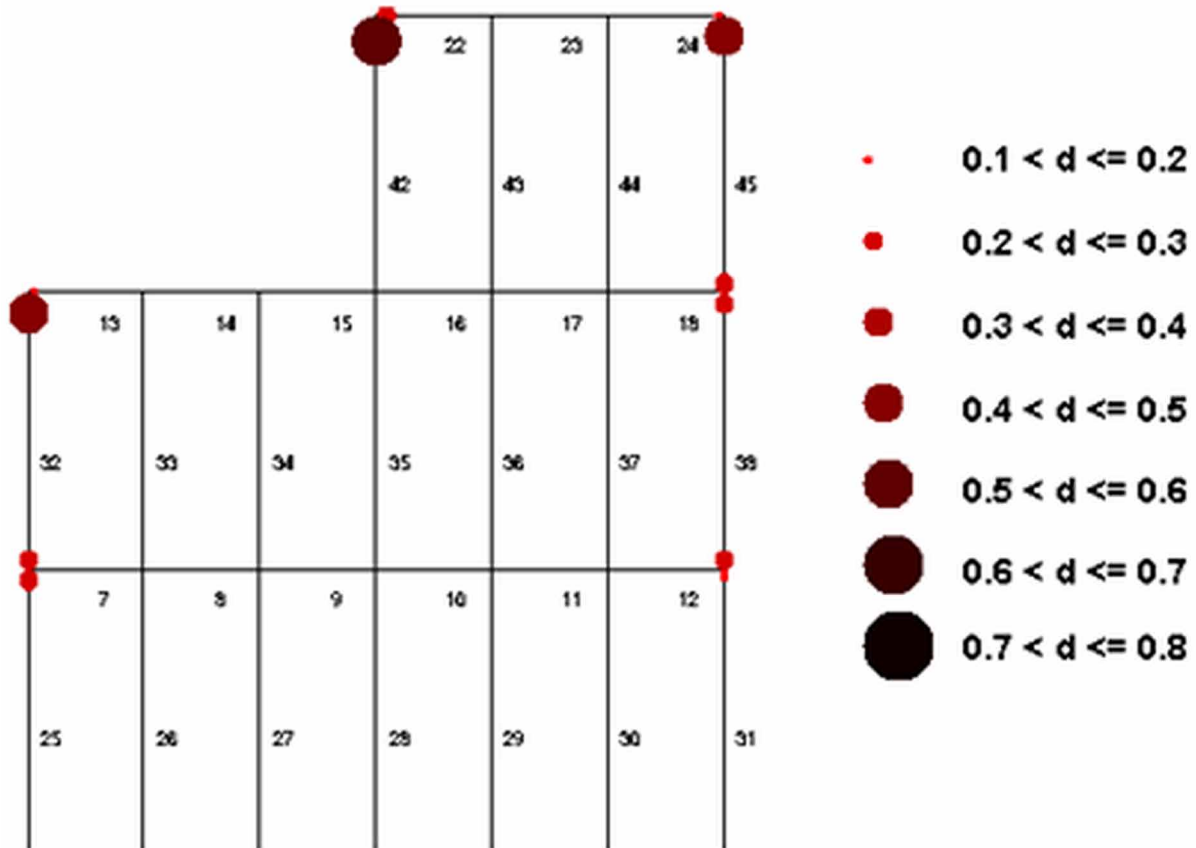


Figure 66. Raimundo Martínez Centeno high school, collapsed during Cariaco Earthquake (Venezuela) in 1997



is a plot of the maximum value of damage for beams and columns as a function of PGA. Thus, this curve is the link between the two tables; through dynamic capacity curve, it is possible to establish what will be the final state of a frame for a given loading and vice versa.

## **Industrial Applications**

In order to obtain the dynamic capacity curve some computational tool is needed. Ideally, the one developed through the sequence of projects that were suggested in the book. Alternatively, a program named Portal of Damage can be used.

## **REFERENCES**

Boore, D. M. (2003). Simulation of ground motion using the stochastic method. *Pure and Applied Geophysics*, 60(3), 635–676. doi:10.1007/PL00012553

Clough, R. W., & Penzien, J. (1975). *Dynamics of structures*. Academic Press.

Fenton, G. A., & Venmarcke, E. H. (1990). Simulation of random fields of earthquake ground vibrations. *Journal of Engineering Mechanics*, 116(8), 1733–1749. doi:10.1061/(ASCE)0733-9399(1990)116:8(1733)

Marante, M. E., Suárez, L., Quero, A., Redondo, J., Vera, B., & Uzcátegui, M. et al. (2005). Portal of damage: A web-based finite element program for the analysis of framed structures subjected to overloads. *Advances in Engineering Software*, 36(5), 346–358. doi:10.1016/j.advengsoft.2004.06.017

Newmark, N. M., & Hall, W. J. (1982). Earthquake spectra and design. *Earth System Dynamics*, 1.

Rojas, R., Vera, B., Picón, R., Marante, M. E., & Flórez-López, J. (2008). Computation of retrofitting of vulnerable RC structures using damage mechanics and experimental analyses. In *Proceedings of 4th International Conference on Structural Defects and Repair* (pp. 25-28). Aveiro, Portugal: Academic Press.

Vanmarcke, E. H., Cornell, C. A., Gasparini, D. A., & Hou, S. N. (1990). *SIMQKE-I: Simulation of earthquake ground motions*. Cambridge, MA: MIT Press.



## Chapter 14

# Lumped Damage Mechanics: Tubular Steel Structures

### ABSTRACT

*This chapter, the last of the book, describes how to use the concepts of damage mechanics for the description of the behavior of tubular frame structures. In the first section of this chapter, the concept of damage of a plastic hinge is used to describe local buckling evolution. It also shows that the technique of the variation of the elastic stiffness, described in Chapter 10, can be utilized to measure the degree of local buckling in the metallic elements. This first section is restricted to the analysis of frames subjected to mono-sign loadings. The second one deals with the behavior of the structures under general loadings in the plane. It shows that in the case of cyclic loadings with reversal of sign a new phenomenon appears: “counter-buckling”; in metaphoric terms, counter-buckling can be described as “ironing the wrinkles.” In this section, this effect is characterized and modeled introducing the concept of “local buckling driving rotation.” Finally, in the third section of the chapter, the analysis of tridimensional frames is addressed.*

### 14.1 LOCAL BUCKLING DAMAGE MODEL FOR PLANAR MONO-SIGN LOADINGS

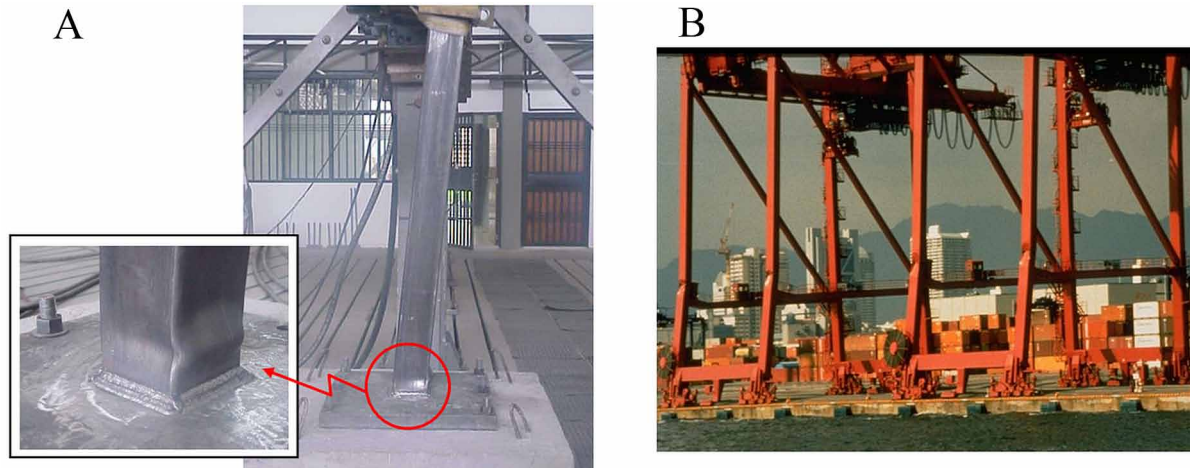
The steel frame structure is the other major alternative in the civil engineering construction industry. During test on both, tubular steel elements and RC frame members, the same phenomena: degradation of stiffness and strength are observed when the specimens are subjected to overloads; however, their fundamental causes are radically different in each case. As it has been discussed at length in the previous chapters, cracking is the phenomenon responsible for these effects in reinforced concrete structures; this is not the case of steel structures. Tubular steel elements are usually built with relatively thin walls; overloads on these components generate the appearance of small waves or wrinkles (see Figure 1a) that do not disappear after unloading the element; this phenomenon is called local buckling. For instance, Figure 1b shows the damage in a crane of the port of Kobe resulting from the 1995 great earthquake. In the picture it can be clearly appreciated the presence of local buckling in its columns.

DOI: 10.4018/978-1-4666-6379-4.ch014

## Lumped Damage Mechanics

Figure 1. a) Local buckling in a tubular steel member of square cross-section b) Buckled crane legs after the 1995 Kobe earthquake Port Crane legs buckled due to soil spreading (UCB-EERC 1995/01) Courtesy of NISEE-PEER, University of California, Berkeley

14.1b Crane legs buckled due to spreading. (1995). Kobe Geotechnical Collection, Japan. University of California, EERC 1995/01 Aug. 1995: 39. Retrieved February 28, 2014 from <http://nisee.berkeley.edu/elibrary/Image/K0127>.



Therefore, it must be concluded that the use of the Griffith criterion and the concepts of fracture mechanics should not be used in the modeling of the behavior of tubular frame members since crack propagation is not the main cause of structural degradation in this case. However, some of the other ideas described in chapter 9 still apply.

### 14.1.1 Experimental Analysis of a Steel Tubular Element

Figure 2 shows the setup of a test on a tube of circular cross-section subjected to a mono-sign loading. The structural response of the element is presented in Figure 3, first in the form of a curve of deflection against force (Figure 3a). From this plot, the curve of plastic deflection vs. stiffness presented in Figure 3b can be built.

The curve 14.3a can be divided into three stages. The first one corresponds to an elastic phase of the behavior. In this stage, the behavior is fully reversible and permanent deflections cannot be appreciated after unloading. If a metallic framed structure is not loaded beyond this phase, the models and techniques described in chapters 3 and 4 are sufficient for the analysis of the structure.

In the second stage, the element exhibits a behavior that can be characterized as elasto-plastic with hardening. Plastic hardening fully develops and large plastic deformations evolve under approximately constant forces. It can be noticed in Figure 3b, that the stiffness of the element is still constant in this phase. Structures that enter this second stage can be modeled using the methods presented in chapters 6 to 8.

The third phase is characterized by significant degradation of the stiffness and strength. The beginning of this last stage is triggered by the appearance of local buckling in the plastic hinge region. The degradation of these mechanical properties increases with the evolution of local buckling. For instance, in the structure shown in the Figure 1b, the columns of the frame have gone through all those phases and their mechanical properties were severely compromised after the seismic event. It is clear that the theory of elasto-plastic frames cannot be used to simulate the behavior of such a structure.

Figure 2. Test on a tube of circular cross-section a) Set up of the test b) Deflection history

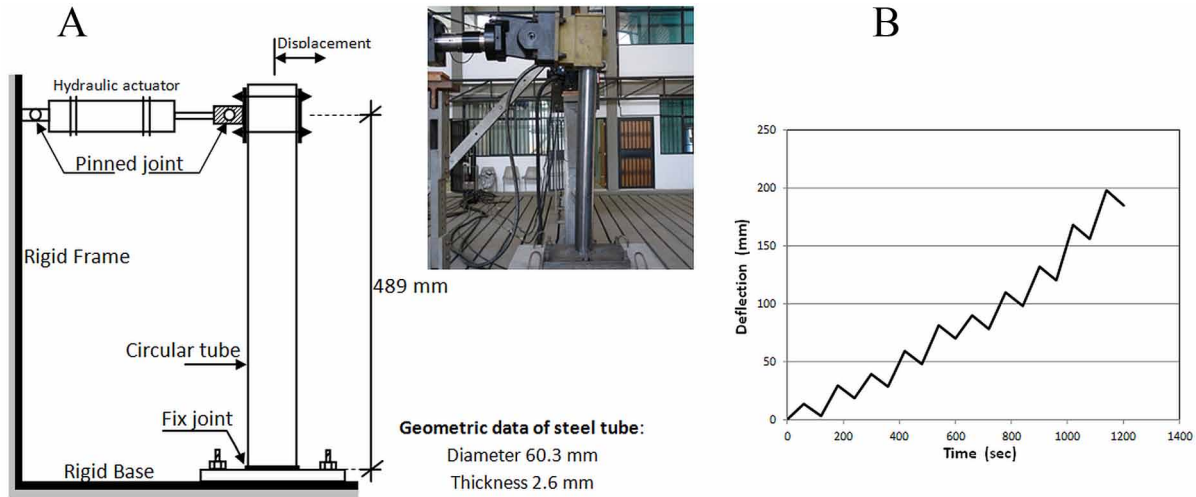
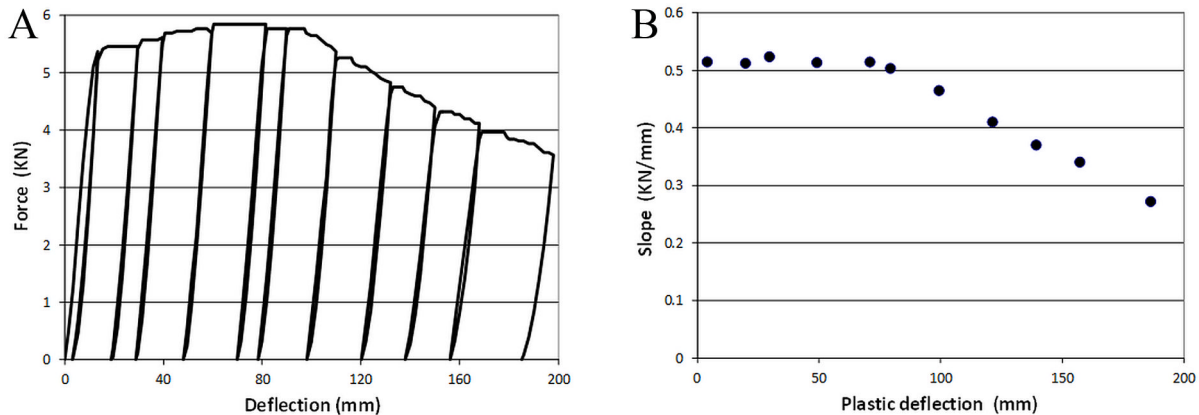


Figure 3. a) Deflection vs. force in the test of Figure 2 b) Plastic deflection vs. Slope



It is important to note that not all metallic tubes are able to develop the three stages in the case of overloads. Those that do, are said to have a “compact cross-section”. If the walls of the tube are too thin with respect to the dimensions of the cross-section, the plastic phase without local buckling is not fully developed or not present at all and local buckling appears more rapidly. Of course, elements with non-compact cross-sections should not be used in the principal elements of any structure; but does not necessarily mean that this is never done.

### 14.1.2 Elasticity Law of a Tubular Frame Element with Local Buckling

The fact that local buckling reduces the elastic limit of the tubular elements (see Figure 3a) as well as the slope of the loading/reloading branches (see Figure 3b) suggests that the concept of plastic hinge with damage can be used for its modeling. Therefore, a tubular frame element can be represented using

### Lumped Damage Mechanics

the same lumped damage model that is described in section 10.1; however, in this case, the damage array  $\{\mathbf{D}\}_b = (d_i, d_j)$  measures the degree of local buckling at the ends of the tube instead of crack densities as illustrated in Figure 4.

Thus, the elasticity law presented in section 10.1, in any of its forms (Equations 10.1.4 or 10.1.5-6), can also be used in this case:

$$\{\Phi - \Phi^p\}_b = [\mathbf{F}(\mathbf{D})]_b \{\mathbf{M}\}_b + \{\Phi^0\}_b; [\mathbf{F}(\mathbf{D})] = \begin{bmatrix} \frac{L_b}{3(1-d_i)EI_b} & -\frac{L_b}{6EI_b} & 0 \\ -\frac{L_b}{6EI_b} & \frac{L_b}{3(1-d_i)EI_b} & 0 \\ 0 & 0 & \frac{L_b}{AE_b} \end{bmatrix};$$

or

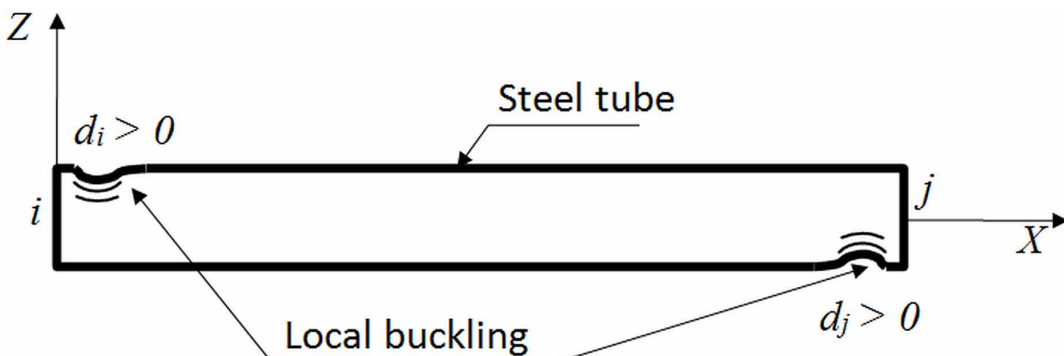
$$\{\mathbf{M}\}_b = [\mathbf{E}(\mathbf{D})]_b \{\Phi - \Phi^p\}_b + \{\mathbf{M}^0(\mathbf{D})\}_b$$

$$[\mathbf{E}(\mathbf{D})]_b = k \begin{bmatrix} 12(1-d_i) & 6(1-d_i)(1-d_j) & 0 \\ 6(1-d_i)(1-d_j) & 12(1-d_j) & 0 \\ 0 & 0 & \frac{EA_b}{kL_b} \end{bmatrix}; k = \frac{1}{4 - (1-d_i)(1-d_j)} \frac{EI_b}{L_b};$$

$$\{\mathbf{M}^0(\mathbf{D})\}_b = -[\mathbf{E}(\mathbf{D})]_b \{\Phi^0\}_b \quad (14.1.1)$$

The matrix  $\{\Phi^0\}_b$  has, again, the initial deformations defined in Table 3 of Chapter 3.

Figure 4. Characterization of local buckling in a tubular element using the lumped damage model



### 14.1.3 Yield Function of a Plastic Hinge with Local Buckling

The second stage of the behavior, assuming that the section is compact, can be described using a yield function with perfect plasticity (Equation 6.2.7) or nonlinear plastic hardening; that is Equations 6.3.1, 6.3.3 and 6.3.5 or 6.3.6 if axial deformations are neglected. If they are not, the perfectly plastic model is defined by the expression (6.4.5).

The third phase, with strength degradation, can be represented assuming again the hypothesis of equivalence in deformations. For instance, the plastic deformation evolution law derived from the yield function (6.2.7) is:

$$\begin{cases} d\phi_i^p = 0 \text{ if } f_i(m_i) < 0 \text{ (hinge } i \text{ locked)} \\ f_i(m_i) = 0 \text{ if } d\phi_i^p \neq 0 \text{ (hinge } i \text{ active)} \end{cases}; f_i = \left| \frac{m_i}{1-d_i} \right| - M_u \leq 0;$$

$$\delta_p = 0$$

$$\begin{cases} d\phi_j^p = 0 \text{ if } f_j(m_j) < 0 \text{ (hinge } j \text{ locked)} \\ f_j(m_j) = 0 \text{ if } d\phi_j^p \neq 0 \text{ (hinge } j \text{ active)} \end{cases}; f_j = \left| \frac{m_j}{1-d_j} \right| - M_u \leq 0 \quad (14.1.2)$$

where  $M_u$  is, as usual, the ultimate moment of the cross-section as defined in chapter 6. If the more sophisticated model with plastic hardening is chosen, the yield functions become:

$$f_i = \left| \frac{m_i}{1-d_i} \right| - \left( M_p + (M_u - M_p)(1 - e^{-\alpha p_i}) \right) \leq 0$$

$$f_j = \left| \frac{m_j}{1-d_j} \right| - \left( M_p + (M_u - M_p)(1 - e^{-\alpha p_j}) \right) \leq 0 \quad (14.1.3)$$

where  $M_p$  is the first plastic moment and  $\alpha$  is the plastic hardening parameter as defined in chapter 6. The terms  $p_i$  and  $p_j$  represent in this case the accumulated plastic deformations:

$$dp_i = |d\phi_i^p| \text{ and } dp_j = |d\phi_j^p| \quad (14.1.4)$$

The plastic deformation evolution laws remain the same.

Plastic elongations can be included in the model if desired, by introducing the following yield functions:

$$f_i = \left( \frac{n}{N_u} \right)^2 + \left( \frac{m_i}{M_u(1-d_i)} \right)^2 - 1; f_j = \left( \frac{n}{N_u} \right)^2 + \left( \frac{m_j}{M_u(1-d_j)} \right)^2 - 1 \quad (14.1.5)$$

### Lumped Damage Mechanics

With the normality rules:

$$d\phi_i^p = d\lambda_i \frac{\partial f_i}{\partial m_i}; d\phi_j^p = d\lambda_j \frac{\partial f_j}{\partial m_j}; d\delta_p = d\lambda_i \frac{\partial f_i}{\partial n} + d\lambda_j \frac{\partial f_j}{\partial n} \quad (14.1.6)$$

and the plastic multipliers evolution laws:

$$\begin{cases} d\lambda_i = 0 \text{ if } f_i < 0 \text{ (hinge } i \text{ is locked)} \\ f_i = 0 \text{ if } d\lambda_i \neq 0 \text{ (hinge } i \text{ is active)} \end{cases};$$

$$\begin{cases} d\lambda_j = 0 \text{ if } f_j < 0 \text{ (hinge } j \text{ is locked)} \\ f_j = 0 \text{ if } d\lambda_j \neq 0 \text{ (hinge } j \text{ is active)} \end{cases} \quad (14.1.7)$$

$\lambda_i$  and  $\lambda_j$  are the plastic multipliers of hinges  $i$  and  $j$ .

Notice that in the last model, the influence of local buckling on the permanent elongation is not fully taken into account; thus it should be used only when axial loads are relatively small with respect to the bending moments.

#### 14.1.4 Local Buckling Evolution Law

The experimental procedure to measure damage in a hinge presented in section 10.3.1 can also be used to quantify the degree of local buckling in a tubular element. The curve of plastic rotation vs. local buckling damage corresponding to the test of Figure 2 can be built from the data presented in the Figure 3a and is shown in Figure 5; in that curve, the variables are computed as:

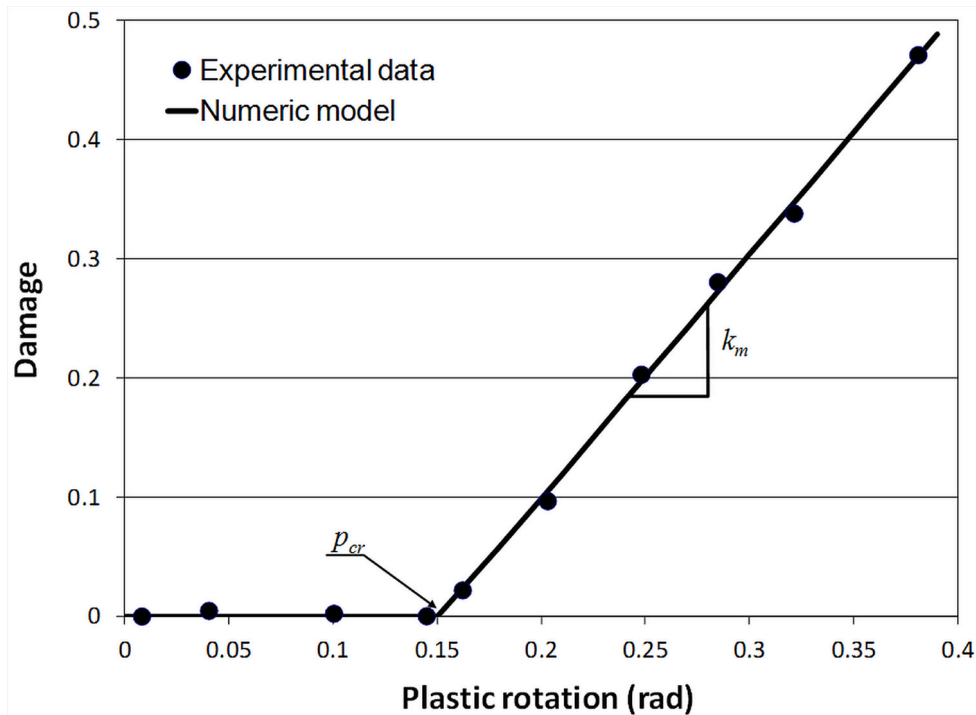
$$\phi^p = \frac{t_p}{L}; d = 1 - \frac{Z(d)}{Z_0} \quad (14.1.8)$$

As usual,  $\phi^p$  is the plastic rotation,  $t_p$  the plastic deflection,  $Z_0$  is the initial slope (without local buckling) and  $Z(d)$  the damaged ones.

The simplest expression describing these results is:

$$d_i = \kappa_m \langle p_i - p_{cr} \rangle \quad (14.1.9)$$

Figure 5. Plastic rotation vs. local buckling damage in the test of Figure 2



where  $p_{cr}$  is the critical plastic rotation that initiates local buckling and  $\kappa_m$  is the slope of the line as indicated in Figure 5. Notice that this evolution law is similar to the one proposed for ductile materials in the uniaxial case discussed in section 9.2.5.

The parameters  $p_{cr}$  and  $\kappa_m$  can be identified from the moment vs. rotation graph as it is shown in Figure 6.

### 14.1.5 Numerical Simulations

The model introduced in this section is defined by the elasticity law (14.1.1), the plastic deformation evolution law (14.1.2) with the yield functions (14.1.2-7) and the local buckling evolution law (14.1.9). The test of Figure 2 was simulated with the model using the parameter values  $p_{cr} = 0.152 \text{ rad}$  and  $\kappa = 2.05$  obtained in the former section. The experimental and numerical deflection vs. force curves are shown in Figure 7.

The test that is shown in Figure 8a was simulated using the described model too. The element has a 120 mm square cross-section, 4 mm thickness and is subjected to the loading path presented in Figure 8b. The model parameters  $p_{cr}$  and  $\kappa$  were identified from the rotation vs. bending moment curve as it is shown in Figure 9.

The experimental and numerical Displacement vs. force curves are shown in Figure 10.

In Figure 10b are indicated the damage values at the beginning of some elastic unloading.

Figure 6. Parameter determination in test of Figure 2

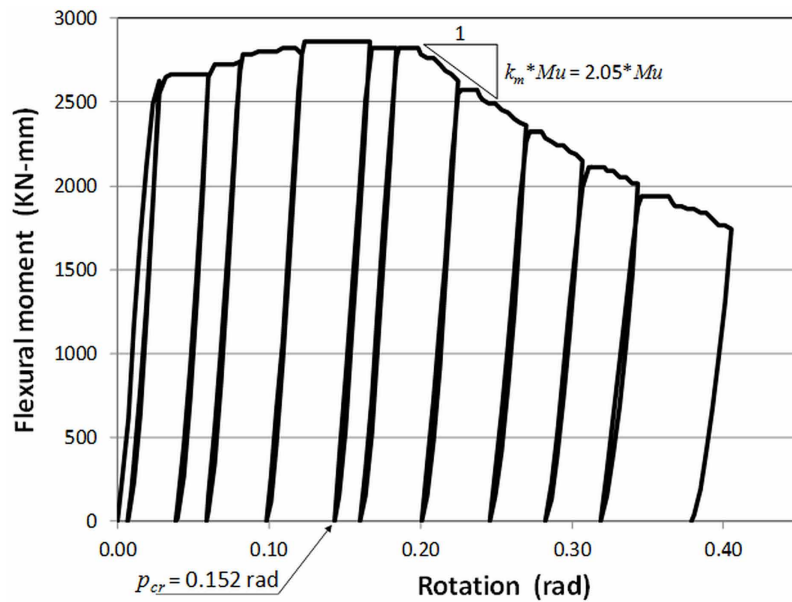
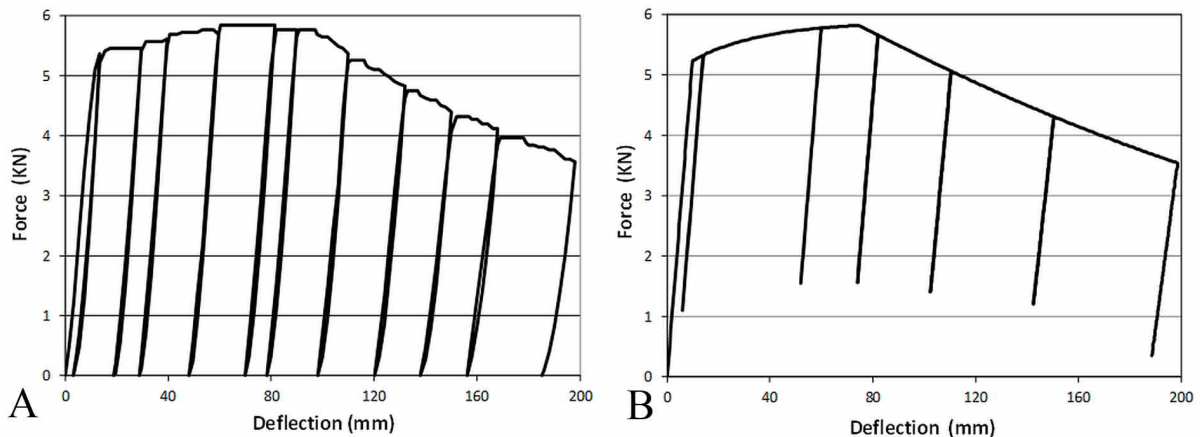


Figure 7. Deflection vs. force curves of the test of Figure 2 a) Experimental b) Numerical simulation



## 14.2 THE COUNTER-BUCKLING EFFECT AND A MODEL FOR GENERAL PLANAR LOADINGS

### 14.2.1 Experimental Analysis of the Behavior of Steel Tubes Subjected to Cyclic Loading

Consider the same experimental test presented in Figure 2. If a cyclic loading is applied (see Figure 11a), the response of the element in a curve of deflection vs. force is the one shown in Figure 11b. For large values of displacements, the local buckling phenomenon appears again but this time in a more complex form. As it can be appreciated in Figure 12 two distinct “wrinkled” zones emerge in the plastic hinge zone.



Figure 8. Test on a tube of square cross-section a) Set up of the test b) Deflection history

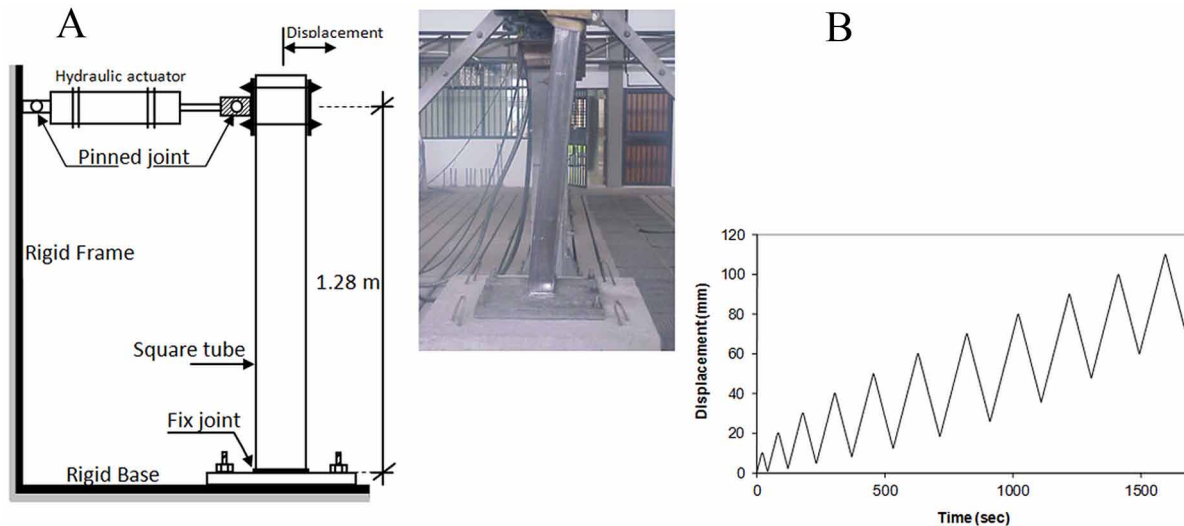
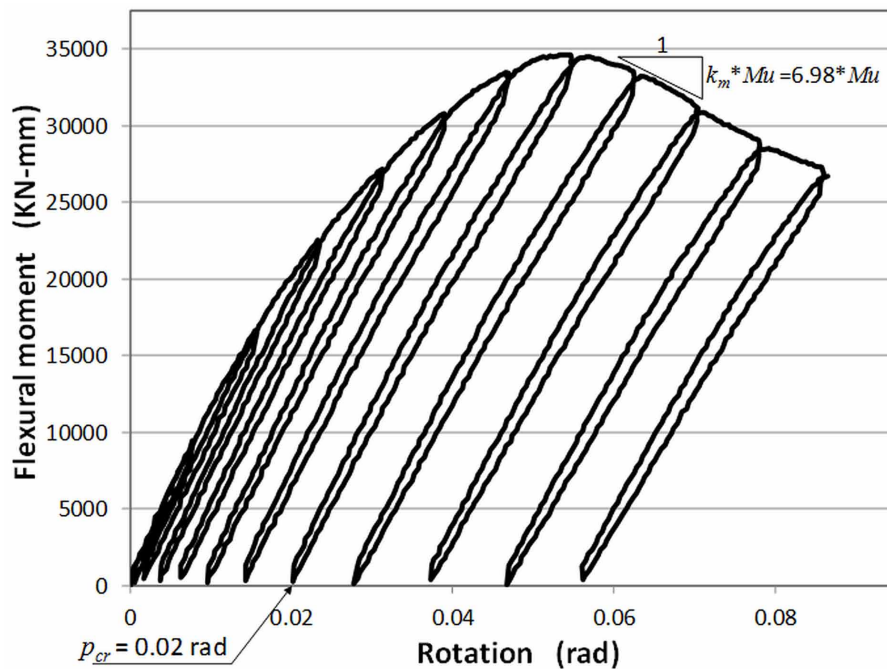


Figure 9. Parameter determination in test of Figure 8



One of the wrinkled surfaces on the plastic hinge zone is produced by positive bending moments; while the other, on the opposite face, is the result of the action of negative bending moments; those wrinkled regions will be called, respectively, “positive local buckling” and “negative local buckling”.

Figure 13 shows only the isolated unloading branches of the graph of Figure 11b; this is a plot of the absolute value of deflection vs. the absolute value of force during the unloading of the tube from positive and negative forces.

## Lumped Damage Mechanics

Figure 10. Displacement vs. force curves in the test of Figure 8 a) Experimental b) Numerical simulation

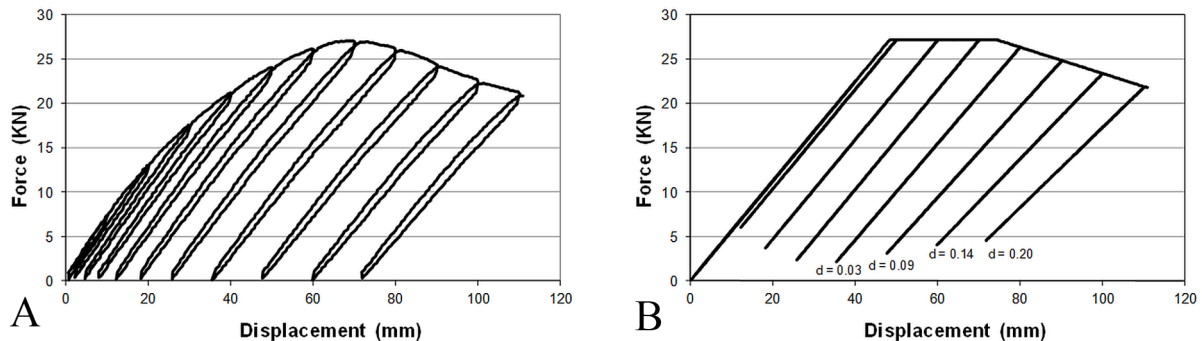
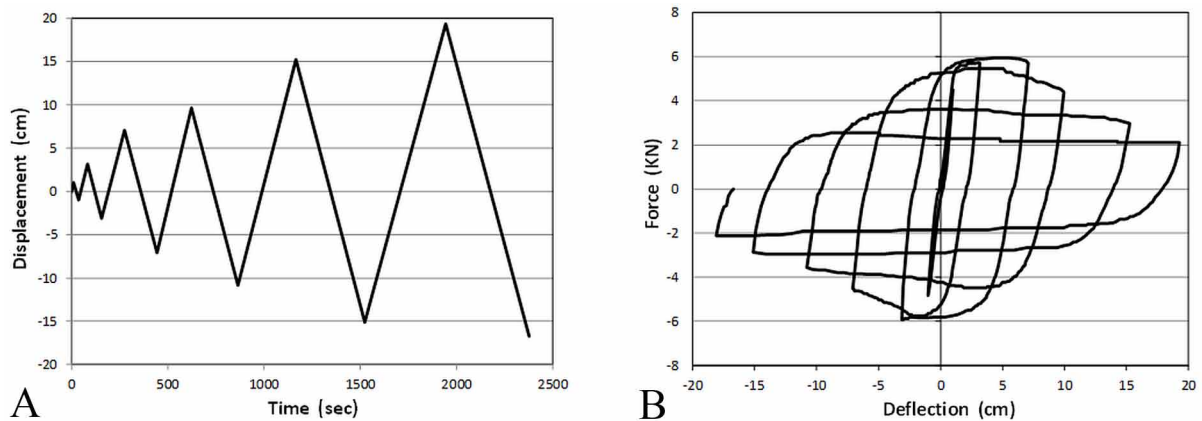


Figure 11. a) History of displacements in a cyclic test b) Deflection vs. force in a cyclic test



The unloading branches under positive forces are called “positive”; if the force is negative the unloading will be called “negative”. The unloading curves are labeled by pairs. One curve of the pair corresponds to a positive unloading and the other to a negative one; in this way the elastic stiffness of the tube under positive and negative forces can be compared.

Local buckling in the tube appeared after the occurrence of the unloading branches marked as number 2; the progressive loss of stiffness can be appreciated in the remaining pairs. On the other hand, notice that the slope is the same in both branches of each pair regardless of the sign of the unloading. However, physically, the phenomenon is not completely symmetric; i.e. positive local buckling appears or grows first and the negative local buckling does the same but latter in the cycle. Thus, the positive unloading branches occur with only the maximum positive local buckling of the cycle while each negative unloading happens with both maximum degrees of local buckling, positive as well as negative. Therefore, it appears that negative local buckling has little effects on the stiffness under positive forces. This observation allows concluding that the unilateral hypothesis presented in chapter 9 (section 9.2.6) and that is used for the modeling of the behavior of reinforced concrete elements (chapter 12) can also be utilized in the case of steel tubes with local buckling.

Figure 12. Local buckling in a cyclic test

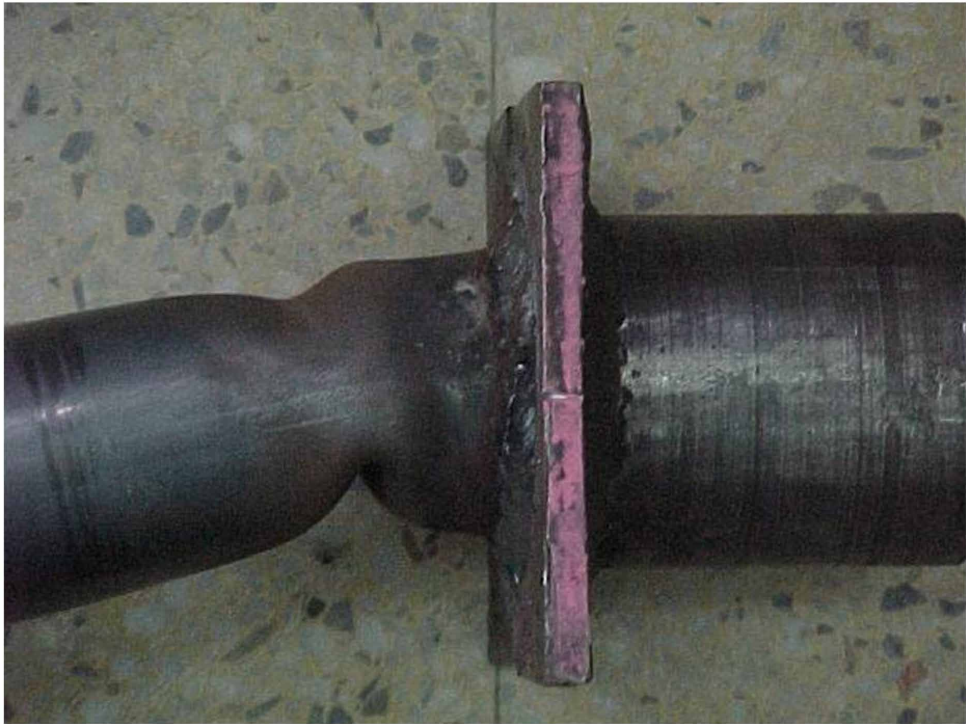
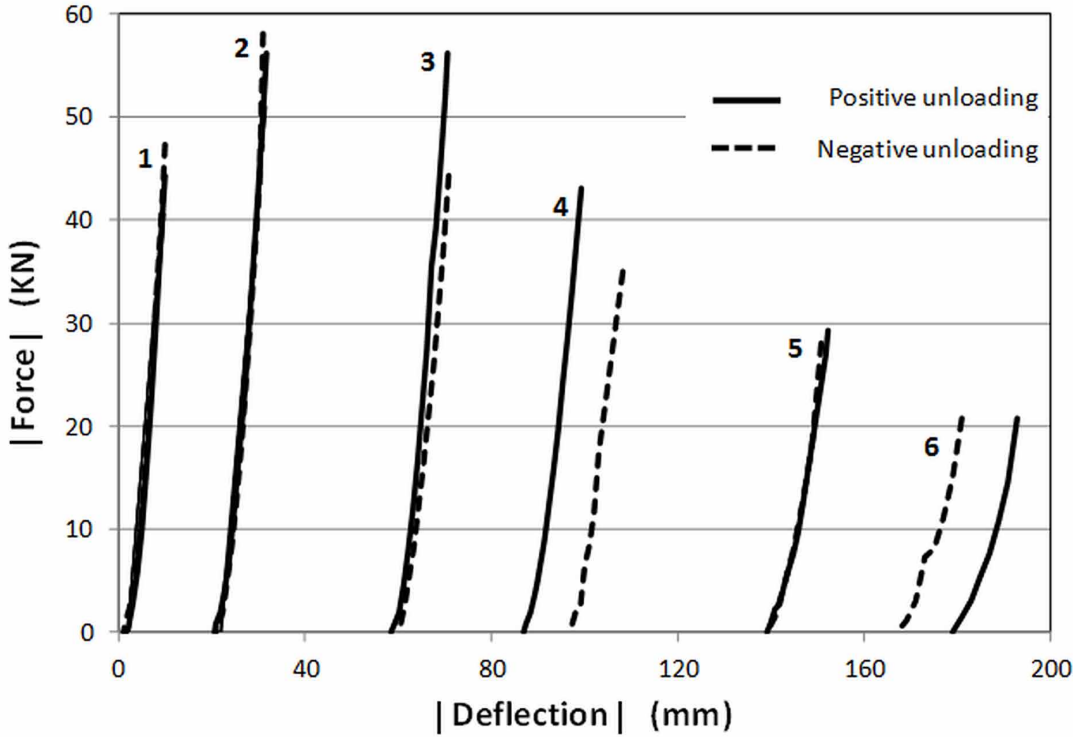


Figure 13. Absolute value of force against the absolute value of deflection during the unloading branches in a cyclic test



### 14.2.2 Unilateral Elasticity Law for Steel Frame Elements with Hollow Cross-Sections

The experimental results described in the previous section show that the unilateral elasticity law can be used to describe the behavior of steel tubes. Thus, two sets of local buckling damage  $(\mathbf{D}^+)_b = (d_i^+, d_j^+)$  and  $(\mathbf{D}^-)_b = (d_i^-, d_j^-)$  are introduced; they characterize the state of local buckling in the element as is represented in Figure 14.

Then, the unilateral elasticity law of a frame element of hollow cross-section is:

$$\{\Phi\}_b - \{\Phi^p\}_b = [\mathbf{F}(\mathbf{D}^+)] \langle \mathbf{M} \rangle_b^+ + [\mathbf{F}(\mathbf{D}^-)] \langle \mathbf{M} \rangle_b^- + \{\Phi^0\}_b$$

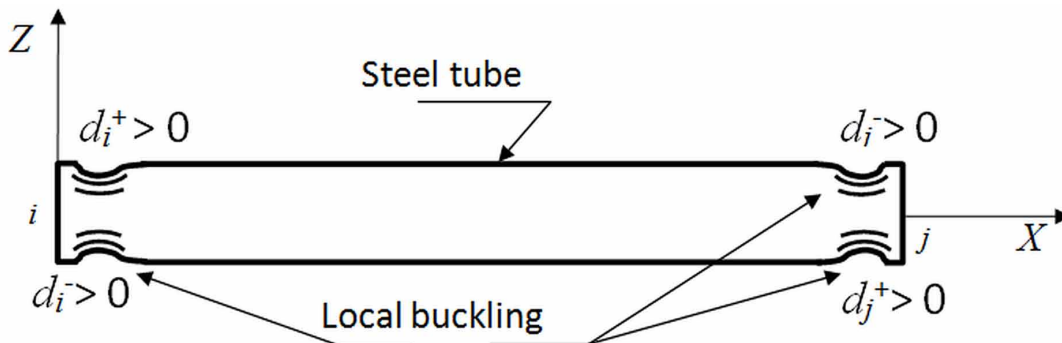
$$[\mathbf{F}(\mathbf{D}^{+/-})] = \begin{bmatrix} \frac{L_b}{3EI_b (1 - d_i^{+/-})} & -\frac{L_b}{6EI_b} & 0 \\ -\frac{L_b}{6EI_b} & \frac{L_b}{3EI_b (1 - d_j^{+/-})} & 0 \\ 0 & 0 & \frac{L_b}{EA_b} \end{bmatrix}; \quad (14.2.1)$$

$\{\Phi\}_b$  and  $\{\Phi^p\}_b$  represent, respectively, the deformation and plastic deformation matrices in the planar case, of course; the terms  $\langle \mathbf{M} \rangle_b^+$  and  $\langle \mathbf{M} \rangle_b^-$  correspond to the positive and negative parts of the stress matrix, such as is defined in chapter 12.

### 14.2.3 Unilateral Yield Function

In order to evaluate the validity of the unilateral hypothesis on the yield function, a different type of test is carried out. Again, the same set up of Figure 2 is used; but this time the loading is not mono-sign or cyclic but a combination of both. It consists first in a mono-sign loading that produces a significant

Figure 14. Representation of the local buckling state in tubular frame element using damage variables



amount of positive local buckling; then the load is reversed so the negative local buckling is achieved; the test is finished with a cyclic loading. This kind of loading is called “mixed”. The results of this mixed test on a tube of circular cross-section are presented in Figure 15.

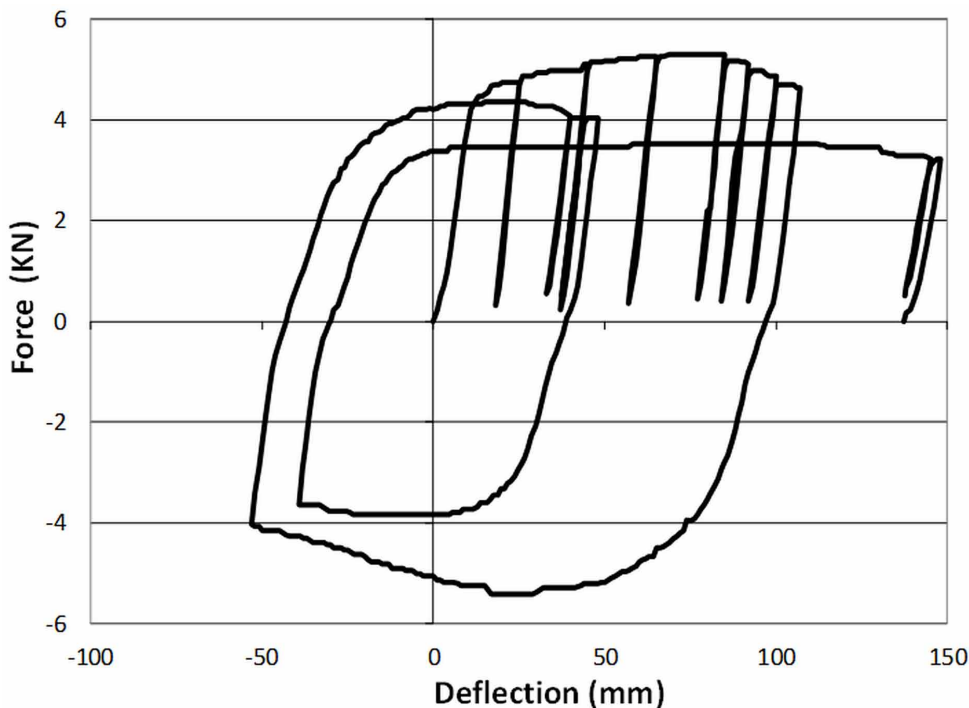
Notice that the value of the force corresponding to the formation of positive local buckling (the first one) is 5.30 KN. Then, the loading reversal produced negative local buckling with a value of 5.41 KN. Thus, when the negative local buckling occurs, positive local buckling had already been formed and yet the strength of the element has been not been modified. This result validates the hypothesis of unilaterality, not only at the level of stiffness degradation, but also for strength degradation. Of course, this assumption, as any other one, has a limit of validity. For very high values of local buckling there seems to be some degree of coupling between negative local buckling and positive strength and vice versa. Therefore, the corresponding unilateral yield function derived from (14.1.2) is:

$$f_i = \text{Max} \left( \frac{m_i}{1 - d_i^+} - M_u, -\frac{m_i}{1 - d_i^-} - M_u \right) \leq 0 \quad (14.2.2)$$

With, of course, the same plastic deformation evolution laws (14.1.2); i.e.:

$$\begin{cases} d\phi_i^p = 0 & \text{if } f_i < 0 \text{ (hinge } i \text{ locked)} \\ f_i = 0 & \text{if } d\phi_i^p \neq 0 \text{ (hinge } i \text{ active)} \end{cases};$$

*Figure 15. Deflection vs. force in a mixed test*



### Lumped Damage Mechanics

$$\delta_p = 0$$

$$\begin{cases} d\phi_j^p = 0 \text{ if } f_j < 0 \text{ (hinge } j \text{ locked)} \\ f_j = 0 \text{ if } d\phi_j^p \neq 0 \text{ (hinge } j \text{ active)} \end{cases} \quad (14.2.3)$$

The previous yield function neglects the plastic hardening and the Bauschinger effect observed during the cyclic tests (see Figure 12b); however for most practical applications, this model should give good-enough precision with engineering purposes. If desired, a more sophisticated, but much more complex, model can be obtained by using unilateral the yield functions with nonlinear isotropic and kinematic hardening described in chapter 7 (section 7.1.6):

$$f_i(m_i, p_i, x_i) = \text{Max} \left( \frac{m_i}{1 - d_i^+} - x_i - (M_p + Q(p_i)); -\frac{m_i}{1 - d_i^-} + x_i - (M_p + Q(p_i)) \right) \leq 0 \quad (14.2.4)$$

where  $x_i$  is the kinematic hardening term,  $Q(p_i)$  the isotropic hardening term and  $M_p$  the yield moment of the cross-section.

The plastic deformation evolution law (14.2.3) remains unchanged. All the options for the evolution of the hardening parameters  $x_i$  and  $Q(p_i)$  presented in section 7.1.6 can also be used unmodified; i.e. nonlinear Equations (7.1.15a and 7.1.16a) or multilinear (7.1.15b and 7.1.16b).

### 14.2.4 The Local Buckling Driving Rotation and the Local Buckling Evolution Laws

As aforementioned, during a cyclic loading occurs a new phenomenon denoted “counter-buckling” that can be described as follows: in the process of local buckling, a wrinkle is formed on the compression side of the tube in the plastic hinge region. When the load is reversed, that wrinkle is subjected to tension stresses; metaphorically speaking, it can be said that these tractions tend to “iron” the wrinkle. Of course, simultaneously the compression stresses resulting from the same bending moment create or increase the wrinkle on the opposite side of the plastic hinge zone. This “ironing” process on the tension side is the counter-buckling effect. Figure 12 shows the plastic hinge region of a tube with local buckling produced by positive and negative bending moments of the same intensity; in the figure both buckled surfaces can be appreciated; the result of the counter-buckling process on one of them, the upper part, can also be noticed.

In order to model the counter-buckling process, new variables, called local buckling driving rotations, are introduced. These variables are defined for positive and negative local buckling as:

$$\begin{aligned} db_i^+ &= \langle d\phi_i^p \rangle_+ + CBf \langle d\phi_i^p \rangle_- ; \text{ if } b_i^+ \geq 0; db_i^+ = 0 \text{ otherwise} \\ db_i^- &= -\langle d\phi_i^p \rangle_- - CBf \langle d\phi_i^p \rangle_+ ; \text{ if } b_i^- \geq 0; db_i^- = 0 \text{ otherwise} \end{aligned} \quad (14.2.5)$$

The term  $CBf$  is denoted counter-buckling factor and can take values between zero and one. A value of  $CBf$  that can be used in many applications is:

$$CBf = 0.7 \tag{14.2.6}$$

Notice that both local buckling driving rotations are always positive.  $b_i^+$  increases with positive increments of the plastic rotation and decreases with the negative one. The opposite occurs with  $b_i^-$ ; that is, it increases with negative increments of the plastic rotation and decreases with the positive one. The counter-buckling process occurs slower than the buckling one by a factor 0.7.

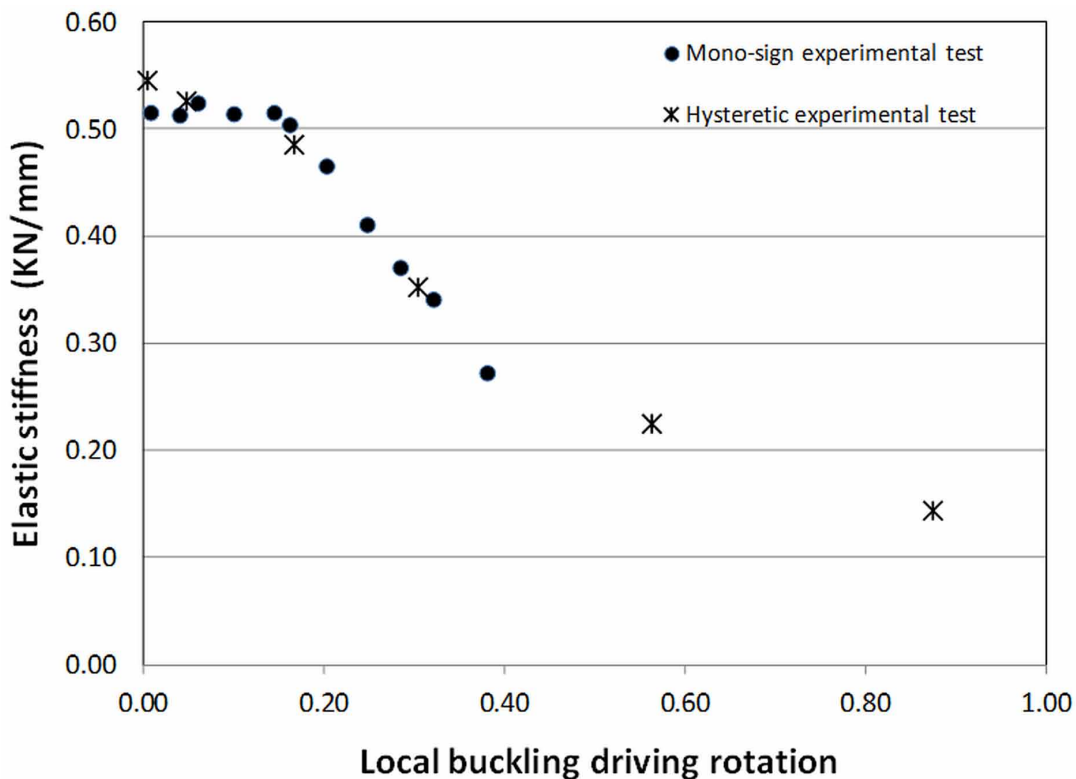
Notice also that in the case of a mono-sign loading, for example, a positive one, one of the local buckling driving rotation becomes the accumulated plastic rotation while the other is equal to zero:  $b_i^+ = p_i, b_i^- = 0$ .

Figure 16 shows a plot of the slope of the elastic unloading branches vs. the local buckling driving rotation in two tests, one corresponding to a mono-sign loading, the other to a cyclic one. Notice that, indeed, the loss of elastic stiffness can be correlated by the local buckling driving rotation.

Then, the local buckling evolution law can be written as:

$$\begin{cases} \Delta d_i^+ = 0 \text{ if } b_i^+ < R(d_i^+) \\ b_i^+ = R(d_i^+) \text{ if } \Delta d_i^+ > 0 \end{cases}, \begin{cases} \Delta d_i^- = 0 \text{ if } b_i^- < R(d_i^-) \\ b_i^- = R(d_i^-) \text{ if } \Delta d_i^- > 0 \end{cases} \tag{14.2.7}$$

Figure 16. Local buckling driving rotation, with  $CBf = 0.7$  vs. elastic stiffness



### Lumped Damage Mechanics

where  $R(d_i^{+/-})$  is, this time, the local buckling resistance function. This resistance function can be identified using the results presented in Figure 16 by computing the local buckling damage again as indicated in section 14.1.4. A graph of damage vs. driving rotation is presented in Figure 17.

From this graph, two expressions can be proposed for the local buckling resistance function. The simplest one generalizes the evolution law for mono-sign loadings presented in section 14.1.4 to the case of cyclic loading with counter-buckling:

$$R(d_{i/j}^{+/-}) = p_{cr} + \frac{d_{i/j}^{+/-}}{\kappa_m} \quad (14.2.8)$$

A more accurate alternative for large values of damage consists in the use of logarithmic function:

$$R(d_{i/j}^{+/-}) = p_{cr} - \frac{1}{\kappa_c} \ln \left( 1 - \frac{d_{i/j}^{+/-}}{0.9} \right) \quad (14.2.9)$$

Figure 18 shows the incorporation of the expressions (14.2.8) and (14.2.9) in the Figure 17 and 5. The parameters  $p_{cr}$  and  $\kappa_m$  were identified in section 14.1.4 and a value of  $\kappa_c = 2.60$  is estimated from the experimental results.

Figure 17. Local buckling damage vs. local buckling driving rotation

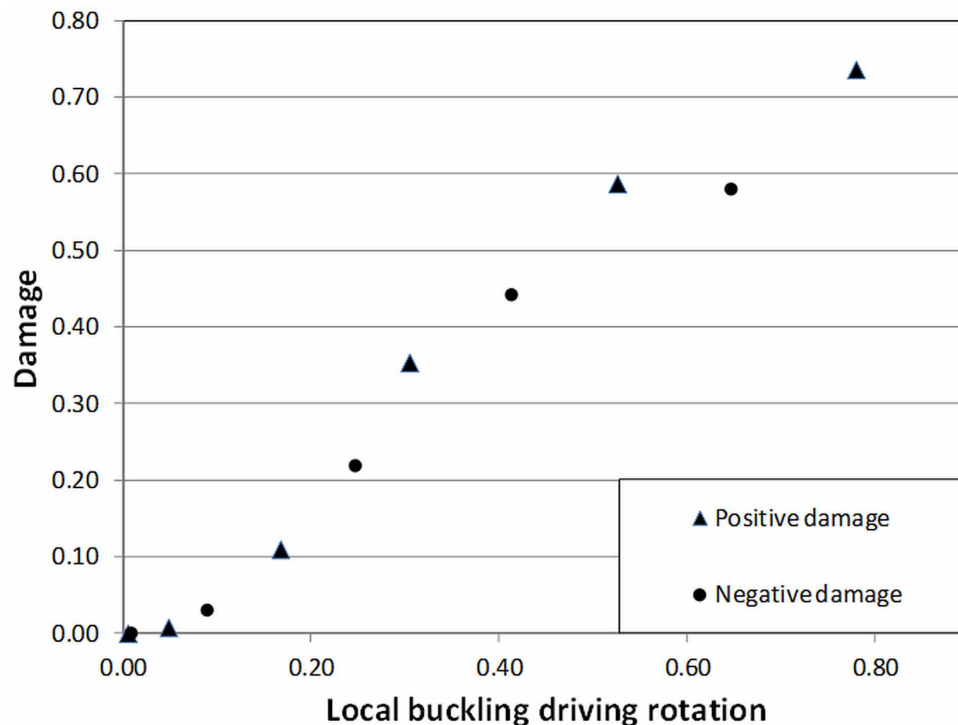
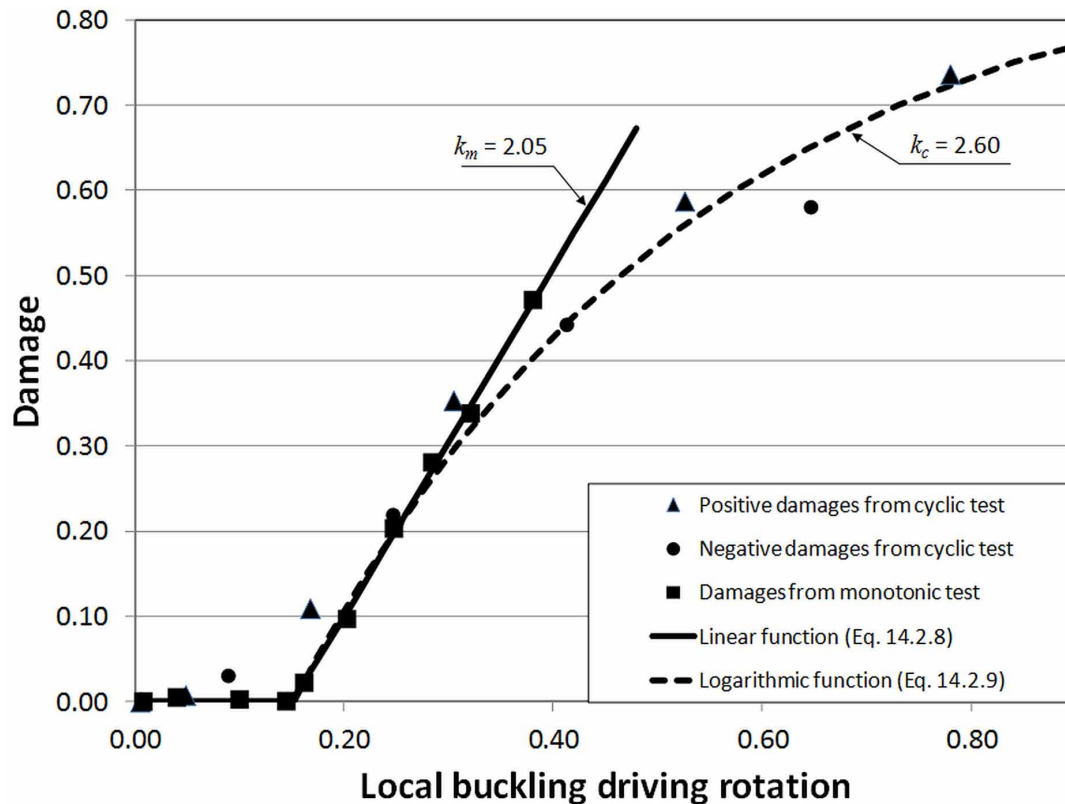




Figure 18. Local buckling resistance functions



In this figure it can be appreciated that the expression (14.2.9) represents in a better way the results for the cyclic test.

### 14.2.5 Numerical Simulations

In this section the numerical simulations corresponding to the cyclic test presented in Figure 11 and the mixed test of Figure 15 are presented. The experimental curves are shown again in order to facilitate the comparison of the results. In the first case, the curve deflection vs. force is shown in Figure 19 and for the second one, in Figure 20. The values of the constants used in these simulations are:  $p_{cr} = 0.152$  rad and  $\kappa_c = 2.60$ .

## 14.3 DAMAGE MODEL FOR TRIDIMENSIONAL STEEL FRAMES

### 14.3.1 Experimental Analysis of a Steel Tubular Element Subjected to Biaxial Loadings

Consider the experimental set up that is shown in Figure 21a. Notice that it is a tube fixed at its base but subjected to two perpendicular lateral forces. The specimens consisted in steel hollow structural elements

### Lumped Damage Mechanics

Figure 19. Deflection vs. force curves corresponding to a circular element subjected to the cyclic loading path of Figure 11a a) Experimental curve b) Numerical simulation

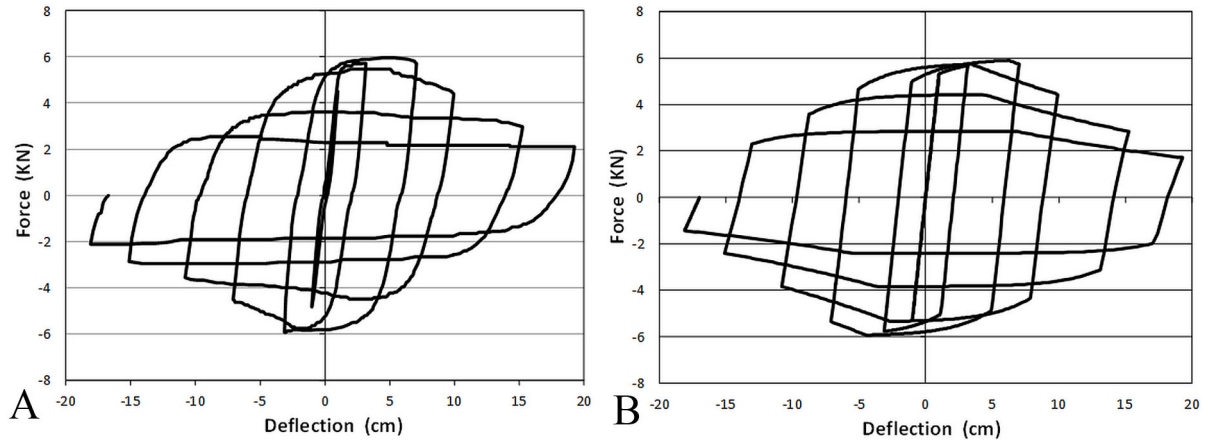
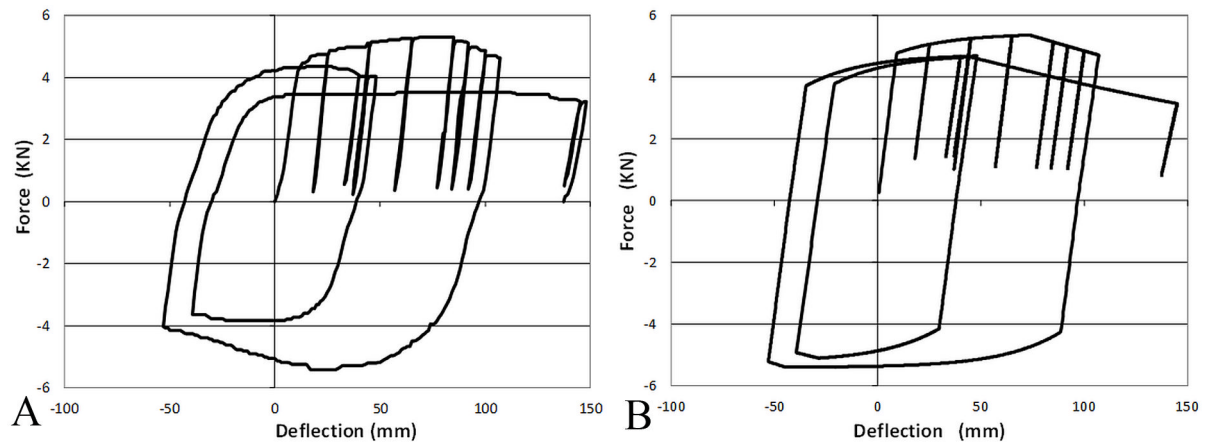


Figure 20. Deflection vs. force curves corresponding to a circular element subjected to mixed loading a) Experimental curve b) Numerical simulation



with 120 mm square cross-section, 4 mm thickness and a free length of 1.28 m. The loading history of controlled displacement for the test is presented in Figure 21b. Notice that this experiment has many aspects in common with the mono-sign test discussed in section 14.1.1, except that the displacements in the Y and Z directions are applied sequentially; at the end of each cycle the corresponding force is carried to zero.

The response of the element is presented in Figure 22 in the form of two graphs of displacement vs. force, one in each direction. The aspect of the plastic hinge region of the tube at the end of the test is shown in Figure 23.

Notice that again two distinct wrinkles can be appreciated in the element; but this time they are not in opposite faces of the tube, as in the cyclic test of section 14.2.1, but in two adjacent ones.

Figure 21. a) Experimental set up for biaxial loading b) Loading history

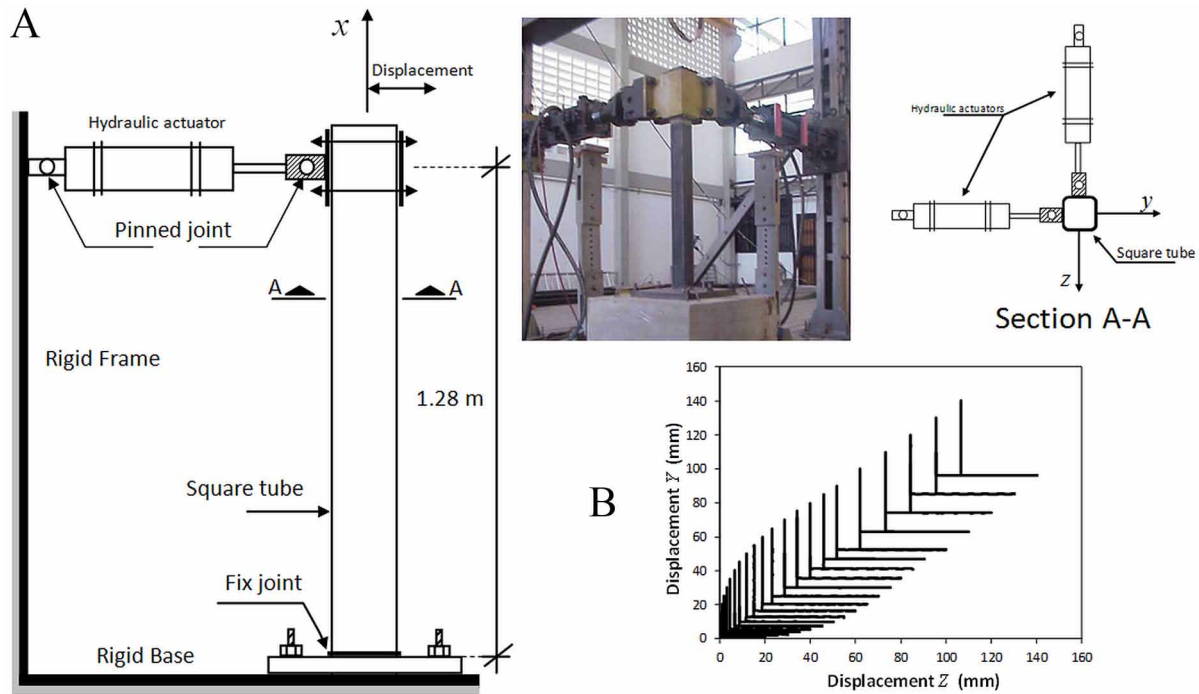
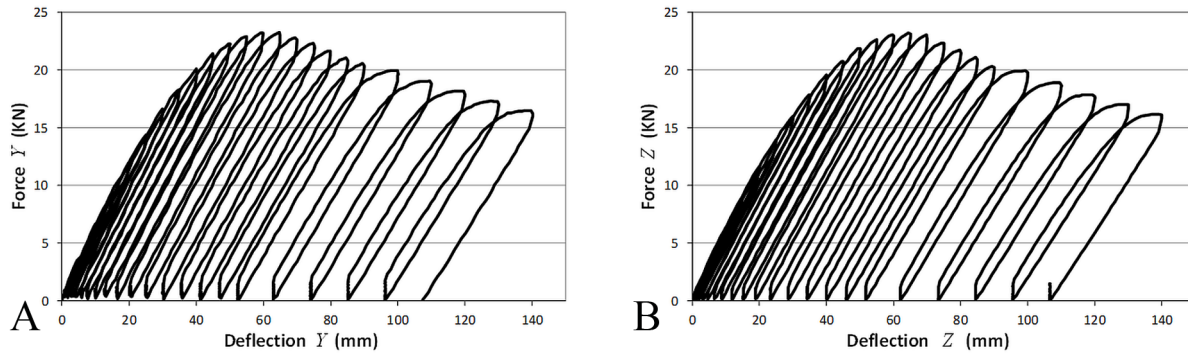


Figure 22. a) Deflection vs. force in the Y direction b) Deflection vs. force in the Z direction



### 14.3.2 Elasticity Law for a Tubular Element in Tridimensional Frame

In order to model a behavior such as the one described in the previous section it is necessary to consider the tridimensional case. The matrix of damage that was defined in section 14.1.2 is extended to  $(\mathbf{D})_b = (d_{iy}, d_{iz}, d_{jy}, d_{jz})$ ; where  $d_{iy}$  characterizes the local buckling resulting from the bending moment around the local axis  $Y$  at the end  $i$  of the element,  $d_{iz}$  is the local buckling damage due to bending moments around the local axis  $Z$  at the same extreme;  $d_{jy}$  and  $d_{jz}$  represent the two damage variables at the end  $j$  (see Figure 24).

*Figure 23. Local buckling in a biaxial test*



The elasticity law has the same general form (Equation 14.1.1) but now all its terms correspond to the tridimensional case:

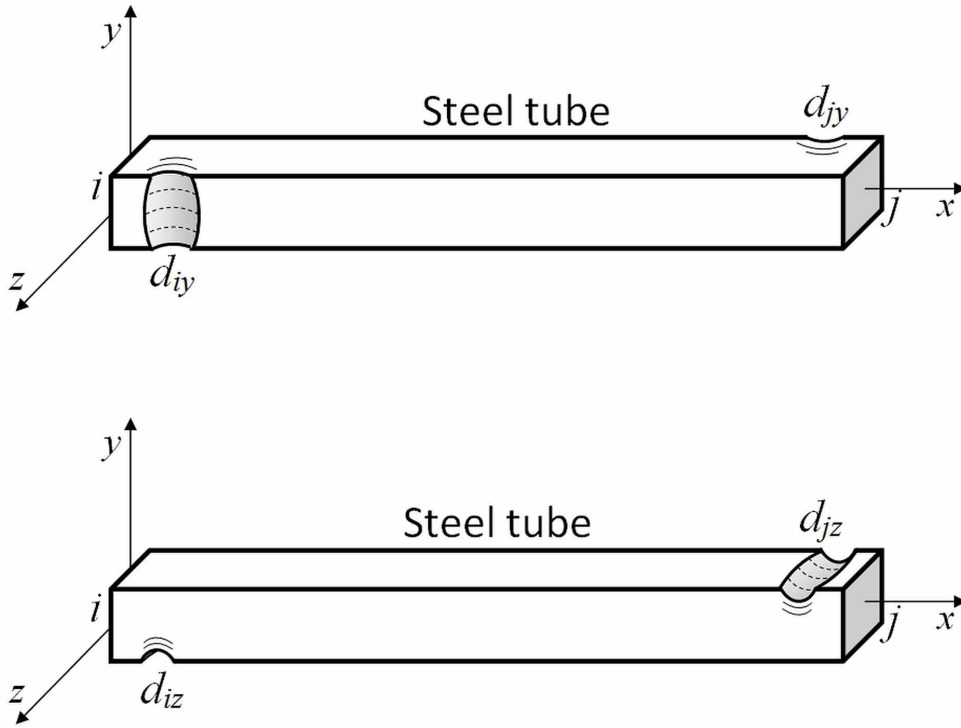
$$\{\Phi - \Phi^p\}_b = [\mathbf{F}(\mathbf{D})]_b \{\mathbf{M}\}_b + \{\Phi^0\}_b;$$

$$\{\Phi\}_b^t = (\phi_{iy}^b, \phi_{jy}^b, \delta_b, \phi_{iz}^b, \phi_{jz}^b, \phi_x^b); \{\mathbf{M}\}_b^t = (m_{iy}^b, m_{jy}^b, n_b, m_{iz}^b, m_{jz}^b, m_x^b) \quad (14.3.1)$$

$$\{\Phi^p\}_b^t = (\phi_{iy}^p, \phi_{jy}^p, \delta_p, \phi_{iz}^p, \phi_{jz}^p, \phi_x^p); \{\Phi^0\}_b^t = (\phi_{iy}^0, \phi_{jy}^0, 0, \phi_{iz}^p, \phi_{jz}^p, 0) \quad (14.3.2)$$

The initial deformations are computed by using twice Table 3 from Chapter 3. The flexibility matrix is given by:

Figure 24. Representation of local buckling in the biaxial case using damage variables



$$[\mathbf{F}(\mathbf{D})] = \begin{bmatrix} \frac{L_b}{3(1-d_{iy})EI_y^b} & \frac{-L_b}{6EI_y^b} & 0 & 0 & 0 & 0 \\ \frac{-L_b}{6EI_y^b} & \frac{L_b}{3(1-d_{jy})EI_y^b} & 0 & 0 & 0 & 0 \\ 0 & 0 & \frac{L_b}{AE_b} & 0 & 0 & 0 \\ 0 & 0 & 0 & \frac{L_b}{3(1-d_{iz})EI_z^b} & \frac{-L_b}{6EI_z^b} & 0 \\ 0 & 0 & 0 & \frac{-L_b}{6EI_z^b} & \frac{L_b}{3(1-d_{jz})EI_z^b} & 0 \\ 0 & 0 & 0 & 0 & 0 & \frac{L_b}{GJ_b} \end{bmatrix} \quad (14.3.3)$$

Notice that this elasticity law does not take into account unilateral behavior (or torsion damage). It is possible to inverse the relationship and to compute the elasticity matrix:

$$\{\mathbf{M}\}_b = [\mathbf{E}(\mathbf{D})]_b \{\Phi - \Phi^p\}_b + \{\mathbf{M}^0(\mathbf{D})\}_b \quad (14.3.4)$$

## Lumped Damage Mechanics

$$[\mathbf{E}(\mathbf{D})]_b = [\mathbf{F}(\mathbf{D})]_b^{-1} =$$

$$\begin{bmatrix} \frac{12EI_y^b}{L_b} \frac{(1-d_{iy})}{4-(1-d_{iy})(1-d_{jy})} & \frac{-6EI_y^b}{L_b} \frac{(1-d_{iy})(1-d_{jy})}{4-(1-d_{iy})(1-d_{jy})} & 0 & 0 & 0 & 0 \\ \frac{-6EI_y^b}{L_b} \frac{(1-d_{iy})(1-d_{jy})}{4-(1-d_{iy})(1-d_{jy})} & \frac{12EI_y^b}{L_b} \frac{(1-d_{iy})}{4-(1-d_{iy})(1-d_{jy})} & 0 & 0 & 0 & 0 \\ 0 & 0 & \frac{AE_b}{L_b} & 0 & 0 & 0 \\ 0 & 0 & 0 & \frac{12EI_z^b}{L_b} \frac{(1-d_{iz})}{4-(1-d_{iz})(1-d_{jz})} & \frac{-6EI_z^b}{L_b} \frac{(1-d_{iz})(1-d_{jz})}{4-(1-d_{iz})(1-d_{jz})} & 0 \\ 0 & 0 & 0 & \frac{-6EI_z^b}{L_b} \frac{(1-d_{iz})(1-d_{jz})}{4-(1-d_{iz})(1-d_{jz})} & \frac{12EI_z^b}{L_b} \frac{(1-d_{iz})}{4-(1-d_{iz})(1-d_{jz})} & 0 \\ 0 & 0 & 0 & 0 & 0 & \frac{GJ_b}{L_b} \end{bmatrix} \quad (14.3.5)$$

### 14.3.3 Yield Functions

The yield functions with damage can be obtained by using the hypothesis of equivalence in deformation and the expression introduced for biaxial plasticity (Equation 6.4.13) without damage:

$$f_{i/j} = \left( \frac{n}{N_u} \right)^{\nu_1} + \left( \frac{m_{iy/jy}}{M_{uy}(1-d_{iy/jy})} \right)^{\nu_2} + \left( \frac{m_{iz/jz}}{M_{uz}(1-d_{iz/jz})} \right)^{\nu_3} - 1 \quad (14.3.6)$$

The parameters  $\nu_1$ ,  $\nu_2$  and  $\nu_3$  can be taken equal to 2. The usual normality laws and plastic multiplier evolution laws accompanying these yield functions allow for the description of the plastic state of the element:

$$d\phi_{iy/jy}^p = d\lambda_{i/j} \frac{\partial f_{i/j}}{\partial m_{iy/jy}}; \quad d\phi_{iz/jz}^p = d\lambda_{i/j} \frac{\partial f_{i/j}}{\partial m_{iz/jz}}; \quad d\delta_p = d\lambda_i \frac{\partial f_i}{\partial n} + d\lambda_j \frac{\partial f_j}{\partial n};$$

$$\begin{cases} d\lambda_{i/j} = 0 & \text{if } f_{i/j}(m_{i/j}, n) < 0 \\ f_{i/j}(m_{i/j}, n) = 0 & \text{if } d\lambda_{i/j} > 0 \end{cases}; \quad \begin{cases} d\phi_x^p = 0 & \text{if } f_x(m_x) < 0 \\ f_x(m_x) = 0 & \text{if } d\phi_x^p > 0 \end{cases} \quad (14.3.7)$$

### 14.3.4 Local Buckling Damage Function and Evolution Laws

A new concept, similar to the yield function, is now introduced: the local buckling damage function for the inelastic hinge  $i$ ,  $g_i$ . This function depends on two accumulated plastic rotations and the local buckling damages:

$$g_i = g_i(p_{iy}, p_{iz}, d_{iy}, d_{iz}) \leq 0 \quad (14.3.8)$$

where these accumulated plastic rotations are defined as follows:

$$dp_{iy} = |d\phi_{iy}^p| \text{ and } dp_{iz} = |d\phi_{iz}^p| \quad (14.3.9)$$

The local buckling evolution of an inelastic hinge  $i$  is now determined assuming that local buckling also obeys a normality law:

$$\Delta d_{iy} = \Delta \mu_i \frac{\partial g_i}{\partial p_{iy}}; \Delta d_{iz} = \Delta \mu_i \frac{\partial g_i}{\partial p_{iz}} \quad (14.3.10)$$

The variable  $\mu$  is the damage multiplier whose evolution law is:

$$\begin{cases} \Delta \mu_i = 0 & \text{if } g_i < 0 \\ g_i = 0 & \text{if } \Delta \mu_i > 0 \end{cases} \quad (14.3.11)$$

### 14.3.5 Experimental Identification of the Local Buckling Damage Function for a Tube of Square Cross-Section

Consider again the experimental set up shown in Figure 21. The determination of the damage function for a tube of square cross-section is carried out by subjecting several elements of this characteristic to the set of biaxial loadings defined in Figure 25.

Notice that these are displacement controlled loadings that are represented by straight lines in the displacement space. These four lines form different angles with the horizontal axis: zero degrees, fifteen degrees, thirty degrees and forty five degrees and they are denoted SBH-0°, SBH-15°, SBH-30° and SBH-45°. The results of those tests are presented in Figures 26 in two graphs of deflection vs. force, one for each local axis

As aforementioned, softening in these curves initiates with local buckling. The values of the plastic deflection at the instant of local buckling initiation can be measured using the elastic stiffness identified at the beginning of the tests and the total deflection corresponding to the point of maximum force. The pairs of plastic deflection in the  $Y$  and  $Z$  directions at the moment of local buckling initiation for a tube of square cross-section are represented in the plot of Figure 27.

Figure 25. Loading paths in the displacement space

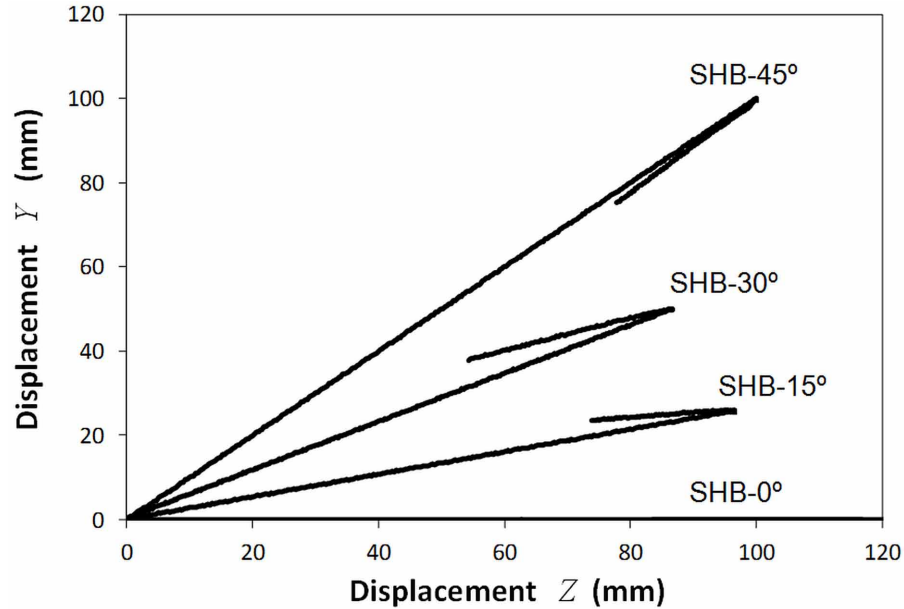
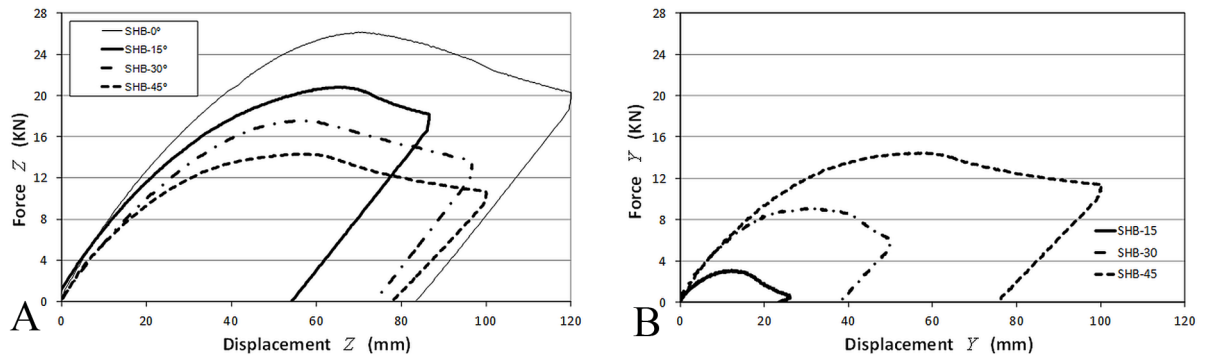


Figure 26. Displacement vs. force in the SHB-0°, SHB-15°, SHB-30° and SHB-45° tests a) in the Z direction b) in the Y direction



This graph shows that the domain of no local buckling forms a square region in the space. After local buckling initiation in any of the local axes, this domain experiences a hardening process; i.e. larger plastic rotations are needed in order to generate local buckling evolution. A generalization of the damage evolution law presented in section 14.1.4 is obtained with the no buckling domain presented in Figure 28.

Notice that the normality and evolution laws (Equation 14.3.10-11) with the no local buckling domain of Figure 28 give the following relationship between damages and accumulated plastic rotations:

$$d_{iy} = \kappa \langle p_{iy} - p_{cr} \rangle; d_{iz} = \kappa \langle p_{iz} - p_{cr} \rangle \quad (14.3.12)$$



Figure 27. Experimental determination of the local buckling function

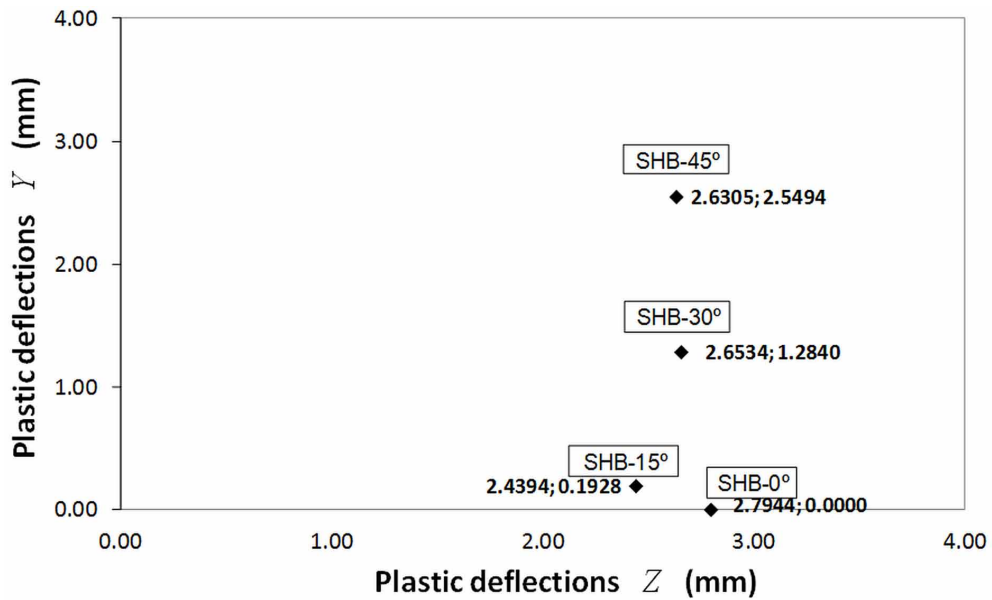
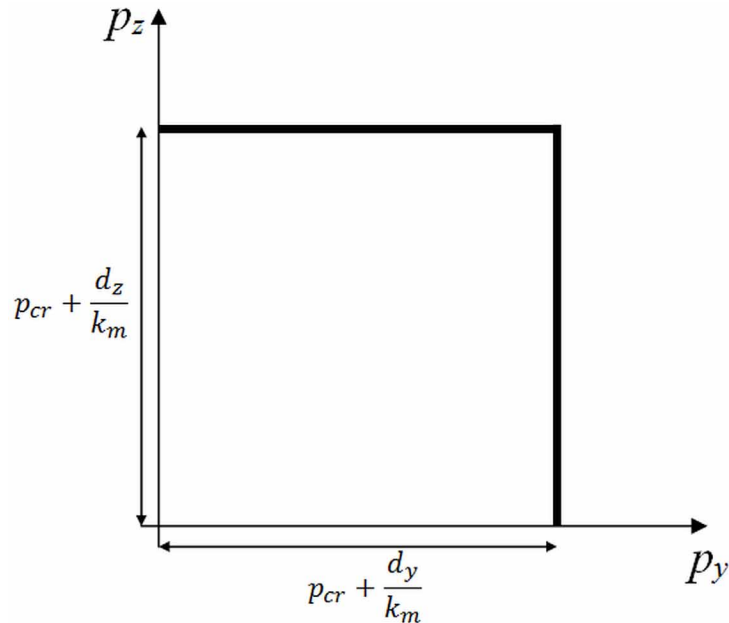


Figure 28. Elastic domain of no local buckling for a tube of square cross-section



### 14.3.6 Numerical Simulations

This section presents numerical simulations of tests carried out on square beams subjected to several loading paths. The first one corresponds to the test presented in Figure 21. As it can be appreciated in Figure 21b, uniaxial displacements in pairs of linearly increasing amplitude were alternatively applied

### Lumped Damage Mechanics

in the two transverse directions. The model parameters  $p_{cr}$  and  $\kappa_m$  were identified from the rotation vs. flexural moment curve that is shown in Figure 29. In Figure 30a the experimental deflection vs. force curves are presented again and in Figure 30b the corresponding numerical simulations. The values of damage computed at the beginning of some elastic unloadings are indicated in later figure.

The second and third numerical simulations correspond to square beams subjected to the loading histories presented in Figures 31a-b. In the square shaped loading path, displacements of the same magnitude were sequentially applied in the two orthogonal directions; then, the specimen was unloaded to zero force in the same sequence. In the triangular-shaped loading path, displacements of the same magnitude were sequentially applied in the two orthogonal directions but the specimen was unloaded simultaneously to zero force.

In Figures 32a is presented the experimental force  $Z$  vs. force  $Y$  curves corresponding to the square-shaped loading path and in Figure 32b the corresponding numerical simulation.

In Figures 33a is presented the experimental deflection vs. force curves in the  $Y$  direction corresponding to the square-shaped loading path and in Figure 33b the numerical simulation. Values of damage computed at the beginning of some elastic unloadings are indicated in the numerical simulation curve.

Finally in Figure 34 are shown the curves corresponding to  $Z$  direction.

The results of the simulation corresponding to the triangular-shaped loading path are presented in Figure 35 b. The set of experimental curves are shown in Figure 35 a.

### 14.3.7 Experimental Identification of the Local Buckling Damage Function for a Tube of Rectangular Cross-Section

Figures 36-39 show the results of the identification tests described in the previous section in the case of a tube of 120 mm x 60 mm cross-section, 2.5 mm thickness and a free length of 1.28 m.

Notice that this time, the no local buckling domain can be represented by a rectangular area. Now, the normality and evolution laws (Equation 14.3.10-11) with the no local buckling domain of Figure 40 give:

$$d_{iy} = \kappa_y \langle p_{iy} - p_{cry} \rangle; d_{iz} = \kappa_z \langle p_{iz} - p_{crz} \rangle \quad (14.3.13)$$

Figure 29. Parameter determination in test of Figure 21

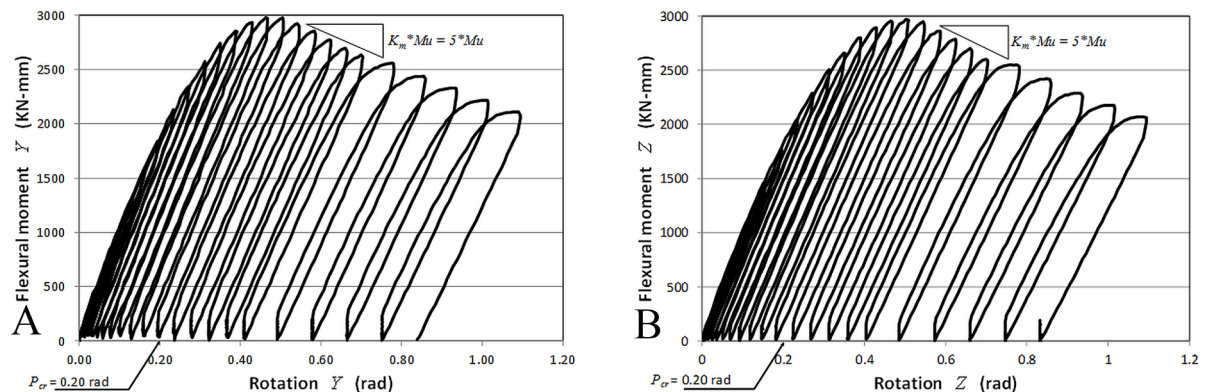
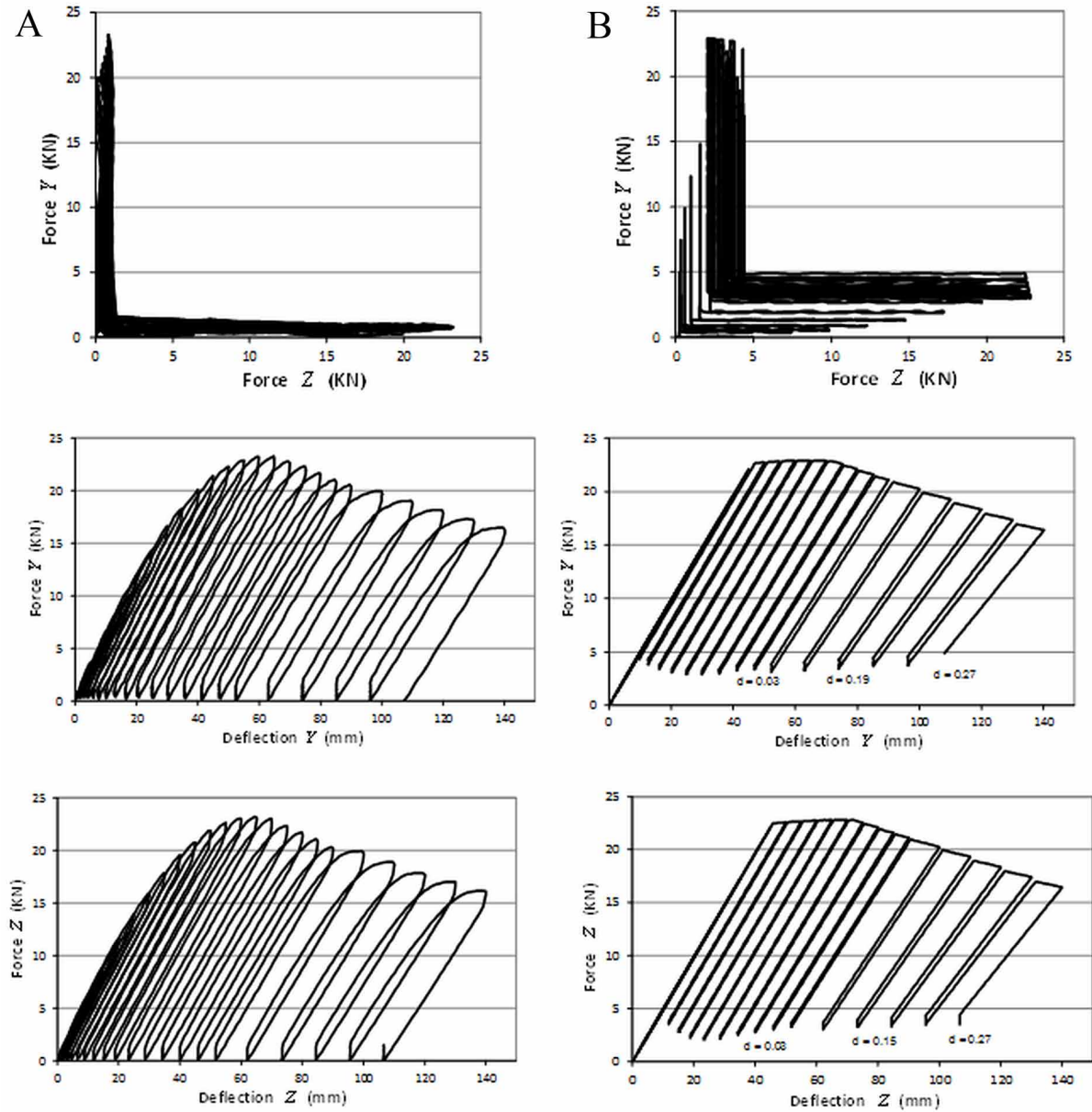


Figure 30. Deflection vs. force curves in the test shown in Figure 21 a) Experimental b) Numerical simulation



### 14.3.8 Numerical Simulations

Same rectangular specimens were subjected to the square-shaped and triangular shaped loading paths shown in Figure 41. Values of damage at the beginning of some elastic unloadings are indicated in the numerical simulation curves.

In Figures 42a is presented the experimental force Z vs. force Y curves corresponding to the square-shaped loading path and in Figure 42b the numerical simulation.

**Lumped Damage Mechanics**

Figure 31. Loading paths applied to 120 mm square beams a) Square-shaped b) Triangular-shaped

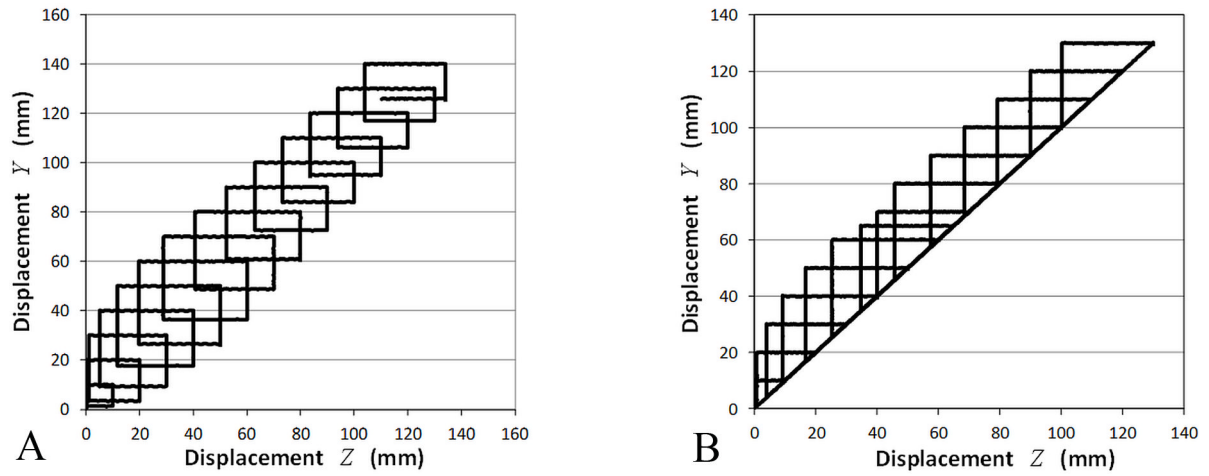


Figure 32. Beam subjected to square-shaped loading path a) Experimental force Z vs. force Y b) Numerical simulation

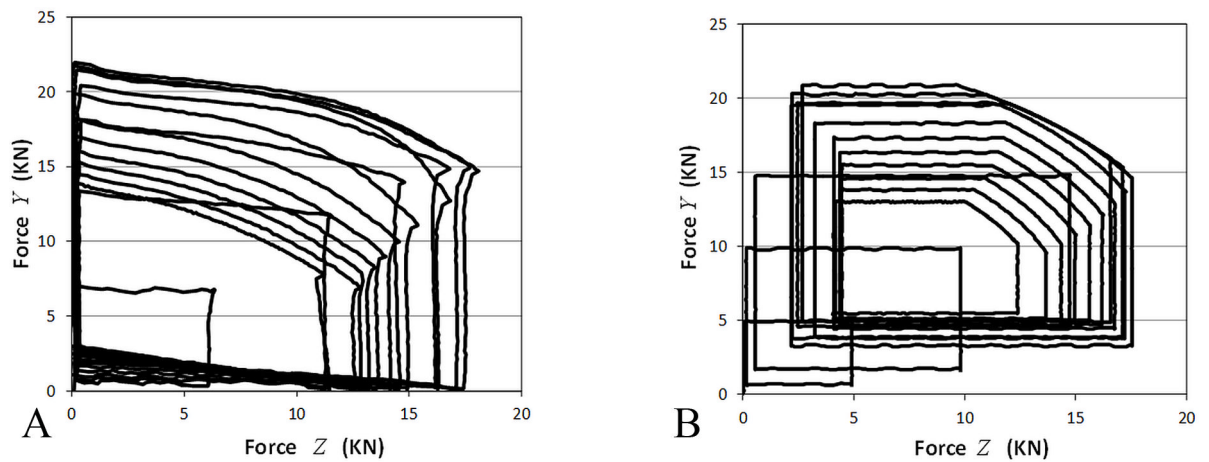


Figure 33. Beam subjected to square-shaped loading path a) Experimental deflection vs. force in the Y direction b) Numerical simulation

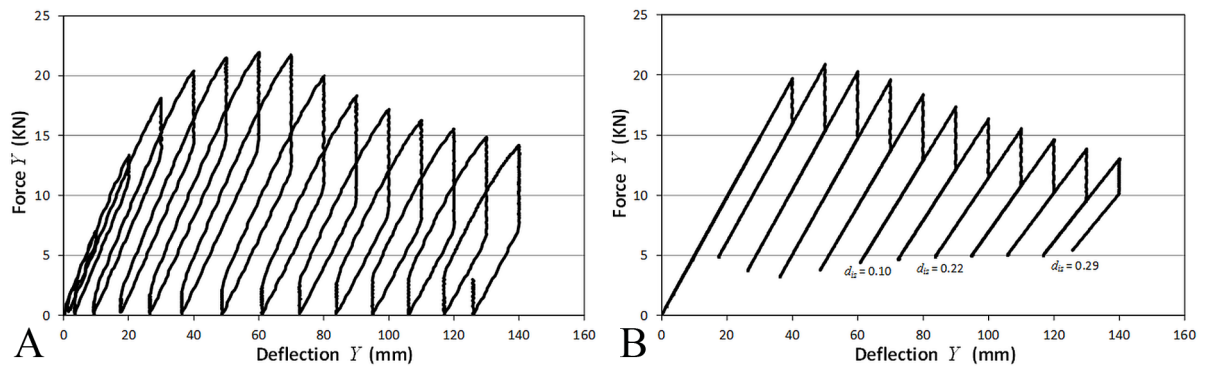
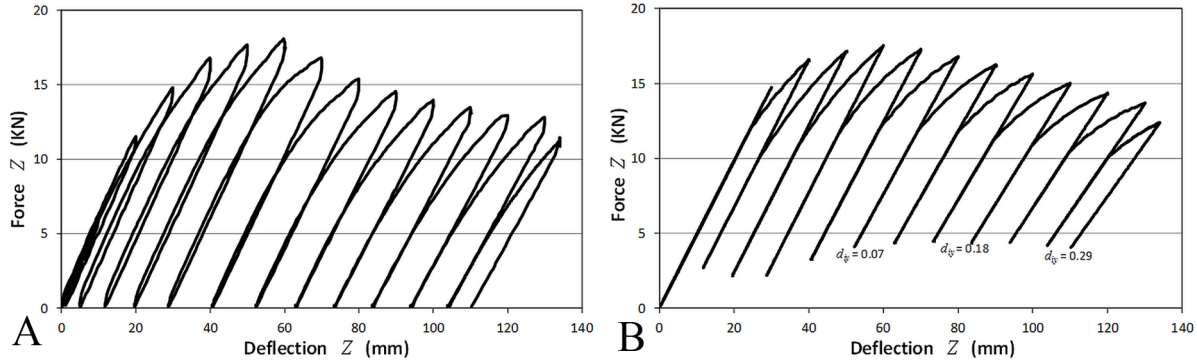


Figure 34. Beam subjected to square-shaped loading path a) Experimental deflection vs. force in the Z direction b) Numerical simulation



In Figures 43a is presented the experimental deflection vs. force curve in the Y direction corresponding to the square-shaped loading path and in Figure 43b the numerical simulation. Values of damage computed at the beginning of the last elastic unloading are indicated in the numerical simulation curve.

In Figure 44 are presented the results corresponding to the Z direction.

The results of the simulation corresponding to the triangular-shaped loading path are presented in Figure 45 b. The experimental curve is shown in Figure 45 a.

### 14.3.9 Local Buckling Damage Function for a Tube of Circular Cross-Section

Consider now a tubular element of circular cross-section; assuming a perfect radial symmetry in the tube, the initial no local buckling domain is also a circle. In the particular case of an element subjected only to actions in the local axes directions Y and Z, the circumference may become an ellipse with the damage hardening process. The local buckling damage function is in this case:

$$g_i = \left( \frac{p_{iy}}{p_{cr} + d_{iy}/\kappa} \right)^2 + \left( \frac{p_{iz}}{p_{cr} + d_{iz}/\kappa} \right)^2 - 1 \quad (14.3.14)$$

The representation of the no local buckling domain is shown in Figure 46.

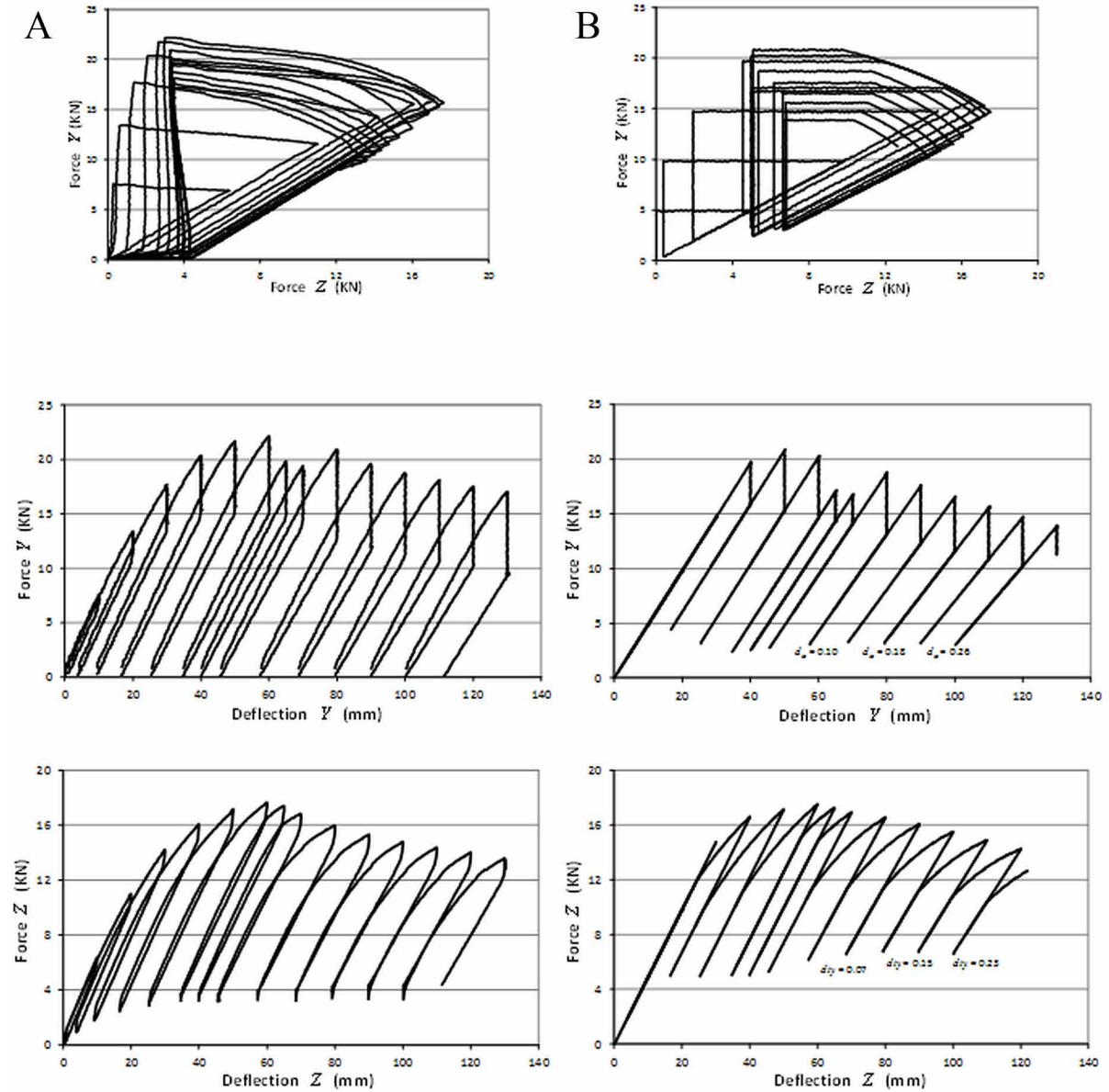
### 14.3.10 Numerical Simulations

Circular specimens with 120 mm external diameter and 3 mm thickness were subjected to the loading paths of the Figure 47.

The experimental results of the L-shaped loading path of Figure 47a are presented in the Figure 48a and in Figure 48b the corresponding numerical simulations.

**Lumped Damage Mechanics**

Figure 35. Responses of square beam subjected to the triangular-shaped loading path a) Experimental b) Numerical simulation



The experimental results of the square-shaped loading path of Figure 47b are presented in the Figure 49a and in Figure 49b the corresponding numerical simulations.

The experimental results of the triangular-shaped loading path of Figure 47c are presented in the Figure 50a and in Figure 50b the corresponding numerical simulations.

Figure 36. Loading paths

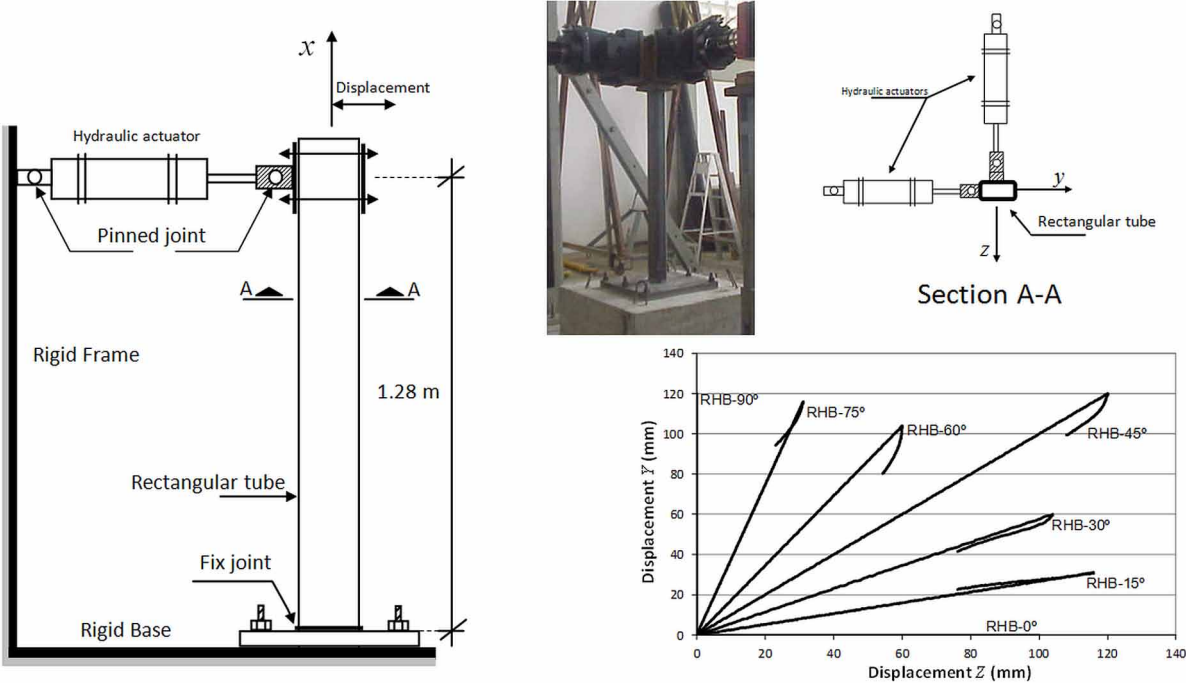


Figure 37. Deflection vs. force in the Y direction

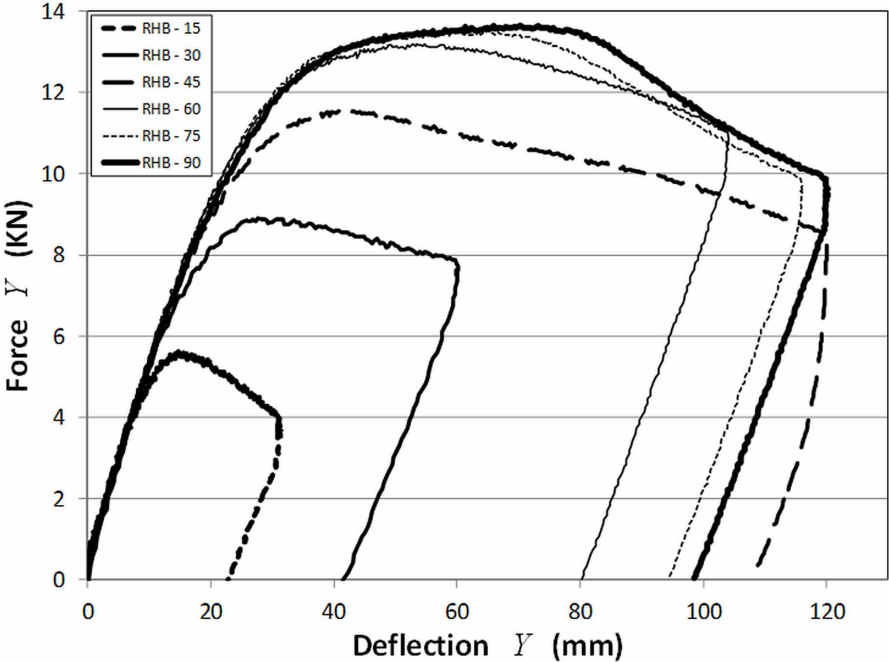


Figure 38. Deflection vs. force in the Z direction

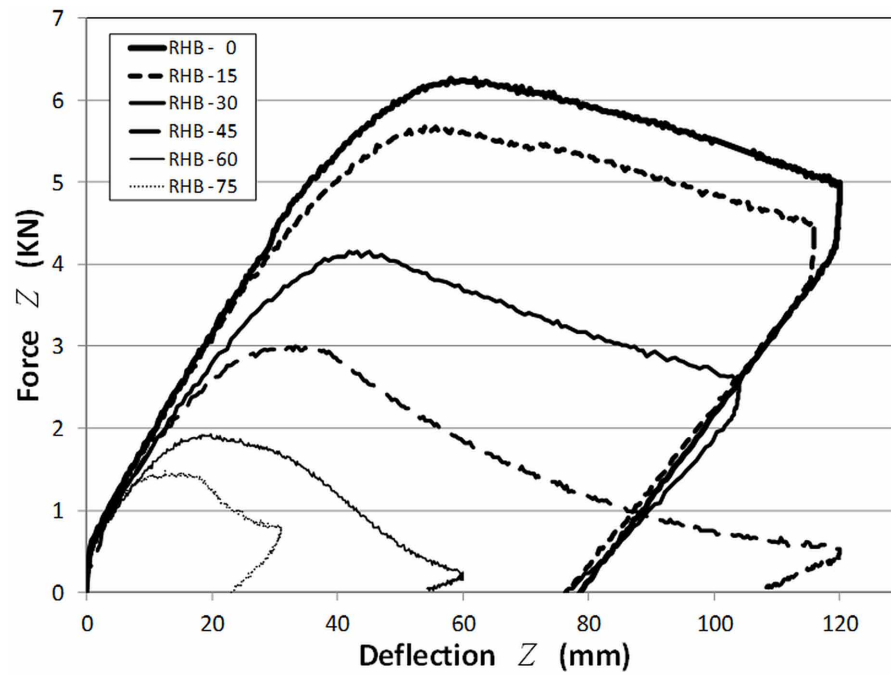


Figure 39. Experimental determination of the local buckling function

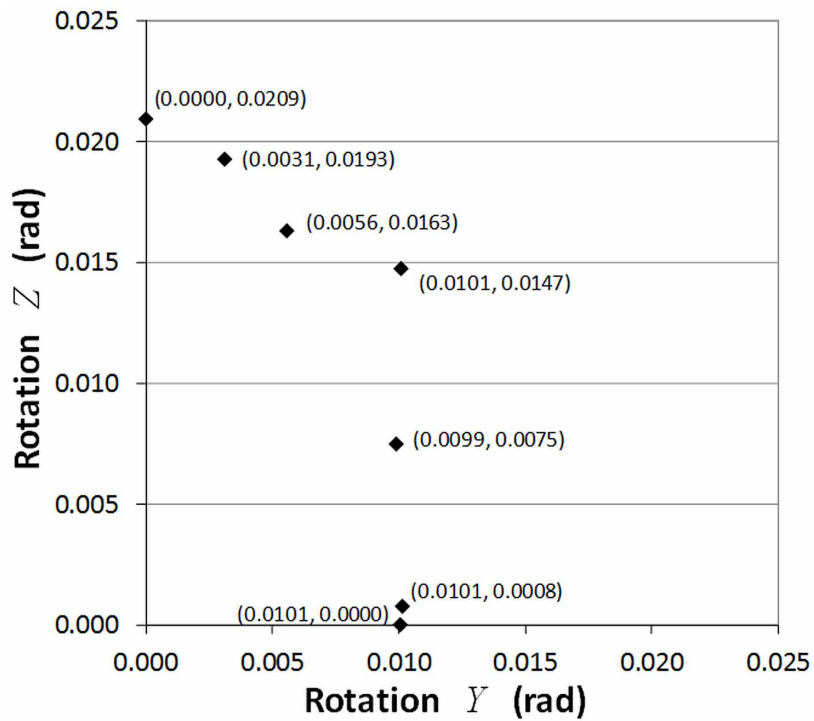
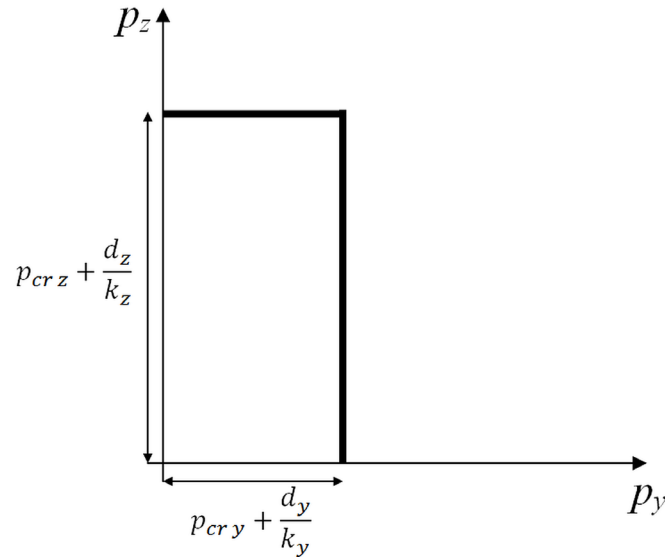




Figure 40. Elastic domain of no local buckling for a tube of rectangular cross-section



## 14.4 ANALYSIS OF STEEL FRAMES WITH LOCAL BUCKLING

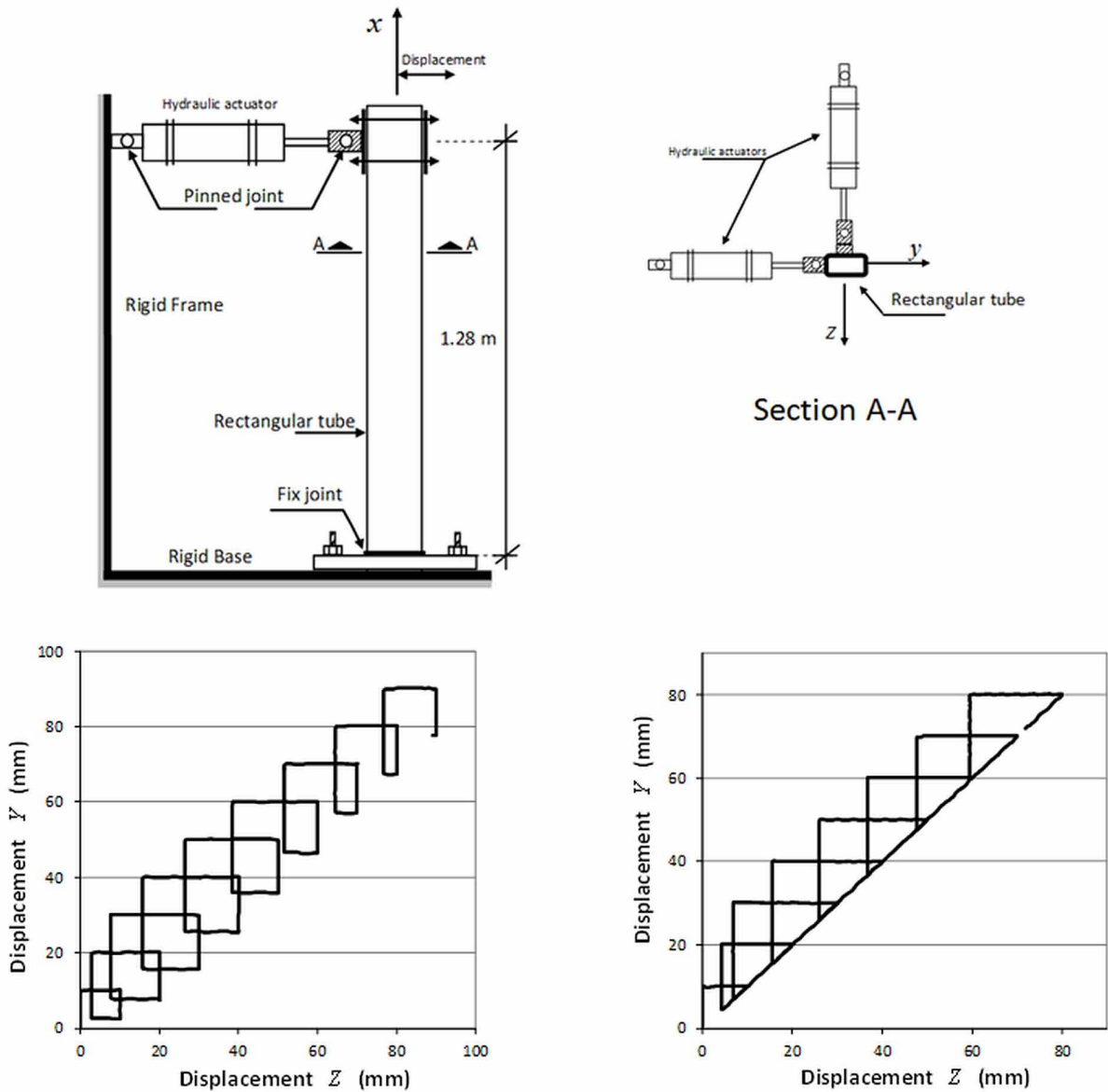
### 14.4.1 Planar Frame Subjected to Mono-Sign Loading

The steel frame of two levels and two spans shown in Figure 51 is subjected to a mono-sign loading. The elements had rectangular hollow cross-section and were welded at the joints. The frame is simulated using the model described in section 14.1. Single elements of the frame were tested in order to identify the parameters of the model and are presented in Table 1. The Figure 52 shows the comparison between model and experimental results in the case of a frame. For the sake of clarity, only four of the elastic unloadings are represented in the simulation.

The Figure 53 indicates the state of damage at the end of the four unloading. The numbers beside the hinges represent the damage values. The first distribution presents six plastic hinges with no damage, i.e. without local buckling. It can be noticed that this state corresponds to the plastic hardening phase of the test. The maximum resistance of the frame is reached between the first and second elastic unloading of the simulation where a sudden change of the tangent slope can be appreciated. In the simulation, this modification of the tangent stiffness is due to the appearance of local buckling in the same six plastic hinges. Four new plastic hinges appear in the frame without local buckling while damage continues to evolve in the first six hinges. After the third unloading, local buckling appears also in the four remaining hinges. In the simulation, a slight additional modification in the tangent stiffness can be appreciated when that happens. The test was stopped after the fourth unloading and the computed final state of damage is shown in the last of Figure 53.

## Lumped Damage Mechanics

Figure 41. Loading paths applied rectangular cross-section beams



### 14.4.2 Planar Frame Subjected to Cyclic Loading

The simulation of the frame, shown in Figure 51, subjected to cyclic loading is presented in this section. This time it is used the model described in section 14.2 considering the parameters  $\kappa_c = 1.45$ ,  $CBf = 0.60$ . In Figures 54 are presented the experimental and numerical force vs. deflection curves.

It can be appreciated that the predicted and observed levels of force in Figure 54 are very close. The damage distribution at the end of the simulation is presented in the Figure 55. Local buckling could be observed in the specimen in the locations predicted by the analysis.

Figure 42. Rectangular beam subjected to square-shaped loading path a) Experimental force Z vs. force Y b) Numerical simulation

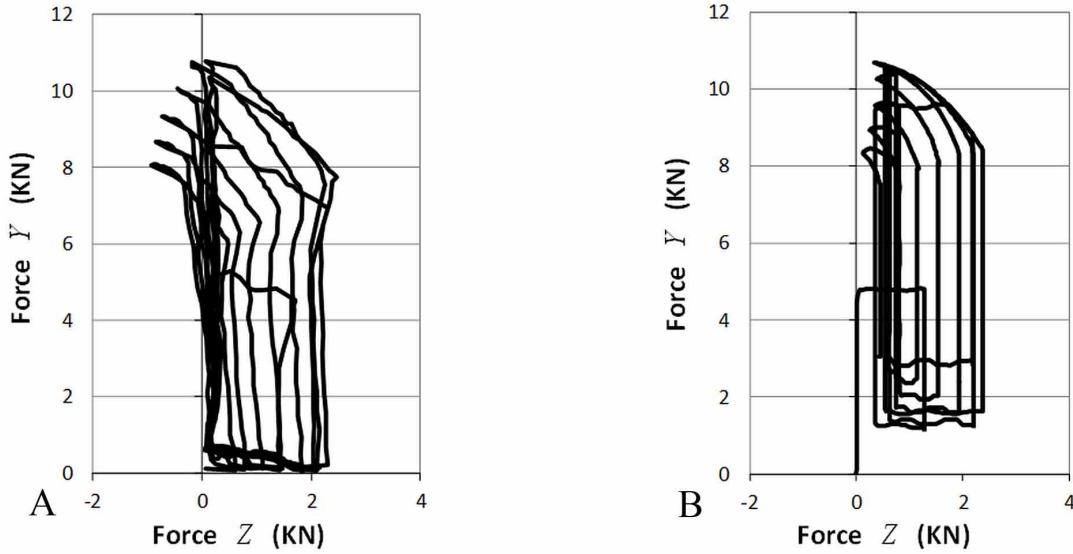


Figure 43. Deflection Y vs. force Y curves corresponding to the square-shaped loading path of Figure 41a a) Experimental b) Numerical simulation

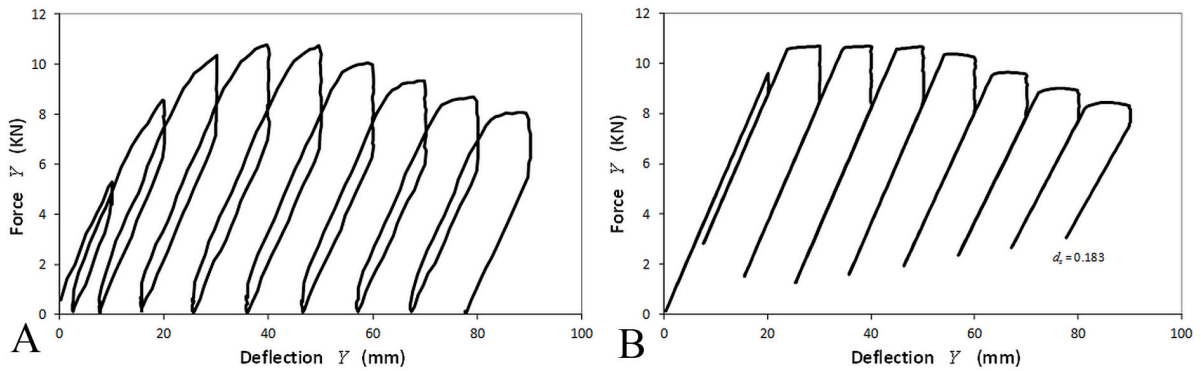
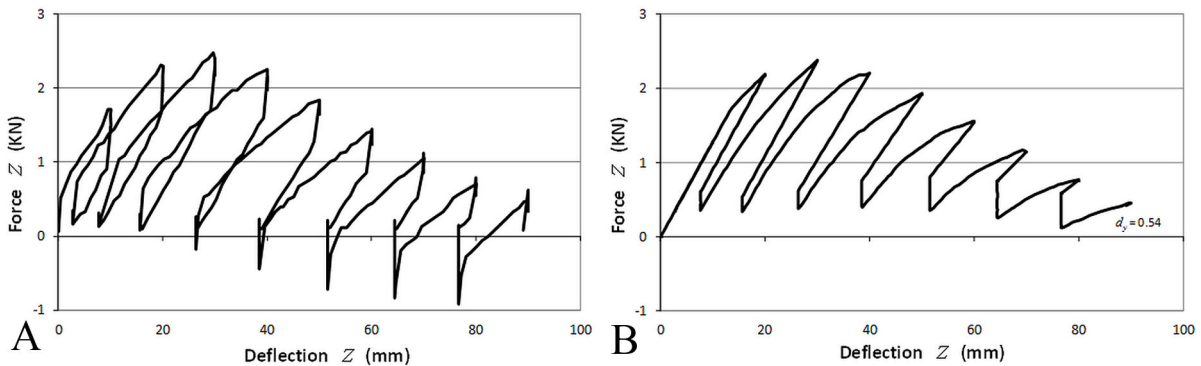
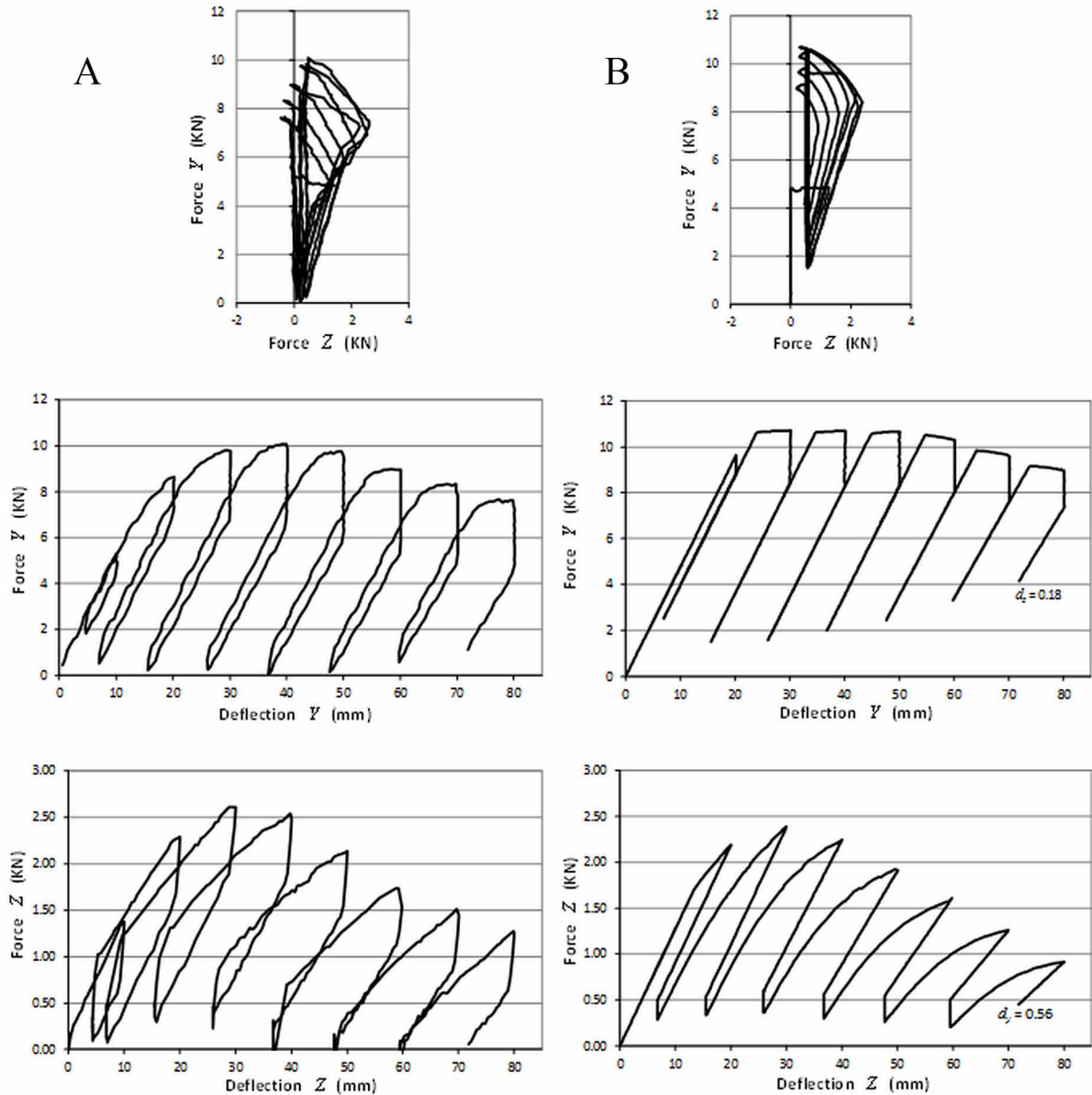


Figure 44. Deflection Z vs. force Z curves corresponding to the square-shaped loading path of Figure 41a a) Experimental b) Numerical simulation



## Lumped Damage Mechanics

Figure 45. Responses of rectangular beam subjected to the triangular-shaped loading path a) Experimental b) Numerical simulation



### 14.4.3 Tridimensional Frames Subjected to Mono-Sign Loading

The tridimensional frame presented in Figure 56a is subjected to the loading path of the Figure 56b.

The frame was built with steel hollow elements of 120 mm square cross-section and 4 mm thickness. The geometry of the structure is shown in Figure 57. The displacements were imposed in the middle of this structure through a steel device specially designed for this purpose as can be appreciated in Figure 56a. The response was obtained in the displacement application point.

Figure 46. Elastic domain of no local buckling for a tube of circular cross-section

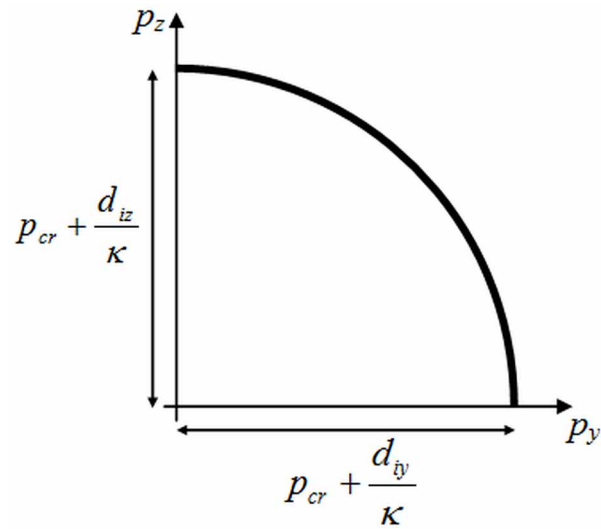


Figure 47. Loading paths applied to elements of circular cross-section

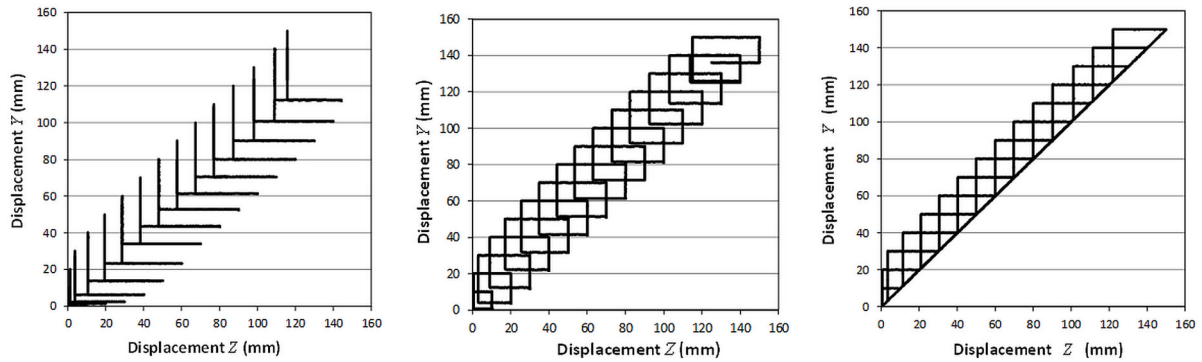


Table 1. Parameters of the elements

Element	$K_m$	$p_{cr}$	$M_p$ (kgf-cm.)	$M_u$ (kgf-cm.)	$A$
Beams	1.45	0.190	669.30	850.73	19.50
Columns	1.45	0.195	674.21	833.57	19.25

### Lumped Damage Mechanics

Figure 48. Responses of a circular beam subjected to the L-shaped loading path a) Experimental b) Numerical simulation

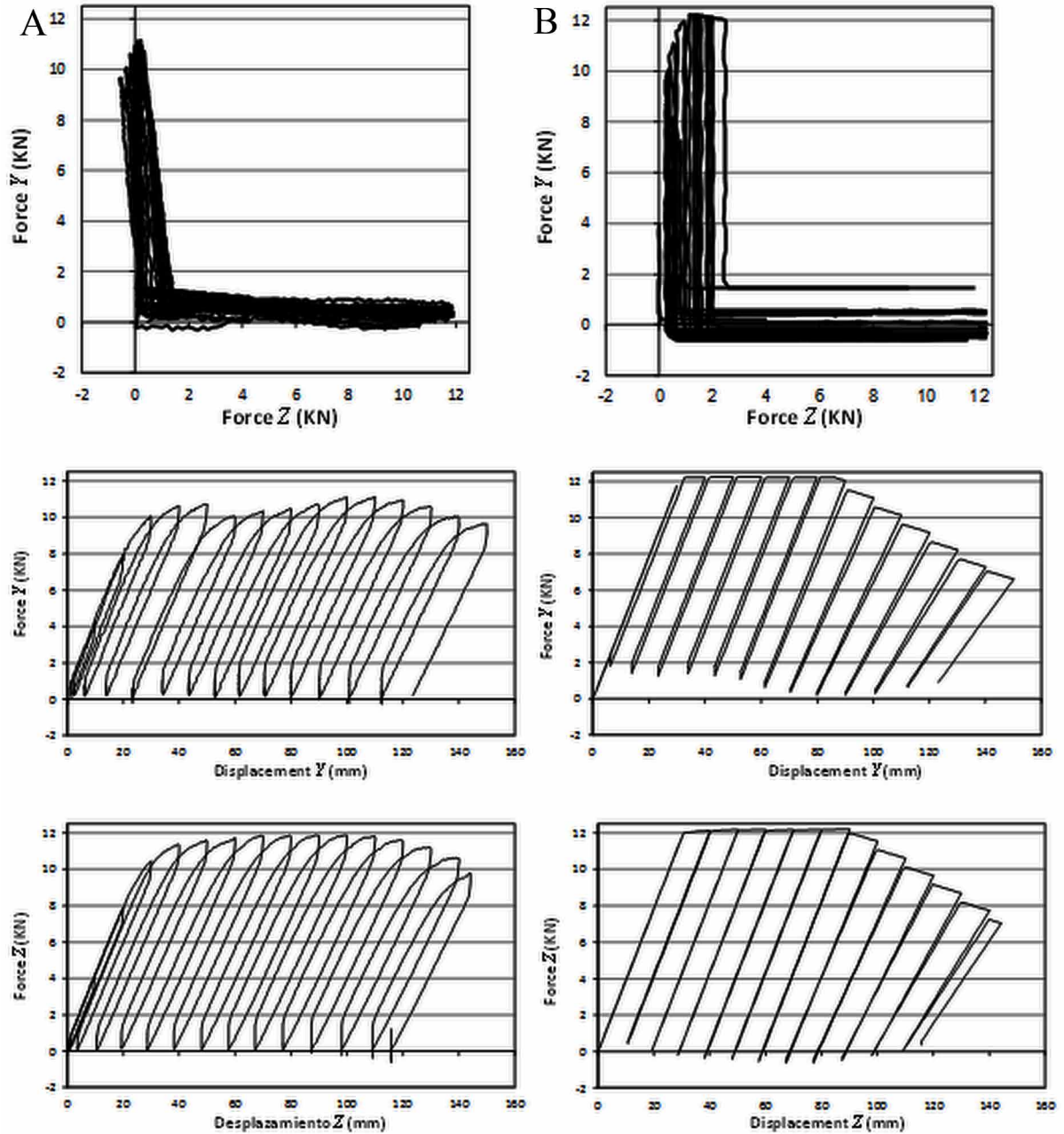
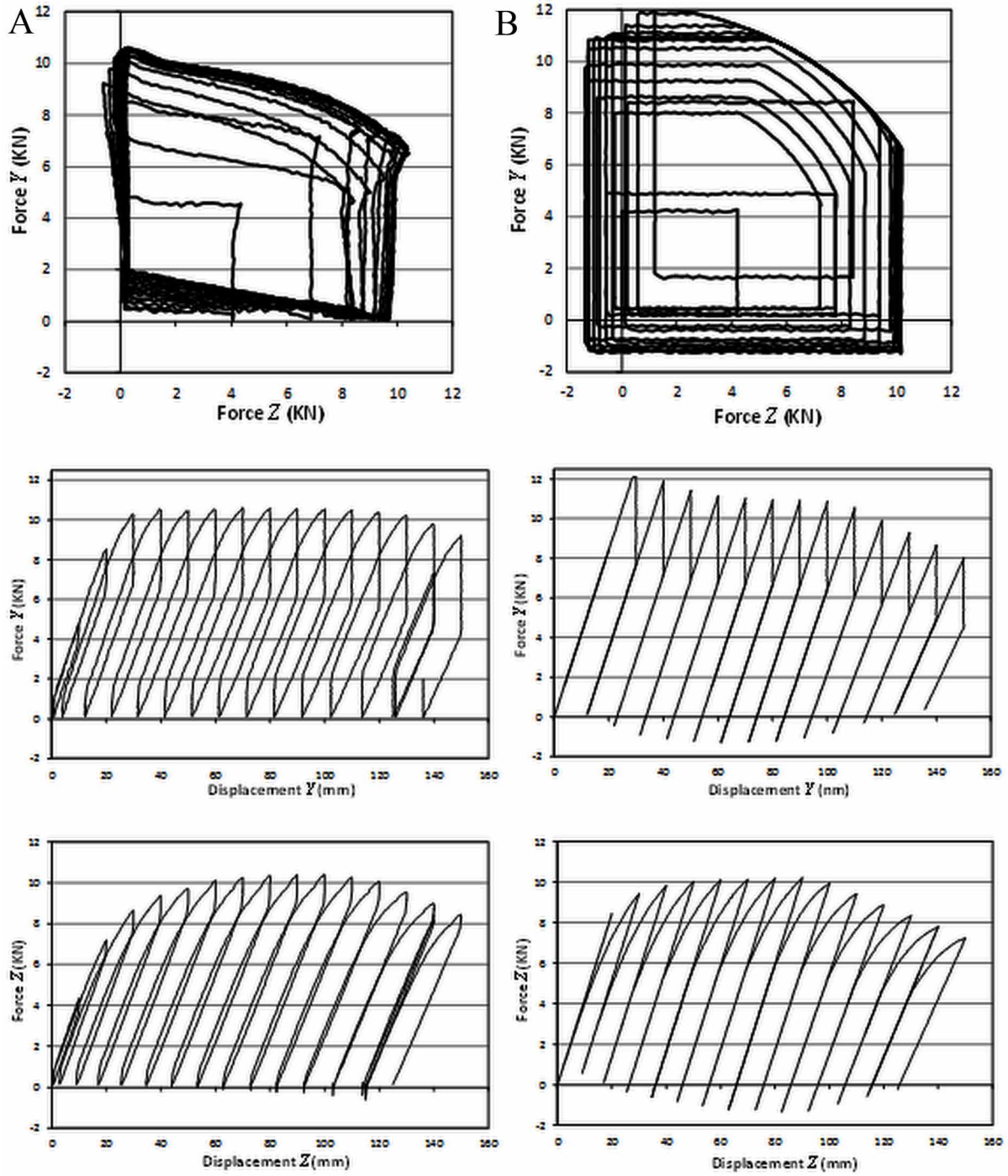


Figure 49. Responses of a circular beam subjected to the square-shaped loading path a) Experimental b) Numerical simulation



## Lumped Damage Mechanics

Figure 50. Responses of circular beam subjected to the triangular-shaped loading path a) Experimental b) Numerical simulation

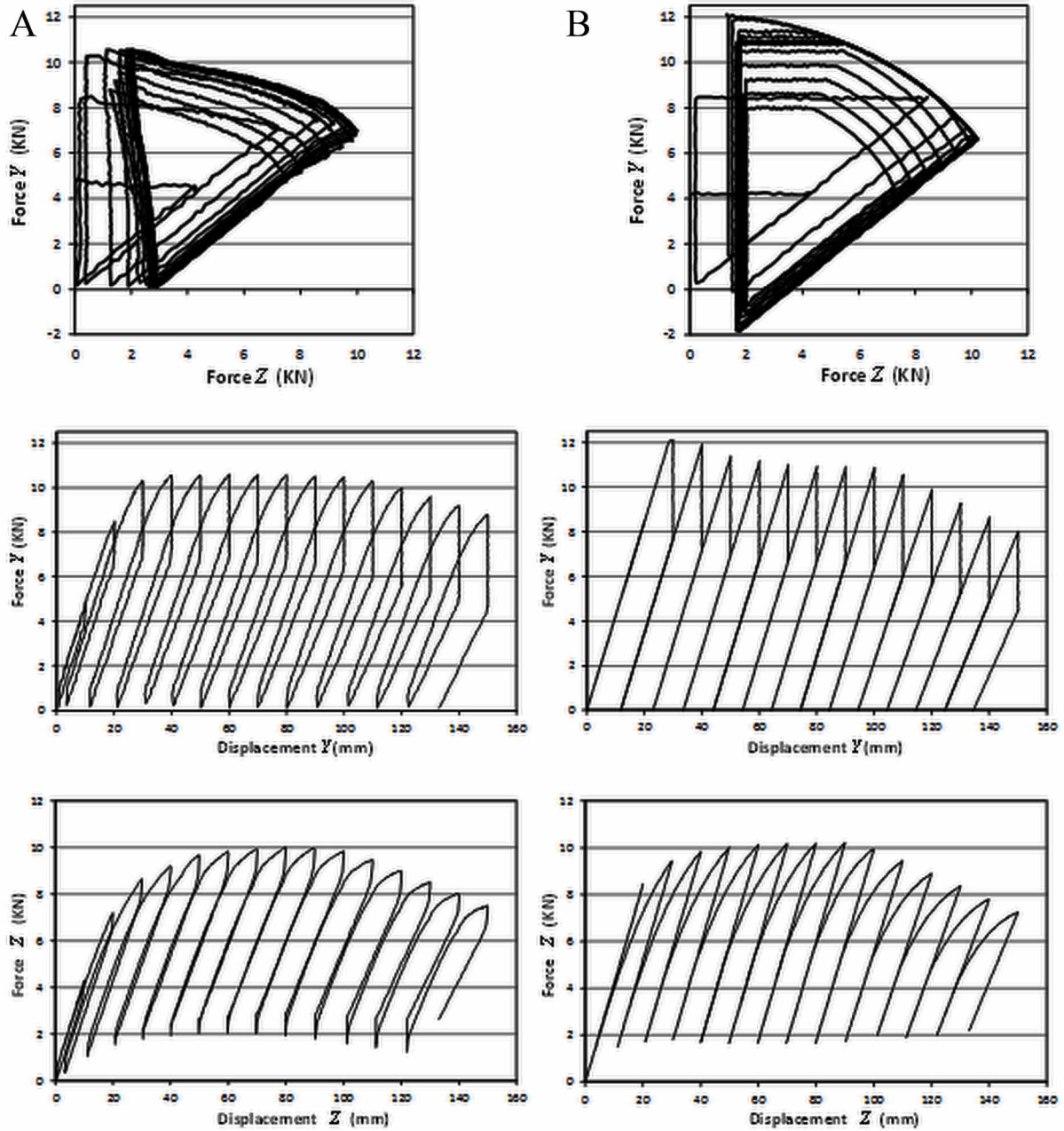




Figure 51. Steel frame subjected to mono-sign loading

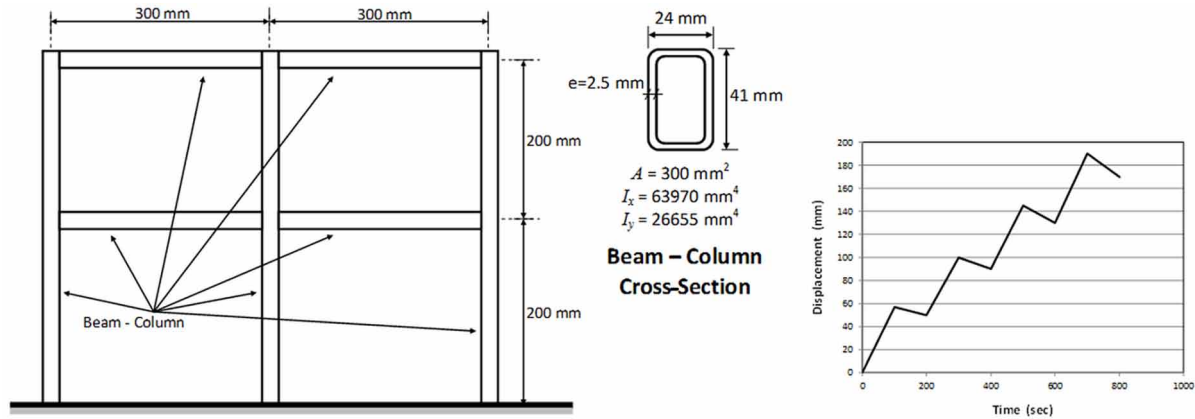
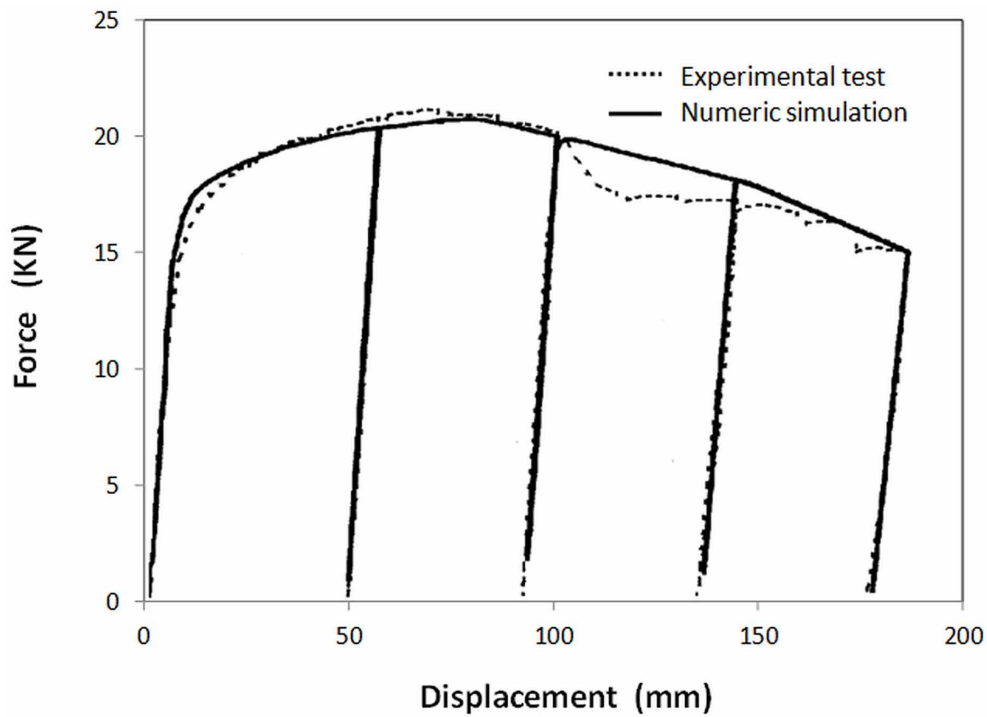


Figure 52. Force vs. displacement curve



For the numerical simulation of the test, beams and columns of the structure were represented by the finite element, described in section 14.3, one element for frame member (a total of eight elements). The slab was represented by multiple elastic elements with high stiffness to assess a uniform distribution of the displacements in the tridimensional frame.

**Lumped Damage Mechanics**

Figure 53. Damage distribution in the frame a) End 1st unloading b) End 2nd unloading c) End 3th unloading d) End 4th unloading

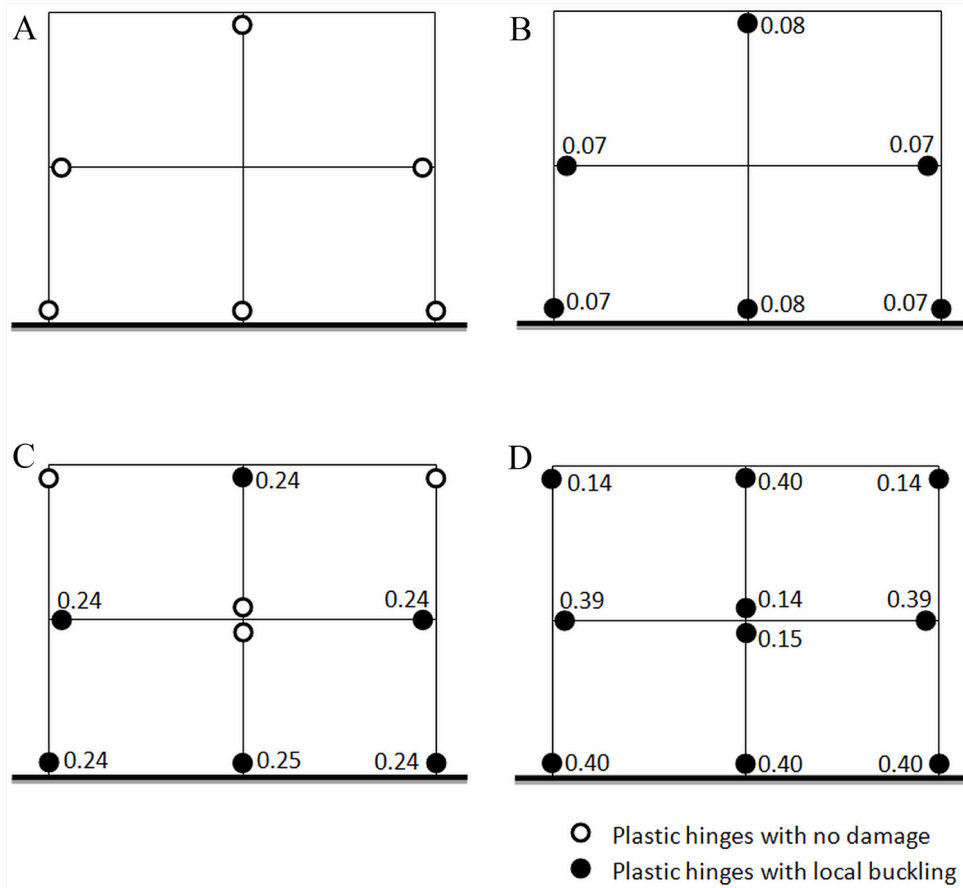


Figure 54. Deflection vs. force curves a) Experimental b) Numerical

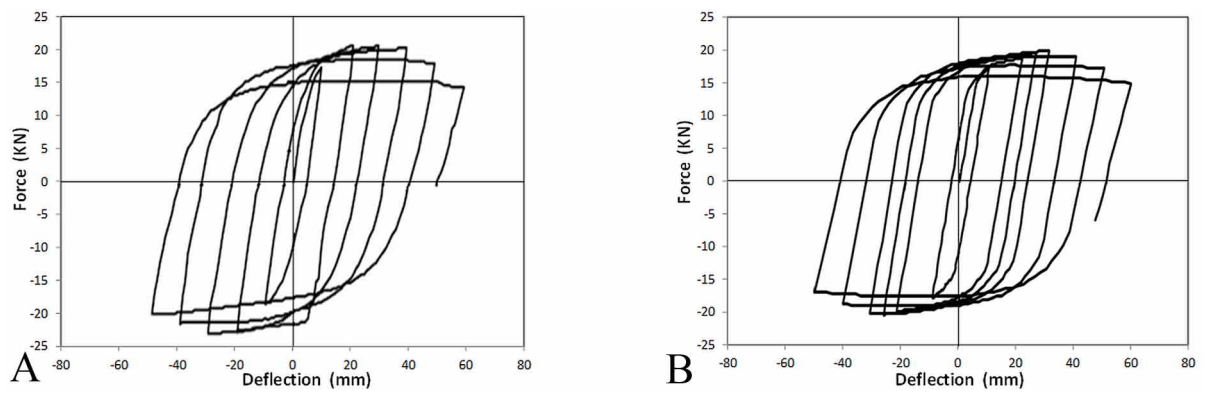


Figure 55. Damage distribution in the frame a) Positive Local Buckling b) Negative Local Buckling

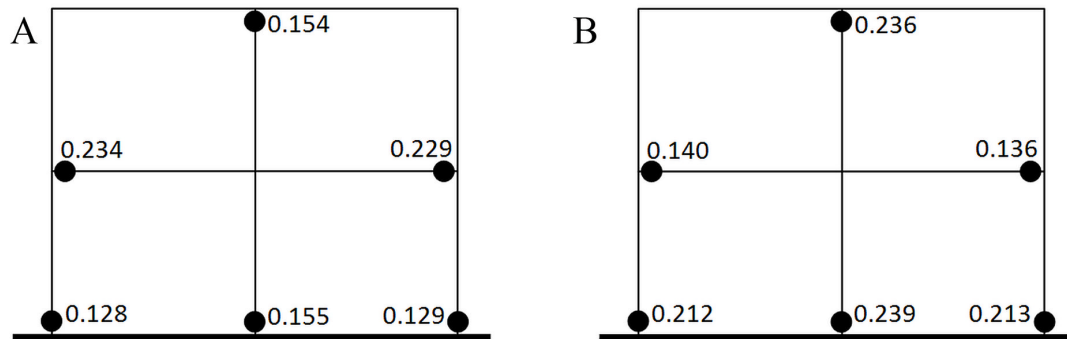
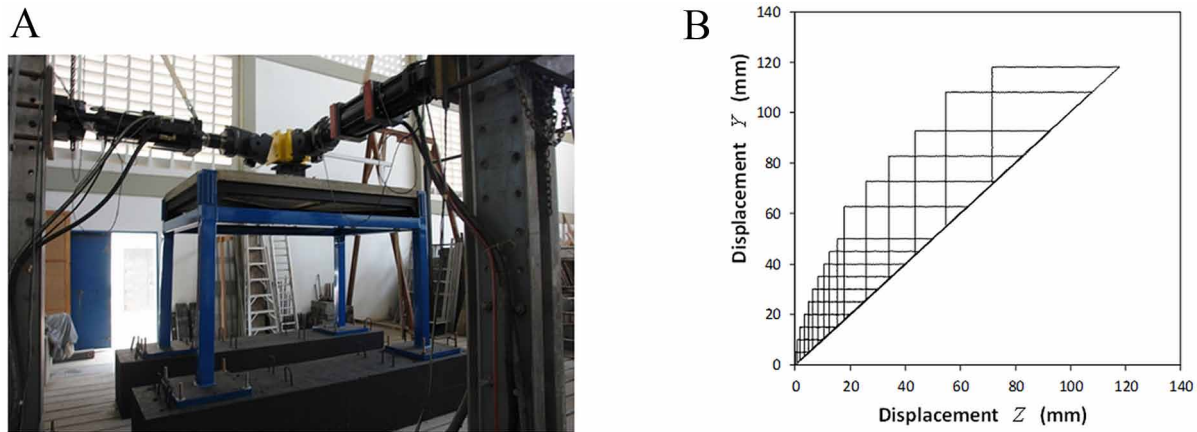


Figure 56. a) Tridimensional Steel frame and b) the loading path



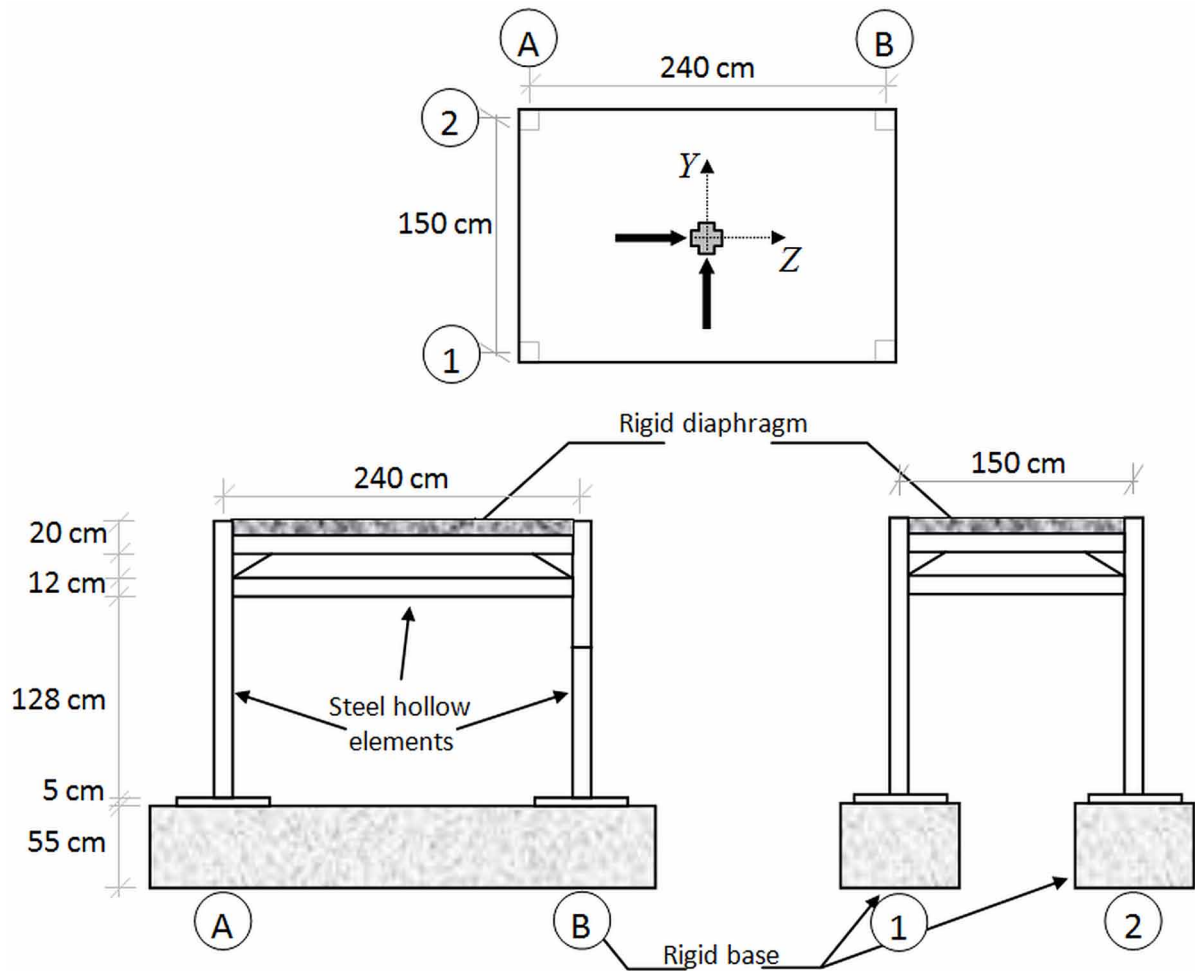
In Figure 58a it is shown the experimental force  $Z$  vs. force  $Y$  curve and in Figure 58b the corresponding numerical simulation. The experimental displacements vs. force curves are presented in Figures 58c and 58e and the corresponding numerical simulations in Figures 58d and 58f.

The damage values and the local buckling aspect in the most damaged column at the end of the test are shown in Figure 59.

## 14.5 SUMMARY AND EQUATIONS QUICK REFERENCE

This chapter describes how the concepts of fracture and damage mechanics can be used for modeling the behavior of tubular frame structures. Tubular steel elements are usually built with relatively thin walls; overloads on these components generate the appearance of small waves or wrinkles that do not

Figure 57. Geometry of the tridimensional frame

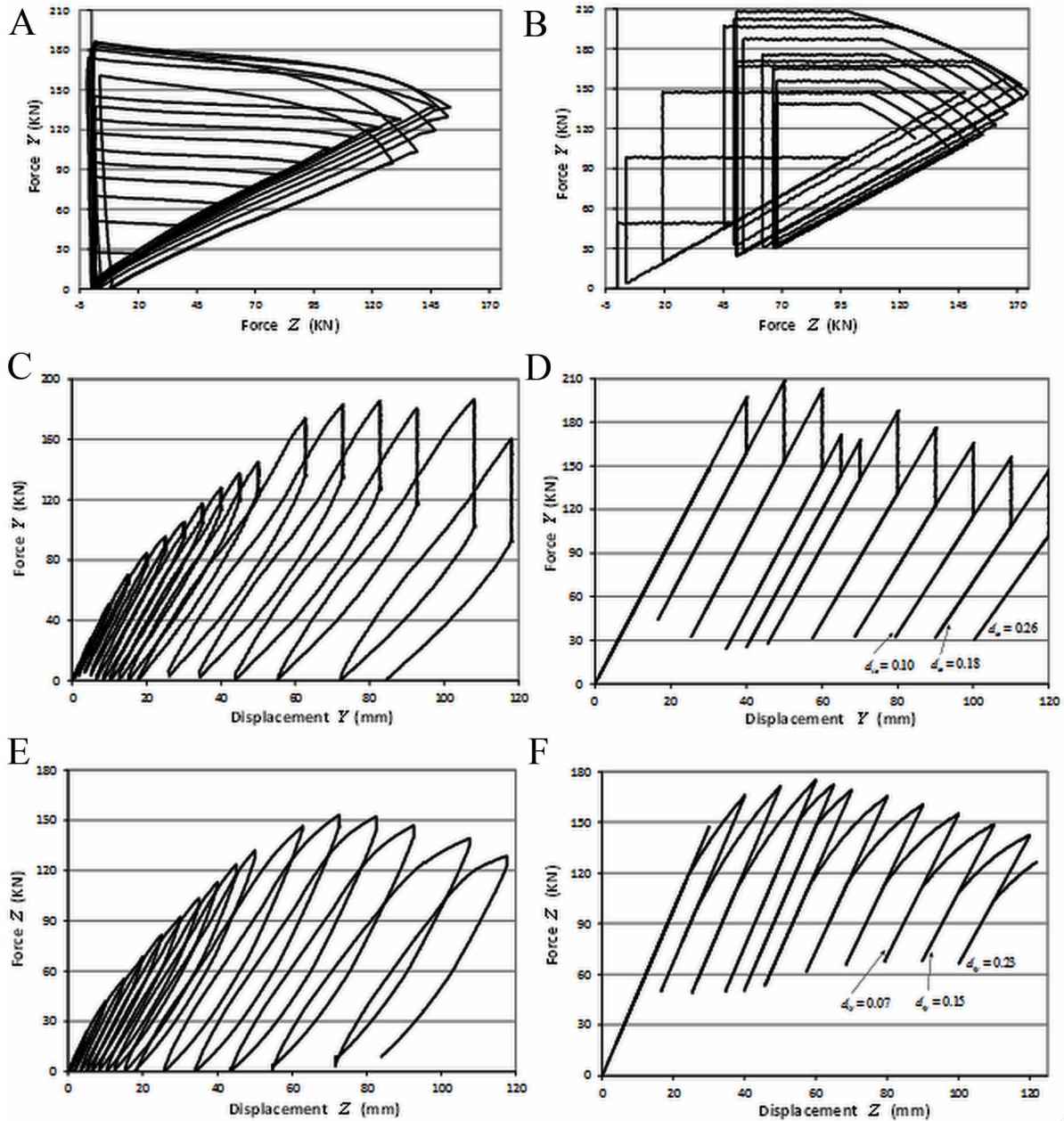


disappear after unloading the element; this phenomenon is called local buckling. This phenomenon is the responsible for the degradation of stiffness and strength in structures built with tubular elements when are subjected to severe overloads.

Experimental tests on tubular columns subjected to mono-sign displacements shown that the buckling reduces the elastic limit of the elements as well as the slope of the loading/reloading branches. This fact allows using the concept of plastic hinge with damage for its modeling. In this case the damage variable measures the degree of local buckling at the ends of the tube.

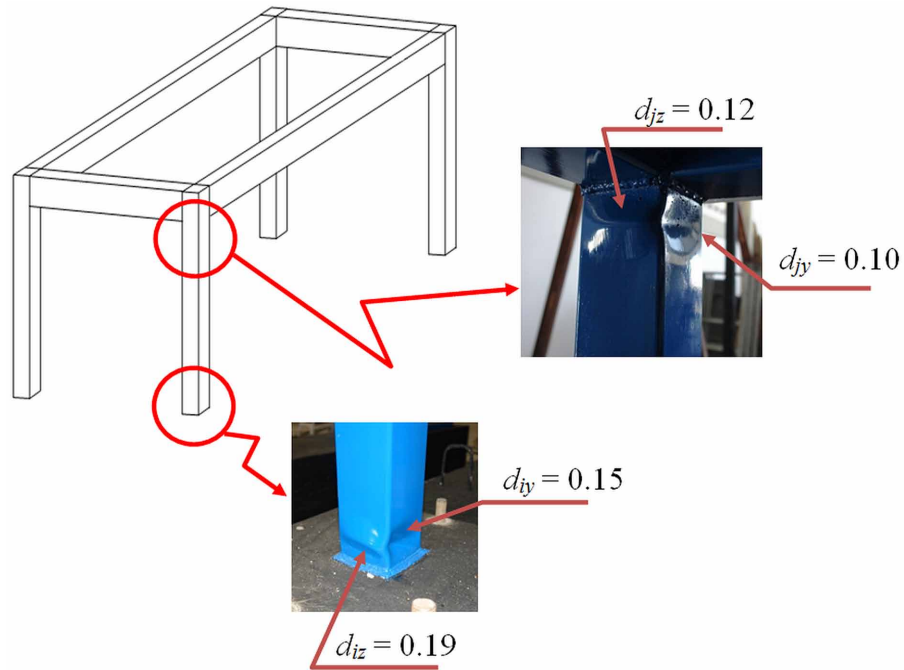
The elasticity and plasticity laws are obtained based on the hypothesis of equivalence on deformations as in the model for RC elements. It can be used a yield function with perfect plasticity or nonlinear plastic hardening.

Figure 58. Tridimensional frame structure: test and simulation. a) Experimental force Y vs. force Z curve. b) Numerical simulation. c) Experimental displacements vs. force curve in Y direction. d) Numerical simulation. e) Experimental displacements vs. force curve in Z direction. f) Numerical simulation.



**Lumped Damage Mechanics**

Figure 59. Damage values and local buckling aspect at the end of the test



A new concept, the counter-buckling, is introduced in order to represent the behavior of this kind of structures when are subjected to cyclic loading with reversal of sign. Metaphorically, the counter-buckling effect can be described as the ironing of the wrinkles. This effect is characterized and modeled introducing the concept of “local buckling driving rotation” (See Table 2).

Table 2.

LOCAL BUCKLING DAMAGE MODEL FOR PLANAR MONO-SIGN LOADINGS	
<i>Elasticity Law of a Tubular Frame Element with Local Buckling</i>	

*continued on following page*

Table 2. Continued

<p>Elasticity law</p> $\{\Phi - \Phi^p\}_b = [\mathbf{F}(\mathbf{D})]_b \{\mathbf{M}\}_b + \{\Phi^0\}_b; [\mathbf{F}(\mathbf{D})] = \begin{bmatrix} \frac{L_b}{3(1-d_i)EI_b} & -\frac{L_b}{6EI_b} & 0 \\ -\frac{L_b}{6EI_b} & \frac{L_b}{3(1-d_i)EI_b} & 0 \\ 0 & 0 & \frac{L_b}{AE_b} \end{bmatrix}$ <p>(14.1.1)</p> <p>or <math>\{\mathbf{M}\}_b = [\mathbf{E}(\mathbf{D})]_b \{\Phi - \Phi^p\}_b + \{\mathbf{M}^0(\mathbf{D})\}_b</math></p> $[\mathbf{E}(\mathbf{D})]_b = k \begin{bmatrix} 12(1-d_i) & 6(1-d_i)(1-d_j) & 0 \\ 6(1-d_i)(1-d_j) & 12(1-d_j) & 0 \\ 0 & 0 & \frac{EA_b}{kL_b} \end{bmatrix}; k = \frac{1}{4 - (1-d_i)(1-d_j)} \frac{EI_b}{L_b};$ <p><math>\{\mathbf{M}^0(\mathbf{D})\}_b = -[\mathbf{E}(\mathbf{D})]_b \{\Phi^0\}_b</math>  <math>\{\Phi^0\}_b</math>: initial deformations defined in Table 3 of Chapter 3</p>
<b>Yield Function of a Plastic Hinge with Local Buckling</b>
<p>Plastic deformation evolution law and yield function</p> $\begin{cases} d\phi_i^p = 0 \text{ if } f_i(m_i) < 0 \text{ (hinge } i \text{ locked)} \\ f_i(m_i) = 0 \text{ if } d\phi_i^p \neq 0 \text{ (hinge } i \text{ active)} \end{cases}; f_i = \left  \frac{m_i}{1-d_i} \right  - M_u \leq 0$ <p><math>\delta_p = 0</math> (14.1.2)</p> $\begin{cases} d\phi_j^p = 0 \text{ if } f_j(m_j) < 0 \text{ (hinge } j \text{ locked)} \\ f_j(m_j) = 0 \text{ if } d\phi_j^p \neq 0 \text{ (hinge } j \text{ active)} \end{cases}; f_j = \left  \frac{m_j}{1-d_j} \right  - M_u \leq 0$ <p><math>M_u</math>: ultimate moment of the cross-section</p>
<p>Yield functions with hardening</p> $f_i = \left  \frac{m_i}{1-d_i} \right  - \left( M_p + (M_u - M_p)(1 - e^{-\alpha p_i}) \right) \leq 0$ $f_j = \left  \frac{m_j}{1-d_j} \right  - \left( M_p + (M_u - M_p)(1 - e^{-\alpha p_j}) \right) \leq 0$ <p style="text-align: right;">(14.1.3)</p> <p><math>M_p</math>: first plastic moment  <math>\alpha</math>: plastic hardening parameter  <math>p_i</math> and <math>p_j</math>: accumulated plastic deformations</p>
<p>Accumulated plastic deformations</p> $dp_i =  d\phi_i^p ; dp_j =  d\phi_j^p $ <p style="text-align: right;">(14.1.4)</p>

continued on following page

**Lumped Damage Mechanics**

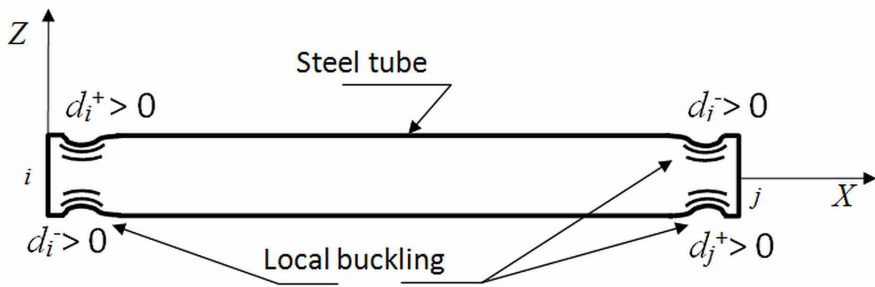
Table 2. Continued

<p>Yield functions</p> $f_i = \left(\frac{n}{N_u}\right)^2 + \left(\frac{m_i}{M_u(1-d_i)}\right)^2 - 1 \quad ; \quad f_j = \left(\frac{n}{N_u}\right)^2 + \left(\frac{m_j}{M_u(1-d_j)}\right)^2 - 1 \quad (14.1.5)$
<p>Normality rules</p> $d\phi_i^p = d\lambda_i \frac{\partial f_i}{\partial m_i} \quad ; \quad d\phi_j^p = d\lambda_j \frac{\partial f_j}{\partial m_j} \quad ; \quad d\delta_p = d\lambda_i \frac{\partial f_i}{\partial n} + d\lambda_j \frac{\partial f_j}{\partial n} \quad (14.1.6)$
<p>Plastic multipliers evolution laws</p> $\begin{cases} d\lambda_i = 0 \text{ if } f_i < 0 \text{ (hinge } i \text{ is locked)} \\ f_i = 0 \text{ if } d\lambda_i \neq 0 \text{ (hinge } i \text{ is active)} \end{cases} \quad ; \quad \begin{cases} d\lambda_j = 0 \text{ if } f_j < 0 \text{ (hinge } j \text{ is locked)} \\ f_j = 0 \text{ if } d\lambda_j \neq 0 \text{ (hinge } j \text{ is active)} \end{cases} \quad (14.1.7)$ <p><math>\lambda_i, \lambda_j</math>: plastic multipliers of hinges <math>i</math> and <math>j</math>.</p>
<p><b>Local Buckling Evolution Law</b></p>
<p>Plastic rotation and damage</p> $\phi^p = \frac{t_p}{L} \quad ; \quad d = 1 - \frac{Z(d)}{Z_0} \quad (14.1.8)$ <p><math>t_p</math>: plastic deflection  <math>Z_0</math>: initial, un-buckled, slope of the deflection vs. force curve (Figure 3a)  <math>Z(d)</math>: the damaged slopes</p>
<p>Damage</p> $d_i = \kappa_m \langle p_i - p_{cr} \rangle \quad (14.1.9)$ <p><math>p_{cr}</math>: critical plastic rotation that initiates local buckling  <math>\kappa_m</math>: slope of the line as indicated in Figure 5.</p>

continued on following page



Table 2. Continued

THE COUNTER-BUCKLING EFFECT AND A MODEL FOR GENERAL PLANAR LOADINGS
<i>Unilateral Elasticity Law for Steel Frame Elements with Hollow Cross-Sections</i>

<p>Local buckling damages: <math>(\mathbf{D}^+)_b = (d_i^+, d_j^+)</math> and <math>(\mathbf{D}^-)_b = (d_i^-, d_j^-)</math></p>
<p>Unilateral elasticity law</p> $\{\Phi\}_b - \{\Phi^p\}_b = [\mathbf{F}(\mathbf{D}^+)] \langle \mathbf{M} \rangle_b^+ + [\mathbf{F}(\mathbf{D}^-)] \langle \mathbf{M} \rangle_b^- + \{\Phi^0\}_b$ $[\mathbf{F}(\mathbf{D}^{+/-})] = \begin{bmatrix} \frac{L_b}{3EI_b (1 - d_i^{+/-})} & -\frac{L_b}{6EI_b} & 0 \\ -\frac{L_b}{6EI_b} & \frac{L_b}{3EI_b (1 - d_j^{+/-})} & 0 \\ 0 & 0 & \frac{L_b}{EA_b} \end{bmatrix} \quad (14.2.1)$
<p><math>\{\Phi\}_b</math> : deformation matrix  <math>\{\Phi^p\}_b</math> : plastic deformation matrix  <math>\langle \mathbf{M} \rangle_b^+, \langle \mathbf{M} \rangle_b^-</math> : positive and negative parts of the stress matrix.</p>
<b>Unilateral Yield Function</b>
<p>Unilateral yield function</p> $f_i = \text{Max} \left( \frac{m_i}{1 - d_i^+} - M_u, -\frac{m_i}{1 - d_i^-} - M_u \right) \leq 0 \quad (14.2.2)$

*continued on following page*

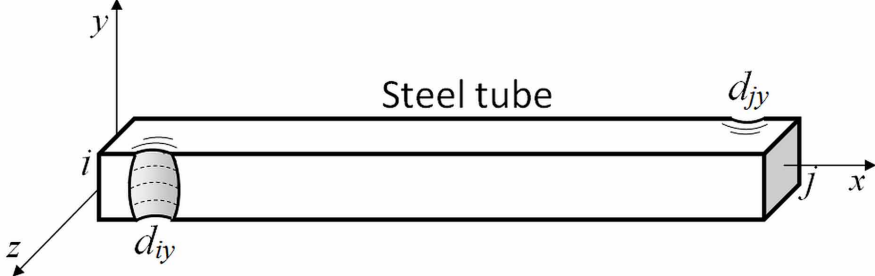
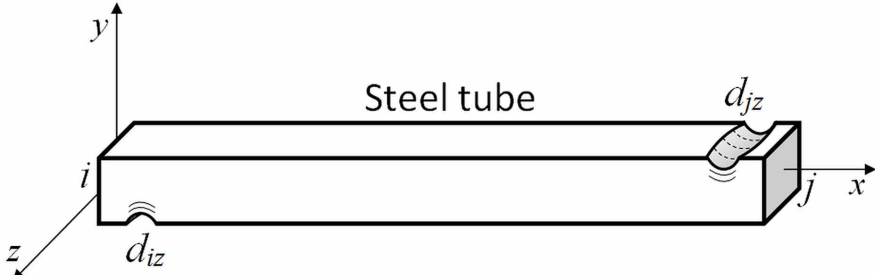
## Lumped Damage Mechanics

Table 2. Continued

<p>Plastic deformation evolution laws</p> $\begin{cases} d\phi_i^p = 0 \text{ if } f_i < 0 \text{ (hinge } i \text{ locked)} \\ f_i = 0 \text{ if } d\phi_i^p \neq 0 \text{ (hinge } i \text{ active)} \end{cases}$ $\delta_p = 0$ $\begin{cases} d\phi_j^p = 0 \text{ if } f_j < 0 \text{ (hinge } j \text{ locked)} \\ f_j = 0 \text{ if } d\phi_j^p \neq 0 \text{ (hinge } j \text{ active)} \end{cases} \quad (14.2.3)$
<p>Yield functions with nonlinear isotropic and kinematic hardening</p> $f_i(m_i, p_i, x_i) = \text{Max} \left( \frac{m_i}{1 - d_i^+} - x_i - (M_p + Q(p_i)); -\frac{m_i}{1 - d_i^-} + x_i - (M_p + Q(p_i)) \right) \leq 0 \quad (14.2.4)$ <p><math>x_i</math>: kinematic hardening term  <math>Q(p_i)</math>: isotropic hardening term  <math>M_p</math>: yield moment of the cross-section.</p>
<p><b>The Local Buckling Driving Rotation and the Local Buckling Evolution Laws</b></p>
<p>Local buckling driving rotations</p> $db_i^+ = \langle d\phi_i^p \rangle_+ + CBf \langle d\phi_i^p \rangle_- ; \text{ if } b_i^+ \geq 0; db_i^+ = 0 \text{ otherwise}$ $db_i^- = -\langle d\phi_i^p \rangle_- - CBf \langle d\phi_i^p \rangle_+ ; \text{ if } b_i^- \geq 0; db_i^- = 0 \text{ otherwise} \quad (14.2.5)$ <p><math>CBf</math>: counter-buckling factor (Can take values between 0 and 1). Good value: 0.7</p>
<p>Local buckling evolution law</p> $\begin{cases} \Delta d_i^+ = 0 \text{ if } b_i^+ < R(d_i^+) \\ b_i^+ = R(d_i^+) \text{ if } \Delta d_i^+ > 0 \end{cases} ; \begin{cases} \Delta d_i^- = 0 \text{ if } b_i^- < R(d_i^-) \\ b_i^- = R(d_i^-) \text{ if } \Delta d_i^- > 0 \end{cases} \quad (14.2.7)$ <p><math>R(d_i^{+/-})</math>: local buckling resistance function</p>
<p>Local buckling resistance function</p> $R(d_{i/j}^{+/-}) = p_{cr} + \frac{d_{i/j}^{+/-}}{\kappa_m} \quad (14.2.8)$ $R(d_{i/j}^{+/-}) = p_{cr} - \frac{1}{\kappa_c} \ln \left( 1 - \frac{d_{i/j}^{+/-}}{0.9} \right) \quad (14.2.9)$ <p><math>\kappa_c = 2.60</math> is estimated from the experimental results.</p>

continued on following page

Table 2. Continued

Damage Model for Tridimensional Steel Frames	
	
	
<p>Matrix of Damage</p> $(\mathbf{D})_b = (d_{iy}, d_{iz}, d_{jy}, d_{jz})$ <p> <math>d_{iy}</math>: local buckling damage due to bending moment around the local axis Y at the end <math>i</math>  <math>d_{iz}</math>: local buckling damage due to bending moments around the local axis Z at the end <math>i</math>  <math>d_{jy}</math>: local buckling damage due to bending moment around the local axis Y at the end <math>j</math>  <math>d_{jz}</math>: local buckling damage due to bending moments around the local axis Z at the end <math>j</math> </p>	

continued on following page

*Table 2. Continued*

Elasticity law

$$\{\Phi - \Phi^p\}_b = [\mathbf{F}(\mathbf{D})]_b \{\mathbf{M}\}_b + \{\Phi^0\}_b \quad (14.3.1)$$

$$\{\Phi\}_b^t = (\phi_{iy}^b, \phi_{jy}^b, \delta_b, \phi_{iz}^b, \phi_{jz}^b, \phi_x^b) \quad \{\mathbf{M}\}_b^t = (m_{iy}^b, m_{jy}^b, n_b, m_{iz}^b, m_{jz}^b, m_x^b)$$

$$\{\Phi^p\}_b^t = (\phi_{iy}^p, \phi_{jy}^p, \delta_p, \phi_{iz}^p, \phi_{jz}^p, \phi_x^p) \quad \{\Phi^0\}_b^t = (\phi_{iy}^0, \phi_{jy}^0, 0, \phi_{iz}^0, \phi_{jz}^0, 0) \quad (14.3.2)$$

$$[\mathbf{F}(\mathbf{D})] = \begin{bmatrix} \frac{L_b}{3(1-d_{iy})EI_y^b} & \frac{-L_b}{6EI_y^b} & 0 & 0 & 0 & 0 \\ \frac{-L_b}{6EI_y^b} & \frac{L_b}{3(1-d_{jy})EI_y^b} & 0 & 0 & 0 & 0 \\ 0 & 0 & \frac{L_b}{AE_b} & 0 & 0 & 0 \\ 0 & 0 & 0 & \frac{L_b}{3(1-d_{iz})EI_z^b} & \frac{-L_b}{6EI_z^b} & 0 \\ 0 & 0 & 0 & \frac{-L_b}{6EI_z^b} & \frac{L_b}{3(1-d_{jz})EI_z^b} & 0 \\ 0 & 0 & 0 & 0 & 0 & \frac{L_b}{GJ_b} \end{bmatrix} \quad (14.3.3)$$

$$\{\mathbf{M}\}_b = [\mathbf{E}(\mathbf{D})]_b \{\Phi - \Phi^p\}_b + \{\mathbf{M}^0(\mathbf{D})\}_b \quad (14.3.4)$$

$$[\mathbf{E}(\mathbf{D})]_b = [\mathbf{F}(\mathbf{D})]_b^{-1} =$$

$$\begin{bmatrix} \frac{12EI_y^b}{L_b} \frac{(1-d_{iy})}{4-(1-d_{iy})(1-d_{jy})} & \frac{-6EI_y^b}{L_b} \frac{(1-d_{iy})(1-d_{jy})}{4-(1-d_{iy})(1-d_{jy})} & 0 & 0 & 0 & 0 \\ \frac{-6EI_y^b}{L_b} \frac{(1-d_{iy})(1-d_{jy})}{4-(1-d_{iy})(1-d_{jy})} & \frac{12EI_y^b}{L_b} \frac{(1-d_{jy})}{4-(1-d_{iy})(1-d_{jy})} & 0 & 0 & 0 & 0 \\ 0 & 0 & \frac{AE_b}{L_b} & 0 & 0 & 0 \\ 0 & 0 & 0 & \frac{12EI_z^b}{L_b} \frac{(1-d_{iz})}{4-(1-d_{iz})(1-d_{jz})} & \frac{-6EI_z^b}{L_b} \frac{(1-d_{iz})(1-d_{jz})}{4-(1-d_{iz})(1-d_{jz})} & 0 \\ 0 & 0 & 0 & \frac{-6EI_z^b}{L_b} \frac{(1-d_{iz})(1-d_{jz})}{4-(1-d_{iz})(1-d_{jz})} & \frac{12EI_z^b}{L_b} \frac{(1-d_{jz})}{4-(1-d_{iz})(1-d_{jz})} & 0 \\ 0 & 0 & 0 & 0 & 0 & \frac{GJ_b}{L_b} \end{bmatrix} \quad (14.3.5)$$

*continued on following page*

<b>Yield Functions</b>
<p>Yield functions</p> $f_{i/j} = \left( \frac{n}{N_u} \right)^{\nu_1} + \left( \frac{m_{iy/jy}}{M_{uy}(1-d_{iy/jy})} \right)^{\nu_2} + \left( \frac{m_{iz/jz}}{M_{uz}(1-d_{iz/jz})} \right)^{\nu_3} - 1 \quad (14.3.6)$ <p>Parameters <math>\nu_1</math>, <math>\nu_2</math> and <math>\nu_3</math> can be taken equal to 2.</p>
<p>Normality laws and plastic multiplier evolution laws</p> $d\phi_{iy/jy}^p = d\lambda_{i/j} \frac{\partial f_{i/j}}{\partial m_{iy/jy}} \quad d\phi_{iz/jz}^p = d\lambda_{i/j} \frac{\partial f_{i/j}}{\partial m_{iz/jz}} \quad d\delta_p = d\lambda_i \frac{\partial f_i}{\partial n} + d\lambda_j \frac{\partial f_j}{\partial n}$ $\begin{cases} d\lambda_{i/j} = 0 \text{ if } f_{i/j}(m_{i/j}, n) < 0 \\ f_{i/j}(m_{i/j}, n) = 0 \text{ if } d\lambda_{i/j} > 0 \end{cases} \quad \begin{cases} d\phi_x^p = 0 \text{ if } f_x(m_x) < 0 \\ f_x(m_x) = 0 \text{ if } d\phi_x^p > 0 \end{cases} \quad (14.3.7)$
<b>Local Buckling Damage Function and Evolution Laws</b>
<p>Local buckling damage function for the inelastic hinge <math>i</math></p> $g_i = g_i(p_{iy}, p_{iz}, d_{iy}, d_{iz}) \leq 0 \quad (14.3.8)$
<p>Accumulated plastic rotations</p> $dp_{iy} = \left  d\phi_{iy}^p \right  \quad \text{and} \quad dp_{iz} = \left  d\phi_{iz}^p \right  \quad (14.3.9)$
<p>Local buckling evolution of an inelastic hinge <math>i</math></p> $\Delta d_{iy} = \Delta \mu_i \frac{\partial g_i}{\partial p_{iy}} \quad \Delta d_{iz} = \Delta \mu_i \frac{\partial g_i}{\partial p_{iz}} \quad (14.3.10)$ <p><math>\mu</math>: damage multiplier</p>
<p>Damage multiplier whose evolution law</p> $\begin{cases} \Delta \mu_i = 0 \text{ if } g_i < 0 \\ g_i = 0 \text{ if } \Delta \mu_i > 0 \end{cases} \quad (14.3.11)$
<b>Experimental Identification of the Local Buckling Damage Function for a Tube of Square Cross-Section</b>
<p>No local buckling domain</p> $d_{iy} = \kappa \langle p_{iy} - p_{cr} \rangle \quad ; \quad d_{iz} = \kappa \langle p_{iz} - p_{cr} \rangle \quad (14.3.12)$
<b>Experimental Identification of the Local Buckling Damage Function for a Tube of Rectangular Cross-Section</b>
<p>No local buckling domain</p> $d_{iy} = \kappa_y \langle p_{iy} - p_{cry} \rangle \quad ; \quad d_{iz} = \kappa_z \langle p_{iz} - p_{crz} \rangle \quad (14.3.13)$
<b>Local Buckling Damage Function for a Tube of Circular Cross-Section</b>
<p>Local buckling damage function</p> $g_i = \left( \frac{p_{iy}}{p_{cr} + d_{iy}/\kappa} \right)^2 + \left( \frac{p_{iz}}{p_{cr} + d_{iz}/\kappa} \right)^2 - 1 \quad (14.3.14)$

## REFERENCES

- Febres, R., Inglessis, P., & Flórez-López, J. (2003). Modeling of local buckling in tubular steel frames subjected to cyclic loading. *Computers & Structures*, 81(22), 2237–2247. doi:10.1016/S0045-7949(03)00292-X
- Florez-Lopez, J. (1999). *Plasticidad y fractura en estructuras aporticadas*. Centro Internacional de Métodos Numéricos en Ingeniería.
- Guerrero, N. (2007). *Análisis teórico-experimental del daño y del pandeo local en estructuras de ingeniería civil*. (Unpublished doctoral dissertation). University of Los Andes, Los Andes, Venezuela.
- Guerrero, N., Marante, M. E., Picón, R., & Flórez-López, J. (2007). Model of local buckling in steel hollow structural elements subjected to biaxial bending. *Journal of Constructional Steel Research*, 63(6), 779–790. doi:10.1016/j.jcsr.2006.08.006
- Inglessis, P., Gómez, G., Quintero, G., & Flórez-López, J. (1999). Model of damage for steel frame members. *Engineering Structures*, 21(10), 954–964. doi:10.1016/S0141-0296(98)00038-8
- Inglessis, P., Medina, S., López, A., Febres, R., & Flórez-López, J. (2002). Modeling of local buckling in tubular steel frames by using plastic hinges with damage. *Steel and Composite Structures*, 2(1), 21–34. doi:10.12989/scs.2002.2.1.021

## Compilation of References

- ACI Committee, American Concrete Institute, & International Organization for Standardization. (2005). Building code requirements for structural concrete (ACI 318-05) and commentary. American Concrete Institute.
- Alarcón, E., Recuero, A., Perera, R., López, C., Gutiérrez, J. P., & De Diego, A. et al. (2001). A reparability index for reinforced concrete members based on fracture mechanics. *Engineering Structures*, 23(6), 687–697. doi:10.1016/S0141-0296(00)00075-4
- Alva, G. M. S., & El Debs, A. L. H. C. (2010). Application of lumped dissipation model in nonlinear analysis of reinforced concrete structures. *Engineering Structures*, 32(4), 974–981. doi:10.1016/j.engstruct.2009.12.024
- Anderson, T. L. (2005). *Fracture mechanics: Fundamentals and applications*. CRC Press.
- Araujo, F., & Proença, S. P. B. (2008). Application of a lumped dissipation model to reinforced concrete structures with the consideration of residual strains and cycles of hysteresis. *Journal of Mechanics of Materials and Structures*, 3(5), 1011–1031. doi:10.2140/jomms.2008.3.1011
- Atkinson, K. E. (1989). *An introduction to numerical analysis*. New York, NY: John Wiley & Sons.
- Avon, D. T., Marante, M. E., & Flórez-López, J. (2002). El doble paso de INTEGRACIÓN: Un algoritmo computacional para mejorar la convergencia en problemas altamente no lineales. In *Proceedings of the Conference CIMENICS, Numerical Methods in Engineering and Applied Sciences (TM1-TM8)*. Caracas, Venezuela: SVMNI.
- Avon, D., Marante, M. E., Picón, R., & Flórez-López, J. (2009). Modelo de daño para elementos de concreto armado sometidos a solicitaciones monotónicas de torsión. In *Proceedings of IX Venezuelan Congress on Seismology and Seismic Engineering*. Caracas, Venezuela: Academic Press.
- Bathe, J. (1996). *Finite element procedures in engineering analysis*. Prentice Hall.
- Batoz, J. L., & Dhatt, G. (1992). *Modélisation des structures par éléments finis: Poutres et plaques* (Vol. 2). Paris, France: Hermès.
- Batoz, J. L., & Dhatt, G. (1992). *Modélisation des structures par éléments finis: Solides élastiques* (Vol. 1). Paris, France: Hermès.
- Boore, D. M. (2003). Simulation of ground motion using the stochastic method. *Pure and Applied Geophysics*, 60(3), 635–676. doi:10.1007/PL00012553
- Bousias, S. N., Verzeletti, G., Fardis, M. N., & Gutiérrez, E. (1995). Load-path effects in column biaxial bending with axial force. *Journal of Engineering Mechanics*, 121(5), 596–605. doi:10.1061/(ASCE)0733-9399(1995)121:5(596)
- Broek, D. (1986). *Elementary engineering fracture mechanics*. The Hague, The Netherlands: Martinus Nijhoff Publishers; doi:10.1007/978-94-009-4333-9
- Carnahan, B., Luther, H., & Wilkes, J. (1969). *Applied numerical methods*. New York, NY: John Wiley & Sons.

## Compilation of References

- Chen, W. F., & Sohal, I. (1995). *Plastic design and second-order analysis of steel frames*. New York, NY: Springer-Verlag. doi:10.1007/978-1-4613-8428-1
- Cipollina, A., López-Inojosa, A., & Flórez-López, J. (1995). A simplified damage mechanics approach to nonlinear analysis of frames. *Computers & Structures*, 54(6), 1113–1126. doi:10.1016/0045-7949(94)00394-I
- Clough, R. W., & Penzien, J. (1993). *Dynamics of structures*. New York, NY: McGraw-Hill.
- Colombo, A., & Negro, P. (2005). A damage index of generalized applicability. *Engineering Structures*, 27(8), 1164–1174. doi:10.1016/j.engstruct.2005.02.014
- Corradi, L., De Donato, O., & Maier, G. (1974). Inelastic analysis of reinforced concrete frames. *Journal of the Structural Division*, 100(9), 1925–1942.
- Cosenza, E., & Manfredi, G. (2000). Damage indices and damage measures. *Progress in Structural Engineering and Materials*, 2(1), 50–59. doi:10.1002/(SICI)1528-2716(200001/03)2:1<50::AID-PSE7>3.0.CO;2-S
- Craig, R. R. (1981). *Structural dynamics—An introduction to computer methods*. New York, NY: John Wiley & Sons.
- Faleiro, J., Oller, S., & Barbat, A. H. (2010). Plastic-damage analysis of reinforced concrete frames. *Engineering Computations*, 27(1), 57–83. doi:10.1108/02644401011008522
- Febres, R., Inghlessi, P., & Flórez-López, J. (2003). Modeling of local buckling in tubular steel frames subjected to cyclic loading. *Computers & Structures*, 81(22), 2237–2247. doi:10.1016/S0045-7949(03)00292-X
- Fenton, G. A., & Venmarcke, E. H. (1990). Simulation of random fields of earthquake ground vibrations. *Journal of Engineering Mechanics*, 116(8), 1733–1749. doi:10.1061/(ASCE)0733-9399(1990)116:8(1733)
- Flórez-López, J. (1995). A simplified model of unilateral damage for RC frames. *Journal of Structural Engineering*, 121(12), 1765–1772. doi:10.1061/(ASCE)0733-9445(1995)121:12(1765)
- Florez-Lopez, J. (1999). *Plasticidad y fractura en estructuras aporticadas*. Centro Internacional de Métodos Numéricos en Ingeniería.
- Friedlander, F. G., & Joshi, M. S. (1998). *Introduction to the theory of distributions*. Cambridge, UK: University Press.
- Guerrero, N. (2007). *Análisis teórico-experimental del daño y del pandeo local en estructuras de ingeniería civil*. (Unpublished doctoral dissertation). University of Los Andes, Los Andes, Venezuela.
- Guerrero, N., Marante, M. E., Picón, R., & Flórez-López, J. (2007). Model of local buckling in steel hollow structural elements subjected to biaxial bending. *Journal of Constructional Steel Research*, 63(6), 779–790. doi:10.1016/j.jcsr.2006.08.006
- Hsu, T. (1984). *Torsion of reinforced concrete members*. New York, NY: Van Nostrand Reinhold.
- Hsu, T. C., & Mo, Y. L. (2010). *Unified theory of concrete structures*. West Sussex, UK: John Wiley and Sons. doi:10.1002/9780470688892
- Inghlessi, P., Gómez, G., Quintero, G., & Flórez-López, J. (1999). Model of damage for steel frame members. *Engineering Structures*, 21(10), 954–964. doi:10.1016/S0141-0296(98)00038-8
- Inghlessi, P., Medina, S., López, A., Fébres, R., & Flórez-López, J. (2002). Modeling of local buckling in tubular steel frames by using plastic hinges with damage. *Steel and Composite Structures*, 2(1), 21–34. doi:10.12989/scs.2002.2.1.021
- Jenkins, W. M. (1982). *Structural mechanics and analysis*. Berkshire, UK: Van Nostrand Reinhold Co. LTD.
- Kappos, A. J. (1997). Seismic damage indices for RC buildings: Evaluation of concepts and procedures. *Progress in Structural Engineering and Materials*, 1(1), 78–87. doi:10.1002/pse.2260010113
- Kent, D. C., & Park, R. (1971). Flexural members with confined concrete. *Journal of the Structural Division*, 97, 1960–1990.
- Lampert, P., & Collins, M. P. (1972). Torsion, bending and confusion – An attempt to establish the facts. *ACI Journal*, 69-45, 500-504.
- Leckie, F. A., & Bello, D. J. (2009). *Strength and stiffness of engineering systems*. New York, NY: Springer.



- Lemaitre, J. (1992). *A course on damage mechanics*. Berlin, Germany: Springer-Verlag. doi:10.1007/978-3-662-02761-5
- Lemaitre, J., & Chaboche, J. L. (1985). *Mécanique des matériaux solides*. Paris, France: Dunod Bordas.
- Lemaitre, J., & Desmorat, R. (2005). *Engineering damage mechanics, ductile, creep, fatigue and brittle failures*. Berlin: Springer.
- Li, G. Q., & Li, J. J. (2007). *Advanced analysis and design of steel frames*. John Wiley & Sons. doi:10.1002/9780470319949
- Liu, Y. B., & Liu, J. B. (2004). A damage beam element model for nonlinear analysis of reinforced concrete member. *Earthquake Engineering and Engineering Vibration-Chinese Edition*, 24(2), 95-100.
- Marante, M. E., Benallal, A., & Flórez-López, J. (2007). Análisis de falla de sólidos inelásticos mediante la teoría de localización. *Acta Científica Venezolana*, 58(2), 43–51.
- Marante, M. E., & Flórez-López, J. (2002). Model of damage for RC elements subjected to biaxial bending. *Engineering Structures*, 24(9), 1141–1152. doi:10.1016/S0141-0296(02)00044-5
- Marante, M. E., & Flórez-López, J. (2003). Three dimensional analysis of reinforced concrete frames based on lumped damage mechanics. *International Journal of Solids and Structures*, 40(19), 5109–5123. doi:10.1016/S0020-7683(03)00258-0
- Marante, M. E., & Flórez-López, J. (2004). Plastic localization revisited. *Journal of Applied Mechanics*, 71(2), 283–284. doi:10.1115/1.1636790
- Marante, M. E., Suárez, L., Quero, A., Redondo, J., Vera, B., & Uzcátegui, M. et al. (2005). Portal of damage: A web-based finite element program for the analysis of framed structures subjected to overloads. *Advances in Engineering Software*, 36(5), 346–358. doi:10.1016/j.advengsoft.2004.06.017
- McGuire, W., Gallagher, R. H., & Ziemian, R. D. (1979). *Matrix structural analysis*. New York, NY: John Wiley & Sons.
- Negro, P., Verzeletti, G., Magonette, G. E., & Pinto, A. V. (1994). *Tests on a four-storey full-scale R/C frame designed according to Eurocodes 8 and 2: Preliminary report (EUR 15879EN)*. Ispra, Italy: ELSA Laboratory.
- Newmark, N. M., & Hall, W. J. (1982). Earthquake spectra and design. *Earth System Dynamics*, 1.
- Oliva, M. G. (1980). *Shaking table testing of a reinforced concrete frame with biaxial response: Report No. EERC 80-28*. Berkeley, CA: Earthquake Engineering Research Center, University of California.
- Oliva, M. G., & Clough, R. W. (1987). Biaxial seismic response of R/C frames. *Journal of Structural Engineering*, 113(6), 1264–1281. doi:10.1061/(ASCE)0733-9445(1987)113:6(1264)
- Ortiz, J., & Hernando, J. I. (2002). *Estructuras de edificación: Análisis lineal y no lineal*. Barcelona, Spain: Ariel.
- Padilla, D., & Rodriguez, M. (2009). A damage index for the seismic analysis of reinforced concrete members. *Journal of Earthquake Engineering*, 13(3), 364–383. doi:10.1080/13632460802597893
- Park, R., & Paulay, T. (1975). *Reinforced concrete structures*. New York, NY: John Wiley and Sons. doi:10.1002/9780470172834
- Park, Y. J., & Ang, A. H. S. (1985). Mechanistic seismic damage model for reinforced concrete. *Journal of Structural Engineering*, 111(4), 722–739. doi:10.1061/(ASCE)0733-9445(1985)111:4(722)
- Paz, M. (1997). *Structural dynamics-Theory and computation*. Boston, MA: Springer. doi:10.1007/978-1-4684-0018-2
- Perdomo, M. E. (2010). *Fractura y daño en estructuras duales de concreto armado*. (Unpublished doctoral dissertation). University of Los Andes, Los Andes, Venezuela.
- Perdomo, M. E., Picón, R., Marante, M. E., Hild, F., Roux, S., & Flórez-López, J. (2013). Experimental analysis and mathematical modeling of fracture in RC elements with any aspect ratio. *Engineering Structures*, 46, 407–416. doi:10.1016/j.engstruct.2012.07.005

## Compilation of References

- Picón, R. (2004). *Modelo simplificado para el comportamiento dinámico de pórticos con vigas plana-columna de concreto armado considerando el deslizamiento entre el refuerzo y el concreto en las junta*. (Unpublished Doctoral Dissertation). University of Los Andes, Los Andes, Venezuela.
- Picon-Rodriguez, R., Quintero-Febres, C., & Florez-Lopez, J. (2007). Modeling of cyclic bond deterioration in RC beam-column connections. *Structural Engineering & Mechanics*, 26(5), 569–589. doi:10.12989/sem.2007.26.5.569
- Powell, G. H. (1969). Theory of nonlinear elastic structures. *Structural Division Journal*, 95, 2687–2701.
- Priestley, M. J. N., Verma, R., & Xiao, Y. (1994). Seismic shear strength of reinforced concrete columns. *ASCE Journal of Structural Engineering*, 120(8), 2310–2329.
- Rajasankar, J., Iyer, N. R., & Prasad, A. P. (2009). Modeling inelastic hinges using CDM for nonlinear analysis of reinforced concrete frame structures. *Computers and Concrete*, 6(4), 319–341. doi:10.12989/cac.2009.6.4.319
- Rice, J. R. (2010). *Solid mechanics*. Retrieved from [http://esag.harvard.edu/rice/e0\\_Solid\\_Mechanics\\_94\\_10.pdf](http://esag.harvard.edu/rice/e0_Solid_Mechanics_94_10.pdf)
- Rojas, R., Vera, B., Picón, R., Marante, M. E., & Flórez-López, J. (2008). Computation of retrofitting of vulnerable RC structures using damage mechanics and experimental analyses. In *Proceedings of 4th International Conference on Structural Defects and Repair* (pp. 25-28). Aveiro, Portugal: Academic Press.
- Sezen, H., & Moehle, J. P. (2004). Shear strength model for lightly reinforced columns. *Journal of Structural Engineering*, 130(11), 1692–1703.
- Sezen, H., & Moehle, J. P. (2007). Seismic test of concrete columns with light transverse reinforcement. *ACI Structural Journal*, 133(11), 864–870.
- Shi, Z. (2009). *Crack analysis in structural concrete: Theory and applications*. Burlington, MA: Butterworth-Heinemann.
- Simo, J. C., Kennedy, J. G., & Govindjee, S. (1988). Non-smooth multisurface plasticity and viscoplasticity: Loading/unloading conditions and numerical algorithms. *International Journal for Numerical Methods in Engineering*, 26(10), 2161–2185. doi:10.1002/nme.1620261003
- Sinha, R., & Shiradhonkar, S. R. (2012). Seismic damage index for classification of structural damage – Closing the loop. In *Proceedings of the 15th World Conference on Earthquake Engineering*. Lisboa, Portugal: Academic Press.
- Sterling, J. (1958). *Indeterminate structural analysis*. Reading, MA: Addison-Wesley Pub. Co.
- Tang, X. S., Zhang, J. R., Li, C. X., Xu, F. H., & Pan, J. (2005). Damage analysis and numerical simulation for failure process of a reinforced concrete arch structure. *Computers & Structures*, 83(31), 2609–2631. doi:10.1016/j.compstruc.2005.03.017
- Teng, T., & Teng, S. (2004). Effective torsional rigidity of reinforced concrete members. *ACI Structural Journal*, 101(2).
- Thomson, E. (2004). *Modelo simplificado para la evaluación del daño en muros estructurales bajos de concreto armado sujetos a cargas laterales*. (Unpublished doctoral dissertation). University of Los Andes, Los Andes, Venezuela.
- Thomson, E., Perdomo, M. E., Picón, R., Marante, M. E., & Flórez López, J. (2009). Simplified model for damage in squat RC shear wall. *Engineering Structures*, 31(10), 2215–2223. doi:10.1016/j.engstruct.2009.05.020
- Timoshenko, S. (1955). *Strength of materials, part I, elementary theory and problems*. New York, NY: D. Van Nostrand Company.
- Timoshenko, S. (1956). *Strength of materials, part II, advanced theory and problems*. New York, NY: D. Van Nostrand Company.
- Vanmarcke, E. H., Cornell, C. A., Gasparini, D. A., & Hou, S. N. (1990). *SIMQKE-I: Simulation of earthquake ground motions*. Cambridge, MA: MIT Press.

## Compilation of References

Von Ramin, M., & Matamoros, A. (2006). Shear strength of reinforced concrete members subjected to monotonic loads. *ACI Structural Journal*, 103(1), 83–92.

Whittaker, B. N., Singh, R. N., & Sun, G. (1992). *Rock fracture mechanics: Principles, design, and applications*. Amsterdam: Elsevier.

*Wikipedia*. (2010). Retrieved from <http://en.wikipedia.org/wiki/Wikipedia>

Williams, M. S., & Sexsmith, R. G. (1995). Seismic damage indices for concrete structures: A state-of-the-art. *Earthquake Spectra*, 11(2), 740–757. doi:10.1193/1.1585817

Yang, T. S., & Wang, J. L. (2010). Damage analysis of three-dimensional frame structure suffering from impact. *Journal of Vibration and Shock*, 29(12), 177–180.

## About the Authors

**Julio Flórez-López** is a Professor of Structural Engineering at the University of Los Andes in Venezuela. He has a degree in Civil Engineering of the University of Los Andes. He did his postgraduate studies at the Laboratoire de Mécanique et Technologie, Cachan, France, where he got a Doctoral degree on Applied Solid Mechanics. He has been visiting professor at the Polytechnic University of Madrid, University of Paris VI, University of São Paulo, and Kyoto University. He works on the theoretical and computational aspects of damage mechanics and its applications to civil engineering problems.

**María Eugenia Marante** is a Professor of Structural Engineering at Lisandro Alvarado University, Venezuela. She majored in Structural Mechanics at the University of Los Andes, Venezuela, attended Rutgers University, New Jersey, as an exchange student, and received a Doctoral degree in Applied Science from the University of Los Andes in 2004. Her research interests include modeling and simulation of the behavior of solids and structures, numerical methods in engineering, damage theory and its applications in earthquake engineering problems. Maria Eugenia Marante co-directs Structural Mechanics Laboratory (LME) at Lisandro Alvarado University, Venezuela, an environment for experimental research in the above-mentioned areas, and is involved in several research projects.

**Ricardo Picón** is a Professor of Structural Engineering at Lisandro Alvarado University in Venezuela. He got a Civil Engineer Degree at Experimental University of the Armed Forces, Venezuela, in 1992, a Master's degree in Structural Engineering in 2000, and the Doctoral degree in Applied Sciences in 2004 at the University of Los Andes, Venezuela. Professor Ricardo Picón was a postdoctoral scholar at Ferguson Structural Engineering Laboratory, University of Texas at Austin, in 2006. His research interests include experimental test to real scale in laboratory of reinforced concrete and steel structures. He co-directs Structural Mechanics Laboratory (LME), an experimental research institute at Lisandro Alvarado University, Venezuela.

# Index

## A

acceleration 14, 42, 100-101, 292, 334, 385-386, 454, 479, 503-504, 506, 509, 526, 533  
 algebraic manipulation program 30, 139, 157, 166-169, 490  
 algorithm 86-87, 90-91, 93-94, 96-97, 99-101, 276, 280-281, 284-290, 292, 382-384, 388-389, 451  
 Assemblage 3-4, 85-88, 91, 94, 112-114, 116, 139, 232, 243, 247, 280, 420

## B

beam 4-6, 8-23, 26-30, 32, 41, 46, 48, 73-74, 76-79, 81-82, 85, 105-106, 109, 112, 172-179, 181-183, 198-199, 202, 222, 238, 273, 330, 375-376, 398, 400, 406, 414, 432-435, 437-438, 460, 463, 466, 470, 488-489, 565-567, 572-573, 575-577  
 beam-column 31, 181, 197-198, 202, 227, 232-233, 236, 241-243, 247, 257, 269, 363, 365-366, 460, 463, 465-467  
 behavior 2, 4-5, 7, 31, 46, 48, 141-146, 148-149, 151, 153, 157-158, 160, 164, 167, 169, 172-173, 177, 179-181, 185-189, 198-199, 201-203, 233, 236-238, 244, 260, 264, 266, 288-289, 337, 339, 341, 343, 345-346, 355-357, 359, 362, 365, 371, 376-377, 380, 383, 389, 400, 412, 432-436, 448, 450-451, 462, 466, 472, 479-481, 493-494, 498, 500, 503, 506-507, 526, 538-539, 542, 545, 547, 549, 556, 558, 580, 583  
 bending 15-18, 20-21, 23, 26-27, 40, 46, 138, 172-177, 181-186, 191-198, 205, 222-223, 225-227, 238, 244, 259-261, 264, 266, 348, 365, 370-373, 388, 396, 400-402, 406-407, 414-415, 424, 428-430, 438, 445, 450, 470-471, 473-474, 477-478, 543-544, 546, 551, 556

## C

Capacity 151, 505-506, 526-527, 533, 536-537  
 component 1, 3-6, 86, 90, 96, 99-101, 186, 243-244, 247, 363, 420  
 constitutive 3-4, 7, 10, 18-20, 23, 27, 45-48, 51-52, 59-60, 76, 85, 92-93, 101, 143-145, 148-149, 151, 156, 160, 172, 177, 185, 231, 233-236, 238-239, 243-244, 285, 290, 338, 346-347, 374, 382, 398, 460, 467, 473  
 coordinate axes 20, 35-37, 46, 48, 54, 56  
 Corrector 276, 284-286, 288-290, 292  
 cracking 7-8, 241, 332, 334-338, 340, 343-344, 362-364, 368-372, 374, 379, 388-389, 396, 398, 412, 414-419, 421-422, 424-428, 435, 437-438, 445-450, 460, 462, 466, 468, 470-471, 473-475, 479, 493, 497, 506, 538  
 Crack Resistance Function 336-337, 341, 349, 355, 365, 367-369, 379-380, 389, 404, 425, 427-428, 449, 470  
 cross-section 4-5, 10-12, 17-23, 28, 34, 41, 46, 51, 54, 60, 172-174, 179, 181, 183-187, 190-196, 198, 202, 217-224, 226-228, 233-235, 239, 242, 245-246, 326, 333, 338, 346, 370, 385, 396, 410, 449, 451-453, 463, 471-472, 506-507, 539-540, 542, 544, 546, 549-551, 555, 560, 562-563, 566, 570-571, 573-574  
 curve 7, 148, 151-152, 157, 164-166, 170-171, 185, 188-189, 199, 233, 237-238, 259, 261, 266, 272, 334-336, 341, 345, 348, 355-357, 359, 365, 375, 379, 398, 400, 402-403, 405-406, 408-409, 425, 428, 453, 462, 494, 496-498, 500, 505-506, 526-527, 533, 536-537, 539, 543-545, 547, 554-555, 563, 566, 578, 580, 582  
 Cycle Fatigue 379, 389, 406, 429

## D

dimensionless coefficient 241

## Index

Direct 38, 84, 90, 94-95, 101, 105, 109, 116, 121, 139, 277, 280, 282, 305, 365  
Displacements 3, 10, 12-13, 15, 18, 20, 23, 31-38, 42-45, 54, 56, 59-60, 73, 85-86, 90, 92-95, 97, 101, 105-106, 108-109, 111-112, 116, 120-121, 124, 126-127, 129-133, 135, 138, 141, 156, 160, 231-232, 277, 280, 282, 285, 305, 308-310, 313-316, 318-319, 323-324, 326, 331, 365, 376, 378-379, 383, 388, 414, 425, 454, 479-480, 489, 506-507, 545, 547, 555, 562-563, 573, 578, 580-582  
distribution 8, 46, 158, 172-176, 181-183, 190-191, 194, 199, 202, 218-219, 221, 232, 239, 372, 449, 453, 456, 460-461, 463, 466, 468, 481, 507, 570-571, 578-580  
dynamic 2-4, 8-9, 14-15, 31, 40, 44, 58, 84, 99, 101, 276, 292, 383, 386, 503, 505-506, 526-527, 533, 536-537

## E

earthquake 9, 39, 93, 99, 198, 231-232, 385-386, 445, 454, 479, 503, 506, 509, 523, 526, 533, 536, 538-539  
elasticity 6-7, 10, 18-19, 31, 43, 45-46, 48, 51, 54, 60, 76-81, 84-85, 92, 99, 107, 109-110, 112, 114, 116, 124, 141-146, 148-154, 156-157, 160, 164, 166-167, 169, 172-174, 176-177, 180-181, 183-184, 186-188, 205, 217-218, 220, 222, 231-239, 243-245, 247, 259, 264, 276-279, 284-286, 288-292, 302, 326, 332-335, 337-342, 344, 347, 355, 357-359, 363-365, 367, 382-383, 388-389, 399, 401-402, 404, 406-407, 412, 418, 420, 423-426, 445-446, 448, 451, 454, 460, 468, 470, 472-474, 479, 492, 538-541, 544, 547, 549, 552, 556-558, 560, 562-564, 566, 570, 574, 578, 581  
elasto-plastic 141, 144, 149-153, 157-158, 160, 172-173, 182, 185, 189, 205, 231, 233, 235, 238, 241, 243-244, 247, 259, 261, 266, 276-277, 290, 292, 328-329, 332, 337, 339, 342, 362, 368, 374-376, 382, 389, 398-399, 420, 473, 539  
energy release 335-337, 340, 345, 349, 355, 358, 364, 367-368, 379-380, 389, 404, 424, 427, 449, 470-471, 473, 477  
equilibrium 3-4, 8-10, 14-15, 17-19, 23, 26-27, 38, 40, 44-46, 59-60, 74-75, 85, 90, 92-94, 96-97, 100-101, 109, 158, 181, 191, 193-195, 202, 246, 285, 290, 292, 346-347, 365, 399, 401-402, 407, 425, 491

evolution 144-146, 148-151, 156-157, 160, 166-167, 177, 179-181, 197-198, 202, 205, 234-237, 239, 244-245, 259-260, 264, 266, 268-269, 272-273, 278, 338, 340-343, 345, 349, 364-365, 368, 373, 379-380, 400, 404, 408, 415-419, 421-422, 424, 429-436, 438, 449-451, 460, 462, 538-539, 542-544, 550-553, 559-561, 563  
external forces 1, 3, 14, 17-18, 20, 23, 42-43, 45-46, 59-60, 74, 85, 91, 94, 101, 160, 277-278, 335-336, 388, 412, 445

## F

force 15-19, 23, 26-27, 30, 40-42, 46-47, 51, 58, 91, 112, 121, 159, 172-173, 177, 181-183, 186-187, 189-196, 201-203, 223, 225, 228, 235, 240-242, 246, 256-260, 264, 266, 269, 333-338, 346, 348-349, 365, 367-369, 371-373, 377-379, 388, 398, 400-403, 406-409, 414-416, 418-419, 421-422, 424-430, 432-437, 446, 451-455, 468, 470-472, 477, 494, 496-498, 500, 539-540, 544-548, 550, 554-556, 560-561, 563-566, 568-569, 571-572, 578-580, 582  
forces applied 7-8, 43, 85  
Formulation 10, 31, 82, 84, 171, 181, 276-277, 284, 290, 328-329, 339, 380, 420, 430  
Fracture mechanics 2, 332-333, 337, 341, 349, 362, 365, 503, 539

## G

Generalized 7-8, 10-12, 14-16, 23, 31-35, 39-42, 54-56, 58-60, 74-77, 86, 90, 100-101, 105, 108-109, 111, 116, 120-121, 130, 160, 186, 205, 232-233, 244, 276, 290-291, 307, 340, 343, 363-364, 389, 404, 412, 460, 473, 489, 507  
global 37, 56, 89, 118, 120, 282, 284-285, 290, 292, 337, 382-383, 386, 388-389  
Griffith Criterion 335-336, 341, 358, 368-369, 375, 379-380, 388-389, 400, 402, 404-405, 407, 424, 429

## H

hand term 14, 18, 85, 94, 97, 101  
hardening 141, 149-158, 160, 164, 166-169, 171, 178-181, 185, 189, 194, 198, 201-202, 205, 235-236, 240, 246, 259-261, 266, 290, 342-343, 368, 373, 398, 429, 450, 539, 542, 551, 561, 566, 570, 581

Hinge-By-Hinge 276-277, 280-282, 284, 292, 301  
 hinges 6, 141, 172, 174, 177-181, 183-186, 189,  
 196-205, 227, 231-238, 243-245, 247, 277-280,  
 282, 286-289, 291-292, 307, 309-311, 313,  
 315-316, 318-319, 321, 323, 325-326, 348,  
 350, 362, 364-365, 368, 373, 376, 388-389,  
 414, 420, 423-424, 429, 437, 445, 450, 460,  
 462, 473-474, 477, 479, 488, 491, 538-540,  
 542-543, 545-546, 551, 555, 560, 570, 581  
 hypothesis 4, 10-11, 19-22, 172, 187, 199, 205, 247,  
 332, 338-339, 341, 344, 349, 363, 373, 375,  
 389, 423, 429, 462, 468, 471, 477, 542, 547,  
 549-550, 559, 581

## I

inelastic 6, 31, 93, 160, 198, 202-204, 232, 236, 238,  
 276, 288-289, 362, 364-365, 383, 389, 420,  
 423, 429, 450, 460, 462, 477, 560  
 infinite number solutions 345, 348-349  
 Isotropic 28, 141, 149, 151-157, 160, 164, 178-181,  
 205, 236, 240, 245, 259-260, 398, 450, 551

## K

Kinematic 3-4, 9, 12-13, 17, 19, 23, 35, 37-39,  
 44-46, 54-58, 60, 73, 85, 92-93, 100-101, 141,  
 153, 156-158, 160, 166, 176, 179-181, 202,  
 205, 236, 240, 245, 259-261, 266, 282, 285,  
 290, 346, 365, 373, 398, 401-402, 406-407,  
 425, 429, 450, 491, 551

## L

left hand term 14, 85, 94, 97, 101  
 longitudinal 17, 23, 187, 189, 198, 236, 240-241,  
 246, 388-389, 415, 425, 457-458, 460, 472,  
 480, 506, 509

## M

material properties 46, 375, 385, 410, 426, 489  
 matrix 10-11, 15, 32-34, 36-38, 40-44, 47-48, 51-  
 52, 54-56, 58-60, 74-75, 78-81, 84-91, 93-94,  
 97-101, 106-114, 116, 118-119, 124, 126-132,  
 134, 136-137, 139, 185, 232-233, 238-239,  
 244-245, 276-280, 282, 286-287, 290, 305,  
 310-311, 315-316, 320-321, 325-327, 363-364,  
 382-383, 404, 420, 424, 446, 448, 490, 541,  
 549, 556-558

method 38, 84-85, 90, 93-95, 97-99, 101, 105, 109,  
 116, 121, 139, 144, 241, 276-277, 280, 282,  
 287, 290, 292, 301, 305, 365, 382-383, 425,  
 431, 470  
 moment 8, 15-19, 21-23, 26-27, 40-42, 46, 59-60,  
 109, 113, 121-122, 138, 158, 172-177, 179-  
 183, 190, 192-193, 195-196, 198-199, 201-202,  
 217-225, 227, 232-235, 269, 280, 309, 313,  
 367-370, 372, 374, 376, 388, 396, 398, 400,  
 402, 404, 406-407, 414, 424, 461, 493-494,  
 497-498, 500, 506, 542, 544, 551, 556, 560,  
 563  
 moment-curvature 174, 205  
 Mono-sign 142-144, 149, 152-153, 365, 379-380,  
 398, 414-416, 430, 435, 437, 446, 450, 466-  
 467, 473, 475, 538-539, 549, 552-553, 555,  
 570, 573, 578, 581

## N

Newton-Raphson 97, 101, 139, 285, 287  
 Nonlinear 9, 31, 38, 45-46, 84, 92-94, 96-97, 101,  
 121, 124, 151, 153-155, 157-158, 160, 164,  
 166, 178-180, 187, 189, 233, 236, 240, 276-  
 277, 284-285, 287, 290, 292, 382, 494, 498,  
 500, 503, 506, 542, 551, 581

## P

peak 188, 335-336, 346-348, 365, 415, 454, 479,  
 503-504, 509, 526, 533  
 phenomena 143, 149, 151, 157, 160, 202, 343, 388,  
 418, 444, 460, 538  
 Planar 10-11, 15, 17, 19, 23, 31-33, 40, 59-60, 81,  
 85-87, 89-90, 99, 113, 136-137, 189, 231, 362,  
 366, 380, 430, 473, 481, 538, 545, 549, 570-  
 571  
 plasticity 2, 6-7, 141-157, 160, 164, 166-167, 169,  
 171-183, 185-186, 189-193, 195-202, 205,  
 217-222, 224, 226-227, 231-245, 247, 256-260,  
 264, 266, 268-269, 272, 276-280, 282, 284-  
 292, 307, 309-310, 313, 315, 318-319, 323,  
 325-326, 328, 332, 337-338, 340, 342-343,  
 348, 350, 355-356, 362-363, 365, 368, 370,  
 373-374, 376-377, 388-389, 400-402, 404, 406,  
 412, 414, 420, 423-424, 429-430, 437, 444-  
 445, 450-451, 468, 471-474, 488, 491, 494,  
 498, 506-507, 538-540, 542-546, 549-552, 555,  
 559-561, 570, 581  
 Portal 506-509, 526, 537

## Index

positive direction 156-157, 334  
Predictor 96-97, 284-286, 288-290, 292

## R

RC 186-187, 189-198, 201-202, 205, 228-229, 233, 235-238, 240-241, 243, 245, 247, 256-257, 259, 261, 266, 269, 274, 301, 310, 315, 319, 326, 337, 362-364, 368-370, 373, 375-376, 379-380, 383, 388-389, 412-416, 418, 424, 427, 430, 432-438, 445-448, 451-453, 455-456, 460, 466, 468-469, 472, 477-478, 481, 538, 581  
reinforcement 187-191, 194-196, 198-202, 205, 235, 240-243, 256, 258, 362, 368, 374, 388-389, 415-416, 425, 449, 451-454, 457, 460, 462-463, 466-468, 506, 509, 511-522, 528-533  
Release Rate 335-337, 340, 345, 349, 355, 358, 367-368, 379-380, 389, 424, 427, 470-471  
residential 506, 509, 511-522  
rotation 11, 13, 19, 21, 27, 32, 34, 37, 51, 57, 73, 106, 158, 176-181, 185-186, 195-197, 201-202, 205, 233, 259-260, 264, 266, 268-269, 272, 291, 374, 376-377, 400-401, 406, 450, 468, 471, 506, 538, 543-544, 551-553, 563, 583

## S

seismic 33, 92, 231, 362, 503-504, 509, 526, 533, 539  
shear 4, 15-19, 21, 23, 26-27, 46, 48, 51-52, 59, 109-110, 112-113, 121-122, 158-160, 187, 200, 231, 238-244, 246-247, 256-261, 264, 266, 290-291, 388, 414-416, 424-430, 432, 435, 437-438, 445-448, 450-451, 453-454, 459-460, 470-473, 488  
Slender 19, 29, 45-46, 48, 52, 85, 231-234, 238, 243-244, 247, 257, 276, 362-363, 412, 414, 432, 435, 438, 445-446, 448, 453, 473, 488, 506  
solid differential 3, 14-15, 21, 340  
steel 41, 155, 172, 180, 184, 186-187, 189, 194-195, 198-201, 203, 205, 231, 233-234, 236, 243, 245-246, 273, 349, 368, 370, 376, 388, 457-458, 472, 538-539, 545, 547, 549, 554, 570, 573, 578, 580  
Stiffness 7, 38, 84-88, 90-91, 94, 97-99, 101, 105, 107-114, 116, 124, 126-127, 129, 131-132, 134, 137, 139, 142, 160, 233, 277, 280, 282, 305, 310-311, 315-316, 320-321, 325, 334, 336-337, 339, 341, 349, 364-365, 367, 375-376, 379, 388, 425, 470, 538-539, 547, 550, 552, 560, 570, 578, 581

strain 3, 7, 11-12, 14, 19, 21, 23, 141, 144-146, 148-153, 155-160, 164-167, 169-173, 177, 187-196, 202, 234, 243, 339-349, 355-359, 370-372, 414  
Stresses 3, 7, 10, 15-16, 18-19, 21, 23, 40, 45-46, 48, 52, 58, 60, 76-81, 85, 92, 101, 111, 121, 130, 138, 144, 147-148, 160, 165, 167-168, 170, 187, 198-200, 233, 239, 244, 246, 280, 285-287, 290, 309, 314, 318, 324, 333-334, 343, 346, 355, 363, 383, 404, 448, 490, 507, 551

## T

theory 1, 3-7, 10-11, 19, 21, 23, 27-31, 34, 46, 48, 52, 76-77, 79, 81, 85, 112, 116, 124, 139, 143, 154, 172, 174, 176, 178, 181, 189, 191, 201, 205, 238, 247, 337, 345, 349, 368-370, 372, 374, 376, 389, 424, 428, 479, 506-507, 539  
Timoshenko 4-5, 10, 14, 18-19, 23, 26-31, 48, 52, 76, 79, 81, 85, 109, 112, 116, 139, 238, 247  
transformation 36, 38, 42, 44, 55-56, 59, 75, 85, 90, 93, 106-107, 109-110, 112, 114, 118, 124, 126-128, 130, 132, 134, 136, 282  
transversal 12, 17, 187, 240-241, 243, 256, 258, 330, 480, 506, 509  
Tridimensional 10, 20-21, 23, 31-32, 54-56, 58-60, 82, 86, 90, 99, 139, 186, 197, 205, 231, 244-245, 247, 290, 329, 383, 445, 473, 476-477, 481, 538, 554, 556-557, 573, 578, 580-582  
tubular 538-541, 543, 549, 554, 556, 566, 580-581

## U

Ultra-low Cycle Fatigue 379, 389, 406, 429  
Unilateral 343-344, 346, 349, 359, 445-447, 450-451, 460, 473-474, 477, 481, 488, 547, 549-551, 558

## Y

yield function 141, 144-145, 148-151, 154, 156-157, 160, 164, 169, 171, 178, 180, 183-186, 197-198, 202, 205, 239-240, 245, 259-260, 264, 266, 269, 287, 291, 325-326, 340, 343, 356, 373-374, 401-402, 404, 429-430, 450, 471, 473, 477, 542, 549-551, 560, 581